東京帝國大學

地震研究所彙報

第十號

昭和七年

BULLETIN

OF THE

EARTHQUAKE RESEARCH INSTITUTE

TOKYO IMPERIAL UNIVERSITY

Vol. X.

1932.

目次

第十號

第一册（昭和七年三月）

			頁
1.	地震波によつて土地の固有振動が誘起される可能度第三報（英文）	妹澤克惟 金井清	1
2.	粘彈性體中の波動の問題に就て（英文）	妹澤克惟	19
3.	表面層を有し表面荷重を受ける彈性體の變形（英文）	西村源六郎	23
4.	地震群に就て（英文）	寺田寅彦	29
5.	本邦地震と世界各地地震の頻度間に存する統計的關係（英文）	山口生知	36
6.	地震回数の統計的研究（豫報）（邦文）	井上宇胤	43
7.	本邦各地の地震前の氣壓勾配に就いて（英文）	井上宇胤 長谷川惠副	55
8.	地震と脈動（豫報）（邦文）	井上宇胤	83
9.	地震波の傳播（第一報）（英文）	河角廣	94
10.	筑波山に於ける傾斜變化觀測報告（英文）	井上宇胤	130
11.	川奈に於ける傾斜變化觀測（英文）	高橋龍太郎	145
12.	東京市内二ケ所（本郷、丸ノ內）における地震動加速度比較（佛文）	石本巳四雄	171
13.	携帶用水平動地震計（英文）	岸上冬彦	188
14.	秦野に於ける山崩（邦文）	寺田寅彦 宮部直巳	192
15.	北條凹地帶（英文）	矢部長克 田山利三郎	200
16.	四國東南部の海岸地形とその地殼運動に對する意義（英文）	渡邊光	209
17.	狩野川冲積層地域の地形と昭和五年十一月二十六日伊豆地震の際にその地域に生じた地變及び地殼變形との關係（英文）	大塚彌之助	235
18.	第三紀以後に於ける伊豆地方の火山活動に就いて（豫報）（英文）	津屋弘逵	247

19. 伊豆震災地一二等三角點水平移動成果報告(邦文)……………… 261
20. 地震觀測報告(自昭和六年七月至同年九月)(英文)……………… 264

第二册 (昭和七年六月)

21. 地震波によつて土地の固有振動が誘起される可能度第四報(英文)…… 妹澤克惟 金井清 273
22. P波S波の振幅が震源距離によつて變化する割合(英文) 妹澤克惟 金井清 299
23. 溫度變化による半無限彈性體の變形式(英文)…… 西村源六郎 335
24. 地殼內部に存在する空窩が地殼の平衡に及ぼす影響(英文)…… 西村源六郎 高山威雄 352
25. 測量結果より得たる三角點變位の吟味(英文)…… 武藤勝彥 384
26. 地震と漁獲との關係(英文)…… 寺田寅彥 393
27. 三鷹村菱形基線の變形と關東地方に於ける地震頻度との關係(英文)…… 寺田寅彥 402
28. 昭和二年丹後地震に關聯せる丹後地方の地殼變形に關する研究(第四報)(英文)…… 坪井忠二 411
29. 昭和五年伊豆地震に關聯せる伊豆地方の地殼變形に關する研究(英文)…… 坪井忠二 435
30. 地震初動方向分布より震源に四重源の推定(佛文)…… 石本巳四雄 449
31. 伊豆半島、熱海町附近の二つの試錐(英文)…… 大塚彌之助 久野久 472
32. 硝子板のワレメに就て(英文)…… 西村源六郎 高山威雄 476
33. 興津、串本間一等水準線檢測成果報告(邦文)…… 490
34. 地震觀測報告(自昭和六年十月至同年十二月)(英文)…… 492

第三册 (昭和七年九月)

35. 關東地方の二三の地震に現はれた著しい波群及地震動の先驅部分(第三)(獨文)…… 松澤武雄 福富孝治 499
36. 本郷、三鷹に於ける初動入射角に就て(英文)…… 鈴木武夫 517
37. 旅順に於ける地殼傾斜變化の觀測(英文)…… 高橋龍太郎 531
38. 土佐灣の海底變化(英文)…… 寺田寅彥 560
39. 相異なる期間に於ける同一地域の地殼の垂直變動の比較(英文)…… 坪井忠二 570
40. 東京附近に於ける水準點の垂直變動に就て(英文)…… 宮部直巳 597
41. 震度階と地震最大加速度(佛文)…… 石本巳四雄 614

42. 關西地方に於ける地震の分布(英文)…………………… 矢島祐利 627

43. 名草地方の地震群(英文)………………………… 今村明恒・小平孝雄・今村久 636

44. 地震に伴ふ發光現象の調査(邦文)…………………… 武者金吉 649

45. 大阪地辷の研究(英文)……………………………… 那須信治 674

46. 大阪府堅上村峠に於ける地辷に關する調査報告(英文)‥ 宮部直巳 694

47. 西南日本外帶とフォッサ・マグナとに於ける鮮新世以後の地殼運動(其一)(英文)…………… 大塚彌之助 701

48. 重力の働ける楔形彈性體を貫通する水平圓形孔附近の應力(英文)…………………… 西村源六郎・高山威雄 723

49. 單層架構構造の震動(英文)…………………………… 妹澤克惟・金井清 767

第四册(昭和七年十二月)

50. 地表に一つの層があるときの地震波の反射及屈折(英文) 妹澤克惟・金井清 805

51. 三鷹村二十五米比較基線長の變化について(英文)…… 武藤勝彥・篠邦彥 817

52. 仁川に於て觀測された地殼の傾斜運動に就いて(英文)‥ 高橋龍太郎 826

53. 本所及び深川に於ける土地の沈降(英文)……………… 宮部直巳 844

54. ピボットに働く摩擦力率の測定(邦文)………………… 石本巳四雄・萩原尊禮・吉田幸雄 858

55. 日本海海底より採集せられたる礫に就いて(英文)…… 津屋弘逵 864

56. 休火山秋田駒ケ岳の活動(英文)……………………… 大塚彌之助 876

57. 地震時土壓の實驗的研究(英文)……………………… 物部長穂・松尾春雄 884

58. 二層又は三層架構の屈曲振動(英文)………………… 妹澤克惟・金井清 903

Contents.

Vol. X.

Part 1.—March, 1932.

Page

1. K. Sezawa and K. Kanai, Possibility of Free Oscillations of Strata exited by Seismic Waves. Part III. (in English) 1
2. K. Sezawa, Notes on the Waves in Visco-Elastic Solid Bodies. (in English) 19
3. G. Nishimura, On the Deformation of a Semi-infinite Elastic Body having a Surface Layer due to the Surface Loading. (in English) 23
4. T. Terada, On Swarm Earthquakes. (in English) 29
5. S. Yamaguti, Statistical Relation between the Frequencies of Earthquakes in Japan and Other Parts of the World. (in English) 36
6. W. Inouye, Statistical Investigations on Earthquake Numbers. (in Japanese) 43
7. W. Inouye and K. Hasegawa, On the Barometric Gradients at the Epochs of the Earthquakes in Japan. (in English) .. 55
8. W. Inouye, Earthquake and Pulsation. (in Japanese) 83
9. H. Kawasumi, Study on the Propagation of Seismic Waves. (The first paper). (in English) 94
10. W. Inouye. On Earth-tiltings observed at Mt. Tukuba. (in English) 130
11. R. Takahasi, Tilting Motion of the Earth's Crust observed at Kawana. (in English) 145
12. M. Ishimoto, Comparaison accélérométrique des secousses sismiques dans deux parties de la ville de Tôkyô. (en français) 171

13. F. KISHINOUYE, A Portable Horizontal Pendulum Seismometer. (in English) 188
14. T. TERADA and N. MIYABE, Landslide at Hatano. (in Japanese) 192
15. H. YABE and R. TAYAMA, Hôjô Trough. (in English) 200
16. A. WATANABE, The Geomorphology of the Coastal District of Southeastern Sikoku; a Contribution to the Knowledge of the Recent Crustal Movements of the Area under Discussion. (in English) 209
17. Y. ÔTUKA, The Geomorphology of the Kano-gawa Alluvial Plain, the Earthquake Fissures of Nov. 26, 1930, and the Pre- and Post-seismic Crust Deformations. (in English) 235
18. H. TSUYA, Neogene and Quaternary Vulcanism in the Idu District. (Preliminary Report). (in English) 247
19. Horizontal Displacements of the Primary and Secondary Triangulation Points in Idu Earthquake Districts. (in Japanese) 261
20. Seismometrical Report. (July—September, 1931). (in English) .. 264

Part 2.—June, 1932.

21. K. SEZAWA und K. KANAI, Possibility of Free Oscillations of Strata exited by Seismic Waves. Part IV. (in English) ... 273
22. K. SEZAWA and K. KANAI, Amplitudes of P- and S-waves at Different Focal Distances. (in English) 299
23. G. NISHIMURA, On the Expressions of the Deformation of a Semi-infinite Elastic Body due to the Temperature Variation. (in English) 335
24. G. NISHIMURA and T. TAKAYAMA, On the Effect of a Spherical Cavity on the Equilibrium of the Gravitating Semi-infinite Elastic Solid. (in English) 352
25. K. MUTO, A Study of Displacements of Triangulation Points. (in English) 384
26. T. TERADA, On some Probable Influence of Earthquakes upon Fisheries. (in English) 393
27. T. TERADA, Deformation of the Rhombic Base Lines at Mitaka

Contents.

Vol. X.

Part 1.—March, 1932.

Page

1. K. Sezawa and K. Kanai, Possibility of Free Oscillations of Strata exited by Seismic Waves. Part III. (in English) 1
2. K. Sezawa, Notes on the Waves in Visco-Elastic Solid Bodies. (in English) 19
3. G. Nishimura, On the Deformation of a Semi-infinite Elastic Body having a Surface Layer due to the Surface Loading. (in English) 23
4. T. Terada, On Swarm Earthquakes. (in English) 29
5. S. Yamaguti, Statistical Relation between the Frequencies of Earthquakes in Japan and Other Parts of the World. (in English) 36
6. W. Inouye, Statistical Investigations on Earthquake Numbers. (in Japanese) 43
7. W. Inouye and K. Hasegawa, On the Barometric Gradients at the Epochs of the Earthquakes in Japan. (in English) .. 55
8. W. Inouye, Earthquake and Pulsation. (in Japanese) 83
9. H. Kawasumi, Study on the Propagation of Seismic Waves. (The first paper). (in English) 94
10. W. Inouye. On Earth-tiltings observed at Mt. Tukuba. (in English) 130
11. R. Takahasi, Tilting Motion of the Earth's Crust observed at Kawana. (in English) 145
12. M. Ishimoto, Comparaison accélérométrique des secousses sismiques dans deux parties de la ville de Tôkyô. (en français) 171

13. F. KISHINOUYE, A Portable Horizontal Pendulum Seismometer. (in English) 188

14. T. TERADA and N. MIYABE, Landslide at Hatano. (in Japanese) 192

15. H. YABE and R. TAYAMA, Hôjô Trough. (in English) 200

16. A. WATANABE, The Geomorphology of the Coastal District of Southeastern Sikoku; a Contribution to the Knowledge of the Recent Crustal Movements of the Area under Discussion. (in English) 209

17. Y. ÔTUKA, The Geomorphology of the Kano-gawa Alluvial Plain, the Earthquake Fissures of Nov. 26, 1930, and the Pre- and Post-seismic Crust Deformations. (in English) 235

18. H. TSUYA, Neogene and Quaternary Vulcanism in the Idu District. (Preliminary Report). (in English) 247

19. Horizontal Displacements of the Primary and Secondary Triangulation Points in Idu Earthquake Districts. (in Japanese) 261

20. Seismometrical Report. (July—September, 1931). (in English) .. 264

Part 2.—June, 1932.

21. K. SEZAWA und K. KANAI, Possibility of Free Oscillations of Strata exited by Seismic Waves. Part IV. (in English) 273

22. K. SEZAWA and K. KANAI, Amplitudes of P- and S-waves at Different Focal Distances. (in English) 299

23. G. NISHIMURA, On the Expressions of the Deformation of a Semi-infinite Elastic Body due to the Temperature Variation. (in English) 335

24. G. NISHIMURA and T. TAKAYAMA, On the Effect of a Spherical Cavity on the Equilibrium of the Gravitating Semi-infinite Elastic Solid. (in English) 352

25. K. MUTO, A Study of Displacements of Triangulation Points. (in English) 384

26. T. TERADA, On some Probable Influence of Earthquakes upon Fisheries. (in English) 393

27. T. TERADA, Deformation of the Rhombic Base Lines at Mitaka

and Earthquake Frequency in Kwantô Districts. (in English) 402

28. C. Tsuboi, Investigation on the Deformation of the Earth's Crust in the Tango District connected with the Tango Earthquake of 1927. (Part 4). (in English) 411

29. C. Tsuboi, Investigation on the Deformation of the Earth's Crust in Idu Peninsula connected with the Idu Earthquake of Nov. 26, 1930. (in English).......................... 435

30. M. Ishimoto, Existence d'une source quadruple au foyer sismique d'après l'étude de la distribution des mouvements initiaux des secousses sismiques. (en français) 449

31. Y. Ôtuka and H. Kuno, On Two Borings near Atami-mati, Idu Peninsula. (in English)............................ 472

32. G. Nishimura and T. Takayama, Some Experiments on Crack Formation in a Glass Plate. (in English)................. 476

33. Precise Levellings along a Route from Okitu to Kusimoto. (in Japanese) 490

34. Seismometrical Report. (October—December, 1931) (in English) 492

Part 3.—September, 1932.

35. T. Matuzawa und T. Fukutomi, Zwei merkwürdige Wellengruppen bei einigen Erdbeben in Kwantô und die dritte Mitteilung über den vorlaufenden Teil der Erdbebenbewegungen. (in deutsch). 499

36. T. Suzuki, On the Angle of Incidence of the Initial Motion observed at Hongô and Mitaka. (in English) 517

37. R. Takahasi, Tilting Motion of the Earth's Crust observed at Ryozyun (Port Arthur). (in English) 531

38. T. Terada, Change of Depth in the Bay of Tosa. (in English) 560

39. C. Tsuboi, Comparison of the Modes of the Vertical Deformations of the Earth's Crust in the Same District during Different Time Intervals. (in English) 570

40. N. Miyabe, On Different Types of Time-variation in the Rate of Vertical Displacement of Bench-marks in Tôkyô and its

Vicinity. (in English).. 597

41. M. Ishimoto, Echelle d'intensité sismique et accélération maxima. (en français) 614

42. S. Yazima, On Statistical Distributions of Earthquakes in Kwansai District. (in English).. 627

43. A. Imamura, T. Kodaira and H. Imamura, The Earthquake Swarms of Nagusa and Vicinity. (in English) 636

44. K. Musya, Investigations into the Luminous Phenomena accompanying Earthquakes. (in Japanese) 649

45. N. Nasu, A Study of the Osaka Landslide. (in English) 674

46. N. Miyabe, Landslide at Tôge, Katagami-mura, Osaka-Hu. (in English) 694

47. Y. Ôtuka, Post Pliocene Crustal Movements in the Outer Zone of Southwest Japan and in the "Fosa Magna". (I). (in English).. 701

48. G. Nishimura and T. Takayama, On the Stress Distribution in the Vicinity of a Horizontal Circular Hole in a Gravitating Wedge-Shaped Elastic Solid. (in English) 723

49. K. Sezawa and K. Kanai, Vibrations of a Singled-storyed Framed Structure. (in English) 767

Part 4.—December, 1932.

50. K. Sezawa and K. Kanai, Reflection and Refraction of Seismic Waves in a Stratified Body. (in English).. 805

51. K. Muto and K. Sino, On Variations in the Length of the Mitaka Comparison Base Line. (in English) 817

52. R. Takahasi, A Note on the Tilting Motion of the Earth's Crust observed at Zinsen (Chemulpo). (in English) 826

53. N. Miyabe, On Depression of the Earth's Crust in Honzyô and Hukagawa, Tokyo. (in English).. 844

54. M. Ishimoto, T. Hagiwara et Y. Yosida, Mesure du moment de frottement au pivot. (en japonais) 858

55. H. Tsuya, On Some Pebbles collected from the Floor of the

Japan Sea. (in English) 864
56. Y. Ôtuka, Recent Activity of the Long-Dormant Akita-Komagatake Volcano in North-East Japan. (in English) 876
57. N. Mononobe and H. Matsuo, Experimental Investigation of Lateral Earth Pressure during Earthquakes. (in English) .. 884
58. K. Sezawa and K. Kanai, Vibrations of a Two- or Three-storeyed Structure. (in English) 903

第十號索引

頁

福富孝治、松澤武雄；松澤武雄、福富孝治　參照

萩原尊禮、吉田幸雄、石本巳四雄；石本巳四雄、萩原尊禮、吉田幸雄　參照

長谷川惠副、井上宇胤；井上宇胤、長谷川惠副　參照

金井清、妹澤克惟；妹澤克惟、金井清　參照

河角廣　(9) 地震波の傳播(第一報)(英文)………………………… 94

岸上冬彥　(13) 携帶用水平動地震計(英文)………………………… 188

小平孝雄、今村久、今村明恒；今村明恒、小平孝雄、今村久　參照

久野久、大塚彌之助；大塚彌之助、久野久　參照

今村明恒、小平孝雄、今村久 (43) 名草地方の地震群(英文)………… 636

今村久、今村明恒、小平孝雄；今村明恒、小平孝雄、今村久　參照

井上宇胤　(6) 地震回數の統計的研究(豫報)(邦文)………………… 43

井上宇胤　(8) 地震と脈動(豫報)(邦文)………………………… 83

井上宇胤　(10) 筑波山に於ける傾斜變化觀測報告(英文)………… 130

井上宇胤、長谷川惠副　(7) 本邦各地の地震前の氣壓勾配に就いて(英文)…… 55

石本巳四雄　(12) 東京市内二ケ所(本鄉、丸ノ内)における地震動加速度比較(佛文)………………………… 171

石本巳四雄　(30) 地震初動方向分布より震源に四重源の推定(佛文)………… 449

石本巳四雄　(41) 震度階と地震最大加速度(佛文)………………… 614

石本巳四雄、萩原尊禮、吉田幸雄　(54) ピボットに働く摩擦力率の測定(邦文)… 858

松尾春雄、物部長穗；物部長穗、松尾春雄　參照

松澤武雄、福富孝治　(35) 關東地方の二三の地震に現はれた著しい波群及地震動の先驅部分(第三)(獨文)………………………… 499

宮部直巳　(40) 東京附近に於ける水準點の垂直變動に就て(英文)………… 597

宮部直巳　(46) 大阪府堅上村峠に於ける地辷に關する調査報告(英文)……… 694

宮部直巳　(53) 本所及び深川に於ける土地の沈降(英文)………… 844

宮部直巳、寺田寅彥；寺田寅彥、宮部直巳　參照

物部長穗、松尾春雄　(57) 地震時土壓の實驗的研究(英文)………… 884

武者金吉　(44) 地震に伴ふ發光現象の調査(邦文)……………… 649

武藤勝彦　(25) 測量結果より得たる三角點變位の吟味(英文) ……………… 384
武藤勝彦、篠邦彦　(51) 三鷹村二十五米比較基線長の變化について(英文) …… 817
那須信治　(45) 大阪地辷の研究(英文) ……………………………………… 674
西村源六郎　(3) 表面層を有し表面荷重を受ける彈性體の變形(英文) ………… 23
西村源六郎　(23) 溫度變化による半無限彈性體の變形式(英文) ……………… 335
西村源六郎、高山威雄　(24) 地殼內部に存在する空窩が地殼の平衡に及ぼす影響
(英文)……………………………………………………………………… 352
西村源六郎、高山威雄　(32) 硝子板のワレメに就て(英文) ………………… 476
西村源六郎、高山威雄　(48) 重力の働ける楔形彈性體を貫通する水平圓形孔附近
の應力(英文)……………………………………………………………… 723
大塚彌之助　(17) 狩野川冲積層地域の地形と昭和五年十一月二十六日伊豆地震の
際にその地域に生じた地變及び地殼變形との關係(英文)……………… 235
大塚彌之助　(47) 西南日本外帶とフオッサ・マグナとに於ける鮮新世以後の地殼
運動(其一)(英文)………………………………………………………… 701
大塚彌之助　(56) 休火山秋田駒ヶ岳の活動(英文)……………………………… 876
大塚彌之助、久野久　(31) 伊豆半島、熱海町附近の二つの試錐(英文)………… 472
妹澤克惟　(2) 粘彈性體中の波動の問題に就て(英文) ………………………… 19
妹澤克惟、金井清　(1) 地震波によつて土地の固有振動が誘起される可能度　第
三報(英文)……………………………………………………………………… 1
妹澤克惟、金井清　(21) 地震波によつて土地の固有振動が誘起される可能度　第
四報(英文)……………………………………………………………………… 273
妹澤克惟、金井清　(22) P波S波の振幅が震源距離によつて變化する割合(英文) 299
妹澤克惟、金井清　(50) 地表に一つの層があるときの地震波の反射及屈折(英文) 805
妹澤克惟、金井清　(49) 單層架構構造の震動(英文)…………………………… 767
妹澤克惟、金井清　(58) 二層又は三層架構の屈曲振動(英文)………………… 903
篠邦彦、武藤勝彦；武藤勝彦、篠邦彦　參照
鈴木武夫　(36) 本郷、三鷹に於ける初動入射角に就て(英文)………………… 517
高橋龍太郎　(11) 川奈に於ける傾斜變化觀測(英文)…………………………… 145
高橋龍太郎　(37) 旅順に於ける地殼傾斜變化の觀測(英文)…………………… 531
高橋龍太郎　(52) 仁川に於て觀測された地殼の傾斜運動に就いて(英文)……… 826
高山威雄、西村源六郎；西村源六郎、高山威雄　參照

田山利三郎、矢部長克；矢部長克、田山利三郎 參照
寺田寅彦 (4) 地震群に就て(英文)…… 29
寺田寅彦 (26) 地震と漁獲との關係(英文)…… 393
寺田寅彦 (27) 三鷹村菱形基線の變形と關東地方に於ける地震頻度との關係(英文)…… 402
寺田寅彦 (38) 土佐灣の海底變化(英文)…… 560
寺田寅彦、宮部直巳 (14) 秦野に於ける山崩(邦文)…… 192
坪井忠二 (28) 昭和二年丹後地震に關聯せる丹後地方の地殼變形に關する研究(第四報)(英文)…… 411
坪井忠二 (29) 昭和五年伊豆地震に關聯せる伊豆地方の地殼變形に關する研究(英文)…… 435
坪井忠二 (39) 相異なる期間に於ける同一地域の地殼の垂直變動の比較(英文)…… 570
津屋弘逵 (18) 第三紀以後に於ける伊豆地方の火山活動に就いて(豫報)(英文)…… 247
津屋弘逵 (55) 日本海海底より採集せられたる礫に就いて(英文)…… 864
渡邊 光 (16) 四國東南部の海岸地形とその地殼運動に對する意義(英文)…… 209
矢部長克、田山利三郎 (15) 北條凹地帶(英文)…… 200
矢島祐利 (42) 關西地方に於ける地震の分布(英文)…… 627
山口生知 (5) 本邦地震と世界各地地震の頻度間に存する統計的關係(英文)…… 36
吉田幸雄、石本巳四雄、荻原尊禮；石本巳四雄、荻原尊禮、吉田幸雄 參照
地震研究所 (19) 伊豆震災地一二等三角點水平移動成果報告(邦文)…… 261
地震研究所 (33) 興津、串本間一等水準線檢測成果報告(邦文)…… 490
地震研究所 (20) 地震觀測報告(自昭和六年七月至同年九月)(英文)…… 264
地震研究所 (34) 地震觀測報告(自昭和六年十月至同年十二月)(英文)…… 492

Index to Vol. X.

Page

FUKUTOMI, T. and MATUZAWA, T.; *See* MATUZAWA, T. and FUKUTOMI, T.

HAGIWARA, T., YOSIDA, Y. and ISHIMOTO, M.; *See* ISHIMOTO, M., HAGIWARA, T. and YOSIDA, Y.

HASEGAWA, K. and INOUYE, W.; *See* INOUYE, W. and HASEGAWA, K.

KANAI, K. and SEZAWA, K.; *See* SEZAWA, K. and KANAI, K.

KAWASUMI, H. (9) Study on the Propagation of Seismic Waves. (The first paper). (in English) 94

KISHINOUYE. F. (13) A Portable Horizontal Pendulum Seismometer. (in English) 188

KODAIRA, T., IMAMURA, K. and IMAMURA, A.; *See* IMAMURA, A., KODAIRA, T. and IMAMURA, H.

KUNO, H. and ÔTUKA, Y.; *See* ÔTUKA, Y. and KUNO, H.

IMAMURA, A., KODAIRA, T. and IMAMURA, H. (43) The Earthquake Swarms of Nagusa and Vicinity. (in English) 636

IMAMURA, H., IMAMURA, A. and KODAIRA, T.; *See* IMAMURA, A., KODAIRA, T. and IMAMURA, H.

INOUYE, W. (6) Statistical Investigations on Earthquake Numbers. (in Japanese) 43

INOUYE, W. (8) Earthquake and Pulsation. (in Japanese) 83

INOUYE, W. (10) On Earth-tiltings observed at Mt. Tukuba. (in English) 130

INOUYE, W. and HASEGAWA, K. (7) On the Barometric Gradients at the Epochs of the Earthquakes in Japan. (in English) 55

ISHIMOTO, M. (12) Comparaison accélérométrique des secousses sismiques dans deux parties de la ville de Tôkyô (en français) 171

ISHIMOTO, M. (30) Existence d'une source quadruple au foyer sismique d'après l'étude de la distribution des mouvements initiaux des secousses sismiques. (en français) 449

ISHIMOTO, M. (41) Echelle d'intensité sismique et accélération maxima. (en français) 614

ISHIMOTO, M., HAGIWARA, T. et YOSIDA, Y. (54) Mesure du moment de frottement au pivot. (en japonais) 858

MATSUO, H. and MONONOBE, N.; *See* MONONOBE, N. and MATSUO, H.

MATUZAWA, T. und FUKUTOMI, T. (35) Zwei merkwürdige Wellengruppen bei einigen Erdbeben in Kwantô und die dritte Mitteilung über den vorlaufenden Teil der Erdbebenbewegungen. (in deutsch) 499

MIYABE, N. (40) On Different Types of Time-variation in the Rate of Vertical Displacement of Bench-marks in Tôkyô and its Vicinity. (in English) 597

MIYABE, N. (46) Landslide at Tôge, Katagami-mura, Osaka-Hu. (in English) 694

MIYABE, N. (53) On Depression of the Earth's Crust in Honzyô and Hukagawa, Tokyo. (in English) 844

MIYABE, N. and TERADA, T.; *See* TERADA, T. and MIYABE, N.

MONONOBE, N. and MATSUO, H. (57) Experimental Investigation of Lateral Earth Pressure during Earthquakes. (in English) 884

MUSYA, K. (44) Investigations into the Luminous Phenomena accompanying Earthquakes. (in Japanese) 649

MUTO, K. (25) A Study of Displacements of Triangulation Points. (in English) 384

MUTO, K. and SINO, K. (51) On Variations in the Length of the Mitaka Comparison Base Line. (in English) 817

NASU, N. (45) A Study of Osaka Landslide. (in English) 674

NISHIMURA, G. (3) On the Deformation of a Semi-infinite Elastic Body having a Surface Layer due to the Surface Loading. (in English) 23

NISHIMURA, G. (23) On the Expressions of the Deformation of a Semi-infinite Elastic Body due to the Temperature Variation. (in English) 335

NISHIMURA, G. and TAKAYAMA, T. (24) On the Effect of a Spherical Cavity on the Equilibrium of the Gravitating Semi-infinite Elastic Solid. (in English) 352

NISHIMURA, G. and TAKAYAMA, T. (32) Some Experiments on Crack

Formation in a Glass Plate. (in English)........................ 476
NISHIMURA, G. and TAKAYAMA, T. (48) On the Stress Distribution in the Vicinity of a Horizontal Circular Hole in a Gravitating Wedge-Shaped Elastic Solid. (in English) 723
ÔTUKA, Y. (17) The Geomorphology of the Kano-gawa Alluvial Plain, the Earthquake Fissures of Nov. 26, 1930, and the Pre- and Post-seismic Crust Deformations. (in English).............. 235
ÔTUKA, Y. (47) Post Pliocene Crustal Movements in the Outer Zone of Southwest Japan and in the "Fossa Magna." (I). (in English) 701
ÔTUKA, Y. (56) Recent Activity of the Long-Dormant Akita-Komagatake Volcano in North-East Japan. (in English) 876
ÔTUKA, Y. and KUNO, H. (31) On Two Borings near Atami-mati, Idu Peninsula. (in English) 472
SEZAWA, K. (2) Notes on the Waves in Visco-Elastic Solid Bodies. (in English) 19
SEZAWA, K. and KANAI, K. (1) Possibility of Free Oscillations of Strata excited by Seismic Waves. Part III. (in English) 1
SEZAWA, K. and KANAI, K. (21) Possibility of Free Oscillations of Strata exited by Seismic Waves. Part IV. (in English) 273
SEZAWA, K. and KANAI, K. (22) Amplitudes of P- and S-Waves at Different Focal Distances. (in English) 299
SEZAWA, K. and KANAI, K. (50) Reflection and Refraction of Seismic Waves in a Stratified Body. (in English) 805
SEZAWA, K. and KANAI, K. (49) Vibration of a Singled-storyed Framed Elastic Solid. (in English)............................ 767
SEZAWA, K. and KANAI, K. (58) Vibrations of a Two- or Three-storeyed Structure. (in English) 903
SINO, K. and MUTO, K.; *See* MUTO, K. and SINO, K.
SUZUKI, T. (36) On the Angle of Incidence of the Initial Motion observed at Hongô and Mitaka. (in English) 517
TAKAHASI, R. (11) Tilting Motion of the Earth's Crust observed at Kawana. (in English) 145
TAKAHASI, R. (37) Tilting Motion of the Earth's Crust observed

at Ryozyun (Port Arthur). (in English) 531
TAKAHASI, R. (52) A Note on the Tilting Motion of the Earth's Crust observed at Zinsen (Chemulpo). (in English) 826
TAKAYAMA, T. and NISHIMURA, G.; *See* NISIMURA, G. and TAKAYAMA, T.
TAYAMA, R. and YABE, H.; *See* YABE, H. and TAYAMA, R.
TERADA, T. (4) On Swarm Earthquakes. (in English) 29
TERADA, T. (26) On Some Probable Influence of Earthquakes upon Fisheries. (in English) 393
TERADA, T. (27) Deformation of the Rhombic Base Lines at Mitaka and Earthquake Frequency in Kwantô Districts. (in English) 402
TERADA, T. (38) Change of Depth in the Bay of Tosa. (in English) 560
TERADA, T. and MIYABE, N. (14) Landslide at Hatano. (in Japanese) 192
TSUBOI, C. (28) Investigation on the Deformation of the Earth's Crust in the Tango District connected with the Tango Earthquake of 1927. (Part 4). (in English) 411
TSUBOI, C. (29) Investigation on the Deformation of the Earth's Crust in Idu Peninsula connected with the Idu Earthquake of Nov. 26, 1930. (in English) 435
TSUBOI, C. (39) Comparison of the Modes of the Vertical Deformations of the Earth's Crust in the Same District during Different Time Intervals. (in English) 570
TSUYA, H. (18) Neogene and Quaternary Vulcanism in the Idu District. (Preliminary Report). (in English) 247
TSUYA, H. (55) On Some Pebbles collected from the Floor of the Japan Sea. (in English) 864
WATANABE, A. (16) The Geomorphology of the Coastal District of South-eastern Sikoku; a Contribution to the Knowledge of the Recent Crustal Movements of the Area under Discussion. (in English) 209
YABE, H. and TAYAMA, R. (15) Hôjô Trough. (in English) 200
YAZIMA, S. (42) On Statistical Distributions of Earthquakes in Kwansai District. (in English) 627

YAMAGUTI, S. (5) Statistical Relation between the Frequencies of Earthquakes in Japan and Other Parts of the World. (in English) 36

YOSIDA, Y., ISHIMOTO, M. and HAGIWARA, T.; *See* ISHIMOTO, M., HAGIWARA, T. and YOSIDA, Y.

EARTHQUAKE RESEARCH INSTITUTE. (19) Horizontal Displacements of the Primary and Secondary Triangulation Points in Idu Earthquake Districts. (in Japanese) 261

EARTHQUAKE RESEARCH INSTITUTE. (33) Precise Levellings along a Route from Okitu to Kusimoto. (in Japanese).................. 490

EARTHQUAKE RESEARCH INSTITUTE. (20) Seismometrical Report. (July–September, 1931). (in English) 264

EARTHQUAKE RESERCH INSTITUTE. (34) Seismometrical Report. (October–December, 1931). (in English)......................... 492

――所　報――

○ 談話會記事

第六十六回談話會（昭和六年十二月十五日）

1. 我が國に於ける地震波傳播異常に就て	和達清夫
1. 海岸地形より見たる四國東南部の地殼運動	渡邊光
1. 伊豆地方に於ける第三紀以後の火山活動に就て（豫報）	津屋弘逵
1. 永久變移を受けた場合の振子の振動	坪井忠二
1. 三鷹菱形基線の變形と關東地方地震頻度との關係（續報）	寺田寅彦
1. 川奈に於ける傾斜變化觀測	高橋龍太郎
1. 地震波によつて土地の固有振動が誘起される可能性度（第二報）	妹澤克惟 金井清
1. 地震に伴ふ經度の變化	白井俊明
1. 地震動と地震記象	河角廣

第六十七回談話會（昭和七年一月十九日）

1. 地震と漁獲	寺田寅彦 渡部哲
1. 南日向地震に伴ひたる發光現象に就て	武者金吉
1. 地殼内部に存在する空窩が地殼の平衡に及ぼす影響	西村源六郎 高山威雄
1. 相模灣海底測量結果	海軍水路部
1. 熱海町附近の試錐	大塚彌之助 久野久
1. 上下動加速度地震計	石本巳四雄

○ 出　張

1. 昭和六年十二月十日地震事項調査の爲め東京府下（三鷹村）へ出張	那須信治
1. 昭和六年十二月十五日地震計据付の爲め靜岡縣下へ出張	小平孝雄
1. 昭和六年十二月二十三日地質調査の爲め靜岡縣下へ出張	津屋弘逵
1. 昭和七年一月二十九日地震事項調査の爲め大阪府下へ出張	那須信治
1. 昭和七年一月二十九日地震事項調査の爲め大阪府下へ出張	宮部直巳

——所　報——

○談話會記事

第六十八回談話會（昭和七年二月十六日）

1. 大阪府下の地辷りに關する調査報告	宮部直巳 那須信治
1. 溫度變化が半無限彈性體の變形に及ぼす影響(其の二)	西村源六郎
1. 地殼內部に存在する空窩が地殼の平衡に及ぼす影響(其の二)	西村源六郎 高山威雄
1. 硝子板のワレメに就て(其の二)	西村源六郎 高山威雄
1. 地震波によつて土地の固有振動が誘起される可能度(第三報)	妹澤克惟 金井清
1. P波及S波の振幅が震源距離によつて變化する割合	妹澤克惟 金井清

第六十九回談話會（昭和七年三月十五日）

1. 關東方面に於ける震源の移動方向に就て(續報)	山口生知
1. 北伊豆の地質（其一　丹那・畑毛間）	津屋弘逵
1. 地震初動方向分布より震源に四重源存在の推定	石本巳四雄
1. 伊豆地震に關係せる地殼變動	坪井忠二
1. 旅順に於ける地表傾斜變化の觀測	高橋龍太郎
1. 山脈や段丘の安定に關する問題(其の一)	西村源六郎 高山威雄
1. 硝子板のワレメに就て(其の三)	西村源六郎 高山威雄
1. 大阪府中河內郡峠地辷調査報告(續報)	那須信治
1. 地震動の大きさに就て(發震機巧との關係)	河角廣

第七十回談話會（昭和七年四月廿六日）

1. 上諏訪溫泉地帶地下水の混合狀態	吉村信吉
1. 基線長の伸縮に就いて	武藤勝彥
1. 地震と脈動(第二報)	井上宇胤
1. 平面波屈折の一例	河角廣 鈴木武夫
1. 關西地方に於ける地震の分布に就いて	矢島祐利
1. 東北・北海道方面並に日本全國に於ける震源の移動方向に就いて	山口生知

○ 出　張

1. 昭和七年二月二日地震事項調査の爲大阪府下へ出張　石　本　巳　四　雄
1. 昭和七年二月八日地震事項調査の爲大阪府下へ出張　宮　部　直　巳
1. 昭和七年二月十三日地震事項調査の爲大阪府下へ出張　那　須　信　治
1. 昭和七年三月三十一日學術上取調の爲大阪、京都二府下へ出張　大　塚　彌　之　助
1. 昭和七年三月十一日地震事項調査の爲長野縣下へ出張　高　橋　龍　太　郎
1. 昭和七年五月三日地震計觀測用務の爲千葉縣下へ出張　囑託　小　平　孝　雄
1. 昭和七年五月四日地震事項調査の爲和歌山縣下へ出張　岸　上　冬　彦

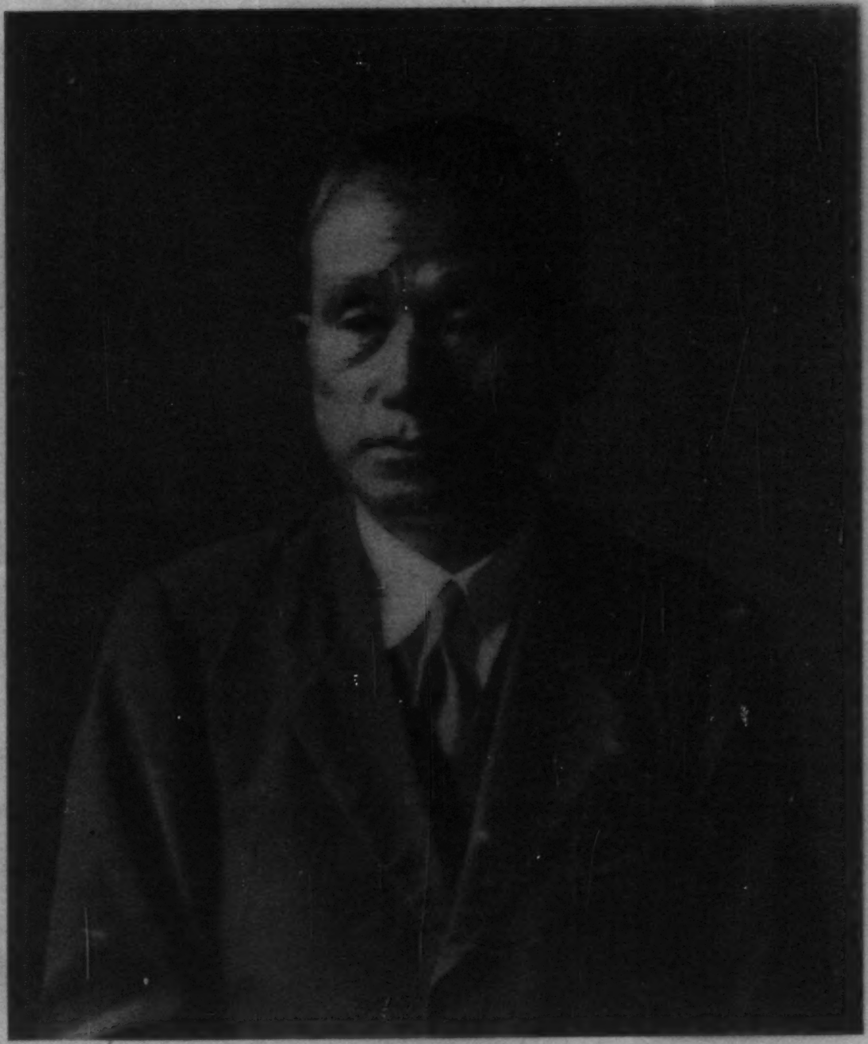

Kyoji Suyehiro

○出　張

1. 昭和七年二月二日地震事項調査の爲大阪府下へ出張　石本巳四雄
1. 昭和七年二月八日地震事項調査の爲大阪府下へ出張　宮部直巳
1. 昭和七年二月十三日地震事項調査の爲大阪府下へ出張　那須信治
1. 昭和七年三月三十一日學術上取調の爲大阪、京都二府下へ出張　大塚彌之助
1. 昭和七年三月十一日地震事項調査の爲長野縣下へ出張　高橋龍太郎
1. 昭和七年五月三日地震計觀測用務の爲千葉縣下へ出張　囑託　小平孝雄
1. 昭和七年五月四日地震事項調査の爲和歌山縣下へ出張　岸上冬彦

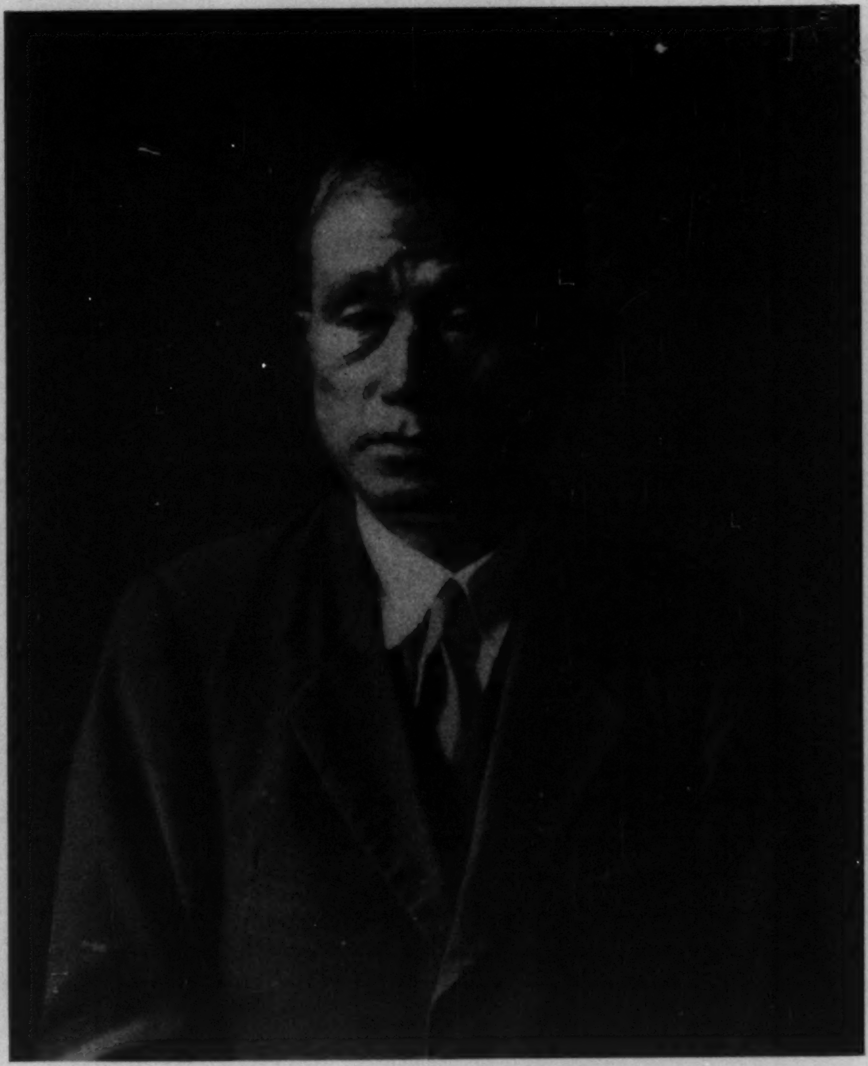

Kyoji Suyehiro

Obituaire du Professeur Kyoji Suyehiro, Directeur de l'Institut de Recherches sur les Tremblements de terre.

Le 9 avril 1932 au matin on apprenait que Monsieur le Professeur Kyoji Suyehiro de l'Université Impériale de Tôkyô était tombé gravement malade ; il mourait le jour même, à 8 heures du soir d'une pneumonie. Sa disparition si soudaine nous à douloureusement surpris, et sa perte nous laisse de vifs regrets. Les funérailles eurent lieu le 12 avril à Aoyama-saidyô et l'enterrement au cimetière de Somei.

Notre regretté Professeur naquit le 24 janvier 1877 à Tôkyô ; il était le second fils de Monsieur Sigeyasu Suehiro, écrivain et homme politique bien connu. Sorti du Premier Lycée Supérieur, il suivit les cours de constructions navales à la Faculté du Génie de l'Université Impériale de Tôkyô. Il termina ses études en 1900 et fut nommé en 1902 professeur-assistant à la Faculté. Il passa en 1909 son doctorat, fit en séjour de deux ans à l'étranger, et devint, à son retour, professeur titulaire à l'Université. Il fut élu, en outre, Membre de l'Académie des Sciences en 1927. D'un autre côté, il fonda en 1919 l'Institut Mitubisi, et en 1925 l'Institut de Recherches sur les Tremblements de terre : il avait occupé un poste important dans le premier et fut directeur du second jusqu'à sa mort. De plus il a été président de la Société de Constructions Navales ainsi que de la Société Physico-mathématique.

M. le Professur Suyehiro laissé derrière lui une oeuvre considérable. De ses travaux, nous citerons seulement en ce qui concerne le génie maritime : Discussions sur la résistance de construction des bateaux, Etude du roulis sur des modèles de bateaux au moyen de vagues produites artificiellement, Construction d'un appareil mesurant la torsion d'un arbre tournant, Construction d'une machine capable de balancer un corp tournant ; en ce qui concerne la sismologie : Calcul et mesure de l'oscillation des bâtiments, Constatation de la période propre du terrain dans les secousses sismiques à l'aide d'un sismographe-analysateur. C'est très connu qu'il était le lauréat du prix de l'Académie Impériale des Sciences aussi que de la Société Anglaise de l'Architecture Navale.

L'année dernière, il fut invité par la Société de génie civil des Etats-Unis à donner des conférences sur l'influence des secousses sismiques sur les constructions civiles. Au retour, il visita la France où il donna aussi une conférence sur certaines questions du génie maritime. Il revint au Japon le 9 mars : qui aurait pu supposer alors, qu'un mois

plus tard, il ne serait plus parmi nous!

D'une autre coté, par son enseignement, il a exercé une grande influence sur ses étudiants. Il a dirigé en même temps beaucoup de chercheurs: on retrouvera ses idées dans de nombreux travaux exécutés actuellement dans les deux Instituts, qu'il a fondés et a dirigés jusqu'à sa mort.

東京帝國大學地震研究所長末廣恭二教授小傳

昭和七年四月九日朝、東京帝國大學教授工學博士末廣恭二先生の危篤の報が傳へられ、續いて同日午後八時遂に永眠せられることとなつた。遽かの逝去の事とて人々は驚き且つ悲み、教授の御他界を心から哀惜した。葬儀は四月十二日青山齋場に於て行はれ、後染井墓地に埋葬された。

故末廣教授は明治十年一月二十四日、政治家として又文筆を以て聞えた末廣重恭氏の次男として東京に誕生せられた、第一高等學校を經て東京帝國工科大學造船學科に入學、明治三十三年卒業されると同時に長崎に赴かれた。明治三十五年には同學の助教授に任ぜられ、其後明治四十二年には學位を得られると同時に二年間外遊の途に就かれる事となつた。歸朝後直ちに同學教授に任ぜられ、爾來其の職に居られたが、昭和二年には帝國學士院會員を仰付けられる光榮を擔はれた。他方において故教授は大正八年三菱研究所、大正十四年地震研究所を創設され、逝かれる迄夫々顧問、所長の要職に就任して居られた。又學會方面に於ても學術研究會議工學部々長を初め、且て造船協會々長、日本數學物理學會委員長として斯道の爲め少なからざる盡力を爲されたのである。

故末廣教授は貴重なる多くの研究論文を殘されたが、其中船舶工學方面に於ては、船體强度論、水槽中に於ける船舶模型動搖實驗、振れ計、回轉機械平衡装置等を擧げることが出來るが地震學方面に於ては、構造物振動の理論及び測定、地震動分解器を以て地震動中に存在する土地の固有振動の研究等を主なるものとして擧げることが出來る。なほ振れ計に對しては帝國學士院より、船舶動搖に關しては英國造船協會より、夫々授賞された事は周知の事實である。

昨年米國土木學會の招聘に應じて渡米せられ、各地に於て地震動の構造物に及ぼす影響に就て講演を行はれ、其後佛國に於ては船舶動搖に關する講演を行はれた。三月九日無事歸朝されたが、此時一ヶ月後に他界されるとは誰が想像し得たであろうか。

一面に於て故教授は大學の講義を通じて學生を薫陶せられたが、又多くの研究者を指導するに決して怠られなかつた。その實證としては故教授が創設され指導されて居た二研究所に於て、現在行はれて居る多くの研究を瞥見するならば、故教授の思想が如何に其中に徹底して居るかを窺ふ事が出來るであらう。

——所　報——

○ 談話會記事

第七十一回談話會（昭和七年五月十七日）

1. 土佐沿岸海底の變化	寺田寅彦
1. 關東地方の二三の地震に現はれた著しい波群及地震動の先驅部分（第三）	松澤武雄 福富孝治
1. 地震時土壓の實驗的研究	物部長穂 松尾春雄
1. 本所、深川に於ける水準測量に就て	今井哲
1. 東京附近に於ける水準測點の垂直變動	宮部直巳
1. 單層多張間架構の震動	妹澤克惟 金井清
1. 名草地方地震群に就て	今村明恒 小平孝雄 今村久
1. 紀伊半島に於ける慢性的地塊運動（第二報）	今村明恒
1. 仁川に於ける地殼の傾斜運動	高橋龍太郎
1. 重力の働く楔形彈性體を貫通する圓形孔附近の應力	西村源太郎 高山威雄
1. 鮮新世以後の地殼變動と丹那—興津—串本間の水準測量	大塚彌之助
1. 二萬氣壓による固體の比重の變化	白井俊明

第七十二回談話會（昭和七年六月廿一日）

1. 地震最大加速度と震度階	石本巳四雄
1. 本郷、三鷹に於ける初動入射角と地表速度	鈴木武夫
1. 北伊豆の地質（其二、畑毛——下畑間）	津屋弘逵
1. 京阪地方の地塊運動に就て（第三報）	今村明恒
1. 半島の傾斜と地殼の剛性	寺田寅彦 宮部直巳
1. 地震の分布と觀測所の分布	寺田寅彦
1. 地震波の何れの部分が家屋に損傷を與ふるか	齊田時太郎
1. 大阪府中河內郡峠地辷り調査報告	那須信治
1. 單層二張間架構の震動	妹澤克惟 金井清
1. 初動方向の偏向度に就て	國富信一
1. 縱波初動の大きさより見たる昭和四年六月三日伊勢灣地震の發震機巧に就て	河角廣

第七十三回談話會（昭和七年七月五日）

1. 深川方面に於ける土地の沈降	宮部直巳
1. 紀伊半島の山麓階に關する或る特徴	大塚彌之助
1. 日本の新第三紀以來の地殼運動を知る手段としての地層の對比	大塚彌之助
1. 日本海底より採集せられたる一岩礫に就て	津屋弘逵
1. ピボットに働く摩擦測定	石本巳四雄 萩原尊禮 吉田幸雄
1. 地球自轉期の變異に關する地球物理學意義	長岡半太郎
1. 緯度變化に現はるる地震の影響	長岡半太郎
1. 輝石の結晶作用に現はれたる地下深處と地表との條件の差異	坪井誠太郎

○出　張

1. 昭和七年五月十四日傾斜計測に關する用務の爲め長野縣下へ出張	高橋龍太郎
1. 昭和七年五月二十五日地震觀測に關する用務の爲め東京府下（三鷹村）へ出張	木村一治
1. 昭和七年六月一日地辷り調査の爲め大阪府下へ出張	那須信治
1. 昭和七年六月一日地震事項調査の爲め茨城縣下へ出張	小平孝雄
1. 昭和七年六月二十八日地震事項調査の爲め神奈川縣下へ出張	那須信治
1. 昭和七年七月二日地質調査の爲め靜岡縣下へ出張	津屋弘逵
1. 昭和七年七月七日地形地質取調の爲め岩手、青森兩縣下へ出張	大塚彌之助
1. 昭和七年七月九日地中電流測定に關する取調の爲め千葉縣下へ出張	高橋龍太郎
1. 昭和七年七月十三日學術上取調の爲め東京府下（三鷹村）へ隨時出張	木村一治
1. 昭和七年七月十六日地震事項取調の爲め長野、群馬二縣下へ出張	那須信治
1. 昭和七年七月二十八日器械据付けの爲め千葉縣下へ出張	高橋龍太郎
1. 昭和七年八月一日地質調査の爲め靜岡、神奈川兩縣下へ出張	久野久
1. 昭和七年八月八日地震史料取調の爲め東京府下（砂町）へ出張	宮部直巳
1. 昭和七年八月十日地震事項取調の爲め長野縣下へ出張	石本巳四雄
1. 昭和七年八月十一日地震事項取調の爲め長野縣下へ出張	那須信治

—所　報—

○談話會記事

第七十四回談話會（昭和七年九月廿日）

1. 潮流或は海流による灣内の副振動の可能性	中野猿人
1. 等方不均一球内の一點より起る彈性波（第一報）	吉山良一
1. 地表に一つの層があるときの地震波の反射屈折	妹澤克惟 金井清
1. 多層架構の振動	妹澤克惟 金井清
1. 昭和四年六月廿七日南大西洋地震の地球内核を通過し來れる横波の觀測	今村明恒
1. 淺間山麓に於ける地表傾斜變化の觀測	高橋龍太郎
1. 秋田駒ケ岳爆發調査報告	大塚彌之助
1. 和歌山縣東野上町に於ける土地滑動の測量	岸上冬彦

第七十五回談話會（昭和七年十月十八日）

1. 自動車による道路の振動に就て	星野市郎
1. 地磁氣の分布と日本の構造	寺田寅彦
1. 筑波山に於ける加速度地震計に依る地震觀測報告	井上宇胤
1. 地震機巧に關する二三の問題に就て	河角廣
1. 地殼内部に異物質がある場合の應力釣合（其の一）	西村源六郎 高山威雄
1. 東京富士見間の水準測量の結果に就て	宮部直巳
1. 地殼變動に關する二三の一般的通則	坪井忠二
1. 關東地方中央部の新第三系の厚さ	大塚彌之助

第七十六回談話會（昭和七年十一月十五日）

1. 固體、摩擦の振動倍率に及ぼす影響	萩原尊禮
1. 上部鮮新世の造陸運動的地殼運動	大塚彌之助
1. 昭和七年十月一日以降の草津白根山の爆發に就て	津屋弘逵
1. 地表に一つの層があるときの地震波の反射屈折（續報）	妹澤克惟 金井清
1. 結氷せる諏訪湖に於ける實驗	向井正幸

○出　張

1. 昭和七年九月九日地殻變動取調の爲め東京府下(砂町)へ出張　宮部直巳
1. 昭和七年九月十九日地震事項取調の爲め靜岡縣下へ出張　松澤武雄
1. 昭和七年十月四日地震事項取調の爲め茨城縣下へ出張　木村一治
1. 昭和七年十月六日噴火事項取調の爲め群馬長野兩縣下へ出張　津屋弘逵
1. 昭和七年十月廿五日事務打合の爲め東京府下(三鷹村)へ出張　石本巳四雄
1. 昭和七年十一月一日地震事項取調の爲め茨城縣下へ出張　小平孝雄
1. 昭和七年十一月一日時報受信機修理の爲め神奈川縣下(鎌倉)へ出張　波江野清藏
1. 昭和七年十一月十八日地震事項取調の爲め神奈川縣下へ出張　坪井忠二

正誤表

Errata.

號 Volume	册 Part	頁 Page	行 Line	誤 *for*	正 *read*
X	1	49	7	二十二日十二時迄	二十二時十二分迄
"	"	188	8	costumarily	customarily
"	"	190	5	another	other
"	"	"	10	interest to	interest in
"	3	508	2	$\frac{\mu_1}{\mu_2}=\frac{1}{5}$	$\frac{\mu_1}{\mu_2}=\frac{1}{4}$
"	"	516	9	Cette	Ces

It is very difficult to discriminate seismic data whether the vibratory movements are due to the multiple reflection at layers or due to the originally oscillatory train of disturbance. Professor Ishimoto[3] has recently shown us some seismic records which were obtained by the accelerometer deviced by him. From his records it seems that the elements in question may be more or less identified. Although his result, nevertheless, may in some cases enable us to know the thicknesses of strata and the possibility of free oscillations of those strata from geometrical standpoint it is uncertain that the concluded result may be dynamically possible. Because there is no theory except that in our foregoing paper, that determines the moving type of the ground

1) Being the continuation of our two preceding papers. See footnote 2).

2) K. Sezawa, "Possibility of the Free-oscillations of the Surface-layer excited by the Seismic-waves", *Bull. Earthq. Res. Inst.*, 8 (1930), 1–11.

K. Sezawa and G. Nishimura, "Dispersion of a shock in Echoing- and Dispersive-Elastic Bodies", *Bull. Earthq. Res. Inst.*, 8 (1930), 321–337.

3) M. Ishimoto, Colloq. Meeting, Earthq. Res. Inst., July, 7, 1931. The paper is perhaps being printed.

○出 張

1. 昭和七年九
1. 昭和七年九
1. 昭和七年十
1. 昭和七年十
1. 昭和七年十
1. 昭和七年十
1. 昭和七年十
1. 昭和七年十

1. *Possibility of Free Oscillations of Strata excited by Seismic Waves. Part III.*[1]

By Katsutada SEZAWA and Kiyoshi KANAI,

Earthquake Research Institute.

(Read Dec. 15, 1931.—Received Dec. 20, 1931.)

1. In two recent works[2] one of us studied in collaboration with Dr. Nishimura some problems of possibility of free oscillations of strata due to seismic waves and also the problem of dispersion of the seismic disturbance due to its multiple reflection at these strata. These problems were related to the behaviour of a single shock, but not concerned with oscillatory disturbance. Even though the case of a single shock is especially important for the purpose of ascertaining the essential nature of the propagation of waves in a heterogeneous elastic body, yet the case of oscillatory disturbance with finite extent is not less important from the point of view of actual seismometry owing to the frequent occurrence of such disturbances.

It is very difficult to discriminate seismic data whether the vibratory movements are due to the multiple reflection at layers or due to the originally oscillatory train of disturbance. Professor Ishimoto[3] has recently shown us some seismic records which were obtained by the accelerometer deviced by him. From his records it seems that the elements in question may be more or less identified. Although his result, nevertheless, may in some cases enable us to know the thicknesses of strata and the possibility of free oscillations of those strata from geometrical standpoint it is uncertain that the concluded result may be dynamically possible. Because there is no theory except that in our foregoing paper, that determines the moving type of the ground

---

1) Being the continuation of our two preceding papers. See footnote 2).

2) K. SEZAWA, "Possibility of the Free-oscillations of the Surface-layer excited by the Seismic-waves", *Bull. Earthq. Res. Inst.*, 8 (1930), 1–11.

K. SEZAWA and G. NISHIMURA, "Dispersion of a shock in Echoing- and Dispersive-Elastic Bodies", *Bull. Earthq. Res. Inst.*, 8 (1930), 321–337.

3) M. ISHIMOTO, Colloq. Meeting, Earthq. Res. Inst., July, 7, 1931. The paper is perhaps being printed.

depending upon the thickness of stratum and the forms of waves.

From this consideration we have here dealt with the problem of transmission of seismic waves of oscillatory type and of finite extent through strata of different elasticities, densities and thicknesses, and we have arrived at some conclusions on the nature of the free vibrations of strata due to seismic waves.

2. Let us first take a simple case where there is one discontinuous stratum perpendicular to the direction of propagation of primary waves in an infinitely extended uniform medium and let the waves be of pure plane type. The axis of x is drawn parallel to the direction of propagation, the origin being taken at a boundary surface of the layer. Let, ρ, λ, μ be the density and the elastic constants of the outer medium and ρ', λ', μ' those of the stratum of thickness H. Again, let u_0, u_0', u_1, u_2 be the respective displacements of the primary, reflected, semi-stationary and transmitted waves in the outer media and stratum. The equations of motion of the front and back outer media and of the stratum are as follows:

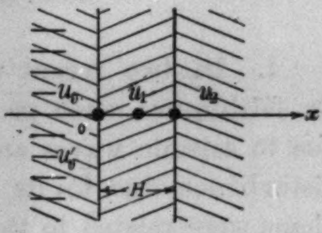

Fig. 1.

$$\frac{\partial^2 (u_0+u_0')}{\partial t^2}=V^2\frac{\partial_2 (u_0+u_0')}{\partial x^2}, \quad \ldots\ldots\ldots\ldots\ldots (1)$$

$$\frac{\partial^2 u_2}{\partial t^2}=V^2\frac{\partial^2 u_2}{\partial x^2}, \quad \ldots\ldots\ldots\ldots\ldots\ldots (2)$$

$$\frac{\partial^2 u_1}{\partial t^2}=V'^2\frac{\partial^2 u_1}{\partial x^2}, \quad \ldots\ldots\ldots\ldots\ldots\ldots (3)$$

where $V^2=(\lambda+2\mu)/\rho$, $V'^2=(\lambda'+2\mu')/\rho'$ for dilatational waves and $V^2=\mu/\rho$, $V'^2=\mu'/\rho'$ for distortional waves.

The typical solutions of these equations can be written by

$$u_0+u_0'=e^{ih(Vt-x)}+C_0e^{ih(Vt+x)}, \quad \ldots\ldots\ldots\ldots\ldots (4)$$

$$u_1=B_1e^{i\beta h(V't-x)}+C_1e^{i\beta h(V't+x)}, \quad \ldots\ldots\ldots\ldots (5)$$

$$u_2=B_2e^{ih(Vt-x)}, \quad \ldots\ldots\ldots\ldots\ldots\ldots\ldots\ldots (6)$$

where $\beta=V/V'$, $2\pi/h$ is wave length of the primary harmonic disturbance, C_0, B_1, C_1, B_2 are arbitrary constants to be determined from the conditions of continuity of displacements and stresses at both boundaries of the stratum. The values thus determined are as follows:

$$\left.\begin{aligned} C_0&=\frac{(1-\alpha^2)(1-e^{-2i\beta hH})}{(1+\alpha)^2-(1-\alpha)^2e^{-2i\beta hH}}, & B_1&=\frac{2(1+\alpha)}{(1+\alpha)^2-(1-\alpha)^2e^{-2i\beta hH}},\\ C_1&=\frac{2(1-\alpha)e^{-2i\beta hH}}{(1+\alpha)^2-(1-\alpha)^2e^{-2i\beta hH}}, & B_2&=\frac{4\alpha e^{-i(\beta-1)hH}}{(1+\alpha)^2-(1-\alpha)^2e^{-2i\beta hH}}, \end{aligned}\right\} \quad ..(7)$$

where $\alpha=(\rho' V')/(\rho V)$.

Decomposing u_0+u_0' in (4) into primary waves u_0 and secondary waves u_0' and applying Fourier's integral we get

$$u_0=\frac{1}{2\pi}\int_{-\infty}^{\infty}dh\int_{-\infty}^{\infty}\varphi(\sigma)e^{ih(Vt-x+\sigma)}d\sigma, \quad \ldots\ldots\ldots\ldots(8)$$

$$u_0'=\frac{1}{2\pi}\int_{-\infty}^{\infty}\frac{(1-\alpha^2)(1-e^{-2i\beta hH})\,dh}{(1+\alpha)^2-(1-\alpha)^2e^{-2i\beta hH}}\int_{-\infty}^{\infty}\varphi(\sigma)e^{ih(Vt-x+\sigma)}d\sigma, \quad \ldots\ldots(9)$$

$$\begin{aligned} u_1=&\frac{1}{\pi}\int_{-\infty}^{\infty}\frac{(1+\alpha)\,dh}{(1+\alpha)^2-(1-\alpha)^2e^{-2i\beta hH}}\int_{-\infty}^{\infty}\varphi(\sigma)\,e^{i\beta h\left(V't-x+\frac{\sigma}{\beta}\right)}d\sigma\\ &-\frac{1}{\pi}\int_{-\infty}^{\infty}\frac{(1-\alpha)e^{-2i\beta hH}dh}{(1+\alpha)^2-(1-\alpha^2)e^{-2i\beta hH}}\int_{-\infty}^{\infty}\varphi(\sigma)\,e^{i\beta h\left(V't+x+\frac{\sigma}{\beta}\right)}d\sigma, \quad (10) \end{aligned}$$

$$u_2=\frac{2}{\pi}\int_{-\infty}^{\infty}\frac{\alpha e^{-i(\beta-1)hH}dh}{(1+\alpha)^2-(1-\alpha)^2e^{-2i\beta hH}}\int_{-\infty}^{\infty}\varphi(\sigma)\,e^{ih(Vt-x+\sigma)}d\sigma, \quad \ldots\ldots(11)$$

where the initial condition

$$t=0;\quad u_0=\varphi(x) \quad \ldots\ldots\ldots\ldots\ldots\ldots(12)$$

for the primary waves is applied.

Again, we know the expression

$$\frac{1}{(1+\alpha)^2-(1-\alpha)^2e^{-2i\beta hH}}=\sum_{m=0}^{\infty}\frac{(1-\alpha)^{2m}}{(1+\alpha)^{2m+2}}e^{-2im\beta hH}. \quad \ldots\ldots (13)$$

Hence (9), (10), (11) reduce to

$$\begin{aligned} u_0'=&\frac{1}{2\pi}\sum_{m=0}^{\infty}\left(\frac{1-\alpha}{1+\alpha}\right)^{2m+1}\int_{-\infty}^{\infty}e^{-2im\beta hH}dh\int_{-\infty}^{\infty}\varphi(\sigma)\,e^{ih(Vt+x+\sigma)}d\sigma\\ &-\frac{1}{2\pi}\sum_{m=0}^{\infty}\left(\frac{1-\alpha}{1+\alpha}\right)^{2m+1}\int_{-\infty}^{\infty}e^{-2i(m+1)\beta hH}dh\int_{-\infty}^{\infty}\varphi(\sigma)\,e^{ih(Vt+x+\sigma)}d\sigma, \quad (9') \end{aligned}$$

$$\begin{aligned} u_1=&\frac{1}{\pi}\sum_{m=0}^{\infty}\frac{(1-\alpha)^{2m}}{(1+\alpha)^{2m+1}}\int_{-\infty}^{\infty}e^{-2im\beta hH}dh\int_{-\infty}^{\infty}\varphi(\sigma)\,e^{i\beta h\left(V't-x+\frac{\sigma}{\beta}\right)}d\sigma\\ &-\frac{1}{\pi}\sum_{m=0}^{\infty}\frac{(1-\alpha)^{2m+1}}{(1+\alpha)^{2m+2}}\int_{-\infty}^{\infty}e^{-2i(m+1)\beta hH}dh\int_{-\infty}^{\infty}\varphi(\sigma)\,e^{i\beta h\left(V't+x+\frac{\sigma}{\beta}\right)}d\sigma, \quad (10') \end{aligned}$$

$$u_2=\frac{2}{\pi}\sum_{m=0}^{\infty}\frac{\alpha(1-\alpha)^{2m}}{(1+\alpha)^{2m+2}}\int_{-\infty}^{\infty}e^{i[(2m+1)\beta-1]hH}dh\int_{-\infty}^{\infty}\varphi(\sigma)\,e^{ih(Vt-x+\sigma)}d\sigma. \quad (11')$$

3. Let the form of the primary waves at $t=0$, which proceed in

the positive direction of x, be

$$\left.\begin{aligned} u_0 &= \cos cx, & [-a<x<0] \\ &= 0, & [0>x] \\ &= 0; & [-a<x] \end{aligned}\right\} \qquad \cdots\cdots\cdots\cdots \quad (14)$$

then, integrating (8), (9′), (10′), (11′) with respect to σ, we get

$$u_0 = \frac{i}{4\pi}\int_{-\infty}^{\infty} e^{ih(Vt-x)}\left[\frac{1}{c-h}-\frac{1}{c+h}-\frac{1}{c-h}e^{i(c-h)a}+\frac{1}{c+h}e^{-i(c+h)a}\right]dh, \quad (15)$$

$$\begin{aligned} u_0' = {} & \frac{i}{4\pi}\sum_{m=0}^{\infty}\left(\frac{1-\alpha}{1+\alpha}\right)^{2m+1}\int_{-\infty}^{\infty} e^{ih(Vt+x-2m\beta H)} \\ & \times\left[\frac{1}{c-h}-\frac{1}{c+h}-\frac{1}{c-h}e^{i(c-h)a}+\frac{1}{c+h}e^{-i(c+h)a}\right]dh \\ & -\frac{i}{4\pi}\sum_{m=0}^{\infty}\left(\frac{1-\alpha}{1+\alpha}\right)^{2m+1}\int_{-\infty}^{\infty} e^{ih[Vt+x-2(m+1)\beta H]} \\ & \times\left[\frac{1}{c-h}-\frac{1}{c+h}-\frac{1}{c-h}e^{i(c-h)a}+\frac{1}{c+h}e^{-i(c+h)a}\right]dh, \quad ..(16) \end{aligned}$$

$$\begin{aligned} u_1 = {} & \frac{i}{2\pi}\sum_{m=0}^{\infty}\frac{(1-\alpha)^{2m}}{(1+\alpha)^{2m+1}}\int_{-\infty}^{\infty} e^{i\beta h(V't-x-2mH)} \\ & \times\left[\frac{1}{c-h}-\frac{1}{c+h}-\frac{1}{c-h}e^{i(c-h)a}+\frac{1}{c+h}e^{-i(c+h)a}\right]dh \\ & -\frac{i}{2\pi}\sum_{m=0}^{\infty}\frac{(1-\alpha)^{2m+1}}{(1+\alpha)^{2m+2}}\int_{-\infty}^{\infty} e^{i\beta h[V't+x-2(m+1)H]} \\ & \times\left[\frac{1}{c-h}-\frac{1}{c+h}-\frac{1}{c-h}e^{i(c-h)a}+\frac{1}{c+h}e^{-i(c+h)a}\right]dh, \quad ..(17) \end{aligned}$$

$$\begin{aligned} u_2 = {} & \frac{i}{\pi}\sum_{m=0}^{\infty}\frac{\alpha(1-\alpha)^{2m}}{(1+\alpha)^{2m+2}}\int_{-\infty}^{\infty} e^{ih[Vt-x+(1-(2m+1)\beta)H]} \\ & \times\left[\frac{1}{c-h}-\frac{1}{c+h}-\frac{1}{c-h}e^{i(c-h)a}+\frac{1}{c+h}e^{-i(c+h)a}\right]dh. \quad ..(18) \end{aligned}$$

The fact that the expressions of displacements are series forms, is not only due to mathematical convenience, but also due to the fact that this indicates the successive formation of the groups of waves by the multiple reflection at the discontinuities.

4. To get these integrals we consider the contour integrations of the type:

$$\int_c \frac{e^{iBZ}}{A-Z}dZ, \quad \int_c \frac{e^{iBZ}}{A+Z}dZ, \quad \int_c \frac{e^{-iBZ}}{A-Z}dZ, \quad \int_c \frac{e^{-iBZ}}{A+Z}dZ$$

$$[A>0, \; B>0] \quad (19)$$

taken respectively round the contours (I), (II), (III), (IV) shown below.

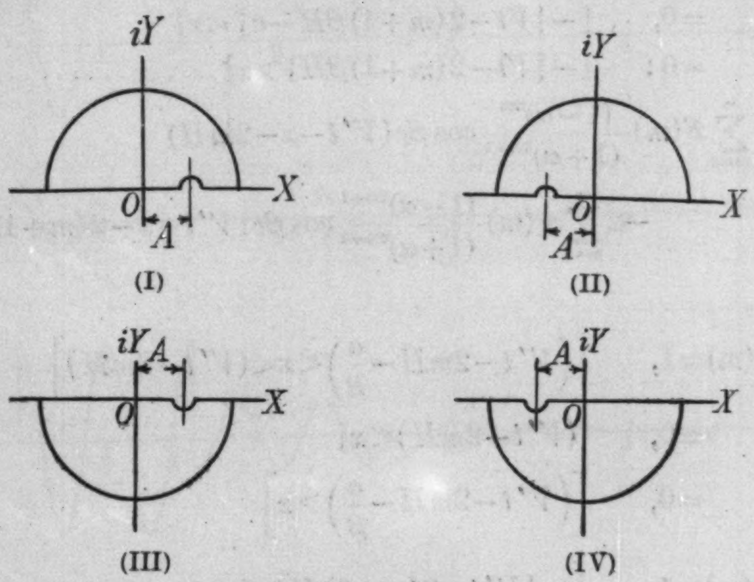

These contour integrations give us the result such that

$$
\left.\begin{aligned}
&\text{(I)} && \int_{-\infty}^{\infty}\frac{e^{iBh}}{A-h}\,dh=-i\pi e^{iAB},\\
&\text{(II)} && \int_{-\infty}^{\infty}\frac{e^{iBh}}{A+h}\,dh=i\pi e^{-iAB},\\
&\text{(III)} && \int_{-\infty}^{\infty}\frac{e^{-iBh}}{A-h}\,dh=i\pi e^{-iAB},\\
&\text{(IV)} && \int_{-\infty}^{\infty}\frac{e^{-iBh}}{A+h}\,dh=-i\pi e^{iAB}.
\end{aligned}\right\}\quad [A>0,\ B>0] \qquad (20)
$$

5. From (15), (16), (17), (18), (20), we find finally

$$
\left.\begin{aligned}
u_0&=\cos c(Vt-x), && [(Vt-a)<x<Vt]\\
&=0, && [Vt<x]\\
&=0; && [(Vt-a)>x]
\end{aligned}\right\}\quad\cdots\cdots\cdots(21)
$$

$$
\begin{aligned}
u_0'=&\sum_{m=0}^{\infty}f(m)\left(\frac{1-\alpha}{1+\alpha}\right)^{2m+1}\cos c(Vt+x-2m\beta H)\\
&-\sum_{m=0}^{\infty}\varphi(m)\left(\frac{1-\alpha}{1+\alpha}\right)^{2m+1}\cos c\{Vt+x-2(m+1)\beta H\},
\end{aligned}
$$

where

$$
\begin{aligned}
f(m)&=1, && [-(Vt-2m\beta H)<x<-(Vt-2m\beta H-a)]\\
&=0, && [-(Vt-2m\beta H-a)<x]\\
&=0, && [-(Vt-2m\beta H)>x]
\end{aligned}
$$

$$\begin{aligned}\varphi(m)&=1, && [-\{Vt-2(m+1)\beta H\}<x<-\{Vt-2(m+1)\beta H-a\}]\\ &=0, && [-\{Vt-2(m+1)\beta H-a\}<x]\\ &=0; && [-\{Vt-2(m+1)\beta H\}>x] \quad \ldots\ldots\ldots\ldots\ldots (22)\end{aligned}$$

$$u_1=2\sum_{m=0}^{\infty}F(m)\frac{(1-\alpha)^{2m}}{(1+\alpha)^{2m+1}}\cos\beta c(V't-x-2mH)$$

$$-2\sum_{m=0}^{\infty}\chi(m)\frac{(1-\alpha)^{2m+1}}{(1+\alpha)^{2m+2}}\cos\beta c\{V't+x-2(m+1)H\},$$

where

$$\begin{aligned}F(m)&=1, && \left[\left(V't-2mH-\frac{a}{\beta}\right)<x<(V't-2mH)\right]\\ &=0, && [(V't-2mH)<x]\\ &=0, && \left[\left(V't-2mH-\frac{a}{\beta}\right)>x\right]\end{aligned}$$

$$\begin{aligned}\chi(m)&=1, && \Big[-\{V't-2(m+1)H\}<x<\\ & && \qquad -\left\{V't-2(m+1)H-\frac{a}{\beta}\right\}\Big]\\ &=0, && \left[-\left\{V't-2(m+1)H-\frac{a}{\beta}\right\}<x\right]\\ &=0; && [-\{V't-2(m+1)H\}>x] \quad \ldots\ldots\ldots\ldots\ldots (23)\end{aligned}$$

$$u_2=4\sum_{m=0}^{\infty}\Psi(m)\frac{\alpha(1-\alpha)^{2m}}{(1+\alpha)^{2m+2}}\cos c[\{1-(2m+1)\beta\}H+Vt-x],$$

where

$$\begin{aligned}\Psi(m)&=1, && [\{1-(2m+1)\beta\}H\\ & && \qquad +Vt-a<x<\{1-(2m+1)\beta\}H+Vt]\\ &=0, && [\{1-(2m+1)\beta\}H+Vt<x]\\ &=0. && [\{1-(2m+1)\beta\}H+Vt-a>x]\end{aligned}$$

The values of u_0 at $x=0$, u_0' at $x=0$, u_1 at $x=H/2$, u_2 at $x=H$ are plotted in Figs. 2, 3, 4, 5, 6, 7. Fig. 2 gives the case, $\alpha=1/2$, $\beta=1$, $H=2L\,(L=2\pi/c)$ and similarly Fig. 3 $\alpha=1/2$, $\beta=1$, $H=L$; Fig. 4 $\alpha=1/2$, $\beta=1$, $H=L/2$; Fig. 5 $\alpha=2$, $\beta=1$, $H=2L$; Fig. 6 $\alpha=2$, $\beta=1$, $H=L$; Fig. 7 $\alpha=2$, $\beta=1$, $H=L/2$.

Fig. 2 a.
($\alpha=1/2$, $\beta=1$)

Figs. 2, 3, 4 show the cases in which the elastic constants in the stratum are smaller than those in the outer medium, while Figs. 5, 6, 7 the cases in which the constants in the stratum are larger than those in

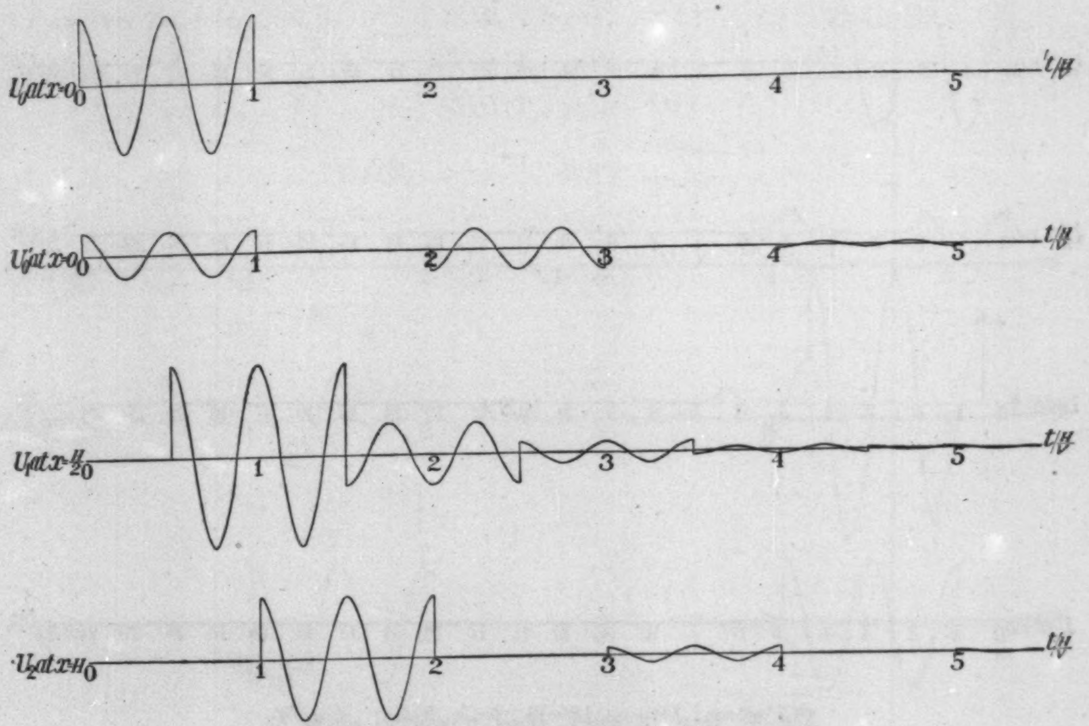

Fig. 2 $(\alpha=1/2,\ \beta=1,\ H=2L,\ a=2L,\ c=2\pi/L)$

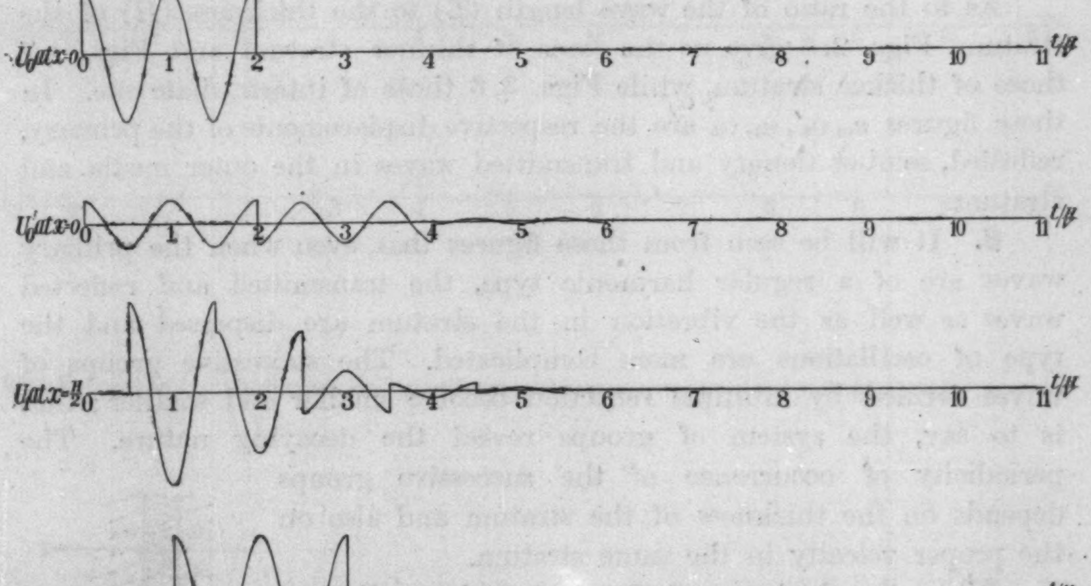

Fig. 3. $(\alpha=1/2,\ \beta=1,\ H=L,\ a=2L,\ c=2\pi/L)$

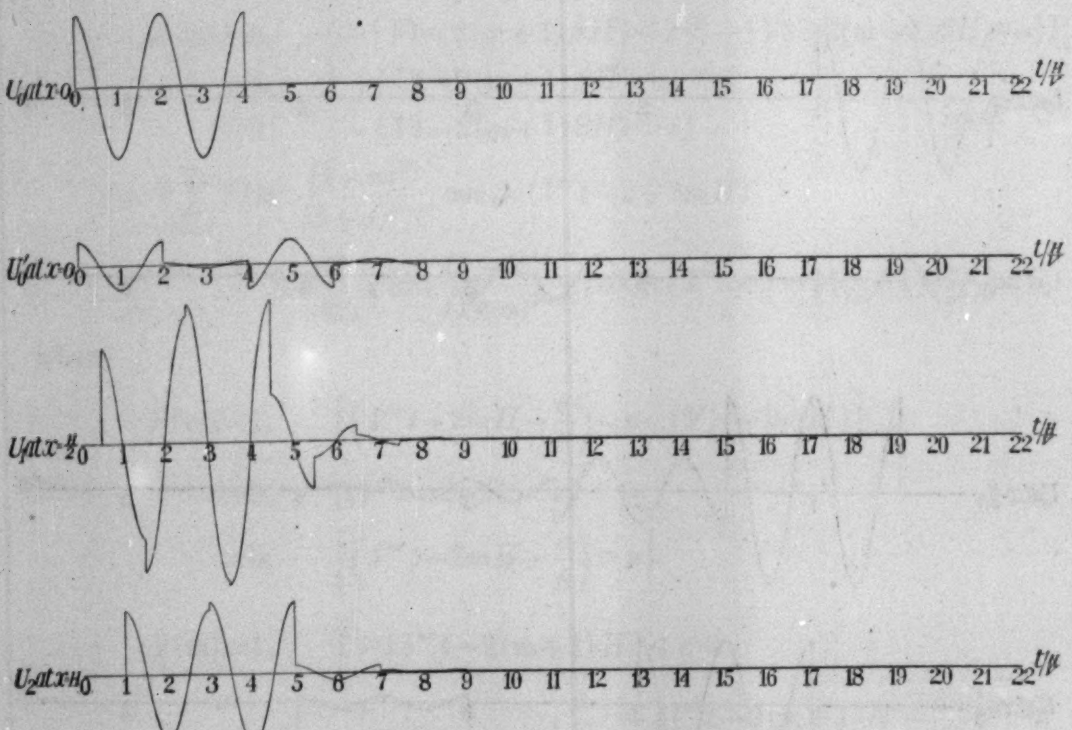

Fig. 4. ($\alpha=1/2$, $\beta=1$, $H=L/2$, $a=2L$, $c=2\pi/L$)

the outer medium.

As to the ratio of the wave length (L) to the thickness (H) of the stratum, Figs. 2, 5 give us the cases of thinner stratum and Figs. 4, 7 those of thicker stratum, while Figs. 3, 6 those of intermediate one. In these figures u_0, u_0', u_1, u_2 are the respective displacements of the primary, reflected, semi-stationary and transmitted waves in the outer media and stratum.

6. It will be seen from these figures that, even when the primary waves are of a regular harmonic type, the transmitted and reflected waves as well as the vibration in the stratum are dispersed and the type of oscillations are more complicated. The successive groups of waves formed by multiple reflection become smaller and smaller; that is to say, the system of groups reveal the decaying nature. The periodicity of occurrence of the successive groups depends on the thickness of the stratum and also on the proper velocity in the same stratum.

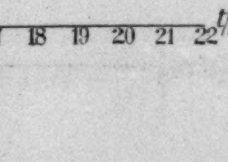

Fig. 5 a.
($\alpha=2$, $\beta=1$)

When the thickness of the stratum is small compared with the length of the disturbed portion, each group in succession appears intermittently in perfect

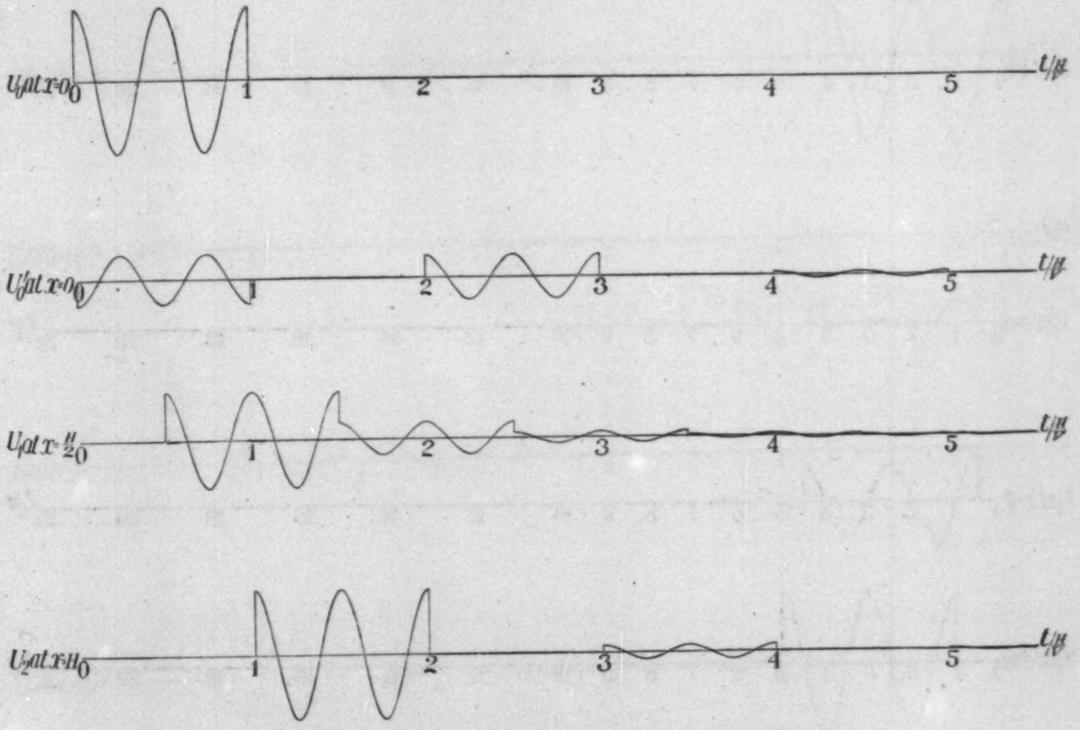

Fig. 5. ($\alpha=2$, $\beta=1$, $H=2L$, $a=2L$, $c=2\pi/L$)

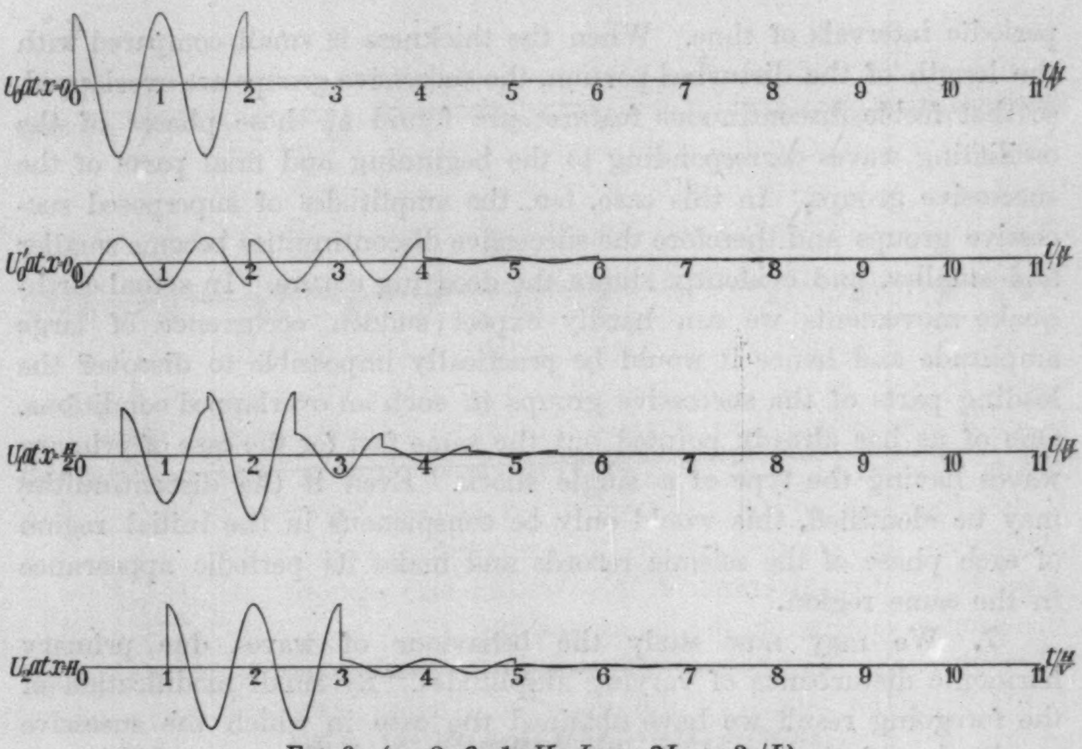

Fig. 6. ($\alpha=2$, $\beta=1$, $H=L$, $a=2L$, $c=2\pi/L$)

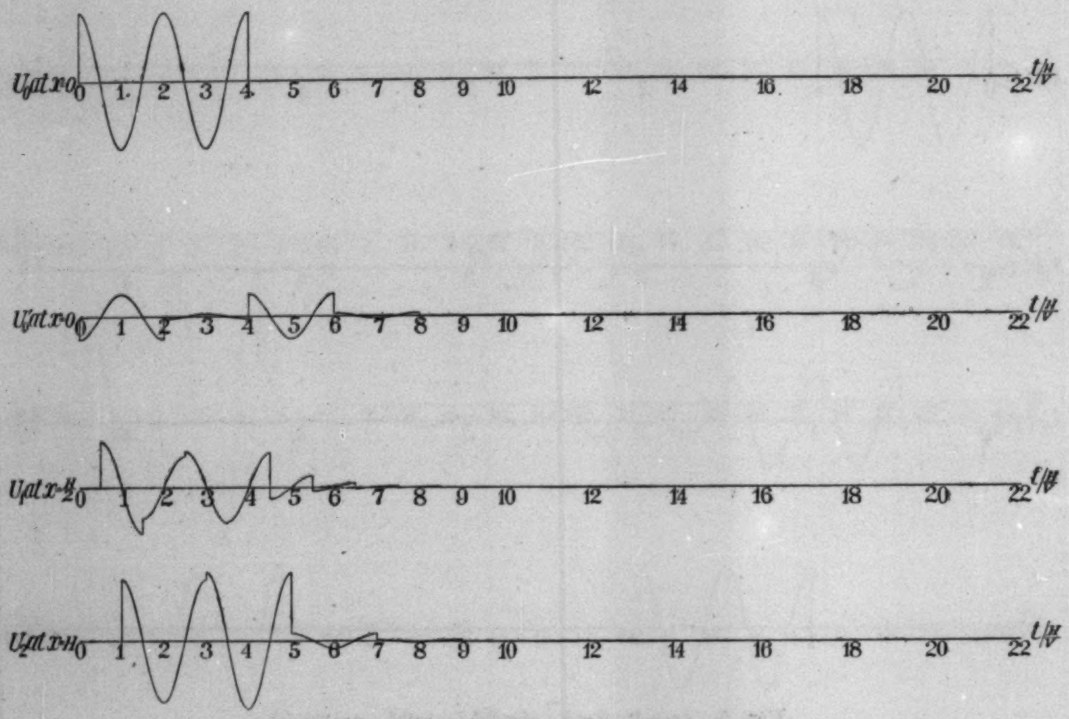

Fig. 7. ($\alpha=2$, $\beta=1$, $H=L/2$, $a=2L$, $c=2\pi/L$)

periodic intervals of time. When the thickness is small compared with the length of the disturbed portion, the successive groups are overlapped, so that feeble discontinuous features are found at those phases of the oscillating waves corresponding to the beginning and final parts of the successive groups. In this case, too, the amplitudes of superposed successive groups and therefore the successive discontinuities become smaller and smaller, and evidently shows the decaying nature. In actual earthquake movements we can hardly expect sudden occurrence of large amplitude and hence it would be practically impossible to discover the leading parts of the successive groups in such an overlapped conditions. One of us has already pointed out the same fact for the case of primary waves having the type of a single shock. Even if the discontinuities may be identified, this would only be conspicuous in the initial region of each phase of the seismic records and make its periodic appearance in the same region.

7. We may now study the behaviour of waves due primary harmonic disturbance of varying amplitudes. By small modification of the foregoing result we have obtained the case in which the sucessive amplitudes of the harmonic disturbance decrease as geometrical pro-

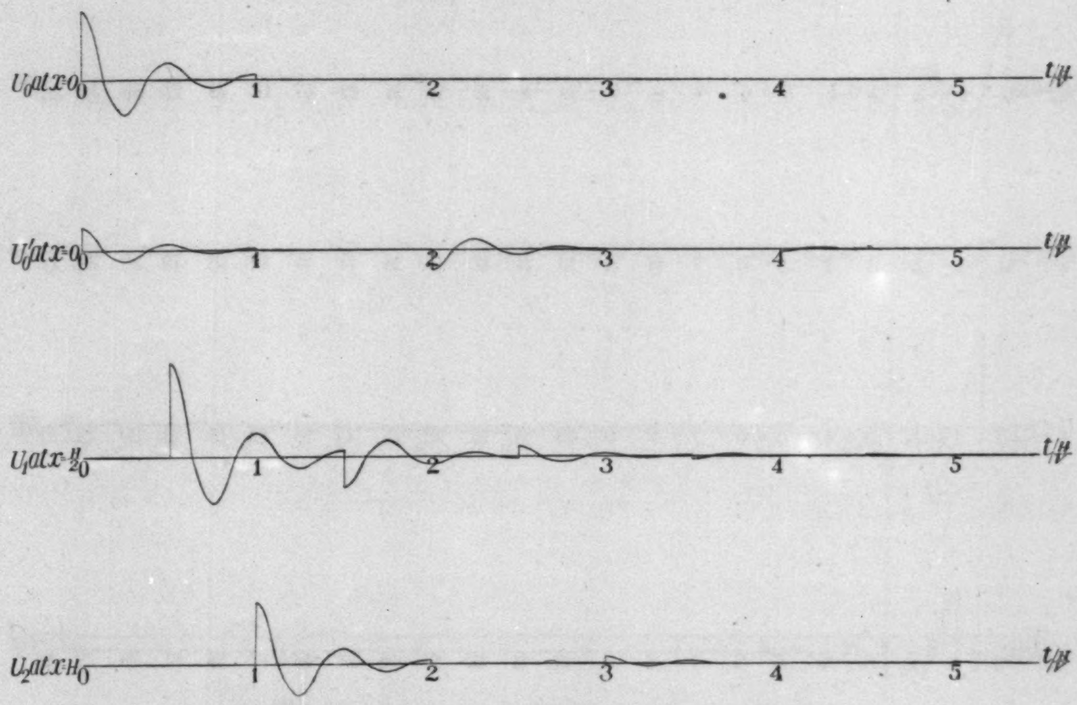

Fig. 8. ($\alpha=1/2$, $\beta=1$, $H=2L$, $a=2L$, $c=2\pi/L$)

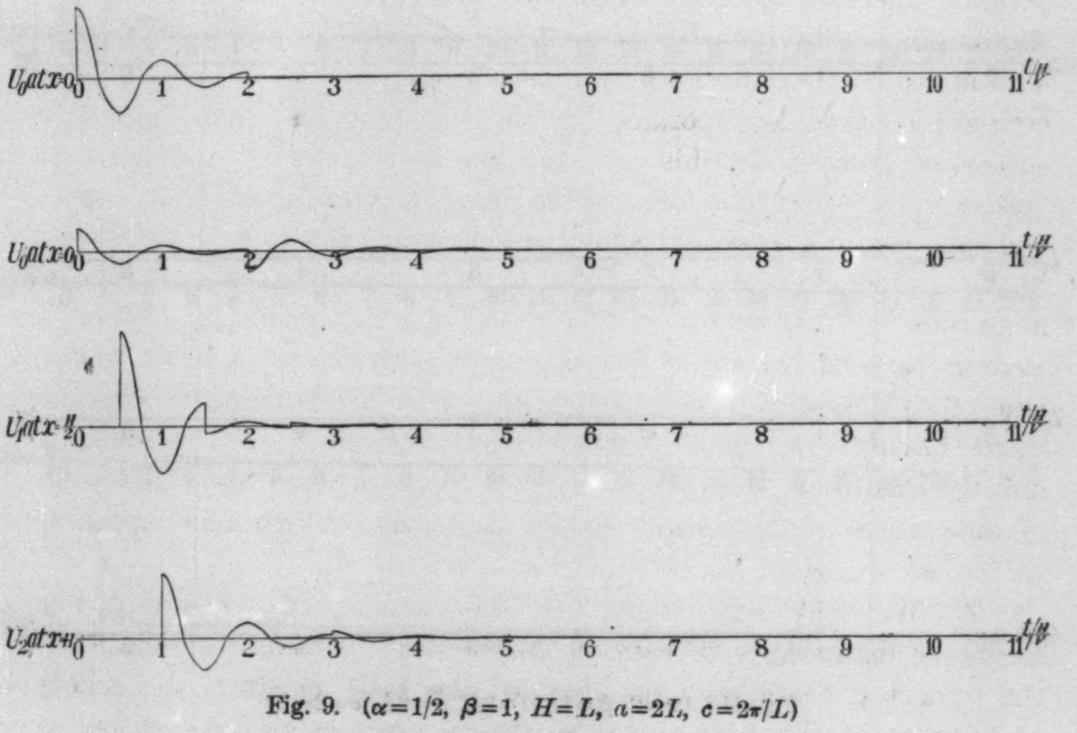

Fig. 9. ($\alpha=1/2$, $\beta=1$, $H=L$, $a=2L$, $c=2\pi/L$)

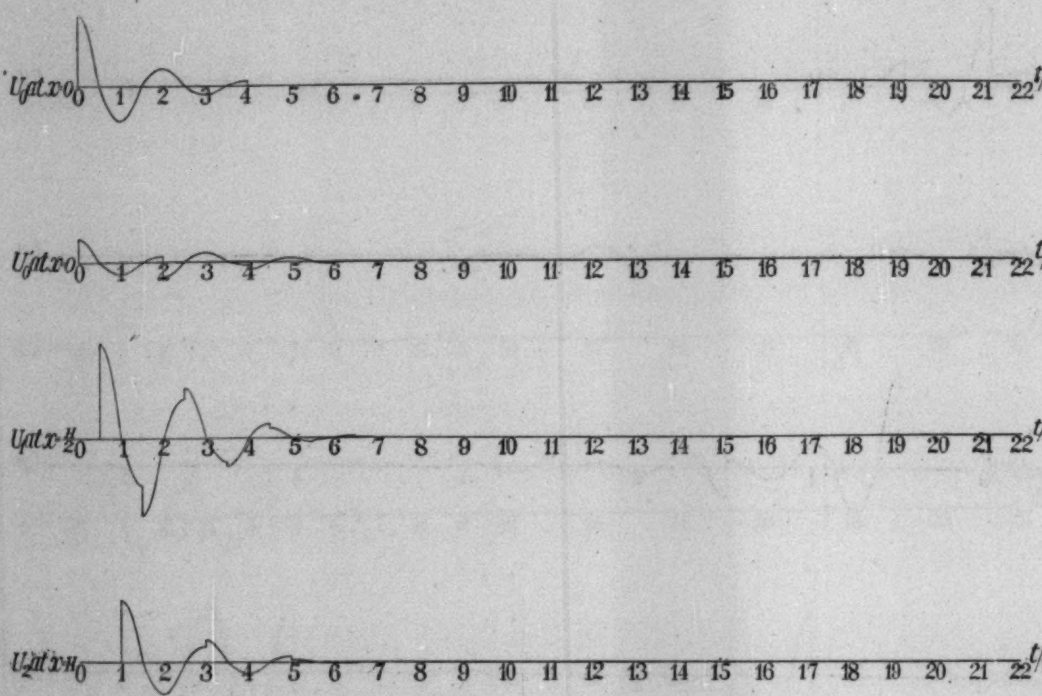

Fig. 10. ($\alpha=1/2$, $\beta=1$, $H=L/2$, $a=2L$, $c=2\pi/L$)

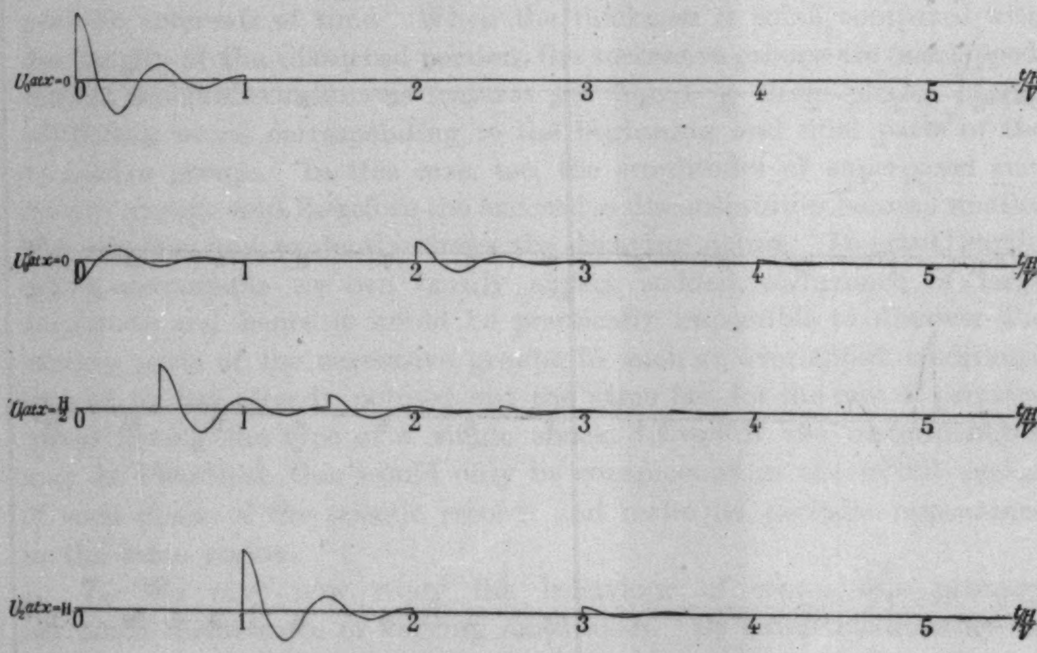

Fig. 11. ($\alpha=2$, $\beta=1$, $H=2L$, $a=2L$, $c=2\pi/L$)

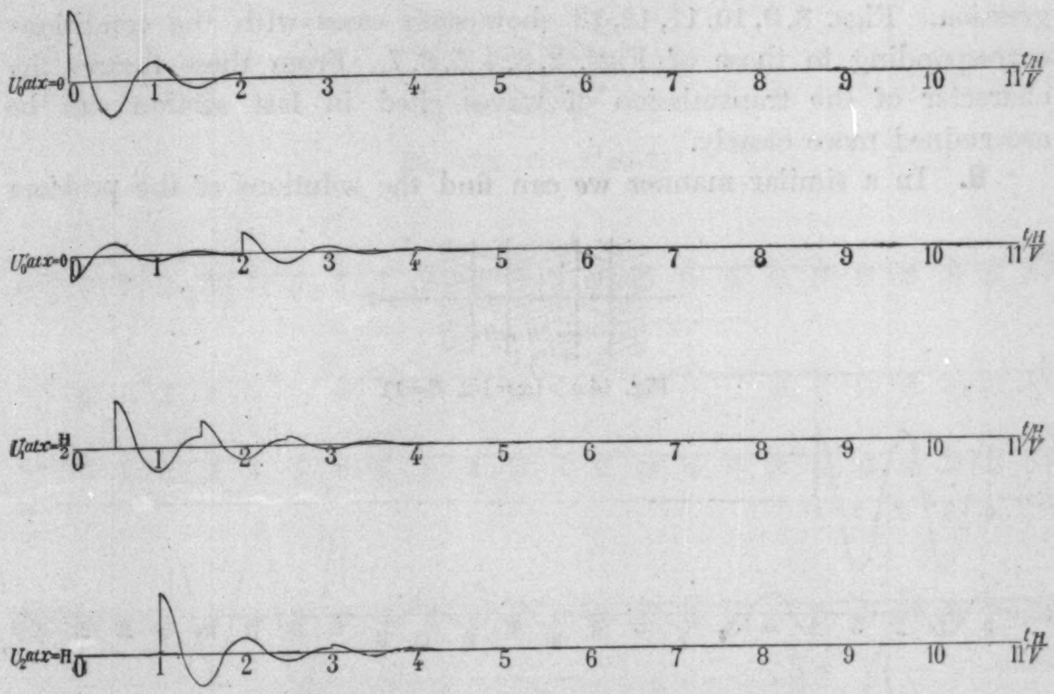

Fig. 12. ($\alpha=2$, $\beta=1$, $H=L$, $a=2L$, $c=2\pi/L$)

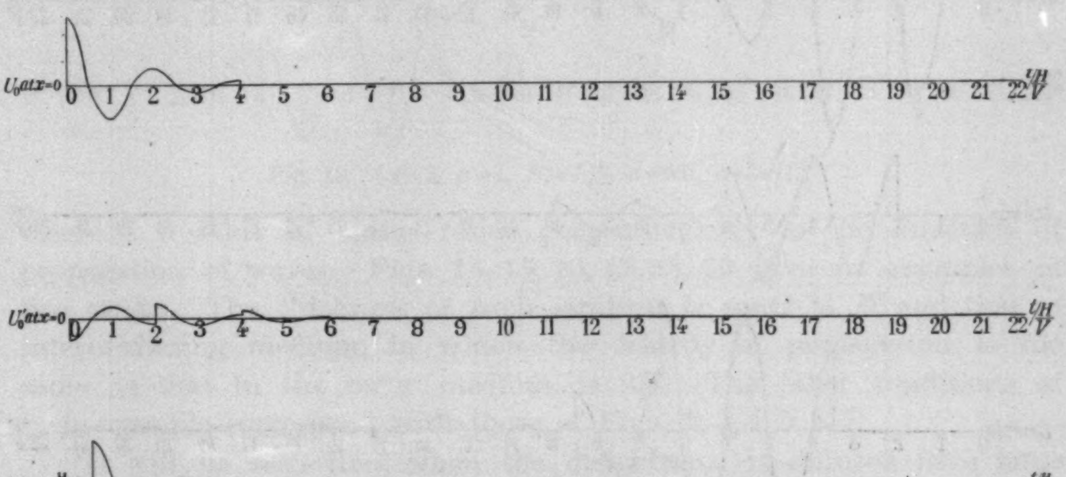

Fig. 13. ($\alpha=2$, $\beta=1$, $H=L/2$, $a=2L$, $c=2\pi/L$)

gression. Figs. 8, 9, 10, 11, 12, 13 show such cases with the conditions corresponding to those of Figs. 2, 3, 4, 5, 6, 7. From these figures the character of the transmission of waves cited in last section can be ascertained more clearly.

8. In a similar manner we can find the solutions of the problem

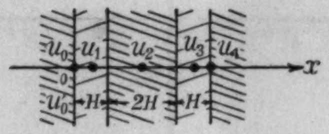

Fig. 14 a. ($\alpha=1/2$, $\beta=1$).

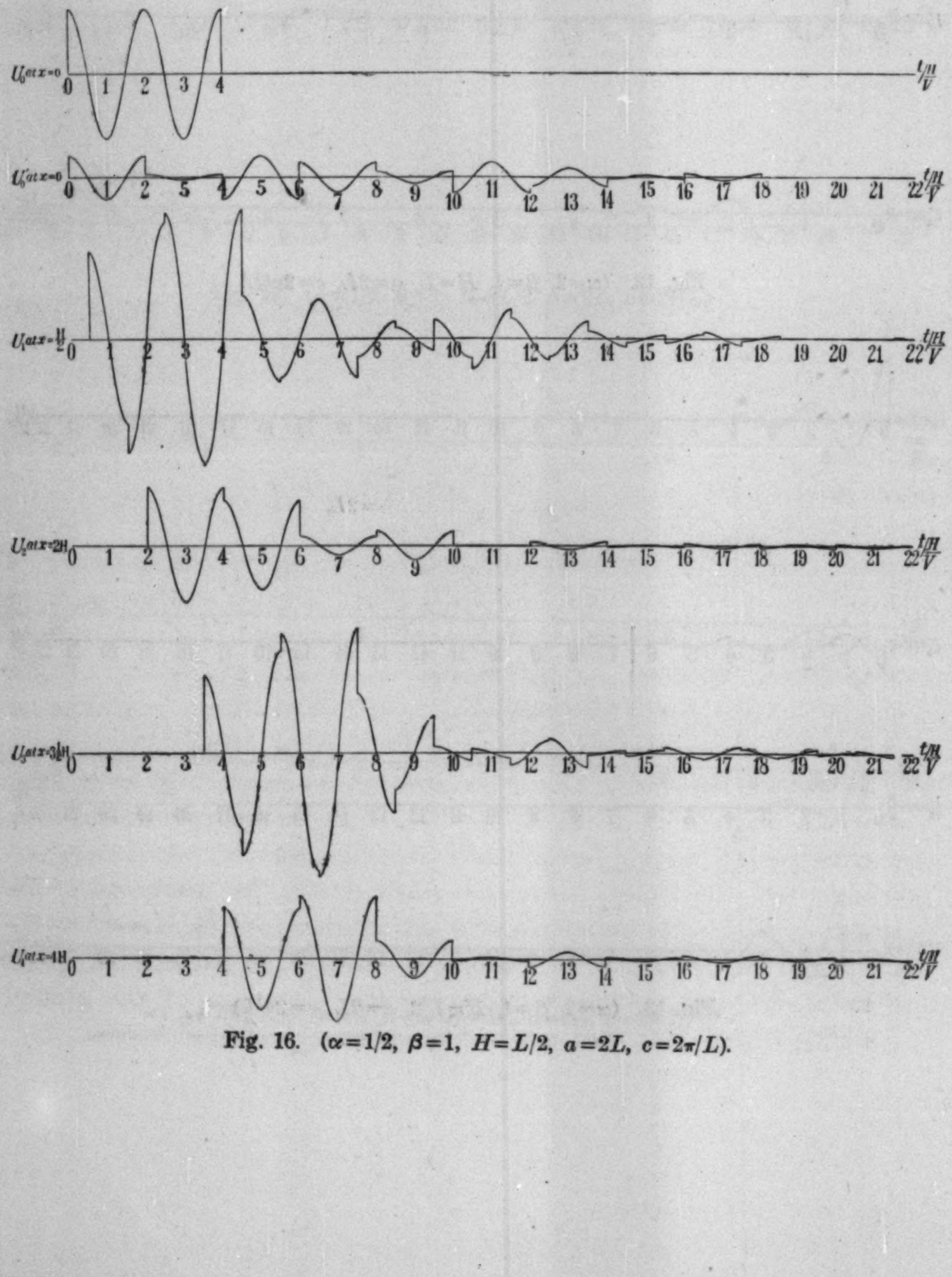

Fig. 16. ($\alpha=1/2$, $\beta=1$, $H=L/2$, $a=2L$, $c=2\pi/L$).

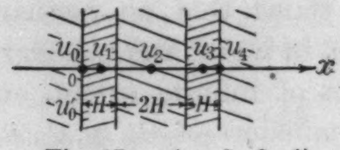

Fig. 17 a. ($\alpha=2,\ \beta=1$).

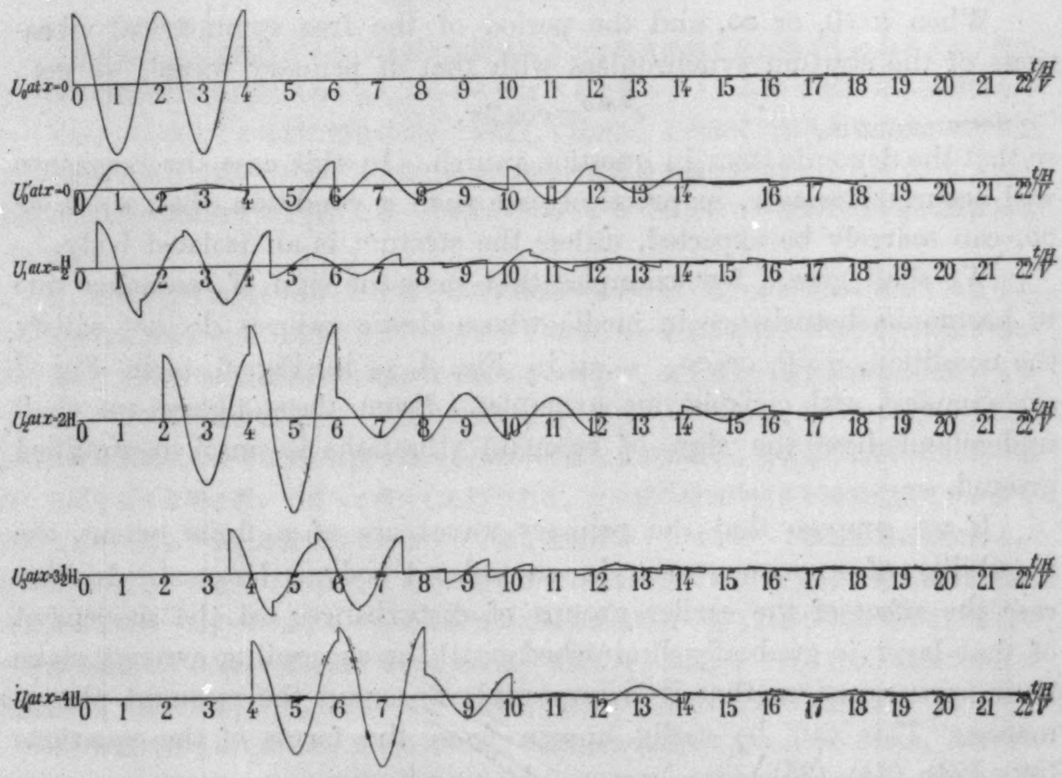

Fig. 19. ($\alpha=2,\ \beta=1,\ H=L/2,\ a=2L,\ c=2\pi/L$)

where a number of strata reside perpendicularly to the direction of propagation of waves. Figs. 14, 15, 16, 17, 18, 19 give us examples of two strata. The thickness of each stratum is equal to H and that of intermediating medium, in which the velocity of propagation is the same as that in the outer medium, is $2H$. The other conditions of each example correspond with those of Figs. 2, 3, 4, 5, 6, 7.

It will be seen that, when the disturbance is diffused in a large extent, the amplitudes of all the vibrations are exceedingly diminished, the principle of energy being thus naturally satisfied. It is also remarkable fact that, when there are many strata, the vibrations of the medium, in which the primary waves are incident, are oscillatory to the same degree as those of the medium in which the transmitted waves are radiated. This nature is proper to the vibrations of the ground due multiple reflection, but not to the ordinary dispersed waves.

9. It may now be stated that no resonant phenomenon can be expected even in the case, in which the primary disturbance consists of a train of harmonic waves of infinite extent, excepting the case $\alpha=0$, or ∞. Because the denominators of C_0, B_1, C_1, B_2 in (7) cannot be zero except the case $\alpha=0$, or ∞.

When $\alpha=0$, or ∞, and the period of the free symmetrical vibrations of the stratum synchronizes with that of primary waves, we get

$$e^{2i\beta hH}=\cos 2\pi,$$

so that the denominators in question vanish. In this case the resonance will occur. However, in practical case such a condition that, $\alpha=0$, or ∞, can scarcely be expected, unless the stratum is an isolated body.

We shall give a few examples that show the sign of resonance due to harmonic disturbance in media whose elastic natures do not satisfy the condition, $\alpha=0$, or ∞. u_1, u_2 in Fig. 4, u_1 in Fig. 6, u_2 in Fig. 7 are simplest and conspicuous examples. From these figures we shall understand how the sign of resonant vibrations is small in stratified ground.

If we suppose that the primary waves are of a finite extent, the possibility of resonance even in an isolated body is lessened. In this case the effect of the earlier groups of disturbances on the movement of that layer is gradually diminished until the succeeding systems make their appearance, so that it is impossible to expect the resonant phenomenon. This can be easily known from the forms of the equations (22), (23), (24), (25).

It is important fact, at any rate, that free vibrations of strata cannot be excited by harmonic waves of infinite extent, and also that they may be more or less excited by arbitrary waves or by harmonic waves of finite extent, under the condition that the excited vibrations are damped away relatively quickly.

10. It is again noted that the period of the intermittent vibrations of the ground is, of course, different according to the kinds of primary waves. As we know from (1), (2), (3), the period $(2H/V)$ is $2H\Big/\sqrt{\dfrac{\lambda'+2\mu'}{\rho'}}$ for dilatational waves and $2H\Big/\sqrt{\dfrac{\mu'}{\rho'}}$ for distortional waves, so that in the case of $\lambda'=\mu'$ the period due to the dilatational waves is $1/\sqrt{3}$ of that of the distortional waves.

1. 地震波によつて土地の固有振動が誘起される可能度 第三報

地震研究所 { 妹 澤 克 惟
金 井 清

この前著者の一人は西村氏と共に地層が地震波によつて固有振動をなし得るものかどうか、又たとへ固有振動をなす可能性があるとしてもどの程度にあり得るかといふ事や如何なる振動型を持つべきかといふ事などを特別な場合について研究して置いた。その論文では入射地震波が衝撃波型をなす場合を論じて置いたけれども、少し違つた場合には多少の疑の餘地があつたので、こゝに入射波が有限長の調和波をなす場合を考へて見たのである。この論文はこの種の研究の第三報告に當つて居る。

一體、土地の固有振動といふと、土地を特別に單獨の振子の如く考へる研究家も可なりあるけれども著者等は其所に大なる誤謬の含まれて居る事を指摘したいと思ふ。如何に地形學的の山や谷が凹凸をなして居つても幾何學的には極めて平坦なものであり、又土地の一部が如何に不均質のものであるといつても結局は固體として隣接の固體と接觸して居るものであり、如何なる理想的模型を以てしても單獨に存在する振子に置き換へる事は不可能なものである。著者等は固體の間に別の彈性や密度を有する層を置いて考へる事にしたのである。この層の物理的性質を極端に變更する事も出來るものであるから、地質學的に想像のつく樣な異同はいくらでも與へる事が出來るのである。ただ計算の方法が複雜になる爲に、ここでは層の厚さのみが一定であつて、長さや幅の擴りが無限であるとして考へたのである。この方向に區切つても力學的性質の變らぬ事は明瞭である。但しその計算で遺憾とする所は波動方向が層の向きに傾いて居る時の問題が、やはり計算の複雜さの爲に後廻しにして置いた事である。此等の問題も次第に手を著けて見たいと考へて居る。

計算の方法は省略して置くが、要するに有限長の調和波が前進して層にぶつかる時は、其層の中で幾回となく重複反射をなし、同時に波動勢力を少しづつ周圍に分散するものである。結果から見ると層の定常振動を誘起させた樣に見えるけれども、實際の機構は上述の如きものである。計算の結果によれば彈性率や密度の割合が層と外部とに於て無限に異なつて居るのでなければ實際の定常振動を起す事が出來ないのである。但し不規則な入射波(有限波長の調和波を含む)や衝擊波が來る時は層の固有振動の週期のみは保つ振動が現れるけれどもそれも後に述べる樣に直ちに減衰するものである。尙又無限に續く等週期調和波がやつて來る時には、其强制振動の週期のみが現はれ層の固有振動の現れぬ事は普通の振動理論にある通りである。この時の共振現象は前にも述べた樣に層の物質と層外の物質との密度や彈性が無限に違つて居るのでなければ勿論起らない。

さて有限長の調和波が層にあたる時にその有限の擾亂部の長さが層の厚さに比較して大なる場合には、振動群が週期的に且つ間歇的に起るものであり、又其次々の振動群は減衰的傾向を持つものである。層の厚さを H とし、其層中の波動速度を V とすれば其間歇的振動は $2H/V$ なる週期を以て起るものである。從て波動が縱波であるか横波であるかによつて其週期も著しく異なる譯である。

有限擾亂部の長さが層の厚さに比較して短い場合には振動群が互に重なり合つて起るから、地震計の記象からその區別をなす事は實際問題として可なり困難を伴ふ。重なり始めや終りのみを拾つて行つて初めて固有振動週期が見つかるのであり、且つこの場合にも後の振動群程どんどん振幅が

小になる規則であるから、稍もすると取違へる恐れがある。此等は計算例とよく照合する事によつて始めて誤りを防ぐ事が出來る事と思ふ。著者等は調和波が等振幅でなくて次々の振幅が減衰する樣な場合の計算例をも示して置いた。斯る形式を有する入射波のある場合には上述の困難は多少減ずるものである。

層が幾つもある場合には波動の振動が非常に長く延びるものであつて振幅もそれにつれて益々減少するものである。此等は勢力保持の法則を數式が自然に表はして異れるものである。但し斯る場合に出る結果で注意すべき事は層列の前面から出る反射波が層列の最後部から出る通過波と同程度に砕けて延びる事である。此は重複反射の場合のみに特有なものであつて普通の分散波の場合と非常に異なるものである事を附記して置く。

[illegible]

[illegible]

[K. Sezawa and K. Kanai.]

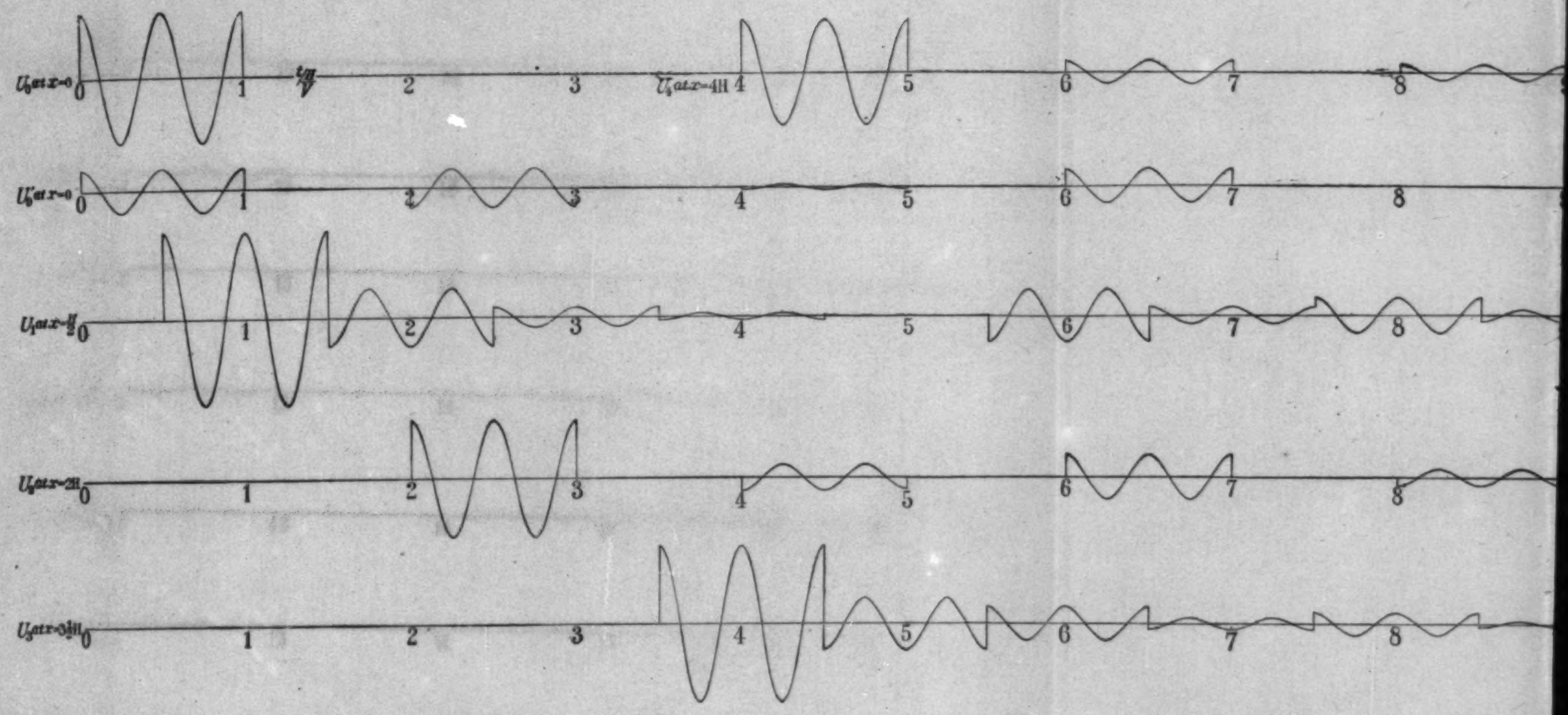

Fig. 14. $\left(\alpha=\frac{1}{2},\ \beta=1,\ H=2L,\ a=\right.$

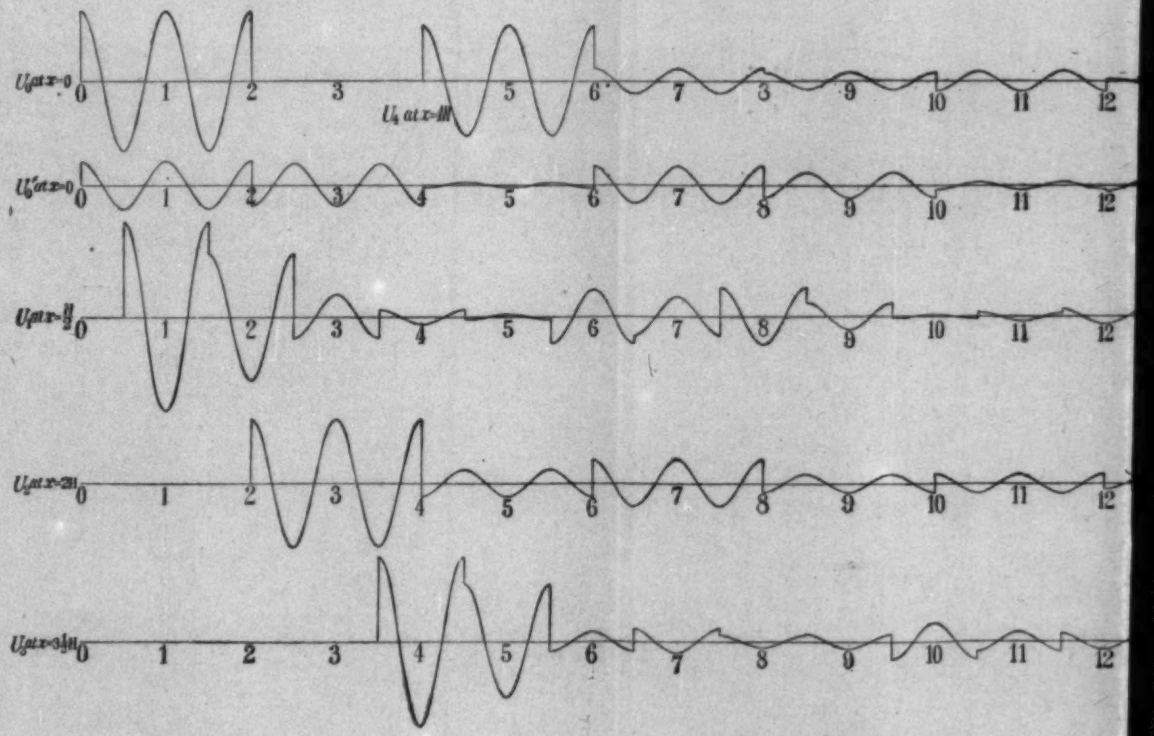

Fig. 15. $\left(\alpha=\frac{1}{2},\ \beta=1,\ H=L,\ a=\right.$

（震研彙報、第十號、圖版、妹澤、金井）

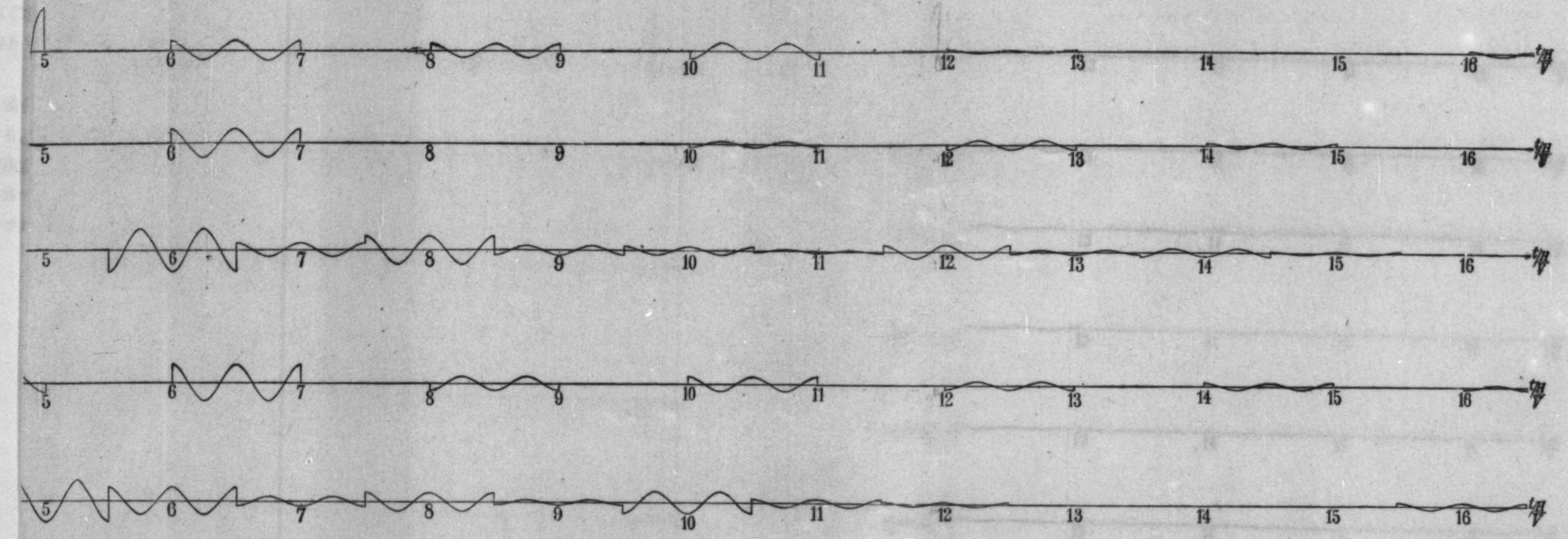

Fig. 14. $\left(\alpha=\frac{1}{2},\ \ \beta=1,\ \ H=2L,\ \ a=2L,\ \ c=\frac{2\pi}{L}\right)$

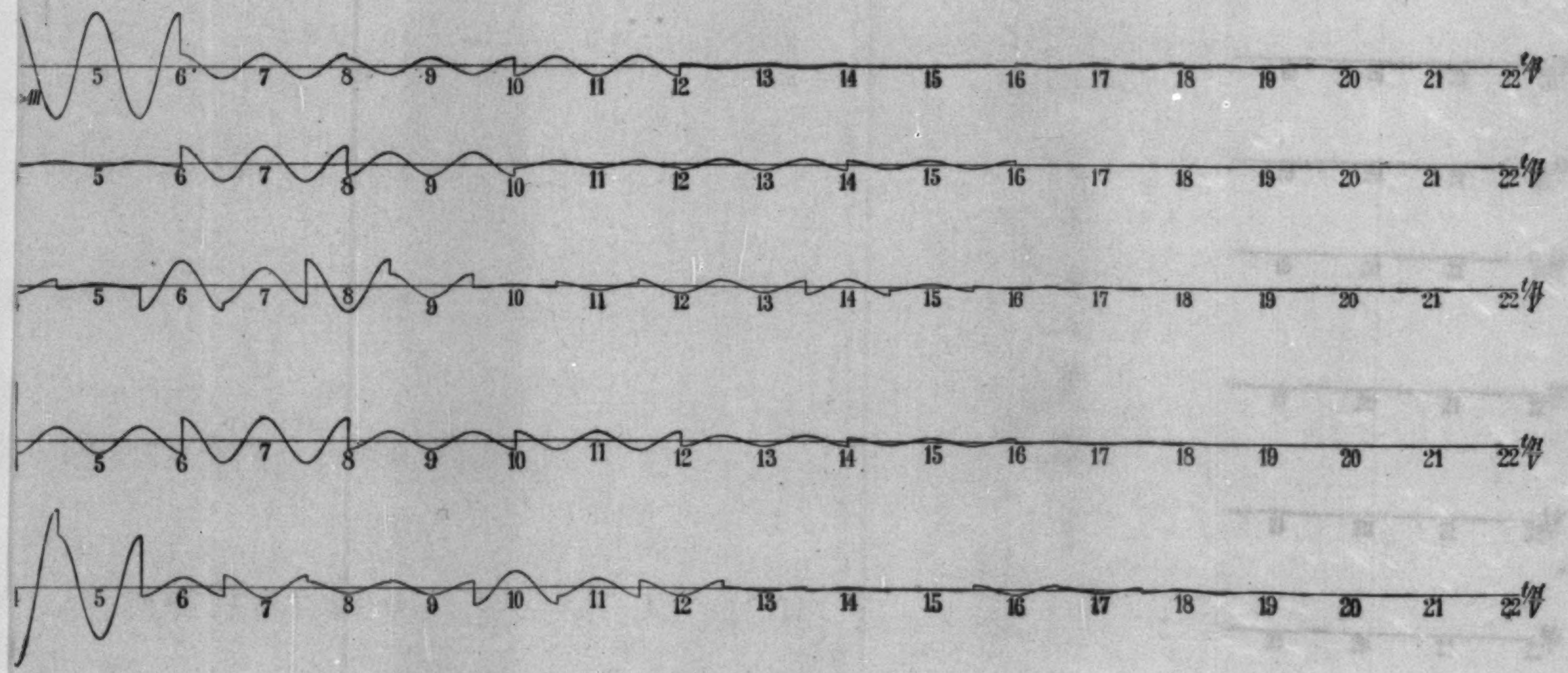

Fig. 15. $\left(\alpha=\frac{1}{2},\ \ \beta=1,\ \ H=L,\ \ a=2L,\ \ c=\frac{2\pi}{L}\right)$

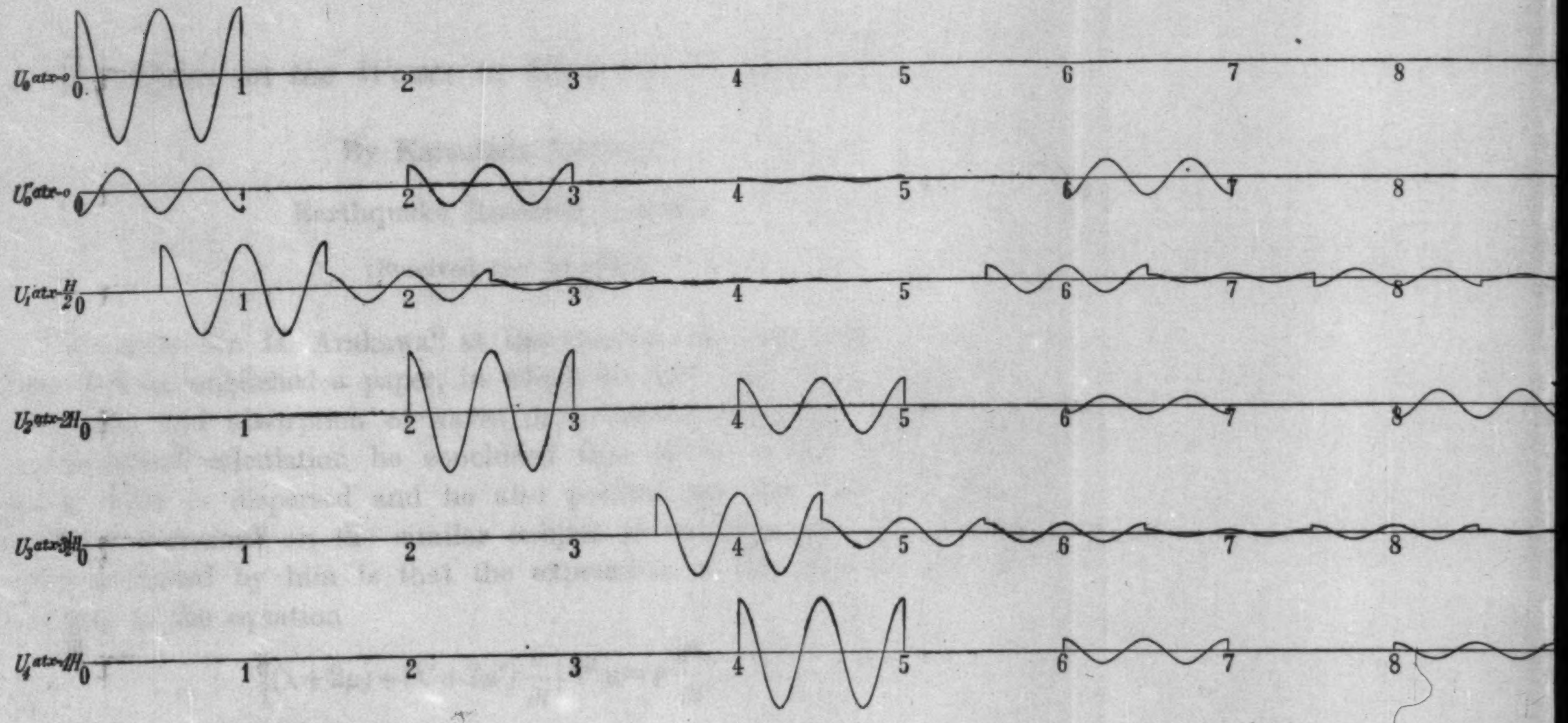

Fig. 17. ($\alpha=2$, $\beta=1$, $H=2L$, $a=$

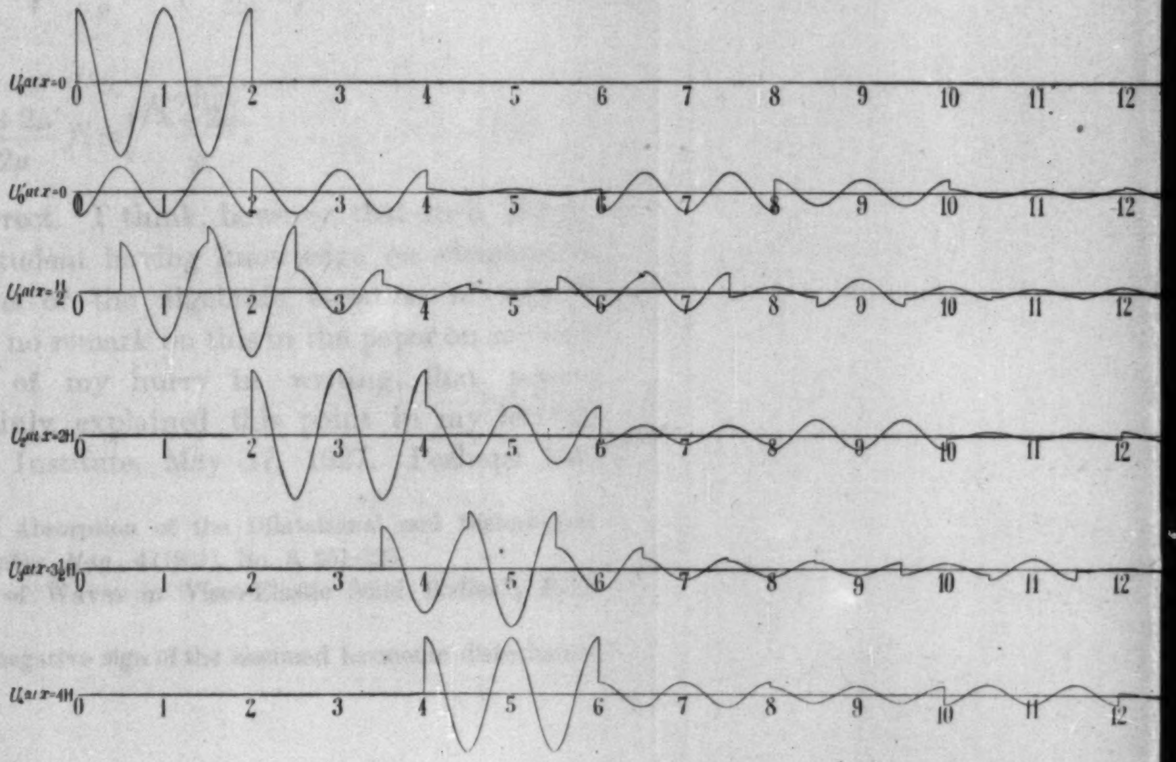

Fig. 18. ($\alpha=2$, $\beta=1$, $H=L$, $a=2$

[Bull. Earthq. Res. Inst., Vol. X, Pl. II.]

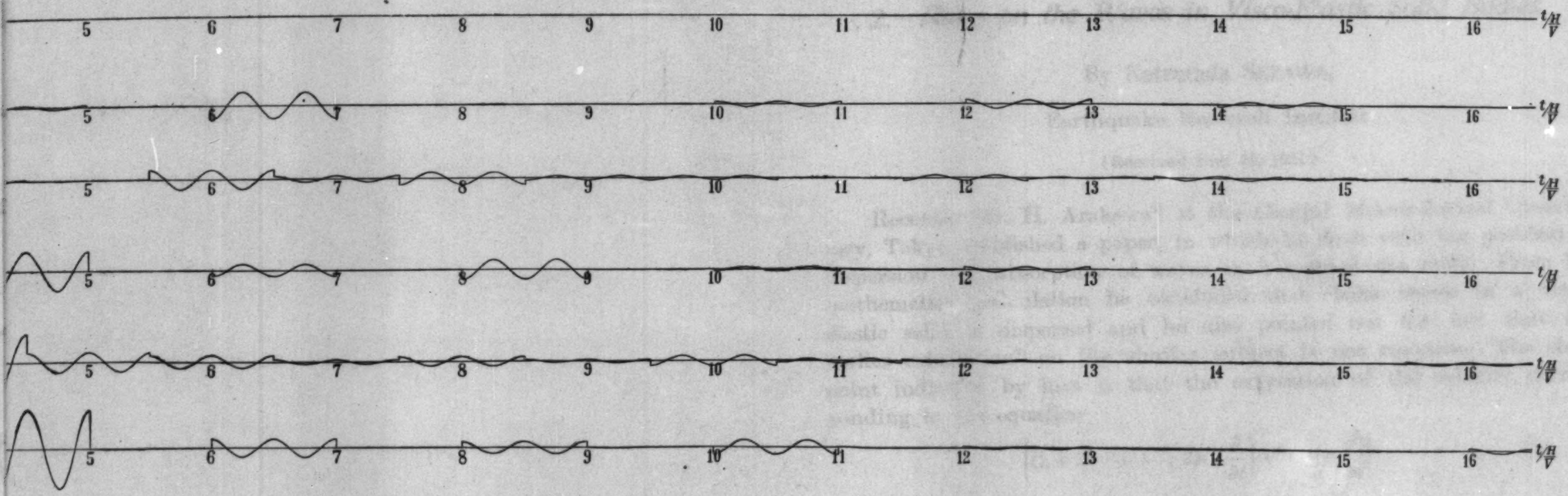

Fig. 17. $\left(\alpha=2,\quad \beta=1,\quad H=2L,\quad a=2L,\quad c=\frac{2\pi}{L}\right)$

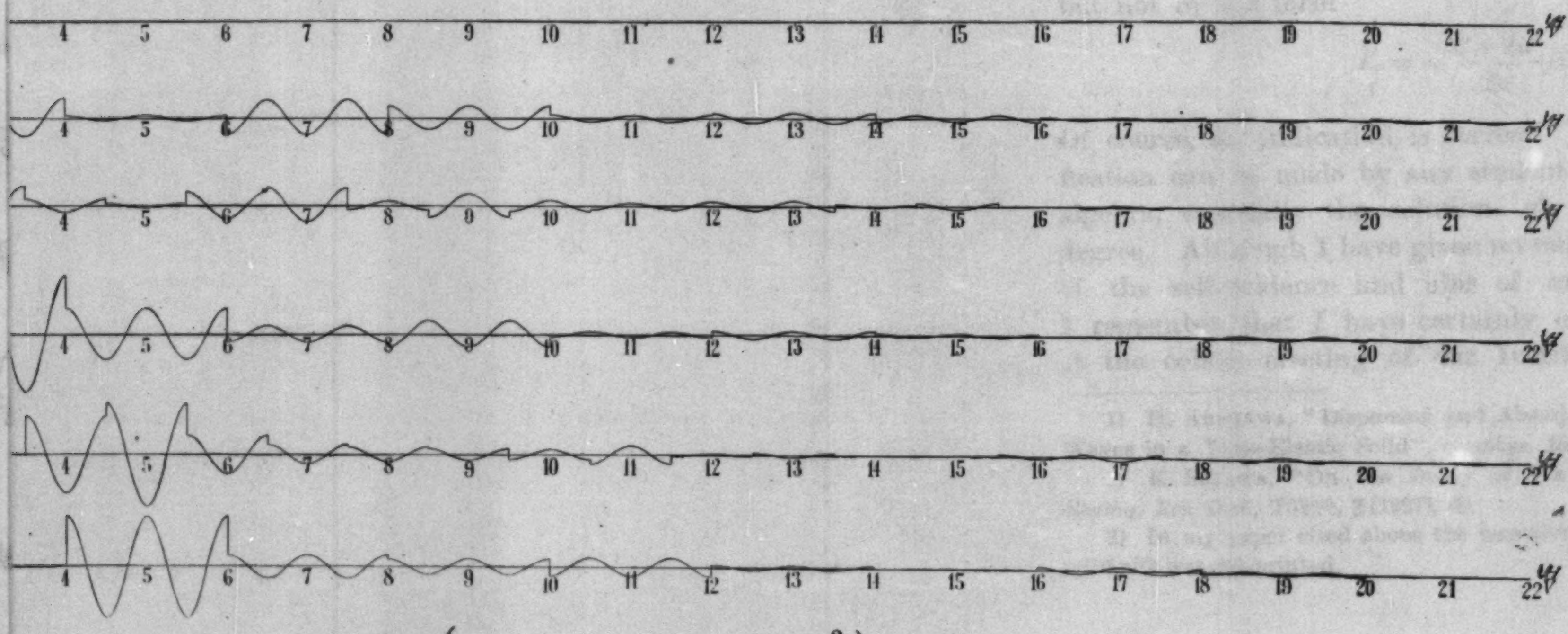

Fig. 18. $\left(\alpha=2,\quad \beta=1,\quad H=L,\quad a=2L,\quad c=\frac{2\pi}{L}\right)$

2. *Notes on the Waves in Visco-Elastic Solid Bodies.*

By Katsutada SEZAWA,

Earthquake Research Institute.

(Received Dec. 20, 1931.)

Recently Mr. H. Arakawa[1] at the Central Meteorological Observatory, Tokyo, published a paper, in which he dealt with the problem of dispersion and absorption of waves in a visco-elastic solid. From his mathematical calculation he concluded that elastic waves in a visco-elastic solid is dispersed and he also pointed out the fact that my earlier calculation[2] on the similar subject is not rigorous. The chief point indicated by him is that the expression of the velocity corresponding to the equation

$$\left\{(\lambda+2\mu)+(\lambda'+2\mu')\frac{\partial}{\partial t}\right\}\nabla^2 u=\rho\frac{\partial^2 u}{\partial t^2} \quad \dots\dots\dots\dots (1)$$

is to be written in the from

$$\frac{p}{f}=-\frac{\lambda'+2\mu'}{2\rho}fi\pm\sqrt{\frac{\lambda+2\mu}{\rho}-\left(\frac{\lambda'+2\mu'}{2\rho}\right)^2 f^2}, \quad \dots\dots\dots (2)$$

but not in the form

$$\frac{p}{f}=-\frac{\lambda'+2\mu'}{2\rho}fi\pm\sqrt{\frac{\lambda+2\mu}{\rho}}. \quad \dots\dots\dots\dots\dots (3)$$ [3]

Of course, his indication is correct. I think, however, that such identification can be made by any student having knowledge on elementary algebra, especially the solutions of the algebraic equation of second degree. Although I have given no remark on this in the paper on account of the self-evidence and also of my hurry in writing that paper, I remember that I have certainly explained this point in my lecture at the colloq. meeting of our Institute, May 17, 1927. Perhaps Mr.

1) H. ARAKAWA, "Dispersion and Absorption of the Dilatational and Distortional Waves in a Visco-Elastic Solid", *Geophys. Mag.*, 4 (1931), No. 3, 251-223.

2) K. SEZAWA, "On the Decay of Waves in Visco-Elastic Solid Bodies", *Bull. Earthq. Res. Inst.*, Tôkyô, 3 (1927), 45.

3) In my paper cited above the negative sign of the assumed harmonic disturbance $e^{-i(pt-fx)}$ was misprinted.

Arakawa has not heard my lecture on this problem. I will make mention of this again in the present paper.

I have omitted the term $\left(\frac{\lambda'+2\mu'}{2\rho}\right)^2 f^2$ in $\sqrt{\frac{\lambda+2\mu}{\rho}-\left(\frac{\lambda'+2\mu'}{2\rho}\right)^2 f^2}$ because of the fact that this term has no influence on the transmission of waves in ordinary substances and also that by the neglect of this term the Fourier's integrals of the types:

$$\left.\begin{aligned}&\frac{1}{\pi}\int_0^\infty df\cos f v_1 t\, e^{-w_1 f^2 t}\int_{-\infty}^\infty \varphi(\lambda)\cos f(x-\lambda)\,d\lambda,\\&\frac{1}{\pi}\int_0^\infty df\, e^{-w_1 f^2 t}\int_{-\infty}^\infty \varphi(\lambda)\cos f(x-v_1 t-\lambda)\,d\lambda\end{aligned}\right\}\quad\ldots\ldots(4)$$

can be easily evaluated. The important point aimed in that paper resided on these integrals. The method of analysis, in which neglecting elements of no practical importance we arrive at final purpose, is, I think, to be employed in all mathematical physics,[4] though it is not correct in the line of pure mathematics.

If we retain the term which I have neglected, it is impossible to evaluate the integrals of the forms (4), and consequently no special feature concerning the decay of waves can be obtained.

The reason, that the term cited above can be neglected, will be seen from the following examples. Let us take $\frac{\lambda+2\mu}{\rho}=10^{12}$ and $\frac{\lambda'+2\mu'}{2\rho}=10^8$, both in C. G. S. units, which are very near to the proper values of ordinary materials. Then, if the wave length$/2\pi=1/f=100$ m, we get by means of (2)

$$p=-i\pm\sqrt{10^4-1},$$

so that the expression of waves becomes

$$e^{-t}\left.\begin{matrix}\cos\\\sin\end{matrix}\right\}(\sqrt{10^4-1}\,t-10^{-4}x),\quad\ldots\ldots\ldots\ldots\ldots(4)$$

where t, x are measured in sec and cm. The velocity of propagation of the case of neglecting the term in question is 10 km per sec and in the case without neglect of the term is $10\left(1-\frac{1}{2\times10^4}\right)$ km, the difference being merely 0·005 %, while the waves are damped away to the amplitude 0·0000454 of that of the initial state during 10 seconds.

If we take $1/f=10$ m, we obtain

4) The harmonic solution of oscillating pendulum may be given as an example. Similar examples are found in various kinds of problems.

$$p=-100\,i\pm 100\sqrt{100-1},$$

so that the expression of the waves becomes

$$e^{-100t}\left.\begin{matrix}\cos\\ \sin\end{matrix}\right\}(100\sqrt{100-1}\,t-10^{-3}x).\ \ldots\ldots\ldots\ldots(5)$$

The velocity of propagation in the case of neglect of the term in question is again 10 km per sec, while in the case without neglect is $10\left(1-\frac{1}{2\times 100}\right)$ km. This seems to be somewhat effective on the dispersives nature, but we can understand from (5) that the amplitudes of waves die away to 0·0000454 of that of the initial state during 1/10 second.

If we take $1/f=1$ km., we get

$$p=-\frac{1}{10^2}i\pm\sqrt{10^2-10^{-4}},$$

so that the expression of waves is

$$e^{-\frac{t}{100}}\left.\begin{matrix}\cos\\ \sin\end{matrix}\right\}(10\sqrt{1-10^{-6}}\,t-10^{-5}x).\ \ldots\ldots\ldots\ldots(6)$$

The velocity of propagation, when the term in question is neglected, is again 10 km per sec, while that of no neglect is $10\left(1-\frac{1}{2\times 10^6}\right)$ km per sec. The damping is very slow and the amplitude decreases to 0·368 of the initial one during 100 seconds.

From these examples it is ascertained that in the possible case of dispersion the waves are damped away during very small fraction of a second, that is to say, they are damped in a short distance even within a fraction of the length of very short waves.

Hence it may be concluded that the waves, whose velocity is affected by the viscosity of the solid, cannot be transmitted to any short distance, so that the investigation of the dispersion of waves due to its damping nature is obviously meaningless.

Although the values of constants $\frac{\lambda+2\mu}{\rho}$ and $\frac{\lambda'+2\mu'}{2\rho}$ are different for different materials, the mutual constraints between the velocity change and the wave decay as imagined from (4), (5), (6) are readily expected, and we can easily show that it is always impossible to consider the dispersion of transmitted waves in a visco-elastic solid body. Therefore, I think that it is rather important to study more fully the own nature of the decay of waves in all cases.

---

2. 粘弾性體中の波動の問題に就て

地震研究所 妹 澤 克 惟

地震波が粘弾性體中で老衰する事は著者が既に研究したが、其波動速度が粘性の影響を受けて多少は變り得るものであるから、波動の分散といふ事が問題になる様にも思ふ。それでこの論文では具體的の數値を入れて果して分散し得るかを考へて見たのである。その結果によると、波長が極めて短く一米位になると無限長のものに比して數百分の一位速度が少くなる事がわかつたが、しかし斯る波では十分の一秒位で振幅が始めのものの數萬分の一位に減少し、從て波長の一米位を傳ると始めのものの數割位になつてしまふ事がわかつた。又一粁位の波長のものは數十秒の間大して減衰せぬ代りに波動速度は無限長のものに比し數百萬分の一も變化せぬ事がわかつた。從て粘弾性體中の波動の分散などを考へる事は殆ど無意味であると考へられる。

それで始めから波動速度を一定として傳播する場合の波動現象を取扱つても差支がない。その樣にする時は計算上種々の定積分が容易に行はれ、其結果波動の老衰問題に忘れてならぬ多くの現象を推定する事が出來るのである。

---

3. *On the Deformation of a Semi-infinite Elastic Body having a Surface Layer due to the Surface Loading.*

By Genrokuro NISHIMURA,

Earthquake Research Institute.

(Read Sept. 15, 1931.—Received Dec. 20, 1931.)

1. The problem of the deformation of a semi-infinite elastic body due to the surface traction has already been studied by many students: Boussinesq,[1] H. Nagaoka,[2] K. Terazawa,[3] H. Lamb,[4] A. E. H. Love[5] and recently M. Matumura.[6] K. Terazawa[7] has obtained, using the theorem of Fourier's double integral formula, the mathematically formal result of the surface deformation of a semi-infinite elastic solid due to any loading symmetrical about the origin. Using this result, he estimated theoretically the amount of the tilt at Chicago due to the tidal loading of the Atlantic Ocean. With the recent development of seismometrical researches, we have obtained much informations regarding the constitution of the earth such as the stratification of layers with different dynamical properties. Thus it is important to investigate the modifications on the theory of the deformation of the earth due to the tidal loading by using the information concerning the structure of the crust of the earth.

R. Takahasi,[8] a member of the Institute, using the tiltmetre devised by M. Ishimoto, studied the tilt of the surface of the crust of the earth due to the tide, and he obtained valuable series of photographic data.

For the purpose of investigating the nature of the depression of the foundation work of building, M. Matumura[9] recently dealt with the same problem. To evaluate definite integral, he used a numerical method of integration. The present author studied, independently

---

1) J. Boussinesq, "Application des Potenties ....", Paris, (1885).
2) H. Nagaoka, *Proc. Math.-Phys. Soc.*, Tôkyô., **6** (1912), 208.
3) K. Terazawa, *Phil. Trans. Roy. Soc.*, (Ser. A), **217** (1916), 35.
4) H. Lamb, *Proc. Roy. Soc.*, London, (Ser. A), **93** (1917), 293.
5) A. E. H. Love, *Phil. Trans. Roy. Soc.*, (Ser. A), **228** (1930), 377.
6) M. Matumura, *Jour. Civil Eng. Soc.*, Tôkyô, **17** (1931), No. 11.
7) K. Terazawa, *loc. cit.*
8) R. Takahasi, *Bull. Earthq. Res. Inst.*, **6** (1929), 85.
9) M. Matumura, *loc. cit.*

M. Matumura for different purpose, the deformation of a semi-infinite body having a surface layer due to the surface loading.

2. For the present purpose, we use the cylindrical coordinates (r, θ, z), and the axis of z being directed downwards from the surface of the upper layer, of which the thickness is H, and the senses of r, θ horizontal.

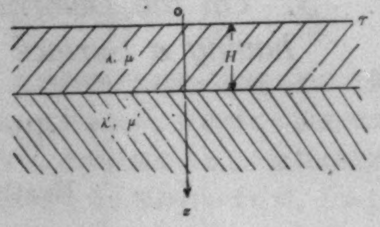

Fig. 1.

We take the following conditions at the upper and the lower surfaces of the layer.

1. The upper surface of the layer is subjected to a symmetrically distributed normal pressure only such that

$$\widehat{zz}_{z=0} = -f(r). \quad \cdots\cdots\cdots\cdots\cdots\cdots \quad (1)$$

2. The displacement of the upper layer and that of the lower solid are continuous in all components at their boundary.

3. The normal and shearing stresses are also continuous at this boundary.

Then we shall have the following expression for the normal component of the upper surface displacement of the layer:

$$w_{z=0} = -\frac{(\lambda+2\mu)}{\mu b^2}\sum_{n=1}^{\infty}\frac{J_0(k_n r)}{k_n J_1^2(k_n b)} \times \frac{\vartheta'_n}{\vartheta_n}\int_0^b f(\mu)J_0(k_n\mu)\mu d\mu, \quad \ldots\ldots (2)$$

in which ϑ_n and ϑ'_n stand for the following determinants,

$$\vartheta_n = \left| \begin{array}{l} \Big[(\lambda+\mu)\{\mu'(\lambda'+\mu')+\mu(\lambda'+3\mu')\}k_nH\,\mathrm{sh}k_nH \\ \quad +\mu'(\lambda'+\mu')(\lambda+2\mu)\mathrm{ch}\,k_nH+(\lambda+\mu)\{\mu'(\lambda'+\mu') \\ \quad +\mu(\lambda'+3\mu')\}k_nH\,\mathrm{ch}k_nH+\{\mu(\lambda+\mu)(\lambda'+3\mu') \\ \quad -\mu\mu'(\lambda'+\mu')\}\,\mathrm{sh}k_nH\Big], \\ \qquad \Big[(\lambda+\mu)\{\mu'(\lambda'+\mu')+\mu(\lambda'+3\mu')\}k_nH\,\mathrm{ch}k_nH \\ \qquad -\mu'(\lambda'+\mu')(\lambda+2\mu)\mathrm{ch}k_nH+(\lambda+\mu)\{\mu'(\lambda'+\mu') \\ \qquad +\mu(\lambda'+3\mu')\}k_nH\,\mathrm{sh}k_nH-\{\mu(\lambda+\mu)(\lambda'+3\mu') \\ \qquad\qquad -\mu\mu'(\lambda'+\mu')\}\,\mathrm{sh}\,k_nH\Big] \\ \Big[\mu(\lambda+\mu)(\lambda'+2\mu')k_nH\,\mathrm{sh}k_nH \\ \quad +\mu'(\lambda+\mu)(\mu+\lambda'+\mu')k_nH\mathrm{ch}k_nH+\mu\mu'(\lambda+\mu \end{array} \right. \quad \ldots (3)$$

$$
\begin{vmatrix}
\qquad -\lambda'-\mu')\mathrm{sh}k_nH\Big], \\
\Big[\mu(\lambda+\mu)(\lambda'+2\mu')k_nH\,\mathrm{ch}k_nH \\
+\mu'(\lambda+\mu)(\mu+\lambda'+\mu')k_nH\,\mathrm{sh}k_nH-\mu(\lambda+\mu) \\
(\lambda'+2\mu')\mathrm{sh}k_nH-\mu'(\lambda'+\mu')(\lambda+2\mu)\mathrm{ch}k_nH\Big]
\end{vmatrix}
$$

$$
\vartheta'_n=\begin{vmatrix}
\Big[(\lambda+\mu)\{\mu'(\lambda'+\mu')+\mu(\lambda'+3\mu')\}k_nH\mathrm{sh}k_nH \\
+\mu'(\lambda'+\mu')(\lambda+2\mu)\mathrm{ch}k_nH+(\lambda+\mu)\{\mu'(\lambda'+\mu') \\
+\mu(\lambda'+3\mu')\}k_nH\mathrm{ch}k_nH+\{\mu(\lambda+\mu)(\lambda'+3\mu') \\
-\mu\mu'(\lambda'+\mu')\}\mathrm{sh}\,k_nH\Big], \\
\{\mu'(\lambda'+\mu')+\mu(\lambda'+3\mu')\}(\mathrm{sh}k_nH+\mathrm{ch}k_nH) \\
\Big[\mu(\lambda+\mu)(\lambda'+2\mu')k_nH\mathrm{sh}k_nH \\
+\mu'(\lambda+\mu)(\mu+\lambda'+\mu')k_nH\mathrm{ch}k_nH \\
+\mu\mu'(\lambda+\mu-\lambda'-\mu')\mathrm{sh}k_nH\Big], \\
\{\mu(\lambda'+2\mu')\mathrm{ch}k_nH+\mu'(\mu+\lambda'+\mu')\mathrm{sh}k_nH\}
\end{vmatrix}, \quad \ldots (4)
$$

λ, μ being the Lame's elastic constants of the upper layer, and λ', μ' those of the lower solid.

To find the expression (2), use has been made of the condition that the normal stress $f(r)$ expressed by (1) may be expanded in the following form:

$$f(r)=\frac{2}{b^2}\sum_{n=1}^{\infty}\frac{J_0(k_nr)}{J_1(k_nb)}\int_0^b f(\mu)J_0(k_n\mu)\mu d\mu, \quad \ldots\ldots\ldots\ldots (5)$$

where k_n is the n th positive root of

$$J_0(k_nb)=0. \quad \ldots\ldots\ldots\ldots\ldots\ldots\ldots (6)$$

The expression (2) is useful for the study of the surface deformation in a limited region whose outer boundary is of radius b.

When b is infinite, we can easily obtain the following expression of the surface normal displacement by using the expressions of (2), (3), (4), (5) and (6):

$$w_{z=0}=-\frac{(\lambda+2\mu)}{2\mu}\int_0^\infty\frac{\vartheta'_n}{\vartheta_n}J_0(k_nr)dk_n\int_0^\infty f(\mu)J_0(k_n\mu)\mu d\mu. \quad \ldots (7)$$

This expression is favourable for the study of the surface deformation in an unlimited region.

When the thickness of the layer H is very small, and $\lambda=\mu$, $\lambda'=\mu'$, we obtain from (7) the following expression of $w_{z=0}$:

$$w_{z=0}=\frac{\mu}{12\mu'^2}\int_0^\infty [9\mu'/\mu+2\{8-\mu'/\mu+2(\mu'/\mu)^2\}k_nH]J_0(k_nr)\mathrm{ch}k_ndk_n \times\int_0^\infty f(\mu)J_0(k_n\mu)\mu d\mu.\ldots\ldots\ldots(8)$$

3. For an example of Section 2, we shall take the following form of the surface normal stress:

$$\left.\begin{aligned}\widehat{zz}_{z=0}&=-\frac{\Pi}{a}(a^2-r^2)^{1/2} &&\text{for } r<a\\ &=0. &&\text{for } r>a\end{aligned}\right\}\ldots\ldots\ldots\ldots(9)$$

Then the normal displacement of the surface of the layer is written in the following form:

$$w_{z=0}=\frac{1}{12\mu}\frac{\Pi a}{(\mu'/\mu)^2}\left[9\mu'/\mu\begin{cases}\frac{1}{2}\left\{\left(1-\frac{1}{2}\frac{r^2}{a^2}\right)\sin^{-1}\frac{a}{r}+\frac{r}{2a}\sqrt{1-\frac{a^2}{r^2}}\right. & \text{for } a\leq r\\ \frac{\pi}{4}\left(1-\frac{r^2}{2a^2}\right) & \text{for } a\geq r\end{cases}\right.$$
$$\left.+2\{8-\mu'/\mu+2(\mu'/\mu)^2\}H/a\begin{cases}0 & \text{for } a\leq r\\ \sqrt{1-\frac{r^2}{a^2}} & \text{for } a\geq r\end{cases}\right].\qquad(10)[10]$$

The surface inclination $\left(\frac{\partial w}{\partial r}\right)_{z=0}$ due to the load of (9) is expressed by

$$\left(\frac{\partial w}{\partial r}\right)_{z=0}=-\frac{\Pi}{12\mu(\mu'/\mu)^2}\left[9\mu'/\mu\begin{cases}\frac{r}{2a}\left\{\sin^{-1}\frac{a}{r}-\frac{a}{r}\left(1-\frac{a^2}{r^2}\right)^{1/2}\right\} & \text{for } r\geq a\\ \frac{\pi}{4}\frac{r}{a} & \text{for } r\leq a\end{cases}\right.$$
$$\left.+2\{8-\mu'/\mu+2(\mu'/\mu)^2\}H/a\begin{cases}0 & \text{for } r\geq a\\ \frac{r}{a}\left(1-\frac{r^2}{a^2}\right)^{-\frac{1}{2}} & \text{for } r\leq a\end{cases}\right].\ldots(11)$$

It may be seen from (10) that when the lower solid is more rigid than the upper layer, the magnitude of the surface normal displacement of the layer is small; and in the reversed case, where the layer is more rigid than the lower solid, the surface displacement of the layer is large. The equation (10) also shows us the relations among the surface defor-

10) To obtain (10), we used the integral formula devised by K. Terazawa. *loc. cit.*

mation, the loading area, and the thickness of the upper layer. Assuming $H/a=10$, we have calculated the magnitude of the surface normal displacement for different values of μ'/μ. (Fig. 2.)

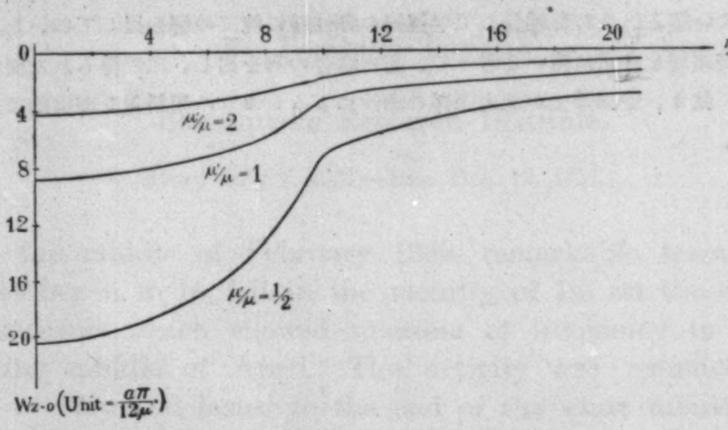

Fig. 2. $\left[\lambda=\mu,\ \lambda'=\mu',\ H/a=\frac{1}{10}.\right]$

If we put $H=\rho g b$ in this example, we have the case of the same loading condition as that of the Terazawa's investigation.[11] Assuming $H=50$ km, $\mu'/\mu=2$ and $\mu=3\times10^{11}$ C. G. S., we obtain the following value of inclination at the position, of which the distance from the centre is 3000 km, by using the equation of (11).

$$\left(\frac{\partial w}{\partial r}\right)_{z=0}=\cdot00028, \quad \ldots\ldots\ldots\ldots\ldots\ldots(12)$$

which is the same value obtained by Terazawa in his example. Regarding the other constants such as a, b, ρ and g, we, of course, used the same values which was applied in Terazawa's example.

In conclusion, the present writer expresses his sincere thanks to Professor K. Sezawa for his kind Guidance.

---

3. 表面層を有し表面荷重を受ける彈性體の變形

地震研究所　西　村　源　六　郎

半無限彈性體の表面荷重による變形問題を取扱ふには現在次の二通りの方法がある。ラーメ、クラペーロン、そしてビジネスク等によつて主に研究された所謂ポテンシヤルの理論から解くものと、寺澤博士、ラム等が提唱してゐる所謂フウリエーの二重積分公式を利用して解いて行く研究方法がそれである。

---

11) K. Terazawa, *loc. cit.*

最近松村工學士は著者と同じ問題を工學的見地から研究され非常に面白い結果を得られてゐる。著者は、本論文に於て、力學的性質を異にする地層の存在を考に入れて、地殼の表面荷重による變形問題を取扱つてみた。解き方は寺澤博士やラブの方法と同じであるが、有限な彈性體の變形問題の研究に都合のよい解と、それを延長して半無限の彈性體に就ての解を出しておいた。そして定積分を解く爲め、表面層を非常に薄いと考へて、其の場合の解を出し、二三得られた面白い性質を擧げ、一つの例題に就き、寺澤博士が北大西洋の潮汐によるシカゴの傾斜量を理論的に出されたものと比較してみた。

4. *On Swarm Earthquakes.*

By Torahiko TERADA,

Earthquake Research Institute.

(Read July 7, 1931.—Rec. Dec. 19, 1931.)

From the middle of February 1930, remarkable trains of swarm earthquakes began to be felt in the vicinity of Itô on the eastern coast of Idu Peninsula which showed maxima of frequency in March and lasted to the middle of April. The activity was resumed from the beginning of May and lasted to the end of the same month. Towards the middle of November another swarm was commenced in northern parts of Idu and culminated in the destructive shock of 26th. Nov. The activity lasted towards the beginning of January 1931. Though somewhat similar phenomena occurred in 1899 at Arima, in 1917 and 1920 at Hakone and in 1922 at the Suwa Lake districts, they are surpassed in frequency and duration as well as in intensity by the recent case of Idu earthquake-swarms with their catastrophal climax of 26th. November.

Fig. 1 will illustrate the characteristic mode of fluctuation in the daily numbers of shocks. In these examples, the earthquakes are crowded within a well defined interval of time and form an apparent group or swarm. Though the daily numbers show a considerable fluctuation we may roughly compare the graph with a kind of probability curve with a definite mean value and dispersion.

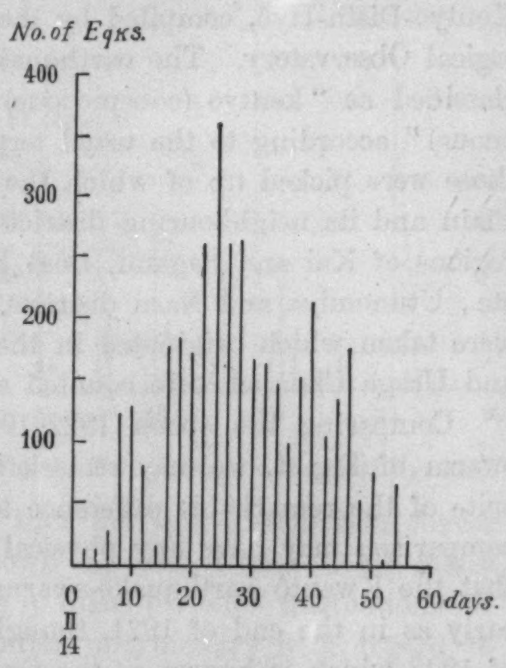

Fig. 1. Itô Earthquakes, Feb. 14–Mar. 11. Sum of successive two days are plotted against the day.

It is the shortness of the intervals of successive shocks that this kind of swarm-earthquakes draw our attention as an unusual

phenomenon. If the time scale be magnified sufficiently people will take no notice of these swarms as such. It is, therefore, of some interest to inquire whether a similar swarm cannot be found with different scales of time and space. For an example, we take the monthly numbers of conspicuous earthquakes in Kwantô Districts which are plotted in Fig. 2. The data for 1920–1927 are taken from Honpô-

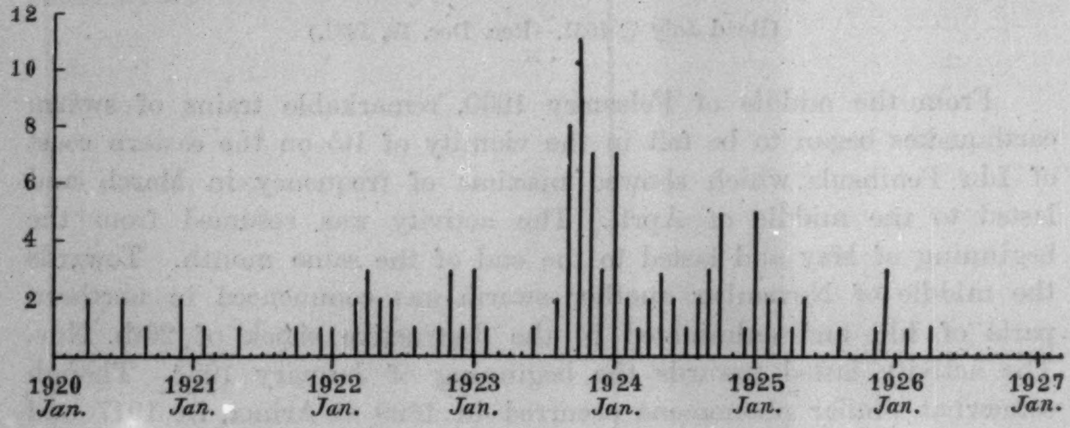

Fig. 2. Earthquakes in Kwantô District 1920–1927.

Kentyo-Disin-Hyô, compiled by the Authorities of the Central Meteorological Observatory. The earthquakes here chosen are those which are classified as "kentyo (conspicuous)" and "yaya kentyo (rather conspicuous)" according to the usual terminology. Among these earthquakes those were picked up of which the epicentres are located within Kwantô Plain and its neighbouring districts such as Idu Peninsula, mountainous regions of Kai and Sagami, Bôsô Peninsula, river basins of Tonegawa etc., Utunomiya and Nasu districts, and Province of Iwaki. Only those were taken which originated in the inland area, though the Tôkyô Bay and Uraga Channel were counted as within this area.

Comparing the epoch 1922–1926 of Fig. 2 with Idu Earthquake-swarm of Fig. 1, we may remark a similarity in features of graphs in spite of the remarkable difference in scales of the coordinates. If such a comparison may have any physical sense, we are led to the inference that the Kwantô earthquake-swarm in question was already begun as early as in the end of 1921, though the climax occurred in September of 1923 which is known as the Great Kwantô Earthquake.

In the case of purely statistical occurrence in which the probability of occurrence of a number n is determined by its mean value ν alone,

we usually resort to Poisson's formula. In the case when the probability p of each element turning out favourable is very small, while the number of the elements, N, concerned is very large so that the mean value $\nu = pN$ is finite, the above assumes the form similar to Gauss's law. In the present case, we may tentatively compare the number, n, of earthquakes in a given day with the number of elementary volumes of a colloidal solution containing a given number of particles. In the latter case the actual statistical distribution will also show some irregularity when the total number of the volume elements taken is finite. The distribution curve in such case cannot, however, be expected to show such a remarkable quasiperiodic fluctuation as shown in Fig. 1 or 2. Hence, we may suspect that there are some causes which give rise to such a characteristic distribution curve.

Among the natural phenomena there seems to be some class which show a quite similar statistical distribution. One of the remarkable examples is afforded by the daily number of falls of camelia flowers. In the last spring, the present writer and Mr. T. Utigasaki of the Institute of Physical and Chemical Research made some observations regarding the fall of this flower. Fig. 3 and 4 show some examples of

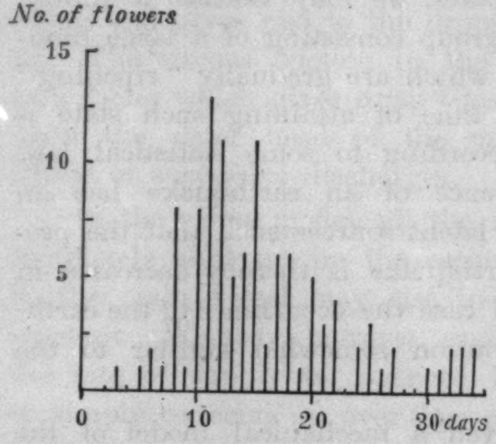

Fig. 3. Fall of camelia flower (Terada).

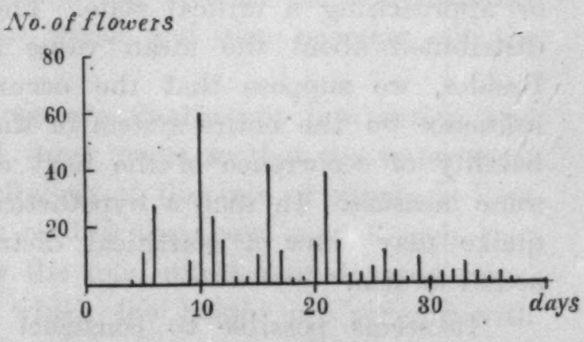

Fig. 4. Fall of camelia flower (Utigasaki).

the results obtained. It will be seen that the time-distribution curves resemble to those of earthquakes shown in Fig. 1 and 2 in many essential points, i. e. the curve shows a quasi-periodic fluctuations of remarkable amplitude and also a similar unsymmetry with regard to the maximum point.

In the case of the flower the meaning of the statistical distribution observed is in some measure apparent. Thus, there are a number of

elements for which the average *life* is assigned and the actual falls take place scattered about this mean. There must, however, be present some cause which gives rise to such a remarkable fluctuation of the distribution curve as is actually observed. Firstly, the weather conditions may considerably affect the fall. It was, however, observed that the number of fall is not necessarily large after a windy or rainy days as may be commonly expected. A very remarkable fact is that the fall takes place almost exclusively during the night hours. Even in a very windy day the fall during the day time is quite rare. Only towards the end of the flower period some of the flowers are rotten before falling, in which case the normal mode of fall is not followed but the pistil and calix drop off attached to the petals. These rotten flowers are sensitive to winds. The normal mode of fall of the petals seems, however, to be determined by some other intrinsic causes. As it is known that the *turgidity* of plants shows a great difference in day and night, we may suppose that the fall of flowers is somewhat connected with it. On the other hand, the fall of a large number of flowers within a short time cannot be without some influence upon the turgidity of the entire organism and therefore affect the later fall in some or other way.

Returning to the case of earthquakes, we may venture a similar conjecture. Thus, we may suppose a group consisting of a large number of "latent" origins of earthquake which are gradually "ripening" or approaching a critical state. The time of attaining such state is distributed about the mean value according to some statistical law. Besides, we suppose that the occurrence of an earthquake has an influence on the entire system of the latent sources such that the probability of occurrence of the next earthquake is thereby decreased in some measure. In such a hypothetical case the occurrence of the earthquake may show a statistical distribution somewhat similar to the actual swarm.

It seems possible to construct even a mechanical model of the system above considered. Suppose, for an instance, a vertical cylindrical vessel containing water, provided with a large number of horizontal side-tubes attached to the wall at nearly constant heights. The end of each tube is provided with a stop such that it is pushed off when the pressure of water inside of it attains a certain value which is not quite constant for all the tubes but varies within a range about the mean value. The stop is connected to a ball or conical secondary stop which lies in the inside of the mouth of the tube, and when the external

primary stop drops out this second stop comes in action and completely shut off the mouth after allowing a certain quantity of water to be discharged, before the complete stoppage is effected. We may also introduce in some part of the tube, between the vessel wall and the stop, some kind of viscous resistance by which means the effect of dropping of a stop upon the water content of the vessel may be made to lag. Suppose now that the vessel is at first empty and water is gradually poured in from above. When the pressure at the depth, where the tubes are arranged, approaches the mean critical value the stops will begin to drop out before the mean value is attained. Others will remain after the mean critical pressure is reached and a few will drop out only when the pressure has considerably surpassed the mean critical value. On account of the discharge of water due to the dropping of a stop the rate of increase of the water head in the main vessel will be retarded. When a large number of stops drop out nearly simultaneously, it may happen that the water head falls down in spite of the continuous supply. In this latter case the further dropping out of the stops may be suspended for a certain time. As, however, the stops which have dropped out are replaced by the inner stops after discharging definite amount of water, the water head soon resumes rising and gives rise to the dropping of another group of stops and so on. The viscous friction in the side-tube as above assumed will serve as a factor which gives some time-lag to the effect of the side-discharge upon the water head of the main vessel and also *smoothes* out the effects of successive discharges.

In the above model, all the stops are finally put into action and completely shut up by the second inner stops so that the water head in the main vessel may rise indefinitely if the rate of supply is kept constant. We may, however, easily modify the above model such that the rate of supply is governed by the total number of dropped stops, or simply conceive an over-flow of which the height are varying with time in a statistical manner. We may also make the same model resume a second period of activity, if the stop of each side-tube consists of a chain of balls made of some substance such as pitch. Under the constant pressure from the inside, the viscous stop will slowly flow out of the mouth opening though in every instant it is a solid stop in the ordinary sense of the words. After the lapse of a certain time average strength of the stops will decrease to a critical amount which is given by the water-head of the main vessel which is assumed here to be

fluctuating as above supposed due to some other external causes. When these second stops drop out the third ones will serve as the complete stop in the next period of repose, and so on.

The above mechanical model could also be replaced by an electrical model in which sparkings of numerous spark gaps replace the dropping out of stops. The destruction of each spark gap after sparking may be attained, for example, by choosing a soap bubble as one of the electrode. A semi-conductor will then play the part of the viscous resistance in the mechanical model.

The practicability of these models are, however, not at all essential in the present discussion, which is aiming at the description of a "Gedankenexperiment" carried out with the purpose of investigating one of the possible mechanism of swarm earthquake.

In comparing the above models with the case of earthquakes the correspondence of the working parts will be quite evident. Thus, falling of each stop represents an earthquake by which the probability of occurence of the next earthquake at the same spot is reduced to zero for a certain time. The water head represents the average state of strain in the entire system including all the latent seismic origins. Each single earthquake is then assumed to contribute to a certain decrease of the average strain of the entire system. The viscous resistance of the model will also correspond to the viscosity of the crustal materials.

Thus, it will be seen that the above model may deserve notice at least as one of the plausible alternatives. The quantitative formulation of this kind of model seems not quite easy as far as the usual method of statistics is resorted to, since the mutual influence of the elements plays here the most essential role, while the usual statistics holds mostly for the case of utterly independent elements. The effect of after-effect as is taken into account in the theory of fluctuation such as applied to the molecula phenomena is of a quite different nature from that here in question.

4. 地震群に就て

地震研究所 寺田寅彦

昭和五年伊豆地方に起つた地震群と比較さるべき地震群が、異なる時間的のスケールに於て關東大地震前後に起つた事に注意を喚起し、又此れと形式的に類似した群起的現象が他の方面にも存在する一例として椿の花の落花数の日々變化を例示し、別に此等に相應ずべき器械的模型を想像して此れに關する思考實驗の經過を述べてある。

5. *Statistical Relation between the Frequencies of Earthquakes in Japan and Other Parts of the World.*

By Seiti YAMAGUTI.

(Read Sep. 15, 1931.—Received Dec. 20, 1931.)

Introduction.

The present investigation was made with the intention of studying the statistical relation between the annual seismic frequencies in Japan and other regions of the world, if such a relation may at all exist. In this respect, South America which is nearly antipodal to Japan, comes first in view, since it was already remarked by some authorities that an earthquake seems to be liable to induce another in the antipodal region. For this reason, South America was taken first and then the other countries have been taken into account one after another. For the statistical investigation, we have tried to apply a method which is somewhat different from the usual method of finding correlation coefficient, as will be described below.

Method of Investigation.

From Rikwa Nenpyô (the Scientific Chronological Table), the conspicuous earthquakes were taken which occurred in different parts of the world, during the period of 30 years, 1900–1930, and they were classified into 7 groups according to the geographical regions of occurrence: those are Japan, South America, Central America, the Coast of the Mediterranean Sea, Continent of Asia, the Philippines with neighbouring oceanic regions, and Australia including the oceanic environments.

The yearly frequency curves were plotted, with the year as the time axis, respectively for these groups, and compared with each other in order to find out some apparent relations among them. In order to smooth out minor irregularities, the number, n, of the earthquakes falling within the successive overlapping time interval of 3 years, was counted and plotted against the middle point of the interval. Next, the deviation, δ, from the mean value of n, was calculated for each region. Also, the reduced value, δ_r, was calculated referred to Japan, i.e. $\delta_r = \delta_x \frac{|\delta_{\text{Japan}}|}{|\delta_x|}$,

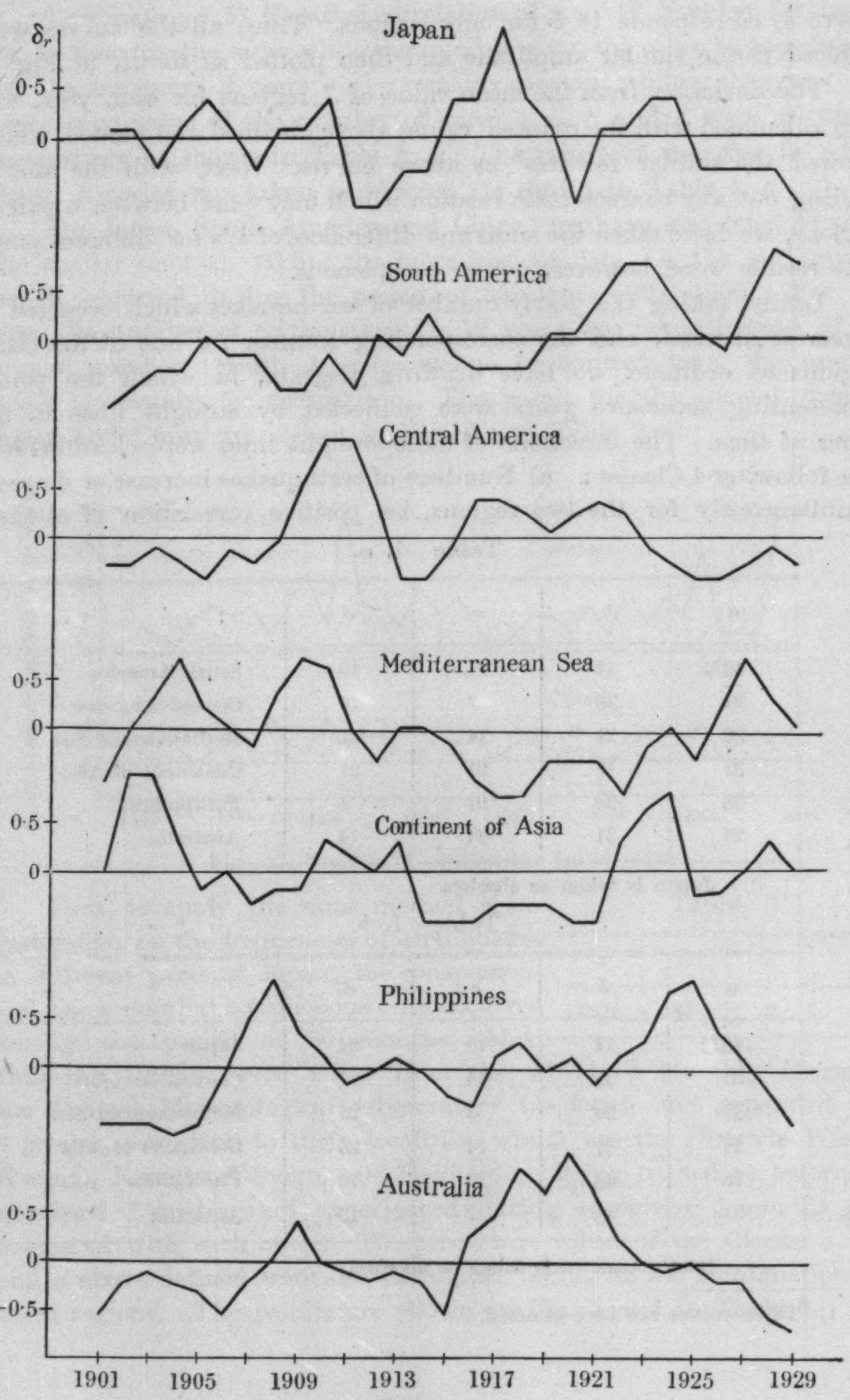

Fig. 1.

$\delta = \frac{n - n_{\text{mean}}}{n_{\text{mean}}}$, $\delta_r = \delta_x \times \frac{|\delta_{\text{Japan}}|}{|\delta_x|}$ reduced to Japan.

where δ_x corresponds to δ for any regions. Thus, all the curves were reduced to the similar amplitude and then plotted as shown in Fig. 1.

The deviation from the mean value of 7 regions for each year, was also calculated with the reduced values above obtained and plotted, which showed the similar features[1] as above curves. Next, with the aim of finding out any characteristic relation which may exist between a pair of regions, we have taken the sums and differences of δ_r's for different pairs. The results were, however, not so conspicuous.

Lastly, taking the yearly number of earthquakes which occurred in Japan as abscissa, and the corresponding number for one of the other regions as ordinate, we have drawn a diagram, in which the points representing successive years were connected by straight lines in the order of time. The directions of these straight lines were classified into the following 4 Classes : *a*) Numbers of earthquakes increase or decrease simultaneously for the two regions, i.e. positive correlation of abscissa

Table 1, *a*.

a	*b*	*c*	*d*	
48%	14	24	10	South America
24	**38**	17	10	Central America
28	24	14	21	Mediterranean Sea
31	17	21	21	Continent of Asia
38	28	21	7	Philippines
24	**31**	24	14	Australia

Japan is taken as abscissa

Table 1, *b*.

a	*b*	*c*	*d*	
48%	14	10	24	Japan
31	**35**	14	21	Central America
31	28	3	28	Mediterranean Sea
28	**31**	14	28	Continent of Asia
28	**48**	10	10	Philippines
31	**45**	7	10	Australia

South America is taken as abscissa

1) These curves are here omitted.

x and ordinate y; b) Negative correlation of x, y; c) Number for Japan, i.e. x, remains the same while the number y for the other region changes for the successive 2 years; d) y remains constant while x changes. The percentage value of the number of cases a, b, c, and d were calculated respectively as shown in Table 1, a. The result of the case in which South America was taken as abscissa, is shown in Table 1, b.

For Japan, South America and China, we have also tried to apply the similar method, taking the more ancient data, i.e. the earthquakes which occurred during the period of 350 years (1550–1900). For this case, the number of earthquakes for 10 years was taken instead of the annual number. South America was to be omitted here, the number being too scanty for comparison. The result for the ancient data of Japan and China are shown in Fig. 2 and Table 2.

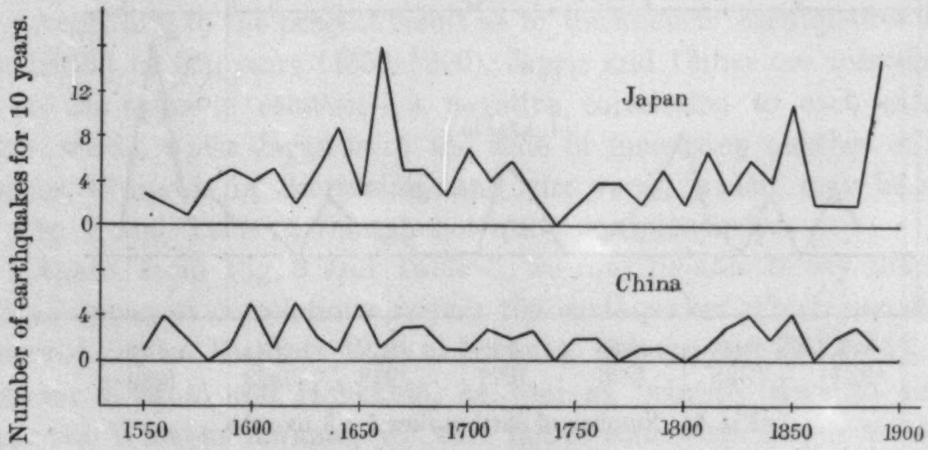

Fig. 2. Number of earthquakes for 10 years.

Table 2.

a	b	c	d
32%	47	9	9

Next, to apply the same method of investigation on the frequencies of earthquakes in different parts of Japan, the conspicuous and the somewhat conspicuous ones occurred during the period of 80 months (May, 1924–Dec., 1930), were taken from the Abridged Monthly Report of the Central Meteorological Observatory in Japan and separated into 4 groups, according to their localities, which are the Districts West to Kwantô, Kwantô, Tôhoku, and Hokkaidô. Being treated as before, the numbers of earthquakes experienced during successive 3 months were compared with each other. The percentage values of the Classes a, b, c and d above defined were also calculated, taking all the combinations of these regions. The results are shown in Fig. 3 and in Table 3.

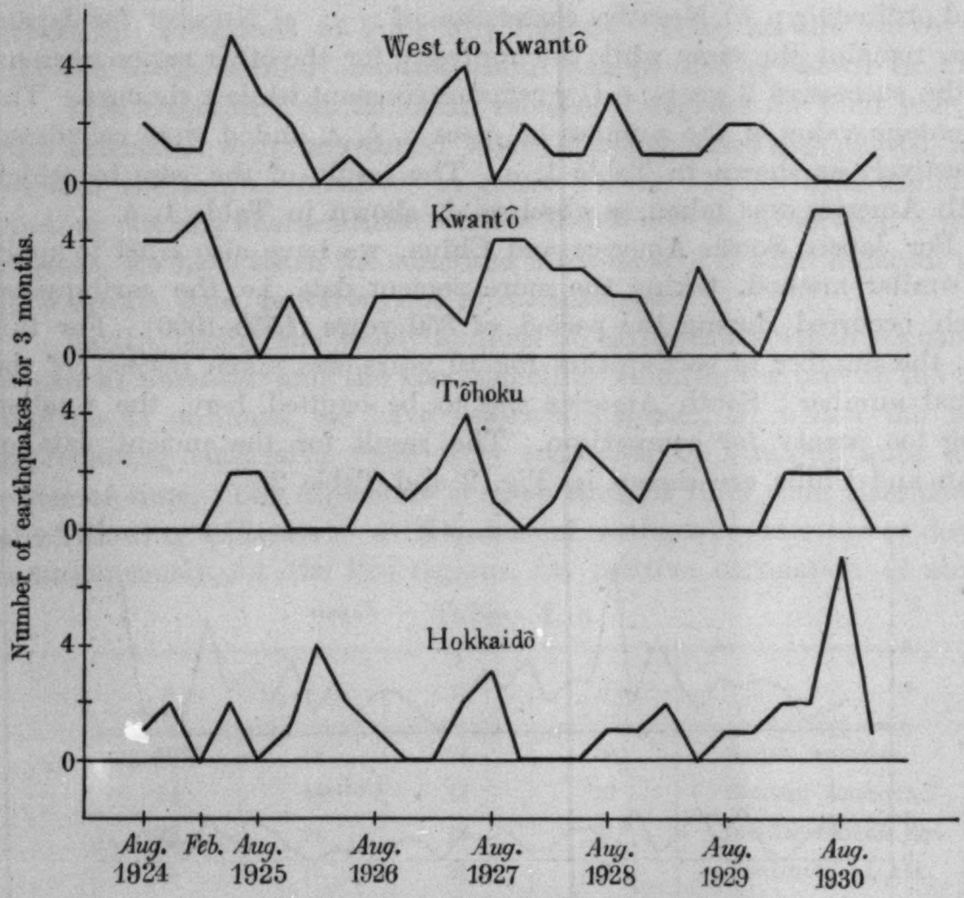

Fig. 3. Number of earthquakes for 3 months.

Table 3.

a	*b*	*c*	*d*	
20%	24	24	20	Kwantô and Tôhoku
20	36	20	12	Kwantô and Hokkaidô
12	40	24	16	Kwantô and West to Kwantô
28	20	32	16	Tôhoku and Hokkaidô
24	32	20	8	Tôhoku and West to Kwantô
24	36	16	16	Hokkaidô and West to Kwantô

Lastly, with the prospect of finding out any relation between the earthquakes occurred in land area and in sea bed respectively in the District of Kwantô, we have taken the "*felt*" earthquakes recorded in the above Report during the period of 80 months. The monthly numbers were treated here as usual. The results are shown in Table 4.

Table 4.

a	*b*	*c*	*d*
40%	53	5	1

Results and Discussions.

Looking at Fig. 1, we may suspect some trace of positive correlation between the seismic frequencies of Japan and South America, though not quite conspicuous. The fact that the value of percentage of *a* in Table 1, is much greater than *b*, may also be considered to show the existence of such a correlation. We can also trace some probable correlation between South America and Philippines referring to Table 1, *b*. For other regions, we can hardly find out any definite relations.

According to the present result as to the ancient earthquakes during the period of 350 years (1550–1900), Japan and China are considered to be in the opposite relation i. e. negative correlation to each other, in other words, when Japan is in the state of increasing number of earthquakes, China is in decreasing, and vice versa, which may be shown in Fig. 2 and Table 2, though not quite conspicuously.

Again, from Fig. 3 and Table 3, we may be able to say that there are no apparent correlations among the earthquakes which respectively occurred in the Districts West to Kwantô, Tôhoku and Hokkaidô, while between Kwantô and Hokkaidô, as well as between Kwantô and the Districts West to Kwantô, we can notice somewhat larger value of *b* than the other cases, which seams to suggest the existence of a negative correlations, as already explained.

Lastly, we can scarcely recognize any definite relations between the earthquakes in the land area and of those in sea bed near the District of Kwantô, except that *b* is somewhat greater than *a*.

In conclusion, I wish to express my best thanks to Prof. T. Terada under whose supervision the entire work has been carried out and who has given me many useful suggestions throughout the course of my investigation.

5. 本邦地震と世界各地地震の頻度間に存する統計的關係

山 口 生 知

本研究は日本に於て年々起る地震の頻度と、世界の他の地方に起る地震の頻度との間には何か或る關係が存在しはせぬかを調べる目的で爲された。

殊に或る地點に起る地震は、地球上之と對蹠的位置にある地點の地震を誘導すると云ふ說が或る學者間に唱へられて居るから、其れが事實か否かを確かめる爲めに、日本と殆ど對蹠的位置に有る南阿米利加の地震を採り日本の地震と比較した。次いで中米、地中海沿岸、亞細亞大陸、フイリッピン群島並に其の附近及び濠洲並びに其の附近の地震をとつて、それ等の間の關係を調べた。

其の結果は第一圖及び第一表に示す通り、日本と南米の地震の頻度間には正の相關關係の有る事が認められる。又南米とフイリツピンとの間には負の相關關係のあることが窺はれる。其の他の國々の間には、一定の關係あることが認められない。又日本と南米及び支那の地震に就いては、更に昔に逆つて 1550 年から 1900 年までの 350 年間に起つた地震をとつて調べて見た。而しこの場合に南米の地震は餘りに數が少ないので止むを得ず取り除いた。

前記 350 年間の昔の地震に就いては、日本と支那との間には負の相關關係がある。即ち日本が地震の數を增す狀態に有る時は、支那は地震の數を減ずる狀態にあり、又日本が數を減ずる時は支那は數を增す樣な傾向があることが認められる。

日本內地の地震に就いても前同樣の調べ方をして見たが、關東と北海道及び關東と關東以西の地震に就いては負の相關關係があるらしく思はれる。

最後に關東地方に於ける內陸地震と海底地震の起り方に就いても關係を調べて見たが、判然とした關係を認むる事は困難であつて僅かに負の相關關係あることを疑はしめるに過ぎない。

6. 地震回數の統計的研究(豫報)

地震研究所　井上宇胤

(昭和六年二月十七日發表——昭和六年十二月二十日受理)

1. 岸上冬彥氏[1]と河角廣氏は大正二年に於ける淺間山の噴火に關し、その活動の長時間繼續せる期間の噴火回數の頻度を統計的に研究されました。其の結果に依ると、火山活動が盛んな時期の方が簡單な統計理論で考へられる場合と同様な經過を取つて居り、勢力の小さい時期には複雜な經過を取つて居りました。此の事實は勢力の小さい時期には副原因の影響を蒙り易い事を暗示して居るものと解釋して居ります。

此の種の現象即ち地震回數及び噴火回數の頻度或は一定の面積に落ちる雨滴及塵埃の數尙又或る場所を通過する人間の數等に應用される統計的理論は次の如きものであります。

一回の試みの内に非常に多くの事柄が含まれて居るとします。此の事柄が期待した事柄であると云ふ確率は非常に小さなものであるが一回の試みの內で此の期待した事柄の起る數は或る有限な數であると致します。すると一回の試みに依つて期待した事柄が x 回起る確率は次のポアツソン氏の數式に依つて與へられます。

$$W(x)=e^{-m}\frac{m^x}{x!}\dots\dots\dots\dots\dots\dots\dots\dots(1)$$

但し m は x の平均値であります。さて私は各種の地震活動に際して地震回數の頻度の消長の經過が上述の統計的理論と如何に一致し或は又如何に異なるかを研究致しました。其の結果として各種の活動とも其の活動中の時期に依つて活動の勢力に消長があるが、其の各々の時期內に於ては其の地震回數の頻度の消長は殆んど上述の統計的理論に依つて與へられるものと一致して居り、從つて一般に地震活動は各時期每に異なる確率を持つて統計的に生起して居ると考へればよい事になりました。

2. さて此の比較研究の方法は次の如きものであります。

或る地震活動に於てある一定の期間內に y 回發生する割合を $W(y)$ とします。此れ

1) 岸上冬彥、河角廣　震研彙報, 4 (1928), 75-83.

は觀測の材料から既知のものであります。今假りに此の現象が統計的理論の示す如く生起して居るものと假定致しますと、其の時の地震發生回數の平均値 m は上述のポアツソン氏の數式に此等の價を代入した

$$W(y)=e^{-m}\frac{m^y}{y!}\cdots\cdots\cdots\cdots(2)$$

なる式を滿足する m に依つて與へられます。即ち此の式に於て y と $W(y)$ を既知の量として m を未知量として求めるのであります。所で此の式を滿足する m なる値は $y=0$ なる場合の外は二箇づゝあります。つまり此の式の右邊は y を常數とすると $y=0$ なる場合を除いて $m=y$ なる場合に最大の値を取りますからもしも $W(y)$ が $m=y$ の時の値卽ち $e^{-y}\frac{y^y}{y!}$ なる量より大きなものであれば上記の式は成立しないのでありますが、もし $W(y)$ が此の値より小さなものとすると上記の式を滿足する m の値は二つある事になります。實際の經驗に依ると一般に $W(y)$ は $e^{-y}\frac{y^y}{y!}$ より小さい値を取りますので上記の式を滿足する m なる量を求める事が出來ます。

さてある一定の期間內に y_1 回發生した割合は $W(y_1)$ であり、y_2 回發生した割合は $W(y_2)$、y_3 回發生した割合は $W(y_3)$ であると云ふ樣にすべての y に就いて其の割合 $W(y)$ が求められたならば此等の各組に就いて上記の樣な m 卽ち $m_1, m_2, m_3\cdots$ 等を求めます。もし此の現象が統計的に發生して居るならばかくして求められた m_1, m_2, m_3 等は皆一定の m なる値卽ち y の平均の値と云ふ一箇の常數になる筈でありますが、もし統計的に生起して居るのでなければ此等の値は一定では無く y の函數として表はされます。但し前記の如く此の m なる値は一般に二箇求められますから統計的に發生して居る場合でも常數の組と然らざる組とに分れます。其の一例とし $m=4{\cdot}3$ の場合に就いて上記の樣な m を求めました。

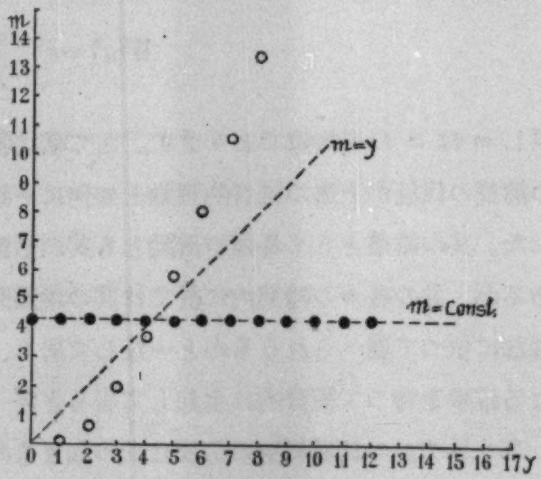

第　一　圖

卽ち此の場合の確率函數は

$$W(y)=e^{-4\cdot3}\frac{4{\cdot}3^y}{y!}$$

でありますから、此れを (2) の式に代入した

$$e^{-m}\frac{m^y}{y!}=e^{-4\cdot3}\frac{4{\cdot}3^y}{y!}$$

なる式を滿足する m を求め此の m を y の函數として第一圖に圖示してあります。此の m を求めるには Pearson[2] の統計表の Table LI. を使用しました。

3. 次に各々の期間毎に現象發生の確率が異なつて居つた、即ち各期間毎に平均値が異なつて居つたとします。もし地震活動であるとすると各期間毎に其の勢力が異なつて居つた樣な場合にあたります。それで此の全期間中の $\frac{1}{n_1}$ の間は此の現象の發生回數が m_1 なる平均値の附近で變化して居り、$\frac{1}{n_2}$ の間は m_2 なる平均値を有して居り、次々に其の樣に成つて居つたと致しますと、此等を全部一緒にして見た時の確率函數は次の樣なものであります。

$$W(y)=\frac{1}{n_1}e^{-m_1}\frac{m_1^y}{y!}+\frac{1}{n_2}e^{-m_2}\frac{m_2^y}{y!}+\dots+\frac{1}{n_n}e^{-m_n}\frac{m_n^y}{y!}\quad\dots(3)$$

此れを (2) の式の $W(y)$ に代入して、それを滿足する m をしらべて見ました。

A) まづ地震活動の或る時期に、一時活動の勢力が減退した場合の一例に就いて調べて見ました。

即ち全期間の大部分は $m=1{\cdot}0$ なる平均値を有して居つたのが其の $\frac{1}{11}$ の期間だけ $m=0{\cdot}1$ であつたと致しますと確率函數は

$$W(y)=\frac{10}{11}e^{-1\cdot0}\frac{1{\cdot}0^y}{y!}+\frac{1}{10}e^{-0\cdot1}\frac{0{\cdot}1^y}{y!}$$

となります。此れを (2) 式に代入して求めた m は第二圖に示してあります。此れに依ると回數の少ない所は統計的の場合より起りにくくなつて居ります。

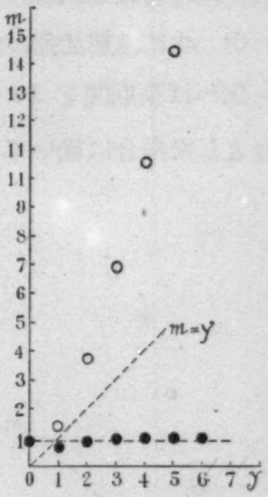

第　二　圖

B) 次に地震活動の或る時期に、一時活動の勢力が增大した場合に就いて調べて見ました。例へば全期間の大部分は $m=6{\cdot}0$ であつたが、$\frac{1}{11}$ の期間だけ $m=15{\cdot}0$ であつたと致しますと其の確率函數は

$$W(y)=\frac{10}{11}e^{-6\cdot0}\frac{6{\cdot}0^y}{y!}+\frac{1}{10}e^{-15\cdot0}\frac{15{\cdot}0^y}{y!}$$

となります。

此れを (2) 式に代入して求めた m は第三圖に示してあります。此れに依ると回數の少ない所は統計的な場合より起り難くなつて居り、回數の多い方は其の反對に起り易くなつて居ります。同樣に全期間の $\frac{19}{20}$ の間は $m=1{\cdot}0$ であり $\frac{1}{20}$ の間は $m=7{\cdot}0$ で

2) K. Pearson, "Tables for Statisticians and Biometricians", Part 1.

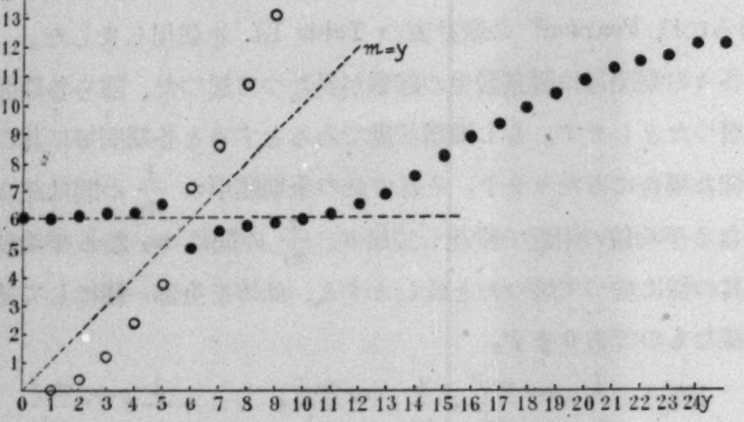

第　三　圖

あつた場合は第四圖に示してあります。

C) 次に地震活動の勢力が直線的に増減した場合に就いて調べて見ました。

例へば全期間を 10 ケに等分した場合に各期間の m が夫々 1, 2, 3, ‥‥ 10 であつたとした場合に就いて y の函數として得られた m の値は第五圖に示してあります。

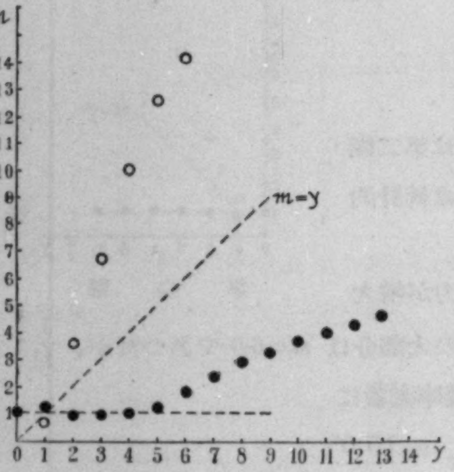

第　四　圖

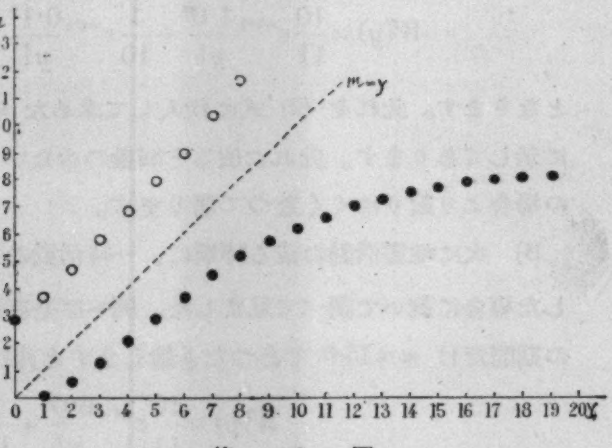

第　五　圖

此れによると回數の少ない所は統計的な場合より生起し難くなつて居りますが、回數の多い方は著しく起り易く成つて居ります。

D) 次に活動の勢力が指數函數的に急に増減した場合の例に就て調べて見ました。

例へば全期間を八ケに等分して各々の期間に於ける m が夫々 0·1, 0·2, 0·4, 0·8, 1·6, 3·2, 6·4, 12·8 であつた場合の y の函數として得られた m の値は第六圖に示してあり

ます。此れによると回數の少ない所は統計的な場合より生起し難くなつて居りますが回數の多い方は著しく起り易くなつて居ります。

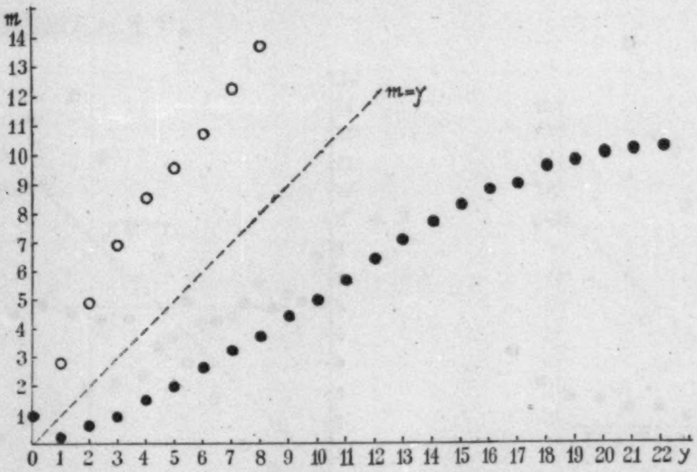

第 六 圖

4. 次に實際の地震活動に就いて、以上と同樣に m を地震回數 y の函數として求めた結果に就いて述べる事に致します。

1) 廣範圍の地震活動。

昭和四年の理科年表に依り 1900 年から 1927 年の間の世界大地震の一月毎の頻度に就いて調べたものが第七圖に示してあります。此れに依ると殆ど統計的に發生して居りますがその間に活動の勢力が衰へた時期が介在して居る事が推察されます。

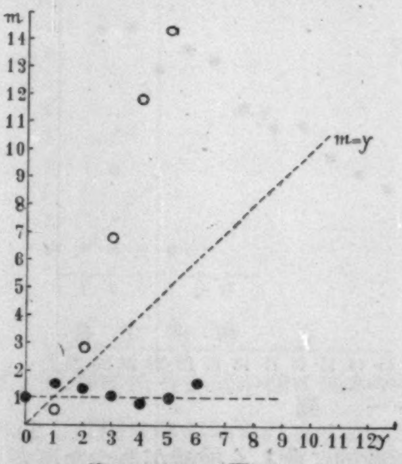

第 七 圖

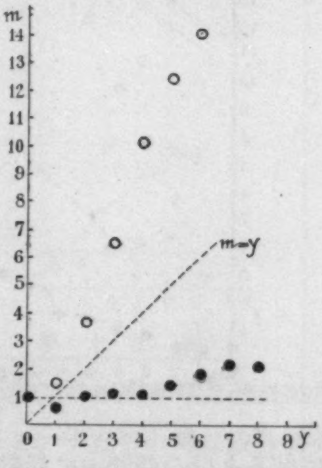

第 八 圖

次に驗震時報第二卷第三號に依り大正元年から大正十四年に至る本邦顯著地震の五日每、十日每、及び一月每の頻度に就いて調べたものが第八、第九と第十圖に示して

あります。此等に依ると殆ど統計的に發生して居りますが、其の間に活動の勢力が增大した時期が介在して居る事が推量されます。

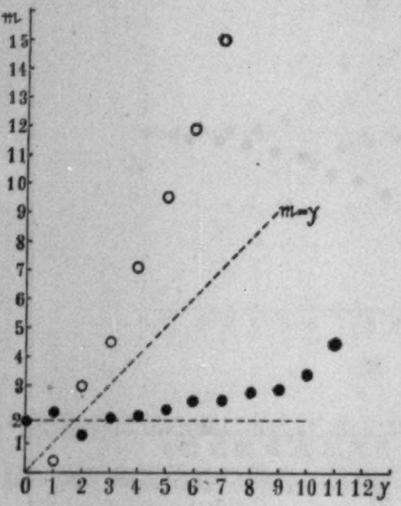

第　九　圖

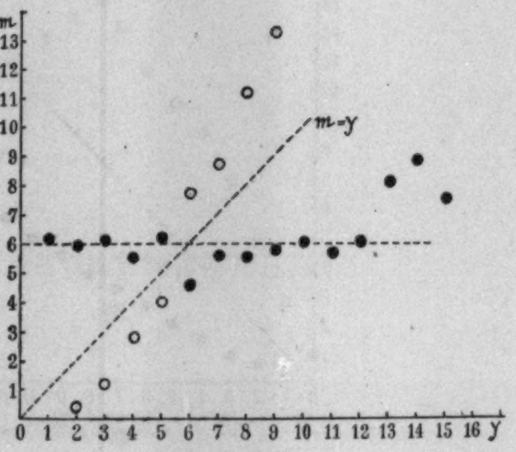

第　十　圖

2) 或る特定の場所に發生した地震群。

昭和五年二月十四日から四月十日迄の伊東地震群[3] の前期の活動を三崎で観測した一時間毎の頻度に就いて調べたものが第十一圖に示してあります。

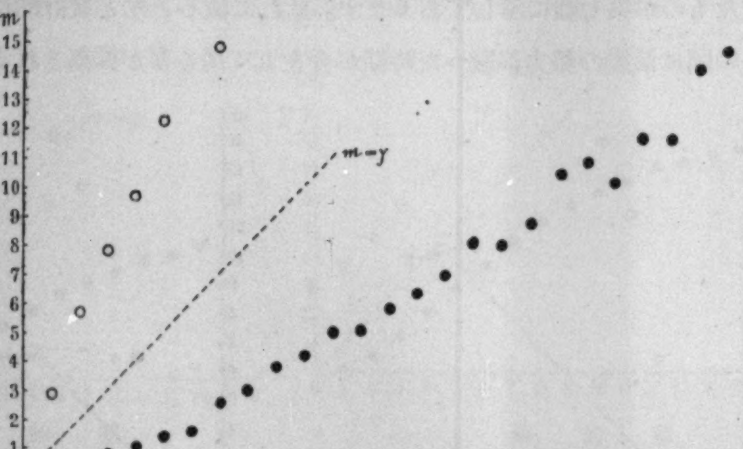

第　十　一　圖

此れに依ると此の期間中に活動の勢力が指數的に著しく增減があつた事がうかゞはれます。次に昭和五年十一月二十六日に發生した伊豆地方の烈震前十一月七日から同

3) 地震, 第二卷 (昭和五年).

月二十六日迄に發生した前震群[4]の一時間毎の頻度に就いて同樣の調査を行つた結果が第十二圖に示してあります。此れによると伊東地震群と同樣に活動の勢力に著しく增減があつた事が知られます。

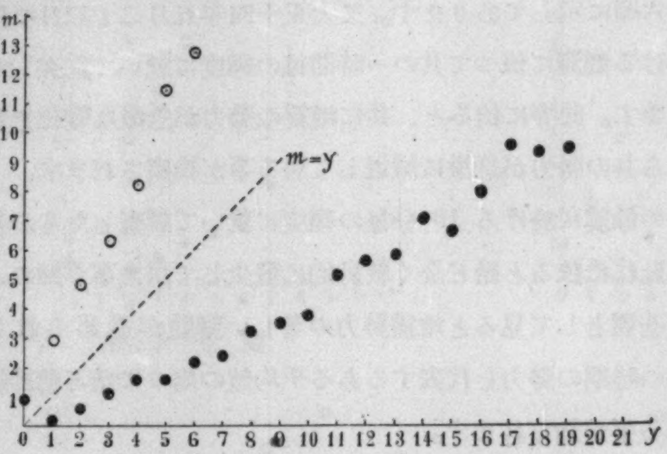

第十二圖

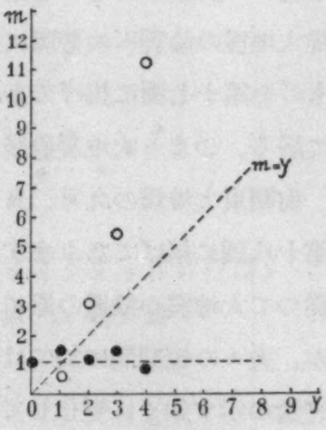

第十三圖

此の前震群の各期間に於ける活動を細かく調べる爲めに氣象要覽に依り經續的に地震が發生して居る十一月十五日十六時五十分から十八時三十分の間の一分毎の頻度及び十六日八時六分から十時二十四分の間の一分毎の頻度及び二十日十九時零分から二十二日十二時迄の間の二分毎の頻度に就いて調べたものが第十三乃至第十五圖に示してあります。

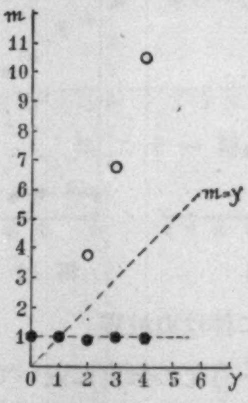

第十四圖

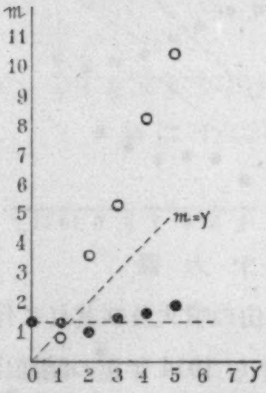

第十五圖

てあります。此等に依ると此の樣に短かい期間中の活動では地震が殆ど統計的な場合と同樣に生起して居る事が知られますが、尙よく見ると、十五日の時は幾分勢力の弱まつた時期が介在して居る傾向が見えるに對し、十六日の際は殆ど一樣な勢力であつたが、二十日の時には幾分活動の勢力が增加した期間が介在して居る傾向が現はれて

4) N. Nasu, F. Kishinouye and T. Kodaira, *Bull. Earthq. Res. Inst.*, 9 (1931), 32.

居ります。

3) 大地震の餘震群。

大正十二年九月一日關東大地震の餘震の九月中の東京有感地震[5] の一時間毎の頻度に就いて調査したものを第十六圖に示してあります。又大正十四年五月二十三日の但馬大地震の餘震[6] の豊岡に於ける觀測に依つて其の一時間毎の頻度に就いて調査したものを第十七圖に掲げてあります。此等に依ると、共に地震の勢力が急激な變化をして居る、つまり大地震直後から其の勢力が急激に減退して居る事が推察されます。

尙關東大地震の九月二日中の餘震に於ける 10 分毎の頻度に就いて調査したものを第十八圖に掲げてあります。此れに依ると殆ど全く統計的に發生して居た事が知れ、從つて大地震の餘震の際にも全體として見ると地震勢力の著しい變動が認められるが、夫々の短期間に於ては夫の時期の勢力を代表するある平均値の周りに殆ど統計的理論の示す如くに變化して居る事が知られます。

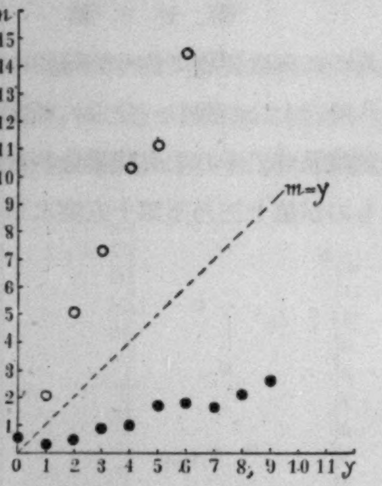

第十六圖

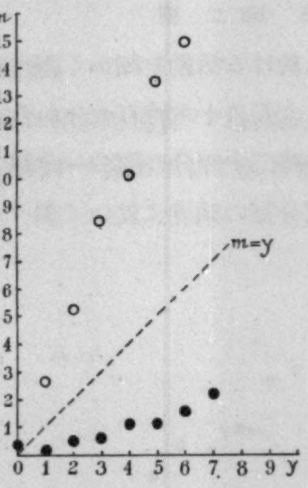

第十七圖

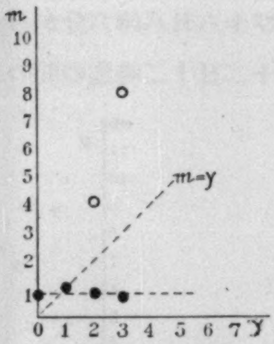

第十八圖

4) 淺間山の噴火及び其れに伴つた地震及び噴火に伴はぬ地震。

1904 年から 1914 年迄の淺間山の著しい噴火[7] の一月毎の頻度に就いて調査したものを第十九圖に示してありますが、此れに依ると勢力の著しい増減があつた事が推察されます。次に 1911 年の六月二十五日から十月二十日迄噴火に伴はぬ地震卽ち大森博士の A 型の地震[8] の日々の頻度に就いて調査したものを第二十圖に示してあります。

5) A. Imamura and K. Hasegawa, *Bull. E. I. C.*, **11** (1928), 27.
6) 今村明恒, 震災豫防調査會報告, **101**, 18.
7) F. Omori, *Bull. E. I. C.*, **8**, 337.
8) F. Omori, *Bull. E. I. C.*, **6**, 243.

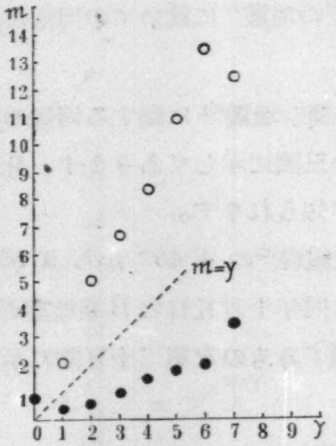

第十九圖

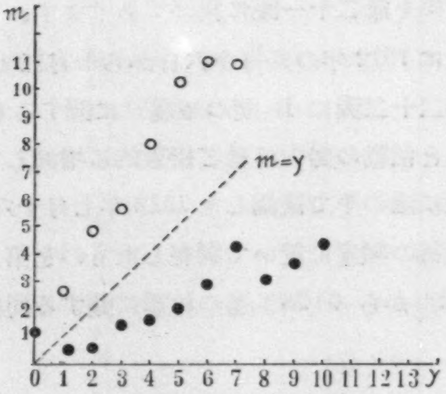

第二十圖

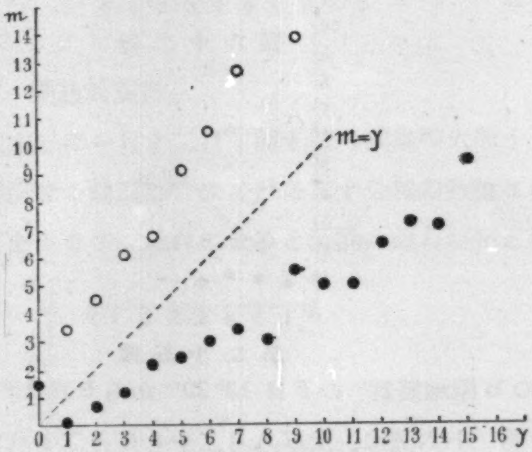

第二十一圖

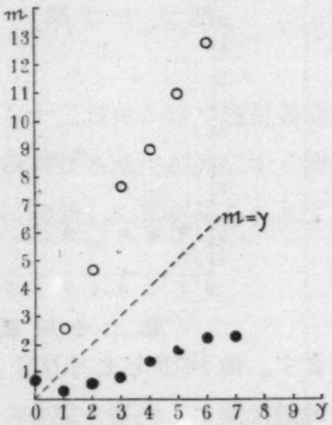

第二十二圖

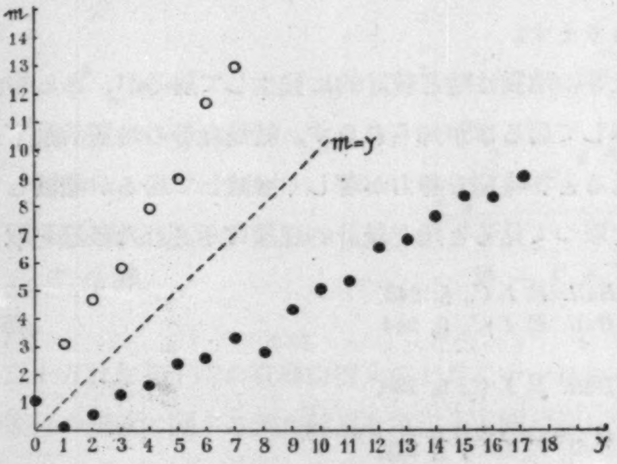

第二十三圖

又同期間内の噴火に伴つた地震即ち大森博士のＢ型の地震[9]に就いての同樣の調査の結果を第二十一圖に揭げてあります。

次に1912年の五月十六日から十月三十一日迄のＡ型の地震[10]に關する同樣の調査を第二十二圖にＢ型の地震[11]に關するものを第二十三圖に示してあります。此等によると活動の勢力は殆ど指數的に增減して居つた事が知られます。

次に湯の平で觀測した1912年七月十六日のＡ型地震群[12]の $4^h 45^m$ から $9^h 55^m$ 迄一分毎の頻度に就いて調査したものを第二十四圖に、同年十月五日のＢ型地震群[13]の $3^h 42^m$ から $6^h 28^m$ 迄の地震に關する同樣の調査に關するものを第二十五圖に示して

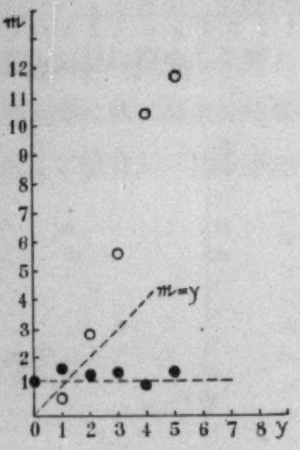

第二十四圖

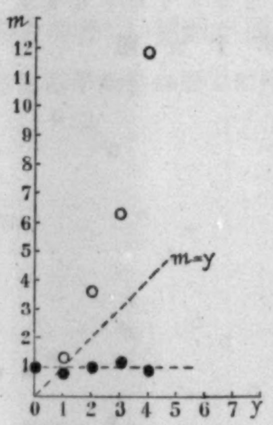

第二十五圖

あります。尙1913年七月五日と六日のＢ型地震群[14]の5日 $13^h 29^m$ から6日 $13^h 53^m$ 迄の地震に關する同樣な調査の結果を第二十六圖に、及び八月二十七日と二十八日のＢ型地震群[15]の二十七日 $19^h 07^m$ から二十八日 $5^h 41^m$ 迄の地震に關するものを第二十七圖に示してあります。

此等によると此等の地震は殆ど統計的に發生して居るが、ある場合には一時勢力が減退した傾向を示して居る事が知られます。結局此等の地震活動も長い期間に亘る活動を全體として見ると各時期で勢力が著しく增減して居るが繼續して活動して居る比較的短かい期間を取つて見ると殆ど統計的理論に示された經過を取つて居る事が分り

9) F. Omori, *Bull. E. I. C.*, **6**, 243.
10) F. Omori, *Bull. E. I. C.*, **6**, 244.
11) Ditto.
12) F. Omori, *Bull. E. I. C.*, **6**, 180,
13) Ditto.
14) F. Omori, *Bull. E. I. C.*, **7**, 219.
15) Ditto.

ます。

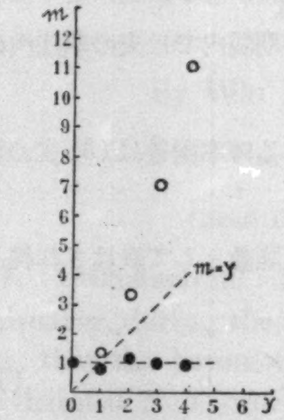

第二十六圖

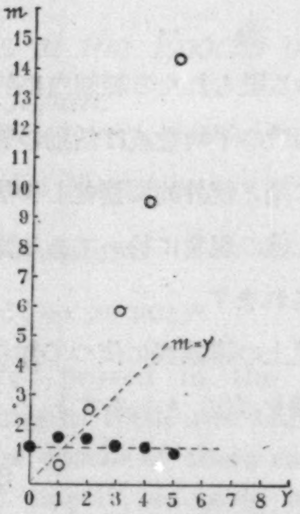

第二十七圖

5) 櫻島前震群。

大正三年一月十二日午前十時の櫻島噴火前十一日から十二日にかけて鹿兒島測候所で觀測せる前震群[16]に於ける二十分毎の頻度に就いて調査せる結果が第二十八圖に示してあります。此れに依ると活動の勢力が殆ど直線的に増減した事が見られます。

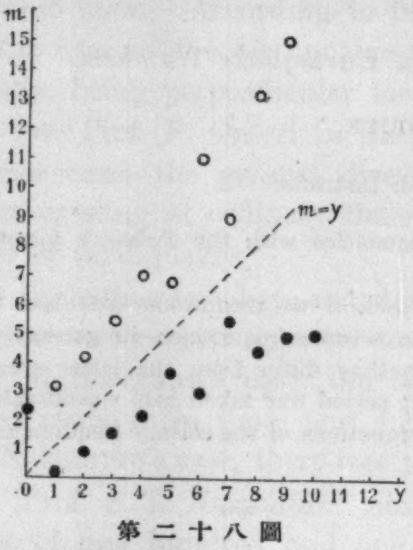

第二十八圖

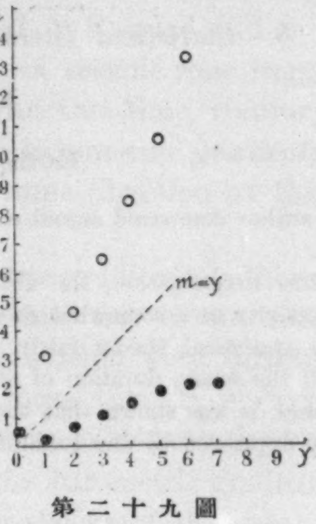

第二十九圖

6) 有珠山前震群。

1910 年の七月二十五日午後十時の有珠山噴火前七月二十一日から札幌で觀測された前震群[17]の一時間毎の頻度に關する調査結果を第二十九圖に示してあります。此れ

16) F. OMORI, *Bull. E. I. C.*, **8**, 360.
17) F. OMORI, *Bull. E. I. C.*, **5**, 11.

に依つても活動の勢力が著しく增減した事が知られます。

4. 結 論

一般にある限られたる範圍內に於ける地震活動の長期間に亙る活動に於ては期間に依り地震回數の平均數或は活動の勢力に消長があるが各期間內では夫の期間內の平均數の周りに殆ど統計的に變化して居る事が分ります。

それで此種の現象に於いてある豫期せる事柄の生起する確率函數は(3)式の型によつて現はされます。

或は又以上の諸圖表に依つて知られる如く m は y の函數として表はされ得ますからその函數を $f(y)$ としますと、

$$W(y)=e^{-f(y)}\frac{f(y)^y}{y!} \quad\ldots\ldots\ldots\ldots\ldots\ldots(4)$$

で表はす事が出來ます。一般には此の $f(y)$ なる函數は複雜でありますが或る場合には割に簡單に表はされます。

---

6. *Statistical Investigations on Earthquake Numbers.*

By Win INOUYE,

Earthquake Research Institute.

The author compared actual earthquake frequencies with the Poisson's formula in statistics.

By this investigation, the author noticed that, if we confine our attention to the seismic activity in a somewhat short period, the seismic frequencies, in general, agree with the statistical theory fairly well, whereas they differ from the latter somewhat greatly, if the whole duration of activity of long period was taken into consideration.

Further, it was shown that the probability functions of the seismic frequencies were generally expressed by the formulas (3) and (4).

---

7. *On the Barometric Gradients at the Epochs of the Earthquakes in Japan.*

By Win INOUYE and Keisuke HASEGAWA,
Earthquake Research Institute.

(Read Dec. 17, 1929.—Received Dec. 20, 1931.)

1. Introduction. Dr. Ken Hasegawa[1] proved in the fifty local earthquakes, during the three years beginning in 1904, near Gihu, central Japan, that the barometric gradients at the epochs of these earthquakes were directed N. E.-ward and S. W.-ward mostly, so as to be perpendicular to the dislocation line which had taken place at the time of the destructive Mino-Owari earthquake of 1891. Moreover, he proved that the general direction of the barometric gradients in question had not coincided with that of the ordinary times at the place.

Prof. S. T. Nakamura[2] next studied the same problem about the fifty small earthquakes in the year 1904, which occurred near Mt. Tukuba, Kwantô basin. According to his investigation, the barometric gradients at the time of the earthquakes were directed N. E.-ward and S. W.-ward mostly, being perpendicular to the Tonegawa seismic zone suggested by the late Prof. F. Omori in the district. But this time, contrary to the former case, the general direction of the barometric gradients at the place existing at ordinary times took the same direction as that of the time of earthquakes.

In both cases above-stated, the barometric gradients gathered in two narrow sectors just opposite to each other and not in one sector only. But in Hasegawa's case, the barometric gradients were directed N. E.-ward about three times and a half much more than S. W.-ward, while in Nakamura's case, there was no such difference between the two senses.

Prof. S. T. Nakamura[3] next studied the barometric gradients at the time of one hundred and one main after-shocks of the great Kwantô earthquake of Sept. 1st, 1923, which had occurred in a half year after the great earthquake. According to his result, it seems that the earth-

1) K. HASEGAWA, *Proc. Math.-Phys. Soc.*, Tôkyô, (1913), 181.
2) S. T. NAKAMURA, *Proc. Math.-Phys. Soc.*, Tôkyô, (1915), 69.
3) S. T. NAKAMURA, *Sinsai-yobô-tyôsakwai-hôkoku*, 100 A.

quakes about Odawara were much more sensible to the barometric gradients than those occurred at other parts of the Kwantô district. They occurred mostly when the barometric gradients had been directed N. W.-ward or when the barometric pressures at the Kôhu basin had been higher than those at the Sagami basin. He says that such a configuration of barometric pressures is generally accompanied by a fine weather. Further, he showed that an earthquke had occurred when the barometric gradient had taken a certain direction peculiar to each parts of the district.

It seems to us, that the fact that the barometric gradients at the epochs of the after-shocks which had occurred in Sagami province were directed N. W.-ward mostly would be intimately connected to the vertical displacements of the earth's crust accompanying the great earthquake, which were revealed by the revised precise levelling carried out by the Military Land Survey Department. The Sagami province and its neighbourhood had undergo a rotating movement about a horizontal axis lying through the center of the province from N. E. to S. W., namely the N. W. and S. E. parts of the province subsided and upheaved respectively.

Dr. K. Suda,[4] of the Marine Meteorological Observatory, obtained interesting results in his research into the barometric gradients at the time of after-shocks in September of the great Kwantô earthquake. He says that, "The frequency of the after-shocks increases when the atmospheric pressure, the rate of the pressure change and the pressure gradient have the contrary sense as those at the instant when the great earthquake happened. On the other hand, it has a tendency to decrease when those factors have the same sense or nearly the same sense as those at the great earthquake occurred."

2. Thus we may take it for granted fact that at the critical state when an earthquake is going to occur the barometric gradient at the epoch do act as a powerful trigger action or secondary cause of the earthquake. Moreover, the barometric gradient at the epoch and place when and where an earthquake occurs, is generally perpendicular to the seismotectonic line in that district. Hence if we make statistics of the barometric gradients at the time of earthquakes in a limited district and if found consequently that these gradients are directed in a narrow sector, then we may infer that the direction of the weak line in this district is perpendicular to the sector.

Now, we tried to examine the barometric gradients at the time of

4) K. SUDA, *Mem. Imp. Marine Observ.*, 1 (1922–1924).

earthquakes in each part of the Japanese arc. The method of statistics is almost the same as had been adopted by the former authorities.

We used the data of those earthquakes as scaled strong and weak in the table of the Japanese strong earthquakes edited by T. Ishikawa[5] of the Central meteorological Observatory for fourteen years beginning in 1912. These earthquakes were devided into eleven groups according as their localities. The position of these localities and the meteorological stations used for the barometric gradients are shown in Fig. 1. and tabulated in Table I.

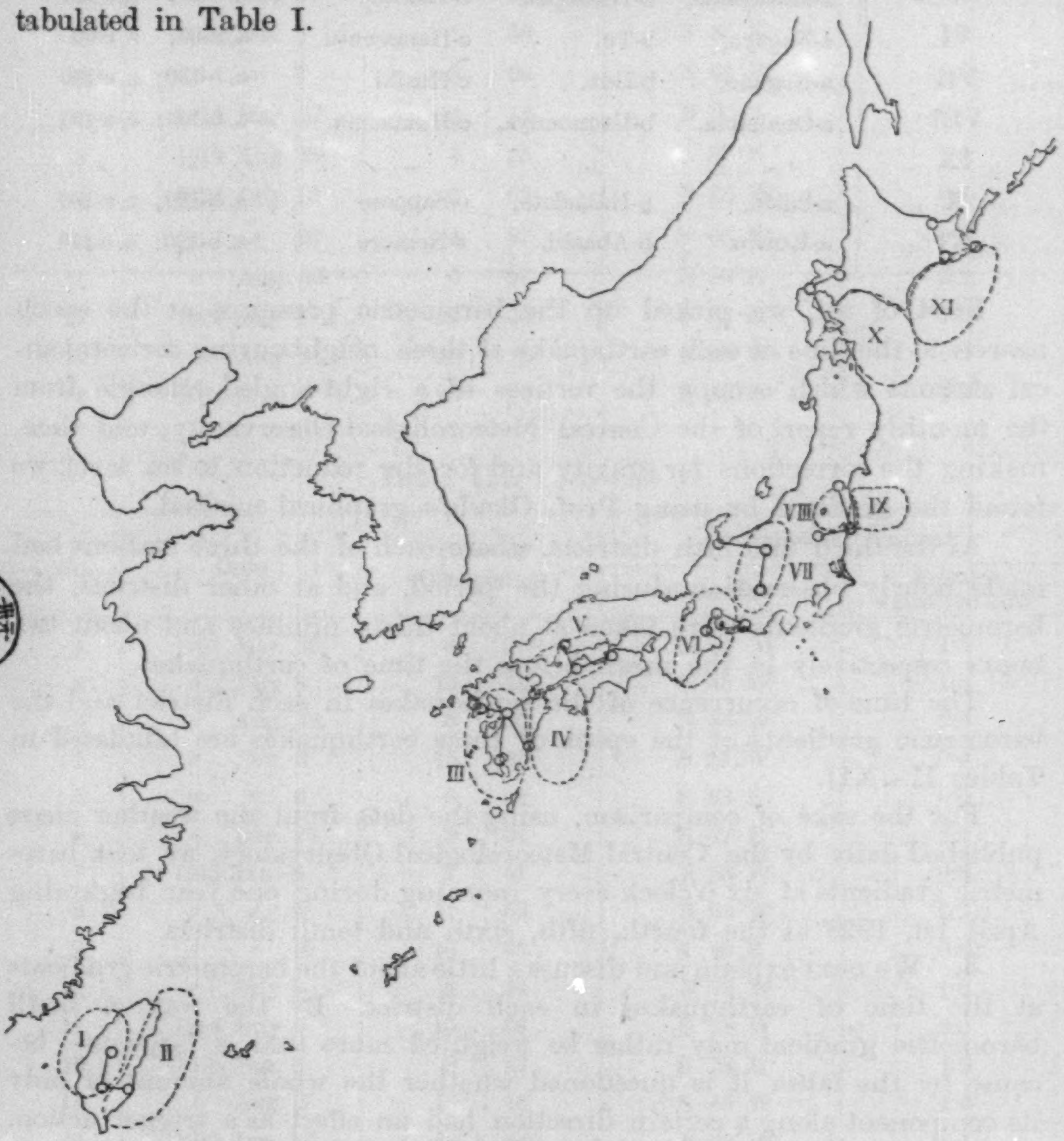

Fig. 1.

5) *Kensin-dihô*, 2 (1926).

[library stamp]

Table I.

District	Meteorological Station			Mutual Distance (in Km)
I	a-Tainan,	b-Taitô,	c-Taityû	a, b-100; a, c-130
II	"	"	"	" "
III	a-Kumamoto,	b-Kagosima,	c-Nagasaki	a, b-140; a, c-80
IV	a-Kumamoto,	b-Miyazaki,	c-Ooita	a, b-120; a, c-100
V	a-Matuyama,	b-Hirosima,	c-Tadotu	a, b-70; a, c-100
VI	a-Nagoya,	b-Tu,	c-Hamamatu	a, b-60; a, c-90
VII	a-Nagano,	b-Iida,	c-Husiki	a, b-130; a, c-100
VIII	a-Onahama,	b-Utunomiya,	c-Hukusima	a, b-100; a, c-100
IX	"	"	"	" "
X	a-Suttu,	b-Hakodate,	c-Sapporo	a, b-120; a, c-100
XI	a-Kusiro,	b-Abasiri,	c-Nemuro	a, b-120; a, c-110

First of all, we picked up the barometric pressures at the epoch nearest to the time of each earthquake at three neighbouring meteorological stations which occupy the vertices of a right-angled triangle from the monthly report of the Central Meteoroligical Observatory, and then, making the corrections for gravity and for the reduction to sea level, we found the gradient by using Prof. Okada's graphical method.

At the third and fifth districts, where each of the three stations had made hourly observation during the period, and at other districts, the barometric gradients were taken at about thirty minutes and about two hours respectively in the mean before the time of earthquakes.

The time of occurrence of the earthquakes in each district and the barometric gradients at the epoch of these earthquakes are tabulated in Tables II～XII.

For the sake of comparison, using the data from the weather chart published daily by the Central Meteorological Observatory, we took barometric gradients at six o'clock every morning during one year beginning April 1st, 1928 at the fourth, fifth, sixth and tenth districts.

3. We next explain and discuss a little about the barometric gradients at the time of earthquakes in each district. By the way, a small barometric gradient may rather be weighted more than a large one, because by the latter it is questioned whether the whole amount or only its component along a certain direction had an effect as a trigger action. But in the following discussion, only the general feature of the barometric gradients is concerned without distinction to their intensities.

Table II. District I.

No.	Date	Time of Occurrence		Barometric Gradient Direction	Amount (mm/100 km)
1	1913 Nov. 1	8h	31m	S 72° E	1·1
2	1916 Aug. 28	16	28	S 66 W	0·2
3	〃 Oct. 21	19	09	S 87 E	1·1
4	〃 Nov. 15	7	32	N 81 E	1·5
5	1917 Jan. 5	1	50	N 85 E	1·2
6	〃 〃 7	3	08	N 01 W	1·0
7	1918 Mar. 27	12	53	N 85 E	0·4
8	1919 Aug. 29	4	35	S 57 E	1·4
9	1921 July 19	2	03	N 65 W	0·4
10	〃 〃 26	4	27	S 68 E	0·8
11	〃 Aug. 30	0	07	N 89 E	2·9
12	1923 May 4	19	40	S 89 E	1·6
13	〃 Aug. 27	20	15	N 28 W	0·9
14	1924 Nov. 2	20	24	S 82 E	1·9

Table III. District II.

No.	Date	Time of Occurrence		Barometric Gradient Direction	Amount (mm/100 km)
1	1912 Mar. 30	3h	31m	N 62° W	1·5
2	〃 July 8	19	21	N 58 W	1·5
3	〃 Aug. 19	6	30	N 85 W	2·0
4	〃 Nov. 3	15	05	S 57 W	0·4
5	〃 〃 6	6	02	S 38 E	0·6
6	〃 Dec. 25	3	07	S 77 E	2·1
7	1913 Jan. 8	7	51	N 53 W	0·8
8	〃 〃 9	11	55	N 59 W	0·7
9	〃 〃 10	16	35	S 40 E	0·6
10	〃 July 9	9	44	N 73 W	1·0
11	1914 July 6	15	38	S 78 W	2·0
12	1915 Jan. 6	8	27	S 78 E	1·0
13	〃 Aug. 2	16	16	S 45 W	1·6
14	1917 Jan. 27	23	54	N 38 W	1·1

(to be continued.)

Table III. District II. (*continued.*)

No.	Date	Time of Occurrence		Barometric Gradient	
				Direction	Amount (mm/100 km)
15	1917 May 5	21h	19m	N 89 E	0·4
16	1918 Jan. 16	0	30	S 64 W	0·5
17	〃 April 1	19	09	S 40 E	0·6
18	〃 Dec. 19	2	17.	N 04 E	0·1
19	1919 Nov. 1	4	03	S 48 E	0·8
20	〃 Dec. 21	4	33	N 60 W	0·6
21	〃 〃 〃	5	36	N 60 W	0·6
22	1920 Jan. 20	13	10	N 33 W	1·0
23	〃 Mar. 13	19	39	N 82 E	0·7
24	〃 May 2c	21	21	S 46 E	0·6
25	〃 June 5	13	21	S 49 E	0·7
26	〃 〃 6	1	39	S 30 E	1·2
27	〃 Oct. 20	19	02	N 52 W	0·8
28	〃 〃 21	4	16	S 35 E	0·4
29	1921 July 25	10	39	N 32 E	0·8
30	〃 〃 30	0	04	N 82 W	2·0
31	〃 Dec. 2	2	51	N 86 E	1·7
32	1922 Jan. 10	22	41	S 72 E	2·5
33	〃 May 23	3	04	N 86 E	0·1
34	〃 July 2	22	29	S 67 E	0·6
35	〃 〃 19	21	55	N 76 E	0·5
36	〃 Aug. 27	4	28	N 61 W	2·7
37	〃 Sept. 2	4	15	N 88 W	2·0
38	〃 〃 7	7	11	N 64 E	0·4
39	〃 〃 8	4	56	S 76 E	0·6
40	〃 〃 15	4	31	S 40 E	0·6
41	〃 〃 17	7	44	S 83 E	2·2
42	〃 〃 〃	10	42	S 83 E	2·2
43	〃 〃 〃	16	22	S 58 E	2·5
44	〃 〃 〃	16	53	S 58 E	2·5
45	〃 〃 〃	18	59	S 58 E	2·5
46	〃 〃 18	15	20	S 78 E	2·5
47	〃 〃 29	7	03	S 12 E	2·7

(*to be continued.*)

Table III. District II. (*continued.*)

No.	Date	Time of Occurrence		Barometric Gradient Direction	Amount (mm/100 km)
48	1922 Oct. 6	2h	12m	S 37 W	0·8
49	〃 〃 12	7	07	S 80 E	1·1
50	〃 〃 14	12	26	N 86 E	0·6
51	〃 〃 〃	16	39	S 32 E	0·6
52	〃 〃 15	18	45	S 63 E	0·7
53	〃 〃 27	23	23	S 40 E	0·6
54	〃 Nov. 5	3	19	S 72 E	1·1
55	〃 〃 19	3	56	N 69 W	0·8
56	〃 Dec. 2	12	46	S 72 E	1·3
57	1923 Jan. 3	7	42	N 90 E	1·8
58	〃 Mar. 8	6	32	S 69 E	0·3
59	〃 〃 18	0	02	S 75 E	2·1
60	〃 April 6	7	09	S 71 E	1·8
61	〃 July 2	11	32	N 87 E	2·0
62	〃 Nov. 19	6	26	S 80 E	0·3
63	〃 〃 〃	6	29	S 74 E	0·3
64	〃 〃 〃	11	18	N 02 W	1·0
65	〃 〃 22	16	21	N 09 W	0·9
66	〃 〃 26	2	02	N 50 E	0·2
67	1924 July 14	21	04	N 58 W	2·0
68	〃 〃 22	23	22	S 55 E	0·8
69	1925 Mar. 1	21	25	N 75 E	1·0
70	〃 May 24	10	24	S 51 E	0·9
71	〃 June 14	9	18	N 29 W	0·1
72	〃 〃 〃	14	48	N 75 W	2·2
73	〃 〃 〃	14	55	N 75 W	2·2

Table IV. District III.

No.	Date	Time of Occurrence		Barometric Gradient	
				Direction	Amount (mm/100 km)
1	1912 Jan. 16	20h	28m	N 42° W	0·2
2	1913 Jan. 6	3	18	N 26 E	0·9
3	〃 June 29	17	23	S 29 W	0·2
4	〃 〃 30	16	08	S 54 W	0·7
5	〃 July 1	22	21	S 50 W	1·2
6	〃 〃 9	10	21	N 45 W	0·2
7	〃 Jan. 12	18	29	N 63 W	3·2
8	〃 Mar. 15	6	45	N 29 W	0·8
9	〃 Dec. 29	6	41	N 18 E	1·0
10	〃 〃 〃	7	47	N 10 W	0·9
11	1919 May 10	14	15	S 15 E	1·0
12	1920 May 26	4	55	N 29 W	0·5
13	〃 Dec. 19	7	51	N 29 W	0·6
14	1921 Oct. 28	23	10	S 91 W	0·2
15	〃 Nov. 12	23	30	N 57 W	0·7
16	1922 Dec. 7	16	17	N 17 E	1·5
17	〃 〃 8	1	50	N 19 E	0·4
18	1923 Dec. 20	21	46	S 03 E	0·2
19	〃 〃 26	5	22	S 24 W	1·0
20	1924 Feb. 3	2	28	N 23 W	0·5
21	〃 July 22	21	42	S 42 W	0·7

Table V. District IV.

No.	Date	Time of Occurrence		Barometric Gradient	
				Direction	Amount (mm/100 km)
1	1912 Jan. 7	23h	26m	N 47° W	0·5
2	〃 〃 21	10	30	S 75 E	0·7
3	〃 Aug. 22	1	29	S 64 E	1·2
4	〃 Oct. 2	12	39	N 61 W	1·2
5	1913 April 3	8	54	N 04 W	1·4
6	〃 〃 〃	10	28	N 50 E	1·4

(*to be continued.*)

Table V. District IV. (*continued.*)

No.	Date	Time of Occurrence		Barometric Gradient Direction	Amount (mm/100 km)
7	1913 April 13	15^h	40^m	N 68° E	1·9
8	〃 〃 20	23	53	N 62 E	0·6
9	〃 Sept. 3	4	02	N 42 W	0·8
10	〃 Nov. 1	9	44	N 84 W	1·3
11	1914 Aug. 4	6	47	S 45 W	1·2
12	〃 Oct. 29	5	13	S 42 W	0·6
13	1915 Mar. 30	8	13	N 87 W	1·4
14	1916 Aug. 28	4	57	S 03 W	0·5
15	1918 Apr. 2	12	34	S 63 E	0·4
16	〃 July 17	6	33	N 83 E	0·9
17	〃 Sept. 15	16	01	N 88 W	1·5
18	〃 Dec. 10	3	49	N 32 W	1·5
19	1920 Dec. 5	3	45	N 76 E	0·8
20	1921 Apr. 19	2	59	N 52 E	1·2
21	〃 Oct. 14	4	33	N 34 W	0·6
22	1922 Aug. 9	6	07	N 88 E	0·3
23	〃 Nov. 27	12	21	S 85 E	1·3
24	〃 Dec. 28	21	04	N 59 W	2·8
25	1923 Dec. 28	21	08	N 59 W	2·8
26	1924 Apr. 1	16	04	S 76 E	4·9
27	〃 Aug. 29	8	50	S 44 E	0·6
28	〃 Nov. 30	10	20	S 41 W	2·0
29	1925 Mar. 16	13	29	N 75 W	0·2

Table VI. District V.

No.	Date	Time of Occurrence		Barometric Gradient Direction	Amount (mm/100 km)
1	1912 Jan. 21	18^h	09^m	N 23° E	1·0
2	〃 April 9	20	37	S 02 E	0·8
3	1913 Jan. 7	17	10	S 31 W	0·2
4	〃 May 26	16	16	N 57 W	0·3

(*to be continued.*)

Teble VI. District V. (*continued.*)

No.	Date	Time of Occurrence		Barometric Gradient Direction	Barometric Gradient Amount (mm/100 km)
5	1913 Sept. 7	1^h	38^m	N 13° E	0·9
6	〃 Oct. 21	12	06	N 60 E	0·2
7	〃 Nov. 8	1	35	N 63 W	0·5
8	1914 Jan. 12	18	12	S 05 W	0·3
9	〃 〃 13	1	00	N 16 W	0·8
10	〃 Sept. 12	14	14	N 53 W	0·4
11	〃 〃 17	5	34	S 53 W	0·9
12	1916 Mar. 6	18	12	S 46 W	1·0
13	〃 〃 15	6	23	S 42 W	0·9
14	〃 Aug. 6	7	53	S 40 W	0·2
15	1919 May 14	21	01	S 20 W	0·2
16	〃 〃 22	22	08	S 23 W	1·5
17	〃 Nov. 1	8	36	N 30 E	0·2
18	〃 〃 2	8	27	N 01 E	1·3
19	〃 〃 3	19	08	N 09 E	0·5
20	〃 Dec. 12	1	41	S 27 W	0·3
21	1920 Feb. 23	15	31	N 23 W	2·2
22	〃 Dec. 14	11	22	S 13 E	2·0
23	1921 Jan. 12	23	53	N 63 W	0·4
24	〃 Apr. 25	16	10	S 29 E	3·5
25	1922 July 12	13	31	N	0·7
26	1923 Sept. 24	22	26	S 62 W	0·1
27	〃 Oct. 3	23	21	N 02 W	2·4
28	〃 Dec. 12	13	03	N 10 E	3·3
29	1924 Mar. 24	9	52	S 61 W	0·9
30	〃 June 26	4	15	S 20 W	1·3
31	1925 May 1	17	16	N 59 W	0·5
32	〃 〃 24	12	52	N 01 W	1·1

Table VII. District VI.

No.	Date	Time of Occurrence		Barometric Gradient	
				Direction	Amount (mm/100 km)
1	1912 Feb. 22	12^h	48^m	S 81° E	1·4
2	〃 〃 23	14	21	N 36 W	2·2
3	〃 Apr. 18	23	37	N 72 E	1·7
4	〃 May 6	8	58	N 43 W	0·1
5	〃 June 24	7	37	S 15 E	0·3
6	〃 Oct. 16	14	23	N 72 W	1·3
7	〃 Dec. 19	19	24	N 44 W	1·3
8	1913 Jan. 6	15	15	N 51 W	1·2
9	〃 〃 17	20	53	N 51 W	3·5
10	〃 〃 27	18	21	S 86 W	1·4
11	〃 Mar. 30	13	10	S 01 E	0·4
12	1914 Jan. 28	4	33	N 82 W	1·6
13	〃 Mar. 23	4	21	S 18 E	0·7
14	〃 Aug. 16	21	16	S 27 E	1·8
15	1915 May 21	0	54	W	2·0
16	1916 Feb. 8	6	11	N 81 W	1·1
17	1917 May 6	12	17	S 81 E	1·9
18	〃 Oct. 19	5	43	S 10 W	0·2
19	1919 Apr. 22	19	12	S 66 E	2·6
20	1920 Apr. 4	20	05	S 27 E	2·6
21	〃 Aug. 15	20	50	N 08 W	2·4
22	〃 Nov. 30	10	27	N 51 W	0·7
23	1922 Feb. 9	23	53	N 48 W	0·6
24	1923 Oct. 28	11	25	S 08 W	6·3
25	1924 Aug. 13	3	19	S 02 E	5·9
26	〃 〃 〃	9	33	S 05 W	5·7
27	〃 Nov. 24	8	28	S 12 W	6·2
28	1925 Feb. 15	16	48	S 24 W	7·5
29	〃 Mar. 20	2	55	S 15 W	7·5
30	〃 July 7	1	46	S 03 E	6·0
31	〃 Aug. 19	21	51	S 01 E	6·3

Table VIII. District VII.

No.	Date	Time of Occurrence		Barometric Gradient	
				Direction	Amount (mm/100 km)
1	1912 Jan. 14	14h	41m	N 04° W	1·1
2	〃 May 26	9	33	S 69 E	2·0
3	〃 〃 〃	19	12	S 78 W	0·8
4	〃 July 13	7	46	S 39 E	1·8
5	〃 〃 28	16	11	N 20 W	2·3
6	〃 Aug. 17	23	22	S 03 W	2·2
7	〃 〃 22	12	36	S 39 E	1·2
8	〃 Sept. 20	23	39	S 35 E	1·7
9	〃 〃 21	11	42	S 22 E	1·9
10	〃 Dec. 11	15	31	N 61 E	1·7
11	1913 Feb. 5	19	27	S 40 E	2·0
12	〃 〃 8	19	07	S 38 W	1·8
13	〃 Aug. 14	11	00	S 72 W	1·5
14	1914 Nov. 15	22	29	S 17 W	1·1
15	1916 Feb. 22	18	12	N 52 W	1·0
16	1917 May 18	4	07	S 34 E	1·3
17	1918 Nov. 11	2	59	S 81 W	1·1
18	1919 Apr. 1	17	52	N 67 W	1·6
19	1920 Feb. 19	13	48	S 03 E	5·5
20	〃 July 4	13	19	S 24 W	1·2
21	1924 Oct. 8	23	01	S 24 W	3·2
22	〃 Dec. 14	5	24	S 02 W	2·6

Table IX. District VIII.

No.	Date	Time of Occurrence		Barometric Gradient	
				Direction	Amount (mm/100 km)
1	1912 Aug. 21	14h	50m	N 48° W	0·6
2	1913 Jan. 22	6	50	N 40 W	2·4
3	〃 Aug. 4	10	23	S 46 W	0·7
4	1914 Sept. 10	6	23	N 30 W	0·5
5	〃 〃 17	2	30	S 32 W	0·7

(*to be continued.*)

Table IX. District VIII. (*continued.*)

No.	Date	Time of Occurrence		Barometric Gradient Direction	Barometric Gradient Amount (mm/100 km)
6	1914 Sept. 19	6h	04m	N 69 W	1·5
7	〃 〃 22	12	53	S 60 W	1·3
8	1920 Apr. 26	11	11	S 77 W	0·2
9	〃 Dec. 20	5	11	S 12 W	0·6
10	1921 Dec. 20	17	04	N 74 E	1·2
11	1923 Jan. 27	14	03	N 82 E	0·5
12	〃 Oct. 23	7	11	N 31 W	0·3
13	〃 Nov. 15	11	14	S 24 W	1·0

Table X. District IX.

No.	Date	Time of Occurrence		Barometric Gradient Direction	Barometric Gradient Amount (mm/100 km)
1	1912 Feb. 17	1h	48m	N 89° W	2·6
2	〃 〃 〃	11	43	S 17 W	0·4
3	〃 Mar. 11	15	24	S 21 E	2·5
4	〃 June 29	3	03	S 72 W	0·9
5	〃 Aug. 18	17	46	S 07 E	1·5
6	〃 〃 23	14	42	S 25 W	1·0
7	〃 Nov. 9	23	05	S 21 W	2·0
8	〃 〃 28	20	59	N 64 W	0·7
9	1913 Feb. 18	22	55	S 13 E	0·7
10	1914 Mar. 21	7	50	S 39 W	1·5
11	〃 May 31	18	05	S 50 E	0·9
12	〃 June 23	11	05	S 15 W	0·6
13	1915 July 9	7	21	S 35 W	1·0
14	〃 〃 26	14	24	S 52 E	1·1
15	〃 Nov. 18	13	04	N 68 W	0·5
16	〃 Dec. 14	5	42	S 50 W	1·2
17	1916 Mar. 8	19	52	N 36 E	0·6
18	〃 Apr. 21	10	08	S 85 W	0·6
19	〃 June 13	7	01	S 10 W	0·4

(*to be continued.*)

Table X. District IX. (*continued.*)

No.	Date	Time of Occurrence		Barometric Gradient	
				Direction	Amount (mm/100 km)
20	1916 June 22	23h	42m	S 19° E	2·4
21	〃 July 19	3	41	S 51 W	0·6
22	〃 Aug. 28	7	43	S 68 W	1·1
23	〃 Oct. 5	10	54	N 23 W	0·4
24	〃 〃 21	21	24	S 18 E	0·5
25	〃 Dec. 17	19	10	S 01 W	1·1
26	1917 Jan. 17	8	31	S 52 W	0·9
27	〃 〃 21	2	40	S 39 W	1·2
28	〃 June 6	1	28	N 45 W	1·3
29	〃 〃 14	22	22	S 02 E	1·0
30	〃 Nov. 10	7	43	N 57 W	1·0
31	1918 Jan. 21	8	37	S 16 E	0·6
32	〃 June 2	8	27	S 17 E	0·4
33	〃 Sept. 13	12	20	N 20 W	0·7
34	〃 Dec. 23	6	04	S 71 E	0·2
35	1919 Feb. 25	10	19	N 23 W	0·7
36	〃 May 16	20	48	N 10 E	1·0
37	〃 Dec. 20	9	28	S 15 W	1·1
38	1920 Jan. 6	12	49	S 44 E	0·5
39	〃 Feb. 2	19	42	N 12 W	1·2
40	〃 Apr. 3	12	46	N 79 E	0·2
41	1921 May 11	21	29	N 54 W	0·3
42	〃 June 14	13	47	S 63 E	0·7
43	1922 Jan. 23	7	05	S 40 E	0·8
44	〃 Feb. 10	22	37	S 20 E	0·8
45	〃 〃 15	10	10	N 10 W	0·8
46	〃 Apr. 23	14	05	S 42 E	3·2
47	〃 〃 27	15	40	S 47 E	1·4
48	〃 June 3	13	56	N 52 W	0·8
49	〃 Sept. 5	19	47	S 86 E	2·0
50	1923 Feb. 1	5	05	N 34 W	3·4
51	〃 〃 6	6	27	S 60 E	0·5
52	〃 〃 22	18	23	N 44 W	0·5

(*to be continued.*)

Table X. District IX. (*continued.*)

No.	Date	Time of Occurrence		Barometric Gradient	
				Direction	Amount (mm/100 km)
53	1923 May 7	22h	10m	N 66° W	0·9
54	〃 July 21	1	50	S 07 E	1·0
55	〃 Sept. 1	5	34	N 32 W	1·1
56	〃 Dec. 27	23	39	S 77 W	0·8
57	1924 June 12	22	11	N 66 W	1·3
58	1925 Jan. 6	0	02	N 64 W	1·4
59	〃 〃 10	21	22	N 69 W	1·1
60	〃 Apr. 20	5	42	S 18 W	0·6
61	〃 〃 〃	11	00	S 34 W	1·6
62	〃 July 26	21	45	N 73 E	0·5
63	〃 Aug. 11	5	40	S 55 E	0·8
64	〃 Sept. 2	7	58	S 27 E	0·8

Table XI. District X.

No.	Date	Time of Occurrence		Barometric Gradient	
				Direction	Amount (mm/100 km)
1	1912 Mar. 22	5h	23m	S 06° E	1·1
2	1913 Jan. 2	9	00	S 53 W	1·9
3	〃 〃 21	22	21	N 10 E	0·3
4	〃 Feb. 20	18	00	S 16 W	0·5
5	〃 July 15	17	21	S 60 E	0·2
6	〃 Aug. 1	7	06	S 56 E	0·5
7	〃 Nov. 10	1	54	S 22 E	2·1
8	1914 Jan. 29	6	50	S 16 W	0·6
9	〃 Feb. 7	15	50	N 32 W	0·4
10	〃 May 11	1	17	S 14 E	1·3
11	〃 〃 31	11	55	S 19 W	0·5
12	〃 July 9	3	31	S 23 E	1·1
13	〃 Sept. 25	14	31	S 43 E	0·6
14	1915 Mar. 18	3	46	S 55 W	0·8
15	〃 July 7	10	39	S 34 W	0·4

(*to be continued.*)

Table XI. District X. (*continued.*)

No.	Date	Time of Occurrence		Barometric Gradient Direction	Barometric Gradient Amount (mm/100 km)
16	1915 Sept. 12	5^h	09^m	S 65 E	0·5
17	〃 Oct. 15	10	10	S 08 E	0·7
18	1916 Feb. 10	7	25	N 60 W	0·5
19	〃 Mar. 9	10	38	S 15 W	1·2
20	〃 〃 25	15	36	S 13 E	0·4
21	〃 Apr. 22	1	48	S 24 E	0·7
22	〃 July 22	6	36	S 53 E	1·4
23	1917 Feb. 12	18	04	N 43 E	1·2
24	〃 July 29	23	34	S 16 W	0·3
25	1918 Aug. 7	0	45	N 72 E	0·4
26	〃 〃 〃	2	21	S 30 E	0·2
27	〃 Sept. 12	23	07	N 17 W	0·8
28	1919 Jan. 4	18	23	N 75 W	2·1
29	〃 Mar. 8	4	57	S 22 E	1·0
30	〃 〃 23	20	32	N 78 E	0·1
31	〃 Aug. 9	21	56	S 20 W	1·1
32	1920 Mar. 27	19	32	N 71 W	0·4
33	〃 Apr. 23	20	35	N 71 W	0·5
34	〃 Sept. 21	5	27	S 51 W	0·7
35	〃 Dec. 22	5	08	S 27 E	1·5
36	1921 Jan. 25	19	28	S 79 W	1·8
37	〃 Apr. 8	13	52	S 73 W	5·6
38	〃 〃 〃	23	35	S 69 W	0·7
39	〃 June 22	20	23	S 17 W	1·2
40	〃 〃 28	7	55	S 02 W	0·2
41	〃 Aug. 28	5	18	N 86 W	1·6
42	〃 〃 〃	20	23	N 83 W	1·3
43	〃 Sept. 5	21	28	S 71 W	0·8
44	〃 〃 9	11	20	S 17 W	0·5
45	〃 〃 〃	18	10	N 87 W	0·6
46	〃 Dec. 11	18	56	N 03 E	0·3
47	〃 〃 12	20	02	S 75 W	0·9
48	1922 Oct. 23	15	25	S 02 W	0·3

(*to be continued.*)

Table XI. District X. (*continued.*)

No.	Date	Time of Occurrence		Barometric Gradient	
				Direction	Amount (mm/100 km)
49	1922 Oct 27	23h	23m	S 27° W	1·1
50	1923 Mar. 12	18	54	S 67 E	0·8
51	〃 Apr. 17	0	09	S 38 W	0·2
52	〃 〃 27	16	15	S 14 W	1·8
53	1923 May 5	2	30	N 65 W	3·4
54	〃 June 28	16	48	S 37 W	1·1
55	〃 July 10	7	13	S 01 E	0·8
56	〃 Aug. 15	2	04	S 51 W	1·3
57	1924 Jan. 22	19	35	S 02 W	0·5
58	〃 May 23	3	08	S 01 E	0·2
59	〃 〃 28	18	53	S 75 W	1·1
60	〃 Nov. 8	11	57	E	1·4
61	〃 〃 26	2	27	S 50 E	0·7
62	1925 June 2	12	43	S 27 W	0·6
63	〃 〃 〃	14	48	S 33 W	0·5
64	〃 〃 23	13	44	S 14 W	0·4
65	〃 Oct. 5	20	08	S 39 E	1·0

Table XII. District XI.

No.	Date	Time of Occurrence		Barometric Gradient	
				Direction	Amount (mm/100 km)
1	1912 Jan. 4	4h	04m	S 29° W	2·8
2	〃 Feb. 19	13	04	N 27 W	2·2
3	〃 June 19	15	57	N 32 E	1·5
4	〃 Aug. 21	13	34	N 71 E	0·7
5	〃 Sept. 4	1	05	N 39 W	0·3
6	〃 Nov. 8	7	22	S 18 W	1·3
7	〃 Dec. 13	14	13	N 47 W	0·4
8	1913 Dec. 6	16	09	S 41 W	0·4
9	1914 Jan. 31	23	20	N 20 W	2·0
10	〃 July 2	4	18	S 29 W	1·3

(*to be continued.*)

Table XII. District XI. (*continued.*)

No.	Date	Time of Occurrence		Barometric Gradient	
				Direction	Amount (mm/100 km)
11	1914 Mar. 3	22^h	15^m	N 63° E	0·5
12	1915 Jan. 19	5	57	S 15 W	1·7
13	〃 Feb. 13	1	36	N 18 W	1·3
14	〃 June 16	14	12	S 29 E	2·4
15	〃 Dec. 7	6	00	S 88 W	1·1
16	〃 〃 14	19	20	S 10 W	4·5
17	〃 Aug. 14	21	38	N 47 E	2·4
18	1916 Jan. 27	20	56	N 40 W	0·4
19	〃 Mar. 8	17	56	S 76 W	0·2
20	〃 Mar. 30	18	20	S 32 E	1·4
21	1917 Mar. 21	16	48	N 04 W	1·0
22	〃 June 8	21	47	N 31 E	1·1
23	〃 July 29	10	58	S 75 E	0·4
24	〃 Aug. 23	14	44	N 01 E	3·2
25	〃 Sept. 29	12	04	N 55 W	0·4
26	1918 Jan. 13	14	48	S 68 E	0·8
27	1919 Mar. 12	19	32	S 11 E	1·6
28	1920 Oct. 20	3	26	S 35 W	1·1
29	1921 Aug. 9	19	38	N 23 E	0·7
30	1922 Feb. 26	17	57	S 16 W	0·5
31	〃 June 8	15	49	S 05 E	2·6
32	〃 〃 12	12	50	N 74 W	1·3
33	〃 Aug. 27	4	28	S 03 E	1·2
34	1924 Apr. 27	9	14	N 49 W	0·6
35	〃 July 1	0	40	N 59 E	0·6
36	〃 Dec. 27	20	22	N 30 E	0·2
37	〃 〃 29	7	56	S 50 E	0·6
38	1925 Jan. 28	13	06	N 45 E	0·5
39	〃 Dec. 5	0	29	N 76 W	0·8

For the sake of reference, the monthly frequencies of the earthquakes in each district are tabulated in Table XIII, and we can see that they are almost equally distributed in time.

1. The First District or Western Formosa. As will be seen from the Fig. 2, the barometric gradients at the epochs of the earthquakes

Table XIII.

Month \ District	I	II	III	IV	V	VI	VII	VIII	IX	X	XI
Jan.	2	9	3	2	5	4	1	2	7	6	6
Feb.	0	0	1	0	1	5	4	0	10	4	3
Mar.	1	4	1	2	3	3	0	0	3	8	4
April	0	2	0	7	2	3	1	1	6	6	1
May	1	5	2	0	5	3	3	0	4	5	1
June	0	5	2	0	1	1	0	0	10	6	5
July	2	10	3	1	1	1	3	0	5	6	3
Aug.	4	3	0	5	1	5	3	2	4	7	5
Sept.	0	11	0	2	4	0	2	4	4	7	2
Oct.	1	8	1	3	2	3	1	1	2	4	1
Nov.	3	10	1	3	4	2	2	1	4	3	1
Dec.	0	6	7	4	3	1	2	2	5	3	7

gathered in Eastward sector. It may be imagined that this fact shows that there is a tectonic line along the central mountain range from North to South. For the sake of reference, it may be mentioned that, according to Prof. Omori's report[6] on the Formosa earthquakes, the shaken areas of the several earthquakes in the year 1904 were elongated extensively to North and South, suggesting the existence of a tectonic line in this direction, while the general trend of the faults which had taken place at the time of the destructive Kagi earthquake on March 17th, 1920[7] was directed to East and West.

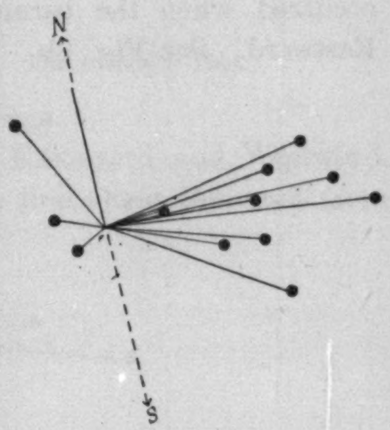

Fig. 2.

2. The Second District or Eastern Formosa and its neighbouring Oceanic Region.

The barometric gradients were directed N. N. W.-ward and S. S. E.-ward, suggesting a weak line to be existed along the coast. See Fig. 3a.

Furthermore, a great earthquake occurred at Sept. 2nd, 1922 and its after-shocks moderate in intensity occurred since that time to November

6) F. Omori, *Sinsai-yobô-tyôsakwai-hôkoku*, 54.

7) F. Omori, *Sinsai-yobô-tyôsakwai-hôkoku*, 63 A.

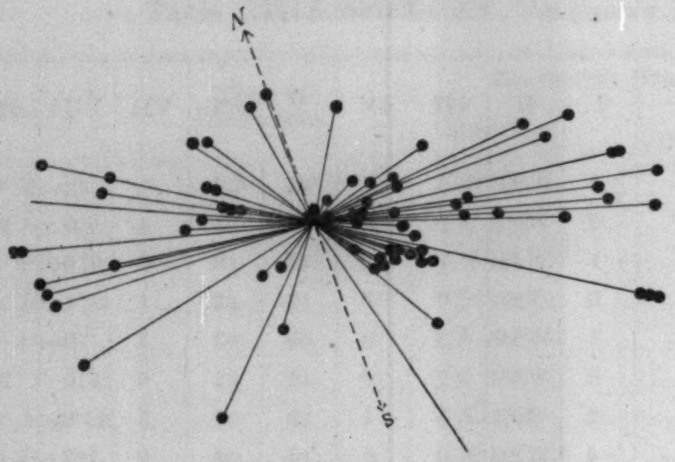

Fig. 3a

19th in the year amounted to eighteen in number. The main part of these after-shocks occurred when the barometric gradients at the place had been directed just opposite to the direction of that of the main earthquake, namely the main earthquake and its after-shocks respectively occurred when the barometric gradients were directed Westward and Eastward. See Fig. 3b. This result is fairly in accordance with that

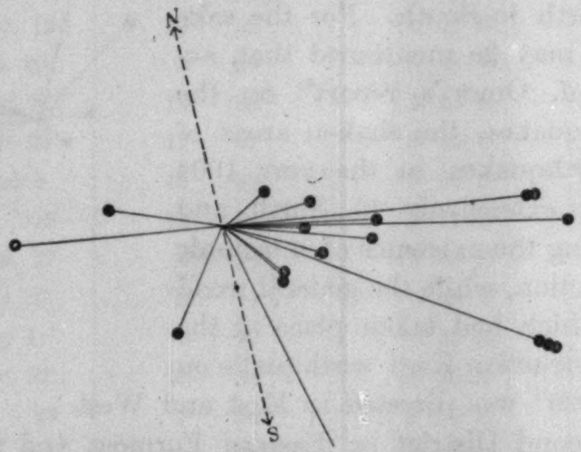

Fig. 3b. The white circle represents the barometric gradient at the time of the great earthquake, and the black circles represent those at the time of after-shocks.

obtained by Dr. Suda in the great Kwantô earthquake and its after-shocks above-stated. But this time, we must keep in mind the existence of a water mass between the atmosphere and the ocean bed.

3. The Third District or Kyûsyû and its Western Sea Area.

This district may be divided into two, northern and southern parts. The earthquakes of the northern part occurred in Professor A. Imamura's Aso seismic zone when the barometric gradients were directed to North and South, so as to be perpendicular to the seismic zone.

The earthquakes of the southern part occurred in the Kirisima seismic zone when the barometric gradients were directed Westward, being normal to the seismic zone. See Figs. 4a & 4b.

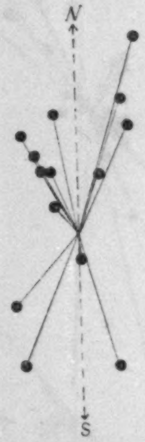

Fig. 4a. The northern Part

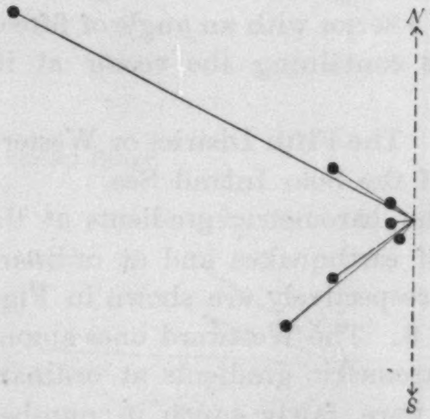

Fig. 4b. The southern Part.

4. The Fourth District or the Sea of Hûga.

The barometric gradients were directed Eastaward and Westward, suggesting a possibility of existing a tectonic line along the coast from North to South. See Fig. 5.

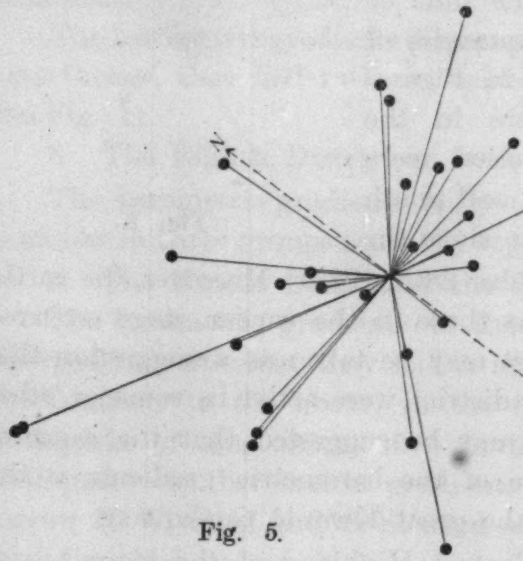

Fig. 5.

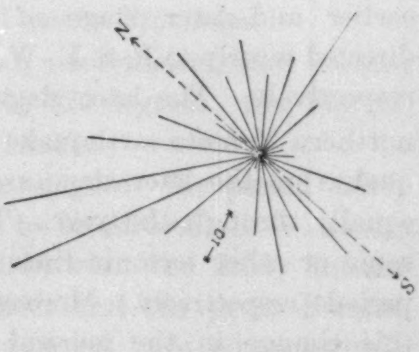

Fig. 6.

For the sake of reference, the barometric gradients at ordinary times at the place are shown in Fig. 6, and we can notice that they are rather equally diverged in all azimuth contrary to those at the time of earthquakes. In the figure, each vector represents the number of the barometric gradients within a sector with an angle of fifteen degrees containing the vector at its center.

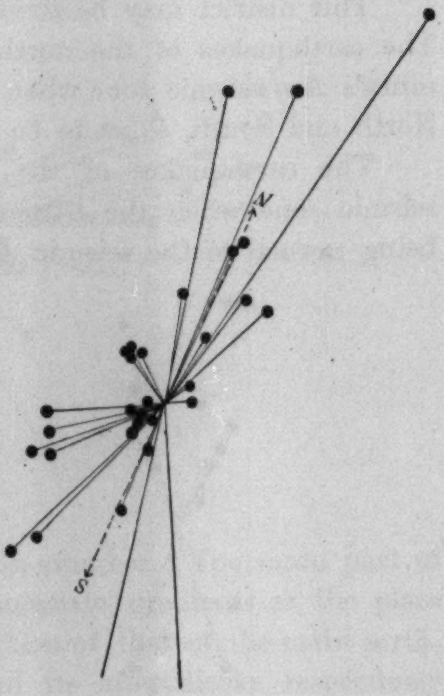

Fig. 7.

5. The Fifth District or Western Part of the Seto Inland Sea.

The barometric gradients at the time of earthquakes and at ordinary times respectively are shown in Figs. 7 and 8. The Westward ones among the barometric gradients at ordinary times were fairly much in number, while those of the barometric gradients at the time of earthquakes were very few, so that the latter were directed mostly to North and South.

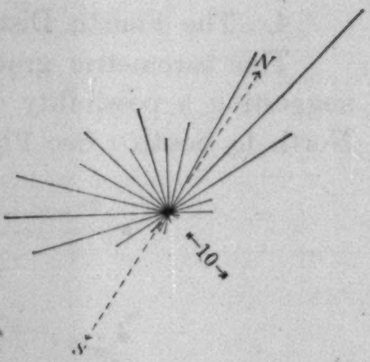

Fig. 8.

6. The Sixth District or Nobi Province and Eastern Part of the Kii Peninsula.

The barometric gradients at the time of earthquakes and the azimuthal frequencies of those at ordinary times are shown in Figs. 9 and 10 respectively. The formers in the earlier and later stage of the period were directed mostly to E. S. E.-W. N. W. and South respectively. The later stage began since the northern Yamato earthquake of October 28th, 1923. Moreover, the earthquakes in the later stage as well as those in the earlier stage occurred equally through the year. This fact may be taken as a suggestion that some or other tectonic lines in the district were active in some or other periods respectively. Moreover, it may be suggested that the cause of this change in the general feature of the barometric gradients at the time of earthquakes might due to the great Kwantô earthquake.

7. The Seventh District or Central Highland of the Main Island

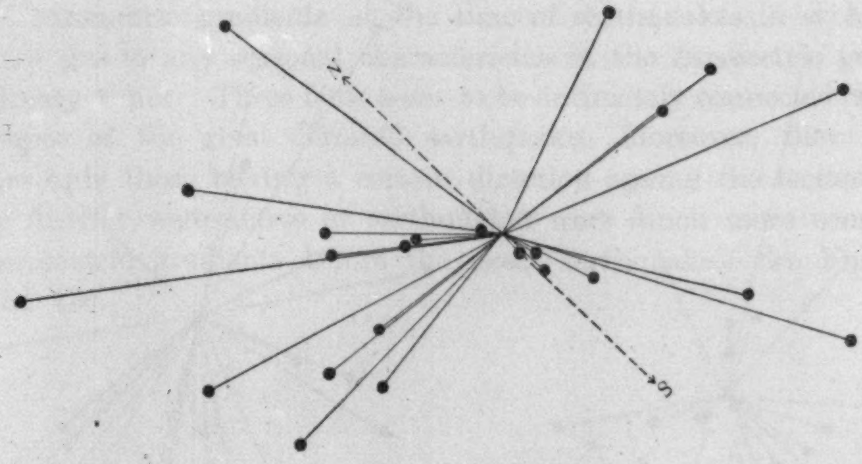

Fig. 9 a. The earlier Stage.

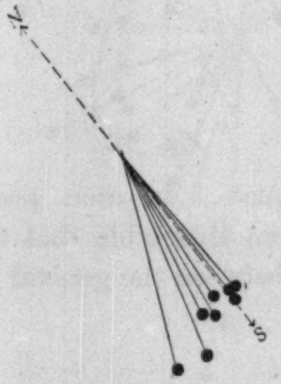

Fig. 9 b. The later Stage.

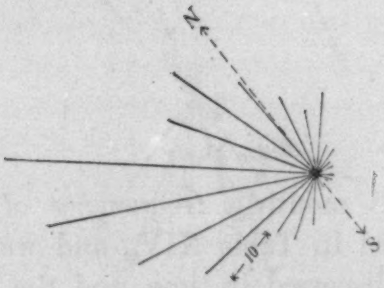

Fig. 10.

of Japan.

The barometric gradients dispersed fairly uniformly in every azimuths, nevertheless, they had rather a tendency to gather in North and South. See Fig. 11.

8. The Eighth District or Iwaki and Iwasiro Provinces.

The barometric gradients fairly dispersed, nevertheless, they seemed to gather in three groups mutually separated by 120 degrees. See Fig. 12.

9. The Nineth District or the Sea of Iwaki.

The barometric gradients in the earlier stage of the period fairly diverged, nevertheless, they had a tendeney to be directed S. W.-ward.

Contrary to the above, in the interval between the fairly intense earthquake of Aug. 28th, 1916 in the district and the great Kwantô earthquake the barometric gradients were directed in a comparatively narrow N. W.-ward and S. E.-ward sectors. After the great earthquake they dispersed again.

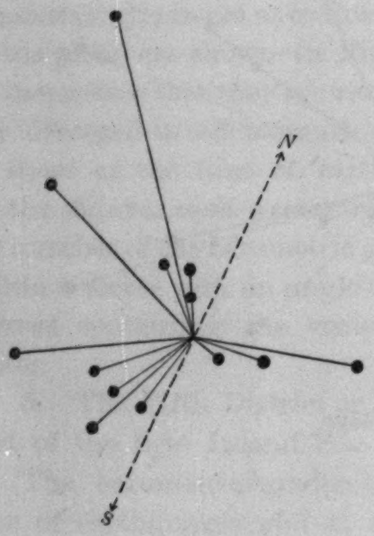

Fig. 11.

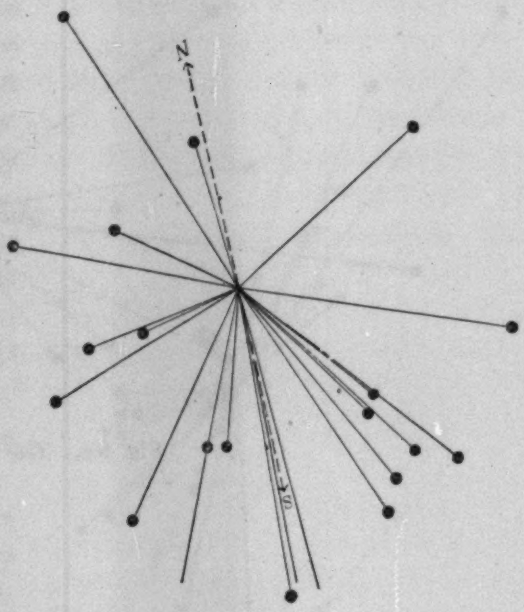

Fig. 12.

The monthly frequencies of the earthquakes in each period are tabulated in Table XIV., and we can see from this table that they are fairly dispersed in time, and the differences between the general features

Table XIV.

	District IX			District X	
	Earlier Stage	Intermediate Stage	Later Stage	Earlier Stage	Later Stage
Jan.	1	4	2	4	2
Feb.	3	7	0	4	0
March	3	0	0	7	1
April	1	3	2	2	4
May	1	3	0	2	3
June	4	5	1	0	6
July	3	1	1	5	1
Aug.	3	0	1	4	3
Sept.	0	3	1	3	4
Oct.	2	0	0	1	3
Nov.	3	1	0	1	2
Dec.	2	2	1	0	3

of the barometric gradients at the time of earthquakes in each period were not due to any seasonal characteristics of the barometric gradients at ordinary times. These facts seem to be intimately connected with the occurrence of the great Kwantô earthquake. Moreover, they suggest whether only those having a certain direction among the tectonic lines in the district were active or earthquakes were much more sensible to the barometric gradients before the great earthquake. See Figs. 13a, 13b and 13c.

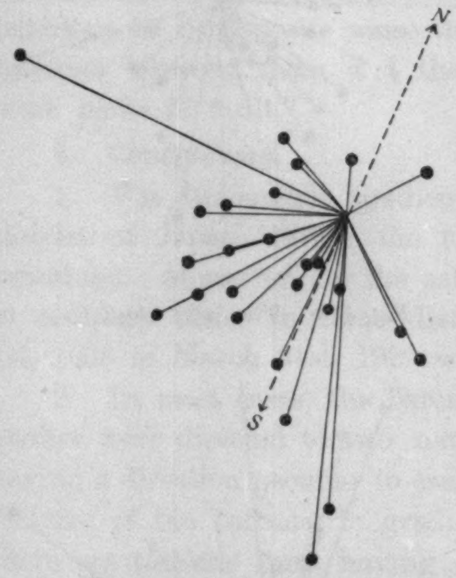

Fig. 13 a. The earlier Stage.

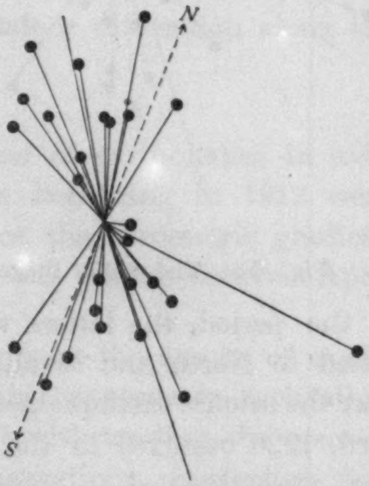

Fig. 13 b. The intermediate Stage.

10. The Tenth District or South-Western Sea of Hokkaidô.

The barometric gradients at ordinary times and at the time of earth-

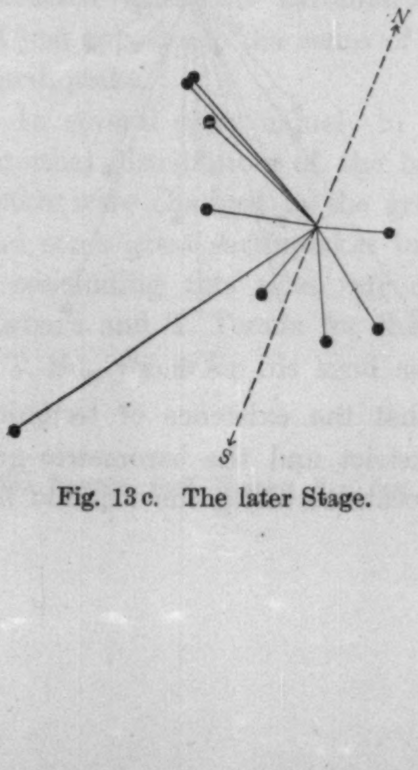

Fig. 13 c. The later Stage.

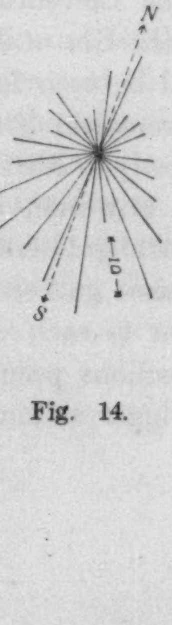

Fig. 14.

quakes are shown respectively in Fig. 14 and Figs. 15a and 15b. The formers dispersed fairly uniformly in all azimuths. In the earlier stage

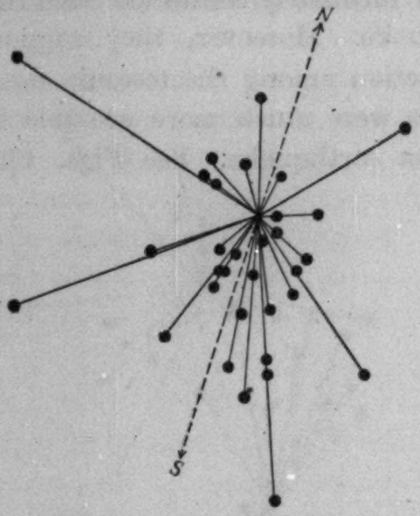

Fig. 15 a. The earlier Stage.

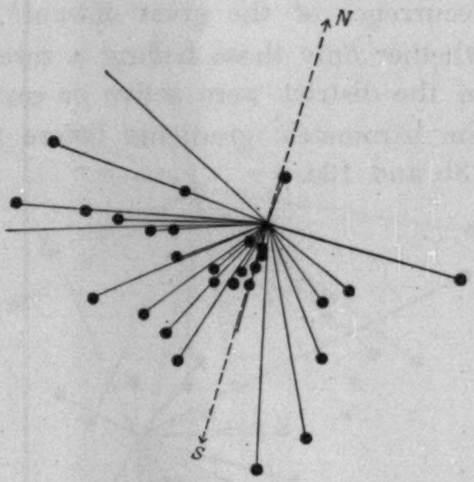

Fig. 15 b. The later Stage.

of the period, the latters were directed to North and South. But after the intense earthquake of April 23rd, 1920 occurred in the district they were directed to South. For the sake of reference, the monthly frequencies of the earthquakes in each period are tabulated in Table XIV, and we will notice that they did not make any important seasonal variations.

11. The Eleventh District or South-Eastern Sea of Hokkaidô.

As will be seen from the Fig. 16, the barometric gradients were directed mostly to North and South.

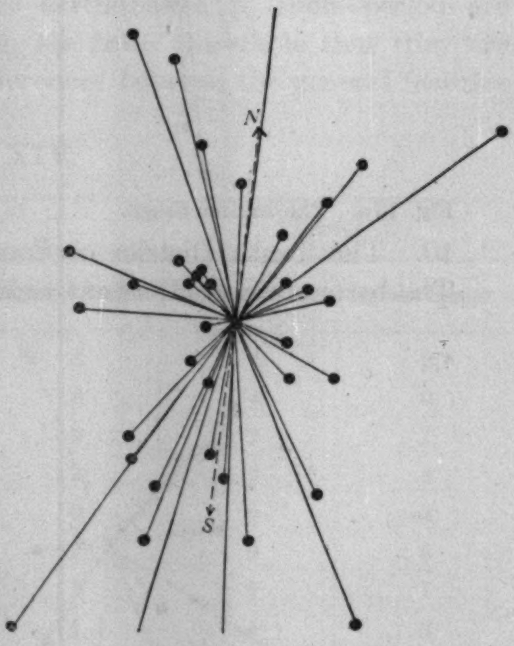

Fig. 16.

4. At any rate, the fact that the barometric gradients at the time of earthquakes gathered in a direction peculiar to each district shows that the existence of tectonic lines having directions peculiar to each district and the barometric gradient act as a trigger action of some dislocations along the tectonic lines or

an earthquake occorrence.

For the sake of reference, it may be mentioned that a model of the mechanism of the trigger action of the barometric gradient was kindly suggested formerly by Professor T. Terada[8], which is as follows, "Suppose two adjacent blocks of the crust be in somewhat loose contact with each other at an inclined fault plane forming the boundary between the blocks. If the atmospheric pressure be higher on the block on the upper side of the inclined boundary plane than on the other, the contact between the two blocks will be tightened, whereas if the pressure distribution be in opposite sense there will ensue a tendency to loosen the junction between them and thence is facilitate a dislocation along the weak plane of fault."

5. Conclusions.

1. The barometric gradients at the time of earthquakes in each district of Japan during the fourteen years beginning in 1912 were examined. Moreover, for the sake of reference, the barometric gradient at ordinary times in some districts during the period between April 1st, 1928 to March 31st, 1929 were taken.

2. In most cases, the barometric gradients at the epochs of earthquakes were directed to two narrow sectors just opposite to each other having a direction peculiar to each district not withstanding the general features of the barometric gradients at ordinary times, suggesting that there are tectonic lines having directions peculiar to each district and the barometric gradient act as a trigger action of some dislocations along these tectonic lines or an earthquake occurrence.

3. The after-shocks of the great Formosa earthquake of Sept. 2nd, 1922 occurred when the barometric gradients at the district had been directed just opposite to the sense of direction of that at the time of the main earthquake.

4. In several cases, namely in the sixth, ninth and tenth districts, the azimuthal distributions of the barometric gradients at the epochs of earthquakes were changed by the great Kwantô earthquake of Sept. 1st, 1923 and some great earthquakes in the very districts.

In concluding this note, our cordial thanks are due to Professors S. Fujiwhara and T. Terada for their kind advices and discussions and to Mr. T. Sugiyama for his kind assistance in preparing the data.

---

8) Win INOUYE, *Bull. Earthq. Res. Inst.*, 5 (1928).

7. 本邦各地の地震前の氣壓勾配に就いて

地震研究所 { 井上宇胤 長谷川惠副

本邦を十一箇の地域に分割して、各地域に於ける顯著地震及び稍顯著地震に就いて、發震前の氣壓勾配を調査しました。

尙比較の爲數箇所に於ける平常時の氣壓勾配の狀態をも調査してあります。

或る地方に於ては時期により地震前の氣壓勾配の集合、離散の狀を異にして居り、夫れが其の地方或は附近の大地震の發生の時期に密接な關係を有して居るらしい事が知られました。

8. 地震と脈動（豫報）

地震研究所　井上宇胤

（昭和六年七月七日發表——昭和六年十二月二十日受理）

1. 大森博士[1] は遠地地震の東京測觀（一橋と本郷）に於ける各相位中に於ける主要な振動週期を驗測されました。其れに依ると、第一初期微動に於ける主要週期は $P_1=4{\cdot}6$ 秒と $P_2=8{\cdot}3$ 秒であり、第二初期微動に於けるものは $P_2=8{\cdot}3$ 秒であつて、東京に於ける脈動の $Q_1=4{\cdot}4$ 秒及び $Q_2=8{\cdot}0$ 秒のものと同じものであると結論されました。卽ち遠地地震に於ける初期微動は地震に依つて土地の自己振動が生起されたものとされて次の様な興味深い事を云はれて居ります。

"The disturbance at the commencement of the 1st preliminary tremor, which has a transit velocity of some 14 km. per. sec., must travel along a layer at some distance below the earth's surface.

These would constitute a progressive source of disturbance and would communicate a sort of stress to the superimcumbent surface layer of the earth's crust in the region about a given station; the latter being, in consequence, thrown into its own proper oscillations, just as the waters of seas are thrown, by great sub-marine earthquakes or by atmospheric disturbances, into destructive waves, whose periods are the same as those of the waves existing at ordinary times and are constant at each given sea-coast place."

次に松澤博士[2] は地震の東京觀測（本郷）に於て、近地地震に於ても、脈動に相當するゆつくりした波が交つて來る事を指てきされました。卽ち相模に發生した地震と涸沼に發生した地震に於ては 2 秒週期の波が現はれて居て q 型の脈動が誘發された事を示し、鹿島灘と襟裳崎の地震に於ては 4 秒週期の波が現はれて居て、Q_1 型に相當して居る事を示されました。尙 1922 年 1 月から 6 月迄の筑波山に於ける地震觀測の記象には、しばしば最初からのろい波が交つて居つて、其の週期は筑波山で觀測される脈動と同程度であつた事を指てきされて居ります。

1) F. Omori, *Pub. E. I. C.*, **13** (1903), 85.
2) T. Matuzawa, *Journ. Fac. Sci., T. I. U.*, **2** (1927).

さて私は次に、筑波山に於ける此の問題を取扱つて見る事に致しました。

2. 筑波山に於ては大森式の微動計二臺に依つて地震觀測をして居りますが、その重りの目方は夫々 35 瓩、週期は 18 秒、倍率は 120 倍のもであります。此等の器械に依つて地震を N. E.—S. W. 向きの動きと N. W.—S. E. 向きの動きとに分解して書かせて居りますが、此の N. W.—S. E. の向きは山の傾斜にそうた向きであり、N. E.—S. W. の向きはそれに直角の向きに當つて居ります。

此等の器械に依つて觀測しますと、筑波山に於ては平常時には殆ど動脈が觀測されませんが、著しい低氣壓が東方の太平洋上を通過する樣な際には脈動が觀測されます。夫等は殆ど皆最大振幅が 2, 3μ 程度のもので、週期は q=2 秒～3 秒及び Q_1=4 秒～5 秒程度のレギュラー型のものであります。其の一例を第一圖に示してあります。卽ち大きさは淺間山で觀測される脈動[3] と同程度で、東京で觀測される大きさの $\frac{1}{10}$ から $\frac{1}{20}$ 程度のものであります。

尙筑波山に於ける脈動は場合に依り一方の成分にのみ良く現はれる事があります。又兩成分に現はれる脈動の週期は低氣壓の位置の如何に依り異なつて居りますが、一般には N. W.—S. E. の成分卽ち山の傾斜にそうた振動に於ては q 型と Q_1 型が現はれますが、q 型の方が現はれ易い。其れに反して N. E.—S. W. の成分卽ち山の傾斜に直角の方向の振動に於ては、主として Q_1 型の脈動が觀測され q 型は殆ど觀測されません。第二圖と第三圖は夫々昭和六年に於ける數回の脈動の N. W.—S. E. 成分及び

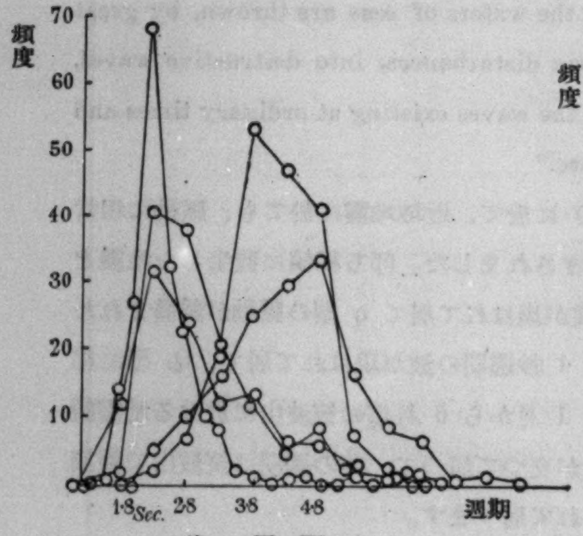

第二圖 Fig. 2.

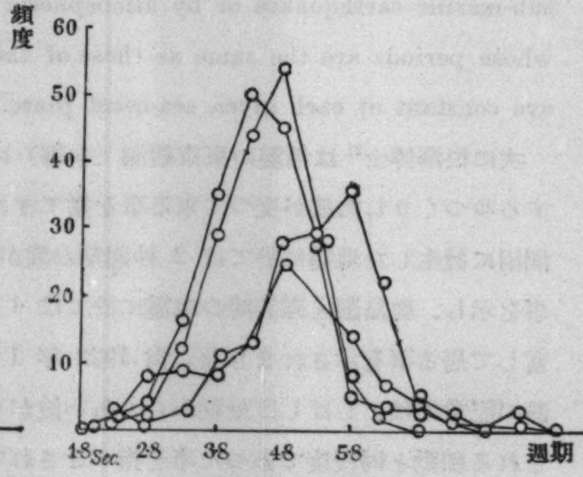

第三圖 Fig. 3.

3) F. OMORI, *Bull. E. I. C.*, 5 (1913).

N. E.—S. W. 成分の週期の半時間內の頻度曲線であります。第四圖は昭和六年六月十二日午後六時前後に於ける脈動の半時間內の兩成分に現はれた週期の頻度曲線であります。此の時には 746 mm. の低氣壓が房總沖にあり、筑波山からの距離は 220 km. でありました。第五圖は昭和六年三月廿四日午後六時の脈動に就いての同樣な頻度曲線でありますが、此の際には筑波山の東北 770 km. の海中に 736 mm. の低氣壓がありました。

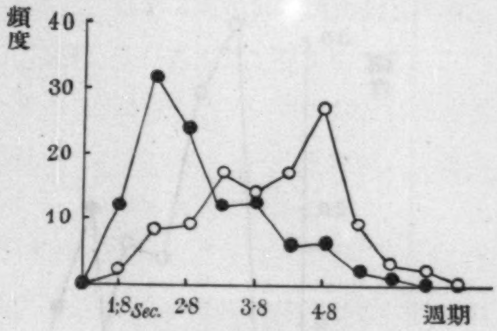

第四圖 Fig. 4.
白玉は N. E.—S. W. 成分
黑玉は N. W.—S. E. 成分

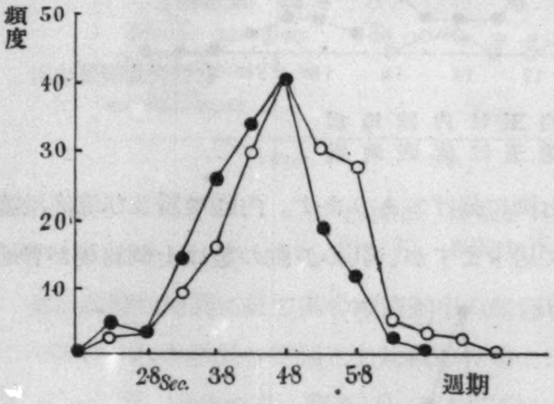

第五圖 Fig. 5.
白玉は N. E.—S. W. 成分
黑玉は N. W.—S. E. 成分

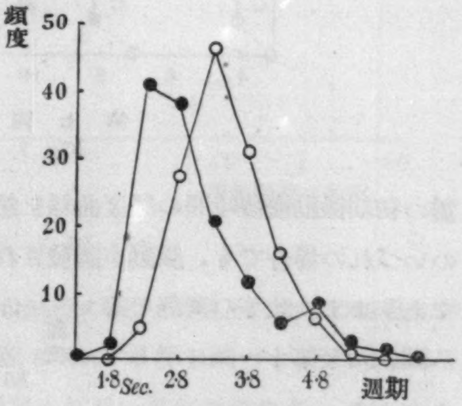

第六圖 Fig. 6.
白玉は N. E.—S. W. 成分
黑玉は N. W.—S. E. 成分

第六圖は昭和六年四月廿二日午後六時の脈動に就いての同樣な頻度曲線でありますが、此の際は低氣壓が北海道方面に過ぎ去つたあとでありました。此等に依ると、場合に依つて兩成分に於ける週期が或は一致し、或は異なる狀が見えて居ります。此の事に依つても筑波山に於ける脈動は此の土地の自己振動が低氣壓或は其れに依つて起された波浪等に依る刺戟に依つて誘發されたものであり、其の刺戟の如何に依つて土地の自己振動のモードが異なる事が知られます。

3. 次に澤松博士の指てきされた如く筑波山に於ては、しばしば地震の最初から此の脈動が誘發されて居りますが、其れに就いて少しくわしく調査して見ませう。

1) 初期微動繼續時間が 20 秒以內の近地地震。

昭和四年一月から昭和六年四月迄の近地地震に於ける誘發された脈動に就いて調査しました。此等の地震を內陸地震と海底地震の二組に分類致しましたが、採用した地

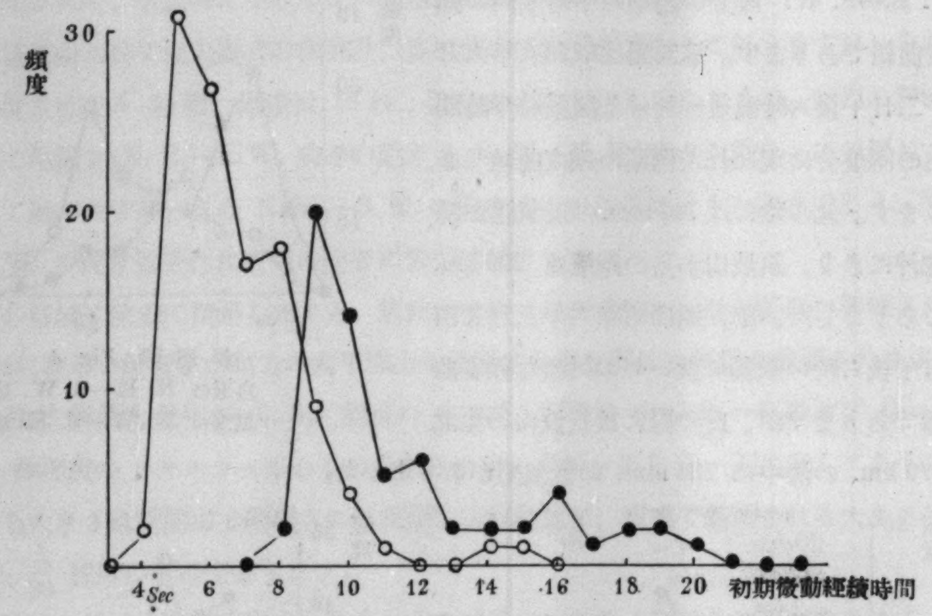

第 七 圖 白玉は內陸地震
Fig. 7. 黑玉は海底地震

震の初期微動繼續時間の頻度曲線を第七圖に揭げてあります。內陸地震及び海底地震のいづれの場合でも、脈動が誘發されて居りますが、其の波動の數は十個前後が普通であります。此等の實例を第八圖、乃至第十一圖に示してあります。

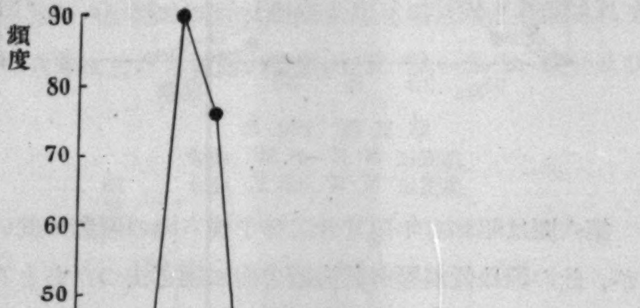

第十二圖 白玉は N.E.—S.W. 成分
Fig. 12. 黑玉は N.W.—S.E. 成分

先づ內陸地震に就いて、此の誘發された脈動の兩成分の週期の頻度曲線を求め第十二圖に示してあります。此れに依ると、N.W.—S.E. 成分に於ては普段の脈動の際に此の成分に現はれ易い q 型の脈動が誘發されて居ります。同樣に N.E.—S.W. 成分に於ては普段の脈動の際に此の成分に現はれ易い Q_1 型の脈動が誘發されて居ります。

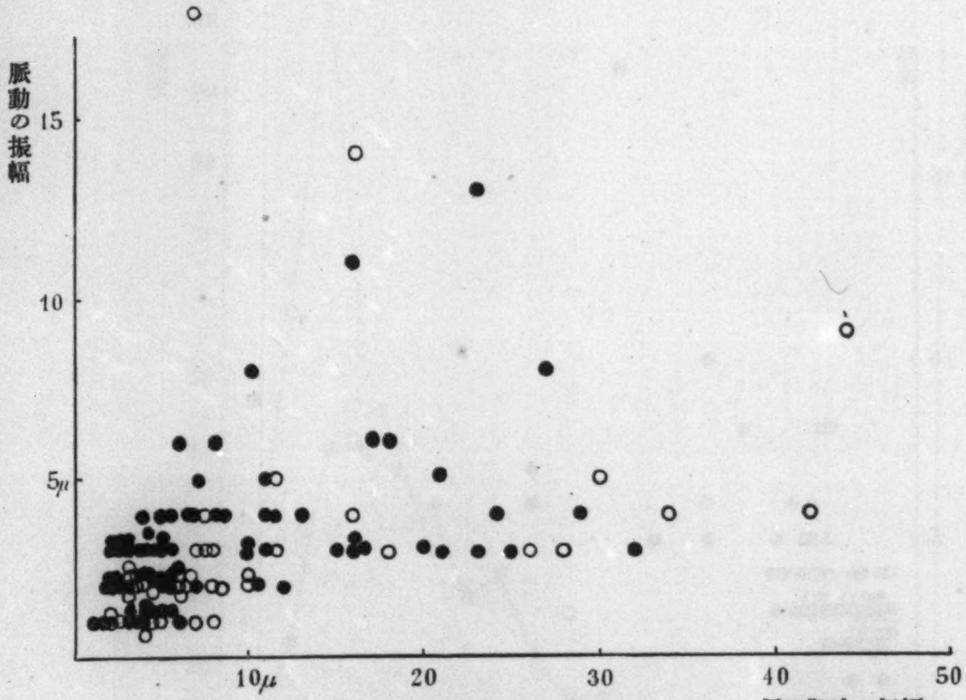

第十三圖　白玉は N.W.—S.E. 成分
Fig. 13.　黒玉は N.E.—S.W. 成分

次に此等の地震に於て其の地震動中の短週期の波動の最大振幅と、此等の地震に依つて誘發された脈動の振幅とを比較して第十三圖に示してあります。此れに依ると N.E.—S.W. 成分の方、即ち Q_1 型の脈動が誘發され易い事が知れます。

次に海底地震に就いて、誘發された脈動の兩成分に於ける週期の頻度曲線を求めて第十四圖に示してあります。此れに依ると內陸地震の場合と全く同樣に N.E.—S.W. 成分には主として q 型の脈動、N.W.—S.E. 成分には、主として Q_1 型の脈動が誘發されてをります。

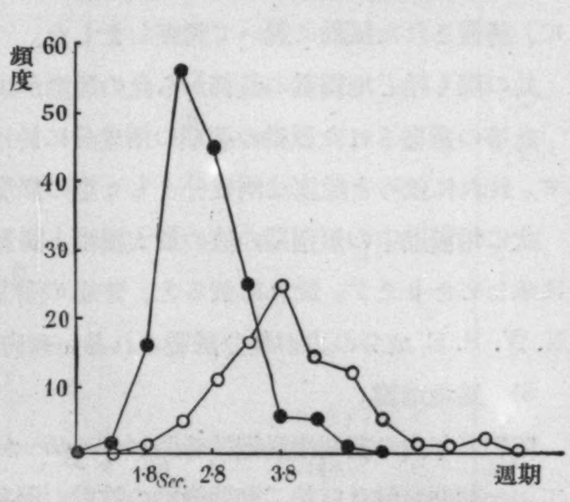

第十四圖　白玉は N.E.—S.W. 成分
Fig. 14.　黒玉は N.W.—S.E. 成分

尙內陸地震の場合と同樣に、地震動中の短週期の波の最大振幅と誘發された脈動の振幅とを比較して第十五圖に揭げてあります。

此れに依ると此度は兩成分が、即

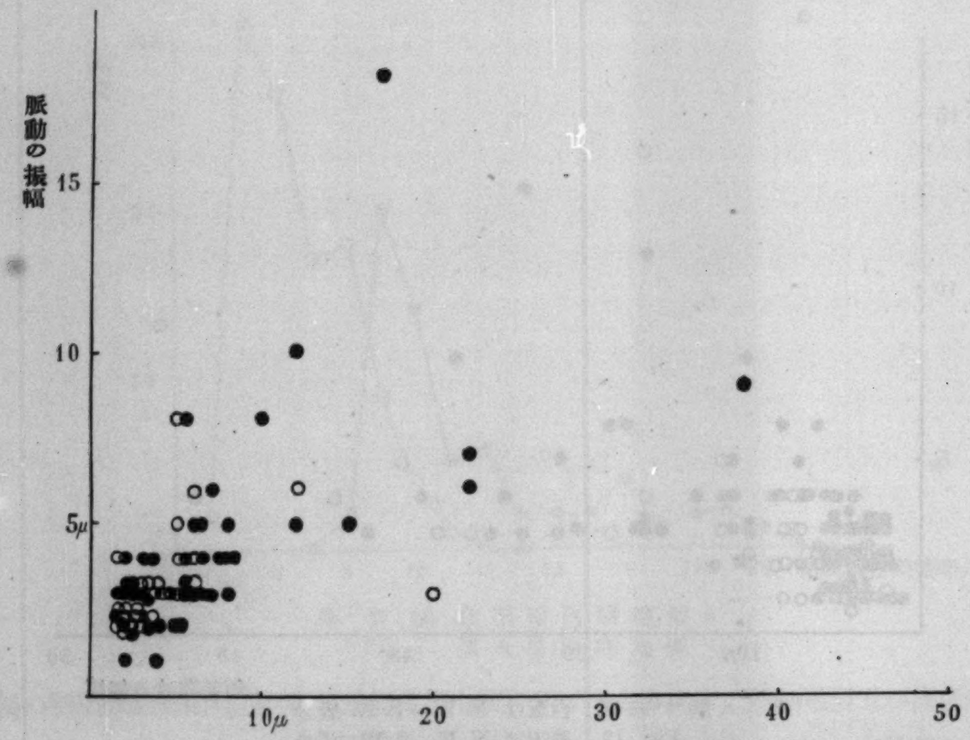

第十五圖 白玉は N.W.—S.E. 成分
Fig. 15. 黒玉は N.E.—S.W. 成分

ち q 型と Q_1 型とが殆ど同程度に誘發される事が知られます。

2) 中距離地震。

昭和六年の一月から四月中の初期微動繼續時間が一分前後の中距離地震八個に就いて、誘發された脈動に就いて調査しました。

此の際も殆ど地震動の最初から此の脈動が現はれて居ります。

此等の誘發された脈動の週期の兩成分に於ける頻度曲線を第十六圖に示してあります。此れに依ると此度は兩成分とも q 型の脈動が主であります。

次に地震動中の短週期の波の最大振幅と誘發された脈動の振幅との比較を第十七圖に示してあります。此れに依ると、普通の脈動の際に主として q 型が觀測される N.W.-S.E 成分の方が幾分誘發され易い傾向が見えて居ります。

3) 遠地地震。

昭和五年内の初期微動繼續時間が $6^m 45^s$ から $29^m 55^s$ 迄の四個の遠地地震に就いて第一初期微動及び第二初期微動の波動の週期の頻度曲線を求めて第十八圖及び第十九圖に示してあります。此れに依ると兩成分とも第一初期微動に於ては q 型と Q_1 型

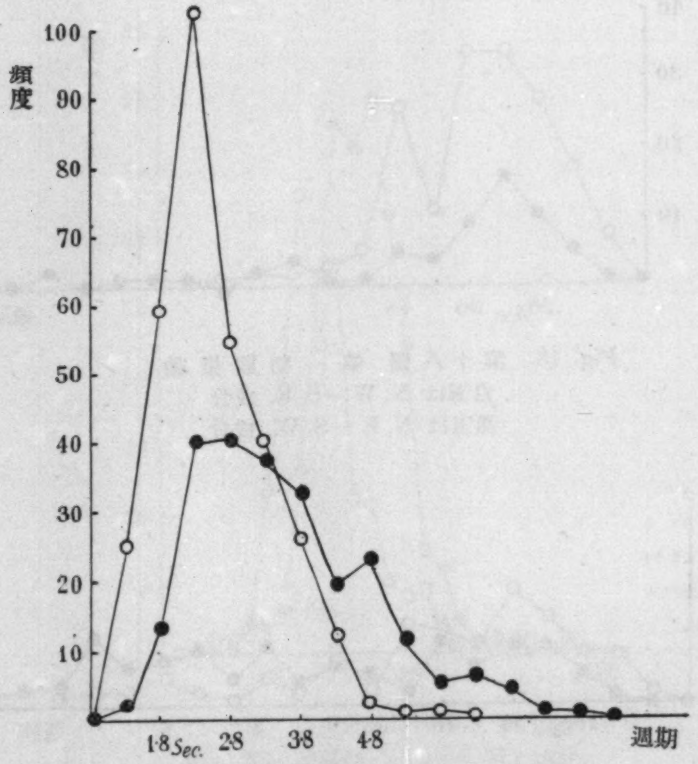

第十六圖 白玉は N. W.—S. E. 成分
Fig. 16. 黒玉は N. E.—S. W. 成分

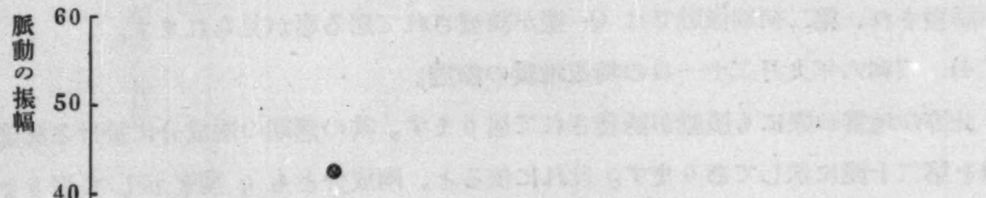

第十七圖 白玉は N. W.—S. E. 成分
Fig. 17. 黒玉は N. E.—S. W. 成分

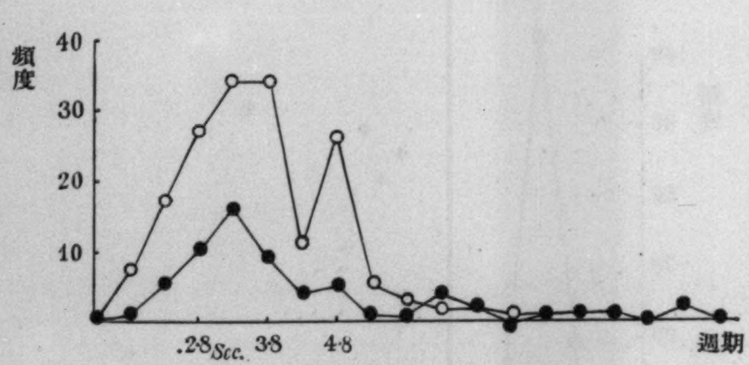

Fig. 18. 第十八圖 第一初期微動
白玉は N. W.—S. E. 成分
黑玉は N. E.—S. W. 成分

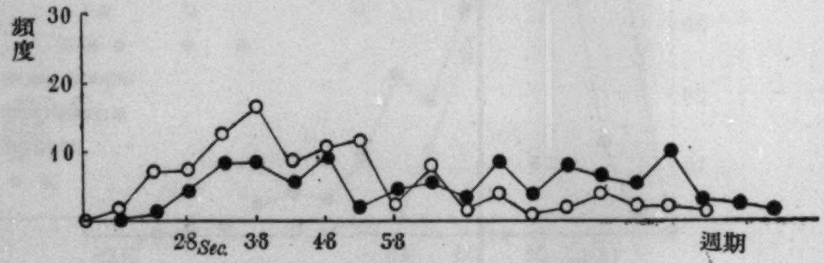

Fig. 19. 第十九圖 第二初期微動
白玉は N. W.—S. E. 成分
黑玉は N. E.—S. W. 成分

が誘發され、第二初期微動では Q_1 型が誘發されて居る事が見られます。

4) 昭和六年九月二十一日の埼玉地震の餘震。

此等の地震の際にも脈動が誘發されて居ります。其の週期の兩成分に於ける頻度曲線を第二十圖に示してあります。此れに依ると、兩成分とも q 型を示して居りますが、N. E.—S. W. 成分の方が幾分週期が長く成つて居ります。

次に地震動中の短週期の波の最大振幅と此等の誘發された脈動の振幅とを比較して第二十一圖及び二十二圖に示してあります。此れに依ると N. E.—S. W. 方向の脈動の方が幾分誘發され易い事が知れます。所で此の方向は此等の地震群の震源地と筑波山とを結ぶ線にそうて居ります。結局、兩成分に於ける誘發された脈動は共に q 型であるが、震源地に向ふ成分の方が幾分週期も長く、且つ誘發され易い事を示して居ります。

4. さて筑波山に於ける地震動中の短週期の波の週期は約 0·1 秒～0·3 秒程度のものであつて、此の波の大部分もやはり地震動の刺戟に依つて起された土地の別種のモ

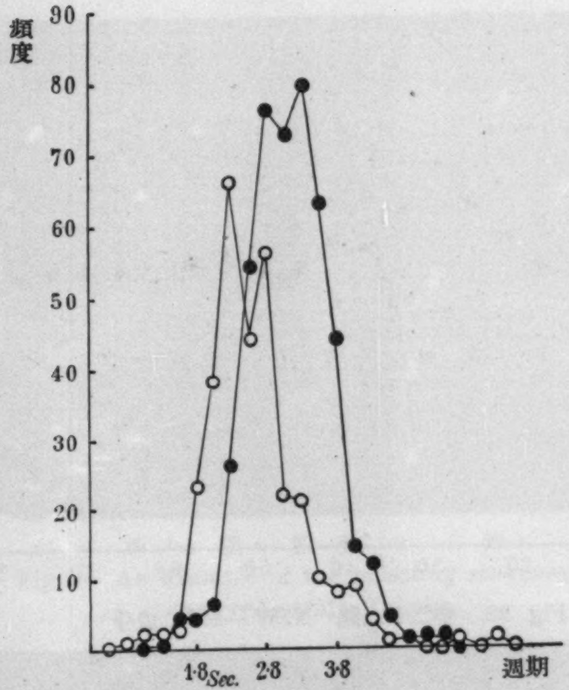

第二十圖 白玉は N. W.—S. E. 成分
Fig. 20. 黒玉は N. E.—S. W. 成分

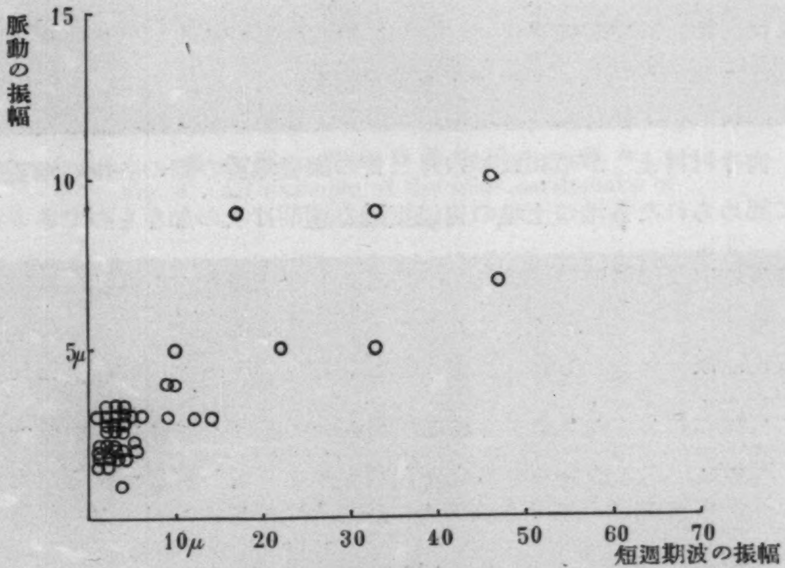

第二十一圖 N. E.—S. W. 成分
Fig. 21.

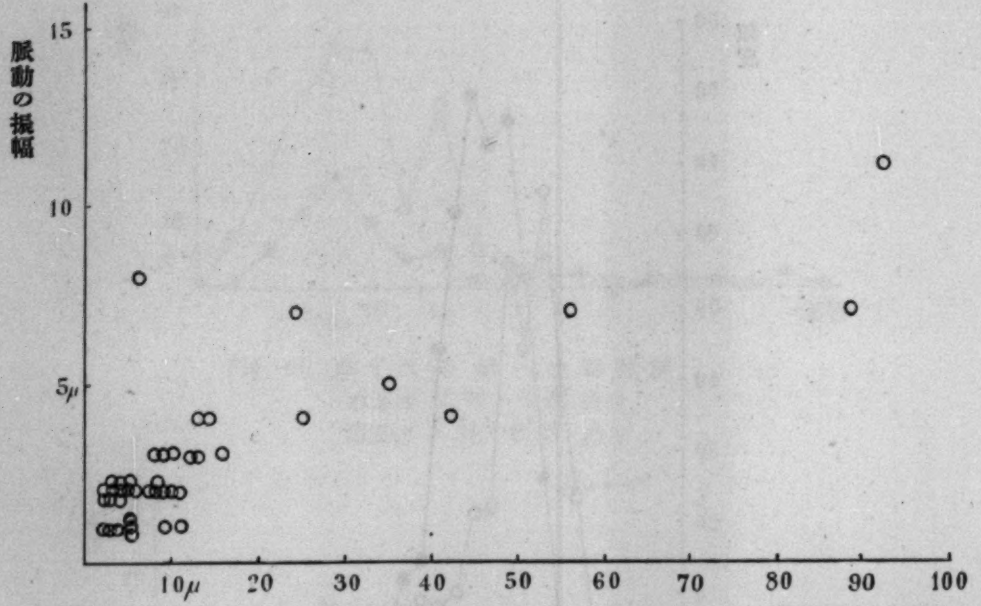

Fig. 22. 第二十二圖 N. W.—S. E. 成分

ードの自己振動でないかと思はれます。然し現在筑波山で使用して居る地震計に依つては、倍率が小さい爲と殊に記錄の速度がおそい爲に此の點を明にする事が出來ないのは遺憾であります。

東京に於ては、大森博士[4] が本郷に於て microtremor の際及び地震の際に 0·29 秒と云ふ自己振動が現はれる事を指てきされました。尙一橋に於ける自己振動は 0·7〜0·8 秒大阪に於ては 0·8 秒である事を示された。

次に末廣博士[5] も地震動の分解器に依つて本郷臺に 0·3 秒の自己震動がある事を示された。尙今村博士[6] が昭和五年六月三日の深發地震の際の各地の地震記象の御研究に依つて認められた各地の土地の自己振動の週期は次の如きものであります。

即ち紀伊半島の目方では 0·55 秒であり、關東では表土が 0·2〜0·3 秒、洪積地が 0·4 秒、第三紀層が 0·6 秒であります。

それで、筑波山に於ても此の程度の波動、即ち 0·1〜0·3 秒程度の短週期の波も土地の自己振動としますと、此の振動と脈動の週期に相當する比較的長週期の自己振動とは或る聯立系（カツプルド・システム）を成して居るものと考へられます。それで、此の聯立系が地震動（上述の大森博士の意見と同樣にインパルスの性質をおびたもの

4) F. Omori, *Bull. E. I. C.*, 2 (1908).
5) K. Suyehiro, *Bull. Earthq. Res. Inst.*, 7 (1929).
6) 今村明恒、地震研究所彙報 第七號。

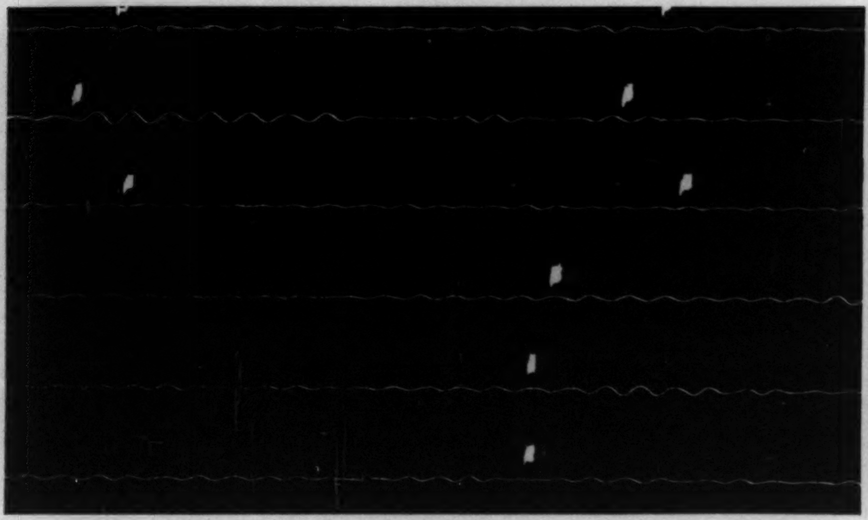

第一圖　脈動の一例

Fig. 1. An example of the pulsatory movements observed at Mt. Tukuba.

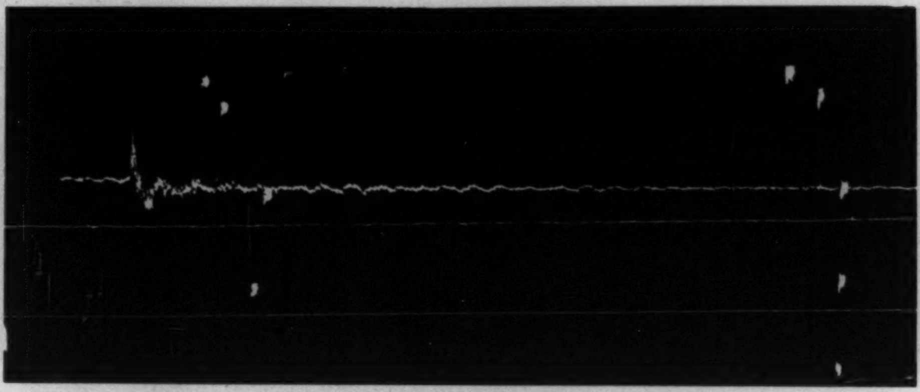

第八圖　內陸近地地震の一例

Fig. 8. An example of the near earthquake of inland origin.

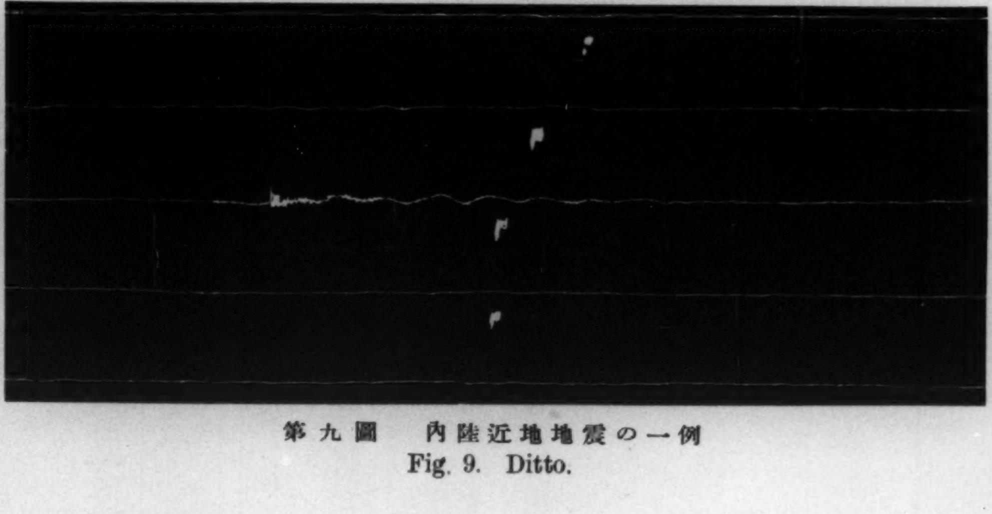

第九圖　內陸近地地震の一例

Fig. 9. Ditto.

(震研彙報、第十號、圖版、井上)

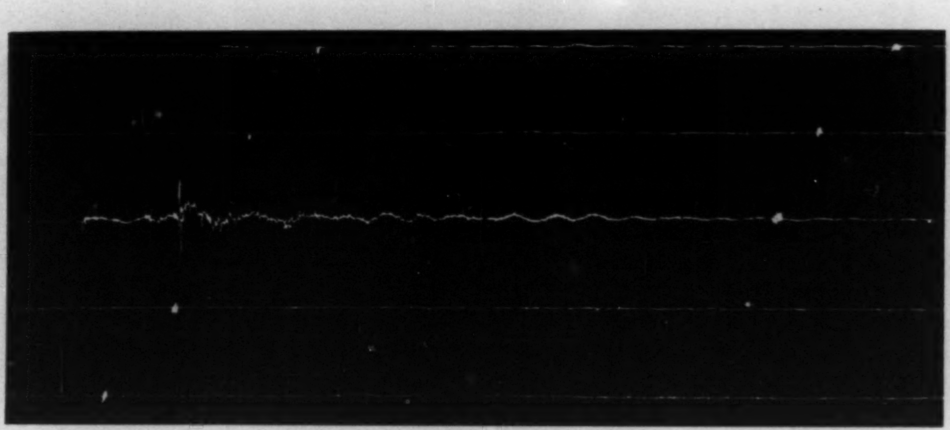

第十圖　海底近地地震の一例
Fig. 10. An example of the near earthquake of oceanic origin

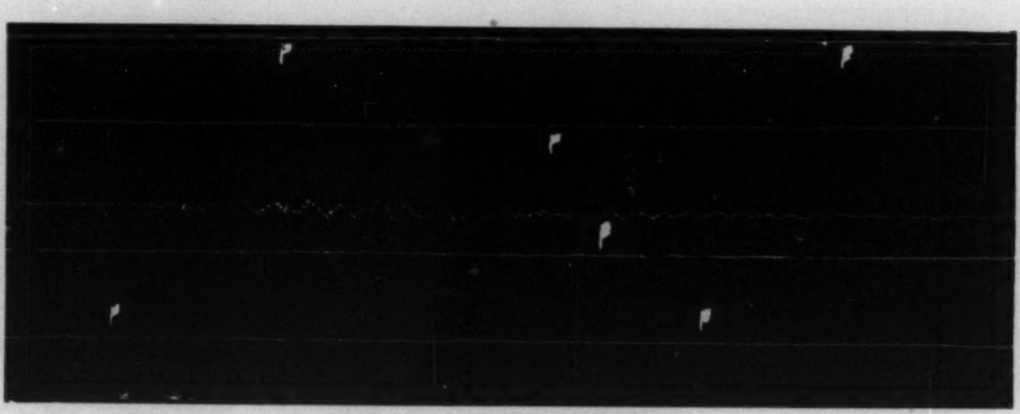

第十一圖　海底近地地震の一例
Fig. 11. Ditto.

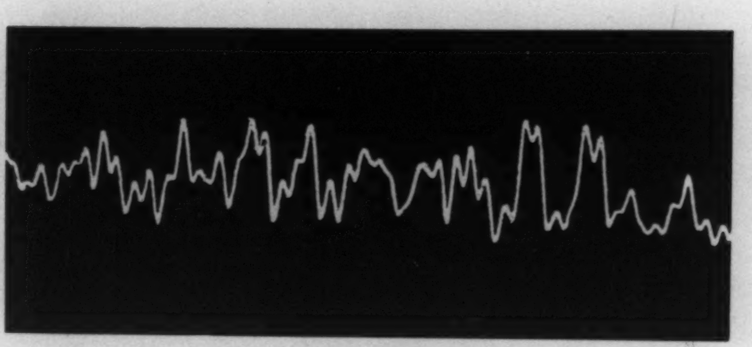

第二十三圖
Fig. 23.

(震研彙報、第十號、圖版、井上)

と考へます)の刺戟に依つて複雑な自己振動を起したものが地震計の記錄に現はれるのであると考へられます。尙地震の際には、此の兩方の振動が起されますが、普段の脈動の際には短週期の方が現はれない事からして、短週期の振動が長週期の振動に及ぼすカツプリングの係數の方が此の逆の場合のものよりも遙に大きいと考へられます。

それで、一つの模型として、二つの週期の異なる單振子をバネでカツプルさせて、短週期の方に鋼鐵の球の群を傾斜した管から衝突させた場合の長週期の方の動きを記錄したものを第二十三圖に示してあります。

此れに依ると幾分實際の地震記象に類似して居りますが、尙兩方の振子の慣性能率を加減したり、カツプリングの種類を變へたりして見たいと思つて居ります。

---

8. *Earthquake and Pulsation.*

By Win INOUYE,

Earthquake Research Institute.

The pulsatory movements observed at Mt. Tukuba are generally consisted of Omori's q- and Q_1-types.

They appear in different manner in their intensities and periods in the two components; the one (N. W.-S. E.) being the component along the mountain slope there, while the other is that perpendicular to this direction; according to the characters of the barometric depressions. A few examples of the frequeney distributions of the periods in two components respectively of the pulsations under different meteorological conditions are shown in Figs. 4, 5 and 6. The black and white circles respectiely represent the N. W.-S. E. and N. E.-S. W. components.

Thus we may infer that they are some modes of the proper oscillations of the earth's crust about the mountain.

Moreover, in general, they are fairly exited by some earthquakes.

The author studied about this excited or induced pulsatory movements by some earthquakes. See Figs, 8, 9, 10 and 11.

The frequency distributions of the periods in two components respetively of the pulsatory movements excited by different earthquakes are shown in Figs. 12, 14, 16, 18 and 19.

---

9. *Study on the Propagation of Seismic Waves.*

(*The first paper*)

By Hirosi KAWASUMI,

Seismological Institute.

(Receive Dec. 20, 1931.)

Introduction.

The ultimate object of seismometry is the elucidation of the waves propagated through the earth in case of earthquake. The entire feature of seismic waves reflects all the characteristics of mechanisms of their origin and properties of the media through which they propagate. The investigation in this line, as is well-known, is the best way to investigate the interior of the earth, but is no less important for the people in the land of earthquake as it enables them to know the mechanisms of the occurrence of earthquake.[1] Only the results of systematic determinatin of the position of hypocentre will reveal the activity of seismic zones, moreover if mechanisms of the origin of individual earthquake are known we may be able to get some clew to the cause of earthquake origin. The investigation in this line pursued regionally and chronologically will throw some light on the foretelling earthquake occurrence. The only way to the purpose is the quantitative study of seismic waves. All kinds of modifications of the waves on the path of propagtion, such as reflexion, refraction, dispersion, absorption and generation of other kinds of waves, depend upon the structure of the media through which the waves propagate.

---

1) Distribution of pull and push of initial motion of earthquake was first found to indicate the mechanism of earthquake origin by T. Shida. Complete earlier bibliography is in "A Historical Sketch of Development of Seismology in Japan." by Proffessors T. Terada and T. Matuzawa in 'Scientific Japan' published for the third Pan-Pacific Science Congress, 1926. Among the later studies on this point, theoretical studies of H. Nakano, [*Geophys. Mag.*, **1** (1928), 255; **2** (1929), 37; **2** (1930), 189] and K. Sezawa [*Bull. Earthq. Res. Inst.*, **7** (1929), 41], on surface waves corresponding more general mechnisms of origin; and the study of seismogram type corresponding the mechanism of origin [*Journ. Met. Soc.*, Japan, ii, **6** (1928), 326] by K. Sagisaka will be most notable. After this paper was written H. Honda published a very interesting quantitative study on this point. [*Journ Meteorol. Soc.*, Japan, ii, **9** (1931), 293.]

The structure of the earth's crust in Japan has been worked out by many investigators,[2] though the discrepancies of the results cannot be disregarded. The effects of viscocity and plasticity have not yet been determined. And surface waves in near earthquake have not yet been decidedly identified. All these problems above mentioned together with a number of other problems as the effect local geology, the possible effect of the dimension of hypocentre[3] etc. are to be solved ultimately by the accurate knowledge of velocity of propagation and the structure of the earth. So my first study must be chiefly directed to this point.

Determination of the velocity of P-wave (*undae normal primae*) is given in chapter I and that of S-wave (*undae normal secundae*) in chapter II. The results of chapter I and II are formulated into practically convenient form and time distance curves for various hypocentral depths and some auxiliary tables for the determination of hypocentre and the wave velocity are calculated in chapter III.

The principal aim of this paper is the introduction of the quantitative study and nothing new is contributed here except the method for these purposes. The main objects stated above will be pursued in the following contributions.

The accuracy of seismometrical observations needed for the above quantitative study have now been attained in Japan, as will be seen from the following results, by the ardent endevour to complete the organization of the systematic observing net under the Central Meteorological Observatory and smaller and denser regional nets under Earthquake Research Institute. I am very much obliged to these observations and especially the results given in chapter II are greatly due to the generocity of the director of the Central Meteorological Observatory who accepted my request through the director of the Earthquake Research Institute to see the photographic copies of seismograms due to the earthquake on May 21, 1928 obtained at more than 20 meteorological stations in Japan.

---

2) Dr. A. Imamura introduced the idea of stratified structure of the crust [*Report. of Earthq. Inv. Com.*, **53** (1906), 9] in 1906, and Mohorovičić layer was found in Japan by K. Wadati [*Journ. Met. Soc.*, Japan, ii, **3** (1925), 53, or Geophys. Mag., **1** (1927), 89], Two layer cust was introduced in Japan by T. Matuzawa. [*Bull. Earthq. Res. Inst.*, **5** (1928), 1] Recently continuous variation of velocity with no discontinuity surface was suggested by S. Sagisaka [*Kensin Zihô*, **5** (1931), 55.] and H. Honda [*Geophys. Mag.*, **3** (1931) and *Journ. Met. Soc.*, Japan, ii, **9** (1931), 293.] The discrepancies in the velocity of P- and S-wave are seen in Chap. I and II of this paper.

3) K. Sezawa, *Bull. Earthq. Res. Inst.*, **3** (1927).

Chapter I. Determination of the velocity of P-wave, from the analysis of travel-times of the earthquake on May 21, 1928, which occurred in Tiba prefecture.[4)]

The velocity of P-wave (undae normal primae) in the so called urtrabasaltic layer has been estimated differently by several authorities in Europe and Japan. For example

K. Zoeppritz, L. Geiger[5)]	$v=7{\cdot}2$ km./sec.		
S. Mohorovičić[6)]	$v=8{\cdot}0$		
B. Gutenberg[7)]	$v=8{\cdot}0$		
V. Conrad[8)]	$v=7{\cdot}83$	8·12	
H. Jeffreys[9)]	$v=7{\cdot}41$	7·70	7·80
K. Wadati[10)]	$v=7{\cdot}5$	7·6	8·0
T. Matuzawa[11)]	$v=7{\cdot}55$		
T. Hirano[12)]	$v=7{\cdot}79$		

The great discrepancies, ranging from 7·4 km./sec. to 8·2 km./sec. compelled me to examine it completely. The determination of the velocity of propagation is closely connected not only with the accuracy of observation but also with the structure of earth's interior and the mechnisms of seismic waves.[13)] The theory of isostacy postulate the non-uniform structure of the earth's crust and the relief on the surfacc is said to be ten times magnified at the intersurface of the crust. The effect of sedimentary layers near the surface has recently occupied the interest of many authorities.[14)] As the determination of the velocity by the observation of an earthquake inevitablly relies upon the law of

4) This part was read before the meeting of the Earthquake Research Institute on May 21st 1929, and published (in Japanese) in the "Disin" or the Journ. Soc. Japan. [1 (1929), 477.]

5) K. ZOEPPRITZ und L. GEIGER, "*Über Erdbebenwellen, III,*" Gött., Nachr. math-phys. Kl. (1909).

6) S. MOHOROVIČIĆ, *Beitr. z. Geophys.*, **13** (194), 217., **14** (1916), 187.

7) B. GUTENBERG, *Handbuch d. Geophys*, **4** (1929).

8) V. CONRAD, *Mitt. d. Erdbeben-kommission.*, Wien, **59** (1925). *Beitr. z. Geophys.*, **20** (1928), 240.

9) H. JEFFREYS, *M. N. R. A. S., Geophys. Supple.*, **1** (1926), 385, 483.

10) K. WADATI, *Journ. Met. Soc.*, Japan. ii, **3** (1925), 53; *Geophys. Mag.*, **1** (1927), 89., **1** (1928), 162., **2** (1929), 1.

11) T. MATUZAWA, *Bull. Earthq. Res. Inst.*, **5** (1928), 25., **6** (1929), 205.

12) T. HIRANO, *Kensin Zihô*, **3** (1929), 243.

13) K. SEZAWA, *Bull. Earthq. Res. Inst.*, **3** (1921).

14) B. GUTENBERG, *Beitr. z. Geophys.*, **15** (1926), 51.

A. IMAMURA, F. KISINOUYE, T. KODAIRA, *Bull. Earthq. Res. Inst.*, **7** (1929), 471.

geometrical optics, departure of the mechanism of seismic waves from the proposition of the geometrical optics (wave length being so short that the front can be seen as plane, and origin being one point[15]) should affect the results in some way or another. The variation of velocity in the horizontal direction[16] or the regional variation of velocity cannot be denied beforehand.

To step in the study in these directions means the entrance into quantitative study which sooner or later has to replace the qualitative study that has lost their power at these divergent questions. The accuracy of the observations has hitherto been considered inadequate for these studies, but in reviewing the determination of the origins of earthquakes in 1928 I came across the data[17], with unusual accuracy, of the earthquake on May the 21st, 1928 which originated in Tiba Prefecture, the greatert eathquake in intencity during the year in Japan, with its rich observations near the epicentre as well as at distant stations, and my study was commenced.

Selection of the method.

The determination of the velocity is almost entirely carried out by the analysis of time-distance curve. If the focal depth is zero, the velocity is determined by the Wiechert-Herglotz-Bateman's method. But when the focal depth is taken into consideration, Mohorovičić's method of "reduzierte Laufzeitkurve"[18] with the aid of Wiechert-Herglotz-Bateman's method or the methód of Galitzin[19] is usually employed. But when we use Mohorovičić's method we must know beforehand the velocity distribution from the surface down to hypocentre. As for the Galitzin's method, it also requires the value of the velocity at the surface, moreover

---

15) T. Matuzawa, *Jap. Journ. Astr. Geophys.*, 4 (1926) 1; *Bull. Earthq. Res. Inst.*, 5 (1928), 25.

16) S. Kunitomi, *Journ. Met. Soc.*, Japan. ii, 3 (1925), 55, 176, 281 etc.; *Beitr. z. Geophys.* H. Honda, *Kensin Zihô*, 5 (1931), 111.

17) *Kisyô Yôran*, (1928), This earthquake was also investigated by Mr. S. Sagisaka [*Journ. Met. Soc.*, Japan, ii 6 (1928) 326.] of the Central Meteorological Observatory, and very interesting features of seismograms were noticed in connection to the mechanism of their origin, though the determination of hypocentral depth by the method of von Seebach is not free from objections because earth's crust is not homogeneous. And travel-time T and Epicentral distance Θ have to be corrected by the amount δT and $\delta\Theta$ for the effect of the crust, and δT does not vanish with $\delta\Theta$. So the focal depth deduced by von Seebach's method should be much shallower than it should be when the hypocentre is beneath the crust.

18) S. Mohorovičić, *Beitr. z. Geophys.*, 13 (1914), 217.

19) B. Galitzin, *Vorlesungen*, (1914), 143–147.
K. Wadati, *Geophys. Mag.*, 1 (1928), 162.
H. Kawasumi, *Journ. Met. Soc.*, Japan, ii, 5 (1927).

the series employed is of bad comvergence and observations beyond the inflexion point of time-distance curve cannot be used. In addition to these, all these methods are not free from the practical difficulty to construct time distance curve without arbitrarieness affecting the results. This objection was recently suppressed by Jeffreys' investigation[20] that linear time-distance curves are sufficient for near earthquakes at the present state of observational accuracy. H. Jeffreys identified the surface velocity with the space velocity beneath the surface layers, and this was already objected by S. Mohorovičic.[21] That the depth of hypocentre and the rate of increase of the velocity with the depth should affect the surface velocity is clear *a priori* and will be shown afterwards.

To construct time-distance curve we must know the epicentre. Current procedure of the determination of epicentre other than those in which the durations of preliminaly tremor are used, is that of V. Inglada,[22] i.e. assuming linearity of seismic rays and constant velocity of propagation, the coordinates of epicentre is determined by means of the method of least squares using a few of the observations of time of occurrence. But in the present case several disturving factors and the unknown velocity forgive me to follow the method. Then the Jeffreys' assumption of linearity of time-distance curve may be thought of. And I determined the coordinates of epicentre and the linear time-distance curve by the method of least squares using the observations at epicentral distances between 200 km. and 600 km. But the result was not satisfactory as the time-distance curve constructed using resulted epicentre showed a discontinuity of inclination at the upper boundary, that is $\Delta=600$ km., although the fitting is very good within the domain considered, and surface velocity came out 8·3 km/sec.

At last I was compelled to use all the observations to determin at one time the coordinates of hypocentre, the velocity with its variation with the depth from the surface and the time of occurrence of the earthquake at the hypocentre. In order that the analysis may be as feasible as possible satisfying above requirements I adopted the assumption of circular trajectory of seismic rays, i.e. the velocity of seismic wave within the ultra-basaltic layer is assumed to be

$$v=a-br^2 \quad \text{(1)}^{23)}$$

20) H. JEFFREYS, *M. M. R. A. S., Geopys. Suppl.*, 1 (1927), 385.
21) S. MOHOROVIČIĆ, *Beitr. z. Geophys.*, (1928).
22) V. INGLADA, *Beitr. z. Geophys.*, 19 (1927), 83.
23) M. P. RUDZKI, *Beitr. z. Geophys.*, 3 (1898), 595. **According to Rudzki Aug. Sch-**

Though the legitimacy of this simple assumption is not yet clear, the examination of this assumption and generalzation into $v=a-br-cr^2-\ldots$ will be postponed for future occasions.[24]

The equation of time-distance curve for this case was deduced long ago by E. Rosental[25] in a very elegant form. (Cf. Fig. 1.)

$$t=\frac{1}{4\sqrt{ab}}\left\{\log\frac{1+2K\sqrt{ab}\tan\alpha}{1-2K\sqrt{ab}\tan\alpha}+\log\frac{1+2K\sqrt{ab}\tan(\Theta'-\alpha)}{1-2K\sqrt{ab}\tan(\Theta'-\alpha)}\right\}\ldots \quad (2)$$

where t is the travel time from H (hypocentre) to S' and α is angles indicated in Fig. 1, (the radius OS' is used throughout for the unit of length) and K is a constant of a seismic ray

$$\frac{V}{r}\cos e=\frac{dt}{d\Theta'}=K \quad \ldots(3)$$

The right hand side of the equation (2) was expanded into a very good converging series by E. Rosental.[26]

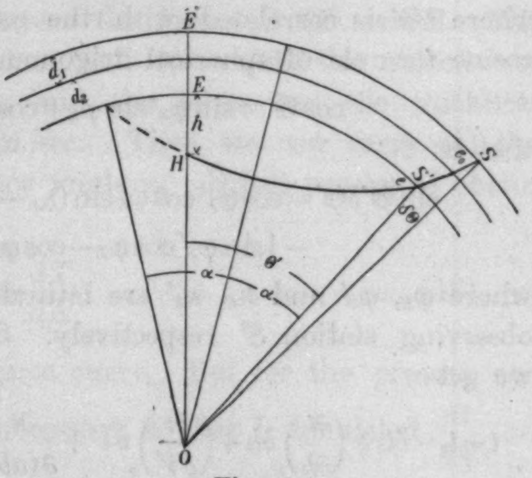

Fig. 1.

$$t=p-\frac{1}{6}abp^3+\frac{3}{40}(ab)p^5-\frac{5}{112}(ab)^3p^7+\ldots\ldots\ldots \quad (4)$$

and $p=d/V$, d being the distance of H and S' and V the geometrical mean of the velocities at the surface and at the hypocentre, that is

$$d=\sqrt{h^2+4(1-h)\sin^2\frac{1}{2}\Theta'} \quad \ldots\ldots\ldots\ldots (5)$$

$$V=\sqrt{(a-b)\{a-b(1-h)^2\}} \quad \ldots\ldots\ldots\ldots\ldots (6)$$

The determination of unkown constants h, V, $\sqrt{ab}$ and time of occurrence of the earthquake at the hypocentre t_0 by method of least

midt assumed circular trajectory as early as 1896.

E. Wiechert, "*Ueber Erdbenwellen,*" Gött. Nachr. math.-phys. Kl. (1907).

E. Rosental, *Beitr. z. Geophys.*, **13** (1914), 28, 106.

24) This point were examined afterwards by the present author to prove the legitimacy of this assumption in Japanese Journ. Astro. Geophys. **9** (1931) 15. see also appendix.

25) E. Rosental, *loc. cit.*

26) As will be supposed from this series this equation is easily shown to be equal to

$$t=\frac{1}{\sqrt{ab}}\ \text{arcsinh}\,\frac{\sqrt{ab}d}{V}.$$

This form was adopted in Chapter III.

squares will be carried out by expanding this formula into Taylor's series, as was deduced by E. Rosental.

$$t-t_0=\delta t_0+\left(\frac{\partial t}{\partial h}\right)_0\delta h+\left(\frac{\partial t}{\partial V}\right)_0\delta V+\left(\frac{\partial t}{\partial(ab)}\right)_0\delta(ab) \quad \ldots\ldots \quad (7)$$

To determine the epicentre, this formula must be extended into

$$t-t_0=\delta t_0+\left(\frac{\partial t}{\partial h}\right)_0\delta h+\left(\frac{\partial t}{\partial V}\right)_0\delta V+\left(\frac{\partial t}{\partial(ab)}\right)_0\delta(ab)+\left(\frac{\partial t}{\partial\Theta'}\right)_0\delta\Theta', \quad (8)$$

where $\delta\Theta'$ is correlated with the coordinates of epicentre through the cosine formula of spherical trigonometry.

$$\cos\Theta'=\sin\varphi_S'\sin\varphi_E+\cos\varphi_S'\cos\varphi_E\cos(\lambda_S'-\lambda_E), \ldots\ldots (9)$$

that is

$$\sin\Theta'\delta\Theta'=\cos\varphi_S'\cos\varphi_E\sin(\lambda_S'-\lambda_E)\delta\lambda_E$$
$$-\{\sin\varphi_S'\cos\varphi_E-\cos\varphi_S'\sin\varphi_E\cos(\lambda_S'-\lambda_E)\}\delta\varphi_E, \quad (10)$$

where φ_E, φ_S' and λ_E, λ_S' are latitudes and longitudes of epicentre and observing station S' respectively. Substituting this into equation (8) we get

$$t-t_0=\delta t_0+\left(\frac{\partial t}{\partial h}\right)_0\delta h+\left(\frac{\partial t}{\partial V}\right)_0\delta V+\frac{\partial t}{\partial(ab)}\delta(ab)+\left(\frac{\partial t}{\partial\lambda_E}\right)_0\delta\lambda_E+\left(\frac{\partial t}{\partial\varphi_E}\right)_0\delta\varphi_F, \quad (11)$$

where

$$\left.\begin{aligned}
&\frac{\partial t}{\partial h}=\frac{1}{Vd}\cdot f\cdot\left(h-\sin^2\frac{1}{2}\Theta'\right)\\
&\frac{\partial t}{\partial V}=-\frac{p}{V}\cdot f\\
&\frac{\partial t}{\partial(ab)}=-\frac{1}{6}p^3+\frac{3}{20}abp^5-\frac{15}{112}(ab)^2p^7+\ldots\\
&\frac{\partial t}{\partial\lambda_E}=\frac{-2(1-h)}{Vd}\cdot f\cdot\cos\varphi_S\cos\varphi_E\sin(\lambda_S-\lambda_E)\\
&\frac{\partial t}{\partial\varphi_E}=\frac{2(1-h)}{Vd}\cdot f\cdot\{\sin\varphi_S\cos\varphi_E-\cos\varphi_S\sin\varphi_E\cos(\lambda_S-\lambda_E)\}\\
&f=1-\frac{ab}{2}p^2+\frac{2}{8}(ab)^2p^4-\frac{5}{16}(ab)^3p^6+\ldots
\end{aligned}\right\} \quad (12)$$

Effect of the surface crust and reduction to the level surface of the ultra-basaltic layer.

To carry out the above procedure, it is necessary to remove the effect of the crust which does not satisfy the condition expressed in

equation (1). For this purpose the observation on the earth's surface must be reduced to the level surface of the ultra-basaltic layer. The structure of the earth's crust in Japan has been well studied by Prof. T. Matuzawa[27], and if at most numerical values may require some modifications, the problem under consideration is to study the propagation of P-wave beneath the crust, and simple assumption will not be fatal to the present purpose. So I will assume following Prof. Matuzawa, that the crust consists of two layers the first and the second. The former has the thickness $d_1=20$ km. and in which the velocity of longitudinal wave $v_1=5.0$ km./sec., and the latter has the thickness $d_2=30$ km. and velocity $v_2=6.1$ km./sec. Then we can carry out the reduction if we know the emergency angle e_0. Direct process to obtain $\cos e_0$ is by the formula

$$\cos e_0 = v_0 \cdot \frac{dT}{d\Delta} \quad \ldots\ldots\ldots\ldots\ldots\ldots (13)$$

calculating $\frac{dT}{d\Delta}$ from the time distance curve. But for the present analysis by the equation (11) $\frac{\partial t}{\partial \theta'}$ is necessary, so that I calculated $\frac{dt}{d\theta'}$ on the earth's surface and thence the travel time δt and distance $\delta\theta$ from S to S' are calculated and represented graphycally as functions of epicentral distance on the earth's surface

$$\theta = \theta' + \delta\theta \ldots\ldots\ldots\ldots\ldots\ldots\ldots\ldots (14)$$

$\delta\theta$ and δt for every station were determined from this graph. Next azimuths, A, of epicentre at the stations were calculated and $\delta\theta$ was decomposed into $\delta\varphi_s$ and $\delta\lambda_s$ and the position was reduced to the level surface of ultra-basaltic layer at the depth of 50 km. by the following formulae.

$$\left.\begin{aligned} \sin A &= \frac{\cos\varphi_E \sin(\lambda_S - \lambda_E)}{\sin\theta'} \\ \delta\varphi_S &= \delta\theta \cos A \\ \delta\lambda_S &= \delta\theta \sin A / \cos\varphi_S \end{aligned}\right\} \ldots\ldots\ldots\ldots (15)$$

$$\left.\begin{aligned} \varphi_S' &= \varphi_S - \delta\varphi_S \\ \lambda_S' &= \lambda_S - \delta\lambda_S \\ T_S &= T - \delta t \\ \theta' &= \theta - \delta\theta. \end{aligned}\right\} \ldots\ldots\ldots\ldots (16)$$

27) T. Matuzawa, *Bull. Earthq. Res. Inst.*, **5** (1928), 25; **6** (1929).

Numerical calculation.

Now that the method has been determined, to step into the numerical calculation I have only to know the coordinates of hypocentre and the velocity (with its variation with depth) and time of occurrence of the earthquake at the hypocentre approximately.

I take the values stated above which were determined by the assumption of linear time-distance curve as the epicentre and depth was estimated from the duration of preliminary tremor near the epicentre. V and (ab) are determined tentatively to fit the observation approximately. The assumed values are as follows:

$$\lambda_E=140^\circ\ 01'\ E$$
$$\varphi_E=35^\circ\ 35'\ N$$
$$h=0{\cdot}003$$
$$V=0{\cdot}00124$$
$$ab=0{\cdot}00004$$
$$t_0=1^h\ 29^m\ 11^s{\cdot}0 \text{ (Local mean time of longitude } 135^\circ E)$$

where t_0 is determined to annul the difference of the observation at Tokyo and the calculated value with the above assumption.

Now I will tabulate the data, taken from the Kisyô Yôran, and important values in the course of calculation in the following Tables. The epicentral distance θ in table I is the distance from the resulting epicentre calculated by the cosine formula of spherical trigonometry, but θ_0' in Table II is that from the epicentre assumed above.

Compiling these data into time-distance curve and 39 stations where observations seemed accurate were at first selected, and after one trial of least square solution, 33 stations were at last adopted and complete calculations were performed as follows.

Table I. The data of the earthquake on May 21, 1928, which originated in Tiba prefecture.

Station	Θ	$T_{(ob)}$	Station	Θ	$T_{(ob)}$
	° ′	h m sec		° ′	h m
Tôkyô	29	1 29+23·1	Kakioka	50·5	24·8
Yokohama	29	24·6	Kumagaya	59	28·5
Mera	35	25·6	Mito	1 00	25
Tyôsi	36	26·3	Utunomiya	1 11	28·9
Tukubasan	49	27·4	Numadu	1 11	33·0

(to be continued.)

Table I. (*continued.*)

Station	Θ (°)	Θ (′)	$T_{(ob)}$ (sec)	Station	Θ (°)	Θ (′)	$T_{(ob)}$ (sec)
Maebasi	1	22	30·0	Toyooka	4	24	74·6
Kôhu	1	22	27·4	Miyako	4	26	77
Onahama	1	35	45·0	Sumoto	4	31	77·2
Oiwake	1	37	38·4	Tokusima	4	51	89·5
Iida	1	57	44·3	Tadotu	5	25·5	$96(+1^m)$
Matumoto	1	59	52	Muroto	5	27	$83(+1^m)$
Nagano	2	04	43·6	Sakai	5	36	109·3
Hamamatu	2	08	33	Kôti	5	49	96·1
Aidu	2	08	48	Okayama	5	50	74·7
Takada	2	19	48·6	Hakodate	6	23·5	121
Hukusima	2	20	47	Hirosima	6	27·5	105·3
Hatizyozima	2	20		Hamada	6	41·5	109·2
Takayama	2	31	46·6	Muroran	6	57	110·0
Niigata	2	40	42·6	Ooita	7	25·5	120·0
Nagoya	2	41	52·7	Obihiro	7	40	129
Gihu	2	49	58·6	Sapporo	7	43	122·5
Yamagata	2	51	50·5	Simonoseki	7	47	166
Sendai	2	53	54·1	Miyasaki	8	06	128·8
Husiki	2	53	47·7	Kusiro	8	14	
Tu	3	07	46·2	Hukuoka	8	17	130·8
Kanazawa	3	07	52·3	Kumamoto	8	19	139·8
Isinomaki	3	09	52·3	Titizima	8	28·5	131·0
Hikone	3	15	64·8	Asahigawa	8	32·5	154
Hukui	3	18	78	Unzendake	8	39	141·8
Kyôto	3	41	66·0	Nemuro	8	56	140·2
Yagi	3	44	66·0	Nagasaki	8	59	139·6
Midusawa	3	48	68	Haboro	9	03	137
Miyadu	3	58	118·5	Ituhara	9	03·5	150·4
Oosaka	4	00	74·2	Husan	9	09·5	150
Siomisaki	4	09	65·5	Zinsen	11	19·5	169·5
Kôbe	4	11	72·9	Ootomari	11	23·5	184·8
Akita	4	17	76·7	Taihoku	19	10	
Wakayama	4	20	75·0	Kôsyun	21	37·5	285·9
Morioka	4	22	75·1				

Table II.

Station	Θ_0 (°)	(′)	$\delta\Theta$ (′)	δt (sec)	$\delta\lambda_s$ (′)	$\delta\varphi_s$ (′)	t_{cal} (sec)	t_0-t_c (sec)	ε (sec)
Tôkyô		14·5	9·4	9·42	10·4	4·1	12·1	0	−0·88
Yokohama		20·0	12·4	9·80	10·3	51·5	12·8	0·8	−0·83
Mera		40·8	22·0	11·43	5·9	21·5	16·5	−1·9	1·91
Tyôsi		41·6	22·2	11·46	26·7	4·7	16·1	−1·3	2·68
Kakioka		40·0	21·8	11·40	5·5	21·3	16·3	−2·5	−2·04
Kumagaya		46	23·3	11·70	19·4	17·3	17·5	0·0	−0·63
Oiwake	1	25·1	27·0	12·54	28·2	14·6	26·4	1·0	1·25
Nagano	1	49·7	27·8	12·66	28·0	16·4	32·0	0·6	0·75
Takada	2	05·1	27·9	12·69	24·1	20·2	35·6	2·0	1·94
Hukusima	2	11·5	28·0	12·70	5·0	27·7	37·0	−1·0	0·46
Takayama	2	17·3	28·0	12·71	34·1	5·2	38·4	−2·8	−2·36
Nagoya	2	29·3	28·0	12·72	34·6	2·3	41·2	0·6	2·06
Sendai	2	46·7	28·0	12·72	9·2	27·0	45·2	−2·1	−0·40
Kyôto	3	32·4	28·0	12·72	33·6	5·0	55·0	0·0	0·93
Yagi	3	36·8	28·0	12·72	32·2	8·9	56·9	−1·9	−0·16
Midusawa	3	39·8	27·9	12·72	8·9	27·0	57·7	−0·7	0·63
Kôbe	4	32	27·9	12·70	32·9	7·0	63·1	0·0	−0·14
Wakayama	4	13·0	27·9	12·70	31·7	9·6	65·4	−1·4	−0·09
Morioka	4	13·5	27·8	12·70	7·9	27·1	65·5	−1·3	−0·69
Toyooka	4	14·5	27·8	12·70	34·0	2·3	65·7	−2·1	−2·10
Miyako	4	21·4	27·8	12·69	13·3	25·9	67·3	−1·3	0·17
Sumoto	4	23·3	27·8	12·69	32·0	8·6	67·7	−1·5	−0·28
Kôti	5	42·7	27·7	12·61	30·7	10·7	86·1	−1·0	−0·05
Hirosima	6	19·3	27·3	12·58	32·2	6·4	94·6	−0·3	0·34
Hamada	6	31·2	27·2	12·56	32·9	3·7	97·4	−0·8	−0·83
Ooita	7	19	27·0	12·50	30·1	9·7	108·3	−0·6	−0·27
Sapporo	7	33·5	26·9	12·49	5·3	26·6	111·7	−0·2	−0·22
Miyasaki	8	01·7	26·7	12·46	27·4	13·1	118·1	−0·3	0·48
Hukuoka	8	08·7	26·7	12·45	30·7	7·7	119·7	0·1	−0·02
Nemuro	8	54·0	26·4	12·38	18·5	22·7	130·0	−0·8	0·08
Nagasaki	8	51·8	26·4	12·39	29·2	9·7	129·5	−0·9	−0·67
Zinsen	11	02·5	25·5	12·18	31·9	2·6	159·0	−0·5	−1·40
Kôsyun	21	34·9	21·2	11·3	16·7	14·5	292·6	−7·7	0·36

First the observations were reduced to the level surface at the depth of 50 km. as stated above by the formulae (15) and (16), and travel-times

were calculated by the formula (4), and t_0-t_c were obtained. (Table II)

Then $\frac{\partial t}{\partial h}, \frac{\partial t}{\partial V}, \frac{\partial t}{\partial(ab)}, \frac{\partial t}{\partial\lambda_E} \frac{\partial t}{\lambda\varphi_E}$ were calculated for these stations, and normal equations of (8) were determined whose numerical coefficients are tabulated in Table III, where simplicities sake a, b, c, d, e, and f were used for the coefficients of δt_0, δh, δV, $\delta(ab)$, $\delta\lambda_E$ and $\delta\varphi_E$ respectively, and l stands for t_0-t_c.

Table III. Coefficients of normal equation.

[aa] 33	[ab] 3·076	[ac] −15·379	[ad] −5·215	[ae] 11·479	[af] −5·631	[al] −30·8
	[bb] 1·573	[bc] 0·296	[bd] 0·443	[be] 0·497	[bf] −0·683	[bl] −0·692
		[cc] 12·881	[cd] 8·071	[ce] −6·242	[cf] 0·441	[cl] 25·249
			[dd] 9·645	[de] −2·324	[df] −0·901	[dl] 24·634
				[ee] 7·915	[ef] 1·571	[el] −8·215
					[ff] 7·873	[fl] −0·716

Solving the normal equations we get the following results. The residuals (ε) of the observational equations are tabulated in the last column of table II, and the sum of which comes out −0·02sec. proving the accuracy of calculations.

$\delta t_0 = -4{\cdot}89^{\text{sec}} \pm 0{\cdot}74^{\text{sec}}$ (P.E.) $\qquad 10^6 \times \delta(ab) = 4{\cdot}2 \pm 0{\cdot}6$ (P.E.)

$10^3 \times \delta h = 6{\cdot}3 \pm 1{\cdot}5 \qquad 10^3 \times \delta\lambda_E = 3{\cdot}8 \pm 0{\cdot}8$

$10^5 \times \delta V = 4{\cdot}7 \pm 1{\cdot}1 \qquad 10^3 \times \delta\varphi_E = -3{\cdot}1 \pm 0{\cdot}6$

Thus the coordinates of hypocentre and the time of occurrence at the origin and the velocity come out as follows:

$t_0 = 1^{\text{h}}\ 29^{\text{m}}\ 6{\cdot}1^{\text{sec}} \pm 0{\cdot}7^{\text{sec}}$ (P.E.)

$\lambda_E = 140°\ 14' E \pm 2'{\cdot}5$

$\varphi_E = 35°\ 24' N \pm 1'{\cdot}9$

hypocentral depth $= 108{\cdot}8^{\text{km}} \pm 9{\cdot}5^{\text{km}}$

$V = 0{\cdot}001193 \pm 0{\cdot}00011 = 7{\cdot}55 \pm 0{\cdot}07$ km./sec.

$v = 0{\cdot}003509 - 0{\cdot}002337\, r^2$ ....(17)

Probale error of individual observation comes out

$$\rho = 0{\cdot}6745\sqrt{\frac{[\varepsilon\varepsilon]}{33-6}} = 0{\cdot}85 \text{ sec.}$$

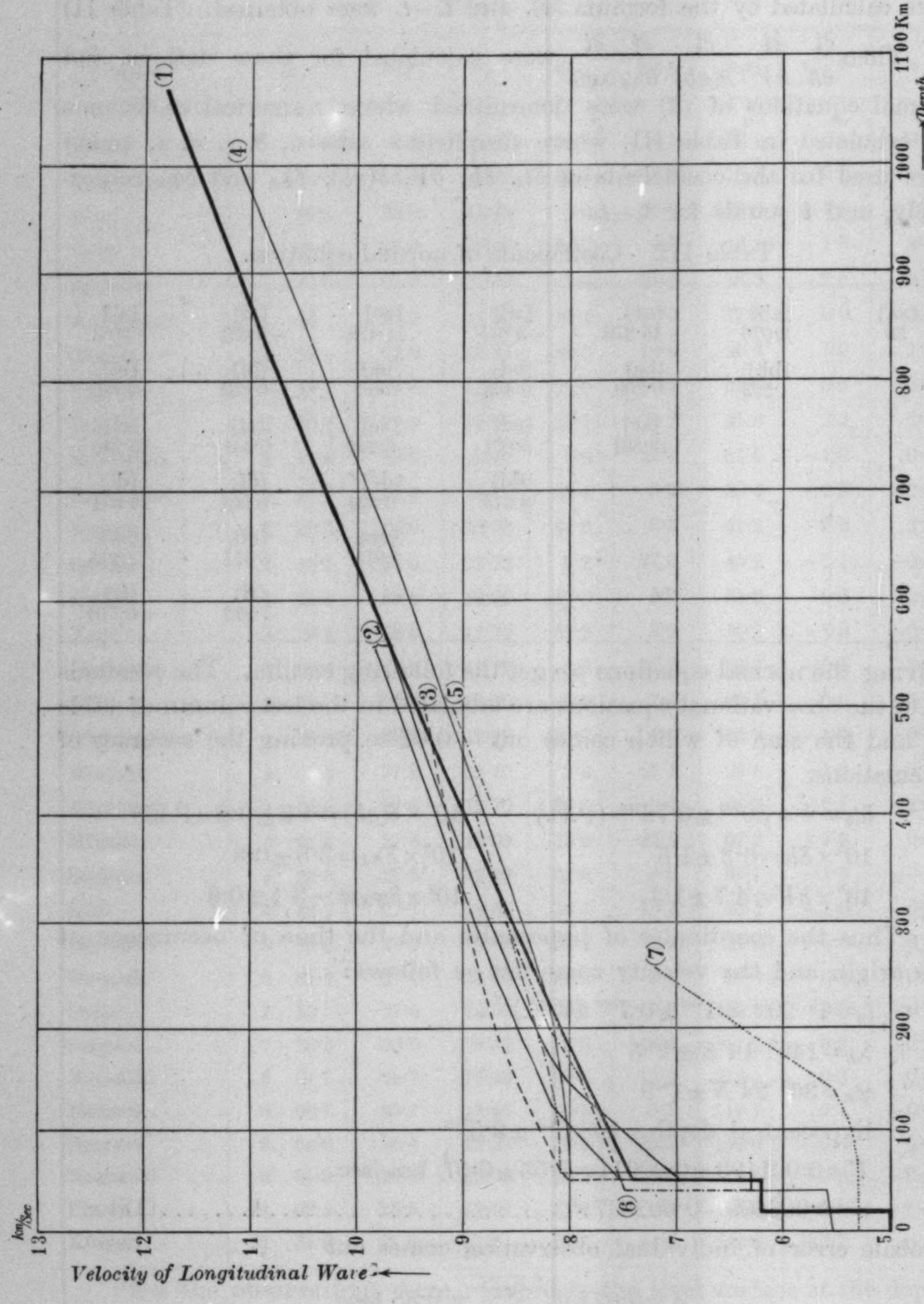

Fig. 2. Comparison of the velocity here obtained with those of senior anthorities.

(1) Results obtained in Chapter I.
(2) By Prof. T. Matuzawa.
(3) By Dr. K. Wadati.
(4) By Prof. B. Gutemberg.
(5) By Prof. S. Mohorovicic.
(6) Mean value obtained by K. Sagisaka.
(7) By Prof. Saem Nakamura.

and among the 33 observations used in the above calculation a half of them is expected to have smaller errors than this value. This number actually comes out 23, to prove the accuracy, amounting more than two thirds of the total.

Discussion of the results.

Seeing the results we may conclude that the accuracy of observations in Japan which have hitherto been depreciated is sufficient for these quantitative study, and the accuracy of the resulting values seems never inferior to European determinations.

The velocity within the earth calculated from the formula (17) are shown in graphical representation side by side with the former determinations of senior authorities. (Fig. 2)

The velocity at the boundary of the ultra-basaltic layer comes out

$$v=0{\cdot}001172=7{\cdot}41 \text{ km./sec.}$$

and is smaller than current values of European authorities. (Cf. p 9.5) I have discussed on the values determined from the surface velocity, which are always larger than the actual space velocity. The value obtained here coincides with the smallest recent values of H. Jeffreys from the Kulpa Vally Earthquake on Oct. 8, 1908, and very near to the values of Prof. T. Matuzawa and former values of Dr. K. Wadati, 7·5 km./sec. This seems to account the legitimacy of the present determination which is the first quantitative determination ever made. I will here present a comparison of the values of travel-times calculated (T_{cal}) from the resulting values with those actually observed including all the other stations than those considered in the above analysis, in Table IV. The frequency curve of the residuals in Table IV (Fig. 3) shows very conspicuous accumulation of the residuals at zero and nearly symmetrical to the maximum, proving legitimacy of present enumeration.

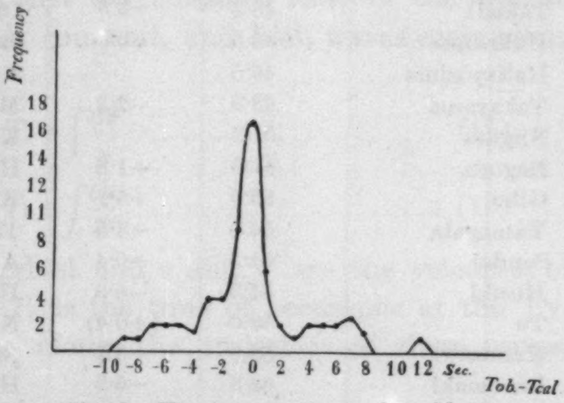

Fig. 3. Frequency curve of residuals.

Table IV. Comparison of the values of arrival times of P-wave observed with those calculated from the constants of least square solution.

Station	T_{cal}	$T_{ob}-T_{cal}$	Station	T_{cal}	$T_{ob}-T_{cal}$
	h 1 m 29+ sec	sec		h 1 m 29+ sec	sec
Tôkyô	24·6	−1·5	Siomisaki	72·7	−7·2
Yokohama	24·6	0	Kôbe	73·2	−0·3
Mera	25·4	+0·1	Akita	74·6	+2·1
Tyôsi	25·5	+0·8	Wakayama	75·2	−0·2
Tukubasan	27·6	−0·2	Morioka	75·8	−0·7
Kakioka	27·8	−3·0	Toyooka	76·2	−1·6
Kumagaya	29·5	−1·0	Miyako	76·7	+0·3
Mito	29·7	−4·7	Sumoto	78·0	−0·8
Utunomiya	32·0	−3·1	Tokusima	82·5	+7·0
Numadu	32·0	+1·0	Tadotu	90·9	(+5·9)
Maebasi	34·2	−4·2	Muroto	91·3	(−8·3)
Kôhu	34·2		Sakai	93·4	+15·9
Onahama	36·9		Kôti	96·4	−0·3
Oiwake	37·4	+1·0	Okayama	96·6	
Iida	41·6	+2·7	Hakodate	104·5	+16·5
Matumoto	42·0	+10·0	Hirosima	106·5	−1·2
Nagano	43·1	+0·5	Hamada	108·7	+0·5
Hamamatu	43·9	−10·9	Muroran	112·4	−2·4
Aidu	43·9	+4·1	Ooita	119·0	+1·0
Takada	46·3	+2·3	Obihiro	122·4	+6·6
Hukusima	46·5	+0·5	Sapporo	123·1	−0·6
Hatizyôzima	46·5		Simonoseki	124·1	
Takayama	48·9	−2·3	Miyasaki	128·4	+0·4
Niigata	51·2		Kusiro	130·2	
Nagoya	51·5	+1·2	Hukuoka	130·9	−0·1
Gihu	53·5	+5·1	Kumamoto	131·4	+8·4
Yamagata	54·0	−3·5	Titizima	133·6	−2·6
Sendai	54·5	−0·4	Asahigawa	134·5	+19·5
Husiki	54·5	−6·8	Unzendake	136·0	+5·8
Tu	58·0	(+0·4)	Nemuro	139·8	+0·4
Kanazawa	58·0	−5·7	Nagasaki	140·6	−1·0
Isinomaki	58·5	−6·2	Haboro	141·6	−4·6
Hikone	60·0	+4·8	Ituhara	141·7	+8·5
Hukui	60·6	(+17·4)	Husan	142·5	+7·5
Kyôto	66·2	−0·2	Zinsen	172·0	−2·5
Yagi	66·9	−0·9	Ootomari	172·8	+12·0
Midusawa	67·8	+0·2	Taihoku		
Miyadu	70·1		Kôsyun	285·7	+0·3
Oosaka	70·6	+3·6			

Chapter II. Determination of the velocity of S-wave.[28]

Velocity of S-wave (*undae normal secundae*) from near earthquake have been obtained from the inclination of linear time-distance curve and, as is necessary the case from the assumption, the values varies in so wide a range that, as for P-wave, the variation of the velocity within the earth must be taken into consideration. But identification of S phase in near earthquake is very difficult owing to the complexity of the mecanism of its origin and interference with the surface waves. And the classification of the phases into the preliminary tremor and principal portion is very umbiguous and so called duration of preliminary tremor has very much complicated meanings. Elucidation from the complexity of the waves propagated through the different paths through stratified layers has been done by Prof. T. Matuzawa[29] and Mr. Hayata,[30] and others. Though the surface waves in near earthquake have not yet been decidedly identified, these will also have to be taken into account to the enunciation of principal portion, and this being now under investigation the results will be reported in near future.

Under these circumstances the determination of the velocity variation of the S-wave within the earth is less accurate than that of P-wave. But I found a linear relation between the time of occurrence of P-wave and the duration of preliminary tremor or the travel-time difference of S- and P-wave in near earthquake within the accuracy of present observations. From this we know that the Poisson's ratio or the ratio of the velocities of P- and S-wave is constant, and both waves come along the same path.

$$T_p = T_0 + \int \frac{ds}{v} \quad \text{.................... (18)}$$

$$T_s = T_0 + \int \frac{ds}{V} \quad \text{.................... (19)}$$

where T_p and T_s are times of arrival and v and V are the velocities of P- and S-wave respectively and T_0 is the time of occurence at the hypocentre and S is the distance along the trajectory of these waves. Then we have

$$T_s - T_p = \int \frac{1}{v}\left(\frac{v}{V} - 1\right) ds \equiv \tau \quad \text{.............. (20)}$$

or

28) Read before the meeting of Earthquake Research Institute on Feb. 17, 1931.

29) T. Matuzawa, *Bull. Earthq. Res. Inst.*, 6 (1929), 177.

30) Hayata, *Kensin Zihô*, 4 (1930), 17–43, (Reprint).

$$\tau=\left(\frac{v}{V}-1\right)(T_p-T_0). \quad \ldots\ldots\ldots\ldots\ldots\ldots \quad (21)$$

As the velocity of P-wave has been determined in chapter I, we can know that of S-wave if we determine the ratio of the velocities by the equation (21).

Through the kindness of the director of the Central Meteorological Observatory I was able to examine photographic copies of the seismograms obtained at 24 stations in Japan due to the earthquake on May 21, 1928, which has been dealt with in preceding chapter.

Examining these copies the author read off several phases and plotting the time intervals from P phase to these phases against the time of arrival of P phase. The discrimination of S phase from other phases is very easy by this diagram. The points representing the travel-time difference of S- and P-wave fairly lies on a straight line (Fig. 4). Leaving aside comments of other phases for the present, this line was determined by the method of least squares from the data of τ

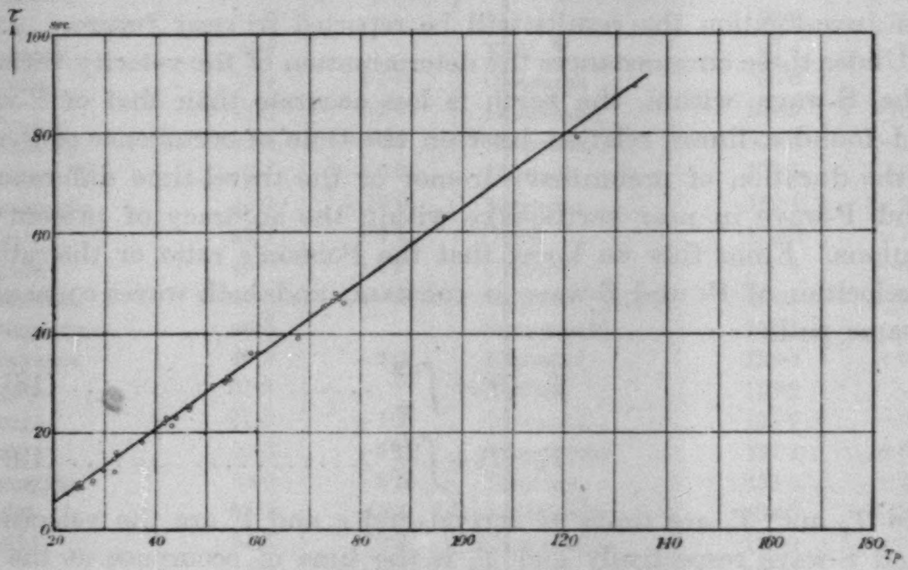

Fig. 4. $\tau-T_p$ Diagram of the earthquake, of May 21, 1928.

observed above supplemented with those reported in Kisyô Yôran where copies were not at my disposal, and for arrival-times of P were used firstly the values calculated by me in capter I (Table IV) ($T_{p(cal)}$) and secondly the values actually observed ($T_{p(ob)}$) supplemented by those calculated where the errors seemed great. The data and results are as follows.

Table V.

Station	$T_{p(cal)}$	$T_{p(ob)} - T_{p(cal)}$	τ	ΔT_p
	sec	sec	sec	sec
Tôkyô	24·6	−1·5	8·7	0·5
Yokohama	24·6	0·0	9·6	−0·7
Mera	25·4	0·1	9·9	−0·3
Tyôsi	25·5	0·8	8·8	1·2
Tukubasan	27·6	−0·2	9·6	2·3
Kakioka	27·8	−3·0	10·0	1·9
Kumagaya	29·5	−1·0	12·6	0·1
Mito	29·7	−4·7	12·3	0·7
Utunomiya	32·0	−3·1	12·0	−3·4
Numadu	32·0	1·0	14.7	−0·3
Maebasi	34·2	−4·2	16·0	0·2
Kôhu	34·2		16·0	0·2
Oiwake	37·4	1·0	18·0	0·7
Iida	41·6	2·7	22·0	−0·5
Matsumoto	42·0	10·0	23	−1·5
Nagano	43·1	0·5	21·4	1·8
Hamamatu	43·9	−10·9	23	0·4
Takada	46·3	2·3	25·5	−0·6
Hukusima	46·5	0·5	24·9	0·4
Hatidyôzima	46·5		25·5	−0·4
Niigata	51·2		29·5	−1 1
Gihu	53·5	5·1	30·0	0·5
Yamagata	54·0	−3·5	31·2	−0·6
Sendai	54·5	−0·4	30·7	0·6
Isinomaki	58·5	−6 2	36·2	−2·9
Hikone	60·0	4·8	36·0	−1·1
Midusawa	67·8	0·2	39·0	2·6
Siomisaki	72·7	−7·2	45·3	−1·0
Kôbe	73·2	−0·3	45·7	−1·1
Akita	74·6	2·1	46·5	−0·8
Wakayama	75·2	−0·2	48	−2·2
Morioka	75·8	−0·7	47·0	−0·2
Miyako	76·7		46	2·0
Kôti	96·4	−0·3	63·0	−1·3
Obihiro	122·4	6·6	79	3·0
Titizima	133·6	−2·6	89·3	0·2

$$T_p = 12{\cdot}33^{\text{sec}} + \frac{\tau}{0{\cdot}738} \quad \text{for the first case}$$

$$\pm 0{\cdot}44^{\text{sec}} \pm 0{\cdot}007$$

and

$$T_p = 12{\cdot}13^{\text{sec}} + \frac{\tau}{0{\cdot}736} \quad \text{for the second case.}$$

Thus the ratio of the velocities of P- and S-wave comes out

$$\frac{v}{V}=1\cdot738\pm0\cdot007 \quad \text{or} \quad 1\cdot736,$$

and Poisson's ratio

$$\sigma=0\cdot2524 \quad \text{or} \quad 0\cdot2516$$

The velocity of S wave at the boundary of the crust comes out 4·26 km./sec. from the values of $v_0=7\cdot41$ km./sec. obtained in chapter I by deviding with 1·738.

The above values somewhat differ from those by European Seismologists[31] and sole result will be subjected to suspition of its accuracy. The τ, T_p diagrams have hitherto been expediently used for the descrimination of τ from others among so called duration of preliminary tremor and for discerning the accuracy of time of occurrence of earthquakes occurred of late in Japan. The innacuracy of T_p causes some divergence of points in the diagrams, but systematic grouping on a straight line with $\frac{d\tau}{dT_p}=07\cdot4$, 0·73 were conspicuous as will be seen from the following table and frequency curve of $(v/V-1)$ i.e. $\frac{d\tau}{dT_p}$. (Table VI; Fig. 5)

Table VI

Earthquake				$\frac{d\tau}{dT_p}=(v/V-1)$				
Date			Epicentre					
1927	I	15	Off the promontory Kyôgasaki	0·73				
1927	II	27	Off the island Hatidyô-zima	0·70				
1926	V	20	Near Titibu	0·73	0·83		1·15	
1927	VI	18		0·72				
1927	VIII	6	Off the Mouth of the River Abukuma		0·80		1·15	
1928	II	12	The Kogaigawa	0·72		0·99	1·14	
1928	III	29	Off the island of Hatidyo-zima	0·71		1·04		
1928	V	21	Tiba prefecture	0·73		0·95	1·12	1·20
1928	IX	23	Bay of Koidumi	0·72			1·15	
1928	IX	25	Suô-nada	0·73			1·15	

(to be continued.)

31) K. Zöppritz and L. Geiger, $\sigma=0\cdot272$ $v/V=1\cdot79$
B. Guttenberg, $v/V=1\cdot789$
H. Jeffreys, $v/V=7\cdot8/4\cdot35=1\cdot79$

Table VI. (*continued.*)

Earthquake				$\frac{d\tau}{dT_p}=(v/V-1)$		
Date			Epicentre			
1928	XII	14	Off the coast of Kudyûkuri	0·70	1·03	1·15
1929	I	9	Kasima-nada	0·71		1·14
1929	I	21	The Sakawagawa	0·72(0·47?)	0·94	
1929	II	24	N.E. off the promontory Siriyazaki	0·73		
1929	IV	16	Kasimanada	0·72	0.98	
1929	IV	18	Kasimanada	0·75	0·98	
1929	IV	23	The Kogaigawa	0·77		
1929	VI	3		0·73	0·79	
1929	VII	27	Mount Tanzawa		0·81	1·16
1929	VIII	8	Hukuoka	0·69		
1629	VIII	16	Near promontory Erimozaki	0·74	0·95	1·15
1929	IX	20		0·73		1·13
1929	X	6	Near promontory Otiisi	0·73	0·84	
1929	X	10	Mount Aso	0·74		
1929	X	25	Mount Unzendake	0·73	0·93	
1929	X	28			0·96	
1930	VII	27	Sagami	0·75		
1930	VIII	17	Uraga strait	0·76		
1930	VIII	21	S. off the promontory Erimozaki	0·78		
1930	VIII	26	S. off the promontory Erimozaki	0·74		
1930	IX	29	Bay of Kagosima	0·74		

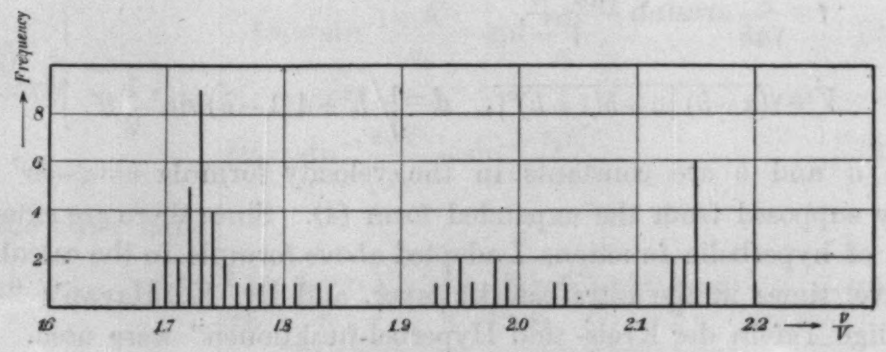

Fig. 5. Frequency curve of $\frac{v}{V}=1+\frac{d\tau}{dT_p}$

It will, thus, be concluded that at least in the region near this country the material of the earth to a depth of about a few hundred kilometres does not much differ from the Poisson's hypothesis, or in other words, the Poisson's ratio is $\frac{1}{4}$ and the velocity of P-wave is about $\sqrt{3}$ times of that of S-wave.

The result will be of some interest and convenience from the theoretical point of view. Thus the velocity of S-wave to presumablly a depth of 1200 km. will be expressed by

$$V=\frac{1}{\sqrt{3}}(0{\cdot}003509-0{\cdot}002337\,r^2)$$

in the unit earth's radius per second.

Chapter III. Provisional Calculation of Time-distance Curves for various Hypocentral Depths up to 500 km.[32]

In chapter I and II, I have determined the velocity of P- and S-wave in the ultra-basaltic layer, and as I have shown there, the results agrees torerablly well with those determined from distant earthquakes by Prof. S. Moharovičić and Prof. B. Gutenberg, and moreover travel times of P-wave up to 2000 km. by Prof. T. Matuzawa nearly coincide with those calculated from the values above obtained. I, therefore, determined to calculate time-distance curves for the sake of convenience for our further study with the method used in preçeding chapters. The mear results of my present calculation will also find some merit in practical use as a first apploximation. So I will present them here.

The equation of time-distance curve (2) in Chapter I by E. Rosental may be easilly transformed into

$$\left.\begin{aligned} &t=\frac{1}{\sqrt{ab}}\operatorname{arcsinh}\frac{\sqrt{ab}\cdot d}{V},\\ &V=\sqrt{(a-b)\{a-b(1-h)^2\}},\quad d=\sqrt{h^2+4(1-h)\sin^2\frac{1}{2}\theta'} \end{aligned}\right\}\qquad(22)$$

where a and b are constants in the velocity formula $v=a-br^2$ as is clearly supposed from the expanded form (4). Since there are extensive tables of hyperbolic functions I adopted above formula in the calculation of travel times in the ultra-basaltic layer, and Dr. K. Hayasi's "Siebenstellige Tafeln der Kreis- und Hyperbel-funktionen" were used.

32) Read before the meeting of the Earthquake Research Institute on Feb. 18, 1931.

The travel times in the ultra-basaltic layer t to epicentral distance θ' of every $20'$ of arc up to $\theta'=15°$ are calculated for 19 hypocentral depths(h) of every $0{\cdot}004R$ from $h=0$ to $h=0{\cdot}072R$, where R stands for the radius of the surface of ultra-basaltic layer ($R=6321$ km.). The results are tabulated in Table VII at the end of this paper.

For the sake of convenience of direct application to observed data, the travel times up to the earth's surface are calculated upon the same assumption as in chapter I, following Prof. Matusawa, though some discrepancies of opinion concerning the structure of the earth's crust near Japan are existing. The procedure is just the same as in chapter I, but as I have not given accunt about this, I will give here briefly.

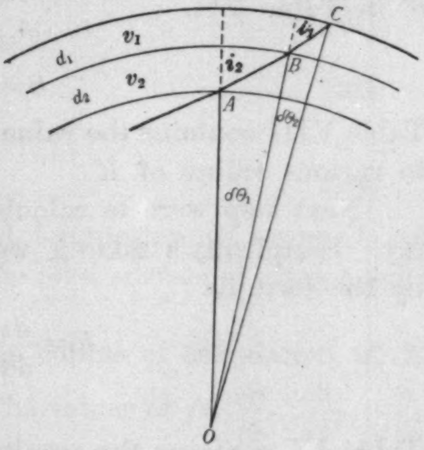

Fig. 6.

From the equation of seismic ray

$$\frac{r}{v}\sin i=\frac{dT}{d\theta}=\frac{dt}{d\theta'}=K \ldots. \quad (23)$$

follows (see Fig. 6, $OC=r_0$, $OB=r_1$, $OA=r_2$)

$$\left.\begin{aligned} i_1&=\sin^{-1}\frac{v_1}{r_1}K \\ i_2&=\sin^{-1}\frac{v_2}{r_2}K \end{aligned}\right\} \ldots\ldots\ldots\ldots\ldots\ldots\ldots \quad (24)$$

and from the triangle OBC

$$\frac{\sin i_1}{r_0}=\frac{\sin(i_1-\delta\theta_1)}{r_1} \ldots\ldots\ldots\ldots\ldots\ldots \quad (25)$$

Then

$$\delta\theta_1=\sin^{-1}\frac{v_1K}{r_1}-\sin\frac{v_1K}{r_0} \ldots\ldots\ldots\ldots\ldots \quad (26)$$

Similarly

$$\delta\theta_2=\sin^{-1}\frac{v_2K}{r_2}-\sin^{-1}\frac{v_2K}{r_1} \ldots\ldots\ldots\ldots\ldots \quad (27)$$

On the other hand

$$\delta t_1=\frac{1}{v_1}\sqrt{\left(\frac{r_0-r_1}{r_0}\right)^2+4\left(1-\frac{r_0-r_1}{r_0}\right)\sin^2\frac{1}{2}\delta\theta_1} \ldots\ldots \quad (28)$$

$$\delta t_2=\frac{1}{v_2}\sqrt{\left(\frac{r_1-r_2}{r_1}\right)^2+4\left(1-\frac{r_1-r_2}{r_1}\right)\sin^2\frac{1}{2}\delta\theta_2} \ldots\ldots \quad (29)$$

The correction to travel time and epicentral distance due to the earth's crust are accordingly,

$$\left.\begin{aligned}\delta\theta&=\delta\theta_1+\delta\theta_2\\ \delta t&=\delta t_1+\delta t_2\end{aligned}\right\}\quad\cdots\cdots\cdots\cdots\cdots\cdots\cdots\quad(30)$$

and we can get the travel time (T) and epicentral distance (θ) from the hypocentre to the earth's surface by adding these correction to t and θ' in Table VII.

$$\left.\begin{aligned}T&=t+\delta t\\ \theta&=\theta'+\delta\theta'\end{aligned}\right\}\quad\cdots\cdots\cdots\cdots\cdots\cdots\cdots\quad(31)$$

Table VIII contains the value of $\delta\theta_1$, $\delta\theta_2$, $\delta\theta$, δt_1, δt_2 and δt corresponding to various values of K.

Next step were to calculate K for individual trajectory of seismic ray. Simplisitiy's sake K were calculated for every 1° of θ' up to 15°, by the formula

$$K=\frac{dt}{d\theta'}=\frac{r\sin\theta'}{Vd\sqrt{ab\frac{d^2}{V_2}+1}}\quad\cdots\cdots\cdots\cdots\cdots\quad(32)$$

Table IX contains the results. The corresponding $\delta\theta$ and δt to these K were determined by graphical interpolation and were added to the corresponding θ' and t in Table VII and T and θ were obtained. These values are tabulated in Table X. The two figures in Table X represent epicentral distance (above) and travel-time (below, in gothic) respectively.

Now I will add a little on the use of these tables. Travel time of S-wave or the duration of preliminary tremor, i.e. travel time difference of S- and P-waves are obtained by multiplying those of P-wave calculated above by v/V or $(v/V-1)$, which were determined in chapter II to be $\sqrt{3}$ or $(\sqrt{3}-1)$ respectively.

Reversely, if we reduce arrival time of S-wave or the duration of preliminary tremor by the above relation to time of occurrence of P-wave, we can use them equally for the determination of the position of hypocentre and the law of velocity variation within the earth with the aid of above tables by the equatian

$$t-t_0=\delta t_0+\left(\frac{\partial t}{\partial\varphi}\right)_0\delta\varphi_0+\left(\frac{\partial t}{\partial\lambda}\right)_0\delta\lambda_0+\left(\frac{\partial t}{\partial h}\right)_0\delta h$$
$$+\left(\frac{\partial t}{\partial V}\right)_0\delta V+\left(\frac{\partial t}{\partial\sqrt{ab}}\right)\delta(\sqrt{ab})\quad\cdots\cdots\quad(33)$$

in which

$$\frac{\partial t}{\partial\varphi}=fr\{\sin\varphi\cos\varphi_0-\sin\varphi_0\cos\varphi\cos(\lambda-\lambda_0)\}\quad\cdots\quad(34)$$

$$\frac{\partial t}{\partial \lambda}=fr\cos\varphi_0\cos\varphi\sin(\lambda-\lambda_0) \quad \dots\dots\dots \quad (34)$$

$$\frac{\partial t}{\partial h}=f(\cos\theta'-r) \quad \dots\dots\dots \quad (35)$$

$$\frac{\partial t}{\partial V}=-f\frac{d^2}{V} \quad \dots\dots\dots \quad (36)$$

$$\frac{\partial t}{\partial\sqrt{ab}}=\frac{1}{\sqrt{ab}}(-t+fd^2) \quad \dots\dots\dots \quad (37)$$

$$f=\frac{1}{Vd\sqrt{ab\frac{d^2}{V}+1}} \quad \dots\dots\dots \quad (38)$$

$$r=1-h \quad \dots\dots\dots \quad (39)$$

where (φ_0, λ_0) and (φ, λ) are latitudes and longitudes of assumed epicentre and observing station reduced to the level surface of ultra-basaltic layer respectively.

As I have already calculated fr on the course of calculation of K, $\frac{\partial t}{\partial h}$, $\frac{\partial t}{\partial V}$, $\frac{\partial t}{\partial\sqrt{ab}}$ etc. are evaluated at once. The values of fr, $\frac{\partial t}{\partial h}$, $\frac{\partial t}{\partial V}$, $\frac{\partial t}{\partial\sqrt{ab}}$ Are tabulated in Table XI, XII, XIII and XIV.

Appendix. Re-examination of the velocity of P-wave[33], and the accuracy of the values calculated in chapter III.

The velocity of the P-wave in the substratum up to the Wiechert discontinuity has been re-estimated by the same method as in chapter I, using the mean travel times to long distances of 85 earthquakes recently obtained by Dr. H. Jeffreys.[34] The results coincided within almost one per cent, with the determination in chapter I, for both assumptions of hypocentral depth of 0 km. (I) and 20 km. (II). The results are compared in the following tables.

Table XV.

Correction to the velocity constants of chapter I.

Assumed focal depth		$\delta(a-b)/(a-b)$	$\delta\sqrt{ab}/\sqrt{ab}$
(I)	0 km.	$-0{\cdot}21\pm0{\cdot}95$	$-0{\cdot}07\pm1{\cdot}83$
(II)	20 km.	$-0{\cdot}03\pm0{\cdot}93$	$-1{\cdot}06\pm1{\cdot}80$

33) Being the abstract of the author's "On the velocity of the P-wave, with special reference to the discontinuity recently suggested by Dr. H. Jeffreys. [*Japanese Journ. Astr. Geophys.* **9** (1931), 15–22.] Added on Dec. 20, 1931.

34) H. Jeffreys, *M.N.R.A.S., Geophys. Suppl.*, **2** (1931), 329–348.

Table XVI.

Comparison of old and new velocity constants.

	$(a-b)\times 10^3$	$\sqrt{ba}\times 10^3$	v
(0)	$1{\cdot}172\pm 0{\cdot}011$ (P.E)	$2{\cdot}837\pm 0{\cdot}105$ (P.E)	$0{\cdot}003509-0{\cdot}002337\,r^2$
(I)	$1{\cdot}169\pm 0{\cdot}011$	$2{\cdot}835\pm 0{\cdot}052$	$0{\cdot}003479-0{\cdot}002310\,r^2$
(II)	$1{\cdot}171\pm 0{\cdot}011$	$2{\cdot}807\pm 0{\cdot}051$	$0{\cdot}003453-0{\cdot}002381\,r^2$

The depth of the Wiechert discontinuity came out

(I) 1177 km. (II) 1166 km.

Thus the velocity formula $v=a-br^2$ above determined is sufficient for the present so far as it concerns the accuracy of determining the travel-time.

The travel-time t calculated from the value of (I) or (II) differs only 0·7 sec. or 1·4 sec. at $\theta=3{\cdot}75°$ and 0·4 sec. at $\theta=17{\cdot}5°$ compared with the values calculated with the constants used in chapter III. So there will be no need of corrections to the values calculated in chapter III.

---

9. 地震波の傳播（第一報）

河角廣

地震計測の最後の目的は地震の際の波動の解釋に盡きる。地震波の凡ての部分は地震發生の機巧と此の波動を傳へる媒質の凡ての特異性を反影する。此の方面の研究は地球內部の構造を究める最も適確な方法である事旣に周知の事實であるが，我々地震國民にとつて更に重要な點は地震發生の機巧を知る事が出來る事にある。單に震原の位置の正確な統計的研究も地質學的地球物理學的の適當なる解釋を得ればば地震發生の原因を推察するに難くないであらう。加之地震發生の機巧をも合せ知る事が出來たならば單に地震の原因を推察し得るに止らないであらう。かかる研究が地方的に又時間的に推進められて行く時所謂地震豫知の問題に如何なる光明が投げられるか想像に難くない事と思ふ。此の樣な目的に到達する道は地震波動の定量的研究より外はない。今迄此の方面の研究は餘りにも輕んぜられ，現在の我國の觀測については到底其の樣な問題を論ずるに足る精度を望み得ない樣に考へられて來た。勿論地震計改良の將來に待つべきものも多々あらうが我々は只拱手して其の日を待つべきではない。地球內部の地震波傳波の速度の測定の如き定量的問題を論じ得べき時間測定の精度も旣に我が國の觀測に存在する事は第一章に示す通りである。斯學に從事するもの此等の進步に對し當事者の尊き努力に對し感謝に耐へない次第である。

筆者本論文の目的は上述の主目的に向ふ筆者の第一步の報告にして，此の樣な定量的研究の最初として其の方法以外には殊別に新しい事はない。

一地點に於て觀測される地震波は前述の如き複雜な諸條件を反映するが其の傳播の途中に起る一般的變化は箇々の地震の發生機巧を知る上に先づ第一に必要な問題である。此の傳播の途中に於ける變化としては新しい波の生成と，反射，屈折，分散，吸收等を上げる事が出來る。此等は何れも媒質の構造性質に關係する。即定量的研究の第一歩は此の地球内部の構造を第一に反映する地震波速度の研究である。斯の如き定量的議論には平均の走時曲線による時は其の際の走時曲線の引方一つに内部の速度分布は關係する故此の樣な不確定さを避ける爲に直接各地に於ける發震時から震原の位置，震原に於ける發震時，地球内部の縱波の速度變化等を最小二乘法を用ひて一時に決定し此等の數値の公算誤差をも示し始めて定量的研究の實を示した。(第一章)材料は昭和三年五月二十一日千葉縣に起つた强震である。

次の問題は S 波 (P 波と同じく地殼の下即超鹽基性層を傳はる横波) の速度の決定である。地殼表層の複雜なる構造震央附近に於ける表面波の問題等は此の横波の認定を困難ならしむる結果，此と縱波との走時差と考へられて居る所謂初期微動繼續時間と云ふものが決して一義的のものでない事は既によく知られて居る所である。此に關して第一章に用ひた地震の地震記象の統一的研究と統計的研究の結果ポアソン此が一定で四分の一に近い事を確めて居る (第二章)。

第三章には既に P 波 S 波の速度は定められたるを以て此を用ひて走時曲線を計算し震原の深さ，速度の値の修正，地殼の構造等の調査等の便宜の爲の諸種の補助の表をも計算してある。

最後に「附」として第一章の速度の數値の精度，其の時得られた速度の式の適用範圍，及第三章の諸表の精度について述べ實用上殆ど修正の必要なき事を示して居る。

Table VII.

Travel time of P-wave in ultra-basaltic layer. $\left(t=\frac{1}{\sqrt{ab}}\operatorname{arc\,sinh}\frac{\sqrt{abd}}{V}\right)$

Θ′ / h	0° 0′	20′	40′	1° 0′	20′	40′	2° 0′	20′	40′	3° 0′	20′	40′	4° 0′	20′	40′
0·000	0	4·93	9·93	15·23	19·85	24·80	29·75	34·68	39·63	44·55	49·47	54·37	59·27	64·16	69·03
0·004	3 39	5·97	10·40	15·12	19·94	24·78	29·65	34·51	39·38	44·24	49·10	53·95	58·79	63·62	68·44
0·008	6·72	8·29	11·83	16·07	20·59	25·22	29·93	34·67	39·43	44·20	48·97	53·74	58·51	63·27	68·02
0·012	10·00	11·10	13·89	17·58	21·71	26·07	30·53	35·14	39·75	44·40	49·07	53·74	58·42	63·11	67·78
0·016	13·24	14·07	16·32	19·50	23·22	27·27	31·52	35·89	40·34	44·84	49·38	53·95	58·53	63·12	67·71
0·020	16·42	17·09	18·95	21·70	25·04	28·77	32·75	36·90	41·16	45·50	49·90	54·34	58·81	63·30	67·79
0·024	19·56	20·12	21·69	24·08	27·08	30·51	34·21	38·13	42·19	46·37	50·61	54·92	59·26	63·64	68·03
0·028	22·66	23·13	24·48	26·59	29·28	32·41	35·87	39·55	43·42	47·41	51·50	55·66	59·87	64·13	68·41
0·032	25·71	26·12	27·31	29·17	31·60	34·47	37·68	41·42	44·80	48·61	52·54	56·55	60·63	64·76	68·93
0·036	28·72	29·08	30·13	31·80	34·01	36·64	39·62	42·87	46·33	49·96	53·72	57·44	61·52	65·52	69·58
0·040	31·70	32·01	32·95	34·46	36·47	38·89	41·66	44·71	47·98	51·43	55·02	58·65	62·53	66·41	70·34
0·044	34·63	34·91	35·76	37·13	38·97	41·20	43·78	46·64	49·73	53·01	56·44	60·00	63·66	67·74	71·34
0·048	37·52	37·78	38·55	39·80	41·49	43·56	45·96	48·64	51·56	54·68	57·95	61·36	64·88	68·50	72·18
0·052	40·38	40·62	41·32	42·47	44·03	45·95	48·19	50·71	53·47	56·53	59·55	62·82	66·20	69·68	73·25
0·056	43·20	43·42	44·07	45·13	46·57	48·36	50·46	52·83	55·43	58·24	61·22	64·35	67·60	70·96	74·40
0·060	45·99	46·20	46·79	47·77	49·11	50·78	52·75	54·98	57·45	60·11	62·96	65·95	69·07	72·30	75·63
0·064	48·74	48·93	49·49	50·40	51·65	53·21	55·06	57·17	59·50	62·04	64·78	67 61	70·60	73·72	76·93
0·068	51·46	51·63	52·15	53·01	54·18	55·64	57·38	59·37	61·58	63·99	66·58	69·32	71·50	75·16	77·95
0·072	54·15	54·31	54·80	55·60	56·69	58·07	59·71	61·59	63·69	65·99	68·43	71·08	73·84	76·72	79·71

(*to be continued.*)

Table VII. (*continued.*)

Θ' / h	5° 0′	20′	40′	6° 0′	20′	40′	7° 0′	20′	40′	8° 0′	20′	40′	9° 0′	20′	40′
0·000	73·89	78·73	83·55	88·37	97·90	97·90	102·69	107·43	112·15	116·85	121·52	126·18	130·81	135·42	140·00
0·004	73·24	78·03	82·81	87·58	97·05	97·05	101·76	106·45	111·13	115·78	120·42	125·03	129·62	134·19	138·73
0·008	72·77		82·22	86·93	96·34	96·29	100·96	105·60	110·23	114·83	119·42	123·99	128·53	133·06	137·56
0·012	72·46	77·12	81·78	86·42	91·06	95·68	100·28	104·87	109·45	114·00	118·54	123·06	127·56	132·04	136·49
0·016	72·30	76·89	81·48	86·06	90·63	95·18	99·73	104·26	108·78	113·28	117·64	122·23	126·66	131·11	135·52
0·020	72·30	76·81	81·32	85·82	90·32	94·81	99·29	103·76	108·22	112·67	117·10	121·51	125·91	130·29	134·65
0·024	72·44	76·86	81·29	85·71	90·14	94·55	98·97	103·38	107·77	112·16	116·53	120·89	125·23	129·56	133·87
0·028	72·72	77·05	81·39	85·73	90·08	94·42	98·76	103·10	107·43	111·76	116·07	120·37	124·66	128·93	133·19
0·032	73·14	77·36	81·61	85·86	90·13	94·39	98·66	102·93	107·19	111·45	115·70	119·94	124·17	128·39	132·59
0·036	73·67	77·79	81·94	86·11	90·29	94·47	98·66	102·86	107·05	111·24	115·43	119·61	123·78	127·93	132 08
0·040	74·32	78·34	82·39	86·46	90·55	94·65	98·77	102·88	107·01	111·13	115·25	119·36	123·47	127·57	131·66
0·044	75·08	78·99	82·94	86·92	90·92	94·93	98·96	103·31	107·05	111·10	115·15	119·20	123·24	127·28	131·32
0·048	75·94	79·74	83·58	87·47	91·37	95·30	99·25	103·51	107·18	111·16	115·14	119·12	123·10	127·08	131·05
0·052	76·55	80·58	84·32	88·11	91·92	95·76	99·63	103·51	107·40	111·30	115·21	119·13	123·01	126·96	130·87
0·056	77·92	81·51	85·15	88·83	92·55	96·31	100·08	103·88	107·70	111·53	115·36	119·21	123·06	126·91	130·76
0·060	79·04	82·51	86·05	89·64	93·26	96·93	100·62	104·33	108·07	111·82	115·59	119·36	123·14	126·93	130·72
0·064	80·22	83·59	87·03	90·51	94·05	97·62	101·23	104·86	108·52	112·19	115·89	119·59	123·30	127·02	130·75
0·068	81·41	84·74	88·07	91·46	94·90	98·39	101·91	105·46	109·04	112·63	116·25	119·89	123·53	127·18	130·84
0·072	82·79	85·95	89·18	92·47	95·82	99·22	102·65	106·12	109·62	113·14	116·69	120·26	123·82	127·41	131·00

(*to be continued.*)

Table VII. (*continued.*)

h \ Θ′	10° 0′	20′	40′	11° 0′	20′	40′	12° 0′	20′	40′	13° 0′	20′	40′	14° 0′	20′	40′	15° 0′
0·000	144·57	149·10	153·62	158·10	162·56	167·00	171·41	175·79	180·15	184·48	188·78	193·06	197·30	201·51	205·71	209·88
0·004	143·27	147·75	152·23	156·67	161·10	165·50	169·87	174·22	178·53	182·84	187·11	191·35	195·56	199·75	203·91	208·05
0·008	142·04	146·50	150·93	155·34	159·73	164·09	168·43	172·74	177·03	181·29	185·52	189·73	193·91	198·07	202·52	206·30
0·012	140·93	145·34	149·74	154·11	158·45	162·77	167·07	171·35	175·60	178·82	184·02	187·59	192·34	196·47	200·56	204·63
0·016	139·91	144·28	148·63	152·96	157·26	161·55	165·81	170·04	174·25	178·44	182·60	186·74	190·86	194·94	199·01	203·05
0·020	138·99	143·32	147·62	151·91	136·17	160·41	164·62	168·82	172·99	177·14	181·27	182·37	189·45	193·50	197·53	201·54
0·024	138·17	142·44	146·70	150.94	155·16	159·35	163·53	167·68	171·82	175·93	180·02	184·08	188·12	192·53	196·14	200·11
0·028	137·43	141·66	145·87	150·06	154·23	158·38	162·52	166·63	170·72	174·79	178·84	182·87	186·87	190·85	194·81	198·75
0·032	136·78	140·96	145·12	149·26	153·39	157·49	161·58	165·65	169·72	173·73	177·74	181·73	185·70	189·64	193·57	197·47
0·036	136·22	140·34	144·45	148·54	152·62	156·68	160·73	164·75	168·76	172·75	177·06	180·66	184·60	188·50	192·39	196·25
0·040	135·74	139·81	143·87	147·91	151·94	155·95	159·95	163·93	167·89	171·84	175·76	179·67	183·56	187·43	191·28	195·11
0·044	135·34	139·07	143·36	147·35	151·33	155·29	159·24	163·18	167·10	171·00	174·88	178·75	182·60	186·43	190·24	194·03
0·048	135·02	138·98	142·93	146·86	150·79	154·71	158·61	162·50	166·37	170·23	174·07	177·9)	181·71	185·50	189·27	193·02
0·052	134·77	138·68	142·57	146·46	150·33	154·20	158·05	161·89	165·72	169·53	173·32	177·11	180·88	184·63	188·36	192·08
0·056	134·60	138·45	142·28	146·12	149·94	153·75	157·56	161·35	165·13	168·90	172·65	175·86	180·10	183·82	187·52	191·20
0·060	134·50	138·29	142·28	145·85	149·62	153·38	157·13	160·87	164·61	168·33	172·04	175·73	179·42	183·08	186·74	190·38
0·064	134·47	138·20	141·29	145·64	149·36	153·07	156·77	160·46	164·15	167·82	171·49	175·14	178·78	182·41	186·02	189·64
0·068	134·51	138·17	141·84	145·50	149·16	152·82	156·47	160·12	163·75	167·38	171·00	174·61	178·20	181·78	185·36	188·91
0·072	134.60	138·21	141·82	145·42	149·03	152·64	156·23	159·83	163·42	167·00	170·57	174·13	177·68	181·22	184·75	188·27

Table VIII. Correction to time-distance curve due to the effect of earth's crust.

K	$\delta\Theta_1$	$\delta\Theta_2$	$\delta\Theta$	δt_1	δt_2	δt
	° ′	° ′	° ′	sec	sec	sec
0	0·0	0·0	0·0	4·00	4·84	8·84
100	0·9	1·6	2·5	4·01	4·86	8·87
200	1·7	3·3	5·0	4·05	4·93	8·98
300	2·6	5·0	7·6	4·12	5·06	9·18
400	3·6	6·9	10·5	4·21	5·26	9·47
500	4·6	9·1	13·7	4·35	5·55	9·90
600	5·9	11·8	17·7	4·56	5·98	10·54
700	7·1	14·9	22·0	4·79	6·56	11·35
800	8·7	20·5	29·2	5·14	7·77	12·91
900	10·8	30·3	41·1	5·66	10·21	15·87
1000	13·3	1 16·5	1 30·3	6·47	23·24	29·71

Table IX. $K = fr \sin \theta'$

h \ Θ	0°	1°	2°	3°	4°	5°	6°	7°	8°	9°	10°	11°	12°	13°	14°	15°
0·000	(853·2)	852·4	850·0	846·1	840·6	833·8	825·5	816·1	805·6	794·2	781·9	769·1	755·7	741·8	727·6	713·2
0·004	0	822·5	836·1	835·3	831·0	824·8	815·3	808·1	798·1	787·0	775·2	762·6	749·5	736·0	722·1	707·0
0·008	0	759·2	812·2	821·6	819·1	814·6	807·8	799·6	790·1	779·6	768·1	756·0	743·3	730·1	716·6	702·9
0·012	0	680·7	780·0	800·7	804·7	802·9	797·5	790·2	781·5	771·6	760·7	749·1	736·5	724·0	710·9	697·5
0·016	0	601·9	742·0	777·7	788·2	789·4	786·1	780·2	772·4	763·2	753·0	741·8	730·1	717·8	705·0	691·9
0·020	0	530·5	700·6	752·0	769·7	774·8	773·8	769·5	762·4	754·4	746·6	734·4	723·1	711·2	698·9	686·3
0·024	0	469·0	656·7	724·2	749·6	759·0	760·7	758·1	752·7	645·3	736·5	726·7	716·0	705·4	692·8	680·6
0·028	0	416·8	615·9	695·2	728·4	742·3	746·9	746·5	742·2	735·9	727·9	710·5	708·7	697·9	686·5	674·7
0·032	0	372·8	575·5	665·4	706·1	724·8	732·3	733·7	731·2	726·0	719·0	710·6	701·2	690·9	680·0	668·7
0·036	0	335·7	537·2	635·7	683·2	706·5	717·3	710·8	723·5	715·9	709·9	702·3	693·5	683·8	673·5	662·6
0·040	0	304·1	501·6	606·3	660·1	687·8	701·7	707·4	707·4	705·5	700·5	693·7	686·5	676·6	666·8	656·4
0·044	0	277·3	468·6	577·6	636·8	668·8	685·8	694·1	696·2	694·9	691·1	685·0	677·7	669·2	660·0	650·1
0·048	0	253·9	438·3	550·0	613·6	649·6	669·5	679·8	684·0	684·0	681·2	676·1	669·5	661·8	653·1	643·7
0·052	0	233·6	410·6	523·4	590·8	630·3	653·1	665·7	671·5	672·9	671·2	667·1	661·3	654·2	646·1	637·2
0·056	0	216·0	384·3	498·1	568·4	611·1	636·8	651·3	658·9	661·7	661·0	657·9	652·8	646·4	638·9	630·6
0·060	0	200·4	362·0	474·1	545·3	592·1	620·1	636·9	646·2	650·3	650·8	648·6	644·4	637·6	632·5	624·0
0·064	0	186·2	340·7	451·4	525·4	573·2	603·6	622·4	633·3	638·8	640·4	639·1	635·7	630·7	624·5	617·2
0·068	0	174·3	321·2	430·0	505·0	554·8	587·2	607·9	620·4	627·3	630·0	629·7	624·2	622·9	617·1	610·4
0·072	0	163·3	303·3	409·9	485·3	536·7	571·0	593·3	607·5	615·6	619·4	620·1	618·3	614·7	609·7	603·5

Table X.

Time-distace curves of P-wave for various hypocentral depth on the earth's surface.

[Gothic figure, below, represents travel time T in sec; the above figure is $\delta\Theta$ in minutes of arc which are to be added to Θ' at the top of the column to get epicentral distance Θ.]

Depth from the surface	h \ Θ'	0°	1°	2°	3°	4°	5°	6°	7°	8°	9°	10°	11°	12°	13°	14°	15°
km. 0	—	68·3 28·6	68·2 43·8	67·7 58·2	66·8 72·8	65·7 87·2	64·6 101·4	62·8 115·4	61·1 129·3	59·4 143·0	57·3 156·5	55·2 169·7	53·3 182·8	51·5 195·7	49·4 208·3	47·6 220·7	45·8 232·9
20	—	58·5 23·2	58·4 38·4	58·0 52·8	57·1 67·4	56·2 81·9	55·2 86·1	53·6 110·2	52·1 124·0	50·5 137·8	48·7 151·3	46·9 164·6	45·1 177·7	43·6 190·7	41·7 203·4	40·1 215·9	38·5 228·1
50	0·000	34·2 14·3	34·1 29·5	33·9 43·9	33·4 58·7	32·9 73·2	32·3 89·0	31·4 101·9	30·6 116·0	29·7 129·9	28·7 143·7	27·6 157·2	26·6 170·5	25·8 183·6	24·7 196·5	23·8 211·2	22·9 223·6
75·3	0·004	0 12·2	31·4 28·5	32·8 42·8	32·8 58·0	32·3 72·4	31·6 86·7	30·6 101·8	30·0 114·9	29·1 128·7	28·2 142·3	27·4 155·8	26·5 169·0	25·6 182·0	24·6 194·7	23·8 209·3	22·8 221·5
100·6	0·008	0 15·6	26·3 28·3	30·2 43·1	31·2 57·6	31·0 71·9	30·5 86·0	30·0 100·0	29·2 113·9	28·5 127·7	27·7 141·2	26·9 154·4	26·0 167·5	25·1 180·4	24·3 193·1	23·4 207·5	22·6 219·7
125·9	0·012	0 18·8	21·4 28·8	27·7 43·1	29·2 57·4	29·6 71·4	29·5 85·5	29·0 99·3	28·4 113·0	27·7 126·6	27·1 140·0	26·2 153·1	25·5 166·2	24·7 179·0	23·9 190·6	23·0 205·8	22·3 217·9
151·1	0·016	0 22·1	17·8 30·1	25·0 43·5	27·5 57·3	28·3 71·2	28·4 85·1	23·1 98·7	27·7 112·3	27·2 125·7	26·5 139·0	25·9 152·1	25·0 164·9	24·3 177·7	23·5 190·1	22·7 204·3	22·0 216·2
176·4	0·020	0 25·3	14·8 31·8	22·5 44·2	25·6 57·6	27·0 71·2	27·3 84·8	27·2 98·2	27·0 111·7	26·4 124·9	25·9 138·1	25·3 151·0	24·6 163·8	23·9 176·4	23·1 188·7	22·4 202·8	21·7 214·6
201·7	0·024	0 28·4	12·6 33·9	20·2 45·2	24·0 58·1	25·6 71·4	26·2 84·6	26·3 98·0	26·2 111·2	25·7 124·3	25·2 137·2	24·7 150·1	24·0 162·7	23·4 175·2	22·8 187·4	22·0 201·3	21·4 213·1
227·0	0·028	0 31·5	11·0 36·1	18·4 46·5	22·2 58·8	24·1 71·7	25·1 84·7	25·3 97·7	25·3 110·8	25·1 123·8	24·6 136·6	24·1 149·2	23·1 162·6	22·9 174·1	22·3 186·2	21·8 200·0	21·1 211·7

(*to be continued.*)

Table X. *(continued.)*

Depth from the surface	h \ Θ'	0°	1°	2°	3°	4°	5°	6°	7°	8°	9°	10°	11°	12°	13°	14°	15°
252·3	0·032	0 34·6	9·7 38·5	16·6 48·0	20·6 59·7	22·8 72·1	24·0 84·9	24·4 97·7	24·5 110·5	24·4 123·3	24·0 135·9	23·6 148·5	23·0 160·9	22·5 173·0	21·9 185·1	21·4 198·7	20·8 210·3
277·6	0·036	0 37·6	8·5 41·0	15·1 49·7	19·7 60·9	21.6 72·8	22·4 85.1	23·1 97·7	23·1 110·3	23·7 122·8	24·3 135·4	23·0 147·8	22·6 160·0	22·1 172·1	21·6 184·1	21·1 197·5	20·3 209·0
302·8	0·040	0 40·5	7·6 43·6	13·8 51·6	18 0 62·0	20·4 73·6	21·8 85·6	22·6 98 0	22·9 110·3	22·8 122·6	22.8 135·0	22·5 147·2	22·1 159·3	21·7 171·3	21·2 183·0	20·7 196·4	20·2 207·8
328·1	0·044	0 43·5	8·8 46·2	12·6 53·5	16·6 63·5	19·3 74 5	20·8 86·2	21·7 98·2	22·0 110·3	22·2 122·5	22·2 134·6	22·0 146·7	21·6 158·6	21·3 170·4	20·8 182·1	20·4 195·3	19·9 206·6
353·4	0·048	0 46·4	6·2 48·9	11·7 55·6	15·6 64·8	18·3 75·5	19·9 86·9	20·9 98·6	21·4 110·5	21·6 122·5	21·6 134·4	21·4 146·2	21·2 158·1	20·9 169·8	20·5 181·3	20·1 194·4	19·6 205·5
378·7	0·052	0 49·2	5·8 51·5	10·8 56·7	14·6 66·5	17·2 76·7	19 0 87·4	20·1 99·1	20·7 110·7	21·0 122·5	21·0 134·2	20·9 145·9	20·8 157·6	20·4 169 1	20·1 180·5	19·7 193·4	19·4 204·5
404·0	0·056	0 52·0	5·3 54·1	10·0 59·9	13·6 68·1	16 3 77·9	18·1 88·5	19 3 99 6	20·0 111·8	20·4 122·6	20·5 134·1	20·4 145·7	20·3 157·2	20·0 168·5	19.8 179·8	19·4 192·5	19·0 203·5
429·3	0·060	0 54·8	5·0 56·8	9·4 62·1	12 8 69·9	15·4 79·2	17·3 89·5	18·6 100·3	19·3 111·4	19 7 122·7	20·0 134·1	20·0 145·5	19·9 156·8	19·7 167·9	19·4 179·2	19·1 191·7	18·7 202·6
454·5	0·064	0 57·6	4·6 59·4	8·7 64·3	12·1 71·7	14·6 80·6	16·5 90·6	17·9 101·1	18·8 111·9	19·2 123·0	19·4 134·2	19·4 145·3	19·4 156·4	19·2 167·6	19·0 178·6	18·8 191·0	18·4 201·8
479·8	0·068	0 60·3	4·2 62·0	8.0 66·6	11·2 73·5	13·9 81·4	15·8 91·6	17·1 101·9	18·1 112·5	18·6 123·3	18·8 134·2	19·0 145·3	19·0 156·3	18·8 167·2	18·7 178·1	18·4 190·4	18·1 201·0
505·1	0·072	0 63·0	4·0 64·6	7·6 68·8	10·8 75·5	13·2 83·6	15·1 92·9	16·4 102·8	17·4 113·2	18·0 123·7	18·4 134·5	18·6 145·3	18·6 156·1	18·5 166·9	18·3 177·7	18·1 189·7	17·8 200·3

$\log_{10} f\bar{r}$

Table XI.

h \ Θ'	0°	1°	2°	3°	4°	5°	6°	7°	8°	9°	10°	11°	12°	13°	14°	15°
0·000	∞	4·68881	4·38659	4·20860	4·08099	3·98074	3·89749	3·82584	3·76258	3·70562	3·65249	3·60539	3·55046	3·51821	3·47822	3·44021
0·004	5·32380	4·67327	4·37942	4·30303	4·07603	3·97607	3·89306	3·82158	3·75847	3·70162	3·64972	3·60169	3·55689	3·51477	3·47492	3·43702
0·008	5·01762	4·63848	4·36683	4·19585	4·06978	3·97063	3·88809	3·81700	3·75414	3·69752	3·64577	3·59793	3·55329	3·51131	3·47160	3·43386
0·012	4·83640	4·59107	4·34926	4·18466	4·06207	3·96424	3·88249	3·81187	3·74936	3·69306	3·64155	3·59392	3·54929	3·50766	3·46812	3·43051
0·016	4·70631	4·56766	4·32756	4·17203	4·05304	3·95700	3·87626	3·80631	3·74429	3·68832	3·63711	3·58971	3·54548	3·50388	3·46450	3·42707
0·020	4·60430	4·48286	4·30264	4·15740	4·04273	3·94888	3·86942	3·80029	3·73882	3·68329	3·63241	3·58531	3·54130	3·49992	3·46075	3·42351
0·024	4·52001	4·42927	4·27452	4·14106	4·03126	3·93995	3·86199	3·79482	3·73303	5·67801	3·62752	3·58073	3·53701	3·49637	3·45691	3·41986
0·028	4·44800	4·37808	4·24668	4·12328	4·01876	3·93030	3·85402	3·78715	3·72693	3·67246	3·62241	3·57599	3·53257	3·49167	3·45295	3·41610
0·032	4·38493	4·32964	4·21719	4·10430	4·00530	3·91989	3·84547	3·77961	3·72045	3·66660	3·61708	3·57103	3·52794	3·48734	3·44885	3·41223
0·036	4·32876	4·28396	4·18732	4·08442	3·99099	3·90883	3·83644	3·77189	3·71367	3·66052	3·61151	3·56590	3·52317	3·48286	3·44464	3·40824
0·040	4·27795	4·24118	4·15750	4·06388	3·97601	3·89719	3·82690	3·76380	3·70609	3·65417	3·60571	3·56059	3·51874	3·47825	3·44032	3·40417
0·044	4·23157	4·20112	4·12800	4·04285	3·96041	3·88501	3·81694	3·75532	3·69919	3·64757	3·59988	3·55508	3·51313	3·47349	3·43585	3·39998
0·048	4·18877	4·16273	4·09899	4·02153	3·94433	3·87235	3·80654	3·74651	3·69149	3·64072	3·59357	3·54941	3·50789	3·46861	3·43128	3·39568
0·052	4·14904	4·12668	4·07057	4·00005	3·92784	3·85925	3·79558	3·73738	3·68351	3·63363	3·58715	3·54357	3·50250	3·46360	3·42659	3·39127
0·056	4·11187	4·09252	4·04282	3·97853	3·91106	3·84581	3·78480	3·72790	3·67527	3·62630		3·53754	3·49692	3·45844	3·42176	3·38673
0·060	4·07698	4·06007	4·01580	3·95610	3·89408	3·83206	3·77324	3·71818	3·66680	3·61879	3·37377	3·53136	3·49125	3·45317	3·41736	3·38215
0·064	4·04400	4·02909	3·98950	3·93579	3·87693	3·81804	3·76153	3·70816	3·65808	3·61103	3·56678	3·52500	3·48540	3·44775	3·41187	3·37741
0·068	4·01276	3·99954	3·96395	3·91469	3·85969	3·80387	3·74959	3·69794	3·66913	3·60316	3·55964	3·51850	3·47943	3·44233	3·40667	3·37259
0·072	3·98302	3·97111	3·93907	3·88383	3·84242	3·78944	3·73743	3·68748	3·63998	3·59496	3·55231	3·51183	3·47331	3·43655	3·40140	3·36766

Table XII. $\log_{10}\left|\frac{\partial t}{\partial h}\right| = \log_{10}|f\{\cos\theta' - r\}|$

[Natural numbers of the logarithms above the boundary of thick line are all negative.]

h \ Θ'	0°	1°	2°	3°	4°	5°	6°	7°	8°	9°	10°	11°	12°	13°	14°	15°
0·000	2·93107	0·87151	1·17135	1·34548	1·46765	1·56112	1·63612	1·69822	1·75078	1·79595	1·83511	1·86957	1·89996	1·91253	1·95104	1·97276
0·004	2·92760	2·26021	1·91147	1·62465	1·27204	0·26718	1·06450	1·36162	1·51851	1·62305	1·70037	1·76098	1·81032	1·85157	1·88666	1·91695
0·008	2·92420	2·53671	2·23901	2·02082	1·81867	1·59682	1·29331	0·56290	0·99615	1·33566	1·50612	1·61733	1·69829	1·76105	1·81163	1·85356
0·012	2·92082	2·66996	2·41106	2·21643	2·04796	1·88301	1·70210	1·57571	1·11029	0·19104	1·15088	1·40349	1·54807	1·64740	1·72143	1·77963
0·016	2·91743	2·74464	2·52183	2·34427	2·19243	2·05018	1·90536	1·74559	1·54843	1·26215	0·55141	0·97197	1·31981	1·49406	1·60835	1·69113
0·020	2·91410	2·78935	2·59901	2·43638	2·29612	2·16702	2·03842	1·90791	1·75908	1·57789	1·32312	0·80552	0·81781	1·25919	1·45649	1·58069
0·024	2·91077	2·81727	2·65412	2·50629	2·37554	2·25575	2·16306	2·02333	1·89792	1·75630	1·58294	1·34158	0·87851	0·71908	1·22366	1·43361
0·028	2·90749	2·83521	2·69662	2·56093	2·43872	2·32645	2·21896	2·11242	2·00095	1·88036	1·74222	1·56682	1·33360	0·87876	0·69683	1·21192
0·032	2·90420	2·83299	2·72811	2·60457	2·49018	2·38419	2·28319	2·18389	2·08226	1·97492	1·85671	1·71955	1·54844	1·30561	0·82388	0·74324
0·036	2·90098	2·85445	2·75213	2·63979	2·53278	2·43254	2·33697	2·24351	2·14902	2·05097	1·94566	1·82800	1·68979	1·51456	1·25960	0·70878
0·040	2·89774	2·84828	2·77063	2·66853	2·56851	2·47357	2·38273	2·29416	2·20480	2·11419	2·01803	1·91332	1·81859	1·65344	1·47072	1·19465
0·044	2·89456	2·86261	2·78494	2·69211	2·59867	2·50873	2·42219	2·33782	2·25362	2·16800	2·07893	1·98332	1·87800	1·75714	1·61061	1·41628
0·048	2·89137	2·86395	2·79605	2·70156	2·62031	2·53908	2·45651	2·37693	2·29569	2·2146	2·13091	2·04246	1·94669	1·83964	1·71499	1·56087
0·052	2·88823	2·86460	2·80465	2·72765	2·64620	2·56545	2·48663	2·40948	2·33271	2·25548	2·17629	2·09345	2·00495	1·90790	1·79800	1·66794
0·056	2·88509	2·86455	2·81129	2·74099	2·65496	2·58847	2·51331	2·43917	2·36558	2·29169	2·21631	2·13807	2·05531	1·96591	1·86668	1·75272
0·060	2·88200	2·86398	2·81639	2·75209	2·68110	2·60863	2·53669	2·46567	2·39496	2·32407	2·25199	2·17761	2·09959	1·91622	1·92561	1·82275
0·064	2·87890	2·86296	2·(79910)	2·76129	2·69498	2·62632	2·55757	2·47946	2·42134	2·35314	2·28399	2·21294	2·13890	2·06046	1·97583	1·88218
0·068	2·87585	2·86165	2·82314	2·76894	2·70694	2·64195	2·57620	2·51068	2·44314	2·37950	2·31292	2·24480	2·17416	2·09997	2·03041	1·93370
0·072	2·87280	2·85998	2·82517	2·77527	2·71725	2·65554	2·59285	2·52987	2·46670	2·40330	2·33916	2·27367	2·20601	2·13524	2·06015	1·98905

Table XIII. $\log_{10}\dfrac{\partial t}{\partial V}=\log_{10}f\dfrac{d^2}{V}$

h \ Θ'	0°	1°	2°	3°	4°	5°	6°	7°	8°	9°	10°	11°	12°	13°	14°	15°
0·000	−∞	4·10361	4·40345	4·57758	4·69975	4·80323	4·86821	4·93033	4·98288	5·02823	5·06721	5·10167	5·13206	5·15906		5·20494
0·004	3·45730	4·10698	4·39853	4·57111	4·68278	4·78594	4·86098	4.92310	4·97570	5·02089	5·05924	5·09473	5·12522	5·15233	5·17652	5·19822
0·008	3·75157	4·12999	4·39934	4·56659	4·68747	4·78000	4·85461	4·91657	4·96909	5·01429	5·05363	5·08809	5·11875	5·14593	5·17021	5·19202
0·012	3·92099	4·16556	4·40512	4·56605	4·68355	4·77489	4·84889	4·91050	4·96284	5·00796	5·04727	5·08184	5·11225	5·13966	5·16402	5·18590
0·016	4·03930	4·20725	4·41514	4·56706	4·68107	4·77076	4·84386	4·90498	4·95703	5·00197	5·04121	5·07573	5·10634	5·13360	5·15799	5·18192
0·020	4·12970	4·25037	4·42847	4·57007	4·67993	4·76755	4·83953	4·89999	5·05164	4·99635	5·03543	5·06988	5·10044	5·12771	5·15214	5·17412
0·024	4·20243	4·29243	4·44331	4·57511	4·68006	4·76525	4·83587	4·89554	4·94669	4·99109	5·02997	5·06431	5·09482	5·12257	5·14650	5·16851
0·028	4·26305	4·33227	4·46151	4·58162	4·68138	4·76386	4·83291	4·89183	4·94220	4·98621	5·02484	5·05802	5·08944	5·11663	5·14105	5·16306
0·032	4·31474	4·36936	4·47979	4·58934	4·68371	4·76322	4·83056	4·88819	4 93905	4·99161	5·01997	5·05365	5·08424	5·11137	5·13570	5·15776
0·036	4·35971	4·40370	4·49846	4·59808	4·68694	4·76332	4·82880	4·88523	4·93433	4·97738	5·01540	5·04914	5·07928	5·10630	5·13064	5·15261
0·040	4·39933	4·43545	4·51719	4·60762	4·69302	4·76414	4·82759	4·88276	4·93053	4·97350	5·01109	5·04459	5·07506	5·10145	5·12571	5·14765
0·044	4·43469	4·46510	4·53569	4·61769	4·69574	4·76557	4·82693	4·88074	4·92807	4·96992	5·00724	5·04027	5·07001	5·09677	5·12094	5·14283
0 048	4·46649	4·49194	4·55380	4·62815	4·70105	4·76756	4·82675	4·87913	4·92550	4·96667	5 00338	5·03620	5·06570	5·09230	5·11635	5·13817
0·052	4·49536	4·51703	4·57136	4·63885	4·70682	4·77003	4·82686	4·86794	4·92327	4·96371	4·99989	5·03237	5·06161	5·08862	5·11193	5·13366
0·056	4·52169	4·54043	4·58833	4·64963	4·71296	4·77293	4·82758	4·87709	4·92135	4·96103	4·99665	5·02875	5·05768	5·08490	5·10766	5·12927
0·060	4·54590	4·56222	4·60469	4·67027	4·71942	4·77625	4·82884	4·87664	4·91978	4·95867	4·99372	5·02537	5·05401	5·07999	5·10409	5·12510
0·064	4·56820	4·58251	4·62037	4·67121	4·72709	4·77987	4·83025	4·87648	4·91849	4·95654	4·99098	5·02219	5·05049	5·07622	5·09970	5·12101
0·068	4·58441	4·60156	4·63577	4·68186	4·73293	4·78382	4·83201	4·87666	4·91751	4·95478	4·98852	5·01925	5·04720	5·07277	5·09590	5·11711
0·072	4·60814	4·61930	4·64988	4·69234	4·73988	4·78793	4·83403	4·87710	4·91679	4·95312	4·98627	5·01650	5·04409	5·06926	5·09229	5·11334

Table XIV. $\log_{10}\left|\left(\frac{dt}{d\sqrt{ab}}\right)\right|$

[Natural numbers are all negative.]

h \ Θ′	0°	1°	2°	3°	4°	5°	6°	7°	8°	9°	10°	11°	12°	13°	14°	15°
0·000	−∞	0·54307	1·44616	1·92328	2·29116	2·58050	2·81024	2·99944	3·16425	3·30198	3·43237	3·54264	3·64206	3·73172	3·81607	3·88727
0·004	$\bar{2}$·54307	0·54307	1·44616	1·92328	2·28343	2·57649	2·80076	2·99023	3·15373	3·29358	3·42159	3·53163	3·63156	3·72147	3·80290	3·87732
0·008	$\bar{2}$·84410	0·54307	1·38817	1·92328	2·31546	2·56010	2·78611	2·97764	3·13857	3·28343	3·40936	3·52216	3·62044	3·71039	3·79227	3·86653
0·012	$\bar{1}$·02020	0·84410	1·44616	1·92328	2·27546	2·55591	2·77860	2·96958	3·13190	3·27466	3·39919	3·51062	3·61274	3·70053	3·78212	3·85673
0·016	0·32123	0·84410	1·49731	1·92328	2·27546	2·54739	2·77607	2·96303	3·12399	3·26406	3·39064	3·50163	3·60112	3·69106	3·77301	3·84778
0·020	0·58448	1·02019	1·54307	1·95804	2·28343	2·55167	2·77096	2·95637	3·11826	3·25824	3·38192	3·49343	3·59268	3·68232	3·76422	3·83886
0·024	0·84411	1·14513	1·58446	1·97443	2·29126	2·55167	2·76838	2·95131	3·11127	3·25064	3·37494	3·48508	3·58407	3·67437	3·75552	3·82998
0·028	1·03443	1·24204	1·65701	2·00547	2·30650	2·55591	2·77096	2·94790	3·10774	3·24550	3·37685	3·47754	3·57649	3·66594	3·74746	3·82182
0·032	1·20583	1·32122	1·71916	2·03443	2·32840	2·56838	2·77096	2·94790	3·10417	3·24117	3·36196	3·47095	3·56919	3·65868	3·74035	3·81421
0·036	1·34926	1·46616	1·77352	2·07455	2·34241	2·57649	2·77352	2·94790	3·10178	3·23680	3·35665	3·46476	3·56302	3·65164	3·73256	3·80671
0·040	1·49247	1·58446	1·84410	2·11127	2·36261	2·58446	2·78112	2·95131	3·09937	3·23327	3·35263	3·45952	3·55675	3·64516	3·72548	3·79955
0·044	1·59230	1·65701	1·90480	2·15585	2·38817	2·59997	2·78858	2·95131	3·09937	3·23060	3·34857	3·45476	3·55124	3·63928	3·71916	3·79276
0·048	1·70145	1·77352	1·94101	2·19628	2·40659	2·61495	2·79592	2·95637	3·10058	3·22881	3·34516	3·45048	3·54653	3·63368	3·71363	3·78660
0·052	1·79594	1·86529	2·02019	2·23327	2·43516	2·62943	2·80552	2·96137	3·10178	3·22881	3·34310	3·44779	3·54220	3·62836	3·70772	3·78061
0·056	1·88550	1·84101	2·08714	2·26735	2·46215	2·64687	2·81491	2·96632	3·10417	3·22971	3·34241	3·44453	3·53871	3·62406	3·70204	3·77556
0·060	1·96304	2·00547	2·14513	2·30650	2·49246	2·66692	2·82637	2·97443	3·10774	3·22971	3·34103	3·44234		3·61971	3·69719	3·76993
0·064	2·04277	2·08714	2·19628	2·35598	2·51620	2·68295	2·83754	2·98240	3·11127	3·23149	3·34103	3·44070	3·53296	3·61605	3·69290	3·76579
0·068	2·11012	2·15585	2·22204	2·28817	2·54307	2·69841	2·85057	2·99023	3·11710	3·23238	3·34172	3·43960	3·52984	3·61126	3·68951	3·76055
0·072	1·17857	2·22431	2·29894	2·43516	2·57649	2·71333	2·86529	2·99944	3·12285	3·23680	3·34172	3·43849	3·52760	3·61014	3·68577	3·75659

10. *On Earth-tiltings observed at Mt. Tukuba.*

By Win INOUYE,

Earthquake Research Institute.

(Read Oct. 20, 1931.–Received Dec. 20, 1931.)

1. Introduction. The previously published note[1] under the same title as that of this paper contained results of observations made by a pair of Ishimoto all-silica tiltmeters in a room of fairly uniform temperature and continued for about two years and a half since the beginning on December 23, 1927 to June 10th, 1930.

The present note which is a continuation of the previous one, deals with observatons made during the three years and nine months since the beginning to September 30th, 1931.

2. Method of procedure. In his previous note the author tried to study the general features of the variations in the earth-tilts by smoothing out the minute irregularities, because, at times, for several days running, the photographs would receive no impression whatsoever, while, at other times, the records obtained would be hopelessly confused by the presence of short period fluctuations in the earth-tiltings.

This time, the variations in the earth-tiltings have been separated into two parts, one being fluctuations in a period of about one or two weeks and the other being those of longer periods. The separation is made as follows; first, the means ($\bar{n}_3$) of three consecutive values of the daily means of the earth-tiltings are taken, then the means ($\bar{n}_{13}$) of thirteen consecutive values of the terms of $\bar{n}_3$, and finally, eath term of $\bar{n}_{13}$ is subtracted from the corresponding term $\bar{n}_3$. The values obtained by this substruction represent the short period fluctuations in the earth-tiltings; $\bar{n}_{13}$ represents variations in the earth-tiltings of the longer periods.

The variations in the air temperature at Mt. Tukuba are also separated into two parts, the short period and the long period, the process of analysis of which is the same as in the case of variations in the earth-tiltings above-stated.

Owing however to the fact that fluctuations of the air temperature

1) W. INOUYE and T. SUGIYAMA, *Bull. Earthq. Research Inst.*, 8 (1930), 346.

are much more active than those of earth-tiltings, the author adopted a somewhat different method of analysis, as follows: First, the means ($\bar{n}_5$) of five consecutive values of the daily means of the air temperature are taken, next the means ($\bar{n}_{19}$) of nineteen consecutive values of the terms of $\bar{n}_5$, and finaly, each term of $\bar{n}_{19}$ is subtracted from the correspondding term of $\bar{n}_5$. The value of $\bar{n}_5-\bar{n}_{19}$ represents the fluctuations of the air temperature during a few weeks, while $\bar{n}_{19}$ represents those during a longer period.

3. Short period fluctuations. The two components of the short period fluctuations in the earth-tiltings and short period fluctuations in the air temperature for year 1928 are shown in Fig. 1.

As seen in the figure, the fluctuations of each component of the earth-tilting fairly resembles those of the air temperature.

The fluctuations in the NW-SE component of the earth-tiltings in particular, are practically correlated with those of the air temperature, except in the period between April 19th and May 10th, when the relation is inverted. This component of the earth-tilting represents that one along the mountain slope at the station. The mountain slopes down S. E.-wards here, so that increase of the air temperature causes decrease of the inclination of the mountain slope. As will be shown presently, the daily variations of the earth-tiltings take place practically in this component only. Moreover, the relation between the senses of the daily variations in the earth-tilts and those of the air temperature is the same as in the case above-stated; that is, the inclination of the mountain slope decreases as the air temperature increases. At all events

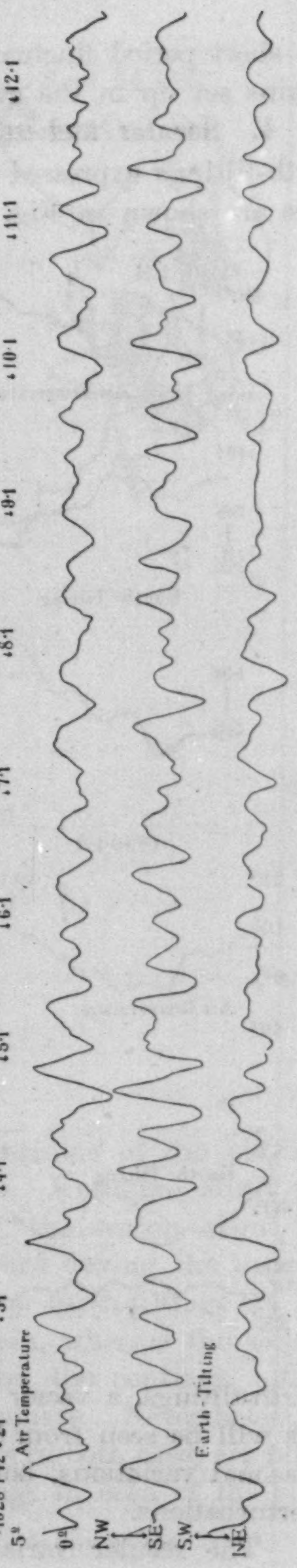

Fig. 1

the short period fluctuation in the earth-tiltings are caused by thermal strains set up in the ground by the sun's heat.

4. Secular and seasonal variations. The slow variations in the earth-tiltings expressed in two components and those in the air temperature are shown in Fig. 2. Taking the resultant of the two component

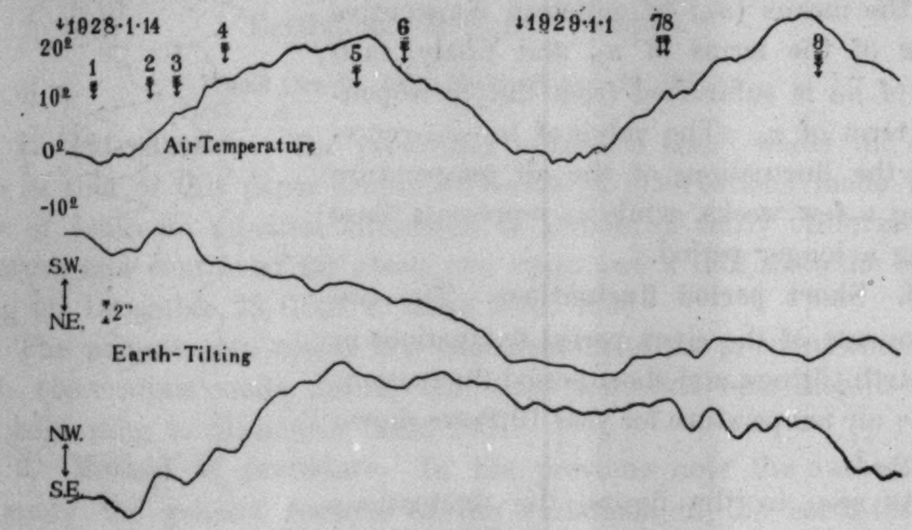

Fig. 2a.

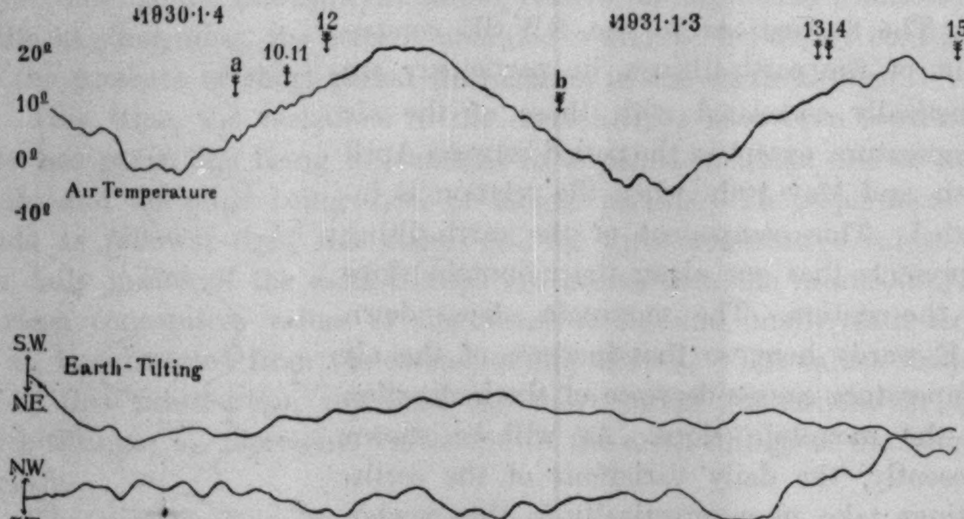

Fig. 2b.

earth-tiltings, a vector diagram was obtained as illustrated in Fig. 3. As will be seen from those figures, the earth-tiltings exhibit secular and seasonal variations, both of which were disturbed several times by stormy perturbations.

The secular variation amounted to 18 second N. N. E.-wards. It

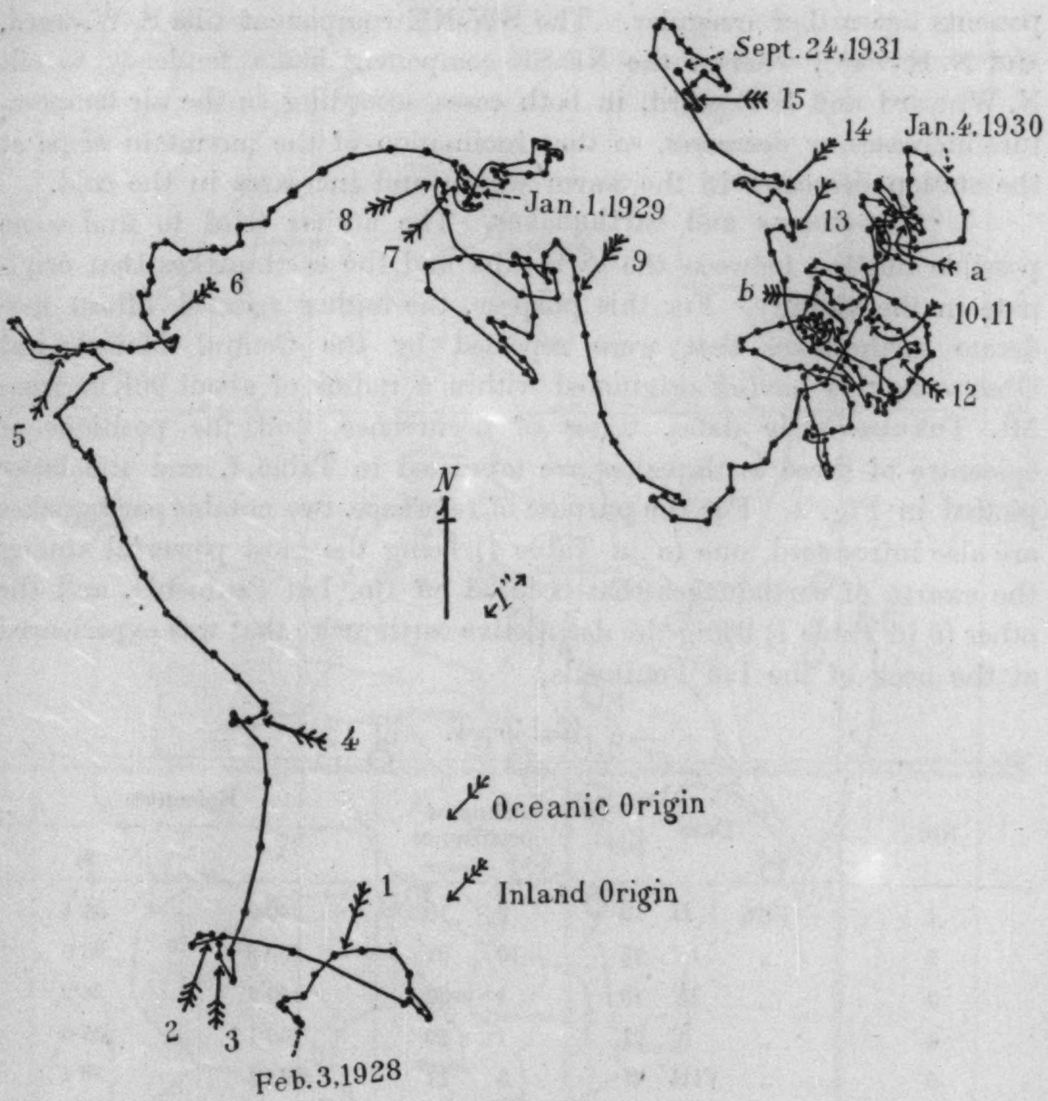

Fig. 3.

may be mentioned that, according to the comparisons of the old and new levellings in the Kwantô district by Messrs. Katuhiko Mutô and Keiryô Atumi[2] of the Millitary Land Survey, the region about Mt. Tukuba has tilted a little short of 1 sec. N. E.-ward during the interval between the two surveys. The variations in the earth-tiltings at Mt. Tukuba is confined to a small area at the station, whereas the secular tilting of the earth's crust about Mt. Tukuba, on the contrary, affects an extensive area of not less than fifty Kms. square. Nevertheless, it is significant that the senses of the earth-tiltings in both cases are fairly alike. The seasonal variations in the earth-tiltings in each of the com-

2) K. Mutô and K. Atumi, *Bull. Earthq. Research Inst.*, 7 (1929), 495.

ponents are rather irregular. The SW-NE component tilts S. W.-ward, and N. E.-ward, whereas the NE-SE component has a tendency to tilt N. W.-ward and S. E.-ward, in both cases according as the air temperature increases or decreases, so that inclination of the mountain slope at the station decreases in the warm season and increases in the cold.

5. **Tilt-storms and earthquakes.** The author tried to find some possible relation between the earth-tilts and the earthquakes that originate in the vicinity. For this purpose, the author selected fifteen moderate earthquakes that were reported by the Central Meteological Observatory as having originated within a radius of about 90Km. from Mt. Tukuba. The dates, times of occurrence, and the positions of epicentre of these earthquakes are tabulated in Table I, and the latter plotted in Fig. 4. For the purpose of reference, two notable earthquakes are also introduced, one (*a* in Table I) being the most powerful among the swarm of earthquakes that occured off Ito, Izu Peninsula, and the other (*b* in Table I) being the destructive earthquake that was experienced at the neck of the Izu Peninsula.

Table I.

No.	Date			Time of occurrence		Epicentre	
						λ	φ
1	1928	II	12	6^h	10^m	140°0	36°1
2	„	III	23	10	21	139·8	36·0
3	„	IV	13	1	36	140·1	36·2
4	„	V	21	1	29	140·1	35·6
5	„	VIII	27	3	11	141·1	36·4
6	„	X	5	15	58	139·6	36·1
7	1929	IV	18	3	33	140·9	36·3
8	„	IV	23	23	16	140·0	36·1
9	„	VIII	16	22	21	140·2	36·5
a	1930	III	22	17	50	139·1	35·0
10	„	V	1	9	58	140·8	35·7
11	„	V	1	13	20	140·8	35·7
12	„	VI	1	2	58	140·4	36·4
b	„	XI	26	4	03	139·0	35·1
13	1931	VI	9	14	07	140·9	36·5
14	„	VI	17	21	09	139·4	35·6
15	„	IX	21	11	20	139·3	36·0

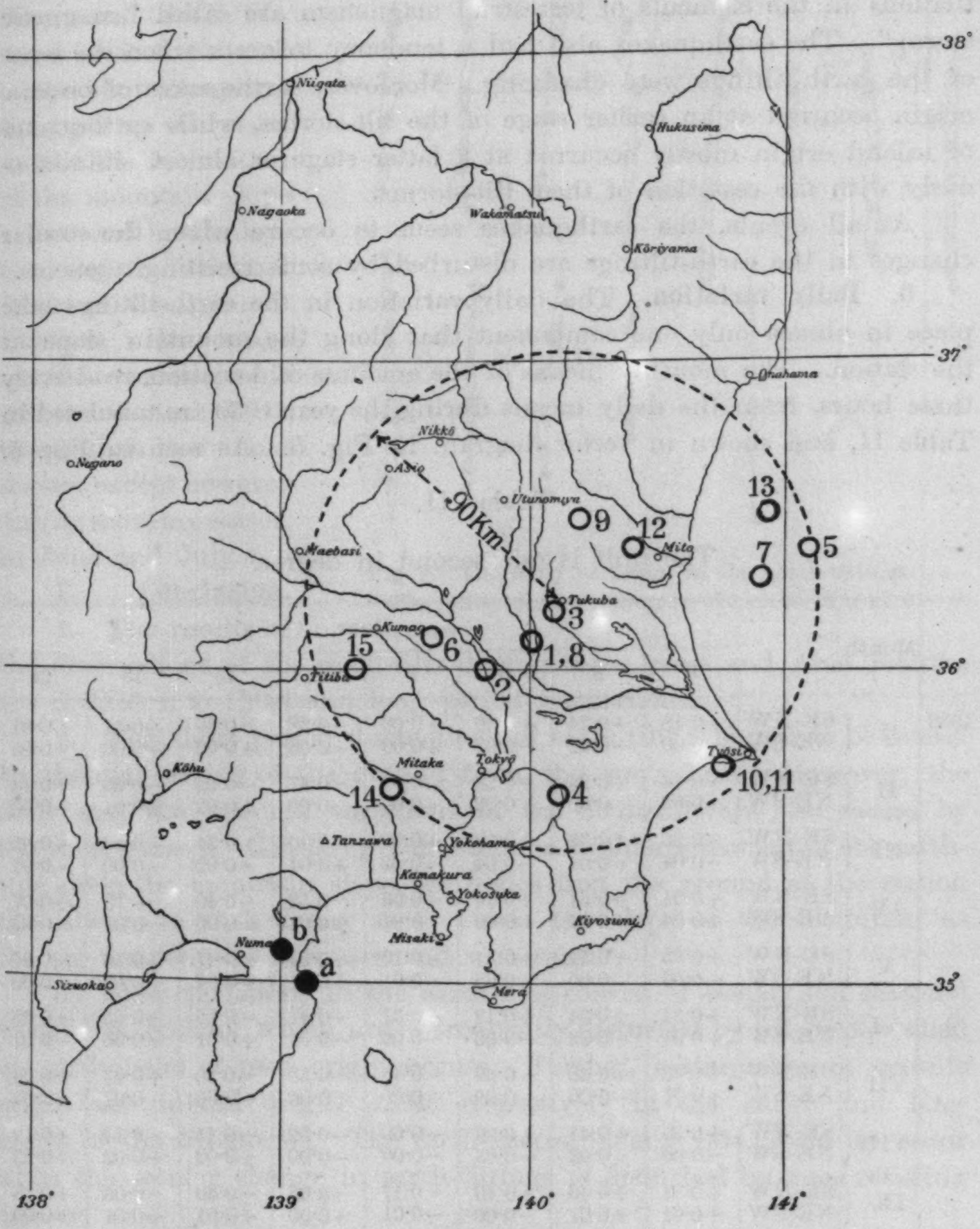

Fig. 4.

As will been seen from Fig. 3, the earthquakes generally occurred when the secular change in earth-tiltings were undergoing irregular fluctuations of comparatively short period. The irregular fluctuations in the earth-tiltings may be called "tilt-storm" just as irregular fluc-

tuations in the elements of terrestrial magnetism are called "magnetic storm". The earthquakes also had a tendency to occur when the sense of the earth-tiltings were changing. Moreover, earthquakes of oceanic origin occurred at an earlier stage of the tilt-storms, while earthquakes of inland origin mostly occurred at a latter stage or almost simultaneously with the cessation of these tilt-storms.

At all events, the earthquakes seem to occure when the secular changes in the earth-tiltings are disturbed by some resisting agencies.

6. Daily variation. The daily variation in the earth-tiltings take place in almost only one component that along the mountain slope at the station. The monthly means of the amounts of deviation, read every three hours, from the daily means during the year 1930 are tabulated in Table II, and shown in vector diagram in Fig. 5. As seen in Fig. 5,

Table II.

The unit is one second in degree.

	Month		Hour							
			0	3	6	9	12	15	18	21
1930	I	SE-NW	+0·18	+0·24	+0·30	+0·06	−0·38	−0·29	−0·11	−0·01
		NE-SW	−0·00	−0·02	−0·03	+0·00	+0·03	+0·02	+0·00	−0·05
	II	SE-NW	+0·14	+0·24	+0·28	−0·01	−0·47	−0·32	−0·05	+0·14
		NE-SW	+0·02	0·00	−0·02	−0·00	−0·00	+0·02	+0·01	−0·00
	III	SE-NW	+0·20	+0·30	+0·29	+0·02	−0·40	−0·34	−0·14	+0·05
		NE-SW	−0·04	−0·04	−0·04	−0·02	+0·04	+0·02	−0·00	−0·01
	IV	SE-NW	+0·21	+0·31	+0·34	−0·03	−0·52	−0·40	−0·13	+0·07
		NE-SW	+0·04	+0·01	+0·00	−0·01	+0·01	−0·00	−0·03	−0·03
	V	SE-NW	+0·33	+0·54	+0·31	−0·10	−0·54	−0·47	−0·16	+0·07
		NE-SW	−0·03	−0·05	−0·05	−0·01	+0·01	+0·04	+0·02	+0·00
	VI	SE-NW	+0·31	+0·34	+0·12	−0·31	−0·41	−0·25	+0·03	+0·25
		NE-SW	+0·01	−0·02	−0·00	−0·00	−0·01	+0·01	+0·00	−0·01
	VII	SE-NW	+0·38	+0·28	−0·09	−0·35	−0·38	−0·20	+0·03	+0·24
		NE-SW	+0·01	−0·00	−0·00	−0·00	+0·00	+0·00	−0·01	+0·01
	VIII	SE-NW	+0·30	+0·41	+0·29	−0·09	−0·52	−0·45	−0·14	+0·12
		NE-SW	−0·00	−0·02	−0·03	−0·00	−0·00	+0·02	+0·02	+0·02
	IX	SE-NW	+0·31	+0·46	+0·40	−0·17	−0·65	−0·40	−0·08	+0·18
		NE-SW	+0·01	+0·01	−0·00	−0·01	+0·00	+0·01	+0·01	+0·00
	X	SE-NW	+0·23	+0·33	+0·34	−0·09	−0·47	−0·37	−0·13	+0·06
		NE-SW	−0·02	−0·04	−0·02	−0·00	+0·02	+0·01	+0·01	−0·00
	XI	SE-NW	+0·14	+0·26	+0·33	+0·13	−0·29	−0·39	−0·20	+0·00
		NE-SW	−0·02	−0·06	−0·04	−0·01	+0·04	+0·03	+0·03	+0·03
	XII	SE-NW	+0·09	+0·15	+0·20	+0·08	−0·20	−0·25	−0·15	−0·01
		NE-SW	−0·02	+0·01	−0·01	+0·00	+0·02	+0·01	0·00	−0·00

the ground tilts N. W.-ward and S. E.-ward as the air temperature increases or dicreases, so that the inclination of the mountain slope is lessened in the day-time by the thermal strain of the ground. Further, the range of the variations is greatre in the warm season than in the cold season, except however during the rainy season in June and July.

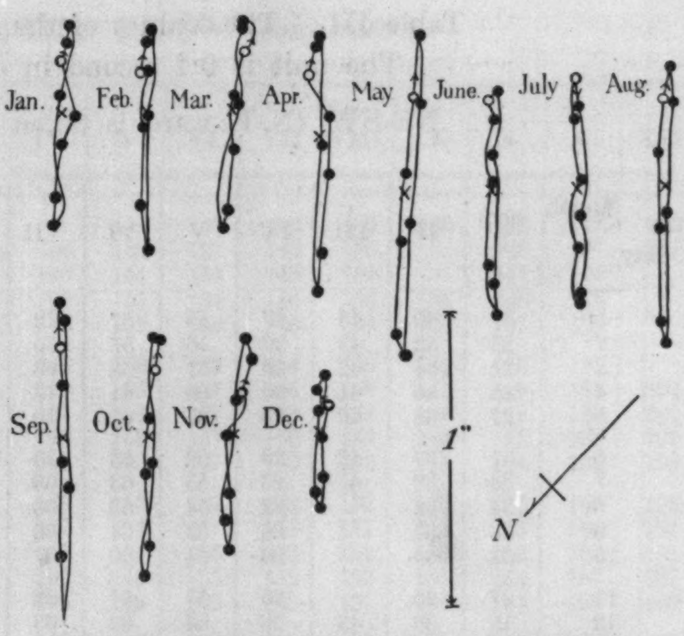

Fig. 5. The daily variation in the earth-tiltings. The white circles represent the earth-tilts at 0 o'clock.

7. Conclusion.

1. The results of the observations of the earth-tilts during three years and nine months are divided into short and long period fluctuations.

2. The short period fluctuations of earth-tilts is shown to be caused by thermal strains of the ground from the sun's heat. Moreover, the daily and the seasonal variations in the earth-tilts are also caused by the same reason. Confining our attention to the component of the earth-tilts along the mountain slope, we notice that the ground at the station tilts always in such a way as to lesson the slope of the mountain as the air temperature increases and vice versa.

3. Slow variations in the earth-tilts consist of secular and seasonal variations, both of which are of frequently disturbed by tilt-storms when an earthquake of near origin occurs. Further, earthquakes of oceanic origin and inland origin occur respectively in the ealier and later stages of the tilt-storms. The earthquakes, at any rate, seem to occur when the secular change in earth-tiltings is disturbed by some resisting agency.

Table III_1. The Values of the Earth-tilts.
The unit is 0·1 second in degree.

NE-SW. (N. E.-ward is taken positive.)

Day \ Month	1928 I	II	III	IV	V	VI	VII	VIII	IX	X	XI	XII
1	17	30	43	27	55	57	72	76	81	91	105	128
2	23	32	43	29	56	57	75	77		92	105	128
3	22	34	42	30	57	58	76	77		91	109	128
4	25	35	41	30	60	61	73	76		90	110	128
5	27	36	40	29	61	62	70	77		91	111	129
6	31	33	42	28	59	63	70	77		95	112	130
7	33	32	47	23	55	63	68	76	83	99	110	133
8	34	32		22	54	63	66	76	84	100	108	135
9	33	34		26	53	61	66	76	85	100	108	138
10	32	35		26	54	60	67	79	86	98	108	142
11	27	35		26	55	61	68	80	87	96	111	143
12	19	36	43	26	54	62	69	81	87	96	114	147
13	18	40	42	26	54	62	70	82	88	96	116	147
14	20	42	42	20	55	62	71	81	89	95	118	148
15	26	49	44	20	55	62	73	76	91	96	118	148
16	27		45	21	55	61	76	75	91	96	115	148
17	28		43	22	55	65	78	75	89	96	111	150
18	27		40	22	57	67	78	75	89	95	113	151
19	26		37	22	59	70	78	74	93	99	117	152
20	25		32	23	61	69	79	74	95	101	119	153
21	28		23	24	61	70	80	76	97	101	119	
22	30		19	26	61	72	83	78	97	103	119	
23	31	48	17	36	62	72	86	78		103	119	
24	29	42	18	40	62	71	89	78	98	104	120	
25	26	42	19	41	63	70	91	78	99	106	120	
26	23	42	20	40	62	69	91	78	99	105	122	
27	21	42	19	41	62	68	89	80	98	105	121	154
28	19	42	21	44	63	69	87	81	96	104	123	153
29	21	42	22	51	64	69	84	81	93	103	125	152
30	24		22	55	60	70	79	81	92	103	128	149
31	27		24		57		79	81		105		147

Table III_2. NE-SW.

Day \ Month	1929 I	II	III	IV	V	VI	VII	VIII	IX	X	XI	XII
1	145	156	169	152	139	136	139	155	137	140	170	194
2	148	157	165	152	138	134	139	156	139	140	170	194
3	152	157	164	152	137	134	139	155	139	142	172	194
4	154	155	167		137	135	142	155	138	144	176	194
5	155	156	167		143	135	142	155	138	147	177	196

(to be continued.)

Table III_2. NE-SW. (*continued.*)

Day \ Month	1929 I	II	III	IV	V	VI	VII	VIII	IX	X	XI	XII
6	154	156	167		151	137	142	155	136	148	178	203
7	153	157	167	153	152	137	143	155		148	177	207
8	154	158	167	146	151	134	145	157		147	177	
9	153	159	166	166	151	134	146	158	138	146	178	
10	152	160	165	149	152	136	145	158	134	147	179	
11	151	161	165	149	152	137	144	158	132	149	181	
12	151	163	166	149	153	137	145	156	141	149	186	204
13	151	165	165	147	154	137	149	154	144	149	186	201
14	153	166	165	148	153	137	150	153	144	152	189	197
15	153	166	169	148	153	137	150	152	144	154	189	193
16	153	165	170	149	153	137	153	152	143	155	185	192
17		165	170	149	153	137	155	151	141	153	184	191
18		164	169	147	151	136	153	151	138	153	185	191
19	157	164	165	145	149	135	152	152	137	153	187	187
20	157	165	162	146	148	136	150	151	134	154	189	190
21	156	166	159	148	143	136	149	150	131	152	192	198
22	156	166	156	151	134	137	145	149	132	154	193	202
23	157	167	154	151	127	138	146	149	133	157	194	206
24	157	167	153	151	131	138	147	145	135	158	197	207
25	157	166	151	151	134	138	148	142		161	200	
26	158	166	148	150	135	137	149	140		161	200	
27	157	168	147	147	135	137	149	140		162	200	
28	156	169	148	146	137	138	151	141		164	200	
29	157		148	144	135	137	152	140		163	200	
30	157		149	140	136	138	153	140		162	198	
31	156		151		136		155	138		165		

Table III_3. NE-SW.

Day \ Month	1930 I	II	III	IV	V	VI	VII	VIII	IX	X	XI	XII
1	214	205	202	200	182	190	179	175	175	165	172	178
2	214	205	203	206	185	181	178	172	175	163	171	178
3	213	205	202	210	188		177	171	175	162	173	178
4	213	205	201	211	189	178	178	174	174	164	174	178
5	210	204	200	212	185	177	176	175	173	167	175	179
6	212	200	201	210	185	177	176	176	172	166	176	179
7		199	203	205	188	180	170	169	174	165	176	179
8	215	199	202	203	188	181	170	169	174	163	176	178
9	215	198	205	202	189	178	170	167	173	160	173	178
10	214	198	207	201	188	178	171	166	172	159	171	177
11	213	199	208	200	188	177	179	166	172	159	170	176
12	212	203	208	198	186	178	180	165	172	160	171	175

(*to be continued.*)

Table III$_3$. NE-SW. (*continued.*)

Day \ Month	1930 I	II	III	IV	V	VI	VII	VIII	IX	X	XI	XII
13	211	203	207	196	186	178	180	164	171	160	173	174
14	210	203	205	197	187	178	180	164	170	160	178	175
15	209	202	202	197	188	177	182	164	166	161	178	177
16		201	203	198	187	175	180	164	164	162	177	180
17		199	202	199	188	178	181	165	163	162	177	180
18		198	202	197	189	183	180	166	162	161	177	178
19	206	197	202	196	189	184	179	167	163	162	177	178
20	208	197	201	195	187	185	179	169		161	177	177
21	208	197	202	191	187	184	178	168	164	163	176	176
22	208	196	206	190	187	181	179	170	164	165	175	176
23	207	195	207	188	187	180	180	171	163	167	175	178
24	206	195	207	185	188	180	180	170	164	168	177	179
25	205	196	201	185	187	177	180		164	168	178	179
26	205	195	200	185	188	177	179		164	167	178	179
27	205	192	200		189	177	178	170	165	170	180	178
28	204	195	200	187	188	176	178	170	165	170	181	178
29	203		199	184	190	177	179	171	166	169	181	176
30	204		199	181	190	178	178	173	166	169	180	175
31	205		198		191		177	175		171		

Table III$_4$. NE-SW.

Day \ Month	1931 I	II	III	IV	V	VI	VII	VIII	IX
1	178	183	184	188		186	186	192	199
2	177	183	184	188	177	186	188	194	196
3	177	183	183	189	179	185	189	194	196
4	177	185	185	189	178	184	188	194	196
5	177	185	185	187	174	185	188	194	196
6	176	186	185	180	175	186	187	195	196
7	175	187	186	180	173	185	187	195	195
8	176	191	188	181	171	185	187	196	196
9	178	191	189	182	170	185	188	198	196
10	179	192	189	181	170	186	189	199	197
11	180	192	189	180	173	188	191	199	197
12	181	191	190	180	176	189	192	199	195
13	184	190	191	180	178	193	192	197	192
14	187	188	192		181	193	194	198	186
15	188	185	192	179	183	192	194	199	185
16	188	183	192	175	182	190	195	198	187
17	187	184	192	175	184	189	194	197	189
18	185	185	191	175	181	190	193	197	191
19	183	188	191	176	178	191	191	196	190
20	183	188	192	177	178	193	185	196	191

(*to be continued.*)

Table III_4. NE-SW. (*continued.*)

Day \ Month	1931 I	II	III	IV	V	VI	VII	VIII	IX
21	182	186	193	177	179	193	183	198	192
22	183	186	194	177	178	192	184	198	193
23	183	186	194	178	181	189	185	197	190
24	183	186	192	177	183	187	188	197	190
25	183	186	191		185	183	191	195	192
26	183	186	190		185	183	190	196	192
27	183	185	190		185	184	188	197	198
28	183	184	190		188	184	187	199	199
29	185		191		188	185	187	199	197
30	186		192		188	185	190	200	197
31	185		191		187		193	200	

Table III_5. SE-NW. (S. E.-ward is taken positive.)

Day \ Month	1928 I	II	III	IV	V	VI	VII	VIII	IX	X	XI	XII
1	7	24	35	11	6	−32	−73	− 90	−87	−73		
2	14	31	43	12	− 7	−32	−74	− 92	−89	−76		−73
3	17	29	34	8	−16	−38	−71	− 90	−88	−73	−98	−76
4	20	25	40		−13	−37	−64	− 91	−88	−69	−88	−77
5	21	25	49		−16	−36	−69	− 93	−90	−70	−87	−75
6	25	27	48	− 2	−18	−38	−74	− 96	−90	−78	−85	−77
7	30	15	45	− 1	−22	−39	−71	−100	−85	−81	−81	−76
8	32	22	42		−21	−46	−73	− 95	−85	−92	−81	−76
9	34	18	43		−23	−47	−75	− 96	−87	−94	−82	−76
10	27	14	39	12	−21	−54	−77	− 99	−83	−86	−77	−81
11	16	20	28	10	−23	−55	−82	− 98	−81	−84	−72	−75
12	19	19	29	11	−21		−82	−105	−79	−88	−71	−75
13	22	19	35	9	−22	−63	−83	−105	−80	−85	−73	−75
14	24	20	33	6	−26	−63	−85	−108	−82	−88		−74
15	25	24	27	5	−27	−58	−88	−100	−83	−82		−72
16	26	34	24	13	−20	−54	−90	− 97	−84	−87	−91	−73
17	24	32	23	21	−13	−53	−87	− 96	−72	−82	−86	−68
18	26	31	16	17	− 8	−60	−84	− 99	−69	−74	−77	−65
19	28	30	12	15	−11	−60	−80	− 93	−70	−80	−76	−62
20	29	32	5	20	− 8	−64	−76	− 93	−72	−86	−81	−56
21	31	28	0	11	−10	−70	−73	−101	−74	−85	−77	−60
22	29	28	0	7	−20	−70	−71	−102		−90	−75	−59
23	27	25	− 1			−72	−72	− 95		−88	−74	−61
24		33	− 1	−12		−73	−78		−78	−89	−75	−60
25	18	41	− 3	− 7		−76	−83	− 89	−80	−90	−79	−58
26	16	40	− 3	− 3		−74	−83	− 84	−70	−91	−81	−56
27	14	39	0	− 1	−21	−71	−83	− 86	−73	−92	−79	−57
28	14	42	− 2	0	−21	−72	−88	− 84	−73	−88		−56
29	20	43	3	− 3	−21	−71	−87	− 81	−74	−90		−56
30	21		7	3	−23	−71	−84	− 80	−70	−84		−52
31	24		9		−26		−85	− 82				−52

Table III$_6$. SE-NW.

Day \ Month	1929 I	II	III	IV	V	VI	VII	VIII	IX	X	XI	XII
1	−53	−52	−54	−55	−49	−32	−33		−9	21	16	−2
2	−46	−51	−46	−49	−49	−40	−31		−9	28	22	−5
3	−43	−53	−41		−33	−40	−26		−8	31	16	−3
4	−50	−54	−46		−25	−40	−30	−44	−4	23	15	−2
5	−56	−59	−47		−25	−38	−31	−35	−6	12	9	4
6	−60	−57	−51		−26	−32	−25	−36		12	12	8
7	−57	−54	−52	−55	−22	−22	−19	−26		11	11	11
8	−56	−57	−55	−54	−28	−13	−17	−32		13	13	8
9	−59	−56	−58	−57	−33	−18	−22	−32			15	10
10	−62	−49	−59	−60	−30	−26	−22	−35			20	11
11	−65	−45	−56	−48	−32	−32	−29	−32			21	10
12	−66	−39	−54	−47	−33	−29	−43	−31	21		13	6
13	−64	−40	−51	−59	−34	−22	−53	−30	24		12	0
14	−65	−40	−41	−57	−31	−18	−56	−29	17		9	−4
15	−61	−41	−41	−59	−35	−16	−56	−26	12		4	−3
16	−53	−46		−66	−35	−16	−56	−25	9		6	0
17	−50	−48		−68	−40	−25	−46	−30	8	14	7	−3
18	−50	−48	−52	−62	−41	−22	−40	−30	5	10	9	−6
19	−48	−50	−55	−57	−42	−32	−40	−27	−2	16	11	4
20	−47	−51	−54	−55	−51	−36	−37	−28	−4	19	13	11
21	−46	−52	−49	−61	−48	−32	−27	−31	3	18	10	
22	−43	−58	−51	−55	−48	−41	−23	−30	4	23	11	15
23	−48	−58	−55	−56	−47	−35	−29	−18	6	25	12	15
24	−51	−52	−57	−56	−55	−31		−13	9	18	15	
25	−53	−46	−57	−59	−60	−33		−9	10	22	9	
26	−55	−42	−53	−62	−58	−39		−6	16	15	6	
27	−57	−42	−56	−64	−59	−40	−31	−11	12	0	0	
28	−53	−42	−64	−64	−58	−39	−31	−10	13	10	−2	
29	−55		−60	−55	−52	−40	−39	−12	13	14	−1	
30	−52		−57	−55	−46	−39	−41	−11	18	14	−2	
31	−52		−53		−36			−7		11		

Table III$_7$. SE-NW.

Day \ Month	1930 I	II	III	IV	V	VI	VII	VIII	IX	X	XI	XII
1	17	7	12		20	10	12	2	15	21	15	10
2	16	8	11		18	15	10	2	13	21	9	16
3	11	5	11	12	5		2		11	24	11	12
4	3	8	9	−1	5		−5		13	23	11	14
5	−5	5	12	−6	7	28	−2		14	21	14	15
6	−3	3	13	−3	12	22	9	5	20	24	13	9
7	0	0	10	−4	14	19	12	−7	26	29	11	2
8		2	3	5	13	21	13	−3	28	23	10	4

(to be continued.)

Table III_7. SE-NW. (*continued.*)

Day \ Month	1930 I	II	III	IV	V	VI	VII	VIII	IX	X	XI	XII
9		3	−2	2	14	26	17	6	27	24	14	2
10	0	−1	−4	3	10	24	20	1	23	26	9	2
11	−4		−4	−3	11	29	15	−2	21	27	11	4
12	−2		−6	9	21	22	9	−2	22	25	14	−1
13	−2		−10	8	21	22	6	−2	23	24	18	2
14	−2		−15	5	21	28	−5	−3	25	24	26	10
15	−6	−8	−8	7	18	31	−7	−2	26	30	24	10
16		−7	−5	4	18	36	−10	−3	23	31	23	11
17		−6	−2	2	19	31	−5	0	20	31	24	11
18		−1	−4	−2	14	23	−1	3	21	30	25	8
19		2	3	−6	21	25	3	3	26	25	30	6
20	2	−2	5	2	19	17	10	1		27	26	5
21	3	4	5	8	22		17	6		26	11	8
22	5	7	5	8	23		21	2	22	24	12	12
23	3	8	3	12	20		18	2	12	19	14	13
24	1	5	2	15	29		15	3	17	19	15	11
25	4	5	7	11	32		14		15	14	17	7
26	5	16	7	9	25	21	8		19	10	18	7
27	6	22	7	6	30	25	4		22	4	11	6
28	7	22	8	10	29	20	1	18	19	8	11	5
29	5		5	21	20	22	1	20	17	9	13	8
30	2		11	20	19	10	5	15	19	12	12	10
31	3		18		13		5	13		17		8

Table III_8. SE-NW.

Day \ Month	1931 I	II	III	IV	V	VI	VII	VIII	IX
1		9	1	26	28	−11	−27	−44	−31
2	8	3	1	22	27	−12	−27	−48	−30
3	5	7	−2	26	25	−8	−30	−47	−31
4	2	9	3	24	24	−3	−27	−45	−33
5	0		−1	27	22	−7	−24	−49	−41
6	6		1	27	10	−7	−19	−56	−36
7	6	11	−4	30	8	−4	−17	−56	−36
8	8	13	3	27	20	−2	−16	−56	−40
9	8	9	3	24	30	−3	−11	−60	−37
10	4	12	8	22	30	0	−8	−54	−45
11	5	10	7	25	28	−6	−6	−52	−47
12	5	12	8	30	30	2	−10	−50	−45
13	2	13	12	28	13	−22	−12	−42	−45
14	−1	5	13	22	5	−24	−11	−45	−37
15	0	−2	14	24	6	−21	−17	−46	−32

(*to be continued.*)

Table III_8. SE-NW. (*continued.*)

Day \ Month	1931 I	II	III	IV	V	VI	VII	VIII	IX
16	1	−1	14	19	1	−10	−21	−47	−33
17	−1	−2	13	19	−13	−13	−21	−47	−36
18	−1	1	17	29	−8	−12	−22	−45	−34
19	−2	0	23	29	−3	−12	· 28	−50	−38
20	0	−6	20	32		−14	−22	−52	−40
21	3	0	18	30		−16	−19	−51	−35
22	3	1	17	26		−15	−18	−49	−36
23	3	−2	13	26		−15	−19	−47	−38
24	3	−1	22	31		−14	−21	−42	−37
25	9	−3	23	25		−13	−23	−31	−38
26	8	−2	20	20		−13	−24	−36	−35
27	10	−7	23	23		−17	−24	−38	−55
28	7	3	26	22	−11	−17	−30	−43	−60
29	6		25	25	−16	−19	−36	−38	−61
30	5		23	19	−18	−21	−48	−30	
31	11		24		−17		−46	−26	

---

10. 筑波山に於ける傾斜變化觀測報告

地震研究所　井　上　宇　胤

1. 筑波山に於ける三年九ケ月に亙る傾斜變化觀測の結果を二週間程の短週期の部分と長週期の部分に分解しました。

2. 此の短週期の變化は太陽の輻射熱に依つて起される地表面の熱變形の爲に起るものであります。尙傾斜變化の日々變化及び季節變化も共に同樣な原因に依るものであります。今此等の變化の內觀測所に於ける山の傾斜の方向の成分のみに就いて考へますと、いずれの場合も外界の氣溫の上昇に伴つて山の傾斜の度を減ずる如く傾斜變化が起つて居ります。

3. 長週期の變化は、しばしば傾斜嵐に依つて亂されて居ります。此の傾斜嵐の際に筑波山附近の地震が發生して居ります。尙其の內、海底地震は傾斜嵐の初期に於て、內陸地震は終期に於て發生して居ります。

4. 兎に角、傾斜變化の積年變化が何物かにさまたげられる期間に此の附近の地震が發生して居るものと解釋されるかも知れません。

11. Tilting Motion of the Earth's crust observed at Kawana.

By Ryûtarô TAKAHASI,

Earthquake Research Institute.

(Read Dec. 15, 1931.—Received Dec. 20, 1931.)

In a short time of only three months, beginning on the 23th. of March, 1930, Itô and its neighbouring region have experienced numerous earthquakes of moderate strength, which exceed 3715 in number[1]. In the case of these earthquakes, various kinds of seismological research[2] were executed by many investigators.

One of the aims of these researches was to observe the movement of land-blocks which lie in the epicentral region of the earthquakes. For this purpose, tiltmeters were installed at Itô and Kawana, the nearest villages to the epicentral region of the earthquakes. The results obtained by these tiltmeters showed that the movements of the Itô and Kawana blocks were related very closely with the activity of the earthquake centres.[3]

It was also noticed in the reseach above that a regular tilting motion which have the same period, and is very similar in form with tides, is superposed on the cumulative tilt of Kawana block. Similar phenomena with this have been observed at Aburatubo Bay, Misaki, and were attributed to the deformation of the earth's crust caused by the varying load of tides.[4] The present paper deals with this regular tilting motion of the earth's crust observed at Kawana and describes the relation of this tilt with tides.

The village of Kawana is situated at the eastern coast of Idu penninsula, Japan (34°57′N; 139°08′E). The village is surrounded by steep cliffs on all sides except north-east, in which direction it faces to the

1) A. Imamura, *Disin.* 2 (1930), 291.

2) Military Land Survey Department, *Bull. Earthq. Res. Inst.*, 8 (1930), 375; 9 (1931), 109.

M. Ishimoto and R. Takahasi, *Bull. Earthq. Res. Inst.*, 8 (1930), 427.

N. Nasu, F. Kishinouye and T. Kodaira, *Bull. Earthq. Res. Inst.*, 9 (1931), 22.

H. Tsuya, *Bull. Earthq. Res. Inst.*, 8 (1930), 409.

3) R. Takahasi, *loc. cit.*, 437.

4) R. Takahasi, *Bull. Earthq. Res. Inst.*, 6 (1929), 85; 7 (1929), 95.

bay of Kawana, a part of the Sagami Bay. Topographical features of the neighbourhood of Kawana can be seen in Fig. 1, in which the tiltmeter station is indicated by *A*. Tiltmeters were installed in a cave bored in a natural layer of volcanic scolia which is appearing on the west side of the village. The cave is about 3m. × 2·5m. × 2·5m. in size and has on the south-east side a narrow entrance provided with a wooden door. Inner surface of the cave is not lined at all, and the tiltmeters were installed directly on the floor of the cave in the directions N-S and E-W. The cave is 20 m. above the mean sea level and 80 m. distant from the nearest beach line. General ideas of the cave can be obtained from Fig. 2.

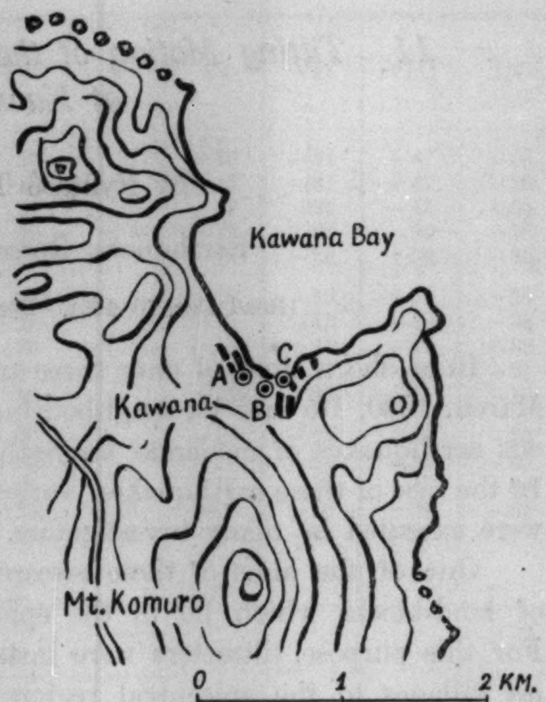

Fig. 1. *A*....Tiltmeter station
B.... „
C....Tide guage
(Based on the chart No. 80 issued from the Hydrographic Department, Japan).

The tiltmeter is a horizontal pendulum of the Zöllner suspension type, of which the frame work, the movable horizontal rod and suspension fibres are all made of fused silica. The instrument is therefore entirely free from elastic after-effect and the effect of temperature variation. Details of the instrument will be omitted in this paper, as it has often been described in other papers.[5] In the tiltmeter used in the present research, however, a slight modification was made in recording the time-marks. As it was desired to obtain a perfect correspondence of time between the records of E-W and N-S components of tilt, the light sources of both components, which are connected in parallel, were lighten for two minutes every an hour by making the electric circuit by a clock work so as to obtain such dotted records of tilt as shown in Fig. 3. In this and the following figures the letters E, W, N, S indicates the directions *toward which the ground tilts.*

The original purpose of the installation of these tiltmeters was, as was already stated in the above, to detect the movement of Kawana block

5) M. ISHIMOTO, *Jap. Journ. Astro. Geophys.*, 6 (1928), 83.

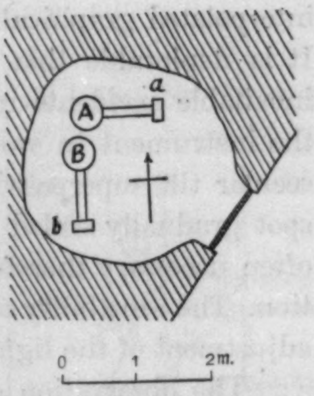

Fig. 2. Tiltmeter station.
A E-W component horizontal pendulum.
B N-S component horizontal pendulum.
$\left.\begin{matrix} a \\ b \end{matrix}\right\}$ Recording parts.

related with the Itô earthqukes. Because the epicentres of the Itô earthquakes were all in a small area which lie a few kilometers off the coast of Kawana,[6] the variation of tilt of the Kawana block was supposed, at the beginning of the observation, to be very large. Under this expectation, the sensibility of the tiltmeter was adjusted to give an deflection of 1 cm. on the record for the variation of tilt of 1 second of arc. The sensibility, however, was doubled afterwards, as the amount of tilt of the block was found later not to be so large as expected.

At the same time with the tiltmeter observation, the tides of Kawana Bay was recorded at *C* indicated in Fig. 1 by a portable tide-guage. This tide-guage is based on the same principle with that described formerly by the author[7] but is modified to record automatically the height of mercury column that is balancing with the water-head between the tide-guage and the sea surface. Magnification coefficient of this tide-guage is 1/26·2. As the Bay of Kawana has a broad mouth, great waves often attack the shore when north-east wind blow strongly. The tide-guage was sometimes swallowed by a greate surf and other times was forced to dismount lest it is swayed off by waves.

The observation of tilt was commenced on the 19th. of March, 1930, and continued till the 12th. of July of the same year. Attendance and management of the tiltmeters and tide-guage were carried out by Mr. I. Kikuma during the whole period of observation. The results of observation of tilt are all given in Table I below. The numbers contained in the table are the hourly readings of the distance between the tilt-curve and the datum line on the record. Because they were measured in unit of 0·1 mm., 1″ corresponds to 100 in the earlier part, and to 200 in the later part of the period of observation. As the period of observation has fallen in the active period of the Itô earthquakes, intermittent lightings of the light source have sometimes coincided with the occurrence of an earthquake. In such cases the tilt could not be recorded, because the horizontal pendulums were in oscillation by the disturbance of the earthquake. The values of tilt for such instants were

6) N. Nasu, F. Kishinouye and T. Kodaira, *loc. cit.*, 23.
7) *Bull. Earthq. Res. Inst.*, 7 (1929), 97.

interpolated graphically from the values 1 hour before and after them. It is deplorable that the observation was often interrupted by various inevitable accidents in spite of the great effort of Mr. Kikuma to keep the instrument in working condition. Since there existed a remarkable secular tilt superposed on short perioded variations, the recording light spot gradually scaled out from the recording part of the tiltmeter; it was often necessary therefore to bring back the light spot to its normal position. The sensibility of the instrument was measured in every time of this adjustment of the light spot, and was kept at the standard sensibility.

The observation of tides was commenced on the 22th. of April and continued till the 12th. of July. In this interval the observation was often interrupted by various causes such as storms. It is very difficult to obtain a long continuous record by a portable tide-guage in such a drear coast as Kawana. Hourly readings of the height of tides are given in Table II below in which unity corresponds to 2·62 cm.

In Fig. 4a are given the tide curve in comparison with the curves of the E-W and N-S components of tilt. As can be seen in the figure, variations of tilt are the same in period and are very similar in form with tides; there is no doubt that this tilt variation is in close relation with tides though there exist considerable phase laggs among these three curves. To the right of Fig. 4 is given the vector-diagram of tilt corresponding to the period from April 25 th. 12 h. 30 m. to 26 th. 12 h. 30 m. Because there is a phase lagg between two components of tilt, the vector diagram describes elliptic loops of very complicated character. The instances of high water and low water, indicated in Fig. 4 b by the letters H. W. and L. W., do not coincide with the time of maximum tilt, but occur about two hours before it. As these curves show, the relations existing between the tilts and the tides are so complicated that it is better for the further study of the phenomena to analyse the tilt-curves and tidal curve into their harmonic components with different periods.

The period of observation of tilt selected for the harmonic analysis is 15 days beginning at 0 h. 30 m. of April 22th., 1930. Because on the tilt-curves are superposed cumulative tilts, we must in the first step of the analysis eliminate this disturbing components. For this purpose, daily means of hourly readings were calculated overlapping by 12 hours and the values obtained were assigned to the central hour. Successive mean values, thus obtained, were connected by a smooth curve, which was taken as zero-line. Hourly readings of this zero-line are given in Table III.

Deflection of the curve from this zero-line was sought and analysed

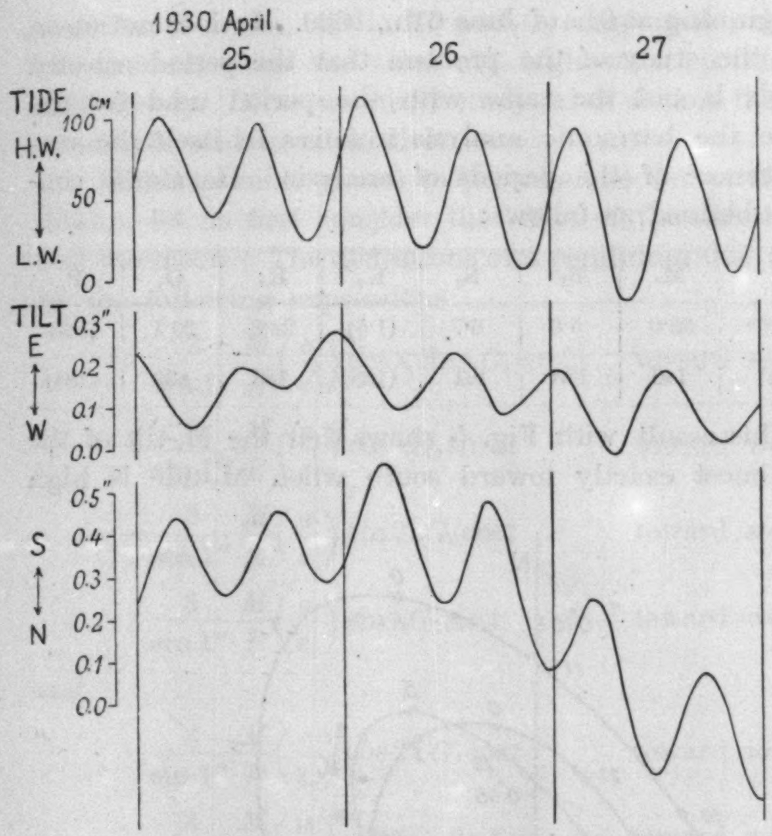

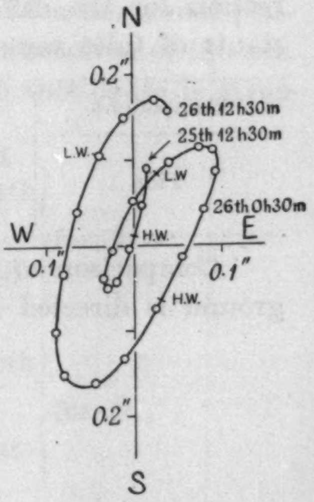

Fig. 4b.
Vector-diagram of tilt.

Fig. 4a. Tides and tilt observed at Kawana.

by the schedule of harmonic analysis given by A. T. Doodson.[8] The method need not be explained here, but the results of this analysis are obtained after making all such corrections as that due to the factor of reduction, acceleration in epoch, disturbances among different components, reduction to local time, etc. Results obtained are as follows:

		M_2	S_2	N_2	K_2	K_1	O_1	P_1
Tilt toward west	H''	0·082	0·028	0·030	(0·008)	0·053	0·050	(0·018)
	$\kappa°$	241	253	201	(253)	228	256	(228)
Tilt toward south	H''	0·110	0·052	0·017	(0·014)	0·076	0·072	(0·025)
	$\kappa°$	186	209	179	(209)	183	189	(183)

In Fig. 5 the vector diagram of M_2 K_1 and O_1 component tilts are shown. In order to compare with this result, we must next analyse the tidal observations obtained at Kawana. The period used for the analysis

8) A. T. Doodson, *Phil. Transact.*, **227 A** (1927), 223.

of tides is 15 days beginning at 0h. of June 6th., 1930. It does not mean any impediment for the study of the problem that the period selected for the tidal analysis is not the same with the period used for the analysis of tilt, since the harmonic analysis involves in itself the correction for the differenece of the periods of analysis. Harmonic constants of tides were obtained as follows:

Component		M_2	S_2	N_2	K_2	K_1	O_1	P_1
Tide	H^{cm}	36·0	5·6	6·7	(1·5)	22·8	20·1	(7·5)
	κ°	146	188	161	(188)	188	163	(188)

Comparison of this result with Fig. 5 shows that the M_2-tilt of the ground is directed almost exactly toward south when M_2-tide is high

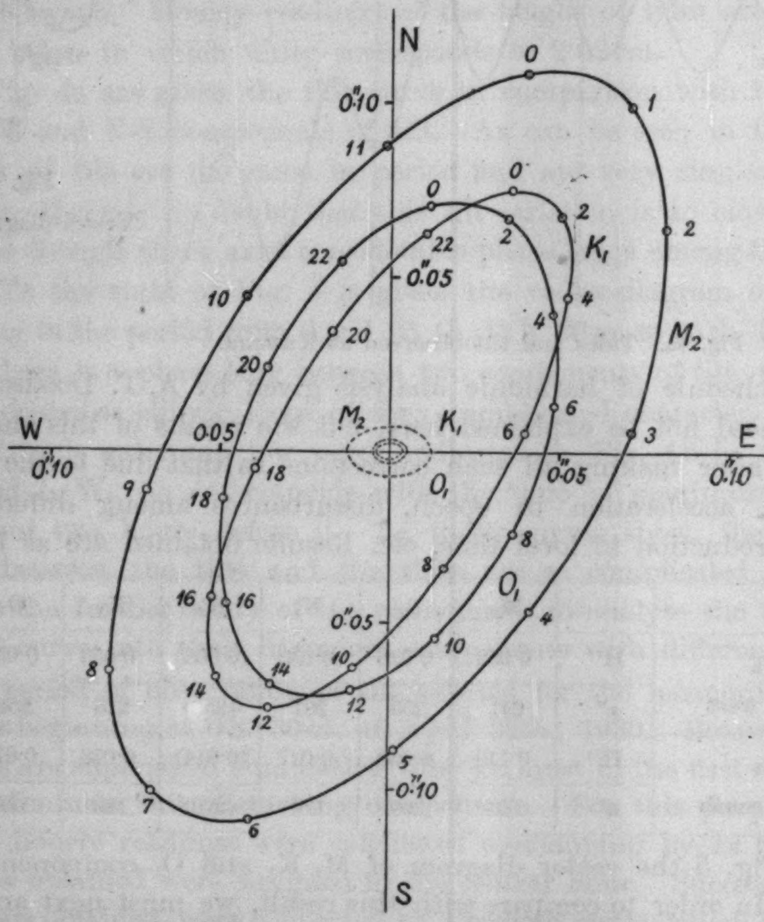

Fig. 5. Full lines Observed component-tilts.
Dotted lines Component-deviation of plumb line due to direct attraction.
Numerical figures indicate component hours.

water at Kawana. As to K_1 and O_1 components, the directions of tilt of the ground when the tides are high water point SSW. and S by W. respectively. Now we must study what makes the ground tilt in such a manner and in such directions.

Of all possible causes to provoke the deflection of a horizontal pendulum, let us first consider the effect of the direct attraction of the sun and the moon. The deflections of a pendulum due to this cause is given by the following expressions:

$$\left.\begin{array}{ll}\dfrac{3}{\sin 1''}\dfrac{M}{E}\left(\dfrac{a}{c}\right)^3\cos\lambda\sin\lambda G_1\cos 2t & \text{toward south}\\[2ex] \dfrac{3}{\sin 1''}\dfrac{M}{E}\left(\dfrac{a}{c}\right)^3\cos\lambda G_1\sin 2t & \text{toward west}\end{array}\right\}\text{for } M_2;$$

$$\left.\begin{array}{ll}-\dfrac{3}{\sin 1''}\dfrac{M}{E}\left(\dfrac{a}{c}\right)^3\cos 2\lambda G_2\cos t & \text{toward south}\\[2ex] \dfrac{3}{\sin 1''}\dfrac{M}{E}\left(\dfrac{a}{c}\right)^3\sin\lambda G_2\sin t & \text{toward west}\end{array}\right\}\text{for } O_1;$$

and

$$\left.\begin{array}{ll}-\dfrac{3}{\sin 1''}\dfrac{M}{E}\left(\dfrac{a}{c}\right)^3\cos 2\lambda\, G_3\cos t & \text{toward south}\\[2ex] \dfrac{3}{\sin 1''}\dfrac{M}{E}\left(\dfrac{a}{c}\right)^3\sin\lambda G_3\sin t & \text{toward west}\end{array}\right\}\text{for } K_1;$$

where

$$G_1=\left(\frac{1}{2}-\frac{5}{4}e^2\right)\cos^4\frac{I}{2},$$

$$G_2=\left(\frac{1}{2}-\frac{5}{4}e^2\right)\sin I\cos^2\frac{I}{2},$$

$$G_3=\left[\left(\frac{1}{4}-\frac{3}{8}e^2\right)^2\sin^4 I+\left(\frac{1}{4}+\frac{3}{8}e_1^2\right)^2G^2\sin^4\omega+2\left(\frac{1}{4}+\frac{3}{8}e^2\right)\left(\frac{1}{4}+\frac{3}{8}e_1^2\right)G\sin^2 I\sin^2\omega\cos 2\nu\right]^{\frac{1}{2}},$$

$$G=\frac{\text{mass of sun}}{\text{mass of moon}}\times\left(\frac{\text{mean distance of moon}}{\text{mean distance of sun}}\right)^3=0{\cdot}46164,$$

M is mass of moon,
E is mass of earth,
a is radius of earth,
c is mean distance of moon,
λ is latitude of the place,

t is hour angle of component fictious star or component hour,
ϵ is eccentricity of moon's orbit,
I is inclination of moon's orbit to equator,
ω is inclination of earth's equator to the ecliptic,
e_1 is eccentricity of earth's orbit,
and ν is R. A. of intersection of moon's orbit with equator. The amplitude and phase of the attraction calculated for Kawana by these expressions are, as follows:

Component		M_2	O_1	K_1
Toward west	H″	0·0128	0·0037	0·0053
	$\kappa°$	90	90	90
Toward south	H″	0·0074	0·0022	0·0032
	$\kappa°$	0	180	180

As will be seen in the table above, the contributions to the deflection of a horizontal pendulum from the direct attraction of the sun and the moon are very small compared with the tilt which was actually observed. These contributions are shown in Fig. 5 by dotted ellipses. If we consider that the earth deforms under the action of tide-generating force, this contribution to the deflection of a horizontal pendulum must bocome still less. Even if we make an unnatural assumption that the earth is everywhere covered with fluid of density 5·5 except at Kawana, where the crust is perfectly rigid, the contribution now in question becomes no more than 2·5 times as large as the original value. Therefore the effect of the direct attraction of the sun and the moon can by no means account for the main part of the actually observed tilt, though there must be some small percentage due to this cause.

Next we will consider the attraction of oceanic tides. The deflection of a horizontal pendulum due to the attraction of tides in the sectorial elementary area limited by r_1, r_2 and θ_1, θ_2 can be calculated by the expressions

$$-\frac{100\,\kappa\rho h}{g\sin 1''}(\log r_2-\log r_1)(\sin\theta_2-\sin\theta_1) \quad \text{toward south}$$

$$\frac{100\,\kappa\rho h}{g\sin 1''}(\log r_2-\log r_1)(\cos\theta_2-\cos\theta_1) \quad \text{toward west,}$$

where

r is the distance from the station,
θ is the azimuth mesaured from the north in the clockwise sense,

κ is the gravitational constant,

ρ is the density of sea water,

and h is the height of tides above mean sea level measured in meter.

Putting $2t_1 = 2t - 146°$, the attraction of M_2-tides were calculated for the domain within 610 km. of the tiltmeter station of Kawana. Results of the calculation is as follows.

r	Toward south		Toward west	
	$\cos 2t_1$	$\sin 2t_1$	$\cos 2t_1$	$\sin 2t_1$
100 m – 1 km	$-0''.001329$	0	$-0''.001240$	0
1 km – 5 km	-0.000854	0	-0.001289	0
5 km – 20 km	-0.000152	0	-0.001354	0
20 km – 100 km	$+0.000862$	0	-0.000737	0
100 km – 610 km	$+0.001186$	$-0''.000408$	-0.000723	$-0''.000720$
total	$-0''.000236$	$-0''.000408$	-0.005343	$-0''.000720$

This is equivalent to

$$-0''.000498 \cos(2t_1 - 55°) \quad \text{toward south}$$

$$-0''.005391 \cos(2t_1 - 8°) \quad \text{toward west,}$$

or in local lunar time t

$$+0''.000498 \cos(2t - 21°) \quad \text{toward south}$$

$$+0''.005391 \cos(2t + 26°) \quad \text{toward west.}$$

For the region beyond 610 km. of the station, we may use without introducing much errors the value of the attraction of M_2-tides for Kyôto, calculated by T. Shida[9]. This is

$$0''.001125 \cos(2t + 166°) \quad \text{toward south}$$

$$0''.001402 \cos(2t + 113°) \quad \text{toward west,}$$

where t is the Kyôtô lunar time; in the Kawana lunar time these become

$$0''.001125 \cos(2t + 159°) \quad \text{toward south}$$

$$0''.001402 \cos(2t + 106°) \quad \text{toward west.}$$

Therefore the total amount of the attraction of M_2-tides is

$$0''.000626 \cos(2t - 200°) \quad \text{toward south}$$

$$0''.006001 \cos(2t - 321°) \quad \text{toward west.}$$

The attraction component directed toward west is ten times as large as that

9) T. Shida, *Mem. Coll. Sci., Kyôto Imp. Univ.*, 4 (1910), 1.

directed toward south. The vector diagram of the attraction of M_2-tide is therefore a very flat ellipse, as shown in Fig. 6, having the longer axis nearly in E-W direction. The attraction attains to its maximum value at t=4h. 42m. and this maximum attraction points nearly to the east.

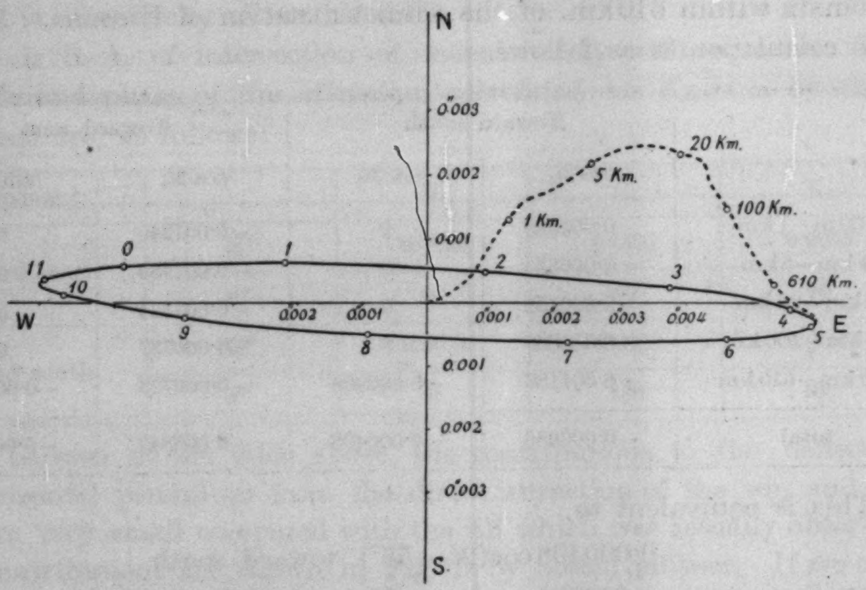

Fig. 6. Full line:—Attraction of tides.
Broken line:—Locus of the end of the longer axis of the ellipse when the calculation of attraction is extended to successive steps of distance.

The attraction of M_2-tide, being only 0·″006 at the maximum, as calculated just above, cannot account for the actually observed M_2-tilt. Then, we must attribute the observed tilt to the deformation of the earth's crust caused by the tidal loading, because there are no other possible causes which can provoke a tilt large enough to account for the actually observed value. It is well-known by the theory of elasticity that the tilt of the surface of a semi-infinite elastic body due to loads distributed on the surface is equivalent to the attraction of that load multiplied by $\frac{1}{4\pi}\frac{(\lambda+2\mu)}{\mu(\lambda+\mu)}\frac{g^2}{\kappa}$,[10] where λ, μ are Lamé's constants and κ is the gravitational constant. If the theory of elasticity holds good in the case of the actual earth, calculated tilt must be represented by an flat ellipse which is entirely similar and similarly situated with the ellipse given in Fig. 6. The maximum value of the calculated tilt amount to 0·″1, if we assume the rigidity of the earth's crust to be 10^{11} c. g. s. This amount of tilt is of the same order with the maximum value of

10) LOVE, "*Math. Theory Elasticity*", 193. Cambridge Univ. Press (1927)

the actual tilt. It can however easily be seen by the comparison of Fig. 5 with Fig. 6 that there is no resemblance between the two ellipses representing the calculated and the observed tilts. Calculated maximum tilt occur when $t=141°$ in the direction of nearly east, while the actually observed tilt is directed nearly to south at that time.

How can we elucidate this discordance in the direction of tilt which exist between the observed and calculated ones? If the rigidity of the earth's crust increases with depth, distant load from the station must be less effective than near load in producing the tilt of the ground at the station, because the greater the distance between the load and the station is, the deeper will be the portion of the crust that comes into play. This consideration is equivalent to assume the rigidity involved in the multiplyer $\frac{1}{4\pi}\frac{(\lambda+2\mu)}{\mu(\lambda+\mu)}\frac{g^2}{\kappa}$ to be a function of the distance of the load from the station.

On the other hand, the end of the longer axis of the ellipse representing the calculated attraction of M_2-tide approaches the origin by the way indicated in Fig. 6, by a dotted curve, as we curtail the calculation and take account only of the load distributed within successive steps of distance. Therefore if we select the functional form of the rigidity in such a way as to make the distant loads ineffective in producing the tilt at the station we can make the calculated tilt to point to any direction between E and NE. In fact, if we assume that the load distributed beyond 1 km. of the station is not effective in producing the tilt at the station, the calculated tilt turns toward NE. It is however impossible to make the calculated tilt to point to the south when $t=146°$, or to describe such a ellipse as actually observed, as long as we are dealing with the theory of Boussinesq or regarding the crust to be perfectly elastic. We must therefore consider some alternatives for the elucidation of the present phenomena. Let us for a while turn our attension to the geologic structure of the neighbourhood of Kawana tiltmeter station. The volcanic scolia into which the observing chamber is bored is very soft, being the most recent effusive of Mt. Komuro. The thickness of this effusive is probably between 100 m. and 200 m. Under this layer of new effusive, there are rocks of considerable rigidities belonging to the tertiary era, which are widely extended in the southern part of Idu penninsula.[11]

---

11) H. Tsuya, "On the Geologic Structure of Itô district, Idu." *Bull. Earthq. Res. Inst.*, 8 (1930), 409.

Geology of Kawana is therefore represented very well by a layer of sand placed on a sheet of rigid board. If a vertical force was applyed to such a layer of sand, it is very probable that the zone sourrounding the load swell out above the original position and tilt in the direction opposit to the load. If the position of the tiltmeter station correspond to the part of this swelling, the direction of the observed tilt must necessarily differ from that given by the theory of Boussinesq.

Boussinesq's solution of the problem of surface loading assumes, moreover, a semi-infinite non-gravitating homogeneous elastic solid and vertical pressure. In reality, however, the earth's surface of Kawana can never be said to be even, the tiltmeter station being on the foot of a steep cliff of a height comparable with the distance to the beach line. Beside this, the layer of scolia is intricated by the presence of lava-flows, and in the sea, there may be unknown faults. In these complicated conditions of the topography and geology the tilt does not necessarily occur in the direction toward the load. It is very probable that the actually observed tilt does not coincide with the calculated one but differ from it by all possible ways.

In short, the tilt observed at Kawana must be attributed to the deformation of the crust caused by the tidal loading, though we cannot explain by which cause such disaccordance in the direction occurs between the observed and calculated tilt. Further study of the problem depends largely on the developement of the dynamics of such materials as sand and soil, and also on tiltmeter observations similar with this which will be executed at different places in the future.

The writer wishes to express here his heartly thanks to Mr. I. Kikuma for his faithfull management of tiltmeters and to Mr. R. Takei for the preparation of tables and figures contained in the present paper.

Table I. Tilt observed at Kawana.

1930 III Unit=0."01

day	19		20		21		22		23		24		25	
Components	E-W	S-N	E-W	S-N	E-W	S-N	E-W	S-N	E-W	S-N	E-W	S-N		
h m 0 30	—	—	+222	−45	+257	−55	+243	−52	+312	−14	+272	+19	—	—
1 30	—	—	211	48	257	55	241	53	312	13	271	20	—	—
2 30	—	—	212	50	257	56	240	52	315	13	269	22	—	—
3 30	—	—	211	52	256	57	239	52	—	12	266	22	—	—
4 30	—	—	211	52	256	56	239	52	315	11	262	22	—	—
5 30	—	—	209	50	255	56	238	52	317	11	260	22	—	—
6 30	—	—	208	48	257	53	236	53	309	10	258	22	—	—
7 30	—	—	204	47	250	50	235	52	310	9	258	23	—	—
8 30	—	—	202	47	251	49	236	52	309	9	259	23	—	—
9 30	—	—	201	48	249	47	236	51	310	8	260	23	—	—
10 30	—	—	198	48	251	48	238	51	312	7	261	25	—	—
11 30	—	—	197	53	252	49	239	52	310	7	255	27	—	—
12 30	—	—	198	58	254	53	239	56	307	9	252	27	—	—
13 30	—	—	200	62	255	55	240	58	300	9	251	28	—	—
14 30	—	—	202	65	256	58	240	59	297	10	250	28	—	—
15 30	—	—	+273	67	258	59	240	62	295	10	251	30	—	—
16 30	—	—	272	65	258	60	241	64	294	12	252	30	—	—
17 30	—	—	268	—	257	61	241	66	293	13	252	28	—	—
18 30	—	—	267	63	256	59	+328	−22	299	—	251	27	—	—
19 30	+210	—	267	60	253	58	322	20	+279	+15	252	27	—	—
20 30	213	−23	264	58	250	57	320	19	279	13	252	27	—	—
21 30	215	21	261	57	249	56	318	17	279	16	252	28	—	—
22 30	217	25	260	55	247	54	317	17	278	16	252	28	—	—
23 30	217	38	258	54	—	50	313	15	275	18	251	29	—	—

day	26		27		28		29		30		31	
Components	E-W	S-N	E-W	S-N	E-W	S-N	E-W	S-N	E.W	S-N	E-W	S-N
h m 0 30	—	—	—	—	+218	− 2	—	—	—	—	+153	−21
1 30	—	—	—	—	219	2	—	—	—	—	—	—
2 30	—	—	—	—	219	7	—	—	-	—	—	—
3 30	—	—	—	—	218	9	—	—	—	—	—	—
4 30	—	—	—	—	216	13	—	—	—	—	—	—
5 30	—	—	—	—	212	16	—	—	—	—	—	—
6 30	—	—	—	—	210	18	—	—	—	—	—	—
7 30	—	—	—	—	208	18	—	—	—	—	—	—
8 30	—	—	—	—	208	17	—	—	—	—	—	—
9 30	—	—	—	—	207	13	—	—	—	—	—	—
10 30	—	—	—	—	208	11	—	—	—	—	—	—
11 30	—	—	—	—	209	11	+187	−19	+165	−24	—	—
12 30	—	—	—	—	210	10	—	—	—	—	—	—
13 30	—	—	—	—	211	10	—	—	—	—	—	—
14 30	—	—	+212	—	211	11	—	—	—	—	+147	−19
15 30	—	—	216	—	210	16	—	—	—	—	—	—
16 30	—	—	—	−17	208	18	—	—	+162	—	—	—
17 30	—	—	—	19	203	19	—	—	159	−36	—	—
18 30	—	—	—	18	200	20	—	—	156	39	—	—
19 30	—	—	213	16	198	18	—	—	153	39	—	—
20 30	—	—	213	13	198	14	—	—	151	37	—	—
21 30	—	—	214	9	199	10	—	—	151	33	—	—
22 30	—	—	214	7	200	6	—	—	151	31	—	—
23 30	—	—	216	4	—	—	—	—	153	27	—	—

Table I. Tilt observed at Kawana. (continued.)

1930 IV Unit=0."01

day	1		2		3		4		5		6		7	
Components (h m)	E-W	S-N	E-W	S-N	E-W	S-N	E-W	S-N	E-W	S-N	E-W	S-N	E-W	S-N
0 30	—	—	—	—	+132	−172	+133	−167	+119	−165	+115	−162	+111	−162
1 30	—	—	—	—	131	173	134	169	118	167	114	162	109	163
2 30	—	—	—	—	132	173	134	170	117	167	114	162	108	164
3 30	—	—	—	—	132	172	134	169	117	168	114	162	108	166
4 30	—	—	—	—	132	168	133	168	117	167	114	161	108	167
5 30	—	—	—	—	131	166	131	164	116	166	113	160	107	165
6 30	—	—	—	—	130	163	129	162	114	162	112	159	106	164
7 30	—	—	—	—	128	162	128	160	112	161	111	158	106	162
8 30	—	—	—	—	126	163	126	160	112	160	110	157	106	167
9 30	—	—	—	—	128	167	126	162	112	162	108	157	108	161
10 30	—	—	—	—	129	171	127	165	116	164	105	169	102	162
11 30	—	—	—	—	132	173	131	170	112	166	105	161	103	165
12 30	—	—	—	—	137	179	131	175	112	169	106	164	103	166
13 30	—	—	—	—	140	180	132	177	114	172	108	169	104	169
14 30	+154	−13	—	—	143	182	133	180	118	174	109	171	105	171
15 30	—	—	—	—	146	181	133	180	119	177	111	172	106	173
16 30	—	—	—	—	147	178	133	179	121	177	113	174	108	176
17 30	—	—	+143	− 19	148	174	133	177	122	175	114	174	109	178
18 30	—	—	147	174	145	170	132	172	122	172	115	173	110	179
19 30	—	—	143	172	143	166	130	169	121	169	115	171	111	178
20 30	—	—	140	167	140	164	127	166	121	168	115	169	112	178
21 30	—	—	136	166	136	162	125	163	119	165	114	168	111	176
22 30	—	—	132	168	134	163	123	163	117	163	113	164	110	173
23 30	—	—	132	170	133	164	120	164	116	163	112	163	109	170

day	8		9		10		11		12		13		14	
Components (h m)	E-W	S-N	E-W	S-N	E-W	S-N	E-W	S-N	E-W	S-N	E-W	S-N	E-W	S-N
0 30	+108	−168	+107	−168	+97	−175	+92	−178	+91	−186	+81	−198	+77	−209
1 30	107	167	102	164	97	171	92	175	92	184	82	197	79	209
2 30	105	165	99	162	96	167	91	171	91	181	81	193	79	202
3 30	103	164	97	161	93	164	89	167	90	177	79	190	79	199
4 30	102	164	94	159	92	163	87	165	88	173	78	188	77	196
5 30	101	163	92	159	89	162	84	163	86	172	74	185	74	194
6 30	101	164	91	160	88	163	82	164	83	172	72	187	73	192
7 30	101	163	90	162	87	166	82	166	82	174	70	189	72	196
8 30	100	162	92	160	88	168	83	172	82	179	71	193	76	200
9 30	100	162	92	163	89	170	88	178	83	183	72	197	75	202
10 30	99	162	92	163	90	171	90	178	85	187	74	201	77	207
11 30	98	162	92	162	91	171	91	178	88	189	76	204	80	212
12 30	98	163	92	162	91	170	92	176	88	189	78	205	83	214
13 30	98	165	91	161	92	168	91	175	88	188	79	204	86	214
14 30	111	160	91	160	91	164	89	171	87	185	79	202	—	191
15 30	104	162	91	160	89	163	88	168	84	182	80	198	—	188
16 30	103	164	91	163	86	163	86	166	82	180	79	193	—	180
17 30	105	168	92	167	85	166	83	167	78	179	76	189	89	175
18 30	107	171	93	171	86	172	82	169	76	179	73	189	86	172
19 30	108	173	93	174	84	173	82	172	74	182	72	190	83	171
20 30	110	174	94	177	86	177	83	179	75	187	72	193	81	172
21 30	110	174	96	178	88	179	87	182	76	190	73	197	79	174
22 30	109	173	97	179	90	181	88	186	78	195	74	202	79	177
23 30	109	171	98	178	91	180	90	187	80	199	76	204	81	181

Table I. Tilt observed at Kawana. (continued.)

1930 IV Unit=0·''01

day	15		16		17		18		19		20		21	
Components	E-W	S-N	E-W	S-N	E-W	S-N	E-W	S-N	E-W	S-N	E-W	S-N	E-W	S-N
h m														
0 30	+82	−182	+78	180	—	−179	—	−178	—	−176	—	−178	+87	−176
1 30	83	182	79	180	—	182	—	179	—	177	—	178	84	175
2 30	84	180	79	179	—	182	—	179	—	177	—	177	82	174
3 30	83	178	79	177	—	181	—	177	—	177	—	177	81	173
4 30	82	173	78	175	—	177	—	176	—	176	—	177	80	173
5 30	80	171	77	172	—	177	—	173	—	174	—	176	80	173
6 30	78	170	73	170	—	175	—	172	—	173	—	174	79	173
7 30	77	171	72	171	—	175	—	172	—	172	—	173	78	173
8 30	74	174	84	176	—	177	—	176	—	174	—	173	78	174
9 30	77	179	78	177	—	182	—	177	—	175	—	173	—	—
10 30	78	184	81	182	—	184	—	178	—	176	—	176	−97*	−41*
11 30	81	188	83	186	—	188	—	181	—	179	—	178	110	51
12 30	83	190	87	190	—	192	—	183	—	182	—	182	114	59
13 30	86	191	90	191	—	195	—	187	—	186	—	183	115	69
14 30	88	189	91	191	—	196	—	188	—	188	—	187	114	81
15 30	88	186	93	189	—	193	—	189	—	190	—	188	114	91
16 30	88	182	93	186	—	190	—	188	—	190	—	189	110	98
17 30	86	178	93	183	—	187	—	186	—	189	—	189	107	103
18 30	83	173	91	178	—	185	—	183	—	188	—	188	107	106
19 30	81	172	89	175	—	180	—	180	—	186	—	186	106	103
20 30	79	171	86	174	—	176	—	178	—	182	—	184	108	102
21 30	77	171	83	175	—	176	—	176	—	181	+91	181	112	98
22 30	76	175	81	176	—	177	—	175	—	179	89	180	118	90
23 30	77	177	—	179	—	177	—	175	—	178	88	178	124	82

day	22		23		24		25		26		27		28	
Components	E-W	S-N	E-W	S-N	E-W	S-N	E-W	S-N	E-W	S-N	E-W	S-N	E-W	S-N
h m														
0 30	−131	− 78	−152	−109	−158	−123	−156	−147	−152	−129	−167	−183	−182	−249
1 30	139	76	158	103	165	113	161	136	154	117	166	178	179	242
2 30	149	77	165	100	171	105	168	125	160	102	172	168	180	232
3 30	157	78	172	98	178	99	174	116	166	93	180	158	183	221
4 30	162	80	179	98	186	98	182	112	175	88	190	153	187	216
5 30	169	82	182	100	189	100	187	115	181	90	198	156	189	217
6 30	173	86	183	104	191	104	190	123	183	100	203	165	190	222
7 30	173	86	188	107	190	111	188	133	181	113	206	184	184	238
8 30	171	98	179	116	187	150	178	140	179	126	200	203	177	260
9 30	169	100	174	120	182	153	173	146	172	141	187	222	161	272
10 30	168	99	172	118	180	155	169	148	167	149	179	233	149	298
11 30	169	98	172	114	179	150	164	144	160	154	173	237	141	304
12 30	170	101	173	111	179	144	160	138	157	151	169	234	136	304
13 30	169	106	174	110	180	139	163	129	157	143	168	224	131	297
14 30	168	111	175	111	183	134	165	118	163	134	172	211	132	283
15 30	164	119	176	116	186	134	169	111	165	120	177	200	136	266
16 30	161	126	173	121	187	138	171	110	170	106	185	191	142	252
17 30	158	133	170	130	179	146	168	111	183	112	194	189	150	240
18 30	153	138	165	140	172	150	170	118	187	122	199	192	158	238
19 30	148	139	159	142	169	157	166	130	184	136	202	201	165	242
20 30	147	136	156	145	165	161	153	138	181	152	201	213	169	253
21 30	141	132	152	143	160	164	150	141	177	169	197	230	164	268
22 30	146	129	153	140	158	163	147	142	172	181	190	242	159	281
23 30	149	118	156	133	156	157	150	139	168	187	186	249	154	289

* Unit=0·''005 hereafter.

Table I. Tilt observed at Kawana. (continued.)

1930 IV-V Unit=0·″005

day	29		30		1		2		3		4		5	
Components (h m)	E-W	S-N	E-W	S-N	E-W	S-N	E-W	S-N	E-W	S-N	E-W	S-N	E-W	S-N
0 30	−150	−290	−169	−312	−176	−359	−161	−386	−155	−339	−137	−421	−122	−451
1 30	148	283	165	312	173	361	158	389	153	401	138	425	123	453
2 30	149	272	166	307	172	358	156	384	150	401	139	428	126	454
3 30	154	261	170	296	172	349	157	379	152	397	139	429	128	455
4 30	162	252	176	286	175	339	160	371	153	391	141	426	130	453
5 30	171	247	183	282	180	332	165	362	156	384	143	422	130	452
6 30	179	252	190	283	185	330	171	358	162	380	147	418	132	449
7 30	182	263	195	294	188	337	178	361	168	380	152	419	137	448
8 30	179	284	191	313	188	351	181	372	168	394	156	424	140	448
9 30	171	306	184	339	181	372	178	390	162	407	154	435	141	453
10 30	161	326	173	361	171	398	169	412	156	427	149	448	143	461
11 30	150	338	160	383	157	418	157	437	147	449	142	464	140	471
12 30	142	343	149	397	142	433	132	463	133	463	135	482	134	483
13 30	137	340	142	400	133	441	122	476	124	478	125	498	125	489
14 30	134	328	138	393	126	440	112	478	111	487	103	508	118	503
15 30	137	313	134	384	121	430	—	—	104	490	99	516	111	514
16 30	143	293	138	367	121	412	108	458	99	486	92	518	102	522
17 30	153	279	145	348	127	396	110	442	99	475	88	513	97	526
18 30	163	270	154	333	133	378	117	—	100	459	87	504	93	521
19 30	175	270	166	324	142	363	127	—	105	443	89	491	91	513
20 30	181	274	174	324	150	366	135	—	112	430	95	479	93	504
21 30	181	286	181	330	156	365	144	—	120	420	102	468	98	492
22 30	179	297	182	342	161	371	152	389	128	418	108	499	105	481
23 30	173	307	179	352	162	379	155	394	134	419	115	453	—	—

day	6		7		8		9		10		11		12	
Components (h m)	E-W	S-N	E-W	S-N	E-W	S-N	E-W	S-N	E-W	S-N	E-W	S-N	E-W	S-N
0 30	−115	—	−114	−500	− 91	−547	−112	−588	−123	−643	−152	—	−158	—
1 30	121	—	120	494	98	533	110	—	132	630	155	−669	157	—
2 30	126	−461	126	492	106	528	118	571	138	620	162	658	149	—
3 30	131	461	129	493	112	527	127	569	144	611	171	—	132	—
4 30	132	461	132	496	117	530	132	—	148	612	179	644	122	—
5 30	129	461	133	500	—	—	137	582	152	619	182	651	116	—
6 30	131	461	132	504	119	552	136	595	152	634	183	664	109	—
7 30	135	462	131	509	117	563	132	608	152	652	179		98	—
8 30	129	464	—	—	106	579	126	619	147	665	171	—	86	—
9 30	133	463	105	518	96	581	119	—	144	—	160	—	72	—
10 30	137	465	107	515	95	577	116	—	141	—	149	—	59	—
11 30	—	471	108	512	96	571	113	622	138	—	141	—	47	—
12 30	—	480	111	513	96	563	—	—	138	—	138	—	39	—
13 30	—	491	113	519	100	560	97	—	141	668	138	—	34	—
14 30	130	503	114	529	104	559	—	600	146	654	142	—	36	—
15 30	122	518	110	540	109	563	127	592	153	643	148	—	39	—
16 30	116	529	108	553	103	573	141	597	160	633	157	—	48	—
17 30	109	536	102	565	100	582	144	606	170	637	153	—	57	—
18 30	104	539	94	576	112	593	142	618	172	645	171	—	69	—
19 30	98	540	78	584	109	603	138	634	173	658	177	—	79	—
20 30	97	537	83	582	106	611	133	646	168	668	176	—	—	—
21 30	100	528	82	577	103	612	129	655	161	—	170	—	—	—
22 30	103	517	83	569	105	608	126	658	156	—	166	—	97	—
23 30	108	508	80	558	107	600	127	654	152	—	161	—	95	—

Table I. Tilt observed at Kawana. (continued.)

1930 V Unit=0.″005

day	13		14		15		16		17		18		19	
Components	E-W	S-N	E-W	S-N	E-W	S-N	E-W	S-N	E-W	S-N	E-W	S-N	E-W	S-N
h m														
0 30	− 90	—	−155	—	—	−10	—	−17	−281	− 10	−139	−198	−58	− 58
1 30	91	—	156	—	—	—	—	20	281	—	139	199	62	59
2 30	92	—	158	—	—	02	—	17	282	13	139	201	65	60
3 30	100	—	164	—	—	11	—	12	284	09	139	200	67	61
4 30	111	—	172	—	—	19	—	04	286	—	140	198	68	59
5 30	121	—	182	—	—	23	—	00	—	—	141	195	71	58
6 30	129	—	194	—	—	22	—	—	136	177	—	—	73	54
7 30	132	—	200	—	—	15	—	—	141	177	148	188	78	52
8 30	130	—	198	—	—	03	—	—	139	182	151	192	81	52
9 30	126	—	179	—	—	21	—	—	140	192	27	46	83	56
10 30	117	—	164	—	—	39	—	−39	136	207	57	56	83	61
11 30	105	—	—	—	—	56	—	57	128	222	56	68	80	71
12 30	—	—	—	—	—	69	—	71	119	238	50	82	77	82
13 30	98	—	—	−39	—	73	—	78	109	249	42	93	72	92
14 30	96	—	—	34	—	74	—	80	99	254	35	102	66	99
15 30	99	—	—	21	—	74	—	76	94	254	32	—	60	106
16 30	108	—	—	05	—	52	—	67	94	249	28	—	56	107
17 30	118	—	—	09	—	39	−240	51	97	238	23	—	53	104
18 30	131	—	—	12	—	26	243	—	103	227	22	—	51	—
19 30	139	—	—	29	—	—	252	23	107	219	28	83	—	—
20 30	149	—	—	30	—	02	262	13	117	208	33	71	—	—
21 30	155	—	—	27	—	01	270	—	124	200	40	62	—	—
22 30	156	—	—	22	—	07	276	06	133	196	47	59	—	—
23 30	156	—	—	14	—	13	277	09	137	197	52	56	78	67

day	20		21		22		23		24		25		26	
Components	E-W	S-N	E-W	S-N	E-W	S-N	E-W	S-N	E-W	S-N	E-W	S-N	E-W	S-N
h m														
0 30	−83	− 63	− 98	− 70	−109	− 91	−104	−102	−110	−114	−128	−133	−139	−140
1 30	89	62	102	69	112	87	111	96	115	107	133	126	143	131
2 30	92	62	105	71	118	88	114	91	120	103	139	119	151	123
3 30	—	—	107	73	112	86	122	92	126	104	146	116	158	119
4 30	—	—	108	77	114	90	126	93	130	110	150	118	164	119
5 30	97	—	109	80	113	96	125	100	131	119	152	127	169	128
6 30	—	—	109	82	111	100	123	111	130	129	151	140	166	141
7 30	—	—	106	83	109	104	119	116	126	141	147	152	161	157
8 30	—	—	107	84	107	106	111	121	122	150	140	166	148	173
9 30	—	—	107	84	104	107	109	122	116	157	131	171	139	184
10 30	—	—	108	84	105	106	105	118	112	157	127	171	132	189
11 30	—	—	109	86	107	103	115	114	112	151	124	167	127	187
12 30	—	—	109	89	107	102	121	110	113	145	123	159	122	180
13 30	—	—	109	94	108	103	121	105	118	137	126	147	122	165
14 30	—	—	103	101	108	107	123	104	122	130	131	136	127	150
15 30	—	—	100	110	106	112	126	107	127	127	136	130	123	140
16 30	76	110	96	118	104	120	125	111	130	128	140	126	102	—
17 30	71	110	91	122	101	126	123	119	132	131	144	127	112	127
18 30	70	108	89	125	99	131	120	128	132	138	147	132	122	119
19 30	—	—	88	124	96	134	118	133	129	144	147	140	128	118
20 30	—	—	81	124	95	132	96	139	128	150	144	146	130	121
21 30	82	88	90	113	93	128	109	133	124	152	142	152	127	130
22 30	88	—	97	105	98	120	108	129	123	149	139	152	125	137
23 30	92	—	102	98	99	110	108	124	125	132	138	148	122	142

Table 1. Tilt observed at Kawana. (continued.)

1930 V–VI Unit = 0.″005

day	27		28		29		30		31		1		2	
Components	E-W	S-N	E-W	S-N	E-W	S-N	E-W	S-N	E-W	S-N	E-W	S-N	E-W	S-N
h m														
0 30	−122	−142	−138	−144	−147	−133	−161	−130	−176	−128	−181	−131	−194	—
1 30	126	137	139	140	146	—	159	130	173	129	181	132	194	—
2 30	132	129	145	131	149	119	159	124	172	125	180	132	195	—
3 30	138	120	152	121	152	109	161	115	173	118	—	—	194	—
4 30	142	113	159	113	159	102	167	108	178	112	185	122	195	—
5 30	150	112	165	108	165	100	173	103	182	107	188	116	197	—
6 30	151	118	170	110	170	106	179	104	188	105	196	108	201	—
7 30	147	130	168	120	169	120	181	113	192	110	199	109	206	—
8 30	138	149	161	137	162	141	177	131	190	122	203	116	211	—
9 30	130	166	151	157	151	162	169	152	186	139	204	128	212	—
10 30	119	182	139	178	138	182	158	173	177	159	200	143	212	—
11 30	110	193	129	192	123	197	146	192	165	182	190	162	209	—
12 30	105	198	122	201	112	205	140	205	154	199	179	180	207	—
13 30	103	194	118	201	107	203	138	210	146	207	167	197	200	—
14 30	104	182	116	192	110	194	132	205	140	210	154	201	195	—
15 30	110	167	120	179	119	179	129	193	138	205	147	206	187	—
16 30	117	150	126	159	125	161	130	174	136	193	147	198	179	—
17 30	127	134	134	140	131	142	135	155	139	176	153	185	173	—
18 20	132	126	142	127	139	128	143	137	146	158	157	170	175	—
19 30	139	122	147	117	—	120	149	127	152	142	162	—	—	—
20 30	142	123	153	—	159	116	163	116	161	131	169	139	—	—
21 30	141	129	155	—	164	117	172	113	169	123	177	—	—	—
22 30	140	137	154	125	165	122	176	117	174	125	183	—	—	—
23 30	139	141	150	131	162	129	177	121	180	126	188	—	195	—

day	3		4		5		6		7		8		9	
Components	E-W	S-N	E-W	S-N	E-W	S-N	E-W	S-N	E-W	S-N	E-W	S-N	E-W	S-N
h m														
0 30	—	—	—	−121	—	—	—	−123	—	−131	—	—	—	—
1 30	−211	—	—	123	—	—	—	—	—	128	—	—	—	—
2 30	213	—	—	127	—	—	—	—	—	126	—	—	—	—
3 30	214	—	—	132	—	—	—	—	—	129	—	—	—	—
4 30	212	—	—	138	—	—	—	—	—	137	—	—	—	—
5 30	211	—	—	139	—	—	—	—	—	—	—	—	—	—
6 30	—	—	—	—	—	—	—	—	—	—	—	—	—	—
7 30	—	−103	—	—	—	—	—	—	—	—	—	—	—	—
8 30	—	97	—	133	—	—	—	—	—	—	—	—	—	—
9 30	—	97	—	131	—	−144	—	—	—	—	—	—	—	—
10 30	—	104	—	129	—	138	—	—	—	—	—	—	—	—
11 30	—	113	—	131	—	136	—	−152	—	—	—	—	—	—
12 30	—	127	—	136	—	136	—	137	—	—	—	—	—	—
13 30	—	142	—	144	—	137	—	134	—	—	—	—	—	—
14 30	—	158	—	156	—	141	—	137	—	—	—	—	—	—
15 30	—	169	—	167	—	150	—	139	—	—	—	—	—	—
16 30	—	177	—	172	—	157	—	147	—	—	—	—	—	—
17 30	—	178	—	178	—	162	—	153	—	—	—	—	—	—
18 30	—	173	—	—	—	166	—	159	—	—	—	—	—	—
19 30	—	163	—	—	—	165	—	161	—	—	—	—	—	—
20 30	—	151	—	—	—	—	—	158	—	—	—	—	—	−151
21 30	—	139	—	—	—	—	—	156	—	—	—	—	—	158
22 30	—	129	—	—	—	—	—	149	—	—	—	—	—	160
23 30	—	122	—	—	—	—	—	139	—	—	—	—	—	161

Table I. Tilt observed at Kawana. (continued.)

1930 VI Unit=0″·005

day	10		11		12		13		14		15		16	
Components	E-W	S-N	E-W	S-N	E-W	S-N	E-W	S-N	E-W	S-N	E-W	S-N	E-W	S-N
h m														
0 30	—	−156	−241	−165	−263	−153	−273	−150	—	—	−293	−156	−302	−157
1 30	—	148	242	161	263	150	271	147	—	—	293	158	301	160
2 30	—	141	246	150	267	143	272	142	—	—	291	157	300	161
3 30	—	136	252	140	271	133	276	136	—	—	292	150	300	160
4 30	—	138	257	137	275	128	279	129	—	—	294	146	300	156
5 30	—	144	262	140	281	127	287	126	—	—	298	139	302	149
6 30	—	159	264	150	285	133	291	129	—	—	304	136	309	143
7 30	—	178	263	168	285	146	292	139	−293	−127	309	137	316	141
8 30	—	195	256	186	280	182	289	153	300	141	312	144	323	146
9 30	—	212	247	203	274	199	281	173	—	—	310	158	329	155
10 30	—	223	—	—	263	215	270	191	—	—	306	174	329	167
11 39	—	227	225	225	251	227	—	—	—	—	297	191	324	180
12 30	—	225	218	224	243	230	—	—	—	—	288	202	318	194
13 30	—	—	212	218	239	222	—	—	260	218	278	213	309	207
14 30	−207	200	213	203	234	207	—	—	264	215	269	220	300	214
15 30	211	183	217	186	236	192	—	—	258	209	262	217	295	216
16 30	219	168	222	168	228	173	—	—	257	198	260	208	291	210
17 30	226	158	231	152	243	154	—	—	260	182	262	196	288	203
18 30	233	152	239	143	252	142	—	—	266	168	268	181	291	188
19 30	240	151	249	139	261	135	258	151	273	156	275	168	295	174
20 30	243	154	257	140	270	133	—	—	282	148	283	158	302	161
21 30	245	160	261	145	274	137	—	—	288	144	291	151	308	153
22 30	245	163	260	150	276	142	—	—	293	147	299	150	314	150
23 30	242	164	261	154	277	147	—	—	295	152	300	152	319	150

day	17		18		19		20		21		22		23	
Components	E-W	S-N	E-W	S-E	E-W	S-N	E-W	S-N	E-W	S-N	E-W	S-N	E-W	S-N
h m														
0 30	−321	−155	−327	−161	−331	−161	−330	−159	−333	−165	−338	−170	−346	−177
1 30	321	160	329	156	333	167	332	161	337	165	341	168	350	172
2 30	320	163	328	171	334	171	333	169	338	170	346	169	354	170
3 30	319	164	326	175	333	178	332	175	338	179	349	173	356	177
4 30	319	162	326	176	330	180	331	182	337	187	348	183	357	181
5 30	322	159	324	173	329	181	327	187	332	196	344	196	356	200
6 30	325	152	326	170	328	180	325	190	328	201	339	206	350	213
7 30	329	149	329	164	328	178	321	190	322	204	333	220	341	230
8 30	333	149	331	162	330	173	320	189	320	203	327	227	334	240
9 30	336	154	331	162	332	171	320	184	318	200	322	224	329	245
10 30	338	162	331	166	333	171	321	181	319	194	321	221	322	242
11 30	334	177	329	174	334	173	322	178	327	188	322	221	321	233
12 30	328	190	324	184	333	178	322	180	332	183	325	201	322	222
13 30	321	202	317	196	330	185	323	182	337	182	331	189	328	210
14 30	314	213	310	203	327	192	323	188	337	184	337	183	334	200
15 30	307	218	304	211	320	198	326	193	337	187	342	184	340	193
16 30	300	217	300	213	314	202	327	199	336	191	346	185	346	189
17 30	298	210	302	210	310	203	325	202	332	197	347	190	351	190
18 30	278	198	305	203	303	201	320	202	330	199	344	194	354	192
19 30	302	187	309	192	317	191	318	198	329	200	341	197	351	198
20 30	306	174	313	181	316	183	314	192	328	196	338	198	348	201
21 30	310	169	317	174	317	175	319	184	322	190	338	199	350	201
22 30	318	161	322	168	320	167	322	177	329	182	340	189	350	198
23 30	323	159	328	161	323	161	326	170	333	174	341	182	351	194

Table I. Tilt observed at Kawana. (continued.)

1930 VI Unit=0″005

day	24		25		26		27		28		29		30	
Components	E-W	S-N	E-W	S-N	E-W	S-N	E-W	S-N	E-W	S-N	E-W	S-N	E-W	S-N
h m														
0 30	−353	−187	−358	−192	−381	−178	−392	−193	—	--201	—	−200	−341	−211
1 30	358	180	361	183	383	—	394	187	—	197	—	203	340	216
2 30	362	179	367	178	388	—	397	181	—	189	—	198	339	217
3 30	368	180	373	177	391	160	400	173	—	181	—	193	341	212
4 30	370	190	378	180	398	163	—	170	—	177	—	186	342	206
5 30	369	203	380	192	—	170	—	—	—	173	—	179	348	199
6 30	362	219	378	207	—	189	—	—	—	—	—	176	352	191
7 30	358	238	371	229	—	214	—	—	—	188	—	181	359	190
8 30	348	252	359	247	—	231	—	—	—	210	—	194	363	196
9 30	338	261	346	261	380	250	392	—	—	235	—	216	366	209
10 30	330	263	337	269	370	265	380	—	—	263	—	237	361	226
11 30	328	259	329	268	359	275	366	—	—	281	−326	255	351	247
12 30	326	248	330	254	352	274	357	—	−387	290	314	276	340	267
13 30	330	233	339	242	350	263	350	286	377	292	303	288	328	283
14 30	334	219	340	223	352	251	348	274	370	284	296	291	318	290
15 30	341	209	343	207	360	233	350	254	369	269	291	296	308	290
16 30	349	197	350	190	367	216	355	236	371	248	290	270	302	280
17 30	355	192	360	181	374	199	363	219	378	228	292	252	302	266
18 30	360	191	369	178	384	187	374	200	386	207	300	231	304	247
18 30	360	197	375	—	393	176	383	190	394	191	309	216	311	229
20 30	360	199	376	—	396	178	392	189	—	187	319	207	319	215
21 30	359	201	379	182	397	186	—	191	—	186	329	200	329	207
22 30	358	200	380	185	398	190	—	198	—	190	336	200	334	207
23 30	358	200	380	185	395	193	—	201	—	196	339	206	338	213

1930 VII

day	1		2		3		4		5		6		7	
Components	E-W	S-N	E-W	S-N	E-W	S-N	E-W	S-N	E-W	S-N	E-W	S-N	E-W	S-N
h m														
0 30	−338	−224	−336	−229	−346	−237	−89	−233	—	—	−106	−231	—	—
1 30	332	232	336	238	345	244	93	239	—	—	109	231	−116	—
2 30	325	241	330	247	343	253	92	249	—	—	112	239	119	—
3 30	320	245	329	250	339	261	90	257	—	—	112	249	121	—
4 30	318	242	325	252	336	267	81	268	—	—	110	252	119	—
5 30	319	237	323	247	333	269	82	275	—	—	103	276	114	—
6 30	322	229	324	240	—	—	78	280	− 88	—	98	289	108	—
7 30	—	—	329	234	—	263	73	—	81	—	89	296	—	—
8 30	—	—	334	229	336	254	72	272	78	—	84	303	—	—
9 30	—	—	340	227	337	249	73	263	78	—	81	302	93	—
10 30	—	—	347	231	339	247	77	259	79	—	79	297	87	−320
11 30	—	—	350	237	342	248	84	251	82	−268	80	289	80	322
12 30	—	—	344	252	338	250	92	249	89	258	82	281	79	316
13 30	—	—	339	267	84	—	93	251	92	254	—	271	79	306
14 30	—	—	331	278	83	—	92	255	93	—	89	264	81	291
15 30	—	—	324	286	75	270	89	261	92	—	93	259	—	—
16 30	—	—	318	290	71	276	87	265	94	—	98	258	91	—
17 30	—	—	315	284	68	277	83	267	—	—	—	—	96	—
18 30	—	—	313	275	66	272	80	263	92	—	100	200	101	—
19 30	—	—	316	262	67	263	81	260	—	—	99	262	104	266
20 30	—	—	321	250	68	254	81	253	90	—	95	261	106	268
21 30	316	216	328	238	73	—	84	246	—	—	95	255	107	270
22 30	327	222	336	233	80	236	89	239	98	239	102	247	105	270
23 30	331	224	341	232	86	231	92	231	101	235	107	—	106	267

Table I. Tilt observed at Kawana. (continued.)

1930 VII Unit=0.″005

day	8		9		10		11		12		13		14	
Components	E-W	S-N	E-W	S-N	E-W	S-N	E-W	S-N	E-W	S-N	E-W	S-N	E-W	S-N
h m 0 30	—	−262	−113	−271	−125	−281	−141	−291	—	—	—	—	—	—
1 30	−110	259	115	267	125	—	—	—	−126	—	—	—	—	—
2 30	114	256	118	261	128	—	—	—	125	−277	—	—	—	—
3 30	118	255	121	258	131	—	—	—	128	269	—	—	—	—
4 30	124	—	126	257	—	—	—	—	130	261	—	—	—	—
5 30	122	258	129	261	—	—	151	—	134	259	—	—	—	—
6 30	120	281	131	271	—	—	158	—	140	262	—	—	—	—
7 30	117	297	130		—	—	162	—	142	272	—	—	—	—
8 30	109	312	125	304	—	—	—	—	140	289	—	—	—	—
9 30	100	327	118	321	—	—	—	—	133	311	—	—	—	—
10 30	91	337	109	337	124	—	—	—	126	331	—	—	—	—
11 30	82	339	101	344	115	—	140	—	—	—	—	—	—	—
12 30	76	332	94	349	108	—	127	—	—	—	—	—	—	—
13 30	74	324	91	341	100	—	—	—	—	—	—	—	—	—
14 30	74	311	88	332	98	—	—	—	—	—	—	—	—	—
15 30	78	294	90	316	98	333	108	—	—	—	—	—	—	—
16 30	86	284	93	299	102	313	107	—	—	—	—	—	—	—
17 30	106	272	100	286	110	300	109	—	—	—	—	—	—	—
18 30	112	265	108	276	118	—	115	—	—	—	—	—	—	—
19 30	113	261	116	270	123	281	121	—	—	—	—	—	—	—
20 30	117	267	121	270	132	278	129	−274	—	—	—	—	—	—
21 30	118	269	123	273	137	279	131	271	—	—	—	—	—	—
22 30	116	272	124	278	141	283	—	—	—	—	—	—	—	—
23 30	115	274	125	281	—	—	—	—	—	—	—	—	—	—

Table II. Tides observed at Kawana.

1930 Unit=26·2 mm.

month	IV									V					
day / hour	22	23	24	25	26	27	28	29	30	1	2	3	4	5	6
h 0	—	61	58	59	64	51	48	47	—	—	—	—	42	47	53
1	—	64	65	66	72	61	54	63	—	—	—	—	41	45	52
2	—	66	68	72	78	67	61	68	—	—	—	—	40	44	52
3	—	65	68	74	77	69	67	73	—	—	—	—	39	45	51
4	—	63	64	72	72	67	70	73	—	—	—	—	39	47	51
5	—	61	60	69	67	59	67	68	—	—	—	—	40	49	52
6	—	59	54	63	59	48	61	59	—	—	—	—	39	51	53
7	—	57	52	58	54	37	49	47	—	—	—	—	41	53	54
8	—	55	50	53	45	30	37	36	—	—	—	—	40	51	55
9	—	54	51	50	42	28	30	28	—	—	—	—	40	45	54
10	—	55	55	52	42	30	29	23	—	—	—	—	34	40	52
11	—	56	58	57	46	36	28	20	—	—	—	—	26	35	50
12	60	55	61	61	54	46	28	23	—	—	—	—	15	25	44
13	58	55	63	67	61	56	44	28	—	—	—	1	5	20	41
14	55	54	63	72	67	61	54	47	—	—	—	3	3	15	37
15	50	52	60	70	69	66	61	58	—	—	—	6	4	13	27
16	46	48	55	67	69	64	69	—	—	—	—	9	8	14	25
17	40	43	49	57	61	61	67	—	—	—	—	14	14	18	23
18	39	38	47	53	54	53	60	—	—	—	—	20	25	24	22
19	40	37	40	46	46	46	55	—	—	—	—	28	32	34	24
20	42	36	40	44	38	37	47	—	—	—	—	37	38	39	27
21	47	40	40	45	36	34	42	—	—	—	—	43	44	46	34
22	52	44	45	51	38	35	38	—	—	—	—	44	47	51	41
23	57	49	51	59	43	40	38	—	—	—	—	43	48	53	50

Table II. Tides observed at Kawana. (continued.)

1930 Unit = 26·2 mm.

Month	V														
day / hour	7	8	9	10	11	12	13	14	15	16	17	18	19	20	21
0 h	55	45	36	49	39	34	37	32	31	36	39	44	40	51	45
1	57	50	42	57	45	45	45	35	34	38	39	41	39	50	47
2	56	53	50	61	53	52	53	43	38	40	42	40	38	49	47
3	55	51	52	60	55	56	58	53	43	48	47	41	39	47	44
4	53	48	49	55	52	55	57	56	50	51	52	43	43	46	42
5	50	42	45	47	47	47	53	54	54	53	55	47	46	46	39
6	47	37	37	44	37	40	47	49	53	53	52	50	46	47	38
7	45	34	30	44	27	32	38	40	47	48	48	50	47	48	38
8	44	33	25	44	17	20	25	34	38	39	42	47	47	49	38
9	43	34	23	44	10	8	11	20	24	24	40	41	43	49	40
10	45	37	24	43	10	5	5	8	11	14	38	36	37	48	41
11	46	41	30	35	13	11	3	2	2	—	36	17	35	45	40
12	47	44	35	40	19	19	5	3	1	—	25	10	31	46	37
13	47	45	43	47	27	29	13	4	2	—	8	6	22	36	34
14	46	43	48	52	35	37	21	13	9	—	7	8	15	31	30
15	44	39	48	55	45	50	29	23	17	—	10	11	13	25	25
16	38	33	45	55	51	55	36	35	31	—	17	15	13	21	22
17	33	26	38	50	52	57	44	44	41	34	25	20	17	18	21
18	25	21	29	40	47	54	53	49	49	43	33	25	22	20	20
19	19	16	25	33	41	50	55	52	51	49	38	36	29	22	22
20	17	15	24	26	34	40	53	51	49	50	47	40	35	28	24
21	22	17	27	25	27	34	47	47	45	47	50	44	40	32	29
22	28	21	33	28	26	32	39	41	40	44	50	43	46	38	34
23	37	29	39	30	29	32	34	36	37	41	47	42	49	42	39

Month	V										VI				
day / hour	22	23	24	25	26	27	28	29	30	31	1	2	3	4	5
0 h	45	40	42	38	29	34	34	22	25	34	31	49	44	43	44
1	48	49	47	40	31	38	44	26	31	42	30	37	40	39	43
2	49	50	48	41	36	38	47	37	36	46	31	37	38	37	38
3	47	49	47	40	36	36	44	44	44	48	35	40	37	32	34
4	44	47	41	39	33	31	40	45	45	46	40	44	37	31	29
5	40	43	35	35	28	39	34	44	42	40	45	45	41	32	28
6	38	38	27	34	26	27	33	36	39	31	46	53	43	33	28
7	37	34	21	28	23	27	33	24	29	27	43	53	45	35	29
8	37	31	17	24	20	25	33	21	18	24	36	50	45	36	32
9	37	30	19	23	−8	24	28	−8	0	17	26	45	43	37	36
10	39	32	21	24	−5	22	28	−13	−11	15	24	38	38	37	39
11	42	37	27	26	−2	21	27	−13	−13	−15	24	29	32	35	41
12	43	40	30	28	5	14	27	−14	−13	−13	24	23	26	31	41
13	—	43	37	30	15	18	19	−1	−11	−5	24	11	18	25	39
14	—	44	39	30	24	31	27	9	−3	−5	24	6	9	18	34
15	—	44	40	32	32	38	39	18	8	−4	24	6	5	13	28
16	—	40	40	32	34	39	44	30	18	7	24	10	2	9	24
17	—	35	34	29	26	38	41	40	30	18	24	18	4	9	22
18	—	30	33	28	21	34	41	41	37	28	29	25	9	14	22
19	—	25	28	25	15	29	42	40	42	37	31	34	18	18	26
20	—	25	29	24	14	29	35	35	35	41	44	41	27	21	32
21	29	27	32	24	14	29	29	30	30	41	46	47	38	28	40
22	32	32	34	25	18	29	24	25	28	38	45	48	42	34	46
23	40	36	36	27	25	30	23	24	31	34	43	46	44	43	49

Table II Tides observed at Kawana. (continued.)

1930 Unit = 26·2 mm.

Month	VI											
hour \ day	6	7	8	9	10	11	12	13	14	15	16	17
h 0	50	44	36	33	30	31	33	40	44	28	31	36
1	48	44	39	38	36	38	36	46	45	27	29	31
2	45	40	41	41	42	44	42	50	47	29	29	28
3	39	36	39	41	44	47	48	51	48	31	31	28
4	33	29	31	39	42	47	51	50	49	37	34	30
5	28	21	18	32	35	39	50	46	50	41	41	34
6	25	15	9	24	27	28	45	39	49	41	44	38
7	23	12	1	14	18	18	35	29	47	38	46	40
8	24	11	1	4	9	4	25	20	43	30	44	40
9	27	13	4	− 3	− 6	− 3	14	9	37	19	41	35
10	33	18	9	− 4	− 8	− 5	1	2	27	11	37	29
11	37	24	16	0	− 6	− 3	− 4	− 4	18	− 4	28	20
12	39	29	23	7	− 1	1	− 3	− 5	6	− 5	19	13
13	39	33	31	18	6	10	3	− 1	− 5	− 5	10	5
14	38	35	36	27	15	18	11	6	− 9	− 5	4	2
15	34	35	37	35	26	31	26	15	− 9	1	4	2
16	30	33	35	38	34	40	37	29	− 6	9	5	5
17	25	28	31	38	39	46	48	36	20	16	12	11
18	22	23	27	36	42	46	49	54	30	25	20	21
19	21	20	24	30	42	44	46	53	37	36	24	25
20	24	20	21	26	38	39	39	50	38	40	24	34
21	30	23	21	23	31	36	34	44	38	40	40	36
22	36	26	22	23	27	32	32	41	32	37	41	37
23	40	31	27	25	27	32	35	40	30	34	40	35

Month				VI								
hour \ day	18	19	20	21	22	23	24	25	26	27	28	29
h 0	31	32	30	33	47	45	50	43	45	53	—	—
1	28	30	25	18	46	48	50	49	51	57	—	—
2	25	27	20	13	45	49	46	52	53	58	—	—
3	25	23	18	13	42	47	40	50	53	64	—	—
4	27	20	17	15	38	44	33	45	51	62	—	—
5	30	21	16	18	33	38	27	30	43	55	—	—
6	32	22	18	22	27	33	13	15	34	46	—	—
7	34	25	21	25	20	27	7	5	15	34	—	—
8	34	28	23	28	19	18	3	2	5	21	—	—
9	31	29	26	29	19	13	5	2	1	10	—	—
10	27	29	27	28	20	10	11	8	1	6	—	—
11	21	26	27	24	24	10	18	14	1	—	—	—
12	14	23	25	21	28	15	24	20	9	—	—	—
13	8	18	23	18	32	24	33	28	22	—	—	—
14	5	11	20	17	40	32	40	38	34	—	—	—
15	2	8	16	—	37	40	44	46	44	—	—	—
16	2	6	13	—	34	45	45	50	52	—	—	—
17	9	8	11	—	31	45	44	52	53	—	—	—
18	14	13	11	—	29	42	44	52	60	—	—	—
19	19	17	14	—	30	37	40	52	55	—	—	—
20	25	30	22	39	31	33	33	41	50	—	—	—
21	29	35	29	45	34	34	33	38	47	—	—	—
22	32	35	35	47	36	39	35	37	45	—	—	—
23	34	33	36	48	40	47	38	40	47	—	—	—

Table II. Tides observed at Kawana. (continued.)

1930 Unit=26·2 mm.

Month		VII					VII						
hour \ day	30	1	2	3	4	5	6	7	8	9	10	11	12
0	—	—	—	60	53	57	56	72	68	—	—	43	41
1	—	—	46	55	48	54	53	70	70	—	—	48	44
2	—	—	45	50	43	56	43	66	69	—	—	55	48
3	—	—	48	46	40	40	45	64	67	—	—	57	51
4	—	—	54	44	40	36	45	64	62	—	—	58	55
5	—	—	61	44	40	29	49	65	61	—	—	52	57
6	—	—	46	47	40	27	48	65	61	—	—	47	56
7	—	—	34	52	40	27	48	65	61	—	—	34	48
8	—	—	28	55	40	31	49	65	60	—	—	26	34
9	—	—	25	57	44	36	49	65	59	—	—	16	20
10	—	—	28	57	46	41	48	65	55	—	—	10	12
11	—	—	31	57	48	45	52	64	—	—	—	8	8
12	—	—	38	53	48	47	58	62	—	—	—	12	4
13	—	—	44	47	51	48	62	58	—	—	—	20	6
14	—	—	45	41	43	46	65	59	—	—	—	27	13
15	—	—	—	37	39	43	65	65	—	—	—	35	22
16	—	—	—	36	36	41	63	67	—	—	—	47	34
17	—	—	—	39	33	40	61	67	—	—	—	55	45
18	—	—	—	45	34	41	59	65	—	—	55	57	55
19	—	—	—	52	37	43	58	63	—	—	53	56	53
20	—	—	57	52	43	47	61	60	—	—	49	52	51
21	—	—	65	57	52	51	63	61	—	—	45	47	48
22	—	—	61	59	55	55	61	61	—	—	42	43	41
23	—	—	63	57	57	57	69	67	—	—	40	41	38

Table III. Variation of Zero-line.

1930 April Unit=0·″005

day	22		23		24		25		26		27	
Components	E-W	S-N	E-W	S-N	E-W	S-N	E-W	S-N	E-W	S-N	E-W	S-N
h m 0 30	−152	− 97	−165	−116	−172	−125	−174	−140	−165	−122	−179	−164
1 30	153	97	166	116	172	126	174	140	165	122	180	167
2 30	154	98	166	117	173	127	173	139	165	122	180	170
3 30	154	98	166	117	173	128	173	139	165	122	181	173
4 30	155	99	167	117	173	129	172	138	166	122	181	177
5 30	155	99	167	117	174	130	171	137	166	123	182	180
6 30	156	100	167	118	174	131	171	136	167	123	182	184
7 30	156	101	168	118	174	131	170	135	167	123	183	188
8 30	157	101	168	118	175	132	170	135	168	124	184	191
9 30	157	102	168	118	175	133	169	134	169	125	184	193
10 30	158	103	169	118	175	134	169	132	169	126	185	196
11 30	158	104	169	118	176	135	168	131	170	128	185	199
12 30	159	104	169	118	176	135	168	130	171	129	186	201
13 30	160	105	169	118	176	136	168	129	171	131	186	204
14 30	160	106	170	119	176	136	167	129	172	134	186	206
15 30	161	108	170	119	176	137	167	128	173	137	186	209
16 30	161	109	170	120	177	138	166	127	173	140	186	211
17 30	162	110	170	120	177	138	166	126	174	143	186	214
18 30	162	111	171	121	177	139	166	125	175	146	185	217
19 30	163	112	171	121	176	139	165	124	175	150	185	219
20 30	163	113	171	122	176	140	165	124	176	153	184	222
21 30	164	113	171	123	176	140	165	123	177	156	184	224
22 30	164	114	172	124	175	140	165	123	177	159	183	226
23 30	165	115	172	125	174	140	165	122	178	162	182	228

Table III. Variation of Zero-line. (continued.)

1930 April—May Unit=0''005

day	28		29		30		1		2		3	
Components	E-W	S-N	E-W	S-N	E-W	S-N	E-W	S-N	E-W	S-N	E-W	S-N
h m												
0 30	−181	−231	−156	−274	−168	−307	−167	−358	−153	−391	−141	−416
1 30	179	233	156	275	168	309	167	359	152	392	141	417
2 30	178	236	156	277	169	311	166	361	152	393	140	418
3 30	177	238	156	278	169	312	166	363	151	394	140	418
4 30	175	240	156	280	169	314	165	365	151	395	139	419
5 30	173	243	157	281	169	316	165	366	151	396	138	421
6 30	172	245	157	282	168	318	164	368	150	398	138	421
7 30	170	247	158	284	168	321	163	370	150	399	137	422
8 30	168	249	158	285	168	323	162	372	149	401	137	423
9 30	167	252	159	287	168	327	161	374	148	403	136	424
10 30	165	254	159	288	168	330	160	375	148	404	136	425
11 30	164	256	160	290	167	333	159	377	147	406	135	426
12 30	162	258	161	291	167	336	158	378	146	407	135	428
13 30	161	260	162	292	167	339	157	379	146	408	134	429
14 30	160	262	162	293	167	341	157	381	146	409	134	430
15 30	160	263	163	295	166	343	156	382	145	410	133	431
16 30	159	264	164	296	166	345	156	383	145	411	133	433
17 30	159	266	164	298	166	347	155	384	144	412	132	434
18 30	158	267	165	299	166	349	155	385	144	412	132	435
19 30	157	269	165	300	166	351	155	386	144	413	131	436
20 30	157	270	166	301	166	352	154	387	143	413	131	438
21 30	157	271	167	302	167	353	154	388	143	414	130	439
22 30	156	272	167	304	167	355	154	389	142	415	130	440
23 30	156	273	168	305	167	356	153	390	142	415	130	442

day	4		5		6		7	
Components	E-W	S-N	E-W	S-N	E-W	S-N	E-W	S-N
h m								
0 30	−129	−443	−118	−474	−114	−483	—	—
1 30	129	445	118	474	114	484	—	—
2 30	128	446	117	475	115	484	—	—
3 30	128	448	117	475	115	485	—	—
4 30	127	450	117	476	116	486	—	—
5 30	127	451	117	476	117	486	—	—
6 30	126	453	116	477	118	487	—	—
7 30	126	454	116	477	119	488	—	—
8 30	125	456	116	477	120	489	—	—
9 30	125	458	116	478	121	490	—	—
10 30	124	459	116	478	121	490	—	—
11 30	124	460	115	478	122	491	—	—
12 30	124	462	115	478	122	491	—	—
13 30	123	463	115	479	122	493	—	—
14 30	123	465	115	479	122	495	—	—
15 30	122	466	115	479	122	496	—	—
16 30	122	467	115	480	122	497	—	—
17 30	121	468	114	480	121	499	—	—
18 30	121	469	114	480	121	501	—	—
19 30	120	470	114	481	120	503	—	—
20 30	120	471	114	481	120	505	—	—
21 30	119	472	114	482	119	507	—	—
22 30	119	473	114	482	118	509	—	—
23 30	118	473	114	483	118	511	—	—

11. 川奈に於ける傾斜變化觀測

地震研究所 高橋龍太郎

昭和五年三月より約三ケ月の間に亘つて數千の有感地震を發生して静岡縣伊東町の附近を怖した伊東地震に際して、伊東町及川奈村へ傾斜計を設置して、伊東地震に關聯せる地塊の運動を調査したのであつたが、川奈に於て得られたる傾斜變化の曲線には川奈地塊の集積的傾斜變化の外に規則的な短週期變化の重なつてゐる事が判明したのである。其の有様は第三圖に於て示されてゐる通りである。本論文は此の規則的變化に就て研究したものである。第四圖に於て見らるゝ如く此の規則的變化が潮汐と密接なる關係にある事は明であるが潮汐、傾斜東西性分、傾斜南北性分の三曲線の間に二時間乃至四時間の位相差が存在するので傾斜を表すヴェクトル圖は東北、西南の方向に長軸を有する楕圓の連續になり、川奈に於ける高潮及び低潮の時は夫々傾斜の極大になる二時間前に起り高潮の時には南に低潮の時には略北に傾くのである。此の潮汐と傾斜との關係を更に詳細に研究する爲に其の各を調和分解して各分潮に就て比較研究したのである。傾斜計の偏差を起す可き種々の原因の内第一に太陽及太陰の直接の引力と地殼潮汐とを考へたが此は到底實測された丈の傾斜變化を生じ得ない事が判明した。次に海水の潮汐の引力を計算したが、此も觀測値を說明し得る程大きくはなり得ない事が判明した。此等三つの原因の外に尙傾斜計の變化を起す可き原因は種々考へられるが何れも極小量の變化しか生じ得ないものであつて、只其の中にて潮汐の荷重による地殼の變形のみが相當の偏位を生ぜしめ得るので、結局觀測せられたる値は潮汐の荷重に依る地殼の變形に起因するものであると考へられる。然るに彈性力學の計算に依れば、傾斜の變化は第六圖に示せるものと全然相似にして大きさのみが異る楕圓を畫いて變化する筈であるが、一方實際に觀測される傾斜變化は第五圖 M_2 の如き變化であるから、理論と際實との間に非常な差違があるのである。此の相違を生ずる原因が色々と考へられたが結局川奈の地形の不規則なる事、地質構造の複雜なる事と川奈の地表層を構成する火山噴出物の彈性的性質に歸するであらう事が論ぜられた。

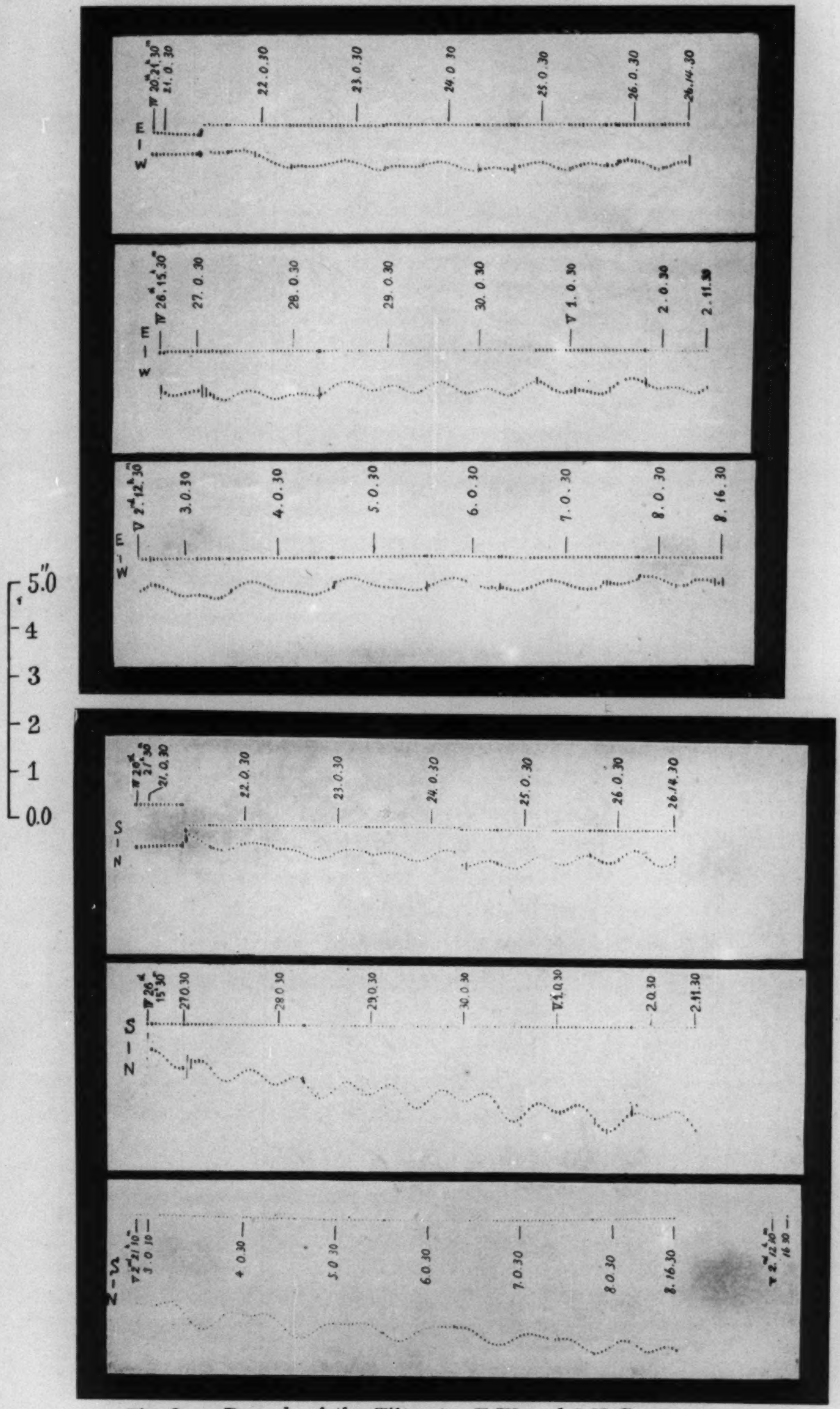

Fig. 3. Records of the Tiltmeter E-W and S-N Components From April 2nd 21h 30m to May 8th 16h 30m, 1930.

12. *Comparaison accélérométrique des secousses sismiques dans deux parties de la ville de Tôkyô*

par Mishio ISHIMOTO,

Institut de Recherches sur les Tremblements de terre.

(Lu le 20 octobre 1931, reçu le 20 decembre 1931.)

1. Introduction.

Dans le mémoire précédent,[1] nous avons remarqué que les secousses sismiques observées à la surface terrestre n'ont plus les caractéristiques des ondes envoyées directement du foyer sismique. Quand les ondes primaires arrivent dans la couche superficielle, elles provoquent des ondes secondaires ; ces dernières sont considérées comme des ondes stationnaires ayant 0·3 seconde de période produites à la surface et elles constituent la plupart des inscriptions sismographiques. Nous affirmons ceci surtout d'après les inscriptions obtenues à Hongô, à notre Institut, avec notre sismographe accélérométrique.

Certes, on sait depuis l'invention du sismographe qu'il y a toujours une telle période d'oscillation[2] dans les secousses sismiques surtout dans le cas de faibles séismes. Néanmoins, pour les séismes de grande intensité, l'apparition habituelle des ondes, dont la période et l'amplitude sont aussi grandes, nous empêchaient de constater l'existence d'ondes ayant 0·3 seconde de période ; lesquelles, donc, ont échappé aux yeux des sismologues depuis une cinquantaine d'année.

Il n'est pas rigoureux, certainement, de vouloir discuter toutes les caractéristiques des secousses sismiques d'après les inscriptions faites par le sismographe du type ordinaire. On sait que le sismographe du type ordinaire inscrit toujours le déplacement du terrain et son inscription sismique ne peut pas s'appliquer tout de suite pour étudier les conditions

1) M. ISHIMOTO, *Bull. Earthq. Res. Inst.*, 9 (1931), 473.

2) Le Prof. F. Omori a compilé les résultats sismiques obtenus en deux stations, Hongô et Hitotubasi qui se trouve dans la partie basse de Tôkyô. (Publ. Earthq. Inv. Comm., No. 10 et 11) Dans ces publications, le Prof. Omori emploie le mot "rides" pour les secousses dont l'amplitude et la période sont également petites. Il a trouvé que la période moyenne des rides est de 0·3 s. près de Hongô et a pensé qu'elles étaient indépendantes des secousses principales, parce qu'elles n'ont pas une grande amplitude.

dynamiques des bâtiments sous l'action sismique. Pour étudier ce problème, on est bien obligé d'adopter le sismographe accéléromètrique.

Comme nous l'avons signalé dans le mémoire précédent, il y a des ondes prédominantes dans les secousses sismiques à Hongô et ce fait sera expliqué en introduisant la période propre du terrain. Cette considération nous suggère que les ondes sismiques observées seraient une sorte d'ondes stationaires dans une couche superficielle de terrain ayant des paramètres d'élasticité un peu différents. Partant de cette idée, nous voulons, donc, exécuter une observation sur les ondes prédominantes, et savoir s'il y en a à Sitamati, la partie basse de Tôkyô. Une station a été installée ainsi à Marunouti, juste en face de la gare centrale de Tôkyô. L'observation a été effectuée à partir du 3 août avec un sismographe accéléromètrique du même type. Certes, nous pouvons considérer la station de Hongô comme représentative de Yamanoté, la partie haute de la ville; et la station de Marunouti comme celle de Sitamati, la partie basse de la ville.

Nous avons, de suite, réussi à enregistrer un certain nombre de séismes ayant une intensité assez grande pour nous permettre de comparer les caractéristiques des secousses sismiques produites dans deux parties de la ville. D'après cela, nous pouvons constater que les ébranlements sismiques aux deux stations sont tout à fait différents, soit en période, soit en amplitude. Nous pouvons, donc, conclure que les ondes primaires jouent un rôle important pour provoquer les changements de phase dans les secousses, mais la période, l'amplitude et la durée des secousses seront déterminées entièrement par les conditions de la couche superficielle, sur laquelle nous faisons l'observation.

2. Géologie de Tôkyô.

La ville de Tôkyô se trouve au bord de la mer, sur le golfe de même nom. Une terrasse ayant 30 m de hauteur occupe la partie ouest de la ville. La couche superficielle à cet endroit se compose de la couche diluviale (la couche de Narita et celle d'akatuti[3]): sous cette couche nous trouvons la couche de Tôkyô qui serait une couche tertiaire. L'autre partie de la ville, plate et basse, est composée par la couche alluviale et le fleuve Sumida la traverse presque en son milieu. Nous trouvons aussi la couche de Tôkyô sous cette couche. La partie basse de ville est divisée en deux, Sitamati et Kôtô par le fleuve. (Fig. 1).

3) C'est une matière d'origine volcanique qui forme la couche superficielle dans la région de Kantô: on lui donne souvent le nom de "loam".

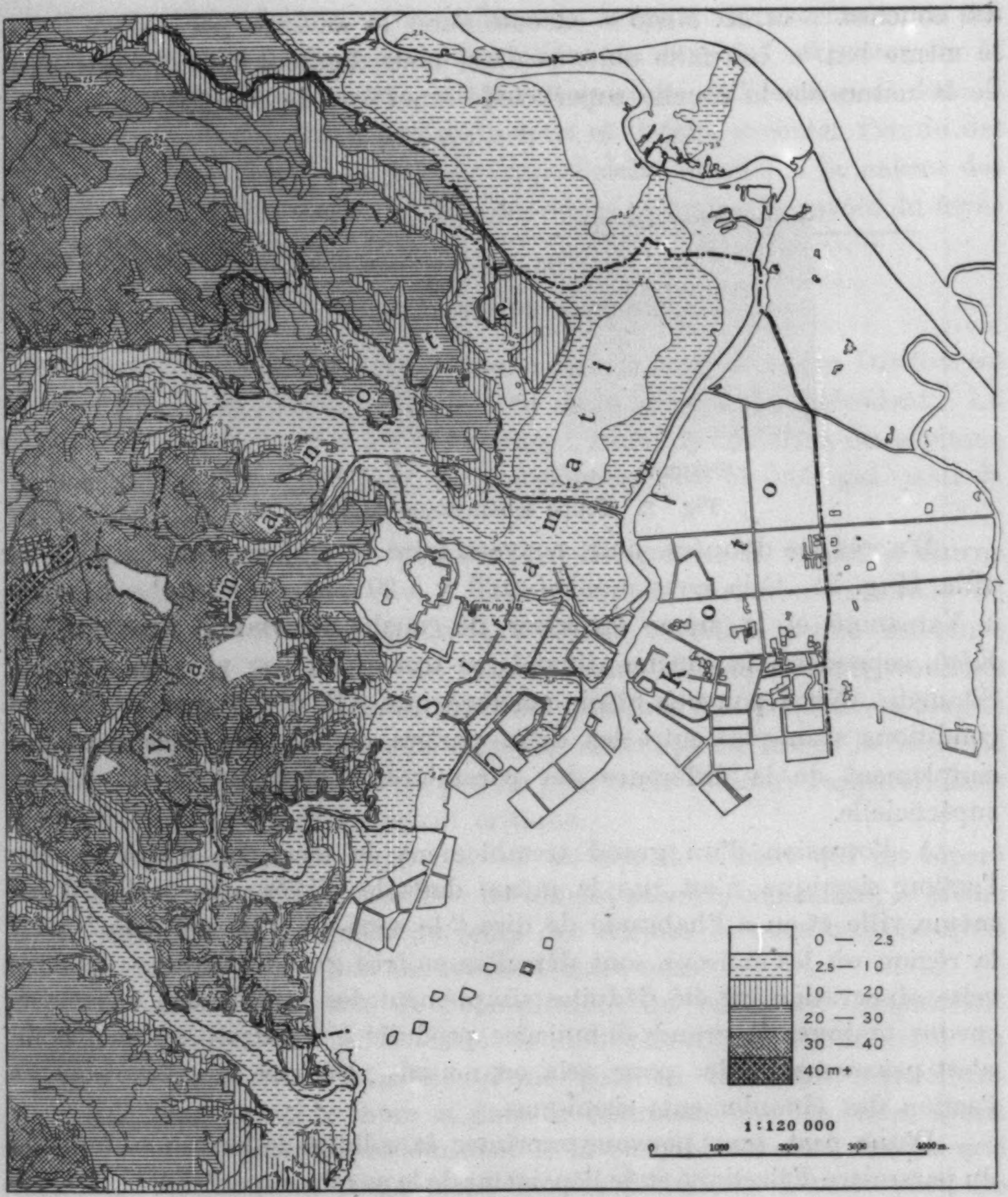

Fig. 1. Carte topographique de Tôkyô.

Les études géologiques de Tôkyô ont été poursuivies surtout après la grande catastrophe de 1923: c'est parce que le Bureau pour la reconstruction de la ville, institué juste après la catastrophe, a exécuté des sondages à la tige partout dans la ville pour connaître la résistance

des couches.[4] M. K. Nisio a exécuté aussi le sondage par rodage dans le même but.[5] Les faits obtenus ainsi nous donnent une certaine idée de la nature de la couche superficielle ainsi que de son épaisseur.

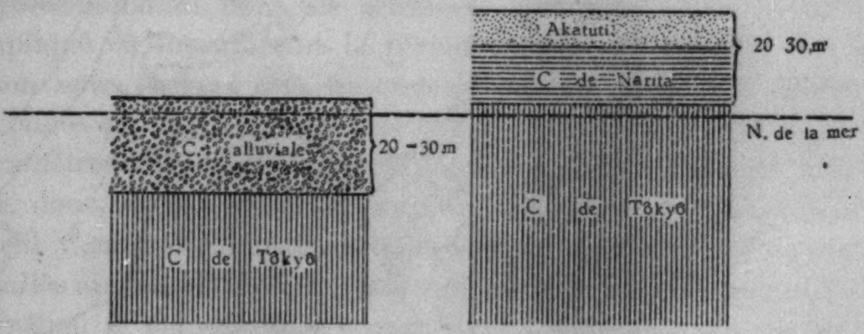

Fig. 2. Coupe schématique de Tôkyô.

D'après les données, nous pouvons faire le schéma de la coupe de la ville. (Fig. 2) Cela nous montre qu'il y a 20 à 30 m de couche diluviale à Yamanoté et la même épaisseur de couche alluviale à Sitamati. A Kôtô, cependant, la couche alluviale se trouve un peu plus épaisse qu'à Sitamati. Nous pouvons ainsi conclure que s'il n'y a pas les mêmes conditions sismiques entre les deux parties de la ville, cela dependra simplement de la différence des paramètres d'élasticité de la couche superficielle.

A l'occasion d'un grand tremblement de terre, on s'aperçoit que l'action sismique n'est pas la même dans les différentes parties d'une même ville et on a l'habitude de dire " le sous-sol n'est pas bon " pour la région où les maisons sont détruites en très grand nombre. Quoique cette observation ait été déduites simplement des expériences, nous apercevons toujours de grands dommages produits à l'endroit où le terrain n'est pas assez solide: pour cela on ne sait rien sur le mécanisme de l'action des ébranlements sismiques.

D'une part, nous pouvons exprimer la solidité de terrain en fonction du paramètre d'élasticité et de l'épaisseur de la couche superficielle. D'autre part on peut adopter la période propre d'oscillation de la couche, si elle existe, comme la mesure de la solidité du terrain. Il est certain que la période propre d'oscillation de la couche est sensiblement grande à l'endroit où les sédiments sont de date récente. En comparant les secousses sismiques aux deux endroits, nous avons constaté le fait comme

4) Mémoire sur la géologie de Tôkyô et Yokohama, (1929) publié par ce Bureau.
5) K. Nisio, *Journ. Min. Inst.*, Japan, 45 (1929), 811 ; 46 (1930), 29 et 109.

on le verra plus loin que la différence la plus importante entre les secousses est celle de la période prédominante dans les secousses de la couche superficielle du terrain. Il paraît que cette différence peut donner la différence de dommage aux bâtiments et il faut exécuter l'étude des propriétés élastiques de la couche superficielle ainsi que la nature des ébranlements produits sous l'action des ondes primaires envoyées du foyer sismique.

3. Observation à Hongô.

L'appareil que nous avons installé dans la cave de notre Institut est le sismographe accélérométrique décrit dans le mémoire précédent. La sensibilité de l'appareil a été déterminée : 1 mm de déviation de la plume correspond à 0·98 gal pour la composante N-S et 0·99 gal pour la composante E-O.

Certainement, nous ne pouvons pas déterminer la variation diurne de température dans la cave ; néanmoins la variation annuelle de température se trouve de 10°–25° C. et cette variation a une influence sur la viscosité de l'huile de l'amortisseur. Quoique nous voulions éviter cette influence, nous la trouvons quelques fois pendant la longue période. Nous faisons, cependant, régler de temps en temps la viscosité de l'huile en la mélangeant de pétrole pour tenir toujours l'appareil dans les conditions de l'amortissement critique.

Nous avons installé l'appareil sur un bloc de ciment qui est séparé de la base du bâtiment. Ce bloc de ciment montre, cependant, le même mouvement que le bâtiment au temp des séismes et nous croyons qu'il n'y a aucune différence de mouvement entre eux.

Nous avons déjà parlé de l'ébranlement du bâtiment[6] considérant qu'il y a certaine différence entre le mouvement du sol et celui du bâtiment. Nous avons constaté, d'une part en installant séparément deux microsismographes hors et dans le bâtiment, que les ondes ayant 0·1 seconde de période prédominent à la surface terrestre, tandis que ces ondes disparaîssent entièrement dans le bâtiment. D'autre part, les ondes ayant 0·3 seconde de période apparaissent toujours aux deux endroits. Conséquemment, nous avons conclu que le bâtiment oscille avec une période propre. Mais, maintenant, il faut revoir ce phénomène, parce que ces petites ondes existent à la surface du sol. Il est plausible que ces ondes ne paraissent pas dans le bâtiment, dont les fondations se trouvent 3 mètres de profondeur de la surface, où nous n'observons

6) M. Ishimoto et R. Takahasi, *Bull. Earthq. Res. Inst.*, 7 (1929), 175.

que les ondes ayant 0·3 seconde de période. D'après ce fait, nous pouvons conclure que les secousses sismiques inscrites sur le bloc de ciment de la cave sont considérées comme celles produites nettement dans le terrain, sauf pour les ondes dont la période demeure assez courte.

Nous pouvons tirer ces considérations aussi dans le même mémoire par les mots: "le bâtiment s'incline comme faisant partie du terrain, suivant la pente des ondes" ou "nous pouvons supposer que les mouvements d'un point du bâtiment représentent ceux des ondes superficielles."

Comme nous le verrons plus tard, dans les inscriptions obtenues sur le bloc de ciment, nous trouvons des valeurs diverses de périodes pour certain type de séisme: ce fait nous donne une preuve que le bâtiment n'a en aucune façon d'ébranlements faisant penser à une oscillation propre.

Les inscriptions obtenues à Hongô surtout pour les forts séismes nous montrent certaines caractéristiques des ébranlements. Nous remarquons quelquefois une seule onde solitaire apparue au début de la phase S: ondes ayant une amplitude plusieurs fois plus gande que les autres. Ce fait nous suggère que les ondes préliminaires ont une propriété analogue aux ondes de choc autant que les ondes restent dans la croûte. Il y a deux ou trois beaux exemples dans les inscriptions ci-jointes.[7] L'existence des ondes solitaires dans les secousses sismiques a été prouvée depuis le premier mémoire sur l'observation accélérométrique. Cette fois-ci, nous remarquons très nettement l'existence d'une onde solitaire au début de la phase S qui nous fait entrevoir une autre nature des ondes sismiques de grande intensité issues du foyer.

4. Observation à Marunouti.

La station de Marunouti se trouve, dans la partie basse de Tôkyô, à 3·5 km au sud de la station de Hongô. Comme l'appareil a été installé sur le sol même, il inscrit toujours une succession de secousses produites par des trains, des camions, etc. Cependant, ces amplitudes restent comparativement petites et elles ne gênent en rien les inscriptions sismiques. La sensibilité de l'appareil a été déterminée et est de 1 mm de déviation de la plume pour 0·78 gal pour la composante N-S, et pour 0·89 gal pour la composposante E-0.

Comme nous n'avons pris aucune précaution pour éviter les variations

7) Voir les inscriptions des séismes du 16 et du 18 Sept. (1931).

thermiques d'air, il y a eu quelque changement de la viscosité de l'huile dans l'amortisseur. Quoique la viscosité varie dans certaines limites, il n'y a que peu de changement dans la valeur de la sensibilité surtout au voisinage de la période propre de l'appareil et il ne donne aucune objection pour relever des secousses sismiques ayant 0·6 seconde de période, considérées comme prédominantes à Marunouti.

Nous avons aperçu tout de suite une différence de type des secousses en comparant les inscriptions obtenues aux deux stations. Nous voulons, cependant, faire une discussion de la différence de période prédominante aux deux stations dans le chapitre suivant.

Nous constatons généralement que la durée des secousses est toujours longue à Marunouti, tandis que l'onde solitaire apparaît dans les secousses à Hongô. Quant à la durée des secousses il nous paraît qu'elles s'amortissent très vite à Hongô mais elles s'amortissent très peu à Marunouti. Ce fait nous donne quelque idée sur la constitution de la série des ondes primaires. Il nous semble que les périodes des ondes primaires restent comparativement petites au début tandis qu'elles augmentent progressivement vers la queue. Nous voyons, donc, que la durée des secousses est assez longue à Marunouti où la période propre du terrain se trouve comparativement grande et que les amplitudes des secousses augmentent suivant le passage du séisme. Nous pouvons relever un exemple de secousses produites à Marunouti, dont l'amplitude maxima a eu lieu 50 secondes après le début de la phase S.[8)]

L'apparition des ondes solitaires dans les secousses n'est pas distincte à Marunouti. Cela dépend certainement de ce que la période propre d'oscillation est comparativement grande à cet endroit: les propriétés des ondes primaires seront perdues quand elles viennent à la couche superficielle du terrain et la perte sera d'autant plus grande que la période propre de la couche est plus grande. En tout cas, il faut faire remarquer que les secousses ne restent plus pareilles en deux stations qui sont éloignées seulement de 3·5 km. Nous nous inclinons à considérer, donc, que le rôle de la couche superficielle est très important pour déterminer la condition locale des secousses. Nous voulons, en effet, examiner le phénomène sismique rapporté à l'existence de la couche superficielle du terrain.

5. Comparaison de la période prédominante.

Nous avons réussi à enregistrer aux deux stations un certain nombre

8) Voir l'inscription obtenue pour le séisme du 28 Septembre 14^h (Fig. 9bis).

de séismes pendant les mois d'août et de septembre. Le tableau I montre les forts séismes ressentis à Tôkyô et leurs épicentres sont indiqués sur la carte. (Fig. 3.) Dans le tableau I, nous marquons toujours la différence de la valeur d'accélération: le plus grand rapport de l'accélération est de 3·6 à l'occasion du séisme apparu le 10 août. Nous pouvons distinguer très bien que les rapports dépendent généralement de la distance épicentrale: Hongô oscille plus que Marunouti pour les séismes dont la distance épicentrale est petite. Pour expliquer cela, nous pensons simplement au fait que le terrain possède une période propre d'oscillation qui n'est pas la même en chaque endroit. Les ondes primaires conservent les ondes de courte période autant qu'elles ne voyagent pas à une grande distance. Conséquemment elles peuvent provoquer une grande accélération des secousses dans une région où la période propre d'oscillation demeure assez courte.

Or, nous savons, d'ailleurs, que dans un grand tremblement de terre,

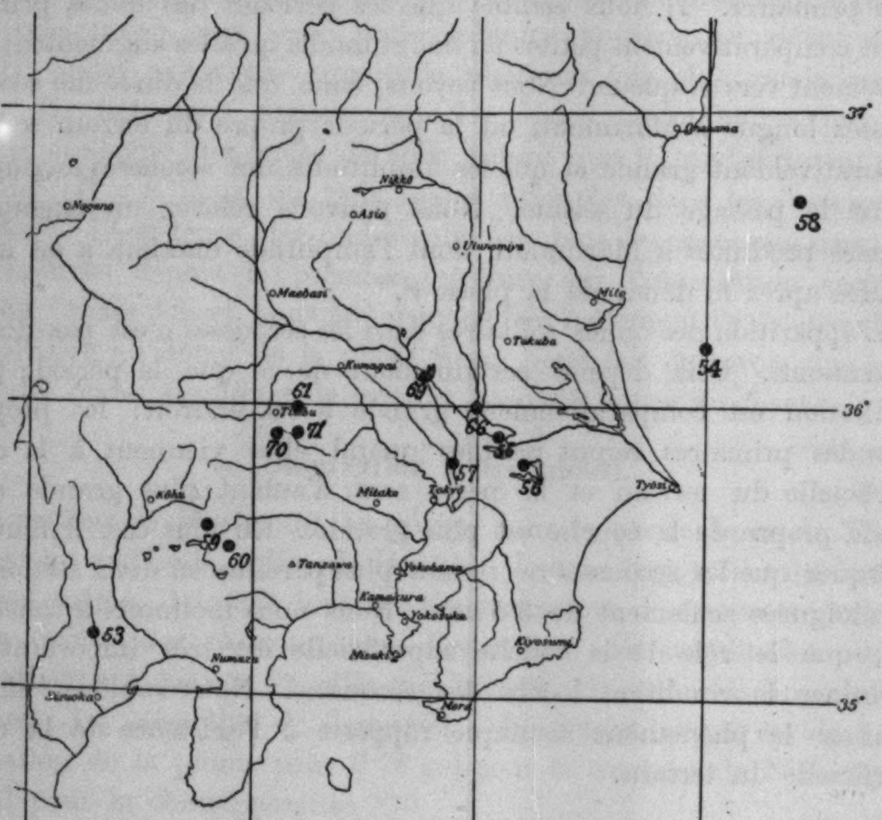

Fig. 3. Positions épicentrales.

Tableau I.

No.	temps d'occurence (1931)					accélération maxima			épicentre		distance épicentrale
		j	h	m	s	Hongô	Marunouti	rapport	λ(*E*)	φ(*N*)	
53	Août.	10	23	34	32	3·3 gal (N)	12·0 gal (O)	3·63	138°3	35°2	141km
54		18	14	40	42	3·5 (S)	6·5 (O)	1·86	141·0	36·2	120
55		19	8	43	45	1·5 (N)	2·0 (O)	1·33	140·1	35·9	36
56		27	8	49	33	3·3 (E)	2·2 (S)	0·67	140·2	35·8	38
57	Sept.	7	5	35	05	31·5 (S)	20·0 (E)	0·64	139·9	35·8	17
58		9	4	09	31	3·5 (N)	2·7 (E)	0·77	141·4	36·7	180
59		16	21	43	23	41·9 (O)	27·0 (N)	0·64	138·8	35·6	88
60		18	15	13	45	19·8 (S)	13·4 (O)	0·63	138·9	35·5	82
61		21	11	20	10	74·6 (O)	——	——	139·2	36·0	64
66		24	13	26	25	3·9 (E)	4·4 (N)	1·13	140·0	36·0	19
69		28	4	50	40	11·9 (N)	8·7 (N)	0·73	139·8	36·1	48
70		28	13	54	28	5·6 (N)	6·4 (O)	1·14	139·1	35·9	67
71	Oct.	3	2	36	55	6·9 (N)	9·1 (E)	1·32	139·2	35·9	59

la distribution catastrophique ne se réalise pas simplement. Nous voyons souvent des maisons détruites dans une région située assez loin de l'épicentre, sans avoir aucune destruction dans la région intermédiaire.

Nous savons aussi que l'on observe le même phénomène dans le cas d'un séisme né dans le sein de la croûte assez profonde. Les propriétés générales de ce type de séisme ont été déjà étudiées spécialement par un sismologue japonais[9]: on a constaté que ce type de séisme donne toujours une distribution anormale de l'intensité sismique. D'après notre considération, cependant, cela est simplement une conséquence de l'existence d'une période propre d'oscillation à chaque région dépendant de l'épaisseur et du paramètre d'élasticité de la couche superficielle. Nous reverrons ce type de séisme encore plus loin.

Nous avons essayé de chercher la période propre des deux stations d'après la méthode suivante. Prenant une valeur d'accélération (3 gal) comme référence, nous avons lu les positions des ondes dans les inscriptions agrandies 4 fois par un procédé photographieque et les chiffres sont lus jusqu'au dixième de millimètre, qui correspond à 0·02 seconde. Il est certain que l'intervalle de deux positions successives mesure la période des secousses. En déterminant le nombre d'ondes (n) pour

9) K. Wadati, *Geophys. Mag.*, 1 (1928), 162 et 2 (1929), 1.

chaque intervalle, nous avons obtenu la courbe en cloche[10] correspondant à chaque séisme; la période prédominante des secousses se trouve au maximum de l'ordonnée de la courbe.

Les courbes en cloche obtenues sont représentées dans les figures. Nous pouvons tout de suite distinguer deux valeurs de la période prédominante dans les secousses aux deux stations: elle est 0·3 seconde à Hongô et 0·6 seconde à Marunouti. Il est très remarquable que la distribution de la période dans la courbe varie surtout avec la distance épicentrale du séisme. Nous pouvons tirer un bel exemple de la courbe obtenue avec le séisme du 10 août. (Fig. 4) La distance épicentrale de ce séisme a été fixée à 140 km environ qui est une des plus grandes distances épicentrales. Il a provoqué une accélération plusieurs fois plus gande à Marunouti comme nous avons déjà dit.

Ce fait nous laisse à considérer le mécanisme de la production des secousses à la surface terrestre. Un séisme voisin peut produire des secousses dans une région où la période propre d'oscillation demeure assez courte, tandis que le séisme lointain ne peut que provoquer des secousses dans une région où la période propre d'oscillation reste assez longue. Nous pouvons, donc, conclure que les ondes primaires sont constituées par celles de courte période, qu'autant qu'elles restent près du foyer.

Les discussions sur ce sujet ont été faites mathématiquement par K. Sezawa[11] qui nous a montré que les ondes peuvent provoquer des

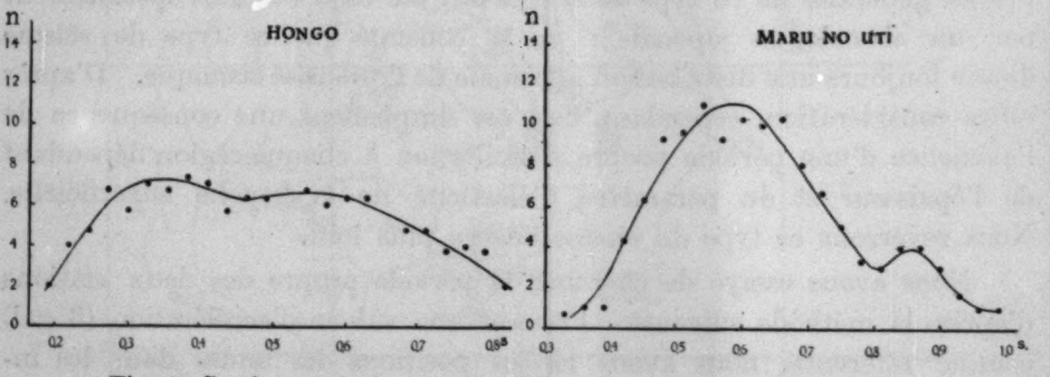

Fig. 4 Courbe en cloche pour le séisme du 10 Août (1931) No. 53.

10) Pour avoir les courbes en cloche, on pense quelque fois qu'il est mieux de prendre n × période pour l'ordonnée, mais cette fois-ci nous prendrons simplement n: c'est parce que nous voulons regarder le nombre d'oscillations dans la série de secousses qui a un rapport serré avec les actions sismiques sur les problèmes du génie.

11) K. SEZAWA, *Bull. Earthq. Res. Inst.*, 8 (1930), 1.

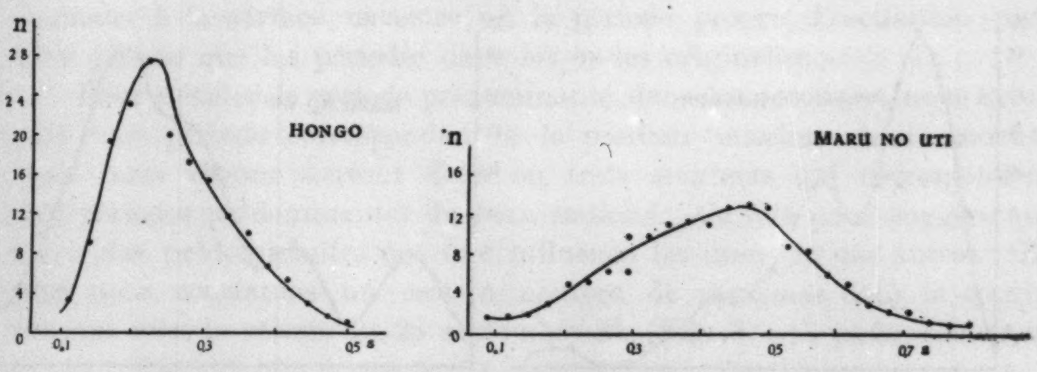

Fig. 5. Courbe en cloche pour le séisme du 7 Sept. (1931) 57.

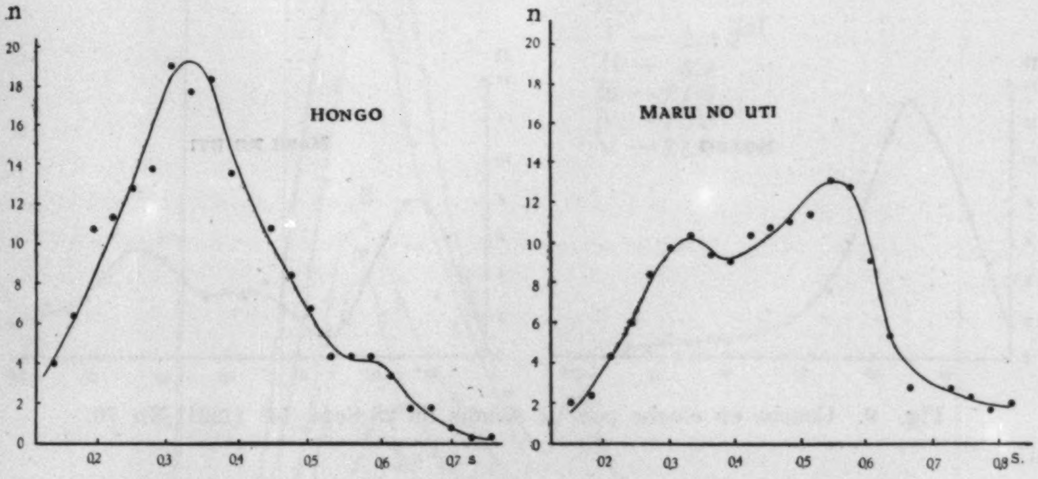

Fig. 6. Courbe en cloche pour le séisme du 16 Sept. (1931) No. 59.

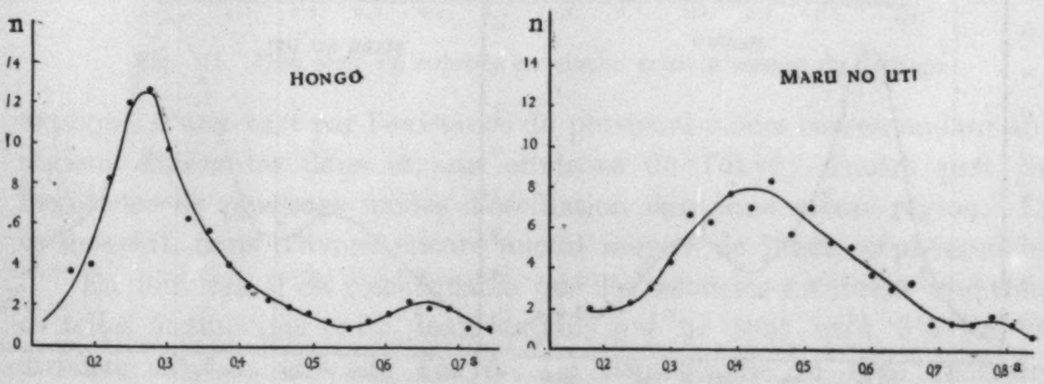

Fig. 7. Courbe en cloche pour le séisme du 18 Sept. (1931) No. 60.

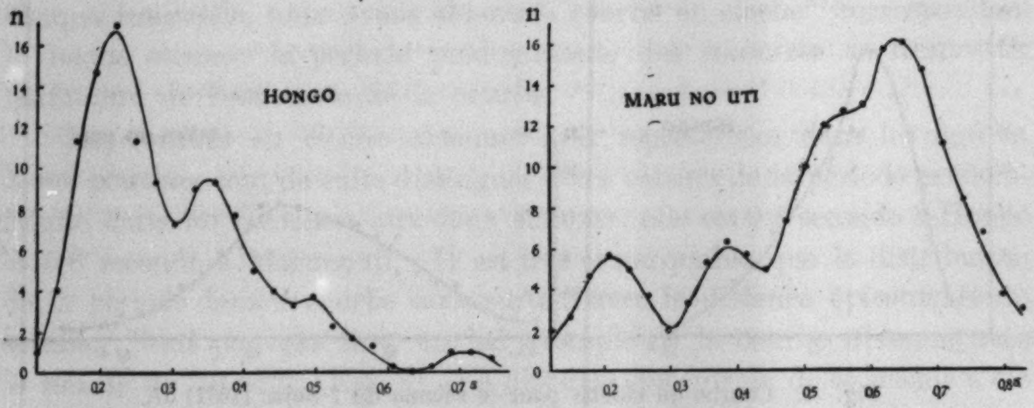

Fig. 8. Courbe en cloche pour le séisme du 28 Sept. 5^h (1931) No. 69.

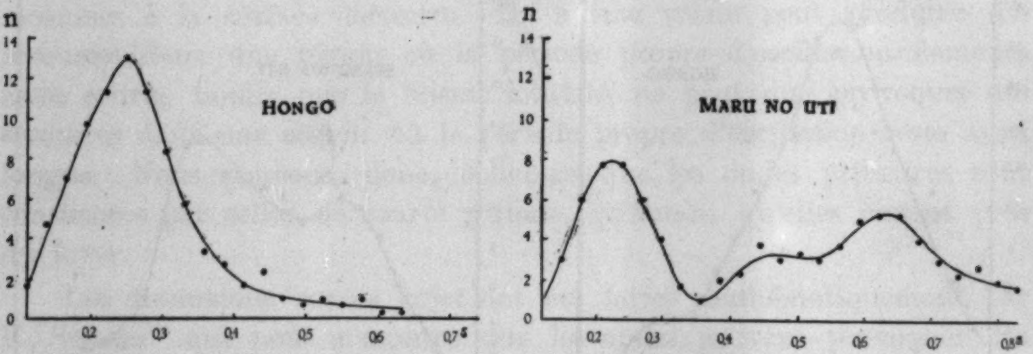

Fig. 9. Courbe en cloche pour le séisme du 28 Sept. 14^h (1931) No. 70.

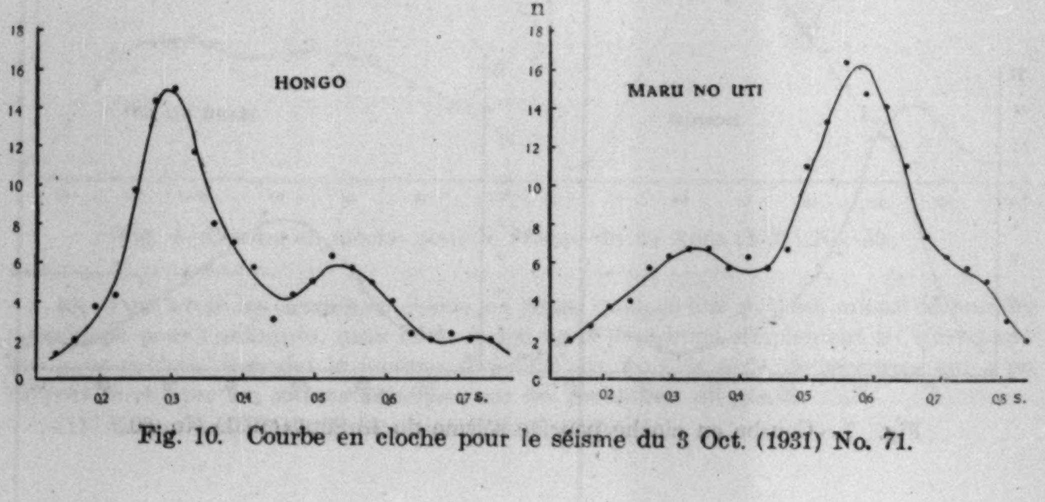

Fig. 10. Courbe en cloche pour le séisme du 3 Oct. (1931) No. 71.

secousses à la surface terrestre où la période propre d'oscillation reste plus grande que les périodes dans les ondes originelles.

Pour décider la période prédominante dans les secousses, nous avons pris une période correspondant à la position maxima de la courbe: mais nous voyons seuvent deux ou trois maximas qui correspondent aux périodes prédominantes de deux stations. Ce fait nous suggère que les ondes prédominantes ont une influence les unes sur les autres. De plus nous constatons un certain nombre de maximas dans la courbe obtenue avec le séisme du 28 septembre 5^h. (Fig. 8) Ce phénomène sera

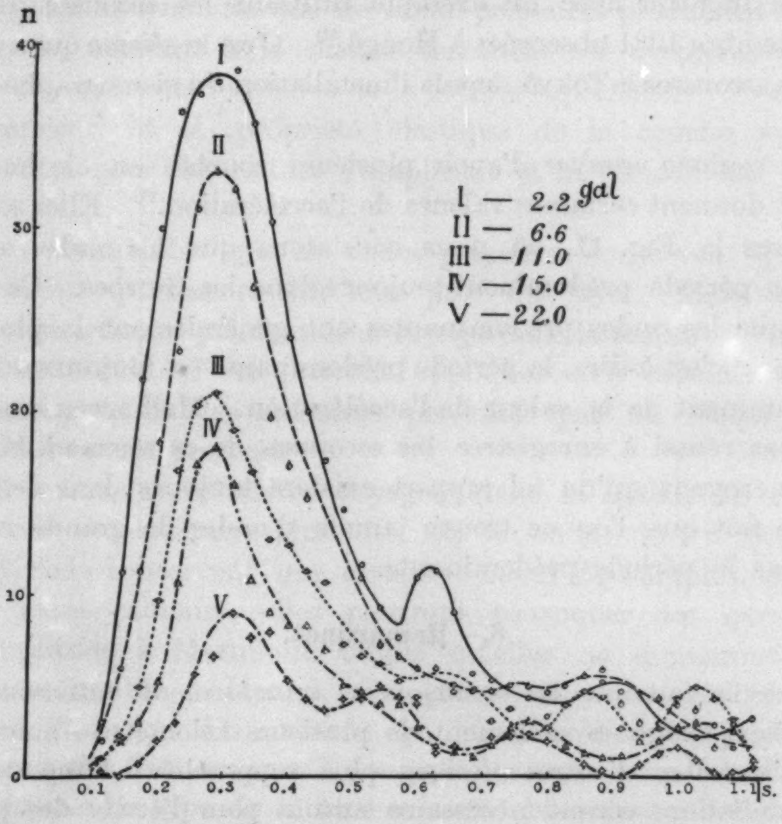

Fig. 11. Une sèrie de courbes en cloche pour le séisme du 21 Sept.

expliqué d'une part par l'existance de plusieurs modes correspondant aux régions différentes dans et aux environs de Tôkyô; d'autre part par l'existence de plusieurs modes d'oscillation dans une même région. En ce moment, nous n'avons encore aucun moyen de juger ce phénomène.

En tout cas, il est remarquable que les secousses sismiques montrent de telles distinctions entre deux stations qui ne sont qu'à 3·5 km de distance dans la ville de Tôkyô. Le sismographe du type ordinaire servira bien pour savoir le temps d'occurence ou l'apparition des différentes

phases dans les secousses sismiques surtout pour les séismes lointains: mais il n'est pas commode pour inscrire les ondes ayant une plus grande accélération qui sont toujours masquées par des ondes dont la période et l'amplitude sont grandes. En employant le sismographe accélérométrique, il est certain, comme nous l'avons déjà dit qu'on peut tirer les caractéristiques des secousses sismiques qui ont un rapport serré avec la nature de la couche superficielle du terrain.

Il y a encore un problème inaperçu: ce sont les ondes de la période prédominante: détiennent-elles toujours les grandes amplitudes ? Nous voulons le montrer avec un exemple utilisant les secousses du séisme du 21 septembre 1931 observées à Hongô.[12] C'est le séisme qui a donné les plus fortes secousses à Tôkyô depuis l'installation du sismographe accélérométrique.

Nous voulons essayer d'avoir plusieurs courbes en cloche avec les ondes qui donnent certaines valeurs de l'accélération.[13] Elles sont représentées dans la Fig. 11. où nous constatons que les ondes ayant 0·3 seconde de période prédominent toujours dans les courbes. Ce fait nous apprend que les ondes prédominantes ont généralement la plus grande accélération: c'est-à-dire, la période prédominante est toujours 0·3 seconde indépendamment de la valeur de l'accélération. Malheureusement, nous n'avons pas réussi à enregistrer les secousses de ce séisme à Marunouti, mais nous croyons qu'un tel rapport existera toujours dans cette région suivant le fait que l'on ne trouve jamais d'ondes de grande amplitude n'ayant pas la période prédominante.

6. Remarques.

D'après le fait que les secousses se transforment entièrement dans deux stations éloignées seulement de plusieurs kilomètres, nous sommes obligés d'installer d'autres stations plus rapprochées l'une de l'autre. Telles installations seront nécéssaire surtout pour l'étude des propriétés des secousses sismiques en relation avec la nature de la couche superficielle.

Presque toutes les villes du Japon ont été construites sur une couche sédimentée récemment par le fleuve: la période propre d'oscillation d'un tel endroit se trouve toujours grande. D'autre part, nous savons que les maisons bâties en un tel endroit sont attaquées fréquemment par les

---

12) Son inscription est montrée dans ce Bulltin 10 (1932), 264. Fig. 12.

13) Nous n'avons pas pu mesurer la période dans un certaine partie de secousses, étant mal inscrites: mais, l'aspect général des courbes restera le même.

secousses sismiques. Ce fait sera expliqué par les secousses prédominantes de longue période[14] qui peuvent causer la destruction surtout de maisons en bois. On conclut souvent du fait qu'il y a beaucoup de dommages le long du bassin du fleuve, que les secousses sismiques ont un rapport serré avec les failles tectoniques. Vraiment, on s'incline à fixer la position épicentrale sur le fleuve, en observant que là ont eu lieu les plus grands dommages; mais cela n'est pas juste en tout cas suivant nos idées. Nous avons des exemples pour lesquels la région épicentrale n'est pas le centre du dommage.

Nous pouvons conclure que les ondes primaires produisent des ondes secondaires en arrivant à la surface terrestre: ces dernières sont probablement des ondes stationnaires de la couche superficielle. Conséquemment l'épaisseur et la propriété élastique de la couche jouent un rôle important pour déterminer l'amplitude et la période des secousses produites.

Il est vraisemblable que les ondes primaires conservent les courtes périodes autant qu'elles restent tout près du foyer. Mais les ondes primaires s'amortissent pendant leur voyage dans la croûte où l'on trouve de la viscosité solide. Nous pouvons appliquer cette considération à la distribution anormale des secousses produites par un séisme dont le foyer se trouve assez profond.

Quand les ondes primaires voyagent dans la croûte, les ondes de courte période s'amortissent plus vite. Si les ondes de 0·6 seconde environ de période conservent une certaine valeur de l'amplitude dans la série des ondes primaire, elles pourront provoquer des secousses de grande amplitude à Marunouti tandis qu'elles ne donneront aucune secousse remarquable à Hongô. Tel phénomène sera réalisé partout au Japon à l'occasion d'un séisme ayant un foyer assez profond qui pourra donner des ébranlements à peu près dans une même condition. Il nous semble que ce type de séisme conserve bien les ondes de courte période; suivant la raison que les ondes traversent toujours la partie profonde de la croûte. En arrivant à la surface terrestre, elles peuvent provoquer une oscillation propre à chaque endroit: cette période varie suivant les conditions élastiques de la couche surperficielle. Nous voyons, en conséquence, une distribution anormale des ébranlements sismiques.

Un phénomène analogue est aussi remarqué à l'occasion d'un grand tremblement de terre. Naturellement, la région où la distribution anormale des secousses apparaît, est limitée par le fait que le foyer ne

14) Elle sera probablement plus de 0·6 seconde.

se trouve pas assez profond. Nous pouvons le constater dans les cartes montrant le degré des secousses: le degré est déterminé généralement par le pourcentage des maisons détruites. Nous en avons deux exemples: le grand tremblement de terre de Kantô[15] et le grand tremblement de terre de Tango.[16] Les ébranlements sont toujours grands à l'endroit où il y a une couche alluviale. Pour le grand tremblement de terre d'Idu, nous avons remarqué une distribution anormale de secousses surtout dans le bassin de la rivière Kanô.

Il faut remarquer, en tout cas, que même dans la ville de Tôkyô nous pouvons relever une distribution anormale de secousses sismiques. Nous croyons que la cause d'une telle distribution a son origine dans les propriétés élastiques de la couche superficielle du terrain. Nous voulons, en effet, discuter prochainement les propriétés élastiques du sol d'après les observations des secousses sismiques.

---

12. 東京市內二ヶ所（本郷、丸ノ內）における地震動加速度比較

地震研究所 石 本 巳 四 雄

1. 地表において觀測される地震動は、表面層の自己振動が誘發される結果として、地殼內における一次波動とは著しく異つたものである事は前論文において述べたものである。實際、本郷においては約 0·3 秒と云ふ自己振動周期が見出されて居る。

元來地震動中に各土地固有の振動の存在する事實は相當以前から認められた事であつたが、變位地震計を使用して居た事から、强震程度の地震においては脈動性振動に邪魔されて表面層固有振動の影響を認める事は困難の狀態にあつた。

各土地に固有振動の存在する事實を確める爲めに、八月上旬から丸ノ內、東京驛前に加速度地震計を設置して觀測を開始し、相當震度の大である多くの地震について記象を得、本郷、丸ノ內における地震動特性を比較して見たのである。

2. 東京の地形は大別して山手、下町となり、本郷は山ノ手代表、丸ノ內は下町代表と考へる事が出來る。山ノ手は約 20 m の厚さの洪積層と其の下部の東京層、下町は $20^{m}-30^{m}$ の沖積層と其の下部の東京層とから成つて居る關係上、若し山手、下町において地震動中表面層の影響がありとすれば、其れは全く洪積層、沖積層の厚さと彈性係數とに專ら關係するものであると推定出來る。從來大地震の場合、家屋の倒壞を標準として地盤が惡いと云ふ言葉が屢々用ひられて居るが、之れは大略表面層の彈性狀況を言ひ表はしたものと見られる。

---

15) T. MATSUZAWA, *Bull. Earthq. Inv. Comm.*, No. 100. A.
16) H. HOMMA, *Tikyû*, 9 (1928), 357.

Hongô

Marunouti

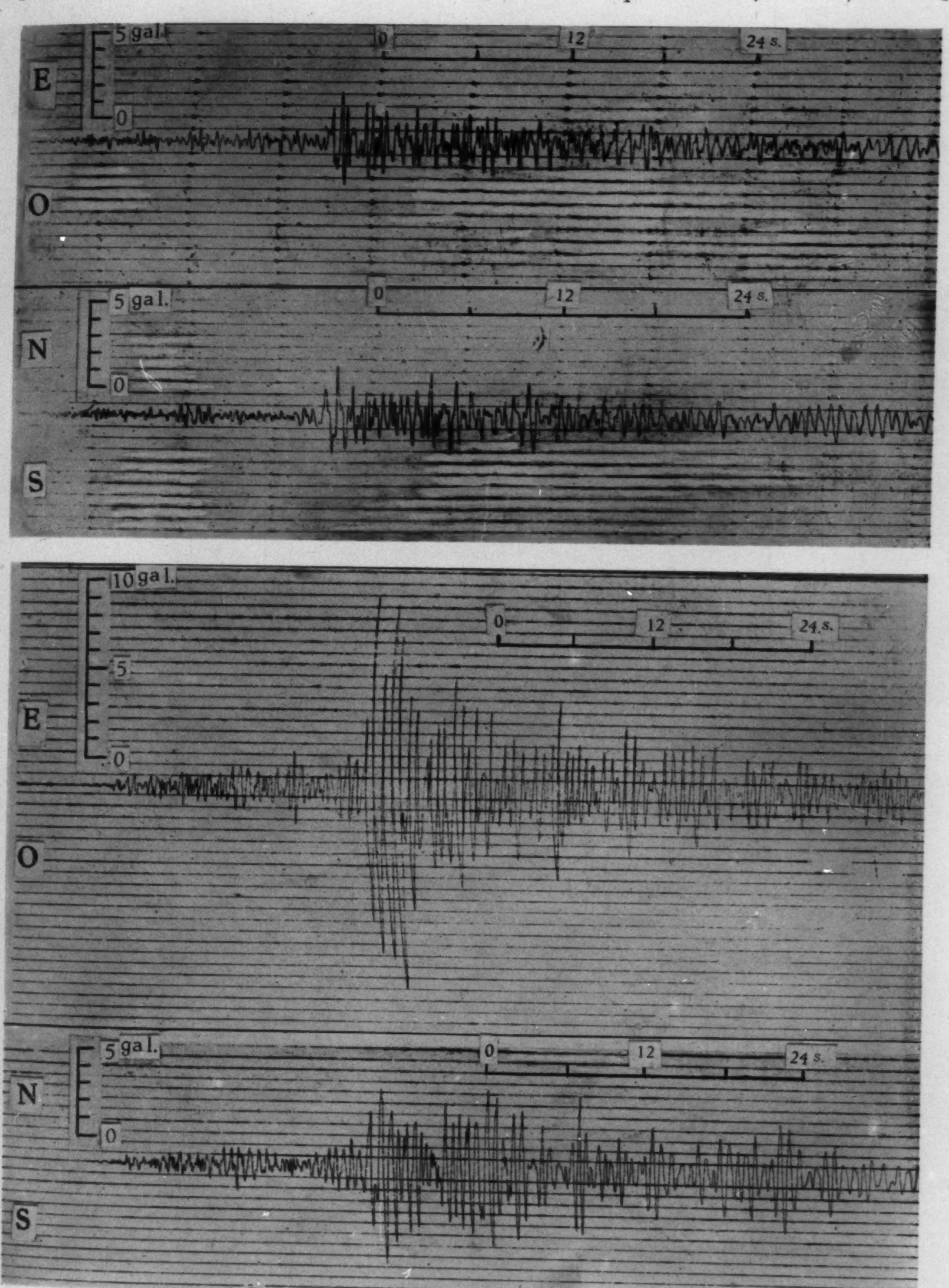

Fig. 4bis Inscription obtenue pour le séisme du 10 Août. (1931) No. 53.

(震研彙報、第十號、圖版、石本)

Hongô

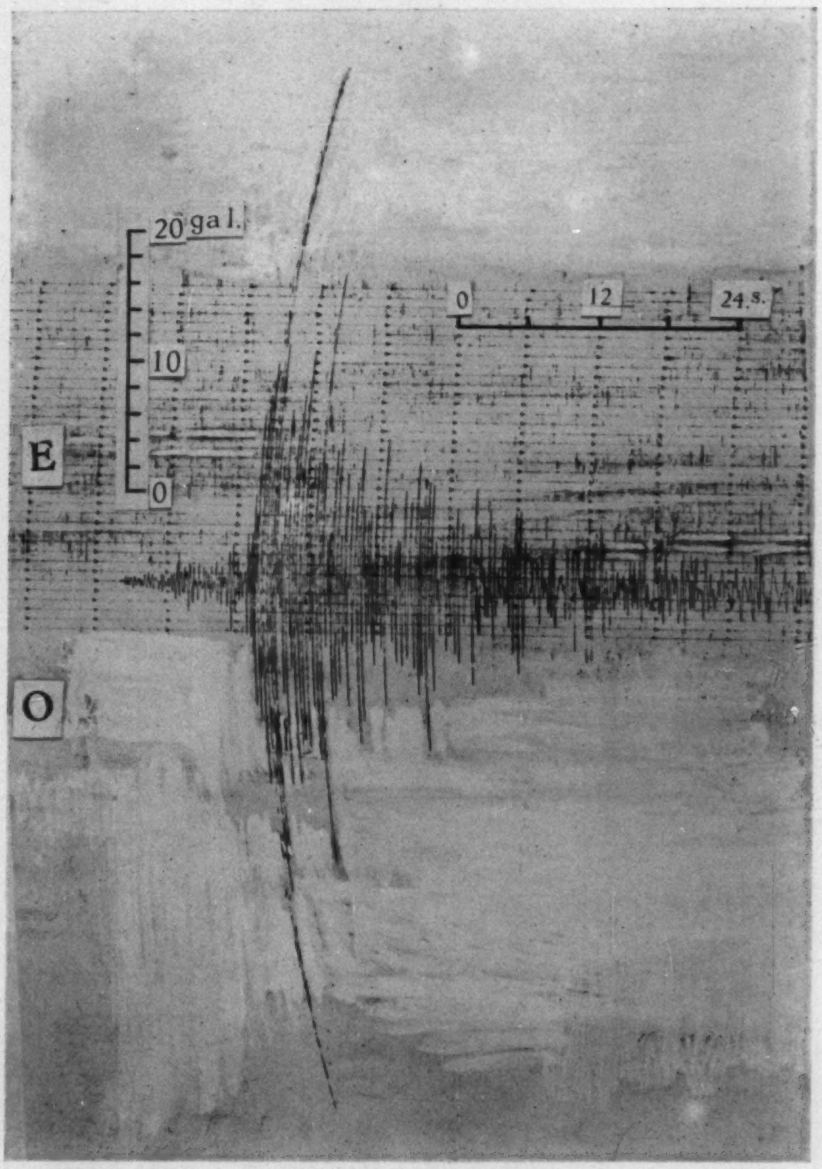

Hongô

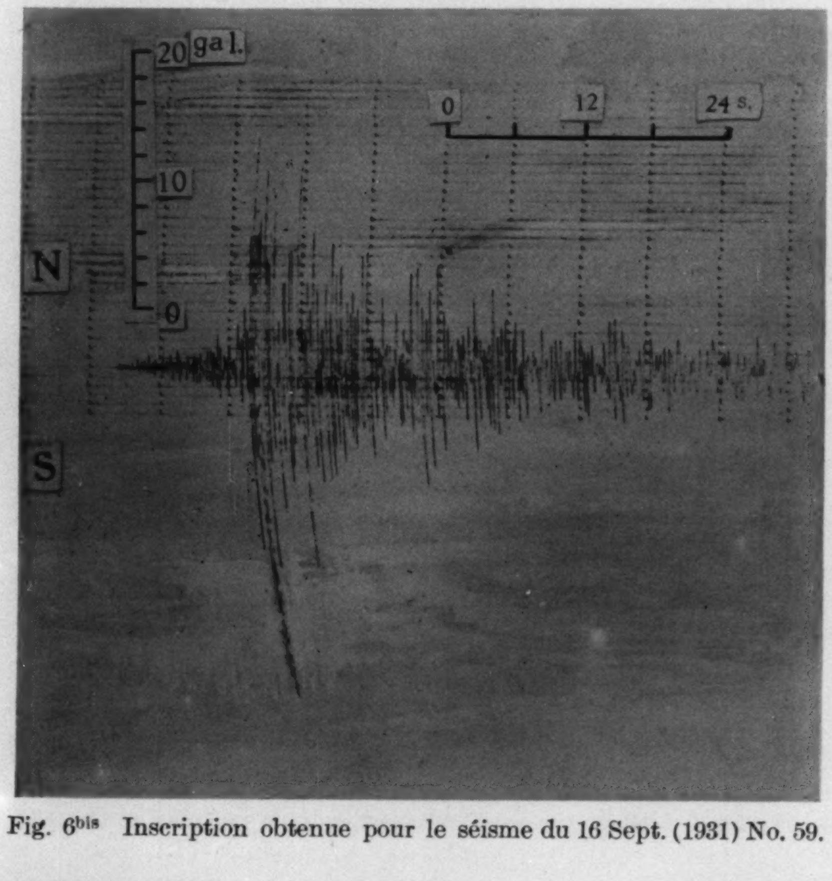

Fig. 6bis Inscription obtenue pour le séisme du 16 Sept. (1931) No. 59.

(實研彙報、第十號、圖版、石本)

Marunouti

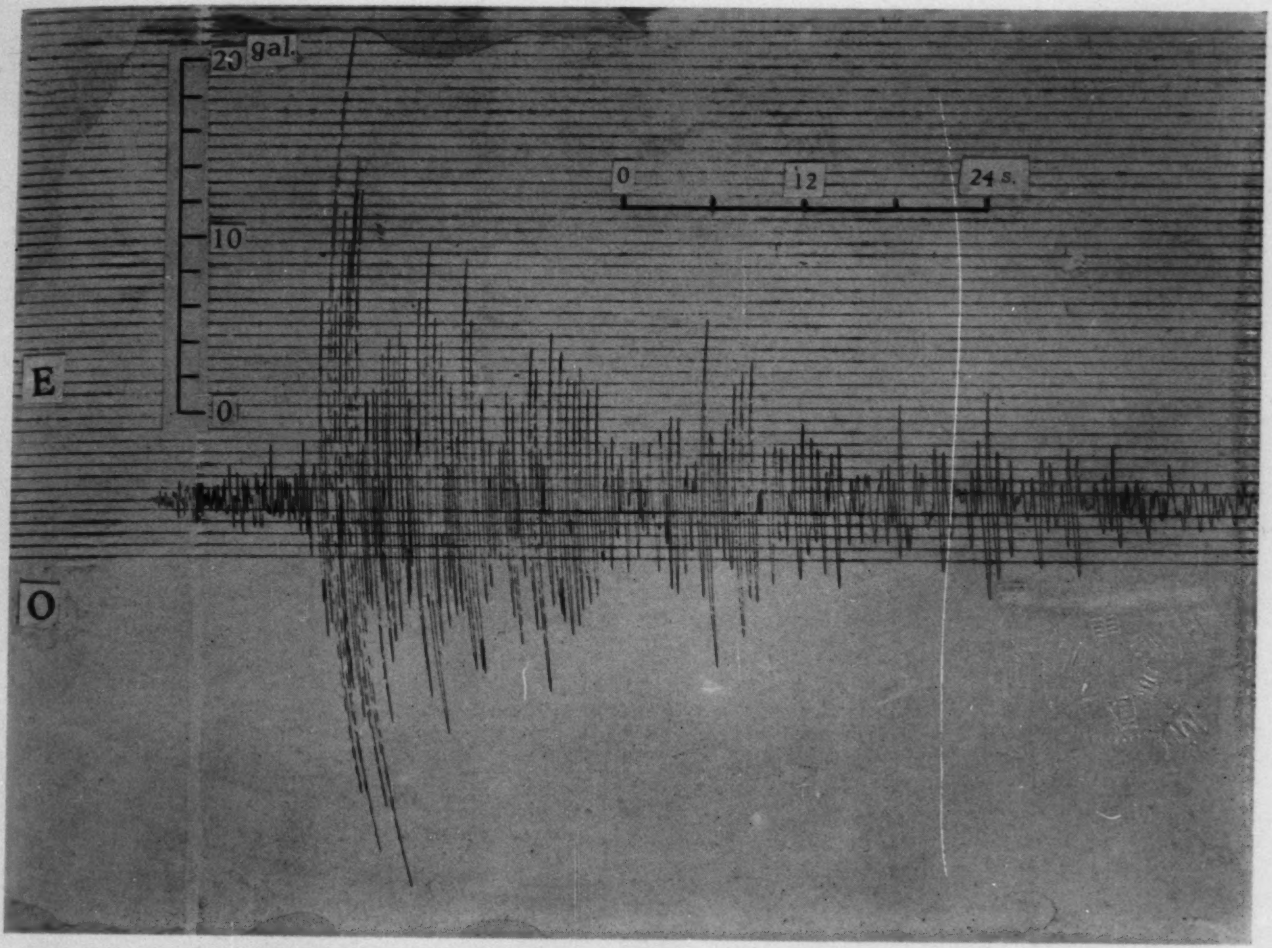

Marunouti

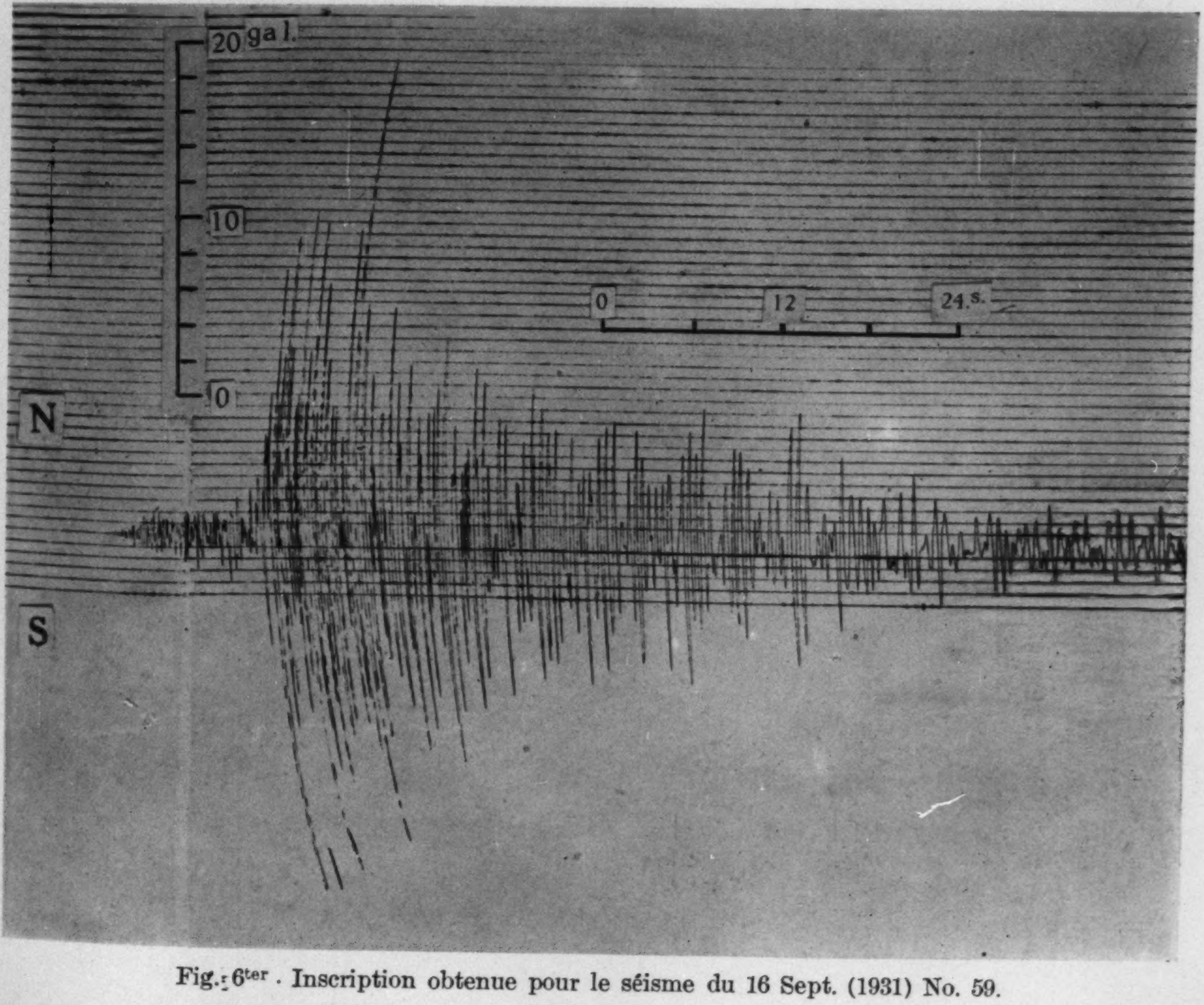

Fig. 6ter. Inscription obtenue pour le séisme du 16 Sept. (1931) No. 59.

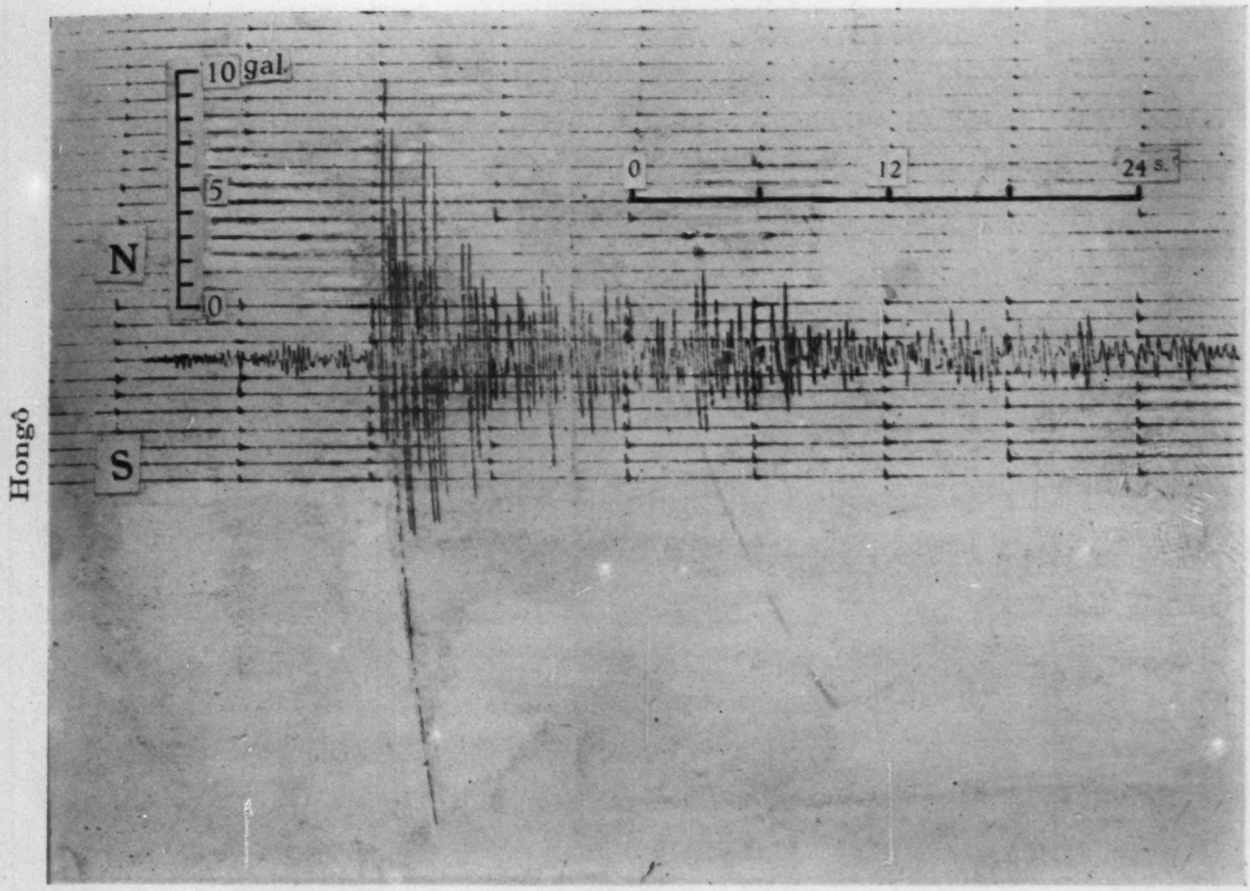

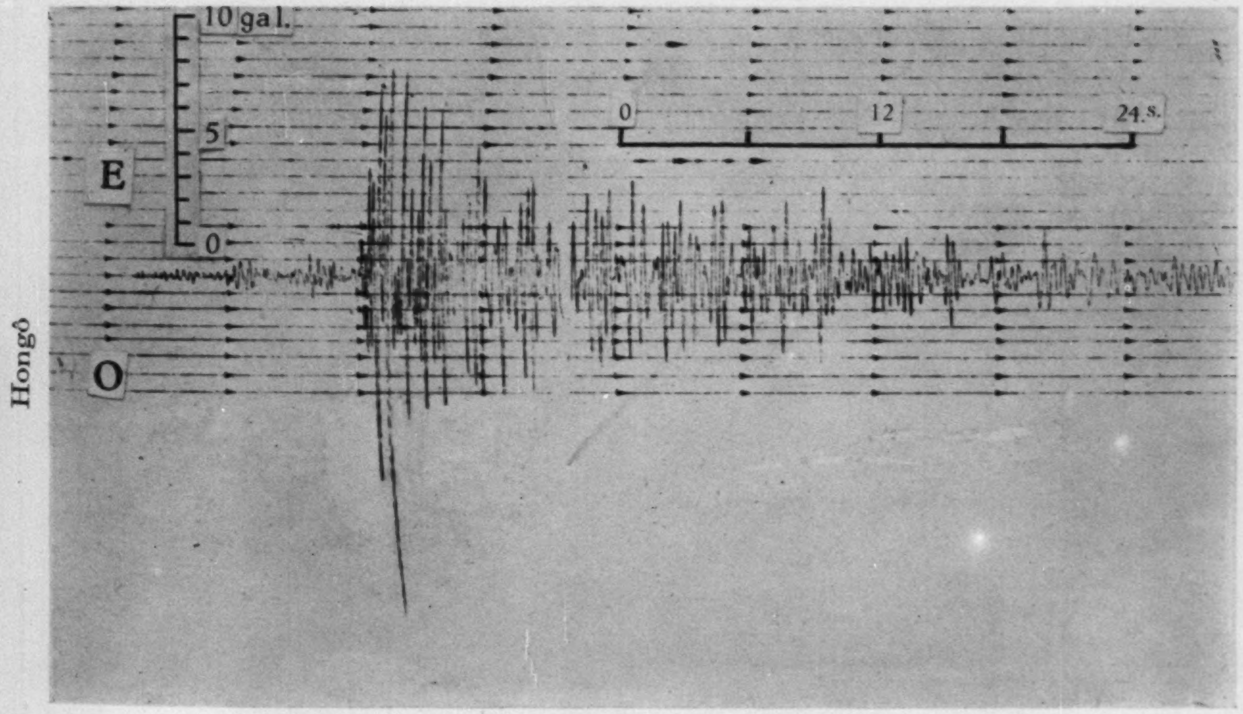

Eig. 7bis Inscription obtenue pour le séisme du 18 Sept. (1931) No. 60.

（石本、圖版、第十號、震研彙報）

(震研彙報、第十號、圖版、石本)

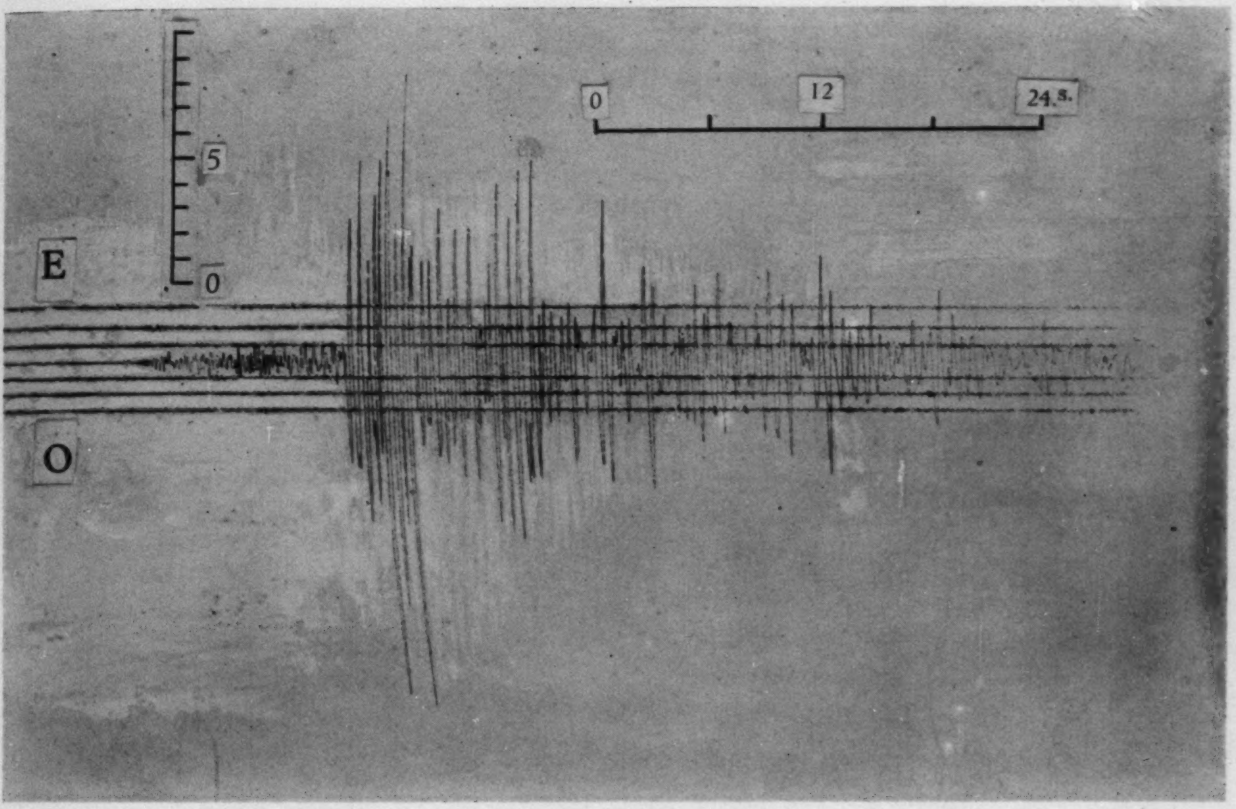

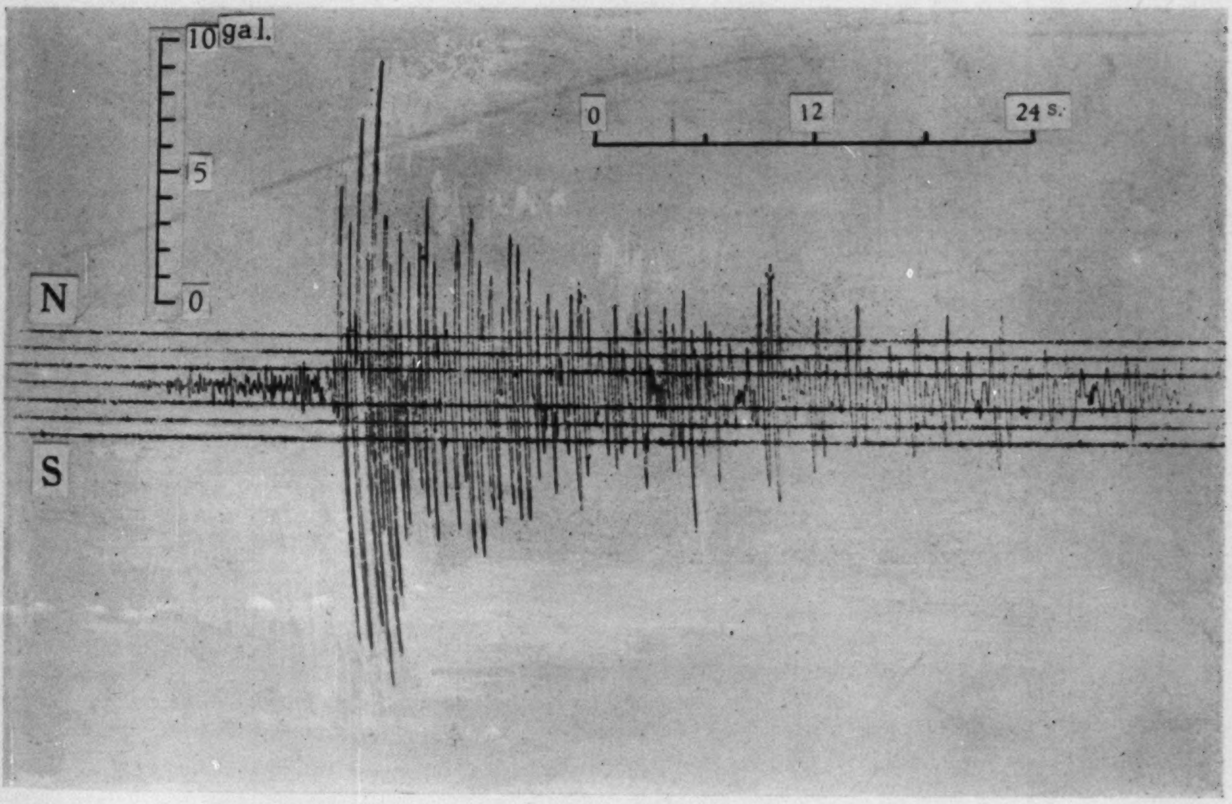

Fig. 7ter Inscription obteune pour le séisme du 18 Sept. (1931) No. 60.

（震研彙報、第十號、圖版、石本）

Hongô

Marunouti

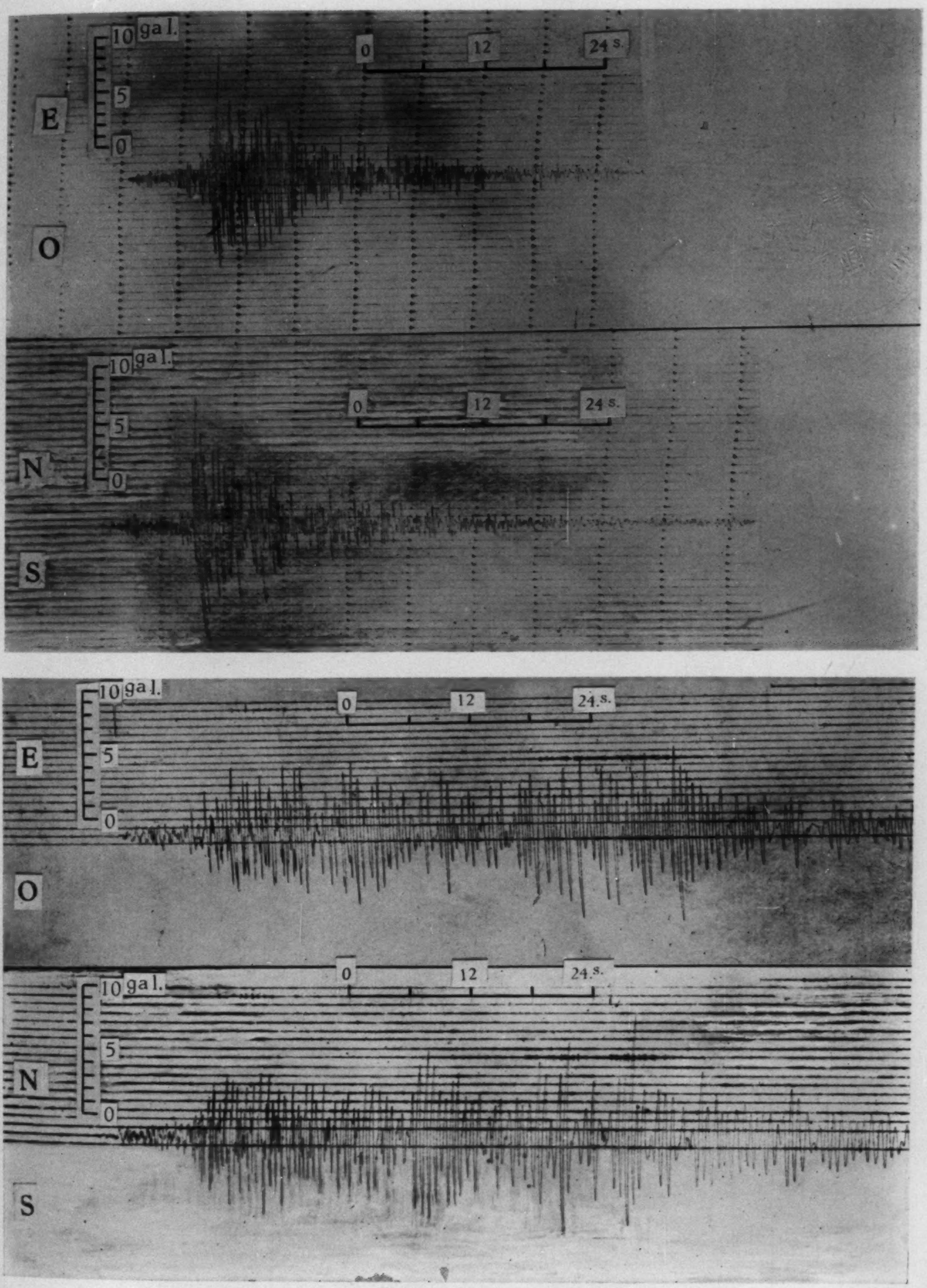

Fig. 8bis Inscription obtenue pour le séisme du 28 Sept. 5h (1931) No. 69.

(震研彙報、第十號、圖版、石本)

（燕京學報、第十號、圖版、石本）

Hongô

Marunouti

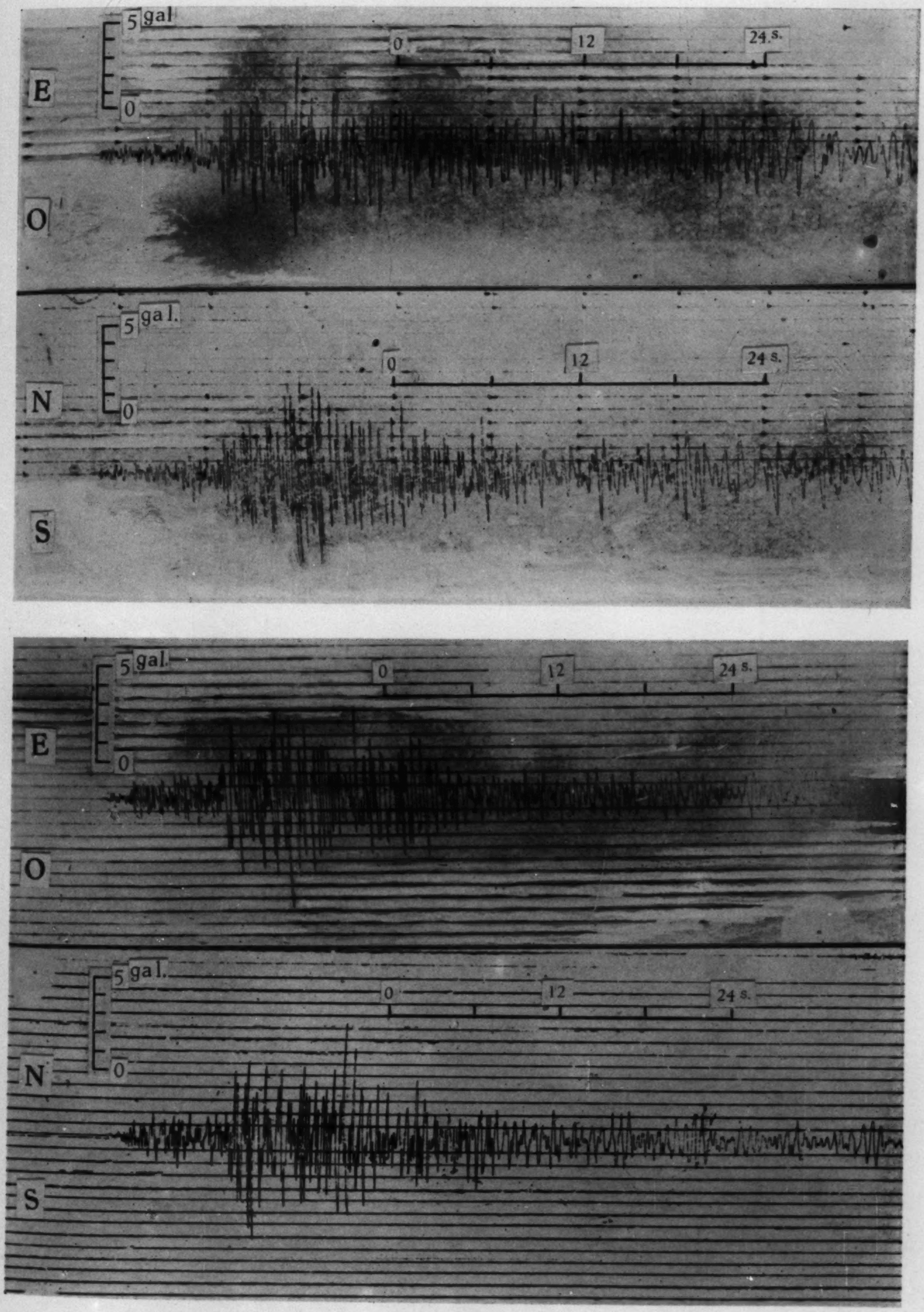

Fig. 9bis Inscription obtenue pour le séisme du 28 Sept. 14h (1931) No. 70.

(震研彙報、第十號、圖版、石本)

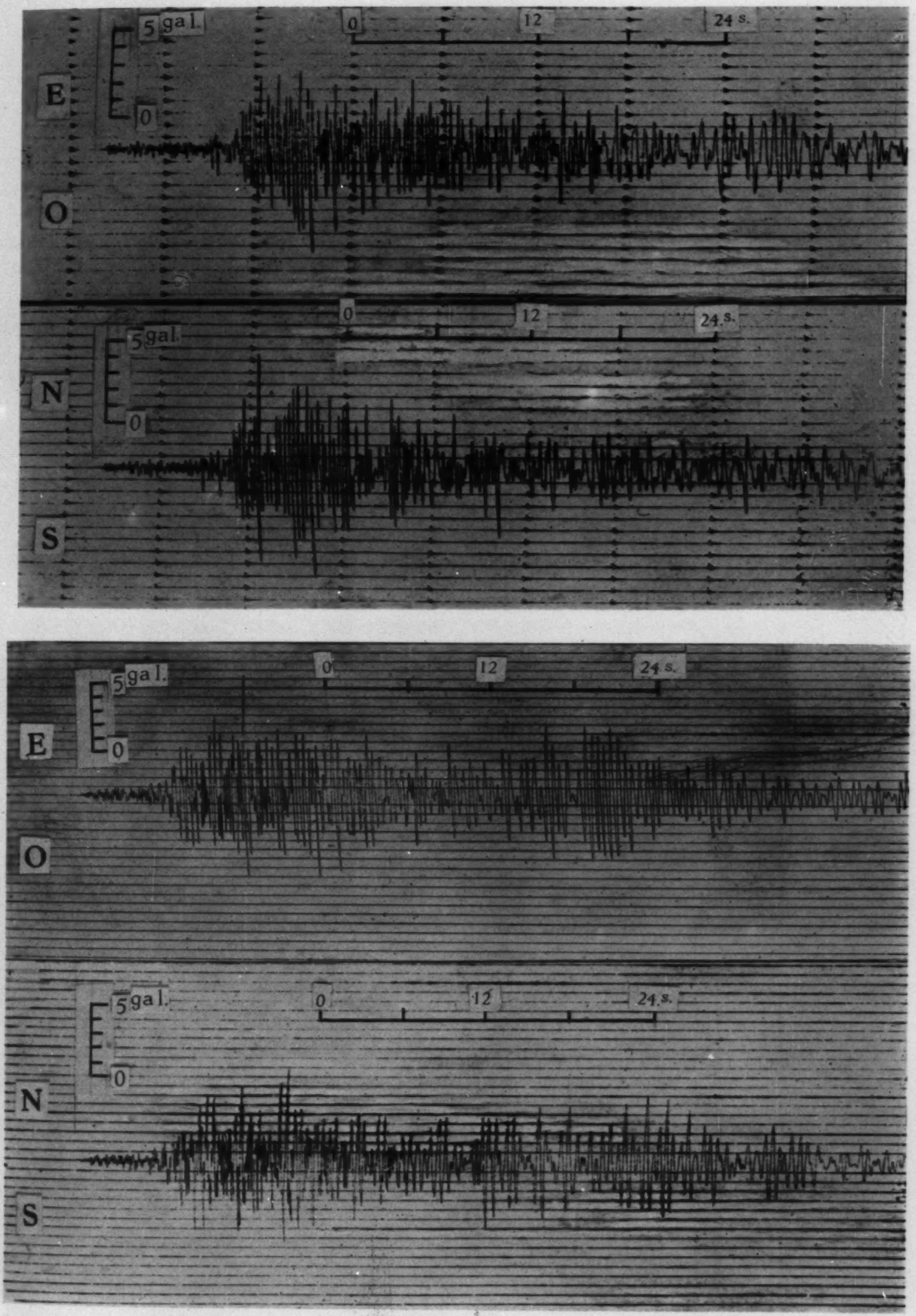

Fig. 10bis Inscription obtenue pour le séisme du 3 Oct. (1931) No. 71.

（石本、圖版、第十巻、震研彙報）

3. 本郷における觀測は地震研究所地下室において行はれたものであるが、建物と土地との間に振動差違がないと云ふ事は種々の觀測から證明されて居る。

得られた地震記象中、S 波の初めにおいて一般震動に比較して數倍の加速度を有する單獨波の出現が見受けられるが、之れは相當震度の大である地震に特有のものであると同時に、地震の本性が全く衝擊性を帶びた波動であると云ふ證明を與へるものである。

4. 丸ノ内における觀測は器械を地表に設置した關係上、自働車、汽車による土地の微動も絕えず記錄されて居るが、地震動記錄上には障碍をなさない。地震動中單獨波の殆ど見受けられない事は、表面層の固有振動周期が比較的大である結果と信ぜられる。

5. 兩觀測所における地震動の根本的差違は震動中に卓越する周期が異る事であつて、兩地點の記象を基として周期の頻度曲線を畫き、その極大値に相當して卓越周期を見出す事から其の土地の固有振動周期が決定された。本郷においては 0·3 秒、丸ノ内においては 0·6 秒が固有振動周期として見出された。

又加速度の値については、近い地震においては本郷の方が大、一般に遠い地震においては丸ノ内の方が大となる。之れは地震波が地殼内を通過する間に固體粘度の影響を受けて、小周期のの波が次第に消失する結果と見られる。即ち近い地震は小周期の波動を多分に含有する事から、本郷は大なる振動をなすに引替へ、遠い地震は大なる周期をもつ地震波動から成立する爲めに、丸ノ内が大なる振動を爲すものと見られる。

なほ九月廿一日秩父地震の本郷觀測結果からは卓越周期を有する振動が同時に大なる加速度を生ぜしめるものである事が判明した。

6. 吾々が經驗する地震動は全く表面層の影響を受けて居る事から、地震動の研究も此の方面から爲す必要がある。日本の都市は多くの場合、自己振動周期の大なる沖積層上に建設されて居るが、沖積層は多く地殼構造線、例へば川、斷層等と場所的關係を保つて居る。沖積層上の地震被害が大である事から、地震學者の中には構造線と地震被害との間に密接な關係を考へる者もあるが、上述の理由により適當でない。震央は地震被害と全く別場所であつて差支へなく、斯樣な實例もある。

深層地震に關して異常震域の存在が認められて居るが、之れも上述の如く地震波の本性と表面層存在との必然的結果と考へられる。深層地震は震源が比較的深い關係上、相當廣範圍に亘つて同樣の波動を與へるが、若し其の際地殼内部を通過して表面に達せんとする地震波中，0·6 秒附近の周期を有する波が卓越して居るならば、各土地の自己周期も此の附近にある關係上所によつて比較的大なる震動が誘起される所と小なる震動が誘起される所との別が生ずる筈である。大地震の際に認められる異常被害分布も同樣の考の下に說明される。

13. A Portable Horizontal Pendulum Seismometer.

By Fuyuhiko KISHINOUYE,

Seismological Institute.

(Read Nov. 18, 1930.—Received Dec. 20, 1931.)

After the eruption of the Volcano Usu, Hokkaidô, in 1910, late Prof. Omori set up a portable seismometer which he had constructed, near the volcano to record earthquakes of volcanic origin. Since then after some great earthquakes, portable seismometers are costumarily set in the seismic area to observe after-shocks by members of the Seismological Institute and the Earthquake Research Institute of the Tokyo Imperial University. And seismometrical trianguration and other noteworthy studies were made with seismometers like above mentioned, after the great Tango earthquake of 1927[1] and the Idu earthquake of 1930.

The writer made a new portable seismometer lighter than those which have been made before, and it may be easily carried by a motor-car or two men on foot.

The Portable Horizontal Pendulum Seismometer.

In the first place, the writer decided that for registering earthquakes mechanical method is applied to the seismometer, because optical method is unhandy in field work. Some merits in mechanical registering are that seismograms are seen directly and no need of dark room, electric cells. But petroleum to smoke recording papers and vanish to fix soot on the paper are ought to be carried with the instrument when it registers mechanically, and these are very troublesome to transport.

The recording drum is a hollow aluminium cylinder 25·5 cm. long, 18 cm. in diameter and its rotation axle 52 cm. long. Recording point displaces 0·75 mm. sideways after a revolution which takes ten minutes. In other words, the velocity of index is about 5·6 cm. per min. on the smoked paper.

1) N. NASU, "A stereometrical study of the aftershocks of the great Tango earthquake," *Journ. Fac. Sci., Tôkyô Imp. Univ.*, Sect. II, 3 (1929), 29.
In this paper, descriptions on the Imamura Portable Seismometer are given.

On a chlumin—a light aluminium alloy invented by Dr. Iidaka—plate, two horizontal pendulums are set up to record two components of horizontal motion of earthquake separately. The pendulum is consisted of a brass framework which suspends a lead cylindrical bob with two steel ribbons. The steel ribbons are used, because they are strong and seldom broken in transit. The bob is 5 kg. in weight, and fixed in the framework with two screws at its top and bottom. It is taken off from the frame when the seismometer in transportation. The framework stands with three screws on the bed-plate, and the period of self-vibration may be changed by adjustment of levelling-screw. The seismometer has been operated successfully when the period is between 3·5 and 5 sec., and the recording magnification is usually set forty. Then instrumental constants at some time, are shown as follows.

$$V=40,\quad T_0=3{\cdot}79,\quad \varepsilon=0{\cdot}144,\quad r/T_0^2=0{\cdot}122.$$

The instrument is not equipped with damper, for damping of the pendulum is somewhat sufficient in this case. But the writer intends to put a damper on the pendulum. Time signals are made by lifting of the recording index with a electromagnet, which is operated once a minute by a clock.

The seismometer at transportation is packed in a box covering the bed-plate with a steel lid 54 cm. long, 38 cm. wide and 25 cm. high, after the two bobs are taken off and the frameworks are clamped on the plate. The weight of the above-mentioned part is 18·5 kg. After removed from the frame, the two bobs are put in another box with the clock-work which drives the recording drum, and the latter box weighs 17 kg in all. When the seismometer is set at places where electric power supplied all day, a simple synchronous motor designed by the writer is used in place of the clock-work as shown in figures on Pl. XIV. Details of the motor will be described below.

A Synchronous Motor for Driving the Recording Drum.

The rotor of the motor is a circular disc, axle of which is supported with two ball-bearings. Twenty small and short circular iron rods are inserted in equal distance near the edge of disc. The rods pass through between two poles of the electromagnet when the disc rotates around its axle. The coil of the electromagnet is charged with alternating current of frequency fifty per sec. So when the disc made revolve at the rate of five turns per second, rotation of the rotor synchronize with the variation of the magnetic force. Then the motor continues its rotation in

a uniform speed. But its velocity is too fast for the recording drum, so the rotation of the drum is made slow by means of worm-gears to the rate of one revolution in ten minutes. It is inconvenient that the motor comes to a halt with the shutting off the current, and it does not turn automatically when current supplied again. So in some cases, another self-operating synchronous motors of the like construction are in use.

Remarks.

The seismometer and the synchronous motor are both made to be portable and easy to handle. Moreover the writer wishes these instruments serve to seismic observations made by anyone who has interest to earthquake. And when some improvements are made, it may be of use even at seismological stations as an auxiliary instrument. The several instruments of the type here stated were already used to record the after shocks of the *Daisyôzi* earthquake which occurred in *Kaga* Province on Oct. 17, 1930[2], the *Idu* earthquake of Nov. 26, 1930 and the *Saitama* earthquake of Sept. 21, 1931.

In conclusion, the writer desires to express his most cordinal thanks to Proffesor M. Ishimoto for his kind advices and supervision.

---

13. 携帶用水平動地震計

岸　上　冬　彦

大地震の後で餘震調査の爲に屢〻携帶用地震計が地震のあつた地方に据えられるが、筆者は從來のものより輕くて取扱の簡單なものをつくつた。未だ完全なものではないが、此處に簡單に其の器械について報告する。

携帶用地震計には記錄裝置は光學的にするよりも煤紙の上に機械的にした方が適當と考へた。次に記錄用の回轉圓筒の大さを決め、其の大さは長さ 25·5 cm. 直徑 18 cm で、回轉の軸の全長は 52 cm とした。回轉の速さは 10 分間に 1 回轉にして、其故記錄用の針は 1 分間に約 5·6 cm 圓筒上を進むることなる。

地震計は二つの水平振子から成立ち、水平動を二つの方向に分けて記錄する。振子の重錘は 5 kg の鉛で、二枚の鋼の薄板で吊るされてゐる。鋼の板を用ひたのは其が運搬中に毀れ難いからであつて、重錘は運ぶ時は取外して、記錄用圓筒を廻はす時計仕掛と一緒に一つの箱に入れる。地震計は三菱造船研究所の飯高博士の發明されたクルミンといふ輕い合金で造られた臺の上に載つてゐて、運搬するときは、夫に鋼鐵製の蓋をして長さ 54 cm. 幅 38 cm. 高さ 25 cm. の箱とする。此の重

2) F. KISHINOUYE, "Report of the strong earthquake of the southwestern part of Kaga Province, Oct. 17, 1930," *Bull. Earthq. Res. Inst.*, 9 (1931), 216.

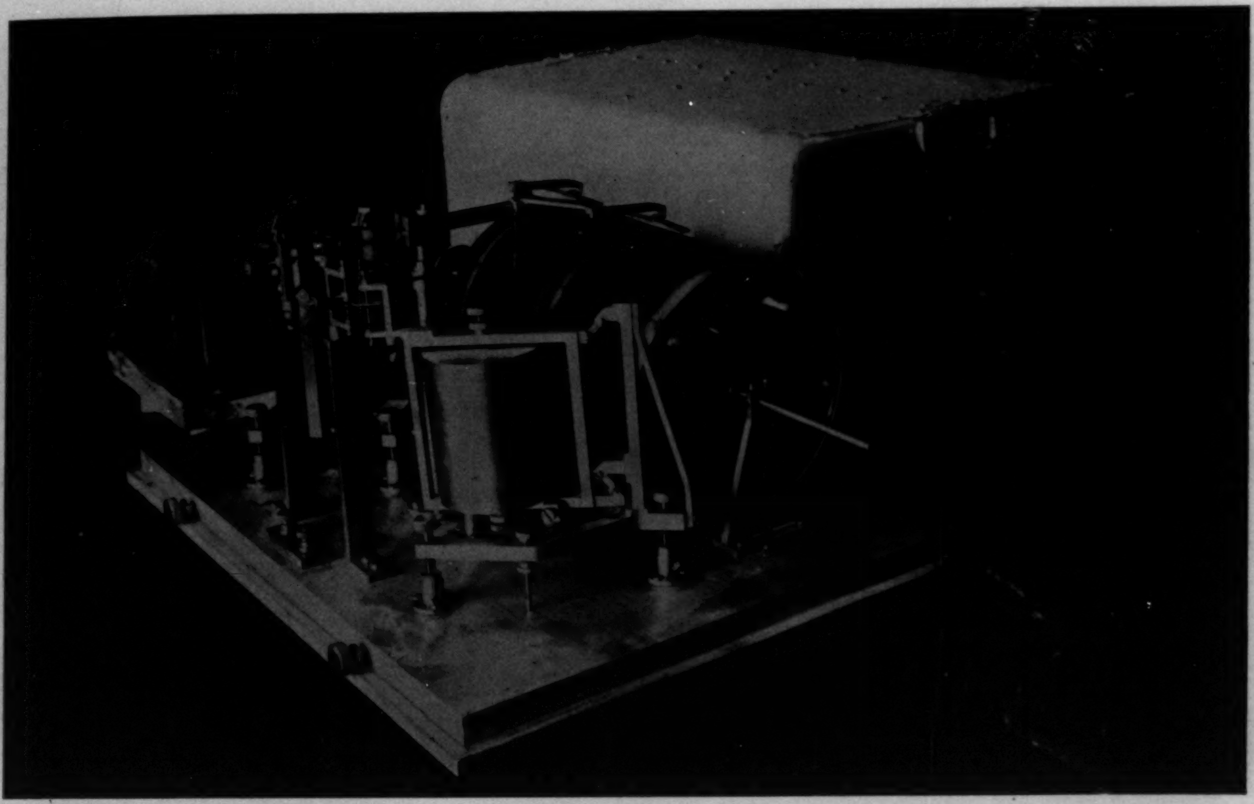

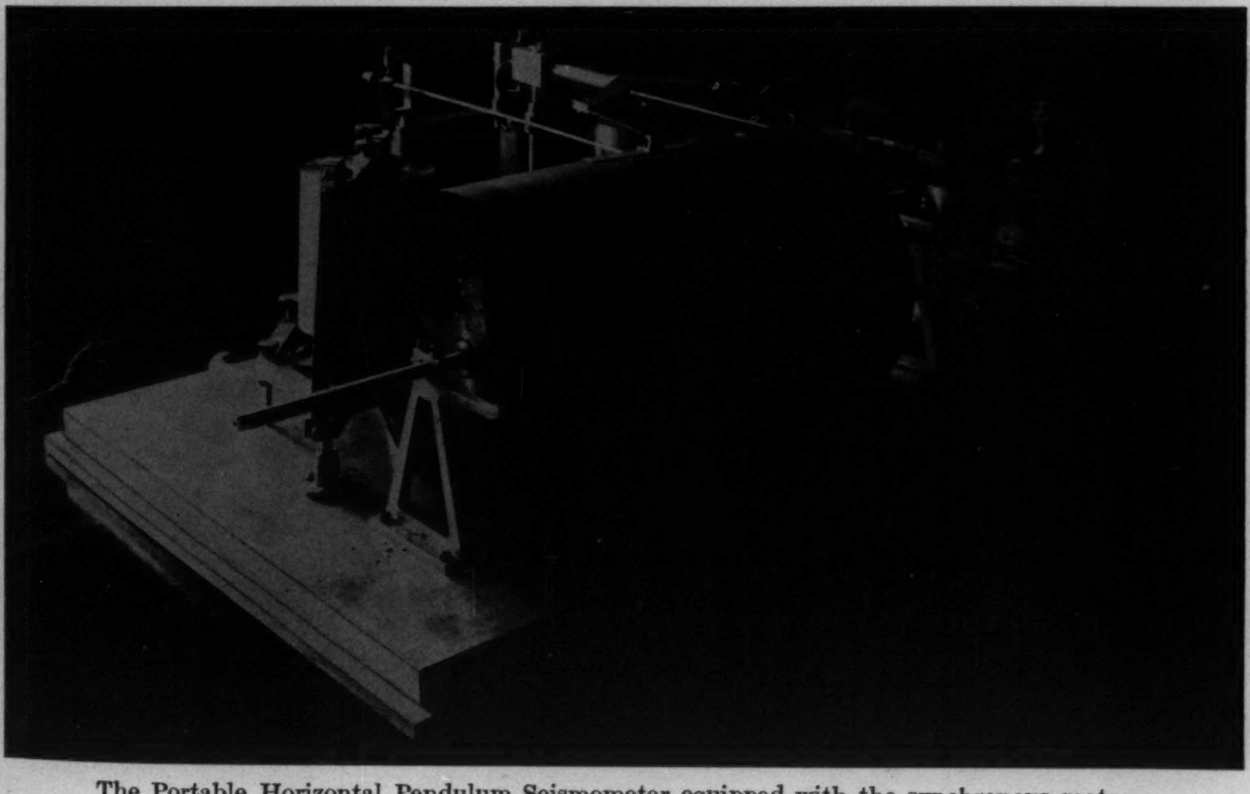

The Portable Horizontal Pendulum Seismometer equipped with the synchronous motor.

(震研彙報、第十號、圖版、岸上)

量が 18·5 kg. で、前記の重錘と時計仕掛の重量が 17 kg. である。自動車、サイドカー付の自動自轉車によれば容易に持運ばれ、又場合によつては二人で分けて運び得る位のものである。

記錄用圓筒を廻轉させるには通常は時計仕掛を用ひるが、終日送電されてゐる所では次に述べる同期電動機を用ひる方が良い結果が得られる。圓板に鐵の鋲を 20 嵌入して、その鋲を週波數 50 の交流を通じた電磁石の極の間を通過する樣にして圓板を廻はしてやる。圓板の回轉が 1 秒に 5 回になると、交流によつて生ずる磁力變化と回轉とが共鳴作用を起し、圓板は一樣に回轉を繼續する。記錄するには此の儘の速度では速すぎるのでウォーム、ギヤアで記錄用圓筒は 10 分間に 1 回轉する樣にする。以上の樣な電動機は停電があると、假令電流が再び來ても回はり始めないのが缺點である。併し、同樣な原理で自動的に回轉を開始する一層精巧なものも用ひられてゐる。

此等の器械は携帶用計りでなく、地震に興味を持つてゐる人は誰でも觀測が出來る樣にしたつもりで製作されたものである。併し又少し手をかければ、觀測所に置く器械としても用ひられるであらうと思ふ。今迄には大聖寺地震、伊豆地震、埼玉地震の餘震觀測等に用ひられた。

---

14. 秦野に於ける山崩

地震研究所 { 寺田寅彦 / 宮部直巳

(昭和六年十二月十九日受理)

1. 1923年9月1日、關東地震の際、神奈川縣秦野町の南方、南秦野村地内に山崩が起つた。

原地は低い丘陵の起伏してゐる地帶で、山崩は東西の方向に刻まれた谷に面する南向きの傾斜地に起つたものである。この山崩で崩壞した土砂は谷の一部を埋め、その爲に流水が阻まれて東西二個の小湖が湛えられてゐる。

この丘陵地帶は、東側を流れる花水川と、西側を流れる中津川との間に夾まれ、東の方の部分に於いて稍ゝ低く、200—150 m. 位であり、西の方の部分に於いて稍ゝ高く、300 m. 位である。この地帶の丘陵は、圓頂多く、點々として散在し、その間に、池ノ窪、中ノ窪、窪ノ庭、篠窪、等といふ名稱を持つた窪地が存在する。(第一圖參照)。

多田助教授によれば、この丘陵地帶に於いて、千村—大槻間に斷層線が引かれ(第一圖、破線)、その斷層の存在は次の如き事實によつて證據立られてゐる。即ち、その山麓線の一直線なること、其の斜面の急なること、千村に remaining hill のあること、南斜面が緩傾斜で consequent valley 多く、且つ、behead された狀態にあることなどがそれである。又、大山山體を刻んだ多くの澤が、この斷層によつて遮斷されて流路を失ひ、南部丘陵に空谷又は小なる川として殘つてゐるといふ事も注意されてゐる。

故山崎博士は此處で問題となつて居る山崩が、陶稜地塊の北邊をなす斷層線附近に起つたものとして注意されてゐる。[1]

この山崩のある谷に沿ふては、嘗て崩れたことのあることを想像させる樣な地形や、最近崩れたと思はれる樣な痕跡がかなり多くある樣に見られた。

この附近の地質は、秦野盆地の北では、第三紀の tuff 及び mudstone 竝に agglomerate であり、南の丘陵地、山崩のある附近では、第三紀の soft tuff より成り、盆地內は gravel bed にて滿され、その上に loam を頂くといふことである。崩壞した現場を見ても loam と loam 下の地層とを區別することが出來る。

1) 山崎直方 震災豫防調査會報告 第100號 乙 (1925).

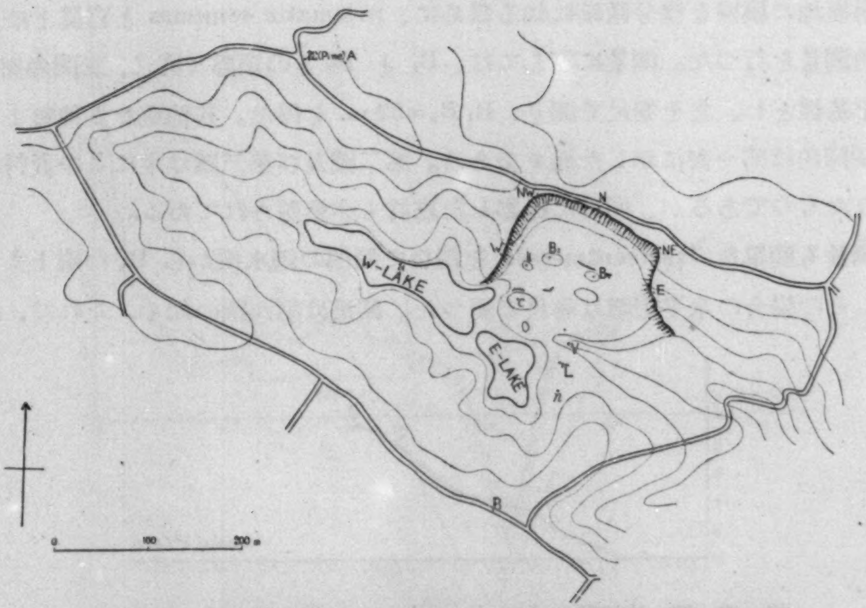

第 二 圖 南秦野村、崩壞地（崩崖附近の地形。・は覘標點）
Fig. 2. Topographical Map in the Neighbourhood of the Landslide (・ Triangulation Points for the Present Survey).

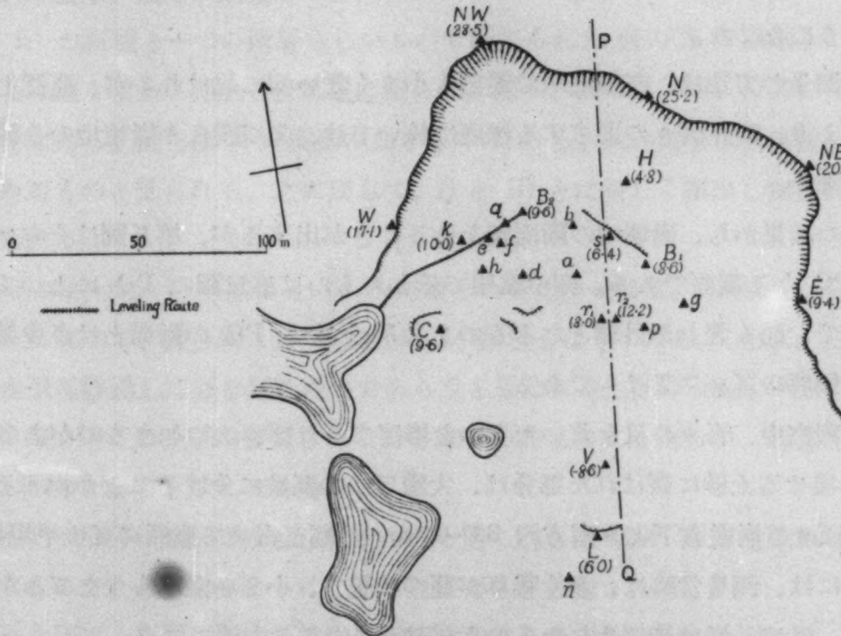

第 三 圖 南秦野村、崩壞地（▲は覘標點を示す）
Fig. 3. Map showing the Distribution of the Points ▲, of which the Positions and Heights were measured.

2. 崩壞地の模樣を幾分精確に知る爲めに、prismatic compass と寫眞とによる簡單な三角測量を行つた。測量に際しては、B_1 と B_2 との頂點（第二、三圖參照）の間の距離を基線とし、之を卷尺で測り、$B_1 B_2 = 52$ m. を得た。其他重なる地點よりの方位角及び仰角は第一表に示した通りである。第二圖及び第三圖は主にこの資料によつて畫かれたものであるが、同時に撮影した寫眞も亦參照されてゐる。

水準測量も簡單な Horizontmesser を用ひて西側の湖水面から B_2 の頂上まで之を行つた，その場合の水平距離は卷尺で測つた。結果は第四圖の如く、これで、湖水面

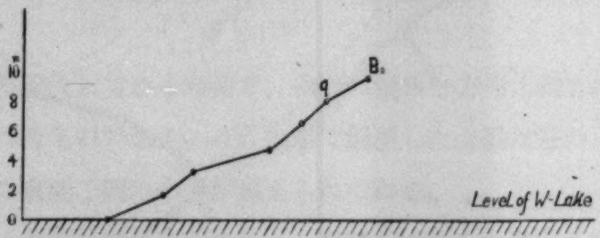

第 四 圖 第三圖の Leveling Route に沿うてのプロファイル
(Leveling の結果)
Fig. 4. Profile along the Leveling Route in Fig. 3.

と比較して、各地點の高さを求めることが出來、第二圖に於ける等高線も大體誤なく引けるやうになつた。

以上の測量の方法は、至極簡單で誤差も小さくない樣に思はれるが、寫眞を參照することにより、現在吾々の要求する程度に於いては、先づ誤なき崩壞地の全貌を畫くことが出來た。

尙、この結果から、崩壞地の斷面圖を作ることが出來るが、第五圖はその一で、第三圖の PQ なる斷面である。圖中點線で示したものは第三圖の PQ によつてきられない部分で、而も著しき目標となるものを含み、且つ PQ の斷面とは多少異つた斷面を示す個所のプロフアイルである。

以上の觀察中、吾々の目を惹いたものを擧げてみれば、次の如きものがある。

a). 崩壞せる土砂に蔽はれた部分は、大體三つの區域に分けることが出來る。

i). 南面せる崩崖直下より南方約 30—40 m. の幅を占めて東西に亘る平坦な部分。この部分には、測量當時は、多く雜草が蔓つて居り、小さい灌木も生えてゐた。是等の灌木は、凡て、崩壞後に生じたものと思はれる。

ii). 圓頂の小山が起伏してゐる區域、是等の小突起の主なるものとしては、B_1B_2 を始め r_1, r_2, d, e, f, g, h, k 等がある（寫眞 Plate XVI 參照）。是等の小突起は凡て、

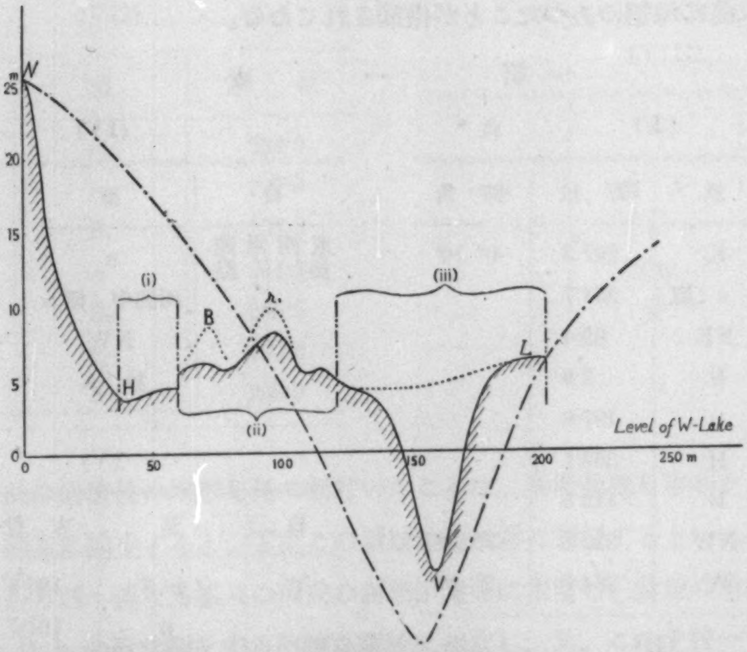

第 五 圖　第三圖に於ける PQ の斷面圖（鎖線は舊の谷のプロファイルを示す）
Fig. 5. Profile of the Section PQ of Fig. 3. (Chains Line shows the Profile of the Valley before the Landslide).

禿山で、小灌木、叢等が點綴してゐた，

iii). ii) の區域と一つの斷層らしいもので距てられた南の方の區域。この區域では、表面は極く軟かい泥土で、草根に綴られ、灌木、叢も多いが、可成、年を經た樹木も生えてゐる。例へば c の樅樹の如きものである。此の部分は崩壞前の地表を現存してゐるものと見られる。之に反して、i) と ii) とは新しく露出した表面から成ると認められる。

b). a) に於ける i) の區域と ii) の區域との境界の一部は、B_1 附近から西の方へ約 30 m. に亘つて、高さ約 1 m. の截然たる小斷崖をなしてゐる。(第二、三圖參照)。

c). 水平に移動して谷を埋めたのであらうと思はれる土砂の mass の上に生えてゐる樅樹 c は、附近の土砂の擾亂されてゐる樣子の甚しいにも拘らず、直立して何事も知らざるが如き容姿を示してゐる。

d). iii) の部分の樹間の水溜、軟土の深く陷ち込んだ個所 V 等を連ねる線は舊谷線を示すもので、是は原高よりは高められてゐると推定される。

e). 谷を隔てゝ崩崖に對する北向の傾斜地內にある L 及び n の附近は、土質が著しく軟弱となつて居り、iii) の區域の延長と思はれる樣な部分がある。

f). 以上の如き、吾々の直接の觀察の外に、土地の人の記憶によれば、崩壞地の附

近に、崩壊以前に地割のあつたことが指摘されてゐる。

第一表

(I)

自	至	方位	仰角
B_1	B_2	297°3	0° 10′
	c (縦)	254·7	
	NE	66·4	
	N	3·9	
	n	197·0	
	H	352·1	
	E	112·5	
	NW	329·8	7° 20′
	W	284·6	3° 40′

(II)

自	至	方位
B_2	B_1	118°3
	E	114·9
	NE	88·5
	N	57·9
	NW	356·4
	W	270·2
	c (縦)	218·7
	n	179·5
	r_1	144·9
	H	77·4

(III)

自	至	方位	仰角
H	B_1	—	3° 40′
	B_2	—	4 20
	r_1	188°5	5 50
	r_2	181·2	4 20
	N	24·0	25 10
	NW	320·9	16 0
	W	263·5	6 40

(IV)

自	至	方位
東西兩湖接點	n	125°6
	西湖中ノ樹 α	324·4
	NW	29·5
	松 A	332·3

(V)

自	至	方位	仰角
W	p. 3	185°5	
	n	161·7	
	r_1	121·5	
	B_1	107·5	
	H	96·5	
	N	74·0	
	B_2	95·7	
	二湖ノ接點	206·2	
	西湖中ノ樹 α	269·8	
	c	166·5	−11° 20′

(VI)

自	至	方位
NW	B_1	151°4
	H	141·4
	B_2	179·2
	c	197·6
	n	179·2
	NE	119·1
	E	135·8
	r_1	164·0
	r_2	160·4
	p_3	195·7
	松 A	304·6

(VII)

自	至	方位
NE	r_2	222°·9
	r_1	227·9
	B_1	232·3
	c	244·5
	B_2	259·5
	E	179·2
	n	209·9

(VIII)

自	至	方位
p. 3	松 A	341°
	c	10
	NW	11
	N	22

〔附記〕 此の崩壞後の地形を見て氣付いたことは、秦野盆地を中心とする附近の地形が、之を適當に縮少すると、丁度この崩壞地の地形に類似するといふ事實である。先づ、大山から西へ連なる峯々の南向の斜面が崖面に相當し、盆地の南側を走る斷層が第三圖の B_1 b の東北側を走る明瞭な斷層に相當し、又、この千村一大槻斷層線の南にある丘陵地が、現在の場合の ii) の地帶、即ち、小丘起伏した區域に相當する樣に見える、是等は少くも外形上からは著しい肖似と云はなければならない。

試に、秦野盆地を南北に縱斷する縱斷面を六個、互に平行に且つ等間隔で作り、その六個のプロファイル曲線を平均したもの（第六圖に點線で示す）と、東西兩端の二個を除いて、殘りの四個に就き平均したもの（第六圖に實線で示す）とを作つてみると、實線で示した後者には明に第五圖に示した崩壞地のプロファイルとの肖似が示されて居る。尤も後者では前面に谷の向ひの崖があるのに、前者では、前面は海であるから此點は比較には成らない。

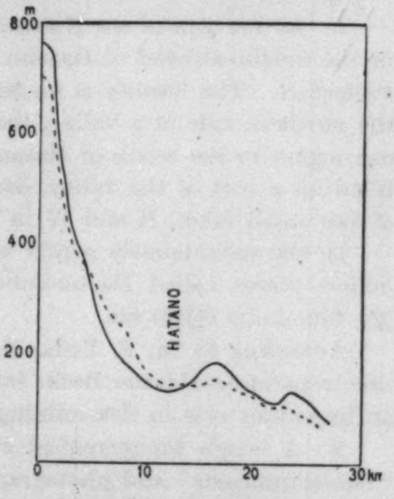

第　六　圖
秦野附近の斷面
（實線は四個の斷面の平均
點線〃六〃　〃　〃）

Fig. 6. Profile Curves of the Lines across Hatano Basin in N-S Direction.

秦野盆地が果して現在の崖崩れと同じやうな機巧で生じたものであるかどうかは勿論外形丈けから判斷することは出來ないので、最後の判斷は地質學者の研究に待つ外はないのであるが、併し、上記の形式的類似の事實は一つの事實として可成顯著なものであるから、玆に特記して讀者の注意を促した所以である。

最も注意すべきは盆地から松田町の方に通ずる

谷の兩側に於ける地質の比較であらう。

次に、この崩壞によつて谷間の池の出來た事實から、次のやうな考が示唆される。即ち、五萬分一地形圖で見て圖上に無數の池沼が點々として存在する地域が往々あるが、さういふ地帶には又往々崩壞地形が多數記入されて居る場合が多い。此に就ては他の機會に詳しく述べたいと思ふのであるが、兎も角も此種の池沼の中には現在の秦野の池と同樣な機巧で生じたものも多數にあるであらうといふ想像は充分合理的であると云つてもよいかと思はれる。

勿論、池沼の多い地方では、人間が此を利用して色々に加工されて居る場合が多いが、併し、凡てを始から人間が開鑿したのではなくて、既存の天然の地形を人間が利用した場合が多いであらうと想像される。

以上の考がある程度迄眞實であるとすると次に起る問題は、池沼地帶と過去の地震との關係である。此れも一顧の價値ある問題であらうと思はれる。

---

14. Landslide at Hatano.

By Torahiko Terada and Naomi Miyabe,

Earthquake Research Institute.

1. At the time of the Kwantô Earthquake of 1923, a typical case of landslide occurred in the neighbourhood of Hatano, a small town to the west of R. Sagami in Kanagawa Prefecture. The locality is marked by ● in Fig. 1. It occurred on the slope forming the northern side of a valley, the trend of which is in E-W direction, in the mountainous region to the south of Hatano. The crumbled earth mass produced by the landslide filled up a part of the valley, dammed up the water-flow, and resulted in the formation of two small lakes, E and W in Figs. 2 and 3.

In the mountainous region where the present landslide occurred, we notice many hollow places called Ike-no-kubo[2] (池ノ窪), Naka-no-kubo (中ノ窪), Kubo-no-niwa (窪ノ庭), Sino-kubo (篠窪) etc.

According to Dr. F. Tada, there are several evidences for the existence of a fault line, separating Hatano Basin from the southern mountainous region, which had played an important role in determining the present topography of the basin.

2. A rough topographical survey was carried out by means of prismatic compass, "Horizontmesser" and photographic camera. The result of the survey is shown in the maps of Figs. 2, 3 and 5, the last one showing the sectional profile PQ of Fig. 3.

Following points may be noticed as regards the features of the landslide.

a) The whole area covered with crumbled earth mass may be divided into the three parts; i. e. (i) A flat zone extending E-W with a breadth of 30–40 m., directly adjoining to the southern foot of the main cliff. This area was over-grown with weeds and shrubs

---

2) The Japanese word 窪 (Kubo) means hollow place.

(震研彙報、第十號、圖版、寺田、宮部)

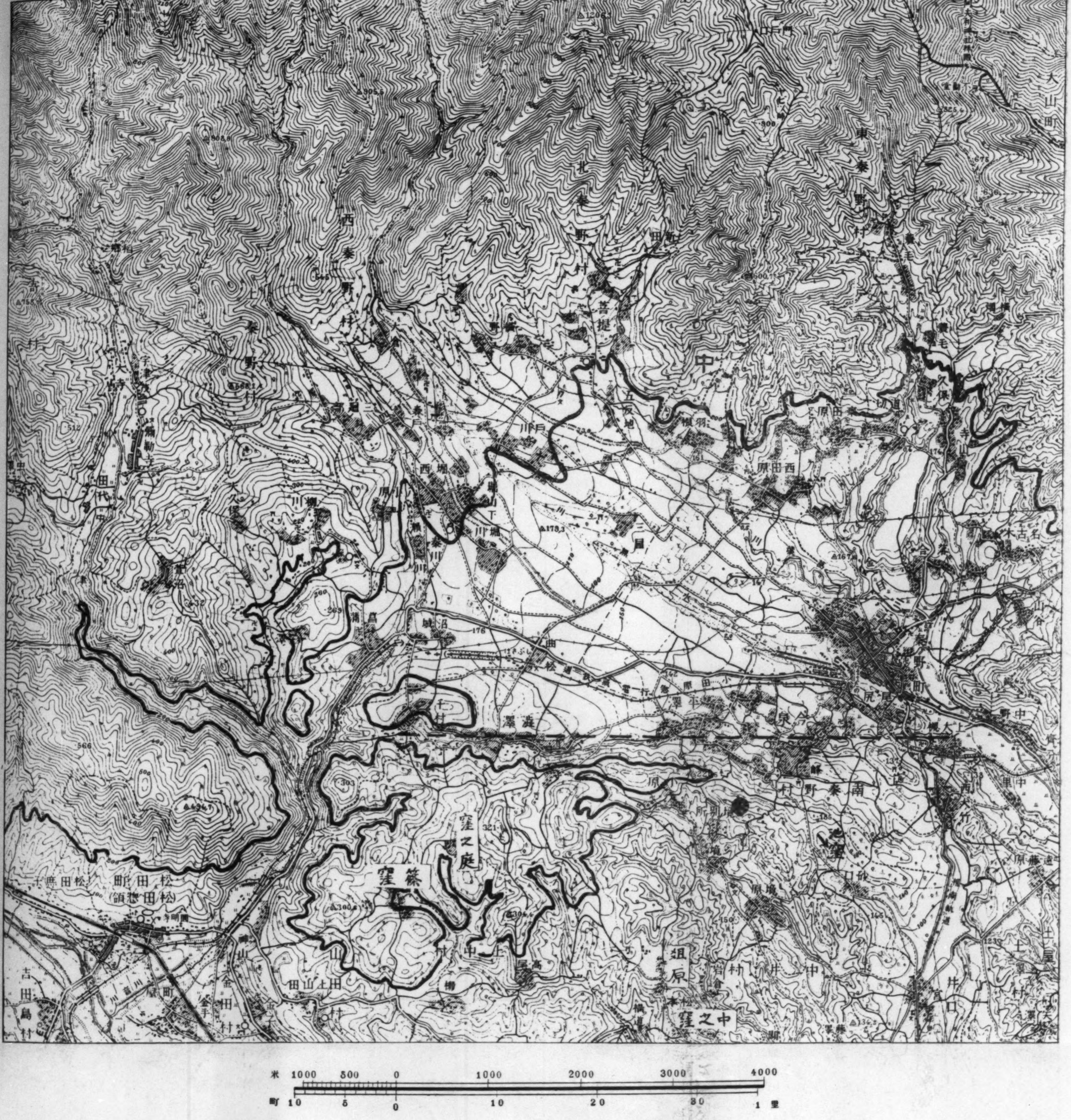

第一圖 秦野町附近の地形圖。(太い等高線は 200 m. の等高線 / 破線は千村—大槻斷層線 / ● は山崩の起つた場所を示す)

Fig. 1. Topographical Map in the neighbourhood of Hatano. (Thick Contours : Contours of 200 m. / Thick Broken Line : Fault Line; Timura-Ootuki. / ● : Locality of Landslide.)

Fig. 7

(第三圖の NW と W との中間附近より E の方を望む)

Landslide in the neighbourhood of Hatano. (Viewed easterly from a Point between the Points NW and W in Fig. 3).

(震研彙報、第十號、圖版、寺田、宮部)

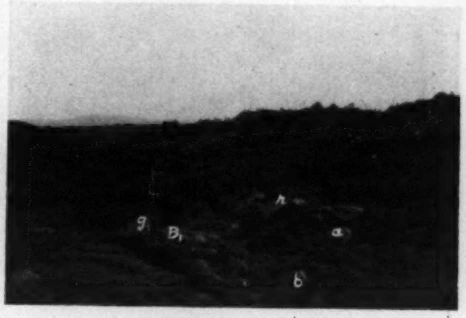

Fig. 8

(NW 附近より東南の方を望む).

Landslide in the neighbourhood of Hatano (Viewed south-easterly form the Point NW in Fig. 3).

Fig. 9

(NW 附近より南方を望む).

Landslide in the neighbourhood of Hatano. (View southerly from the Point NW in Fig. 3).

at the time of our observation; (ii) An area with knolls and hollows, adjoining to the south of (i). Knolls are named as B_1, B_2, r_1, r_2, d, e, f, g, h, k etc. in the maps and photos; (iii) An area adjoining to the south of (ii), from which it is separated by a distinct fault-like boundary. In this area, the ground surface consists of soft humus, on which the shrubberies and full grown trees stand.

b) A part of the boundary between the areas (i) and (ii) makes a small cliff of 1 m. in height and 30 m. in length

c) The surface mass of the earth in the area (iii) is seen much disturbed and yet aged trees (for instance *c* in Fig. 2 or 3) standing upirght in this area shows no indication of being disturbed.

d) There are several hollow places in the area of (iii), for instance V and a small pond which seems to show the trend of central line of the original valley.

e) In the neighbourhood of points *L* and *n*, the surface mass of the earth was sensibly softened, with indications of being disturbed. The points *L* and *n* are situated on the slope on the opposite side of the valley facing the slide-cliff.

3) A striking resemblance was noticed which exists between the topography of the present lande-slide area and that of the much larger region including the Hatano Basin together with the northern mountain range and the southern hilly district. The profile curves (Fig. 6) along the lines drawn across the Basin in N-S direction are compared with the profile of the present land-slide area.

4) It may be suggested that examples of the ponds formed by the process similar to the present case may be numerous, especially in the country frequently disturbed by earthquakes. Peculiar topographical features of some districts characterised by a remarkable swarm of ponds might have been due to the similar cause.

---

15. *Hôjô Trough.*

By Hisakatsu YABE and Risaburô TAYAMA,

(Read Oct. 20, 1931.—Received Oct. 20, 1931.)

(With 1 Text-Figure and 1 Plate.)

The Bôsô Peninsula, which is one of the major geotectonic divisions of the Kwantô Region,[1] consists of seven parts, each trending east-west and geotectonically as well as physiographically distinct from the other.[2] Counted from the north they are (Figure 1)

1. Kimitsu tilted block, sloping northwards with its tilt-edge along the Nokogiri-Kiyozumi ridge.
2. Kamogawa graben, with the valley of Hoda-gawa on the western prolongation, the real nature of which is still unknown.
3. Mineoka horst.
4. Soro-Iwai fault-line valley.
5. Middle Awa (or Chûbô) plateau, sloping southwards.
6. Hôjô trough.
7. South Awa (or Nanbô) plateau, sloping northwestwards.

Of these seven parts, the Hôjô trough only is dealt with in the present article, while certain features of the Middle and South Awa plateaux are taken into consideration.

The depressed zone lying between the Middle Awa plateau and the South Awa plateau was often called the "Hôjô graben"[3] or "Kagamigaura graben" on account of its graben-like aspect; it was found, however, that the depression in its greater length is a trough and not

---

1) H. YABE and R. AOKI, "The Great Kwantô Earthquake of September 1, 1923, Geologically Considered", *Ann. Rep. Saitô Gratitude Foundation*, No. 1 (1926), 70 et seq.

2) H. YABE, "Bôsô Peninsula", *Gendai no Kagaku* (*Science Gazette*), Vol. II, No. 4 (1914), (in Japanese). In this paper is given my first notion about the block-structure of the peninsula, which is essentially the same as our present view at least as to the major divisions.

3) For instance, H. YABE and R. TAYAMA, "On Some Remarkable Examples of Drowned Valleys found around the Japanese Islands", *Rec. Oceanogr. Wks.*, Japan, II (1929), 12: It is the "depression of Tateyama" or "depressed zone of Tateyama" of the late Professor Yamasaki: "Physiographical Studies of the Great Earthquake of the Kwantô District, 1923", *Jour. Fac. Sci., Imp. Univ.*, Tôkyô, Ser. II, Vol. 1 (1926).

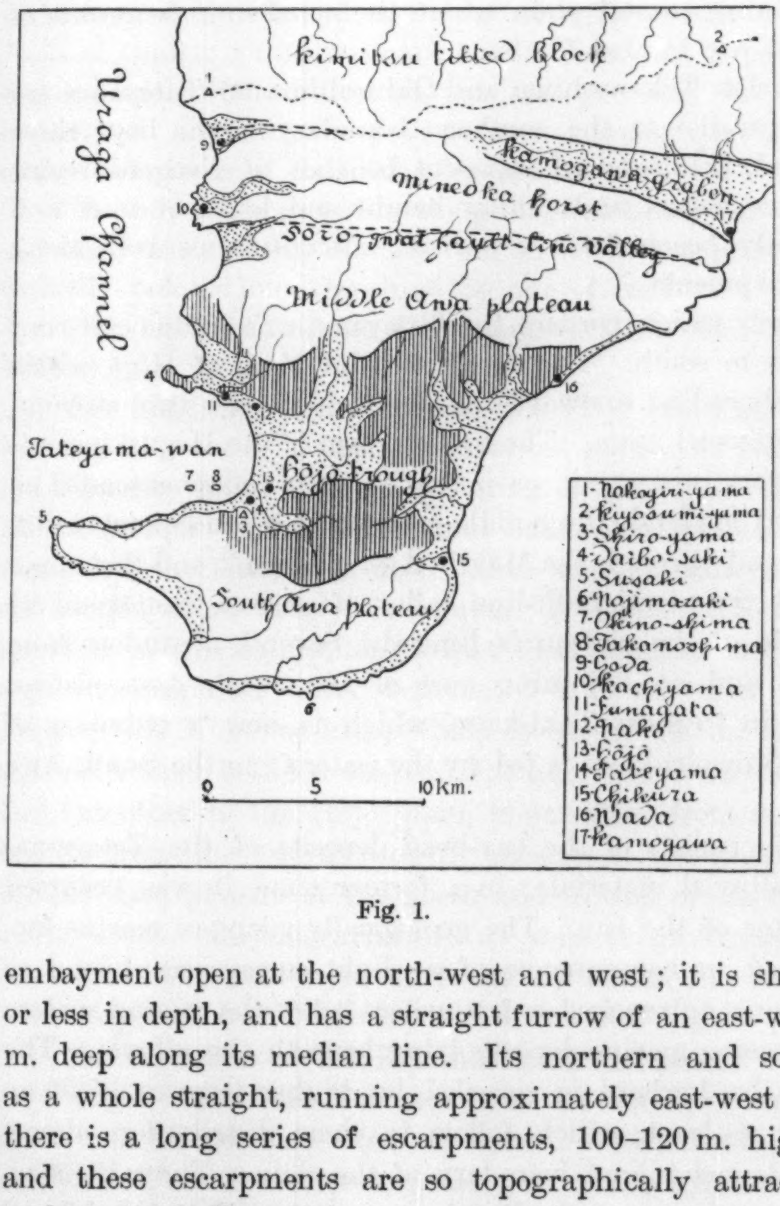

Fig. 1.

a graben, and the name Hôjô trough is prefered to Hôjô graben.

The depressed zone in question consists of four parts of different physiognomy; counted from the west, they are: the Tateyama-wan (bay of Tateyama),[4] the alluvial plain of Hôjô or Hôjô plain, Kokonoe hills, and the alluvial plain of Chitose or Chitose plain.

The Tateyama-wan is a four kilometers broad rectangular embayment open at the north-west and west; it is shallow, being 30 m. or less in depth, and has a straight furrow of an east-west trend, 327–662 m. deep along its median line. Its northern and southern coasts are as a whole straight, running approximately east-west; in a distant view there is a long series of escarpments, 100–120 m. high on both coasts, and these escarpments are so topographically attractive that several authors, including Yabe, regarded them as fault-scarps. Concerning them, the late Professor N. Yamazaki stated in his "Physiographical Studies of the Great Kwantô Earthquake of the Kwantô District, 1923," that "the northern wall of this zone is well marked by the scarp which extends from the cliffy promontory of Daibozaki farther eastward, passing by the bluff of Nako, where stands the well-known temple of Kannon, while the hills to the east of Cape Susaki form the southern boundary. Between these fault-lines extends the beautiful bay of Tate-

4) Also sometimes called Kagamigaura.

yama and an adjoining coastal plain where the noted summer resorts of Hôjô and Tateyama are located."[5]

The two small islets Takanoshima and Okinoshima off Tateyama are on a line nearly parallel to the southern boundary of the bay; these islets are flat topped, being raised wave-cut benches of Neogene rocks. Terraces of the same nature and similar height and lcwer ones as well as the present sandy beach form a narrow, discontinuous belt along the foot of the escarpments.

The sandy beach which borders the Tateyama-wan at the east runs straight from north to south. The broad alluvial plain of Hôjô which extends from the shore-line eastwards, is drained by the two streams, Heguri-gawa and Shiwoiri-gawa. The main stream of the Heguri-gawa is physiographically very interesting, as it has its lower course extended on a new grown coastal lowland, the middle course cut a consequent valley of a north-south trend through the Middle Awa plateau,[6] and the upper course lying in the Soro-Iwai fault-line valley of an east-west trend by which the back-side of the plateau is limited. Several streamlets from the Kokonoe hills and an adjoining part of the South Awa plateau coalesce on the plain to form Taki-kawa which is now a tributary of the Heguri. The Shiwoiri-kawa is fed by the water from the South Awa plateau.

The Hôjô plain consits of the bay-head deposits of the Tateyama-wan, overlain by alluvial materials; in a former time it was occupied by the marine water of the bay. The geologically youngest marine formation was uplifted in consequence of a slight emergence of land as shown by the streams intrenched a few meters below the ground surface and sometimes exposing marine deposits lying beneath the alluvia. The earlier history of the lowland is revealed by higher terraces 15-20 m. above the present sea-level, which follow in their distribution almost thoroughly the indented inland boundary of the plain. These 15-20 m. terraces belong to a category of the Post-loam terraces (PL.) of Aoki and Tayama[7] in the Kwantô region north of the Bôsô peninsula, and are believed by us to be of marine origin; the 20 m. terraces are rock ben-

5) Yamasaki assumed rift valleys for the middle course of the Heguri-gawa and the adjacent middle course of the Maruyama-gawa which are parallel to one another, an opinion which we can not accept Yamasaki, "Physiographical Studies", 89.

6) YAMASAKI, "Physiographical Studies", 89.

7) R. AOKI and R. TAYAMA, "Morphology and Geology of the Kwantô Tectonic Basin, with Special Reference to Its Western Marginal Part", *Saito Gratitude Foundation*, Sci. Rep. VIII (1930), (in Japanese).

ches covered by alluvial or detrial materials while the 15 m. terraces are built of contemporaneous marine sediments. At a post-Pleistocene time, the sea-level of the Tateyama-wan was preceded by a submergence far superior in amount; the present coastal topography still retains the incontestable trace of that submergence of land.

These latest episodes in the geological history are quite the same in the other parts of the Kwantô region as in the present district, as repeatedly pointed out elsewhere by one of us.[8)]

The depression of the Hôjō zone certainly took place prior to this submergence of land.

The hilly land lying between the Hôjô plain and Chitose plain on the Pacific coast is a strongly dissected plateau of Neogene rocks called the Kokonoe hills; it is quite similar in geological and early topographical growth to the Middle and South Awa plateaux. At present it lies below the latter two, or in other words it shows an aspect of having submerged more deeply in alluvia. A fact which merits our special mention in this connection is that there is absolutely no trace of an abrupt topographical break between it and the other two. The highest ridge of the Kokonoe hills, which is hardly 100 m. high and serves as the water-shed between the two streams, one down to the Chitose plain and the other to the Hôjô plain, is extended from north to south and has its crest line uninterruptedly passing to the ground surface of the Middle Awa plateau at the north and to that of the South Awa plateau at the south. Physiographically as well as geologically we could find no trustworthy indication of faults by which the lower Kokonoe hills were suspected to be separated from the two higher plateaux.

The crest line of the Kokonoe hills lies nearer to the Pacific shore than to the shore ofthe Tateyama-wan, its distance from the former being about one half of that from the latter. The hilly land is further asymmetrical in another respect, namely as to the altitude of terraces along its western and eastern borders. The 20–15 m. terraces on the west side are equivalent to the 30–20 m. ones on the east side; likewise the lower or younger terraces hold higher altitudes on the eastern side than on the western. This peculiar feature suggests an asymmetrical emergence of land, the amount being greater on the eastern side than on the western.

---

8) H. Yabe and R. Aoki, "A Summary of the Stratigraphical and Palaeontological Studies of the Cenozoic of Japan, 1920–1923", *Proc. Pan-Pacific Sci. Congr.*, Australia, (1923), 969.

The inland boundary of the Chitose plain very rich in indentations shows nowhere any sharp topographical and geological breaks reminding us of dislocation lines which seem to have contributed on the origin of the lowland.

By cartographical studies as well as in field observations we could not succeed in tracing any faults or fault-scarps on either side of the Hôjô plain, Kokonoe hills and Chitose plain, as stated above. Actual faults do not exist on either side of these parts of the Hôjô depression and neither in a position as plotted by Yamasaki[9] and Yabe[10] independently on their tectonic maps of the Kwantô region, nor elsewhere near any position apt to bring up the idea that the depression is a graben in strict sense; on the contrary, the physiographical relation of the Middle and South Awa plateaux to the depressed zone suggests its origin as a trough rather than a graben, due to a gentle downwarp of the earth's supercrust.

The escarpment on the north and south coasts of the Tateyama-wan are arranged on straight lines, of which the northern one is 5 km. and the southern one 10 km. long. The escarpments on the north coasts are, however, too discontinuous and separated to be safely assumed as the remnants of a once continuous fault scarp. These on the south coasts are more continuous and can be said as still retaining a vestige of an ancient fault scarp, though we have no geological evidence to support this interpretation; we can restore a fault scarp along the line of these escarpments, but it may or may not have existed there actually. Therefore what we can say now at most about the westernmost section of the Hôjô depression is merely that it has a certain evidence, though not a conclusive one, of a graben.

The depressed zone of Hôjô gives us a false impression of a graben; this is due to the remarkable panoramic views from its lowlands to the north and to the south. On both sides of the lowlands there is visible in a distance a series of escarpments which are nothing but the edge of terraces.

The Middle Awa plateau with its ground-surface as a whole is sloping southwards carrying two distinct planes of denudation which are correlated with the Lower Tama terrace (T_2) and the Upper Tama terrace (T_1) of Aoki and Tayama in the other parts of the Kwantô region. Higher areas above them are the relics of the Pre-Tama land with an

9) YAMASAKI, *op. cit.*, Pl. IX.
10) YABE and AOKI, *op. cit.*, Pl. II.

aspect of a dissected peneplane.

The terminal slope or face of the Upper Tama terrace is fairly continuous and magnificient in a distant view; it is usually 40–80 m. high and its base lies 100–120 m. above the sea level. In a top view, it is interrupted by a few large valleys where it always makes a broad backward bent; hence, the total aspect of the line is a series of curves convex southwards, and their front lies approximately on a line west by south to east by north in extension. By way it must be added that there is no trace of major fault geologically recognised to play an important rôle on the growth of these escarpments.

This upper series of escarpments lies 2 km. north of the restored line of escarpments between Daibôzaki and Nako and of its imaginary eastward prolongation.

In the South Awa plateau the Pre-Tama land-surface is reduced almost to nil and only a small area at the valley-head of the Nagaogawa close to the southeastern border of the plateau is thought by us with some doubt to be a remnant of it. From the highest part which is about 200 m. high, the ground-surface of the plateau slopes gently to the north-west, with an abrupt break at a height of 100–120 m., where the Upper and Lower Tama terraces are separated by a steep wall 40–80 m. high and facing the depressed zone of Hôjô; the wall is most conspicuous for a distance of 3 km. and has a trend west-south-west to east-north-east. According to F. Ueda, a fault runs parallel to and 1 km. north of the escarpment; it is either a simple escarpment by erosion more or less controled by an old dislocation line, or a retired fault scarp, according to the pre-Upper Tama or pre-Lower Tama origin of the fault.

The two escarpments along the edge of the Upper Tama terraces on the northern and southern sides of the depressed zone of Hôjô are some nine kilometers apart; they are not only parallel to one another but also parallel to the general trend of the Hôjô zone. This feature is important, because it tells us that the first downwarping of the earth's supercrust along the Hôjô zone was already displayed in the post-Upper Tama time.

In the other parts of the Kwantô region, the Upper and Lower Tama terraces are succeeded by the next lower Musashino terraces, and these in their turn by the Post-loam terraces. As a matter of fact, the Musashino terraces are developed very poorly, if any at all, in the Hôjô zone; a narrow terrace on the mid-slope of a small hill called Shiro-

yama near Tateyama is thought by us with some doubt to be one example of them and all others are similarly very limited in extension and of doubtful nature. The Shiroyama has a broad belt of the Post-loam terraces around its base, 20 m. above the sea-level.

In p. 4 we have already stated that the downwarping of the Hôjô zone in the present state is an earlier event than the submergence of land which preceded the building of 15–20 m. terraces. Further, that the building of the Lower Tama terraces anteceded the downwarping is quite evident from the distribution and topographical features of the Lower and Upper Tama terraces given above. Now the question arises whether the downwarping is older than the building of the Musashino terraces or younger ?. Any sound discrimination of the pre-Musashino (terrace) or post-Musashino (terrace) date of the crustal movement is rendered difficult by the very scanty development of the Musashino terraces in the district; but we hold the view that the district was primarily destitute of the Musashino terraces in any significant extension and the downwarping took place there after the building of the Musashino terraces in other places and before the submergence of land which preceded the building of the 15–20 m. terraces, for, otherwise, the Musashino terraces must be found in more extended distribution.

Summary: The depressed zone of Hôjô is probably not a graben, but a trough in its greater length; the possibility of its being a graben can be still maintained at most only in its westernmost section, the Tateyama-wan. The downwarping of the earth's supercrust took place most vividly at a time later than the building of the Musashino terraces and earlier than the submergence of land which preceded the emergence of the 15–20 m. terraces. The similar trough-making process seems to have been once active on the same line after the building of the Upper Tama terraces and before that of the Lower Tama.

Finally it remains to be added that there are two other troughs on the South Awa plateau, which are more or less similar in nature to, but much smaller in size than the Hôjô trough. One of them is 4 km. by 2 km., elongated from west to east, transversal to the eastern border of the plateau, and drained by the Kawajiri-gawa which has its mouth near Chikura on the Pacific coast. It is recognisable as a trough of the Lower Tama terraces by restoration, along the border of which the Musashino terraces are scarcely tracable.

The other trough of a more topographical interest is situated close

to the southern border of the South Awa plateau which is limitted in the south by a bold escarpment, 60–100 m. high, facing the sea; it is elongated from east-north-east to west-south-west and 3·5 km. by 6 km. in extension. In front of the escarpment which is a fault scarp (Shirahama fault) is a lowland, a kilometer broad and consisting of 20–30 m., 12–20 m. and lower terraces, including rock benches elevated at the occasion of Kwantô earthquake of Genroku era (1703)[11] and that of 1923. This trough is now provisionally called Nagao-gawa trough, as it is drained by the stream of that name.

The Nagao-gawa trough is a trough of the Upper and Lower Tama terraces, with the almost horizontal Musashino terraces well developed over the sunken area and still preserved rather fresh. The Musashino terraces have an elevation of 50–80 m. above the sea-level; through them the main stream and large tributaries of the Nagao-gawa makes their incised meander. Hence the Nagao-gawa trough is a product of supercrustal deformation at a date before the building of the Musashino terraces and after that of the Lower Tama terraces.

The Nagao-gawa cuts a narrow gorge just before its debouch from the plateau-border to the coastal lowland, thereby enclosing a small basin some 30 m. high near a village of the name Hongô; the basin traversed by the incised meander course of the main stream of the Nagao-gawa is due to the northward tilting of the very marginal part of the border of the South Awa plateau since the building of the Musashino terraces.

---

11) A. Imamura, "Change of the Coast Line in Bôsô Peninsula", *Rep. Imp. Earthq. Inv. Comm.*, No. 100, B (1925), 91, (in Japanese).

15. 北條凹地帶

地震研究所 矢部長克
田山利三郎

在來房總半島南部に於て所謂「北條地溝帶」「館山灣地溝帶」と稱せられたるものは地溝と稱すべきに十分なる斷層を兩側に缺き寧ろ凹地帶と見做すを適當とすべし。唯館山灣南側の多少一直線狀に配列する急崖の列は斷層崖を想起せしめざるにあらざるも實際は然らず。地形上著しき兩側の急崖は T_1, T_2 兩段丘の境にありて、北側にあつては北より南に、南側にあつては南より北に傾き殊に T_2 面は北條凹地帶內の九重丘陵地の表面に連る。

M 面は發達不十分なれど PL_1, PL_2 面は北條平野と千歲平野の周緣に發達す。この PL_1 面は千歲平野に於ては北條平野に於けるものより多く隆起す。

北條凹地帶の形成は既に T_2 面形成後に始り最新の著しき運動は恐らくM-面形成後なるべし。而して PL_1 面形成後東西兩側に於て非對稱的の上昇を示す。

尙この以外に長尾川と川尻川の兩凹地帶あり前者は半島の南端白濱斷層に接し恐らく M 面形成後の地盤彎曲に歸するものなるべし。

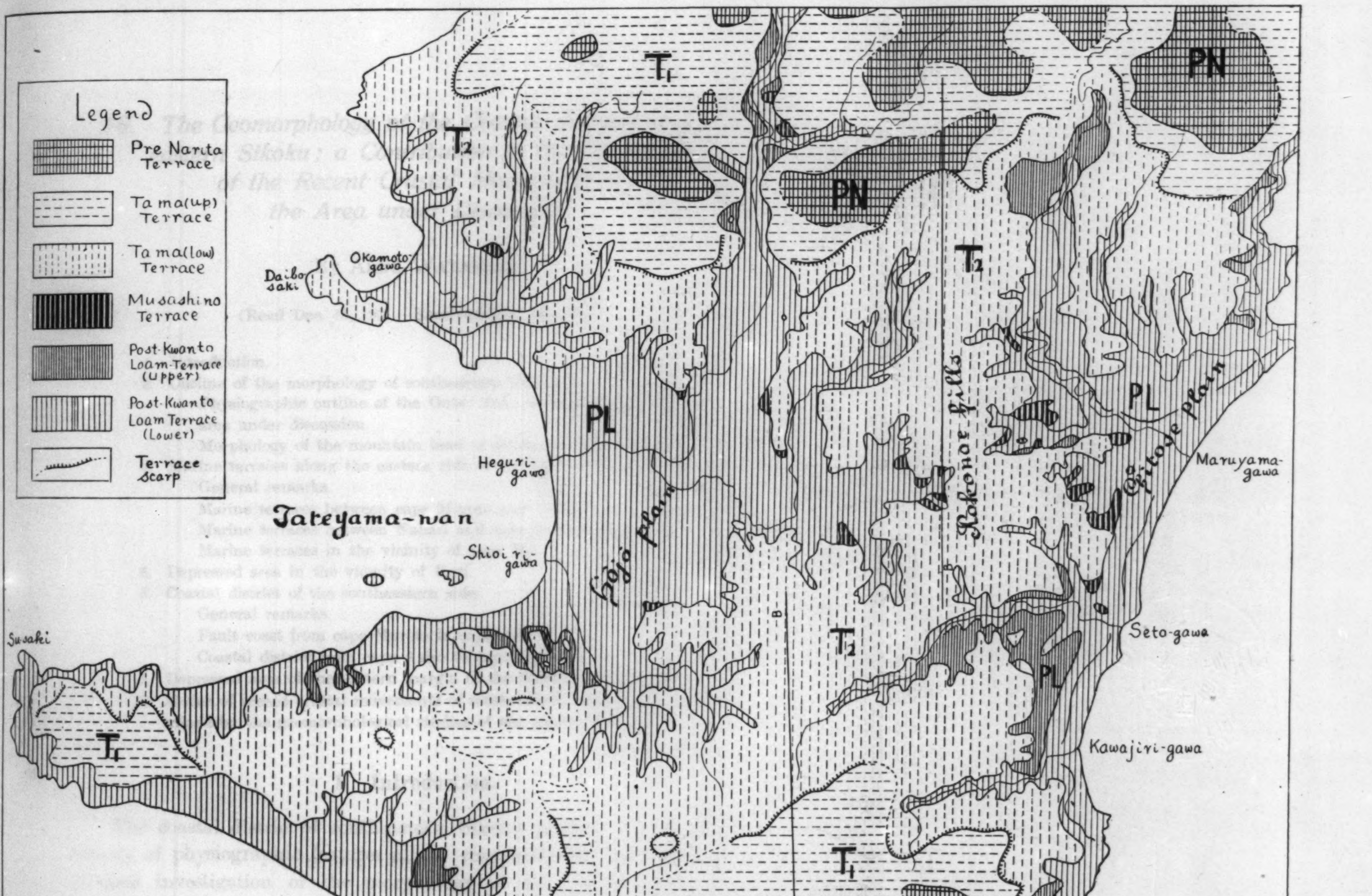

Fig. 2. Terrace Map of the Middle and Southern Parts of Bôsô Peninsula. (Originally it accompanies two profiles along the lines A-B and C-D; but these are excluded from the present paper).

16. *The Geomorphology of the Coastal District of Southeastern Sikoku; a Contribution to the Knowledge of the Recent Crustal Movements of the Area under Discussion.*

By Akira WATANABE,

(Read Dec. 15, 1931.—Received Dec. 20, 1931.)

1. Introduction.
2. Outline of the morphology of southeastern Sikoku.
   Physiographic outline of the Outer Zone and its relation to the area under discussion.
   Morphology of the mountain land of southeastern Sikoku.
3. Marine terraces along the eastern side of the bay of Tosa.
   General remarks.
   Marine terraces between cape Muroto and Nahari.
   Marine terraces between Nahari and cape Gotennohana.
   Marine terraces in the vicinity of cape Tei.
4. Depressed area in the vicinity of Koti.
5. Coastal district of the southeastern side.
   General remarks.
   Fault coast from cape Muroto to cape Aziro.
   Coastal district from cape Aziro to cape Gamoda.
6. Depressed area of the eastern margin of the Sikoku mountain land.
7. Modes of recent crustal movements of southeastern Sikoku as determined by the geomorphological studies of the coastal district.

1. Introduction.

The coastal district of southeastern Sikoku presents a multifarious variety of physiographic features all of comparatively modern growth. A close investigation of the morphology of the area in question has proved to be a contribution to the knowlege of the recent crustal deformations of considerable differential nature.

Several steps of marine terraces that are very well developed along the eastern side of the bay of Tosa are the distinguishing marks of the intermittent type of uplift,[1] while the immediate western continuation

1) Short statements of the marine terraces of this region were given by T. Ogawa and Y. Ôtuki some thirty years ago.

in the vicinity of the city of Koti bears strong evidences of the recent date of depression represented by deep embayments, partly submerged ridges, and isolated hills protruding well above the level floor of the delta plain.[2] In speaking of the eastern side of the area, the tectonic nature of the steep cliff bordering the southern coast has been noted out by some predecessors,[3] and in the north along the Kitan strait, the recent marginal downwarping has resulted in the penetration of the sea water into the maturely dissected margin of the mountain land at the rear.[4]

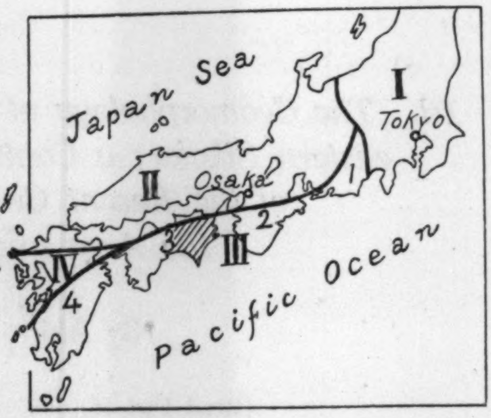

Fig. 1. Map showing the location of the area under discussion.

I. Northeast Japan.
II. Inner Zone of Soutwest Japan.
III. Outer Zone of Southwest Japan.
1. Akaisi. 2. Kii. 3. Sikoku.
4. Kyushu.
IV. Nagasaki Dreiecke.

It is here proposed to discuss the certain important shoreline features of the area, and to elucidate the modes of recent crustal movements so far as can be traced back by the geomorphologic evidences. The observations on which the present report is based were made once in the summer of 1928 for two weeks, and again for one week in the same season of the next year.

Before taking up the specific area of this report it seems desirable to note the salient geomorphologic features of southeastern Sikoku as a

---

T. OGAWA, Expl. Text Geol. Map of Japan, "Koti" sheet, 1:200.000, (1905).

Y. ÔTUKI, Expl. Text Geol. Map of Japan, "Muroto" sheet, 1:200.000, (1902).

In recent years T. Tuzimura and H. Simomura rendered short but suggestive discussions of the marine terraces of this region in their more ambitious works.

T. TUZIMURA, "Regional Physiography of Japan," Tôkyô, (1929).

H. SIMOMURA, "Some Consideration Concerning the Coastal Terraces in Japan," *Geogr. Rev. of Japan*, 6 (1930), 860–862.

2) The characteristic landforms of this area was noted by T. Terada.

T. TERADA, "On the Relief of the Earth Crust on the Southern Coast of the Province of Tosa, Sikoku," *Bull., Earthq. Res. Inst.*, 4 (1929), 67–73.

3) Y. ÔTUKI, Expl. Text Geol. Map of Japan, "Hiwasa" Sheet, 1:2000.000, (1908).

H. SIMOMURA, "Some Consideration Concerning the Coastal Terraces in Japan," *Geogr. Rev. of Japan*, 6 (1930), 861.

4) T. TUZIMURA, "Coast Topography of Japan," *Gendai no Kagaku*, 8 (1920), 256.

whole, because the skeleton or the foundation of the coastal district is seemed to bear an important relation to the genesis and the subsequent development of the coast topography.

2. Outline of the Morphology of Southeastern Sikoku.

Physiographic Outline of the Outer Zone and its Relation to the Area under Discussion: The mountain lands of the Outer Zone of Southwestern Japan, extending from central Honshu westward to the southwestern corner of the island of Kyushu, have a remarkable similarity in geologic structures as well as in morphologic features.[5] The regular zonal arrangement of Chrystalline schists and much distorted Paleozoic and Mesozoic formations in chronological order from north to south characterizes throughout the entire extent, and they run in accordance with the general trend of the insular arc of this portion. The northern boundary of the Outer Zone is continuously marked by the Median Line along which the land of the Inner Zone is regarded to have been overthrusted upon that of the Outer Zone.

The morphologic similarity throughout the whole stretch of the Outer Zone is none the less conspicuous. Leveled or subdued surfaces are recognizable even near the culminations. Since their formation the rhythmic alternation of the periods of uplifts and of quiescences in the course of the successive growth of the mountain lands has resulted in the development of many steps of erosion levels, although their present extension is exceedingly limitted owing to the vigorous late erosion, and the area as a whole may well be regarded as a maturely dissected mountain land of strong relief.

There is every reason to believe that the type of crustal deformation has been taking the form of warping, which is accompanied by steep marginal flexure along the coast. The northern margin has been dropped down by a bold and contiguous fault scarp throughout the entire extent of the Median Line. It is just adjacent to this fault scarp that the highest portion of each locality is found. From this portion there is a gradual decrease in altitude southward. Mountain building is still in the course of its growth, and owing to the vigorous downward corrasion still going on none of the river has extensive flood plain along

5) The instructive general statements of the physiographic features of this region are found in T. Tuzimura's book on the "Regional Physiography of Japan" Tôkyô, (1929).

the course. Intrenched meandering course characterizes most of the important rivers, and the effect of the accumulation of sediments is almost negligible with the exception of small areas along the coast.

Intense downwarping of the earth's crust has caused the separation of this once continuous range into four independent blocks of land. They are from east to west, the mountain lands of Akaisi, Kii, Sikoku, and Kyushu, which are separated by the Ise bay, the Kitan strait, and the Bungo strait respectively. The regular occurrence of these straits as well as the steep seaward inclination of the mountain lands to these straits suggest the existence of troughs of a stationary earth wave that proceeds in equatorial direction, or in accordance with the general trend of the island arc of this portion. The recent continuation of this movement is well evidenced by the submerged type of shoreline features along the coast of these straits. On the other hand, many signs of uplifts are found in abraded terraces, elevated deltas, and coastal plains in the southern periphery of these mountain lands.

Without considering the occurrence of these straits, the mountain lands of the Outer Zone of Southwestern Japan have a remarkable continuity within themselves. Contrary to the Inner Zone where the complicated systems of the geomorphologic fault structures have broken the lands in a most profused manner, the Outer Zone has scarcely any sign of morphologic fault with the exception of Sikoku where two rows of fault scarps traverse the interior of the mountain land.

Morphology of the Mountain Land of southeastern Sikoku; Although a few segments of land that belong to the Inner Zone are attached in the north, the Sikoku mountain land in the south constitutes the main body of the island. Eastward the island is detached off from the Kii mountain land by the Kitan strait and westward from the Kyushu mountain land by the Bungo strait. It has been shown in the altitude distribution as well as in the major configuration of the island that the Sikoku mountain land is divided into two mountain masses by a lower portion in the center. The highest part of the eastern mass lies in the north central portion where Turugisan attains to 1955 m. The western mass has, in common with the other land area of the Outer Zone, its culmination just adjacent to the northern margin where Isizutisan and Ninomori reach 1921 m and 1930 m respectively.

A steep northward descent from these culmination is recognizable as a bold fault scarp along the Median Line, but descent to the other directions is comparatively gradual. The low portion of the summit

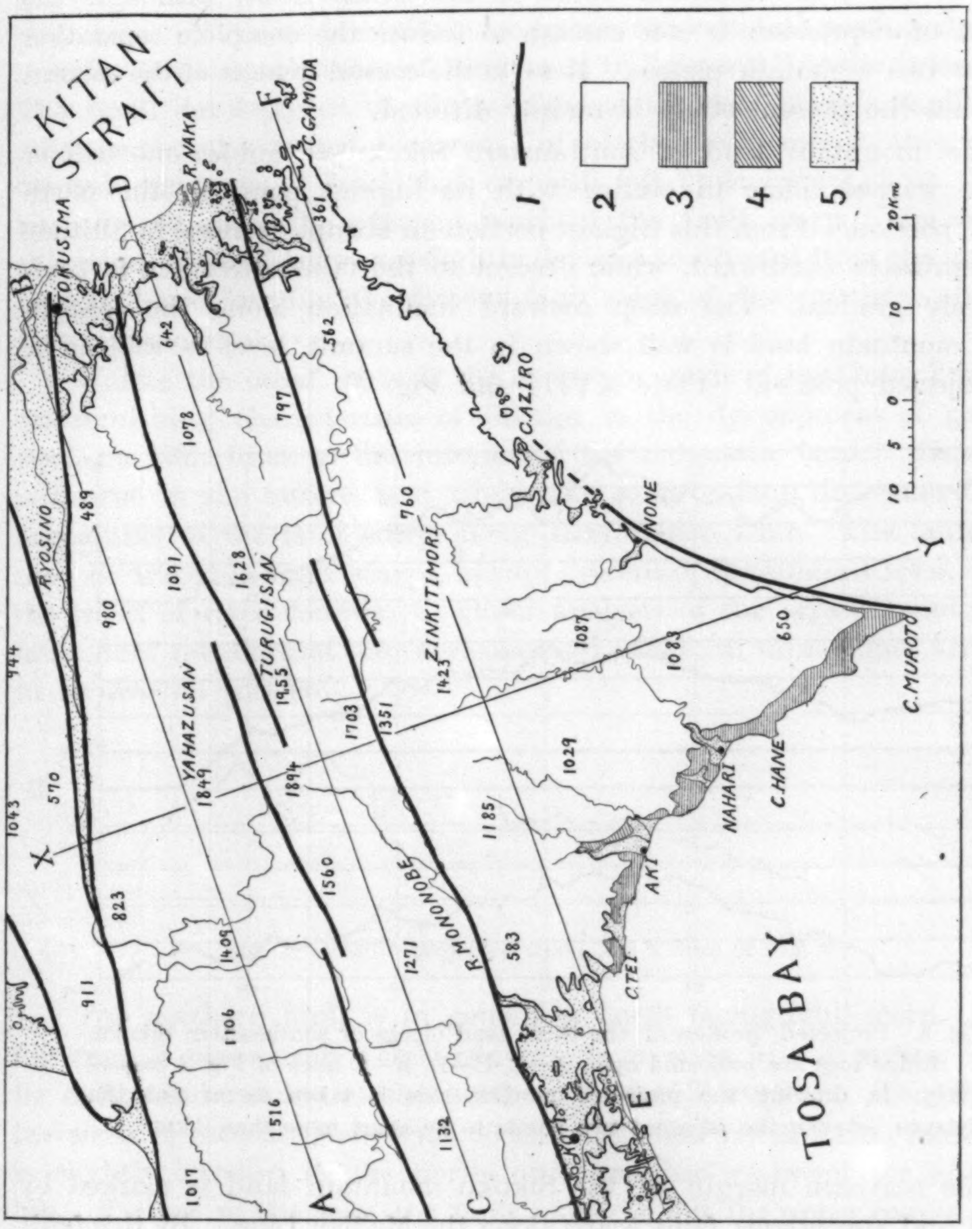

Fig. 2. Geomorphologic map of southeastern Sikoku.

1. Geomorphologic fault line. 2. Mountainous area.
3. Marine terrace. 4. River terrace. 5. Alluvial plain.

level lying between these mountain masses suggests the existence of a trough of the earth wave which has caused the formation and the separation of the four mountain lands of the Outer Zone, although the amount of depression is not enough to induce the complete separation of these two mountain masses. It is to the coastal district of the eastern mass that the present study is mainly directed.

The mountain land of southeastern Sikoku resembles one half of a huge warped dome in outline with its highest point in the north central portion. From this highest portion an abrupt decrease in altitude is recognizable northward, while descent to the other direction is comparatively gradual. The steep seaward inclination along the margin of the mountain land is well shown in the summit level as well as in the projected profiles. (Plate XVIII and Fig. 3)

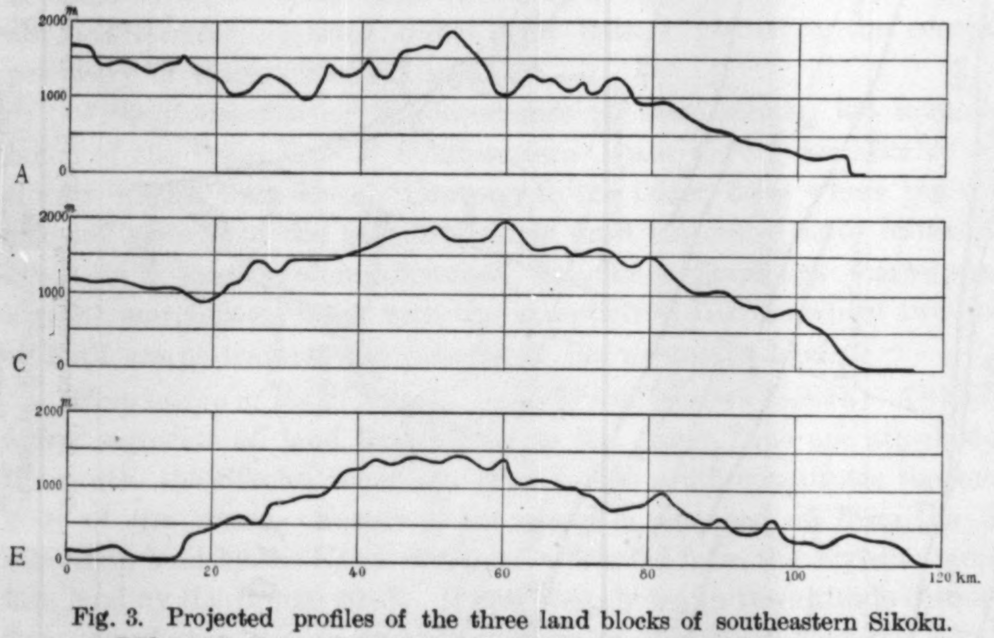

Fig. 3. Projected profiles of the three land blocks of southeastern Sikoku. Ridge tops are projected upon A—B, C—D, E—F lines of Fig. 2 respectively. In drawing the projected profiles, care is taken so as not the distance between the adjacent two points to be apart more than 4 km.

The northern margin of the Sikoku mountain land is marked by a bold and contiguous fault scarp along the Median Line. By this fault the mountain land drops down to the depressional area of the famous "Setouti" or the Inland Sea and the Yosinogawa Graben.[6] The height of

6) T. TUZIMURA, "Geomorphologic Significances of the Median Line of Southwestern Japan," *Jour. Geol. Soc.*, Tôkyô, 31 (1924), 130.

this fault scarp exceeds 1000 m in the center from where there is a gradual decrease in height both eastward and westward. In the east the fault scarp embraces the Yosinogawa Graben with the Horst of Sanuki range to the north. With its precipitous escarpment the central portion descends directly to the spacious sea of Bingonada in "Setouti" or the Inland Sea. The small development of alluvial fans at the foot of this fault scarp tells the recent repeated occurrence of block movements in this region. Several segments of land that are still left undepressed above the sea level are found to the adjacent north of the fault scarp. The western extension of this fault scarp slightly deviates southward from the geologic Median Line, forming the famous fault coast of the northern shore of cape Sadanomisaki.

Unlike the other parts of the mountain lands of the Outer Zone, the distinguishing characteristic of Sikoku is the development of geomorphologic fault lines in the interior of the mountain land.[7] Especially is it true in the eastern part where two rows of fault lines are running subparallel to the fault scarp along the Median Line. The fault lines may be traced in fault scarps, abrupt descent of the summit level, and in the trend of river courses. A closer analysis of the arrangement of the fault lines reveals that they are composed of several minor lines arranged in *en échelon* pattern.

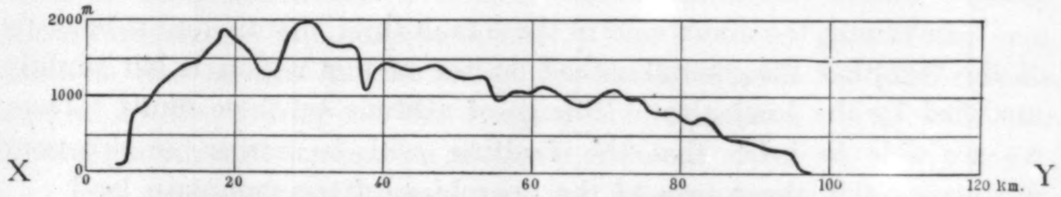

Fig. 4. Profile projected upon X—Y line of Fig. 2.

The northern fault is in general a north facing fault scarp. Starting from a place near Komatusima, a fault runs in a direction of west by south, and reaches at the northern foot of Turugisan. The distance traversed is measured as about 60 km. Another north-facing fault scarp is slightly offsetted to the north, and stretches westward for about 40 km. Farther to the west the fault valley along the upper course of the river Yosino is still offsetted to the north.

The southern fault is in general a south-facing fault scarp which

---

7) T. Tuzimura, "Nature of Fault Valleys and the Geomorphologic Fault Structures of a Portion of the Japanese Islands," *Geogr. Rev. of Japan.* 2 (1926), 215.

runs almost in the same direction as that to the north. From the eastern end of the mountain land the fault stretches along the drainage basin of the river Naka for 50 km. Near its western extremity an offsetted fault is found to the north. The course of this fault line practically coincides with that of the river Mononobe. This fault line can be traced westward to the northern margin of the Koti plain, and the entire length is measured as about 80 km. An abrupt descent of the summit level bounded by this fault is clearly manifested in Plate XVIII.

In this way, the eastern part of the Sikoku mountain land is divided into three land blocks each of which runs subparallel in accordance with the trend of the fault lines. The central block is an elongated Horst whose northern and southern margins are bounded by the fault scarps above noted. Turugisan, the highest portion of the island of Sikoku, is nearly in the center. The northern block is somewhat inferior in elevation, and the maximum height reaches 1849 m at Yahazusan.

The southern block, which is abruptly dropped down from the Turugisan Horst, is wedge shape in outline. The highest portion lies in the north central part where Zinkitimori attains to 1423 m. From this portion descent to the east, west and south is gradual until the present coastal district is reached.

Concerning the occurrence of these fault lines, mention must be made of the fact that the general arched outline of this region is but slightly modified by the local abrupt change of altitude by these faults. Thus, we are able to infer that the faulting will be rather an accessory phenomenon in the course of the uparching of the mountain land.

The trend of the important divides coincides with that of the fault lines. Flat topped surfaces are recognizable upon many of the interstream ridges, and subdued topography is found even near the culminating point at Turugisan. The extension of these surfaces is exceedingly limitted in area owing to the late obliteration by erosion. There is every reason to believe that these levels do not necessarily indicate the existence of a once extensive peneplain, but may be divided into many steps of erosion levels that have been formed in the course of the successive growth of the mountain land.

Most of the important rivers of this region that are vigorously corrading downward have no flood plain along the courses, and the effect of sedimentation is almost negligible except in a small portion

near the mouths of the large rivers. Steep valley walls and numerous rapids along the river courses are the characteristics of the valley forms. Discordant junctions of tributaries with main streams are often seen in the interior of the mountain. We may therefore conclude that the mountainous area is still in the course of its rapid upgrowth.

From what has been presented so far, we are able to consider that the major configuration of the skelton of the area has been formed by the two wavy motions of the earth's crust which intersect at right angle each other. One wave proceeds nearly equatorial in direction, in other words, parallel to the major trend of the insular arc of this portion.[8] The troughs of the wave are occupied by the straits at present in case the amount of depression is enough to induce the invasion of the sea water. The lower portion in the center of Sikoku will be of the same nature although the amount of depression is not enough to cause the complete separation of the mountain masses to the east and the west.

Another wave proceeds in meridional direction, or normal to the trend of the insular arc. The movement is associated with faulting, and the fault scarp along the Median Line as well as the two rows of fault lines in the interior have separated the mountain land of Sikoku into the three elongated land blocks. The form of this wave is assymmetric with its steep northward inclination from the crest and the gentle southward slant. The cuspate outline of the southern part of the area may be due to the intersection of the sea level with the land surface formed by the overlap of the crest of the equatorial wave with the gradual southward inclination of the meridional wave.

The steep marginal descent of the summit level of the mountain land is presumably due to flexure, although occasionally replaced by faulting. The existence of marine terraces along the eastern shore of the bay of Tosa is not enough to obscure the steep marginal inclination of the summit level of this portion.

The major outline of the skeleton of the coastal district has thus been made clear, the general and the sectional statements of the coast topography will be given in the succeeding chapters.

---

8) Recently Y. Ôtuka pointed out the same type of crustal movements of this region in the early Pliocene time.

Y. Ôtuka, "Early Pliocene Crustal Movement in the Outer Zone of Southwest Japan and in the Naumann's Fossa Magna," *Bull. Earth. Res. Inst.*, 9 (1931), 340-352.

3. Marine Terraces along the Eastern Side of the Bay of Tosa.

General Remarks: Along the eastern side of the bay of Tosa, the geomorphologic features of the coastal district are dominated by the development of several steps of marine terraces. They can be traced throughout the entire coast from cape Muroto to cape Tei. The terraces are in most cases abrasion surfaces with thin veneer of gravels not exceeding few meters in thickness. The maximum elevation so far identified by morphologic evidences is about 300 m in the east. The surfaces of the marine terraces have a gentle seaward slant, with complementary sea cliffs of varying height at the rear.

Remnants of abandoned stacks with wave cut notches are numerously found upon the abrasion surfaces, and elevated sea caves are in places recognized at the foot of the former sea cliffs. In the accompanying map (Plate 19) the distribution of the marine terraces as well as their profiles of the respective sections are indicated. The marine terraces are shown in three different symbols classified by the present altitude, and their elevation measured at the foot of the former sea cliffs are shown in the profiles below.

The lowest terrace of very recent origin is represented by vertical lines. It can be traced from the southern tip at cape Muroto to as far northeastward as cape Gotennohana. The intermediate terraces are shown in cross lines. They comprise the terraces less than 200 m in height. Marine terraces higher than 200 m are shown in black. It should be noted that the terraces represented by these respective symbols do not necessarily indicate the ones of contemporeneous origin, and that the classification is merely done for convenience sake.

In regard to the upper terraces, a great differences in the degree of dissection as well as in the modes of formation are found from east to west. For, in speaking of the intermediate terraces, while extensive initial surfaces with a continuous seaward slant are preserved in the east, those in the west are much obliterated by late erosion, and the continuity of the surfaces themselves is often interrupted by many steps of former sea cliffs.

The highest terraces are greatly obliterated by erosion, although their distinguishing characteristics of marine origin are still recognized. The best development of these surfaces is in the east, with diminishing degree of their preservation westward.

Marine Terraces between Cape Muroto and Nahari: The above noted three steps are typically developed in this portion. The lowest one is fringing the entire extent along the coast. The height measured at the foot of the back cliff is from 8 to 10 m and the breadth does not exceed 600 m. This is an abrasion terrace with gravels strewn over the surface. Stacks are scattered upon the surface and the clear remnants of wave cut notches are recognizable at their base. A closer analysis of the surface indicates that this level is not a continuously slanting abrasion surface which was formed under the sea level at a time of long quiescence, but is composed of several minor steps,[9] and wave cut notches which show the approximate position of the former strand line are found in various height at present. We may, therefore, with confidence assert that this abrasion surface was formed by several intermittent uplifts with intervals of quiescence during which the time was not long enough to entirely cut back the surface by wave action. The latest movements of this upheaval occurred on the occasion of the great earthquakes of 1707 and 1854 when uplifts of 5 feet and 4 feet were reported respectively near cape Muroto.[10]

The surface has a sand dune cover near the mouths of the large rivers. Each river has an alluvial plain along the lower course, and the surface of the plain is now slightly rejuvenated in sympathy with the recent uplifts. In the western part between cape Hane and Nahari the abrasion terrace is almost cut back by late wave action, although signs of recent uplifts are clearly observable as elevated sea caves and wave cut notches.

The intermediate terrace is very well preserved in this area. Where it is typically developed the terrace surface has a characteristic seaward slope from the foot of the back cliff. The height measured at the foot of the former sea cliff is about 180 m throughout the entire extent, and the gradual slant of the terrace surface is seen until 120 m is reached. The steep sea cliff exceeding 100 m in height bounds the intermediate terrace and the lowest one. In places the terrace surface reaches as low as 40 m. The maximum breadth of the terrace is about 2000 m near cape Gyoto.

---

9) The writer described the same characteristic feature on his report on the marine terrace of Bôsô peninsula.

A. WATANABE, "Marine Terraces of the Southern Part of Boso Peninsula," *Geogr. Rev. of Japan*, **5** (1929), 121.

10) A. IMAMURA, "On the Chronic and the Acute Crustal Deformation of the Southern part of Sikoku," *Disin*, **2** (1930), 359.

This terrace is now in the incipient stage of dissection separated only by sharp canyons. Small streams that come from the back cliff are occasionally seen to emerge on the terrace surface and flow out over its surface for some length in a very shallow trench, sometimes reaching to the head of the steep sea cliff at the rear of the lowest terrace, showing that the recession of the cliff in front was scarcely less rapid than that of the gorges in the cliff.

The surface of the terrace is well supplied with water worn pebbles which are in places accumulated to a thickness of several meters. Stacks are numerously found upon the surface, and wave cut notches are still preserved at the foot. The distinct character of the terrace surface, in common with the lowest terrace, is the occurrence of many minor steps of wave wrought terraces. Also wave cut notches are found in various altitude upon the surface. From these it is evident that the formation of this abrasion surface was not accomplished under the long stable condition of the earth's crust, but was under the rhythmic alternation of minor intermittent uplifts and short intervals of repose which is not long enough to induce the entire obliteration of the newly emerged surface in front. Therefore, the present seaward slope of the terrace surface as a whole is by no means the natural inclination of the abrasion surface, but is somewhat steeper than the surface formed under the sea level.

The distribution of this terrace is restricted in a belt that is almost parallel to the present shoreline, and no penetration of the surface is recognizable in the inland. This fact, together with the absence of the thick veneer of gravel will teach that scarcely any appreciable amount of subsidence took place in this area since the emergence of this terrace.

From what have been said above, we are able to consider that after the interval of repose, during which the sea cliff at the rear of the intermediate terrace was formed, numerous minor intermittent type of uplifts caused the emergence of this terrace. The high front cliff would have been formed at the time of slow uplift during which the power of cliff recession was strong enough to cut back the newly attached abrasion surfaces.

The development of the uppermost terrace is distinctly observable in this area. The surface is much dissected by late stream erosion. The most distinct portion is found near the mouth of the river Nisi. Here the terrace is a completely truncated surface sloping down seaward from 290 m to 220 m. The elevated sea cliff at the rear is not so clearly

recognized owing to the late modification. The surface is covered by an unconsolidated gravel bed with the thickness of about 4 m. The completely truncated surface is observed beneath the cap of gravels. This highest terrace is well developed as far northwestward as in the vicinity of Nahari, and the extension is also limitted along a belt that is nearly parallel to the shoreline. To the southeast from cape Gyoto this terrace is not a completely truncated plain which is regarded as the distinct character of the abrasion surface, but is an undulating surface of slight relief, although the sky line seen from a distance is quite uniform in elevation. Near cape Gyoto this surface is about 300 m in height. The surface near cape Muroto is found upon the long ridge projecting southward from the main body of the mountain land. The maximum height is found at an elevation of 258 m in the south of the ridge. This surface may be regarded as the denudation level of old stage by fluviatile erosion. No gravel is strewn over the surface, as is naturally expected upon the gently undulating surface of subaerial origin. It should be noted, however, that these levels are almost equal or somewhat inferior to the adjacent marine terraces in elevation, and that their occurrence is confined to a belt nearly parallel to the present shoreline. From these it is not impossible to consider that the surfaces were originally of marine origin, and was later modified by subaerial action when the initial surface was still near the sea level.

Marine Terraces between Nahari and Cape Gotennohana: The lowest terrace above noted is continuously fringing the coast as far westward as cape Gotennohana. The height is about 10 m at the foot of the back cliff. Stacks and beach gravels are strewn over the surface, and relics of sea caves are in places found at the foot of the back cliff. Extensive flood plain is developed at the mouth of the river Aki. The surface has subjected a slight rejuvenation in sympathy with the recent uplift of the adjacent area.

The relative height of the back cliff is about 40 m which is much inferior to that to the east. Also the height of the intermediate terrace is gradually decreasing westward. Just to the west of Nahari lies a flat level with the maximum height of 78 m. Unlike the other marine terraces of this region, this terrace is of depositional origin, and the gravel bed of 20 m in thickness is resting in unconformity upon the Pliocene foundation. Farther to the west, the predominating height of terraces ranges from 120 m to 140 m, from where there is an appreciable seaward slope till 50 m is reached. The surface is composed of many

minute steps just the same as the intermediate terraces to the east. This surface is almost continuously fringing along a narrow belt only interrupted by the extensive flood plain at the mouth of the river Aki. There is a tendency to decrease the height westward, for while 140 m is measured to the east of the river Aki, 100 m is the predominating height to the west, and farther westward in the vicinity of cape Gotennohana the intermediate terrace comes as low as 80 m in height. However, with the exception of the inferiority in elevation, the terrace surface has the same features as that to the east of Nahari.

Many terraces of higher altitude is recognized at the back of this level. They are still found upon the narrow ridges that are projected off from the main body of the mountain land. The height ranges from 300 m to 160 m to the east of the river Aki, but a gradual decrease in altitude is recognizable westward, and at the western end near Gotennohana many terraces of minute extension comes as low as 120 m.

Attention must be paid to the fact that while the marine terraces with 180 m in height are well preserved to the east of Nahari, that with the same morphologic features are decreasing the height westward, and although many terraces of nearly equal in elevation are found to the west, they are all in more advanced stage of dissection. In regard to the degree of dissection the latter may be compared to the highest terrace to the east of Nahari. The entire extent of the coastal district is composed of shale or sandy shale of Mesozoic formation with small patches of Pliocene foundation to the west of Nahari, and no great difference in the resistance for erosion is considered so far as the lithologic nature is concerned. Drainage condition can not explain the difference in the degree of dissection, as the development of river nets is almost in the same condition throughout the entire coast.

These facts will be easily understood when we consider the gentle westward decrease in the amount of uplift from Nahari. Eastward from Nahari the universally equal amount of uplift may be postulated.

Marine Terraces in the Vicinity of Cape Tei: Many steps of marine terraces are found in the vicinity of cape Tei. The highest one is found at an elevation of 120 m. These surfaces are bounded each other by conspicuous sea cliffs. They are in most cases abrasion surfaces although occasionally covered by thin veneer of gravels. These terraces are in an advanced stage of dissection in spite of the low elevation. Traces of uplift disappear to the west of this place, and gradually

merges into the depressed area of the koti plain represented by the well indentated type of the piedmont line.

In concluding this chapter, mention must be made of the shoreline feature before the emergence of the marine terraces. The present coast line has a sinuous outline with rounded projections and spacious engulf-ments. Parallelism of the present coast line to the former strand lines behind the intermediate and the highest terraces has already been noted out, and it is quite evident that the coastal outline proir to the emer-gence of these terraces was of the same type as at present. The positions of the present rounded projections coincide with the tips of the main spurs from the mountain land, and although the back cliffs of the highest terraces are now very inconspicuous, yet their former existence is supposed by the steep seaward inclination of the spurs down to the surfaces of the highest terraces.

For these reasons, we may be able to infer that the shoreline features prior to the emergence of the marine terraces in this coastal district was of the depressed type, although the initial indentation had been greatly obliterated by the recession of the projecting headlands. In other words, the coastal features at that time must have been the mature stage of the depressed coast.

4. Depressed Area in the Vicinity of Koti.

Westward from cape Tei, signs of uplift disappear and the rich indentation of the maturely dissected mountain margin tells the recent date of depression. The eastern part of the area has almost entirely been buried by the delta plain of the river Mononobe and some other minor streams, although the depressed remnants of the former ridge tops are scattered on the plain as isolated hills. Proceeding westward, the power of aggradation gradually decreases, and not only many bays and inlets are still left unburied by the waste, but also the delta plains that have partly filled the former embayments are very low and swampy; in most cases the elevation scarcely exceeds 2 meters.

The distinguishing characteristic of this region is a marked paral-lism of the partly submerged ridges to the present shoreline; a feature that reminds us of the famous example of Dalmatian coast. Four major rows of ridges are recognizable, which are separated one another either by drowned valleys or waste-filled plains. These ridges are pro-jected out from the spurs of the mountain land to the west, and they

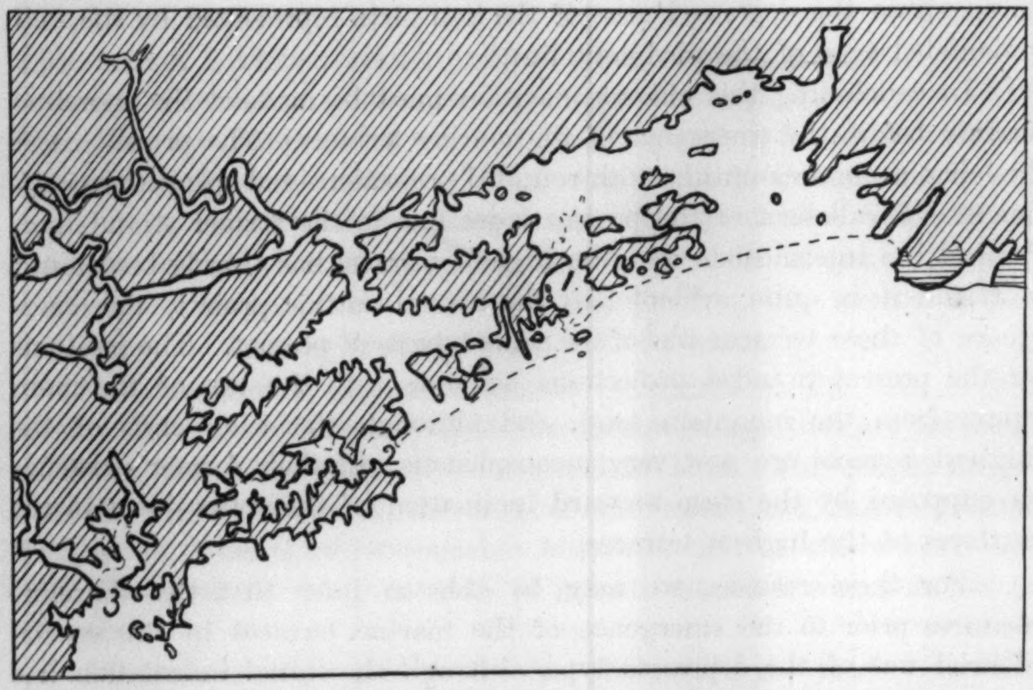

Fig. 5. Showing the depressed area in the vicinity of Koti. Note the rich indentation of the piedmont lines and the partly submerged ridges that run parallel to the present shoreline.
1. Urato Bay. 2. Uranouti Bay. 3. Susaki Bay.

are detached off from the corresponding ridges of the mountain land to the east, although the presumable former continuation is readily understood.

Direction of these ridges accords with the major geologic as well as the geomorphologic trend of the Sikoku mountain land. However, the present morphological features can only tell that they are the former ridge tops of the maturely dissected mountain land, although subsequent or tectonic nature of the origin of the inserted valleys is not an impossible inference.

The northern margin of the waste-filled plain of Koti is bounded by a bold and continuous cliff exceeding 300 m in height. The cliff extends in a direction of E. by N. No trace of subsidence is noticeable to the north of this cliff, and no penetration of the waste-filled valley is recognizable in the valleys that have been formed in the cliff, while many signs of the depression of land are found to the south. We may, therefore, safely infer that there must be a boundary line of upheaval and depression along this cliff. The eastern extension of this cliff penetrates into the valleys of Mononobe and Makiyama. There is

a marked difference in general altitude between the mountain lands to the north and the south of these valleys as shown in Plate XVIII. From these morphological evidences, it is not impossible to believe the tectonic origin of this cliff either by faulting or by a very steep flexure.

The eastern margin of this area is marked by the penetration of the flood plain into the peripheral portion of the maturely dissected mountain land to the east. It has been already stated in the foregoing chapter that no trace of recent depression is noticeable in the immediate eastern shore of this area. This is also true in the inland where the river terraces can be traced almost along the entire course of the river Mononobe down to its outlet from the mountainous area. The type of the movement that has caused these physiographic differences between the two areas must be a gentle flexure, as no trace of a slope of tectonic origin is noticeable in this region. In short, the western margin of the southern block of southeastern Sikoku has been dropped down to the depressed area of the Koti plain by a gentle westward downwarping of the earth crust.

5. Coastal District of the Southeastern Side.

General Remarks: Marked morphologic differences are found between the coastal districts of the eastern and the western sides of southeastern Sikoku. No trace of marine terrace that is so distinguishing a characteristic of the east coast of the Tosa bay is recognizable northeastward from cape Muroto. Simple outline of the coast with its concave side toward the ocean as well as an abrupt seaward descent of the bordering cliff characterize throughout the coast from cape Muroto to as far northeastward as cape Gamoda, and no appreciable breadth of littoral plain is attached at the foot of the cliff.

Although the entire coast line has a similarity in broader aspects, it differs in details. For, while the southern portion is fringed with a steep cliff exceeding 500 m in height, the northeastern portion has numerous short embayments along the steeply inclined slope. The difference is also found in submarine relief. In the south submarine continuation of the steep subaerial cliff can be traced to a depth of more than 1000 m, but there is a gentle submarine slope in the north. In this way, the coastal district of this region may be divided into two portions of somewhat dissimilar geomorphologic features. They will be treated separately in the following.

Fault Coast from Cape Muroto to Cape Aziro: Northward from cape Muroto to None, a high cliff is bordering the coast with a narrow littoral plain not exceeding 200 m in breadth at its foot. The height of the cliff ranges from 500 m to 700 m. Submarine relief of this portion teaches us the submarine continuation of this cliff without accompanied by a continental shelf. The following three possible origin of this steep slope will be presented in order to afford some clue to the interpretation of the genesis of this coastal district. That is; a) that the steep cliff represents the mature stage of shoreline cycle due to the prolonged marine erosion; b) that the region as a whole is a depressed remnant of the once extensive mountain land of considerable relief, and the present steep cliff bordering the coast is originally of subaerial origin, and is happened to be at the present level by a prolonged later subsidence, or c) that the steep cliff was essentially formed by a tectonic event either by faulting or by steep flexure.

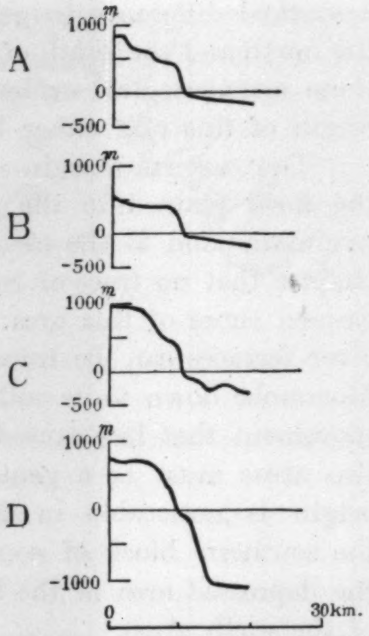

Fig. 6. Profiles of the southeastern coast in alphabetical order from the northeast to the southwest.

If the first assumption may be valid, the present sea-facing escarpment must be a sea cliff formed by the long continued marine erosion, and the simple outline of the coast is explained by the action of the refraction of waves. Admitting this explanation, there must be a complementary extensive abrasion surface at the foot of the cliff. Submarine chart of this region teaches us the direct continuation of the bold subaerial cliff to the steep submarine slope without accompanied by any appreciable abrasion surface in front. This is well shown in Plate 18 and D of Fig. 6. Therefore, we can not expect the validity of this explanation for the formation of this cliff.

In regard to the second assumption, we notice that the end of the long spurs that are projected seaward from the main divide of the mountain land of this portion are cut by this bordering cliff. In other words, the end of these long spurs are intersecting with this steep cliff with high angle; a fact that can not find a due explanation when we consider the origin of this cliff as mainly of subaerial erosion.

The third assumption that the steep bordering cliff is of tectonic nature has already been proposed by Y. Ôtuki and H. Simomura. The intersection of the trend of the coast line with that of the projecting spurs, the absence of a complementary abrasion surface in front, the direct continuation of the cliff to the submarine slope down to an extraordinary depth of more than 1000 m, the remarkable simple outline of the coast; all these geomorphologic features will be explained satisfactory by considering the coastal cliff as of tectonic origin. The steep inclination of the subaerial as well as the submarine slope of this cliff will be explained better by faulting than by flexure, as has already been stated by H. Simomura. At present, marine erosion has caused the slight recession of the cliff.

The absence of marine terraces along this side will be well explained by the earth-movement of this kind. It is evident from what has been stated, that while intermittent type of uplift has been in progress along the western side, faulting has been taking place along the southeastern margin of the mountain land of Sikoku.

Northward from None the simple outline of the coast is replaced by the submerged type of shoreline dominated by many embayments and outlying islands, although the shoreline as a whole maintains the same trend. Also the width of the continental shelf in front is greatly increased, and there is a comparatively gradual descent of the sea floor from the coast. Between None and cape Aziro short embayments are embraced by the projecting spurs. Depression that has allowed the penetration of the sea water into the former valleys of fluviatil origin must have been marginal in nature, as vigorous downward corrasion that is taking place in the immediate interior tells the recent progress of mountain growth in the inland. Thus the marginal downwarping to the east has been made clear. This movement is the northward continuation of the faulting above noted.

Coastal District from Cape Aziro to Cape Gamoda: To the north of cape Aziro the coastal outline changes the general trend somewhat eastward until cape Gamoda is reached at the eastern tip of the island. The characteristic common throughout the area is the accordance of the general trend of the coast line with that of the main ridges in the adjacent interior. The important ridges of the mountainous interior of this region are the eastern extremities of the main divides of the island, and parallel valleys with intervenning ridges are the distinguishing characteristics of this region. From the top of the southern-most ridge

there is an abrupt southward descent down to the sea level, and thus the trend of the present coast line is determined. The height of this ridge top ranges up to 450 m. Short embayments not exceeding 2 km in length are developed along the shore, and a row of islands projects off eastward from cape Gamoda. Also in the south another row of islands is shooting off from cape Aziro eastward, taking a subparallel trend to the ridges, and consequently to the coast line now under discussion. A longitudinal valley is enclosed between this ridge and the one further to the north; all run subparallel to the present coast line.

From what has been stated so far, we are able to consider that the present coast line has been determined by a considerable amount of the depression of land by which the northern side of a former longitudinal valley has happened to meet with the sea level. A row of islands that projects eastward from cape Aziro will be the depressed remnant of a ridge farther to the south. As no sign of recent depression is recognizable in the inland to the north of the coastal district, we must postulate the marginal flexure near the present shoreline.

It is highly probable that this movement belongs to the same system as that which has caused the formation of the fault coast in the southern portion, although the amount of vertical displacement is far inferior to the latter. Taking the entire stretch of the coast discussed in the present chapter, we find out that the intense vertical movement represented by the profound faulting in the southwestern portion gradually gives way to a gentle marginal downwarping with decreasing amount of vertical movement as we proceed northeastward.

6. Depressed Area of the Eastern End of the Sikoku Mountain Land.

Along the eastern end of the Sikoku mountain land, the edge of the maturely dissected margin has many characteristic features of the depressed coast. Especially is it true in the southern part where several rows of promontories are embracing long estuaries between them. The promontories are the eastward continuation of the ridges of the mountain land, and naturally, the enclosing estuaries can be traced landward into the longitudinal valleys between. Many outlying islands are projected off farther eastward from the tips of the promontories. The small development of deltas at the bay heads as well as the absence of

high sea cliff along the shore indicate the youthful stage of marine cycle of the depressed coast.

The coast line of the northern portion of the area has been greatly simplified by the delta building, although irregular outline of piedmont line with projecting spurs and wide waste-filled valleys bear evidences of the recent date of depression. Also many isolated hills are protruding above the level floor of the alluvial plain. Steep valleys in these small hills have every characteristic of the upper stream region of the maturely dissected mountain land of considerable relief, showing that the hills are the depressed remnants of the former ridge tops. Relics of wave action are well preserved around the foot of the isolated hills.

These minor differences in the coastal outline of the north and the south will be mainly due to the difference in the transportation power of the waste by the rivers. For while the rivers that are vigorously prograding the northern portion are of considerable size whose source can be traced far up in the interior part of the mountain land, those of the southern portion are of local origin, and are only sufficient to build minor deltas in the tranquil water of the heads of the embayments.

Depression that has induced the drowning of the maturely dissected margin of the mountain land of this region must have been marginal in type, as no delay of downward corrasion is recognizable in the immediate inland. We see also that only the eastern extremity of the maturely dissected fault scarp along the Median Line has distinct marks of depression represented by detached hills and wide waste-filled valleys, and that the steep marginal inclination of the general altitude eastward is recognized as shown in Plate XVIII and Fig. 3.

Along the western coast of the Kii mountain land, the genesis and the subsequent development of the morphology of the coastal district is the mere duplication of this region. We are able to consider that the steep downwarping will account for the separation of Sikoku from Kii, and thus the formation of the Kitan strait. The recent continuation of this movement is clearly manifested by the absence of the high sea cliff around the partly submerged ridges and islands, and by the small development of deltas at the bay heads. This is a type of movement that has induced the separation of the once continuous mountain range of the Outer Zone into the four separated mountain lands.

Lastly, attention must be drawn to the fact that although the two rows of fault lines that traverse the interior part of the mountain land terminate in this region, no differential movement bounded by these fault

lines is noticed so far as the coastal features are concerned, although in the west a marked differential movement by the activity of the fault is well evidenced in the Kôti plain. Shortly speaking, downwarping that has resulted in the formation of the Kitan strait is the dominant factor in determining the present coastal features.

7. Modes of Recent Crustal Movements of Southeastern Sikoku as Determind by the Geomorphological Studies of the Coastal District.

We have now come to the end of our inquiry, and the modes of crustal movements that can be inferred from the morphological studies of the coastal district should be briefly summarized in the following.

1) From the morphological studies of the mountain land of southeastern Sikoku, it is perhaps possible to state that the present configuration of the area in question is an outcome of the overlap of two stationary earth waves, one proceeds in equatorial direction, or in accordance with the general trend of the insular arc of this portion, and the other proceeds in meridional direction or normal to the former. It is at the point of the present highest altitude where the crests of these two waves are supposed to have overlapped one above the other. The troughs of the equatorial wave are represented by the straits by which the mountain range of the Outer Zone is separated into the four independent mountain lands. A trough lying between the two mountain masses of Sikoku is not deep enough to induce the complete separation of these two land masses.

The meridional wave is accompanied by faulting as an accessory phenomenon. Three rows of fault lines that run subparallel one another in equatorial direction have divided southeastern Sikoku into three separated blocks of lands each of which is elongated in accordance with the trend of the fault lines.

While the outline of the equatorial wave is rather symmetric in spite of the shallower western trough, the meridional wave in general is much assymmetric with its steep northward inclination and gentle southward slant from the crest. The overlap of the waves of these sorts will account for the present major configuration of southeastern Sikoku.

It has been suggested, also, by the existence of many steps of erosion levels that the mountain growth by these wavy motions of the earth's crust was of more or less intermittent in type.

2) After the establishment of the major configuration, the area has undergone steep marginal flexure which is well revealed in a steep seaward inclination of the summit level along the coast. The marginal flexure is in places replaced by faulting. The continuous fault scarp along the northern margin and the fault coast along the southeastern shore will account for this type of movement.

3) The recent activity of this marginal flexure is well manifested in the present coastal features. This movement is likened to that of a seesaw rotating upon its axis, that is, the upheaval toward landward and the depression toward seaward. Here the axis line is regarded as a boundary line of upheaval and depression in reference to the sea level. The coastal district is fringed with marine terraces if the axis line lies off from the coast. On the other hand, the coastal district has distinct characteristics of the depressed type if the axis line lies in the inland. The considerable variety of the coastal features of this region is mainly explained in this way.

4) Signs of uplift are found in several steps of marine terraces along the southeastern coast of the bay of Tosa. Frequent alternation

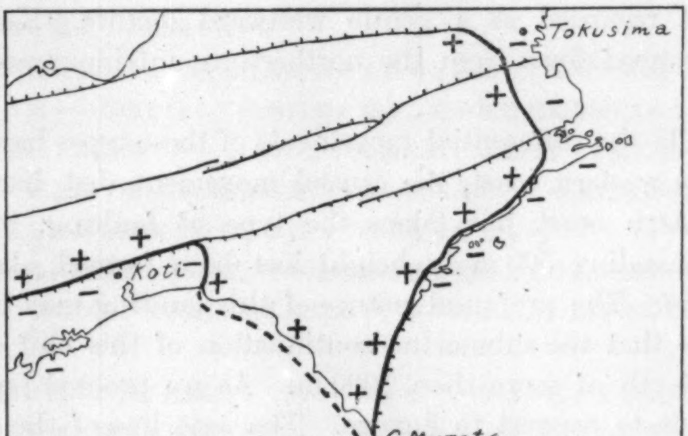

Fig. 7. Showing the distribution of the upheaved and the depressed areas as determined by the geomorphological studies of the coastal district.

+ Upheaved area
— Depressed area

The boundary line of upheaval and depression in reference to the sea level is drawn with a specially thick line.

of intermittent uplifts with periods of comparative quiescence is inferred from the several steps of marine terraces with their complementary sea

cliffs at the rear.

The periods of rapid uplifts during which the abrasion surfaces were emerged may be again analysed into frequent alternation of intermittent uplifts of minute amount with intervals of repose during which the time was not long enough to completely cut back the narrow abrasion surfaces in front. The uplifts of about 5 feet and 4 feet on the occasions of the great earthquakes of 1707 and 1854 respectively were the latest movements of this type.

In the southeastern portion, three major steps of abrasion surfaces with their corresponding sea cliffs suggest the thrice repeated periods of rapid uplifts with intervals of comparative quiescence. No appreciable amount of depression is considered in the course of the successive formation of these terraces. The gradual decrease in the amount of uplift westward from Nahari throughout the entire duration of the formation of these terraces is revealed in the gentle westward decrease in their altitude respectively.

5) To the west of cape Tei, the area of recent uplift gradually merges into the depressed area of the Koti plain. The type of this crustal movement is regarded as a gentle westward flexure. Koti plain has also been dropped down from the northern mountainous area by a fault scarp.

6) While the differential movements of these types have been going on along the western coast, the crustal movement that has determined the southeastern coast has taken the type of faulting, by which the steep cliff exceeding 500 m in height has been formed along the present shoreline. The profound nature of this faulting may be understood when we see that the submarine continuation of this cliff can be traced down to a depth of more than 1000 m. As we proceed northward, the faulting tends to convert to flexure. The axis line of the movement is assumed in the inland close to the present shoreline, and thus the short drowned valleys and outlying islands are accounted for.

7) The eastern end of the Sikoku mountain land has been dropped down by a steep marginal downwarping. This movement is well evidenced by the steep eastward inclination of the summit level, by the development of submerged features along the coast as well as the definit signs of mountain growth in the adjacent interior. The axis line of the crustal movement must have passed through somewhat inland from the present shore. This movement, together with the westward downwarping of the western end of the Kii mountain land, accounts for the formation

of the Kitan strait. The idea of the recent continuation of this movement is evidenced by the youthful stage of the shoreline of depression represented by the absence of high sea cliffs around the projecting promontories and outlying islands.

---

16. 四國東南部の海岸地形とその地殼運動に對する意義

渡　邊　光

東部四國山地の海岸地帶の地形學的研究から、この地域に如何なる樣式の地殼運動が近時行はれたかを知らうと試みた。取扱つた地域は德島から室戶岬を經て高知に至る迄の海岸である。結論を要約すれば

1) 今日の東部四國山地の大體の輪廓は二つの別の方向を有する地殼の定常波に依つて生じたものであると思はれる。一は大體東西の方向の波であつて、即ち島孤の方向に略〻一致するものであり、他の一は南北の方向をとり、島弧に對しては略々直角に交るものである。この二つの波の峯が略々一致した箇所が今日の山地の最高部を構成して居る。東西方向の波の谷の部分は外帶山地を分離して居る所の海峽に依つて代表されて居る。四國山地の東部と西部との間に在る底い部分も一の谷であらうが、海峽を構成する程深くない。

南北方向の波には隨伴現象として斷層運動が認められる。最北をなすは中央線に沿ふ北面斷層崖であり、それと略々同一の方向を持して山地內部を切る二條の地形的斷層が認められる。而してこの波は其の形狀が著しく非對稱であつて、北の方中央線に對して急に下り、南に徐々に傾いて居る。室戶岬附近のカスプ狀をなす海岸線の輪郭は東西方向の波の峯と、この南北方向の波の南方への徐々の傾きに依つて生じた面と海面との交りに依つて說明さる可きものであらう。

2) この山地の輪郭が出來上つてから、その邊緣部は急な撓曲を受けた。撓曲は所に依つては斷層に移化して居るのであつて、中央線に沿ふ斷層崖や、室戶岬東北方の斷層海岸の如きはそれである。

3) この邊緣撓曲は近時に到る迄繼續して居るのであつて、今日の種々多樣の海岸地形は、この撓曲が行はれる際に海面に對する相對的の隆起と沈降の境界線に當る箇所の位置の相異に依つて生じたものに他ならない。即ち、若しこの境界線が陸地內にあれば、陸地のその箇所より海の方にあたる部分は溺れて沈降形の海岸地形を示し、これに反して若しそれが海中にあれば、海岸線附近は隆起して海岸段丘の發達を見るに到つたのである。

4) 隆起の證跡は土佐灣の東岸に海岸段丘として見出される。海岸段丘は東南部に於て三段を數へ、最高のものは 300 m 位から 220 m 位迄徐々に下る面であり、中段はそれと 40 m 程の海蝕崖を以て境され、180 m より 120 m 位迄下る海蝕面、最下段は約 100 m の高さの海蝕崖を以て中段と接し、舊汀線を 10 m 程の所に有する極めて最近の起原のものである。この事實から、最高段の背後の海蝕崖を生じた比較的地盤の垂直運動の激しくなかつた時代以來三回の比較的地盤運動の激しかつた時代と、その間に狹まれた二回の緩漫な時代とが在つた事が解る。而して今この時代を通じて海蝕力が一定と假定するならば、最下段の段丘の背後にある 100 m 以上の海蝕崖を形

成した地殻運動の緩漫な時代は、中段の背後にある 40 m の海蝕崖を生じた時代よりも長時期に亘つた事が言へる。

これらの段丘面を更に精しく吟味する時は各が更に多くの細かい段より成る事を知り得べく、これらの段丘面は海蝕面そのままの傾斜よりも急になつて居る。從つてこれら海蝕面を隆起せしめた運動の様式は短時日間に行はれた急激の垂直運動ではなく、何回にも亘つて間歇的に行はれた小隆起の積算に依るものである事が解る。ただその間に狹まれた比較的靜止の時代が新に前面に附加された隆起海蝕面を全然破壞し去る程長時に亘つたものでなかつたのである。寶永四年の大地震の際行はれた室津附近の約 5 尺の隆起及び安政元年の 4 尺程度の隆起はこの種の間歇的隆起の最近のものに外ならない。

最高の段丘が形成されて以來著しい沈降運動は行はれなかつた。尙海蝕崖形成の時代にもこの間歇的小隆起は行はれて居たのであらうが、隆起の量が尠かつたか、或はその間の靜止の時代が長かつたかの爲に、新に前面に附加された海蝕面が海蝕に依つて取り去られたものであらう。

以上の段丘は尖端室戸岬より奈波利迄は略々同様の發達狀態をなして舊海蝕崖の高さも一致して居るがそれより西に行くに從つて各々その高さを減じ、手結岬迄及んで居る。

5) 手結岬の西には隆起の證跡はなく、高知平野の沈降區域に移化して居る。この差異は手結岬以西に於ける西方への下撓曲に依るものと思はれる。尙高知平野はその北方の山地から比高約 300 m の斷層崖を以て陷落して居る。

6) 土佐灣の沿岸に於て此の様な差別運動か行はれて居た間に、此の地域の東南岸には斷層運動が行はれ、斯て室戸岬より北々東に走る斷層海岸を生ずるに至つた。この斷層運動の垂直變位の甚しかつた事は約 500 m の高さを有する陸上の急崖がその下に殆ど海蝕面を作ることなく 1000 m 以上の深さ迄海中に追跡することが出來る事からも想定される。東北方に赴くにつれて斷層は撓曲に移化して居り、海面に對する隆起と沈降の境界線が岸に接して陸方に在つた爲に現在見る短い溺れ谷が生じたのである。

7) 四國山地の東緣は急な下撓曲に依つて東方に下つて居る。この運動は紀伊半島の西緣の西方への下撓曲と相俟つて紀淡海峽の成因をなすものである。この際隆起と沈降の境界線は多少現在の海岸線から距れて陸方に在つた爲に壯年的に開折された山地の邊緣部が溺れて沈降形海岸地形を現して居るのである。又この下撓曲が最近に至る迄も繼續して行はれて居る事はこの沈降海岸の海蝕輪廻が未だ殆んど進んで居らないことからも了解する事が出來る。

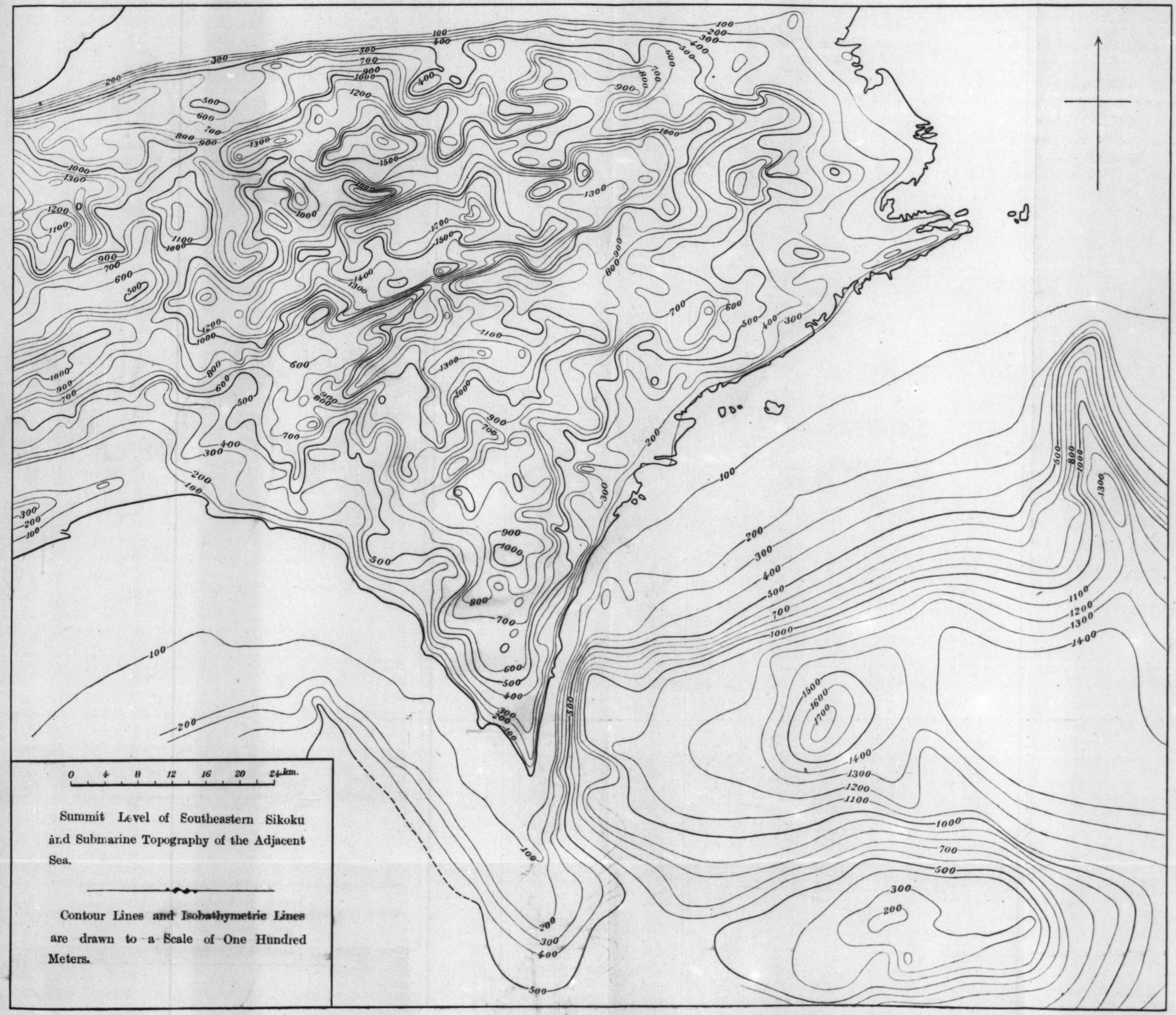

(震研彙報、第十號、圖版、渡邊)

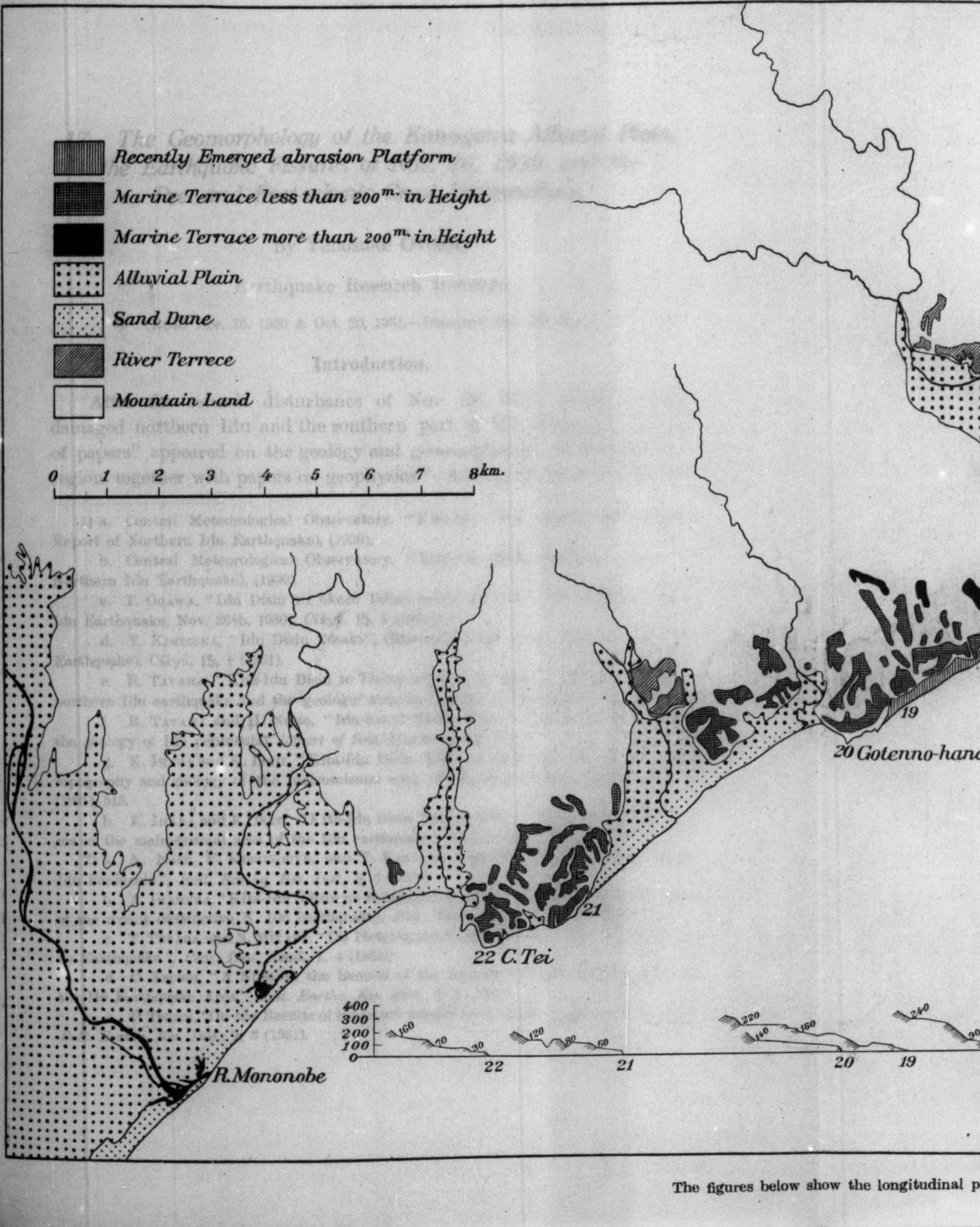

The figures below show the longitudinal p

(震研彙報、第十號、圖版、渡邊)

Distribution of marine terraces along the east coast of the bay of Tosa

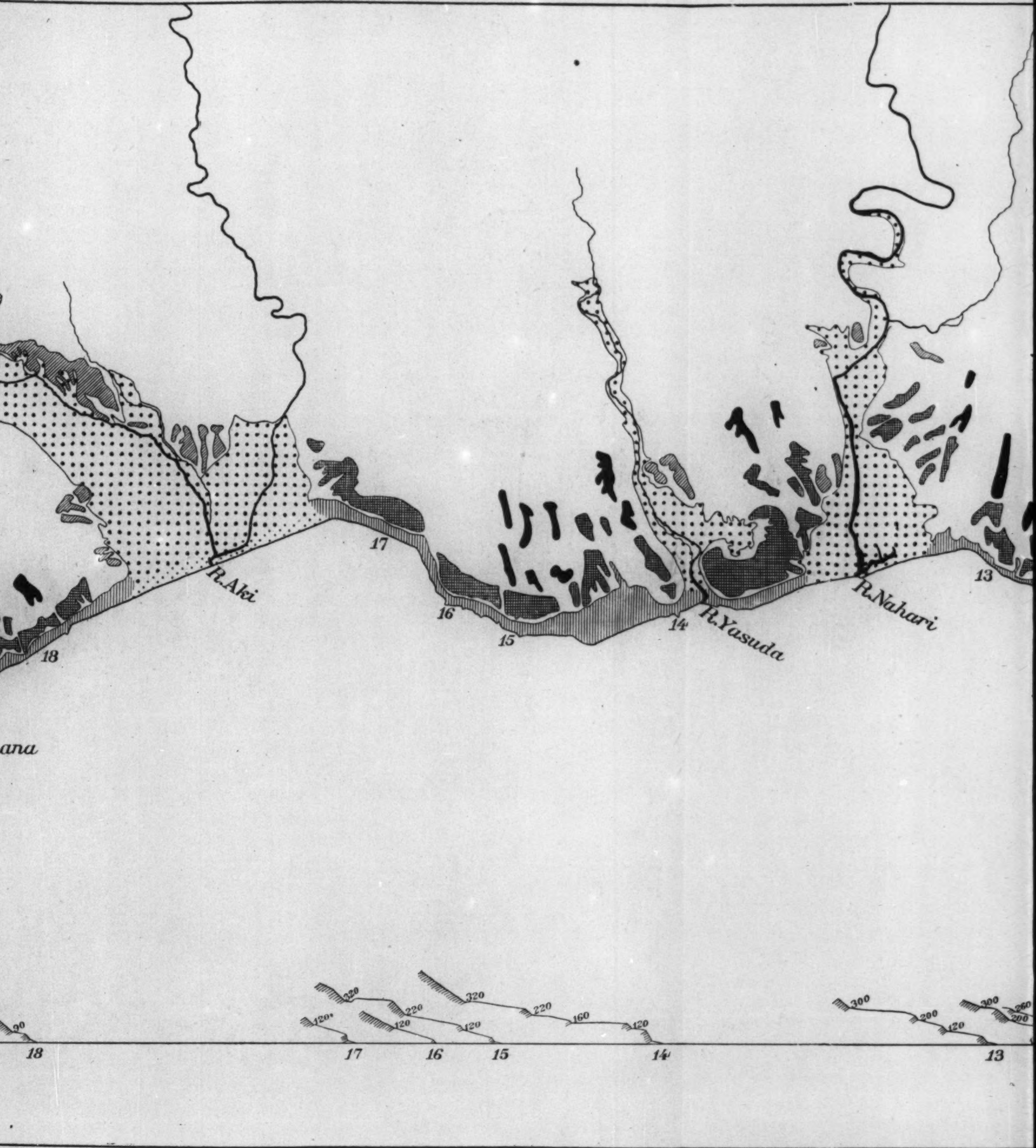

l profiles of marine terraces. The height of the terraces is shown by the arabic figures in meter. Numbers along the shore indicate the sites

Distribution of marine terraces along the east coast of the bay of Tosa

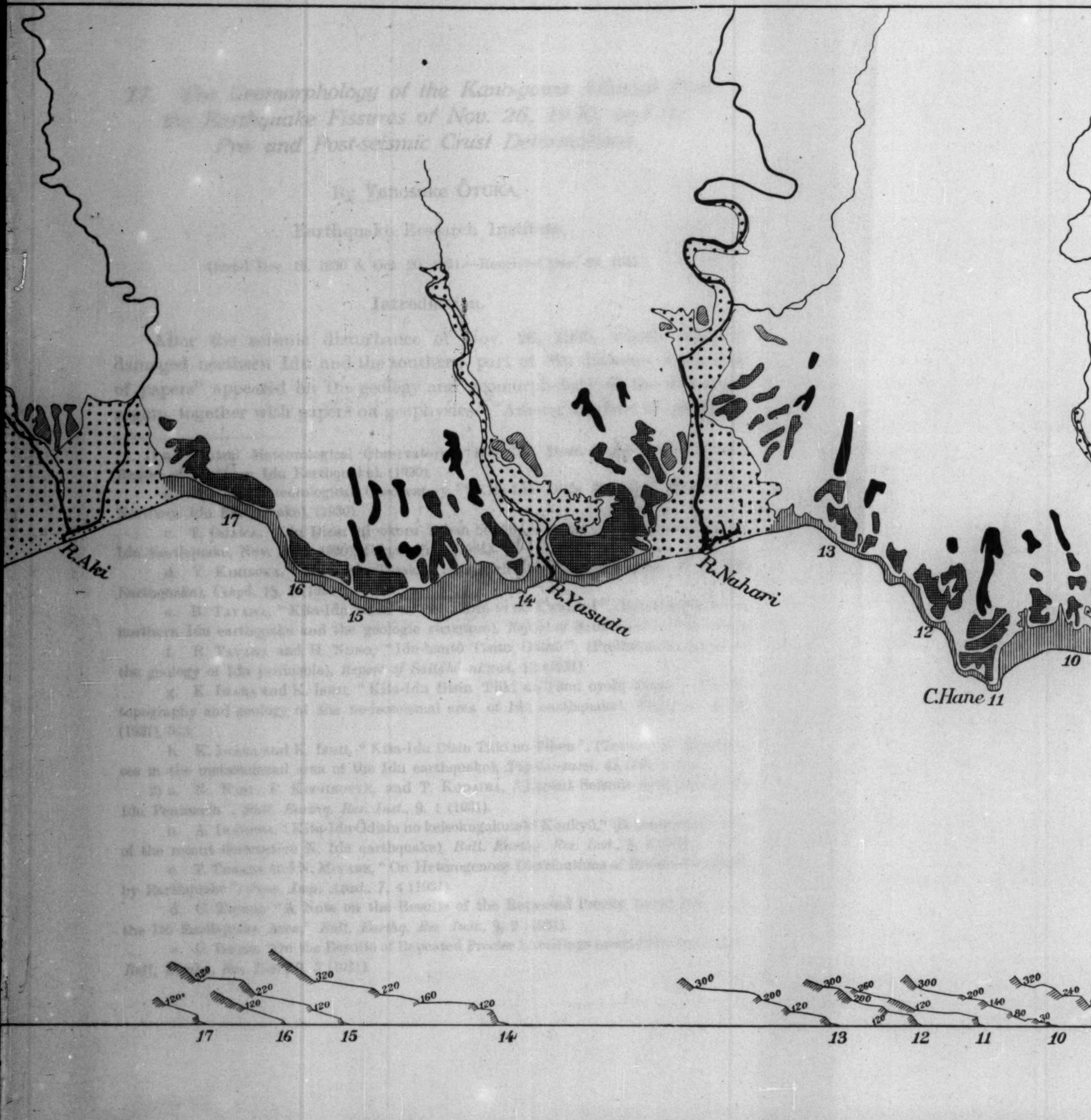

terraces. The height of the terraces is shown by the arabic figures in meter. Numbers along the shore indicate the sites of the starting points of the

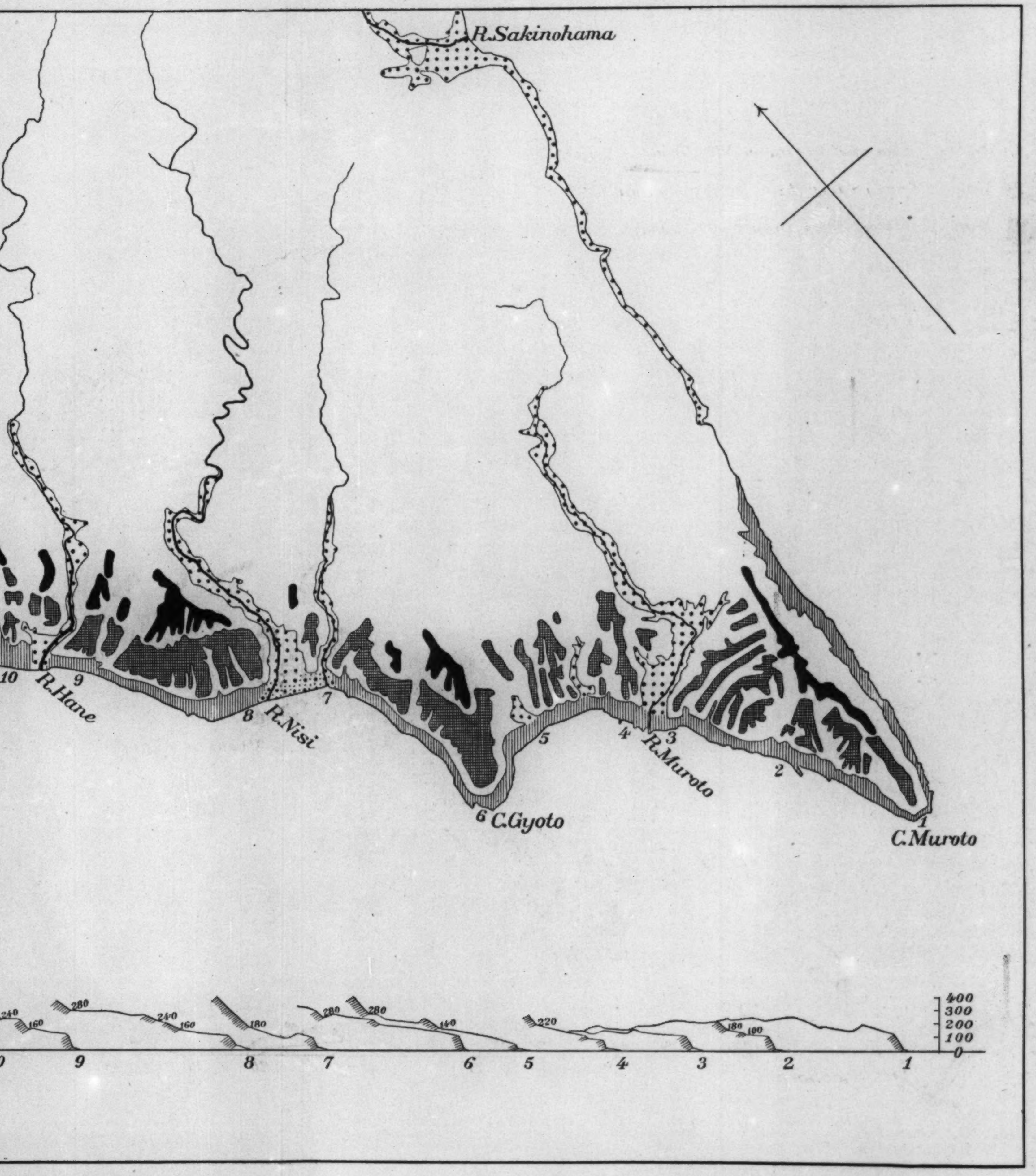

the corresponding profiles below.

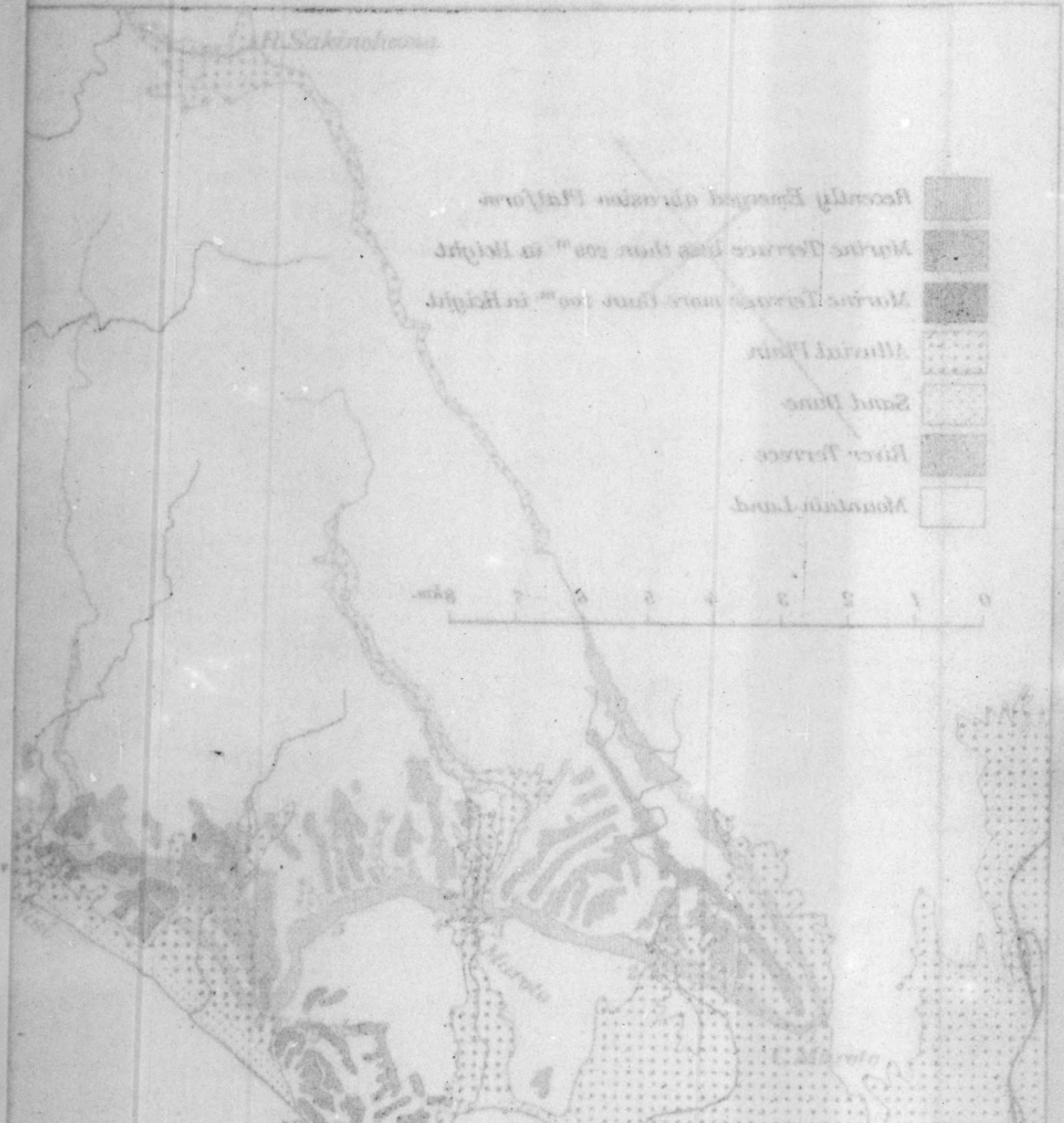

The figures below sh

17. *The Geomorphology of the Kano-gawa Alluvial Plain, the Earthquake Fissures of Nov. 26, 1930, and the Pre- and Post-seismic Crust Deformations.*

By Yanosuke ÔTUKA,

Earthquake Research Institute.

(Read Dec. 16, 1930 & Oct. 20, 1931.—Received Dec. 20, 1931.)

Introduction.

After the seismic disturbance of Nov. 26, 1930, which severely damaged northern Idu and the southern part of Mt. Hakone, a number of papers[1] appeared on the geology and geomorphology of the disturbed region, together with papers on geophysics.[2] Among the host of questions

1) a. Central Meteorological Observatory, "Kita-Idu Disin Gaihô", (Preliminary Report of Northern Idu Earthquake), (1930).

b. Central Meteorological Observatory, "Kita-Idu Disin Hôkoku," (Report of Northern Idu Earthquake), (1930).

c. T. OGAWA, "Idu Disin ni okeru Diban-hendô ni tuite", (Dislocations of the Idu Earthquake, Nov. 26th, 1930), *Cikyû*, **15**, 1 (1931).

d. Y. KIMIZUKA, "Idu Disin Tôsaki", (Research Trips to the Regions of the Idu Earthquake), *Cikyû*, **15**, 1 (1931).

e. R. TAYAMA, "Kita-Idu Disin to Tisitukôzô to no Kwankei", (Relations between northern Idu earthquake and the geologic structure), *Report of Saitôhôonkwai*, **11** (1931).

f. R. TAYAMA and H. NIINO, "Idu-hantô Tisitu Gaihô", (Preliminary report of the geology of Idu peninsula), *Report of Saitôhôonkwai*, **13** (1931).

g. K. IHARA and K. ISHII, "Kita-Idu Disin Tiiki no Tikei oyobi Tisitu", (On the topography and geology of the meizoseismal area of Idu earthquake), *Tigaku-zassi*, **43** (1931), 513.

h. K. IHARA and K. ISHII, "Kita-Idu Disin Tiiki no Tihen", (Terrestrial disturbances in the meizoseismal area of the Idu earthquake), *Tigaku-zassi*, **43** (1931), 514.

2) a. N. NASU, F. KISHINOUYE, and T. KODAIRA, "Recent Seismic Activities in the Idu Peninsula", *Bull. Earthq. Res. Inst.*, **9**, 1 (1931).

b. A. IMAMURA, "Kita-Idu Ôdisin no keisokugakuteki Kenkyû," (Seismometric study of the recent destructive N. Idu earthquake), *Bull. Earthq. Res. Inst.*, **9**, 1 (1931).

c. T. TERADA and N. MIYABE, "On Heterogenous Distributions of Houses Destroyed by Earthquake", *Proc. Imp. Acad.*, **7**, 4 (1931).

d. C. TSUBOI, "A Note on the Results of the Repeated Precise Levellings across the Itô Earthquake Area," *Bull. Earthq. Res. Inst.*, **9**, 2 (1931).

e. C. TSUBOI, "On the Results of Repeated Precise Levellings around Idu Peninsula," *Bull. Earthq. Res. Inst.*, **9**, 3 (1931).

that this earthquake has raised, what geologists and geomorphologists would in particular like to have answered are: What are the relations between the earthquake fissures and the geology and geomorphology of this disturbed region? What connections have the earthquake fissures with the crustal displacements as revealed by levellings made both before and after the catastrophe?; and what relations have the crustal displacements that went on during the last 35 years with the present geomorphological features?

From the tectonic point of view, the Idu Peninsula, which projects into Sagami Bay, in the bottom of which Bay were located the epicenters of the great Kwantô earthquake of Sept. 1, 1923, is situated on the southern part of Naumann's *fossa magna*, where the early Pliocene strata were severely disturbed, and between the two geotectonic lines of Itoigawa-Siduoka and Nirasaki-Suntô. Many volcanoes of the Hudi (Fuji) volcanic group which are connected with these geotectonic lines are distributed in this peninsula. Geologically speaking, the basement complex of the peninsula is built up of igneous and also pyroclastic Neogene rocks. After they had been deposited, these pyroclastic formations were deformed into complicated structures by crustal movements during late Tertiary[3] and were sculptured into more or less rugged reliefs by subaerial denudation. After that, these regions suffered in part through transgression of the lowest Peistocene. On these reliefs the early Quaternary volcanoes, such as Atami,[4] Yugawara,[5] Hakone,[6] and Amagi[7] became active, in the order named, with numerous block movements.

Then the basal reliefs that were sculptured in the late Tertiary were thickly covered with the younger volcanic materials (lava and ashes), and were changed into smooth reliefs (e.g., western slope of Tan'na,[8] Tanakayama[9] Forest, etc.) which contrast strongly with the older reliefs, which are destitute of younger volcanic material (e. g., Kanuki-yama,[10] Tokura-yama,[11] Wasidu-yama,[12] etc.). Pl. XXI, Fig. 1.

The recent fluviatile erosion that dissected these two reliefs, both rugged and smooth, made some erosion valleys filled with young fluviatile deposits of the Kano-gawa,[13] the Kise-gawa,[14] and others. The Kano-gawa Alluvial plain is a plain composed of these young fluviatile materials.

It is worth noting that although the severely shaken regions of the

3) Y. ÔTUKA, *Bull. Earthq. Res. Inst.*, 9, 3 (1931).

4) 熱海. 5) 湯河原. 6) 箱根. 7) 天城. 8) 丹那. 9) 田中山. 10) 香貫山. 11) 戸倉山. 12) 鷲頭山. 13) 狩野川. 14) 黄瀬川.

Idu earthquake of 1930 consist of these younger formations, the area of the older reliefs of basement complex were hardly scarred by any marks of disturbance.

The writer believes that two distinct aggregations of geologic forces were at work in bringing about that Idu earthquake, one being the forces that were responsible for the formation of the complicated Tertiary structures and the other the forces that were responsible for the distribution of the volcanoes of the Hudi (Fuji) volcanic group. It is unfortunate that hardly any study worthy of the name has been made of this region by Japanese geologists, with the result that there is very little data for the study of the Idu earthquake from the geological side. In these circumstances Professor S. Tsuboi, Ass't Professor H. Tsuya, Mr. H. Kuno, and the writer, all members of the Institute, are now occupied with the geological survey of the region, so that the results of their geologic studies of the Idu earthquake should be available at no distant date.

In this paper will be discussed the tectonic relations of the most recent topography—the Alluvial plain—to the ground disturbances and to the pre- and post-seismic crustal displacements in the Kano-gawa Alluvial plain.

The writer takes this opportunity of thanking the members of the Earthquake Research Institute, the Military Land Survey, the Central Meteorological observatory, Tôkyô, and others for prompt publication of their reports on the Idu earthquake, for by means of these reports his field studies were greatly assisted and facilitated.

Geomorphology of the Kano-gawa Alluvial Plain (Pl. XX)

The Misima fan. The equatorially elongated coastal plain, Ukisimagahara,[15] that fringes the southern foot of Mt. Hudi and Mt. Asitaka,[16] is a very young plain of deposition, so young in fact that not long while ago it was only a lagoonal region. Therefore this young plain may be young Alluvium, contemporaneous with the Sitamati plain of Tôkyô, i.e., the writer's geomorphological plain A_{II}.[17] In that case it is the young deposit that covers the foot of Mt. Hudi.

The southeastern base of Mt. Hudi converges southward and develops a beautiful fan-shaped slope towards the south as far as Misima[18] and Numadu,[19] through the narrow part where the base of Mt. Hudi and that

15) 浮島ヶ原. 16) 愛鷹山.
17) Y. Ôtuka, "Daisiki" (The Quaternary), *Iwanami Kôza.*
18) 三島. 19) 沼津.

of Mt. Asitaka come close to that of Mt. Hakone. This fan-shaped slope is the "Misima Fan."

The materials composing this fan are mostly wastes derived from Mt. Hudi, such as lava flows, ashes, etc. To the writer, intercalation of lava flows with other materials is of no importance in dealing with the large topography of the fan, for the reason that distribution of lava flows does not point to any geomorphological anomalies. (The destroyed houses in the town of Misima were in alignment with these lava flows).[20] The geologic age of the Misima fan is then contemporaneous with or slightly later than that of the coastal plain, Ukisimagahara, although the boundary of the latter is so concordant that no definite line of demarcation can be drawn between them.

The boundary of the fan may be traced from Higasinôdô[20], in the village of Kaneoka-mura,[22] through the northern foot of Kanuki-yama, where the surface of the fan touches the Wasidu mountainland, with discordant boundaries, to Tanita,[23] south-east of Misima town. The boundaries along which run two rivers, Kise-gawa and Sakai-gawa,[24] from the vertex of the fan to both margins, are topographically discordant with the base of Mt. Asitaka on the west and that of Mt. Hakone on the east.

According to Mr. Murata,[25] the special character of the surface contours of the fan is such that the form of the fan is not likely to be affected by the presence at its front, or toe, of any obstacle, even a mountain. If this is so, then the theory of upwarping of the crust will have to be invoked in order to explain the Misima fan, which has a greater southward convexity of contour line than a normal fan.

Rivers on the Fan. The fan is dissected by incisive meandering rivers having a depth of 10 m. As stated by Mr. Murata, their courses are straight from the vertex to the front of the fan. Two of them, the Sakai-gawa and Tama-gawa,[26] turn southwest-ward in their lower courses, where the slope of the fan disappears. The Kise-gawa meanders incisively and excavates laterally in its lower course. It confluxes with the Kano-gawa at the front of the fan, where the Kano-gawa had

20) T. Terada and N. Miyabe, *Proc. Imp. Acad.*, 7, 4 (1931), 146.

21) 東能堂. 22) 金岡村. 23) 谷田. 24) 境川.

25) T. Murata, "Theoretical Consideration on the Forms of Alluvial Fans," *Geogr. Rev.*, Japan, 7, 7 (1931).

T. Murata, "Relation between the Form of an Alluvial Fan and its Marginal Topography," *Geogr. Rev.*, Japan, 7, 8 (1931).

26) 玉川.

dissected it previously; and where the peculiar southward convexity of the contour lines of the fan are exhibited.

Alluvial plain near Daiba.[27] The Kano-gawa Alluvial plain between the Wasidu mountainland and the Tanaka-yama Forest, as shown in Pl. XX, gradually slopes down northward to the southern part of the Kakizawa river,[28] which drains the Tan'na basin; while on the northern side of the river its slope rises to the north and passes into the Misima fan with a concordant boundary. The meandering Kano river, whose course antedates the Misima fan, runs past the fan along the boundary between the Wasidu mountainland and the Alluvial plain to the northwest in a direction opposite to that shown by the contours of the Alluvial plain.

The Alluvial plain near Daiba and the Hatake[29] Hot Springs are parts of the Kano-gawa that were dammed up by the Misima fan and the Wasidu mountainland, so that geologically it is younger than the Misima fan. The plains near Daiba, especially Misono[30] and Simo,[31] Nakasato-mura,[32] Nirayama-mura,[33] and Oohira-mura,[34] being the lowest parts of this region, are subject to floods during the rainy season, with the result that the crust here is weak due to settling of insufficient deposits. Should, however, the width of the valley be proportional to its depth, then the Alluvial deposits may be thicker than has been supposed, although it is only an inference based on the foregoing assumptions, boring being the only way to decide the point. The incised meander courses, as already shown, may have been caused by the very gentle grade of the river floor.

Summarising now what has been said, the Misima fan is a peculiar fan, being intercalated with lava flows. Its topographic characters, however, agree well with the results of Murata's study. One peculiarity that never fails to strike the observer is the greater convexity of its contour lines near the course of the Kise-gawa. The Alluvial plain near Nakasato-mura and Nirayama-mura is a younger plain than the surface of the Misima fan, with a weak crust.

Ground Disturbances of the Alluvial Plain.

For convenience the ground disturbances of the Alluvial plain have been grouped by locality as follows: (1) Matoba, Simidu-mura[35];

---

27) 大場. 28) 柿澤川. 29) 畑毛. 30) 御園. 31) 下. 32) 中郷村.
33) 韮山村. 34) 大平村. 35) 清水村的場.

Nagahusi and Simo, Nakasato-mura;[36] (2) Nitta, Kan'nami-mura;[37] (3) Yatumizo and Akô, Nakasato-mura;[38] (4) Idunagaoka railway station, Nirayama-mura,[39] and Kona, Kawanisi-mura.[40]

(1). Matoba, Simidu-mura, and Nagahusi and Simo, Nakasato-mura. Nagahusi and Matoba were severely damaged but no trace of any ground disturbances could be found except near Matoba, where water spurted from a small earthquake fissure. Southeast of these villages many earthquake fissures were noticed on the Alluvial plain. The sense of these fissures seemed to agree with those of the crust deformations that were measured after the earthquake. Fig. 1, Pl. XXI, shows their distribution.

(a). Across a small road connecting Simo and Misono, small parallel fissures ran N. 80°E. The largest one measured 120 m. in length (Pl. XXII, Fig. 2). Its horizontal and vertical displacements were small. A little north of these fissures were many small ones at the junction of the bed rock and a bank of soil, where the road crosses a small valley. These fissures, or *rifts* as they will be called, must be distinguished from true earthquake fissures. It is notable, as will be seen later, that these rifts occur at the junction of two or more formations having different crust strengths (text fig. a).

(b). A group of large rifts (text fig. b and Pl. XXII, Fig. 4) appears 100 m. east of locality (a), where a path 1 metre wide, and crossed by these rifts, has been displaced 1/3 metre horizontally, but not vertically. This group consists of two large ones and some smaller ones, the larger one of which is traceable for about 200 m. in a N. 65°W.-N. 20° W.-N. 65° W. direction, having the shape of the letter "Z", but with the stem of the letter slanting in the opposite direction. The ground on the southern side of this rift had shifted 1/3 m. westward, relatively to its northern side (Pl. XXIII, Fig. 5). The shorter rift runs N. 60° W. Its displacement is in the same sense as that of the larger rift just mentioned. Paddy

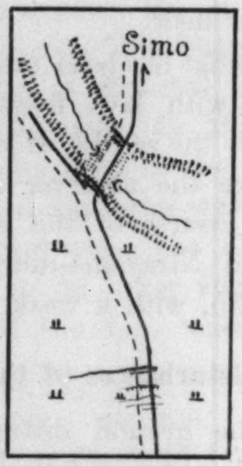

Text fig. a.

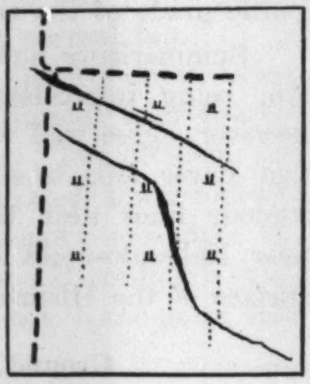

Text fig. b.

36) 中郷村長伏、下. 37) 函南村仁田. 38) 中郷村八溝、赤王. 39) 韮山村伊豆長岡.
40) 河西村古奈.

field dykes that were formerly straight and ran parallel, N-S, were severed and thrown out of alignment about 1/3 m. by the earthquake rifts, the southern side towards the west and the northern side towards the east.

(c). In a dry rice-field along the road just mentioned, and 200 m. south of locality (b), we also find earthquake rifts, which however do not extend as far as the road but run N. 60° W. across the rice-field dykes. Their displacements are the same as those last mentioned (text fig. c, Fig. 3, Pl. XXII). These three groups of earthquake rifts show very small displacements, vertically or laterally.

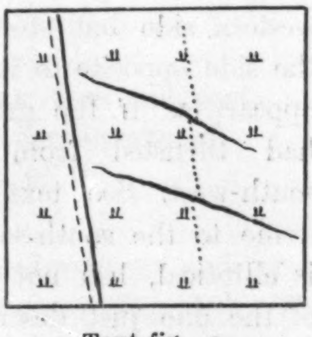

Text fig. c.

(2). Nitta, Kan'nami-mura. On the Sundu Railway line,[41] about 800 m. north of Idunitta station, appears a group of parallel rifts. These rifts, which ran roughly N. 70° E., had bent and even cut the track rails. The ground between these parallel rifts, which were broken and discontinuous lines, had subsided and tilted like a small *graben*, or a small fault angle basin. To a slight extent horizontal shiftings occurred in all directions. Fig. 6, Pl. XXIII shows the rifts with their positions in line with the direction of the said horizontal displacement, while Figs. 7-10 show other examples.

(3). Yatumizo and Akô, Nakasato-mura The mouth of the Akô valley was disturbed in such a way as to appear that the Alluvial deposits which filled this valley had slid down south- or south-westwards. On the southern side of the small spur of the valley that pushes out westwards (Fig. 2, Pl. XXII), the Alluvial deposits slid down southward carrying the railway track about 1 m. south-ward with it, while the ground on the eastern side of the part that had slid was raised relatively about 1/3 m. by a local rift in a N-S direction, (Fig. 11, 12, Pl. XXIV) and formed a meridionally elongated depression between an elongated swell, or elevation, in the same direction and the western slope of the spur (Fig. 2, Pl. XXI). These features resembles that of the landslide in Niigata Prefecture as described by Mr. T. Tokuda.[42]

At *d* in Fig. 2, Pl. XXI, will be seen two domed swells in the rice fields, 300 m. S.S.E. of *a* in Fig. 2, Pl. XXI. (Fig. 13, 14, Pl. XXV). These elevations have a diameter of about 5 m., with a depression between

41) 駿豆鐵道.

42) T. Tokuda, *Geogr. Rev.*, Japan, **3**, 5 (1927), 371-381.

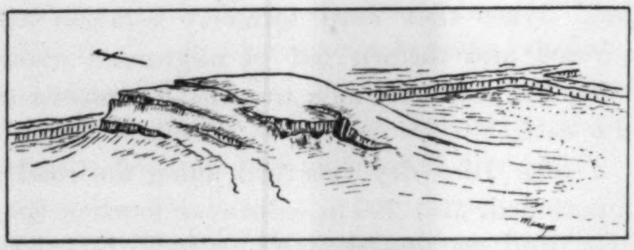

Text fig. d.

them in which water has accumulated. The slope of the dome on the north-east is gentle on its south-western side but steep on the side opposite to it. It appears as if the ground had thrusted from the south-west. See text fig. *d.* The dome to the south-south-east, which is elliptical, has not the steep slope of the one just described, as shown in plan in text fig. *e.* These swells are about 1 m. high.

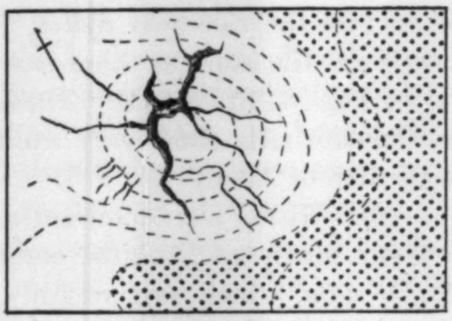

Text fig. e.
(Drowned area is dotted.)

(4). Nagaoka railway station, Nirayama-mura, and Kona, Kawanisi-mura. The earthquake rifts near Nagaoka station on the Sundu railway are on a small scale. Ground water spurted out from a few of them. Their trends are N. 60°W. or N. 40°W. According to Mr. Tanahashi,[43] who studied these earthquake rifts in detail, those near Nanzyô[44] and Kona run N. 40° E. and may be traced for about 100 m.

The conclusion from the foregoing is that the distribution of disturbances indicates the presence of a tectonic zone as marked by a group of rifts on the way from Simo through Nitta and Yatumizo to Akô. It is possible that there are other tectonic centers of earthquake rifts near Nagaoka railway station besides the zone just mentioned.

The foregoing practically covers all the earthquake rifts on the Alluvial plain that were observed by the writer. As to the possible objection that some rifts might have escaped detection, the writer is confident that even should this objection turn out to be not unfounded, it will not adversely affect any future studies that may be based on the inferences stated in the preceding pages.

Disturbances on the Alluvial Plain. The disturbances on the Alluvial plain are divided as follows:

(1). Disturbances caused by differential "strength of crust"; e.g., Kona, Nirayama Matiya,[45] Nanzyô, Hatake, and Tada.[46]

43) TANAHASHI, *Umi to Sora*, **11**, 3 (1931).
44) 南條. 45) 町屋. 46) 多田.

(2). Disturbances caused by differential strength of rocks in the Alluvium; e.g., Misima-mati.

(3). Disturbances caused by the terrestrially disturbed zone; Daiba, Matoba, Nagabusi, Yatumizo, Idunagaoka station.

(4). Disturbances the causes of which are still unknown.

Ground Disturbances and Crust Deformations, Pre- and post-Seismic Disturbances associated with the earthquake of Nov. 1930, and the Geomorphology of the Alluvial Plain.

Soon after the Idu earthquake of 1930, precise levellings and triangulations were repeated by the Military Land Survey (Fig. 15). The results of these measurements were recently discussed by Mr. C. Tsuboi[47]

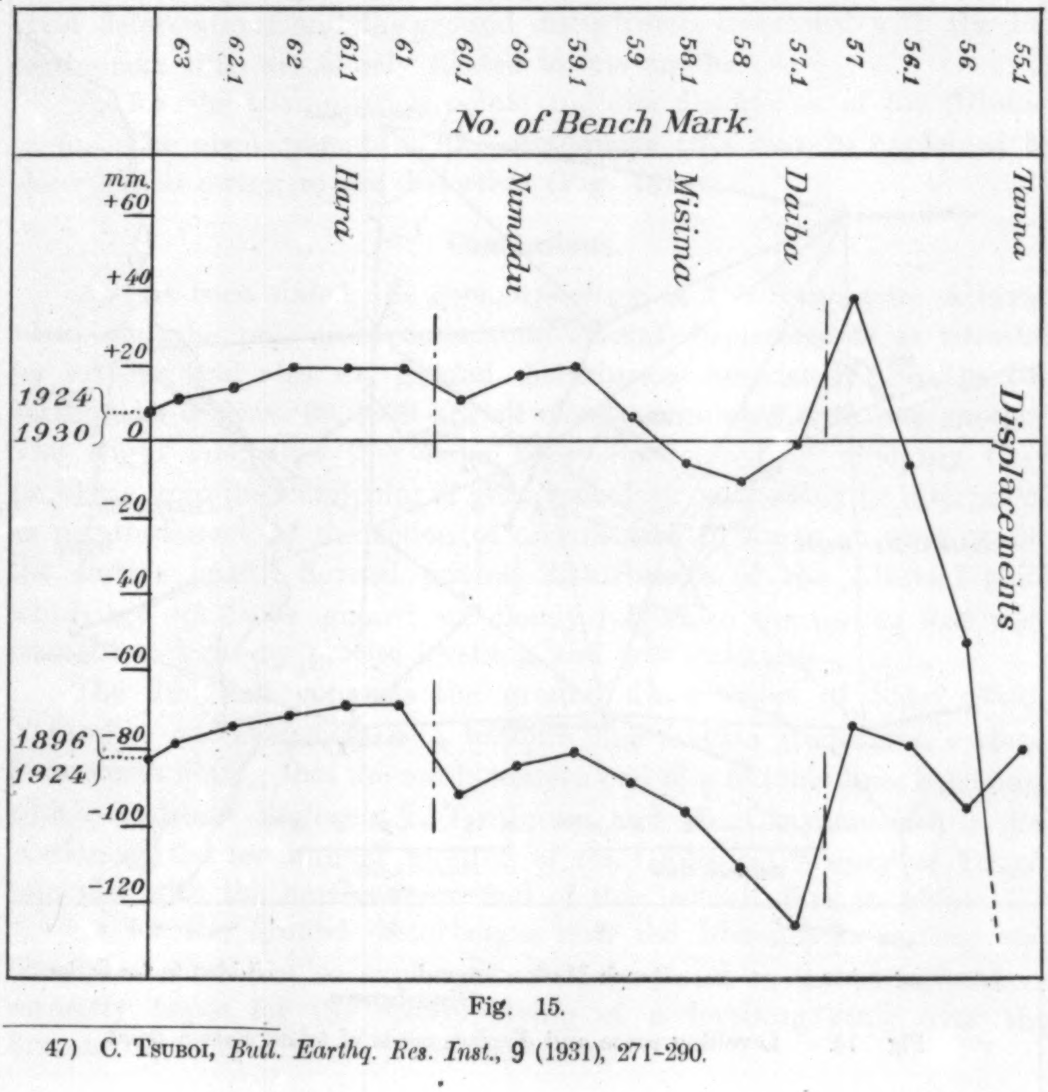

Fig. 15.

47) C. Tsuboi, *Bull. Earthq. Res. Inst.*, 9 (1931), 271-290.

in this bulletin. According to him, in the Kano-gawa Alluvial plain there are block boundaries between bench-marks Nos. 57 and 57.1, between Nos. 59 and 59.1, and between Nos. 9404 and 9405. The mean displacement that occured between bench marks Nos. 57 and 57.1 during the period between 1896 and 1924, as measured in 1924, is smaller than that for the period between 1924 and 1931, during which last period occurred the Idu earthquake. This means that if the pre-seismic change had occurred at a uniform rate, then it is equivalent to the acute changes associated with the 1930 earthquakes. The inferred tectonic zone as previously described, crosses the levelling route between bench-marks No. 57 and No. 57.1, where Mr. C. Tsuboi has marked the boundary line of blocks.

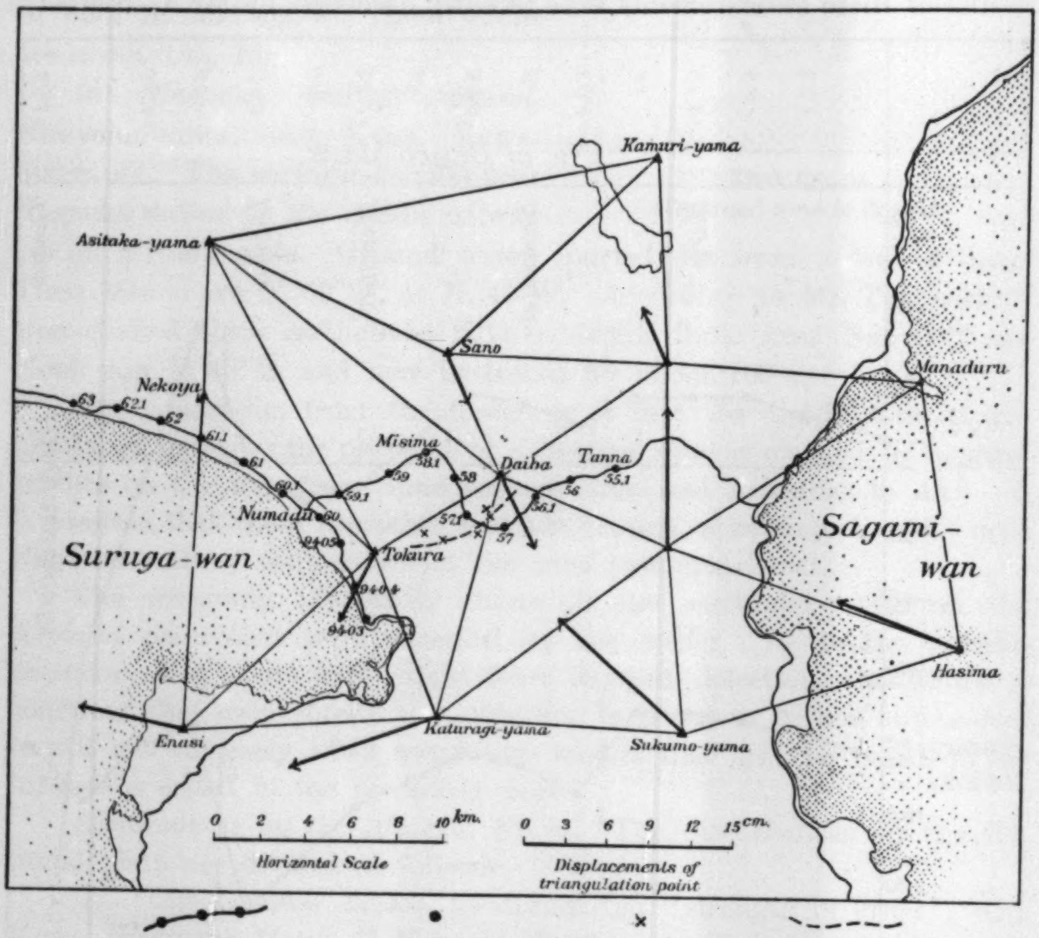

Levelling route Bench Mark Ground Disturbances Hidden tectonic line?

Fig. 16. Levelling route and displacements of triangulation point.

According to the same investigator, post-seismic displacements of bench-marks between No. 57.1 and No. 58 show tilting of the block towards N. 50° E. This tilting is not inconsistent with the ground disturbances near Akô, referred to above. Record of displacements for the past 35 years show tilting of the block farther to the southeast, and it is seen to enhance the grade of the Misima fan. The displacements during 36 years of bench-marks Nos. 57.1, and 58, 58.1, 59, 59.1, and 60 show an anticlinal warping. This is not inconsistent with the sense shown by the peculiar convexity of the contour line of the Misima fan. According to Mr. C. Tsuboi again, there is a block boundary between bench-mark Nos. 59.1 and 60, but it may be regarded as an earth flexure.

From these considerations it will be seen that on the Kano-gawa Alluvial plain, at any rate, the topography, and the pre- and post-seismic crust deformations and the ground disturbances associated with the Idu earthquake 1930 are closely related to one another.

As for the triangulation points indicate distortions of the Alluvial plain. The displacements of the earthquake rifts may be explained by shear action owing to the distortion (Fig. 16).

Conclusions.

As has been stated, the geomorphology of the Kano-gawa Alluvial plain and the pre- and post-seismic crustal displacements as revealed by surveys, and also the ground disturbances associated with the Idu earthquake of Nov. 30, 1930 are all closely connected with one another. The slight anomalies that have been encountered in studying these problems from the standpoint of geomorphology may safely be interpreted as manifestations of the action of certain hidden forces at work under the earth's crust. Several ground disturbances of the Alluvial plain which are apt to be ignored are closely related to the results that were brought to light by precise levelling and triangulations.

The line that connects the ground disturbances of Simo, Nitta, Yatumizo, and Akô may be a tectonic line hidden under the surface. It is worth noting that the south-western end of a tectonic line, regarding which Assistant Professor T. Tsujimura and Mr. Okayama had a discussion at the last annual meeting of the Geological Society of Tôkyô, coincides with the north-eastern end of this tectonic line at Akô.

As for the ground disturbances near the Idunagaoka railway station, the writer has no explanation to offer; and in the circumstances earnestly hopes for the speedy laying of a levelling route over the Simoda highway through Nirayama-mura.

17. 狩野川冲積層地域の地形と昭和五年十一月二十六日伊豆地震の際にその地域に生じた地變及び地殼變形との關係

地震研究所 大塚彌之助

最も新しい地質時代に出來たと考へられる冲積層堆積地域の地形、卽ち三島扇狀地及び狩野川冲積地の地形、とその地表面にできた伊豆地震の際の地變と、伊豆地震の前後に行はれた一等水準點檢測の結果及び伊豆地震前後の一等三角點檢測の結果とはかなり關係があるやうに見える。

そして地形から知られる僅な異常も地殼に絕えず作用してゐる或る力の或る表現とも解することができる。

又一般に輕視されがちな冲積地の種々な地變も水準點の檢測の結果や、三角點の檢測の結果やと比べると密接な關係が生じてくる。

地震の被害もよく吟味してみると地質學的に意味のあるところに分布されてゐるやうであるが、試錐を要する地域では原因不明の被害が相當ある。

中鄕村下から伊豆仁田、八ツ溝を經て赤王に至る地域には地質構造上特異な線、恐らく斷層線が存在するのであらうが、冲積層下に隱れて知られない。唯だ 1931 年の東京地質學會總會の席上に於て辻村助教授、岡山學士によりて注意された山中新田の東南側を走る地形學的異常線の南端が赤王附近に達してゐることは今後の硏究の際に注意する必要があると思ふ。

(震研彙報、第十號、圖版、大塚)

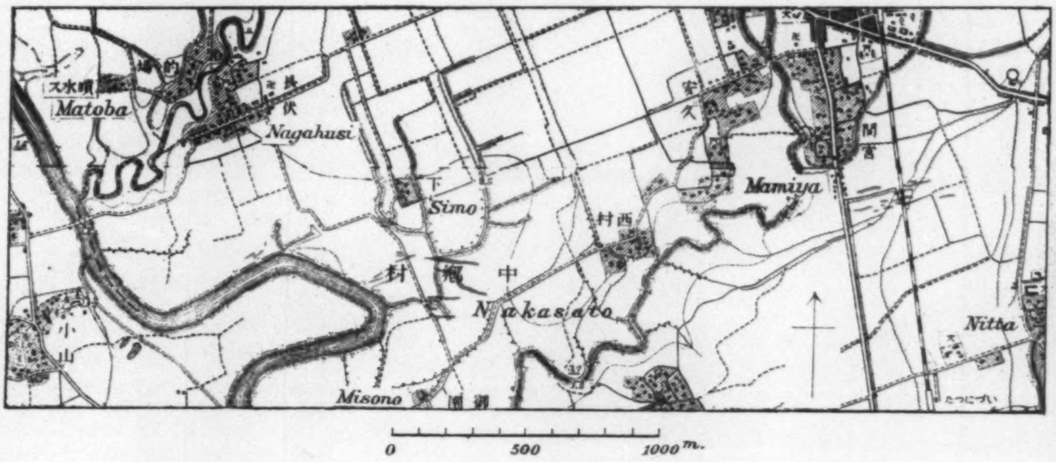
Matoba
Nagahusi
Simo
Mamiya
Nakasato
Misono
Nitta
0
500
1000 m.

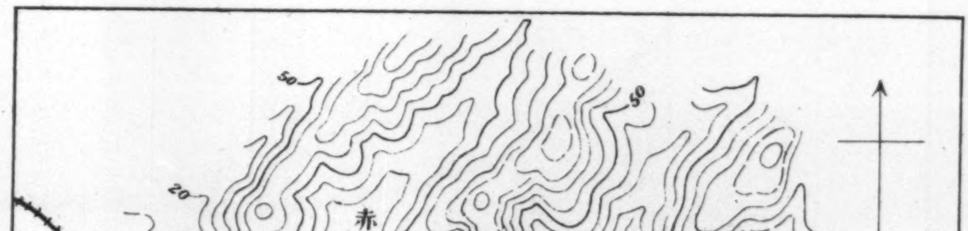
赤王
Akô
上沢
呂多
大場
DAIBA
八ッ溝
Yatumizo
平井
50
20
40
30
0
500
1000 m.

Fig. 1. Kano-gawa Alluvial Plain and Wasidu Mountainland.

Fig. 2. Earthquake rift nr. Simo

Fig. 3. Earthquake rift nr. Simo. Fig. shows the displacement of a rice-field dyke.

Fig. 4. Earthquake rift nr. Simo.

Fig. 5. Earthquake rift nr. Simo. Fig. shows the displacements of troughs.

Fig. 7. Earthquake rift nr. Nitta.

Fig 6. Earthquake rifts nr. Nitta.

Fig. 8. Earthquake rift nr. Nitta.

Fig. 9. Earthquake rift nr. Nitta.

Fig. 11. Earthquake rift nr. Akô.

Fig. 10. Earthquake rift nr. nitta.

Fig. 12. Earthquake rift nr. Akô.

Fig. 13. Earthquake swell nr. Yatumizo.

Fig. 14. Earthquake swell nr. Yatumizo.

(震研彙報、第十號、圖版、大塚)

18. *Neogene and Quaternary Vulcanism in the Idu*[1] *District.* (*Preliminary report*)

By Hiromichi TSUYA,

Earthquake Research Institute.

(Read Dec. 15, 1931.—Received Dec. 20, 1931.)

I. Introduction.

The Idu district, which comprises, in addition to the peninsula of that name, the outlying group of small islands called the Idu Sititô (Idu Seven Islands)[2], is well known for its numerous volcanoes. This whole region is a series of volcanic rocks intercalated with sedimentaries, the oldest of which is a series of volcanics that were erupted during the Tertiary in the peninsula itself, while the youngest is the still active volcano of Ôsima[3], the most northerly member of the Sititô group. This active volcano forms a link in the volcanic chain known as the Huzi Volcanic Zone[4] which basaltic vulcanism had built up on the *fossa magna* since the Pleistocene. Consequently there is here a profusion of phenomena portraying the intensive volcanic activities that characterized this region since the time of the Tertiary.

In the winter of 1925-6, the writer visited the southern part of the Idu peninsula with the object of examining the geological correlation between the peninsula itself and the outlying liparitic insular volcanoes (Kôdusima[5] and Niizima[6]) of the Idu Sititô[7]. After the earthquakes of the first half of 1930 that shook the northeastern coast-belt of the peninsula, the writer investigated the geologic structure of the meizoseismal area[8]. Again, after the destructive earthquake of Nov. 26, 1930 that convulsed the northern part of the peninsula, the writer renewed with increased interest the investigation of the Idu district, in which investigation he is still engaged. A preliminary account of the volcanic history of the district as generalized from fragmental results already

1) 伊豆. 2) 伊豆七島. 3) 大島. 4) 富士火山帶. 5) 神津島. 6) 新島.
7) H. TSUYA, "Volcanoes of Kôzu-shima", *Bull. Earthq. Res. Inst.*, 7 (1929), 269-334.
8) H. TSUYA, "On the Geologic Structure of Itô District, Idu", *Ibid.*, 8 (1930), 409-426.

communicated, together with some hitherto unpublished details, are presented in this report.

II. Tertiary Vulcanism.

Tertiary volcanics are distributed extensively over the Idu peninsula. They are altered andesites, liparites, dacites, and fresh andesites, all accompanying their own pyroclastics; besides solid lavas. As a consequence of their complicated modes of occurrence and dislocation, and partly because of the alterations to which some of them have been subjected, their sequence is interpreted in different ways by different authors. H. Ishiwara[9] tried to show that the Tertiary volcanics of the peninsula are accompanied by sedimentary rocks containing the uppermost Tertiary faunas, and that they must therefore belong to submarine eruptions of that time. He regarded these as eruptions from a Tertiary central volcano ("Nekko Volcano")[10] and also as from local fissure-eruptions. But, although he distinguished the eight kinds of propylite, dacite, pyroxene-andesite, tuffite, tuff-conglomerate, agglomerate, shale, and sandstone, and indicated their respective type-localities, he made no attempt to unravel the sequence of eruption of these volcanic materials. According to S. Kozu[11], the geological sequence of the southern part of the Idu peninsula is plagioliparite, potash-liparite, propylite, liparite, Tertiary sediments, dacite, and pyroxene-andesite. In his opinion, the vulcanism there began in the middle Tertiary with the eruption of the plagioliparite and ended in the later Tertiary with the eruption of pyroxene-andesite, on the sea-floor throughout the whole period, with repeated fluctuations in activity. The statements of the above two authors constituted until recently the main information regarding the general geology of the peninsula. Recently, R. Tayama[12] and H. Niino[13] attempted a systematic examination of the peninsula from the stratigraphical side, and discriminated numerous Tertiary volcanic rocks according to their stratigraphic succession.

---

9) H. Ishiwara, "Geology of the Volcanoes of Idu Peninsula", *Report Earthq. Invest. Com.*, **17** (1898), 3–49, (in Japanese).

10) 猫越火山.

11) S. Kōzu, "Geology of the Southern Part of Idu Peninsula", *Report Geol. Survey*, **38** (1913), 1–19, (in Japanese).

12) R. Tayama, "Relation between the N. Idu Earthquake on Nov. 26, 1930 and the Geological Structure of N. Idu", *Report Sci. Res., Saitō Gratitude Foundation*, **11** (1931), 1–53, (in Japanese).

13) R. Tayama and H. Niino, "An Introduction to the Geology of Idu Peninsula", *Ibid.*, **13** (1931), 1–81, (in Japanese).

So far as the writer's observations go, the sequence of Tertiary vulcanism of the Idu peninsula is as follows:

1. Miocene vulcanism.

The first eruption phase in the Tertiary is represented by the altered andesites that are so widely distributed in the Idu peninsula, and which form the oldest formation now exposed there. Their age has not yet been definitely proved, but the upper limit to their possible range of age is fixed by the lower Miocene formations that overlie them unconformably.

The altered andesites, which occur as lava-flows interstratified with their pyroclastics, are associated with shale, sandstone, and conglomerate. As the last-named contains well-rounded pebbles of altered andesites, it is inferred that, although the altered andesites are largely from submarine eruptions, volcanic islands were built up on the Tertiary sea-floor and afterwards reduced by wave-action. From the thickness of the volcanics and the sizes of the pyroclastics, it is evident that the eruptions then were as wide-spread as they were energetic. These eruptions may have been alternately effusive and explosive, taking place from local vents which, however, have not yet been found.

The altered andesites vary considerably in megascopical as well as microscopical characters: they have not been uniformly effected by propylitization, although even in their freshest parts, their primary constituents are more or less replaced by secondary calcite, chlorite, silica, etc., while the base is devitrified. The freshest and most typical specimen of the altered andesites that could be obtained had phenocrysts of calcic plagioclase, augite, and hypersthene. The pyroclastic products had also been similarly altered.

The next series in the volcanic sequence suggests that subsequent to eruptions of the altered andesites, when possibly the oldest formation had been dislocated, a renewed outbreak of volcanic activity gave rise to eruptions of another and wholly different class of materials. This time the rocks were of a markedly acid type. They include varieties that range from potash-liparite, through plagioliparite, into dacite, and are distributed in the southern part and also in the western half of the northern part of the peninsula. The volcanic discharges consist largely of fragmentary materials (tuffs, tuff-breccias, and agglomerates), solid lavas being comparatively insignificant in amount and local in origin, though intrusive sheets, necks, and dikes frequently occur. None of

the erupted materials thicken sufficiently towards centres that might be taken to mark volcanoes of the central eruption type. The fragmentary materials form stratified beds containing marine fossils. As these materials become more calcareous, so do the fossils become more numerous. The few intercalated limestones have yielded fossils that indicate the age of the volcanics to be lower Miocene.

As to the succession of the volcanic events, no regular order in the eruptions of the various acidic rocks of this age has yet been established, although from certain available data the writer inferrs that these rocks, in the order of eruption, are: Potash-liparite, biotite-plagioliparite, hornblende-dacite, and hornblende-augite-dacite. These rocks, which have been subjected to more or less alteration, show their primary constituents to be silicified and sometimes sericitized, and the base devitrified, while its pore spaces are filled with recrystallized secondary quartz.

After the eruptions of the acidic rocks, there followed once more a period of volcanic activity, like that of the earliest andesites, but probably of less intensity. The andesites of this period occur as dikes, cutting through the lower Miocene beds. Like the earliest andesites, they also have been subjected to alteration. Whether or not they are the last manifestations of Miocene vulcanism in the district it is not possible yet to say, although another group of andesitic rocks that overlie them is quite fresh and seems much younger.

2. *Pliocene vulcanism.*

Vulcanism in later Miocene and earlier Pliocene cannot very well be ascertained as only a few rocks that probably belong to these periods have been found, and these few have yielded so far only fossils that are of small value as age-markers.

Vulcanism in the latest Pliocene is established by fossil evidence. Andesites and dacites are the rock-types represented. They occur in the central part of the Idu peninsula, accompanying their own tuffs, tuff-breccias, and agglomerates; besides solid lavas. They include various rocks which, in the order of eruption, are hornblende-pyroxene-dacite, pyroxene-dacite, pyroxene-andesite, and olivine-bearing pyroxene-andesite. The tuffs, both dacitic and andesitic, have yielded marine fossils by which we can assign them to submarine eruptions towards the close of the Pliocene. A number of andesitic bodies (dikes, lava-flows, and agglomerates) that intrude into and extend over the Miocene series in other parts of the peninsula are probably of this period.

III. Quaternary Vulcanism.

Either at the end of the Pliocene age or in the beginning of the Pleistocene, the Idu peninsula underwent elevation, and the submarine formations rose in one part, at least, above the sea-level of that time. In the southern part of the peninsula, wide-spread Tertiary vulcanism was succeeded by Quaternary relative quiescence; while probably some time later, in the northern part, subaerial vulcanism became active, when a sedimentary series[14] of the earliest Pleistocene had been more or less deformed, and continued its activity the whole of the Pleistocene. At the present day vulcanism is confined to activities of insular volcanoes in the Idu Sititô group.

Not a few investigators have studied this Quaternary vulcanism, and in the following review of the subject the writer has combined the results of their studies with data of his own.

3. Pleistocene vulcanism.

Pleistocene vulcanism built up numerous andesitic and basaltic volcanoes of central type. Of these volcanoes, Amagi[15], Usami[16], Taga[17], and Yugawara[18] are aligned from south to north in the northeastern part of the peninsula. Usami, which is the oldest of these four volcanoes, is built up of lava-flows of pyroxene-andesite and olivine-pyroxene-andesite, with intercalations of pyroclastic products. The next in age is Taga and then Yugawara. Their products are olivine-pyroxene-andesite accompanying pyroclastic material; besides solid lavas.

In the vicinity of the Atami hot-spring resort[19] we find pyroxene-dacite masses, which, according to H. Kuno, extruded later than the products of volcano Taga, but earlier than the products of volcano

14) This series consists of gravels, tufaceous sandstone, and shale. It has yielded abundant plant fossils.

15) 天城火山.

16) 宇佐美火山. This name is proposed here for the first time to designate the volcanic body that extends to the west of Usami, a village about 4 km. north of the Itô hot-spring resort (伊東溫泉).

17) 多賀火山. This was proposed to represent a volcanic body adjacent to the north of the volcano Usami, by H. Kuno who is studying that body. The term "Atami Volcano" in the writer's previous paper (*Bull. Earthq. Res. Inst.*, **8** (1930), 409-426) comprises these two volcanoes—Usami and Taga.

18) 湯ヶ原火山. The existence of this volcano was first suggested by T. Hirabayashi (*Report Earthq. Invest. Com.*, **16** (1898), 58-73), and was affirmed lately by H. Kuno.

19) 熱海溫泉.

Yugawara. It is therefore clear that dacitic and andesitic vulcanism acted alternately in the Pleistocene age.

Amagi, which is the largest volcano in the peninsula, and occupies the eastern half of the central part of the latter, consists, besides the main volcano, of numerous parasitic cones. It appears to be younger than the three above-mentioned—Usami, Taga, and Yugawara. According to J. Suzuki[20], who studied the volcano in detail, the main body is built up of fragmental ejecta and repeated lava-flows of pyroxene-andesite; while the parasitic cones, which are younger than the main body, may be divided into three groups, in the order of eruption and also according to the nature of the products: the parasitic cones of the first stage (pyroxene-andesite, hornblende-bearing pyroxene-andesite, and olivine-bearing pyroxene-andesite), the parasitic cones of the second stage (products similar to those of the first), and the parasitic cones of the third stage (olivine-bearing pyroxene-andesite and olivine-basalt). The writer observed at the northern foot of the volcano that a lava-flow of pyroxene-andesite (a product of one of the parasitic cones of the second stage ?) covers an olivine-pyroxene-andesite from volcano Usami.

Outside the boundary of the northeastern foot of volcano Amagi, there is a group of basaltic volcanoes—the Oomuroyama group—which J. Suzuki regarded as third stage parasitic cones of the former. The youngest volcano in this group is Oomuroyama[21], which consists of a cinder-cone (Oomuroyama proper) and extensive lava-flows, morphologically representing a typical aspi-conide. Besides this, the group comprises the volcanoes Komuroyama[22], Jôbosi[23], and Umenokidaira[24], and the Itô scoria-bed. These volcanic bodies might have been built up by vulcanism of a later date, when the volcanoes Amagi, Usami, and Taga had been more or less dislocated and dissected[25]. Considering the youngest volcano, the vulcanism in this group seems to be the last to have occurred in the Idu peninsula, the time being the late Pleistocene. The morphological features of Oomuroyama indicate youth: so youthful in fact that it may well date from a much later age.

In addition to the foregoing, there are a number of Pleistocene volcanoes in the northwestern part of the peninsula. Their structural details and their products, however, have not yet been investigated.

---

20) J. Suzuki, "Geology of the Amagi Volcanic Group, Prov. Idu", *Jour. Geol. Soc., Tôkyô*, **28** (1921), 431-448, (in Japanese).

21) 大室山. 22) 小室山. 23) 城星火山. 24) 梅ノ木平火山.

25) H. Tsuya, *Bull. Earthq. Res. Inst.*, **8** (1930), 409-426.

4. *Recent vulcanism.*

In the Idu peninsula, Pleistocene vulcanism was succeeded by a period (Recent) of relative quiescence, while the present numerous hot-springs there represent a stage of post-volcanic thermal activity. In the Idu Sititô territory, on the contrary, vulcanism, both basaltic and liparitic, has been active in recent times. This recent vulcanism has already been discussed in a previous paper[26], in which the writer endorsed the views that were put forward independently by T. Tsujimura[27] and S. Tsuboi[28].

IV. Correlation of the Vulcanism in the Idu District with that in Adjoining Districts.

In the preceding pages the writer gave the sequence of the vulcanism in the Idu district since the Neogene time. To present as one

	Basic Effusives	Volcanic Bodies	Acidic Effusives	Volcanic Bodies
Recent	Basalts and basaltic andesites	Ôsima group in Idu Sititô	Plagioliparites	Niizima group in Idu Sititô
Pleistocene	Basalts Olivine-pyroxene-andesites Pyroxene-andesites	Oomuroyama group Volcanoes: Amagi Yugawara Taga Usami	Dacites	Lava-flows in the vicinity of Atami
Pliocene	Olivine-bearing pyroxene-andesite Pyroxene-andesite	Lavas and pyroclastics intercalated with sediments (Hiyekawa[29] beds)	Dacites	Lavas and pyroclastics intercalated with sediments (Hiyekawa beds)
Miocene	Altered andesites	Lava-flows ? and dikes	Dacites Plagioliparites Potash-liparites	Lava-flows, necks, and dikes; besides pyroclastics
	Altered andesites (propylite)	Lava-flows and pyroclastics intercalated with sediments		

26) H. Tsuya, *Bull. Earthq. Res. Inst.*, **7** (1929), 269–334.

27) T. Tsujimura, "On the Topography of Kôzu-shima and Nii-jima Islands (Izu)", *Report Earthq. Invest. Com.*, **89** (1918), 57–96, (in Japanese).

28) S. Tsuboi, "Volcano Ôshima, Idzu", *Jour. Col. Sci., Tokyo Imp. Univ.*, Art. 6, **43** (1920), 1–146.

29) 冷川

whole view the leading rock-types that erupted during the vulcanism, the general rock-sequence as they erupted is tabulated in page 7.

As will be seen from the table, Neogene vulcanism began with eruptions of andesite which was afterward subjected to alteration, so that succeeding vulcanism was alternately liparitic (or dacitic) and andesitic. This seems to be the case not only with the Idu district, but also with of the much larger region of the *fossa magna*, of which Idu district forms but a very small fraction. In view of this it is possible to correlate the Idu peninsula with several adjoining districts:

1. In the central part of Sinano province[30], according to F. Homma[31], vulcanism dates from the Miocene as shown in the following rock-sequence:

1) Two-pyroxene-andesite, olivine-andesite, and hornblende-andesite .... Lower Miocene.
2) Biotite-liparite and augite-hornblende-biotite-dacite (with quartz-diorite and diorite) ... Upper Miocene.
3) Two-pyroxene-andesite (with diorite-porphyrite) .. .. Lower Pliocene.
4) Biotite-andesite, hornblende-andesite, and two-pyroxene-andesite .... Pleistocene.
5) Olivine-bearing two-pyroxene-andesite .... Recent.

Of these, the oldest andesites are particularly worthy of notice in that they are from submarine eruption, and have been subjected to alteration (silicification and chloritization) as recognized in the oldest andesites in the Idu district.

2. In the Asigara district[32] adjoining the north part of the Idu peninsula is developed the so-called Misaka series, which practically consists of andesitic-basaltic lavas and basic pyroclastic rocks with local intercalations of limestone and clastic rocks[33]. This series is of Miocene age, and the volcanics in it seem to be products of submarine eruptions of that time. This volcanic phase was succeeded by the intrusion of a large mass of quartz-diorite which may be correlated with a similar one of later Miocene age in Sinano province. The intrusion of the quartz-

30) 信濃國.

31) F. HOMMA, *Geology of the Central Part of Sinano Province*, (Tokyo, 1931), 79-84, (in Japanese).

32) 足柄地方.

33) K. SUGI, "On the Metamorphic Facies of the Misaka Series in the Vicinity of Nakagawa, Prov. Sagami", *Jap. Jour. Geol. Geogr.*, **9** (1931), 88-142.

diorite was followed by renewed eruptions of pyroxene-andesite, both solid and fragmental, which, with intercalations of clastic rocks, constitute the Pliocene formation (Asigara bed) of the district.

3. In the Ôiso district[34], adjoining the northeast part of the Idu peninsula, the oldest volcanic material is the pyroxene-andesite fragments contained in a siliceous sandstone of Miocene or older age; while at least, four stages of vulcanism in the succeeding ages may be recognized in the succession of the volcanics there developed, the first being represented by hypersthene-hornblende-dacite (lower Miocene), the second by pyroxene-andesite (Miocene-Pliocene), the third by hornblende-pyroxene-dacite (lower Pleistocene), and the fourth by olivine-pyroxene-andesite (upper Pleistocene)[35].

The districts above cited are a few examples of regions that are within the *fossa magna*, in which Tertiary vulcanism is generally characterized by the earliest eruptions of andesites during early Miocene or earlier. It is probable that these early eruptions took place in the *fossa magna*, which diastrophism had caused to be formed during early Tertiary at the boundary between southwestern and northeastern Japan. It is particularly noteworthy that in these districts, as in the Idu district, andesitic rocks and liparitic or dacitic rocks erupted alternately.

V. On the Distributions of the Andesitic and the Liparitic or Dacitic Rocks in the Idu District.

The relation of vulcanism to crustal disturbances in the Idu district is a subject that calls for further investigation. At the same time several important facts regarding the locations of volcanic vents are clearly known to the writer. Leaving aside for a while the Tertiary andesitic rocks, the location of the original vents of which have not yet been found, the Quaternary andesitic and basaltic rocks mostly erupted from volcanoes in the northern part of the Idu peninsula and in the Idu Sititô territory. These volcanoes lie in the so-called Huzi Volcanic Zone, which Quaternary vulcanism built up in the *fossa magna* that traverses central Japan in N. N. W.-S. S. E. direction.

Liparitic and dacitic rocks erupted from vents as shown by their dikes, necks, and dome-shaped lava-masses that are distributed in the Idu peninsula. These vents may be grouped in a system of parallel

---

34) 大磯地方.

35) H. Tsuya, "Petrographic Notes on the Sedimentary Rocks of Southwest Sagami Province", *Bull. Earthq. Res. Inst.*, **9** (1931), 354-373.

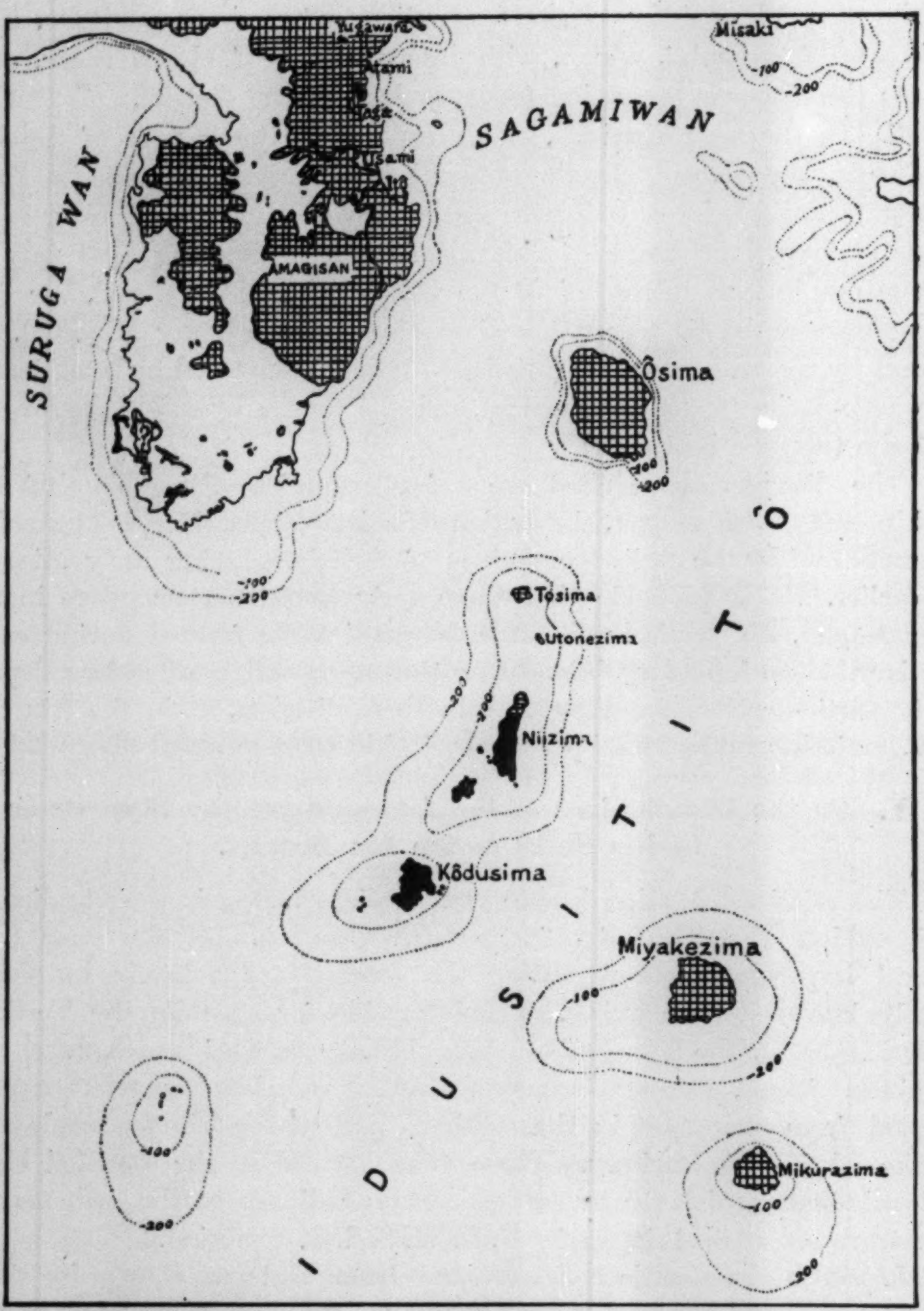

Fig. 1. Sketch map showing distribution of some volcanic rocks in the Idu district.
Cross-hatched areas: Quaternary andesitic and basaltic masses.
Black areas: Liparitic and dacitic masses, except their pyroclastics. (Tertiary and Quaternary.)
All Tertiary rocks, except liparites and dacites, and Quaternary sediments are left blank.

zones having a general direction, N. E.-S. W. Parallel to these zones is the line connecting the liparitic insular volcanoes of Idu Sititô. (See Fig. 1.)

These two trends—the N. N. W.-S. S. E. trend of andesitic volcanoes and the N. E.-S. W. trend of liparitic volcanoes or vents—seem to be surface manifestations of the ground structure of the district; the former representing a principal fracture and the latter a subsidiary one. But, these trends were not determined by any visible structural lines in the rocks, but by the presence of volcanic vents. If the sites of the volcanic vents had been fixed by dislocation or lines of weakness in the earth's crust, they should lie below the formations that are now visible at the surface.

VI. Summary and Conclusions.

Owing to a tectonic disturbance that occurred during the Eogene, central Japan was subjected to dislocation, resulting in a great fracture —Naumann's *fossa magna* or Yabe's *Itoigawa-Sunto Line*—that severed the geological continuation of Japan between southwestern and northeastern Japan. It is highly probable that this disturbance was responsible for the vulcanism that operated at the boundary of these two large geologic units of Japan in the early Neogene. So great was the vulcanism that in many districts at the boundary, volcanic rocks and pyroclastic sediments are the chief representatives of the lower Neogene formations. Since that time vulcanism has operated in these districts repeatedly with alternate renewal and decay of activity. The Idu district occupies the Pacific side of the boundary between southwestern and northeastern Japan. The volcanic history, as inferred from the sequence of volcanic rocks of this district, is briefly summarized as follows:

1. Miocene vulcanism. The oldest vulcanism occurred during early Miocene or a little before it, with submarine eruptions of andesites. This oldest vulcanism was followed, probably some time later when the formations practically composed of the oldest andesites had more or less deformed, by submarine eruptions of liparites and dacites. This phase of vulcanism, was succeeded by a subordinate phase of activity, characterized by minor extrusions of andesites. All these Miocene volcanic rocks were subjected more or less to alterations—chloritization, silicification, sericitization, etc. The succession of these rocks implies considerable time, although its actual duration is a question we have no means of answering at present. The only precise datum is that

afforded by faunal evidence, which assigns the dacitic volcanics lying some distance above the base of the complex to lower Miocene.

2. Pliocene vulcanism. Regarding vulcanism during late Miocene and early Pliocene, we are largely in the dark as only a few rocks have been identified with these ages. In the latest Pliocene age, eruptions of dacites and andesites took place. They were again largely submarine eruptions.

3. Pleistocene vulcanism. At the close of the Tertiary, or in the beginning of the Pleistocene, Idu peninsula was subjected to crustal movement, generally in the sense of uplift. It was not until some time after the movement that raised so much of the Tertiary sea-floor into land had taken place, that Pleistocene vulcanism became vigorous. It was chiefly concentrated in the northern part of the peninsula; while in the southern part, Tertiary vulcanism was succeeded by Pleistocene and Recent relative quiescence. The andesitic volcanoes Amagi, Usami, Taga and Yugawara, together with other yet uninvestigated volcanoes in the northwestern part of the peninsula, are, as also the dacitic masses in the vicinity of Atami, products of Pleistocene vulcanism. The basaltic Oomuroyama group represents the last vulcanism, which probably occurred some time later, at the time when the early Pleistocene volcanoes Usami, Taga, etc., were subjected to more or less dislocation and dissection.

4. Recent vulcanism. In the Idu peninsula, none of the latest volcanoes is known to have erupted in historic times; while the numerous hot-springs there are displaying post-volcanic thermal activity. In the Idu Sititô, on the contrary, liparitic and basaltic vulcanism was active during historic times.

An examination of the materials that were erupted during the whole course of the vulcanism and so fully recorded in the geology of the Idu district, reveals the fact that andesitic and liparitic or dacitic rocks have played their rôle in every age from lower Miocene up to Recent. Thus, a discrimination of the two lineages—andesitic and liparitic or dacitic—is essential to a proper understanding of the vulcanism of the district. As to the genetical relationship between the two lineages, very little can be said now. If we assume in the meantime that the rocks of these two lineages were derived from a common stock-magma, then their differentiation from this magma must be explained by one or other of two alternatives: (1) Either the partial magmas that separated out during early Tertiary had remained throughout suc-

ceeding ages as available sources of the andesitic rocks on the one hand and of the liparitic or dacitic rocks on the other, and that further differentiation had gone on within them; or (2) that differentiation to an advanced stage had proceeded repeatedly along definite lines at wide intervals of time. Of these two alternatives, the writer is inclined to accept the former, agreeing with S. Tsuboi in the opinion that the basaltic and liparitic rocks which erupted during Recent time in the Idu Sititô territory are descendants respectively of the andesitic and liparitic or dacitic rocks that erupted during the Tertiary and early Pleistocene in the Idu peninsula.

Examples presenting close analogies with the volcanic sequence of the Idu district could be cited from adjoining districts: Sinano, Asigara, and Ôiso.

The distribution of the sites of vents of liparitic and dacitic rocks shows distinct zones parallel with each other in the direction from N. E. to S. W. The directions of these zones are very remarkable in contrast with the Huzi Volcanic Zone, which runs in the N. N. W.-S. S. E. direction, and in which direction the Quaternary andesitic and basaltic volcanoes of the district are aligned. The zones of these two directions—N. E.-S. W. and N. N. W.-S. S. E.—seem to represent the underground fracture lines connected with available sources, respectively, of the acidic volcanic rocks and the basic volcanic rocks.

---

18. 第三紀以後に於ける伊豆地方の火山活動に就いて（豫報）

地震研究所　津　屋　弘　逵

昭和五年十一月二十六日の北伊豆地震以後北伊豆地方の地質を研究してゐる間に同地方に於ける火山岩の噴出順序を或程度まで確めることが出來た。本論文はその結果に既に以前公けにしたものを加へて伊豆地方全般の火山活動を總括したものである。

伊豆地方に於ては安山岩類と流紋岩類（或は石英安山岩類）とが第三紀及び以後の火山活動によつて同時或は交互に噴出してゐる。既に坪井誠太郎博士はこの事實を認められ、筆者も斷片的に認めてゐたのであるが、最近の研究によつて一層詳かにすることが出來た。即、伊豆地方に於て知ることが出來る最初の火山活動は中新世初期或はそれより稍古期の安山岩の噴出に初まり、其後同地方の火山活動は鮮新世、更新世を經て現世に至るまで各時代毎に安山岩類及び流紋岩類（或は石英安山岩類）の噴出によつて繰返されてゐる。所謂フォツサマグナの中に在る他の地方（例へば信濃地方、足柄地方等）と伊豆地方とを火山岩の噴出順序の上から對比すると何處でも大體同様であることが認められる。

伊豆地方に於ける火山岩の分布を見るに、第三紀の安山岩は伊豆半島一帶に分布してゐて今の所

その噴出の中心が明かでないが、第四紀の安山岩類は主として北伊豆と伊豆七島中の大島、三宅島、八丈島等との所謂富士火山帶に相當する部分に限られてゐる。これに反して流紋岩類の分布をその岩脈、岩頸、火山體等の分布によつて見ると北東一南西に走る數帶に分たれてゐる樣に見える。その最も著しいものは伊豆七島に於ける流紋岩火山島の配列に見られるが、伊豆半島に於ても、殊にその南部に於て、認められる。この北東一南西の酸性火山岩帶ともいふべきものはこの火山岩に貫かれてゐる地層の構造線とは一致してゐない樣である。從つて、一般に火山岩噴出地點が地殼の弱線に支配されるものとすれば火山帶を決定する地殼の弱線は地表に近い部分の地層に見られる構造線では示されない場合がある樣に考へられる。富士火山帶とこれに斜交する酸性火山岩帶は伊豆地方を通過する二方向の地殼の弱線を示し、これらが夫々基性火山岩類及び酸性火山岩類の本源と連絡あるものと考へることが出來る。

尙、本論文は伊豆地方の火山活動に關する總括的研究の豫報で、詳しいことは更に研究の結果報告したいと思つてゐる。

---

19. 伊豆震災地一二等三角點水平移動成果報告

大正十二年關東大地震後伊豆半島をも包む關東一帶の三角測量が陸地測量部の手によりて行はれたり。最近伊豆地震の直後、同測量部が我地震研究所の委囑によりて更に同地方の一二等三角點につき二等三角測量を行へり。此を明治十七年に行はれたる舊測量結果と比較せるもの及び關東大地震後の測量結果と舊測量結果とを比較せるものを對照せしめたるものを第一圖に示す。又、伊豆地震直後の測量結果を關東大地震後の測量結果と比較せるものを第二圖に示す。

倘、各観測に關する詳細事項を示せば下記の如し。

1. 觀測年次

舊測量	明治十七年
關東震災復舊測量（以下關東と略稱す）	大正十四•五年
新測量	昭和六年二月及三月

2. 觀測法

各觀測共に二等經緯儀を用ひ六測回の方向觀測法による。

3. 計算の要領

三角點の移動量は舊觀測値、關東觀測値及新觀測値を以て次の假定及方法により算定したる舊經緯度、關東經緯度及新經緯度に基き舊位置に對する關東震災（- - →）及伊豆震災（——→）の移動量を算出せり。（第一圖）

但し根古屋村三角點は關東測量に際し再設したるものなるを以て之を除く。

a. 經緯度計算に關する假定

各測量共に愛鷹山三角點を不動とし同點より冠ヶ岳三角點に對する方位を不變と假定せり。

b. 觀測角の平均

各測量の觀測値につき同一順序を以て網の平均法により計算せり。但關東測量に關しては其實施したる北半部につき算定せり。

c. 距離の計算

各三角點相互の距離は前項により決定したる平均角と次に示す與邊とによ

り算定せり。

舊 與 邊	愛鷹山—冠ケ岳とし關東震災比較計算に於ける舊値
關東與邊	同 新値
新 與 邊	德倉山—大場村とし昭和六年五月田方郡函南村に在る農學校西側に選定したる基線より發し二回の増大により決定したる値

4. 測量の精度

網の平均による一方向の中等誤差を $\pm\sqrt{\frac{Pvv}{r}}$ により算定す。其の値次の如し。

舊 測 量	$\pm\ 2''\cdot52$	P は重量
關東測量	$\pm\ 1''\cdot87$	v は剩餘
新 測 量	$\pm\ 0''\cdot99$	r は規約方程式の數

〔昭和六年十二月二日・地震研究所〕

---

19. Horizontal Displacements of the Primary and Secondary Triangulation Points in Idu Earthquake Districts.

After the great Kwantô earthquake of September 1, 1923, a revision of the triangulation in the disturbed region including the Province of Idu was carried out by the Land Survey Department. At our request the Department made, again, a trigonometrical survey in the same province during a period, which is just after the recent Idu earthquake of November 26, 1930, in order to know the magnitudes of horizontal movements of certain primary and secondary triangulation points due to the earthquake occurrence.

The full arrows in Fig. 1 show the relative horizontal displacements of the triangulation points obtained by the comparison of the result of the earlier measurements before the Kwantô earthquake and that after the Idu earthquake, while the broken arrows in the same figure represent the similar relative displacements obtained by the comparison of the results of the measurements before and after the Kwantô earthquake. Fig. 2 give the relative horizontal displacements acquired by the comparison between the result of measurements after Kwantô earthquake and that after Idu earthquake. The periods of the field works for the three measurements were as follows:

I. The earlier survey: in 1884.
II. Survey after the great Kwantô earthquake: 1925–1926.
III. Survey after the Idu earthquake: February–March, 1931.

For each survey, the coordinates of Asitakayama and the direction of the line joining this point and Kamurigatake were assumed unchanged. The distances between respective triangulation points were culculated from each mean of observed angles and

(震研彙報、第十號、圖版、地震研究所)

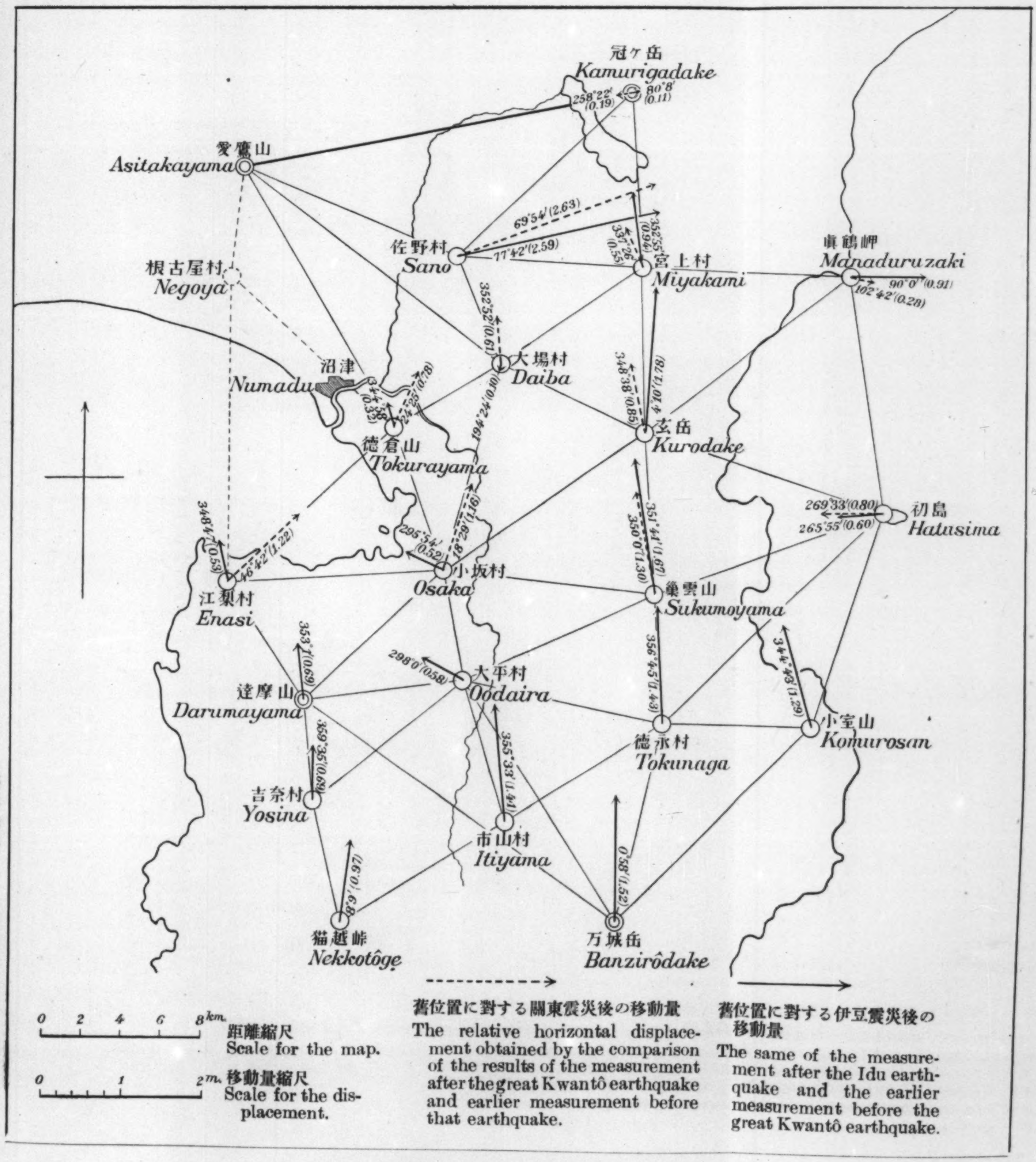

第一圖 伊豆震災地一二等三角點水平移動圖 (A)

Fig. 1. Map showing the Horizontal Displacements of the Primary and Secondary Triangulation Points in Idu Earthquake Districts. (A)

latic
Surv
surv
qual
of c

latic
the
the
of th
the
mea
the

joini
resp

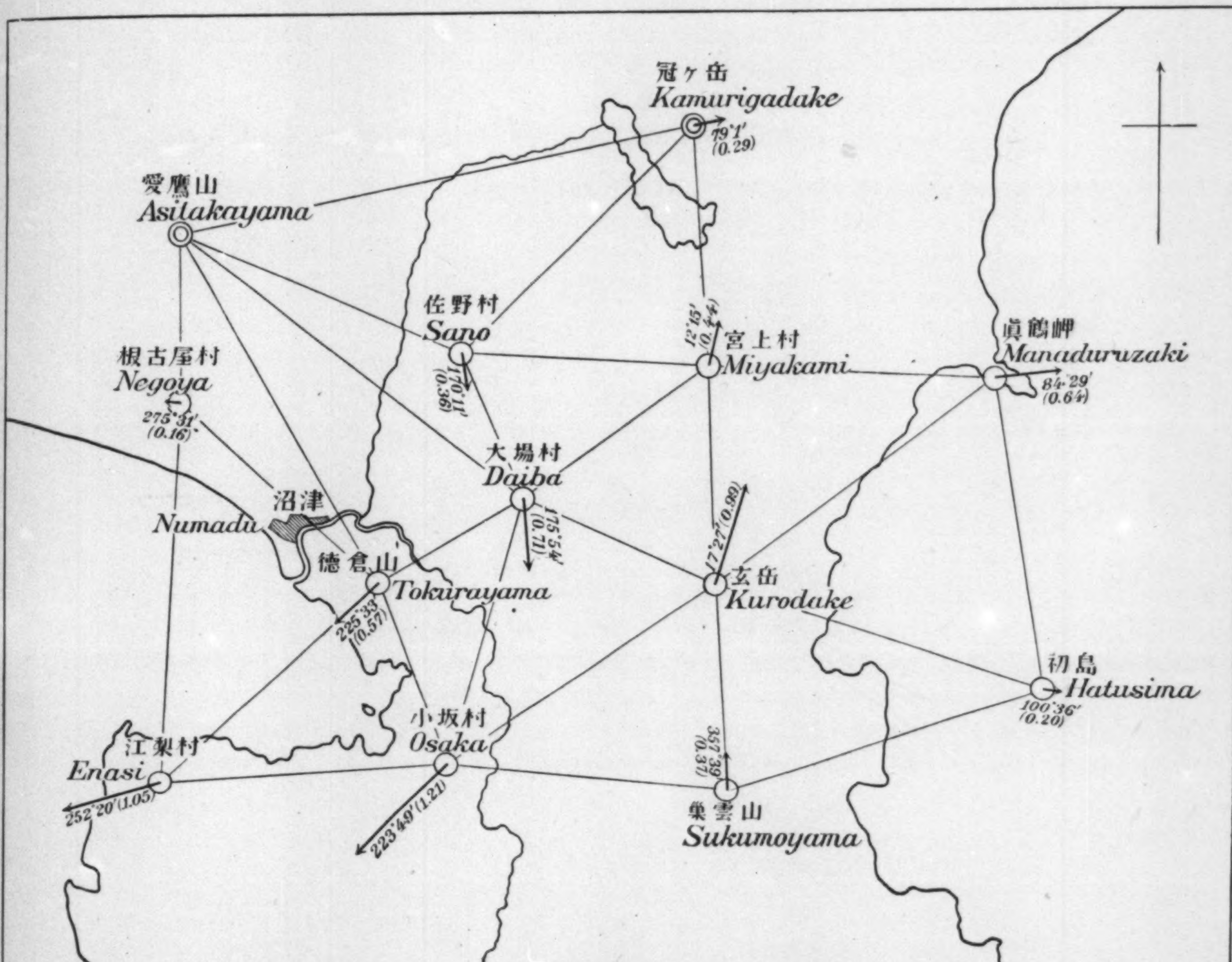

第二圖 伊豆震災地一二等三角點水平移動圖 (B)

Fig. 2. Map showing the Horizontal Displacements of the Primary and Secondary Triangulation Points in Idu Earthquake Districts (B)

(震研彙報、第十號、圖版、地震研究所)

the length of the base line shown below:

I. The earlier survey: the distance between Asitakayama and Kamurigatake.

II. Survey after the great Kwantô earthquake: the postseismic distance between the same two points.

III. Survey after Idu earthquake: the distance between Tokurayama and Daiba.

The probable errors of measurements are as follows:

	I	II	III
$m=\pm\sqrt{\dfrac{Pvv}{r}}$	$\pm 2''\cdot 52$	$\pm 1''\cdot 87$	$\pm 0''\cdot 99$

where P is the weight, v the residual and r the number of equations.

(Dec. 2, 1931. Earthquake Research Institute.)

20. *Seismometrical Report.*

地震觀測報告

(Earthquake Research Institute, Tôkyô, Japan.)

(July 1—September 30, 1931.)

(1) Sensible earthquakes in Tôkyô for the period July 1—September 30, 1931.

List I.

Time = Central standard time of Japan (Civil mean time of the meridian 135°E).

Notation:

Prel. tr. = Preliminary tremors.
N. S. = North-South component.
E. W. = East-West component.
2A = Range of motion.
T = Period of earthquake motion.
λ = Longitude.
φ = Latitude.
D = Depth of focus.

Intensity: I (slight), II (rather weak), III (weak), IV (rather strong), V (strong), VI (violent).

No.	Station	Date	Time of occurrence	Duration		Maximum motion				Direction of initial motion	Epicentre		D	Intensity
				Prel. tr.	Total	N. S.		E. W.			λ (E)	φ (N)		
						2A	T	2A	T					
			h m s	s	m	mm	s	mm	s				km	
41	Tôkyô	July 1	14 52 23·9	8·6	4	0·455	0·67	0·391	0·78		140°16	35°90	60	I
	Kamakura		14 52 28·4	10·0	3	0·086	0·57	0·072	0·48					
	Misaki			11·6	4	0·079	0·6	0·063	0·4					
	Kiyosumi			11·4	3	0·020	0·4	0·034	0·4					I
	Titibu			13·7	3	0·016	0·8	0·024	0·4					
	Tôgane			9·2	3	0·040	1·0	0·068	1·0					
	Tukuba		14 52 22·3	8·7	4									I
	Mitaka													

(to be continued.)

List I. (*continued.*)

No.	Station	Date	Time of occurrence	Duration: Prel. tr.	Duration: Total	Maximum motion N. S. 2A	Maximum motion N. S. T	Maximum motion E. W. 2A	Maximum motion E. W. T	Direction of initial motion	Epicentre λ (E)	Epicentre φ (N)	D	Intensity
			h m s	s	m	mm	s	mm	s				km	
42	Tôkyô	July 2	7 47 12 8	16·9	3	0·125	0·5	0·112	0·4		139°·60	34°·95		I
	Kamakura		7 47 10·0	14·2	2	0·034	0·7	0·046	0·7					
	Misaki			—	2	0·012	0·3	0·025	0·3					
	Kiyosumi			15·8	3	0·008	0·4	0·020	0·4					
	Titibu			—										
	Tôgane			18·6	2	0·014	0 3	0·010	0·2					
	Tukuba			—										
	Mitaka													
43	Tôkyô	8	5 46 24·7	8·3	5	0·420	0·68	0·570	0·68	N67°W	139·32	35·84	40	II
	Kamakura			6·3	3	0·250	0·60	0·176	0·60	N34°E,d				II
	Misaki			—										
	Kiyosumi			—										
	Titibu			7·0	4	0·106	0·30	0·112	0 30					
	Tôgane			14·3	5	0·044	0·60	0·034	0·60					
	Tukuba		5 46 27·5	10·2	4									
	Mitaka													
44	Tôkyo	10	14 59 16·6	11·4	6	0·186	1·13	0·260	1·13		140·65	35·66	14	I
	Kamakura													
	Misaki			13·2	4	0·108	1·3	0·075	0·6					
	Kiyosumi			9·4	7	0·088	1·7	0·036	1·4					
	Titibu			18·2	4	0·028	1·5	0·028	1·4					
	Tôgane			7 5	8	1·030	1·5	0·800	1·4					
	Tukuba		14 59 11·3	15·6	9									
	Mitaka													
45	Tôkyô	10	22 10 41·5	12·8	13	0 842	1·30	1·762	1·67	E sl.S	140·83	35·59	26·5	II
	Kamakura		22 11 —	17·1	9	0·800	0·57	0·380	0·57	S36°W,d				II
	Misaki			15·8	5	0·440	1·4	0·550	1·8					
	Kiyosumi			10 3	12	0·350	3·3	0·400	2·8					
	Titibu			22·8	6	0·160	1·3	0·156	0·6					
	Tôgane			8·0	11	—	—	2·950	2·0					
	Tukuba		22 10 38·4	15 6	13									II
	Mitaka													
46	Tôkyô	19	21 23 57·5	20·7	10	0·137	0·48	0·106	0·42		140·41	37·31		I
	Kamakura		21 23 —	20·7	6	0·054	0·55	0·066	0·55					
	Misaki			31·0	7	0·035	0 50	0·030	0·60					
	Kiyosumi			28·5	7	0·060	1·2	0·024	0·80					
	Titibu			21·0	8·5	0·188	1·0	0·270	1·20					
	Tôgane			20·0	8	0·044	0·6	0·064	0·6					
	Tukuba		21 23 45·0	16·2	10									I
	Mitaka													
47	Tôkyô	20	8 29 28·1	8·2	2	0·121	0·48	0·054	0·51		139·36	35·66		I
	Kamakura		8 29 30·0	6·5	2	0·078	0·46	0·036	0·38					
	Misaki			7·5	2	0·025	1·00	0·017	0·70					
	Kiyosumi			—										
	Titibu			8·4	1									
	Tôgane			20·0	1	0·004	1·00	0·020	0·60					
	Tukuba		8 29 37·6	12·4	2									
	Mitaka													

(*to be continued.*)

List I. *(continued.)*

No.	Station	Date	Time of occurrence	Duration: Prel. tr.	Duration: Total	Maximum motion N.S. 2A	N.S. T	E.W. 2A	E.W. T	Direction of initial motion	Epicentre λ (E)	Epicentre φ (N)	D	Intensity
			h m s	s	m	mm	s	mm	s				km	
48	Tôkyô	July 26	10 41 19·9	8·8	7	2·475	0·74	2·365	0·75		140°09	35°85	58	III
	Kamakura		10 41 23·7	11·1	6	0·560	0·78	0·460	0·39					II
	Misaki			13·6	6	0·470	0·7	0·413	0·6					
	Kiyosumi			10·0	6	0·146	0·5	0·200	0·7					II
	Titibu			11·8	5	0·064	0·6	0·052	0·6					
	Tôgane			9·4	6	0·260	0·8	0·350	0·9					
	Tukuba		10 41 21·5	9·3	8									I
	Mitaka													
49	Tôkyô	28	11 5 42·0	10·8	15	0·333	0·95	0·329	0·94		140·25	35·95	60	II
	Kamakura		11 5 46·4	13·6	5	0·060	1·2	0·140	1·2					
	Misaki			14·4	5	0·067	1·6	0·067	1·5					
	Kiyosumi			14·7	6	0·026	0·8	0·036	1·4					
	Titibu			13·0	4	0·056	0·8	0·080	0·8					
	Tôgane			10·6	12	0·132	1·2	0·200	1·2					
	Tukuba		11 5 38·3	6·6	9									II
	Mitaka													
50	Tôkyô	28	11 27 29·2	9·9	3	0·112	0·63	0·063	0·50		139·85	36·22	46	I
	Kamakura			13·6	5	0·060	0·38	0·140	0·63					I
	Misaki			14·6	2	0·008	0·3	0·010	0·6					
	Kiyosumi			—	2	0·006	0·6	0·008	0·6					
	Titibu			11·0	1	0·008	0·3	0·004	0·2					
	Tôgane			13·1	2	0·028	0·4	0·020	0·6					
	Tukuba		11 27 25·6	7·1	2									I
	Mitaka													
51	Tôkyô	30	1 30 12·8	9·2	2·5	0·044	0·23	0·036	0·23		139·68	36·49	18	I
	Kamakura													
	Misaki			16·0	1	0·005	0·5	0·001	0·4					
	Kiyosumi			—										
	Titibu			8·5	1	0·008	0·2	0·010	0·2					
	Tôgane			13·8	1	0·004	0·3	0·002	0·2					II
	Tukuba		1 30 11·0	5·5	2									
	Mitaka													
52	Tôkyô	31	4 46 21·4	14·6	14	0·078	0·57	0·065	0·45		140·79	36·29		I
	Kamakura		4 46 24·6	22·5	5	0·020	0·36	0·030	0·36					
	Misaki			21·0	4	0·082	1·00	0·047	1·0					
	Kiyosumi			18·0	4	0·020	0·8	0·020	0·7					
	Titibu			19·4	3	0·032	0·7	0·034	1·0					
	Tôgane			12·7	7	0·040	0·6	0·060	0·8					
	Tukuba		4 46 12·5	9·6	7									I
	Mitaka													
53	Tôkyô	Aug. 10	23 34 32·0	19·8	12	0·911	1·04	0·622	1·04	N80°E,u	138·31	35·15		II
	Kamakura		23 34 24·4	17·0	9·5	0·606	0·20	1·040	0·50	N58°E				II
	Misaki			16·0	10	0·530	2·7	0·790	2·7	E				II
	Kiyosumi			23·0	11	0·720	4·8	0·580	5·0					
	Titibu			16·0	6	0·560	3·5	0·530	2·5	S45°W				
	Tôgane			25·6	12	0·350	2·0	0·420	3·5					
	Tukuba		23 34 34·4	27·6	28									
	Mitaka													

(to be continued.)

List I. (*continued.*)

No.	Station	Date	Time of occurrence	Duration: Prel. tr.	Duration: Total	Maximum motion N. S. 2A	Maximum motion N. S. T	Maximum motion E. W. 2A	Maximum motion E. W. T	Direction of initial motion	Epicentre λ (E)	Epicentre φ (N)	D	Intensity
			h m s	s	m	mm	s	mm	s		°	°	km	
54	Tôkyô	Aug. 18	14 40 42·3	20·5	30	1·720	2·6	1·130	3·1		141·00	36·15		I
	Kamakura		14 40 47·8	24·3	15	0·474	1·7	0·596	1·0					II
	Misaki													
	Kiyosumi			20·0	14	0·540	3·8	0·400	2·5					
	Titibu			23·5	11	0·170	1·8	0·170	1·6					
	Tôgane			13·6	21	0·640	1·1	0·450	1·5					II
	Tukuba		14 40 32·5	9·4	11									II
	Mitaka													
55	Tôkyô	19	8 43 45·2	7·1	3	0·054	0·30	0·082	0·20		140·14	35·86	40	I
	Kamakura		8 43 49·0	13·1	2	0·028	0·49	0·028	0·49					
	Misaki			14·1	3	0·014	0·5	0·023	1·0					
	Kiyosumi			14·8	2	0·004	0·3	0·004	0·3					
	Titibu													
	Tôgane			8·0	2	0·016	0·4	0·012	0·4					
	Tukuba		8 43 41·4	6·0	2									I
	Mitaka													
56	Tôkyô	27	8 49 32·7	8·7	4	0·348	0·62	0·245	0·76	N81°E	140·23	35·75	50	II
	Kamakura		8 49 35·9	9·4	3	0·026	0·28	0·038	0·34					
	Misaki			10·9	3	0·050	0·5	0·028	0·3					
	Kiyosumi			11·4	3	0·016	0·4	0·028	0·8					
	Titibu			8·0	2·5	0·008	0·4	0·008	0·5					
	Tôgane													
	Tukuba		8 49 29·8	8·1	3									I
	Mitaka													
57	Tôkyô	Sept. 7	5 35 5·2	8·3	7	1·453	0·52	1·160	0·59	N69°E,d	139·91	35·77	60	III
	Kamakura		5 35 6·8	9·4	5	0·580	0·45	0·490	0·45					II
	Misaki			10·4	5	0·395	0·75	0·325	0·75	N25°E				II
	Kiyosumi		5 35 5·5	9·8	6	0·120	0·56	0·232	0·56					II
	Titibu			12·2	5	0·110	0·54	0·132	0·77					
	Tôgane			9·6	5	0·180	0·50	0·170	0·56					II
	Tukuba		5 35 0·4	9·6	6									II
	Mitaka													
58	Tôkyô	9	4 9 31·4	24·5	30	1·480	2·9	1·480	3·5	S50°W,u	141·43	36·70		I
	Kamakura		4 9 34 2	25·8	15	2·46	5·6	0·56	2·8					I
	Misaki			33·0	30	0·367	1·9	0·565	2·8					II
	Kiyosumi			27·3	30	0·530	2·58	1·150	4·8					
	Titibu			29·7	20	0·310	1·62	0·230	2·37					
	Tôgane			21·3	30	0·590	2·85	0·490	3·45					II
	Tukuba		4 9 21·4	32·0	40									
	Mitaka													
59	Tôkyô	16	21 43 23·4	12·0	35	8·340	2·61	2·000	0·45	E sl.N,u	138·82	35·55	20	III
	Kamakura		21 43 16·3	8·7	17	7·85	0·81	12·800	0·81	N82W,d				III
	Misaki			10·0	20					N45°W				III
	Kiyosumi			17·0	25	2·200	4·7	1·90	4·7					III
	Titibu			7·5	20			3·04	2·0	S23°W				III
	Tôgane			18·0	30			2·10	2·3					III
	Tukuba		21 43 20·5	15·8	22									II
	Mitaka													

(to be continued.)

List I. (*continued.*)

No.	Station	Date	Time of occurrence	Duration: Prel. tr.	Duration: Total	Maximum motion N.S. 2A	N.S. T	E.W. 2A	E.W. T	Direction of initial motion	Epicentre λ (E)	Epicentre φ (N)	D	Intensity
			h m s	s	m	mm	s	mm	s		°	°	km	
60	Tôkyô	Sept. 18	15 13 45·4	11·6	7	1·720	0·76	1·240	0·34	N77°E,u	138·91	35·54		II
	Kamakura		15 13 44·0	7·9	7·5	2·400	0·5	6·000	0·5	N78°W,d				III
	Misaki			10·7	6	0·540	0·7	1·100	1·2					II
	Kiyosumi													
	Titibu			8 0	5	0·124	0·4	0·280	0·5					
	Tôgane			15·5	8	0·164	0·8	0·080	0·7					II
	Tukuba		15 13 54·1	15·4	8									I
	Mitaka													
61	Tôkyô	21	11 20 10·3	9·7	40	54·000	6·8	25·000	5·8	S71°E,u	139·12	36·0	16	V
	Kamakura		11 20 15·0	12·5	22	32·000	1·1	8·500	1·1	S8°E,u				IV
	Misaki			14·2						S22°E				IV
	Kiyosumi		11 20 21·0	17·8						S25°E				III
	Titibu			2·8						N48°E				V
	Tôgane			15·0						S46°E				IV
	Tukuba		11 20 11·9	10·0										III
	Mitaka		11 26 33·8	8·0						S38°E				V
62	Tôkyô	21	15 21 37·3	9·6	5	0·080	0·35	0·060	0·35		139·18	35·99	16	I
	Kamakura													
	Misaki			14·5	4	0·050	0·51	0·037	0·51					
	Kiyosumi			18·0	6	0·020	0·91	0 024	0·91					
	Titibu			3·2				0·350	0·37					
	Tôgane			16·1	6	0·100	0·85	0·084	0·85					I
	Tukuba		15 21 45·0	9·4	3									II
	Mitaka			7·9	5	0·122	0·20	0·130	0·2					I
63	Tôkyô	21	15 49 13·0	9·6	7	0·166	0·40	0·062	0·40		139·19	36·01	12	I
	Kamakura		15 49 17·8	12·5	5	0·110	0·65	0·098	0·52					
	Misaki			15·0	4	0·067	1·16	0·083	0·94					
	Kiyosumi			18·2	6	0·032	0·91	0·020	0·91					
	Titibu			2·6				0·890	0·35					
	Tôgane			16·0	6	0·084	0·90	0·120	0·90					I
	Tukuba		15 49 20·3	9·8										I
	Mitaka			7·9	7	0·156	0·37	0·140	0·37					I
64	Tôkyô	23	21 46 18·5	9·0	7	0·060	0·37	0·088	0·37		139·17	36·01	17	I
	Kamakura		21 46 24·6	11·2	5									
	Misaki			14·2	5	0·032	1·23	0·040	0·87					
	Kiyosumi		21 46 31·8	16·6	6	0·014	0·47	0·016	0·75					
	Titibu			3·2	2	0·200	0·30	0·264	0·40					
	Tôgane													
	Tukuba		21 46 19·1	8·6	3									I
	Mitaka			7·7	6	0·160	0·60	0·208	0·40					
65	Tôkyô	24	1 22 41·1	9·1	10	0·120	0·26	0·150	0·35	S58°E	139·10	36·02	30	I
	Kamakura		1 22 45·7	9·9	5	0·080	0·37	0·140	0·62					
	Misaki			12·8	6	0·065	0·52	0·046	0·52					
	Kiyosumi			18·2	6	0·030	0·49	0·020	0·49					
	Titibu			4·0	2	0·308	0·34	0·288	0·33	N62°E				
	Tôgane			15·7	7	0·162	0·77	0·118	0·77					I
	Tukuba		1 22 41·7	8·3	3·5									
	Mitaka			7·1	7	0·160	0·32	0·108	0·43					

(*to be continued.*)

List I. (*continued.*)

No.	Station	Date	Time of occurrence	Duration		Maximum motion				Direction of initial motion	Epicentre		D	Intensity
				Prel. tr.	Total	N. S. 2A	N. S. T	E. W. 2A	E. W. T		λ (E)	φ (N)		
			h m s	s	m	mm	s	mm	s		°	°	km	
66	Tôkyô	Sept. 24	13 26 25·0	8·5	8	0·485	0·78	0·466	0·78		140·04	35·98	10	I
	Kamakura		13 26 28·4	11·8	5	0·070	0·38	0·060	0·38					
	Misaki			11·9	5	0·063	0·58	0·090	0·43					
	Kiyosumi		13 26 26·1	13·6	5	0·040	0·56	0·036	0·56					I
	Titibu			14·3	3	0·052	0·84	0·048	0·53					
	Tôgane			11·0	7	0·070	0·43	0·116	0·43					I
	Tukuba		13 26 21·9	7·5	3									
	Mitaka			10 6	5	0·166	0·29	0·120	0·29					I
67	Tôkyô	24	21 11 26·3	9·8	5	0·058	0·34	0·076	0·36	S58°E	139·11	36·01	18	I
	Kamakura		21 11 32·4	11·5	5	0·060	0·47	0·036	0·39					
	Misaki			15·0	5	0·025	0·45	0·042	0·56					
	Kiyosumi			18·3	5	0·001	0·84	0·016	1·02					
	Titibu			2·9	2			0·392	0·43					
	Tôgane			14·9	7	0·086	0 69	0·054	0·69					I
	Tukuba													
	Mitaka			7·8	7	0·116	0·40	0·136	0·4					II
68	Tôkyô	26	12 37 43·4	9·7	2	0·070	0·27	0·030	0·27		139·08	36·05	17	I
	Kamakura		12 37 44·8	11·4	2	0·040	0·47	0·030	0·47					
	Misaki			15·6	4	0·015	0·53	0·018	0·53					
	Kiyosumi		12 37 50·8	17·7	2	0·008	0·58	0·004	0·58					
	Titibu			2·9	1·5	0·092	0·30	0·110	0·35					
	Tôgane			15·4	3	0·036	0·84	0·026	0·85					
	Tukuba		12 37 43·6	9·6	2									I
	Mitaka			8 0	3	0·062	0·38	0·036	0·38					
69	Tôkyô	28	4 50 40·0	7·9	7	0·650	0·7	0·590	0·7		139·76	36·10	40	II
	Kamakura		4 50 44·2	11·7	6	0·050	0·5	0·240	0·5					II
	Misaki			14·5	8	0·233	1·3	0·150	2·4					
	Kiyosumi			15·6	5	0·200	3·0	0·170	2·0					
	Titibu			9 0	4	0·180	0·9	0·072	0·5					
	Tôgane			11·8	4	0·096	1·0	0·146	0·6					
	Tukuba		4 50 38·3	5·5	5									II
	Mitaka			9·0	7	0·160	0 86	0·530	0·86					II
70	Tôkyô	28	13 54 27·6	8·7	13	0·420	1·13	0·580	1·13	S40°E,u.	139·18	35·96	25	II
	Kamakura		13 54 31·1	11·6	8·5	0·260	0·8	0·840	0·8	S10°E				II
	Misaki			16·2	10	0·700	3·0	0·241	1·5					
	Kiyosumi			18·2	12	0·220	3·5	0·120	1·5					
	Titibu			4·0	7	1·640	0·7	2·460	0·6					
	Tôgane			15·4	9	0·900	1·6	1·000	2·4					
	Tukuba		13 54 37·4	8·4	12					S81°W				I
	Mitaka		13 54 27·5	8·3	10	0·480	0·42	0·730	0·42	S30°E,u.				II

(2) *Important distant earthquake as observed in Tôkyô, Hongô.*

The most important distant earthquake observed during this period was the Sin Kiang earthquake of August 10, 1931. A pair of Imamura long period (3-min.) horizontal pendulums gave the following

results[1];

Phase	Time			Period	Amplitude		Azimuth
					N. S.	E. W.	
P	21h	26m	12s	33s	−30μ	50μ	S 59° E
			〃	8	26	33	S 52° E
PP		27	31				
PPP		28	1				
S		32	10	54	−2000	4700	S 67° E
SS		34	28	88	−3000	0	due S
L		35	16	90	22000	10400	N 25° E
L		36	46	48	20700	23400	N 48° E
L		37	34	42	22700	10000	N 24° E
L		38	16	34	15000	16000	N 47° E
L		38	50	31	18700	11800	N 31° E
							(mean N 35° E)
M		42	15	13	8500	−11000	N 52° W
M		42	38	13	8400	−13800	N 59° W
M		42	51	12	7200	− 9600	N 53° W
							(mean N 55° W)

Deducing from the duration of the preliminary tremors the epicentral distance becomes 4300 kms. The initial phase P gives S 59° E. Thus epicentre lies at a point 89° E, 45° N, that is, in the northern part of Sin Kiang, China. (See Fig. 14).

Note on the strong Saitama earthquake of September 21, 1931.

The earthquake of September 21, 1931, was the strongest experienced in Tôkyô since January of this year.

Intensity of the earthquake.

According to the Ishimoto Acceleration seismograph diagrams (Fig. 12) obtained at the Earthquake Research Institute the intensity of motion, or the maximum component accelerations were as follows:

N. S. component	55·5 gal. ?
E. W. component	74·6 gal.

which are approximately equal to 1·5 times of those on the occasion of the strong earthquake of June 17, 1931. (See Seism. R., Jan.-March, 1931.)

1) A. Imamura, "The world-shaking earthquake of August 10, 1931, as observed with a three-minute horizontal pendulum," *Japanese Journ. Astron. and Geophys.*, Vol. IX, No. 1 (1931).

Durations of the preliminary tremors and directions of the initial motion.

Station	Duration of preliminary tremors	Direction of initial motion
Tôkyô	9·7 sec.	S 71° E up
Kamakura	12·5	S 8° E up
Misaki	14·2	S 22° E
Kiyosumi	17·8 ?	S 25° E
Titibu	2·8 ?	N 48° E
Tôgane	15·0	S 45° E
Tukuba	10·0 ?	
Mitaka	8·0 ?	S 38° E
Itô	15·6	Due S
Koyama	9·1	S slight W
Yosiwara	13·8	N 11° E
Tanna	14·6	S slight W up

Earthquake Damage.

The following list gives the damage in four prefectures which are situated near the seismic origin.

Prefecture	Killed	Wounded	Totally collapsed house and godown	Partially collapsed house and godown	Broken chimney
Saitama	11	122	169	262	82
Gunma	5	30	33	5	48
Ibaraki		1	2	1	1
Tôkyô		1			

(N. Nasu and Ch. Yasuda.)

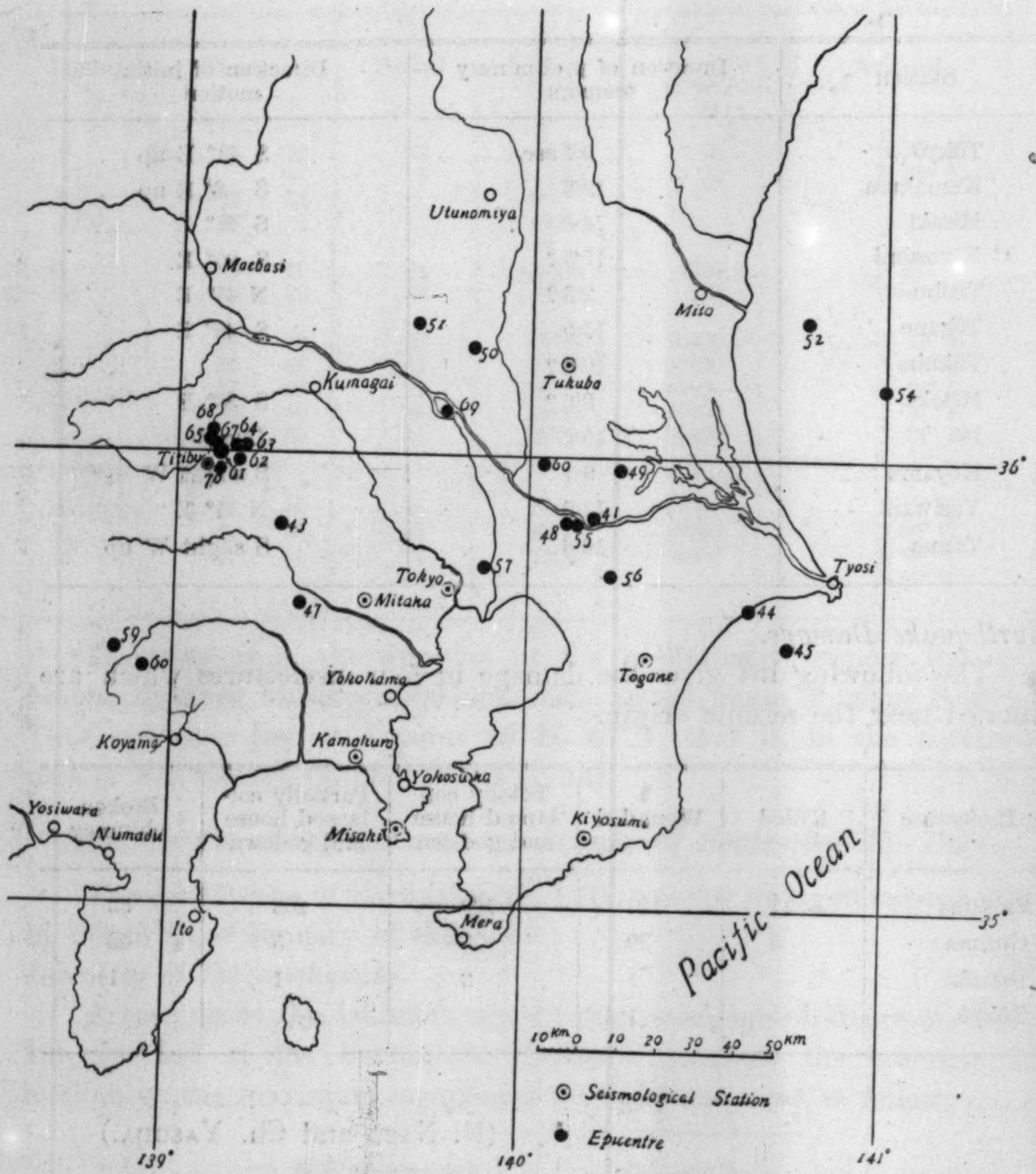

Fig. 1. Distribution of the epicentres of the earthquakes that originated within 160 kms. from Tôkyô and felt there during the period July 1-September 30, 1931. (Figures attached to each epicentre indicate the earthquake number.)

Instrument: No. 5.
Instrumental constants:

Component	Natural period	Magnification	Damping ratio
N.S.	7 sec.	50	1·50
E.W.	7	50	1·50
Vert.	7	28	1·50

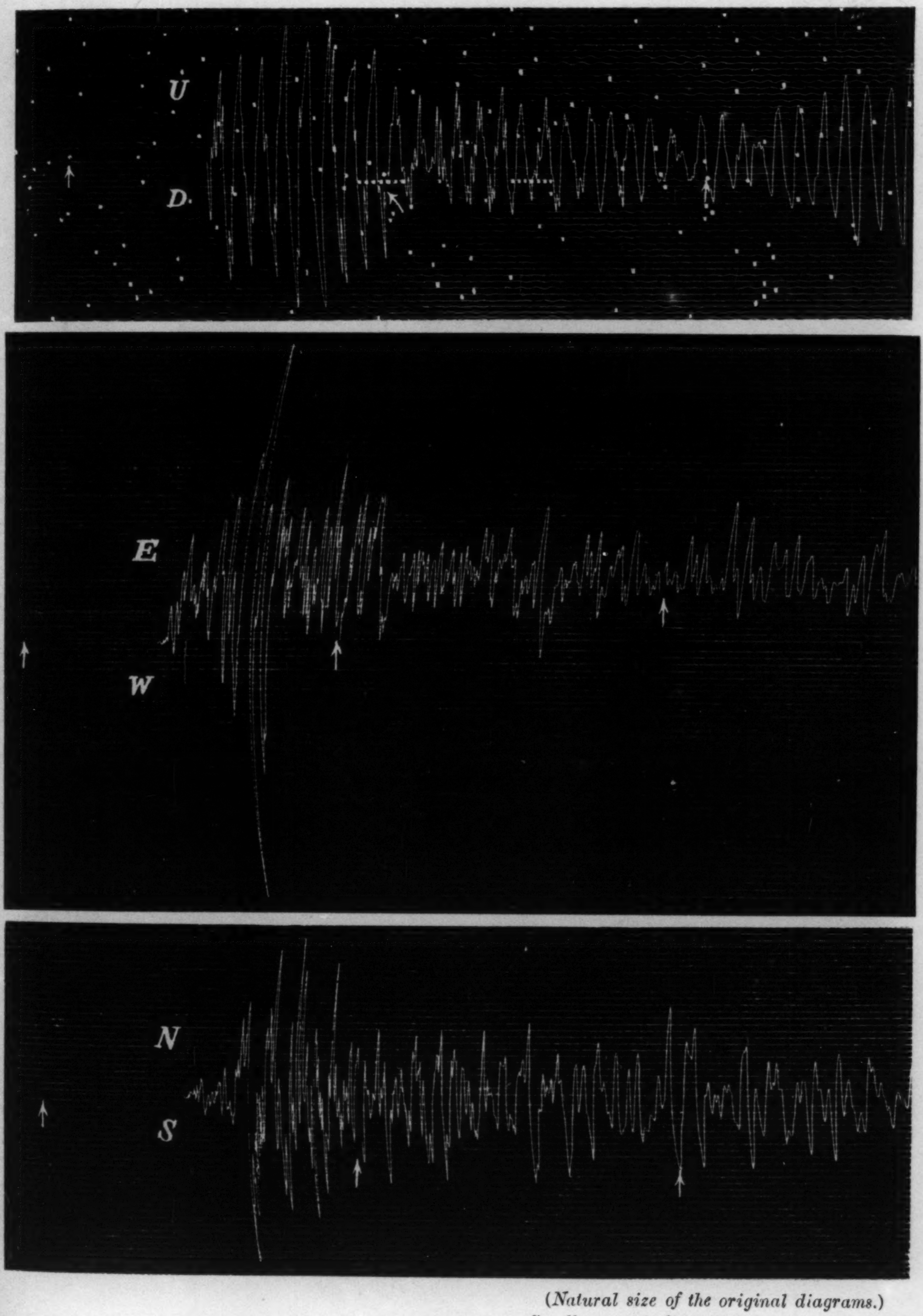

(*Natural size of the original diagrams.*)
Small arrow indicates the minute-break.

Fig. 2. Tôkyô Observation of the Earthquake of July 10, 1931.

（震研彙報、第十號、圖版、震報）

Instrument : No. 4.

Instrumental constants :

Component	Natural period	Magnification	Damping ratio
E.W.	7 sec.	50	1·50
N.S.	7	50	1·50

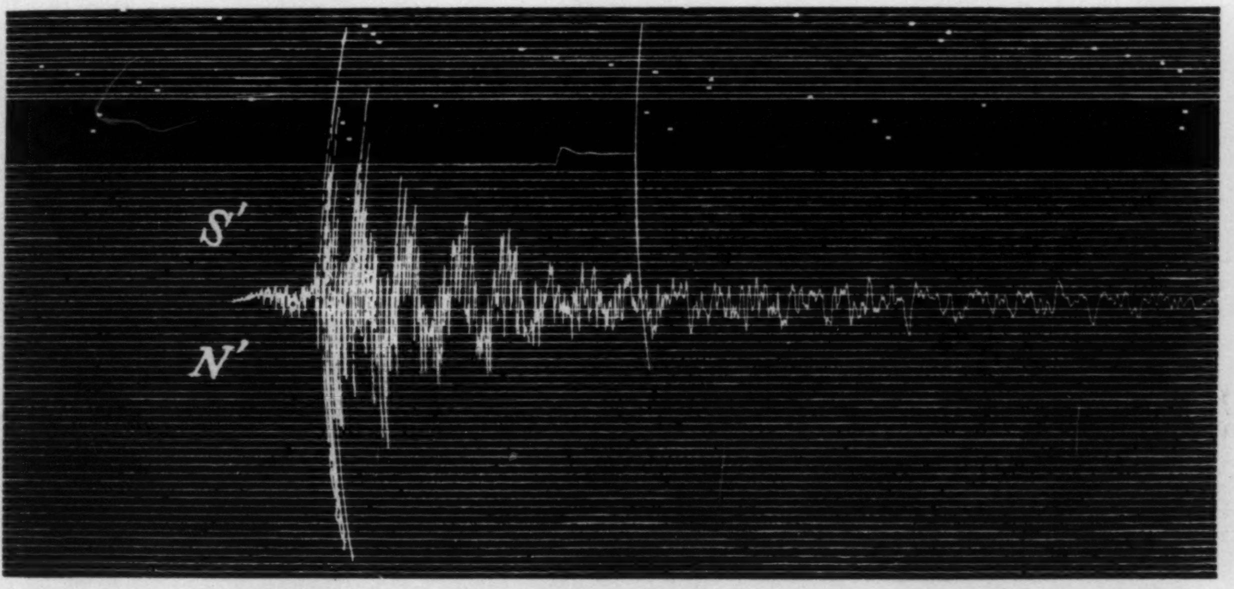

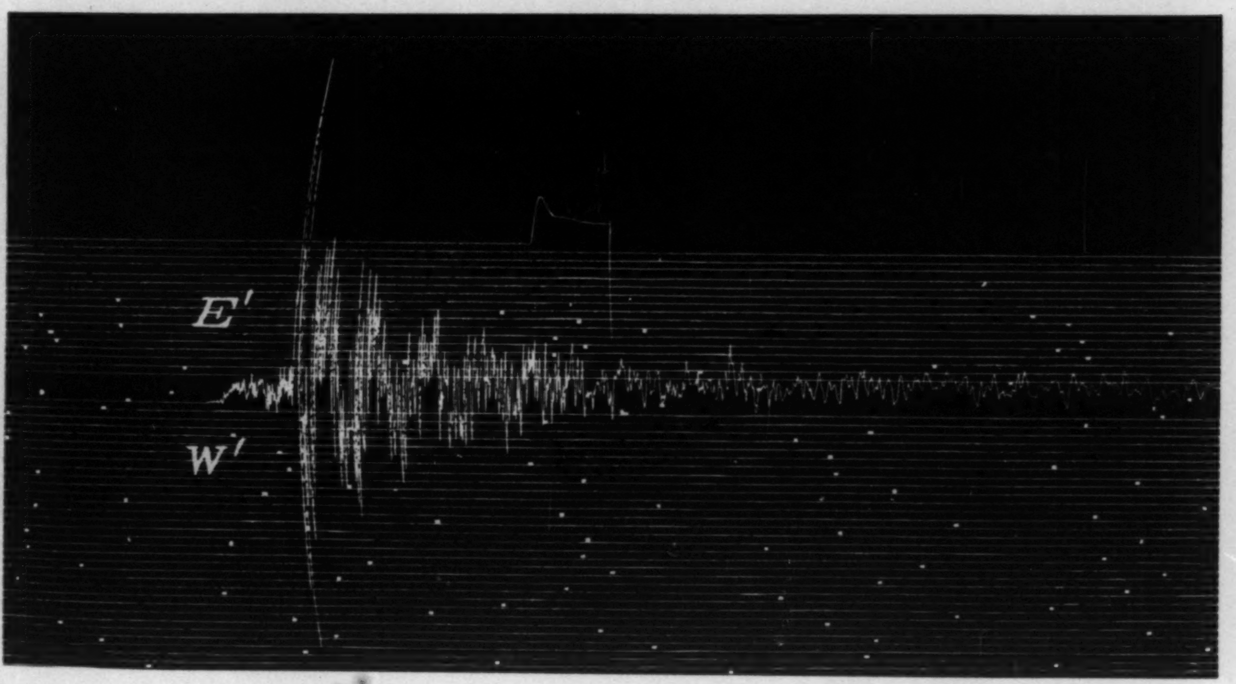

N' = N 13° W, S' = S 13° E.
E' = N 77° E, W' = S 77° W.

(*Natural size of the original Diagrams.*)

Fig. 3. Tôkyô Observation of the Earthquake of September 7, 1931.

Instrumental constants:

Instrument:
N. S. Component=No. 15.
E.W. Component=No. 14.

Component	Natural period	Magnification	Damping ratio
N S.	60 sec.	20	2·0
E.W.	60	15	3·2

N.S. Component.

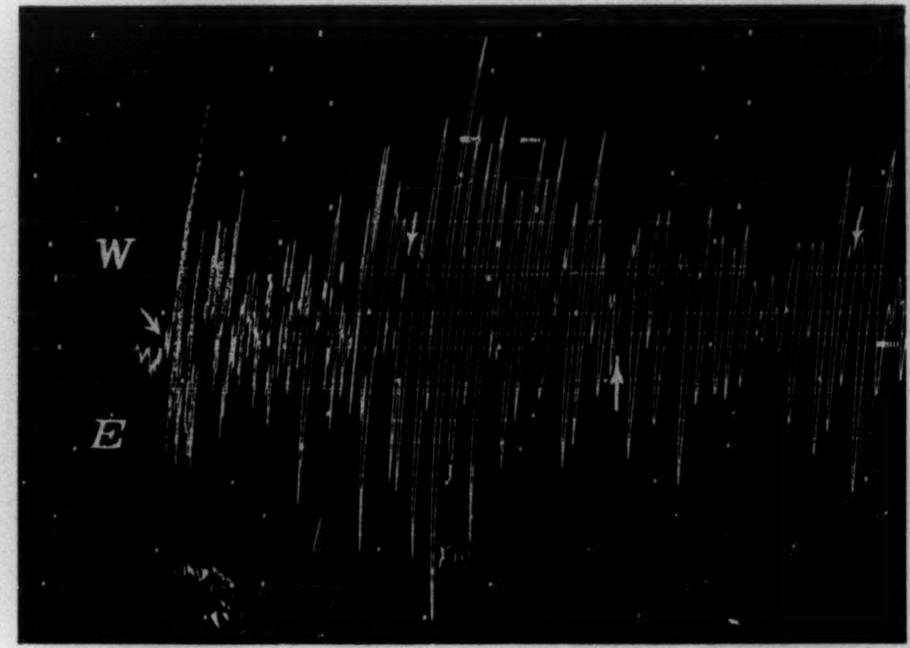

E.W. Component.

(Natural size of the original diagrams.)
Small arrow indicates the minute-break.

Fig. 4. Tôkyô Observation of the Earthquake of September 16, 1931.

Instrument : No. 3.

Instrumental constants :

Component	Natural period	Magnification	Damping ratio
N.S.	60 sec.	1·5	1·50
E.W.	60	1·5	1·50

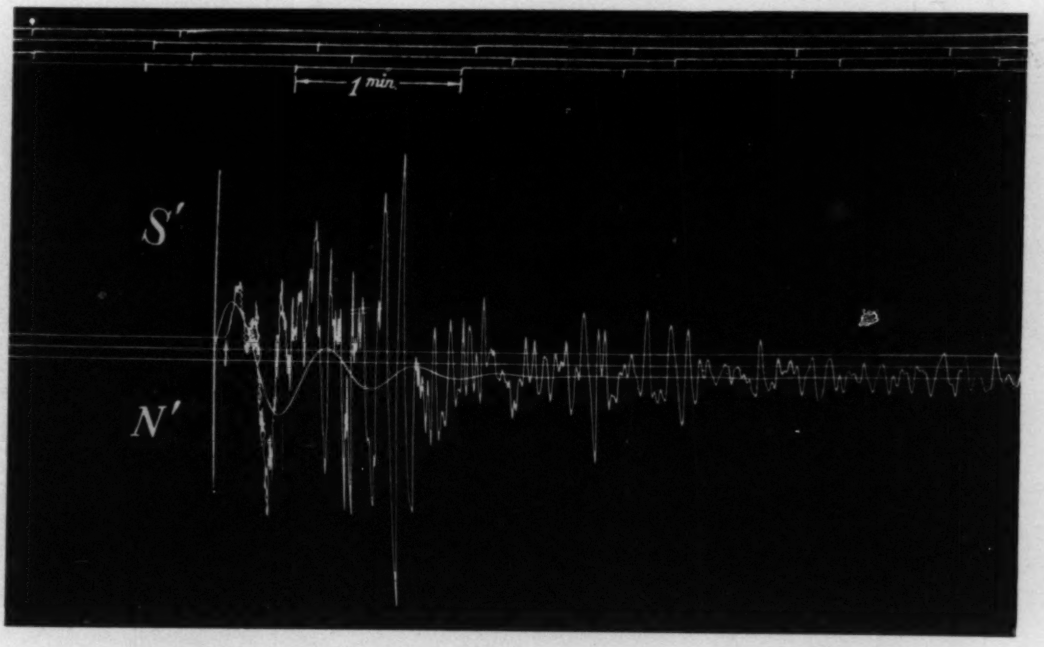

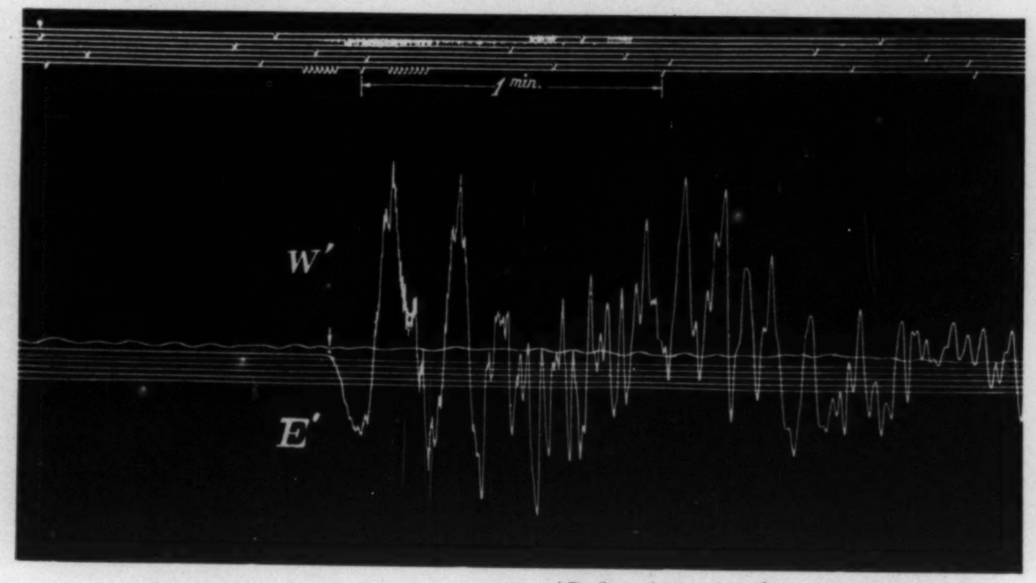

(Reduced to 2/3 of the original diagrams.)

N′ = N 13° W, S′ = S 13° E.

E′ = N 77° E, W′ = S 77° W.

Fig. 5. Tôkyô Observation of the Strong Saitama Earthquake of September 21, 1931.

(震研彙報、第十號、圖版、震報)

Instruments: No. 5.

Instrumental constants:

Component	Natural period	Magnification	Damping ratio
N.S.	7 sec.	50	1·50
E.W.	7	50	1·50
Vert.	7	28	1·50

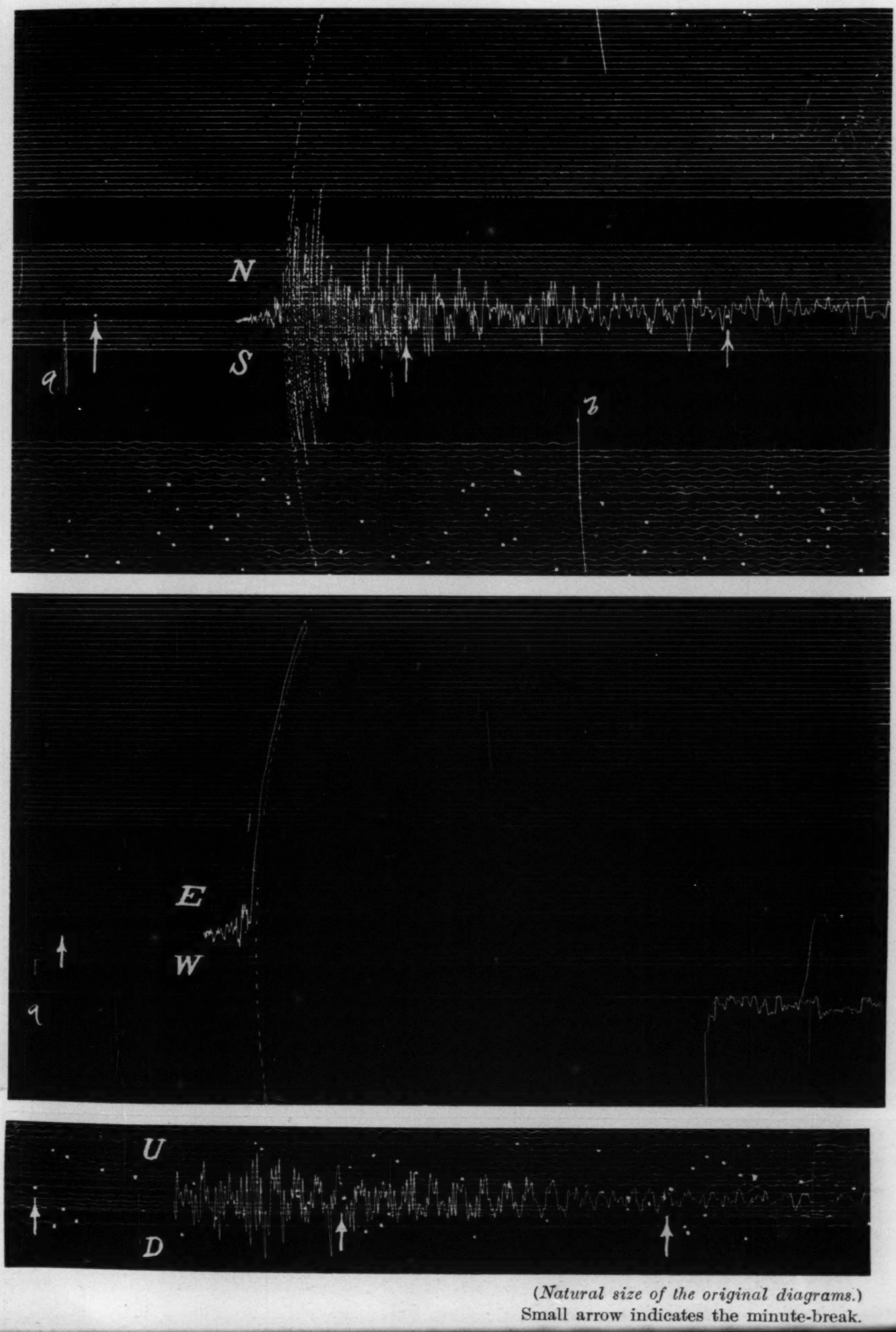

(*Natural size of the original diagrams.*)
Small arrow indicates the minute-break.

（震研彙報、第十號、圖版、震報）

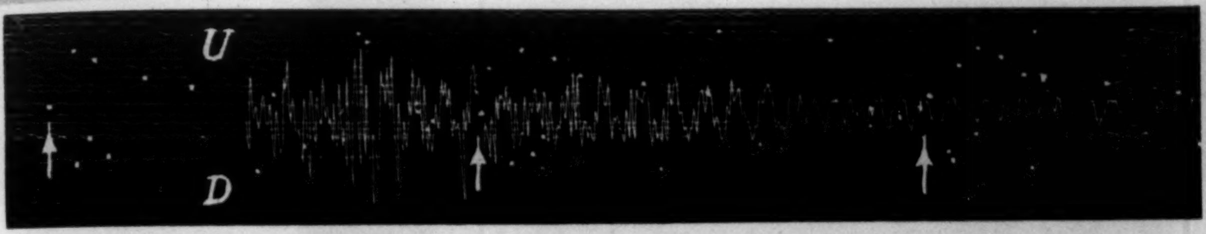

(*Natural size of the original diagrams.*)
Small arrow indicates the minute-break.

Fig. 6. Tôkyô Observation of the Earthquake of September 28, 1931.

Instrument : No. 5.

Instrumental constant :

Component	Natural period	Magnification	Damping ratio
N.S.	7 sec.	50	1·50
E.W.	7	50	1·50

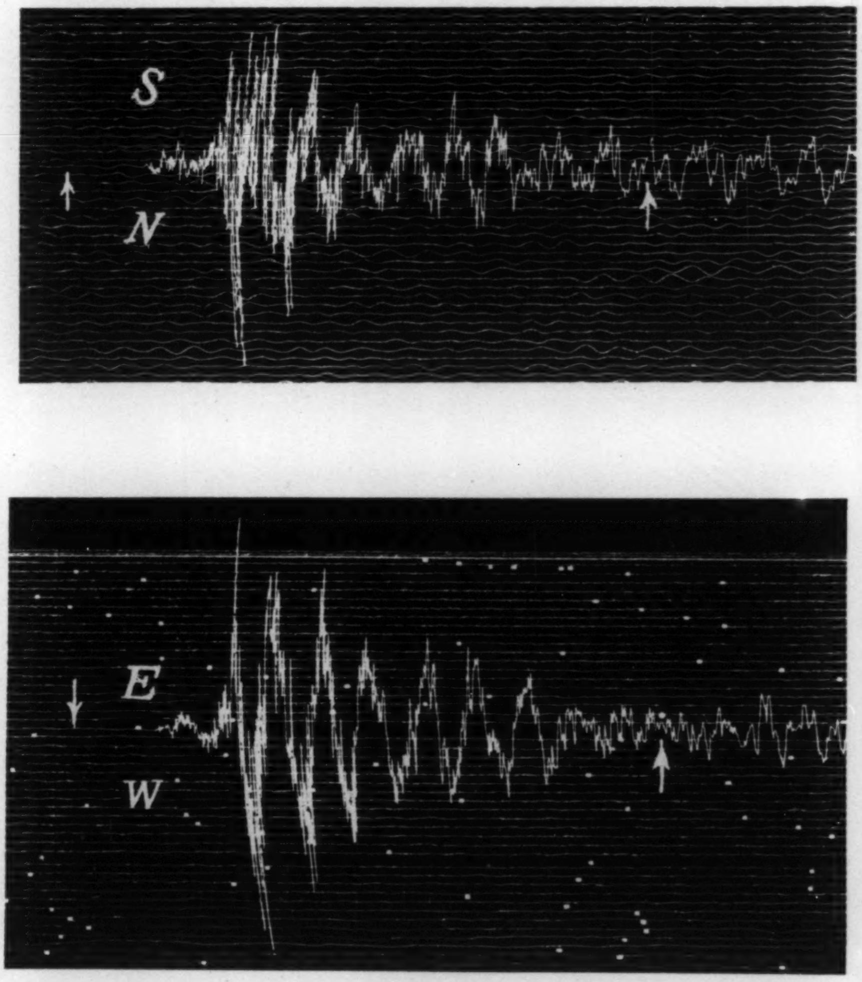

(*Natural size of the original diagrams.*)
Small arrow indicates the minute-break.

Fig. 7. Tôkyô Observation of the Earthquake of September 28, 1931.

（震研彙報、第十號、圖版、震報）

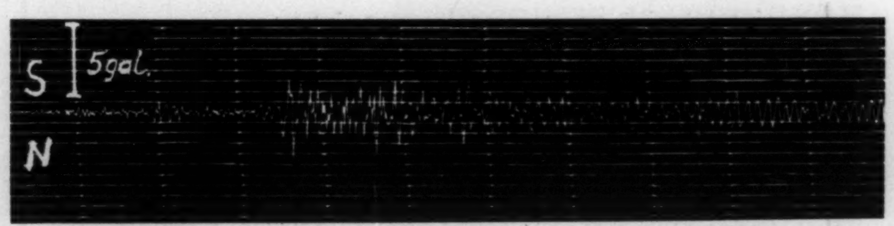

N.S. Component.

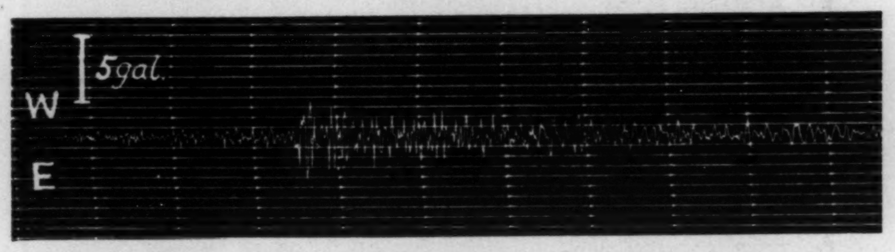

E.W. Component. Fig. 8.

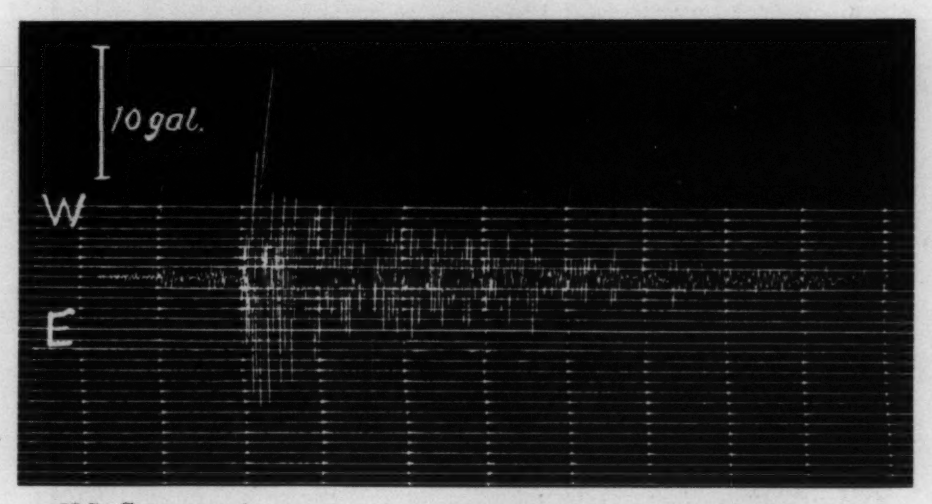

N S. Component.

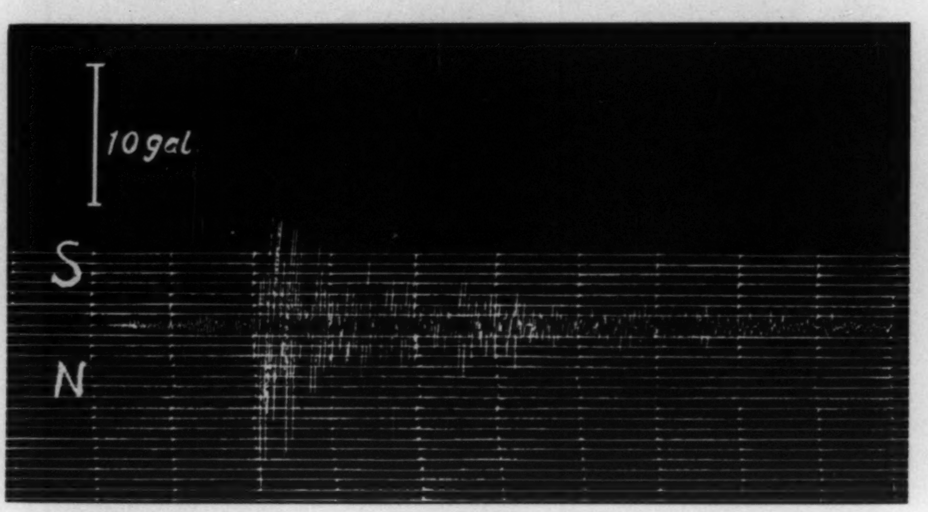

E.W. Component. Fig. 11.

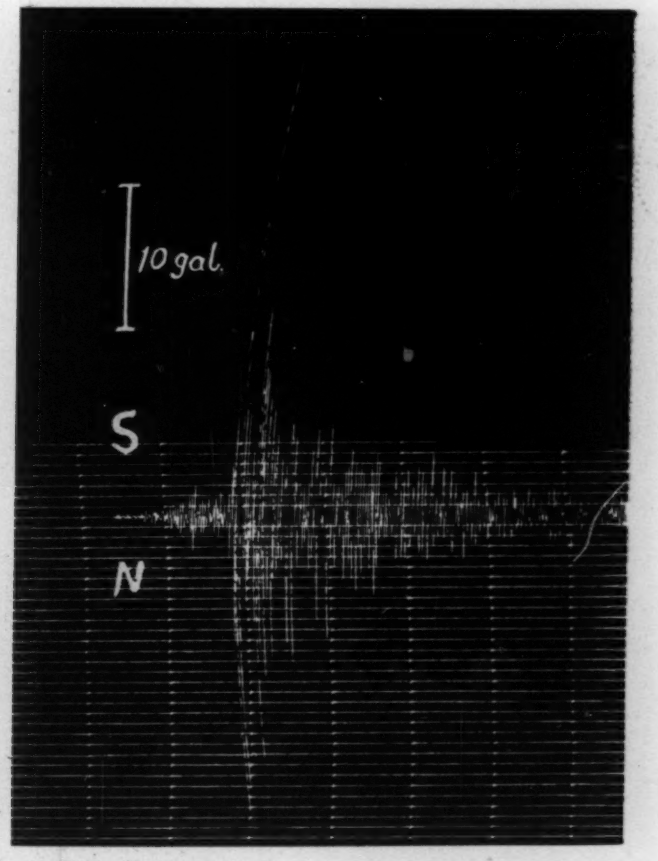

N.S. Component.

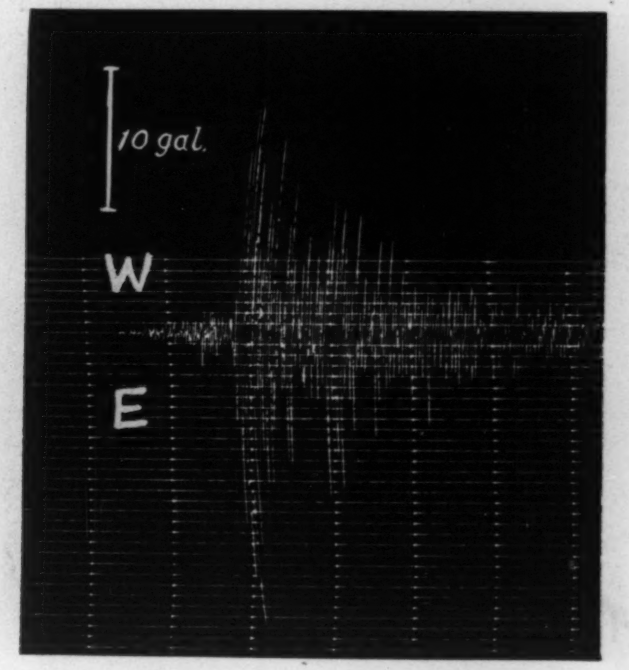

E.W. Component.

Fig. 8. Tôkyô Observation of the Earthquake of August 10, 1931
Fig 11. „ „ „ September 18, 1931.

Fig. 9. Tôkyô Observation of the Earthquake of September 7, 1931.

Ishimoto Acceleration Seismograph Diagrams.

(Time between consecutive two marks=6 sec.)

（震研彙報、第十號、圖版、震報）

([illegible] 第十號 附屬 [illegible])

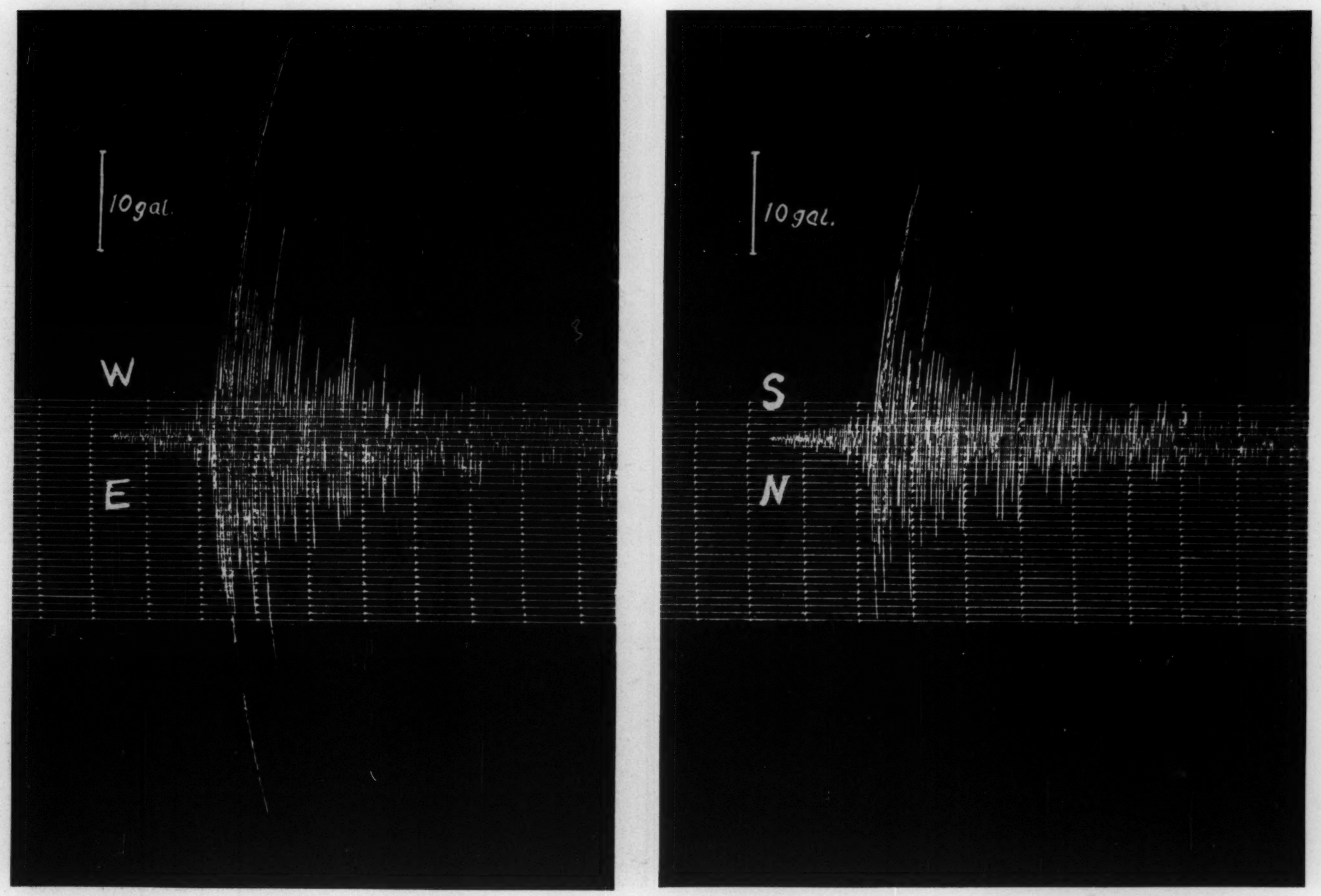

E.W. Component. N.S. Component.

Fig. 10. Tôkyô Observation of the Earthquake of September 16, 1931.
Ishimoto Acceleration Seismograph Diagram.
(Time between consecutive two marks=6 sec.)

（震研彙報、第十號、圖版、震報）

（震研彙報、第十號、圖版、震報）

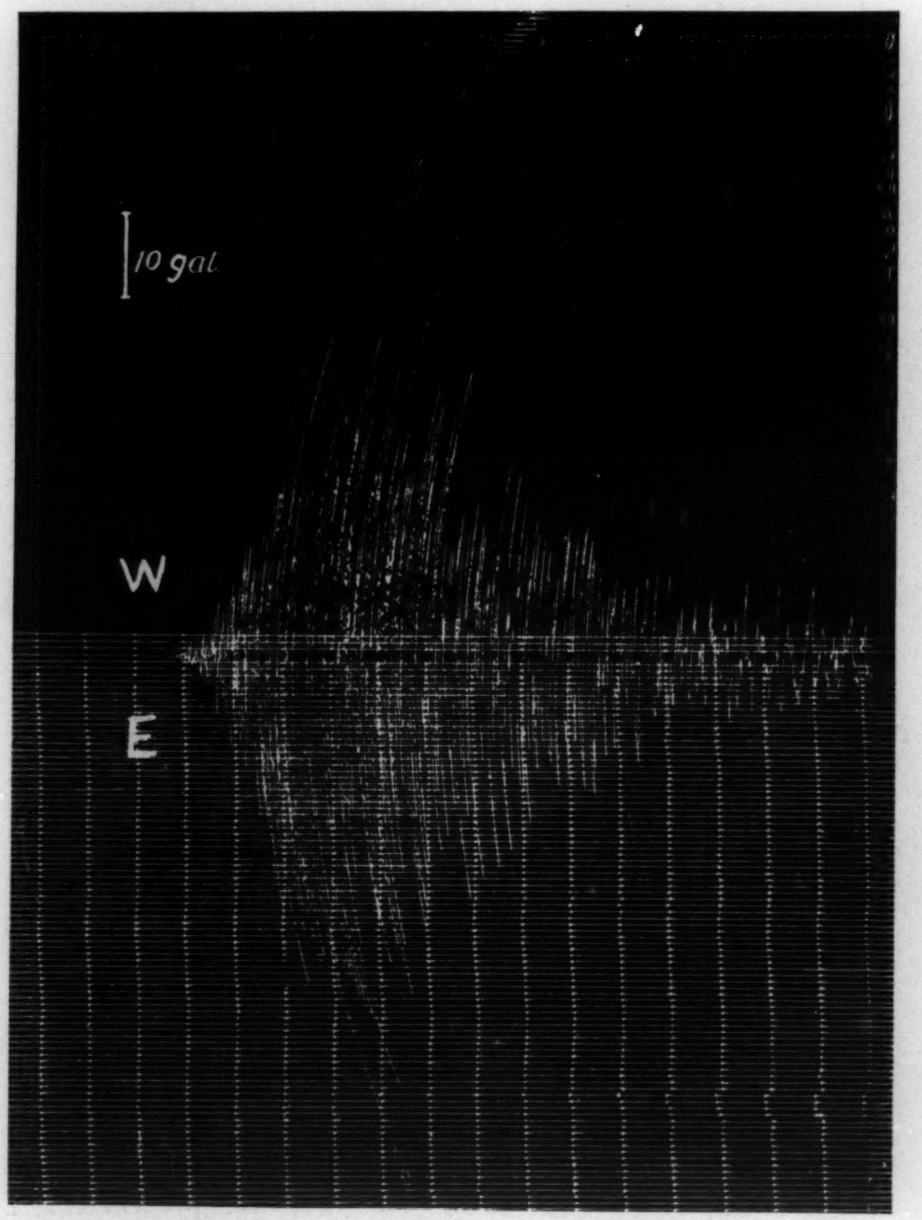

E.W. Component.

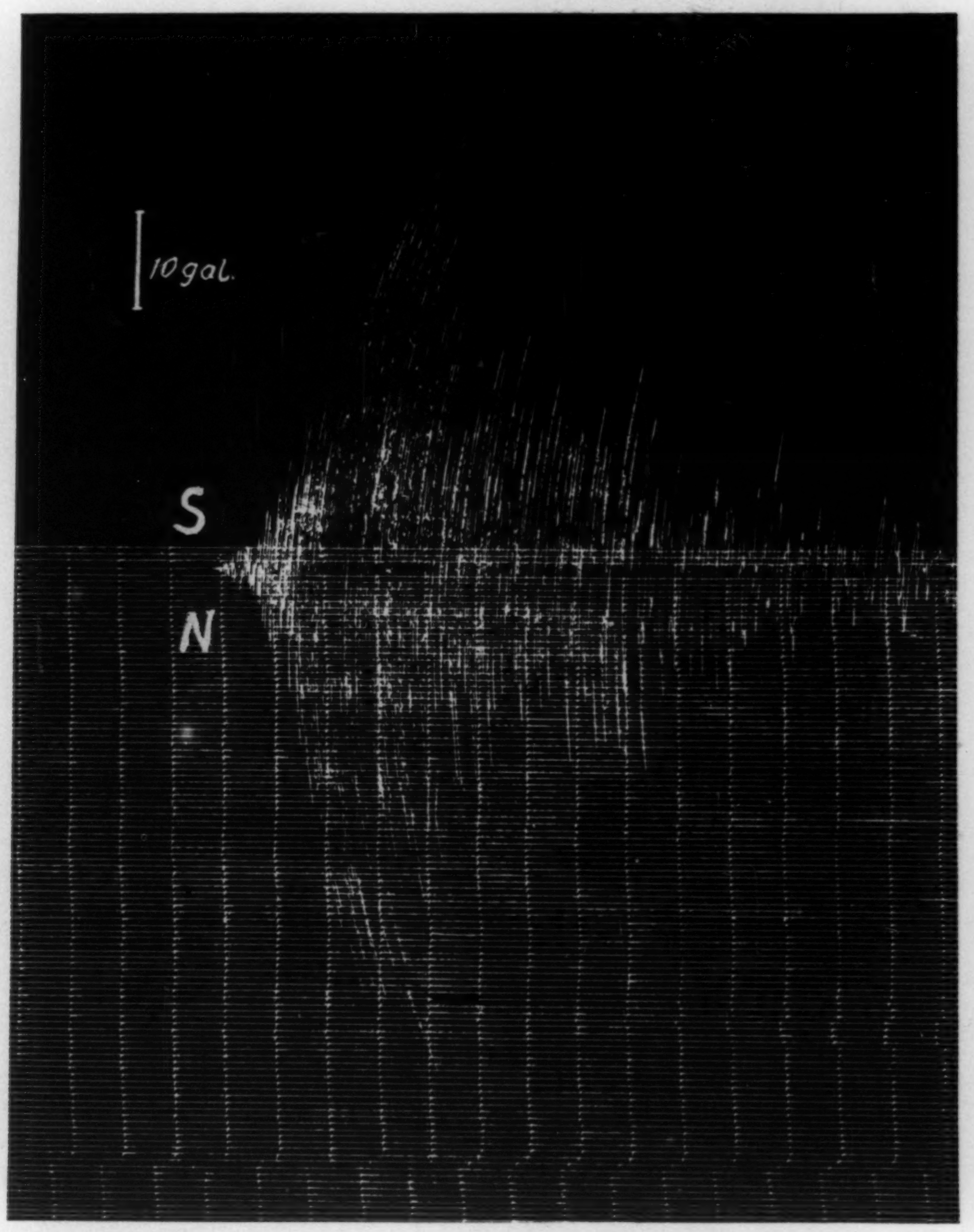

N.S. Component.

Fig. 12. Tôkyô Observation of the Strong Saitama Earthquake of September 21, 1931.
Ishimoto Acceleration Seismograph Diagrams.
(Time between consecutive two marks=6 sec.)

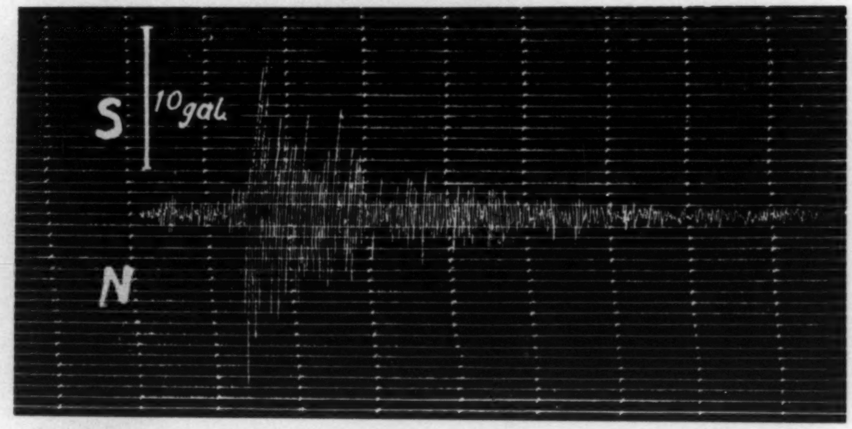

N.S. Component.

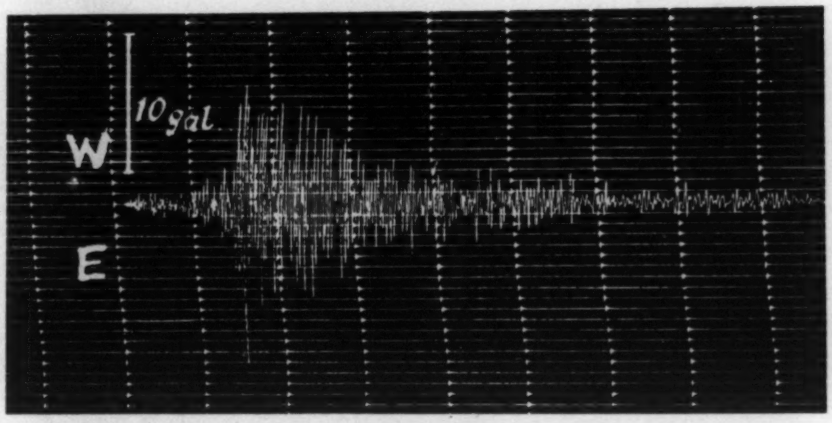

E.W. Component.

(震研彙報、第十號、圖版、震報)

Fig. 13. Tôkyô Observation of the Earthquake of September 28, 1931.
Ishimoto Acceleration Seismograph Diagrams.
(Time between consecutive two marks=6 sec.)

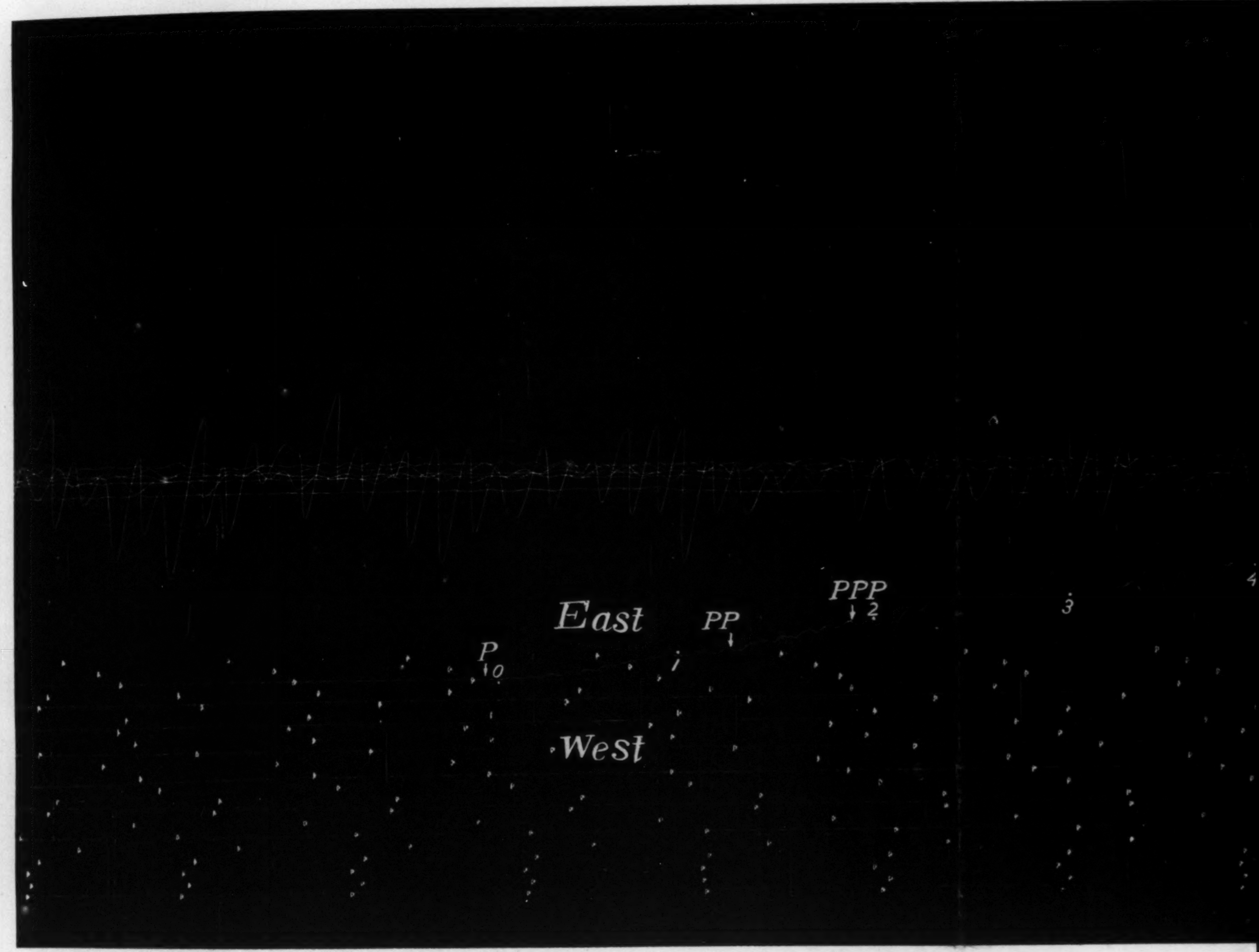

E. W. Component. Free vibration period = 2^{m} 11^{s}. Magnification = 5

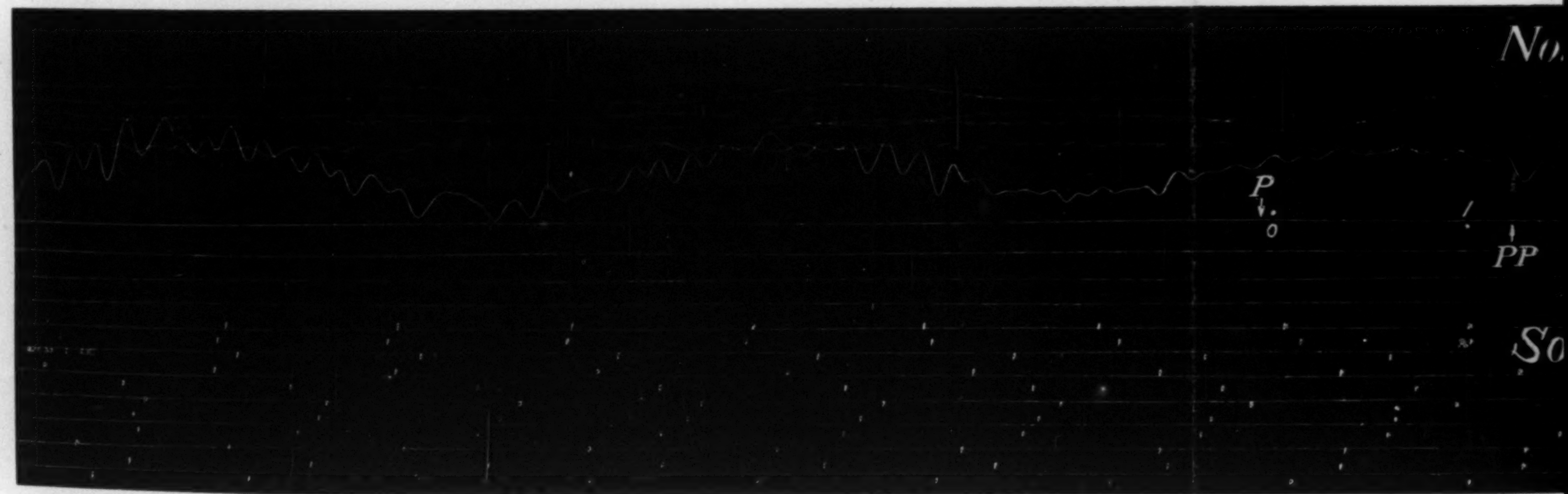

N. S. Component. Free vibration period = 3^{m} 31^{s}. Magnification = 1·5

(震研彙報、第十號、圖版、震報)

S
3
4
5
6
7

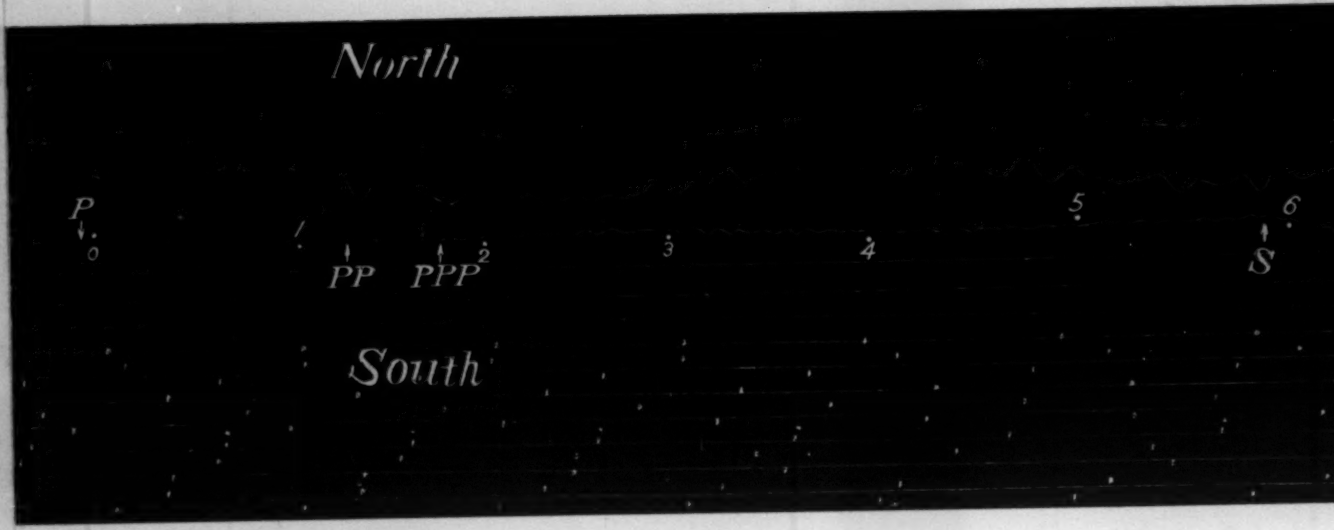
North
P
0
1
PP
PPP
2
3
4
5
6
S
South

Fig. 14. The Sin Kiang Earthquake of August 10, 1931, observed at (Tôkyô) Hongô.

Imamura Long Period Horizontal Pendulum Seismograph Record.

Time of commencement $= 21^{h}\ 26^{m}\ 12^{s}$ (G.M.T.)

(Minute mark is shown with dot.)

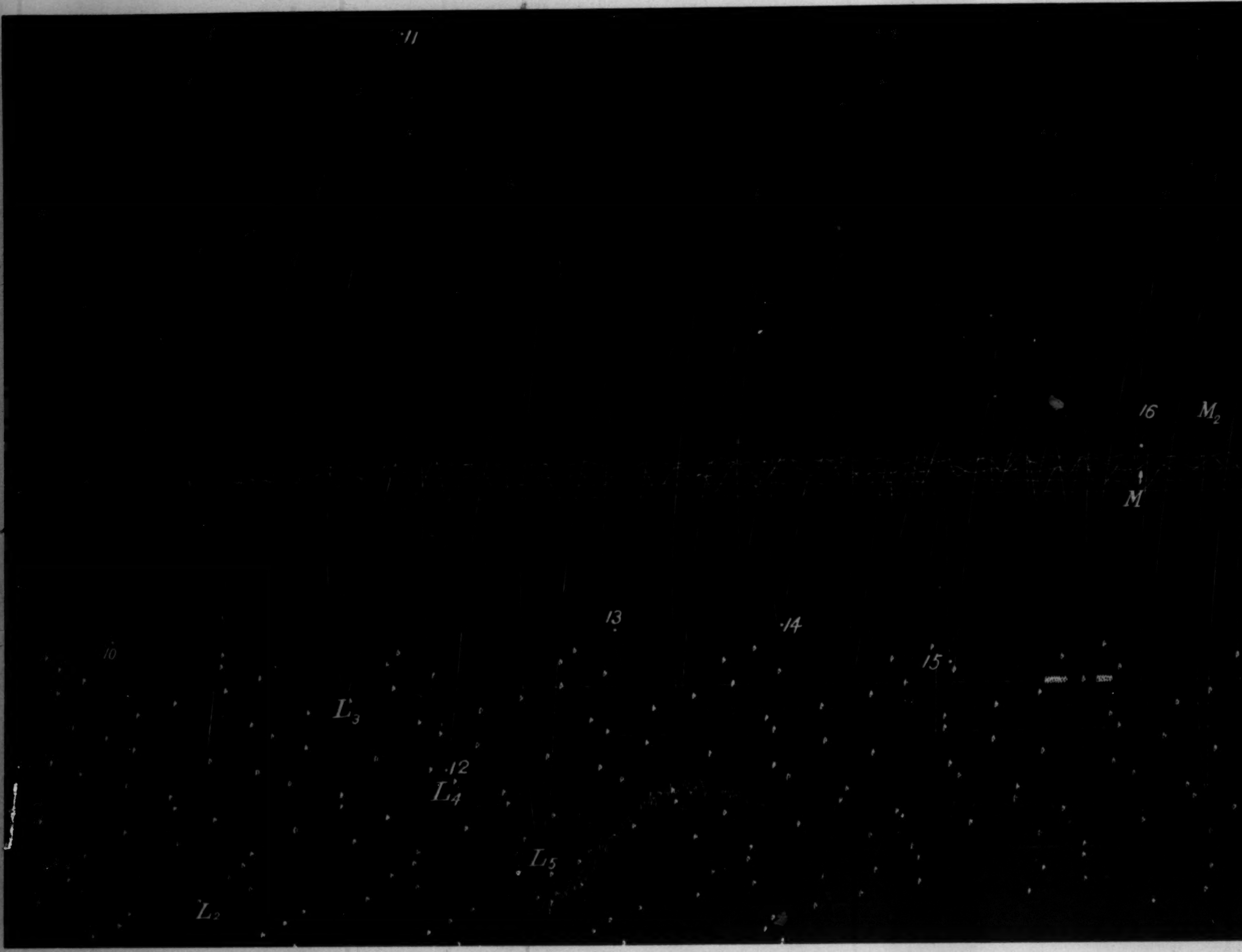

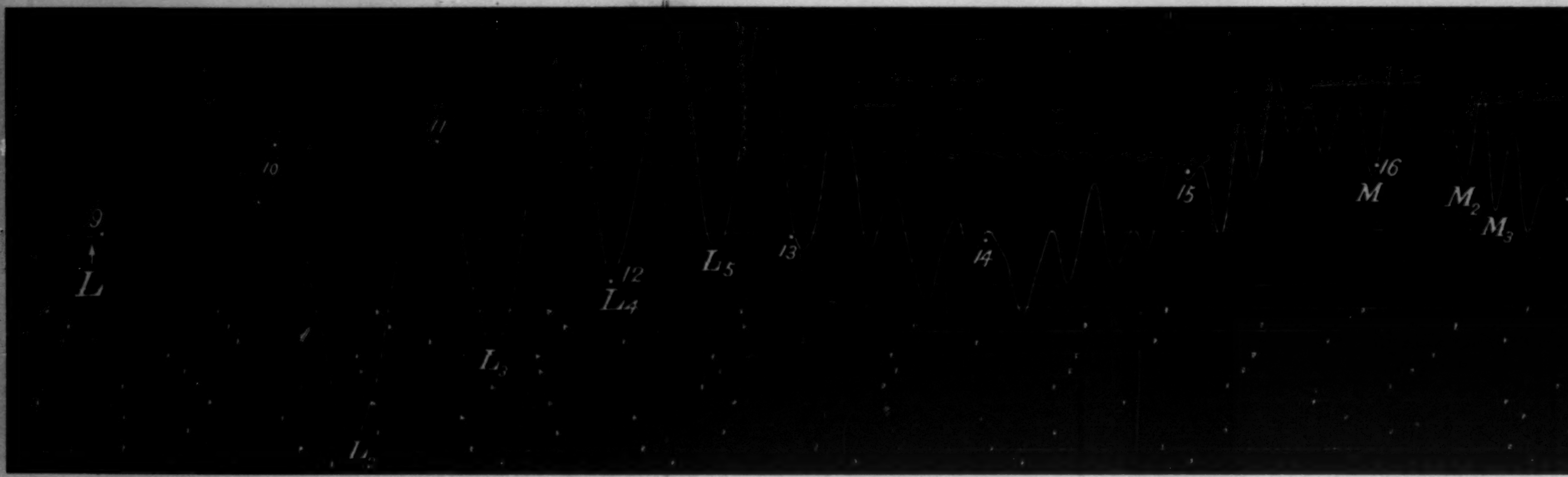

of August 10, 1931, observed at (Tôkyô) Hongô.

ntal Pendulum Seismograph Record.

nent = 21^h 26^m 12^s (G.M.T.)

is shown with dot.)

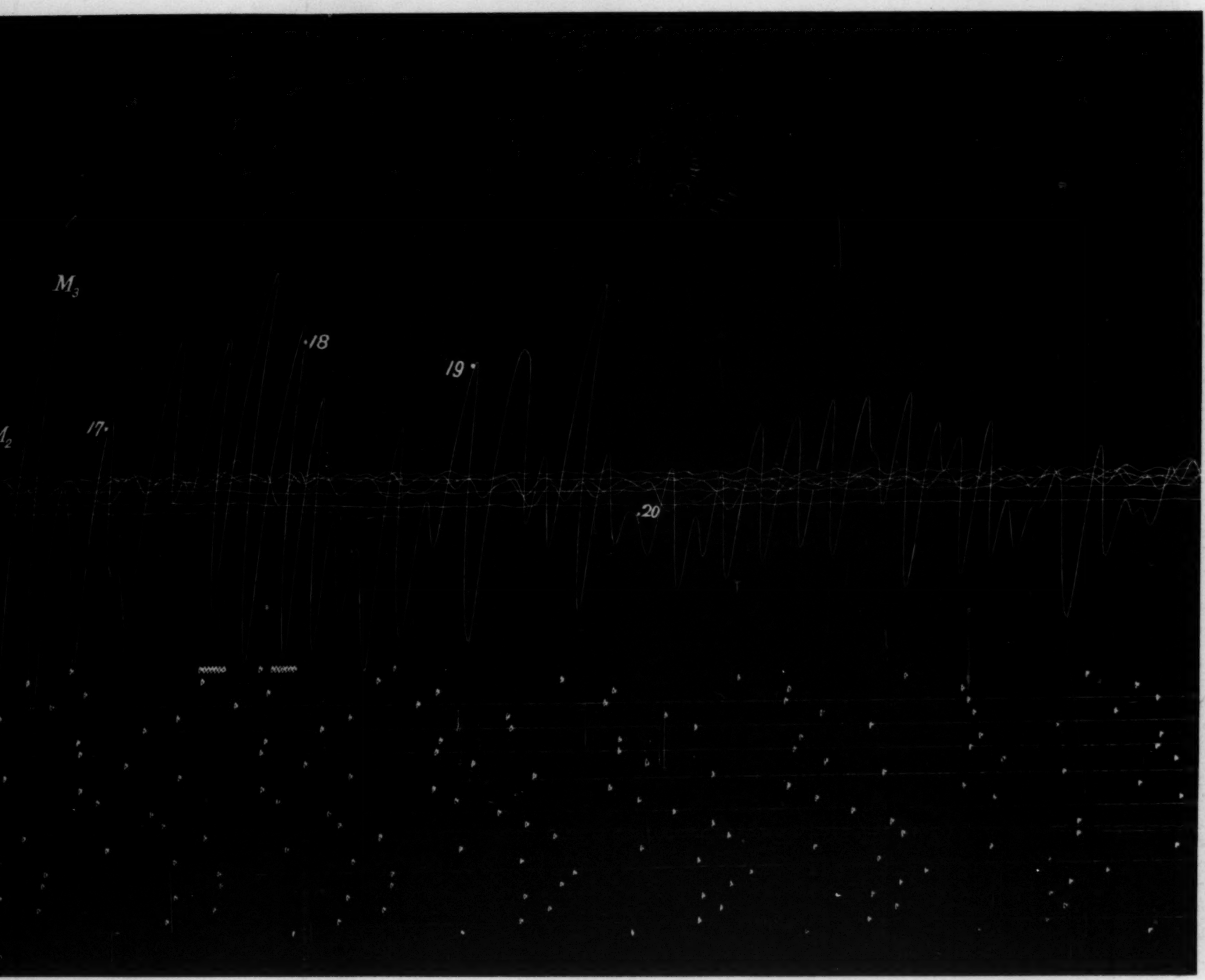
M_3
18
19
M_2
17
20

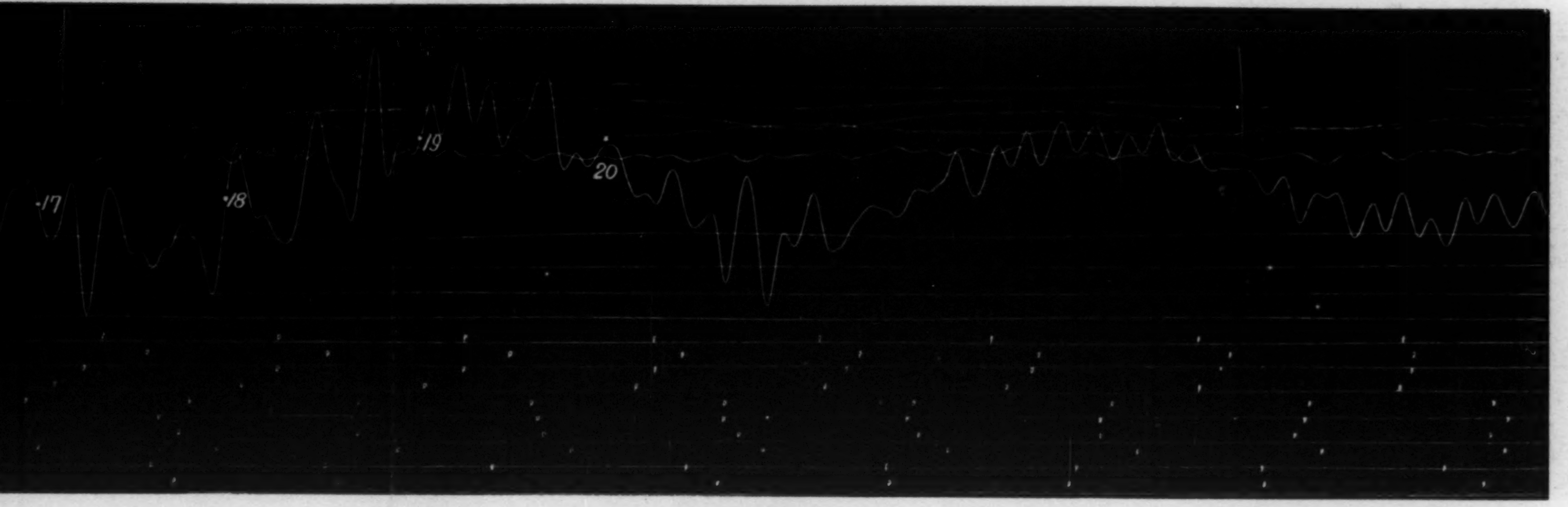
17
18
19
20

21. *Possibility of Free Oscillations of Strata excited by Seismic Waves. Part IV.*

By Katsutada SEZAWA and Kiyoshi KANAI,

Earthquake Research Institute.

(Read Feb. 16, 1932.—Received March 19, 1932.)

1. The present paper is the continuation of our research work on the determination of the possible range of free oscillations of strata due to seismic disturbances and deals with the case where primary seismic waves are incident upwards normally to doubly stratified layers residing on the surface of a semi-infinite body.

As to the thicknesses, densities and elastic constants of two layers and the bottom medium, we have employed the results of investigations due to a certain degree to Dr. Matuzawa[1] etc., and completely to Prof. Imamura[2] etc.. These are approximated as follows.

Layer	Thickness	Density	V for P-waves	V for S-waves
Upper layer (Granitic)	$H'-H=20$km	$\rho''=2{\cdot}7$	5·0 km/sec	3·15 km/sec
Second layer (Basaltic)	$H=30$km	$\rho'=3{\cdot}0$	6·1 km/sec	3·70 km/sec
Bottom medium (Ultrabasic)	∞	$\rho=3{\cdot}5$	7·5 km/sec	4·45 km/sec

2. Let ρ, λ, μ be the density and elastic constants of the bottom solid, ρ', λ', μ' those of the second layer of thickness H and ρ'', λ'', μ'' those of the first or upper layer of thickness $H'-H$. Again, let u, u', u'' be the respective displacements in the bottom medium, the second layer and the first layer; then the equations of motion of each medium are written as follows:

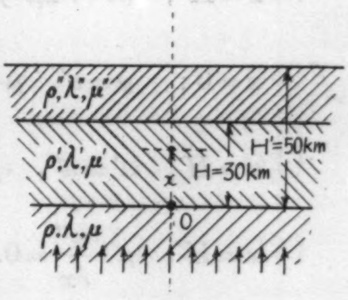

Fig. 1.

1) T. MATUZAWA, K. YAMADA and T. SUZUKI, "On the Forerunners of Earthquake-motions (The Second Paper)," *Bull. Earthq. Res. Inst.*, **7** (1929), 241–260.

2) A. IMAMURA, F. KISHINOUYE and T. KODAIRA, "The Effect of Superficial Sedimentary Layers upon the Transmission of Seismic Waves," *Bull. Earthq. Res. Inst.*, **7** (1929), 471–487, (in Japanese).

$$\left.\begin{aligned}\frac{\partial^2 u}{\partial t^2}&=V_1^2\frac{\partial^2 u}{\partial x^2},\\ \frac{\partial^2 u'}{\partial t^2}&=V_2^2\frac{\partial^2 u'}{\partial x^2},\\ \frac{\partial^2 u''}{\partial t^2}&=V_3^2\frac{\partial^2 u''}{\partial x^2},\end{aligned}\right\}\quad\cdots\cdots\cdots(1)$$

where $V_1^2=(\lambda+2\mu)/\rho$, $V_2^2=(\lambda'+2\mu')/\rho'$, $V_3^2=(\lambda''+2\mu'')/\rho''$ for dilatational waves and $V_1^2=\mu/\rho$, $V_2^2=\mu'/\rho'$, $V_3^2=\mu''/\rho''$ for distortional waves. The typical solutions of these equations are expressed by

$$\left.\begin{aligned}u&=e^{ih(V_1t-x)}+Ae^{ih(V_1t+x)}\\ u'&=Be^{ih'(V_2t-x)}+Ce^{ih'(V_2t+x)},\\ u''&=De^{ih''(V_3t-x)}+Ee^{ih''(V_3t+x)},\end{aligned}\right\}\quad\cdots\cdots\cdots(2)$$

where A, B, C, D, E are arbitrary constants and h, h' and h'' have the meaning such that

$$h=p/V_1,\quad h'=p/V_2,\quad h''=p/V_3,\quad\cdots\cdots\cdots(3)$$

in which $p/2\pi$ is the frequency of waves.

The boundary conditions at the planes, $x=0$, $x=H$, $x=H'$ are as follows:

$$\left.\begin{aligned}&x=0;\quad u=u',\quad (\lambda+2\mu)\frac{\partial u}{\partial x}=(\lambda'+2\mu')\frac{\partial u'}{\partial x},\\ &x=H;\quad u'=u'',\quad (\lambda'+2\mu')\frac{\partial u'}{\partial x}=(\lambda''+2\mu'')\frac{\partial u''}{\partial x},\\ &x=H';\quad (\lambda''+2\mu'')\frac{\partial u''}{\partial x}=0,\end{aligned}\right\}\ \text{for dilatational waves,}\quad(4)$$

$$\left.\begin{aligned}&x=0;\quad u=u',\quad \mu\frac{\partial u}{\partial x}=\mu'\frac{\partial u'}{\partial x},\\ &x=H;\quad u'=u'',\quad \mu'\frac{\partial u'}{\partial x}=\mu''\frac{\partial u''}{\partial x},\\ &x=H';\quad \mu''\frac{\partial u''}{\partial x}=0.\end{aligned}\right\}\ \text{for distortional waves.}\quad(5)$$

Substituting (2) in (4) and (5) by means of (3), and using the following notations:

$$\left.\begin{aligned}\alpha&=\sqrt{\frac{\rho'(\lambda'+2\mu')}{\rho(\lambda+2\mu)}},\quad \alpha'=\sqrt{\frac{\rho''(\lambda''+2\mu'')}{\rho'(\lambda'+2\mu')}},\\ \beta&=\sqrt{\frac{\rho'(\lambda+2\mu)}{\rho(\lambda'+2\mu')}},\quad \beta'=\sqrt{\frac{\rho''(\lambda'+2\mu')}{\rho'(\lambda''+2\mu'')}}\end{aligned}\right\}\quad\cdots\cdots(6)$$

for dilatational waves ; and

$$\left.\begin{aligned} \alpha=\sqrt{\frac{\rho'\mu'}{\rho\mu}}\,, \quad \alpha'=\sqrt{\frac{\rho''\mu''}{\rho'\mu'}}\,, \\ \beta=\sqrt{\frac{\rho'\mu}{\rho\mu'}}\,, \quad \beta'=\sqrt{\frac{\rho''\mu'}{\rho'\mu''}} \end{aligned}\right\} \quad \ldots\ldots\ldots\ldots\ldots(7)$$

for distortional waves, we find finally

$$A=\frac{(1-\alpha)(1+\alpha')e^{2i\beta\beta'h(H'-H)}e^{2i\beta hH}+(1+\alpha)(1-\alpha')e^{2i\beta\beta'h(H'-H)}+(1-\alpha)(1-\alpha')e^{2i\beta hH}+(1+\alpha)(1+\alpha')}{(1+\alpha)(1+\alpha')e^{2i\beta\beta'h(H'-H)}e^{2i\beta hH}+(1-\alpha)(1-\alpha')e^{2i\beta\beta'h(H'-H)}+(1+\alpha)(1-\alpha')e^{2i\beta hH}+(1-\alpha)(1+\alpha')}, \quad \ldots\ldots\ldots\ldots(8)$$

$$B=\frac{2\{(1+\alpha')e^{2i\beta\beta'hH'}+(1-\alpha')e^{2i\beta hH}\}}{(1+\alpha)(1+\alpha')e^{2i\beta\beta'h(H'-H)}e^{2i\beta hH}+(1-\alpha)(1-\alpha')e^{2i\beta\beta'h(H'-H)}+(1+\alpha)(1-\alpha')e^{2i\beta hH}+(1-\alpha)(1+\alpha')}, \quad \ldots\ldots\ldots\ldots(9)$$

$$C=\frac{2\{(1-\alpha')e^{2i\beta\beta'h(H'-H)}+(1+\alpha')\}}{(1+\alpha)(1+\alpha')e^{2i\beta\beta'h(H'-H)}e^{2i\beta hH}+(1-\alpha)(1-\alpha')e^{2i\beta\beta'h(H'-H)}+(1+\alpha)(1-\alpha')e^{2i\beta hH}+(1-\alpha)(1+\alpha')}, \quad \ldots\ldots\ldots\ldots(10)$$

$$D=\frac{4e^{2i\beta\beta'hH'}e^{i\beta hH(1-\beta')}}{(1+\alpha)(1+\alpha')e^{2i\beta\beta'h(H'-H)}e^{2i\beta hH}+(1-\alpha)(1-\alpha')e^{2i\beta\beta'h(H'-H)}+(1+\alpha)(1-\alpha')e^{2i\beta hH}+(1-\alpha)(1+\alpha')}, \quad \ldots\ldots\ldots\ldots(11)$$

$$E=\frac{4e^{i\beta hH(1-\beta')}}{(1+\alpha)(1+\alpha')e^{2i\beta\beta'h(H'-H)}e^{2i\beta hH}+(1-\alpha)(1-\alpha')e^{2i\beta\beta'h(H'-H)}+(1+\alpha)(1-\alpha')e^{2i\beta hH}+(1-\alpha)(1+\alpha')}. \quad \ldots\ldots\ldots\ldots(12)$$

In the special case where $\alpha'=1$, $\beta'=1$ we find

$$A=\frac{(1-\alpha)+(1+\alpha)e^{-2i\beta hH'}}{(1+\alpha)+(1-\alpha)e^{-2i\beta hH'}}, \quad \ldots\ldots\ldots\ldots(8')$$

$$B=\frac{2}{(1+\alpha)+(1-\alpha)e^{-2i\beta hH'}}, \quad \ldots\ldots\ldots\ldots(9')$$

$$C=\frac{2e^{-2i\beta hH'}}{(1+\alpha)+(1-\alpha)e^{-2i\beta hH'}}, \quad \ldots\ldots\ldots\ldots(10')$$

$$D=\frac{2}{(1+\alpha)+(1-\alpha)e^{-2i\beta hH'}}, \quad \ldots\ldots\ldots\ldots(11')$$

$$E=\frac{2e^{-2i\beta hH'}}{(1+\alpha)+(1-\alpha)e^{-2i\beta hH'}} \quad \ldots\ldots\ldots\ldots(12')$$

These are coincident with the result which one[3)] of us obtained a few years ago.

Decomposing u in (2) into primary waves u_1 and reflected waves u_2, and applying Fourier's integral we get

3) K. SEZAWA, "Possibility of the Free-oscillations of the Surface-layer excited by the Seismic-waves," *Bull. Earthq. Res. Inst.*, **8** (1930), 1—11.

$$u_1=\frac{1}{2\pi}\int_{-\infty}^{\infty}dh\int_{-\infty}^{\infty}f(\sigma)e^{ih(V_1t-x+\sigma)}d\sigma, \quad \ldots\ldots\ldots\ldots(13)$$

$$u_2=\frac{1}{2\pi}\int_{-\infty}^{\infty}\left[\frac{(1-\alpha)(1+\alpha')e^{2i\beta\beta'h(H'-H)}e^{2i\beta hH}+(1+\alpha)(1-\alpha')e^{2i\beta\beta'h(H'-H)}+(1-\alpha)(1-\alpha')e^{2i\beta hH}+(1+\alpha)(1+\alpha')}{(1+\alpha)(1+\alpha')e^{2i\beta\beta'h(H'-H)}e^{2i\beta hH}+(1-\alpha)(1-\alpha')e^{2i\beta\beta'h(H'-H)}+(1+\alpha)(1-\alpha')e^{2i\beta hH}+(1-\alpha)(1+\alpha')}\right]dh$$
$$\times\int_{-\infty}^{\infty}f(\sigma)e^{ih(V_1t+x+\sigma)}d\sigma, \qquad (14)$$

$$u'=\frac{1}{\pi}\int_{-\infty}^{\infty}\frac{\{(1+\alpha')e^{2i\beta\beta'hH'}+(1-\alpha')e^{2i\beta hH}\}dh}{(1+\alpha)(1+\alpha')e^{2i\beta\beta'h(H'-H)}e^{2i\beta hH}+(1-\alpha)(1-\alpha')e^{2i\beta\beta'h(H'-H)}+(1+\alpha)(1-\alpha')e^{2i\beta hH}+(1-\alpha)(1+\alpha')}$$
$$\times\int_{-\infty}^{\infty}f(\sigma)e^{i\beta h\left(V_2t-x+\frac{\sigma}{\beta}\right)}d\sigma$$
$$+\frac{1}{\pi}\int_{-\infty}^{\infty}\frac{\{(1-\alpha')e^{2i\beta\beta'h(H'-H)}+(1+\alpha')\}dh}{(1+\alpha)(1+\alpha')e^{2i\beta\beta'h(H'-H)}e^{2i\beta hH}+(1-\alpha)(1-\alpha')e^{2i\beta\beta'h(H'-H)}+(1+\alpha)(1-\alpha')e^{2i\beta hH}+(1-\alpha)(1+\alpha')}$$
$$\times\int_{-\infty}^{\infty}f(\sigma)e^{i\beta h\left(V_2t+x+\frac{\sigma}{\beta}\right)}d\sigma, \qquad (15)$$

$$u''=\frac{2}{\pi}\int_{-\infty}^{\infty}\frac{e^{2i\beta\beta'hH'}e^{i\beta hH(1-\beta')}dh}{(1+\alpha)(1+\alpha')e^{2i\beta\beta'h(H'-H)}e^{2i\beta hH}+(1-\alpha)(1-\alpha')e^{2i\beta\beta'h(H'-H)}+(1+\alpha)(1-\alpha')e^{2i\beta hH}+(1-\alpha)(1+\alpha')}$$
$$\times\int_{-\infty}^{\infty}f(\sigma)e^{i\beta\beta'h\left(V_3t-x+\frac{\sigma}{\beta\beta'}\right)}d\sigma$$
$$+\frac{2}{\pi}\int_{-\infty}^{\infty}\frac{e^{i\beta hH(1-\beta')}dh}{(1+\alpha)(1+\alpha')e^{2i\beta\beta'h(H'-H)}e^{2i\beta hH}+(1-\alpha)(1-\alpha')e^{2i\beta\beta'h(H'-H)}+(1+\alpha)(1-\alpha')e^{2i\beta hH}+(1-\alpha)(1+\alpha')}$$
$$\times\int_{-\infty}^{\infty}f(\sigma)e^{i\beta\beta'h\left(V_3t+x+\frac{\sigma}{\beta\beta'}\right)}d\sigma, \qquad (16)$$

where the initial condition

$$t=0; \qquad u_0=f(x) \quad \ldots\ldots\ldots\ldots\ldots\ldots(17)$$

for the primary waves is applied.

Again, the integrand under the first integral sign of each first term of the right-hand side of (16) is transformed as follows:

$$\frac{e^{2i\beta\beta'hH'}e^{i\beta hH(1-\beta')}}{(1+\alpha)(1+\alpha')e^{2i\beta\beta'h(H'-H)}e^{2i\beta hH}+(1-\alpha)(1-\alpha')e^{2i\beta\beta'h(H'-H)}+(1+\alpha)(1-\alpha')e^{2i\beta hH}+(1-\alpha)(1+\alpha')}$$
$$=\frac{e^{i\beta hH(\beta'-1)}}{(1+\alpha)(1+\alpha')+(1-\alpha)(1-\alpha')e^{-2i\beta hH}+(1+\alpha)(1-\alpha')e^{-2i\beta\beta'h(H'-H)}+(1-\alpha)(1+\alpha')e^{-2i\beta h(\beta'H'-\beta'H+H)}},$$
$$\ldots\ldots\ldots\ldots\ldots\ldots(18)$$

$$\frac{e^{i\beta hH(1-\beta')}}{(1+\alpha)(1+\alpha')e^{2i\beta\beta'h(H'-H)}e^{2i\beta hH}+(1-\alpha)(1-\alpha')e^{2i\beta\beta'h(H'-H)}+(1+\alpha)(1-\alpha')e^{2i\beta hH}+(1-\alpha)(1+\alpha')}$$
$$=\frac{e^{i\beta h(\beta'H-2\beta'H'-H)}}{(1+\alpha)(1+\alpha')+(1-\alpha)(1-\alpha')e^{-2i\beta hH}+(1+\alpha)(1-\alpha')e^{-2i\beta\beta'h(H'-H)}+(1-\alpha)(1+\alpha')e^{-2i\beta h(\beta'H'-\beta'H+H)}}.$$
$$\ldots\ldots\ldots\ldots\ldots\ldots(19)$$

The proper expansion of the factor corresponding to the denominator of the above expressions becomes

$$\{(1+\alpha)(1+\alpha')+(1-\alpha)(1-\alpha')e^{-2i\beta hH}+(1+\alpha)(1-\alpha')e^{-2i\beta\beta' h(H'-H)}$$
$$+(1-\alpha)(1+\alpha')e^{-2i\beta h(\beta' H'-\beta' H+H)}\}^{-1}$$

$$=(1+\alpha)^{-1}(1+\alpha')^{-1}\sum_{m=0}^{\infty}(-1)^m\sum_{n=0}^{m}\frac{m!}{n!(m-n)!}$$
$$\times\sum_{p=0}^{n}\frac{n!}{p!(n-p)!}\,\frac{(1-\alpha)^{m-p}(1-\alpha')^{m+p-n}}{(1+\alpha)^{m-p}(1+\alpha')^{m+p-n}}e^{2ih\beta\{(p-m)H+n\beta' H-n\beta' H'\}}. \quad (20)$$

When we put

$$M=(1+\alpha)^{-1}(1+\alpha')^{-1}\sum_{m=0}^{\infty}(-1)^m\sum_{n=0}^{m}\frac{m!}{n!(m-n)!}\sum_{p=0}^{n}\frac{n!}{p!(n-p)!}, \quad ..(21)$$

the expression (16) of the displacement of the upper layer becomes

$$u''=\frac{2}{\pi}\int_{-\infty}^{\infty}M\frac{(1-\alpha)^{m-p}(1-\alpha')^{m+p-n}}{(1+\alpha)^{m-p}(1+\alpha')^{m+p-n}}e^{ih\beta\{(2p-2m-1)H+(2n+1)\beta' H-2n\beta' H'\}}dh$$
$$\times\int_{-\infty}^{\infty}f(\sigma)e^{i\beta\beta' h\left(V_3t-x+\frac{\sigma}{\beta\beta'}\right)}d\sigma$$
$$+\frac{2}{\pi}\int_{-\infty}^{\infty}M\frac{(1-\alpha)^{m-p}(1-\alpha')^{m+p-n}}{(1+\alpha)^{m-p}(1+\alpha')^{m+p-n}}e^{ih\beta\{(2p-2m-1)H+(2n+1)\beta' H-2(n+1)\beta' H'\}}dh$$
$$\times\int_{-\infty}^{\infty}f(\sigma)e^{i\beta\beta' h\left(V_3t+x+\frac{\sigma}{\beta\beta'}\right)}d\sigma. \quad ..(22)$$

3. Let the form of the primary waves when $t=0$, that proceed upwards, be

$$\left.\begin{array}{ll} u_1=\cos cx, & [-a<x<0] \\ \quad =0, & [0>x] \\ \quad =0; & [-a<x] \end{array}\right\} \quad ....(23)$$

then, integrating (13) and (22) with respect to σ, and again integrating with respect to h, we obtain the expressions of the displacement of the primary waves for any time and of the vibratory movement of the upper layer as follows:

$$\left.\begin{array}{ll} u_1=\cos c(V_1t-x), & [(V_1t-a)<x<V_1t] \\ \quad =0, & [V_1t<x] \\ \quad =0; & [(V_1t-a)>x] \end{array}\right\} \quad ....(24)$$

$$u''=4(1+\alpha)^{-1}(1+\alpha')^{-1}\sum_{m=0}^{\infty}(-1)^m\sum_{n=0}^{m}\frac{m!}{n!(m-n)!}$$
$$\times\sum_{p=0}^{n}\frac{n!}{p!(n-p)!}\,\frac{(1-\alpha)^{m-p}(1-\alpha')^{m+p-n}}{(1+\alpha)^{m-p}(1+\alpha')^{m+p-n}}\,f(m,n,p)$$

$$\times \cos c\beta\{\beta'(V_3t-x)+(2p-2m-1)H+(2n+1)\beta'H-2n\beta'H'\}$$

$$+4(1+\alpha)^{-1}(1+\alpha')^{-1}\sum_{m=0}^{\infty}(-1)^m\sum_{n=0}^{m}\frac{m!}{n!\,(m-n)!}$$

$$\times\sum_{p=0}^{n}\frac{n!}{p!\,(n-p)!}\frac{(1-\alpha)^{m-p}(1-\alpha')^{m+p-n}}{(1+\alpha)^{m-p}(1+\alpha')^{m+p-n}}\ \varphi(m,n,p)$$

$$\times \cos c\beta\{\beta'(V_3t+x)+(2p-2m-1)H+(2n+1)\beta'H-2(n+1)\beta'H'\}, \qquad \ldots\ldots\ldots\ldots(25)$$

where
$$f(m,n,p)=1,\quad \left[\left\{V_3t+\frac{(2p-2m-1)H+(2n+1)\beta'H-2n\beta'H'}{\beta'}\right\} > x > \left\{V_3t+\left\{\frac{(2p-2m-1)H+(2n+1)\beta'H-2n\beta'H'}{\beta'}-\frac{a}{\beta\beta'}\right\}\right]$$

$$=0,\quad \left[\left\{V_3t+\frac{(2p-2m-1)H+(2n+1)\beta'H-2n\beta'H'}{\beta'}\right\}<x\right]$$

$$=0,\quad \left[\left\{V_3t+\frac{(2p-2m-1)H+(2n+1)\beta'H-2n\beta'H'}{\beta'}-\frac{a}{\beta\beta'}\right\}>x\right]$$

$$\varphi(m,n,p)=1,\quad \left[-\left\{V_3t+\frac{(2p-2m-1)H+(2n+1)\beta'H-2(n+1)\beta'H'}{\beta'}\right\} < x < -\left\{V_3t+\frac{(2p-2m-1)H+(2n+1)\beta'H-2(n+1)\beta'H'}{\beta'}-\frac{a}{\beta\beta'}\right\}\right]$$

$$=0,\quad \left[-\left\{V_3t+\frac{(2p-2m-1)H+(2n+1)\beta'H-2(n+1)\beta'H'}{\beta'}\right\}>x\right]$$

$$=0.\quad \left[-\left\{V_3t+\frac{(2p-2m-1)H+(2n+1)\beta'H-2(n+1)\beta'H'}{\beta'}-\frac{a}{\beta\beta'}\right\}<x\right]$$

The values of u_1 at $x=0$ and u'' at $x=H'$ (free surface) are plotted in Figs. 2, 3, 4, 5, 6, 7, 8, 9, 10, 11. In these figures Figs. 2, 3, 4, 5, 6, are related to the transmission of dilatational waves so that the values $V_1=7{\cdot}5$ km/sec, $V_2=6{\cdot}1$ km/sec, $V_3=5{\cdot}0$ km/sec were used in these cases; while Figs. 7, 8, 9, 10, 11 are concerned with the propagation of distortional waves so that the values $V_1=4{\cdot}45$ km/sec, $V_2=3{\cdot}70$ km/sec, $V_3=3{\cdot}15$ km/sec were employed. Fig. 2 gives the case of wave length $L=\frac{2\pi}{c}=10$ km, and similarly Fig. 3 $L=40$ km; Fig. 4 $L=60$ km; Fig. 5 $L=100$ km; Fig. 6 $L=150$ km. The remaining figures correspond with the propagation of distortional waves and Fig. 7 gives the case of wave length $L=\frac{2\pi}{c}=6$ km; Fig. 8 $L=24$ km; Fig. 9 $L=36$ km; Fig. 10 $L=60$km; Fig. 11 $L=90$ km. In all cases we have assumed that $a=2L$.

4. Let the form of the primary waves when $t=0$, that proceed upwards, be

$$u_1=e^{-\frac{\sigma^2}{c^2}}, \qquad \text{(26)}$$

then, integrating (12) and (21) with respect to σ, and again integrating with respect to h, we get the expressions of the displacement of the primary waves for any time and of the movement of the upper layer as follows:

$$u_1=e^{-\frac{(V_1t-x)^2}{c^2}}, \qquad \text{(27)}$$

and

$$\begin{aligned} u'' =& 4(1+\alpha)^{-1}(1+\alpha')^{-1}\sum_{m=0}^{\infty}(-1)^m\sum_{n=0}^{m}\frac{m!}{n!(m-n)!} \\ & \times\sum_{p=0}^{n}\frac{n!}{p!(n-p)!}\frac{(1-\alpha)^{m-p}(1-\alpha')^{m+p-n}}{(1+\alpha)^{m-p}(1+\alpha')^{m+p-n}} \\ & \times e^{\frac{-\beta^2\{\beta'(V_3t-x)+(2p-2m-1)H+(2n+1)\beta'H-2n\beta'H'\}^2}{c^2}} \\ & +4(1+\alpha)^{-1}(1+\alpha')^{-1}\sum_{m=0}^{\infty}(-1)^m\sum_{n=0}^{m}\frac{m!}{n!(m-n)!} \\ & \times\sum_{p=0}^{n}\frac{n!}{p!(n-p)!}\frac{(1-\alpha)^{m-p}(1-\alpha')^{m+p-n}}{(1+\alpha)^{m-p}(1+\alpha')^{m+p-n}} \\ & \times e^{\frac{-\beta^2\{\beta'(V_3t+x)+(2p-2m-1)H+(2n+1)\beta'H-2(n+1)\beta'H'\}^2}{c^2}}. \end{aligned} \qquad \text{(28)}$$

The fact, that the expressions of displacements in (25), (28) are of series forms, is not only due to mathematical convenience, but also due to the nature that the series forms indicate the successive formation of the groups of waves by the multiple reflection at the discontinuities.

The values of u_1 at $x=0$ and u'' at $x=H'$ (free surface) are plotted in Figs. 12, 13, 14, 15, 16, 17, 18, 19, 20, 21. In these figures Figs. 12, 13, 14, 15, 16 give the cases of dilatational waves and correspond respectively to the cases of $c=5$ km, 20 km, 30 km, 50 km, 75 km; while Figs. 17, 18, 19, 20, 21 those of distortional waves and correspond respectively to the cases $c=3$ km, 12 km, 18 km, 30 km, 45 km.

5. It will be seen from these figures that, even when the primary waves are of a regular harmonic type or of a type of a single shock, the movements on the surface of the ground are oscillatory in complicated forms as in the cases of preceding papers. These complicated oscillations, however, may be separated in successive groups, each of which corresponds to the effect of reflection of waves at each discontinuous surface

of the layer. Thus, the periodicity of occurrence of the successive groups depends on the thicknesses of the strata and on the proper velocities in these strata. In the present case, too, the successive groups become smaller and smaller. The intermittence or overlapping of the groups of oscillations according with the ratio of the thicknesses of strata to the length of disturbed portion abides also by the same law as shown in preceding papers.

When the primary disturbance is of a regular harmonic type of a finite extent, each group of the oscillations at the surface may be generally identified by the small steps superposed on the principal oscillatory movement, while in the case of the primary disturbance of a type of a single shock, all fluctuating amplitudes at the surface may be taken as the respective groups. From this consideration it may be concluded that, though in the case of the primary disturbance of the type of a single shock the vibratory movements on the surface indicate the sign of free oscillations of strata, the oscillations on the surface due to primary waves of some oscillatory type are by no means the consequence of self-oscillations of the strata, but each interval between small steps superposed on the principal vibrations corresponds, indeed, with the period of free oscillations of a stratum or of strata.

In actual seismic waves the primary disturbance, either of a pure harmonic type or of a single shock, is of rare occurrence and some intermediate type of disturbance between the above two cases are expected to take place, so that the category belonging to each individual case would not be of a perfect use. As, however, the two cases give critical types of the free-oscillations of strata, it seems possible that the moving type of the ground in general may also be intermediate between the above two.

6. This article is not directly connected with the main part of the present paper. The problem of the transmission of dilatational disturbance of a harmonic type of a finite extent in a body having a single surface layer was dealt with as a supplement to one[4)] of our preceding papers.

Let the axis of x be drawn upwards from the lower boundary of a surface layer, and let u be the displacement of the bottom medium and ρ, λ, μ the density and Lamé's elastic constants of this medium. The similar displacement, density and elastic constants of the surface layer of thickness H are to be expressed by u', ρ', λ', μ'. In the same manner

4) K. SEZAWA, *loc. cit.*, in foot note 3).

of mathematical treatment as in the preceding paper[5] we arrive at

$$u_1=\frac{1}{2\pi}\int_{-\infty}^{\infty}dh\int_{-\infty}^{\infty}f(\sigma)e^{ih(V_1t-x+\sigma)}d\sigma, \quad \ldots\ldots\ldots\ldots(29)$$

$$u_2=\frac{1}{2\pi}\sum_{m=0}^{\infty}(-1)^m\left(\frac{1-\alpha}{1+\alpha}\right)^{m+1}\int_{-\infty}^{\infty}e^{-2im\beta hH}dh\int_{-\infty}^{\infty}f(\sigma)e^{ih(V_1t+x+\sigma)}d\sigma$$
$$+\frac{1}{2\pi}\sum_{m=0}^{\infty}(-1)^m\left(\frac{1-\alpha}{1+\alpha}\right)^{m}\int_{-\infty}^{\infty}e^{-2i(m+1)\beta hH}dh\int_{-\infty}^{\infty}f(\sigma)e^{ih(V_1t+x+\sigma)}d\sigma, [\alpha<1]\ldots(30)$$

$$u'=\frac{1}{\pi}\sum_{m=0}^{\infty}(-1)^m\frac{(1-\alpha)^m}{(1+\alpha)^{m+1}}\int_{-\infty}^{\infty}e^{-2im\beta hH}dh\int_{-\infty}^{\infty}f(\sigma)e^{i\beta h\left(V_2t-x+\frac{\sigma}{\beta}\right)}d\sigma$$
$$+\frac{1}{\pi}\sum_{m=0}^{\infty}(-1)^m\frac{(1-\alpha)^m}{(1+\alpha)^{m+1}}\int_{-\infty}^{\infty}e^{-2i(m+1)\beta hH}dh\int_{-\infty}^{\infty}f(\sigma)e^{i\beta h\left(V_2t+x+\frac{\sigma}{\beta}\right)}d\sigma, \quad [\alpha<1]$$
$$\ldots\ldots(31)$$

$$u_2=-\frac{1}{2\pi}\sum_{m=0}^{\infty}\left(\frac{\alpha-1}{\alpha+1}\right)^{m+1}\int_{-\infty}^{\infty}e^{-2im\beta hH}dh\int_{-\infty}^{\infty}f(\sigma)e^{ih(V_1t+x+\sigma)}d\sigma$$
$$+\frac{1}{2\pi}\sum_{m=0}^{\infty}\left(\frac{\alpha-1}{\alpha+1}\right)^{m}\int_{-\infty}^{\infty}e^{-2i(m+1)\beta hH}dh\int_{-\infty}^{\infty}f(\sigma)e^{ih(V_1t+x+\sigma)}d\sigma, \ [\alpha>1]\ (32)$$

$$u'=\frac{1}{\pi}\sum_{m=0}^{\infty}\frac{(\alpha-1)^m}{(\alpha+1)^{m+1}}\int_{-\infty}^{\infty}e^{-2im\beta hH}dh\int_{-\infty}^{\infty}f(\sigma)e^{i\beta h\left(V_2t-x+\frac{\sigma}{\beta}\right)}d\sigma$$
$$+\frac{1}{\pi}\sum_{m=0}^{\infty}\frac{(\alpha-1)^m}{(\alpha+1)^{m+1}}\int_{-\infty}^{\infty}e^{-2i(m+1)\beta hH}dh\int_{-\infty}^{\infty}f(\sigma)e^{i\beta h\left(V_2t+x+\frac{\sigma}{\beta}\right)}d\sigma, \ [\alpha>1] \quad (33)$$

where

$$\left.\begin{aligned} V_1&=\sqrt{\frac{\lambda+2\mu}{\rho}},\quad V_2=\sqrt{\frac{\lambda'+2\mu'}{\rho'}},\quad h=p/V_1,\\ \alpha&=\sqrt{\frac{\rho'(\lambda'+2\mu')}{\rho(\lambda+2\mu)}},\quad \beta=\sqrt{\frac{\rho'(\lambda+2\mu)}{\rho(\lambda'+2\mu')}},\end{aligned}\right\}\ \ldots\ldots(34)$$

u_1 is incident waves, u_2 reflected waves in the bottom medium and $f(x)$ is the type of the original waves. Now we take the initial disturbance of the type,

$$t=0;\quad f(x)=\cos cx,\quad [-a<x<0]\ \ldots\ldots\ldots\ldots(35)$$

then, substituting this in (29), (30), (31), (32), (33), we find

$$\left.\begin{aligned} u_1&=\cos c(V_1t-x), && [(V_1t-a)<x<V_1t]\\ &=0, && [V_1t<x]\\ &=0, && [(V_1t-a)>x]\end{aligned}\right\}\ \ldots\ldots\ldots(36)$$

5) K. SEZAWA, *loc. cit.*, in foot note 3).

$$u_2=\sum_{m=0}^{\infty} f(m)(-1)^m\left(\frac{1-\alpha}{1+\alpha}\right)^{m+1}\cos c(V_1t+x-2m\beta H)$$
$$+\sum_{m=0}^{\infty}\varphi(m)(-1)^m\left(\frac{1-\alpha}{1+\alpha}\right)^{m}\cos c\{V_1t+x-2(m+1)\beta H\},\ldots\ldots(37)$$

where

$$f(m)=1,\quad [-(V_1t-2m\beta H)<x<-(V_1t-2m\beta H-a)]$$
$$=0,\quad [-(V_1t-2m\beta H)>x]$$
$$=0,\quad [-(V_1t-2m\beta H-a)<x]$$
$$\varphi(m)=1,\quad [-\{V_1t-2(m+1)\beta H\}<x<-\{V_1t-2(m+1)\beta H-a\}]$$
$$=0,\quad [-\{V_1t-2(m+1)\beta H\}>x]$$
$$=0,\quad [-\{V_1t-2(m+1)\beta H-a\}<x]$$

$$u'=2\sum_{m=0}^{\infty} f(m)(-1)^m\frac{(1-\alpha)^m}{(1+\alpha)^{m+1}}\cos c\beta(V_2t-x-2mH)$$
$$+2\sum_{m=0}^{\infty}\varphi(m)(-1)^m\frac{(1-\alpha)^m}{(1+\alpha)^{m+1}}\cos c\beta\{V_2t+x-2(m+1)H\},\ldots(38)$$

where

$$f(m)=1,\quad \left[(V_2t-2mH)>x>\left(V_2t-2mH-\frac{a}{\beta}\right)\right]$$
$$=0,\quad [V_2t-2mH)<x]$$
$$=0,\quad \left[\left(V_2t-2mH-\frac{a}{\beta}>x\right]\right.$$
$$\varphi(m)=1,\quad \left[-\{V_2t-2(m+1)H\}<x<-\left\{V_2t-2(m+1)H-\frac{a}{\beta}\right\}\right]$$
$$=0,\quad [-\{V_2t-2(m+1)H\}>x]$$
$$=0.\quad \left[-\left\{V_2t-2(m+1)H-\frac{a}{\beta}\right\}<x\right]$$

A few numerical examples are shown in Figs. 22, 23, 24, 25, 26, 27. In Figs. 22, 23, 24 the cases of $H=\frac{L}{2}$, $H=L$, $H=2L$, besides the condition that $\alpha=\frac{1}{2}$, $\beta=1$, $a=2L$ in common, are plotted respectively, while in Figs. 25, 26, 27 the cases of $H=\frac{L}{2}$, $H=L$, $H=2L$, besides the conditions that $\alpha=2$, $\beta=1$, $a=2L$ in common, are illustrated.

In conclusion we are indebted to Dr. Nasu who has shown us the proper values of the constants due to Prof. Imamura and Prof. Matuzawa concerning the strata of the ground.

21. 地震波によつて土地の固有振動が誘起される可能度 第四報

地震研究所 妹澤克惟 金井清

この論文は著者等が以前からやつて居る研究の續きであつて、ここでは地表に二つの層がある時に下から垂直に縦波及横波が來る時の地表の振動のしかたを論じたものである。表面の二つの層の性質に關しては種々説があるかも知れぬけれども、今村、松澤兩博士其他の人々の結果が大體に於て正しいものと見て其を適當に調節して下の如く假定した。

層	厚さ	密度	縦波の速度	横波の速度
表面層（花崗岩層）	20 km	2·7	5·0 km/sec	3·15 km/sec
第二層（玄武岩層）	30 km	3·0	6·1 km/sec	3·70 km/sec
下　層（超鹽基性）	∞	3·5	7·5 km/sec	4·45 km/sec

この様な狀態にある層狀體に下方から有限長の調和波と衝撃型單波とを送る場合を考へた。但し調和波と云つても層の厚さに比較して種々の波長を有する場合を計算し、又衝撃型波動についても其の有效長の種々の場合をあたつて見たのである。

有限長調和波を送る時に生ずる表面の振動は非常に複雜ではあるけれども、分析して見ると以前の研究の時と同じく、順々の波動群になり、この波動群が漸次小振幅となるものである。而して此等波動群は計算の結果を圖示せるものに現れて居る様な所々の階段狀のものがそれであつて、大なる繰替しは始めからの振動である。從て層の固有振動に當るものも階段狀の所から次又は其次の階段狀の所までが其週期であつて、大なる繰替しの週期は始めからの振動週期である。

次に送られる波動が單一の衝撃型の時には、次々の振動繰替しが夫々の波動群に相當するものであり、從て此等の振動繰替しの週期が層の大體の固有振動週期であるといふ事が出來る。この場合にも次々の振動が漸次小振幅となる事は他の場合と大差がないのである。

實際の地震波では上述の二つの極限の間にある種々の狀態の波動の事が多いに違ひない。それ故表面の振動型や地層の固有振動の現れ方も大體前記二種の場合の間にある事が多い事と思はれる。從つて固有振動を推定する爲の分析は可なり困難を伴ふかも知れない。それにしても上の様に兩極端がわかつて居る以上は大凡の範圍限界は想像がつく事と思ふ。

尙この論文の末尾には以前の論文の補ひとして、表面層が一つしかなく原波動が有限長の調和波である場合を附加へて置いた。その性質についての委しい説明は省略する事にした。

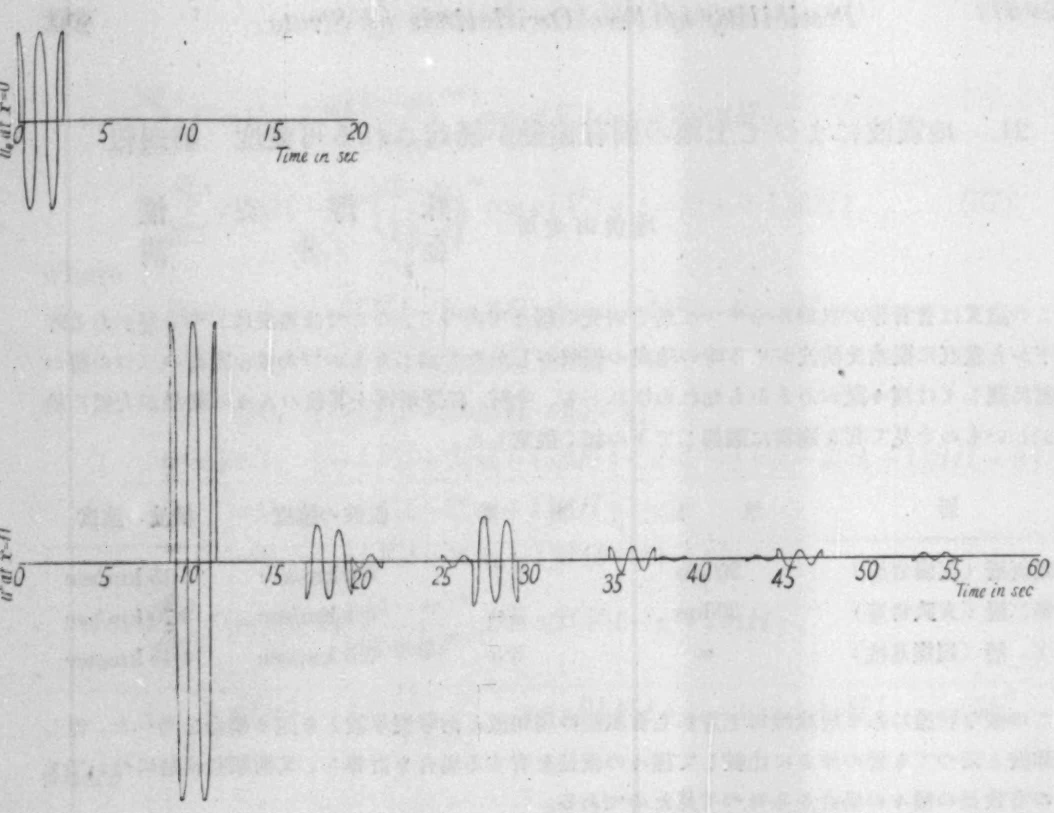

Fig. 2. $V_1=7{\cdot}5$ km/sec, $V_2=6{\cdot}1$ km/sec, $V_3=5{\cdot}0$ km/sec, $L\doteqdot 10$ km.

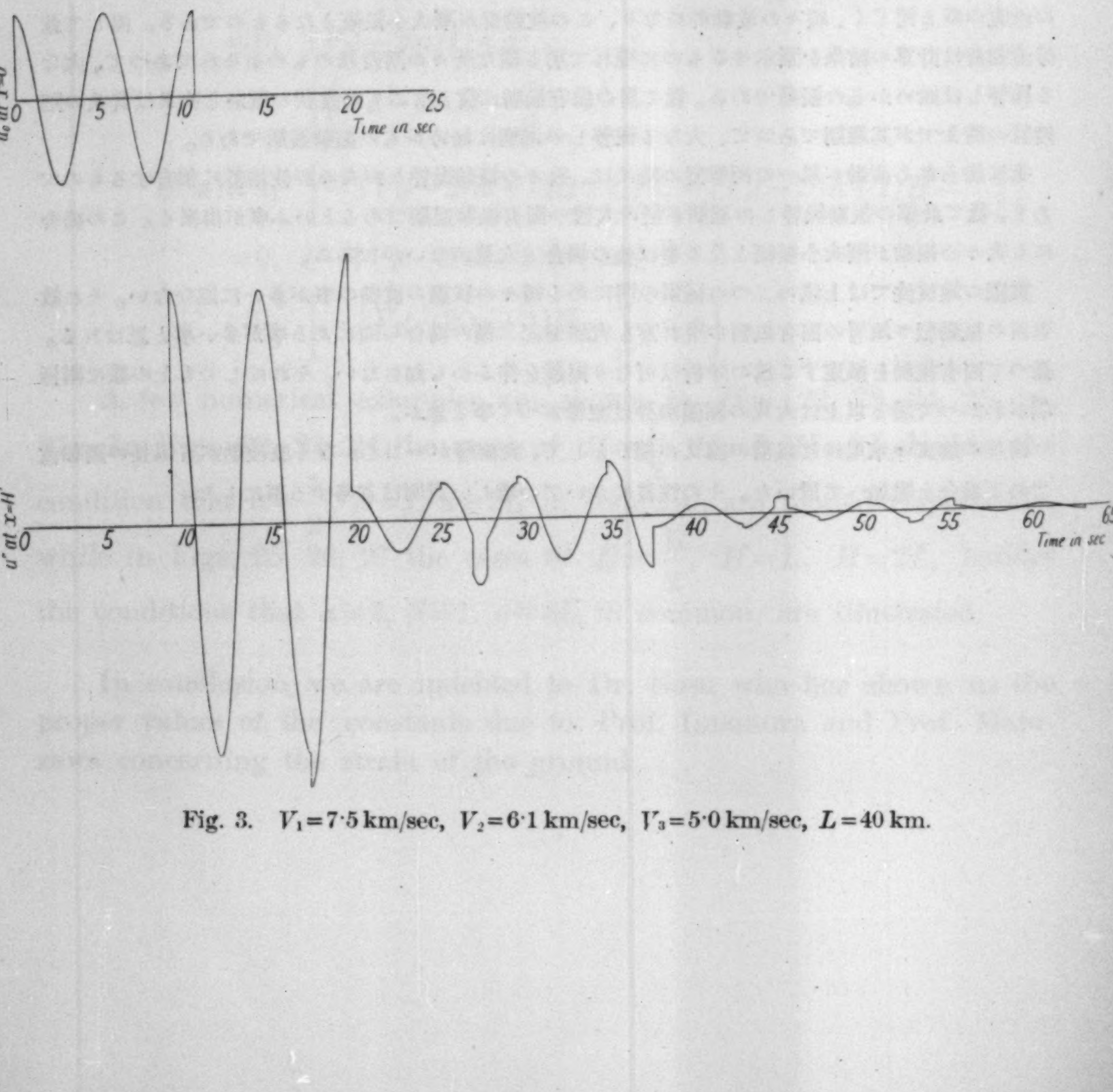

Fig. 3. $V_1=7{\cdot}5$ km/sec, $V_2=6{\cdot}1$ km/sec, $V_3=5{\cdot}0$ km/sec, $L=40$ km.

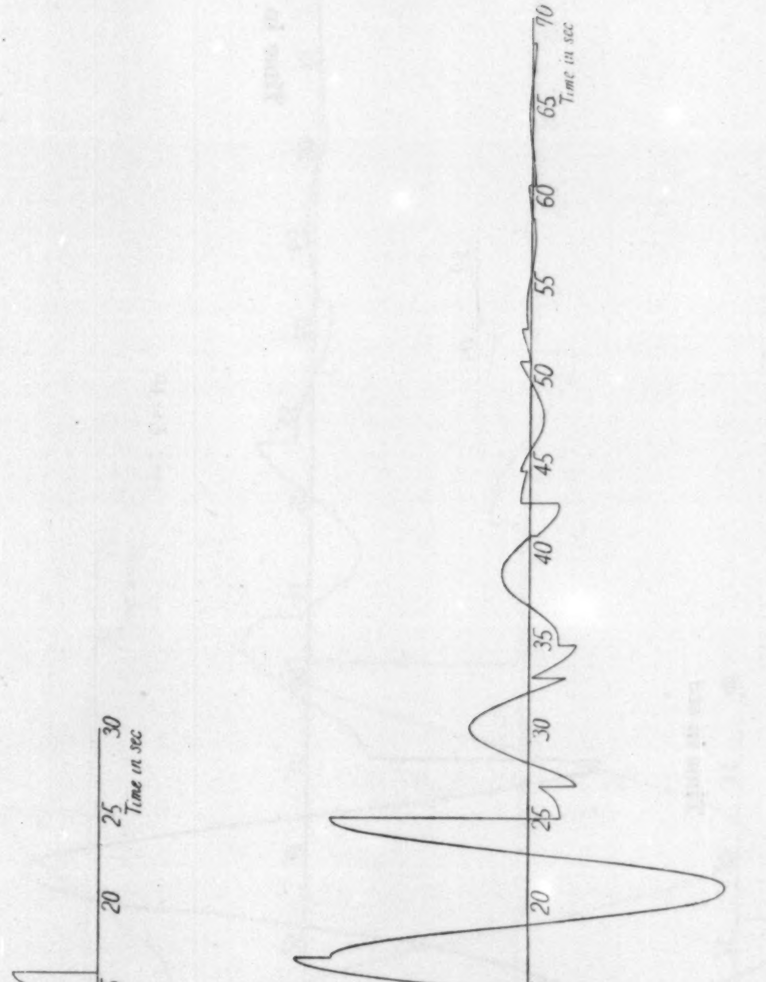

Fig. 4. $V_1 = 7{\cdot}5$ km/sec, $V_2 = 6{\cdot}1$ km/sec, $V_3 = 5{\cdot}0$ km/sec, $L = 60$ km.

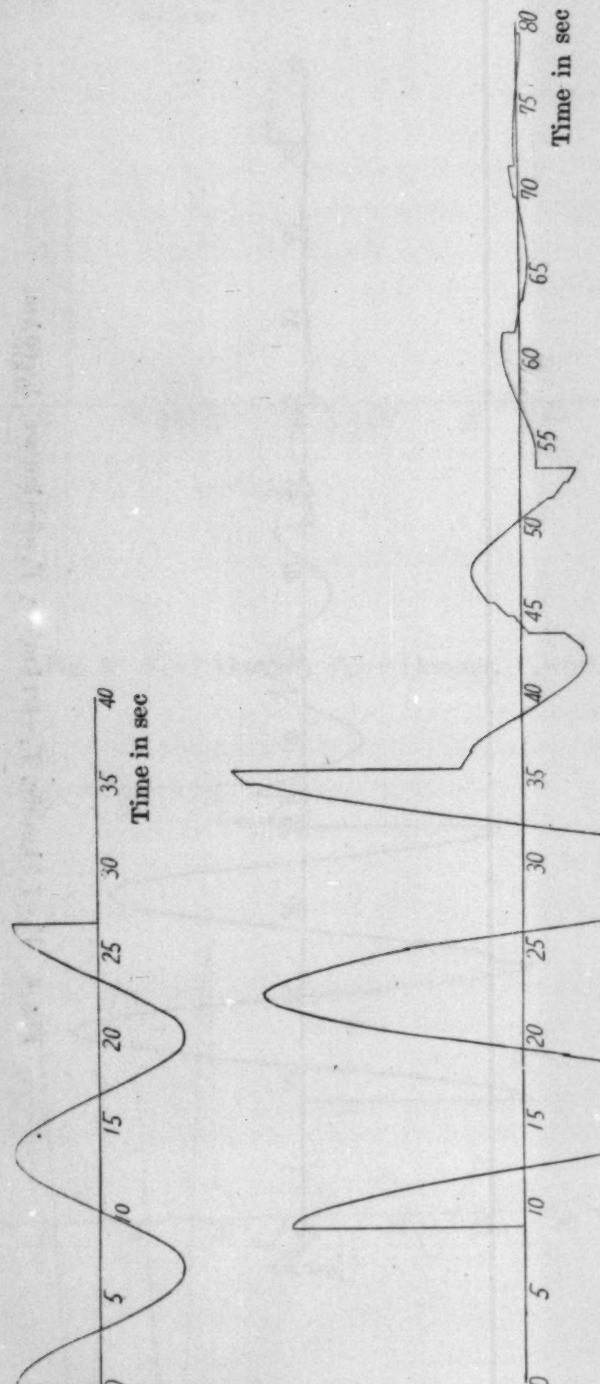

Fig. 5. $V_1=7{\cdot}5$ km/sec, $V_2=6{\cdot}1$ km/sec, $V_3=5{\cdot}0$ km/sec, $L=100$ km.

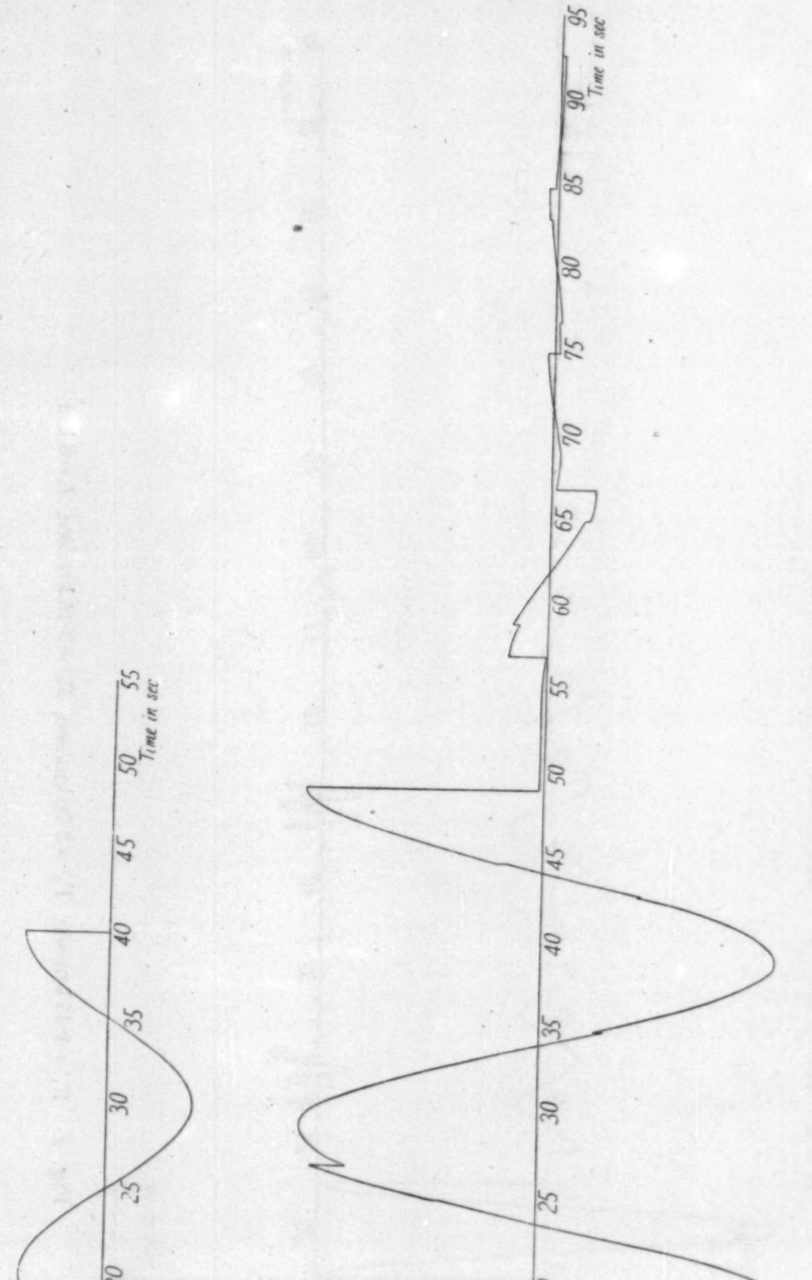

Fig. 6. $V_1 = 7{\cdot}5$ km/sec, $V_2 = 6{\cdot}1$ km/sec, $V_3 = 5{\cdot}0$ km/sec, $L = 150$ km.

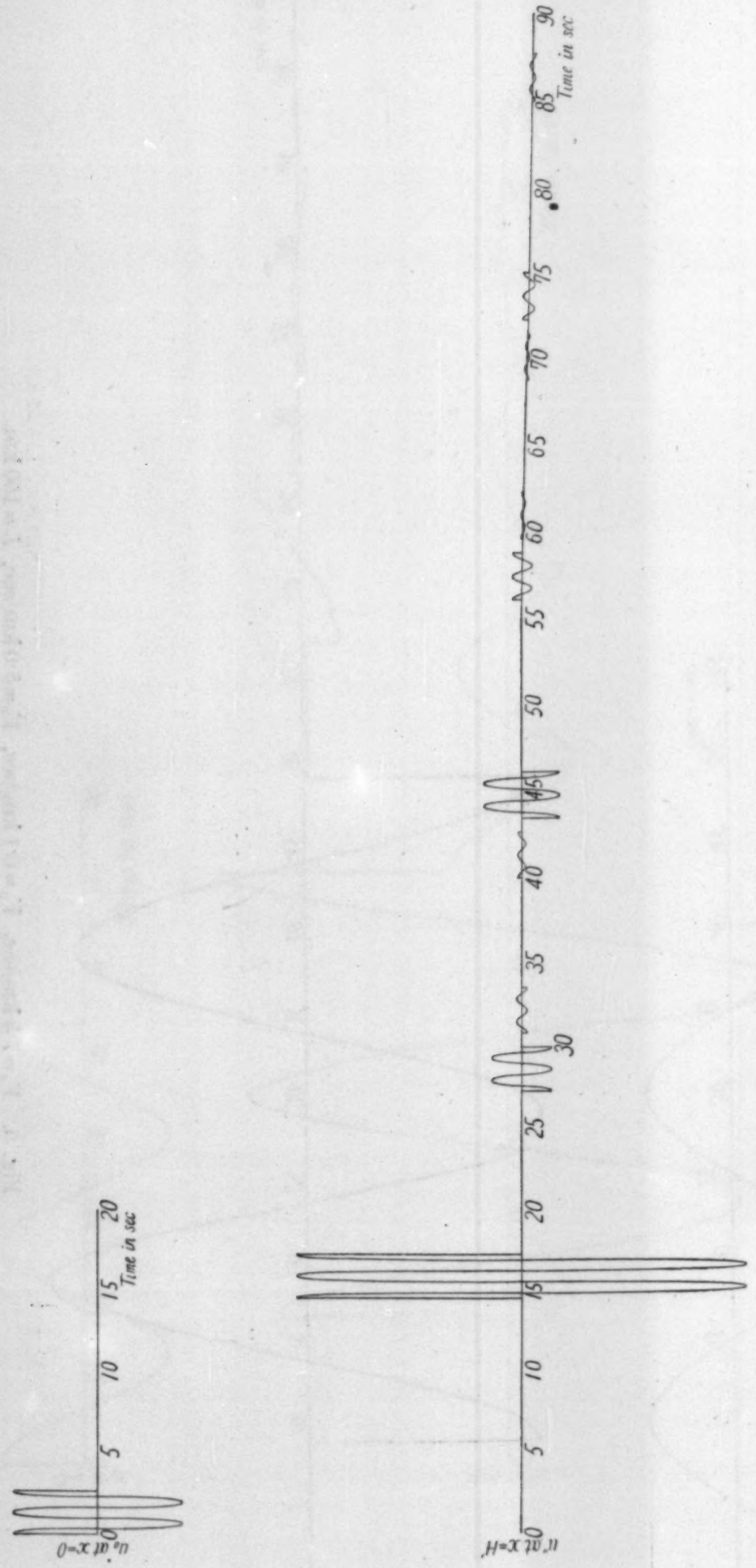

Fig. 7. $V_1'=4{\cdot}45$ km/sec, $V_2'=3{\cdot}70$ km/sec, $V_3'=3{\cdot}15$ km/sec, $L=6$ km.

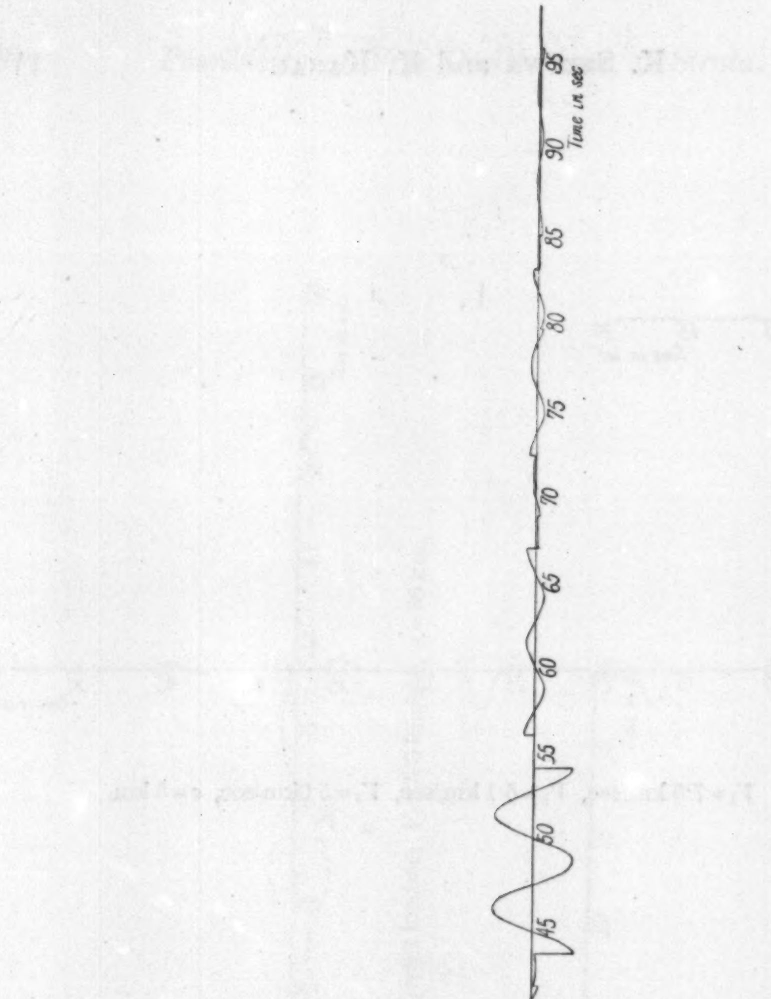

Fig. 8. $V_1' = 4{\cdot}45$ km/sec, $V_2' = 3{\cdot}70$ km/sec, $V_3' = 3{\cdot}17$ km/sec, $L = 24$ km.

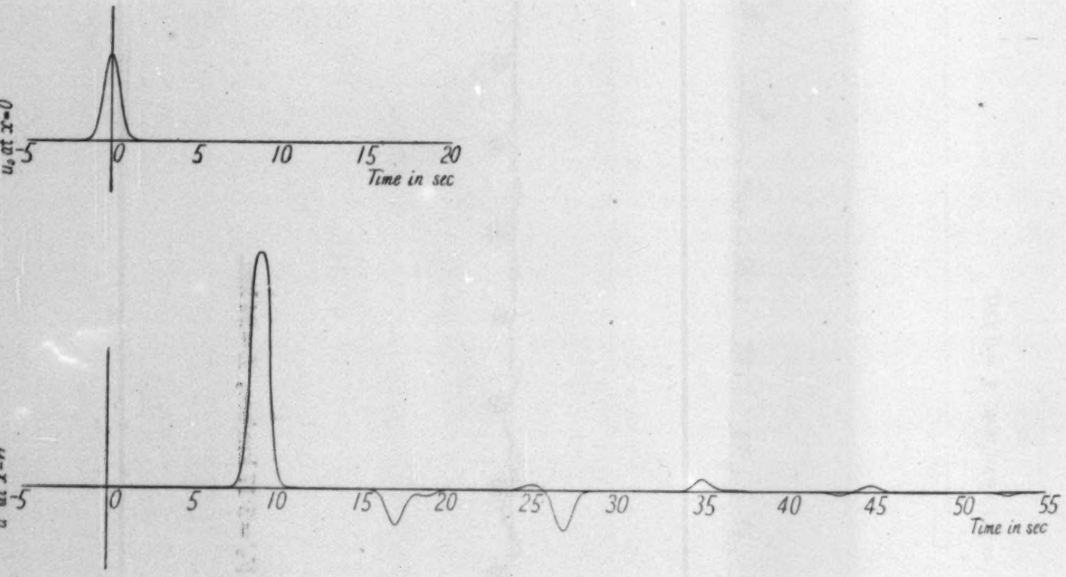

Fig. 12. $V_1=7{\cdot}5$ km/sec, $V_2=6{\cdot}1$ km/sec, $V_3=5{\cdot}0$km/sec, $c=5$ km.

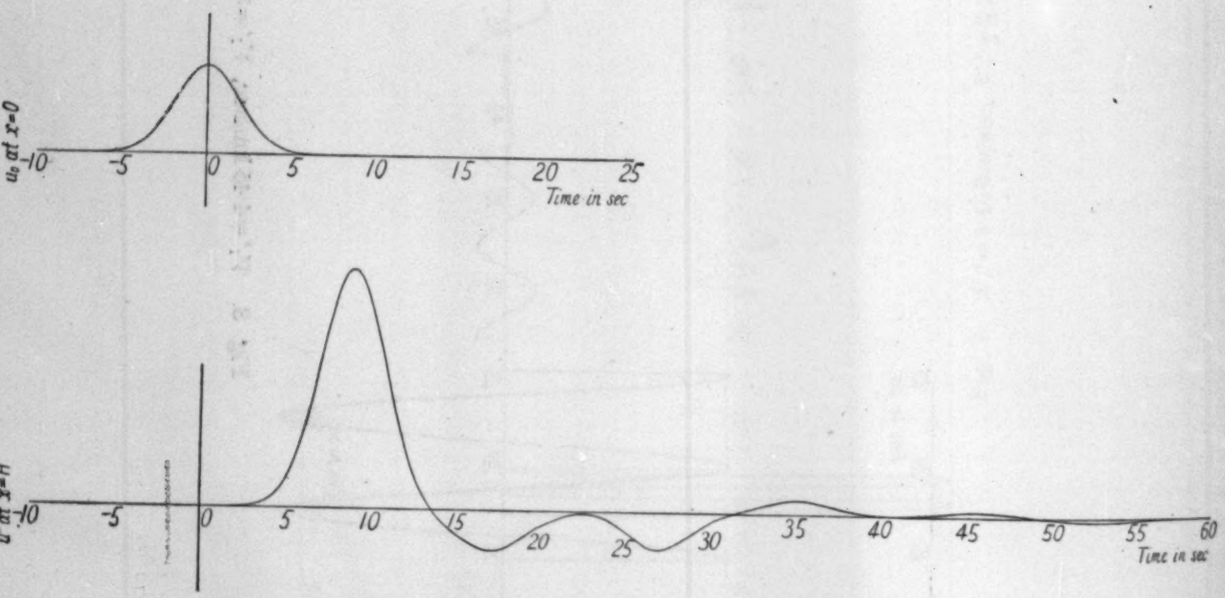

Fig. 13. $V_1=7{\cdot}5$ km/sec, $V_2=6{\cdot}1$ km/sec, $V_3=5{\cdot}0$ km/sec, $c=20$ km.

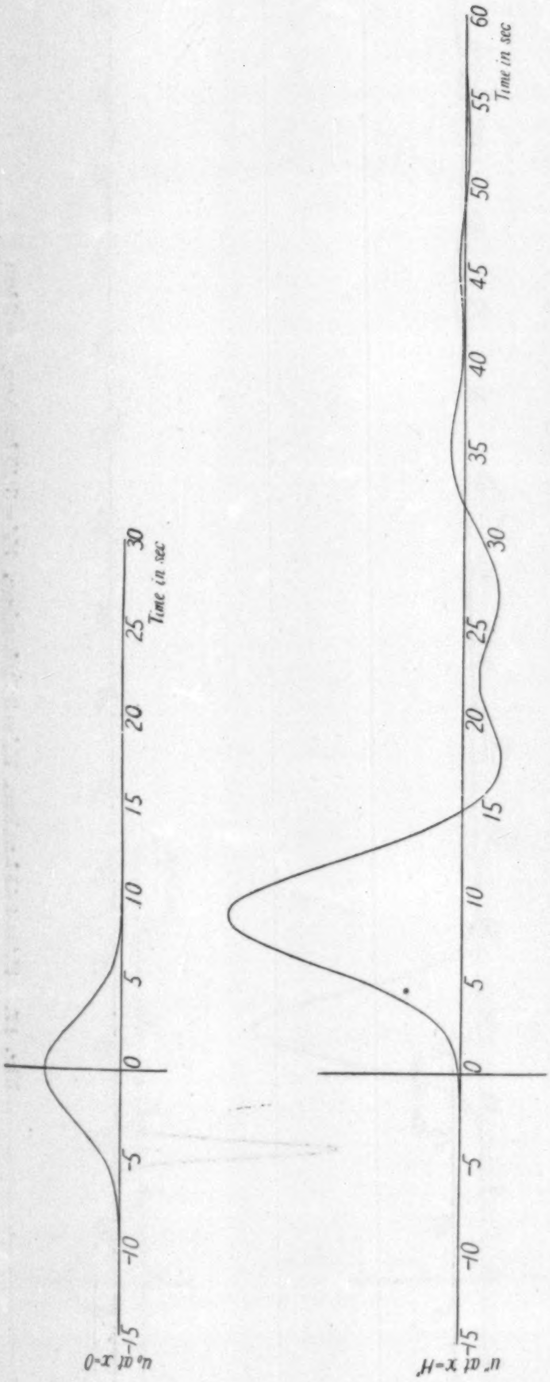

Fig. 14. $V_1=7{\cdot}5$ km/sec, $V_2=6{\cdot}1$ km/sec, $V_3=5{\cdot}0$ km/sec, $c=30$ km.

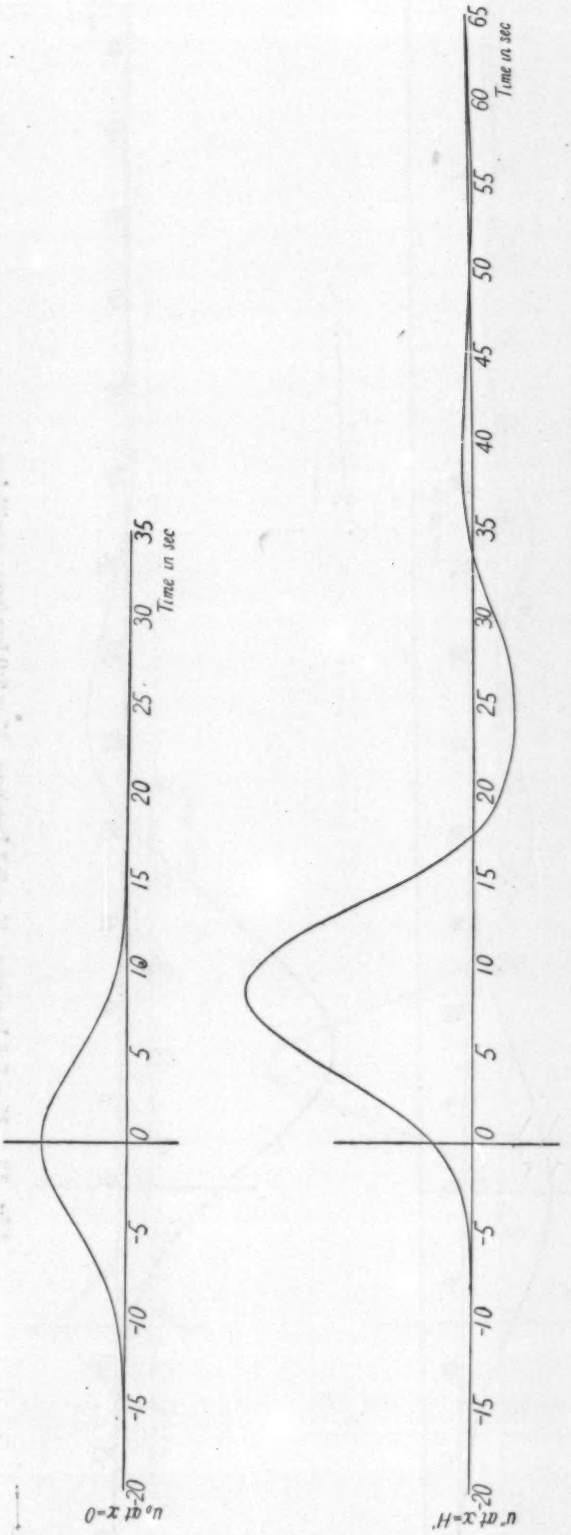

Fig. 15. $V_1=7{\cdot}5$ km/sec, $V_2=6{\cdot}1$ km/sec, $V_3=5{\cdot}0$ km/sec, $c=50$ km.

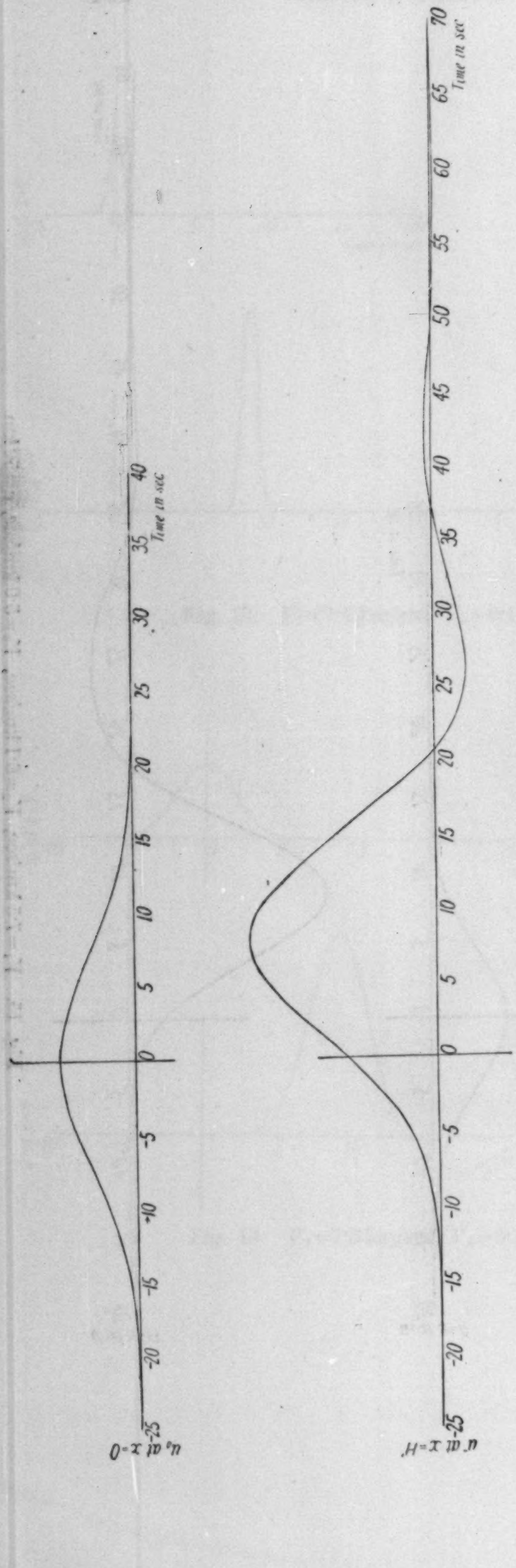

Fig. 16. $V_1=7{\cdot}5$ km/sec, $V_2=6{\cdot}1$ km/sec, $V_3=5{\cdot}0$ km/sec, $c=75$ km.

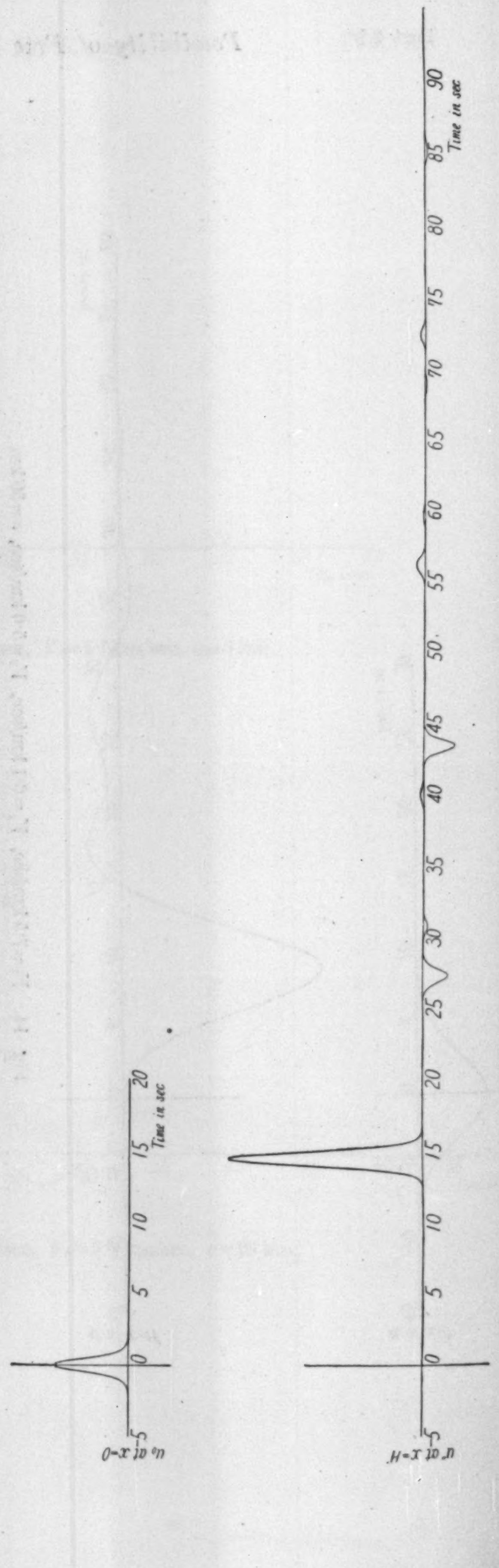

Fig. 17. $V_1'=4{\cdot}45$ km/sec, $V_2'=3{\cdot}70$ km/sec, $V_3'=3{\cdot}15$ km/sec, $c=3$ km

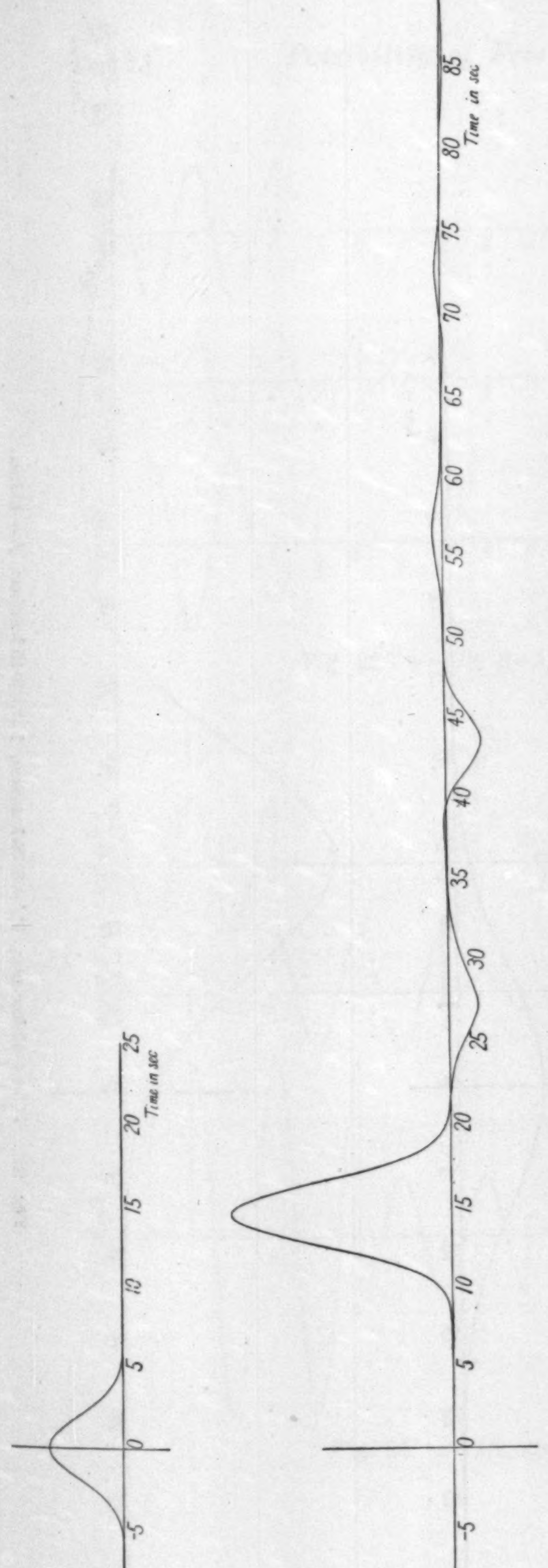

Fig. 18. $V_1'=4{\cdot}45$ km/sec, $V_2'=3{\cdot}70$ km/sec, $V_3'=3{\cdot}15$ km/sec, $c=12$ km.

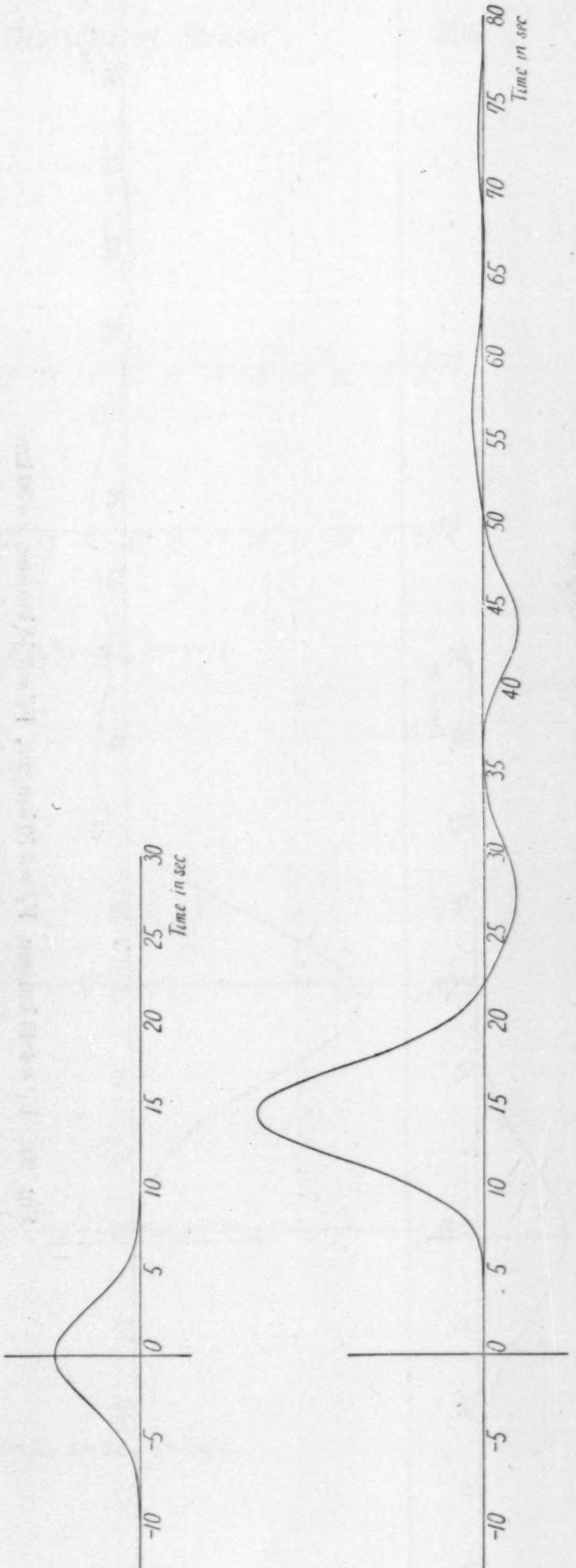

Fig. 19. $V_1'=4{\cdot}45$ km/sec, $V_2'=3{\cdot}70$ km/sec, $V_3'=3{\cdot}15$ km/sec, $c=18$ km.

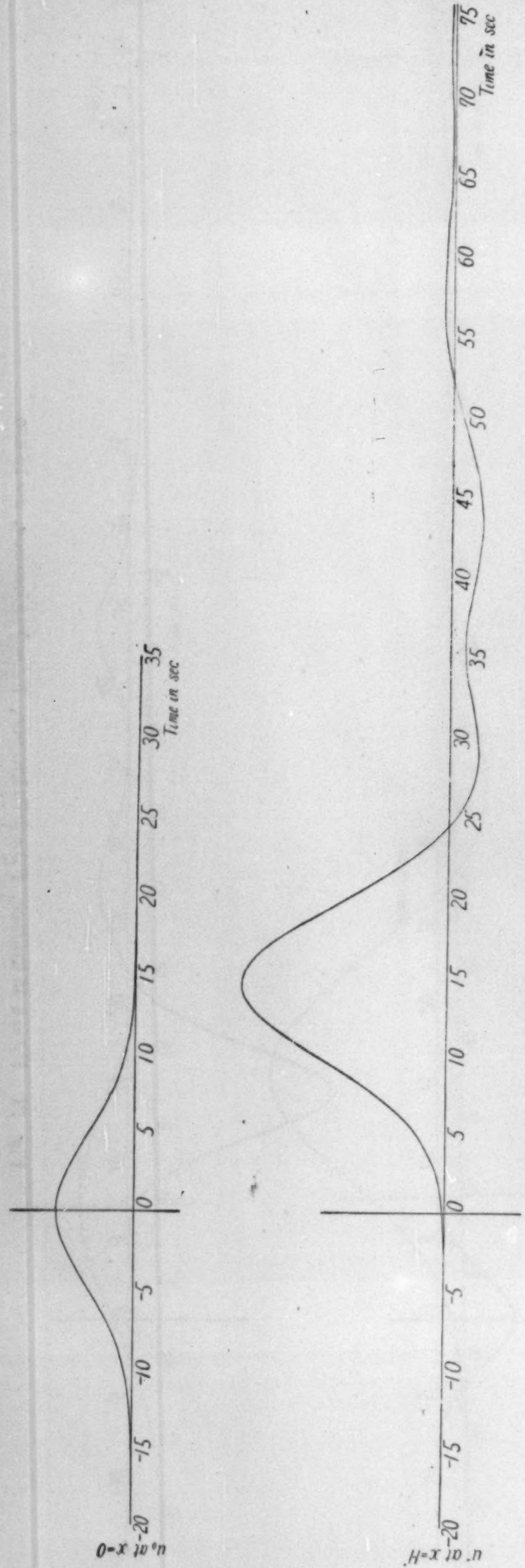

Fig. 20. $V_1' = 4{\cdot}45$ km/sec, $V_2' = 3{\cdot}70$ km/sec, $V_3' = 3{\cdot}15$ km/sec, $c = 30$ km.

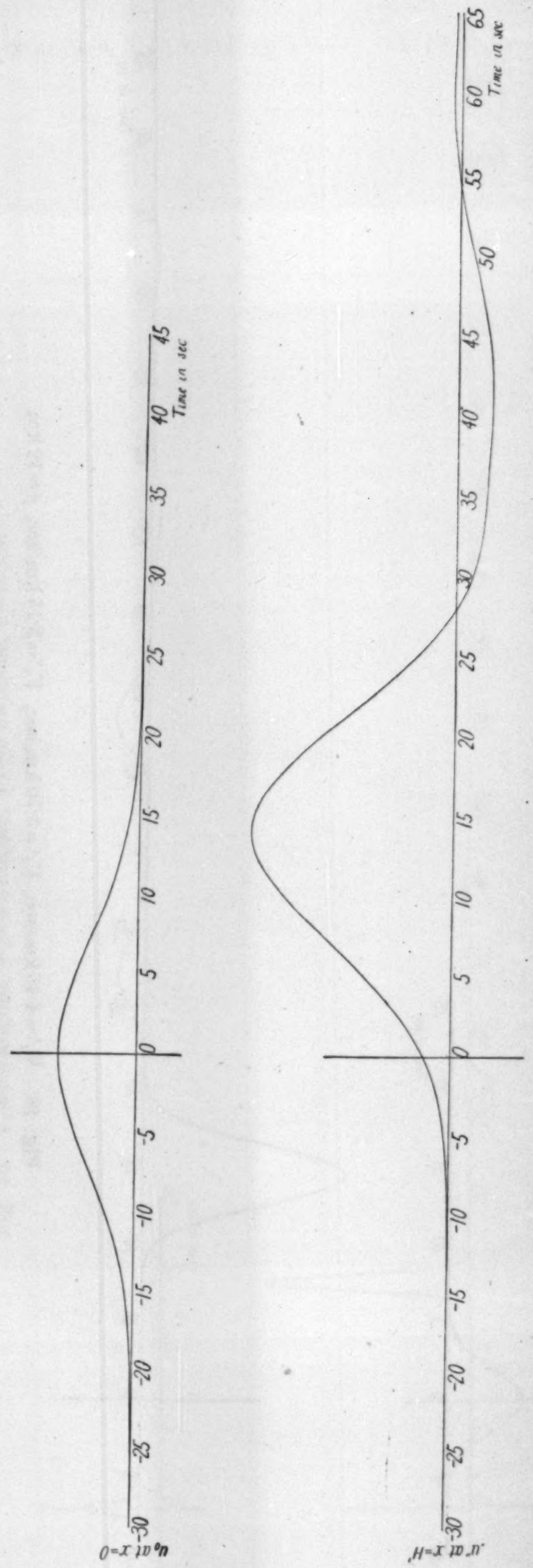

Fig. 21. $V_1' = 4{\cdot}45$ km/sec, $V_2' = 3{\cdot}70$ km/sec, $V_3' = 3{\cdot}15$ km/sec, $L = 45$ km.

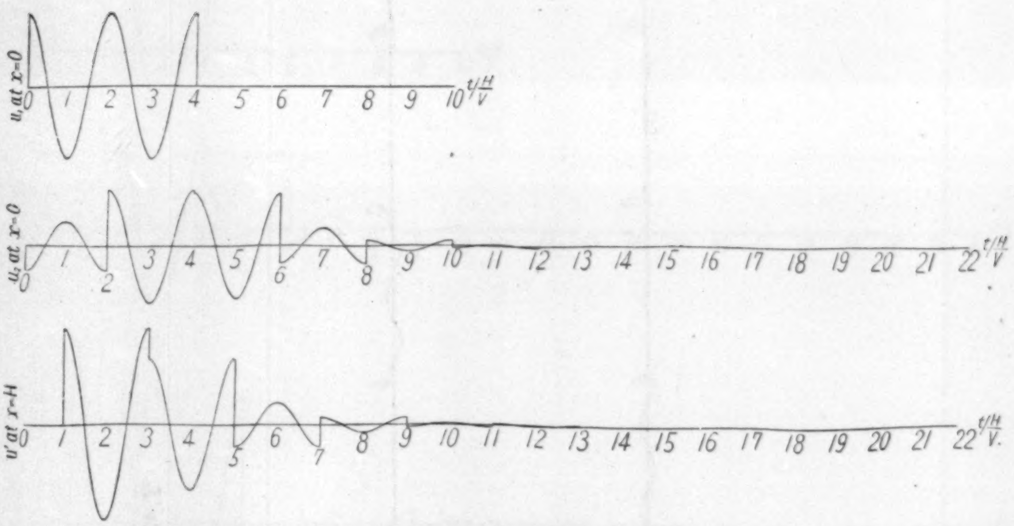

Fig. 22. $\alpha=1/2$, $\beta=1$, $H=L/2$, $a=2L$, $c=2\pi/L$.

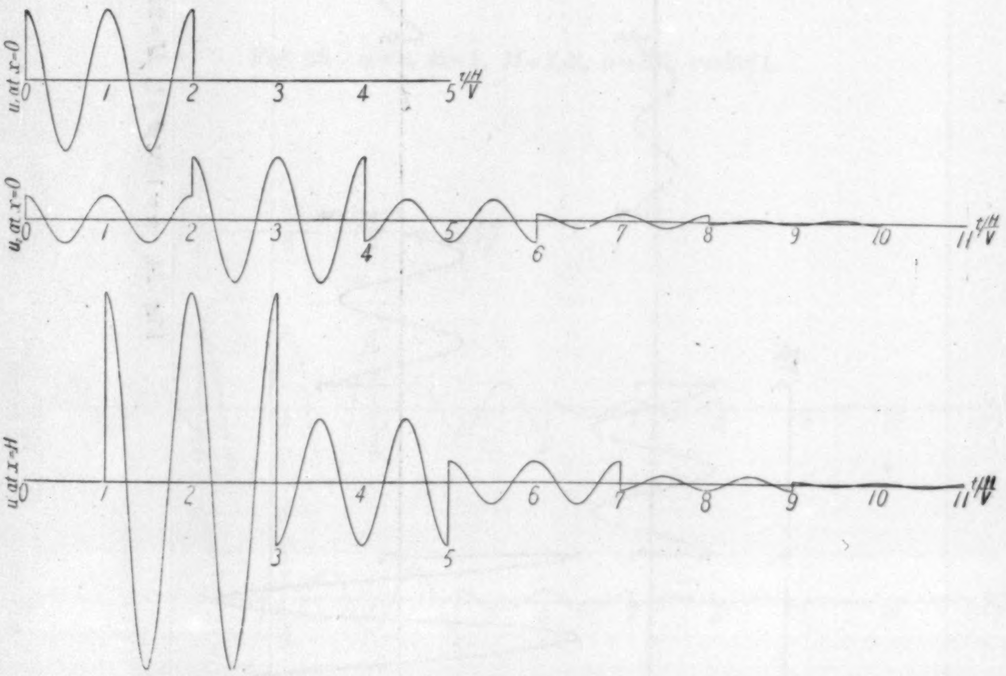

Fig. 23. $\alpha=1/2$, $\beta=1$, $H=L$, $a=2L$, $c=2\pi/L$.

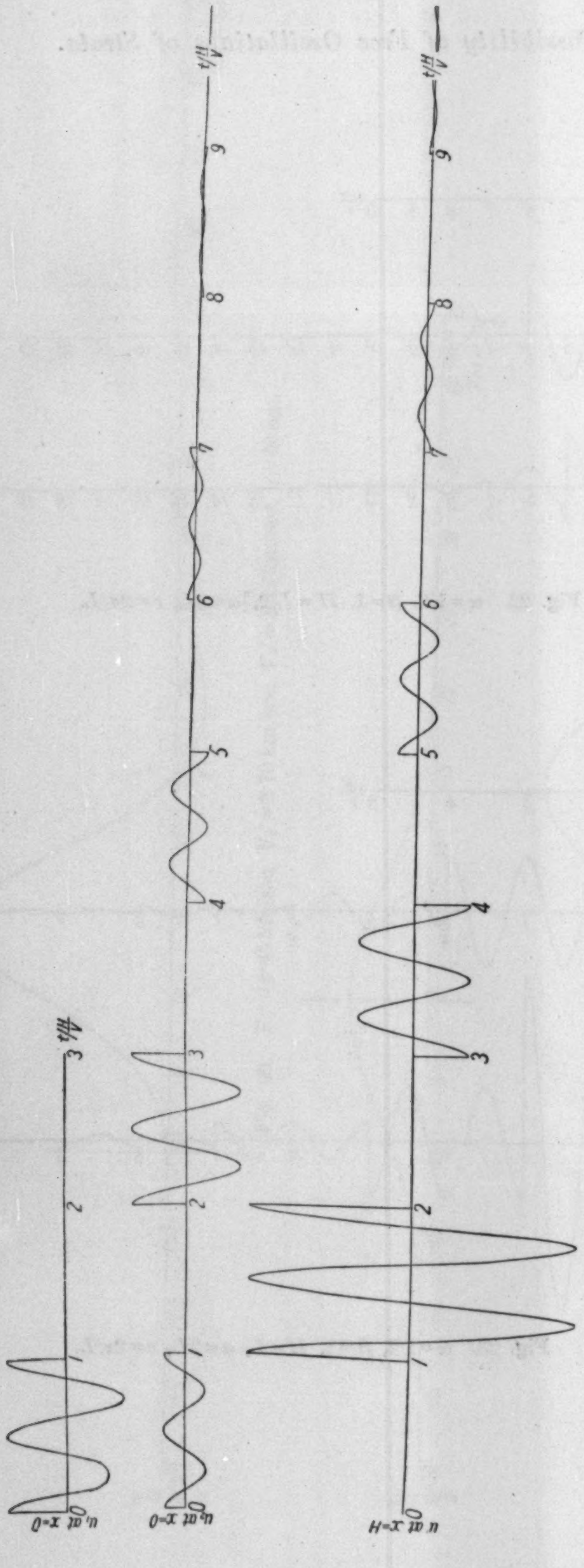

Fig. 24. $\alpha=1/2,\ \beta=1,\ H=2L,\ a=2L,\ c=2\pi/L.$

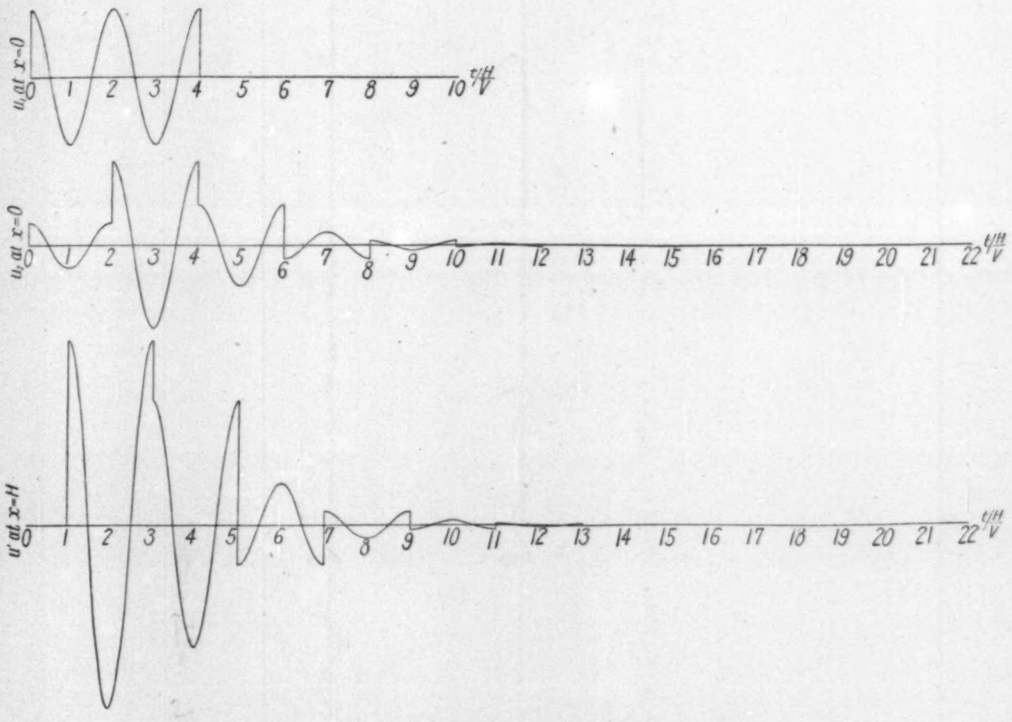

Fig. 25. $\alpha=2$, $\beta=1$, $H=L/2$, $a=2L$, $c=2\pi/L$.

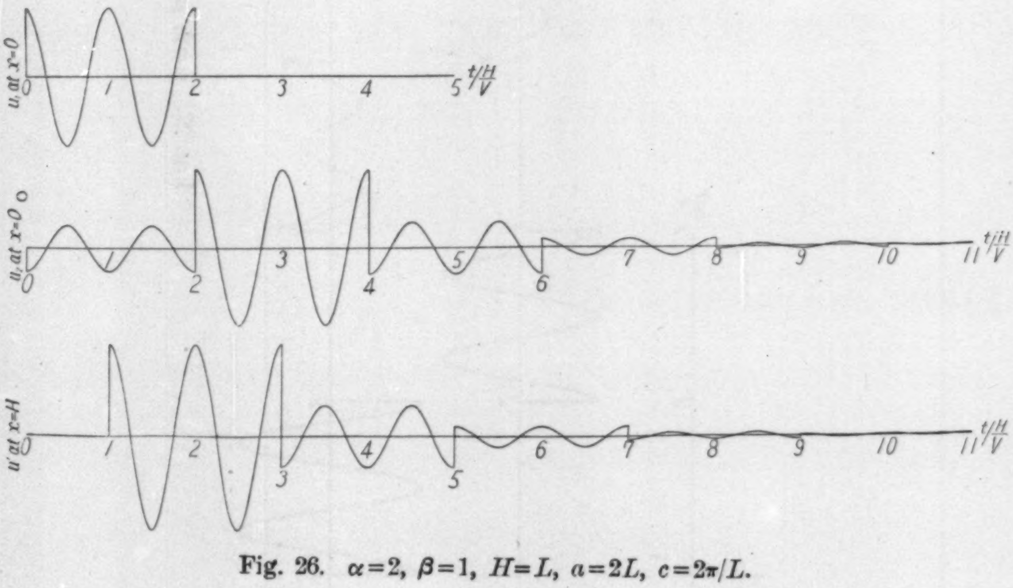

Fig. 26. $\alpha=2$, $\beta=1$, $H=L$, $a=2L$, $c=2\pi/L$.

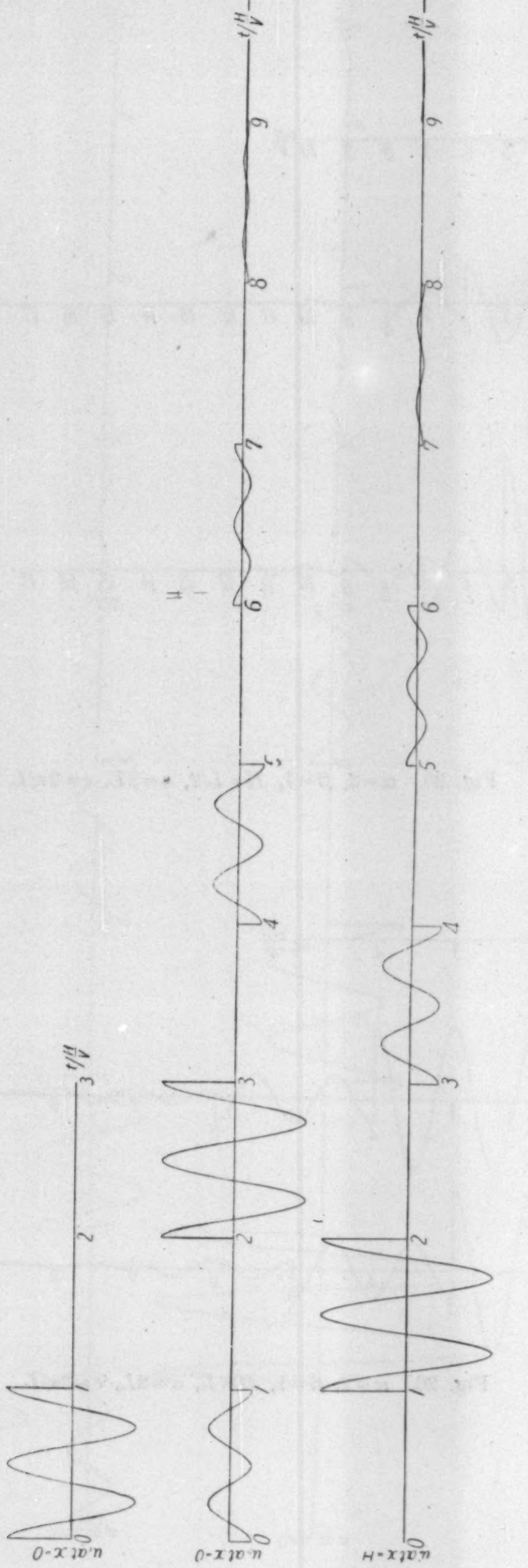

Fig. 27. $\alpha=2$, $\beta=1$, $H=2L$, $a=2L$, $c=2\pi/L$.

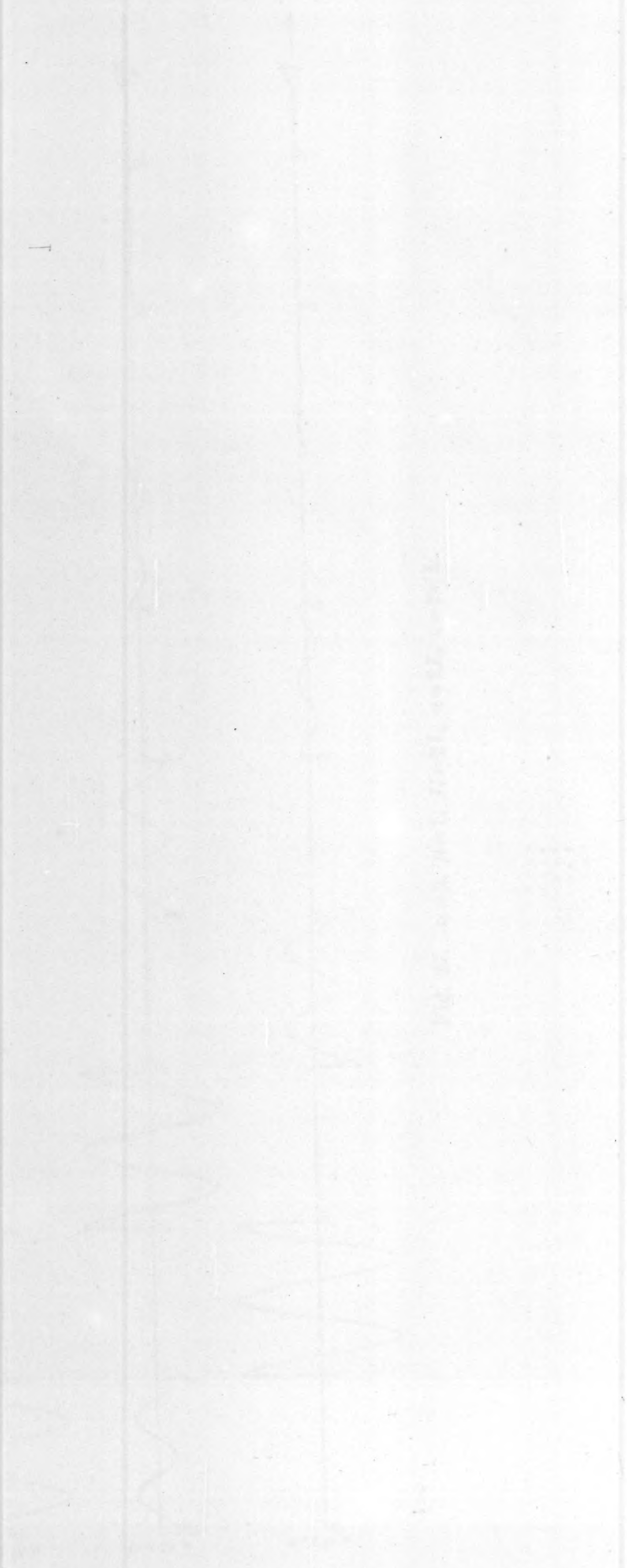

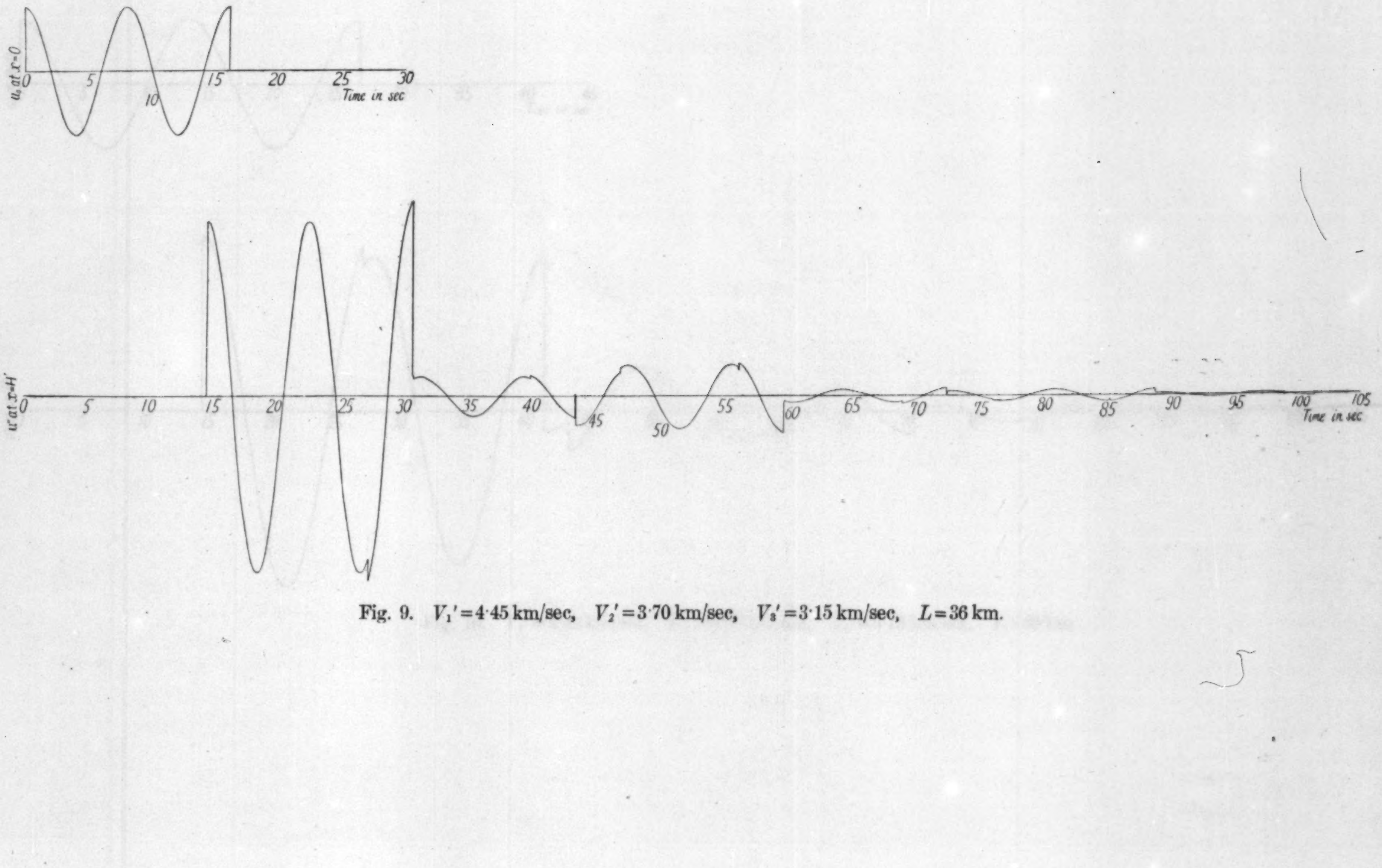

Fig. 9. $V_1'=4{\cdot}45$ km/sec, $V_2'=3{\cdot}70$ km/sec, $V_3'=3{\cdot}15$ km/sec, $L=36$ km.

[Bull. Earthq. Res. Inst., Vol. X, Pl. XL.]

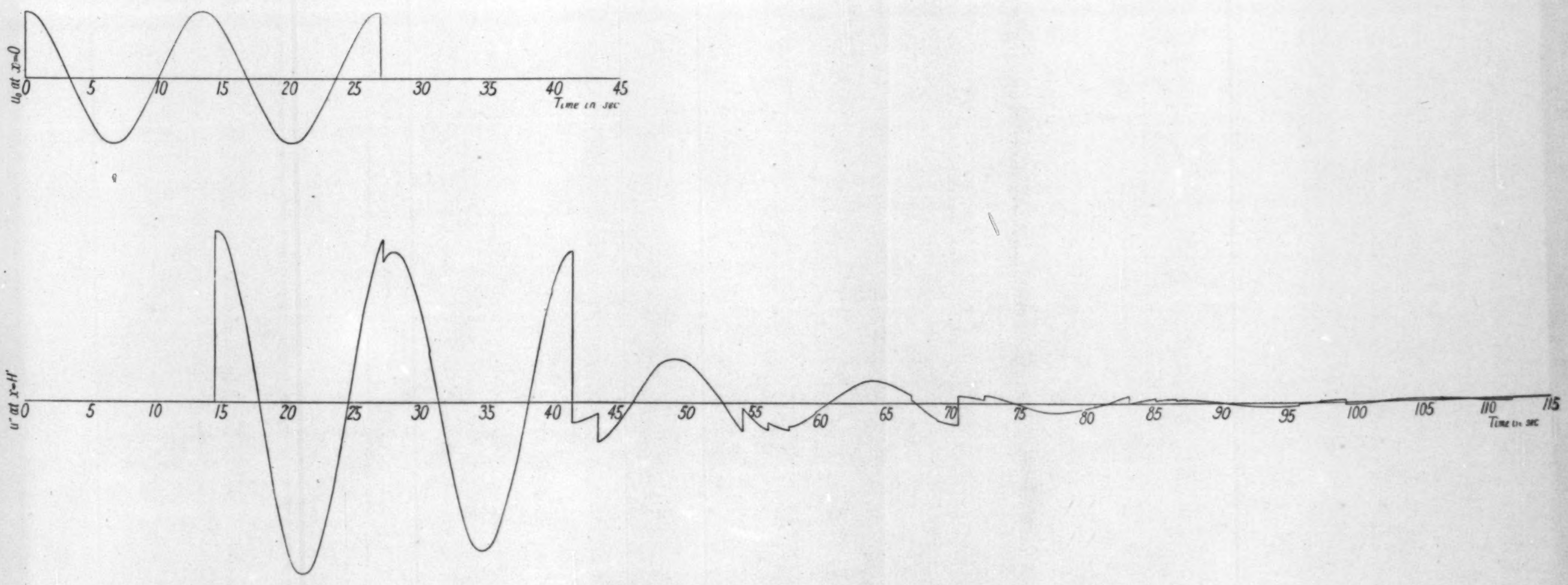

Fig. 10. $V_1'=4{\cdot}45$ km/sec, $V_2'=3{\cdot}70$ km/sec, $V_3'=3{\cdot}15$ km/sec, $L=60$ km.

(震研彙報、第十號、圖版、妹澤、金井)

(震研彙報、第十號、圖版、妹澤、金井)

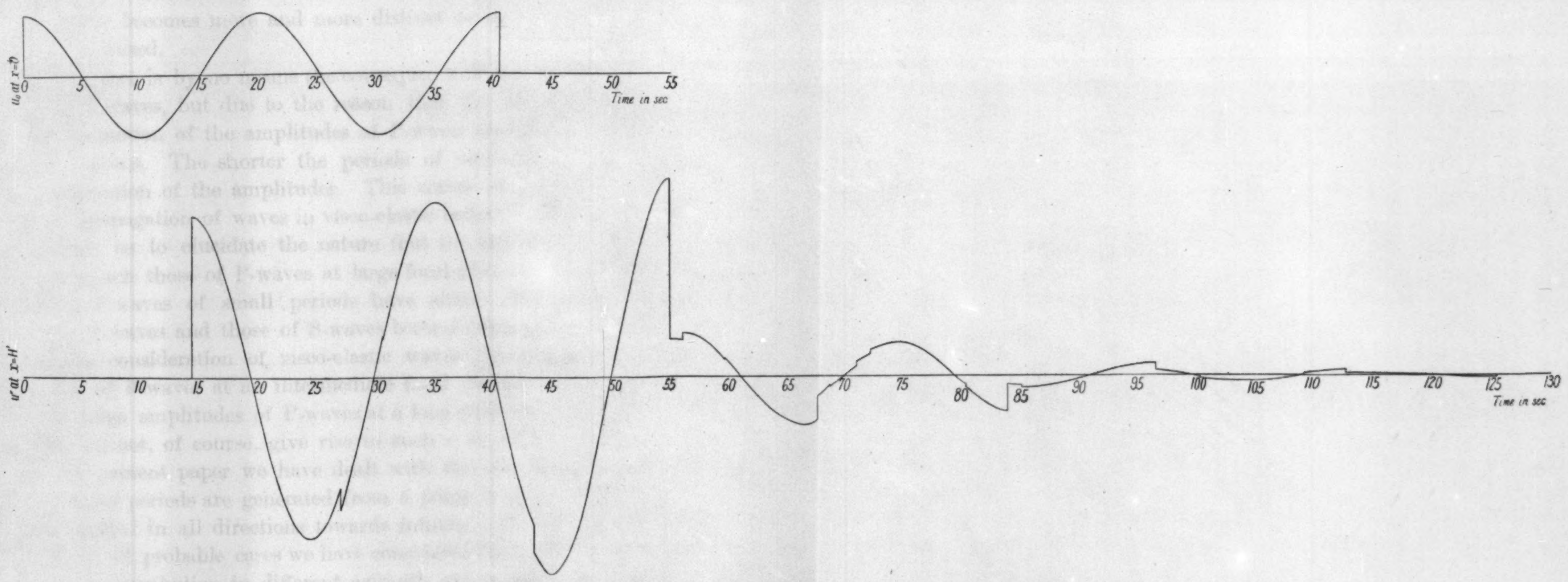

Fig. 11. $V_1' = 4{\cdot}45$ km/sec, $V_2' = 3{\cdot}70$ km/sec, $V_3' = 3{\cdot}15$ km/sec, $L = 90$ km.

22. *Amplitudes of P- and S-waves at Different Focal Distances.*

By Katsutada SEZAWA and Kiyoshi KANAI,

Earthquake Research Institute.

(Read July 7, 1931 and Feb. 16, 1932.—Received March 19, 1932.)

It is well-ascertained fact that the amplitudes of P-waves are smaller than those of S-waves at an intermediate focal distance in general and this character becomes more and more distinct as the distance from the origin is increased.

Such a fact is by no means the consequence of the essential property of P- and S-waves, but due to the reason that the effective periods of original fluctuation of the amplitudes of P-waves are always shorter than those of S-waves. The shorter the periods of oscillations, the quicker is the diminution of the amplitudes. This comes out directly from the theory of propagation of waves in visco-elastic bodies.[1] The same theory also enables us to elucidate the nature that the amplitudes of S-waves rather approach those of P-waves at large focal distances where the oscillations of P-waves of small periods have almost died away and the periods of P-waves and those of S-waves become comparable. No theory without the consideration of visco-elastic waves can explain the small amplitudes of P-waves at an intermediate focal distance as well as the relatively large amplitudes of P-waves at a long distance. Reflection and refraction cannot, of course, give rise to such a result.

In the present paper we have dealt with the case where P- and S-waves of equal periods are generated from a point in a visco-elastic body and transmitted in all directions towards infinity. To get the solutions of waves of all probable cases we have considered the generation of waves of a certain distribution in different azimuth as well as different latitude. The case of some distribution has already been studied by one[2] of us a

1) K. SEZAWA, "On the Decay of Waves in Visco-Elastic Solid Bodies", *Bull. Earthq. Res. Inst.*, 3 (1927), 43-53; "Notes on Waves in Visco-Elastic Solid Bodies", *Bull. Earthq. Res. Inst.*, 10 (1932), 19-22.

2) K. SEZAWA, "Dilatational and Distortional Waves generated from a Cylindrical or a Spherical Origin", *Bull. Earthq. Res. Inst.*, 2 (1927), 13-20.

few years ago. The explanation of the smallness of the periods of the actually generated P-waves is very difficult, and we have left its study to future occasion.

For the sake of simplicity we have taken spherical coordinates. Let u, v, w be radial, colatitudinal and azimuthal components of displacement. The equations of motion of the body are expressed by

$$\left.\begin{aligned}
\rho\frac{\partial^2 u}{\partial t^2}&=\left\{(\lambda+2\mu)+(\lambda'+2\mu')\frac{\partial}{\partial t}\right\}\frac{\partial\Delta}{\partial r}\\
&\qquad-\left(2\mu+2\mu'\frac{\partial}{\partial t}\right)\left\{\frac{1}{r\sin\theta}\frac{\partial(\varpi_\phi\sin\theta)}{\partial\theta}-\frac{1}{r\sin\theta}\frac{\partial\varpi_\theta}{\partial\phi}\right\},\\
\rho\frac{\partial^2 v}{\partial t^2}&=\left\{(\lambda+2\mu)+(\lambda'+2\mu')\frac{\partial}{\partial t}\right\}\frac{1}{r}\frac{\partial\Delta}{\partial\theta}\\
&\qquad-\left(2\mu+2\mu'\frac{\partial}{\partial t}\right)\left\{\frac{1}{r\sin\theta}\frac{\partial\varpi_r}{\partial\phi}-\frac{1}{r}\frac{\partial(r\varpi_\phi)}{\partial r}\right\},\\
\rho\frac{\partial^2 w}{\partial t^2}&=\left\{(\lambda+2\mu)+(\lambda'+2\mu')\frac{\partial}{\partial t}\right\}\frac{1}{r\sin\theta}\frac{\partial\Delta}{\partial\phi}\\
&\qquad-\left(2\mu+2\mu'\frac{\partial}{\partial t}\right)\left\{\frac{1}{r}\frac{\partial(r\varpi_\theta)}{\partial r}-\frac{1}{r}\frac{\partial\varpi_r}{\partial\theta}\right\}.
\end{aligned}\right\}\quad\ldots(1)$$

In these equations r, θ, ϕ are the radial distance, colatitude, and azimuth, the origin being taken at seismic focus; ρ the density: λ, μ Lamé's elastic constants; λ', μ' dilatational and shearing solid viscosities; while $\Delta, \varpi_r, \varpi_\theta, \varpi_\phi$ have the meanings as expressed in the following forms:

$$\left.\begin{aligned}
\Delta&=\frac{1}{r^2\sin\theta}\left[\frac{\partial(ur^2\sin\theta)}{\partial r}+\frac{\partial(vr\sin\theta)}{\partial\theta}+\frac{\partial(wr)}{\partial\phi}\right],\\
2\varpi_r&=\frac{1}{r^2\sin\theta}\left[\frac{\partial}{\partial\theta}(wr\sin\theta)-\frac{\partial}{\partial\phi}(vr)\right],\\
2\varpi_\theta&=\frac{1}{r\sin\theta}\left[\frac{\partial u}{\partial\phi}-\frac{\partial(wr\sin\theta)}{\partial r}\right],\\
2\varpi_\phi&=\frac{1}{r}\left[\frac{\partial(vr)}{\partial r}-\frac{\partial u}{\partial\theta}\right].
\end{aligned}\right\}\quad\ldots(2)$$

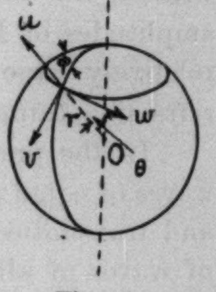

Fig. 1.

Eliminating $u, v, w,$ in (1) by means of (2), we get

$$\begin{aligned}
\rho\frac{\partial^2\Delta}{\partial t^2}&=\left\{(\lambda+2\mu)+(\lambda'+2\mu')\frac{\partial}{\partial t}\right\}\left[\frac{1}{r^2}\frac{\partial}{\partial r}\left(r^2\frac{\partial\Delta}{\partial r}\right)\right.\\
&\qquad\left.+\frac{1}{r^2}\frac{\partial}{\sin\theta\partial\theta}\left(\sin\theta\frac{\partial\Delta}{\partial\theta}\right)+\frac{1}{r^2\sin^2\theta}\frac{\partial^2\Delta}{\partial\phi^2}\right],
\end{aligned}$$

$$
\left.
\begin{aligned}
\rho\frac{\partial^2\varpi_r}{\partial t^2}&=\left\{\mu+\mu'\frac{\partial}{\partial t}\right\}\left[\frac{\partial^2\varpi_r}{\partial r^2}+\frac{4}{r}\frac{\partial\varpi_r}{\partial r}+\frac{2}{r^2}\varpi_r\right.\\
&\qquad\left.+\frac{1}{r^2\sin\theta}\frac{\partial}{\partial\theta}\left(\sin\theta\frac{\partial\varpi_r}{\partial\theta}\right)+\frac{1}{r^2\sin^2\theta}\frac{\partial^2\varpi_r}{\partial\phi^2}\right],\\
\rho\frac{\partial^2\varpi_\theta}{\partial t^2}&=\left\{\mu+\mu'\frac{\partial}{\partial t}\right\}\left[\frac{1}{r}\frac{\partial^2(\varpi_\theta r)}{\partial r^2}+\frac{1}{r^2\sin^2\theta}\frac{\partial^2\varpi_\theta}{\partial\phi^2}\right.\\
&\qquad\left.-\frac{1}{r^2\sin^2\theta}\frac{\partial^2(\varpi_\phi\sin\theta)}{\partial\phi\,\partial\theta}-\frac{1}{r}\frac{\partial^2\varpi_r}{\partial r\partial\theta}\right],\\
\rho\frac{\partial^2\varpi_\phi}{\partial t^2}&=\left\{\mu+\mu'\frac{\partial}{\partial t}\right\}\left[\frac{1}{r}\frac{\partial^2(\varpi_\phi r)}{\partial r^2}+\frac{1}{r^2}\frac{\partial}{\partial\theta}\frac{1}{\sin\theta}\frac{\partial(\varpi_\phi\sin\theta)}{\partial\theta}\right.\\
&\qquad\left.-\frac{1}{r^2}\frac{\partial}{\partial\theta}\frac{1}{\sin\theta}\frac{\partial\varpi_\theta}{\partial\phi}-\frac{1}{r\sin\theta}\frac{\partial^2\varpi_r}{\partial r\partial\phi}\right].
\end{aligned}
\right\}\quad\ldots\ldots(3)
$$

Put in (3)

$$\varDelta=e^{ipt}\varDelta',\quad \varpi_r=e^{ipt}\varpi_r',\quad \varpi_\theta=e^{ipt}\varpi_\theta',\quad \varpi_\phi=e^{ipt}\varpi_\phi',\ldots\ldots\ (4)$$

where $p/2\pi$ is the frequency of all waves; then we get

$$\frac{-\rho p^2}{(\lambda+2\mu)+ip(\lambda'+2\mu')}=\frac{1}{\varDelta'}\left[\frac{1}{r^2}\frac{\partial}{\partial r}\left(r^2\frac{\partial\varDelta'}{\partial r}\right)\right.$$
$$\left.+\frac{1}{r^2\sin\theta d\theta}\left(\sin\theta\frac{\partial\varDelta'}{\partial\theta}\right)+\frac{1}{r^2\sin^2\theta}\frac{\partial^2\varDelta'}{\partial\phi^2}\right]\equiv-h^2,\ \ldots\ldots(5_a)$$

$$\frac{-\rho p^2}{\mu+ip\mu'}=\frac{1}{\varpi'_r}\left[\frac{\partial^2\varpi'_r}{\partial r^2}+\frac{4}{r}\frac{\partial\varpi'_r}{\partial r}+\frac{2}{r^2}\varpi'_r\right.$$
$$\left.+\frac{1}{r^2\sin\theta}\frac{\partial}{\partial\theta}\left(\sin\theta\frac{\partial\varpi'_r}{\partial\theta}\right)+\frac{1}{r^2\sin^2\theta}\frac{\partial^2\varpi'_r}{\partial\phi_2}\right]\equiv-k^2,\ \ldots\ldots(5_b)$$

$$\frac{-\rho p^2}{\mu+ip\mu'}=\frac{1}{\varpi'_\theta}\left[\frac{1}{r}\frac{\partial^2(\varpi'_\theta r)}{\partial r^2}+\frac{1}{r^2\sin^2\theta}\frac{\partial^2\varpi'_\theta}{\partial\phi^2}\right.$$
$$\left.-\frac{1}{r^2\sin^2\theta}\frac{\partial^2(\varpi'_\phi\sin\theta)}{\partial\phi\,\partial\theta}-\frac{1}{r}\frac{\partial^2\varpi'_r}{\partial r\partial\theta}\right]\equiv-k^2,\ \ldots\ldots(5_c)$$

$$\frac{-\rho p^2}{\mu+ip\mu'}=\frac{1}{\varpi'_\phi}\left[\frac{1}{r}\frac{\partial^2(\varpi'_\phi r)}{\partial r^2}+\frac{1}{r^2}\frac{\partial}{\partial\theta}\frac{1}{\sin\theta}\frac{\partial(\varpi'_\phi\sin\theta)}{\partial\theta}\right.$$
$$\left.-\frac{1}{r^2}\frac{\partial}{\partial\theta}\frac{1}{\sin\theta}\frac{\partial\varpi'_\theta}{\partial\phi}-\frac{1}{r\sin\theta}\frac{\partial^2\varpi'_r}{\partial r\partial\phi}\right]\equiv-k^2,\ \ldots\ldots(5_d)$$

where $2\pi/h$, $2\pi/k$ give the approximate wave lengths of P- and S-waves respectively, from which we find

$$\left(\frac{p}{h}\right)^2-\frac{ip}{h}\frac{(\lambda'+2\mu')}{\rho}h-\frac{\lambda+2\mu}{\rho}=0\ \ \ldots\ldots\ldots(6_1)$$

for (5_a) and

$$\left(\frac{p}{k}\right)^2-\frac{ip}{k}\frac{\mu'}{\rho}k-\frac{\mu}{\rho}=0 \quad \ldots\ldots\ldots\ldots\ldots (6_2)$$

for (5_b), (5_c), (5_d); and we also obtain the equations of the types:

$$\left.\begin{aligned}
&\frac{1}{r^2}\frac{\partial}{\partial r}\left(r^2\frac{\partial\Delta'}{\partial r}\right)+\frac{1}{r^2}\frac{1}{\sin\theta}\frac{\partial}{\partial\theta}\left(\sin\theta\frac{\partial\Delta'}{\partial\theta}\right)+\frac{1}{r^2\sin^2\theta}\frac{\partial^2\Delta'}{\partial\phi^2}+h^2\Delta'=0,\\
&\frac{\partial\varpi'_r}{\partial r^2}+\frac{4}{r}\frac{\partial\varpi'_r}{\partial r}+\frac{2}{r^2}\varpi_r'+\frac{1}{r^2\sin\theta}\frac{\partial}{\partial\theta}\left(\sin\theta\frac{\partial\varpi'_r}{\partial\theta}\right)\\
&\qquad\qquad+\frac{1}{r^2\sin^2\theta}\frac{\partial^2\varpi'_r}{\partial\phi^2}+k^2\varpi'_r=0,\\
&\frac{1}{r}\frac{\partial^2(\varpi'_\theta r)}{\partial r^2}+\frac{1}{r^2\sin^2\theta}\frac{\partial^2\varpi'_\theta}{\partial\phi^2}-\frac{1}{r^2\sin^2\theta}\frac{\partial^2(\varpi_\phi'\sin\theta)}{\partial\phi\,\partial\theta}\\
&\qquad\qquad-\frac{1}{r}\frac{\partial^2\varpi_r'}{\partial r\,\partial\theta}+k^2\varpi_\theta'=0,\\
&\frac{1}{r}\frac{\partial^2(\varpi_\phi' r)}{\partial r^2}+\frac{1}{r^2}\frac{\partial}{\partial\theta}\frac{1}{\sin\theta}\frac{\partial(\varpi'_\phi\sin\theta)}{\partial\theta}-\frac{1}{r^2}\frac{\partial}{\partial\theta}\frac{1}{\sin\theta}\frac{\partial\varpi'_\theta}{\partial\phi}\\
&\qquad\qquad-\frac{1}{r\sin\theta}\frac{\partial^2\varpi'_r}{\partial r\,\partial\phi}+k^2\varpi'_\phi=0.
\end{aligned}\right\}\ldots(7)$$

The solutions of (6) are expressed by

$$\left.\begin{aligned}
\frac{p}{h}&=\frac{(\lambda'+2\mu')hi}{2\rho}\pm\sqrt{\frac{\lambda+2\mu}{\rho}-\left(\frac{\lambda'+2\mu'}{2\rho}\right)^2h^2}\\
&\qquad\fallingdotseq\frac{(\lambda'+2\mu')hi}{2\rho}\pm\sqrt{\frac{\lambda+2\mu}{\rho}},\\
\frac{p}{k}&=\frac{\mu'ki}{2\rho}\pm\sqrt{\frac{\mu}{\rho}-\left(\frac{\mu'}{2\rho}\right)^2k^2}\fallingdotseq\frac{\mu'ki}{2\rho}\pm\sqrt{\frac{\mu}{\rho}}.
\end{aligned}\right\}\ldots\ldots(8)$$

Solving (7) and using the result in (8), we obtain

$$\left.\begin{aligned}
\Delta&=A_{mn}\frac{H^{(2)}_{n+\frac{1}{2}}(hr)}{\sqrt{r}}P_n^m(\cos\theta)\cos m\phi\, e^{-\frac{(\lambda'+2\mu')}{2\rho}h^2t}\,e^{i\sqrt{\frac{\lambda+2\mu}{\rho}}ht},\\
2\varpi_r&=B_{mn}\frac{H^{(2)}_{n+\frac{1}{2}}(kr)}{r^{3/2}}P_n^m(\cos\theta)\sin m\phi\, e^{-\frac{\mu'}{2\rho}k^2t}\,e^{i\sqrt{\frac{\mu}{\rho}}kt},\\
2\varpi_\theta&=\Bigg[C_{mn}\frac{H^{(2)}_{n+\frac{1}{2}}(kr)}{\sqrt{r}}\frac{P_n^m(\cos\theta)}{\sin\theta}+\frac{B_{mn}}{n(n+1)}\frac{1}{r}\frac{d}{dr}
\end{aligned}\right\}\ldots(9)$$

$$\times\{\sqrt{r}\,H^{(2)}_{n+\frac{1}{2}}(kr)\}\frac{dP_n^m(\cos\theta)}{d\theta}\Big]\sin m\phi\, e^{-\frac{\mu'}{2\rho}k^2t}\, e^{i\sqrt{\frac{\mu}{\rho}}kt},$$

$$2\varpi_\phi=\Big[C_{mn}\frac{H^{(2)}_{n+\frac{1}{2}}(kr)}{m\sqrt{r}}\frac{dP_n^m(\cos\theta)}{d\theta}+\frac{B_{mn}m}{n(n+1)}\frac{1}{r}\frac{d}{dr}$$

$$\times\{\sqrt{r}\,H^{(2)}_{n+\frac{1}{2}}(kr)\}\frac{P_n^m(\cos\theta)}{\sin\theta}\Big]\cos m\phi\, e^{-\frac{\mu'}{2\rho}k^2t}\, e^{i\sqrt{\frac{\mu}{\rho}}kt}.$$

Displacement (u_1, v_1, w_1) answering to Δ in (9) and satisfying $\varpi_r=\varpi_\theta=\varpi_\phi=0$ is expressed by

$$\left.\begin{aligned}
u_1&=-\frac{A_{mn}}{h^2}\frac{d}{dr}\frac{H^{(2)}_{n+\frac{1}{2}}(hr)}{\sqrt{r}}P_n^m(\cos\theta)\cos m\phi\, e^{-\frac{(\lambda'+2\mu')h^2t}{2\rho}}\, e^{i\sqrt{\frac{\lambda+2\mu}{\rho}}ht},\\
v_1&=-\frac{A_{mn}}{h^2}\frac{H^{(2)}_{n+\frac{1}{2}}(hr)}{r^{3/2}}\frac{dP_n^m(\cos\theta)}{d\theta}\cos m\phi\, e^{-\frac{(\lambda'+2\mu')h^2t}{2\rho}}\, e^{i\sqrt{\frac{\lambda+2\mu}{\rho}}ht},\\
w_1&=\frac{mA_{mn}}{h^2}\frac{H^{(2)}_{n+\frac{1}{2}}(hr)}{r^{3/2}}\frac{P_n^m(\cos\theta)}{\sin\theta}\sin m\phi\, e^{-\frac{(\lambda'+2\mu')h^2t}{2\rho}}\, e^{i\sqrt{\frac{\lambda+2\mu}{\rho}}ht}.
\end{aligned}\right\}\quad ..(10)$$

Displacement (u_2, v_2, w_2) answering to ϖ_r together with second terms in the expressions of ϖ_θ and ϖ_ϕ, under the condition that $\Delta=0$, is expressed by

$$\left.\begin{aligned}
u_2&=0,\\
v_2&=\frac{mB_{mn}}{n(n+1)}\frac{H^{(2)}_{n+\frac{1}{2}}(kr)}{\sqrt{r}}\frac{P_n^m(\cos\theta)}{\sin\theta}\cos m\phi\, e^{-\frac{\mu'}{2\rho}k^2t}\, e^{i\sqrt{\frac{\mu}{\rho}}kt},\\
w_2&=-\frac{B_{mn}}{n(n+1)}\frac{H^{(2)}_{n+\frac{1}{2}}(kr)}{\sqrt{r}}\frac{dP_n^m(\cos\theta)}{d\theta}\sin m\phi\, e^{-\frac{\mu'}{2\rho}k^2t}\, e^{i\sqrt{\frac{\mu}{\rho}}kt}.
\end{aligned}\right\}\quad ..(11)$$

Displacement (u_3, v_3, w_3) derived from the values of the first terms of ϖ_θ and ϖ_ϕ and fulfilling the conditions, $\Delta=\varpi_r=0$, is written by

$$\left.\begin{aligned}
u_3&=-\frac{n(n+1)C_{mn}}{mk^2}\frac{H^{(2)}_{n+\frac{1}{2}}(kr)}{r^{3/2}}P_n^m(\cos\theta)\cos m\phi\, e^{-\frac{\mu'}{2\rho}k^2t}\, e^{i\sqrt{\frac{\mu}{\rho}}kt},\\
v_3&=-\frac{C_{mn}}{mk^2}\frac{1}{r}\frac{d}{dr}\{\sqrt{r}\,H^{(2)}_{n+\frac{1}{2}}(kr)\}\frac{dP_n^m(\cos\theta)}{d\theta}\cos m\phi\, e^{-\frac{\mu'}{2\rho}k^2t}\, e^{i\sqrt{\frac{\mu}{\rho}}kt},\\
w_3&=\frac{C_{mn}}{k^2}\frac{1}{r}\frac{d}{dr}\{\sqrt{r}\,H^{(2)}_{n+\frac{1}{2}}(kr)\}\frac{P_n^m(\cos\theta)}{\sin\theta}\sin m\phi\, e^{-\frac{\mu'}{2\rho}k^2t}\, e^{i\sqrt{\frac{\mu}{\rho}}kt}.
\end{aligned}\right\}\quad (12)$$

The expressions[3] of displacements in (10), (11), (12) give the case of waves decaying with time even at the origin, and they are not suitable to the propagation of waves generated from the origin at a constant rate of energy transmission, so that we have introduced conventionally kinematical relations, such that $hr=pt$ in $exp.\left\{-\frac{(\lambda'+2\mu')}{2\rho}h^2t\right\}$ for (u_1, v_1, w_1) and $kr=pt$ in $exp.\left\{-\frac{\mu'}{2\rho}k^2t\right\}$ for (u_2, v_2, w_2) and (u_3, v_3, w_3). In spite of its incorrectness in strict mathematics we have employed such a manner, as it gives a dynamically equivalent form of expressions of waves transmitted in visco-elastic medium. The expressions thus obtained are as follows:

$$\left.\begin{aligned} u_1&=-\frac{A_{mn}}{h^2}\frac{d}{dr}\frac{H^{(2)}_{n+\frac{1}{2}}(hr)}{\sqrt{r}}e^{-\frac{(\lambda'+2\mu')h^2r}{2\sqrt{\rho(\lambda+2\mu)}}}P_n^m(\cos\theta)\cos m\phi\, e^{i\sqrt{\frac{\lambda+2\mu}{\rho}}ht},\\ v_1&=-\frac{A_{mn}}{h^2}\frac{H^{(2)}_{n+\frac{1}{2}}(hr)}{r^{3/2}}e^{-\frac{(\lambda'+2\mu')h^2r}{2\sqrt{\rho(\lambda+2\mu)}}}\frac{dP_n^m(\cos\theta)}{d\theta}\cos m\phi\, e^{i\sqrt{\frac{\lambda+2\mu}{\rho}}ht},\\ w_1&=\frac{mA_{mn}}{h^2}\frac{H^{(2)}_{n+\frac{1}{2}}(hr)}{r^{3/2}}e^{-\frac{(\lambda'+2\mu')h^2r}{2\sqrt{\rho(\lambda+2\mu)}}}\frac{P_n^m(\cos\theta)}{\sin\theta}\sin m\phi\, e^{i\sqrt{\frac{\lambda+2\mu}{\rho}}ht}. \end{aligned}\right\}\quad\cdots(13)$$

$$\left.\begin{aligned} u_2&=0,\\ v_2&=\frac{mB_{mn}}{n(n+1)}\frac{H^{(2)}_{n+\frac{1}{2}}(kr)}{\sqrt{r}}e^{-\frac{\mu'k^2r}{2\sqrt{\rho\mu}}}\frac{P_n^m(\cos\theta)}{\sin\theta}\cos m\phi\, e^{i\sqrt{\frac{\mu}{\rho}}kt},\\ w_2&=-\frac{B_{mn}}{n(n+1)}\frac{H^{(2)}_{n+\frac{1}{2}}(kr)}{\sqrt{r}}e^{-\frac{\mu'k^2r}{2\sqrt{\rho\mu}}}\frac{dP_n^m(\cos\theta)}{d\theta}\sin m\phi\, e^{i\sqrt{\frac{\mu}{\rho}}kt}. \end{aligned}\right\}\quad\cdots(14)$$

$$\left.\begin{aligned} u_3&=-\frac{n(n+1)C_{mn}}{mk^2}\frac{H^{(2)}_{n+\frac{1}{2}}(kr)}{r^{3/2}}e^{-\frac{\mu'k^2r}{2\sqrt{\rho\mu}}}P_n^m(\cos\theta)\cos m\phi\, e^{i\sqrt{\frac{\mu}{\rho}}kt},\\ v_3&=-\frac{C_{mn}}{mk^2}\frac{1}{r}\frac{d}{dr}\{\sqrt{r}H^{(2)}_{n+\frac{1}{2}}(kr)\}e^{-\frac{\mu'k^2r}{2\sqrt{\rho\mu}}}\frac{dP_n^m(\cos\theta)}{d\theta}\cos m\phi\, e^{i\sqrt{\frac{\mu}{\rho}}kt},\\ w_3&=\frac{C_{mn}}{k^2}\frac{1}{r}\frac{d}{dr}\{\sqrt{r}H^{(2)}_{n+\frac{1}{2}}(kr)\}e^{-\frac{\mu'k^2r}{2\sqrt{\rho\mu}}}\frac{P_n^m(\cos\theta)}{\sin\theta}\sin m\phi\, e^{i\sqrt{\frac{\mu}{\rho}}kt}. \end{aligned}\right\}\quad(15)$$

3) Similar expressions as (10), (11), (12) that are suitable to the propagation of waves on a spherical surface were obtained by one of us a few years ago. See *Bull. Earthq. Res. Inst.* 6 (1929), 14. Solutions (10), (11), (12) in the case $\lambda'=\mu'=0$ were published by one of us on July 7, 1931 and their special case where $m=0$ was published in *Bull. Earthq. Res. Inst.*, 2 (1927), 13-20.

For the purpose of getting numerical values of these displacements, we have used the relations:

$$\left.\begin{aligned} H^{(2)}_{n+\frac{1}{2}}(hr) &\eqsim \sqrt{\frac{2}{\pi hr}}\, e^{-i\left(hr-\frac{n+1}{2}\pi\right)}, \\ H^{(2)}_{n+\frac{1}{2}}(kr) &\eqsim \sqrt{\frac{2}{\pi kr}}\, e^{-i\left(kr-\frac{n+1}{2}\pi\right)}, \\ P_n^m(\cos\theta) &= (-1)^m \frac{d^m P_n(\cos\theta)}{d\theta^m}. \end{aligned}\right\} \quad \ldots\ldots\ldots(16)$$

By means of these expression we have

$$\left.\begin{aligned} u_1 &= -\frac{A_{mn}}{h^2}\sqrt{\frac{2}{\pi h}}\left\{-\frac{ih}{r}e^{-i\left(hr-\frac{n+1}{2}\pi\right)} - \frac{1}{r^2}e^{-i\left(hr-\frac{n+1}{2}\pi\right)}\right\} \\ &\quad \times e^{-\frac{\lambda'+2\mu'}{2\rho}\sqrt{\frac{\rho}{\lambda+2\mu}}h^2 r}(-1)^m\frac{d^m P_n(\cos\theta)}{d\theta^m}\cos m\phi\, e^{i\sqrt{\frac{\lambda+2\mu}{\rho}}ht}, \\ v_1 &= -\frac{A_{mn}}{h^2}\frac{1}{r^2}\sqrt{\frac{2}{\pi h}}\, e^{-i\left(hr-\frac{n+1}{2}\pi\right)} \\ &\quad \times e^{-\frac{\lambda'+2\mu'}{2\rho}\sqrt{\frac{\rho}{\lambda+2\mu}}h^2 r}(-1)^m\frac{d^{m+1} P_n(\cos\theta)}{d\theta^{m+1}}\cos m\phi\, e^{i\sqrt{\frac{\lambda+2\mu}{\rho}}ht}, \\ w_1 &= \frac{mA_{mn}}{h^2}\frac{1}{r^2}\sqrt{\frac{2}{\pi h}}\, e^{-i\left(hr-\frac{n+1}{2}\pi\right)} \\ &\quad \times e^{-\frac{\lambda'+2\mu'}{2\rho}\sqrt{\frac{\rho}{\lambda+2\mu}}h^2 r}\frac{1}{\sin\theta}(-1)^m\frac{d^m P_n(\cos\theta)}{d\theta^m}\sin m\phi\, e^{i\sqrt{\frac{\lambda+2\mu}{\rho}}ht}. \end{aligned}\right\} \quad \ldots(17)$$

$$\left.\begin{aligned} u_2 &= 0, \\ v_2 &= \frac{mB_{mn}}{n(n+1)}\frac{1}{r}\sqrt{\frac{2}{\pi k}}\, e^{-i\left(kr-\frac{n+1}{2}\pi\right)} \\ &\quad \times e^{-\frac{\mu'}{2\rho}\sqrt{\frac{\rho}{\mu}}k^2 r}\frac{1}{\sin\theta}(-1)^m\frac{d^m p_n(\cos\theta)}{d\theta^m}\cos m\phi\, e^{i\sqrt{\frac{\mu}{\rho}}kt}, \\ w_2 &= -\frac{B_{mn}}{n(n+1)}\frac{1}{r}\sqrt{\frac{2}{\pi k}}\, e^{-i\left(kr-\frac{n+1}{2}\pi\right)} \\ &\quad \times e^{-\frac{\mu'}{2\rho}\sqrt{\frac{\rho}{\mu}}k^2 r}(-1)^m\frac{d^{m+1} P_n(\cos\theta)}{d\theta^{m+1}}\sin m\phi\, e^{i\sqrt{\frac{\mu}{\rho}}kt}. \end{aligned}\right\} \quad \ldots(18)$$

$$u_3 = -\frac{n(n+1)}{mk^2}C_{mn}\frac{1}{r_2}\sqrt{\frac{2}{\pi k}}\, e^{-i\left(kr-\frac{n+1}{2}\pi\right)}$$

$$\left.\begin{aligned}
&\times e^{-\frac{\mu'}{2\rho}\sqrt{\frac{\rho}{\mu}}k^2r}(-1)^m\frac{d^mP_n(\cos\theta)}{d\theta^m}\cos m\phi\, e^{i\sqrt{\frac{\mu}{\rho}}kt},\\
&v_3=-\frac{C_{mn}}{mk^2}\frac{1}{r}\sqrt{\frac{2}{\pi k}}\,e^{-i\left(kr-\frac{n+1}{2}\pi\right)}(-ik)\\
&\qquad\times e^{-\frac{\mu'}{2\rho}\sqrt{\frac{\rho}{\mu}}k^2r}(-1)^m\frac{d^{m+1}P_n(\cos\theta)}{d\theta^{m+1}}\cos m\phi\, e^{i\sqrt{\frac{\mu}{\rho}}kt},\\
&w_3=\frac{C_{mn}}{k^2}\frac{1}{r}\sqrt{\frac{2}{\pi k}}\,e^{-i\left(kr-\frac{n+1}{2}\pi\right)}(-ik)\\
&\qquad\times e^{-\frac{\mu'}{2\rho}\sqrt{\frac{\rho}{\mu}}k^2r}\frac{1}{\sin\theta}(-1)^m\frac{d^mP_n(\cos\theta)}{d\theta^m}\sin m\phi\, e^{i\sqrt{\frac{\mu}{\rho}}kt}.
\end{aligned}\right\}\quad ..(19)$$

To make the problem simple we have taken $m=2$, $n=2$, and assumed the density of the solid, the velocities of propagation of P- and S-waves and damping constants for these respective waves as follows.

$$\rho=2{\cdot}7,\quad \sqrt{\frac{\lambda+2\mu}{\rho}}=6{\cdot}0\ \text{km/sec},\quad \sqrt{\frac{\mu}{\rho}}=3{\cdot}7\ \text{km/sec},$$

$$\frac{\lambda'}{2\rho}=\frac{\mu'}{2\rho}=\frac{1}{5{\cdot}4\times10^3}\ \text{km}^2/\text{sec.}^{4)}\quad \left(\begin{array}{l}\text{assuming that } \lambda', \mu' \text{ are}\\ \text{of equal qualification}\end{array}\right)$$

The wave lengths for P-waves are assumed to be 6·0 km, 60 km, and 0·6 km, while those of the corresponding S-waves are taken to be 3.7 km, 37 km, and 0·37 km respectively. The amplitudes of all components of displacements in the directions i) $P_2(\cos\theta)=1$, $\cos2\phi=1$; ii) $P_2(\cos\theta)=1$, $\cos 2\phi=0$; iii) $P_2^2(\cos\theta)=0$, $\cos2\phi=1$; iv) $P_2^2(\cos\theta)=0$, $\cos 2\phi=0$; v) $P_2(\cos\theta)=-\frac{1}{2}$, $\cos2\phi=1$; vi) $P_2(\cos\theta)=-\frac{1}{2}$, $\cos 2\phi=0$; and at the radial distances, $r=30$ km, 60 km, 120 km, 240 km, 480 km, 960 km, 1920 km, 2400 km, are shown in the appended tables and Figs. 2–10.

The expressions of the displacements show that there are two kinds of S-waves, namely (u_2, v_2, w_2) and (u_3, v_3, w_3), while P-waves are only of one kind. We may call the waves of the type (u_3, v_3, w_3) to be S-waves of the first kind and those of the type (u_2, v_2, w_2) to be S-waves of the

4) These values were temporarily taken to be approximately equal to what Professor Suyehiro derived from the results of experiments due to Professor Tanakadate, Professor Omori and Dr. Taniguchi on brick columns. *Bull. Earthq. Res. Inst.*, 6 (1928), 1–8.

second kind. We find many features to distinguish the two kinds of S-waves.

When the effect of damping is neglected, the radial component ot the displacement of P-waves varies inversely as the radial distance from the origin, while the components transverse to the radial one vary as the inverse square of the radial distance.

The radial component of the displacement of S-waves of the first kind under the similar condition varies inversely as the square of the firsf radial disfance, while the components transverse to the radial one vary as the direct inverse of the radial distance.

The radial component of the displacement of S-waves of the second kind under the similar condition is zero for all radial distances, while the components transverse to the radial one vary again the direct inverse of the radial distance.

It may be concluded that in every kind of waves transmitted in a solid body without solid friction damping the main portion of the displacement varies as the inverse of the radial distance from the origin. Thus, with a mere comparison of the main amplitudes of waves we cannot discriminate P- and S-waves, and much less both kinds of S-waves.

When, however, we observe more closely the components of all kinds of waves, it is possible to get the identification of the waves. The transverse components of P-waves diminish very quickly as the radial distance is increased, and the component of S-waves of the first kind diminishes again in the same manner as in the above case, while that of S-waves of the second kind is zero for all radii.

The variation of the displacements in regard to the direction of propagation has a pecuriority corresponding to each kind of waves. In the direction of propagation where the transeverse component of P-waves is polarised in a certain sense, the same component of S-waves of the first kind is also polarised in the same sense, while the sense of polarisation of S-waves of the second kind is independent of that of P-waves as well as S-waves of the first kind. This may be attributed to the mechanism that P-waves should be acompanied by S-waves of the first kind owing to the conditions of displacements or stresses at the origin of seismic waves, but S-waves of the second kind is possible to occur independently.

In the case of coexistence of P-waves and S-waves of the first kind the distributions of the main amplitudes of both waves are different. In the region, where the amplitudes of P-waves are large, those of S-

waves in question are small, and *vice versa*. The amplitudes of S-waves of the second kind, however, are independent of P-waves. These are also due to the mechanism of the seismic focus.

The above consideration is connected merely with the case where the effect of the solid friction of the material is neglected, although the results in the tables and diagrams contain this effect. When such an effect is taken into account and the periods of vibrations of all kinds of waves are the same, the amplitude of S-waves at a certain station is more damped than that of P-waves at the same station and this is due to the fact that the time of transmission of S-waves from the origin to this station is longer than that of P-waves. The shorter the period of both waves, the relative quickness of the rate of decrease of S-waves is more distinct. In order to demonstrate this nature, we have taken up u_1, v_2, v_3 of three cases i) $L_1=60$ km, $L_2=37$ km; ii) $L_1=6$ km; $L_2=3{\cdot}7$ km; iii) $L_1=0{\cdot}6$ km, $L_2=0{\cdot}37$ km; and kept constant the amplitudes of all waves at the focal distance 2400 km and illustrated the result in Figs. 11, 12 and 13. From the amplitudes of waves at other focal distances, we may understand how the damping of S-waves is quick in comparison with that of P-waves.

The foregoing conclusion cannot be much altered even in the cases where there are some boundaries which cause the reflection and refraction of waves and also where the medium of transmission is varying in a certain manner. This may be seen from the results of a number of our theoretical investigations already carried out to get concrete idea on several cases of boundaries etc.. At any rate, the abnormal smallness of the amplitudes of P-waves cannot be ascertained directly from the nature of the propagation of waves, but they may be cleared when the mechanism, that the period of P-waves is small compared with those of S-waves, will be completely determined.

22. P波S波の振幅が震源距離によつて變化する割合

地震研究所 妹澤克惟
金井清

一般に震源距離が遠くなるに従てP波の振幅はS波の振幅に比較して益々小さくなる事はよく知られて居る事柄である。しかしながらこの事實はP波S波の根本的性質の結果として現れるのではなく、P波の振動週期がS波のそれに比して概して短い爲に減衰作用を速に受けるといふ事

に他ならないのである。それで震源距離が一層大になる時は P 波の震幅は反て S 波の振幅に近づくといふ事の説明も出來るものである。減衰作用を用ひなければ、中間の震源距離で P 波が S 波よりも益々小になり、もつと遠方では P 波が S 波に比して再び增大するといふ說明を與へる事が出來ぬ。反射屈折其他の理論は餘り役に立たない事はこれまでの理論的研究で明かである。

計算の方法は震源から種々の方向性を有する P 波と S 波とが出るものと假定し、これまで種々の場合に行つたのと大體同じ様に考へ且つ原點の條件から P 波と S 波とを算出するのである。彈性體は勿論粘性を含むものとする。この樣にして現れる S 波と P 波の形を見ると P 波の方は一種類しかないけれども S 波の方は第一種と第二種とから成立して居り、且つ P 波と第一種の S 波とは震源の條件の爲に必ず組合つて發生する事及び第二種の S 波は震源の適當なる條件によつて單獨に起り得る事がわかる。

次に固體に粘性のない時に P 波のその傳播方向の振幅は震源距離に反比例して小さくなるけれども同じ波のこれに直角の方向の振幅は距離の二乘に反比例して小さくなる事、第一種の S 波は其傳播方向の振幅が震源距離の二乘に反比例して小さくなるのにそれに直角の方向の振幅は距離それ自身に反比例して小さくなる事、又第二種の S 波は傳播方向に直角の方向の振幅は第一種の場合と同じ樣に變化するのに傳播方向のものは始めから零である事が知られるのである。

上の樣に P 波と各種の S 波とは固體粘性のない時振動方向や其他特別な事項は大分相違のある事がわかるけれども、絕對振幅のみの比較では餘り區別がつかない。しかしながら種々の觀測點の P 波や S 波の振幅分布を見ると著しい相違がある。卽ち或場所で P 波の傳播の向に直角方向の變位が或向に polarise して居れば其場所で第一種の S 波の傳播の向に直角方向の變位も同じ向に polarise する事がわかる。又 P 波と第一種の S 波とが共存する時に P 波の振幅が大なる所では S 波の振幅は小さく、逆に P 波の振幅の小なる所では S 波の振幅が大なるものである。然るに第二種の S 波は P 波に無關係となる。此等は震源に於ける應力や變位の條件から定まるものである。

以上は固體の粘性を考へなくても出て來る事柄であるが、若し粘性を考へる時には、模樣が多少變更される。卽ち P 波と S 波との粘性的減衰の作用を同じ割合に取る時は、或震源距離では S 波の方の振幅が同じ週期の P 波に比較して餘計に減衰して來るといふ事がわかるのである。この事は震源距離の非常に遠い所で P 波と S 波との振動週期が可なり近いものしか殘つて居らぬ樣な時に P 波の方が S 波に比較して振幅が餘り縮まないといふ事實とよく符合して居る樣に思はれる。何れにしても適當なる震源距離で P 波が S 波よりも振幅が一般に小であるといふ事柄の說明を一定週期の波についてなす事は出來ぬ。それにはどうしても震源又は原點附近から出る波について P 波の振動週期が S 波のものよりも小であるといふ事を確める事が先決問題である樣に思ふ。

Table I. The Case of $L_1=6\cdot0$ km, $L_2=3\cdot7$ km.

	r in km	30	60	120	240	480	960	1920	2400
$P_2(\cos\theta)=1$, $\cos 2\phi=0$	$u_1/A_{22}\sqrt{\frac{2}{\pi h}}\times\frac{3}{2\pi}$	0·09965	0·04970	0·02470	0·01220	0·00595	0·00284	0·00129	0·00099
	$v_1/A_{22}\sqrt{\frac{2}{\pi h}}\times\frac{3}{2\pi}$	0	0	0	0	0	0	0	0
	$w_1/A_{22}\sqrt{\frac{2}{\pi h}}\times\frac{3}{2\pi}$	0	0	0	0	0	0	0	0
	$u_2\Big/\frac{B_{22}}{2\cdot3}\sqrt{\frac{2k}{\pi}}\times\frac{3}{2\pi}$	0	0	0	0	0	0	0	0
	$v_2\Big/\frac{B_{22}}{2\cdot3}\sqrt{\frac{2k}{\pi}}\times\frac{3}{2\pi}$	—	—	—	—	—	—	—	—
	$w_2\Big/\frac{B_{22}}{2\cdot3}\sqrt{\frac{2k}{\pi}}\times\frac{3}{2\pi}$	0	0	0	0	0	0	0	0
	$u_3/C_{22}\sqrt{\frac{2}{\pi k}}\times\frac{3}{2\pi}$	0·0036143	0·0008997	0·0002230	0·0000548	0·0000132	0·0000031	0·0000007	0·0000004
	$v_3/C_{22}\sqrt{\frac{2}{\pi k}}\times\frac{3}{2\pi}$	0	0	0	0	0	0	0	0
	$w_3/C_{22}\sqrt{\frac{2}{\pi k}}\times\frac{3}{2\pi}$	0	0	0	0	0	0	0	0
	$u_1/A_{22}\sqrt{\frac{2}{\pi h}}\times\frac{3}{2\pi}$	0	0	0	0	0	0	0	0
	$v_1/A_{22}\sqrt{\frac{2}{\pi h}}\times\frac{3}{2\pi}$	0	0	0	0	0	0	0	0
	$w_1/A_{22}\sqrt{\frac{2}{\pi h}}\times\frac{3}{2\pi}$	—	—	—	—	—	—	—	—
	$u_2\Big/\frac{B_{22}}{2\cdot3}\sqrt{\frac{2k}{\pi}}\times\frac{3}{2\pi}$	0	0	0	0	0	0	0	0

(to be continued.)

Table I. (*continued.*)

	r in km	30	60	120	240	480	960	1920	2400
$P_2(\cos\theta)=1$, $\cos 2\phi=0$	$v_2\Big/\frac{B_{22}}{2\cdot 3}\sqrt{\frac{2k}{\pi}}\times\frac{3}{2\pi}$	0	0	0	0	0	0	0	0
	$w_2\Big/\frac{B_{22}}{2\cdot 3}\sqrt{\frac{2k}{\pi}}\times\frac{3}{2\pi}$	0	0	0	0	0	0	0	0
	$u_3/C_{22}\sqrt{\frac{2}{\pi k}}\times\frac{3}{2\pi}$	0	0	0	0	0	0	0	0
	$v_3/C_{22}\sqrt{\frac{2}{\pi k}}\times\frac{3}{2\pi}$	0	0	0	0	0	0	0	0
	$w_3/C_{22}\sqrt{\frac{2}{\pi k}}\times\frac{3}{2\pi}$	—	—	—	—	—	—	—	—
	$u_1/A_{22}\sqrt{\frac{2}{\pi h}}\times\frac{3}{2\pi}$	0	0	0	0	0	0	0	0
	$v_1/A_{22}\sqrt{\frac{2}{\pi h}}\times\frac{3}{2\pi}$	−0·0031709	−0·0007907	−0·0001965	−0·0000485	−0·0000118	−0·0000028	−0·0000006	−0·0000004
	$w_1/A_{22}\sqrt{\frac{2}{\pi h}}\times\frac{3}{2\pi}$	0	0	0	0	0	0	0	0
	$u_2\Big/\frac{B_{22}}{2\cdot 3}\sqrt{\frac{2k}{\pi}}\times\frac{3}{2\pi}$	0	0	0	0	0	0	0	0
$P_2^2(\cos\theta)=0$, $\cos 2\phi=1$	$v_2\Big/\frac{B_{22}}{2\cdot 3}\sqrt{\frac{2k}{\pi}}\times\frac{3}{2\pi}$	0	0	0	0	0	0	0	0
	$w_2\Big/\frac{B_{22}}{2\cdot 3}\sqrt{\frac{2k}{\pi}}\times\frac{3}{2\pi}$	0	0	0	0	0	0	0	0
	$u_3/C_{22}\sqrt{\frac{2}{\pi k}}\times\frac{3}{2\pi}$	0	0	0	0	0	0	0	0
	$v_3/C_{22}\sqrt{\frac{2}{\pi k}}\times\frac{3}{2\pi}$	−0·03070	−0·01528	−0·00758	−0·00372	−0·00180	−0·00084	−0·00036	−0·00027

(*to be continued.*)

Table I. (*continued.*)

	r in km	30	60	120	240	480	960	1920	2400
	$w_3/C_{22}\sqrt{\frac{2}{\pi k}}\times\frac{3}{2\pi}$	0	0	0	0	0	0	0	0
$P_2^2(\cos\theta)=0$, $\cos 2\phi=0$	$u_1/A_{22}\sqrt{\frac{2}{\pi h}}\times\frac{3}{2\pi}$	0	0	0	0	0	0	0	0
	$v_1/A_{22}\sqrt{\frac{2}{\pi h}}\times\frac{3}{2\pi}$	0	0	0	0	0	0	0	0
	$w_1/A_{22}\sqrt{\frac{2}{\pi h}}\times\frac{3}{2\pi}$	0	0	0	0	0	0	0	0
	$u_2\sqrt{\frac{B_{22}}{2\cdot 3}}\sqrt{\frac{2k}{\pi}}\times\frac{3}{2\pi}$	0	0	0	0	0	0	0	0
	$v_2\sqrt{\frac{B_{22}}{2\cdot 3}}\sqrt{\frac{2k}{\pi}}\times\frac{3}{2\pi}$	0	0	0	0	0	0	0	0
	$w_2\sqrt{\frac{B_{22}}{2\cdot 3}}\sqrt{\frac{2k}{\pi}}\times\frac{3}{2\pi}$	−0·06140	−0·03057	−0·01515	−0·00745	−0·00360	−0·00168	−0·00073	−0·00055
	$u_3/C_{22}\sqrt{\frac{2}{\pi k}}\times\frac{3}{2\pi}$	0	0	0	0	0	0	0	0
	$r_3/C_{22}\sqrt{\frac{2}{\pi k}}\times\frac{3}{2\pi}$	0	0	0	0	0	0	0	0
	$w_3/C_{22}\sqrt{\frac{2}{\pi k}}\times\frac{3}{2\pi}$	0	0	0	0	0	0	0	0
	$u_1/A_{22}\sqrt{\frac{2}{\pi h}}\times\frac{3}{2\pi}$	−0·09965	−0·04970	−0·02470	−0·01220	−0·00595	−0·00284	−0·00129	−0·00099
	$v_1/A_{22}\sqrt{\frac{2}{\pi h}}\times\frac{3}{2\pi}$	0	0	0	0	0	0	0	0
	$w_1/A_{22}\sqrt{\frac{2}{\pi h}}\times\frac{3}{2\pi}$	0	0	0	0	0	0	0	0

(*to be continued.*)

Table I. (*continued.*)

	r in km	30	60	120	240	480	960	1920	2400
	$u_2 \Big/ \frac{B_{22}}{2\cdot3}\sqrt{\frac{2k}{\pi}} \times \frac{3}{2\pi}$	0	0	0	0	0	0	0	0
$P_2(\cos\theta) = -\frac{1}{2}$, $\cos 2\phi = 1$	$v_2 \Big/ \frac{B_{22}}{2\cdot3}\sqrt{\frac{2k}{\pi}} \times \frac{3}{2\pi}$	0·12281	0 06114	0·03031	0·01489	0·00719	0 00336	0·00146	0·00109
	$w_2 \Big/ \frac{B_{22}}{2\cdot3}\sqrt{\frac{2k}{\pi}} \times \frac{3}{2\pi}$	0	0	0	0	0	0	0	0
	$u_3/C_{22}\sqrt{\frac{2}{\pi k}} \times \frac{3}{2\pi}$	−0 0036143	−0·0008997	−0·0002230	−0·0000548	−0·0000132	−0·0000031	−0 0000007	−0·0000004
	$v_3/C_{22}\sqrt{\frac{2}{\pi k}} \times \frac{3}{2\pi}$	0	0	0	0	0	0	0	0
	$w_3/C_{22}\sqrt{\frac{2}{\pi k}} \times \frac{3}{2\pi}$	0	0	0	0	0	0	0	0
	$u_1/A_{22}\sqrt{\frac{2}{\pi h}} \times \frac{3}{2\pi}$	0	0	0	0	0	0	0	0
	$v_1/A_{22}\sqrt{\frac{2}{\pi h}} \times \frac{3}{2\pi}$	0	0	0	0	0	0	0	0
	$w_1/A_{22}\sqrt{\frac{2}{\pi h}} \times \frac{3}{2\pi}$	0 0063417	0·0015813	0·0003929	0·0000971	0·0000237	0·0000056	0·0000013	0·0000008
	$u_2 \Big/ \frac{B_{22}}{2\cdot3}\sqrt{\frac{2k}{\pi}} \times \frac{3}{2\pi}$	0	0	0	0	0	0	0	0
$P_2(\cos\theta) = -\frac{1}{2}$, $\cos 2\phi = 0$	$v_2 \Big/ \frac{B_{22}}{2\cdot3}\sqrt{\frac{2k}{\pi}} \times \frac{3}{2\pi}$	0	0	0	0	0	0	0	0
	$w_2 \Big/ \frac{B_{22}}{2\cdot3}\sqrt{\frac{2k}{\pi}} \times \frac{3}{2\pi}$	0	0	0	0	0	0	0	0
	$u_3/C_{22}\sqrt{\frac{2}{\pi k}} \times \frac{3}{2\pi}$	0	0	0	0	0	0	0	0

(*to be continued.*)

Table I. (*contineud.*)

	r in km	30	60	120	240	480	960	1920	2400
	$v_3/C_{22}\sqrt{\frac{2}{\pi k}}\times\frac{3}{2\pi}$	0	0	0	0	0	0	0	0
	$w_3/C_{22}\sqrt{\frac{2}{\pi k}}\times\frac{3}{2\pi}$	0·06140	0·03057	0·01515	0·00745	0 00360	0·00168	0·00073	0·00055

Table II. The Case of $L_1=60$ km, $L_2=37$ km.

	r in km	300	600	1200	2400	4800	9600	19200	24000
	$u_1/A_{22}\sqrt{\frac{2}{\pi h}}\times\frac{3}{2\pi}$	0·09997	0·04997	0·02497	0 01247	0·00622	0·00309	0·00153	0·00122
	$v_1/A_{22}\sqrt{\frac{2}{\pi h}}\times\frac{3}{2\pi}$	0	0	0	0	0	0	0	0
	$w_1/A_{22}\sqrt{\frac{2}{\pi h}}\times\frac{3}{2\pi}$	0	0	0	0	0	0	0	0
	$u_2\Big/\frac{B_{22}}{2\cdot 3}\sqrt{\frac{2k}{\pi}}\times\frac{3}{2\pi}$	0	0	0	0	0	0	0	0
$P_2(\cos\theta)=1$, $\cos 2\phi=1$	$v_2\Big/\frac{B_{22}}{2\cdot 3}\sqrt{\frac{2k}{\pi}}\times\frac{3}{2\pi}$	—	—	—	—	—	—	—	—
	$w_2\Big/\frac{B_{22}}{2\cdot 3}\sqrt{\frac{2k}{\pi}}\times\frac{3}{2\pi}$	0	0	0	0	0	0	0	0
	$u_3/C_{22}\sqrt{\frac{2}{\pi k}}\times\frac{3}{2\pi}$	0·0036285	0·0009066	0·0002265	0 0000565	0 0000141	0·0000035	0 00000086	0·00000055
	$v_3/C_{22}\sqrt{\frac{2}{\pi k}}\times\frac{3}{2\pi}$	0	0	0	0	0	0	0	0

(*to be continued.*)

Table II. (*continued.*)

	r in km	300	600	1200	2400	4800	9600	19200	24000
	$w_3/C_{22}\sqrt{\frac{2}{\pi k}}\times\frac{3}{2\pi}$	0	0	0	0	0	0	0	0
$P_2(\cos\theta)=1$, $\cos 2\phi=0$	$u_1/A_{22}\sqrt{\frac{2}{\pi h}}\times\frac{3}{2\pi}$	0	0	0	0	0	0	0	0
	$v_1/A_{22}\sqrt{\frac{2}{\pi h}}\times\frac{3}{2\pi}$	0	0	0	0	0	0	0	0
	$w_1/A_{22}\sqrt{\frac{2}{\pi h}}\times\frac{3}{2\pi}$	—	—	—	—	—	—	—	—
	$u_2\Big/\frac{B_{22}}{2\cdot 3}\sqrt{\frac{2k}{\pi}}\times\frac{3}{2\pi}$	0	0	0	0	0	0	0	0
	$v_2\Big/\frac{B_{22}}{2\cdot 3}\sqrt{\frac{2k}{\pi}}\times\frac{3}{2\pi}$	0	0	0	0	0	0	0	0
	$w_2\Big/\frac{B_{22}}{2\cdot 3}\sqrt{\frac{2k}{\pi}}\times\frac{3}{2\pi}$	0	0	0	0	0	0	0	0
	$u_3/C_{22}\sqrt{\frac{2}{\pi k}}\times\frac{3}{2\pi}$	0	0	0	0	0	0	0	0
	$v_3/C_{22}\sqrt{\frac{2}{\pi k}}\times\frac{3}{2\pi}$	0	0	0	0	0	0	0	0
	$w_3/C_{22}\sqrt{\frac{2}{\pi k}}\times\frac{3}{2\pi}$	—	—	—	—	—	—	—	—
	$u_1/A_{22}\sqrt{\frac{2}{\pi h}}\times\frac{3}{2\pi}$	0	0	0	0	0	0	0	0
	$v_1/A_{22}\sqrt{\frac{2}{\pi h}}\times\frac{3}{2\pi}$	−0·0031810	−0·0007950	−0 0001986	−0·0000496	−0·0000124	−0·0000031	−0·00000075	−0·0000005
	$w_1/A_{22}\sqrt{\frac{2}{\pi h}}\times\frac{3}{2\pi}$	0	0	0	0	0	0	0	0

(*to be continued.*)

Table II. (*continued.*)

	r in km	300	600	1200	2400	4800	9600	19200	24000
$P_2^2(\cos\theta)=0$ $\cos 2\phi=1$	$u_2\Big/\frac{B_{22}}{2\cdot3}\sqrt{\frac{2k}{\pi}}\times\frac{3}{2\pi}$	0	0	0	0	0	0	0	0
	$v_2\Big/\frac{B_{22}}{2\cdot3}\sqrt{\frac{2k}{\pi}}\times\frac{3}{2\pi}$	0	0	0	0	0	0	0	0
	$w_2\Big/\frac{B_{22}}{2\cdot3}\sqrt{\frac{2k}{\pi}}\times\frac{3}{2\pi}$	0	0	0	0	0	0	0	0
	$u_3/C_{22}\sqrt{\frac{2}{\pi k}}\times\frac{3}{2\pi}$	0	0	0	0	0	0	0	0
	$v_3/C_{22}\sqrt{\frac{2}{\pi k}}\times\frac{3}{2\pi}$	-0·03082	-0·01540	-0·00770	-0·00384	-0·00191	-0·00095	-0·00047	-0·00037
	$w_3/C_{22}\sqrt{\frac{2}{\pi k}}\times\frac{3}{2\pi}$	0	0	0	0	0	0	0	0
$P_2^2(\cos\theta)=0,$ $\cos 2\phi=0$	$u_1/A_{22}\sqrt{\frac{2}{\pi h}}\times\frac{3}{2\pi}$	0	0	0	0	0	0	0	0
	$v_1/A_{22}\sqrt{\frac{2}{\pi h}}\times\frac{3}{2\pi}$	0	0	0	0	0	0	0	0
	$w_1/A_{22}\sqrt{\frac{2}{\pi h}}\times\frac{3}{2\pi}$	0	0	0	0	0	0	0	0
	$u_2\Big/\frac{B_{22}}{2\cdot3}\sqrt{\frac{2k}{\pi}}\times\frac{3}{2\pi}$	0	0	0	0	0	0	0	0
	$v_2\Big/\frac{B_{22}}{2\cdot3}\sqrt{\frac{2k}{\pi}}\times\frac{3}{2\pi}$	0	0	0	0	0	0	0	0
	$w_2\Big/\frac{B_{22}}{2\cdot3}\sqrt{\frac{2k}{\pi}}\times\frac{3}{2\pi}$	-0·06164	-0·03080	-0·01540	-0·00768	-0·00382	-0·00190	-0·00094	-0·00074
	$u_3/C_{22}\sqrt{\frac{2}{\pi k}}\times\frac{3}{2\pi}$	0	0	0	0	0	0	0	0

(*to be continued.*)

Table II. (*continued.*)

	r in km	300	600	1200	2400	4800	9600	19200	24000
	$v_3/C_{22}\sqrt{\frac{2}{\pi k}}\times\frac{3}{2\pi}$	0	0	0	0	0	0	0	0
	$w_3/C_{22}\sqrt{\frac{2}{\pi k}}\times\frac{3}{2\pi}$	0	0	0	0	0	0	0	0
$P_2(\cos\theta)=-\frac{1}{2}$, $\cos 2\phi=1$	$u_1/A_{22}\sqrt{\frac{2}{\pi h}}\times\frac{3}{2\pi}$	−0·09997	−0·04997	−0·02497	−0·01247	−0·00622	−0·00309	−0·00153	−0·00122
	$v_1/A_{22}\sqrt{\frac{2}{\pi h}}\times\frac{3}{2\pi}$	0	0	0	0	0	0	0	0
	$w_1/A_{22}\sqrt{\frac{2}{\pi h}}\times\frac{3}{2\pi}$	0	0	0	0	0	0	0	0
	$u_2\Big/\frac{B_{22}}{2\cdot3}\sqrt{\frac{2k}{\pi}}\times\frac{3}{2\pi}$	0	0	0	0	0	0	0	0
	$v_2\Big/\frac{B_{22}}{2\cdot3}\sqrt{\frac{2k}{\pi}}\times\frac{3}{2\pi}$	0·12329	−0·06161	0·03078	0·01536	0·00766	0·00380	0·00187	0·00149
	$w_2\Big/\frac{B_{22}}{2\cdot3}\sqrt{\frac{2k}{\pi}}\times\frac{3}{2\pi}$	0	0	0	0	0	0	0	0
	$u_3/C_{22}\sqrt{\frac{2}{\pi k}}\times\frac{3}{2\pi}$	−0·0036285	−0·0009066	−0·0002265	−0·0000565	−0·0000141	−0·0000035	−0·00000086	−0·00000055
	$v_3/C_{22}\sqrt{\frac{2}{\pi k}}\times\frac{3}{2\pi}$	0	0	0	0	0	0	0	0
	$w_3/C_{22}\sqrt{\frac{2}{\pi k}}\times\frac{3}{2\pi}$	0	0	0	0	0	0	0	0
	$u_1/A_{22}\sqrt{\frac{2}{\pi h}}\times\frac{3}{2\pi}$	0	0	0	0	0	0	0	0
	$v_1/A_{22}\sqrt{\frac{2}{\pi h}}\times\frac{3}{2\pi}$	0	0	0	0	0	0	0	0

(*to be continued.*)

Table II. (*continued.*)

	r in km	300	600	1200	2400	4800	9600	19200	24000
$P_2(\cos\theta)=-\frac{1}{2}$, $\cos 2\phi=0$	$w_1/A_{22}\sqrt{\frac{2}{\pi h}}\times\frac{3}{2\pi}$	0·0063620	0 0015900	0·0003972	0 0000992	0·0000248	0·0000062	0.0000015	0·0000010
	$u_2\Big/\frac{B_{22}}{2\cdot 3}\sqrt{\frac{2k}{\pi}}\times\frac{3}{2\pi}$	0	0	0	0	0	0	0	0
	$v_2\Big/\frac{B_{22}}{2\cdot 3}\sqrt{\frac{2k}{\pi}}\times\frac{3}{2\pi}$	0	0	0	0	0	0	0	0
	$w_2\Big/\frac{B_{22}}{2\cdot 3}\sqrt{\frac{2k}{\pi}}\times\frac{3}{2\pi}$	0	0	0	0	0	0	0	0
	$u_3/C_{22}\sqrt{\frac{2}{\pi k}}\times\frac{3}{2\pi}$	0	0	0	0	0	0	0	0
	$v_3/C_{22}\sqrt{\frac{2}{\pi k}}\times\frac{3}{2\pi}$	0	0	0	0	0	0	0	0
	$w_3/C_{22}\sqrt{\frac{2}{\pi k}}\times\frac{3}{2\pi}$	0·06164	0·03080	0·01540	0 00768	0·00382	0·00190	0·00094	0·00074

Table III. The Case of $L_1=0\cdot 6$ km, $L_2=0\cdot 37$ km.

r in km	3	6	12	24	48	96	192	240
$u_1/A_{22}\sqrt{\frac{2}{\pi h}}\times\frac{3}{2\pi}$	0·09700	0·04735	0 02213	0·00979	0.00384	0·00118	0·00022	0·00011
$v_1/A_{22}\sqrt{\frac{2}{\pi h}}\times\frac{3}{2\pi}$	0	0	0	0	0	0	0	0
$w_1/A_{22}\sqrt{\frac{2}{\pi h}}\times\frac{3}{2\pi}$	0	0	0	0	0	0	0	0

(*to be continued.*)

Table III. (*continued.*)

	r in km	3	6	12	24	48	96	192	240
$P_2(\cos\theta)=1$, $\cos 2\phi=1$	$u_2\Big/\frac{B_{22}}{2\cdot 3}\sqrt{\frac{2k}{\pi}}\times\frac{3}{2\pi}$	0	0	0	0	0	0	0	0
	$v_2\Big/\frac{B_{22}}{2\cdot 3}\sqrt{\frac{2k}{\pi}}\times\frac{3}{2\pi}$	—	—	—	—	—	—	—	—
	$w_2\Big/\frac{B_{22}}{2\cdot 3}\sqrt{\frac{2k}{\pi}}\times\frac{3}{2\pi}$	0	0	0	0	0	0	0	0
	$u_3/C_{22}\sqrt{\frac{2}{\pi k}}\times\frac{3}{2\pi}$	0·0034760	0·0008322	0·0001908	0·0000401	0·0000071	0·0000009	0·00000006	0·00000002
	$v_3/C_{22}\sqrt{\frac{2}{\pi k}}\times\frac{3}{2\pi}$	0	0	0	0	0	0	0	0
	$w_3/C_{22}\sqrt{\frac{2}{\pi k}}\times\frac{3}{2\pi}$	0	0	0	0	0	0	0	0
$P_2(\cos\theta)=1$, $\cos 2\phi=0$	$u_1/A_{22}\sqrt{\frac{2}{\pi h}}\times\frac{3}{2\pi}$	0	0	0	0	0	0	0	0
	$v_1/A_{22}\sqrt{\frac{2}{\pi h}}\times\frac{3}{2\pi}$	0	0	0	0	0	0	0	0
	$w_1/A_{22}\sqrt{\frac{2}{\pi h}}\times\frac{3}{2\pi}$	—	—	—	—	—	—	—	—
	$u_2\Big/\frac{B_{22}}{2\cdot 3}\sqrt{\frac{2k}{\pi}}\times\frac{3}{2\pi}$	0	0	0	0	0	0	0	0
	$v_2\Big/\frac{B_{22}}{2\cdot 3}\sqrt{\frac{2k}{\pi}}\times\frac{3}{2\pi}$	0	0	0	0	0	0	0	0
	$w_2\Big/\frac{B_{22}}{2\cdot 3}\sqrt{\frac{2k}{\pi}}\times\frac{3}{2\pi}$	0	0	0	0	0	0	0	0
	$u_3/C_{22}\sqrt{\frac{2}{\pi k}}\times\frac{3}{2\pi}$	0	0	0	0	0	0	0	0

(*to be continued.*)

Table III. (*continued.*)

	r in km	3	6	12	24	48	96	192	240
	$v_3/C_{22}\sqrt{\frac{2}{\pi k}}\times\frac{3}{2\pi}$	0	0	0	0	0	0	0	0
	$w_3/C_{22}\sqrt{\frac{2}{\pi k}}\times\frac{3}{2\pi}$	—	—	—	—	—	—	—	—
	$u_1/A_{22}\sqrt{\frac{2}{\pi h}}\times\frac{3}{2\pi}$	0	0	0	0	0	0	0	0
	$v_1/A_{22}\sqrt{\frac{2}{\pi h}}\times\frac{3}{2\pi}$	−0·0030864	−0·0007533	−0·0001760	−0·0000390	−0·0000076	−0·0000012	−0·0000001	−0·00000004
	$w_1/A_{22}\sqrt{\frac{2}{\pi h}}\times\frac{3}{2\pi}$	0	0	0	0	0	0	0	0
	$u_2\Big/\frac{B_{22}}{2\cdot 3}\sqrt{\frac{2k}{\pi}}\times\frac{3}{2\pi}$	0	0	0	0	0	0	0	0
$P_2^2(\cos\theta)=0$ $\cos 2\phi=1$	$v_2\Big/\frac{B_{22}}{2\cdot 3}\sqrt{\frac{2k}{\pi}}\times\frac{3}{2\pi}$	0	0	0	0	0	0	0	0
	$w_2\Big/\frac{B_{22}}{2\cdot 3}\sqrt{\frac{2k}{\pi}}\times\frac{3}{2\pi}$	0	0	0	0	0	0	0	0
	$u_3/C_{22}\sqrt{\frac{2}{\pi k}}\times\frac{3}{2\pi}$	0	0	0	0	0	0	0	0
	$v_3/C_{22}\sqrt{\frac{2}{\pi k}}\times\frac{3}{2\pi}$	−0·02953	−0·01414	−0·00648	−0·00273	−0·00096	−0·00024	−0·00003	−0·00001
	$w_3/C_{22}\sqrt{\frac{2}{\pi k}}\times\frac{3}{2\pi}$	0	0	0	0	0	0	0	0
	$u_1/A_{22}\sqrt{\frac{2}{\pi h}}\times\frac{3}{2\pi}$	0	0	0	0	0	0	0	0
	$v_1/A_{22}\sqrt{\frac{2}{\pi h}}\times\frac{3}{2\pi}$	0	0	0	0	0	0	0	0

(*to be continued.*)

Table III. (*continued.*)

	r in km	3	6	12	24	48	96	192	240
$P_2^2(\cos\theta)=0$, $\cos 2\phi=0$	$w_1/A_{22}\sqrt{\frac{2}{\pi h}}\times\frac{3}{2\pi}$	0	0	0	0	0	0	0	0
	$u_2\Big/\frac{B_{22}}{2\cdot3}\sqrt{\frac{2k}{\pi}}\times\frac{3}{2\pi}$	0	0	0	0	0	0	0	0
	$v_2\Big/\frac{B_{22}}{2\cdot3}\sqrt{\frac{2k}{\pi}}\times\frac{3}{2\pi}$	0	0	0	0	0	0	0	0
	$w_2\Big/\frac{B_{22}}{2\cdot3}\sqrt{\frac{2k}{\pi}}\times\frac{3}{2\pi}$	−0·05905	−0.02828	0·01297	−0·00545	−0·00193	−0·00048	−0·00006	−0·00002
	$u_3/C_{22}\sqrt{\frac{2}{\pi k}}\times\frac{3}{2\pi}$	0	0	0	0	0	0	0	0
	$v_3/C_{22}\sqrt{\frac{2}{\pi k}}\times\frac{3}{2\pi}$	0	0	0	0	0	0	0	0
	$w_3/C_{22}\sqrt{\frac{2}{\pi k}}\times\frac{3}{2\pi}$	0	0	0	0	0	0	0	0
$P_2(\cos\theta)=-\frac{1}{2}$, $\cos 2\phi=1$	$u_1/A_{22}\sqrt{\frac{2}{\pi h}}\times\frac{3}{2\pi}$	−0·09700	−0·04735	−0·02213	−0·00979	−0·00384	−0·00118	−0·00022	−0·00011
	$v_1/A_{22}\sqrt{\frac{2}{\pi h}}\times\frac{3}{2\pi}$	0	0	0	0	0	0	0	0
	$w_1/A_{22}\sqrt{\frac{2}{\pi h}}\times\frac{3}{2\pi}$	0	0	0	0	0	0	0	0
	$u_2\Big/\frac{B_{22}}{2\cdot3}\sqrt{\frac{2k}{\pi}}\times\frac{3}{2\pi}$	0	0	0	0	0	0	0	0
	$v_2\Big/\frac{B_{22}}{2\cdot3}\sqrt{\frac{2k}{\pi}}\times\frac{3}{2\pi}$	0·11811	0·05655	0·02594	0·01091	0·00386	0·00096	0·00012	0·00005
	$w_2\Big/\frac{B_{22}}{2\cdot3}\sqrt{\frac{2k}{\pi}}\times\frac{3}{2\pi}$	0	0	0	0	0	0	0	0

(*to be continued.*)

Table III. (*continued.*)

	r in km	3	6	12	24	48	96	192	240
	$u_3/C_{22}\sqrt{\frac{2}{\pi k}}\times\frac{3}{2\pi}$	−0·0034760	−0·0008322	−0·0001908	−0·0000401	−0·0000071	−0·0000009	−0·00000006	−0·00000002
	$v_3/C_{22}\sqrt{\frac{2}{\pi k}}\times\frac{3}{2\pi}$	0	0	0	0	0	0	0	0
	$w_3/C_{22}\sqrt{\frac{2}{\pi k}}\times\frac{3}{2\pi}$	0	0	0	0	0	0	0	0
$P_2(\cos\theta)=-\frac{1}{2}$, $\cos 2\phi=0$	$u/A_{22}\sqrt{\frac{2}{\pi h}}\times\frac{3}{2\pi}$	0	0	0	0	0	0	0	0
	$v_1/A_{22}\sqrt{\frac{2}{\pi h}}\times\frac{3}{2\pi}$	0	0	0	0	0	0	0	0
	$w_1/A_{22}\sqrt{\frac{2}{\pi h}}\times\frac{3}{2\pi}$	0·0061728	0·0015065	0·0003521	0·0000779	0·0000153	0·0000023	0·0000002	0·0000001
	$u_2\Big/\frac{B_{22}}{2.3}\sqrt{\frac{2k}{\pi}}\times\frac{3}{2\pi}$	0	0	0	0	0	0	0	0
	$v_2\Big/\frac{B_{22}}{2\cdot3}\sqrt{\frac{2k}{\pi}}\times\frac{3}{2\pi}$	0	0	0	0	0	0	0	0
	$w_2\Big/\frac{B_{22}}{2\cdot3}\sqrt{\frac{2k}{\pi}}\times\frac{3}{2\pi}$	0	0	0	0	0	0	0	0
	$u_3/C_{22}\sqrt{\frac{2}{\pi k}}\times\frac{3}{2\pi}$	0	0	0	0	0	0	0	0
	$v_3/C_{22}\sqrt{\frac{2}{\pi k}}\times\frac{3}{2\pi}$	0	0	0	0	0	0	0	0
	$w_3/C_{22}\sqrt{\frac{2}{\pi k}}\times\frac{3}{2\pi}$	0·05905	0·02827	0·01297	0·00545	0·00193	0·00048	0·00006	0·00002

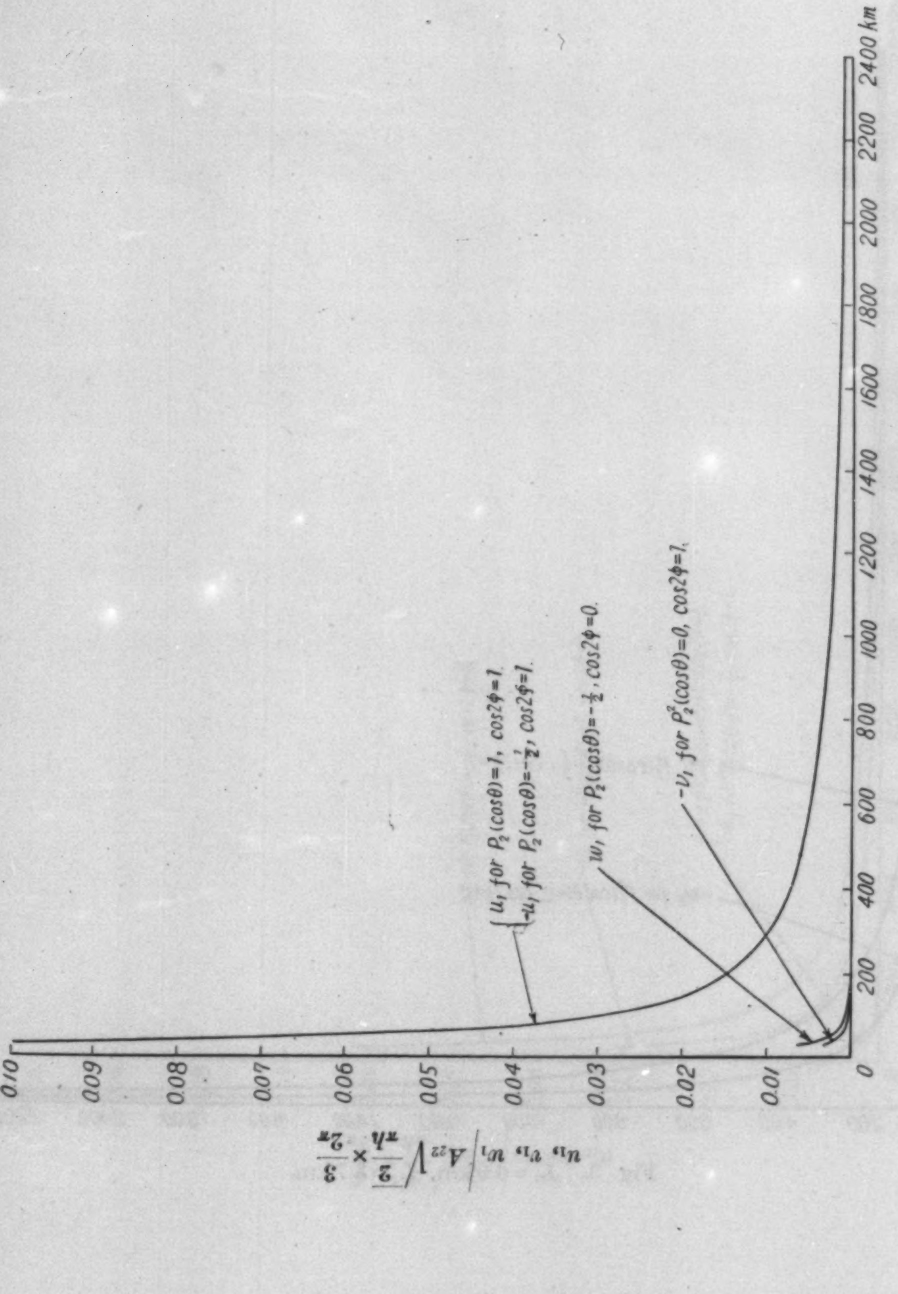

Fig. 2. $L_1=6{\cdot}0\,\text{km}$, $L_2=3{\cdot}7\,\text{km}$

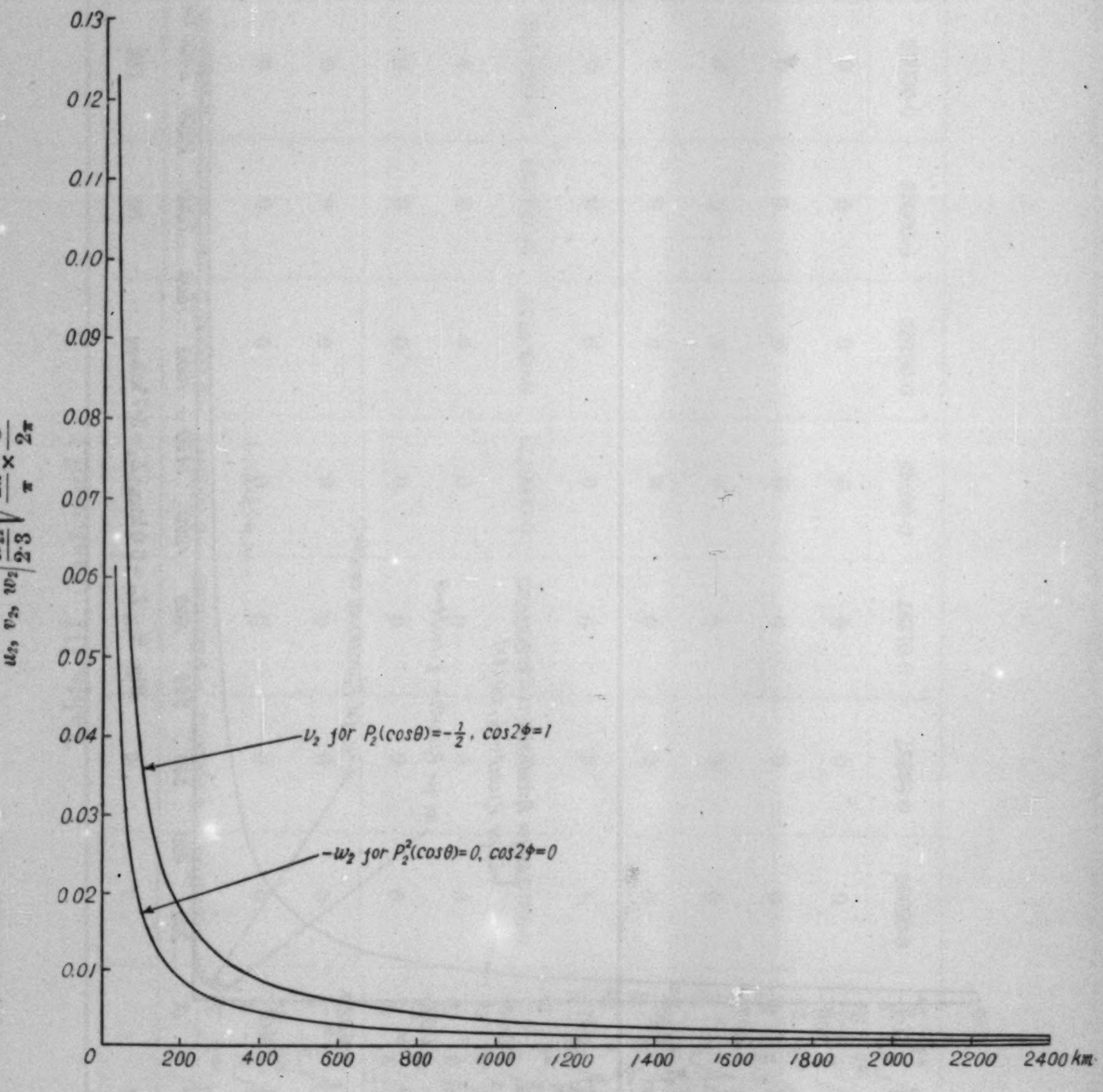

Fig. 3. $L_1 = 6{\cdot}0$ km, $L_2 = 3{\cdot}7$ km.

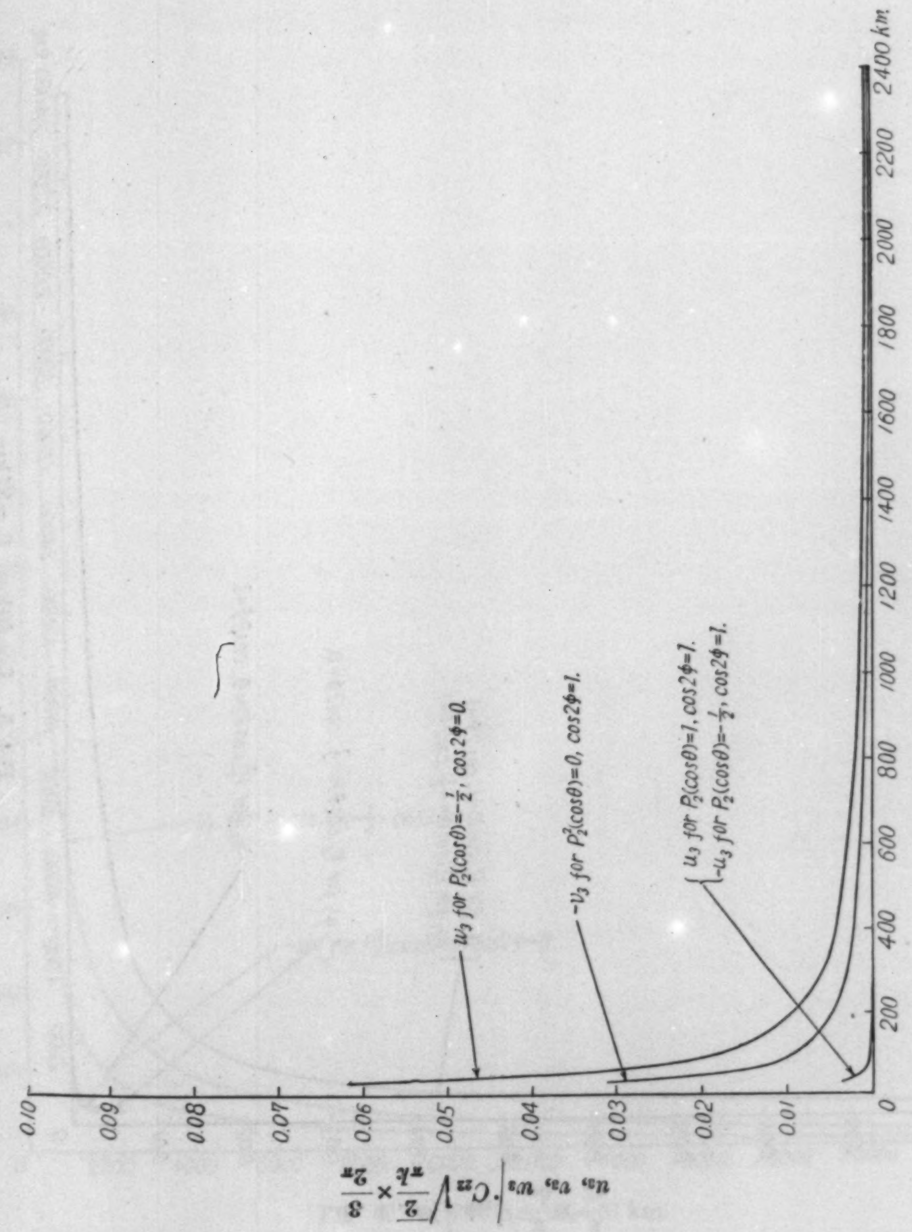

Fig. 4. $L_1=6{\cdot}0$ km, $L_2=3{\cdot}7$ km.

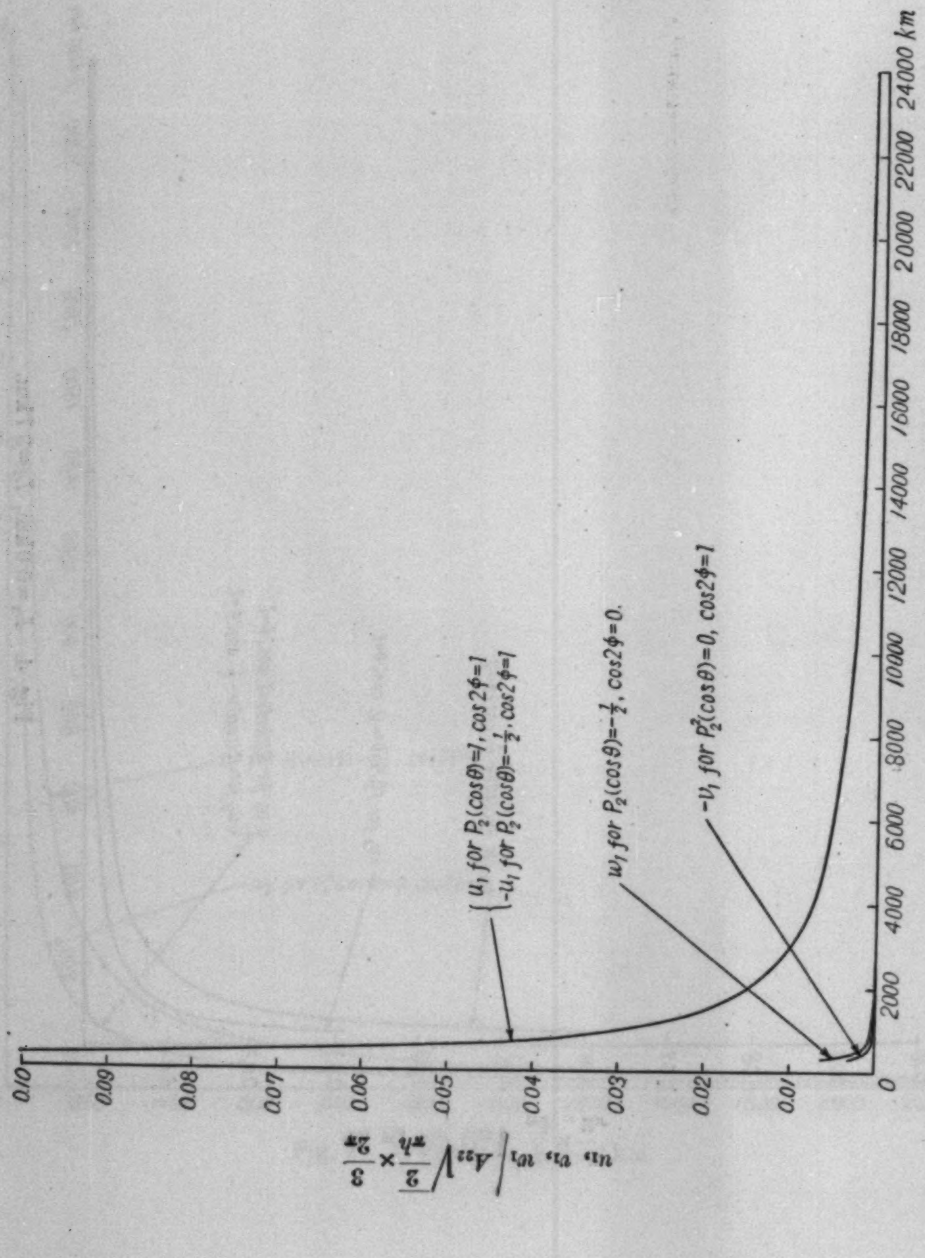

Fig. 5. $L_1=60$ km, $L_2=37$ km.

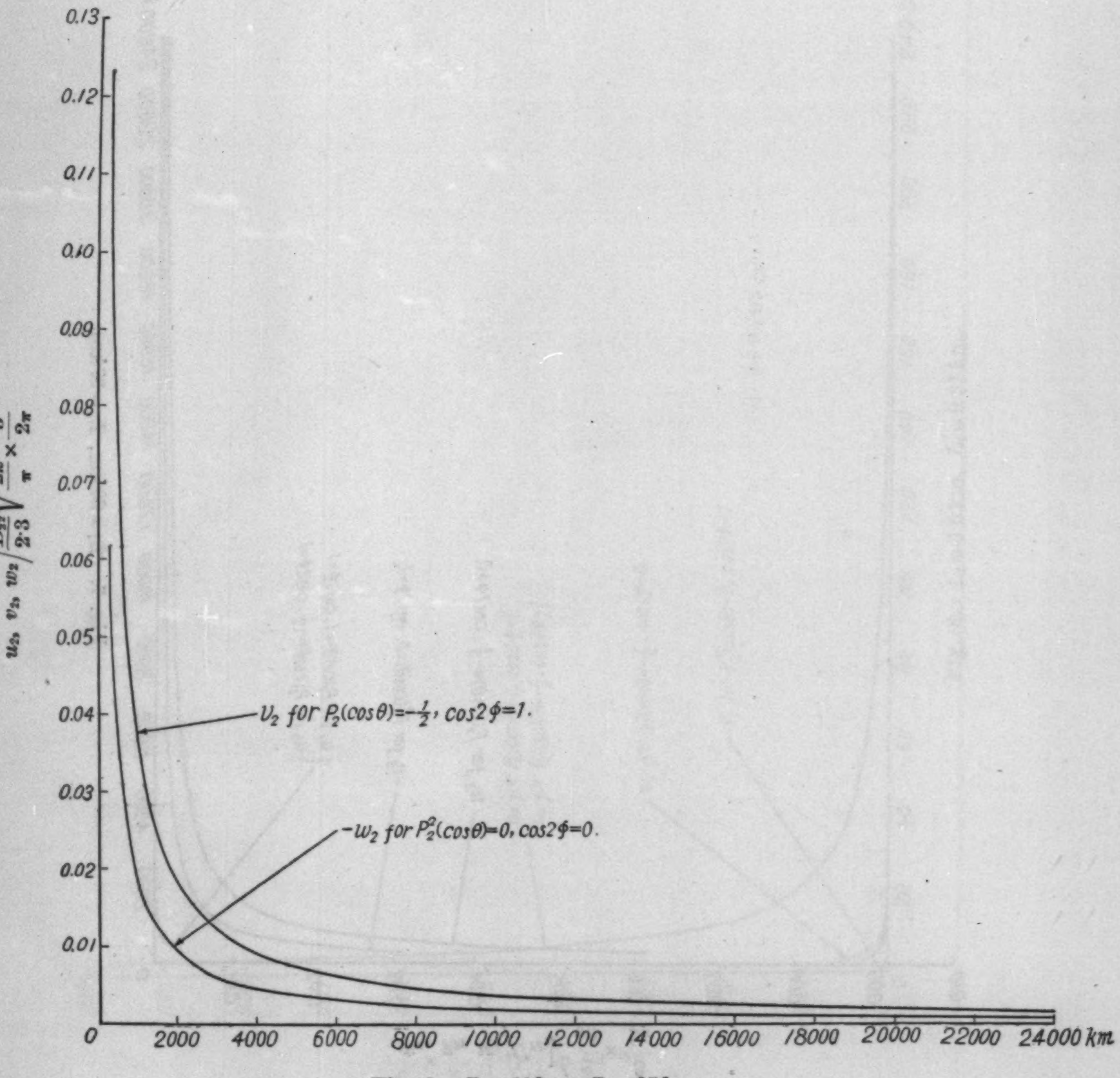

Fig. 6. $L_1=60$ km, $L_2=37$ km.

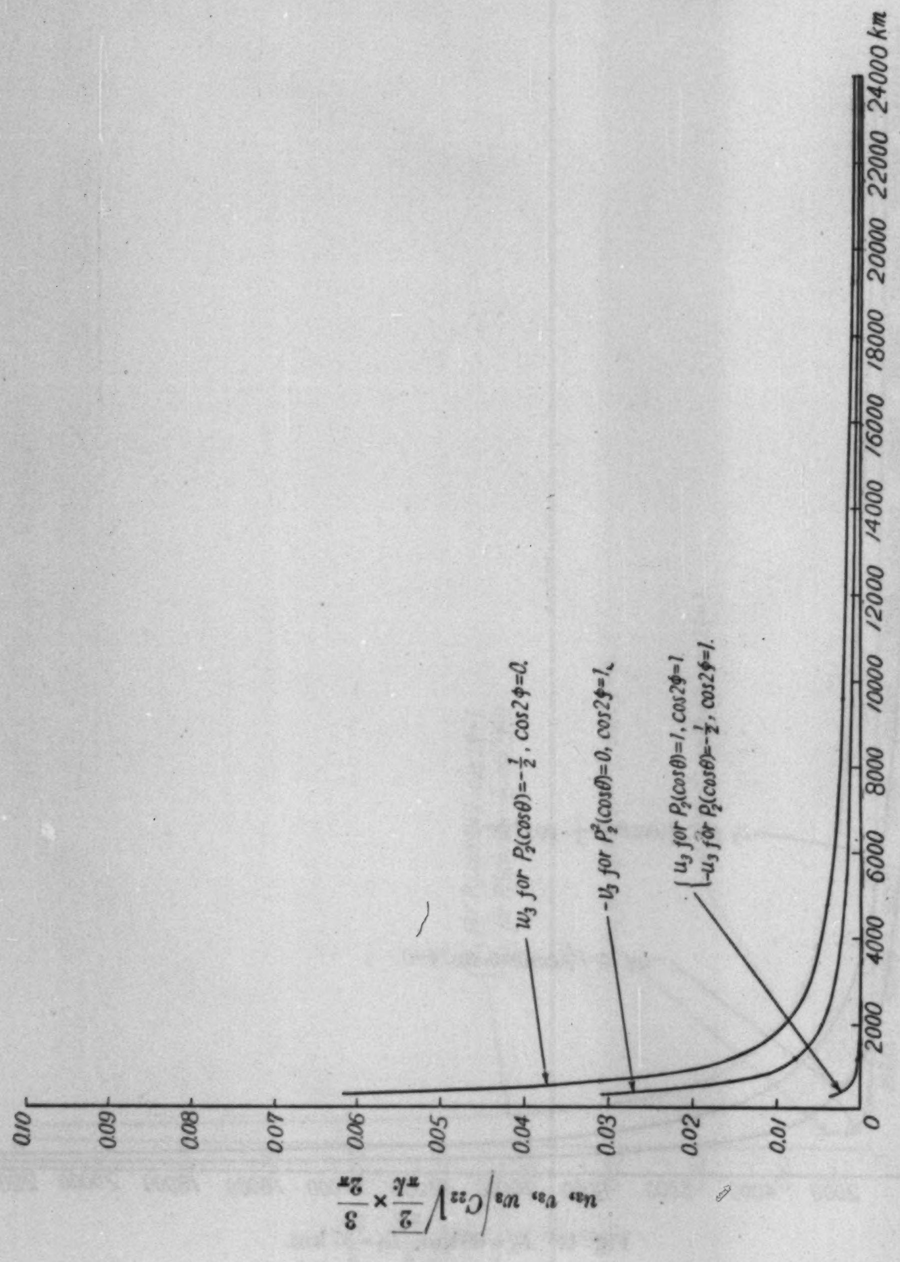

Fig. 7. $L_1=60$ km, $L_2=37$ km.

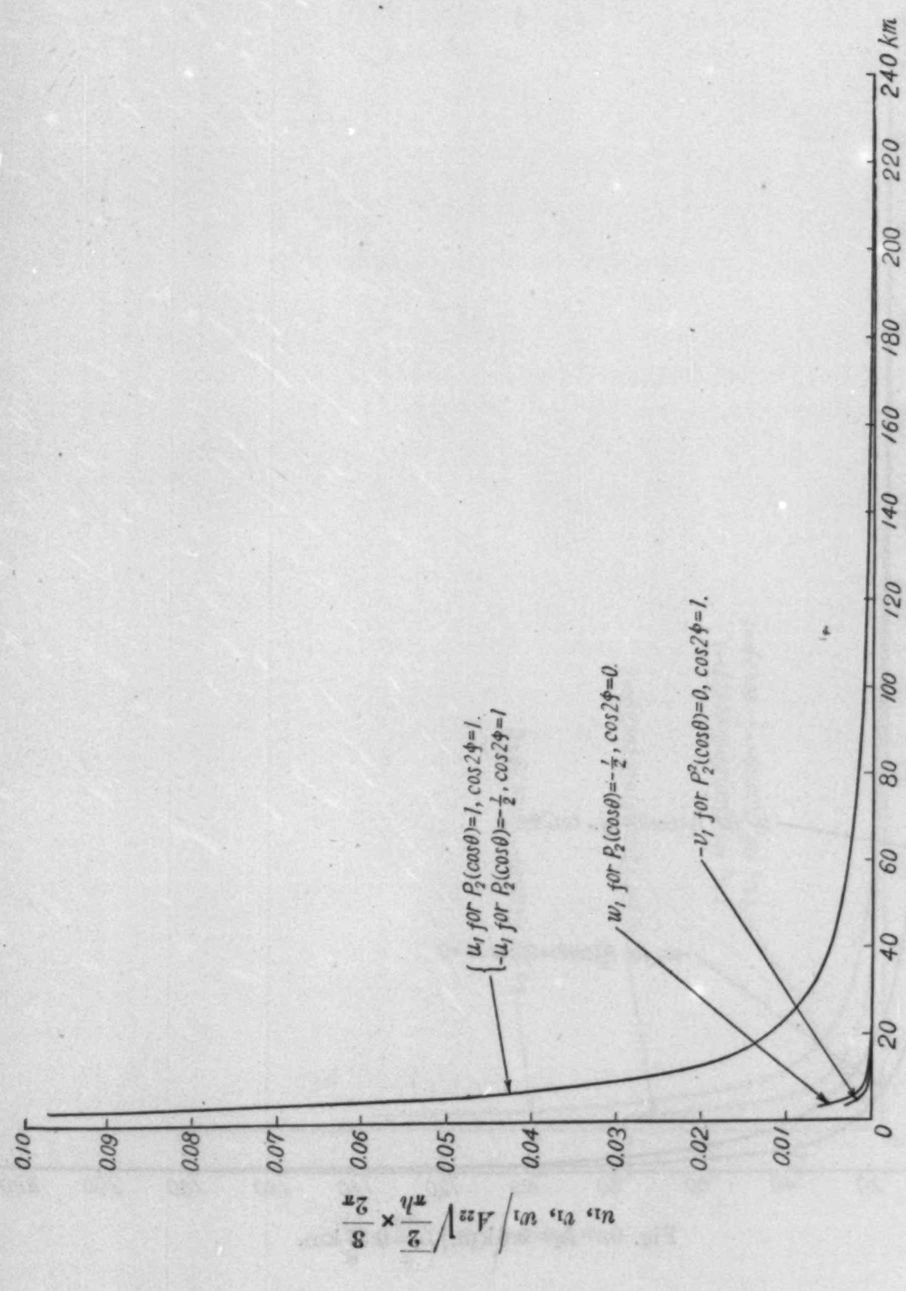

Fig. 8. $L_1 = 0{\cdot}6$ km, $L_2 = 0{\cdot}37$ km.

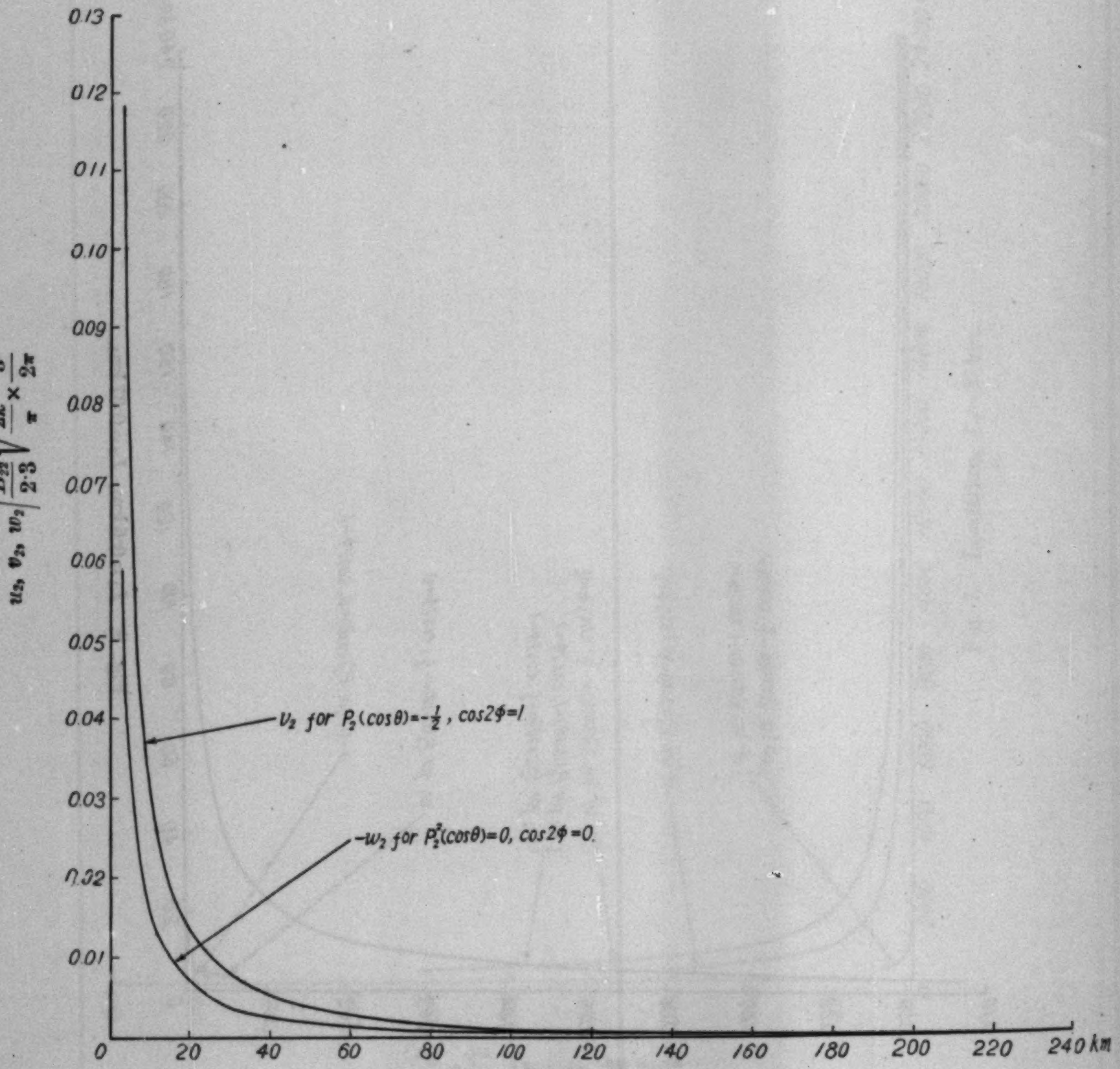

Fig. 9. $L_1=0{\cdot}6$ km, $L_2=0{\cdot}37$ km.

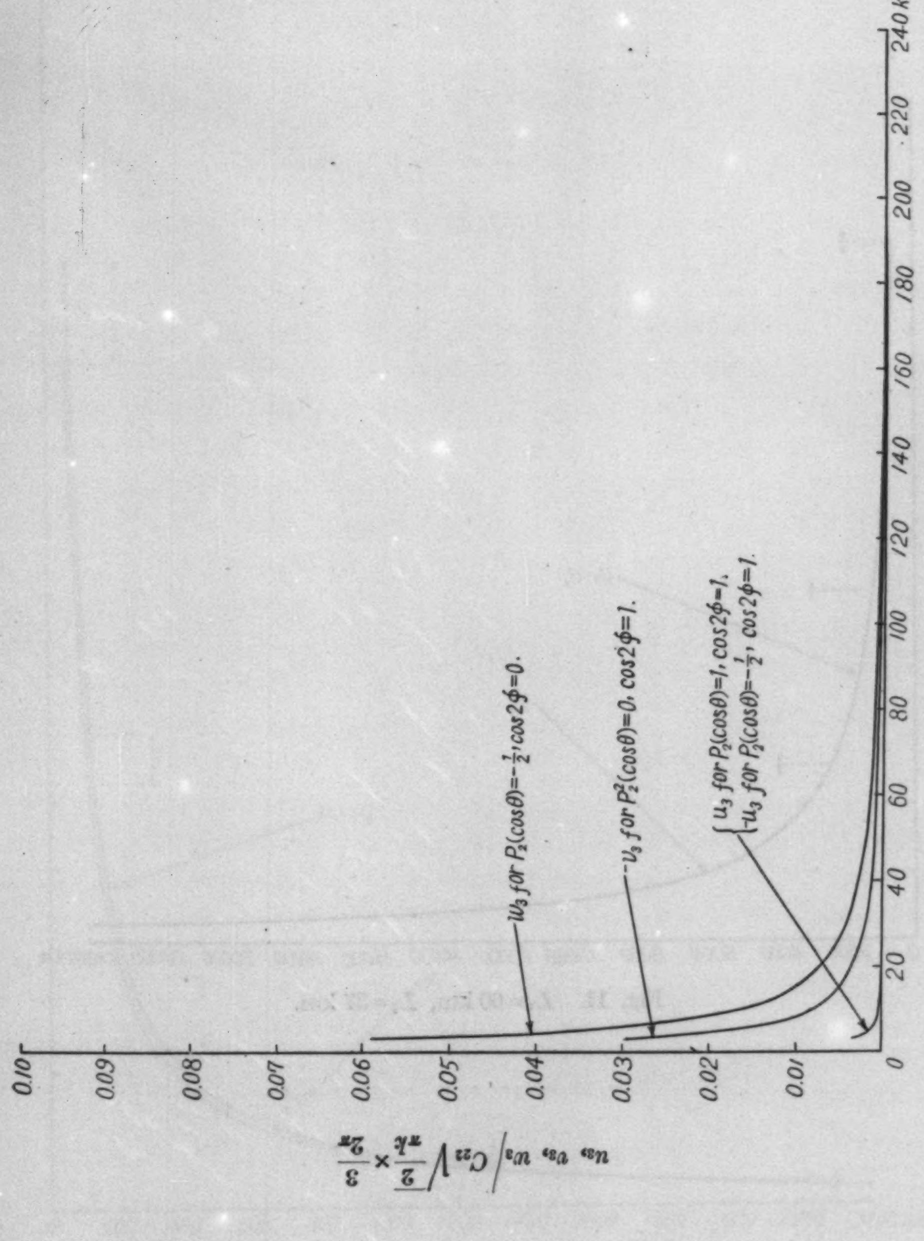

Fig. 10. $L_1 = 0{\cdot}6$ km, $L_2 = 0{\cdot}37$ km.

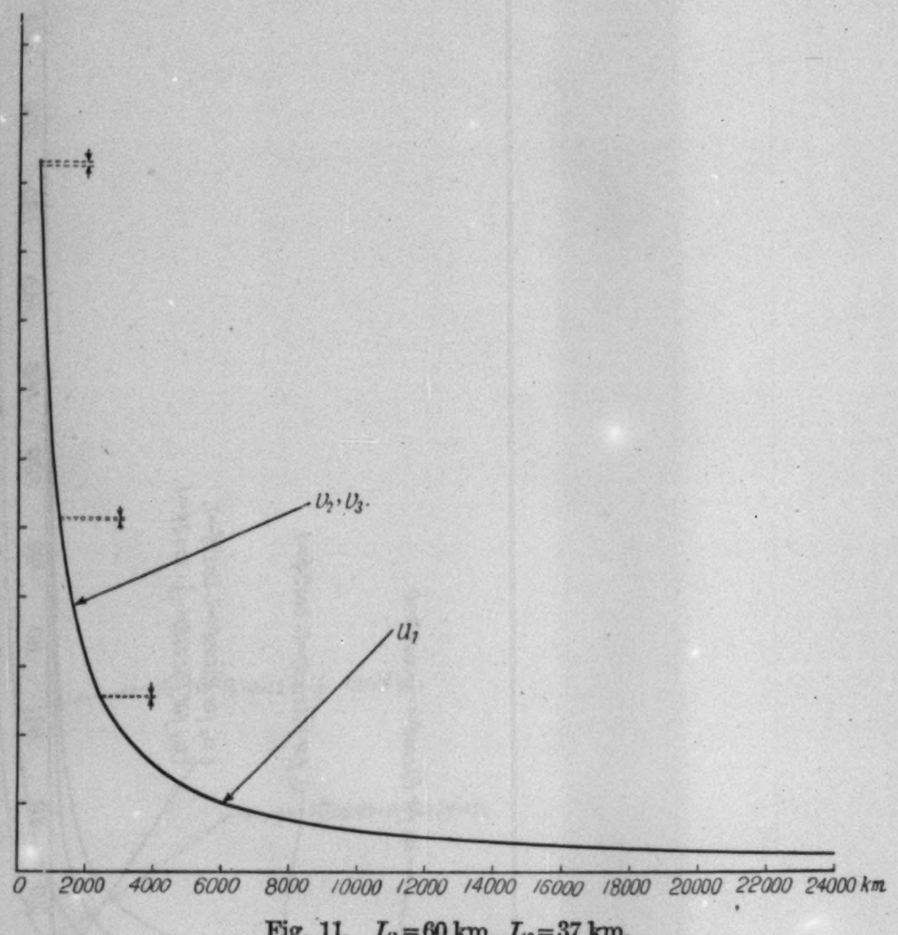

Fig. 11. $L_1=60$ km, $L_2=37$ km.

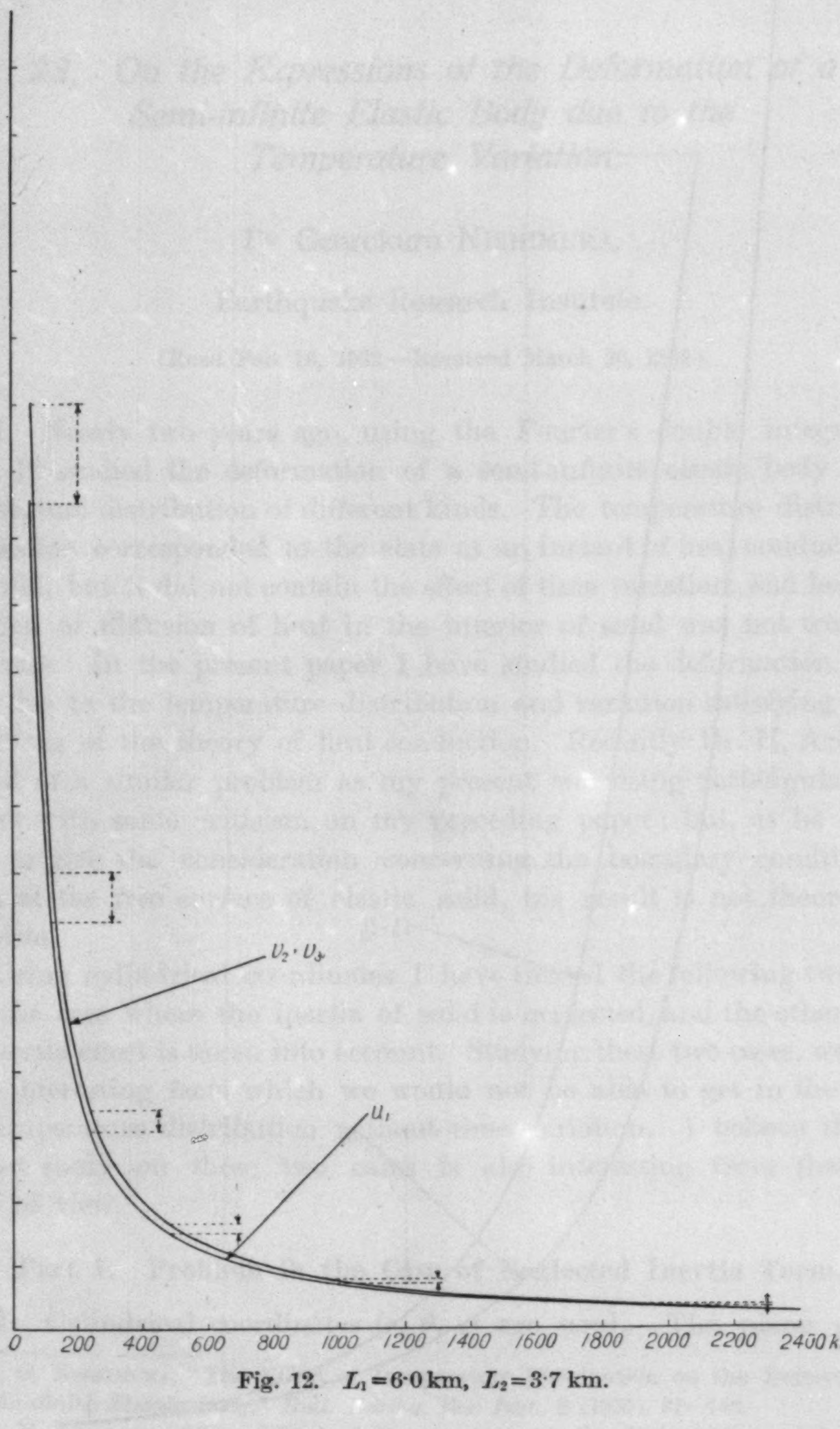

Fig. 12. $L_1=6{\cdot}0$ km, $L_2=3{\cdot}7$ km.

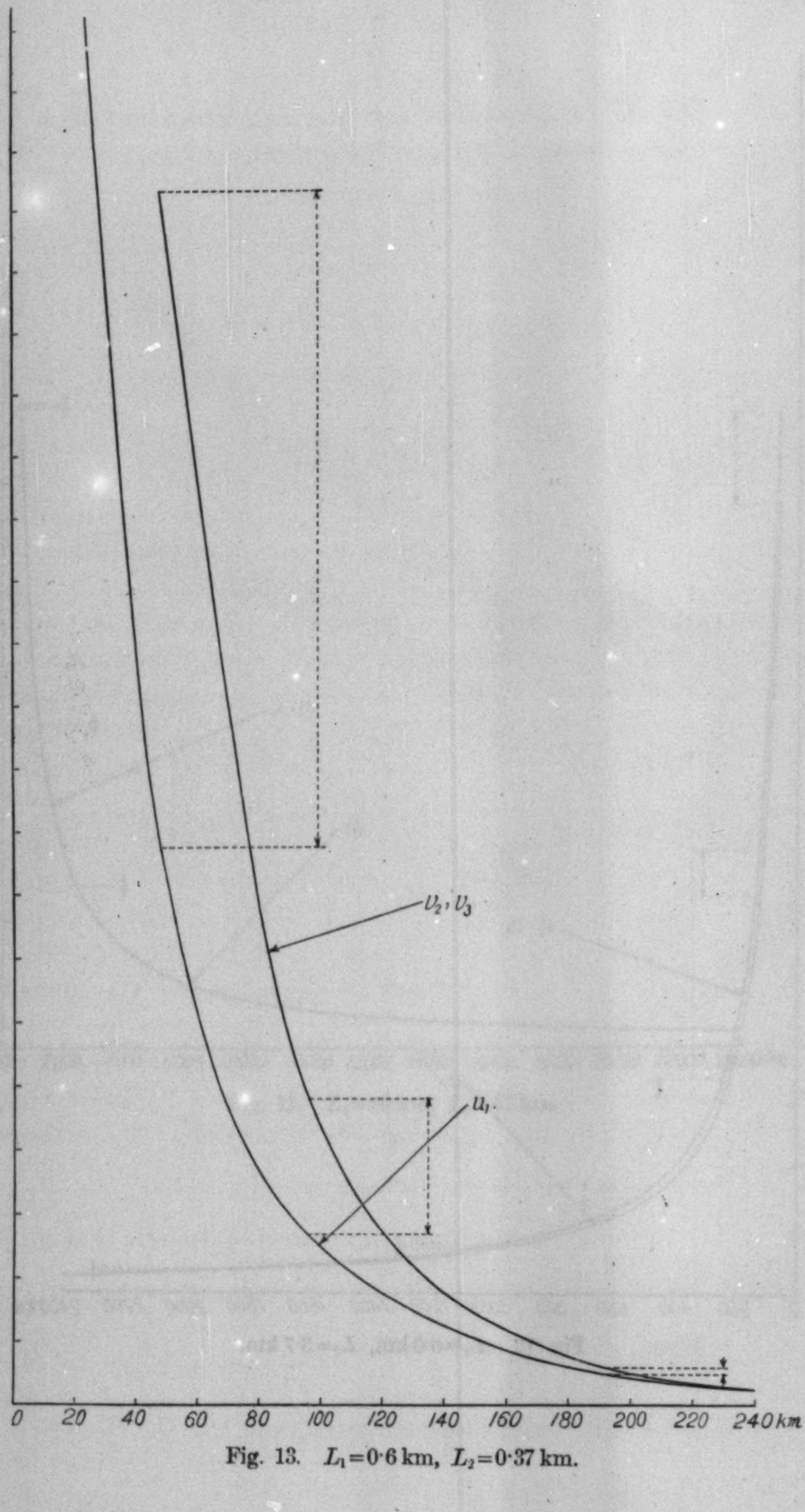

Fig. 13. $L_1=0{\cdot}6$ km, $L_2=0{\cdot}37$ km.

23. *On the Expressions of the Deformation of a Semi-infinite Elastic Body due to the Temperature Variation.*

By Genrokuro NISHIMURA,

Earthquake Research Institute.

(Read Feb. 16, 1932.—Received March 20, 1932.)

1. Nearly two years ago, using the Fourier's double integral formula I[1] studied the deformation of a semi-infinite elastic body due to temperature distribution of different kinds. The temperature distribution in question corresponded to the state at an instant of heat conduction in the solid, but it did not contain the effect of time variation, and hence the problem of diffusion of heat in the interior of solid was not treated in that case. In the present paper I have studied the deformation of the solid due to the temperature distribution and variation satisfying all the conditions of the theory of heat conduction. Recently Dr. H. Arakawa[2] treated of a similar problem as my present one using rectangular coordinates with some critisism on my preceding paper; but, as he did not seem to give the consideration concerning the boundary conditions of stress at the free surface of elastic solid, his result is not theoretically complete.

Using cylindrical coordinates I have treated the following two cases, *i. e.* the case where the inertia of solid is neglected, and the other where the inertia effect is taken into account. Studying these two cases, we found some interesting facts which we would not be able to get in the case of the temperature distribution without time variation. I believe that the present study on these two cases is also interesting from theoretical point of view.

Part I. Problem in the Case of Neglected Inertia Term.

2. Cylindrical coordinates (r, θ, z) are used. The plane $z=0$ is

1) G. NISHIMURA, "The Effect of Temperature Distribution on the Deformation of a Semi-infinite Elastic Body," *Bull. Earthq. Res. Inst.*, 8 (1930), 91—142.

2) H. ARAKAWA, "The Effect of Temperature on the Deformation of Infinite or Semi-infinite Elastic Body," *Geophys. Mag.*, Tôkyô, 64 (1931).

the surface of elastic solid, and r is the distance from the origin o, θ the azimuthal angle around z-axis. The axis of z is taken vertically downwards. (Fig. 1.)

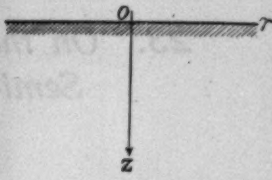

Fig. 1.

The equations of motion of elastic body when temperature variation is taken into consideration, and the inertia force is neglected, are expressed by the following three forms:

$$\left.\begin{aligned}
&(\lambda+2\mu)\frac{\partial \Delta}{\partial r}-\frac{2\mu}{r}\frac{\partial \varpi_z}{\partial \theta}+2\mu\frac{\partial \varpi_\theta}{\partial z}=\alpha\frac{\partial T}{\partial r},\\
&(\lambda+2\mu)\frac{1}{r}\frac{\partial \Delta}{\partial \theta}-2\mu\frac{\partial \varpi_r}{\partial z}+2\mu\frac{\partial \varpi_z}{\partial r}=\alpha\frac{1}{r}\frac{\partial T}{\partial \theta},\\
&(\lambda+2\mu)\frac{\partial \Delta}{\partial z}-\frac{2\mu}{r}\frac{\partial}{\partial r}(r\varpi_\theta)+\frac{2\mu}{r}\frac{\partial \varpi_r}{\partial \theta}=\alpha\frac{\partial T}{\partial z}
\end{aligned}\right\}\quad\ldots\ldots\ldots(1)$$

in which λ, μ are Lamé's elastic constants of solid, T is the temperature variation of the same solid, and

$$\alpha=\left(\lambda+\frac{2}{3}\mu\right)c,\quad\ldots\ldots\ldots\ldots\ldots\ldots(2)^{3)}$$

where c is the cubical expansion coefficient of solid.

The dilatation Δ, and the components of rotation $2\varpi_r$, $2\varpi_\theta$, $2\varpi_z$ are connected with the displacement in the following forms:

$$\left.\begin{aligned}
&2\varpi_r=\frac{1}{r}\frac{\partial w}{\partial \theta}-\frac{\partial v}{\partial z},\\
&2\varpi_\theta=\frac{\partial u}{\partial z}-\frac{\partial w}{\partial v},\\
&2\varpi_z=\frac{1}{r}\frac{\partial}{\partial r}(rv)-\frac{1}{r}\frac{\partial u}{\partial \theta},
\end{aligned}\right\}\quad\ldots\ldots\ldots\ldots(3)$$

where u, v, w are the radial, azimuthal, and axial components of displacement of solid.

For the purpose of finding u, v, w from the equations (1) and (3), we must first find the suitable form of T which satisfies the equation of conduction of heat in elastic solid such that

3) In two-dimensional problems, α should be taken as $\frac{2}{3}(\lambda+\mu)c$. In the second part of my preceding paper, *loc. cit.*, pp. 95—115, the meaning of notation α must be taken to be $\frac{2}{3}(\lambda+\mu)c$. My thanks are due to Dr. H. Arakawa for his kind notice, in his paper, *loc. cit.*, on my inattention on this point in my preceding paper.

$$\frac{\partial T}{\partial t}=\kappa\left(\frac{\partial^2 T}{\partial r^2}+\frac{1}{r}\frac{\partial T}{\partial r}+\frac{1}{r^2}\frac{\partial^2 T}{\partial \theta^2}+\frac{\partial^2 T}{\partial z^2}\right), \quad\dots\dots\dots(4)$$

where t is time and κ the diffusivity of solid such that

$$\kappa=\frac{K}{\gamma\rho}. \quad\dots\dots\dots(5)$$

K is the thermal conductivity, γ the specific heat and ρ the density of solid.

There are many types of elementary solutions of equation (4), and we take the following form of T for our purpose:

$$T=e^{-\kappa(k_s^2+m^2)t}C_n(k_s r)\begin{matrix}\sin\\ \cos\end{matrix}\Big\} mz\begin{matrix}\sin\\ \cos\end{matrix}\Big\} n\theta, \quad\dots\dots\dots(6)$$

where m, n and k_s are any constants to be determined by the initial and boundary conditions of temperature, and $C_n(x)$ is the Cylindrical function of any form of order n.

Now we know the following identical relation between ϖ_r, ϖ_θ and ϖ_z:

$$\frac{1}{r}\frac{\partial(r\varpi_r)}{\partial r}+\frac{1}{r}\frac{\partial\varpi_\theta}{\partial\theta}+\frac{\partial\varpi_z}{\partial z}=0. \quad\dots\dots\dots(7)$$

Using this relation and the equations (1), we obtain the following differential equations:

$$\frac{\partial^2}{\partial r^2}[(\lambda+2\mu)\Delta-\alpha T]+\frac{1}{r}\frac{\partial}{\partial r}[(\lambda+2\mu)\Delta-\alpha T]$$
$$+\frac{1}{r^2}\frac{\partial^2}{\partial\theta^2}[(\lambda+2\mu)\Delta-\alpha T]+\frac{\partial^2}{\partial z^2}[(\lambda+2\mu)\Delta-\alpha T]=0, \quad\dots(8)$$

$$\frac{\partial^2\varpi_z}{\partial r^2}+\frac{1}{r}\frac{\partial\varpi_z}{\partial r}+\frac{1}{r^2}\frac{\partial^2\varpi_z}{\partial\theta^2}+\frac{\partial^2\varpi_z}{\partial z^2}=0. \quad\dots\dots\dots(9)$$

Substituting the expression (6) for T in the equation (8), we obtain the following differential equation:

$$\frac{\partial^2\Delta}{\partial r^2}+\frac{1}{r}\frac{\partial\Delta}{\partial r}+\frac{1}{r^2}\frac{\partial^2\Delta}{\partial\theta^2}+\frac{\partial^2\Delta}{\partial z^2}=-\frac{\alpha(k_s^2+m^2)}{(\lambda+2\mu)}e^{-\kappa(k_s^2+m^2)t}C_n(k_s r)\begin{matrix}\sin\\ \cos\end{matrix}\Big\} mz\begin{matrix}\sin\\ \cos\end{matrix}\Big\} n\theta.$$
$$\dots\dots\dots(10)$$

The particular solution of the equation (10) is written in the form:

$$\Delta_1=\frac{\alpha}{(\lambda+2\mu)}e^{-\kappa(k_s^2+m^2)t}C_n(k_s r)\begin{matrix}\sin\\ \cos\end{matrix}\Big\} mz\begin{matrix}\sin\\ \cos\end{matrix}\Big\} n\theta. \quad\dots\dots(11)$$

The dilatation expressed by (11) is that due to the elementary temperature distribution expressed by (6).

The complementary solution of equation (10), which is useful for the present study, is

$$\Delta_2 = A_m e^{-\kappa(k_s^2+m^2)t} e^{-k_s z} C_n(k_s r) \begin{matrix}\sin\\ \cos\end{matrix}\Big\} n\theta, \quad \dots\dots\dots(12)$$

where A_m is an arbitrary constant to be determined by the boundary conditions of elastic solid.

The solution of (9), which is suitable for our problem, is of the form of

$$2\varpi_z = B_m e^{-\kappa(k_s^2+m^2)t} e^{-k_s z} C_n(k_s r) \begin{matrix}-\cos\\ \sin\end{matrix}\Big\} n\theta, \quad \dots\dots(13)$$

where B_m is also an arbitrary constant to be determined by the elasticity conditions of solid.

Substituting the expressions (6), (11), (12), and (13) for T, Δ and ϖ_z in equations (1), we obtain the following solutions of $2\varpi_r$ and $2\varpi_\theta$:

$$2\varpi_r = \left[\frac{n(\lambda+2\mu)}{k_s\mu} A_m \frac{C_n(k_s r)}{r} - B_m \frac{1}{k_s}\frac{\partial C_n(k_s r)}{\partial r}\right] e^{-k_s z} e^{-\kappa(k_s^2+m^2)t} \begin{matrix}-\cos\\ \sin\end{matrix}\Big\} n\theta, \quad ..(14)$$

$$2\varpi_\theta = \left[\frac{(\lambda+2\mu)}{k_s\mu} A_m \frac{\partial C_n(k_s r)}{\partial r} - B_m \frac{n}{k_s}\frac{C_n(k_s r)}{r}\right] e^{-k_s z} e^{-\kappa(k_s^2+m^2)t} \begin{matrix}\sin\\ \cos\end{matrix}\Big\} n\theta. \quad ...(15)$$

Now we can find the following differential equations concerning ru, rv, w, Δ, $2\varpi_r$, $2\varpi_\theta$ and $2\varpi_z$ by means of the relations of (3):

$$\frac{\partial^2 w}{\partial r^2} + \frac{1}{r}\frac{\partial w}{\partial r} + \frac{1}{r^2}\frac{\partial^2 w}{\partial \theta^2} + \frac{\partial^2 w}{\partial z^2} = \frac{\partial \Delta}{\partial z} + \frac{2}{r}\frac{\partial \varpi_r}{\partial \theta} - \frac{2}{r}\frac{\partial}{\partial r}(r\varpi_\theta), \quad ....(16)$$

$$\frac{\partial^2(rv)}{\partial r^2} + \frac{1}{r}\frac{\partial(rv)}{\partial r} + \frac{1}{r^2}\frac{\partial^2(rv)}{\partial \theta^2} + \frac{\partial^2(rv)}{\partial z^2} = \frac{\partial \Delta}{\partial \theta} - 2r\frac{\partial \varpi_r}{\partial z} + \frac{2}{r}\frac{\partial}{\partial r}(r^2\varpi_z), \quad (17)$$

$$\frac{\partial^2(ru)}{\partial r^2} - \frac{1}{r}\frac{\partial(ru)}{\partial r} + \frac{1}{r^2}\frac{\partial^2(ru)}{\partial \theta^2} + \frac{\partial^2(ru)}{\partial z^2} - \frac{2}{r^2}\frac{\partial(rv)}{\partial \theta}$$
$$= r\frac{\partial \Delta}{\partial r} + 2r\frac{\partial \varpi_\theta}{\partial z} - 2\frac{\partial \varpi_z}{\partial \theta}. \quad ......(18)$$

Substituting (11), (12), (13), (14) and (15) for Δ, $2\varpi_r$, $2\varpi_\theta$ and $2\varpi_z$ in the two differential equations (16), (17), we obtain the particular solutions w, rv in the following forms:

$$w = -\frac{m\alpha e^{-\kappa(k_s^2+m^2)t}}{(\lambda+2\mu)(k_s^2+m^2)} C_n(k_s r) \begin{matrix}\cos\\ -\sin\end{matrix}\Big\} mz \begin{matrix}\sin\\ \cos\end{matrix}\Big\} n\theta$$
$$-\frac{A_m}{2k_s\mu}\left[(\lambda+3\mu)+(\lambda+\mu)k_s z\right] e^{-k_s z} e^{-\kappa(k_s^2+m^2)t} C_n(k_s r) \begin{matrix}\sin\\ \cos\end{matrix}\Big\} n\theta, \quad ..(19)$$

and

$$rv = \frac{n\alpha e^{-\kappa(k_s^2+m^2)t}}{(\lambda+2\mu)(k_s^2+m^2)} C_n(k_s r) \begin{matrix}\sin\\ \cos\end{matrix}\Big\} mz \begin{matrix}-\cos\\ \sin\end{matrix}\Big\} n\theta$$

$$-\frac{n(\lambda+\mu)}{2\mu k_s} A_m z e^{-k_s z} e^{-\kappa(k_s^2+m^2)t} \frac{1}{r} C_n(k_s r) \begin{matrix}-\cos\\ \sin\end{matrix}\Big\} n\theta$$

$$-B_m \frac{e^{-k_s z}}{k_s^2} e^{-\kappa(k_s^2+m^2)t} \frac{\partial C_n(k_s r)}{\partial r} \begin{matrix}-\cos\\ \sin\end{matrix}\Big\} n\theta. \quad \ldots\ldots\ldots\ldots(20)$$

The complementary solution of (16), (17) are written easily in the following forms:

$$w = -k_s E_m e^{-k_s z} e^{-\kappa(k_s^2+m^2)t} C_n(k_s r) \begin{matrix}\sin\\ \cos\end{matrix}\Big\} n\theta, \quad \ldots\ldots(21)$$

$$rv = -nE_m e^{-k_s z} e^{-\kappa(k_s^2+m^2)t} C_n(k_s r) \begin{matrix}-\cos\\ \sin\end{matrix}\Big\} n\theta, \quad \ldots\ldots(22)$$

where E_m is also an arbitrary constant to be determined by the boundary conditions.

Now substituting (11), (12), (13), (15), (20) and (22) for the expressions of Δ, $2\varpi_\theta$, $2\varpi_z$ and rv in the equation (18), we can find the particular solution of ru, which are favourable to the present study, in the following forms:

$$ru = -\frac{\alpha e^{-\kappa(k_s^2+m^2)t}}{(\lambda+2\mu)(k_s^2+m^2)} r\frac{\partial C_n(k_s r)}{\partial r} \begin{matrix}\sin\\ \cos\end{matrix}\Big\} mz \begin{matrix}\sin\\ \cos\end{matrix}\Big\} n\theta$$

$$+\frac{(\lambda+\mu)}{2k_s\mu} A_m z e^{-k_s z} e^{-\kappa(k_s^2+m^2)t} r\frac{\partial C_n(k_s r)}{\partial r} \begin{matrix}\sin\\ \cos\end{matrix}\Big\} n\theta$$

$$+\frac{n}{k_s} B_m e^{-k_s z} e^{-\kappa(k_s^2+m^2)t} C_n(k_s r) \begin{matrix}\sin\\ \cos\end{matrix}\Big\} n\theta$$

$$+E_m e^{-k_s z} e^{-\kappa(k_s^2+m^2)t} r\frac{\partial C_n(k_s r)}{\partial r} \begin{matrix}\sin\\ \cos\end{matrix}\Big\} n\theta. \quad \ldots\ldots\ldots\ldots(23)$$

There is also the complementary solution ru of the equation (18), but it does not satisfy the equation of motion (1).

As the components of stress $\widehat{rr}$, $\widehat{\theta\theta}$, $\widehat{zz}$, $\widehat{r\theta}$, $\widehat{rz}$ and $\widehat{\theta z}$ are expressed by

$$\left.\begin{aligned} &\widehat{rr} = \lambda\Delta + 2\mu\frac{\partial u}{\partial r} - \alpha T, \quad \widehat{\theta\theta} = \lambda\Delta + 2\mu\left(\frac{u}{r} + \frac{1}{r}\frac{\partial v}{\partial\theta}\right) - \alpha T, \\ &\widehat{zz} = \lambda\Delta + 2\mu\frac{\partial w}{\partial z} - \alpha T, \quad \widehat{r\theta} = \mu\left(\frac{\partial v}{\partial r} - \frac{v}{r} + \frac{1}{r}\frac{\partial u}{\partial\theta}\right), \\ &\widehat{rz} = \mu\left(\frac{\partial u}{\partial z} + \frac{\partial w}{\partial z}\right), \quad \widehat{\theta z} = \mu\left(\frac{1}{r}\frac{\partial w}{\partial\theta} + \frac{\partial v}{\partial z}\right), \end{aligned}\right\} \quad (24)$$

we can find the components of stress which are necessary for the present study, by using (6), (11), (12), (19), (20), (21), (22) and (23).

Now the surface ($z=0$) of elastic solid is a free surface, so that we have the following conditions on this surface:

$$z=0\,;\quad \widehat{zz}=0,\ \widehat{rz}=0,\ \widehat{\theta z}=0. \qquad \ldots\ldots\ldots\ldots(25)$$

From these relations we can find the following forms of constants A_m, B_m and E_m:

$$\left.\begin{aligned} A_m&=\frac{2\mu\alpha m k_s}{(\lambda+\mu)(\lambda+2\mu)(k_s^2+m^2)},\quad B_m=0,\\ E_m&=-\frac{m\alpha}{(\lambda+\mu)(k_s^2+m^2)k_s}\,. \end{aligned}\right\} \qquad \ldots\ldots(26)^{4)}$$

Substituting these relations (26) for A_m, B_m and E_m in the components of displacement expressed by (19), (20), (21), (22) and (23), we obtain the components of displacement u, v, w in the following forms:

$$\begin{aligned} u=&-\frac{\alpha e^{-\kappa(k_s^2+m^2)t}}{(\lambda+2\mu)(k_s^2+m^2)}\frac{\partial C_n(k_s r)}{\partial r}\sin mz\left.\begin{matrix}\sin\\ \cos\end{matrix}\right\}n\theta\\ &+\frac{m\alpha e^{-\kappa(k_s^2+m^2)t}}{(\lambda+2\mu)(k_s^2+m^2)}ze^{-k_s z}\frac{\partial C_n(kr)}{\partial r}\left.\begin{matrix}\sin\\ \cos\end{matrix}\right\}n\theta\\ &-\frac{m\alpha e^{-\kappa(k_s^2+m^2)t}}{(\lambda+\mu)(k_s^2+m^2)k_s}e^{-k_s z}\frac{\partial C_n(k_s r)}{\partial r}\left.\begin{matrix}\sin\\ \cos\end{matrix}\right\}n\theta, \end{aligned} \qquad \ldots\ldots\ldots(27)$$

$$\begin{aligned} v=&\frac{n\alpha e^{-\kappa(k_s^2+m^2)t}}{(\lambda+2\mu)(k_s^2+m^2)}\frac{C_n(k_s r)}{r}\sin mz\left.\begin{matrix}-\cos\\ \sin\end{matrix}\right\}n\theta\\ &-\frac{nm\alpha e^{-\kappa(k_s^2+m^2)t}}{(\lambda+2\mu)(k_s^2+m^2)}ze^{-k_s z}\frac{C_n(k_s r)}{r}\left.\begin{matrix}-\cos\\ \sin\end{matrix}\right\}n\theta\\ &+\frac{nm\alpha e^{-\kappa(k_s^2+m^2)t}}{(\lambda+\mu)(k_s^2+m^2)}e^{-k_s z}\frac{C_n(k_s r)}{r}\left.\begin{matrix}-\cos\\ \sin\end{matrix}\right\}n\theta, \end{aligned} \qquad \ldots\ldots\ldots(28)$$

$$\begin{aligned} w=&-\frac{m\alpha e^{-\kappa(k_s^2+m^2)t}}{(\lambda+2\mu)(k_s^2+m^2)}C_n(k_s r)\cos mz\left.\begin{matrix}\sin\\ \cos\end{matrix}\right\}n\theta\\ &-\frac{mk_s\alpha e^{-\kappa(k_s^2+m^2)t}}{(\lambda+2\mu)(k_s^2+m^2)}ze^{-k_s z}C_n(k_s r)\left.\begin{matrix}\sin\\ \cos\end{matrix}\right\}n\theta\\ &-\frac{m\mu\alpha e^{-\kappa(k_s^2+m^2)t}}{(\lambda+\mu)(\lambda+2\mu)(k_s^2+m^2)}e^{-k_s z}C_n(k_s r)\left.\begin{matrix}\sin\\ \cos\end{matrix}\right\}n\theta. \end{aligned} \qquad \ldots(29)$$

4) To obtain these results, we used the upper part of $\left.\begin{matrix}\sin\\ \cos\end{matrix}\right\}mz$ of T expressed by (6).

The displacement thus obtained is of elementary type which corresponds to the temperature variation expressed by (6) and satisfies the boundary conditions at the free surface $z=0$ expressed by (25).

3. When the temperature varies as any function of time t, coordinates r and θ on the free surface $(z=0)$ of elastic solid and the initial temperature is zero at every point in the solid, the problem is more complicated; and I shall show the method of treatment as follows.

Now the conditions with regards to temperature T are as follows (in mathematical notations):

$$t=0; \quad T=0, \quad \ldots\ldots\ldots\ldots\ldots\ldots (30)_1$$

$$z=0; \quad T=f(r, \theta, t), \quad \ldots\ldots\ldots\ldots (30)_2$$

$$z=\infty; \quad T=0, \quad \ldots\ldots\ldots\ldots\ldots\ldots (30)_3$$

$$r=\infty; \quad T=0. \quad \ldots\ldots\ldots\ldots\ldots\ldots (30)_4$$

Substituting the Bessel function of first kind $J_n(k_s r)$ for $C_n(k_s r)$, and taking $\sin mz$ and $\cos n\theta$ in the elementary equation (6), we obtain the following expression of T which satisfies the equation of heat conduction (4) and the initial and boundary conditions expressed by $(30)_1$, $(30)_2$, $(30)_3$ and $(30)_4$:

$$T=\frac{\kappa}{\pi^2}\sum_{n=0}^{\infty}\delta_n\int_0^{\infty}\int_0^{\infty}\int_0^{\infty}\int_0^{2\pi}\int_0^{t} e^{-\kappa(\sigma^2+\xi^2)(t-\eta)}f(\zeta, \varphi, \eta)\cos n(\theta-\varphi)J_n(\sigma r)$$
$$J_n(\sigma\zeta)\sin\xi z\sigma\xi\zeta\, d\eta\, d\varphi\, d\zeta\, d\sigma\, d\xi, \ldots\ldots (31)$$

where $\delta_0=1$, $\delta_1=\delta_2=\delta_3=\ldots\ldots=\delta_n=2$.

Now we have to obtain the displacement corresponding to the temperature variation expressed by (31) and satisfying the boundary conditions (25) in Section 2. Using the elementary solutions expressed by (27), (28) and (29), we obtain the final solutions, which satisfy all conditions, in the following forms:

$$u=-\frac{\kappa\alpha}{\pi^2(\lambda+2\mu)}\sum_{n=0}^{\infty}\delta_n\int_0^{\infty}\int_0^{\infty}\int_0^{\infty}\int_0^{t}\int_0^{2\pi} e^{-\kappa(\sigma^2+\xi^2)(t-\eta)}\frac{\left[\sin\xi z+\left(\xi z-\frac{\xi}{\sigma}\right)e^{-\sigma z}\right]}{(\sigma^2+\xi^2)}$$
$$\cos n(\theta-\varphi)f(\zeta, \varphi, \eta)\frac{\partial J_n(\sigma r)}{\partial r}J_n(\sigma\zeta)\sigma\xi\zeta\, d\eta\, d\varphi\, d\zeta\, d\sigma\, d\xi, \ldots (32)$$

$$v=\frac{\kappa\alpha}{\pi^2(\lambda+2\mu)}\sum_{n=0}^{\infty}\delta_n\int_0^{\infty}\int_0^{\infty}\int_0^{\infty}\int_0^{t}\int_0^{2\pi} e^{-\kappa(\sigma^2+\xi^2)(t-\eta)}$$
$$\frac{n\left[\sin\xi z-\xi z e^{-\sigma z}+\frac{(\lambda+2\mu)}{(\lambda+\mu)}\frac{\xi}{\sigma}e^{-\sigma z}\right]}{(\sigma^2+\xi^2)}$$

$$\sin n(\theta-\varphi)f(\zeta,\varphi,\eta)\frac{J_n(\sigma r)}{r}J_n(\sigma\zeta)\sigma\xi\zeta d\eta d\varphi d\zeta d\sigma d\xi, \quad \ldots.(33)$$

$$w=-\frac{\kappa\alpha}{\pi^2(\lambda+2\mu)}\sum_{n=3}^{\infty}\delta_n\int_0^\infty\int_0^\infty\int_0^\infty\int_0^{2\pi}\int_0^t e^{-\kappa(\sigma^2+\xi^2)(t-\eta)}\frac{\left[\cos\xi z+\frac{\mu}{\lambda+\mu}e^{-\sigma z}+\sigma z e^{-\sigma z}\right]}{(\sigma^2+\xi^2)}$$

$$\cos n(\theta-\varphi)f(\zeta,\varphi,\eta)J_n(\sigma r)J_n(\sigma\zeta)\sigma\xi^2\zeta d\eta d\varphi d\zeta d\sigma d\xi. \quad \ldots.(34)$$

We can easily formulate the components of thermal stress $\widehat{rr}$, $\widehat{\theta\theta}$, $\widehat{zz}$, $\widehat{r\theta}$, $\widehat{rz}$, $\widehat{\theta z}$ at any point in the solid due to the temperature variation expressed by (31), but in the present study we omit this procedure.

In this section, we have obtained the general expressions of displacement u, v, w due to temperature T in the semi-infinite elastic body satisfying the conditions expressed by (30).

4. When the distribution of temperature has no azimuthal variation, and is given by the form:

$$z=0\,; \quad T=\phi(r,t), \quad \ldots\ldots\ldots\ldots\ldots\ldots\ldots.(35)$$

we have the following form of temperature distribution in solid:

$$T=\frac{\kappa}{\pi}\int_0^\infty\int_0^\infty\int_0^\infty\int_0^t e^{-\kappa(\sigma^2+\xi^2)(t-\eta)}\phi(\zeta,\eta)J_0(\sigma r)J_0(\sigma\zeta)\sin\xi z\sigma\xi\zeta d\eta d\zeta d\sigma d\xi. \quad \ldots\ldots\ldots.(36)$$

The equation (36), of cource, satisfies the conditions $(30)_1$, $(30)_3$, $(30)_4$.

The components of displacement (u, w) corresponding to the temperature variation (36) are easily formulated as in the follow:

$$u=-\frac{\kappa\alpha}{\pi(\lambda+2\mu)}\int_0^\infty\int_0^\infty\int_0^\infty\int_0^t e^{-\kappa(\sigma^2+\xi^2)(t-\eta)}\phi(\zeta,\eta)\frac{\left[\sin\xi z+(z+1)e^{-\sigma z}\xi\right]}{(\sigma^2+\xi^2)}\frac{\partial J_0(\sigma r)}{\partial r}$$

$$J_0(\sigma\zeta)\sigma\xi\zeta d\zeta d\eta d\sigma d\xi, \quad \ldots.(37)$$

$$w=-\frac{\kappa\alpha}{\pi(\lambda+\mu)(\lambda+2\mu)}\int_0^\infty\int_0^\infty\int_0^\infty\int_0^t e^{-\kappa(\sigma^2+\xi^2)(t-\eta)}\phi(\zeta,\eta)$$

$$\frac{\left[(\lambda+\mu)\cos\xi z+\zeta e^{-\sigma z}+(\lambda+\mu)\sigma z e^{-\sigma z}\right]}{(\sigma^2+\xi^2)}$$

$$J_0(\sigma r)J_0(\sigma\zeta)\sigma\xi^2\zeta d\zeta d\eta d\sigma d\xi. \quad \ldots\ldots.(38)$$

The surface deformation due to the temperature variation may be studied by the following two components of displacement:

$$u_{z=0}=-\frac{\kappa\alpha}{\pi(\lambda+2\mu)}\int_0^\infty\int_0^\infty\int_0^\infty\int_0^t e^{-\kappa(\sigma^2+\xi^2)(t-\eta)}\phi(\zeta,\eta)\frac{J_0(\sigma\zeta)}{(\sigma^2+\xi^2)}\frac{\partial J_0(\sigma r)}{\partial r}$$

$$\xi^2\zeta d\zeta d\eta d\sigma d\xi, \quad \ldots\ldots.(39)$$

$$w_{z=0}=-\frac{\kappa\alpha}{\pi(\lambda+\mu)}\int_0^\infty\int_0^\infty\int_0^\infty\int_0^t e^{-\kappa(\sigma^2+\xi^2)(t-\eta)}\phi(\zeta,\eta)\frac{J_0(\sigma r)}{(\sigma^2+\xi^2)} J_0(\sigma\zeta)\sigma\xi^2\zeta d\eta d\zeta d\sigma d\xi \quad ..(40)$$

Part II. Problems When the Inertia Effect is Considered.

5. Using the same coordinates as that in Part I, the equations of motion of an elastic body of temperature variation T are expressed by the following forms:

$$\left.\begin{aligned}
\rho\frac{\partial^2 u}{\partial t^2}&=(\lambda+2\mu)\frac{\partial\Delta}{\partial r}-\frac{2\mu}{r}\frac{\partial\varpi_z}{\partial\theta}+2\mu\frac{\partial\varpi_\theta}{\partial z}-\alpha\frac{\partial T}{\partial r},\\
\rho\frac{\partial^2 v}{\partial t^2}&=(\lambda+2\mu)\frac{1}{r}\frac{\partial\Delta}{\partial\theta}-2\mu\frac{\partial\varpi_r}{\partial z}+2\mu\frac{\partial\varpi_z}{\partial r}-\alpha\frac{1}{r}\frac{\partial T}{\partial\theta},\\
\rho\frac{\partial^2 w}{\partial t^2}&=(\lambda+2\mu)\frac{\partial\Delta}{\partial z}-\frac{2\mu}{r}\frac{\partial}{\partial r}(r\varpi_\theta)+\frac{2\mu}{r}\frac{\partial\varpi_r}{\partial\theta}-\alpha\frac{\partial T}{\partial z}.
\end{aligned}\right\} \quad ..(41)$$

For solving the equations (41), we must first find the suitable form of the expression of temperature T. We take the following form of T as that in the preceding part:

$$T=e^{-\kappa(k_s^2+m^2)t}C_n(k_s r)\begin{matrix}\sin\\\cos\end{matrix}\Big\} mz \begin{matrix}\sin\\\cos\end{matrix}\Big\} n\theta. \quad ....(6')$$

Now, using the identical relations expressed by (7) and the relations of (3) in Part I, we find the following equations:[5)]

$$\rho\frac{\partial^2\Delta}{\partial t^2}=\frac{\partial^2}{\partial r^2}[(\lambda+2\mu)\Delta-\alpha T]+\frac{1}{r}\frac{\partial}{\partial r}[(\lambda+2\mu)\Delta-\alpha T] +\frac{1}{r^2}\frac{\partial^2}{\partial\theta^2}[(\lambda+2\mu)\Delta-\alpha T]+\frac{\partial^2}{\partial z^2}[(\lambda+2\mu)\Delta-\alpha T], \quad ....(42)$$

$$\rho\frac{\partial^2\varpi_z}{\partial t^2}=\mu\left[\frac{\partial^2\varpi_z}{\partial r^2}+\frac{1}{r}\frac{\partial\varpi_z}{\partial r}+\frac{1}{r^2}\frac{\partial^2\varpi_z}{\partial\theta^2}+\frac{\partial^2\varpi_z}{\partial z^2}\right], \quad ....(43)$$

$$\rho\frac{\partial^2\varpi_r}{\partial t^2}=\mu\left[\frac{\partial^2\varpi_r}{\partial r^2}+\frac{3}{r}\frac{\partial\varpi_r}{\partial r}+\frac{\varpi_r}{r^2}+\frac{1}{r^2}\frac{\partial^2\varpi_r}{\partial\theta^2}+\frac{\partial^2\varpi_r}{\partial z^2}+\frac{2}{r}\frac{\partial\varpi_z}{\partial z}\right], \quad ....(44)$$

$$\rho\frac{\partial^2\varpi_\theta}{\partial t^2}=\mu\left[\frac{\partial^2\varpi_\theta}{\partial r^2}+\frac{1}{r}\frac{\partial\varpi_\theta}{\partial r}-\frac{\varpi_\theta}{r^2}+\frac{1}{r^2}\frac{\partial^2\varpi_\theta}{\partial\theta^2}+\frac{\partial^2\varpi_\theta}{\partial z^2}+\frac{2}{r^2}\frac{\partial^2\varpi_r}{\partial\theta}\right] \quad ....(45)$$

Substituting (6′) for T in equation (42), we obtain the differential equation of the form:

5) The reductions of these equations when $T=0$ have been made by Prof. K. Sezawa. K. SEZAWA, *Bull. Earthq. Res. Inst.*, 6 (1929).

$$\rho\frac{\partial^2\Delta}{\partial t^2}-(\lambda+2\mu)\left[\frac{\partial^2\Delta}{\partial r^2}+\frac{1}{r}\frac{\partial\Delta}{\partial r}+\frac{1}{r^2}\frac{\partial^2\Delta}{\partial\theta^2}+\frac{\partial^2\Delta}{\partial z^2}\right]$$
$$=\alpha(k_s^2+m^2)e^{-\kappa(k_s^2+m^2)t}C_n(k_s r)\begin{matrix}\sin\\ \cos\end{matrix}\Big\} mz\begin{matrix}\sin\\ \cos\end{matrix}\Big\} n\theta. \quad ..(46)$$

We have the particular solution of equation (46) of the form:

$$\Delta_1=\frac{\alpha e^{-\kappa(k_s^2+m^2)t}}{\{\rho\kappa^2(k_s^2+m^2)+(\lambda+2\mu)\}}C_n(k_s r)\begin{matrix}\sin\\ \cos\end{matrix}\Big\} mz\begin{matrix}\sin\\ \cos\end{matrix}\Big\} n\theta. \quad ..(47)$$

The dilatation expressed by (47) is due to the elementary temperature variation expressed by (6′).

The complementary solution of equation (46), which is necessary for the present study, is

$$\Delta_2=A_m e^{-\kappa(k_s^2+m^2)t}C_n(k_s r)e^{-\left[\frac{\rho\kappa^2(k_s^2+m^2)^2}{(\lambda+2\mu)}+k_s^2\right]^{1/2}z}\begin{matrix}\sin\\ \cos\end{matrix}\Big\} n\theta, \quad ....(48)$$

where A_m is an arbitrary constant to be determined by the boundary conditions of elastic solid.

The solution of (43), which is favourable for the present study, is of the form:

$$2\varpi_z=B_m e^{-\kappa(k_s^2+m^2)t}C_n(k_s r)e^{-\left[\frac{\rho\kappa^2(k_s^2+m^2)^2}{\mu}+k_s^2\right]^{1/2}z}\begin{matrix}\sin\\ -\cos\end{matrix}\Big\} n\theta, \quad ..(49)$$

B_m being also an arbitrary constant to be determined by the boundary conditions.

Substituting (49) for $2\varpi_z$ in equation (44), we obtain the following solution of (44):

$$2\varpi_r=C_m\frac{C_n(k_s r)}{r}e^{-\kappa(k_s^2+m^2)t}e^{-\left[\frac{\rho\kappa^2(k_s^2+m^2)^2}{\mu}+k_s^2\right]^{1/2}z}\begin{matrix}-\cos\\ \sin\end{matrix}\Big\} n\theta$$
$$-B_m\frac{\left[\frac{\rho\kappa^2(k_s^2+m^2)^2}{\mu}+k_s^2\right]^{1/2}}{k_s^2}\frac{\partial C_n(k_s r)}{\partial r}e^{-\left[\frac{\rho\kappa^2(k_s^2+m^2)^2}{\mu}+k_s^2\right]^{1/2}z}\begin{matrix}-\cos\\ \sin\end{matrix}\Big\} n\theta. \quad (50)$$

Using the expression (50), we can find the solution of $2\varpi_\theta$ shown below:

$$2\varpi_\theta=C_m\frac{1}{n}\frac{\partial C_n(k_s r)}{\partial r}e^{-\kappa(k_s^2+m^2)t}e^{-\left[\frac{\rho\kappa^2(k_s^2+m^2)^2}{\mu}+k_s^2\right]^{1/2}z}\begin{matrix}\sin\\ \cos\end{matrix}\Big\} n\theta$$
$$+B_m\frac{n\left[\frac{\rho\kappa^2(k_s^2+m^2)^2}{\mu}+k_s^2\right]^{1/2}}{k_s^2}\frac{C_n(kr)}{r}e^{-\left[\frac{\rho\kappa^2(k_s^2+m^2)^2}{\mu}+k_s^2\right]^{1/2}z}\begin{matrix}\sin\\ \cos\end{matrix}\Big\} n\theta. \quad (51)$$

In the expressions (50), (51), C_m is also an arbitrary constant.

Substituting (47), (48), (49), (50) and (51) for Δ, $2\varpi_r$, $2\varpi_\theta$ and $2\varpi_z$ in the equations (16), (17) and (18), we obtain the following solutions of the components of displacement (u, v, w) after some reductions:

$$u=-\frac{\alpha e^{-\kappa(k_s^2+m^2)t}}{\{\rho\kappa^2(k_s^2+m^2)+(\lambda+2\mu)\}\{k_s^2+m^2\}}\frac{\partial C_n(k_sr)}{\partial r}\begin{matrix}\sin\\ \cos\end{matrix}\Big\}mz\begin{matrix}\sin\\ \cos\end{matrix}\Big\}n\theta$$
$$+\frac{(\lambda+2\mu)A_m e^{-\kappa(k_s^2+m^2)t}}{\rho\kappa^2(k_s^2+m^2)^2}\frac{\partial C_n(k_sr)}{\partial r}e^{-\left[\frac{\rho\kappa^2(k_s^2+m^2)^2}{(\lambda+2\mu)}+k_s^2\right]^{1/2}z}\begin{matrix}\sin\\ \cos\end{matrix}\Big\}n\theta$$
$$-\frac{\mu\left\{\frac{\rho\kappa^2(k_s^2+m^2)^2}{\mu}+k_s^2\right\}^{1/2}}{n\rho\kappa^2(k_s^2+m^2)^2}C_m e^{-\kappa(k_s^2+m^2)t}\frac{\partial C_n(k_sr)}{\partial r}e^{-\left[\frac{\rho\kappa^2(k_s^2+m^2)^2}{\mu}+k_s^2\right]^{1/2}z}\begin{matrix}\sin\\ \cos\end{matrix}\Big\}n\theta$$
$$-\frac{n}{k_s^2}B_m e^{-\kappa(k_s^2+m^2)t}\frac{C_n(k_sr)}{r}e^{-\left[\frac{\rho\kappa^2(k_s^2+m^2)^2}{\mu}+k_s^2\right]^{1/2}z}\begin{matrix}\sin\\ \cos\end{matrix}\Big\}n\theta, \qquad \text{........(52)}$$

$$v=-\frac{n\alpha e^{-\kappa(k_s^2+m^2)t}}{\{\rho\kappa^2(k_s^2+m^2)+(\lambda+2\mu)\}\{k_s^2+m^2\}}\frac{C_n(k_sr)}{r}\begin{matrix}\sin\\ \cos\end{matrix}\Big\}mz\begin{matrix}\cos\\ -\sin\end{matrix}\Big\}n\theta$$
$$+\frac{n(\lambda+2\mu)}{\rho\kappa^2(k_s^2+m^2)^2}A_m e^{-\kappa(k_s^2+m^2)t}\frac{C_n(k_sr)}{r}e^{-\left[\frac{\rho\kappa^2(k_s^2+m^2)^2}{(\lambda+2\mu)}+k_s^2\right]^{1/2}z}\begin{matrix}\cos\\ -\sin\end{matrix}\Big\}n\theta$$
$$-\frac{\mu\left\{\frac{\rho\kappa^2(k_s^2+m^2)^2}{\mu}+k_s^2\right\}^{1/2}}{\rho\kappa^2(k_s^2+m^2)^2}C_m e^{-\kappa(k_s^2+m^2)t}\frac{C_n(k_sr)}{r}e^{-\left[\frac{\rho\kappa^2(k_s^2+m^2)^2}{\mu}+k_s^2\right]^{1/2}z}\begin{matrix}\cos\\ -\sin\end{matrix}\Big\}n\theta$$
$$-\frac{1}{k_s^2}B_m e^{-\kappa(k_s^2+m^2)t}\frac{\partial C_n(k_sr)}{\partial r}e^{-\left[\frac{\rho\kappa^2(k_s^2+m^2)^2}{\mu}+k_s^2\right]^{1/2}z}\begin{matrix}\cos\\ -\sin\end{matrix}\Big\}n\theta, \qquad \text{....(53)}$$

$$w=-\frac{m\alpha e^{-\kappa(k_s^2+m^2)t}}{\{\rho\kappa^2(k_s^2+m^2)+(\lambda+2\mu)\}\{k_s^2+m^2\}}C_n(k_sr)\begin{matrix}\cos\\ -\sin\end{matrix}\Big\}mz\begin{matrix}\sin\\ \cos\end{matrix}\Big\}n\theta$$
$$-\frac{(\lambda+2\mu)}{\rho\kappa^2(k_s^2+m^2)^2}\left[\frac{\rho\kappa^2(k_s^2+m^2)^2}{(\lambda+2\mu)}+k_s^2\right]^{1/2}A_m C_n(k_sr)e^{-\kappa(k_s^2+m^2)t}$$
$$\times e^{-\left[\frac{\rho\kappa^2(k_s^2+m^2)^2}{(\lambda+2\mu)}+k_s^2\right]^{1/2}z}\begin{matrix}\sin\\ \cos\end{matrix}\Big\}n\theta$$
$$+\frac{k_s^2\mu}{n\rho\kappa^2(k_s^2+m^2)^2}C_m e^{-\kappa(k_s^2+m^2)t}C_n(k_sr)e^{-\left[\frac{\rho\kappa^2(k_s^2+m^2)^2}{\mu}+k_s^2\right]^{1/2}z}\begin{matrix}\sin\\ \cos\end{matrix}\Big\}n\theta. \qquad (54)$$

In each expression of the component of displacement, u, v, and w, the first term having the trigonometrical functions of mz corresponds to the temperature variation (6′) only, and the other terms having e-functions of z correspond to the displacement which may be used for the purpose of fulfilment of the boundary conditions of elastic solid.

Using these components of displacement, (52), (53), (54) and dilatations (47), (48), and temperature variation (6′), we can obtain the components of traction $\widehat{rr}$, $\widehat{\theta\theta}$, $\widehat{zz}$, $\widehat{r\theta}$, $\widehat{\theta z}$, $\widehat{rz}$.

Now the surface $(z=0)$ of elastic solid is free from traction as in the case of Part I. Therefore we have

$$z=0\,;\quad \widehat{zz}=0,\ \widehat{rz}=0,\ \widehat{\theta z}=0. \quad \ldots\ldots\ldots\ldots(55)$$

These conditions give us the values of constants A_m, B_m and C_m in the following forms:

$$B_m=0,$$

$$A_m=\frac{-4\mu^2k_s^2m\alpha\rho\kappa^2(k_s^2+m^2)\left\{\dfrac{\rho\kappa^2(k_s^2+m^2)^2}{\mu}+k_s^2\right\}^{1/2}}{(\lambda+2\mu)\{\rho\kappa^2(k_s^2+m^2)+(\lambda+2\mu)\}\left[4\mu^2k_s^2\left\{\dfrac{\rho\kappa^2(k_s^2+m^2)^2}{(\lambda+2\mu)}+k_s^2\right\}^{1/2}\left\{\dfrac{\rho\kappa^2(k_s^2+m^2)^2}{\mu}+k_s^2\right\}^{1/2}-\{\rho\kappa^2(k_s^2+m^2)^2+2\mu k_s^2\}^2\right]},$$

$$C_m=-\frac{2mn\alpha\rho\kappa^2(k_s^2+m^2)\{\rho\kappa^2(k_s^2+m^2)^2+2\mu k_s^2\}}{\{\rho\kappa^2(k_s^2+m^2)+(\lambda+2\mu)\}\left[4\mu^2k_s^2\left\{\dfrac{\rho\kappa^2(k_s^2+m^2)^2}{(\lambda+2\mu)}+k_s^2\right\}^{1/2}\left\{\dfrac{\rho\kappa^2(k_s^2+m^2)^2}{\mu}+k_s^2\right\}^{1/2}-\{\rho\kappa^2(k_s^2+m^2)^2+2\mu k_s^2\}^2\right]}.$$

$$\ldots\ldots\ldots\ldots\ldots\ldots\ldots(56)$$

Then, substituting these expressions (56) for the constants A_m, B_m and C_m in the components of displacement expressed by (52), (53) and (54), we have the components of displacement u, v, w of the forms:

$$u=-\frac{\alpha e^{-\kappa(k_s^2+m^2)t}}{\{\rho\kappa^2(k_s^2+m^2)+(\lambda+2\mu)\}\{k_s^2+m^2\}}\frac{\partial C_n(k_sr)}{\partial r}\begin{matrix}\sin\\ \cos\end{matrix}\Big\}mz\begin{matrix}\sin\\ \cos\end{matrix}\Big\}n\theta$$

$$-\frac{4\mu^2k_s^2m\alpha\left\{\dfrac{\rho\kappa^2(k_s^2+m^2)^2}{\mu}+k_s^2\right\}^{1/2}e^{-\kappa(k_s^2+m^2)t}}{\{\rho\kappa^2(k_s^2+m^2)+(\lambda+2\mu)\}\{k_s^2+m^2\}F(k_s,m)}\frac{\partial C_n(k_sr)}{\partial r}e^{-\left[\frac{\rho\kappa^2(k_s^2+m^2)^2}{(\lambda+2\mu)}+k_s^2\right]^{1/2}}\begin{matrix}\sin\\ \cos\end{matrix}\Big\}n\theta$$

$$+\frac{2m\alpha\mu\{\rho\kappa^2(k_s^2+m^2)^2+2\mu k_s^2\}\left\{\dfrac{\rho\kappa^2(k_s^2+m^2)^2}{\mu}+k_s^2\right\}^{1/2}}{(k_s^2+m^2)\{\rho\kappa^2(k_s^2+m^2)+(\lambda+2\mu)\}F(k_s,m)}\frac{\partial C_n(k_sr)}{\partial r}e^{-\kappa(k_s^2+m^2)t}$$

$$\times e^{-\left[\frac{\rho\kappa^2(k_s^2+m^2)^2}{\mu}+k_s^2\right]^{1/2}z}\begin{matrix}\sin\\ \cos\end{matrix}\Big\}n\theta, \quad \ldots(57)$$

$$v=-\frac{n\alpha e^{-\kappa(k_s^2+m^2)t}}{\{\rho\kappa^2(k_s^2+m^2)+(\lambda+2\mu)\}\{k_s^2+m^2\}}\frac{C_n(k_sr)}{r}\left.\begin{matrix}\sin\\ \cos\end{matrix}\right\}mz\left.\begin{matrix}\cos\\ -\sin\end{matrix}\right\}n\theta$$

$$-\frac{4\mu^2k_s^2mn\alpha\left\{\dfrac{\rho\kappa^2(k_s^2+m^2)^2}{\mu}+k_s^2\right\}^{1/2}e^{-\kappa(k_s^2+m^2)t}}{\{\rho\kappa^2(k_s^2+m^2)+(\lambda+2\mu)\}\{k_s^2+m^2\}F(k_s,m)}\frac{C_n(k_sr)}{r}e^{-\left[\frac{\rho\kappa^2(k_s^2+m^2)^2}{(\lambda+2\mu)}+k_s^2\right]^{1/2}z}\left.\begin{matrix}\cos\\ -\sin\end{matrix}\right\}n\theta$$

$$+\frac{2mn\alpha\mu\{\rho\kappa^2(k_s^2+m^2)^2+2\mu k_s^2\}\left\{\dfrac{\rho\kappa^2(k_s^2+m^2)^2}{\mu}+k_s^2\right\}^{1/2}}{(k_s^2+m^2)\{\rho\kappa^2(k_s^2+m^2)+(\lambda+2\mu)\}F(k_s,m)}\frac{C_n(k_sr)}{r}$$

$$\times e^{-\left[\frac{\rho\kappa^2(k_s^2+m^2)^2}{\mu}+k_s^2\right]^{1/2}z}\left.\begin{matrix}\cos\\ -\sin\end{matrix}\right\}n\theta,\quad\ldots\ldots(58)$$

$$w=-\frac{m\alpha e^{-\kappa(k_s^2+m^2)t}}{(k_s^2+m^2)\{\rho\kappa^2(k_s^2+m^2)+(\lambda+2\mu)\}}C_n(k_sr)\left.\begin{matrix}\cos\\ -\sin\end{matrix}\right\}mz\left.\begin{matrix}\sin\\ \cos\end{matrix}\right\}n\theta$$

$$+\frac{4\mu^2k_s^2m\alpha\left\{\dfrac{\rho\kappa^2(k_s^2+m^2)^2}{(\lambda+2\mu)}+k_s^2\right\}^{1/2}\left\{\dfrac{\rho\kappa^2(k_s^2+m^2)^2}{\mu}+k_s^2\right\}^{1/2}e^{-\kappa(k_s^2+m^2)t}}{(k_s^2+m^2)\{\rho\kappa^2(k_s^2+m^2)+(\lambda+2\mu)\}F(k_s,m)}$$

$$\times C_n(k_sr)e^{-\left[\frac{\rho\kappa^2(k_s^2+m^2)^2}{(\lambda+2\mu)}+k_s^2\right]^{1/2}z}\left.\begin{matrix}\sin\\ \cos\end{matrix}\right\}n\theta$$

$$-\frac{2k_s^2m\mu\alpha\{\rho\kappa^2(k_s^2+m^2)^2+2uk_s^2\}e^{-\kappa(k_s^2+m^2)t}}{(k_s^2+m^2)\{\rho\kappa^2(k_s^2+m^2)+(\lambda+2\mu)\}F(k_s,m)}$$

$$\times C_n(k_sr)e^{-\left[\frac{\rho\kappa^2(k_s^2+m^2)^2}{\mu}+k_s^2\right]^{1/2}z}\left.\begin{matrix}\sin\\ \cos\end{matrix}\right\}n\theta.\qquad(59)$$

In the above expressions (57), (58) and (59), $F(k_s, m)$ represents the relation :

$$F(k_s,m)=\left[4\mu^2k_s^2\left\{\frac{\rho\kappa^2(k_s^2+m^2)^2}{(\lambda+2\mu)}+k_s^2\right\}^{1/2}\left\{\frac{\rho\kappa^2(k_s^2+m^2)^2}{\mu}+k_s^2\right\}^{1/2}\right.$$

$$\left.-\{\rho\kappa^2(k_s^2+m^2)^2+2\mu k_s^2\}^2\right].\qquad(60)$$

The displacement thus obtained is the elementary solution which corresponds to the temperature variation of the type (6′) and satisfies the boundary conditions at the free surface ($z=0$).

6. In this section we shall study the case where the temperature of the semi-infinite solid is subjected to the following conditions :

$$t=0\,; \qquad T=0, \qquad \ldots\ldots\ldots\ldots\ldots\ldots\ldots(61)$$

$$z=0\,; \qquad T=f(r,\theta,t), \qquad \ldots\ldots\ldots\ldots\ldots(62)$$

$$r=\infty\,; \qquad T=0, \qquad \ldots\ldots\ldots\ldots\ldots\ldots\ldots(63)$$

$$z=\infty\,; \qquad T=0. \qquad \ldots\ldots\ldots\ldots\ldots\ldots\ldots(64)$$

These conditions are the same one as that in Section 3, and therefore the form of T is

$$T=\frac{\kappa}{\pi^2}\sum_{n=0}^{\infty}\delta_n\int_0^{\infty}\int_0^{\infty}\int_0^{\infty}\int_0^{2\pi}\int_0^{t}e^{-\kappa(\sigma^2+\xi^2)(t-\eta)}f(\zeta,\varphi,\eta)\cos n(\theta-\varphi)J_n(\sigma r)$$
$$J_n(\sigma\zeta)\sin\xi z\sigma\xi\zeta\,d\eta\,d\varphi\,d\zeta\,d\sigma\,d\xi\ldots.(65)$$

Using the elementary solutions (57), (58), and (59), we obtain the following form of displacement which corresponds to this temperature variation (65) and satisfies the boundary conditions (55):

$$u=-\frac{\kappa\alpha}{\pi^2}\sum_{n=0}^{\infty}\delta_n\int_0^{\infty}\int_0^{\infty}\int_0^{\infty}\int_0^{2\pi}\int_0^{t}\frac{e^{-\kappa(\sigma^2+\xi^2)(t-\eta)}f(\zeta,\varphi,\eta)\cos n(\theta-\varphi)}{\{\rho\kappa^2(\sigma^2+\xi^2)+(\lambda+2\mu)\}\{\sigma^2+\xi^2\}}\frac{\partial J_n(\sigma r)}{\partial r}$$
$$J_n(\sigma\zeta)\sin\xi z\,\sigma\xi\zeta\,d\eta\,d\varphi\,d\zeta\,d\sigma\,d\xi$$

$$-\frac{2\mu\alpha\kappa}{\pi^2}\sum_{n=0}^{\infty}\delta_n\int_0^{\infty}\int_0^{\infty}\int_0^{\infty}\int_0^{2\pi}\int_0^{t}\frac{\xi\left\{\frac{\rho\kappa^2(\sigma^2+\xi^2)^2}{\mu}+\sigma^2\right\}^{1/2}f(\zeta,\varphi,\eta)e^{-\kappa(\sigma^2+\xi^2)(t-\eta)}}{(\sigma^2+\xi^2)\{\rho\kappa^2(\sigma^2+\xi^2)^2+(\lambda+2\mu)\}F(\sigma,\xi)}$$
$$\frac{\partial J_n(\sigma r)}{\partial r}\left[2\mu\sigma^2e^{-\left[\frac{\rho\kappa^2(\sigma^2+\xi^2)^2}{(\lambda+2\mu)}+\sigma^2\right]^{1/2}z}+\{\rho\kappa^2(\sigma^2+\xi^2)^2+2\mu\sigma^2\}e^{-\left[\frac{\rho\kappa^2(\sigma^2+\xi^2)^2}{\mu}+\sigma^2\right]^{1/2}z}\right]$$
$$\cos n(\theta-\varphi)J_n(\sigma\zeta)\sigma\xi\zeta\,d\eta\,d\varphi\,d\zeta\,d\sigma\,d\xi, \quad (66)$$

$$v=\frac{\kappa\alpha}{\pi^2}\sum_{n=0}^{\infty}\delta_n\int_0^{\infty}\int_0^{\infty}\int_0^{\infty}\int_0^{2\pi}\int_0^{t}\frac{e^{-\kappa(\sigma^2+\xi^2)(t-\eta)}n\,f(\zeta,\varphi,\eta)\sin n(\theta-\varphi)}{\{\sigma^2+\xi^2\}\{\rho\kappa^2(\sigma^2+\xi^2)+(\lambda+2\mu)\}}\frac{J_n(\sigma r)}{r}$$
$$J_n(\sigma\zeta)\sin\xi z\sigma\xi\zeta\,d\eta\,d\varphi\,d\zeta\,d\sigma\,d\xi$$

$$+\frac{2\mu\alpha\kappa}{\pi^2}\sum_{n=0}^{\infty}\delta_n\int_0^{\infty}\int_0^{\infty}\int_0^{\infty}\int_0^{2\pi}\int_0^{t}\frac{n e^{-\kappa(\sigma^2+\xi^2)(t-\eta)}f(\zeta,\varphi,\eta)\left\{\frac{\rho\kappa^2(\sigma^2+\xi^2)^2}{\mu}+\sigma^2\right\}^{1/2}\sin n(\theta-\varphi)}{\{\sigma^2+\xi^2\}\{\rho\kappa^2(\sigma^2+\xi^2)+(\lambda+2\mu)\}F(\sigma,\xi)}$$
$$\left[2\mu\sigma^2e^{-\left[\frac{\rho\kappa^2(\sigma^2+\xi^2)^2}{(\lambda+2\mu)}+\sigma^2\right]^{1/2}z}+\{\rho\kappa^2(\sigma^2+\xi^2)^2+2\mu\sigma^2\}e^{-\left[\frac{\rho\kappa^2(\sigma^2+\xi^2)^2}{\mu}+\sigma^2\right]^{1/2}z}\right]$$
$$J_n(\sigma r)J_n(\sigma\zeta)\sigma\xi^2\zeta\,d\eta\,d\varphi\,d\zeta\,d\sigma\,d\xi, \quad (67)$$

$$w=-\frac{\kappa\alpha}{\pi^2}\sum_{n=0}^{\infty}\delta_n\int_0^{\infty}\int_0^{\infty}\int_0^{\infty}\int_0^{2\pi}\int_0^{t}\frac{e^{-\kappa(\sigma^2+\xi^2)(t-\eta)}f(\zeta,\varphi,\eta)\cos n(\theta-\varphi)}{\{\sigma^2+\xi^2\}\{\rho\kappa^2(\sigma^2+\xi^2)+(\lambda+2\mu)\}}J_n(\sigma r)$$

$$J_n(\sigma\zeta)\cos\xi z\sigma\xi^2\zeta\, d\eta d\varphi d\zeta d\sigma d\xi$$

$$+\frac{2\mu\kappa\alpha}{\pi^2}\sum_{n=0}^{\infty}\delta_n\int_0^{\infty}\int_0^{\infty}\int_0^{\infty}\int_0^{2\pi}\int_0^{t}\frac{e^{-\kappa(\sigma^2+\xi^2)(t-\eta)}f(\zeta,\varphi,\eta)\xi\sigma^2\cos n(\theta-\varphi)}{\{\sigma^2+\xi^2\}\{\rho\kappa^2(\sigma^2+\xi^2)+(\lambda+2\mu)\}\,F(\sigma,\xi)}$$

$$J_n(\sigma r)\left[2\mu\left\{\frac{\rho\kappa^2(\sigma^2+\xi^2)^2}{(\lambda+2\mu)}+\sigma^2\right\}^{1/2}\left\{\frac{\rho\kappa^2(\sigma^2+\xi^2)^2}{\mu}+\sigma^2\right\}^{1/2}e^{-\left[\frac{\rho\kappa^2(\sigma^2+\xi^2)^2}{(\lambda+2\mu)}+\sigma^2\right]^{1/2}z}\right.$$

$$\left.-\{\rho\kappa^2(\sigma^2+\xi^2)^2+2\mu\sigma^2\}e^{-\left[\frac{\rho\kappa^2(\sigma^2+\xi^2)^2}{\mu}+\sigma^2\right]^{1/2}z}\right]J_n(\sigma\zeta)\sigma\xi\zeta\, d\eta d\varphi d\zeta d\sigma d\xi. \quad (68)$$

In the above expressions (66), (67) and (68), $F(\sigma,\xi)$ is written in place of

$$F(\sigma,\xi)=\left[4\mu^2\sigma^2\left\{\frac{\rho\kappa^2(\sigma^2+\xi^2)^2}{(\lambda+2\mu)}+\sigma^2\right\}^{1/2}\left\{\frac{\rho\kappa^2(\sigma^2+\xi^2)^2}{\mu}+\sigma^2\right\}^{1/2}\right.$$

$$\left.-\{\rho\kappa^2(\sigma^2+\xi^2)^2+2\mu\sigma^2\}^2\right]. \quad \ldots\ldots(69)$$

7. When the surface distribution of temperature has no azimuthal variation and is given by the form :

$$z=0;\quad T=\phi(r,t), \quad \ldots\ldots\ldots\ldots\ldots(70)$$

the expression of T satisfying (70), (61), (63) and (64) can be written as follows :

$$T=\frac{\kappa}{\pi}\int_0^{\infty}\int_0^{\infty}\int_0^{\infty}\int_0^{t}e^{-\kappa(\sigma^2+\xi^2)(t-\eta)}\phi(\zeta,\eta)J_0(\sigma r)J_0(\sigma\zeta)\sin\xi z\sigma\xi\zeta\, d\eta d\zeta d\sigma d\xi, \quad (71)$$

and the expressions of the components of displacement in the solid are written in the forms :

$$u=-\frac{\kappa\alpha}{\pi}\int_0^{\infty}\int_0^{\infty}\int_0^{\infty}\int_0^{t}\frac{e^{-\kappa(\sigma^2+\xi^2)(t-\eta)}\phi(\zeta,\eta)\sin\xi z}{\{\rho\kappa^2(\sigma^2+\xi^2)^2+(\lambda+2\mu)\}(\sigma^2+\xi^2)}\frac{\partial J_0(\sigma\zeta)}{\partial r}$$

$$J_0(\sigma\zeta)\sigma\xi\zeta\, d\eta d\zeta d\sigma d\xi$$

$$-\frac{2\mu\alpha\kappa}{\pi}\int_0^{\infty}\int_0^{\infty}\int_0^{\infty}\int_0^{t}\frac{\left\{\frac{\rho\kappa^2(\sigma^2+\xi^2)^2}{\mu}+\sigma^2\right\}^{1/2}\phi(\zeta,\eta)J_0(\sigma\zeta)}{\{\sigma^2+\xi^2\}\{\rho\kappa^2(\sigma^2+\xi^2)^2+(\lambda+2\mu)\}F(\sigma,\xi)}\frac{\partial J_0(\sigma r)}{\partial r}$$

$$e^{-\kappa(\sigma^2+\xi^2)(t-\eta)}\left[2\mu\sigma^2 e^{-\left[\frac{\rho\kappa^2(\sigma^2+\xi^2)^2}{(\lambda+2\mu)}+\sigma^2\right]^{1/2}z}\right.$$

$$+\left\{\rho\kappa^2(\sigma^2+\xi^2)^2+2\mu\sigma^2\right\}e^{-\left[\frac{\rho\kappa^2(\sigma^2+\xi^2)^2}{\mu}+\sigma^2\right]^{1/2}z}\Bigg]\sigma\xi^2\zeta\, d\eta\, d\zeta\, d\sigma\, d\xi, \quad \ldots\ldots(72)$$

$$w=-\frac{\kappa\alpha}{\pi}\int_0^\infty\int_0^\infty\int_0^\infty\int_0^t\frac{e^{-\kappa(\sigma^2+\xi^2)(t-\eta)}\phi(\zeta,\eta).J_0(\sigma r)}{\{\sigma^2+\xi^2\}\,\{\rho\kappa^2(\sigma^2+\xi^2)+(\lambda+2\mu)\}}$$

$$J_0(\sigma\zeta)\cos\zeta z\sigma\xi^2\zeta\, d\eta\, d\zeta\, d\sigma\, d\xi$$

$$+\frac{2\mu\kappa\alpha}{\pi}\int_0^\infty\int_0^\infty\int_0^\infty\int_0^t\frac{e^{-\kappa(\sigma^2+\xi^2)(t-\eta)}\phi(\zeta,\eta)\xi\sigma^2J_0(\sigma r).J_0(\sigma\zeta)}{\{\sigma^2+\xi^2\}\{\rho\kappa^2(\sigma^2+\xi^2)+(\lambda+2\mu)\}F(\sigma,\xi)}$$

$$\Bigg[2\mu\left\{\frac{\rho\kappa^2(\sigma^2+\xi^2)^2}{(\lambda+2\mu)}+\sigma^2\right\}^{1/2}\left\{\frac{\rho\kappa^2(\sigma^2+\xi^2)^2}{\mu}+\sigma^2\right\}^{1/2}e^{-\left[\frac{\rho\kappa^2(\sigma^2+\xi^2)^2}{(\lambda+2\mu)}+\sigma^2\right]^{1/2}z}$$

$$-\left\{\rho\kappa^2(\sigma^2+\xi^2)^2+2\mu\sigma^2\right\}e^{-\left[\frac{\rho\kappa^2(\sigma^2+\xi^2)^2}{\mu}+\sigma^2\right]^{1/2}z}\Bigg]\sigma\xi\zeta\, d\eta\, d\zeta\, d\sigma\, d\xi, \quad \ldots\ldots(73)$$

where $F(\sigma,\xi)$ has the same meaning as that of (69) in Section 6.

The surface deformation due to the temperature distribution (71) may be written by the following equations:

$$u_{z=0}=-\frac{2\mu\alpha\kappa}{\pi}\int_0^\infty\int_0^\infty\int_0^\infty\int_0^t\frac{\left\{\frac{\rho\kappa^2(\sigma^2+\xi^2)^2}{\mu}+\sigma^2\right\}^{1/2}\phi(\zeta,\eta)e^{-\kappa(\sigma^2+\xi^2)(t-\eta)}}{\{\sigma^2+\xi^2\}\{\rho\kappa^2(\sigma^2+\xi^2)^2+(\lambda+2\mu)\}F(\sigma,\xi)}$$

$$[\rho\kappa^2(\sigma^2+\xi^2)^2+4\mu\sigma^2]\frac{\partial J_0(\sigma r)}{\partial r}J_0(\sigma\zeta)\sigma\xi^2\zeta\, d\eta\, d\zeta\, d\sigma\, d\xi, \quad \ldots\ldots(74)$$

$$w_{z=0}=\frac{2\kappa^2\alpha\rho}{\pi}\int_0^\infty\int_0^\infty\int_0^\infty\int_0^t\frac{e^{-\kappa(\sigma^2+\xi^2)(t-\eta)}(\sigma^2+\xi^2)\{\rho\kappa^2(\sigma^2+\xi^2)^2+2\mu\sigma^2\}}{\{\rho\kappa^2(\sigma^2+\xi^2)+(\lambda+2\mu)\}F(\sigma,\xi)}\phi(\zeta,\eta)$$

$$J_0(\sigma r)J_0(\sigma\zeta)\sigma\xi^2\zeta\, d\zeta\, d\eta\, d\sigma\, d\xi. \quad \ldots\ldots(75)$$

8. Using the cylindrical coordinates, we have obtained the expressions of the displacement of a semi-infinite elastic solid due to the temperature variation which satisfies completely the equations of heat conduction and the initial and boundary conditions of the solid. We have studied the problem separating into two cases: one of them is the case where the inertia of solid is neglected, and the other the case where the inertia effect is taken into account. In both cases the resulting equations contain the term of density in spite of the fact that the inertia term is neglected in one case and not in the other.

In concluding this paper, my cordial thanks are due to Professor K. Sezawa for his kind advices during the course of this study.

23. 溫度變化による半無限彈性體の變形式

地震研究所 西 村 源 六 郎

曩に「溫度分布が半無限彈性體の變形に及ぼす影響」と題して著者は彈性體の溫度分布によろ變形問題をフリーエーの二重積分公式を利用して色々な溫度分布に就て取扱つてみた事がある。本研究に於ては熱傳導論に基いて、半無限彈性體の變形問題を理論的に取扱つたのである。即ち彈性體中に起る溫度變化を全く傳導論的に取扱ひ、それによつて生ずる變形問題を彈性體の慣性を考へに入れない場合と、彈性體の慣性を入れた場合の二つに就き、變形式を求めてみた。式は可なり復雜であるが兩者を比較研究すると共に、全く時間的の變化を考へに入れない場合の彈性體の變形式との間に、色々面白い事項が含まれてゐる事がわかるのである。

24. *On the Effect of a Spherical Cavity on the Equilibrium of the Gravitating Semi-infinite Elastic Solid.*

By Genrokuro NISHIMURA and Takeo TAKAYAMA,

Earthquake Research Institute.

(Read Jan. 19 and Feb. 16, 1932.—Received March 20, 1932.)

1. Due to Professor M. Ishimoto,[1] there are many pockets of magma in the interior of the crust of the earth and these cavities play an important *rôle* on the occurrence of an earthquake. Thus we think that it may be some importance to investigate the strength of these pockets or cavities under the gravitating body force of the crust.

Professor N. Yamaguti[2] studied the stress distribution in the vicinity of a horizontal circular hole in a gravitating elastic solid for the purpose of investigating the strength of a horizontal tunnel. Recently Dr. T. Sugihara[3] also studied the stress distribution in the neighbourhood of a shaft or of a inclined drift in a gravitating solid with some approximations. But the problem referring to a spherical cavity has not yet been studied.

We shall study, in the first part of this paper, the stress distribution in the neighbourhood of a spherical cavity in the interior of the gravitating semi-infinite elastic solid. In the second part the stress distributions in the neighbourhood of a spherical cavity in a infinite elastic solid under the uniform shearing force are investigated.

2. In the present study, the spherical coordinates (r, θ, ϕ) are used. The density and the gravity constant are taken to be ρ and g. Let the origin O of the coordinates be at the centre of a spherical cavity of the radius a, and the distance from O to the upper horizontal surface of solid be z_0. Fig. 1 indicates the relation between the spherical coordinates (r, θ, ϕ) and the rectangular coordinates (x, y, z). Let u, v, w be the components of displacement in the directions of radius r, co-latitude

1) M. ISHIMOTO, *Bull. Earthq. Res. Inst.*, 6 (1929), (in Japanese).

2) N. YAMAGUTI, "On the Stresses Around a Horizontal Circular Hole in Gravitating Elastic Solid," *Jour. Civil Eng.*, Tokyo, 15 (1929), 291.

3) T. SUGIHARA, *Jour. Mining Inst.*, Japan, 47 (1931), 560, (in Japanese).

θ, and azimuth ϕ, and $\widehat{rr}$, $\widehat{\theta\theta}$, $\widehat{\phi\phi}$ the normal components of traction, $\widehat{r\theta}, \widehat{r\phi}, \widehat{\theta\phi}$ the shearing components of stress with regard to the spherical coordinates. Again, let u', v', w' be the components of displacement in the directions of x, y, and z, and $\widehat{xx}$, $\widehat{yy}, \widehat{zz}$ the normal components of stress and $\widehat{xy}, \widehat{yz}, \widehat{zx}$ the shearing components of stress respectively.

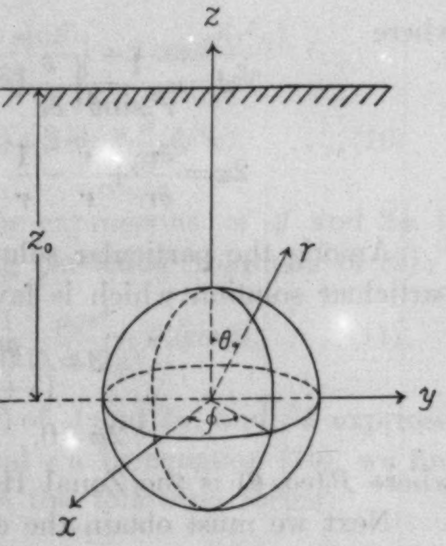

Fig. 1.

Now the top surface ($z=z_0$) of the solid is horizontal, and therefore there is no variation of the azimuthal components of displacement and stress. Then the stress equations of the equilibrium of the solid in the gravitating field are expressed by

$$\left.\begin{aligned}&\frac{\partial\widehat{rr}}{\partial r}+\frac{1}{r}\frac{\partial\widehat{r\theta}}{\partial\theta}+\frac{1}{r}\{2\widehat{rr}-\widehat{\theta\theta}-\widehat{\phi\phi}+\widehat{r\theta}\cot\theta\}=\rho g\cos\theta,\\&\frac{\partial\widehat{r\theta}}{\partial r}+\frac{1}{r}\frac{\partial\widehat{\theta\theta}}{\partial\theta}+\frac{1}{r}\{(\widehat{\theta\theta}-\widehat{\phi\phi})\cot\theta+3\widehat{r\theta}\}=-\rho g\sin\theta.\end{aligned}\right\}\quad\ldots\ldots(1)$$

The normal components of stress, $\widehat{rr}, \widehat{\theta\theta}, \widehat{\phi\phi}$ and the shearing component of stress $\widehat{r\theta}$ are expressed in the following forms:

$$\left.\begin{aligned}&\widehat{rr}=\frac{\lambda}{r^2\sin\theta}\left\{\frac{\partial}{\partial\theta}(r^2u\sin\theta)+\frac{\partial}{\partial r}(rv\sin\theta)\right\}+2\mu\frac{\partial u}{\partial r},\\&\widehat{\theta\theta}=\frac{\lambda}{r^2\sin\theta}\left\{\frac{\partial}{\partial r}(r^2u\sin\theta)+\frac{\partial}{\partial\theta}(rv\sin\theta)\right\}+2\mu\left\{\frac{1}{r}\frac{\partial v}{\partial\theta}+\frac{u}{r}\right\},\\&\widehat{\phi\phi}=\frac{\lambda}{r^2\sin\theta}\left\{\frac{\partial}{\partial r}(r^2u\sin\theta)+\frac{\partial}{\partial\theta}(rv\sin\theta)\right\},\\&\widehat{r\theta}=\mu\left\{\frac{\partial v}{\partial r}-\frac{v}{r}+\frac{1}{r}\frac{\partial u}{\partial\theta}\right\},\end{aligned}\right\}(2)$$

where λ and μ are the Lamé's elastic constants of the solid.

In equation (1), we substitute for the components of stress the expression (2); and we thus obtain the following equations:

$$\left.\begin{aligned}&(\lambda+2\mu)\frac{\partial\varDelta}{\partial r}-\frac{2\mu}{r}\frac{\partial\varpi}{\partial\theta}-\frac{2\mu}{r}\varpi\cot\theta=\rho g\cos\theta,\\&(\lambda+2\mu)\frac{1}{r}\frac{\partial\varDelta}{\partial\theta}+2\mu\frac{\partial\varpi}{\partial r}+2\mu\frac{\varpi}{r}=-\rho g\sin\theta,\end{aligned}\right\}\quad\ldots\ldots(3)$$

where

$$\left.\begin{aligned} \Delta &= \frac{1}{r^2 \sin\theta}\left\{\frac{\partial}{\partial r}(r^2 u \sin\theta) + \frac{\partial}{\partial\theta}(rv\sin\theta)\right\}, \\ 2\varpi &= \frac{\partial v}{\partial r} + \frac{v}{r} - \frac{1}{r}\frac{\partial u}{\partial\theta}. \end{aligned}\right\} \quad \ldots\ldots(4)$$

Among the particular solutions satisfying (3), we take the following particluar solution which is favourable to the present study:

$$\left.\begin{aligned} \Delta &= \frac{\rho g r}{(\lambda+2\mu)} P_1(\cos\theta), \\ 2\varpi &= 0, \end{aligned}\right\} \quad \ldots\ldots\ldots\ldots\ldots(5)$$

where $P_1(\cos\theta)$ is the Zonal Harmonics of the first order.

Next we must obtain the complementary solutions of (3) which are necessary to satisfy the boundary conditions of the solid. Now we obtain the following equation, using the equations (3), after some reductions:

$$\frac{\partial^2\Delta}{\partial r^2} + \frac{2}{r}\frac{\partial\Delta}{\partial r} + \frac{1}{r^2}\frac{\partial^2\Delta}{\partial\theta^2} + \frac{\cot\theta}{r^2}\frac{\partial\Delta}{\partial\theta} = 0. \quad \ldots\ldots\ldots(6)$$

We obtain the following solutions of (6) easily:

$$\begin{aligned} \Delta = &\left\{A_0 + \frac{A_0'}{r}\right\}P_0(\cos\theta) + \left\{A_1 r + \frac{A_1'}{r^2}\right\}P_1(\cos\theta) \\ &+ \left\{A_2 r^2 + \frac{A_2'}{r^3}\right\}P_2(\cos\theta) + \left\{A_3 r^3 + \frac{A_3'}{r^4}\right\}P_3(\cos\theta), \quad \ldots\ldots(7) \end{aligned}$$

where A_0, A_0', A_1, A_1', A_2, A_2', A_3, A_3' are the arbitrary constants, and $P_0(\cos\theta)$, $P_2(\cos\theta)$, $P_3(\cos\theta)$ are the Zonal Harmonics of zero, second and third order.

Using (7), we obtain the following forms of 2ϖ which are the particular solutions of (3):

$$\begin{aligned} 2\varpi = &-\frac{(\lambda+2\mu)}{\mu}\left\{\frac{A_1 r}{2} - \frac{A_1'}{r^2}\right\}\frac{\partial P_1(\cos\theta)}{\partial\vartheta} \\ &-\frac{(\lambda+2\mu)}{\mu}\left\{\frac{A_2 r^2}{3} - \frac{A_2'}{2r^3}\right\}\frac{\partial P_2(\cos\theta)}{\partial\theta} \\ &-\frac{(\lambda+2\mu)}{\mu}\left\{\frac{A_3 r^3}{4} - \frac{A_3'}{3r^3}\right\}\frac{\partial P_3(\cos\theta)}{\partial\theta}. \quad \ldots\ldots\ldots(8) \end{aligned}$$

Now we find the following two differential equations in relation to u, v, Δ and 2ϖ after some reductions from the relations expressed by (4):

$$\frac{\partial^2(r^2u)}{\partial r^2} + \frac{1}{r^2\sin\theta}\frac{\partial}{\partial\theta}\left\{\sin\theta\frac{\partial(r^2u)}{\partial\theta}\right\} = \frac{\partial}{\partial r}(r^2\Delta) - \frac{2r}{\sin\theta}\frac{\partial}{\partial\theta}(\sin\theta\,\varpi), \ldots(9)$$

$$\frac{\partial}{\partial r}\left\{r^2\frac{\partial(rv\sin\theta)}{\partial r}\right\}+\frac{1}{\sin\theta}\frac{\partial}{\partial\theta}\left\{\sin\theta\frac{\partial(rv\sin\theta)}{\partial\theta}\right\}+2\cos\theta\frac{\partial(r^2u)}{\partial r}$$

$$=\frac{r^2}{\sin\theta}\frac{\partial}{\partial\theta}(\sin^2\theta\Delta)+2\sin\theta\frac{\partial}{\partial r}(r^4\varpi). \quad \ldots(10)$$

Substituting the relations (5) for the expressions of Δ and 2ϖ in the equation (9), we obtain the following particular solutions of (9):

$$r^2u=\frac{3}{10}\frac{\rho g r^4}{(\lambda+2\mu)}P_1(\cos\theta)+\frac{1}{5}\frac{\rho g r^4}{(\lambda+2\mu)}P_3(\cos\theta). \quad \ldots(11)$$

Next, substituting the expression (5) of Δ and 2ϖ, and r^2u expressed by (11), for the expressions of Δ, 2ϖ, and r^2u in equation (10), we find the particular solution $rv\sin\theta$ of (10) in the following forms:

$$rv\sin\theta=\frac{1}{10}\frac{\rho g r^3}{(\lambda+2\mu)}\sin\theta\frac{\partial P_1(\cos\theta)}{\partial\theta}+\frac{1}{15}\frac{\rho g r^3}{(\lambda+2\mu)}\sin\theta\frac{\partial P_3(\cos\theta)}{\partial\theta}. \quad (12)$$

Substituting (7) and (8) for the expression of Δ and 2ϖ in the right-hand term of the equation (9), we obtain the following particular solution of (9):

$$\begin{aligned}r^2u=&\left[\frac{1}{3}A_0r^3+\frac{(\lambda+3\mu)}{2\mu}A_0'r^2\right]P_0(\cos\theta)\\&+\left[\frac{(-\lambda+\mu)}{10\mu}r^4A_1-\frac{(\lambda+2\mu)}{\mu}A_1'r\right]P_1(\cos\theta)\\&-\left[\frac{\lambda}{7\mu}A_2r^5+\frac{(3\lambda+5\mu)}{6\mu}A_2'\right]P_2(\cos\theta)\\&-\left[\frac{(3\lambda+\mu)}{18\mu}A_3r^6+\frac{(2\lambda+3\mu)}{5\mu}\frac{A_3'}{r}\right]P_3(\cos\theta). \quad \ldots\ldots(13)\end{aligned}$$

Substituting (7) and (8) and (13) for the expressions of Δ, 2ϖ and r^2u in equation (10), we obtain the particular solution $rv\sin\theta$ of (10) in the following forms:

$$\begin{aligned}rv\sin\theta=&-\left[\frac{(2\lambda+3\mu)}{10\mu}A_1r^3+\frac{(\lambda+3\mu)}{2\mu}A_1'\right]\sin\theta\frac{\partial P_1(\cos\theta)}{\partial\theta}\\&-\left[\frac{(5\lambda+7\mu)}{42\mu}A_2r^4+\frac{A_2'}{6r}\right]\sin\theta\frac{\partial P_2(\cos\theta)}{\partial\theta}\\&-\left[\frac{(3\lambda+4\mu)}{36\mu}A_3r^5+\frac{(-\lambda+\mu)}{30\mu}\frac{A_3'}{r^2}\right]\sin\theta\frac{\partial P_3(\cos\theta)}{\partial\theta}. \quad (14)\end{aligned}$$

As the complementary solutions of the equation (9) we obtain the following expressions of r^2u which are favourable to the present study:

$$r^2u=-C_0'P_0(\cos\theta)+\left[C_1r^2-\frac{2}{r}C_1'\right]P_1(\cos\theta)$$
$$+\left[2r^3C_2-\frac{3}{r^2}C_2'\right]P_2(\cos\theta)+\left[3r^4C_3-\frac{3C_4'}{r^3}\right]P_3(\cos\theta),\quad ..(15)$$

where $C_0', C_1, C_1', C_2, C_2', C_3$ and C_3' are the arbitrary constants which may be determined by the boundary conditions.

Corresponding to r^2u expressed by (15), we obtain the following particular solutions of $rv\sin\theta$ from the equation (10):

$$rv\sin\theta=\left[C_1r+\frac{C_1'}{r^2}\right]\sin\theta\frac{\partial P_1(\cos\theta)}{\partial\theta}+\left[C_2r^2+\frac{C_2'}{r^3}\right]\sin\theta\frac{\partial P_2(\cos\theta)}{\partial\theta}$$
$$+\left[C_3r^3+\frac{C_3'}{r^4}\right]\sin\theta\frac{\partial P_3(\cos\theta)}{\partial\theta}.\quad ....(16)$$

For obtaining the solutions of u and v expressed by (11), (12), (13), (14), (15) and (16), we used the following relations about the Zonal Harmonics:

$$\left.\begin{aligned}\frac{\partial\left[\sin\theta\frac{\partial P_n(\cos\theta)}{\partial\theta}\right]}{\partial\theta}&=-n(n+1)\sin\theta P_n(\cos\theta),\\ \frac{\partial^2}{\partial\theta^2}\left[\sin\theta\frac{\partial P_n(\cos\theta)}{\partial\theta}\right]&=-n(n+1)\sin\theta\frac{\partial P_n(\cos\theta)}{\partial\theta}-n(n+1)\cos\theta P_n(\cos\theta).\end{aligned}\right\}(17)$$

The general solutions of u and v expressed by (11), (12), (13), (14), (15), (16) satisfy, of course, the equation of equilibrium of the elastic solid (3). Using these general expressions of displacement, we find the general expressions of the components of stress $\widehat{rr}$, $\widehat{\theta\theta}$, $\widehat{\phi\phi}$ and $\widehat{r\theta}$ as in the following forms:

$$\widehat{rr}=\left[\left(\lambda+\frac{2\mu}{3}\right)A_0+\frac{\lambda A_0'}{r}+\frac{4\mu}{r^3}C_0'\right]P_0(\cos\theta)$$
$$+\left[\frac{(5\lambda+6\mu)}{5(\lambda+2\mu)}\rho gr+\frac{(3\lambda+2\mu)}{5}A_1r+\frac{(3\lambda+4\mu)}{r^2}A_1'+\frac{12\mu}{r^4}C_1'\right]P_1(\cos\theta)$$
$$+\left[\frac{\lambda}{7}A_2r^2+\frac{(9\lambda+10\mu)}{3r^3}A_2'+4\mu C_2+\frac{24\mu}{r^5}C_2'\right]P_2(\cos\theta)$$
$$+\left[\frac{4\mu}{5(\lambda+2\mu)}\rho gr-\frac{(3\lambda+4\mu)}{9}A_3r^3+\frac{(17\lambda+18\mu)}{5r^4}A_3'\right.$$
$$\left.+12\mu C_3r+\frac{40\mu}{r^6}C_3'\right]P_3(\cos\theta),\quad ..(18)$$

$$\widehat{\theta\theta}=\left[\left(\lambda+\frac{2\mu}{3}\right)A_0+\frac{(2\lambda+3\mu)}{r}A_0'-\frac{2\mu}{r^3}C_0'\right]P_0(\cos\theta)$$

$$+\left[\frac{(5\lambda+3\mu)}{5(\lambda+2\mu)}\rho gr-\frac{(\lambda+4\mu)}{r^2}A_1'+\frac{(4\lambda+\mu)}{5}A_1r+\frac{2\mu}{r}C_1-\frac{4\mu}{r^4}C_1'\right]P_1(\cos\theta)$$

$$+\left[\frac{5}{7}\lambda A_2r^2-\frac{5\mu}{3r^3}A_2'+4\mu C_2-\frac{6\mu}{r^5}C_2'\right]P_2(\cos\theta)$$

$$+\left[\frac{2\mu}{5(\lambda+2\mu)}\rho gr-\frac{(6\lambda+\mu)}{9}A_3r^3+\frac{(\lambda-6\mu)}{5r^4}A_3'+6\mu C_3r-\frac{8\mu}{r^6}C_3'\right]P_3(\cos\theta)$$

$$+\left[\frac{\mu}{5(\lambda+2\mu)}\rho gr-\frac{(2\lambda+3\mu)}{5}A_1r-\frac{(\lambda+3\mu)}{r^2}A_1'+\frac{2\mu}{r}C_1+\frac{2\mu}{r^4}C_1'\right]\frac{\partial^2 P_1(\cos\theta)}{\partial\theta^2}$$

$$+\left[-\frac{(5\lambda+7\mu)}{21}A_2r^2-\frac{\mu}{3}\frac{A_2'}{r^2}+2\mu C_2+\frac{2\mu}{r^5}C_2'\right]\frac{\partial^2 P_2(\cos\theta)}{\partial\theta^2}$$

$$+\left[\frac{2\mu}{15(\lambda+2\mu)}\rho gr-\frac{(3\lambda+4\mu)}{18}A_3r^3+\frac{(\lambda-\mu)}{15r^4}A_3'\right.$$

$$\left.+2\mu C_3r+\frac{2\mu}{r^6}C_3'\right]\frac{\partial^2 P_3(\cos\theta)}{\partial\theta^2},\ (19)$$

$$\widehat{\phi\phi}=\left[\left(\lambda+\frac{2\mu}{3}\right)A_0+\frac{(2\lambda+3\mu)}{r}A_0'-\frac{2\mu}{r^3}C_0'\right]P_0(\cos\theta)$$

$$+\left[\frac{(5\lambda+3\mu)}{5(\lambda+2\mu)}\rho gr+\frac{(4\lambda+\mu)}{5}A_1r-\frac{(\lambda+4\mu)}{r^2}A_1'+\frac{2\mu}{r}C_1-\frac{4\mu}{r^4}C_1'\right]P_1(\cos\theta)$$

$$+\left[\frac{5}{7}\lambda A_2r^2-\frac{5\mu}{3r^3}A_2'+4\mu C_2-\frac{6\mu}{r^5}C_2'\right]P_2(\cos\theta)$$

$$+\left[\frac{2}{5}\frac{\mu\rho gr}{(\lambda+2\mu)}+\frac{(6\lambda-\mu)}{9}A_3r^3+\frac{(\lambda-6\mu)}{5r^4}A_3'+6\mu C_3r-\frac{8\mu}{r^6}C_3'\right]P_3(\cos\theta)$$

$$+\left[\frac{\mu\rho gr}{5(\lambda+2\mu)}-\frac{(2\lambda+3\mu)}{5}A_1r-\frac{(\lambda+3\mu)}{r^2}A_1'\right.$$

$$\left.+\frac{2\mu}{r}C_1+\frac{2\mu}{r^4}C_1'\right]\cot\theta\frac{\partial P_1(\cos\theta)}{\partial\theta}$$

$$+\left[-\frac{(5\lambda+7\mu)}{21}A_2r^2-\frac{\mu}{3r^3}A_2'+2\mu C_2+\frac{2\mu}{r^5}C_2'\right]\cot\theta\frac{\partial P_2(\cos\theta)}{\partial\theta}$$

$$+\left[\frac{2}{15}\frac{\mu\rho gr}{(\lambda+2\mu)}-\frac{(3\lambda+4\mu)}{18}A_3r^3+\frac{(\lambda-\mu)}{15r^4}A_3'\right.$$

$$\left.+2\mu C_3r+\frac{2\mu}{r^6}C_3'\right]\cot\theta\frac{\partial P_3(\cos\theta)}{\partial\theta},\ \ldots\ (20)$$

$$\widehat{r\theta}=\left[\frac{2}{5}\frac{\mu\rho gr}{(\lambda+2\mu)}-\frac{(3\lambda+2\mu)}{10}A_1r+\frac{\mu A_1'}{r^2}-\frac{6\mu}{r^4}C_1'\right]\frac{\partial P_1(\cos\theta)}{\partial\theta}$$

$$+\left[-\frac{(8\lambda+7\mu)}{21}A_2r^2-\frac{8\mu}{r^5}C_2'-\frac{(3\lambda+2\mu)}{6r^3}A_2'+2C_2\mu\right]\frac{\partial P_2(\cos\theta)}{\partial\theta}$$

$$+\left[\frac{4}{15}\frac{\mu\rho g r}{(\lambda+2\mu)}-\frac{(15\lambda+14\mu)}{36}A_3 r^3-\frac{(8\lambda+7\mu)}{15}\frac{A_3'}{r^4}\right.$$

$$\left.+4\mu C_3 r-\frac{10\mu}{r^6}C_3'\right]\frac{\partial P_3(\cos\theta)}{\partial\theta}. \quad \ldots\ldots(21)$$

The general expressions of the components of stresses thus obtained satisfy, of course, the equations of equilibrium of the elastic body under the gravitating field expressed by (1).

Using these general expressions of displacement and traction, we shall study the problem on the effect of an internal spherical cavity on the stresses of the gravitating semi-infinite elastic solid.

Next referring to Fig. 1, we have the following expressions of the components of displacement and stress which are the solutions of the gravitating semi-infinite elastic solid having no cavity in its interior:

$$u'=v'=0, \quad w'=\frac{\rho g}{2(\lambda+2\mu)}(z_0-z)^2, \quad \ldots\ldots\ldots\ldots(22)$$

$$\left.\begin{aligned}\widehat{xx}=\widehat{yy}&=-\frac{\lambda}{\lambda+2\mu}\rho g(z_0-z),\\ \widehat{zz}&=-\rho g(z_0-z),\\ \widehat{xy}=\widehat{yz}&=\widehat{zx}=0.\end{aligned}\right\} \quad \ldots\ldots\ldots\ldots(23)$$

These expressions satisfy, of course, the following conditions: the normal and the tangential components of stress $\widehat{zz}$, $\widehat{yz}$, and $\widehat{zx}$ vanish at the free surface $z=z_0$, and the stress at any point in the gravitating solid increases according to the increase of the position from the upper surface of the solid.

When we transform the components of displacement and stress expressed by (22), (23) into the components of displacement and stress in the polar coordinates (r, θ, ϕ), we have the following forms of them:

$$\left.\begin{aligned}u=&-\frac{\rho g z_0}{2(\lambda+2\mu)}r+\left[\frac{\rho g z_0^2}{2(\lambda+2\mu)}+\frac{3\rho g r^2}{8(\lambda+2\mu)}\right]\cos\theta\\ &-\frac{\rho g z_0 r}{2(\lambda+2\mu)}\cos 2\theta+\frac{\rho g r^2}{8(\lambda+2\mu)}\cos 3\theta,\\ v=&-\left[\frac{\rho g z_0^2}{2(\lambda+2\mu)}+\frac{\rho g r^2}{8(\lambda+2\mu)}\right]\sin\theta+\frac{\rho g z_0 r}{2(\lambda+2\mu)}\sin 2\theta\\ &-\frac{\rho g r^2}{8(\lambda+2\mu)}\sin 3\theta,\end{aligned}\right\} \quad \ldots.(24)$$

$$\left.\begin{aligned}
\widehat{rr} &= -\frac{(\lambda+\mu)}{(\lambda+2\mu)}\rho g z_0 + \frac{(2\lambda+3\mu)}{2(\lambda+2\mu)}\rho g r\cos\theta \\
&\quad -\frac{\mu}{(\lambda+2\mu)}\rho g z_0\cos 2\theta + \frac{\mu}{2(\lambda+2\mu)}\rho g r\cos 3\theta, \\
\widehat{\theta\theta} &= -\frac{(\lambda+\mu)}{(\lambda+2\mu)}\rho g z_0 + \frac{(2\lambda+\mu)}{2(\lambda+2\mu)}\rho g r\cos\theta \\
&\quad +\frac{\mu}{(\lambda+2\mu)}\rho g z_0\cos 2\theta - \frac{\mu}{2(\lambda+2\mu)}\rho g r\cos 3\theta, \\
\widehat{\phi\phi} &= -\frac{\lambda}{(\lambda+2\mu)}\rho g z_0 + \frac{\lambda}{(\lambda+2\mu)}\rho g r\cos\theta, \\
\widehat{r\theta} &= -\frac{\mu}{2(\lambda+2\mu)}\rho g r\sin\theta + \frac{\mu}{(\lambda+2\mu)}\rho g z_0\sin 2\theta \\
&\quad -\frac{\mu}{2(\lambda+2\mu)}\rho g r\sin 3\theta.
\end{aligned}\right\} \quad \ldots\ldots (25)$$

The expressions (24), (25) are favourable to the study of the equilibrium of the gravitating semi-infinite solid containing no cavity as we have previously stated.

Now, the boundary conditions of the present problem are as follows:

1. The surface of the spherical cavity is free from traction.

2. The displacement and the stress at the whole space far from the spherical cavity in the solid are equal to the ones expressed by (24) and (25).

These are denoted by

$$r=a;\quad \widehat{rr}=0,\quad \widehat{r\theta}=0. \quad \ldots\ldots\ldots\ldots\ldots\ldots (26)$$

$$r=\infty;\quad u=u \text{ expressed by (24)},$$

$$\left.\begin{aligned}
v&=v \quad ,, \quad ,, \quad ,, \\
\widehat{rr}&=\widehat{rr} \quad ,, \quad ,, \quad (25), \\
\widehat{\theta\theta}&=\widehat{\theta\theta} \quad ,, \quad ,, \quad ,, \\
\widehat{\phi\phi}&=\widehat{\phi\phi} \quad ,, \quad ,, \quad ,,
\end{aligned}\right\} \quad \ldots\ldots\ldots (27)$$

$$\widehat{r\theta}=\widehat{r\theta} \quad ,, \quad ,, \quad ,,$$

Using the expressions of displacement (11), (12), (13), (14), (15), (16) and that of stress (18), (19), (20), (21) which are the general solutions of the equation of the equilibrium (1) or (3), and also the conditions (26) and (27), we find the following values of the arbitrary constants:

From (26);

$$\left.\begin{aligned} &A_0'=0, \quad A_1=A_2=A_3=C_3=0, \\ &A_0=-\frac{\rho g z_0}{(\lambda+2\mu)}, \quad C_1=\frac{\rho g z_0^2}{2(\lambda+2\mu)}, \quad C_2=-\frac{\rho g z_0}{2(\lambda+2\mu)}. \end{aligned}\right\} \cdots (28)$$

From (26);

$$\left.\begin{aligned} &A_2'=\frac{20\mu\,\rho g z_0 a^3}{(\lambda+2\mu)(9\lambda+14\mu)}, \quad C_0'=\frac{(3\lambda+2\mu)\rho g z_0 a^3}{12\mu(\lambda+2\mu)}, \\ &C_1'=\frac{\rho g a^5}{90(\lambda+2\mu)}, \quad A_1'=-\frac{\rho g a^3}{3(\lambda+2\mu)}, \\ &C_2'=-\frac{2(\lambda+\mu)\rho g z_0 a^5}{(\lambda+2\mu)(9\lambda+14\mu)}, \quad C_3'=\frac{2\rho g(\lambda+\mu)a^7}{(\lambda+2\mu)(19\lambda+26\mu)}, \\ &A_3'=-\frac{28\mu\rho g a^5}{(\lambda+2\mu)(19\lambda+26\mu)}. \end{aligned}\right\} \cdots (29)$$

Substituting these values (28), (29) for C_2', A_3', C_3', A_1', C_1', C_0', A'_0, C_1, C_2, A_0, A_1, A_2, A_3, C_3, A_2', in the expressions (11), (12), (13), (14), (15), (16), (18), (19), (20), (21), we obtain the final results which are favourable to the present study as follows:

$$\begin{aligned} u=&-\left[\frac{\rho g z_0 r}{3(\lambda+2\mu)}+\frac{(3\lambda+2\mu)\rho g z_0 a^3}{12\mu(\lambda+2\mu)r^2}\right]P_0(\cos\theta) \\ &+\left[\frac{3}{10}\frac{\rho g r^2}{(\lambda+2\mu)}+\frac{\rho g a^3}{3\mu r}+\frac{\rho g z_0^2}{2(\lambda+2\mu)}-\frac{2\rho g a^5}{90(\lambda+2\mu)r^3}\right]P_1(\cos\theta) \\ &-\left[\frac{10(3\lambda+5\mu)\rho g z_0 a^3}{3(\lambda+2\mu)(9\lambda+14\mu)r^2}+\frac{2\rho g z_0 r}{3(\lambda+2\mu)}-\frac{6(\lambda+\mu)\rho g z_0 a^5}{(\lambda+2\mu)(9\lambda+14\mu)r^4}\right]P_2(\cos\theta) \\ &+\left[\frac{1}{5}\frac{\rho g r^3}{(\lambda+2\mu)}+\frac{28\rho g(2\lambda+3\mu)a^5}{5(\lambda+2\mu)(19\lambda+26\mu)r^3}-\frac{8(\lambda+\mu)\rho g a^7}{(\lambda+2\mu)(19\lambda+26\mu)r^5}\right]P_3(\cos\theta), \end{aligned}$$

$$\cdots\cdots\cdots\cdots (30)$$

$$\begin{aligned} v=&\left[\frac{1}{10}\frac{\rho g r^2}{(\lambda+2\mu)}+\frac{(\lambda+3\mu)\rho g a^3}{6\mu(\lambda+2\mu)r}+\frac{\rho g z_0^2}{2(\lambda+2\mu)}+\frac{\rho g a^5}{90(\lambda+2\mu)r^3}\right]\frac{\partial P_1(\cos\theta)}{\partial\theta} \\ &-\left[\frac{10\mu\rho g z_0 a^3}{3(\lambda+2\mu)(9\lambda+14\mu)r^2}+\frac{\rho g z_0 r}{3(\lambda+2\mu)}+\frac{2(\lambda+\mu)\rho g z_0 a^5}{(\lambda+2\mu)(9\lambda+14\mu)r^4}\right]\frac{\partial P_2(\cos\theta)}{\partial\theta} \\ &+\left[\frac{\rho g r^2}{15(\lambda+2\mu)}+\frac{14(-\lambda+\mu)\rho g a^5}{15(\lambda+2\mu)(19\lambda+26\mu)r^3}\right. \\ &\left.\qquad+\frac{2(\lambda+\mu)\rho g a^7}{(\lambda+2\mu)(19\lambda+26\mu)r^5}\right]\frac{\partial P_3(\cos\theta)}{\partial\theta}, \quad \cdots (31) \end{aligned}$$

$$\widehat{rr}=\left[-\frac{(3\lambda+2\mu)}{3(\lambda+2\mu)}\rho g z_0+\frac{(3\lambda+2\mu)\rho g z_0 a^3}{3(\lambda+2\mu)r^3}\right]P_0(\cos\theta)$$

$$+\left[\frac{(5\lambda+6\mu)\rho gr}{5(\lambda+2\mu)}-\frac{(3\lambda+4\mu)\rho ga^3}{3(\lambda+2\mu)r^2}+\frac{2\mu\rho ga^5}{15(\lambda+2\mu)r^4}\right]P_1(\cos\theta)$$

$$+\left[-\frac{4\mu\rho gz_0}{3(\lambda+2\mu)}+\frac{20\mu(9\lambda+10\mu)\rho gz_0a^3}{3(\lambda+2\mu)(9\lambda+14\mu)r^3}-\frac{48\mu(\lambda+\mu)\rho gz_0a^5}{(\lambda+2\mu)(9\lambda+14\mu)r^5}\right]P_2(\cos\theta)$$

$$+\left[\frac{4\mu\rho gr}{5(\lambda+2\mu)}-\frac{28\mu(17\lambda+18\mu)\rho ga^5}{5(\lambda+2\mu)(19\lambda+26\mu)r^4}+\frac{80\mu(\lambda+\mu)\rho ga^7}{(\lambda+2\mu)(19\lambda+26\mu)r^6}\right]P_3(\cos\theta), \qquad \ldots\ldots\ldots\ldots(32)$$

$$\widehat{\theta\theta}=-\left[\frac{(3\lambda+2\mu)}{3(\lambda+2\mu)}\rho gz_0+\frac{(3\lambda+2\mu)\rho gz_0a^3}{6(\lambda+2\mu)r^3}\right]P_0(\cos\theta)$$

$$+\left[\frac{(5\lambda+3\mu)}{5(\lambda+2\mu)}\rho gr+\frac{\mu\rho gz_0^2}{(\lambda+2\mu)r}+\frac{(\lambda+4\mu)\rho ga^3}{3(\lambda+2\mu)r^2}-\frac{4\mu\rho ga^5}{90(\lambda+2\mu)r^4}\right]P_1(\cos\theta)$$

$$-\left[\frac{4\mu\rho gz_0}{3(\lambda+2\mu)}+\frac{100\mu^2\rho gz_0a^3}{3(\lambda+2\mu)(9\lambda+14\mu)r^3}-\frac{12\mu(\lambda+\mu)\rho gz_0a^5}{(\lambda+2\mu)(9\lambda+14\mu)r^5}\right]P_2(\cos\theta)$$

$$+\left[\frac{2\mu\rho gr}{5(\lambda+2\mu)}-\frac{28\mu(\lambda-6\mu)\rho ga^5}{5(\lambda+2\mu)(19\lambda+26\mu)r^4}-\frac{16\mu(\lambda+\mu)\rho ga^7}{(\lambda+2\mu)(19\lambda+26\mu)r^6}\right]P_3(\cos\theta)$$

$$+\left[\frac{\mu\rho gr}{5(\lambda+2\mu)}+\frac{\mu\rho gz_0^2}{(\lambda+2\mu)r}+\frac{(\lambda+3\mu)\rho ga^3}{3(\lambda+2\mu)r^2}+\frac{2\mu\rho ga^5}{90(\lambda+2\mu)r^4}\right]\frac{\partial^2P_1(\cos\theta)}{\partial\theta^2}$$

$$-\left[\frac{2\mu\rho gz_0}{3(\lambda+2\mu)}+\frac{20\mu^2\rho gz_0a^3}{3(\lambda+2\mu)(9\lambda+14\mu)r^3}+\frac{4\mu(\lambda+\mu)\rho gz_0a^5}{(\lambda+2\mu)(9\lambda+14\mu)r^5}\right]\frac{\partial^2P_2(\cos\theta)}{\partial\theta^2}$$

$$+\left[\frac{2\mu\rho gr}{15(\lambda+2\mu)}-\frac{28\mu(\lambda-\mu)\rho ga^5}{15(\lambda+2\mu)(19\lambda+26\mu)r^4}+\frac{4\mu(\lambda+\mu)\rho ga^7}{(\lambda+2\mu)(19\lambda+26\mu)r^6}\right]\frac{\partial^2P_3(\cos\theta)}{\partial\theta^2}, \qquad \ldots\ldots(33)$$

$$\widehat{\phi\phi}=-\left[\frac{(3\lambda+2\mu)\rho gz_0}{3(\lambda+2\mu)}+\frac{(3\lambda+2\mu)\rho gz_0a^3}{6(\lambda+2\mu)r^3}\right]P_0(\cos\theta)$$

$$+\left[\frac{(5\lambda+3\mu)}{5(\lambda+2\mu)}\rho gr+\frac{\mu\rho gz_0^2}{(\lambda+2\mu)r}+\frac{(\lambda+4\mu)\rho ga^3}{3(\lambda+2\mu)r^2}\right]P_1(\cos\theta)$$

$$-\left[\frac{4\mu\rho gz_0}{3(\lambda+2\mu)}+\frac{100\mu^2\rho gz_0a^3}{3(\lambda+2\mu)(9\lambda+14\mu)r^3}-\frac{12\mu(\lambda+\mu)\rho gz_0a^5}{(\lambda+2\mu)(9\lambda+14\mu)r^5}\right]P_2(\cos\theta)$$

$$+\left[\frac{2\mu\rho gr}{5(\lambda+2\mu)}-\frac{28\mu(\lambda-6\mu)\rho ga^5}{5(\lambda+2\mu)(19\lambda+26\mu)r^4}-\frac{16\mu(\lambda+\mu)\rho ga^7}{(\lambda+2\mu)(19\lambda+26\mu)r^6}\right]P_3(\cos\theta)$$

$$+\left[\frac{\mu\rho gr}{5(\lambda+2\mu)}+\frac{\mu\rho gz_0^2}{(\lambda+2\mu)r}+\frac{(\lambda+3\mu)\rho ga^3}{3(\lambda+2\mu)r^2}+\frac{2\mu\rho ga^5}{90(\lambda+2\mu)r^4}\right]\cot\theta\frac{\partial P_1(\cos\theta)}{\partial\theta}$$

$$-\left[\frac{2\mu\rho gz_0}{3(\lambda+2\mu)}+\frac{20\mu^2\rho gz_0a^3}{3(\lambda+2\mu)(9\lambda+14\mu)r^3}+\frac{4\mu(\lambda+\mu)\rho gz_0a^5}{(\lambda+2\mu)(9\lambda+14\mu)r^5}\right]\cot\theta\frac{\partial P_2(\cos\theta)}{\partial\theta}$$

$$+\left[\frac{2\mu\rho gr}{15(\lambda+2\mu)}-\frac{28\mu(\lambda-\mu)\rho ga^5}{15(\lambda+2\mu)(19\lambda+26\mu)r^4}+\frac{4\mu(\lambda+\mu)\rho ga^7}{(\lambda+2\mu)(19\lambda+26\mu)r^6}\right]\cot\theta\frac{\partial P_3(\cos\theta)}{\partial\theta}, \quad \ldots(34)$$

$$\widehat{r\theta}=-\left[\frac{\mu\rho ga^3}{3(\lambda+2\mu)r^2}+\frac{6\mu\rho ga^5}{90(\lambda+2\mu)r^4}-\frac{2\mu\rho gr}{5(\lambda+2\mu)}\right]\frac{\partial P_1(\cos\theta)}{\partial\theta}$$
$$-\left[\frac{2\mu\rho gz_0}{3(\lambda+2\mu)}+\frac{10\mu(3\lambda+2\mu)\rho gz_0a^3}{3(\lambda+2\mu)(9\lambda+14\mu)r^3}-\frac{16\mu(\lambda+\mu)\rho gz_0a^5}{(\lambda+2\mu)(9\lambda+14\mu)r^5}\right]\frac{\partial P_2(\cos\theta)}{\partial\theta}$$
$$+\left[\frac{4\mu\rho gr}{15(\lambda+2\mu)}+\frac{28\mu(8\lambda+7\mu)\rho ga^5}{15(\lambda+2\mu)(19\lambda+26\mu)r^4}-\frac{20\mu(\lambda+\mu)\rho ga^7}{(\lambda+2\mu)(19\lambda+26\mu)r^6}\right]\frac{\partial P_3(\cos\theta)}{\partial\theta}. \quad \ldots(35)$$

Now we now the relations such that

$$\left.\begin{aligned}&P_0(\cos\theta)=1,\quad P_1(\cos\theta)=\cos\theta,\quad P_2(\cos\theta)=\frac{3}{4}\cos 2\theta+\frac{1}{4},\\&P_3(\cos\theta)=\left(\frac{5}{8}\cos 3\theta+\frac{3}{8}\cos\theta\right).\end{aligned}\right\} \quad (36)$$

Using these formulae, we rewrite the final solutions (30), (31), (32), (33), (34), (35) in the following forms which are more or less convenient for the study of the natures of the equilibrium in the interior of the solid :

$$u=-\frac{\rho gz_0}{2(\lambda+2\mu)}r-\frac{(9\lambda^2+30\lambda\mu+26\mu^2)\rho gz_0a^3}{4\mu(\lambda+2\mu)(9\lambda+14\mu)r^2}+\frac{3(\lambda+\mu)\rho gz_0a^5}{2(\lambda+2\mu)(9\lambda+14\mu)r^4}$$
$$+\left[\frac{\rho gz_0^2}{2(\lambda+2\mu)}+\frac{3\rho gr^2}{8(\lambda+2\mu)}+\frac{\rho ga^3}{3\mu r}+\frac{(68\lambda+103\mu)\rho ga^5}{18(\lambda+2\mu)(19\lambda+26\mu)r^3}-\frac{3(\lambda+\mu)\rho ga^7}{(\lambda+2\mu)(19\lambda+26\mu)r^5}\right]\cos\theta$$
$$+\left[-\frac{\rho gz_0}{2(\lambda+2\mu)}r-\frac{5(3\lambda+5\mu)\rho gz_0a^3}{2(\lambda+2\mu)(9\lambda+14\mu)r^2}+\frac{9(\lambda+\mu)\rho gz_0a^5}{2(\lambda+2\mu)(9\lambda+14\mu)r^4}\right]\cos 2\theta$$
$$+\left[\frac{\rho gr^2}{8(\lambda+2\mu)}+\frac{7(2\lambda+3\mu)\rho ga^5}{2(\lambda+2\mu)(19\lambda+26\mu)r^3}-\frac{5(\lambda+\mu)\rho ga^7}{(\lambda+2\mu)(19\lambda+26\mu)r^5}\right]\cos 3\theta, \quad \ldots\ldots\ldots\ldots(37)$$

$$v=-\left[\frac{\rho gz_0^2}{2(\lambda+2\mu)}+\frac{\rho gr^2}{8(\lambda+2\mu)}+\frac{(\lambda+3\mu)\rho ga^3}{6\mu(\lambda+2\mu)r}+\frac{(-5\lambda+23\mu)\rho ga^5}{36(\lambda+2\mu)(19\lambda+26\mu)r^3}+\frac{3(\lambda+\mu)\rho ga^7}{4(\lambda+2\mu)(19\lambda+26\mu)r^5}\right]\sin\theta$$

$$+\left[\frac{\rho g z_0 r}{2(\lambda+2\mu)}+\frac{5\mu\rho g z_0 a^3}{(\lambda+2\mu)(9\lambda+14\mu)r^2}+\frac{3\rho g z_0 a^5}{(9\lambda+14\mu)r^4}\right]\sin 2\theta$$

$$-\left[\frac{\rho g r^2}{8(\lambda+2\mu)}+\frac{7(-\lambda+\mu)\rho g a^5}{4(\lambda+2\mu)(19\lambda+26\mu)r^3}+\frac{15(\lambda+\mu)\rho g a^7}{4(\lambda+2\mu)(19\lambda+26\mu)r^5}\right]\sin 3\theta, \quad \ldots\ldots\ldots\ldots(38)$$

$$\widehat{rr}=-\frac{(\lambda+\mu)}{(\lambda+2\mu)}\rho g z_0+\frac{(27\lambda^2+105\lambda\mu+78\mu^2)\rho g z_0 a^3}{3(\lambda+2\mu)(9\lambda+14\mu)r^3}-\frac{12\mu(\lambda+\mu)\rho g z_0 a^5}{(\lambda+2\mu)(9\lambda+14\mu)r^5}$$

$$+\left[\frac{(2\lambda+3\mu)\rho g r}{2(\lambda+2\mu)}-\frac{(3\lambda+4\mu)\rho g a^3}{3(\lambda+2\mu)r^2}-\frac{\mu(199\lambda+206\mu)\rho g a^5}{6(\lambda+2\mu)(19\lambda+26\mu)r^4}\right.$$

$$\left.+\frac{30\mu(\lambda+\mu)\rho g a^7}{(\lambda+2\mu)(19\lambda+26\mu)r^6}\right]\cos\theta-\left[\frac{\mu\rho g z_0}{(\lambda+2\mu)}-\frac{5\mu(9\lambda+10\mu)\rho g z_0 a^3}{(\lambda+2\mu)(9\lambda+14\mu)r^3}\right.$$

$$\left.+\frac{36\mu(\lambda+\mu)\rho g z_0 a^5}{(\lambda+2\mu)(9\lambda+14\mu)r^5}\right]\cos 2\theta+\left[\frac{\mu}{2(\lambda+2\mu)}\rho g r-\frac{7\mu(17\lambda+18\mu)\rho g a^5}{2(\lambda+2\mu)(19\lambda+26\mu)r^4}\right.$$

$$\left.+\frac{50\mu(\lambda+\mu)\rho g a^7}{(\lambda+2\mu)(19\lambda+26\mu)r^6}\right]\cos 3\theta, \quad \ldots\ldots\ldots\ldots(39)$$

$$\widehat{\theta\theta}=-\frac{(\lambda+\mu)\rho g z_0}{(\lambda+2\mu)}-\frac{(9\lambda^2+20\lambda\mu+26\mu^2)\rho g z_0 a^3}{2(\lambda+2\mu)(9\lambda+14\mu)r^3}+\frac{3\mu(\lambda+\mu)\rho g z_0 a^5}{(\lambda+2\mu)(9\lambda+14\mu)r^5}$$

$$+\left[\frac{(2\lambda+\mu)}{2(\lambda+2\mu)}\rho g r+\frac{\mu\rho g a^3}{3(\lambda+2\mu)r^2}-\frac{\mu(16\lambda-61\mu)\rho g a^5}{6(\lambda+2\mu)(19\lambda+26\mu)r^4}\right.$$

$$\left.-\frac{15\mu(\lambda+\mu)\rho g a^7}{2(\lambda+2\mu)(19\lambda+26\mu)r^6}\right]\cos\theta+\left[\frac{\mu}{(\lambda+2\mu)}\rho g z_0-\frac{5\mu^2\rho g z_0 a^3}{(\lambda+2\mu)(9\lambda+14\mu)r^3}\right.$$

$$\left.+\frac{21\mu(\lambda+\mu)\rho g z_0 a^5}{(\lambda+2\mu)(9\lambda+14\mu)r^5}\right]\cos 2\theta-\left[\frac{\mu\rho g r}{2(\lambda+2\mu)}+\frac{7\mu(2\lambda+3\mu)\rho g a^5}{(19\lambda+26\mu)r\,2(\lambda+2\mu)^4}\right.$$

$$\left.+\frac{65\mu(\lambda+\mu)\rho g a^7}{2(\lambda+2\mu)(19\lambda+26\mu)r^6}\right]\cos 3\theta, \quad \ldots\ldots\ldots\ldots(40)$$

$$\widehat{\phi\phi}=-\frac{\lambda}{(\lambda+2\mu)}\rho g z_0-\frac{(9\lambda^2+20\lambda\mu+6\mu^2)\rho g z_0 a^3}{2(\lambda+2\mu)(9\lambda+14\mu)r^3}+\frac{9\mu(\lambda+\mu)\rho g z_0 a^5}{(\lambda+2\mu)(9\lambda+14\mu)r^5}$$

$$+\left[\frac{\lambda}{(\lambda+2\mu)}\rho g r+\frac{\mu\rho g a^3}{3(\lambda+2\mu)r^2}+\frac{\mu(26\lambda+19\mu)\rho g a^5}{6(\lambda+2\mu)(19\lambda+26\mu)r^4}\right.$$

$$\left.-\frac{45\mu(\lambda+\mu)\rho g a^7}{2(\lambda+2\mu)(19\lambda+26\mu)r^6}\right]\cos\theta$$

$$+\left[-\frac{15\mu^2\rho g z_0 a^3}{(\lambda+2\mu)(9\lambda+14\mu)r^3}+\frac{15\mu(\lambda+\mu)\rho g z_0 a^5}{(\lambda+2\mu)(9\lambda+14\mu)r^5}\right]\cos 2\theta$$

$$+\left[\frac{35\mu^2\rho g a^5}{2(\lambda+2\mu)(19\lambda+26\mu)r^4}-\frac{35\mu(\lambda+\mu)\rho g a^7}{2(\lambda+2\mu)(19\lambda+26\mu)r^6}\right]\cos 3\theta, \quad \ldots .(41)$$

$$\widehat{r\theta}=\left[-\frac{\mu}{2(\lambda+2\mu)}\rho g r+\frac{\mu\rho g a^3}{3(\lambda+2\mu)r^2}-\frac{\mu(26\lambda+19\mu)\rho g a^5}{6(\lambda+2\mu)(19\lambda+26\mu)r^4}\right.$$

$$+\frac{15\mu(\lambda+\mu)\rho g a^7}{2(\lambda+2\mu)(19\lambda+26\mu)r^6}\Bigg]\sin\theta+\Bigg[\frac{\mu}{(\lambda+2\mu)}\rho g z_0+\frac{5\mu(3\lambda+2\mu)\rho g z_0 a^3}{(\lambda+2\mu)(9\lambda+14\mu)r^3}$$

$$-\frac{24\mu(\lambda+\mu)\rho g z_0 a^5}{(\lambda+2\mu)(9\lambda+14\mu)r^5}\Bigg]\sin 2\theta+\Bigg[-\frac{\mu}{2(\lambda+2\mu)}\rho g r-\frac{7\mu(8\lambda+7\mu)\rho g a^5}{2(\lambda+2\mu)(19\lambda+26\mu)r^4}$$

$$+\frac{75\mu(\lambda+\mu)\rho g a^7}{2(\lambda+2\mu)(19\lambda+26\mu)r^6}\Bigg]\sin 3\theta. \qquad\qquad (42)$$

These equations shew us the distributions of displacement and stress in the solid of two kinds: one of which is in a plane-symmetry with respect to the plane $\theta=\pi/2$, and the other is unsymmetrical about that plane. The former corresponds to the distributions of displacement and stress in a elastic solid having a spherical cavity due to the uniform compression $\rho g z_0$ at infinity, and the latter corresponds to the different distributions of displacement and stress.

For asertaining the distributions of displacement and stress in the solid, we take the following numerical example. In this example, we tentatively assume that $\lambda=\mu$, the poisson's ratio$=1/4$, and $a/z_0=1/5$. The units of displacement and stress are taken $\rho g z_0^2/5\mu$ and $\rho g z_0$ respectively. Under these assumptions, we have the six tables in which the displacement and stress corresponding to the values of r/a and θ are tabulated. (Table I, II, III, IV, V, VI.)

The values in these tables are also illustrated in six figures. (Fig. 2, 3, 4, 5, 6, 7.) The parameter of each curve in these figures is r/a, while the abscissa of the same figures is the angle of the colatitude θ and the ordinates of the curves represent the magnitude of components of displacement and stress of which the units are $\rho g z_0^2/5\mu$ and $\rho g z_0$ respectively.

From these figures it may be seen that the tractions in the solid are distributed symmetrically about the vertical axis ($\theta=0$) and unsymmetrically with respect to the plane $z=0$ passing the origin, and thus the tractions on the surface of the spherical cavity is largest on the circle of $r/a=1$, $\theta\fallingdotseq 100°$. It may also be seen that the component of stress $\widehat{\theta\theta}$, which is the compression on the surface of the cavity in this case, is larger than the other components of the stress on this surface. In this numerical examples, all the components of stress have the negative sign (compression), but in the other cases where z_0/a is small and the poisson's ratio is less than that of this example, the stress in some portions (at the regions of $\theta=0°$, $\theta=180°$) of spherical surface of the cavity has the positive sign (tension).

As we have discussed, $\widehat{\theta\theta}$ on the surface of the cavity is the important component of stress on the failure of the cavity. We shall study the properties of the component $\theta\theta_{r=a}$ in detail.

We write $\widehat{\theta\theta}$, when $\lambda=\mu$, on the surface of the cavity in the following form:

$$\widehat{\theta\theta}_{r/a=1}=-0{\cdot}979\,\rho g z_0+0{\cdot}444\rho g a\cos\theta$$
$$+0{\cdot}870\rho g z_0\cos 2\theta-0{\cdot}778\rho g a\cos 3\theta.\ \ldots\ldots\ldots(43)$$

Using this equation, we get the result as in the following table (Table VII) which gives us the magnitudes of $\theta\theta_{r=a}$in cases of $z_0/a=3, 5, 7, 9$, and 10, the unit of the magnitude of stress being taken $\rho g a$.

Table VII gives us the following two figures. (Fig. 8 and 9.) The unit of stress $\widehat{\theta\theta}_{r=a}$ in these figures is taken to be $\rho g a$.

Fig. 8 and 9 indicate us that the maximum magnitude of $\widehat{\theta\theta}_{r=a}$ occurs in the vicinity of $\theta=90°-100°$. Again, $\theta\theta_{r=a}$ increases linearly with the increase of depth of the centre of cavity from the upper surface of the elastic solid. The rate of increase of $\theta\theta_{r=a}$ with the depth, therefore, is maximum at $\theta=90°\sim100°$.

Table I.

(Magnitude of the component of displacement u. Unit$=\frac{\rho g z_0^2}{5\mu}$.)

θ \ r/a	1	2	3	4
0°	0·27	0·12	−0·13	−0·39
10°	0·27	0·12	−0·12	−0·37
20°	0·28	0·15	−0·09	−0·34
30°	0·29	0·16	−0·05	−0·29
45°	0·29	0·21	0·03	−0·17
60°	0·27	0·21	0·10	−0·04
70°	0·19	0·18	0·11	0·02
80°	0·09	0·12	0·09	0·04
90°	−0·03	0·01	0·01	0
100°	−0·20	−0·15	−0·14	−0·13
110°	−0·41	−0·36	−0·35	−0·35
120°	−0·64	−0·59	−0·62	−0·64
135°	−1·02	−1·04	−1·05	−1·20
150°	−1·33	−1·35	−1·54	−1·77
160°	−1·50	−1·53	−1·78	−2·07
170°	−1·60	−1·66	−1·94	−2·28
180°	−1·64	−1·70	−1·99	−2·35

Table II.

(Magnitude of the component of displacement v. Unit$=\frac{\rho g z_0^2}{5\mu}$.)

θ \ r/a	1	2	3	4
0°	0	0	0	0
10°	−0·04	−0·05	−0·02	0
20°	−0·08	−0·10	−0·05	−0·01
30°	−0·15	−0·17	−0·09	−0·03
45°	−0·27	−0·29	−0·19	−0·10
60°	−0·45	−0·46	−0·36	−0·26
70°	−0·59	−0·59	−0·50	−0·42
80°	−0·73	−0·73	−0·67	−0·62
90°	−0·87	−0·86	−0·85	−0·85
100°	−0·99	−0·98	−1·02	−1·08
110°	−1·07	−1·05	−1·16	−1·29
120°	−1·09	−1·08	−1·23	−1·43
135°	−1·01	−1·01	−1·21	−1·45
150°	−0·78	−0·79	−0·98	−1·20
160°	−0·56	−0·56	−0·71	−0·88
170°	−0·29	−0·29	−0·37	−0·46
180°	0	0	0	0

Table III.

(Magnitude of the component of stress $\widehat{rr}$. Unit $=\rho g z_0$.)

θ \ r/a	1	2	3	4
0°	0	−0·40	−0·33	−0·17
10°	0	−0·40	−0·34	−0·18
20°	0	−0·40	−0·35	−0·21
30°	0	−0·40	−0·36	−0·24
45°	0	−0·39	−0·36	−0·28
60°	0	−0·37	−0·34	−0·30
70°	0	−0·35	−0·33	−0·30
80°	0	−0·35	−0·33	−0·31
90°	0	−0·36	−0·35	−0·34
100°	0	−0·39	−0·40	−0·41
110°	0	−0·45	−0·49	−0·53
120°	0	−0·54	−0·63	−0·69
135°	0	−0·72	−0·90	−1·02
150°	0	−0·87	−1·19	−1·38
160°	0	−0·97	−1·35	−1·57
170°	0	−1·05	−1·46	−1·70
180°	0	−1·08	−1·50	−1·75

Table IV.

(Magnitude of the component of stress $\widehat{\theta\theta}$. Unit $=\rho g z_0$.)

θ \ r/a	1	2	3	4
0°	−0·17	−0·23	−0·15	−0·07
10°	−0·21	−0·25	−0·16	−0·08
20°	−0·30	−0·29	−0·19	−0·11
30°	−0·47	−0·37	−0·26	−0·16
45°	−0·81	−0·52	−0·40	−0·30
60°	−1·21	−0·72	−0·60	−0·51
70°	−1·48	−0·85	−0·75	−0·68
80°	−1·71	−0·97	−0·89	−0·85
90°	−1·85	−1·06	−1·01	−1·00
100°	−1·89	−1·11	−1·10	−1·12
110°	−1·81	−1·11	−1·13	−1·18
120°	−1·61	−1·06	−1·10	−1·17
135°	−1·15	−0·91	−0·97	−1·05
150°	−0·62	−0·72	−0·78	−0·85
160°	−0·32	−0·61	−0·66	−0·73
170°	−0·11	−0·53	−0·58	−0·64
180°	−0·04	−0·51	−0·55	−0·61

Table V.

(Magnitude of the component of stress $\widehat{\phi\phi}$. Unit $=\rho g z_0$.)

θ \ r/a	1	2	3	4
0°	−0·10	−0·23	−0·15	−0·08
10°	−0·11	−0·23	−0·15	−0·08
20°	−0·14	−0·24	−0·16	−0·09
30°	−0·19	−0·25	−0·17	−0·11
45°	−0·28	−0·26	−0·20	−0·15
60°	−0·39	−0·28	−0·24	−0·20
70°	−0·46	−0·30	−0.27	−0·24
80°	−0·51	−0·32	−0·30	−0·29
90°	−0·54	−0·34	−0·34	−0·33
100°	−0·55	−0·37	−0·37	−0·38
110°	−0·53	−0·39	−0·40	−0·43
120°	−0·48	−0·42	−0·44	−0·47
135°	−0·37	−0·45	−0·48	−0·52
150°	−0·24	−0·48	−0·52	−0·57
160°	−0·18	−0·50	−0·53	−0·59
170°	−0·13	−0·51	−0·54	−0·60
180°	−0·11	−0·51	−0·55	−0·61

Table VI.

(Magnitude of the component of stress $\widehat{r\theta}$. Unit $=\rho g z_0$.)

θ \ r/a	1	2	3	4
0°	0	0	0	0
10°	0	0·08	0·05	0·03
20°	0	0·15	0·10	0·06
30°	0	0·21	0·15	0·10
45°	0	0·27	0·20	0·15
60°	0	0·26	0·21	0·18
70°	0	0·21	0·18	0·16
80°	0	0·12	0·11	0·10
90°	0	0·01	0	0
100°	0	−0·12	−0·13	−0·13
110°	0	−0·25	−0·26	−0·28
120°	0	−0·36	−0·38	−0·41
135°	0	−0·45	−0·48	−0·52
150°	0	−0·41	−0·45	−0·49
160°	0	−0·31	−0·34	−0·38
170°	0	−0·17	−0·18	−0·21
180°	0	0	0	0

Table VII. (The magnitude of $\widehat{\theta\theta}_{r=a}$. Unit$=\rho g a$.)

θ \ z_0/a	3	5	7	9	10
0°	−0·66	−0·88	− 1·10	− 1·32	− 1·42
10°	−0·72	−1·04	− 1·32	− 1·69	− 1·85
20°	−0·91	−1·54	− 2·16	− 2·78	− 3·09
30°	−1·25	−2·34	− 3·42	− 4·52	− 5·06
45°	−2·07	−4·03	− 6·00	− 7·95	− 8·93
60°	−3·24	−6·07	− 8·90	−11·72	−13·14
70°	−4·11	−7·40	−10·70	−13·99	−15·63
80°	−4·92	−8·52	−12·16	−15·71	−17·50
90°	−5·55	−9·25	−12·94	−16·64	−18·49
100°	−5·85	−9·45	−13·09	−16·64	−18·43
110°	−5·76	−9·05	−12·25	−15·64	−17·29
120°	−5·24	−8·07	−10·90	−13·72	−15·14
135°	−3·80	−5·76	− 7·72	− 9·68	−10·65
150°	−2·02	−3·11	− 4·19	− 5·29	− 5·82
160°	−0·97	−1·59	− 2·21	− 2·84	− 3·15
170°	−0·25	−0·57	− 0·84	− 1·21	− 1·38
180°	−0·01	−0·21	− 0·43	− 0·65	− 0·76

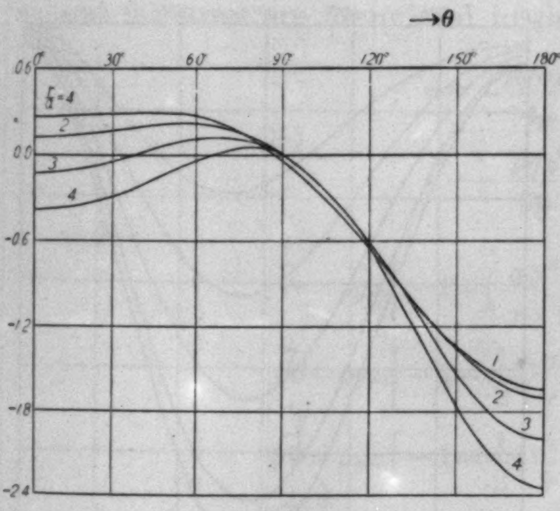

Fig. 2.

[Magnitude of u, $\lambda=\mu$, $\frac{a}{z_0}=\frac{1}{5}$, unit$=\frac{\rho g z_0^2}{5\mu}$.]

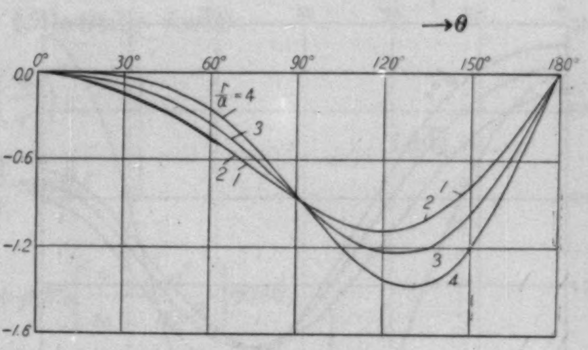

Fig. 3.

[Magnitude of v, $\lambda=\mu$, $\frac{a}{z_0}=\frac{1}{5}$, unit$=\frac{\rho g z_0^2}{5\mu}$.]

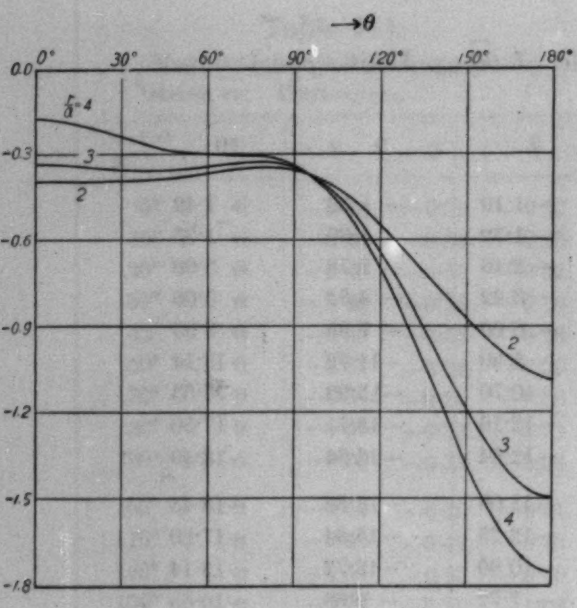

Fig. 4.

[Magnitude of $\widehat{rr}$, $\lambda=\mu$, $\frac{a}{z_0}=\frac{1}{z_0}$, unit$=\rho g z_0$.]

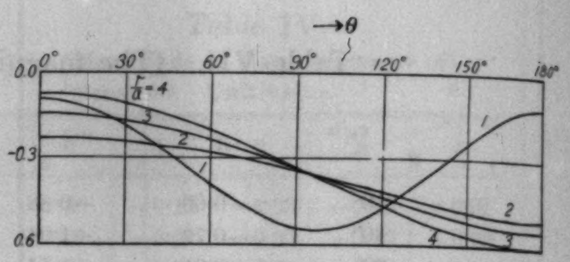

Fig. 6.

[Magnitude of $\widehat{\phi\phi}$, $\lambda=\mu$, $\frac{a}{z_0}=\frac{1}{5}$, unit$=\rho g z_0$.]

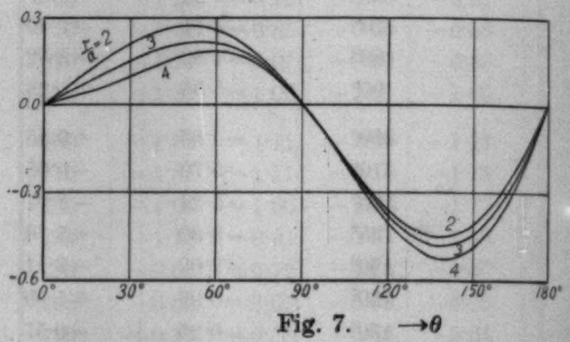

Fig. 7.

[Magnitude of $\widehat{r\theta}$, $\lambda=\mu$, $\frac{a}{z_0}=\frac{1}{5}$, unit$=\rho g z_0$.]

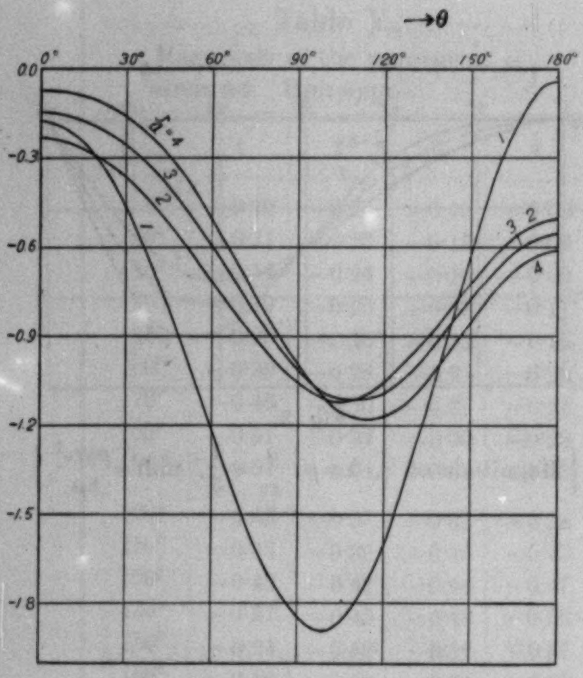

Fig. 5.

[Magnitude of $\widehat{\theta\theta}$, $\lambda=\mu$, $\frac{a}{z_0}=\frac{1}{5}$, unit$=\rho g z_0$.]

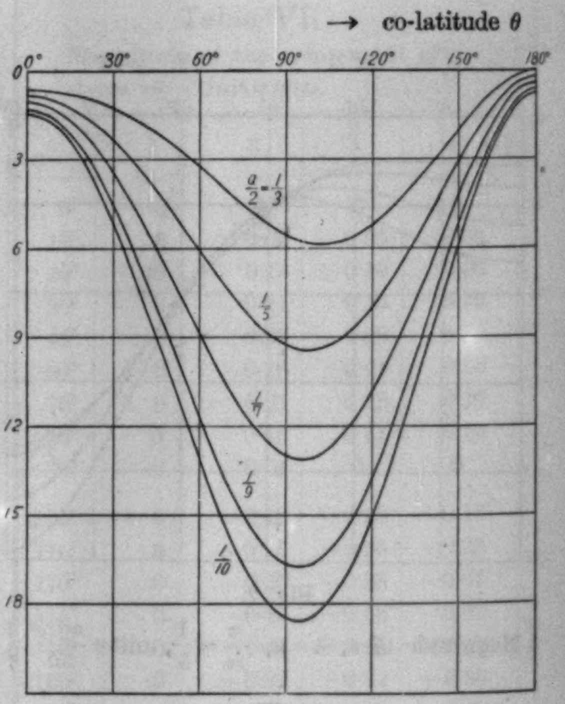

Fig. 8.

[Magnitude of $\widehat{\theta\theta}_{r=a}$, $\lambda=\mu$, unit$=\rho g a$.]

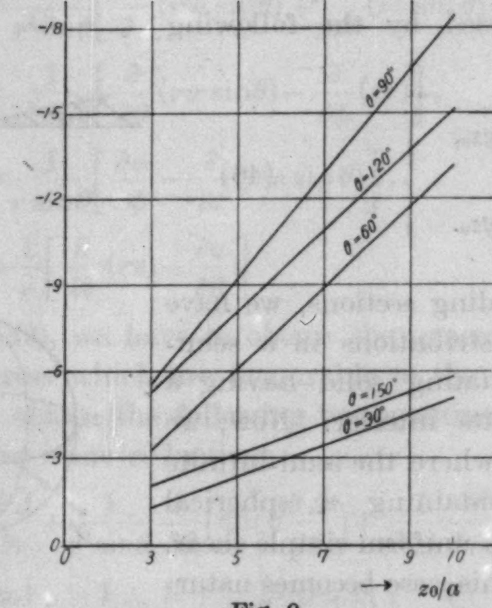

Fig. 9.

[Magnitude of $\widehat{\theta\theta}_{r=a}$, $\lambda=\mu$.
Unit$=\rho g a$.]

3. When the gravitating solid is incompressible, the displacement and the stress are formulated in the following forms:

$$\left.\begin{aligned} u&=-\frac{\rho g a z_0}{4\mu}\left(\frac{a}{r}\right)^2, \\ v&=-\frac{\rho g a^3}{6\mu}\frac{1}{r}\sin\theta, \end{aligned}\right\} \quad \cdots\cdots\cdots(44)$$

and

$$\left.\begin{aligned} \widehat{rr}&=\rho g z_0\left[-1+\left(\frac{a}{r}\right)^3\right]+\rho g z_0\left[\frac{r}{z_0}-\frac{a^3}{z_0 r^2}\right]\cos\theta, \\ \widehat{\theta\theta}&=\rho g z_0\left[-1-\frac{1}{2}\left(\frac{a}{r}\right)^3\right]+\rho g r\cos\theta, \\ \widehat{\phi\phi}&=\rho g z_0\left[-1-\frac{1}{2}\left(\frac{a}{r}\right)^3\right]+\rho g r\cos\theta, \\ \widehat{r\theta}&=0. \end{aligned}\right\} \quad ..(45)$$

It can be seen from the equations (45) that when the gravitating solid is incompressible, the interior of solid is maintained in hydrostatic pressure. The stress on the surface of cavity is compressive, and when the depth of the centre of cavity from the top surface of solid is very

deep, and $a \ll z_0$, the stress components on the surface of cavity are approximately expressed by the following equations:

$$\left.\begin{aligned} \widehat{\theta\theta}_{r=a} &= -\frac{3}{2}\rho g z_0, \\ \widehat{\phi\phi}_{r=a} &= -\frac{3}{2}\rho g z_0. \end{aligned}\right\} \qquad \text{........(46)}$$

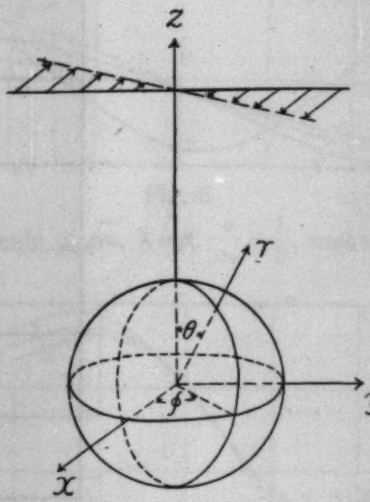

Fig. 10.

4. In the preceding sections, we have studied the stress distributions in a semi-infinite elastic gravitating solid having a spherical cavity in its interior. Now, we shall study the case where the semi-infinite gravitating solid containing a spherical cavity is subjected to a uniform simple shear. As the problem in this case becomes naturally free from gravitating body force, it is sufficient to study the case where the body is strained by the uniform shear. We can obtain the problem of the acutual case by superposing the results thus obtained on those of the preceding sections.

Referring to Fig. 10, we assume that the solid having a spherical cavity of radius a is subjected to a uniform simple shear:[4)]

$$\widehat{xy} = S. \qquad \text{.......................(47)}$$

The equations of equilibrium of elastic solid referring to spherical coordinates are as follows:

$$\left.\begin{aligned} &(\lambda+2\mu)\frac{\partial \Delta}{\partial r} - \frac{2\mu}{r\sin\theta}\frac{\partial(\sin\theta\,\varpi_\phi)}{\partial\theta} + \frac{2\mu}{r\sin\theta}\frac{\partial\varpi_\theta}{\partial\phi} = 0, \\ &(\lambda+2\mu)\frac{1}{r}\frac{\partial \Delta}{\partial\theta} - \frac{2\mu}{r\sin\theta}\frac{\partial\varpi_r}{\partial\phi} + \frac{2\mu}{r}\frac{\partial(r\varpi_\phi)}{\partial r} = 0, \\ &(\lambda+2\mu)\frac{1}{r\sin\theta}\frac{\partial \Delta}{\partial\phi} - \frac{2\mu}{r}\frac{\partial(r\varpi_\theta)}{\partial r} + \frac{2\mu}{r}\frac{\partial\varpi_r}{\partial\theta} = 0, \end{aligned}\right\} \quad \text{....(48)}$$

where

4) Professor Love studied the same problem, using the rectangular coordinates, yet I have fully studied the problem in spherical coordinates in order to get the solutions congruent with that of the preceding sections. LOVE, *The mathematical theory of Elasticity*, 4th ed., 252.

$$\left.\begin{aligned} \varDelta &= \frac{1}{r^2\sin\theta}\left[\frac{\partial}{\partial r}(r^2 u\sin\theta)+\frac{\partial}{\partial\theta}(rv\sin\theta)+\frac{\partial}{\partial\phi}(rw)\right], \\ 2\varpi_r &= \frac{1}{r^2\sin\theta}\left[\frac{\partial}{\partial\theta}(rw\sin\theta)-\frac{\partial}{\partial\phi}(rv)\right], \\ 2\varpi_\theta &= \frac{1}{r\sin\theta}\left[\frac{\partial u}{\partial\phi}-\frac{\partial}{\partial r}(rw\sin\theta)\right], \\ 2\varpi_\phi &= \frac{1}{r}\left[\frac{\partial}{\partial r}(rv)-\frac{\partial u}{\partial\theta}\right]. \end{aligned}\right\} \quad \ldots (49)$$

Using (48), (49), we have to obtain the general expressions of displacement and stress which are favourable to the present study.

Now we can obtain the following two equations concerning to $\varDelta$ and $r\varpi_r$ from (48) after some reductions:

$$\frac{\partial^2\varDelta}{\partial r^2}+\frac{2}{r}\frac{\partial\varDelta}{\partial r}+\frac{1}{r^2\sin\theta}\frac{\partial}{\partial\theta}\left(\sin\theta\frac{\partial\varDelta}{\partial\theta}\right)+\frac{1}{r^2\sin\theta}\frac{\partial^2\varDelta}{\partial\phi^2}=0, \quad \ldots\ldots (50)$$

$$\frac{\partial^2(r\varpi_r)}{\partial r^2}+\frac{2}{r}\frac{\partial(r\varpi_r)}{\partial r}+\frac{1}{r^2\sin\theta}\frac{\partial}{\partial\theta}\left(\sin\theta\frac{\partial(r\varpi_r)}{\partial\theta}\right)+\frac{1}{r^2\sin\theta}\frac{\partial^2}{\partial\phi^2}(r\varpi_r)=0. \quad (51)$$

The solutions of (50), (51), which are necessary for the present study, are expresed by

$$\varDelta=\left[Ar^2+\frac{A'}{r^3}\right]P_2^2(\cos\theta)\sin 2\phi, \ldots\ldots\ldots\ldots\ldots (52)$$

$$2\varpi_r=-\left[Br+\frac{B'}{r^4}\right]P_2^2(\cos\theta)\cos 2\phi, \ldots\ldots\ldots\ldots (53)$$

where $P_m^n(\cos\theta)$ is the associated function of mth order and n^{th} degree, and A, A', B, B' are the arbitrary constants to be determined by the boundary conditions.

Substituting the expressions (52), (53) for $\varDelta$ and $2\varpi_r$ in the equations (48), we can obtain the following forms of $2\varpi_\theta$ and $2\varpi_\phi$:

$$2\varpi_\theta=\frac{2(\lambda+2\mu)}{\mu}\left\{\frac{A}{3}r^2-\frac{A'}{2r^3}\right\}\frac{P_2^2(\cos\theta)}{\sin\theta}\cos 2\phi$$
$$-\left\{\frac{B}{2}r-\frac{B'}{3r^4}\right\}\frac{\partial P_2^2(\cos\theta)}{\partial\theta}\cos 2\phi, \quad \ldots . (54)$$

$$2\varpi_\phi=-\frac{(\lambda+2\mu)}{\mu}\left\{\frac{Ar^2}{3}-\frac{A'}{2r^3}\right\}\frac{\partial P_2^2(\cos\theta)}{\partial\theta}\sin 2\phi$$
$$+\left\{Br-\frac{2}{3}\frac{B'}{r^4}\right\}\frac{P_2^2(\cos\theta)}{\sin\theta}\sin 2\phi. \quad \ldots . (55)$$

Now, we can find the following three equations concerning $rw\sin\theta$,

r^2u, $rv\sin\theta$, Δ, $2\varpi_r$, $2\varpi_\theta$, $2\varpi_\phi$:

$$\frac{\partial}{\partial r}\left\{r^2\frac{\partial(rw\sin\theta)}{\partial r}\right\}+\frac{1}{\sin\theta}\frac{\partial}{\partial\theta}\left\{\sin\theta\frac{\partial}{\partial\theta}(rw\sin\theta)\right\}+\frac{1}{\sin^2\theta}\frac{\partial^2(rw\sin\theta)}{\partial\phi^2}$$

$$=r^2\frac{\partial\Delta}{\partial\phi}+\frac{2r^2}{\sin\theta}\frac{\partial}{\partial\theta}(\sin^2\theta\,\varpi_r)-2\sin\theta\frac{\partial}{\partial r}(r^3\varpi_\theta),\quad\ldots\ldots(56)$$

$$\frac{\partial^2}{\partial r^2}(r^2u)+\frac{1}{r^2\sin\theta}\frac{\partial}{\partial\theta}\left\{\sin\theta\frac{\partial(r^2u)}{\partial\theta}\right\}+\frac{1}{r^2\sin^2\theta}\frac{\partial^2(r^2u)}{\partial\phi^2}$$

$$=\frac{\partial}{\partial r}(r^2\Delta)-\frac{2r}{\sin\theta}\frac{\partial}{\partial\theta}(\sin\theta\,\varpi_\phi)+\frac{2r}{\sin\theta}\frac{\partial\varpi_\theta}{\partial\phi},\quad\ldots\ldots\ldots(57)$$

$$\frac{\partial}{\partial r}\left\{r^2\frac{\partial(rv\sin\theta)}{\partial r}\right\}+\frac{1}{\sin\theta}\frac{\partial}{\partial\theta}\left\{\sin\theta\frac{\partial(rv\sin\theta)}{\partial\theta}\right\}+\frac{1}{\sin^2\theta}\frac{\partial^2}{\partial\phi^2}(rv\sin\theta)$$

$$+2\cos\theta\frac{\partial(r^2u)}{\partial r}=\frac{r^2}{\sin\theta}\frac{\partial}{\partial\theta}(\sin^2\theta\,\Delta)-2r^2\frac{\partial\varpi_r}{\partial\phi}+2\sin\theta\frac{\partial}{\partial r}(r^3\varpi_\phi).\quad(58)$$

Substituting (52), (53), (54), (55) for Δ, $2\varpi_r$, $2\varpi_\theta$, $2\varpi_\phi$ in the equations (56), (57), we obtain the particular solutions concerning $rw\sin\theta$ and r^2u :

$$rw\sin\theta=-\left\{\frac{(5\lambda+7\mu)}{21\mu}r^4A+\frac{1}{3}\frac{A'}{r}\right\}P_2^2(\cos\theta)\cos2\phi$$

$$+\frac{1}{6}\left\{Br^3+\frac{B'}{r^2}\right\}\sin\theta\frac{\partial P_2^2(\cos\theta)}{\partial\theta}\cos2\phi,\quad\ldots\ldots\ldots(59)$$

$$r^2u=-\left\{\frac{\lambda}{7\mu}Ar^5+\frac{(3\lambda+5\mu)}{6\mu}A'\right\}P_2^2(\cos\theta)\sin2\phi.\quad\ldots\ldots(60)$$

For obtaining these solutions, use has been made of the following relations concerning the associated functions :

$$\left.\begin{aligned}&\frac{\partial}{\partial\theta}\left\{\sin\theta\frac{\partial P_2^2(\cos\theta)}{\partial\theta}\right\}=\frac{4}{\sin\theta}P_2^2(\cos\theta)-6\sin\theta P_2^2(\cos\theta),\\&\frac{\partial^2}{\partial\theta^2}\left\{\sin\theta\frac{\partial P_2^2(\cos\theta)}{\partial\theta}\right\}=\frac{4}{\sin\theta}\frac{\partial}{\partial\theta}P_2^2(\cos\theta)-6\left\{\sin\theta\frac{\partial P_2^2(\cos\theta)}{\partial\theta}\right.\\&\qquad\left.+\cos\theta P_2^2(\cos\theta)\right\}-\frac{4\cos\theta}{\sin^2\theta}P_2^2(\cos\theta).\end{aligned}\right\}\ldots(61)$$

The complementary solutions of (56) and (57) are of the forms :

$$rw\sin\theta=2\left\{Cr^2+\frac{C'}{r^3}\right\}P_2^2(\cos\theta)\cos2\phi,\quad\ldots\ldots\ldots(62)$$

$$r^2u=\left\{2Cr^3-\frac{3C'}{r^2}\right\}P_2^2(\cos\theta)\sin2\phi,\quad\ldots\ldots\ldots(63)$$

were C, C' are also the arbitrary constants.

Substituting (52), (53), (55), (60), (63) for Δ, $2\varpi_r$, $2\varpi_\phi$ and r^2u in the equation of (58), we obtain the following particular solutions which are favourable to our present study:

$$rv\sin\theta=-\left\{\frac{(5\lambda+7\mu)}{42\mu}Ar^4-\frac{A'}{6r}\right\}\sin\theta\frac{\partial P_2^2(\cos\theta)}{\partial\theta}\sin 2\phi$$

$$+\left\{\frac{B}{3}r^3+\frac{B'}{3r^2}\right\}P_2^2(\cos\theta)\sin 2\phi$$

$$+\left\{Cr^2+\frac{C'}{r^3}\right\}\sin\theta\frac{\partial P_2^2(\cos\theta)}{\partial\theta}\sin 2\phi. \qquad \text{(64)}$$

Using the general expressions of the components of displacement (59), (60), (62), (63) and (64), we formulate the components of stress $\widehat{rr}$, $\widehat{\theta\theta}$, $\widehat{\phi\phi}$, $\widehat{r\theta}$, $\widehat{r\phi}$, $\widehat{\theta\phi}$ in the following forms[5]:

$$\widehat{rr}=\left\{\frac{\lambda}{7}r^2A+\frac{(9\lambda+10\mu)}{3}\frac{A'}{r^3}+4\mu C+\frac{24\mu}{r^5}C'\right\}P_2^2(\cos\theta)\sin 2\phi, \qquad \text{(65)}$$

$$\widehat{\theta\theta}=\left\{\frac{5\lambda}{7}Ar^2-\frac{5\mu}{3}A'\frac{1}{r^3}+4\mu C-\frac{6\mu C'}{r^5}\right\}P_2^2(\cos\theta)\sin 2\phi$$

$$-\left\{\frac{(5\lambda+7\mu)}{21}Ar^2+\frac{\mu}{3}\frac{A'}{r^3}-2\mu C-\frac{2\mu}{r^5}C'\right\}\frac{\partial^2P_2^2(\cos\theta)}{\partial\theta^2}\sin 2\phi, \qquad \text{(66)}$$

$$\widehat{\phi\phi}=\left\{\frac{5\lambda}{7}Ar^2-\frac{5\mu}{3}A'\frac{1}{r^3}+4\mu C-\frac{6\mu C'}{r^5}\right\}P_2^2(\cos\theta)\sin 2\phi$$

$$+\left\{\frac{4(5\lambda+7\mu)}{21}Ar^2+\frac{4\mu}{3}\frac{A'}{r^3}-8\mu C-8\mu\frac{C'}{r^5}\right\}\frac{P_2^2(\cos\theta)}{\sin^2\theta}\sin 2\phi$$

$$+\left\{-\frac{(5\lambda+7\mu)}{21}Ar^2-\frac{\mu}{3}\frac{A'}{r^3}+2\mu C+\frac{2\mu C'}{r^5}\right\}\cot\theta\frac{\partial P_2^2(\cos\theta)}{\partial\theta}\sin 2\phi, \qquad \text{(67)}$$

$$\widehat{r\theta}=-\left\{\frac{(8\lambda+7\mu)}{6}Ar^2+\frac{(3\lambda+2\mu)}{6r^3}A'-2\mu C+8\mu\frac{C'}{r^5}\right\}\frac{\partial P_2^2(\cos\theta)}{\partial\theta}\sin 2\phi, \qquad \text{(68)}$$

$$\widehat{r\phi}=-\left\{\frac{2(8\lambda+7\mu)}{21}Ar^2+\frac{(3\lambda+2\mu)}{3r^3}A'-4\mu C+\frac{16\mu C'}{r^5}\right\}\frac{P_2^2(\cos\theta)}{\sin\theta}\cos 2\phi, \qquad \text{(69)}$$

$$\widehat{\theta\phi}=\left\{-\frac{(5\lambda+7\mu)}{21}Ar^2-\frac{\mu}{3}\frac{A'}{r^3}+2\mu C+\frac{2\mu C'}{r^5}\right\}\frac{\partial}{\partial\theta}\left(\frac{P_2^2(\cos\theta)}{\sin\theta}\right)\cos 2\phi$$

$$+\left\{\frac{(5\lambda+7\mu)}{21}Ar^2+\frac{\mu}{3}\frac{A'}{r^3}-2\mu C-\frac{2\mu C'}{r^5}\right\}\frac{\cot\theta}{\sin\theta}P_2^2(\cos\theta)\cos 2\phi$$

5) In these expressions we omit the terms concerning to B from the nature of our problem.

$$-\left\{\frac{(5\lambda+7\mu)}{21}Ar^2+\frac{\mu}{3}\frac{A'}{r^3}-2\mu C-2\mu\frac{C'}{r^5}\right\}\frac{1}{\sin\theta}\frac{\partial P_2^2(\cos\theta)}{\partial\theta}\cos 2\phi. \quad \ldots\ldots\ldots(70)$$

Now the boundary conditions which are necessray for the present case are as follows:

$$r=a;\quad \widehat{rr}=0,\ \widehat{r\theta}=0,\ \widehat{r\phi}=0, \quad \ldots\ldots\ldots\ldots\ldots\ldots(71)$$

$$\left.\begin{aligned} r=\infty;\quad \widehat{rr}&=S\sin^2\theta\sin 2\phi,\\ \widehat{\theta\theta}&=S\cos^2\theta\sin 2\phi,\\ \widehat{\phi\phi}&=-S\sin 2\phi,\\ \widehat{r\theta}&=\frac{S}{2}\sin 2\theta\sin 2\phi,\\ \widehat{r\phi}&=S\sin\theta\cos 2\phi,\\ \widehat{\theta\phi}&=S\cos\theta\cos 2\phi.\end{aligned}\right\}\quad \ldots\ldots\ldots\ldots\ldots(72)$$

The conditions expressed by (71) mean that the surface of the spherical cavity is free from tractions, and the conditions (72) has the significance that the portions in the solid far from cavity are subjected to the uniform simple shear expressed by (47).

We find the following values of arbitrary constants in the expressions (65), (66), (67), (68), (69), (70) from the boundary conditions (71), (72):

$$\left.\begin{aligned} &B=B'=0,\quad A=0,\quad C=\frac{S}{12\mu},\\ &C'=\frac{(\lambda+\mu)Sa^5}{2\mu(9\lambda+14\mu)},\quad A'=-\frac{5a^3S}{(9\lambda+14\mu)}.\end{aligned}\right\}\quad \ldots\ldots(73)$$

Substituting these values in the general expressions of displacement and stress (59), (60), (62), (63), (64), (65), (66), (67), (68), (69), (70), we obtain the final results as follows:

$$u=S\left\{\frac{r}{6\mu}+\frac{5}{6}\frac{(3\lambda+5\mu)}{\mu(9\lambda+14\mu)}\frac{a^3}{r^2}-\frac{3}{2}\frac{(\lambda+\mu)}{\mu(9\lambda+14\mu)}\frac{a^5}{r^4}\right\}P_2^2(\cos\theta)\sin 2\phi, \quad \ldots(74)$$

$$v=S\left\{\frac{r}{12\mu}+\frac{5}{6}\frac{1}{(9\lambda+14\mu)}\frac{a^3}{r^2}+\frac{1}{2}\frac{(\lambda+\mu)}{\mu(9\lambda+14\mu)}\frac{a^5}{r^4}\right\}\frac{\partial P_2^2(\cos\theta)}{\partial\theta}\sin 2\phi, \quad \ldots(75)$$

$$w=S\left\{\frac{r}{6\mu}+\frac{5}{3}\frac{1}{(9\lambda+14\mu)}\frac{a^3}{r^2}+\frac{(\lambda+\mu)}{\mu(9\lambda+14\mu)}\frac{a^5}{r^4}\right\}\frac{P_2^2(\cos\theta)}{\sin\theta}\cos 2\phi, \quad \ldots(76)$$

$$\widehat{rr}=S\left\{\frac{1}{3}-\frac{5}{3}\frac{(9\lambda+10\mu)}{(9\lambda+14\mu)}\frac{a^3}{r^3}+\frac{12(\lambda+\mu)}{(9\lambda+14\mu)}\frac{a^5}{r^5}\right\}P_2^2(\cos\theta)\sin 2\phi, \quad \ldots\ldots(77)$$

$$\widehat{\theta\theta}=S\left\{1+\frac{10\mu}{(9\lambda+14\mu)}\frac{a^3}{r^3}+\frac{6(\lambda+\mu)}{(9\lambda+14\mu)}\frac{a^5}{r^5}\right\}\sin 2\phi$$

$$+S\left\{-\frac{1}{3}+\frac{5\mu}{3(9\lambda+14\mu)}\frac{a^3}{r^3}-\frac{7(\lambda+\mu)}{(9\lambda+14\mu)}\frac{a^5}{r^5}\right\}P_2^2(\cos\theta)\sin 2\phi, \quad \ldots(78)$$

$$\widehat{\phi\phi}=S\left\{-1-\frac{10\mu}{(9\lambda+14\mu)}\frac{a^3}{r^3}-\frac{6(\lambda+\mu)}{(9\lambda+14\mu)}\frac{a^5}{r^5}\right\}\sin 2\phi$$

$$+S\left\{\frac{5\mu}{(9\lambda+14\mu)}\frac{a^3}{r^3}-\frac{5(\lambda+\mu)}{(9\lambda+14\mu)}\frac{a^5}{r^5}\right\}P_2^2(\cos\theta)\sin 2\phi, \quad \ldots\ldots\ldots(79)$$

$$\widehat{r\theta}=S\left\{\frac{1}{6}+\frac{5(3\lambda+2\mu)}{6(9\lambda+14\mu)}\frac{a^3}{r^3}-\frac{4(\lambda+\mu)}{(9\lambda+14\mu)}\frac{a^5}{r^5}\right\}\frac{\partial P_2^2(\cos\theta)}{\partial\theta}\sin 2\phi, \quad \ldots\ldots\ldots(80)$$

$$\widehat{r\phi}=S\left\{\frac{1}{3}+\frac{5(3\lambda+2\mu)}{3(9\lambda+14\mu)}\frac{a^3}{r^3}-\frac{8(\lambda+\mu)}{(9\lambda+14\mu)}\frac{a^5}{r^5}\right\}\frac{P_2^2(\cos\theta)}{\sin\theta}\cos 2\phi, \quad \ldots\ldots\ldots(81)$$

$$\widehat{\theta\phi}=S\left\{\frac{1}{6}+\frac{5\mu}{3(9\lambda+14\mu)}\frac{a^3}{r^3}+\frac{(\lambda+\mu)}{(9\lambda+14\mu)}\frac{a^5}{r^5}\right\}\frac{1}{\sin\theta}\frac{\partial P_2^2(\cos\theta)}{\partial\theta}\cos 2\phi. \quad \ldots(82)$$

We understand from these final expressions of displacement and stress that the displacement and the stress are expressed by Tesseral Harmonics of second order and second degree.

For the purpose of knowing the distributions of stress more fully, we take the following numerical example. Putting $\lambda=\mu$ in the expressions (77), (78), (79), (80), (81), (82), we obtain the results in the tables in which the displacement and the stress corresponding to different values of r/a and θ are tabulated. (Table VIII, IX, X, XI, XII, XIII, XIV, XV, XVI.)

These tables also indicate us the following figures. (Fig. 10, 11, 12, 13a, 13b, 14a, 14b, 15a, 15b, 16a, 16b, 17a, 17b, 18a, 18b).

From these tables and figures, we understand that the region effected by the presence of a spherical cavity is limited in the boundary region of that cavity and the effective radius is approximately $4a$ from the centre of the cavity, and stress component $\widehat{\theta\theta}_{r=a}$ is larger than the other components on the surface of cavity.

The values of $\widehat{\theta\theta}$ on the surface of cavity, when $\lambda=\mu$, is of the following form:

$$\widehat{\theta\theta}_{r=a}=\frac{15}{23}S\sin 2\phi+\frac{30}{23}S\cos 2\theta\sin 2\phi. \quad \ldots\ldots\ldots\ldots(83)$$

The expression (83) gives us the results shown in the following tables, in which the magnitudes of $\widehat{\theta\theta}_{r=a}$ are tabulated for different values of θ and ϕ. (Table XVII.)

At $\theta=0$, $\phi=45°$, or $\theta=0$, $\phi=225°$, the tension stress is 1.957 S, and at $\theta=0$, $\phi=135°$, or $\theta=0$, $\phi=315°$, the compression stress is 1·957 S.

Table VIII.

(Magnitude of u, unit $=\frac{Sa}{\mu}\sin 2\phi$, $\lambda=\mu$.)

θ \ r/a	1	2	3	4
0°	0·08	0·03	0·02	0·01
10°	0·10	0·07	0·06	0·07
20°	0·18	0·17	0·20	0·25
30°	0·29	0·32	0·41	0·52
45°	0·49	0·60	0·80	1·03
60°	0·70	0·88	1·19	1·54
70°	0·81	1·03	1·40	1·81
80°	0·88	1·13	1·53	1·99
90°	0·90	1·17	1·58	2·05

Table IX.

(Magnitude of v, unit $=\frac{Sa}{\mu}\sin 2\phi$, $\lambda=\mu$.)

θ \ r/a	1	2	3	4
0°	0	0	0	0
10°	0·17	0·18	0·26	0·34
20°	0·32	0·34	0·49	0·65
30°	0·42	0·46	0·66	0·87
45°	0·49	0·53	0·76	1·00
60°	0.42	0·46	0·66	0·87
70°	0·32	0·34	0·49	0·65
80°	0·17	0·18	0.26	0·34
90°	0	0	0	0

Table X.

(Magnitude of w, unit $=\frac{Sa}{\mu}\cos 2\phi$, $\lambda=\mu$.)

θ \ r/a	1	2	3	4
0°	0	0	0	0
10°	0·17	0·19	0·27	0·35
20°	0·33	0·37	0·52	0·69
30°	0·49	0·53	0·77	1·01
45°	0·69	0·76	1·08	1·42
60°	0·85	0·93	1·32	1·75
70°	0·92	1·01	1·44	1·89
80°	0·96	1·05	1·51	1·99
90°	0·98	1·07	1·53	2·02

Table XI.

(Magnitude of $\widehat{rr}$, unit $=S\sin 2\phi$, $\lambda=\mu$.)

θ \ r/a	1·0	1·05	1·1	1·2	1·25	1·5	1·75	2·0	2·5	2·75	3·0	3·5	3·75	4·0
0°	0	0	0	0	0	0	0	0	0	0	0	0	0	0
10°	0							0·02			0·03			0·03
20°	0							0·07			0·70			0·11
30°	0							0·15			0·22			0·24
45°	0	−0·05	−0·08	- 0.07	−0·04	0·10	0·21	0·29	0·39	0·41	0·43	0·46	0·46	0·47
60°	0							0·44			0·65			0·70
70°	0							0·51			0·76			0·83
80°	0							0·56			0·83			0·91
90°	0	−0·10	−0·16	−0·13	−0·07	0·19	0·42	0·58	0·78	0·82	0·86	0·91	0·93	0·94

Table XII.

(Magnitude of $\widehat{\theta\theta}$, unit $=S\sin 2\phi$, $\lambda=\mu$.)

θ \ r/a	1·0	1·1	1·25	1·5	1·75	2·0	2·5	3·0	3·5	4·0
0°	1·96	1·65	1·39	1·19	1·11	1·07	1·03	1·02	1·01	1·01
10°	1·88					1·04		0·99		0·98
20°	1·65					0·95		0·90		0·89
30°	1·30					0·81		0·77		0·76
45°	0·65	0·66	0·65	0·60	0·58	0·56	0·53	0·52	0·51	0·51
60°	0					0·30		0·27		0·26
70°	−0·35					0·16		0·14		0·13
80°	−0·58					0·07		0·05		0·03
90°	−0·65	−0·33	−0·10	0·01	0·05	0·04	0·03	0·02	0·01	0·01

Table XIII.

(Magnitude of $\widehat{\phi\phi}$, unit $=S\cos 2\phi$, $\lambda=\mu$.)

θ \ r/a	1·0	1·1	1·2	1·25	1·5	1·75	2·0	2·5	3·0	3·5	4·0
0°	−1·96	−1·65	−1·46	−1·39	−1·20	−1·11	−1·07	−1·03	−1·02	−1·01	−1·01
10°	−1·98						−1·07		−1·02		−1·01
20°	−2·03						−1·07		−1·02		−1·01
30°	−2·12						−1·06		−1·01		−1·01
45°	−2·28	−1·81	−1·54	−1·44	−1·19	−1·09	−1·05	−1·02	−1·01	−1·01	−1·00
60°	−2·45						−1·04		−1·00		−1·00
70°	−2·53						−1·03		−1·00		−1·00
80°	−2·59						−1·03		−1·00		−1·00
90°	−2·61	−1·97	−1·61	−1·49	−1·18	−1·07	−1·03	−1·01	−1·00	−1·00	−1·00

Table XIV.

(Magnitude of $\widehat{r\theta}$, unit $=S\sin 2\phi$, $\lambda=\mu$.)

θ \ r/a	1·0	1·1	1·2	1·25	1·5	1·75	2·0	2·5	3·0	3·5	4·0
0°	0	0	0	0	0	0	0	0	0	0	0
10°	0						0·18		0·18		0·17
20°	0						0·35		0·33		0·33
30°	0						0·46		0·45		0·44
45°	0	0·26	0·40	0·44	0·52	0·54	0·54	0·53	0·52	0·51	0·51
60°	0						0·46		0·45		0·44
70°	0						0·35		0·33		0·33
80°	0						0·18		0·18		0·17
90°	0	0	0	0	0	0	0	0	0	0	0

Table XV.

(Magnitude of $\widehat{r\phi}$, unit $= S\cos 2\phi$, $\lambda=\mu$.)

θ \ r/a	1·0	1·1	1·2	1·5	1·75	2·0	2·5	3·0	3·5	4·0
0°	0	0	0	0	0	0	0	0	0	0
10°	0					0·19		0·18		0·18
20°	0					0·37		0·35		0·35
30°	0					0·54		0·53		0·51
45°	0	0·32	0·56	0·74	0·76	0·76	0·74	0·73	0·72	0·72
60°	0					0·93		0·89		0·88
70°	0					1·01		0·97		0·96
80°	0					1·06		1·02		1·00
90°	0	0·52	0·79	1·05	1·08	1·07	1·05	1·03	1·02	1·02

Table XVI.

(Magnitude of $\widehat{\theta\phi}$, unit $= S\cos 2\phi$, $\lambda=\mu$.)

θ \ r/a	1·0	1·1	1·2	1·25	1·5	2·0	2·5	3·0	3·5	4·0
0°	1·33	1·03	0·84	0·77	0·57	0·45	0·41	0·39	0·39	0·38
10°	1·32					0·44		0·39		0·38
20°	1·25					0·42		0·37		0·36
30°	1·15					0·39		0·34		0·33
45°	0·94	0·73	0·59	0·54	0·40	0·31	0·29	0·28	0·27	0·27
60°	0·67					0·22		0·20		0·19
70°	0·46					0·15		0·14		0·13
80°	0·23					0·08		0·07		0·07
90°	0	0	0	0	0	0	0	0	0	0

Table XVII.

(Magnitude of $\widehat{\theta\theta}_{r=a}$)

ϕ \ θ	0°	60°	90°	120°
0°	0	0	0	0
45°	1·957S	0	−0·7S	0
90°	0	0	0	0
135°	−1·957S	0	0·7S	0
180°	0	0	0	0
225°	1·957S	0	−0·7S	0
270°	0	0	0	0
315°	−1·957S	0	0·7S	0

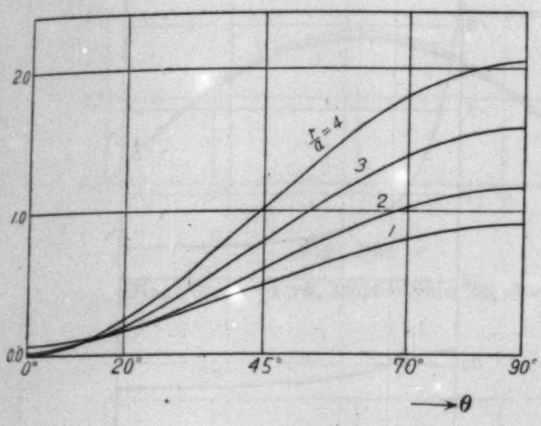

Fig. 10. (Magnitude of u, unit $=\frac{Sa}{\mu}\sin 2\phi$, $\lambda=\mu$.)

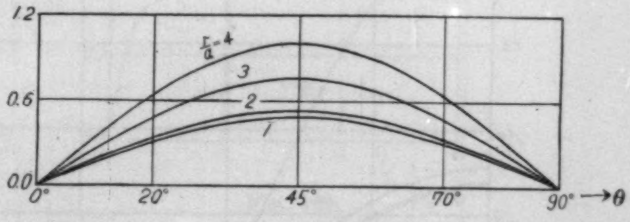

Fig. 11. (Magnitude of v, unit $=\frac{Sa}{\mu}\sin 2\phi$, $\lambda=\mu$.)

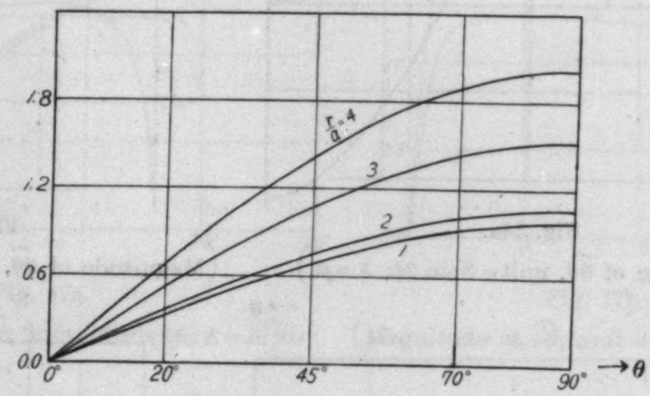

Fig. 12. (Magnitude of w, unit $=\frac{Sa}{\mu}\cos 2\phi$, $\lambda=\mu$.)

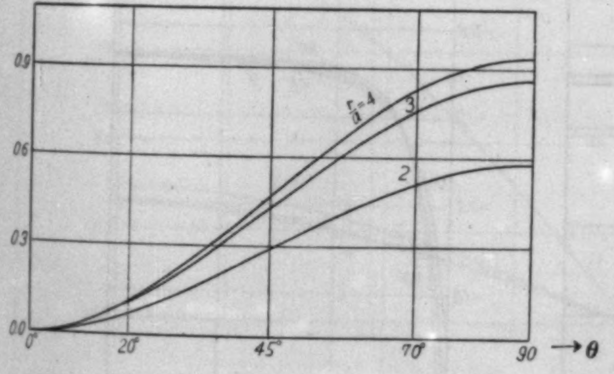

Fig. 13a. (Magnitude of $\widehat{rr}$, unit $=S\sin 2\phi$, $\lambda=\mu$.)

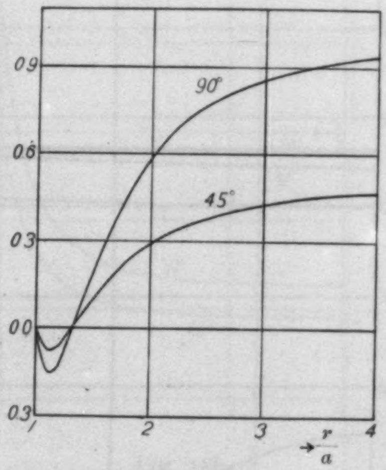

Fig. 13b. (Magnitude of $\widehat{rr}$, unit $=S\sin 2\phi$, $\lambda=\mu$.)

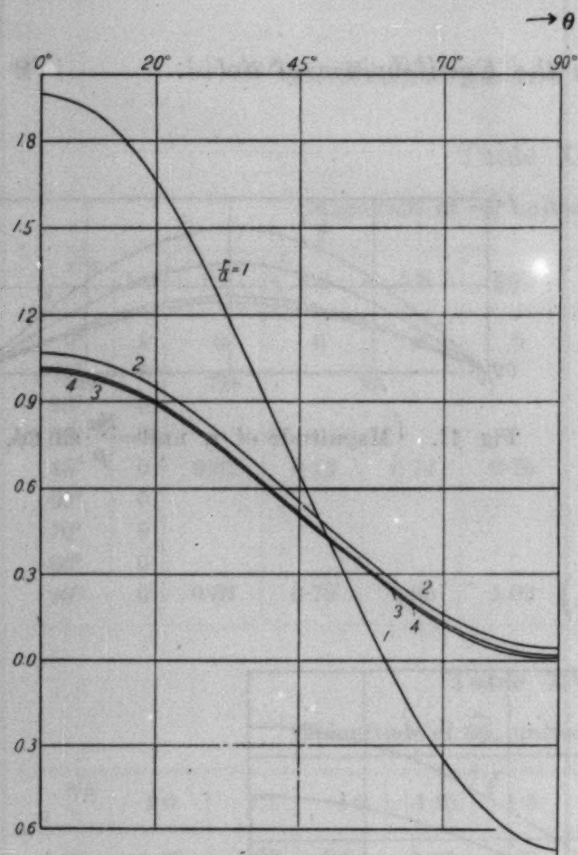

Fig. 14a.

(Magnitude of $\widehat{\theta\theta}$, unit $= S \sin 2\phi$, $\lambda = \mu$.)

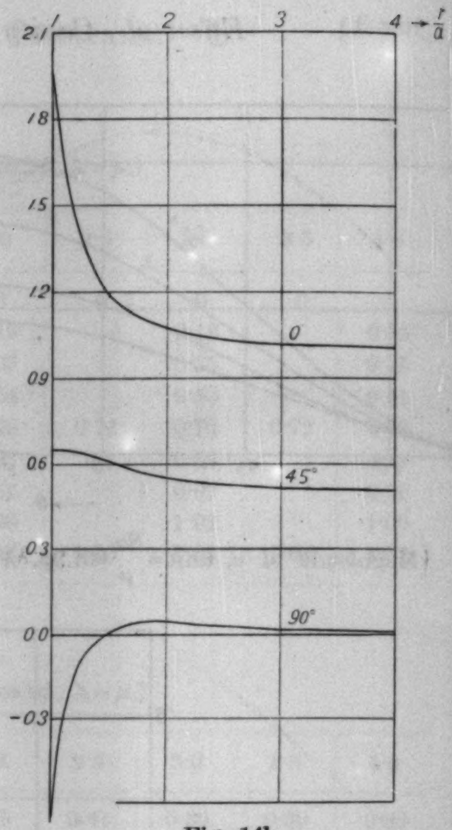

Fig. 14b.

(Magnitude of $\widehat{\theta\theta}$, unit $= S \sin 2\phi$, $\lambda = \mu$.)

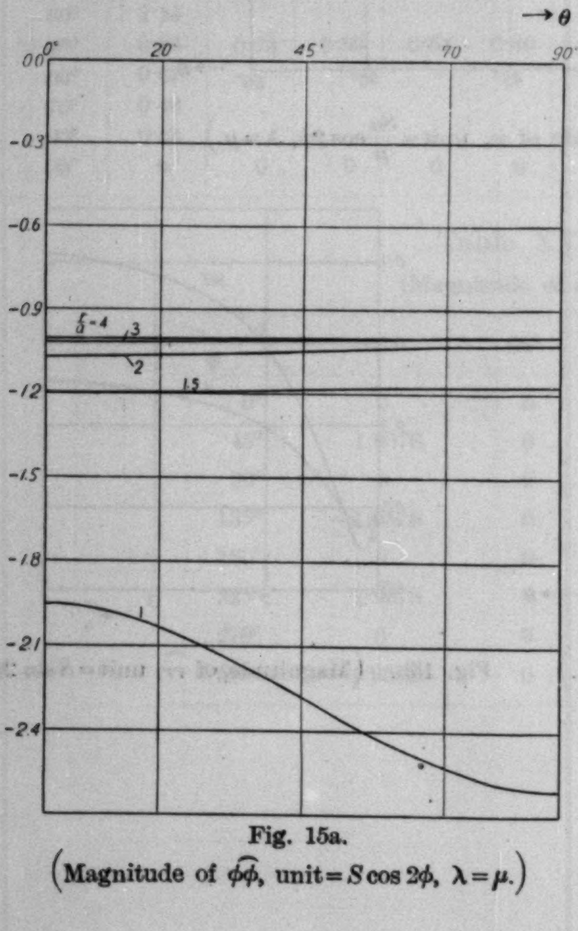

Fig. 15a.

(Magnitude of $\widehat{\phi\phi}$, unit $= S \cos 2\phi$, $\lambda = \mu$.)

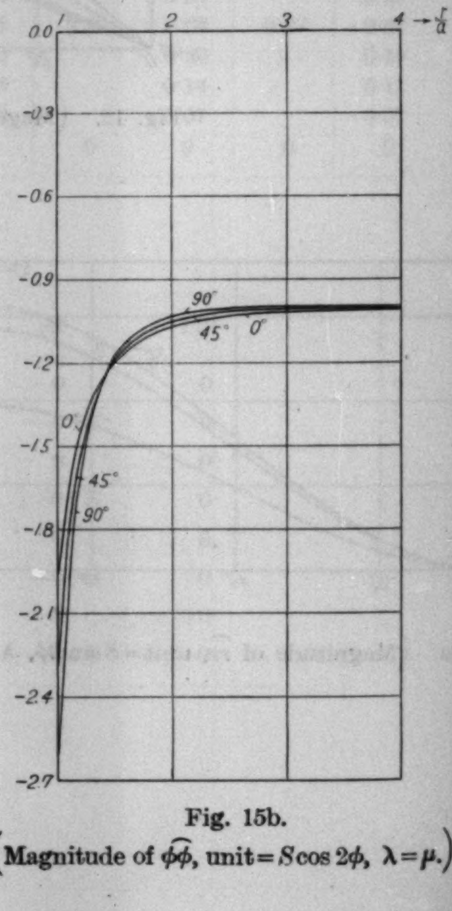

Fig. 15b.

(Magnitude of $\widehat{\phi\phi}$, unit $= S \cos 2\phi$, $\lambda = \mu$.)

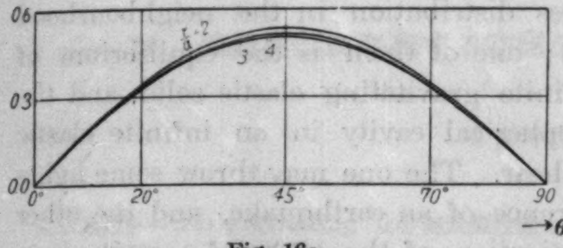

Fig. 16a.

(**Magnitude of $\widehat{r\theta}$, unit = $S\sin 2\phi$, $\lambda=\mu$.**)

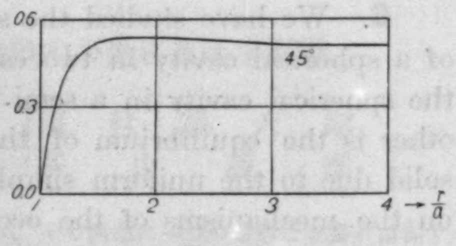

Fig. 16b.

(**Magnitude of $\widehat{r\theta}$, unit = $S\sin 2\phi$, $\lambda=\mu$.**)

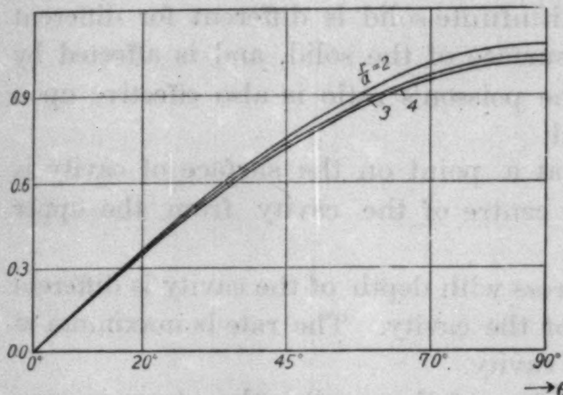

Fig. 17a.

(**Magnitude of $\widehat{r\phi}$, unit = $S\cos 2\phi$, $\lambda=\mu$.**)

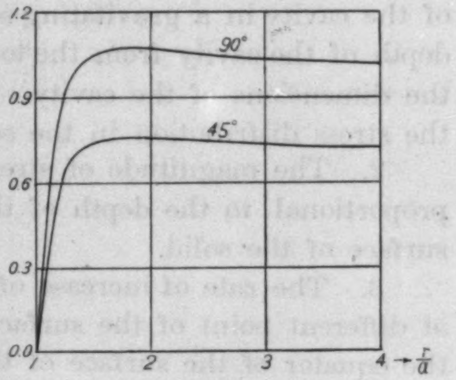

Fig. 17b.

(**Magnitude of $\widehat{r\phi}$, unit = $S\cos 2\phi$, $\lambda=\mu$.**)

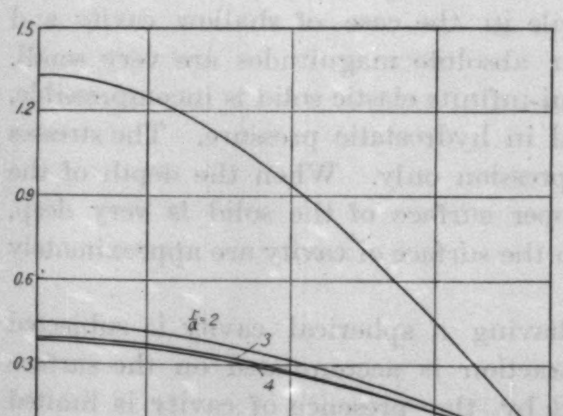

Fig. 18a.

(**Magnitude of $\widehat{\theta\phi}$, unit = $S\cos 2\phi$, $\lambda=\mu$.**)

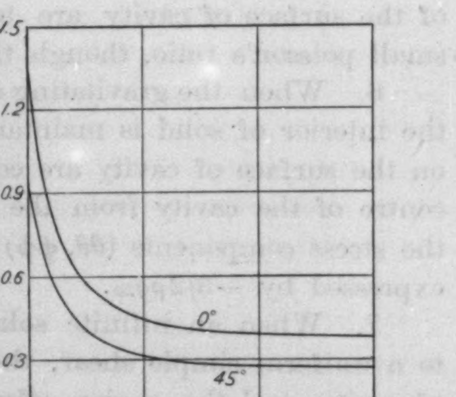

Fig. 18b.

(**Magnitude of $\widehat{\theta\phi}$, unit = $S\cos 2\phi$, $\lambda=\mu$.**)

6. We have studied the stress distribution in the neighbourhood of a spherical cavity in two cases; one of them is the equilibrium of the spherical cavity in a semi-infinite gravitating elastic solid, and the other is the equilibrium of the spherical cavity in an infinite elastic solid due to the uniform simple shear. The one may throw some lights on the mechanisms of the occurrence of an earthquake, and the other may give some clew to the investigations of the effect of a cavity in a semi-infinite gravitating elastic solid under dynamical forces.

We will mention some results obtained from the calculations:

1. The stress distribution in the neighbourhood of the inner surface of the cavity in a gravitating semi-infinite solid is different for different depth of the cavity from the top surface of the solid, and is affected by the dimensions of the cavity. The poisson's ratio is also effective upon the stress distribution in the solid.

2. The magnitude of stress at a point on the surface of cavity is proportional to the depth of the centre of the cavity from the upper surface of the solid.

3. The rate of increase of stress with depth of the cavity is different at different point of the surface of the cavity. The rate is maximum at the equator of the surface of the cavity.

4. At the equator of the surface of the cavity, the stress is compressive and is larger than the other components of tractions at the surface.

5. Some components of stress at the top and the bottom portions of the surface of cavity are tensile in the case of shallow cavity and small poisson's ratio, though their absolute magnitudes are very small.

6. When the gravitating semi-infinite elastic solid is incompressible, the interior of solid is maintained in hydrostatic pressure. The stresses on the surface of cavity are compression only. When the depth of the centre of the cavity from the upper surface of the solid is very deep, the stress components $(\theta\theta, \phi\phi)$ on the surface of cavity are approximately expressed by $-3/2\rho g z_0$.

7. When an infinite solid having a spherical cavity is subjected to a uniform simple shear, the traction is accumulated on the surface of cavity, and the region effected by the presence of cavity is limited in the boundary region of that cavity, and the effective radius from the centre of the cavity is approximately four times the radius of the cavity.

In conclusion, the present authors must express their sincere thanks to Professor K. Sezawa for his kind guidance.

24. 地殼內部に存在する空窩が地殼の平衡に及ぼす影響

地震研究所 { 西村源六郎
高山威雄

先づ地殼を一つの gravitating な半無限彈性體と考へ、その內部に一つの球形な空窩が存在する時の平衡問題を研究し、次にこの彈性體が一樣な剪應力を受ける時どの樣な平衡上の變化を受けるかを研究する目的で一つの無限彈性體が一樣な剪應力を受ける時の平衡問題を取扱つてみた。色々面白いと思はれる結果を得たのであるが多少でも參考になる所があれば幸と思つてゐる。

25. *A Study of Displacements of Triangulation Points.*

By Katsuhiko MUTO,

Imperial Japanese Military Land Survey.

(Read Sept. 15, 1931.—Received Feb. 26, 1932.)

Soon after the great Kwantô and Tango earthquakes the Land Survey executed revisional triangulations with a view to detecting earth movements that had taken place since the previous observations were made a number of years before.[1]

In computing these displacements in the Kwantô region the position of the primary point, Teruisi-yama, and the azimuth of the line from Teruisi-yama to Tukuba-san (the primary point); and in Tango the positions of the primary points, Kasagata-yama and Hyôno-yama, were all assumed not to have changed their positions since the previous triangulation observations were made there.

The reason for not making the same assumption for the two triangulations is that whereas in Kwantô the Sagamino base line was measured and the length of each side of the triangles determined, in Tango no base line was measured so that a side of a triangle had to be used as the base for the new triangulation.

In both Kwantô and Tango the survey was carried into regions where none of the usual earthquake effects were noticed, and the position and azimuth of points in regions where the ground could hardly have been displaced were selected as points for reference. Unless the changes as shown by differences in the position and azimuth as compared with the previous triangulation were absolutely beyond question, no displacement however apparent was recognized.

But since in both triangulations no examinations were made to check possible systematic errors in length, which, needless to say, is of paramount importance, in triangulation, the following investigation, which forms the subject of this paper, was made in order to detect possible displacements of reference points and also errors in length of sides of triangles.

1. When a point in the triangulation net is displaced in a certain

1) THE MILITARY LAND SURVEY, *Bull. Earthq. Res. Inst.*, 4 (1927); 7 (1929), 187.

direction, the change v in the direction angle of this point with reference to another point is given by the following expression in both direct and opposite directions.

$$v = \frac{e}{s}\rho'' \sin(360^\circ - \varphi + \psi),$$

where

- e displaced length,
- s distance between the occupied station and the sighted point,
- φ direction angle of displacement measured clockwise from a specified initial direction,
- ψ direction angle of the sighted point measured clockwise from the same initial direction as that of φ.

When all the distances from a point to several other points are equal then the v of all the directions from that point distribute themselves on the same sine curve, but when the distances differ, v deviate from the sine curve according to the magnitudes of the difference.

2. Fig. 1 shows the changes in the angles at the primary points, Tôkyô and Tanzawa-yama, together with those of the primary points, Tukuba-san, Teruisi-yama, Dôhira-yama, Kokusi-dake, and Kenasi-yama,

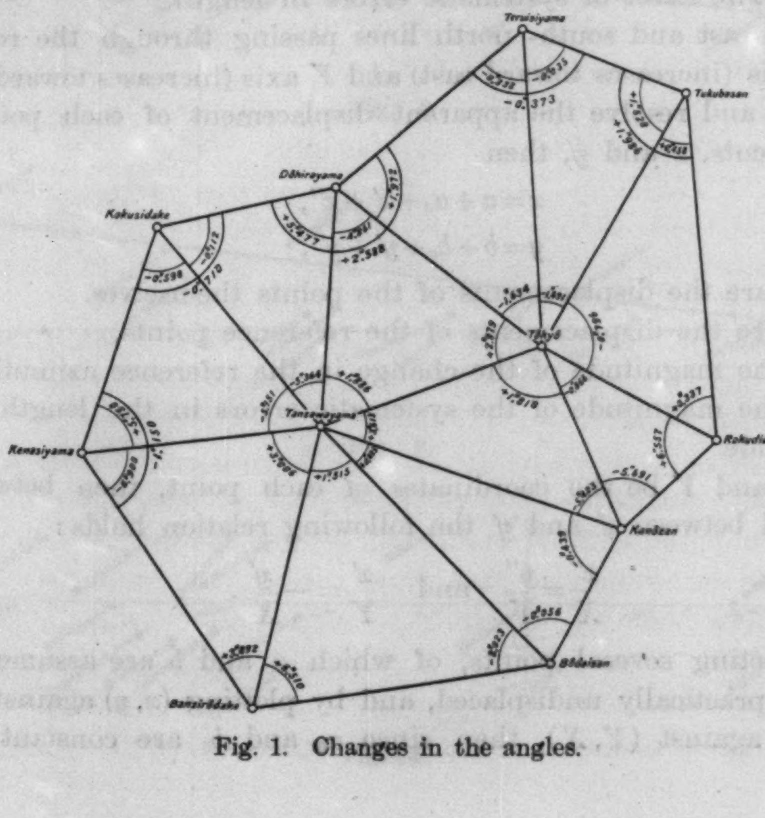

Fig. 1. Changes in the angles.

the last five of which are situated outside of the area devastated by the earthquake. It seems that the changes in the angles at these triangulation points were caused by the displacements of Tôkyô and Tanzawa-yama. Indeed as shown below the change in the angles of Teruisi-yama, Dôhira-yama, etc., are so small that it is evident that these points have practically not changed their positions:

Teruisi-yama	Tukuba-san Dôhira-yama	$-0''\cdot 373$
Dôhira-yama	Teruisi-yama Kokusi-dake	$+2''\cdot 588$
Kokusi-dake	Dôhira-yama Kenasi-yama	$-0''\cdot 710$
Kenasi-yama	Kokusi-dake Banzirô-dake	$-1''\cdot 150$

3. As factors of the displacements ascertained by comparing the old and new triangulations, we may consider

1. The displacement of the point itself,
2. The displacement of the reference point,
3. The effect of the change in the reference azimuth,
4. The effect of systematic errors in length.

Let the west-east and south- north lines passing through the reference point, X axis (increases toward east) and Y axis (increases toward north) respectively, and resolve the apparent displacement of each point into two components, x and y, then

$$x=a+a_0+x'+x'',$$
$$y=b+b_0+y'+y'',$$

where a, b are the displacements of the points themselves.

a_0, b_0 are the displacements of the reference points,

x', y' the magnitude of the change in the reference azimuth,

x'', y'' the magnitude of the systematic errors in the length of the side.

Now let X and Y be the coordinates of each point, then between x'' and y'', and between x' and y' the following relation holds:

$$\frac{x''}{X}=\frac{y''}{Y} \quad \text{and} \quad \frac{x'}{Y}=-\frac{y'}{X}.$$

By selecting several points, of which a and b are assumed to be small, i. e., practically undisplaced, and by plotting (x, y) against (X, Y) as well as against (Y, X), then since a_0 and b_0 are constant for all

points, we can determine the relation between (x'', y'') and (X, Y) and also between (y', x') and (X, Y); because if in the first two terms (x'', y'') and (X, Y) we can treat (x', y') as an accidental error, and in the two second terms (y', x') and (X, Y) treat (x'', y'') as an accidental error, then the systematic error in length, the changes in the azimuth of reference, as well as the magnitudes of a_0 and b_0, can be determined.

4. Figs. 2 and 3 show the relation between (X, x) and (Y, y), that is (X, x'') and (Y, y''), of the triangulation in the Kwantô district, the origin of the coordinate axes being Teruisi-yama. In the figures the thick lines show the mean position of the plotted points. In both figures the mean lines pass through the origin of the coordinate axes and their inclinations are almost the same. This fact shows not that the reference point Teruisi-yama had been displaced during the interval between the old and new triangulations, but that there are systematic errors in the length of the sides of the triangles.

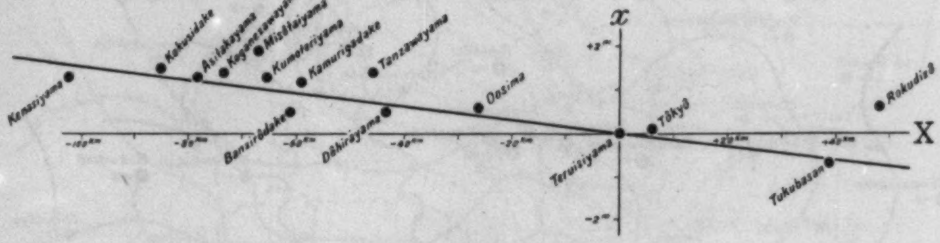

Fig. 2.

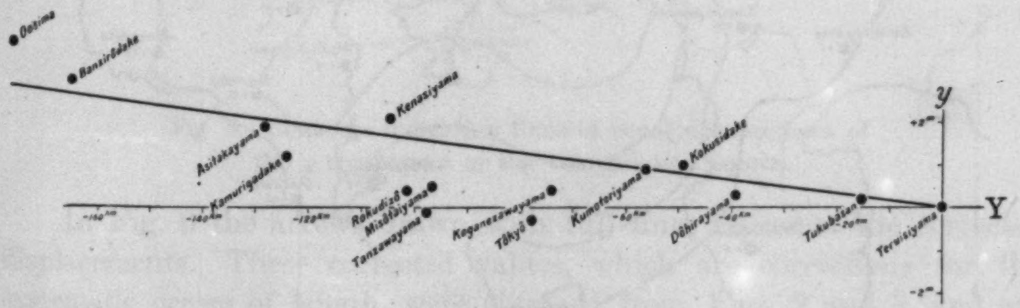

Fig. 3.

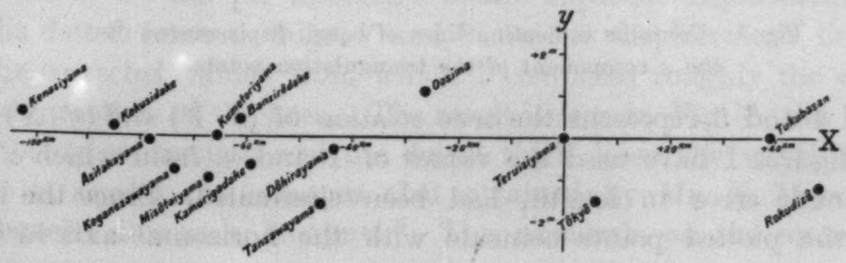

Fig. 4.

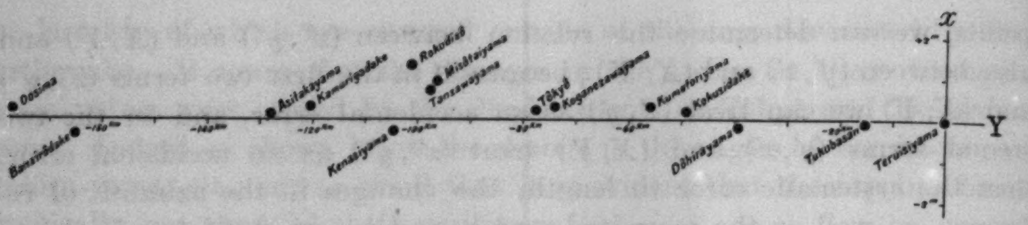

Fig. 5.

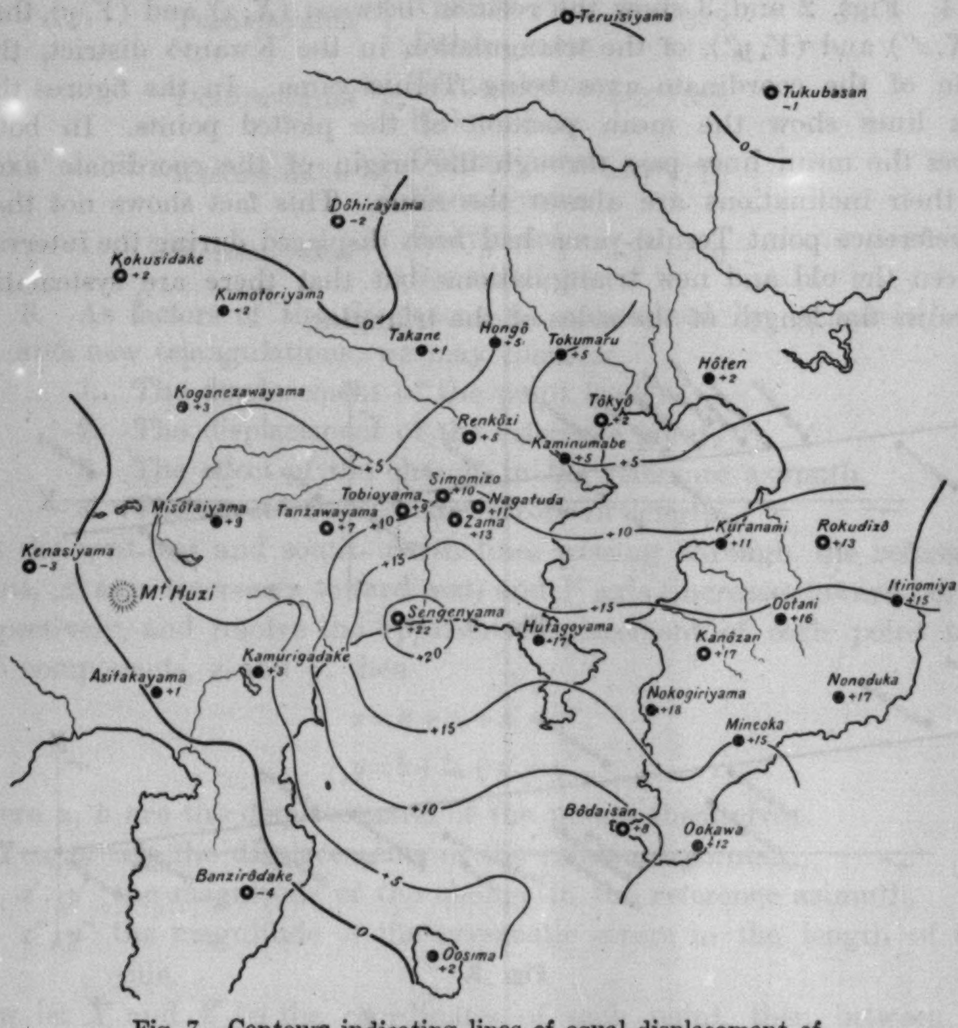

Fig. 7. Contours indicating lines of equal displacement of the x component of the triangulation points.

Figs. 4 and 5 represent the true relation of (x', Y) and (y', X); for in these figures I have used the values of x and y, from which x'', y'', the systematic error in length, had been eliminated. Since the mean lines of the plotted points coincide with the horizontal axis in these figures 4 and 5, the reference azimuth has not changed.

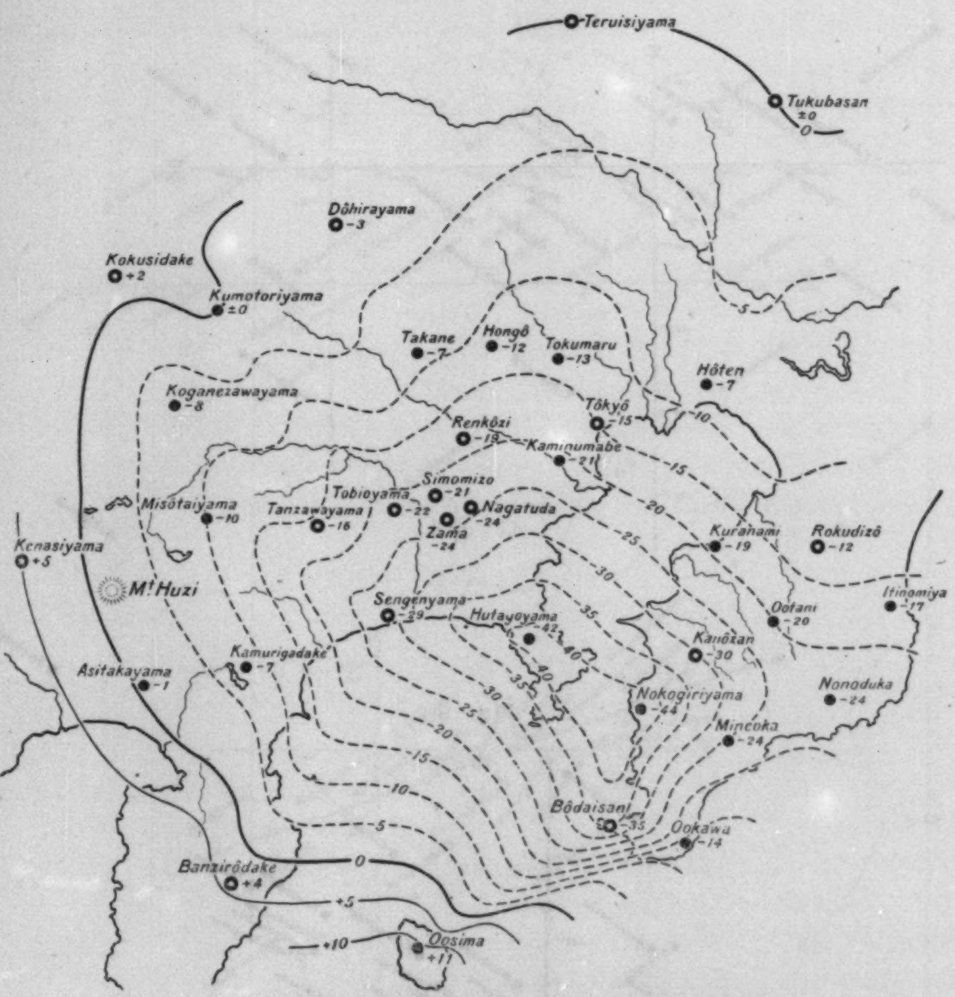

Fig. 8. Contours indicating lines of equal displacement of the y component of the triangulation points.

In Fig. 6 the arrows drawn with full lines represent the corrected displacements. These corrected values, which are corrections for the systematic errors of length, were obtained from Figs. 2 and 3, and are additions of 1·5 cm. per kilometre to the apparent displacements shown by the dotted arrows. Figs. 7 and 8 are the displacement lines based on the corrected values from which I computed roughly the expansion and contraction of the area. The result is seen in Fig. 6, the full thick lines being contraction and the dotted thick lines the expantion. The result is almost the same as that obtained by Mr. N. Miyabe of the Earthquake Research Institute.[2] The numerals on the contours indi-

2) N. MIYABE, *Bull. Earthq. Res. Inst*, **9** (1931), 12.

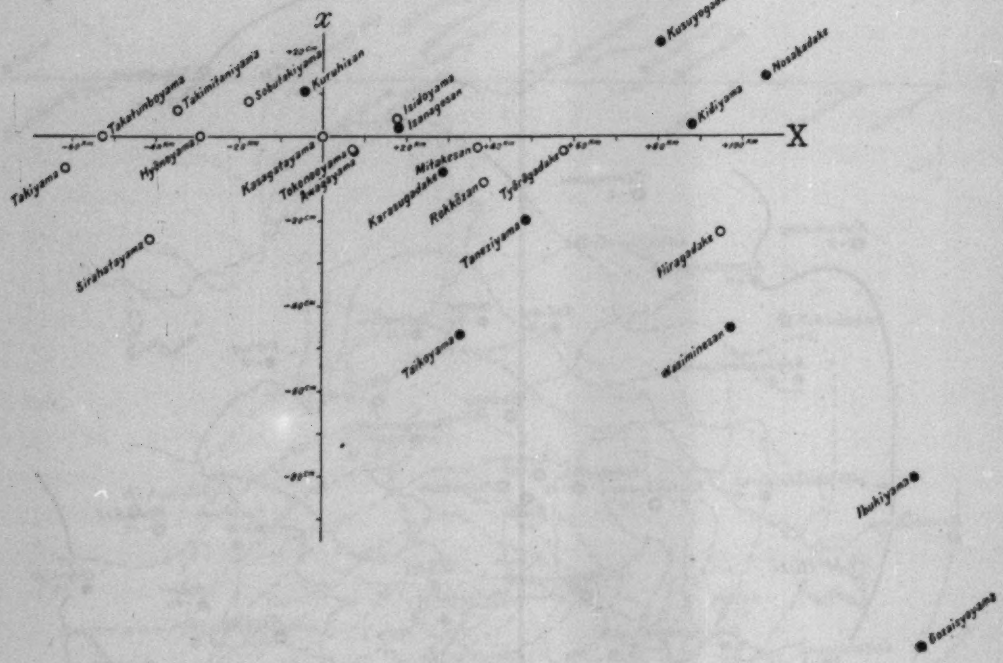

Fig. 9.

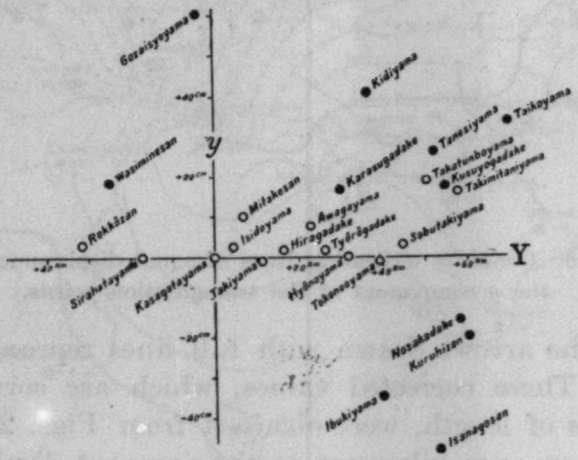

Fig. 10.

cating the lines of equal displacements of x and y components and on the contours indicating expansion and contraction are not true values but only values proportional to them.

5. I applied the same method as that used for the Kwantô to the result of the Tango triangulation, the origin of coordinate axes being the primary point, Kasagata-yama.

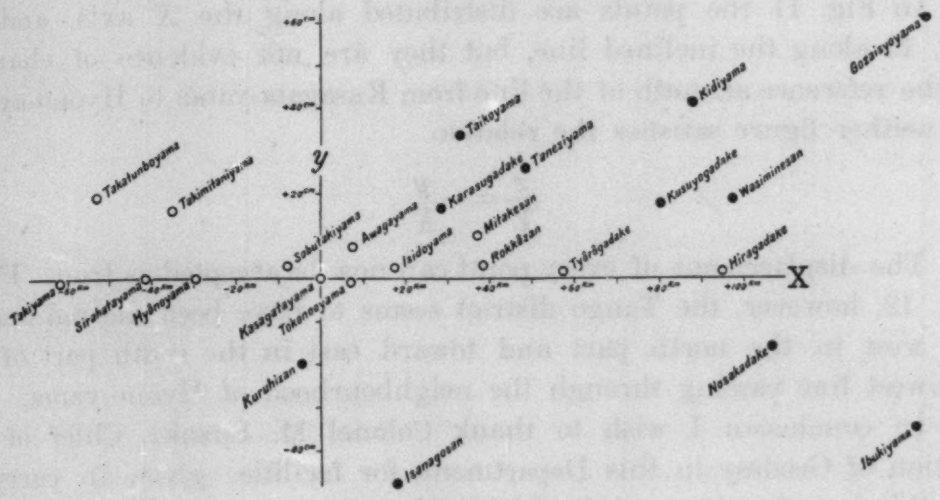

Fig. 11.

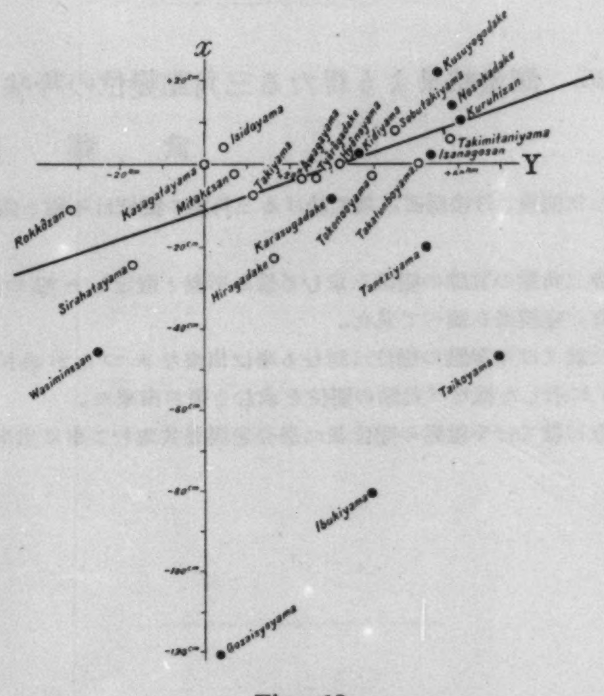

Fig. 12.

Figs. 9, 10, 11, and 12 represent the relations of (x, X) and (y, Y), (x, Y) and (y, X) respectively. The circles in the figures are points situated in regions where changes in the angles was comparatively small. In Figs. 9 and 10 these points are distributed on the X axis. This shows that the side length is free from systematic error.

In Fig. 11 the points are distributed along the X axis, and in Fig. 12 along the inclined line, but they are not evidence of changes in the reference azimuth of the line from Kasagata-yama to Hyôno-ayma, for neither figure satisfies the relation

$$\frac{x}{Y} = -\frac{y}{X} .$$

The displacement of every point can now be accepted as true. From Fig. 12, however, the Tango district seems to have been sheered toward the west in the north part and toward east in the south part of the east-west line passing through the neighbourhood of Hyôno-yama.

In conclusion I wish to thank Colonel M. Suzuki, Chief of the Section of Geodesy in this Department, for facilities given in carrying out this investigation and for his continued interest during its progress.

---

25. 測量結果より得たる三角點變位の吟味

武　藤　勝　彦

陸地測量部が發表した關東、丹後兩震災地に於ける三角點の變位は不動と假定した三角點に關する相對變位である。

此の論文に於ては各三角點の實際の變位を求むる爲め不動と假定した點の運動及び三角形の邊長に存するかも知れない定誤差を調べて見た。

其の結果關東地方に就ては不動點の變位は認むる事は出來なかつたが邊長に定誤差が含まれてゐる事が知れ Fig. 6 に示した樣な三角點の變位を求むる事が出來た。

然しながら丹後地方に就ては不動點の變位並に邊長定誤差共認むる事は出來なかつた。

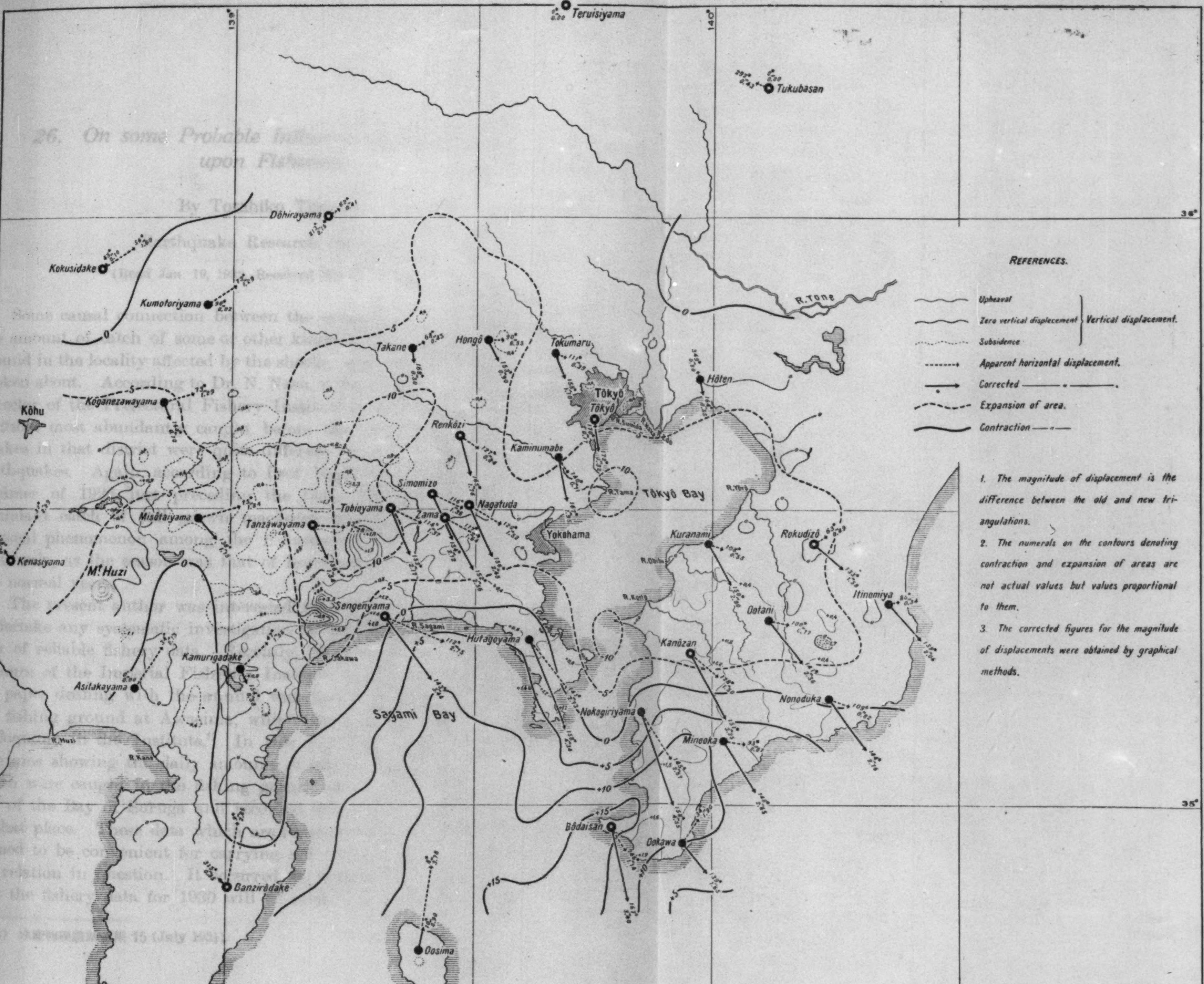

Fig. 6. Relative Horizontal Displacements of Triangulation Points.

(震研彙報、第十號、圖版、武藤)

26. *On some Probable Influence of Earthquakes upon Fisheries.*

By Torahiko TERADA,

Earthquake Research Institute.

(Read Jan. 19, 1932.-Received March 19, 1932.)

Some causal connection between the occurrence of earthquakes and the amount of catch of some or other kinds of fishes on a certain fishing ground in the locality affected by the shocks, have not infrequently been spoken about. According to Dr. N. Nasu, it was remarked by Mr. Miura, Director of the Prefectural Fishery Institute at Itô, Idu, that the kinds of fishes most abundantly caught before the remarkable swarm-earthquakes in that district were quite different from those caught after the earthquakes. Again, according to Prof. Nagaoka, it is said that in the summer of 1923 just preceding the Great Kwantô Earthquake, an abundant catch of full grown mackerels (*Scomber*) was noted as an unusual phenomenon among the fishermen in the vicinity of Miura Peninsula, as the season was that of horse mackerel (*Caranx*) fishery in the normal years.

The present author was interested with this problem but unable to undertake any systematic investigation in this line on account of the lack of reliable fishery data. Recently, he received from Mr. Kinosuke Kimura of the Imperial Fisheries Institute a copy of the reprints of his paper dealing with the annual variation of the status of fisheries on the fishing ground at Awasima, which was read before the meeting of Colloquium in the Institute.[1] In this paper are given a number of diagrams showing the daily amounts of catch of different kinds of fishes which were caught in the fishing ground of Awasima at the northern end of the Bay of Suruga and recorded in the book kept at the Office of that place. These data which are referred to the six years 1924–1929, seemed to be convenient for carrying out a preliminary investigation of the relation in question. It occurred to the present author, however, that the fishery data for 1930 will be most interesting for the first step

1) 水産物理談話會報 15 (July 1931).

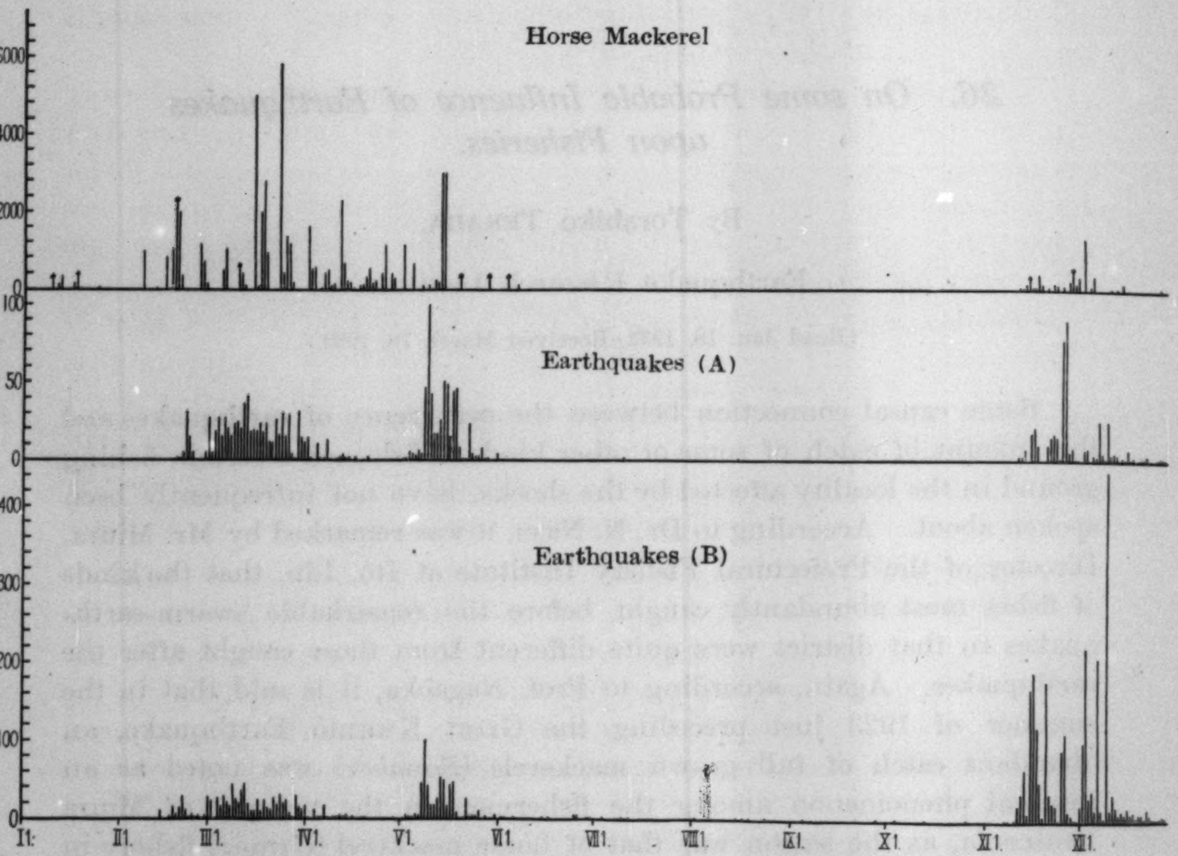

Fig. 1. Earthquakes (A) means the no. of "felt" earthquakes in N-Idu and Itô. Earthquakes (B) means the sum of the numbers of earthquakes, felt and unfelt earthquakes in Idu Peninsula and the Bay of Suruga *plus* the number of conspicuous or rather conspicuous earthquakes in Musasi, Sagami, Suruga and Kai. The mark ★ on fish-diagram means that the amount of catch is not exactly known though abundant.

of investigation, since in this very year there occurred a series of conspicuous swarms of earthquakes in the Province of Idu not far from the said fishing ground. Upon the request of the author, Mr. Kimura kindly took the trouble of preparing a copy of the data for this year, containing the daily numbers of catch for different kinds of fishes and for a number of fishing grounds of the same district. A provisory review of these data revealed a rather remarkable fact that the epochs with abundant catch of horse mackerel, *Caranx*, at Sigedera coincided nearly with the periods in which the seismic activity was at its full display. Fig. 1[2)]

2) The earthquake data here plotted in the diagram are taken from the Report of North Idu Earthquake issued by the Central Meteorogical Observatory.

will illustrate this rather striking coincidence. Especially interesting is the comparison of the two data in Nov.–Dec.

The result of this first trial seemed encouraging so that a further step was taken for a more systematic investigation by taking the data for the other six years given in the paper cited. In the diagrams given there, the daily amounts of catch are plotted as the ordinates y, not proportional to the number n of the fish caught, but in a peculiar deformed scale such that the length of y is multiplied by 3/2 when n is doubled, i. e. $y=n^a$, where $a=\log 3/2 \div \log 2 = 0{\cdot}585$. Such a kind of scale seems not only convenient but also quite rational. Suppose that the number of fishes caught is a fraction f of the total number N of the swarm of fishes present and f may increase with N by different reasons such that $f=\alpha N^b$, α being a constant. Then the catch is $n=\alpha N^{b+1}$ and therefore $N=\frac{1}{\alpha}n^{\frac{1}{b+1}}$. If f be simply proportional to N, we have $b=1$ and $N\propto n^{0\cdot5}$ which is not very different from y as above defined.

At any rate, we could adopt y of these diagrams as an arbitrary measure of the amount of catch in the present investigation where any

Fig. 2. Lowest curve gives the decade number of earthquakes; full line for the sum of unfelt, felt, rather conspicuous and conspicuous earthquakes originated in Idu Peninsula and the Bay of Suruga; dotted line for the sum (No. of felt and unfelt ones in Idu, the Bay of Suruga and W part of the Bay of Sagami)+(No. of conspicuous and rather conspicuous shocks in Musasi, Sagami, Suruga, Kai, Idu). Middle curve gives the decade amount of catch of horse mackerel and top curve that of immature tunny, both in an arbitrary scale.

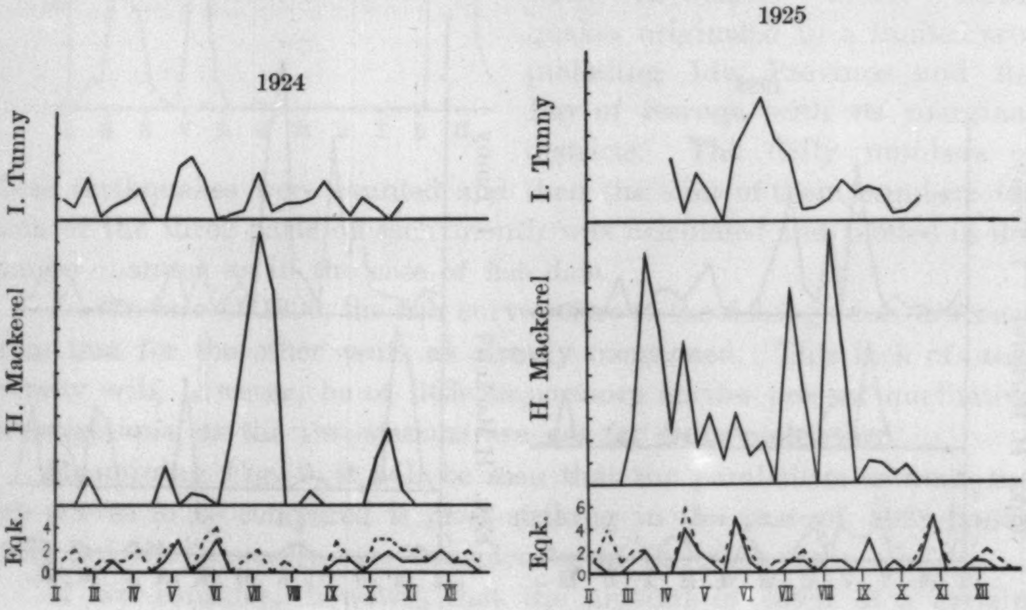

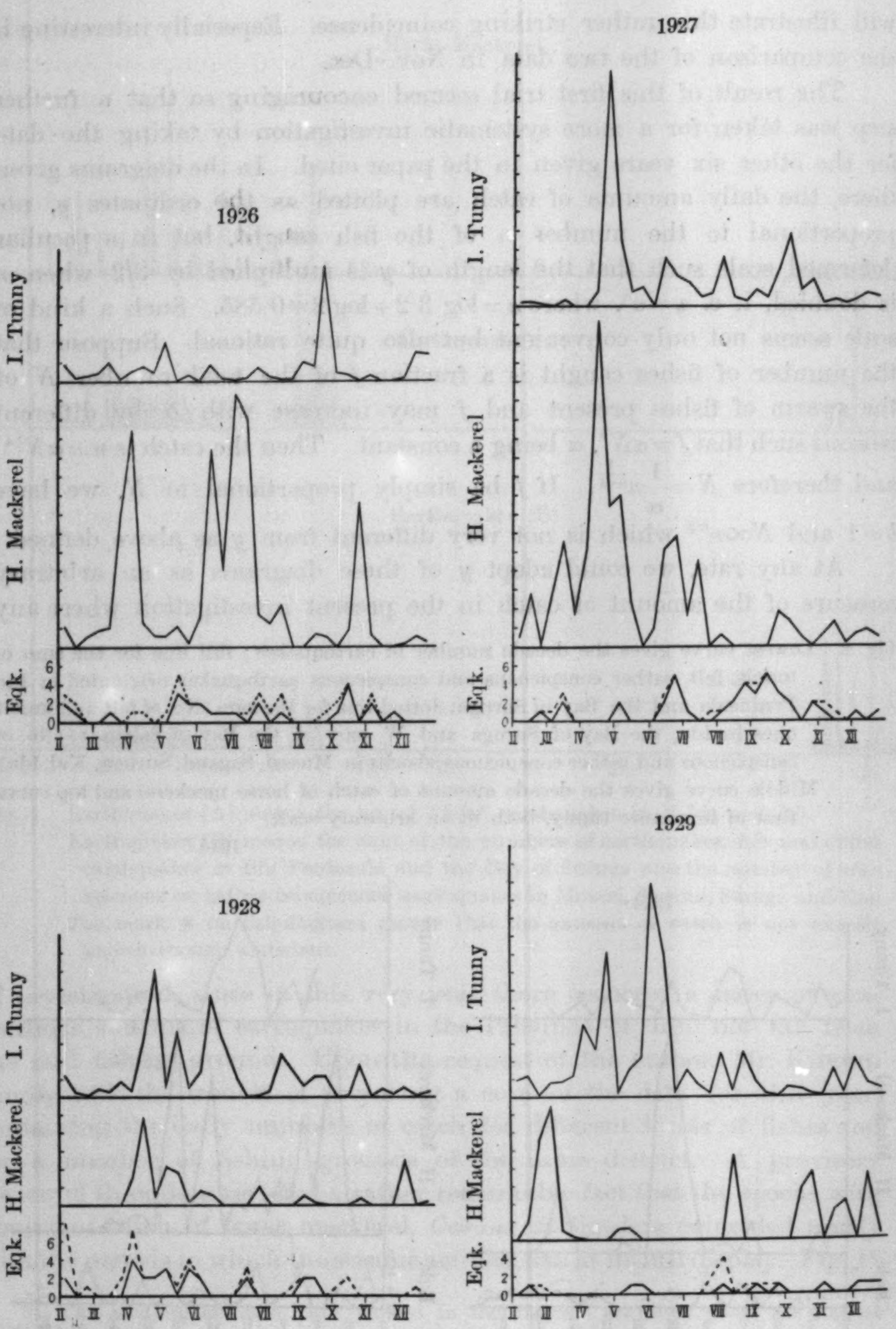
1926
1927
1928
1929
I. Tunny
H. Mackerel
Eqk.
6
4
2
0
I
II
III
IV
V
VI
VII
VIII
IX
X
XI
XII

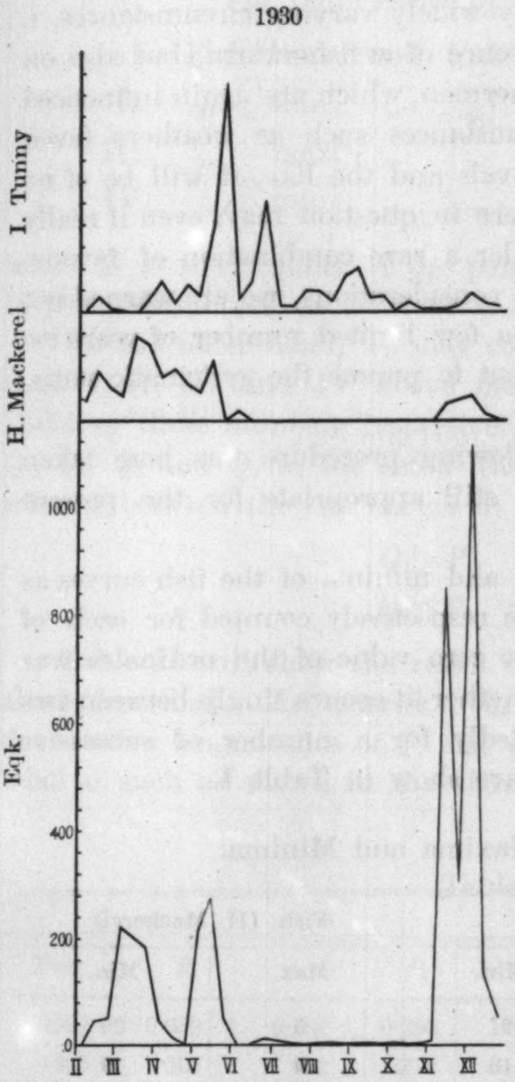

convenient measure may be allowed, as long as it reproduces the relative magnitudes of the daily values in their right order of sequence.

As the daily values of y show very irregular fluctuations which depend partly on natural and partly on artificial circumstances, a smoothing procedure was taken in the following manner. Each month was divided into the three parts: 1–10, 11–20 and 21–end of the month. The sum of y's contained in each of these parts was calculated and plotted as ordinates against the time axis. The result is shown in Fig. 2.

As for the seismic activity to be compared with these fishery data, the materials were exclusively taken from Kisyô-Yoran of the Central Meteorological Observatory, from which we picked out all the "felt" as well as "unfelt" earthquakes originated in a limited area including Idu Province and the Bay of Suruga with its marginal districts. The daily numbers of these earthquakes were counted and then the sum of their numbers for each of the three parts of each month was calculated and plotted in the similar manner as in the case of fish data.

In the case of 1930, the fish curve refers to the fishing place different from that for the other years as already mentioned. This lack of uniformity will, however, be of little importance in the present qualitative investigations, as the two stations are not far from each other.

Examining Fig. 2, it will be seen that the parallelism between the two curves to be compared is most striking in the case of 1928 beside 1930, but not generally very conspicuous in the other years.

If we consider, however, that the amount of catch at a certain

fishing ground may depend upon very widely varying circumstances, i. e. not only upon the arrival and presence of a fish-swarm, but also on the fishing activity on the part of fishermen, which are again influenced by many natural and artificial circumstances such as weathers (even earthquakes!), holidays, religious festivals and the like, it will be of no wonder if the statistical correlation here in question may, even if really existing, reveal itself only seldom under a rare combination of favourable circumstances. In view of these considerations, we are warned not to attribute the above coincidence in a few limited number of years too hastily to a mere play of accidence, but to pursue the systematic statistical investigations a step further.

For this latter purpose, the following procedure was here taken which seemed relatively simple and still appropriate for the present preliminary stage of research.

At first, the numbers of maxima and minima of the fish curves as well as of the earthquake curves were respectively counted for each of the seven years. In this counting the zero value of the ordinates was counted each time as a minimum, whether it occurs singly between two finite ordinates or it appears repeatedly for a number of successive epochs. The numbers thus counted are show in Table I.

Table I. Number of Maxima and Minima.

Year	Earthquake		Fish. (H. Mackerel)	
	Max.	Min.	Max.	Min.
1924	7	21	6	20
1925	13	16	9	19
1926	8	18	9	11
1927	8	18	10	15
1928	7	25	7	21
1929	10	23	6	19
1930	5	20	7	22

From these numbers we could calculate the values of the probability of accidental coincidence for different combinations of maxima or minima of one curve with maxima and minima of the other. Thus, denoting by M and m the numbers of maxima and minima respectively and distinguishing the cases for fish and earthquake respectively by the suffixes f and s, we have

For Coincidence of	Probability
I. Fish max. and Eqk. max.,	$M_f M_s / N^2 = P_1$,
II. „ min. „ „ min.,	$m_f m_s / N^2 = P_2$,
III. „ max. „ „ min.,	$M_f m_s / N^2 = P_3$,
IV. „ min. „ „ max.,	$m_f M_s / N^2 = P_4$,

where N is the number of the points on the time axis, i. e. $3 \times 11 = 33$ in the present case, as January is lacking.

On the other hand, we may count the actual numbers of the four cases I, II, III and IV above mentioned, from the curves of Fig. 2. Dividing these numbers respectively by N we obtain the probabilities Q_1, Q_2, Q_3 and Q_4 in the actual case. If there exists any positive correlation between the two curves to be compared, we may expect that

$$Q_1 > P_1, \qquad Q_2 > P_2,$$
$$Q_3 < P_3, \qquad Q_4 < P_4.$$

Table II will show the result of statistics carried out in the manner above described. The asterisk $*$ in the table marks the cases for which the relative magmitudes of P and Q are in favour of a positive correlation such as shown in the above inequalities.

Table II.

Year	P_1		Q_1	P_2		Q_2	P		Q_3	P_4		Q_4
1924	0·039	*	0·182	0·386		0·333	0·129		0·167	0·116	*	0·061
1925	·107		·030	·279	*	·394	·227	*	·181	·132	*	·121
1926	·066	*	·091	·182		·182	·081	*	·000	·149	*	·091
1927	·073	*	·091	·248		·212	·110		·167	·165		·167
1928	·045	*	·061	·482	*	·546	·135	*	·091	·161		·167
1929	·055	*	061	·401		·394	·175		·182	·127	*	·121
1930	·032	*	·061	·404	*	·455	·101	*	·030	·129	*	·061
Mean	0·059	*	0·081	0·340	*	0·359	0·137	*	0·117	0·139	*	0·113

Thus, for the case I, $Q_1 > P_1$ except for 1925, in which year however II, III and IV show the favourable relations. The year 1930 shows exceptionally favourable relation as already mentioned. Lastly, the mean values of the seven years are all in favour of the positive correlation.

Again, we may calculate the ratios

$$\frac{P_1+P_2}{P_3+P_4} \quad \text{and} \quad \frac{Q_1+Q_2}{Q_3+Q_4}$$

for comparison. Table III shows the result.

Table III.

	$\frac{P_1+P_2}{P_3+P_4}$	$\frac{Q_1+Q_2}{Q_3+Q_4}$
1924	1·74	2·43 *
1925	1·08	1·40 *
1926	1·08	3·00 *
1927	1·17	1·00
1928	1·38	2·50 *
1929	1·52	1·50
1930	1·90	2·33 *
Mean	1·45	2·02 *

* marks the year favourable for the positive correlation.

It will be seen that the ratios are generally larger for the actual case than for the case of purely accidental coincidence.

As for the fishes other than horse mackerel, we remarked a rather striking fact that the catch curve for "*mezi*," immature tunny (*Thynnus*) in 1928 shows a striking similarity with horse mackerel curve as well as the earthquake curve. It seems that the parallelism is better if the *mezi* curve be shifted about a month towards the left, i. e. the apparent effect of earthquake upon *mezi* fishery are seen to have taken place with a sensible time-lag. Such a relation is, however, not so conspicuous in the other years. A further investigation on this latter point must be reserved for a future when a more abundant and reliable data are at our disposal.

Though it will be premature to propose anything like an explanation of the relation of which the existence has just been sheerly shown here as probable, it will not be useless to point out different possibilities conceivable in connection with the present problem, especially for the purpose of drawing the attention of oceanographers and biologists in seismic countries, without whose collaborations it will be difficult to pursue the present investigation any further. Firstly, the seismic shocks or

some kinds of mechanical stimuli associated with them may be directly felt by fishes and induce them to approach the fishing ground in some or other ways. Secondly, the shocks may somehow affect the depth of the layers with the greatest density of some planktons edible for the fishes.[3] Thirdly, the earthquakes may affect the chemical nature of the coastal sea water due to the disturbance of the subterranean water and thus indirectly affect the planktons or fishes. These possibilities could be tested by observations, or by some experiments, if desired. The present result seems at least to encourage than to discourage these kinds of observations or experiments on the sides of marine biologists engaged with the investigation of scientific problems of fisheries.

---

26. 地震と漁獲との關係

地震研究所　寺田寅彦

駿河灣北端にある漁場の漁獲高の日々の變化と、伊豆及駿河灣附近に於ける地震の日々頻度の變化との間の關係を調べた。先づ昭和五年の伊豆に於ける群起地震の日々頻度と、重寺漁場に於ける鰺の漁獲高と比べて見ると著しい相關のある事が認められる。次に 1924–1929 の六年間につきては淡嶋漁場の漁獲、1930 に就ては上記重寺漁場の漁獲を採り、一ケ月を三分した其各部分に於ける地震回數と漁獲との間の關係を調べて見た。其方法としては先づ地震の曲線と漁獲の曲線との最高及最低の數を數へ、それからして、地震と漁獲とが無關係な場合に於ける兩曲線最高最低の重なる確率を計算し、それを實際に兩者の重なつて居る比率と對照した。其結果は兩者が全く無關係でなく互に正の相關をもつて居るらしいといふことになつた。此關係は昭和三年、同五年には著しく明瞭であるが年によつては明瞭でない。併し七年間の平均から云へば矢張多少の正相關があると認めなければならない。鰺の外ではメジが矢張多少の關係を示すやうであるが、此に就ては更に研究をしなければ確かな事は云はれない。

此論文に用ゐた漁獲高の材料は水產試驗場技師木村喜之助君の好意によつて手に入れる事が出來たものである。玆に同君に對する感謝の意を表する。

---

3) Dr. K. Tago who was collecting planktons at the mouth of the Bay of Tôkyô on the very morning of Sept. 1, 1923, i. e. the day of the Great Kwantô Earthquake, observed an unusal abundance of planktons in the surface layer combined with the scantiness of them in the middle layer. At the same time, an unusual swarm of *Katuwo* was observed and caught in the vicinity of Okinosima where such thing occurs quite rarely, *Kwagaku-Tisiki*, **3** (1923), No. 11; *Tigakuzassi*, **36** (1923), No. 420.

27. *Deformation of the Rhombic Base Lines at Mitaka and Earthquake Frequency in Kwantô Districts.*[1]

By Torahiko TERADA,

Earthquake Research Institute.

(Read Nov. 17 and Dec. 15, 1931.—Rec. Mar. 19, 1932.)

The secular variation of the area of the rhombus formed by a set of five geodetic base lines, situated in the compound of the Tôkyô Astronomical Observatory at Mitaka, was already investigated fully by C. Tsuboi,[2] who suspected a possible connection between an abnormal change of this area and the occurrence of a severe earthquake. While dealing with the statistical data of the yearly frequencies of earthquakes in the Kwantô District, the present author happened to remark some trace of apparent relation between the said variation of the frequencies and the variation of the area of the rhombic base lines. An attempt was, therefore, made to investigate in some detail whether such a relation may exist actually.

For the data of the earthquakes to be taken for the basis of the statistical investigation, the List of the "conspicuous" and "rather conspicuous" earthquakes, compiled by Mr. Takami Isikawa[3] of the Central Meteorological Observatory, was utilized. As the List ends with 1925, the later data were taken directly from Kisyô-yôran up to 1931. From these data those earthquakes were picked out of which the epicentres are located in the Kwantô District, i. e. the Provinces of Musasi, Sagami, Awa, Kadusa, Simoosa, Kôduke, Simotuke and Hitati. To these were added those earthquakes originated in Idu, Kai and Iwaki, though the omission of these could scarcely affect the general qualitative feature of the results. Those earthquakes located in the sea area off the Pacific coast of the above district were also taken into account.

For the change of area of the base-line-rhombus, the mean value was taken of the increments of the areas of the two adjacent triangles composing the rhombus, observed during the interval between the two successive measurements. Thus, denoting the mean area by S, we cal-

1) An abstract of this paper is already published in *Proc. Imp. Acad.*, **8** (1932), 8.

2) C. TSUBOI, *Proc. Imp. Acad.*, **6** (1929), 367; *ibid.*, **7** (1931), 155.

3) T. ISHIKAWA, *Kensin-Zihô*, **2** (1926), 87.

culated $\Delta S/S = s$ for the successive intervals. On the other hand, the numbers n of earthquakes recorded during the corresponding intervals were to be counted and compared with the above s. The counting was made in the following three ways: (1) The number was counted regardless of intensity of the earthquake. (2) Those earthquakes were only counted of which the epicentres are located in the land area (including the Tokyo Bay and Uraga Channel). (3) The earthquakes were weighted according to intensities, namely with the weight 1 for the "rather conspicuous," 2 for the "conspicuous" and 3 for those severe ones accompanied with sensible destructive effects and casualities. Denote the numbers respectively by n_1, n_2 and n_3. The difference $n_1 - n_2$ will practically give the number of earthquakes originated from the sea area. The time interval for counting the earthquakes was taken from the day on which the geodetic measurement at the beginning of the said interval was completed to the day on which the next measurement was closed. Table I (A) gives the data used for the comparison.

Table I. (A)

	Time Intervals from — to	No. of Days	s 10^{-5}	n_1	n_2	n_3	$\dot{s}$ 10^{-6}/100d.	$\dot{n}_1$ No./100d.	$\dot{n}_2$ No./100d.	$\dot{n}_3$ No./100d.	$\dot{n}_1-\dot{n}_2$ No./100d.
1.	1916. VI. 11—1917. II. 20	254	−0·045	26	6	33	−0·18	10·2	2·4	13·0	7·9
2.	1917. II. 20— 〃 . X. 17	239	+0·525	17	10	22	+2·20	7·1	4·2	9·2	2·9
3.	〃 . X. 17—1918. II. 10	116	−0·525	11	4	12	−4·53	9·5	3·5	10·3	6·0
4.	1918. II. 10— 〃 . X. 23	255	−0·050	18	8	23	−0·20	7·1	3·1	9·0	3·9
5.	〃 . X. 23—1919. XII. 12	415	+0·345	21	8	23	+0·83	5·1	1·9	5·5	3·1
6.	1919. XII. 12—1920. XI. 24	348	+0·330	23	7	29	+0·95	6 6	2·0	8·3	4·6
7.	1920. XI. 24—1921. XI. 8	349	+0·095	12	9	17	+0·27	3·4	2·6	4·9	0·9
8.	1921. XI. 8—1922. XI. 8	365	−0·215	26	19	39	−0·59	7·1	5·2	10·7	1·9
9.	1922. XI. 8—1923. IX. 6	302	+2·910	33	17	47	+9·64	10·9	5·6	15·6	5·3
10.	1923. IX. 6— 〃 . X. 24	48	−0·545	18	15	26	−11·36	37·5	31·3	54·2	6·3
11.	〃 . X. 24—1924. I. 29	97	−0·260	21	17	26	−2·68	21·7	17·5	26·8	4·1
12.	1924. I. 29— 〃 . VIII. 15	199	−0·345	27	16	32	−1·73	13·6	8·0	16·1	5·5
13.	〃 . VIII. 15—1925. XII. 17	487	+0·380	44	29	46	+0·78	9·0	5·9	9·4	3·1
14.	1925. XII. 17—1927. XII. 16	729	+0·935	37	12	39	+1·28	5·1	1·7	5·4	3·4
15.	1927. XII. 16—1929. III 20	460	−0·195	13	6	16	−0·42	2·8	1·3	3·5	1·5
16.	1929. III. 20—1930. II. 14	331	−0·470	9	3	12	−1·42	2·7	0·9	3·6	1·8
17.	1930. II. 14—1931. X. 6	599	+0·360	28	12	42	+0·60	4·7	2·0	7·0	2·7

Table I (B). For the meaning of n''s and n'''s see later.

Time Interval No.	n_1'	n_2'	n_3'	$\dot{n}_1'$	$\dot{n}_2'$	$\dot{n}_3'$	n_1''	n_2''	n_3''	$\dot{n}_1''$	$\dot{n}_2''$	$\dot{n}_3''$
1	22	4	28	8·7	1·6	11·0	22	4	30	8·7	1·6	11·8
2	19	10	25	8·0	4·2	10·5	18	4	23	7·5	1·7	9·6
3	9	6	9	7·8	5·2	7·8	10	6	14	8·6	5·2	12·1
4	19	7	25	7·5	2·7	9·8	22	10	24	8·6	3·9	9·4
5	22	8	24	5·3	1·9	5·8	24	11	29	5·8	2·7	7·0
6	25	8	31	7·2	2·3	8·9	26	7	32	7·5	2·0	9·2
7	12	9	17	3·4	2·6	4·9	14	8	20	4·0	2·3	5·7
8	24	17	37	6·6	4·7	10·1	18	15	27	5·9	4·1	7·4
9	25	11	28	8·3	3·6	9·3	22	14	27	7·3	4·6	8·9
10	15	11	31	31·3	22·9	64·6	0	0	0	0·0	0·0	0·0
11	26	21	31	26.8	21·6	32·0	13	3	15	13·4	3·1	15·5
12	31	23	38	15·6	11·6	19·1	53	43	78	26·6	21·6	39·2
13	46	29	49	9·4	6·0	10·1	56	36	61	11·5	7·4	12·5
14	38	14	40	5·2	1·9	5·5	36	15	37	4·9	2·1	5·1
15	12	6	14	2·6	1·3	3·0	21	9	24	4·6	2·0	5·2
16	10	3	14	3·0	0·9	4·2	12	3	16	3·6	0·9	4·8
17	25	10	36	4·2	1·7	6·0	18	7	24	3·0	1·2	4·0

At first, the values of s, n_1, n_2, n_3 were respectively plotted as ordinates against the time as abscissa, taking the middle points of the successive intervals as the corresponding time. Some apparent positive correlation was noted between s and n's. It must, however, be taken into consideration that s as well as n's represent the total increments for the common interval of time, so that when the intervals are not constant the above graph will merely serve for the comparison of $ds/dt.\Delta t$ with $dn/dt.\Delta t$, but not of dn/dt with dn/dt. On plotting Δt curve, it may be seen that the above apparent correlation is utterly illusory.

In comparing the time rates of s and n with each other, some difficulty is felt, since the intervals are rather irregular. Disregarding this irregularity, however, ds/dt and dn/dt were estimated by dividing the above values of s and n by the number of days in the corresponding interval. The graphs of these time rates are plotted in Fig. 1, in which the ds/dt curve is drawn inverted. In order to discuss the possible relation between the two quantities ds/dt and dn/dt, the following

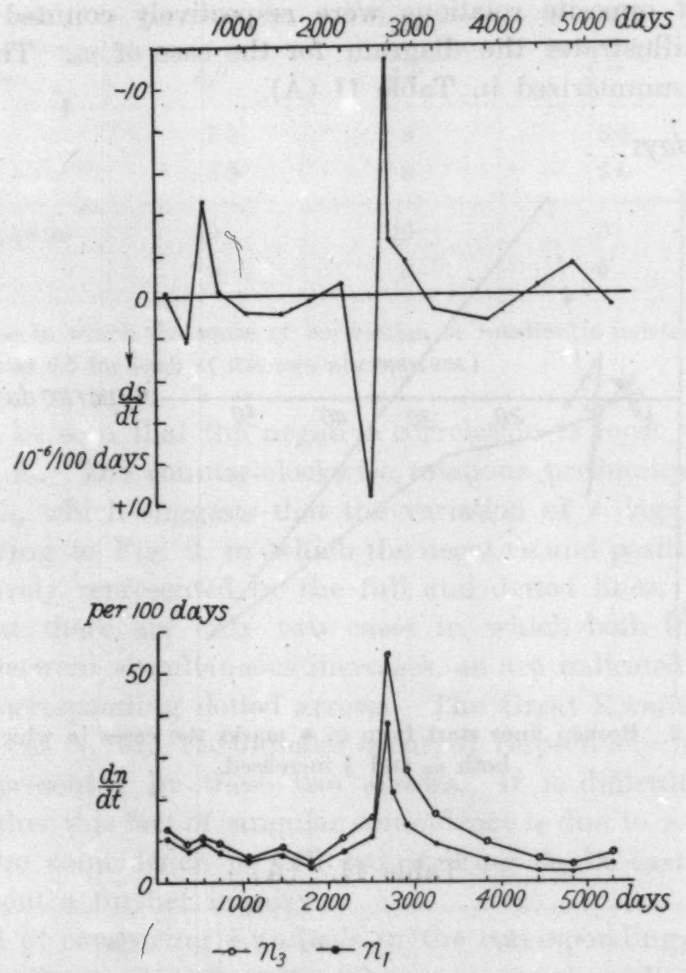

Fig. 1.

graphical method was employed. Taking $dn/dt=\dot{n}$ and $ds/dt=\dot{s}$ respectively as abscissa and ordinate, the points are successively plotted for the successive intervals and the consecutive points are connected by a straight line marked by arrow showing the time sequence. If a positive or negative correlation prevailed between the two quantities these straight lines will show a tendency to make acute or obtuse angle respectively with the positive direction of x. Besides, if there existed some systematic time-lag between the two quantities the successive arrows will show a tendency to be gradually deflected either in clockwise or counter-clockwise sense.

Such diagrams were constructed and the numbers of cases with the positive and negative correlations, as well as of those with the

clockwise and opposite rotations were respectively counted for each of $\dot{n}$'s. Fig. 2 illustrates the diagram for the case of n_3. The results of statistics are summarized in Table II (A).

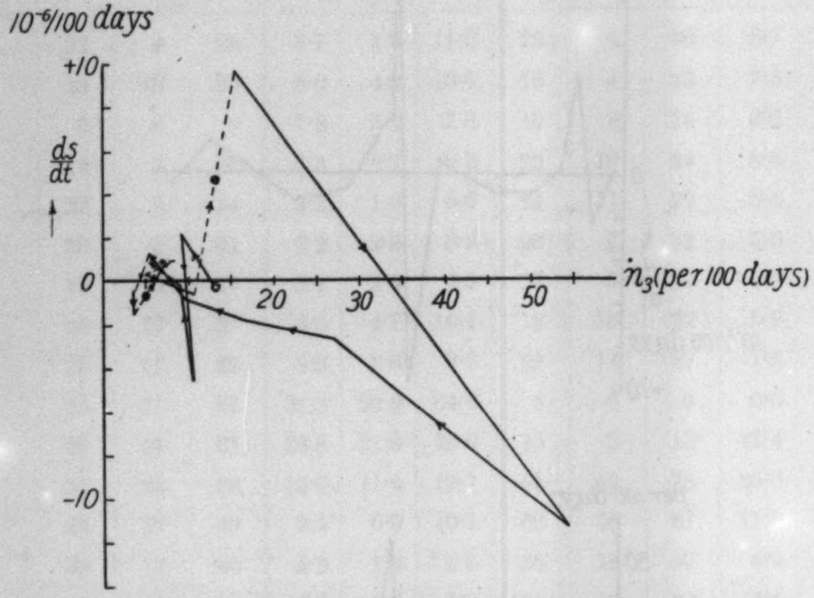

Fig. 2. Broken lines start from ○. ● marks the cases in which both $\dot{n}_3$ and $\dot{s}$ increased.

Table II. (A)

Correlation	$\dot{n}_1$	$\dot{n}_2$	$\dot{n}_3$	$\dot{n}_1-\dot{n}_2$
Negative	10	9	11	9
Positive	6	7	5	7
Counter-clockwise	10	10	9	8
Clockwise	5	5	6	7

(B)

Correlation	$\dot{n}_1'$	$\dot{n}_2'$	$\dot{n}_3'$	$\dot{n}_1'-\dot{n}_2'$
Negative	10	11	10	9
Positive	6	5	6	7
Counter-clockwise	10	6·5	10	10
Clockwise	5	8·5	5	5

(C)

Correlation	$\dot{n}_1''$	$\dot{n}_2''$	$\dot{n}_3''$	$\dot{n}_1''-\dot{n}_2''$
Negative	7·5	8	8·5	7
Positive	8·5	8	7·5	9
Counter-clockwise	10	10	9	8
Clockwise	5	5	6	7

(The case in which the sense of correlation or rotation is indeterminate, is counted as 0.5 for each of the two alternatives.)

It will be seen that the negative correlation is most conspicuous in the case of $\dot{n}_3$. The counter-clockwise rotations predominate in the case of $\dot{n}_1$ and $\dot{n}_2$, which suggests that the variation of $\dot{s}$ lags after that of $\dot{n}$'s. Referring to Fig. 2, in which the negative and positive correlations are respectively represented by the full and dotted lines, it may be remarked that there are only two cases in which both the quantities $\dot{s}$ and $\dot{n}_3$ underwent simultaneous increases, as are indicated by • marked upon the corresponding dotted arrows. The Great Kwantô Earthquake and the recent N. Idu Earthquake occurred respectively in the intervals of time represented by these two arrows. It is difficult at present to decide whether this fact of singular coincidence is due to a mere accident or not. The coincidence is still too striking to be cast off as utterly trivial without a further inquiry.

Instead of comparing $\dot{s}$ and $\dot{n}$'s in the corresponding time intervals the time for the earthquakes was taken one month earlier than that for $\dot{s}$; for example, s in the interval 11 June 1916—20 Feb. 1917 was made to correspond with n for 11 May 1919-20 Jan. 1917. We denote these numbers of earthquakes by n''s which are tabulated in Table I (B). The result of the similar statistics is shown in Table II (B).

Similarly the epochs for n's were taken six months earlier than those for s. Denoting the corresponding n and dn/dt for this epoch by n'' and $\dot{n}''$ which are tabulated in Table I (B), the relation between the variations of $\dot{s}$ and $\dot{n}''$ is summarized in Table II (().

It will be seen that in Table II (B) for n', the negative correlation is preserved and even improved a little for n_2, for which the apparent time-lag has disappeared. In Table II (C), the negative correlation has entirely been obliterated, while the apparent time-lag remains for n_1'' and n_2''.

From these results, it may be concluded that there exists at least some traces of relation between the variations of $\dot{s}$ and $\dot{n}$ here considered. It seems (1) that generally $\dot{s}$ decreases with the increased $\dot{n}$ and (2) that the variation of $\dot{s}$ lags a little behind that of $\dot{n}$.

On the other hand, the semi-annual numbers of earthquakes were counted as shown in Table III, from which the mean values for the successive two half-years were taken and plotted in Fig. 3, together with the inverted $\dot{s}$ curve.

Table III.

Time Interval		No. of Eqks.			Time Interval		No. of Eqks.		
		n_1	n_2	n_3			n_1	n_2	n_3
1916	VII-XII	17	4	22	1924	I-VI	29	18	36
1917	I-VI	15	5	22	〃	VII-XII	22	14	25
〃	VII-XII	15	11	15	1925	I-VI	19	12	19
1918	I-VI	14	4	18	〃	VII-XII	10	7	10
〃	VII-XII	9	4	11	1926	I-VI	11	5	11
1919	I-VI	11	5	12	〃	VII-XII	7	2	8
〃	VII-XII	11	3	15	1927	I-VI	7	1	7
1920	I-VI	15	4	19	〃	VII-XII	13	4	14
〃	VII-XII	10	6	15	1928	I-VI	6	8	8
1921	I-VI	7	5	8	〃	VII-XII	3	3	3
〃	VII-XII	3	3	6	1929	I-VI	8	11	11
1922	I-VI	17	13	27	〃	VII-XII	2	3	3
〃	VII-XII	10	6	10	1930	I-VI	9	11	11
1923	I-VI	20	7	23	〃	VII-XII	5	8	8
〃	VII-XII	42	33	64	1931	I-VI	8	13	13

Though it will be premature to presume a theoretical discussions of the present result based on such a scanty data, the following considerations will be of some interest at least in way of a suggestion. Two alternatives may be proposed regarding the possible relation between s and n, as far as they are not in contradiction with the present results, i. e.

$$\frac{dn}{dt}-f(t)+k\frac{ds}{dt}=0, \qquad (1)$$

$$\frac{d}{dt}\left\{\frac{dn}{dt}-\phi(t)\right\}+k'\frac{ds}{dt}=0, \qquad (2)$$

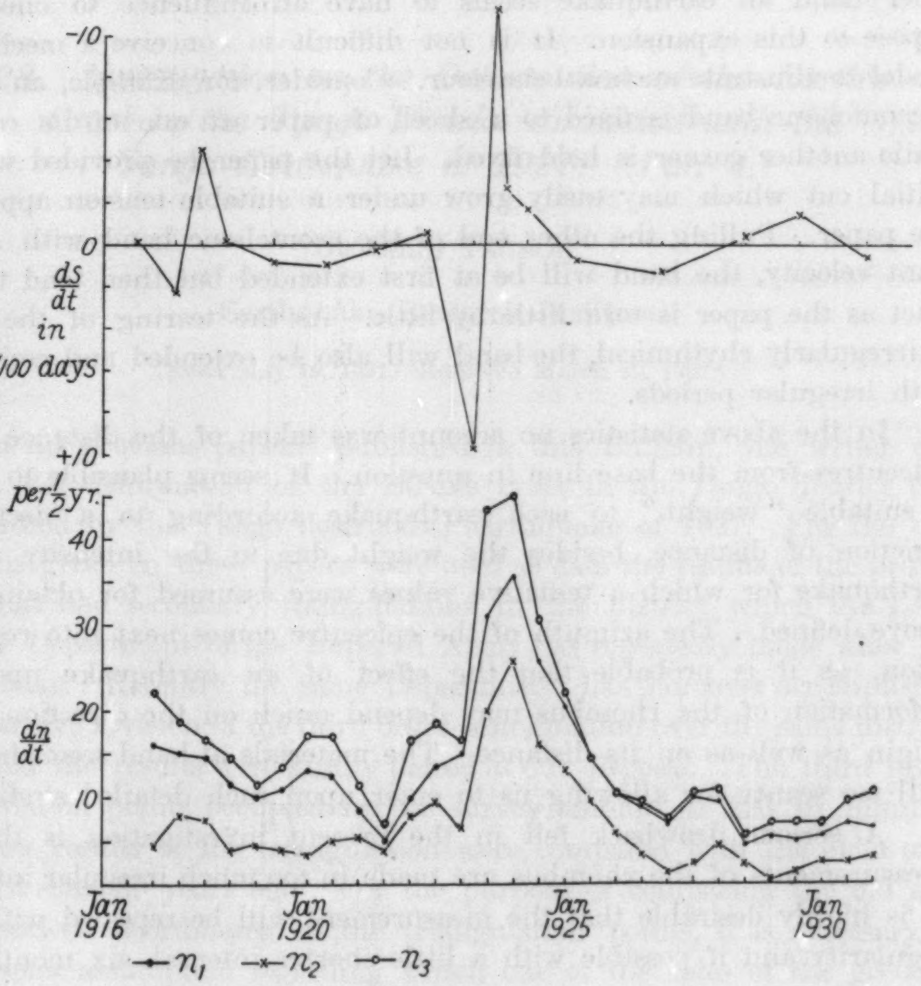

Fig. 3.

where $f(t)$ and $\phi(t)$ are slowly varying functions of time, and k and k' positive constants. From these we obtain respectively

$$k(s-s_0)=\int_0^t f(t)dt-n, \tag{1'}$$

$$k'(s-s_0)=ct+\int_0^t \phi(t)dt-n, \tag{2'}$$

where s_0 and c are constant. Provided with a sufficiently abundunt data, it seems possible to undertake a statistical test of such a relation and even to determine the form of $f(t)$ or $\phi(t)$.

At any rate, it seems that the area of the rombus is subjected to a gradual secular expansion owing to some straining force continuously acting on the part of the earth's crust on which it is situated. On the

other hand an earthquake seems to have an influence to check, or oppose to this expansion. It is not difficult to conceive a mechanical model to illustrate such a behaviour. Consider, for example, an end of a caoutchouc band is fixed to a sheet of paper at one of its corners, while another corner is held fixed. Let the paper be provided with an initial cut which may easily grow under a suitable tension applied to the paper. Pulling the other end of the caoutchouc band with a constant velocity, the band will be at first extended but then tend to contract as the paper is torn little by little. As the tearing of the paper is irregularly rhythmical, the band will also be extended and contracted with irregular periods.

In the above statistics no account was taken of the distance of the epicentres from the base line in question. It seems plausible to assign a suitable "weight" to each earthquake according to a decreasing function of distance, besides the weight due to the intensity of the earthquake for which a tentative values were assumed for obtaining n_3 above defined. The azimuth of the epicentre comes next into consideration, as it is probable that the effect of an earthquake upon the deformation of the rhombus may depend much on the direction of the origin as well as on its distance. The materials at hand seems however still too scanty for allowing us to enter upon such detailed studies.

A serious drawback felt in the present investigation is that the measurements of the rhombus are made in too much irregular intervals. It is highly desirable that the measurement will be repeated with more regularity and if possible with a little shorter interval, six months say.

---

27. 三鷹村菱形基線の變形と關東地方に於ける地震頻度との關係

地震研究所　寺　田　寅　彦

三鷹菱形基線によつて圍まれた面積の變化速度と、關東地方に於ける顯著な地震の頻度との間の統計的關係を調査した結果、兩者の間に多少の相關が存在することを確めることが出來た。面積は地震のない時は增大する傾向があるが、地震があるとそれが減ずるやうな傾向がある。なほ、偶然かも知れないが、關東地震の時と北伊豆地震の時と、此の二つの場合に相當する期間に限つて、面積變化速度と地震頻度との關係の異常が認められる。

---

28. *Investigation on the Deformation of the Earth's Crust in the Tango District connected with the Tango Earthquake of 1927.* (*Part 4.*)

By Chûji TSUBOI,

Earthquake Research Institute.

(Read May 19, 1931.—Received March 20, 1932.)

In his previous papers[1] published in this Bulletin, the writer discussed the deformation of the earth's crust in the Tango district that was caused by the Tango destructive earthquake of 1927. For the discussions given in these papers were used as data the results of the precise levellings and secondary triangulations in the district which the Land Survey Department of the Imperial Army has repeatedly made after the earthquake. Recently the same Department[2] has moreover accomplished an extensive revision of the third order triangulation over the same district, of which the results were kindly placed at our disposal. The third order triangulation points occupied by the survey amount to 226 in number. The new results of the triangulation were compared with the older ones obtained some 30 years ago. For the purpose of comparing the old and new geodetic coordinates of the triangulation points, it is necessary to make some assumption regarding which one of the sides of the geodetic triangles in the district is to be taken as remained unchanged both in its length and azimuth notwithstanding the disturbance of the earthquake. This side must be one of a geodetic trigangle of which the change in shape between the old and new surveys is smallest of all in the district. Among all the primary triangles in the district, the sum of the absolute values of the differences of internal angles between the old and new surveys is smallest for the triangle Hyônoyama, Kasagatayama and Tokonooyama, being 0″298. Among the triangles that are in contact with the above one, the sum of the absolute values of the differences of internal angles between the old and new surveys is smallest for the triangle Hyônoyama, Kasagatayama and Sirahatayama, being 1″924. Being com-

1) C. TSUBOI, *Bull. Earthq. Res. Inst.*, **6** (1929), 71; **8** (1930), 153, 388; **9** (1931), 423.

2) LAND SURVEY DEPARTMENT, "Results of the Revision of the Third Order Triangulations in the Tango District," (1930), (a pamphlet in Japanese).

mon to both triangles, the side Hyônoyama-Kasagatayama was taken to have been unchanged between the old and new surveys both in its length and azimuth. This assumption is of course a tentative one, but so far as we confine ourselves to the discussions of the relative displacements of the triangulation points and of the strain of the earth's crust produced by them, this assumption, though it may differ a little from reality, will produce no serious errors in the discussions besed on it. The horizontal and vertical displacements of the triangulation points as found by the comparison of the old and new surveys in this way are given in Table I, Fig. 1 and Fig. 2. Though these values have already been published in pamphlets by the Land Survey Department in Japanese language, the writer may be allowed to reproduce the values here for the benefit of reference.

Table I.

A. Horizontal and Vertical Displacements of the First Order Triangulation Points in the Tango District.

u Eastward Displacement.
v Northward Displacement.
w Upward Displacement.
$\sqrt{u^2+v^2}$ Resultant Horizontal Displacement.
$tg^{-1}\frac{u}{v}$ Azimuth of Horizontal Displacement Measured Clockwise from North.

Taiangulation Point	u	v	$\sqrt{u^2+v^2}$	$tg^{-1}\frac{u}{v}$	w
	m	m	m		m
Taikoyama	−0·473	+0·339	0·582	305° 38′	+0·04
Kuruhizan	+0·106	−0·197	0·224	151 43	−0·16
Isanagosan	+0·018	−0·484	0·484	177 52	+0·02
Taneziyama	−0·204	+0·259	0·330	321 46	−0·16
Tokonooyama	−0·033	−0·006	0·033	259 42	0·00
Karasugadake	−0·088	+0·169	0·190	332 30	+0·03

B. Horizontal and Vertical Displacements of the Second Order Triangulation Points in the Tango District.

u Eastward Displacement.
v Northward Displacement.
w Upward Displacement.
$\sqrt{u^2+v^2}$ Resultant Horizontal Displacement.
$tg^{-1}\frac{u}{v}$ Azimuth of Horizontal Displacement Measured Clockwise from North.

Triangulation Point	u	v	$\sqrt{u^2+v^2}$	$tg^{-1}\frac{u}{v}$	w
	m	m	m		m
Kwannonzan	−0·023	−0·068	0·072	198° 41′	+0·05
Minato	+0·078	−0·364	0·372	167 54	−0·31
Nyoô	−0·070	−0·807	0·810	184 57	+0·16
Motomiduka	−0·083	−0·151	0·172	208 48	+0·05
Mitani	+0·126	−0·308	0·333	157 45	−0·15
Ooyama	−0·139	+0·243	0·280	330 14	−0·23
Simomura	+0·015	−0·182	0·183	175 17	+0·11
Hatidyômura	+0·003	−0·247	0·247	179 18	−0·08
Ôokadera	−0·136	−0·277	0·309	206 9	−0·01
Isikawamura.	−0·408	+0·425	0·589	316 10	−0·02
Yuragadake	−0·393	+0·295	0·492	306 59	−0·13
Sengenzi	−0·219	+0·265	0·344	320 26	−0·05
Kayaoku	−0·151	−0·009	0·151	266 35	+0·06
Higasimitumatumura	−0·035	+0·243	0·245	351 48	−0·13
Hurudera	+0·066	−0·169	0·182	158 40	+0·06
Amautimura	−0·242	+0·136	0·278	299 20	−0·03
Izamura	+0·020	−0·151	0·152	172 27	+0·10
Sendyôgadake	−0·182	+0·253	0·312	324 16	−0·15
Okadanakamura	−0·272	+0·320	0·420	319 38	+0·15
Yôrôgadake	−0·116	+0·154	0·193	323 1	−0·02
Yabegadake	−0·124	+0·317	0·340	338 38	−0·17
Noboriotôge	−0·124	+0·043	0·131	289 8	−0·17
Kutami	−0·101	+0·210	0·233	334 19	−0·04
Mutuyori	−0·111	+0·154	0·190	324 13	+0·08
Nômi	−0·045	+0·037	0·058	309 26	−0·11
Higasihattamura	−0·048	+0·136	0·144	340 34	+0·17
Hosibara	−0·066	+0·126	0·142	332 21	+0·01
Kamikawagutimura	−0·157	+0·065	0·170	292 29	−0·11

(*to be continued.*)

Table I. B. (*continued*.)

Triangulation Point	u	v	$\sqrt{u^2+v^2}$	$tg^{-1}\frac{u}{v}$	w
	m	m	m		m
Kamanowa	+0·015	+0·049	0·051	17° 1′	+0·02
Oda	-0·056	+0·037	0·067	303 27	+0·27
Kamikawai	+0·013	+0·040	0·042	18 0	-0·18
Simotakeda	-0·094	+0·031	0·099	288 15	+0·02
Nomura	-0·432	+0·376	0·573	311 2	-0·03
Itigao	-0·869	+0·626	1·071	305 46	-0·08
Oohara	-0·588	+0·327	0·673	299 5	-0·17
Simooka	+0·531	-1·128	1·247	154 48	-0·08
Yorizawa	-0·745	+0·804	1·096	317 11	-0·09
Tudumigadake	-0·524	+0·524	0·741	315 0	0·24
Kurosaki	-0·556	+0·487	0·739	311 13	+0·03
Miemura	+0·116	+0·918	0·925	7 12	+0·48
Osima	-0·287	+0·404	0·496	324 37	-0·22

C. Horizontal and Vertical Displacements of the Third Order Triangulation Points in the Tango District.

u Eastward Displacement.
v Northward Displacement.
w Upward Displacement.
$\sqrt{u^2+v^2}$ Resultant Horizontal Displacement.
$tg^{-1}\frac{u}{v}$ Azimuth of Horizontal Displacement Measured Clockwise from North.

Triangulation Point	u	v	$\sqrt{u^2+v^2}$	$tg^{-1}\frac{u}{v}$	w
	m	m	m		m
Kumi	-0·0	-0·277	0·277	180° 00′	-0·08
Kôyama	-0·126	-0·493	0·509	194 20	+0·10
Hakoisi	—	—	—	—	—
Oomukai	+0·050	-0·431	0·434	173 23	-0·20
Kandani	+0·126	-0·277	0·304	155 32	-0·32
Totitani	+0·202	-0·370	0·422	151 22	-0·02
Urake	+0·025	-0·647	0·647	177 47	+0·03
Hasidume	+0·101	-0·493	0·503	168 25	-0·02
Idusumi	+0·101	-0·431	0·443	166 49	-0·18
Suda	+0·202	-0·277	0·343	143 54	-0·09

(to be continued.)

Table I. C. (*continued.*)

Triangulation Point	u	v	$\sqrt{u^2+v^2}$	$tg^{-1}\frac{u}{v}$	w
	m	m	m		m
Itinono	+0·176	−0·431	0·466	157° 47′	−0·16
Sano	+0·126	−0·678	0·690	169 28	+0·19
Nonaka	+0·101	−0·555	0·564	169 41	−0·09
Hutamata	0·000	−0·431	0·431	180 0	−0·13
Arikuma	−0·252	+0·185	0·313	306 17	+0·08
Dannosaka	−0·202	0·000	0·202	270 0	+0·01
Ooeyama	−0·252	+0·339	0·422	323 22	−0·11
Akaisidake	−0·126	+0·247	0·277	332 58	−0·06
Hukôtôge	−0·202	+0·431	0·476	334 53	−0·18
Odamura	−0·277	+0·462	0·539	329 3	−0·08
Iwaya	−0·176	−0·185	0·255	223 34	−0·40
Kanawaridani	−0·504	+0·462	0·684	312 31	−0·02
Tyûda	−0·252	+0·308	0·398	320 43	−0·28
Waki	−0·428	+0·308	0·527	305 44	−0·06
Okuyama	−0·403	+0·370	0·547	312 33	+0·01
Nohara	−0·101	+0·308	0·324	341 51	−0·22
Kannonzi	−0·202	+0·247	0·319	320 43	−0·17
Kawabehara	−0·176	+0·247	0·303	324 32	−0·39
Kuroti	0·0	+0·370	0·370	0 0	−0·24
Uranyûhinata	−0·302	−0·185	0·354	238 31	—
Usiroyama	−0·328	+0·031	0·330	275 24	−0·08
Hukayûo	−0·151	+0·123	0·195	309 10	—
Miyama	−0·151	+0·154	0·216	315 34	−0·02
Usitani	−0·176	+0·154	0·234	311 11	+0·11
Sugiyama	−0·176	+0·186	0·255	316 26	−0·21
Hukuroya	−0·176	+0·123	0·215	304 57	−0·06
Toisigatake	−0·126	+0·370	0·391	341 12	−0·24
Kyôhaku	−0·278	+0·247	0·372	311 37	−0·15
Dinusi	−0·353	+0·277	0·449	308 7	+0·11
Seikôzi	−0·302	+0·308	0·431	315 34	+0·10
Ononai	−0·252	+0·216	0·332	310 36	+0·15
Nakati	−0·202	+0·247	0·319	320 43	−0·03
Kuretani	−0·176	+0·216	0·279	320 50	+0·27
Togura	−0·076	+0·247	0·258	342 54	0·0

(*to be continued.*)

Table I. C. (*continued.*)

Triangulation Point	u	v	$\sqrt{u^2+v^2}$	$tg^{-1}\frac{u}{v}$	w
	m	m	m		m
Huruike	−0·126	+0·185	0·224	325° 45′	−0·15
Dake	+0·126	+0·308	0·333	22 15	−0·11
Yuhune	−0·050	+0·431	0·434	353 23	−0·24
Sôgômura	−0·076	+0·401	0·408	349 16	−0·18
Kômori	−0·126	+0·216	0·250	329 45	+0·05
Tunedu	−0·076	+0·092	0·120	320 26	+0·06
Hiuragatake	−0·101	+0·308	0·324	351 51	−0·23
Sorayama	−0·076	+0·431	0·438	350 0	−0·25
Hamagasira	−0·328	+0·247	0·411	306 59	—
Miyatani	−0·252	+0·185	0·313	306 17	−0·02
Kitisaka	−0·176	+0·247	0·303	324 32	0·0
Kahara	−0·176	+0·154	0·234	311 11	−0·02
Rokudi	−0·227	+0·154	0·274	304 9	+0·04
Iidumi	−0·176	+0·062	0·186	289 24	−0·01
Aodi	−0·176	+0·123	0·215	304 57	−0·06
Hazaki	−0·227	+0·185	0·293	309 10	−0·01
Takabatake	−0·202	+0·185	0·274	312 29	+0·06
Tendai	−0·252	+0·185	0·313	306 17	+0·01
Sengokuzan	−0·252	+0·154	0·295	301 26	+0·02
Nakatakidaki	−0·101	+0·154	0·182	326 44	+0·04
Zyosi	+0·076	+0·185	0·200	22 20	+0·01
Mizono	−0·075	−0·863	0·866	184 58	+0·17
Kidu	−0·101	−1·048	1·053	185 30	+0·20
Tukinami	+0·025	−1·202	1·202	178 49	+0·18
Egasayama	−0·101	+0·092	0·137	312 20	+0·11
Kôsindani	−0·101	+0·123	0·159	320 37	−0·18
Horikiri	−0·101	+0·185	0·211	331 22	−0·03
Kurio	−0·076	−0·031	0·082	247 49	−0·10
Tawa	−0·076	+0·154	0·172	333 44	−0·12
Hata	−0·126	−0·123	0·176	225 41	−0·10
Nagasako	−0·152	+0·031	0·155	281 32	−0·17
Umedani	−0·152	+0·062	0·164	292 11	−0·09
Mitakeyama	−0·202	+0·092	0·222	294 29	−0·18
Itinomiya	−0·101	−0·154	0·184	213 16	−0·14

(*to be continued.*)

Table I. C. (*continued.*)

Triangulation Point	u	v	$\sqrt{u^2+v^2}$	$tg^{-1}\frac{u}{v}$	w
	m	m	m		m
Tatunozyô	−0·076	−0·062	0·098	230° 48′	−0·05
Himegami	−0·025	+0·123	0·125	348 31	−0·18
Okiyama	−0·126	+0·185	0·224	325 45	−0·12
Siroyama	—	—	—	—	—
Hadumaki	−0·202	+0·062	0·211	287 04	−0·13
Simoamadu	−0·227	+0·154	0·274	304 09	−0·11
Kôrinzi	−0·076	+0·185	0·200	337 40	−0·12
Nagayama	−0·126	+0·062	0·140	296 12	−0·22
Nagau	−0·328	0·0	0·328	270 0	−0·11
Kasadani	−0·101	+0·247	0·267	337 46	+0·03
Tengamine	−0·101	+0·216	0·239	334 56	+0·08
Bessyo	−0·101	+0·216	0·239	334 56	−0·12
Sorayama	−0·076	+0·185	0·200	337 40	−0·07
Takadake	−0·152	+0·092	0·178	301 11	−0·10
Sigazato	−0·076	+0·154	0·172	333 44	+0·07
Ootani	+0·025	+0·123	0·125	11 29	−0·05
Okuyama	−0·051	+0·216	0·222	346 43	+0·13
Motomiya	−0·025	+0·154	0·156	350 47	−0·21
Sutizan	0·0	+0·062	0·062	0 0	−0·11
Takasiro	−0·051	+0·123	0·133	337 29	−0·16
Kisaiti	−0·202	+0·123	0·236	301 20	−0·11
Monobe	−0·101	+0·123	0·159	320 37	−0·02
Mikunizan	−0·101	+0·185	0·211	331 22	+0·02
Miseuzan	0·0	+0·123	0·123	0 0	+0·10
Kurotani	−0·126	+0·123	0·176	314 19	0·0
Uesugi	−0·076	+0·062	0·098	309 12	+0·03
Nakamurayama	−0·051	+0·092	0·106	331 0	−0·06
Nanahyakkoku	−0·025	+0·154	0·156	350 47	+0·06
Arigaduku	+0·202	+0·277	0·343	36 6	+0·10
Itibandani	0·0	+0·123	0·123	0 0	+0·01
Oro	−0·101	+0·185	0·211	331 22	−0·08
Ikaruga	−0·101	+0·123	0·159	320 37	−0·19
Takanosu	−0·076	0·0	0·076	270 0	−0·19
Simomiya	+0·025	−0·216	0·217	173 24	+0·19

(*to be continued.*)

Table I. C. (*continued.*)

Triangulation Point	u	v	$\sqrt{u^2+v^2}$	$tg^{-1}\frac{u}{v}$		w
	m	m	m			m
Hinado	+0·050	−0·185	0·192	164°	53′	+0·08
Bazi	+0·050	−0·185	0·192	164	53	+0·12
Simokage	−0·050	−0·123	0·133	202	7	−0·11
Sindô	+0·101	−0·370	0·384	164	44	+0·11
Turui	+0·075	−0·185	0·200	157	56	−0·04
Kaodani	+0·126	−0·247	0·277	152	58	+0·18
Tôzima	0·0	−0·277	0·277	180	0	+0·01
Miyai	−0·101	−0·462	0·473	192	20	+0·02
Yuhune	0·0	−0·216	0·216	180	0	−0·13
Takehana	−0·101	−0·586	0·595	189	47	+0·04
Iwai	−0·076	−0·123	0·145	211	43	+0·01
Takui	+0·503	+0·092	0·511	79	38	−0·22
Kazima	+0·101	−0·123	0·159	140	37	+0·32
Miyasita	−0·050	−0·154	0·162	197	59	+0·21
Simoduka	+0·050	−0·154	0·162	162	1	+0·11
Matumoto	+0·075	−0·062	0·097	129	35	+0·34
Tada	−0·101	0·0	0·101	270	0	+0·08
Takesaka	−0·025	−0·185	0·187	187	42	−0·07
Onmata	−0·025	−0·370	0·371	183	52	+0·08
Tai	+0·176	−0·216	0·279	140	50	−0·36
Tuiyama	+0·151	−0·216	0·264	145	3	−0·27
Kei	+0·050	−0·277	0·281	169	46	−0·16
Yasiro	−0·277	−0·308	0·414	221	58	−0·07
Simoyama	−0·277	−0·586	0·628	201	10	−0·05
Ootani	+0·025	−0·308	0·309	175	22	−0·02
Uyama	+0·126	−0·185	0·224	145	45	−0·06
Komono	−0·101	−0·339	0·354	196	35	+0·06
Aitani	+0·101	−0·123	0·159	140	37	+0·25
Sibayama	0·0	−0·031	0·031	180	0	+0·13
Yasuki	0·0	−0·123	0·123	180	0	+0·16
Ootuki	+0·050	−0·185	0·192	164	53	−0·13
Morio	+0·101	−0·247	0·267	157	46	−0·04
Mihirakisan	+0·050	−0·277	0·281	169	46	−0·08
Hôtaku	−0·076	−0·154	0·172	206	16	−0·12

(*to be continued.*)

Table I. C. (*continued.*)

Triangulation Point	u	v	$\sqrt{u^2+v^2}$	$tg^{-1}\frac{u}{v}$	w
	m	m	m		m
Hyôtani	+0·101	−0·185	0·211	151° 22′	−0·09
Tadati	0·0	−0·216	0·216	180 0	0·0
Nanmeizan	0·0	−0·185	0·185	180 0	−0·08
Kimura	−0·101	−0·154	0·184	213 16	−0·04
Tôridake	−0·126	−0·186	0·224	214 15	+0·18
Nakahudi	−0·227	−0·339	0·408	213 48	−0·10
Okuhudi	−0·151	−0·154	0·216	224 26	−0·04
Akahanamura	−0·076	0·0	0·076	270 0	−0·20
Sidani	+0·050	−0·247	0·252	168 33	+0·08
Idusi	+0·050	−0·247	0·252	168 33	+0·08
Hosomi	+0·151	−0·123	0·195	129 10	+0·10
Terasaka	0·0	−0·123	0·123	180 0	+0·05
Kamimura	+0·202	−0·123	0·236	121 20	+0·10
Nyûdô	+0·050	−0·062	0·080	141 7	+0·11
Kawami	+0·101	+0·247	0·267	22 14	+0·11
Okuyane	+0·025	−0·247	0·248	174 13	−0·02
Hirayama	−0·176	−0·216	0·279	219 10	−0·02
Sirodani	−0·202	−0·185	0·274	227 31	−0·12
Aida	−0·126	−0·185	0·224	214 15	−0·10
Myôkenyama	−0·151	−0·092	0·177	238 39	−0·08
Sasaki	−0·126	−0·031	0·130	256 11	−0·01
Miyama	−0·101	−0·031	0·106	252 56	−0·02
Nisidani	−0·101	0·0	0·101	270 0	−0·01
Katama	−0·176	−0·216	0·229	199 23	+0·07
Zôrayama	−0·126	+0·092	0·156	306 8	−0·05
Kayano	−0·176	+0·154	0·234	311 11	+0·15
Utiumi	0·0	+0·062	0·062	0 0	+0·01
Otomi	−0·126	+0·185	0·224	325 45	−0·39
Okurue	−0·176	+0·123	0·215	304 57	−0·26
Kurogane	+0·151	−0·031	0·154	101 36	−0·16
Isitani	−0·477	+0·678	0·829	324 52	−0·03
Sarugao	−0·452	+0·216	0·501	295 32	0·0
Hê	−0·754	+0·616	0·974	309 15	−0·15
Nimatu	−0·553	+0·431	0·701	307 56	−0·01

(*to be continued.*)

Table I. C. (*continued.*)

Triangulation Point	u	v	$\sqrt{u^2+v^2}$	$tg^{-1}\frac{u}{v}$	w
Oohira	m −0·955	m +0·709	m 1·189	306° 35′	m −0·27
Takinoyama	−0·427	+0·308	0·526	305 48	+0·07
Kasayama	−0·478	+0·401	0·624	310 0	−0·04
Tumo	−0·528	+0·247	0·583	295 4	−0·11
Ooisi	−0·905	+0·586	1·078	302 55	−0·17
Kubo	−0·679	+0·431	0·804	302 24	−0·15
Obama	−0·553	+1·171	1·295	334 43	−0·16
Mitinoku	−0·955	+0·801	1·246	309 59	−0·20
Hatadani	−0·478	+0·339	0·586	305 21	−0·15
Ootani	−0·981	+0·924	1·348	313 17	−0·32
Moriage	−0·503	+0·431	0·662	310 36	+0·04
Gamatani	−0·754	+0·493	0·901	303 11	−0·24
Terayama	−0·553	+0·339	0·649	301 31	−0·08
Inunegasira	−0·629	+0·431	0·762	304 25	−0·27
Naya	−0·880	+0·832	1·212	313 24	−0·13
Wasigasaki	−0.604	+0·247	0·653	292 14	+0·04
Asago	−1·257	+1.048	1·637	309 49	−0·52
Tunoduki	−0·503	+0·308	0·590	301 29	−0·18
Kongôsan	−0·604	+0·678	0·908	318 18	−0·20
Sengokuyama	−0·579	+0·370	0·687	302 35	+0·01
Dake	−0·604	+0·462	0·760	307 25	−0·31
Yada	−0·931	+1·079	1·425	319 13	−0·34
Arai	−0·025	−1·233	1·233	181 10	+0·26
Akasaka	−0·881	+0·832	1·212	313 22	−0·25
Takao	−0·730	+0·647	0·975	311 33	−0·21
Yanaganaru	−0·604	+0·555	0·820	312 35	−0·35
Nisiyama	−0·101	−1.356	1·360	184 16	+0·24
Yasuke	−0·604	+0·431	0·742	305 31	−0·05
Mineyama	−0·906	+1·233	1·530	323 41	−0·22
Ainome	+0·025	−0·986	0·986	178 33	+0·33
Takase	−0·755	+0·955	1·217	321 40	+0·01
Kidumiyama	−0·554	+0·801	0·974	325 20	+0·21
Nisitani	−0·503	+0·555	0·749	317 49	−0·13
Hiziyama	0·0	−0·894	0·894	180 0	0·0

(*to be continued.*)

Table I. C. (*continued.*)

Triangulation Point	u	v	$\sqrt{u^2+v^2}$	$tg^{-1}\frac{u}{v}$	w
	m	m	m		m
Mititani	−0·478	+0·678	0·830	324° 49′	−0·04
Minamitani	−0·579	+0·524	0·781	312 9	−0·16
Byôbuyama	−0·101	−0·555	0·564	190 18	+0·32
Yakedôsi	+0·076	−0·709	0·713	173 53	+0 04
Misakayama	−0·428	+0·894	0·991	334 25	+0·24
Dôgatani	−0·504	+0·462	0·684	312 31	0·0
Kaya	+0·050	−0·524	0·526	174 33	−0·06
Kaitanidake	+0·050	+0·062	0·080	38 53	+0·34
Yosidu	−0·554	+0·431	0·702	307 53	−0·06
Sedoyama	−0·453	+0·431	0·625	313 34	−0·02
Oogatani	−0·403	+0·247	0·473	301 30	−0·31
Kanase	−0·202	+0·277	0·343	323 54	−0·17

Now that we have known the horizontal and vertical displacements of the third order triangulation points densely distributed over the district, we are able to proceed into a more detailed discussion on the crust deformation in this district than have hitherto been. Making use of the results given in the tables, the lines of equal eastward and northward displacements, u and v, are constructed as shown in Fig. 3 and Fig. 4. There were actually remarkable discontinuities in these displacements across the Gômura and Yamada seismic faults which were produced at the time of the earthquake of 1927, but the lines of equal eastward and northward displacements were drawn as if they were continuous throughout and were rapidly varying in these fault regions. This is merely for the sake of simplicity, for our final object is to find how the strain would be distributed on a hypothetical elastic body when the points on it are made to move just in the same manner as the corresponding points on the actual earth's crust in the district. It must be emphasised that by saying so we never assume the earth's crust to be ideally elastic. The lines of equal eastward and northward displacements were given in the writer's previous paper[3] which were constructed using as data the results of the revision of the second order triangulation. There are minor differences between the present figures and the corresponding former ones, which however are by no means essential. At any rate, it is note-

3) C. Tsuboi, *Bull. Earthq. Res. Inst.*, **8** (1930), 153

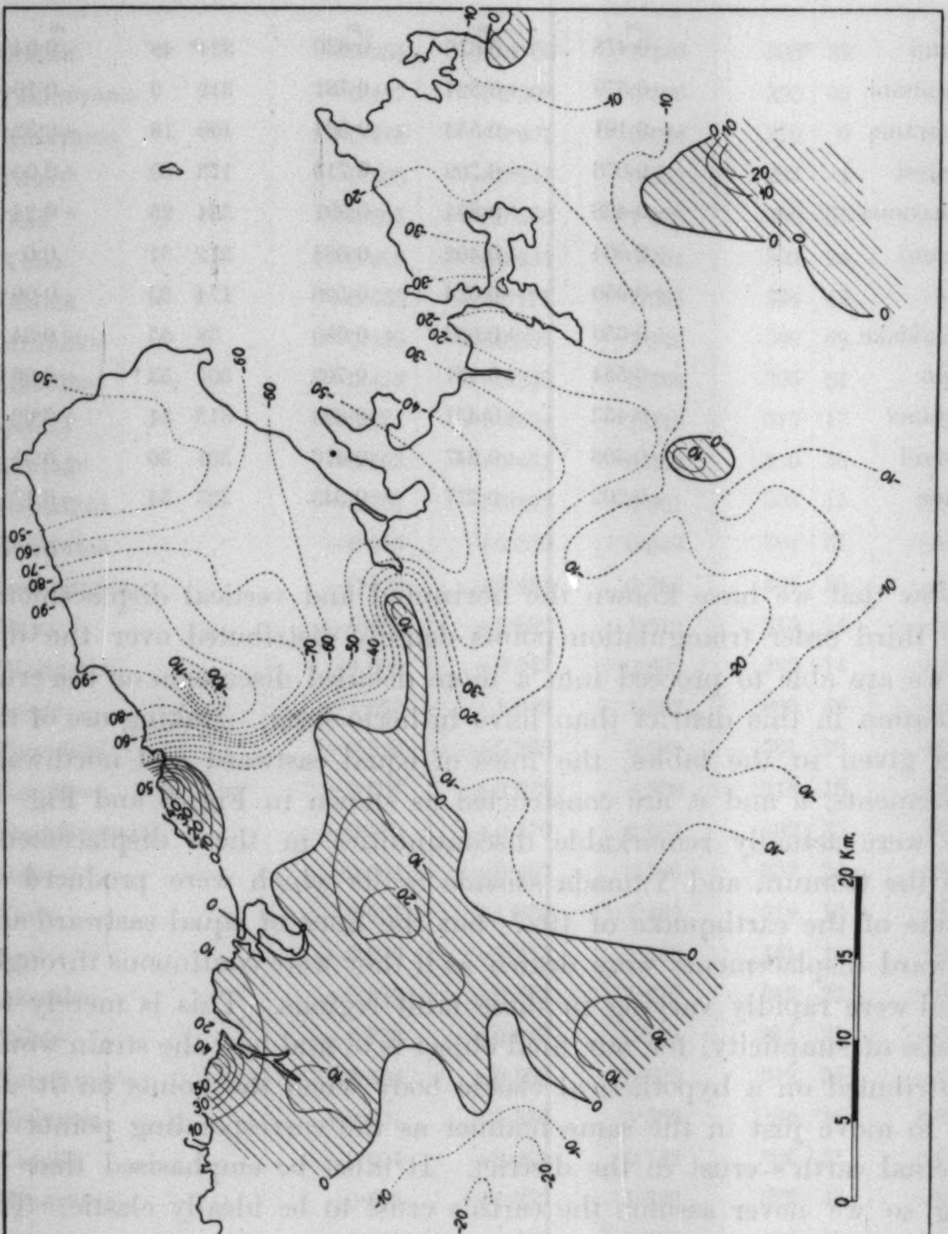

Fig. 3. Lines of Equal Eastward Displacement in cm.

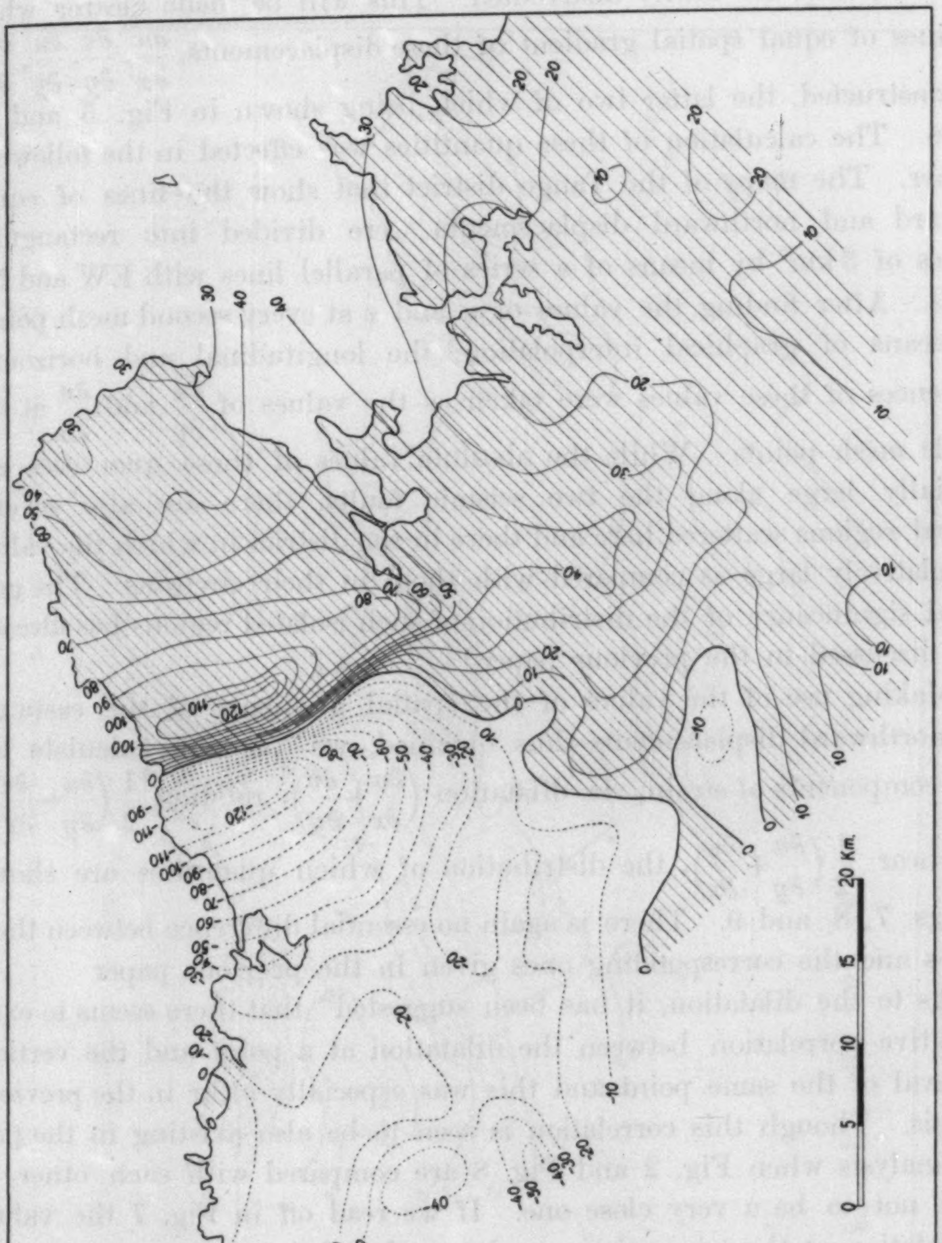

Fig. 4. Lines of Equal Northward Displacement in cm.

worthy that the contour lines are very much crowded along the two seismic faults while in other parts of the district, especially in the Tango peninsula, they are thinly distributed. This will be made clearer when the lines of equal spatial gradient of these displacements, $\frac{\partial u}{\partial x}, \frac{\partial v}{\partial y}, \frac{\partial u}{\partial y}, \frac{\partial v}{\partial x}$, are constructed, the latter two of which being shown in Fig. 5 and in Fig. 6. The calculation of these quantities was effected in the following manner. The maps of the Tango district that show the lines of equal eastward and northward displacements were divided into rectangular meshes of 3 km^2 by means of a series of parallel lines with EW and NS trends. After finding the values of u and v at every second mesh points by means of graphical interpolation, the longitudinal and horizontal differences of these values were taken as the values of $\frac{\partial u}{\partial y}$ and $\frac{\partial v}{\partial x}$ at the middle mesh points. While the aboslute values of these quantities are especially large along the two seismic faults, there are also several isolated regions scattered here and there in the district in which the values are relatively large as compared with those in their environs. The geological significance of the distribution of such isolated regions has already been discussed in the previous paper.[4]

Making use of the values of the spatial gradients of the eastward and northward displacements thus obtained, we can now calculate the three components of strain, viz. dilatation $\left(\frac{\partial u}{\partial x}+\frac{\partial v}{\partial y}\right)$, rotation $\frac{1}{2}\left(\frac{\partial u}{\partial y}-\frac{\partial v}{\partial x}\right)$, and shear $\frac{1}{2}\left(\frac{\partial u}{\partial y}+\frac{\partial v}{\partial x}\right)$, the distribution of which quantities are shown in Figs. 7, 8, and 9. There is again no essential difference between these figures and the corresponding ones given in the previous paper.

As to the dilatation, it has been suggested[5] that there seems to exist a positive correlation between the dilatation at a point and the vertical upheaval of the same point and this was especially clear in the previous analysis. Though this correlation is seen to be also existing in the present analysis when Fig. 2 and Fig. 8 are compared with each other, it seems not to be a very close one. If we read off in Fig. 7 the values of dilatation at the triangulation points and find the amounts of upheaval w for the corresponding points in Table I, we can construct a correlation diagram for these two quantities which is shown in Fig. 10. Though

4) *loc. cit.*

5) T. Terada and N. Miyabe, *Bull. Earthq. Res. Inst.*, **7** (1929), 223.
C. Tsuboi, *ibid.*, **8** (1930), 153.
T. Terada, *Proc. Imp. Acad.*, **6** (1930), 53.

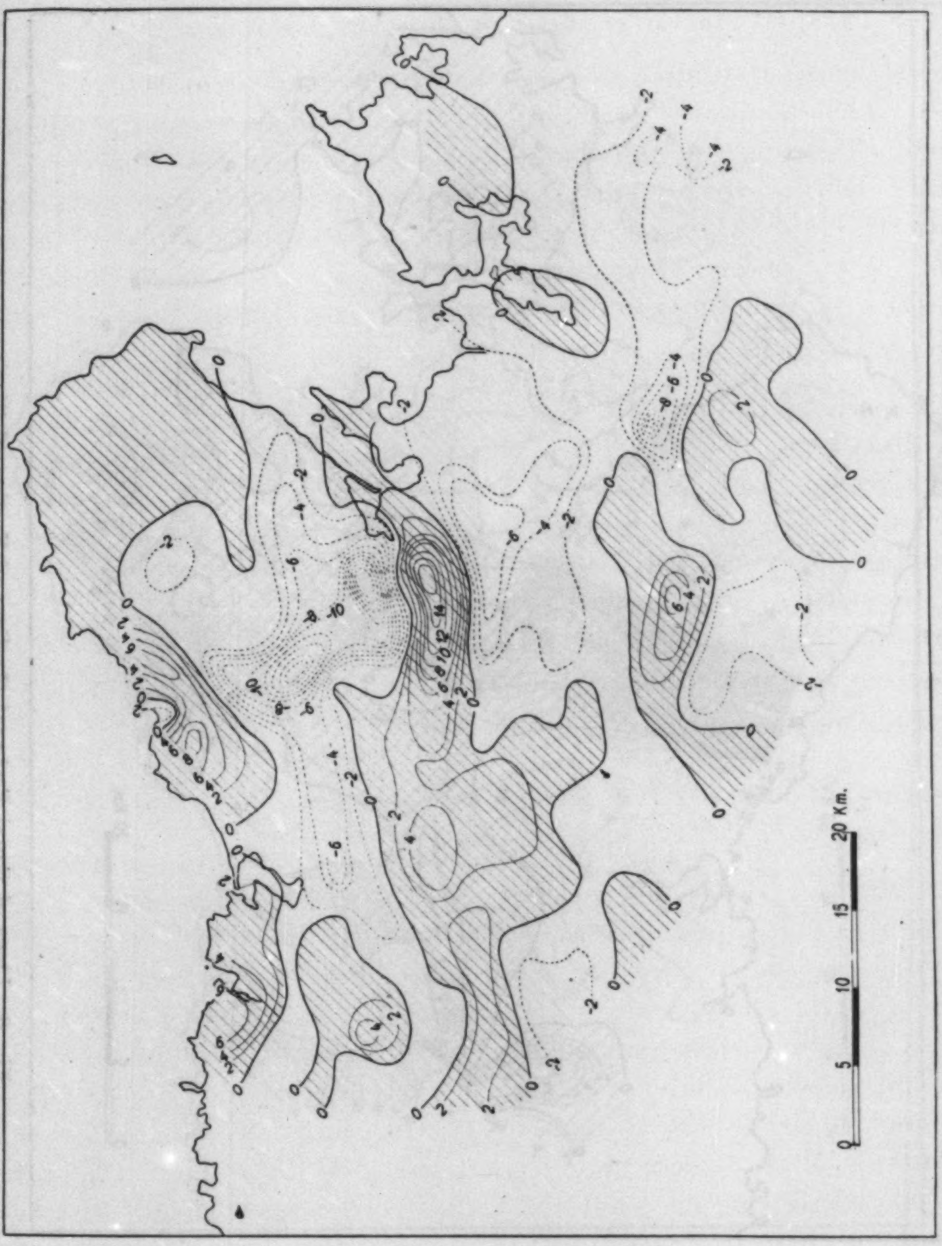

Fig. 5. Lines of Equal Northward Gradient of Eastward Displacement in 10^{-5}.

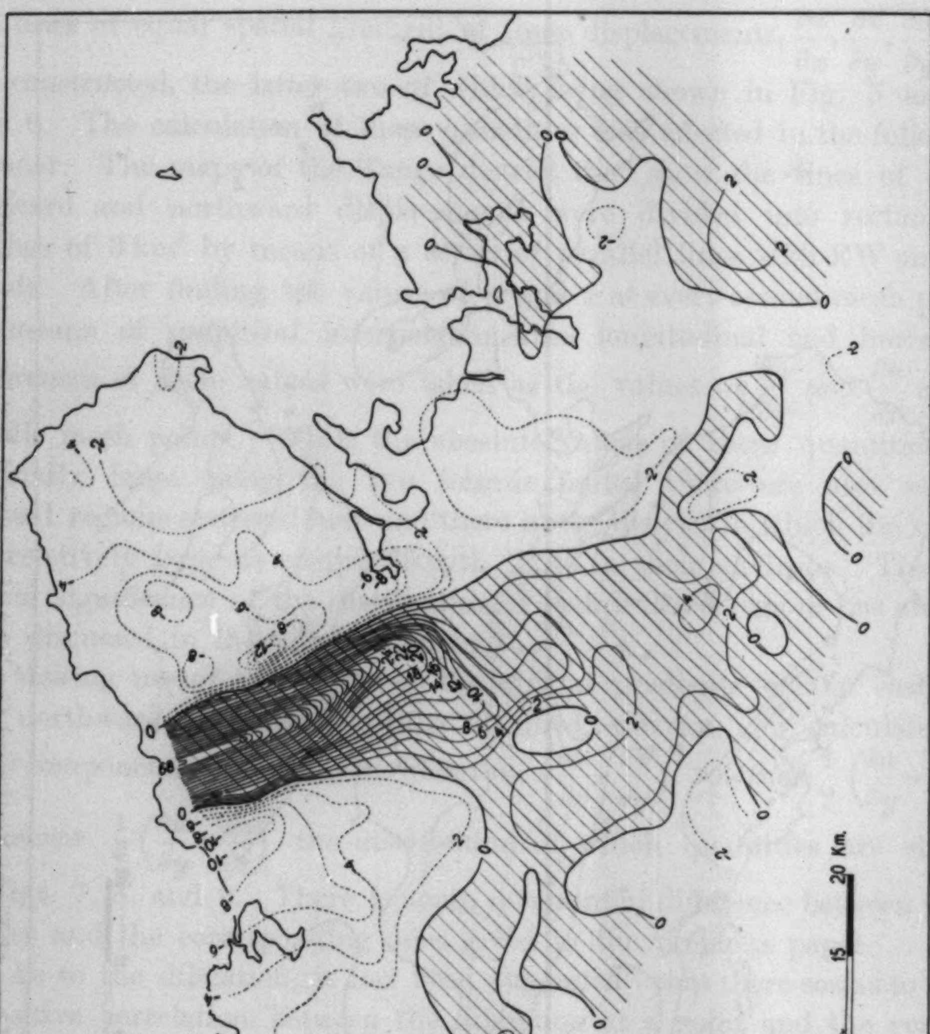

Fig. 6. Lines of Equal Eastward Gradient of Northward Displacement in 10^{-5}

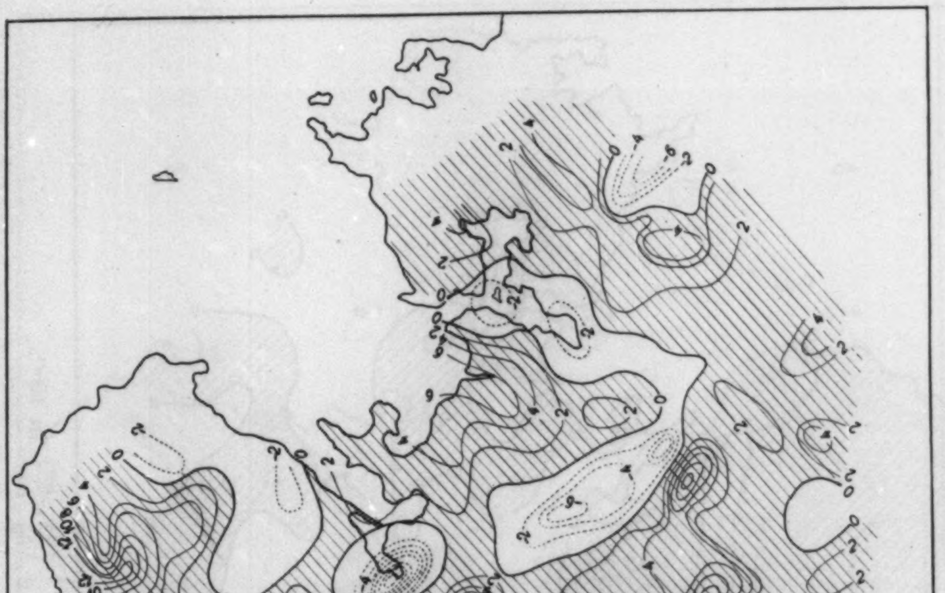

Fig. 7. Lines of Equal Dilatation $\left(\frac{\partial u}{\partial x}+\frac{\partial v}{\partial y}\right)$ in 10^{-5}.

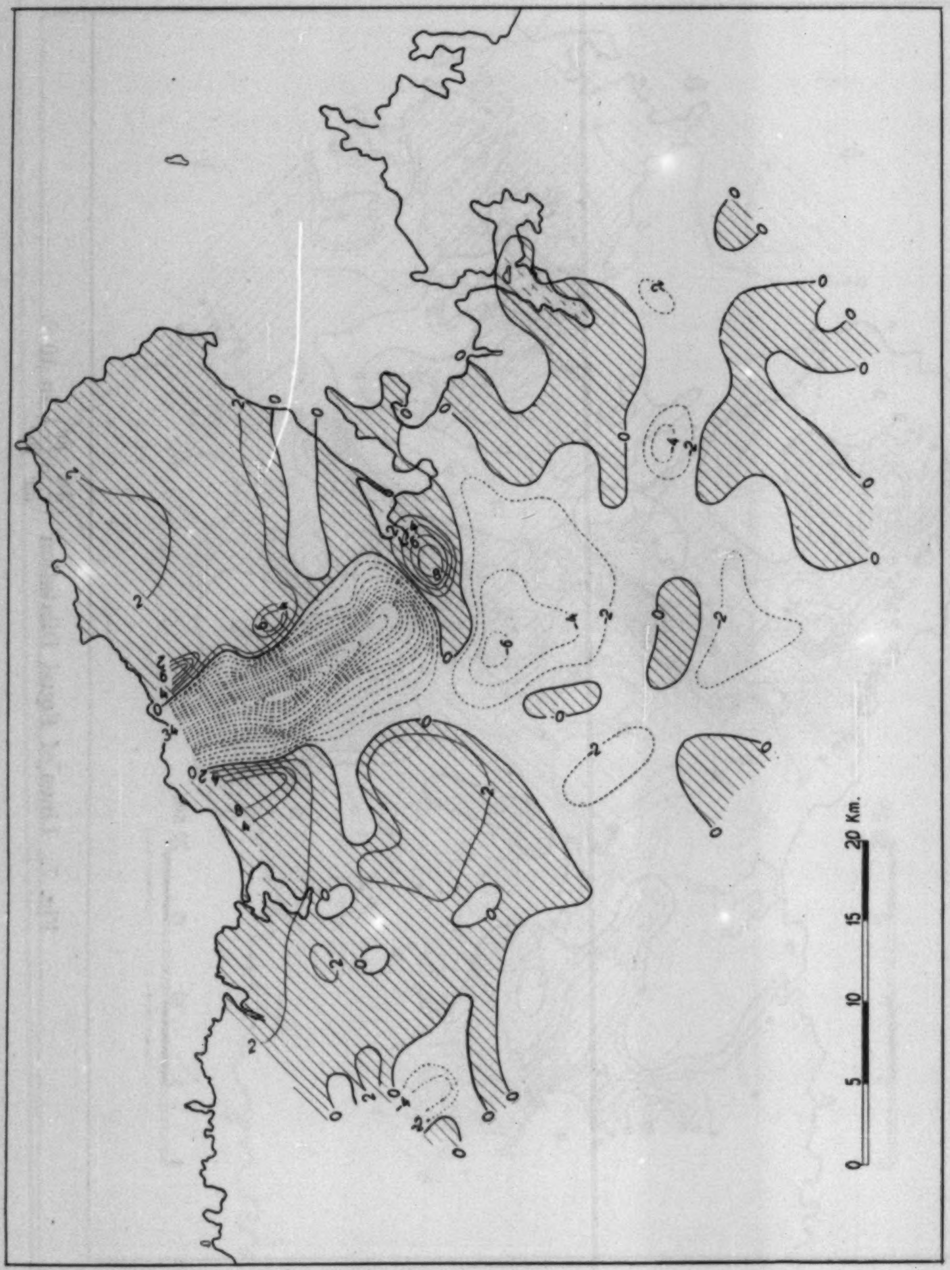

Fig. 8. Lines of Equal Rotation $\frac{1}{2}\left(\frac{\partial u}{\partial y}-\frac{\partial v}{\partial x}\right)$ in 10^{-5}.

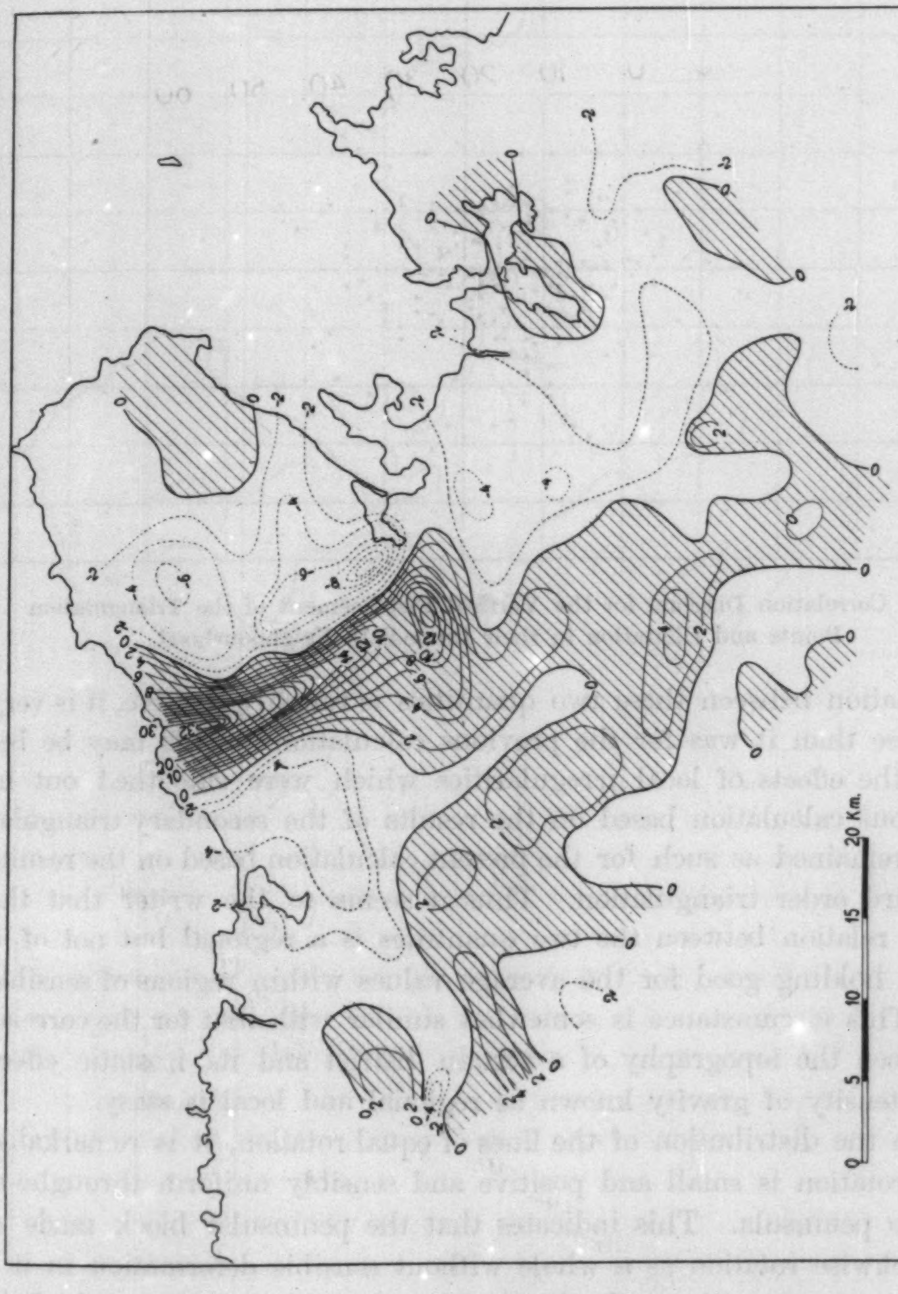

Fig. 9. Lines of Equal Shear $\frac{1}{2}\left(\frac{\partial u}{\partial y}+\frac{\partial v}{\partial x}\right)$ in 10^{-5}.

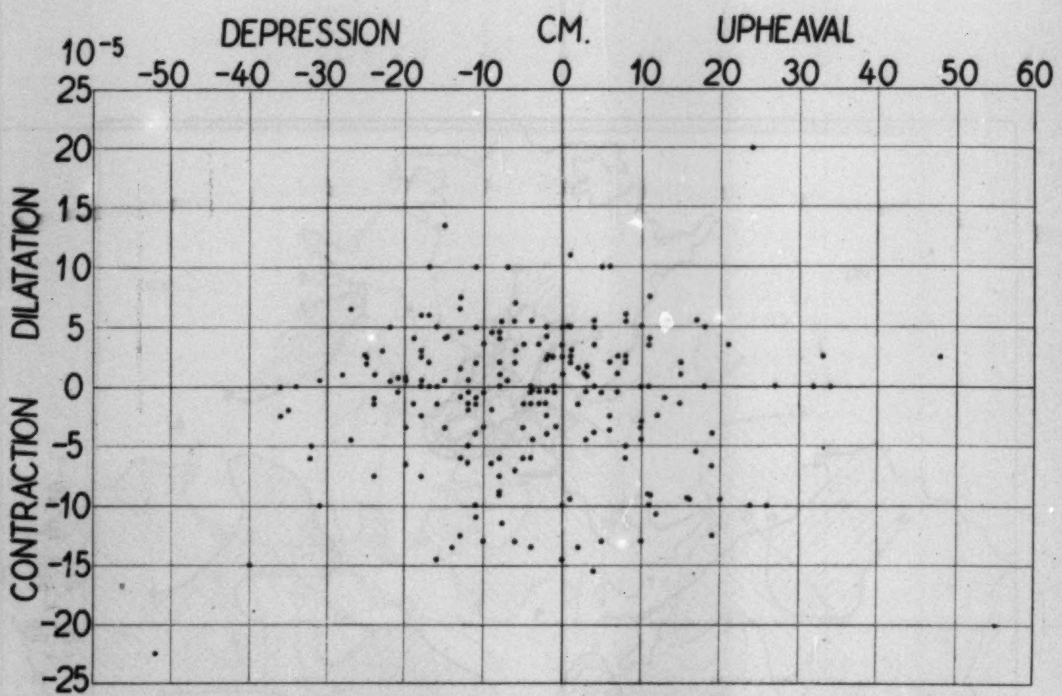

Fig. 10. Correlation Diagram for the Vertical Displacement of the Triangulation Points and Dilatation in their Immediate Neighbourhood.

the correlation between these two quantities is roughly positive, it is very much loose than it was for the provious calculation. This may be because of the effects of local irregularities which were smoothed out in the previous calculation based on the results of the secondary triangulation but remained as such for the present calculation based on the results of the third order triangulation. Thus it seems to the writer that the suggested relation between the two quantities is a regional but not of a local one, holding good for the average values within regions of sensible extent. This circumstance is somewhat similar with that for the correlation between the topography of a certain district and its isostatic effect on the intensity of gravity known as regional and local isostasy.

As to the distribution of the lines of equal rotation, it is remarkable that the rotation is small and positive and sensibly uniform throughout the Tango peninsula. This indicates that the peninsular block made a small clockwise rotation as a whole without sensible deformation in it.

We can now construct the lines of equal maximum shear which is given by

$$\sigma=\sqrt{\left(\frac{\partial u}{\partial x}-\frac{\partial v}{\partial y}\right)^2+\left(\frac{\partial v}{\partial x}+\frac{\partial u}{\partial y}\right)^2}.$$

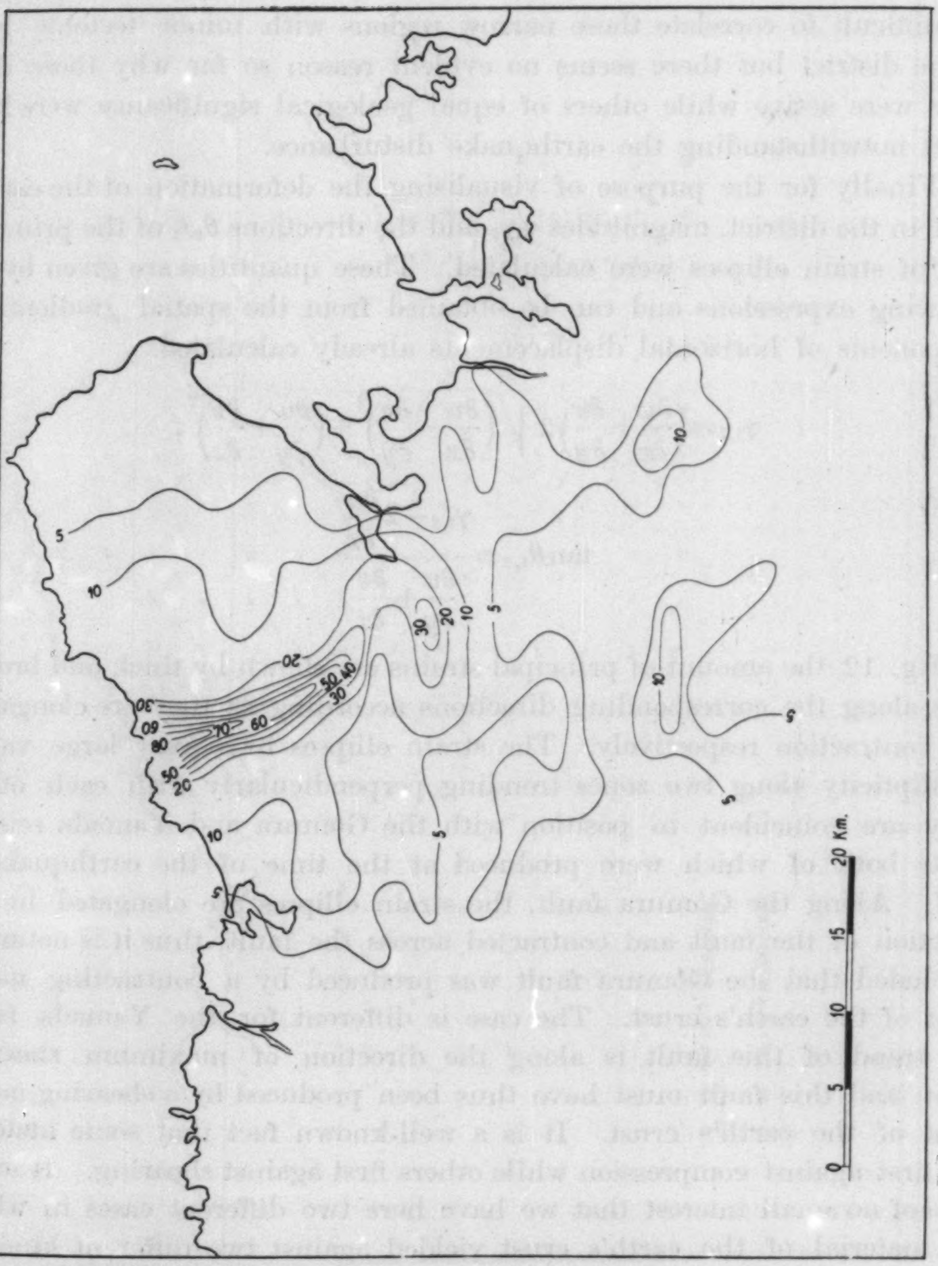

Fig. 11. Lines of Equal Maximum Shear in 10^{-5}

The distribution of this quantity is shown in Fig. 11. This is naturally large along the two seismic faults. There are moreover two isolated regions in which maximum shear exceeds the value of 10×10^{-5}. It is not difficult to correlate these narrow regions with minor tectonic lines in the district but there seems no evident reason so far why these lines alone were active while others of equal geological significance were kept intact notwithstanding the earthquake disturbance.

Finally for the purpose of visualising the deformation of the earth's crust in the district, magnitudes $\gamma_1\gamma_2$ and the directions $\theta_1\theta_2$ of the principal axes of strain ellipses were calculated. These quantities are given by the following expressions and can be obtained from the spatial gradients of components of horizontal displacements already calculated.

$$\gamma_{1,2}=\left(\frac{\partial u}{\partial x}+\frac{\partial v}{\partial y}\right)\pm\sqrt{\left(\frac{\partial u}{\partial x}-\frac{\partial v}{\partial y}\right)^2+\left(\frac{\partial u}{\partial y}+\frac{\partial v}{\partial x}\right)^2},$$

$$\tan\theta_{1,2}=\frac{\gamma_{1,2}-2\dfrac{\partial u}{\partial x}}{\dfrac{\partial u}{\partial y}+\dfrac{\partial v}{\partial x}}.$$

In Fig. 12, the amount of principal strains are shown by thick and broken lines along the corresponding directions according as they are elongation and contraction respectively. The strain ellipses have very large values of ellipticity along two zones trending perpendicularly with each other. They are coincident in position with the Gômura and Yamada seismic faults both of which were produced at the time of the earthquake of 1927. Along the Gômura fault, the strain ellipses are elongated in the direction of the fault and contracted across the fault, thus it is naturally concluded that the Gômura fault was produced by a contracting movement of the earth's crust. The case is different for the Yamada fault. The trend of this fault is along the direction of maximum shearing strain and this fault must have thus been produced by a shearing movement of the earth's crust. It is a well-known fact that some material fail first against compression while others first against shearing. It seems to be of no small interest that we have here two different cases in which the material of the earth's crust yielded against two different kinds of deformations. The distribution of the strain ellipses in the neighbourhood of the Gômura fault seems to indicate that this fault was elongated more southward than it was observable on the surface of the earth's crust at the time of the earthquake of 1927.

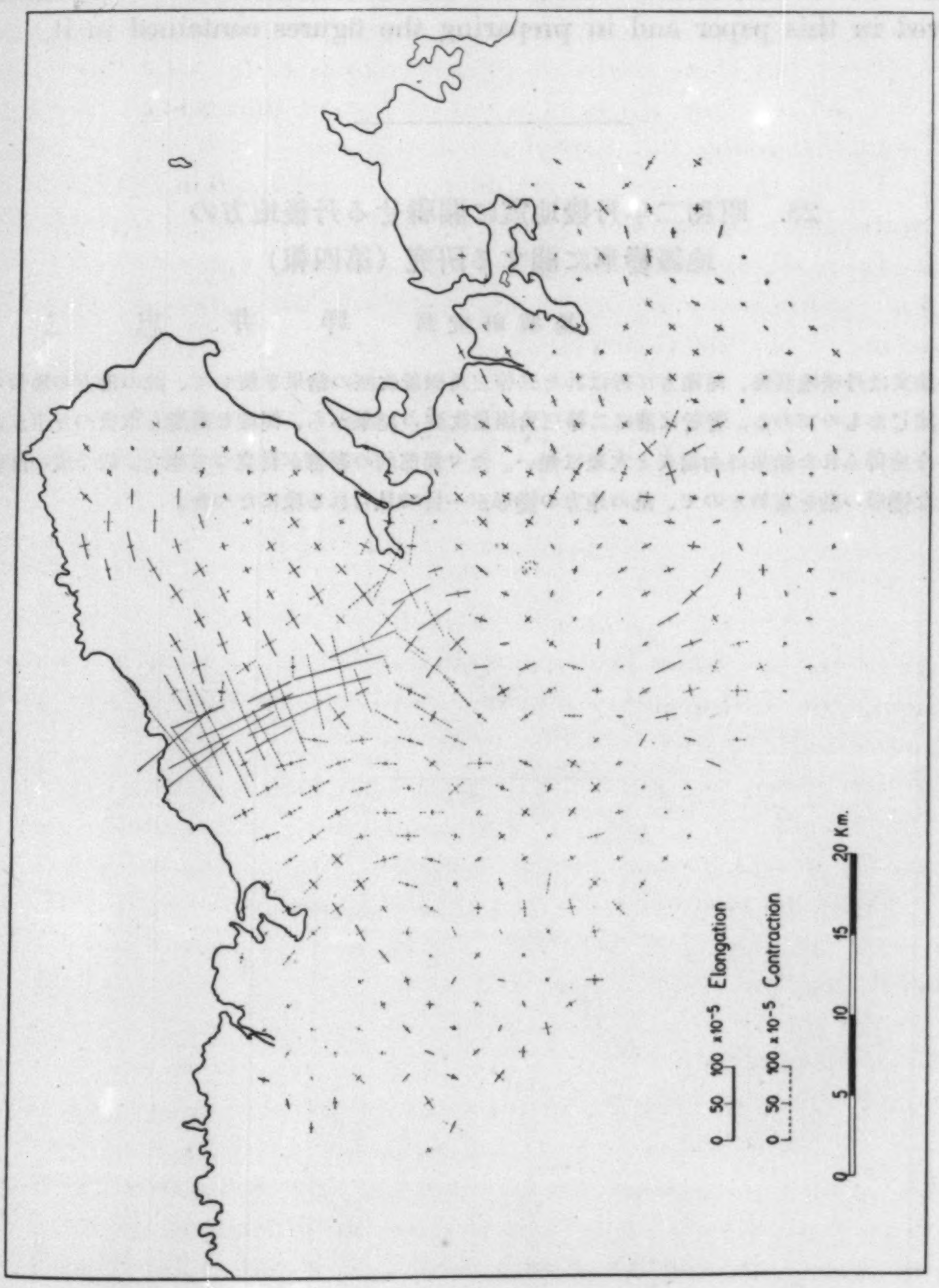

Fig. 12. Principal Axes of Strain Ellipses.

In conclusion, the writer wishes to express his sincere thanks to Professor Torahiko TERADA for his interests in the present work. Thanks are also due to Mr. Akira JITSUKAWA for his assistance in the calculation involved in this paper and in preparing the figures contained in it.

---

28. 昭和二年丹後地震に關聯せる丹後地方の地殼變形に關する研究（第四報）

地震研究所　坪　井　忠　二

此の論文は丹後地震後、同地方に行はれた三等三角測量改測の結果を使つて、此の地方の地殼の變形を論じたものである。著者は前に二等三角測量改測の結果から、同様な問題を取扱つた事があるが、今度得られた結果は勿論夫と大差は無い。たゞ局部的の影響が目立つて來た。尙今度の計算では主な變形の軸を定めたので、此の地方の變形が一目で見られる樣になつた。

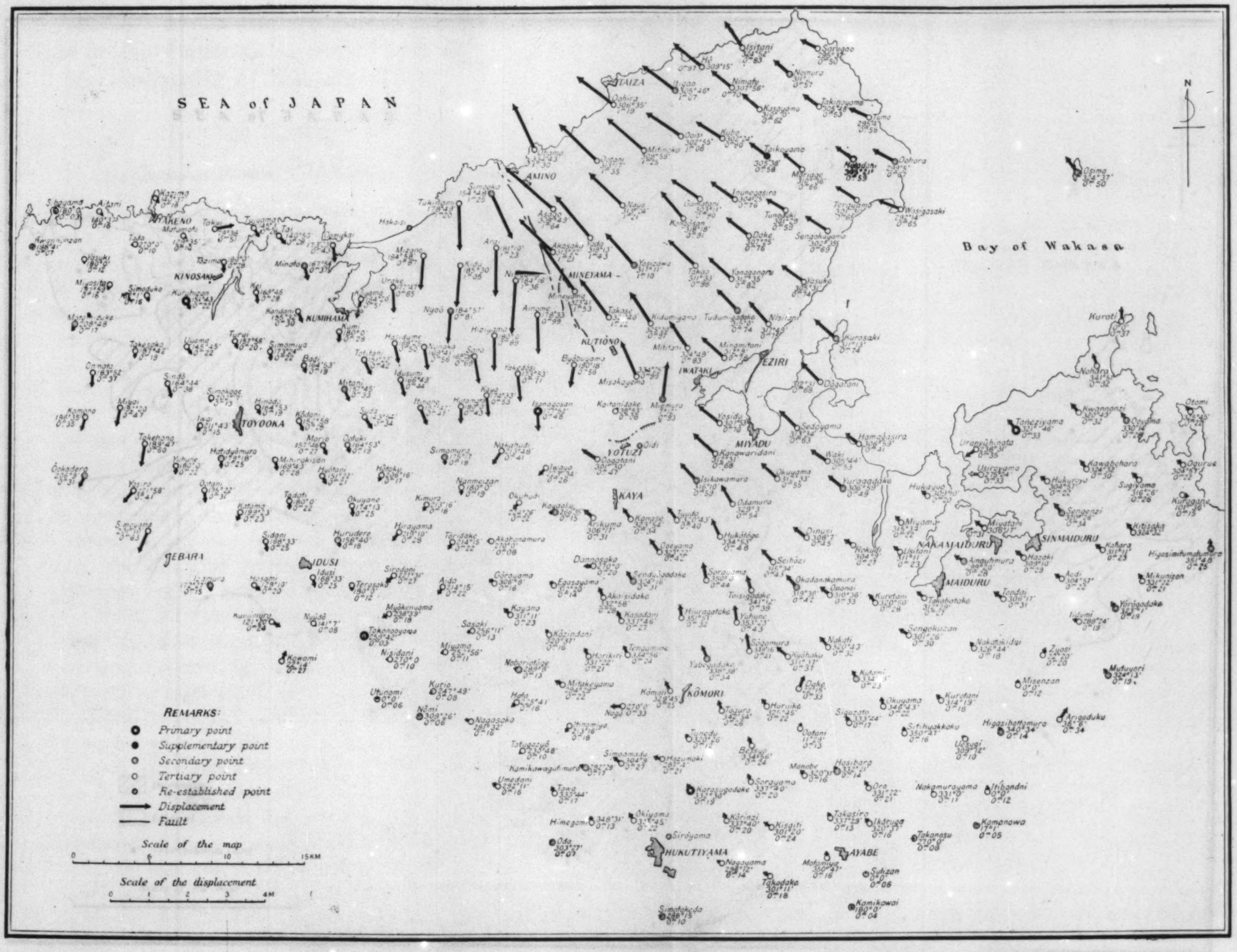

Fig. 1. Horizontal Displacements of the Triangulation Points in the Tango District.

（震研彙報、第十號、圖版、坪井）

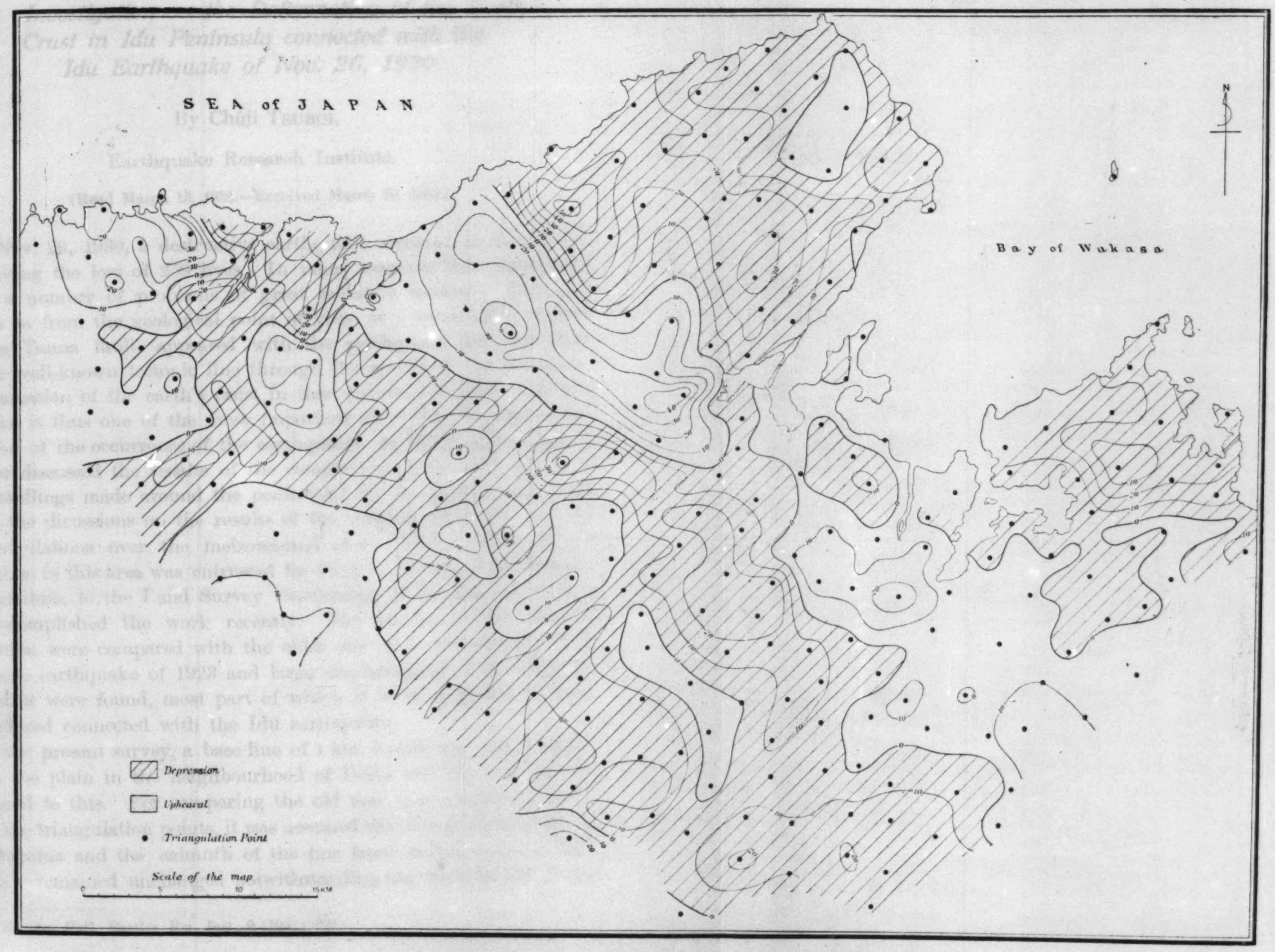

Fig. 2. Vertical Displacements of the Triangulation Points in the Tango District in cm.

（震研彙報、第十號、圖版、坪井）

29. *Investigation on the Deformation of the Earth's Crust in Idu Peninsula connected with the Idu Earthquake of Nov. 26, 1930.*

By Chûji TSUBOI,

Earthquake Research Institute.

(Read March 15, 1932.—Received March 20, 1932.)

On Nov. 26, 1930, a destructive earthquake occurred in Idu Peninsula resulting the loss of 259 lives. In many respects this earthquake afforded a number of problems of great scientific interest. This was especially so from the geological point of view as a remarkable seismic fault, the Tanna fault, appeared with the earthquake that was right along the well-known tectonic line through the middle of the peninsula. The deformation of the earth's crust in this district connected with the earthquake is thus one of the most important clues for elucidating the mechanism of the occurrence of the earthquake. In his previous paper,[1] the writer discussed the results of the comparison of the old and new precise levellings made around the peninsula. In the present paper will be given the dicussions on the results of the comparison of the old and new triangulations over the meizoseismal area. The revision of the triangulation in this area was entrusted by Prof. K. Suyehiro, the director of our Institute, to the Land Survey Department of the Imperial Army which accomplished the work recently. The results of the present triangulation were compared with the older one made immediately after the Kwanto earthquake of 1923 and large displacements of the triangulation points were found, most part of which is to be regarded to have been produced connected with the Idu earthquake.

For the present survey, a base line of 1 km. length was newly established in the plain in the neighbourhood of Daiba and the new survey was referred to this. For comparing the old and new geodetic coordinates of the triangulation points, it was assumed that the geodetic position of Asitakayama and the azimuth of the line from Asitakayama to Kamurigadake remained unchanged notwithstanding the disturbances of the

---

1) C. TSUBOI, *Bull. Earthq. Res. Inst.*, 9 (1931), 271.

earthquake. These assumptions are of course of a tentative nature but so far as we confine ourselves to the discussion of the relative displacements of the triangulation points and the strain on the earth's crust produced by them, they will produce no serious effect on the results of calculation based on it. Similar assumptions have also been necessary in the calculation of the strains in other districts. The effects of these assumptions can easily be considered in the following manner.

Let in Fig. 1, ABC be a triangle before the earthquake disturbance of which AB is assumed to be unchanged both in its length and direction. Let $A'B'C'$ be the true position of the triangle after the disturbance which however we do not know. We have assumed $AB=A'B'$ and $\theta=\theta'$. The error in position of the point C that is produced by this untrue comparison is given as follows:

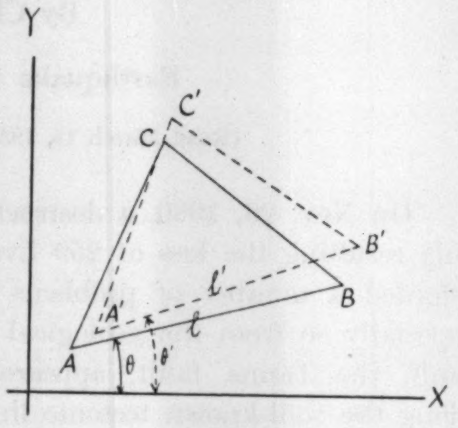

Fig. 1.

$$u=U+u_0+x\frac{d(AB)}{AB}-(\theta-\theta')y,$$

$$v=V+v_0+y\frac{d(AB)}{AB}+(\theta-\theta')x,$$

where U and V are x-, y-components of real displacement of C, u and v those on unreal assumptions, u_0 and v_0, x-, y- components of displacement of the point A, and x and y are the relative co-ordinates of the point C with respect to A. Let AB be denoted by l and $(\theta-\theta')$ by $d\theta$, then

$$\left\{\begin{aligned} u&=U+u_0+x\frac{dl}{l}-yd\theta, \\ v&=V+v_0+y\frac{dl}{l}+xd\theta. \end{aligned}\right.$$

If we calculate the strains from these values, we get

$$\left|\begin{aligned} \frac{\partial u}{\partial x}&=\frac{\partial U}{\partial x}+\frac{dl}{l}, \\ \frac{\partial u}{\partial y}&=\frac{\partial U}{\partial y}-d\theta, \end{aligned}\right.$$

$$\left\{\begin{aligned} \frac{\partial v}{\partial x} &= \frac{\partial V}{\partial x} + d\theta, \\ \frac{\partial v}{\partial y} &= \frac{\partial V}{\partial y} + \frac{dl}{l}. \end{aligned}\right.$$

$$\left\{\begin{aligned} &\frac{\partial u}{\partial x} + \frac{\partial v}{\partial y} = \left(\frac{\partial U}{\partial x} + \frac{\partial V}{\partial y}\right) + 2\frac{dl}{l} \quad \text{...dilatation,} \\ &\frac{1}{2}\left(\frac{\partial u}{\partial y} - \frac{\partial v}{\partial x}\right) = \frac{1}{2}\left(\frac{\partial U}{\partial x} - \frac{\partial V}{\partial x}\right) - d\theta \quad \text{....rotation,} \\ &\frac{1}{2}\left(\frac{\partial u}{\partial y} + \frac{\partial v}{\partial y}\right) = \frac{1}{2}\left(\frac{\partial U}{\partial y} + \frac{\partial V}{\partial x}\right) \quad \text{... shear.} \end{aligned}\right.$$

$$\sigma = \sqrt{\left(\frac{\partial u}{\partial x} - \frac{\partial v}{\partial y}\right)^2 + \left(\frac{\partial v}{\partial x} + \frac{\partial u}{\partial y}\right)^2} = \sqrt{\left(\frac{\partial U}{\partial x} - \frac{\partial V}{\partial y}\right)^2 + \left(\frac{\partial V}{\partial x} + \frac{\partial U}{\partial y}\right)^2}$$

....maximum shear.

$$\gamma_{1,2} = \left(\frac{\partial u}{\partial x} + \frac{\partial v}{\partial y}\right) \pm \sqrt{\left(\frac{\partial u}{\partial x} - \frac{\partial V}{\partial y}\right)^2 + \left(\frac{\partial u}{\partial y} + \frac{\partial v}{\partial x}\right)^2}$$

$$= \left(\frac{\partial U}{\partial x} + \frac{\partial V}{\partial y}\right) \pm \sqrt{\left(\frac{\partial U}{\partial x} - \frac{\partial V}{\partial y}\right)^2 + \left(\frac{\partial V}{\partial x} + \frac{\partial U}{\partial y}\right)^2} + 2\frac{dl}{l}$$

....principal strain.

$$\tan\theta_{1,2} = \frac{\gamma_{1,2} - 2\dfrac{\partial u}{\partial x}}{\dfrac{\partial u}{\partial y} + \dfrac{\partial v}{\partial x}} = \frac{\left(\dfrac{\partial U}{\partial x} + \dfrac{\partial V}{\partial y}\right) \pm \sqrt{\left(\dfrac{\partial U}{\partial x} + \dfrac{\partial V}{\partial y}\right)^2 + \left(\dfrac{\partial V}{\partial x} + \dfrac{\partial U}{\partial y}\right)^2} - 2\dfrac{\partial U}{\partial x}}{\dfrac{\partial U}{\partial y} + \dfrac{\partial V}{\partial x}}$$

...direction of axes of strain ellipse.

Therefore we see that dilatation and rotation and principal strains calculated from the untrue assumption differ from the real ones by a constant term. On the other hand, shear, maximum shear and the direction of the principal axes of strain are just as same as the real ones. Thus the relative distribution of dilatation, rotations and the principal strain are by no means affected by the untrue assumptions, which will only cause some shifts of zero lines.

The displacements of the triangulation points in this district as found by the comparison of their old and new geodetic coordinates are shown in Table I and in Fig. 2.

Table I.

Horizontal Displacements of Triangulation Points in Idu Peninsula.

d	Resultant Displacement in cm.
θ	Azimuth of Displacement Measured Clockwise from North
u	Eastward Component of Displacement in cm.
v	Northward Component of Displacement in cm.

	d	θ	u	v
(1) Asitakayama	—	—	—	—
(2) Kamurigadake	29	79°1′	28·5	5·5
(3) Sano-mura	36	170°11′	6·1	−35·5
(4) Miyakami-mura	44	12°15′	9·3	43·0
(5) Manaduru-zaki	64	84°29′	63·7	6·2
(6) Negoya-mura	16	275°31′	−15·9	1·5
(7) Daiba-mura	71	175°54′	5·1	−70·8
(8) Kurodake	99	17°27′	29·7	94·4
(9) Tokurayama	57	225°33′	−40·7	−39·9
(10) Hasima	20	100°36′	19·7	− 3·7
(11) Osaka-mura	121	223°49′	−83·8	−87·3
(12) Sukumoyama	37	357°39′	− 1·5	37·0
(13) Enasi-mura	105	252°20′	−100·0	−31·9

From these values, the dilatation, rotation and shear were calculated for different triangles following the method, due initially to Prof. T. Terada.[2)]

Consider a triangle of which the vertices are of the co-ordinates (x_1y_1), (x_2y_2) and (x_3y_3). Let the horizontal displacements of these points be (u_1v_1), (u_2v_2) and (u_3v_3) and further assume u and v inside the triangle are given by the following expressions

$$u = ax + by + c,$$
$$v = a'x + b'y + c'$$

subjected to the conditions

$$u_{1,2,3} = ax_{1,2,3} + by_{1,2,3} + c,$$
$$v_{1,2,3} = a'x_{1,2,3} + b'y_{1,2,3} + c'.$$

Then $$\frac{\partial u}{\partial x} = a = \frac{(y_3 - y_1)(u_2 - u_1) - (y_2 - y_1)(u_3 - u_1)}{\Delta},$$

2) T. TERADA and N. MIYABE, *Bull. Earthq. Res Inst.*, 7 (1929), 223.

$$\frac{\partial u}{\partial y}=b=\frac{(x_2-x_1)(u_3-u_1)-(x_3-x_1)(u_2-u_1)}{\Delta},$$

$$\frac{\partial v}{\partial x}=a'=\frac{(y_3-y_1)(v_2-v_1)-(y_2-y_1)(v_3-v_1)}{\Delta},$$

$$\frac{\partial v}{\partial y}=b'=\frac{(x_2-x_1)(v_3-v_1)-(x_3-x_1)(v_2-v_1)}{\Delta},$$

where $$\Delta=(x_2-x_1)(y_3-y_1)-(x_3-x_1)(x_2-x_1).$$

The values obtained in this way were taken to be those of the geometrical centre of the triangle. This is the first approximation. Then we can calculate the dilatation, rotation, shear, maximum shear, principal strain, direction of the axes of strain ellipse for different triangles. The results of the calculations are given in Table II and Figs. 3–9.

Table II.

I	Triangles. Numerals in the brackets correspond to the triangulation points given in Table I.	
II	Eastward Gradient of Eastward Displacement	$\frac{\partial u}{\partial x}$ in 10^{-5}.
III	Northward Gradient of Eastward Displacement	$\frac{\partial u}{\partial y}$ in 10^{-5}.
IV	Eastward Gradient of Northward Displacement	$\frac{\partial v}{\partial x}$ in 10^{-5}.
V	Northward Gradient of Northward Displacement	$\frac{\partial v}{\partial y}$ in 10^{-5}.
VI	Dilatation	$\left(\frac{\partial u}{\partial x}+\frac{\partial v}{\partial y}\right)$ in 10^{-5}.
VII	Rotation	$\frac{1}{2}\left(\frac{\partial u}{\partial y}-\frac{\partial v}{\partial x}\right)$ in 10^{-5}.
VIII	Shear	$\frac{1}{2}\left(\frac{\partial u}{\partial y}+\frac{\partial v}{\partial x}\right)$ in 10^{-5}.
IX	Maximum Shear	$\sqrt{\left(\frac{\partial u}{\partial x}-\frac{\partial v}{\partial y}\right)^2+\left(\frac{\partial v}{\partial x}+\frac{\partial u}{\partial y}\right)^2}$ in 10^{-5}.
X	Principal Strain	$\gamma_1=\left(\frac{\partial u}{\partial x}+\frac{\partial v}{\partial y}\right)+\sqrt{\left(\frac{\partial u}{\partial x}-\frac{\partial v}{\partial y}\right)^2+\left(\frac{\partial u}{\partial y}+\frac{\partial v}{\partial x}\right)^2}$ in 10^{-5}.
XI	"	$\gamma_2=\left(\frac{\partial u}{\partial x}+\frac{\partial v}{\partial u}\right)-\sqrt{\left(\frac{\partial u}{\partial x}-\frac{\partial v}{\partial y}\right)^2+\left(\frac{\partial u}{\partial y}+\frac{\partial v}{\partial x}\right)^2}$ in 10^{-5}.
XII	Direction of One of the Principal Axes of Strain γ_1	

$$\theta=\tan^{-1}\left(\frac{\left(\frac{\partial u}{\partial x}+\frac{\partial v}{\partial y}\right)+\sqrt{\left(\frac{\partial u}{\partial x}-\frac{\partial v}{\partial y}\right)^2+\left(\frac{\partial u}{\partial y}+\frac{\partial v}{\partial x}\right)^2}-2\frac{\partial u}{\partial x}}{\frac{\partial u}{\partial y}+\frac{\partial v}{\partial x}}\right)$$

I	II	III	IV	V	VI	VII	VIII	IX	X	XI	XII
(5)(10)(12)	+0·05	+0·39	−0·36	+0·03	+0·08	+0·38	+0·02	+0·03	+0·11	+0·05	22°
(7) (8)(12)	+0·55	+0·43	+2·76	+0·89	+1·44	−1·17	+1·57	+3·22	+4·64	−1·77	48°
(4) (3) (8)	+0·02	−0·25	+0·82	−0·61	−0 59	−0·54	+0·29	+0·85	+0 26	−1·43	21°
(11) (9)(12)	+0·90	+0·93	+1·32	+1·15	+2·04	−0·20	+1·13	+2·27	+4·32	−0·23	48°
(2) (7) (4)	−0·09	+0·22	+1·89	−0·31	−0·40	−0·84	+1·05	+2·11	+1·72	−2·51	42°
(9)(13)(11)	+0·12	+0·66	−0·55	+0·48	+0·60	+0·60	+0·06	+0·38	+0·98	0·22	81°
(3) (7) (4)	+0·08	+0·04	+0·92	+1·06	+1·09	−0·44	+0·46	+1·40	+2·49	−0·31	68°
(1) (3) (6	+0·17	+0·26	−0·36	−0·03	+0·15	+0·31	−0·05	+0·22	+0·37	−0·08	167°
(1) (3) (2)	+0·13	+0·15	−0·08	+0·59	+0·72	+0·11	+0·04	+0·47	+1·38	+0·25	86°
(7) (9) (8)	+0·57	+0 48	+1·04	−2·78	−2·21	−0·29	+0·76	+3·67	+1·47	−5·88	11°
(7) (8 (11)	+0·67	+0·69	+2·13	−0·45	+0·23	−0·72	+1·41	+3·03	+3·25	−2·80	34°
(2) (3) (7)	+0·17	+0·10	−0·10	+0·61	+0·78	+0·10	−0·01	+0·44	+1·22	0·34	91°
(1) (6) (9)	−0·10	+0·26	−0·59	−0·03	−0·13	+0·42	−0·17	+0·34	+0·22	−0·47	121°
(7)(12)(11)	+0·86	+0·63	+1·18	−0·18	+0·69	−0·27	+0·90	+2·08	+2·77	−1·40	30°
(3) (7) (8)	+0.45	+0·22	+3·34	+2·13	+2·58	−1·56	+1·78	+3·94	+6·51	−1·36	57°
(2) (4) (5)	+0·53	+0·26	−0·38	−0·46	+0 08	+0·32	−0·06	+2·00	+1·07	−0·92	177°
(12) (8) (5)	+0·04	+0·40	−1·34	+0·64	+0·68	+0·87	−0·47	+1·12	+1·79	−0·44	119°
(4) (8)(10)	−0·17	−0·26	−1·03	−0·66	−0·82	+0·39	−0·64	+1·37	+0·55	−2·19	146°
(5) (4)(10)	+0·54	+0·47	−0·35	+0·03	+0·57	+0·41	+0·06	+0·53	+1·09	−0·05	6°
(9) (8)(12)	+0.57	+0·43	+1·09	+0·79	+1·36	−0·34	+0·76	+1·53	+2·89	−0·18	49°
(6) (3)(13)	+0·12	+0·57	−0·40	+0·26	+0·38	+0·49	+0·09	+0·22	+0·59	+0·16	64°
(11) (6)(13)	+0·12	+0·58	−0·54	+0·26	+0·38	+0·56	+0·02	+0 15	+0·53	+0·24	82°
(1) (7) (3)	+0·09	+0·06	−0·07	+0·63	+0·71	+0·06	−0·01	+0 54	+1·25	+0·17	89°
(6) (9)(13)	+0·20	+0·57	−0·33	+0·25	+0·45	+0·40	+0·12	+0·25	+0·69	+0·20	51°
(9) (7)(11)	+0·41	+0·76	−0·80	+0·39	+0·80	+0·78	−0·02	+0·05	+0·84	+0·76	146°
(2) (3) (4)	+0·05	+0·23	+0·83	−0·38	−0.33	−0·32	+0·53	+1·14	+0 81	−1·47	34°
(4) (8) (5)	+0·51	+0·24	−0·39	−0·64	−0·13	+0·08	−0·31	+1·33	+1·20	−1·46	165°
(1) (9) (7)	+0·51	+0·60	−0·57	−0·02	+0·49	+0·58	+0·02	+0·52	+1·01	−0·03	2°
(9) (8)(11)	+0·58	+0·82	+1·10	+1·07	+1·64	−0·14	+0·96	+1·98	+3·62	−0·34	52°
(6) (3) (9)	+0·13	+0·50	−0·39	+0·19	+0·32	+0·45	+0·06	+0·13	+0·45	+0·19	58°
(7) (3) (9)	+0.67	+0·31	−0·76	+0·32	+0·99	+0·54	−0·23	+0·57	+1·55	+0·42	154°
(8)(10) (5)	+0·05	+0·39	−0·83	−0·05	0	+0·61	−0·22	+0·45	+0·45	−0·45	141°
(8) (4) (7)	+0·24	+0·25	+2·08	−0·57	−0·34	−1·16	+0·92	+2·00	+1·69	−2·34	33°
(8)(12)(10)	+0·05	+0·40	−0·59	+0.69	+0·73	+0·49	−0·10	+0·67	+1·40	−0·06	99°
(11) (8)(12)	+0.84	+0·44	+1·28	+0·80	+1·64	−0·42	+0·86	+1·72	+3·36	−0·09	44°

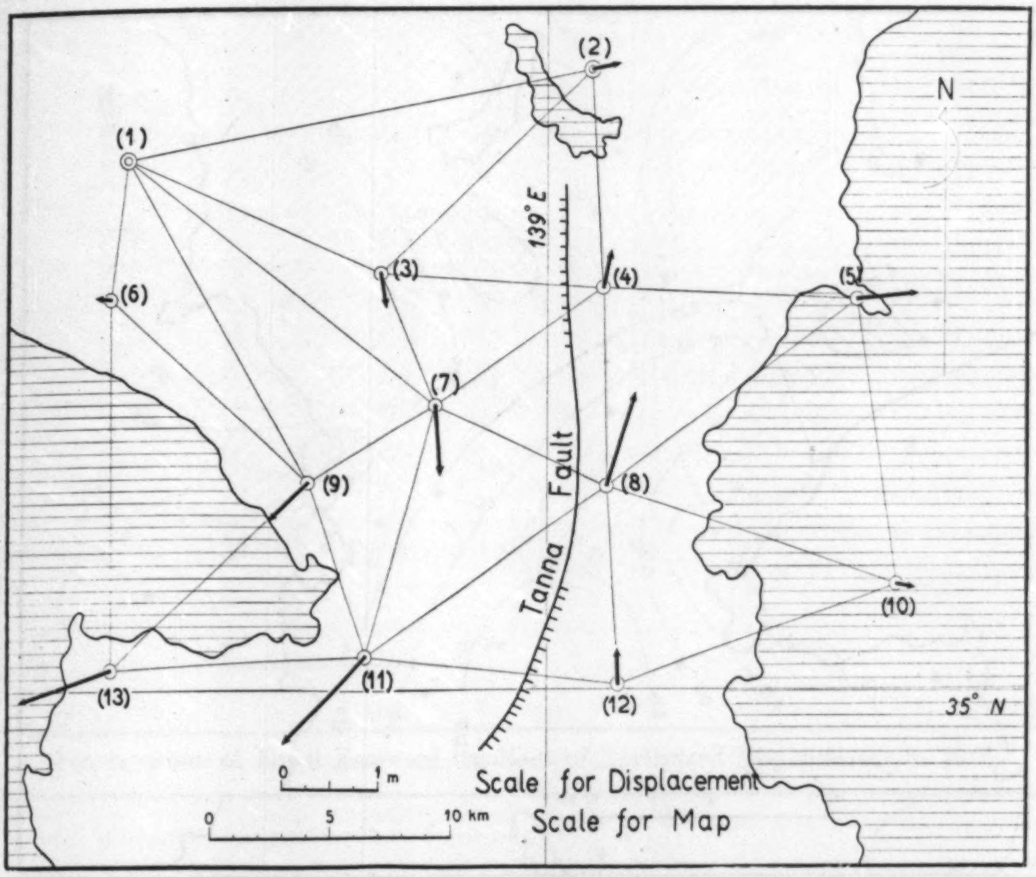

Fig. 2. Horizontal Displacements of the Triangulation Points in Idu Peninsula.

In Fig. 2, the horizontal displacements of the triangulation points are shown by arrows taken to be proportional to their values towards the correspondig directions. It is readily found that the direction of the movement is decidedly opposite on both sides of the Tanna fault. On the western side on the fault, the amount of the displacement is uniformly large throughout, while on its eastern side, they are large only in the immediate neighbourhood of the fault, especially at the point (8). This would seem to indicate that the displacements of the triangulation points on the eastern side of the fault were produced only as a marginal phenomenon. If it is assumed that there was actually some southward component in the displacement of the point (2) then the displacements of the triangulation points on the eastern side of the fault will be of irregular distribution which will be nearly null in their means. In this case, the southwestern displacements of the triangulation points on the western side of the fault will be increased. These circumstances however will not make no influence on the calculation that follows, for which the

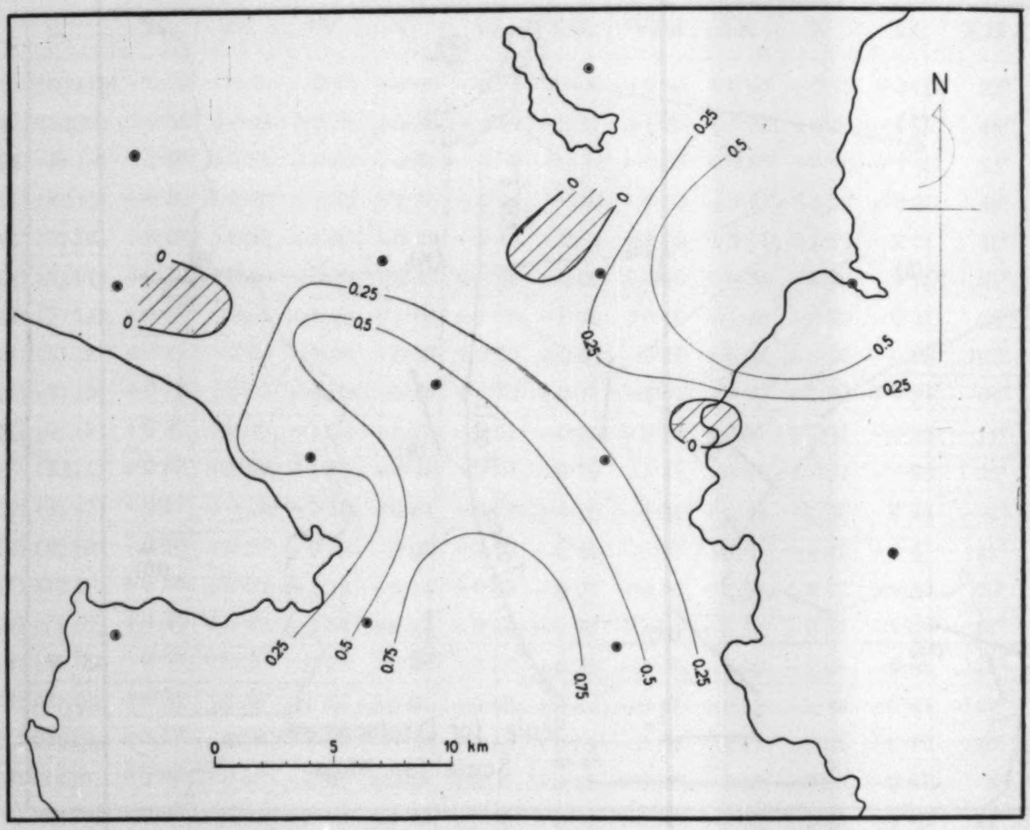

Fig. 3. Lines of Equal Eastward Gradient of Eastward Displacement in 10^{-5}.

reason was proved in the foregoing pages.

In Fig. 3, it is readily seen that the eastward gradient of eastward displacements of the trianglation points are positive almost everywhere in the surveyed area. There is a large difference in amount between them and the northward gradients of northward displacements, which are much larger than the former. The lines of equal eastward gradient of northward displacement in Fig. 4 shows naturally an intimate relation with the trend of the Tanna fault. This quantity is positive along a comparatively narrow zone parallel to the fault. On the eastern and western sides of this zone, the values are negative and their absolute values are much larger on the eastern side than those on the western, which fact indicates hat the displacements of the triangulation points on the eastern side of the fault are large only in the immediate neighbourhood of the fault while on its western side the decrease of the amount of horizontal displacement with distance from the fault is very much smaller, the displacements of the triangulation points sensibly far

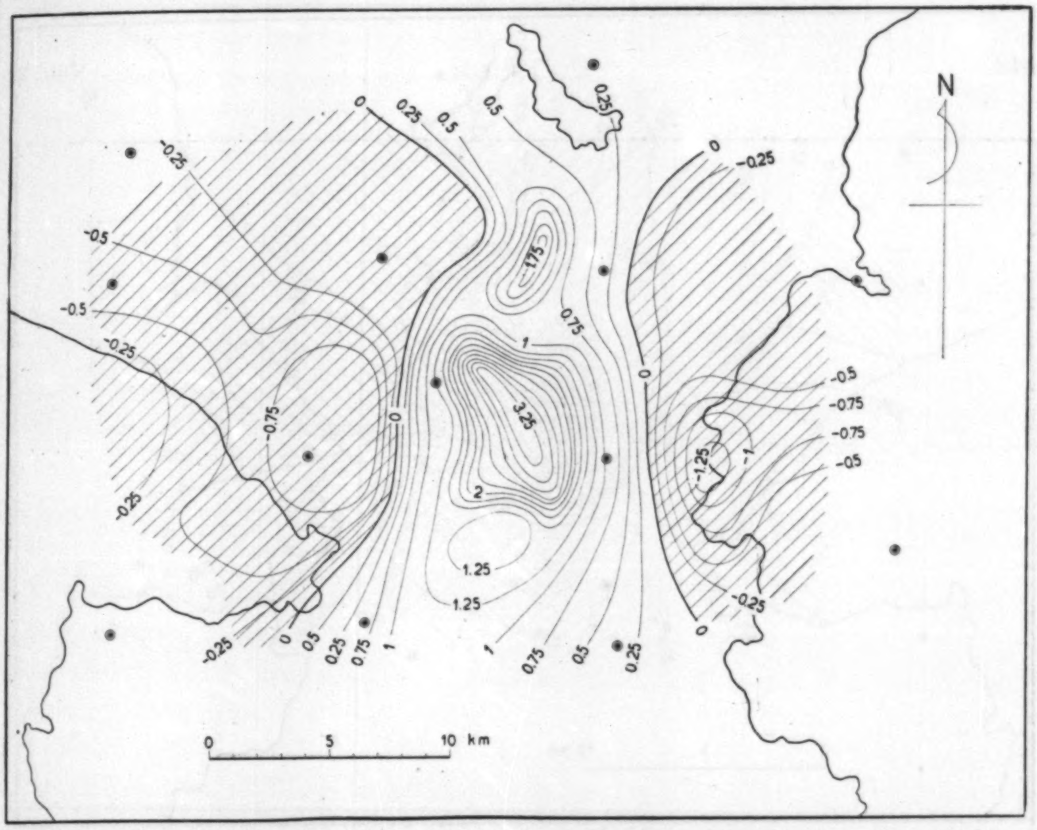

Fig. 4. Lines of Equal Eastward Gradient of Northward Displacement in 10^{-5}.

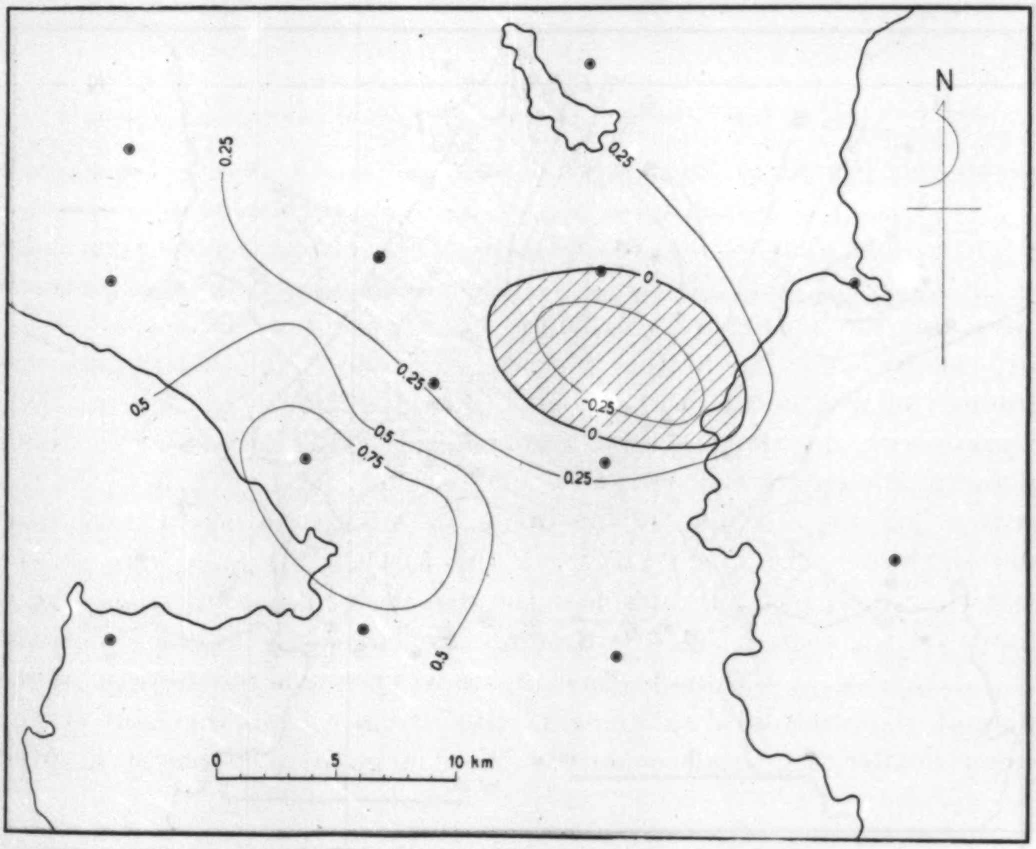

Fig. 5. Lines of Equal Northward Gradient of Eastward Displacement in 10^{-5}.

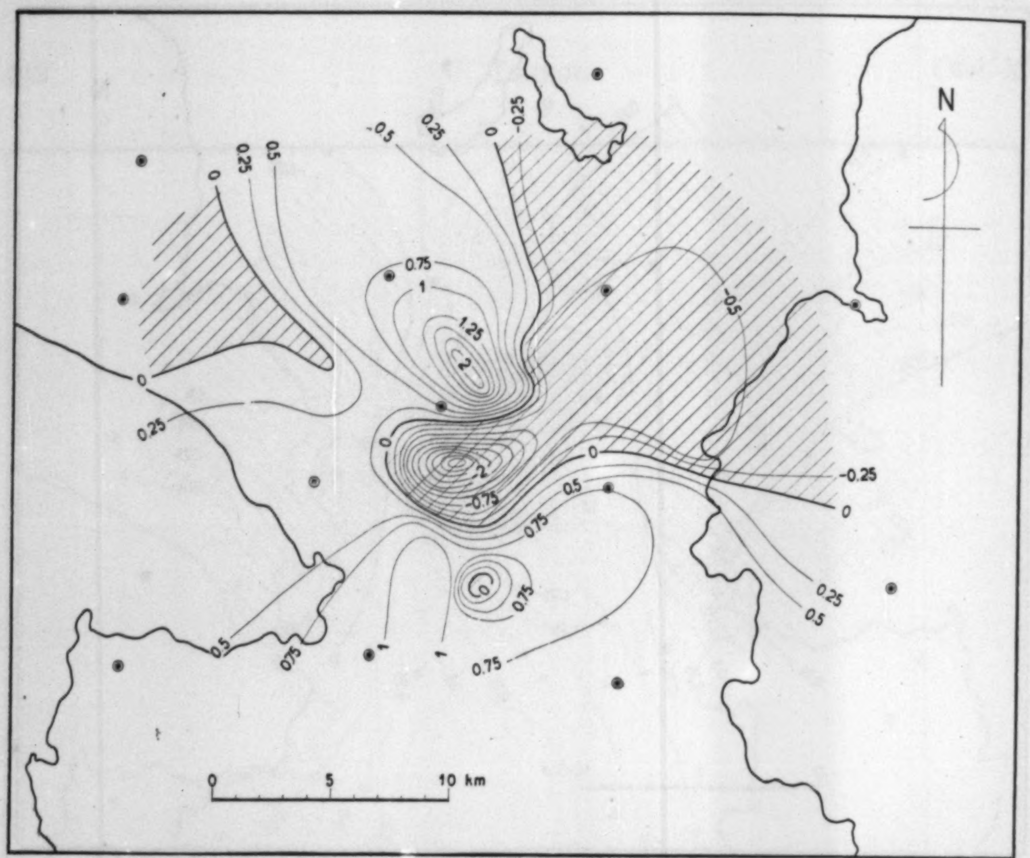

Fig. 6. Lines of Equal Northward Gradient of Northward Displacement in 10^{-5}.

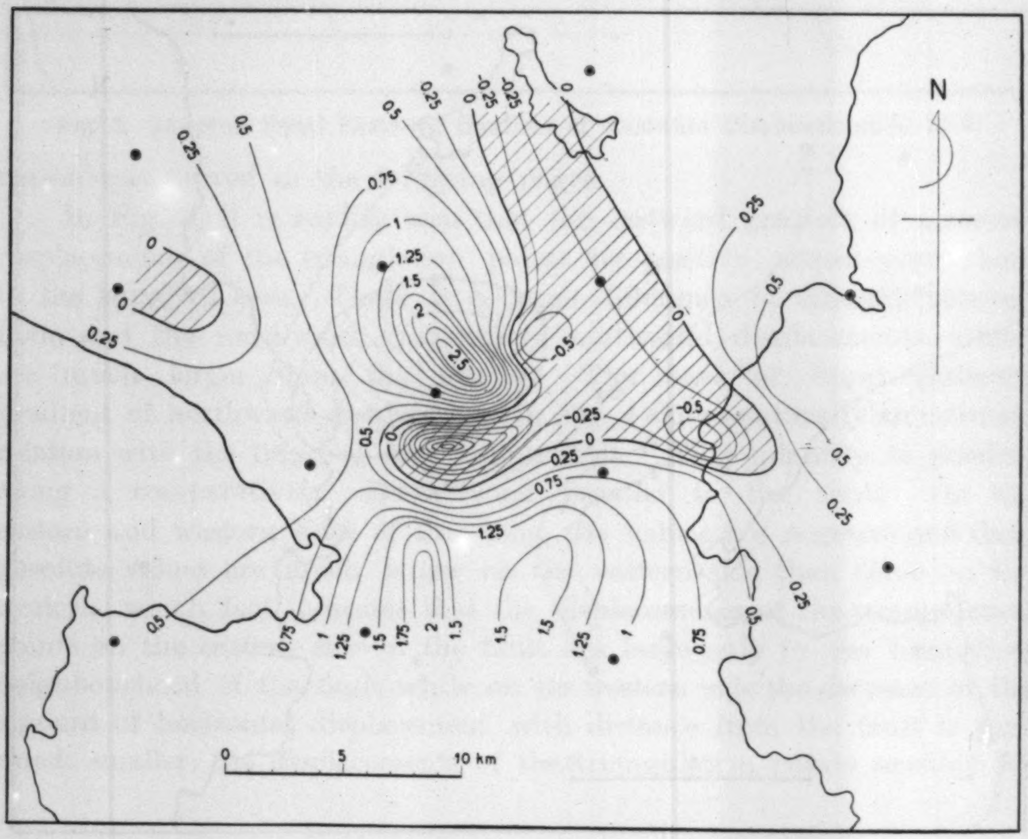

Fig. 7. Lines of Equal Dilatation $\left(\frac{\partial u}{\partial x}+\frac{\partial v}{\partial y}\right)$ in 10^{-5}.

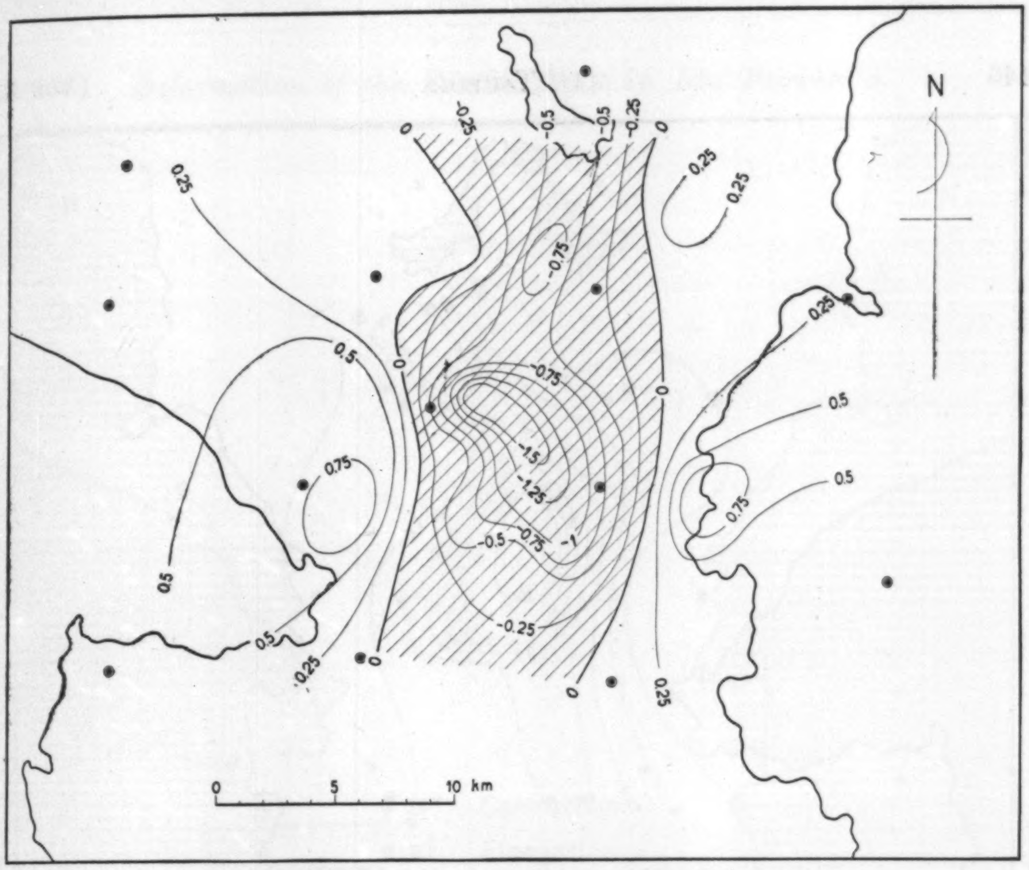

Fig. 8. Lines of Equal Rotation $\frac{1}{2}\left(\frac{\partial u}{\partial y}-\frac{\partial v}{\partial x}\right)$ in 10^{-5}.

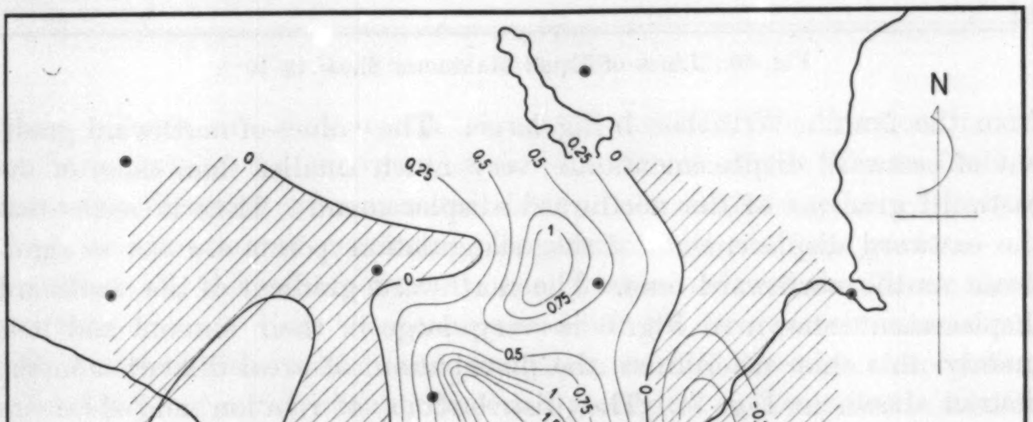

Fig. 9. Lines of Equal Shear $\frac{1}{2}\left(\frac{\partial u}{\partial y}+\frac{\partial v}{\partial x}\right)$ in 10^{-5}.

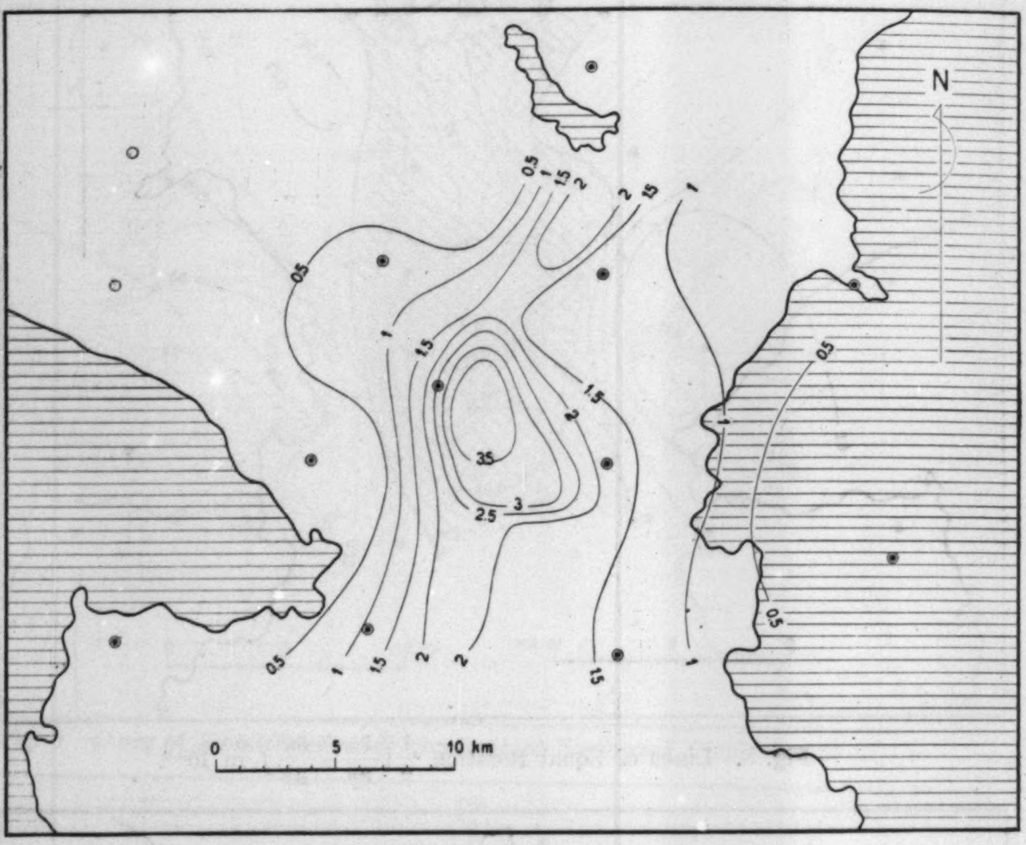

Fig. 10. Lines of Equal Maximum Shear in 10^{-5}.

from the fault nevertheless being large. The values of northward gradient of eastward displacements are very much smaller than those of the eastward gradient of the northward displacement. Thus it seems that the eastward displacements of the triangulation points are not so significant as the northward ones. The northward gradient of the northward displacement shown in Fig. 6 is very large in their amount and it is mainly this that determines the distribution of areal dilatation in the district shown in Fig. 7. The distributions of rotation and shear are nearly the same and this is naturally expected by the smallness of the northward gradient of eastward displacements. The distribution of maximum shear shown in Fig. 10, seems to be interesting in that there are two mutually perpendicular directions along which its value is relatively large. Similar phenomena are also observable with experiments on the rapture of materials.

Finally the distribution of principal axes of strain ellipses in the district shown in Fig. 11 well illustrates the mode of the crust deformations. The principal axes are trending NW-SE and NE-SW and the

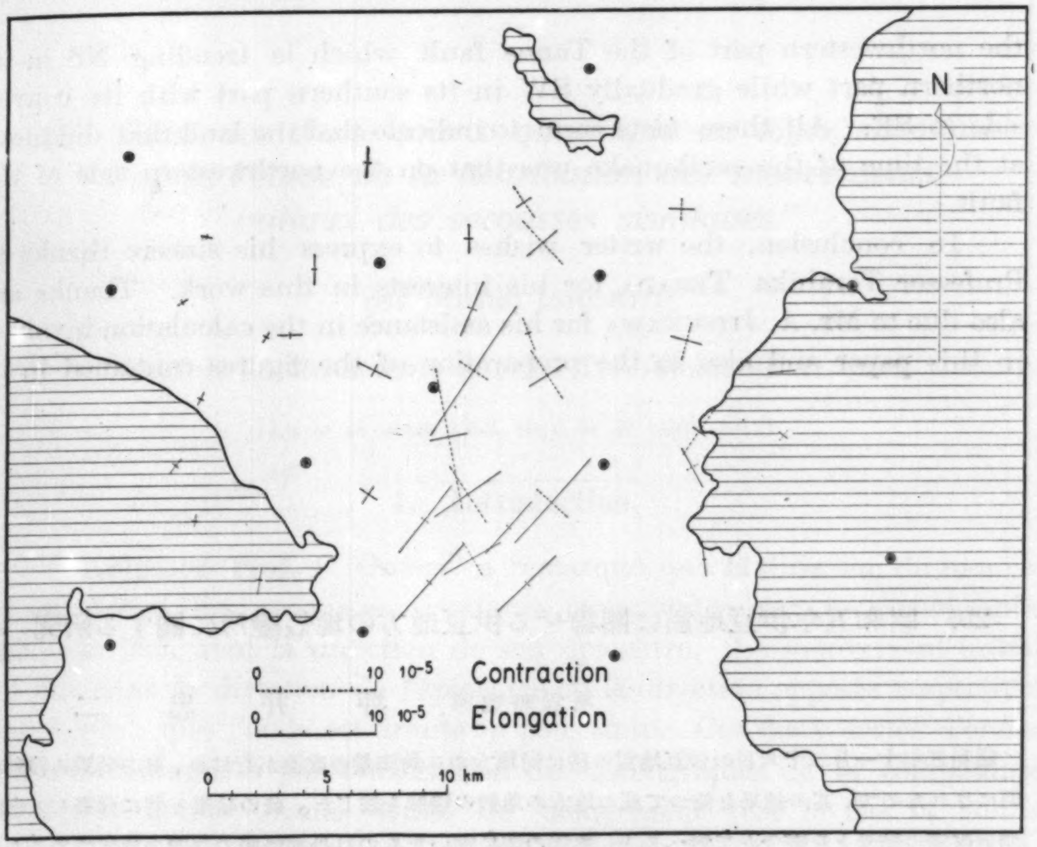

Fig. 11. Principal Axes of Strain Ellipses.

strain ellipses are very much elongated in NE-SW direction in the southern part of the surveyed area. The trend of the Tanna fault is along the direction of maximum shear in its northern part while it is along the direction of maximum elongation in its southern part.

After all, the earth's crust on the western side of the Tanna fault was thus found to have been compressed into SE direction simultaneously with the clockwise rotation and elongation in SW direction. According to H. Tsuya of our Institute, there is a geological evidence that a similar movement of the earth's crust took place in this area in Upper Pleistocene. In his previous paper,[3] on the other hand, the writer showed by the comparison of precise levellings before and after the earthquake that the direction of the tilting of land blocks caused by the earthquake changes itself clockwise as we go from the southern to northern blocks. It was also shown that the block movement of the earth's crust is predominant in that part of the earth's crust in the peninsula that lies on

3) *loc. cit.*

the northwestern part of the Tanna fault which is trending NS in its northern part while gradually SW in its southern part with its convex side to SE. All these facts seem to indicate that the land that did move at the time of the earthquake was that on the northwestern side of the fault.

In conclusion, the writer wishes to express his sincere thanks to Professor Torahika TERADA for his interests in this work. Thanks are also due to Mr. A. JITSUKAWA for his assistance in the calculation involved in this paper and also in the preparation of the figures contained in it.

---

29. 昭和五年伊豆地震に關聯せる伊豆地方の地殼變形に關する研究

地震研究所 坪 井 忠 二

昭和五年十一月二十六日の伊豆地震の後に同地方の三角測量の改測が行はれ、各三角點の移動が明にされたので、其の結果を使つて此の地方の地殼の變形を論じた。此の結果と前に發表した水準測量改測の結果とを綜合して考へると、地震の際に動いたものは丹那斷層の西側の地域であるらしく考へられるのである。

30. *Existence d'une source quadruple au foyer sismique d'après l'étude de la distribution des mouvements initiaux des secousses sismiques.*[1]

par Mishio ISHIMOTO,

Institut de Recherches sur les Tremblements de terre.

(Lu le 15 mars 1932, reçu le 20 mars 1932)

1. Introduction.

Le regretté Prof. F. Omori[2] a remarqué que la direction du mouvement initial des secousses sismiques enregistrées par le sismographe coïncide bien avec la direction de son épicentre. Le mouvement initial se fait dans la direction de l'épicentre ou la direction opposée respectivement selon que l'onde est tirante ou poussante. Ces deux sortes d'ondes ont été distinguées par l'inscription du sismographe de la composante verticale: l'onde tirante donne un mouvement vers le bas et l'onde poussante donne un mouvement vers le haut. Le Prof. Omori a, donc, réussi a déterminer la direction épicentrale: on a employé ce procédé pour connaître la direction épicentrale avec un seul sismogramme.

Le Prof. T. Sida[3] a remarqué cependant, en 1917, que la distribution régionale des mouvements initiaux des secousses sismiques observés en plusieurs stations paraît comparativement simple. Il nous a motré que les mouvements initiaux se distribuent dans quatre quadrants pour le séisme du 18 mai 1917, dont l'épicentre se trouve au fleuve Tenryû. Pour expliquer cette distribution il a supposé au foyer un modèle exécutant l'éloignement brusque de deux disques parallèles dans la direction de leur axe.

Il a constaté aussi pour le séisme du 26 nov. 1916, dont l'épicentre se trouve auprès du détroit d'Akasi, que tous les mouvements initiaux se dirigent vers l'épicentre et il l'a considéré comme d'origine dépressionelle. En tout cas, son procédé nous suggère le mécanisme de la production

---

1) L'étude préliminaire a été publiée dans *Proc. Imp. Acad. Jap.*, **8** (1932), 36.

2) F. OMORI, *Bull. Earthq. Inv. Comm.*, **6** (1912), 11.

3) Il en a parlé, en 1917 à la séance annuelle de la Société japonaise de physique-mathématique.

des ondes sismiques au foyer. Depuis cela tous les sismologues japonais se sont constamment efforcés de développer son procédé. En profitant de tous les forts séismes apparus au Japon, ils ont examiné s'il y avait plusieurs mécanismes de production des ondes.

Pourtant, au cas du séisme de Simabara en 1922, le Prof. Saém. Nakamura a constaté que les deux lignes nodales coïncident très bien avec les lignes tectonique dans la région épicentrale et il a supposé que deux portions de croûte ont exécuté un glissement le long d'une des lignes nodales. Certes, cette manière de voir donne aussi la même distribution. D'après sa considération l'origine du séisme n'est qu'une faille glissante et cela nous fait voir la possibilité de deux sortes de mécanismes au foyer. (Fig. 1)

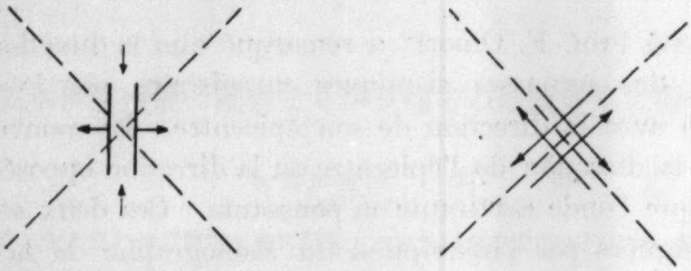

(a) (b)

Fig. 1. Deux modèles représentant deux mécanismes différents.

En tout cas, la distribution régionale des mouvements initiaux des secousses sismiques nous donne une certaine idée du mécanisme de production des ondes sismiques au foyer ; mais la décision d'un de deux modèles restra un problème irrésolu autant qu'on ne considère que le phénomène à deux dimensions. Certes, si nous limitons notre discussion aux séismes dont les foyers restent peu profonds et dont les mouvements du foyer demeurent horizontaux à la surface terrestre, il n'y a pas de préférence : mais quand nous faisons attention surtout aux séismes dont les foyers restent comparativement profonds, nous trouvons le cas où nous aurons quelque moyen de nous décider pour l'un des deux modèles. Mais comme les séismes à foyer profond donnent toujours des distributions anormales pour les mouvements initiaux, on nous dit qu'ils auront au foyer un mécanisme différent de celui des séismes à foyer peu profond.

4) S. NAKAMURA, *Kisyô-syûsi* (2) 1 (1923), 1.

D'autre part, le Prof. M. Matuyama[5] a fait une discussion en adoptant le modèle de deux disques et a conclu que les lignes nodales doivent être représentées par une courbe hyperbolique au lieu de deux lignes droites. Pourtant, comme le Prof. S. Nakamura a adopté le mécanisme de glissement dans le cas du séisme de Simabara, les chercheurs du Bureau Central de Météorologie ont été conduits à considérer le séisme comme ayant un glissement de faille à son foyer.

Or, les conditions des observations sismiques sont bien améliorées aujourd'hui : le Bureau Central de Météorologie s'efforce d'inaugurer des stations partout au Japon, en y installant le même type de sismographe (type de Wiechert). Ainsi, il nous permet d'une part d'obtenir les mouvements initiaux des secousses sismiques avec assez de sûreté, d'autre part d'étudier un grand nombre de séismes quoiqu'ils n'aient pas grande intensité. Nous voulons, ensuite, remarquer surtout les distributions des mouvements initiaux donnés par les séismes dont les foyers demeurent assez profonds, en espérant que nous pourrions tirer certaine influence de la profondeur hypocentrale. Cela nous permetra de considérer de mécanisme de la production des ondes sismiques avec trois dimensions.

2. Distribution des mouvements initiaux déjà étudiées.

Nous avons déjà dit qu'il y a deux sortes de mécanismes pour expliquer la distribution des mouvements initiaux des secousses sismiques. Nous les distingons : a) le mouvement brusque de deux disques parallèles dans la direction de leur axe ; b) deux portions d'écorce font un glissement relatif produisant une faille. Pour le modèle-b, on suppose généralement deux glissements perpendiculaires, quoique un tel glissement n'existe pas dans la nature.

M. S. Kunitomi[6] a proposé, cependant, une façon de distribution avec un seul glissement : cette fois-ci l'amplitude du mouvement devient maxima le long de la faille, tandis que la distribution en quadrants reste sans aucun changement. Nous pourrions vérifier son hypothèse avec des données précises d'observation : mais d'après l'étude de M. K. Honda[7] les mouvements initiaux des secousses se trouvent maximum dans les directions bissectrices des angles donnés par deux lignes nodales.

---

5) M. Matuyama, "Bankin no Disingaku" (livre de sismologie, en japonais), 229.
6) S. Kunitomi, *Geophys. Mag.*, **2** (1930), 65.
7) K. Honda, *ibid.* **4** (1931), 185.

Nous savons, donc, même dans le modèle-b que la question de la distribution des mouvements initiaux n'est pas résolue simplement.

Certes, nous avons un grand nombre de résultats représentant la distribution des mouvements initiaux surtout depuis le grand tremblement de terre de 1923. Nous allons, en effet, passer en revue les résultats recemment rapportés. Quant au grand tremblement de terre de Kantô, (le 1er Sept. 1923) M. S. Kunitomi[8] a publié un mémoire où nous trouvons beaucoup de résultats sismométriques.

En ramassant les données sur les mouvements initiaux des secousses étudiées par plusieurs personnes, il a donné sa conclusion. Il explique la distribution par un effet de réflexion des ondes sur une couche située à 50 km de profondeur. Suivant cette idée il fixe la profondeur hypocentrale à 28 km qui est assez petite quand on la compare aux résultats obtenus par les autres moyens. Il a adopté cette manière d'explication aussi pour le tremblement de terre de Sekihara.[9] (le 27 Oct. 1927.) D'après notre point de vue, cependant, l'adoption d'un phénomène de réflexion n'est pas nécessaire : nous la discuterons dans les chapitres plus loin.

MM. K. Sagisaka et H. Satô[10] ont étudié le tremblement de terre du 3 août 1926, dont l'épicentre se trouve près de Yokohama. Ils supposent une ligne nodale de direction SE-NO qui coïncide avec une ligne tectonique. Ils n'ont pas, cependant, réussi à expliquer l'existence d'une onde poussante enregistrée à Kakioka.

Pour le grand tremblement de terre de Tango (le 7 mai 1927) M. S. Kunitomi[11] a fait une carte représentant la distribution des mouvements initiaux. Il constate dans celle-ci qu'une des deux lignes nodales coïncide avec la faille produite dans la région épicentrale et cherche à expliquer la distribution avec un seul glissement de faille. Naturellement il considère la distribution des mouvements initiaux comme un problème à deux dimensions, parce que la profondeur hypocentrale a été fixé à 15 km.

M. K. Sagisaka[12] a publié un mémoire sur le séisme du 21 mai 1928, dont l'épicentre se trouve auprès de la ville de Tiba. Il a montré qu'il y a une région d'ondes poussantes en forme de lentille. Pour

---

8) S. KUNITOMI, *Geophys. Mag.*, **3** (1931), 149.
9) S. KUNITOMI, *Kisyô-syûsi*, (2) **6** (1928), 59.
10) K. SAGISAKA et H. SATO, *ibid.*, (2) **4** (1926), 301.
11) S. KUNITOMI, *loc. cit.*
12) K. SAGISAKA, *Kisyô-syûsi*, (2) **6** (1928), 326.

expliquer cela il considère une faille au foyer ; mais il est assez difficile de comprendre le mécanisme qui donnera un domaine des ondes poussantes en forme de lentille. Il a aussi exécuté une étude sur un tremblement de terre[13] à foyer profond dont l'épicentre se trouve près de la presqu'île de Sima (le 3 juin 1929) ; nous en parlons au chapitre suivant.

D'autre côté, M. K. Tanahasi[14] a publié un mémoire sur le séisme du 4 juillet 1929 dont l'épicentre se trouve dans la presqu'île de Kii. Il a fait une carte représentant la distribution des mouvements initiaux. Pour expliquer cela il adopte la réflexion des ondes sur une couche dans la croûte. Il a publié aussi une autre mémoire sur le séisme[15] du 2 juin 1931 dont l'épicentre se trouve près de Takayama : comme ce séisme a son foyer assez profond nous voulons en parler au chapitre suivant.

Récemment, M. S. Kunitomi a exécuté des études, d'une part sur un séisme,[16] un de plus grands séisme dans la foule sismique d'Itô ; d'autre part sur le grand tremblement de terre d'Idu[17] du 26 nov. 1930. En constatant que les mouvements initiaux de ces séismes se partagent en quatre quadrants, il conclut que ce sont des séisme d'origne tectonique : c'est-à-dire que les ondes sismiques ont été causées par la production d'une faille. Cette fois-ci, les épicentres restaient auprès de la surface terrestre et nous n'avons aucune préférence parmi les deux modèles. Comme nous l'avons déjà dit, M. K. Honda a étudié surtout les amplitudes des mouvements initiaux sur le dernier tremblement de terre.

M. K. Hukutomi[18] a étudié les séismes apparus dans la région de Kantô où le réseau des stations a des mailles assez serrées. Il a employé l'inscription du sismographe de composante verticale pour distinguer les deux sortes d'ondes. Il constate qu'il y a des séismes qui ne donnent pas de distribution en quadrant, lesquels occupent une certaine partie de Kantô : il a tracé une ligne droite passant par l'épicentre, en considérant qu'elle représente la faille produite.

Ce que nous avons déjà dit sont les résultats des études sur les mouvements initiaux des secousses sismiques ; sur lesquels la plupart des sismologues considèrent le mécanisme de la production d'une faille au foyer avec le rayonnement des ondes sismiques. Comme nous

13) K. Sagisaka, *Kensin-zihô*, **3** (1929), 313 ; *Geophys. Mag.*, **3** (1930), 165.
14) K. Tanahasi, *Umi to Sora*, **9** (1929), 197.
15) K. Tanahasi, *ibid.*, **11** (1391), 277.
16) S. Kunitomi, "Iwanami-Kôza", sur physique et chimie, section physique 8.
17) S. Kunitomi, *Geophys. Mag.*, **4** (1931), 73.
18) K. Hukutomi, *Zisin.*, **3** (1931), 592.

l'avons déjà indiqué, la distribution donnée par deux sortes de mécanismes reste toujours le même autant que nous occuppons des séismes dont l'hypocentre demeure auprès de la surface terrestre. Certes, nous avons dit, que les distributions des mouvements initiaux données par les séismes à foyer profond restent toujours assez irrégulières pour qu'on ne puisse pas tracer de ligne droite nodale. Il nous semble, cependant, qu'il faut examiner tout d'abord la distribution dans les séismes à foyer profond: cette étude nous donnera des idées pour connaître le mécanisme de la production des ondes au foyer en considérant le cas de trois dimensions.

3. Distributions pour les séismes à foyer profond.

Nous avons dit que les distributions des mouvements initiaux pour les séismes à foyer profond donnent quelque chose d'assez irrégulier pour qu'on ne puisse pas tracer de courbe nodale. Nous remarquons, cependant, deux ou trois exemples de distributions déjà rapportées. Nous pouvons d'abord indiquer un mémoire publié par M. K. Tanahasi[19]. La figure 2 représente la distribution des mouvements initiaux obtenue pour le séisme du 2 juin 1931, dont l'épicentre se trouve au près de Takayama et dont la profondeur hypocentrale en de 240 km. En constatant que la courbe nodale ressemble à une hyperbole, il a adopté pour mécanisme de la production des ondes sismiques au foyer avec le modèle-a;

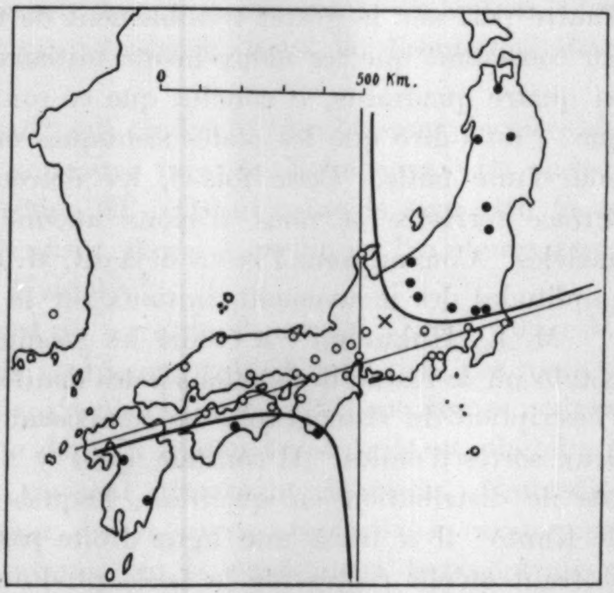

Fig. 2. Distribution des mouvements initiaux pour le séisme du 2 juin 1931. (d'après M. K. Tanahasi) Profondeur hypocentrale 240 km.
● onde poussante, ○ onde tirante, × épicentre.

c'est-à-dire deux disques qui s'éloignent subitement dans la direction de leur axe. Bien que ce modèle ait été proposé premièrement par le prof. T. Sida et puis par le Prof. M. Matuyama, il était abandonné depuis l'apparition du séisme de Simabara. Le moment est venu de

19) K. Tanahasi, *loc. cit.*

réflechir à l'origine des deux modèles de mécanisme. Il nous semble qu'il est presque impossible de rendre compte de la distribution des mouvements initiaux avec le modèle-b manifestant le phénomène du glissement de faille au foyer.

Certes, nous sommes tout à fait libres quant au choix des deux modèles, autant qu'on étudie seulement les séismes à foyer peu profond. Mais, nous inclinons à choisir le modèle-a pour les séismes à foyer profond. Pour appuyer ce point de vue, nous avons essayé de chercher la distribution des mouvements initiaux surtout pour les séismes à foyer profond espérant que cela nous donnerait certaines suggestions.

Un mémoire publié par M. K. Sagisaka[20] nous donne un autre exemple. Il a étudié le séisme du 3 juin 1929, dont l'épicentre se trouve auprès de la presqu'île de Sima et dont la profondeur hypocentrale se trouve à 300 km environ. Il met deux lignes nodales pour représenter la faille produite au foyer et fait passer l'une des deux par l'épicentre. Nous voulons, cependant, représenter la courbe nodale suivant le mécanisme du modèle-a. Nous mettons une ellipse au lieu de deux lignes dont l'intérieur est occupé par les ondes poussantes. (Fig. 3)

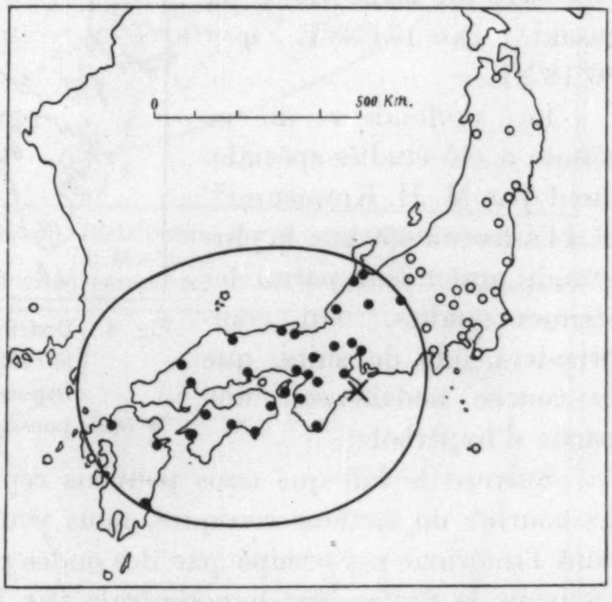

Fig. 3. Distribution des mouvements initiaux pour le séisme du 3 juin 1929. (d'après les données de M. K. Sagisaka) Profondeur hypocentrale 300 km.
• onde poussante, ○ onde tirante, × épicentre.

Représenter la ligne nodale par une ellipse paraîtra étrange surtout pour ceux qui considèrent toujours la production des ondes sismiques comme due au glissement d'une faille. C'est, cependant, une simple conséquence de l'adoption du modèle-a. Nous allons développer cette manière de voir dans les chapitres suivants.

Ces deux exemples nous suggèrent l'idée que les courbes nodales sont les sections d'un cône. Nous avons, donc, essayé étudier les dis-

20) K. Sagisaka, *loc. cit.*

tributions des mouvements initiaux surtout pour les séismes à foyer profond. Bien que nous efforcions de faire la carte avec les données figurant dans Kisyô-yôran, la plupart des séismes ne satisfont pas nos conditions : quelque-fois l'épicentre se place mal dans la mer, quelque-fois l'inscription est faite seulement en plusieurs stations autour de l'épicentre à cause d'une trop petite intensité. En tout cas, nous avons réussi à trouver un exemple montrant les courbes nodales avec les sections coniques. La figure 4 montre la distribution des mouvements initiaux pour le séisme du 15 janvier 1927 dont l'épicentre se trouve au large de Kyô-gasaki. ($\lambda=134°38'$E, $\varphi=36°18'$N)

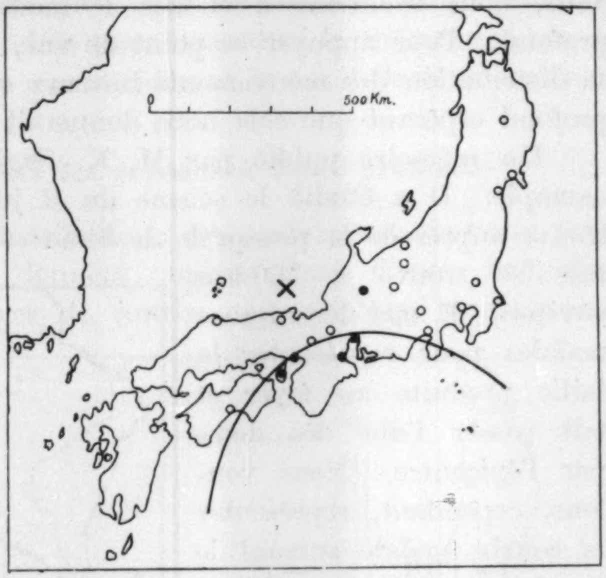

Fig. 4. Distribution des mouvements initiaux pour le séisme du 15 jan. 1927. Profondeur hypocentrale 450 km
● onde poussante, ○ onde tirante, × épicentre.

La profondeur de ce séisme a été étudiés spécialement par M. H. Kawasumi[21] et il l'a fixée à 450 km, la plus grande profondeur parmi les séismes étudiés. On comprendera, tout de suite, que la courbe nodale soit une partie d'hyperbole.

Suivant le fait que nous pouvons représenter les lignes nodales avec les courbes de sections coniques, nous voulons savoir la forme du cône dont l'intérieur est occupé par des ondes poussantes. D'autre part, nous trouvons la profondeur hypocentrale par les données sur l'occurence de temps ou la durée des secousses préliminaires. Quand nous connaissons la forme de le ligne nodale et la profondeur hypocentrale, nous pouvons déterminer du cône en supposant que l'écorce terrestre est un milieu homogène et isotrope. Au moyen de la géométrie perspective, nous trouvons que le cône a un angle de 45° environ : cet angle coïncide, cependant, très bien avec l'angle de deux lignes nodales obetenues surtout pour les séismes à foyer peu profond. Nous pouvons dire, donc, que la grandeur de la courbe dépend de la profondeur hypocentrale et que la forme de la courbe dépend de l'orientation de l'axe du cône.

21) H. KAWASUMI, *Kisyô-syûsi*, (2) 5 (1927), 232.

4. Adoption de la courbe de section conique pour les courbes nodales.

Avec l'idée que les courbes nodales seront représentées par les courbes de section conique, nous avons essayé de faire une revision des résultats, soit d'après les cartes faites par les sismologues, soit d'après les données de Kisyô-yôran.

La figure 5 représente la courbe nodale du grand tremblement de terre de 1923 d'après les données de M. S. Kunitomi[22]: l'épicentre a été déterminé : $\lambda=139°17'E$, $\varphi=35°22'N$. Nous mettons une ellipse pour la courbe nodale. Certes, nous sommes obligés de comparer la profondeur hypocentrale pour décider de la grandeur de l'ellipse. Suivant la grandeur de l'ellipse tracée, il nous semble que le foyer reste assez profond. Mais, d'après la détermination de la profondeur hypocentrale exécutée avec les résultats d'observations surtout des stations voisines, nous constatons que le foyer reste comparativement peu profond. Il nous paraît, donc, que les ondes ont été rayonnées d'un foyer ayant une dimension étendue dans une direction verticale. Il

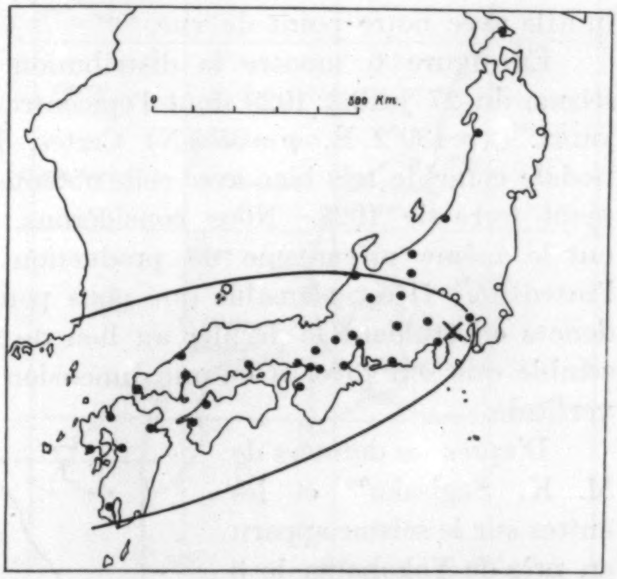

Fig. 5. Distribution des mouvements initiaux pour le séisme du 1er sept. 1923.
● onde poussante, ○ onde tirante, × épicentre.

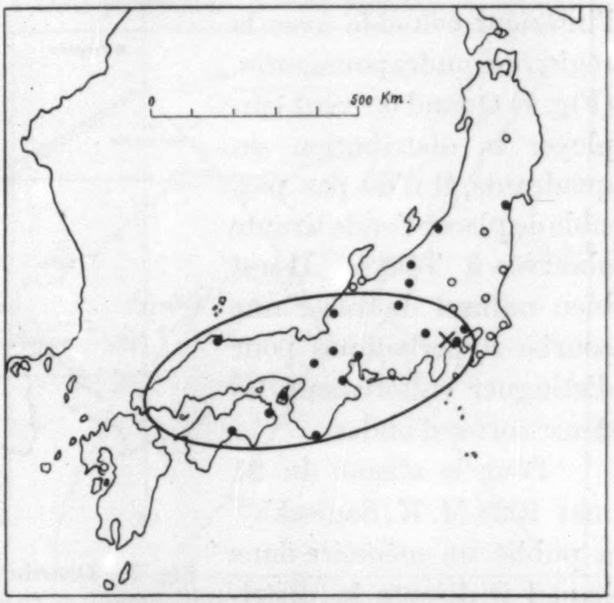

Fig. 6. Distribution des mouvements initiaux pour le séisme du 27 juillet 1929.
● onde poussante, ○ onde tirante, × épicentre

22) S. Kunitomi, *loc. cit.*

est possible que les ondes rayonnées près de la surface aient été aperçues surtout par les stations voisines, les ondes rayonnées au sein de la croûte l'ayant été par les stations lointaines. Quoique M. S. Kunitomi ait considéré la réflexion des ondes sur une couche située plus bas, elle est inutile avec notre point de vue.

La figure 6 montre la distribution des mouvements initiaux du séisme du 27 juillet 1929 dont l'épicentre se trouve au près de Tanzawa-yama. ($\lambda = 139°2$ E, $\varphi = 35°5$ N) Certes, l'ellipse tracée pour la ligne nodale coïncide très bien avec celle obtenue dans le cas du grand tremblement terre de 1923. Nous considérons, donc, que ces deux séismes ont le même mécanisme de production des ondes sismiques malgré l'intensité. Il est plausible que nous pourrions assurer beaucoup d'évidences en étudiant le dernier au lieu du premier. En tout cas, il nous semble que son foyer a eu une dimension étendue aussi dans la direction verticale.

D'après les données de M. K. Sagisaka[23] et les autres sur le séisme apparu au près de Yokohama le 3 août 1926, nous pouvons mettre une hyperbole dont l'intérieur coïncide avec la région des ondes poussantes. (Fig. 7) Quand on veut employer la distribution en quadrants, il n'est pas possible de placer l'onde tirante observée à Tôkyô. Il est bien naturel de tracer une courbe hyperbolique pour distinguer entièrement les deux sortes d'ondes.

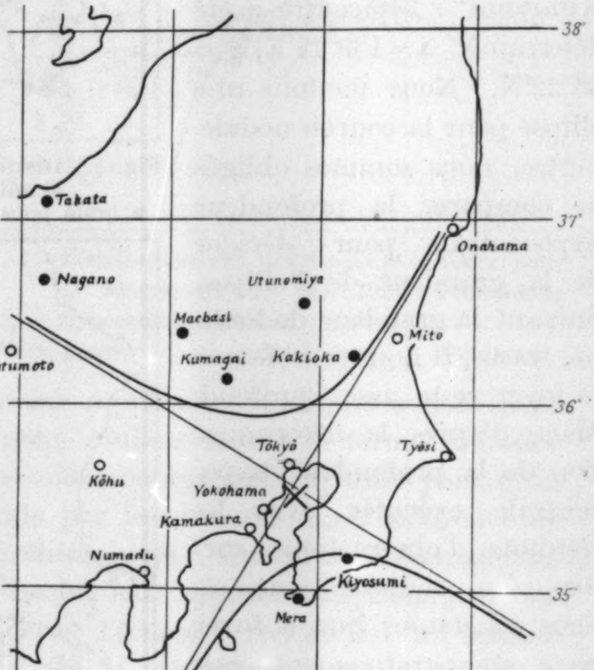

Fig. 7. Distribution des mouvements initiaux pour le séisme du 3 août 1926. Profondeur hypocentrale 40 km ● onde poussante, ○ onde tirante, × épicentre.

Pour le séisme du 21 mai 1928 M. K. Sagisaka[24] a publié un mémoire dans lequel il discute la distribution des movements initi-

23) K. SAGISAKA, *loc. cit.*
24) K. SAGISAKA, *loc. cit.*

aux. (Fig. 8) L'épicentre de ce séisme se trouve au près de Tiba ($\lambda = 140°1$ E $\varphi = 35°6$ N) et le foyer est à 63 km de profondeur. Il a mis une courbe en forme de lentille pour déterminer la région des ondes poussantes. Cette manière d'explication nous paraît qu'il traite une condition assez compliquée. Sa forme, qu'est ce qu'elle signifie? Il est tout à fait naturel de tracer une section conique pour la courbe nodale avec l'idée que la source de la production des ondes sismiques demeure simple. Nous mettons une ellipse pour déterminer la région occupée par les ondes poussantes. Certes, la profondeur hypocentrale détermine la grandeur de l'ellipse. Nous constatons que la profondeur déterminée d'après sa grandeur demeure très voisine de celle calculée par les autres procédés.

D'autre part M. K. Tanahasi[25] a étudié le séisme du 4 juillet 1929 dont l'épicentre se trouve dans le presqu'île de Kii. (Fig. 9) Il a employé la réflexion

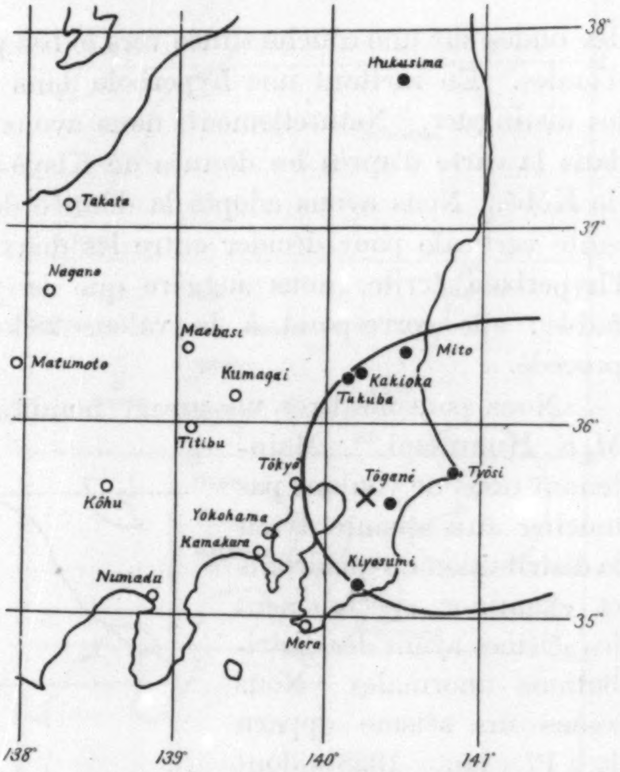

Fig. 8. Distribution des mouvements initiaux pour le séisme du 21 mai 1928. Profondeur hypocentrale 63 km.
● onde poussante, ○ onde tirante, × épicentre.

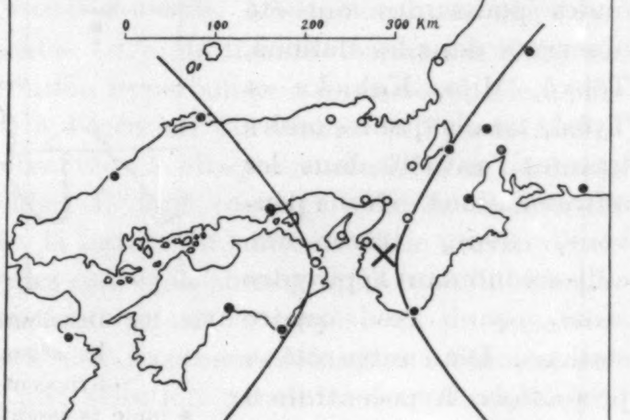

Fig. 9. Distribution des mouvements initiaux pour le séisme du 4 juillet 1929. (d'après les données de M. K. Tanahasi) Profondeur hypocentrale 28 km.
● onde poussante, ○ onde tirante, × épicentre.

25) K. Tanahasi, *loc. cit.*

des ondes sur une couche située vers le bas pour distinguer les deux sortes d'ondes. En mettant une hyperbole dans sa carte, nous avons réussi à les distinguer. Naturellement, nous avons exécuté une petite correction dans la carte d'après les donnés de Kisyô-yôran. C'est pour la donnée de Kôbé. Nous avons adopté la donnée de Kisyô-yôran sur la composante verticale pour décider entre les deux sortes d'ondes. En tout cas l'hyperbole écrite, nous suggère que la profonder hypocentrale reste faible: elle correspond à la valeur 28 km determinée avec un autre procédé.

Nous pouvons tirer un grand nombre d'exemples du mémoire de M. K. Hukutomi.[26] Maintenant nous ne voulons pas toucher aux séismes ayant la distribution en quadrants et examiner spécialement les séismes ayant des distributions anormales. Nous avons un séisme apparu le 1er jan. 1928 dont l'épicentre se trouve sur le fleuve de Kinu ($\lambda = 140°0$E, $\varphi = 36°0$ N). (Fig. 10) Les ondes poussantes ont été observées dans les stations, Tôkyô, Mito, Kakioka et Tyôsi, tandis que les ondes tirantes l'ont été dans les autres stations. Nous pouvons, donc, tracer une ellipse contenant l'épicentre ainsi que ces quatre stations. D'un autre côté sa profondeur hypocentrale a été fixée à 55 km ; laquelle coïncide très bien avec la grandeur d'ellipse supposant que l'angle du cône ait la valeur 45°.

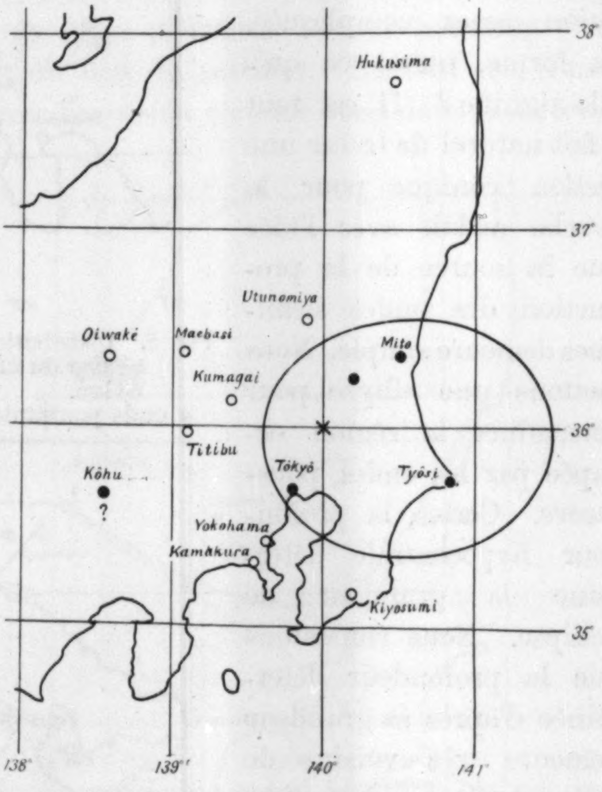

Fig. 10. Distribution des mouvements initiaux pour le séisme du 1er jan. 1928. Profondeur hypocentrale 55 km
• onde poussante, ○ onde tirante, × épicentre.

Pour le séisme du 1er mai 1930, dont l'épicentre se trouve près de Tyôsi ($\lambda = 140°3$ E., $\varphi = 35°7$ N), l'onde poussante a été observée seulement à

26) K. HUKUTOMI, *loc. cit.*

la station Tyôsi et les ondes tirantes aux autres stations. (Fig. 11) Cela nous permet ainsi de tracer une ellipse avec beaucoup de liberté. Mais la région des ondes poussantes sera mieux représentée avec une ellipse qu'avec les courbes autres que l'ellipse.

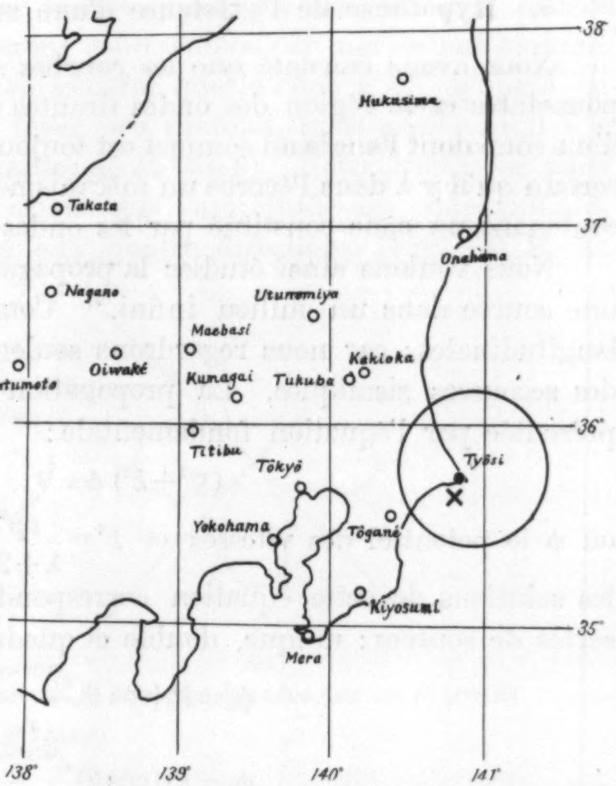

Fig. 11. Distribution des mouvements initiaux pour le séisme du 1er mai 1930. Profondeur hypocentrale 40 km.

• onde poussante, ○ onde tirante, × épicentre.

Nous voulons ajouter quelques mots sur le séisme du 26 nov. 1916 étudié par les Prof. Sida et Matuyama. Quand nous voyons la carte représentant la distribution des mouvements initiaux pour ce séisme, nous comprenons tout de suite que les mouvements sont distingués par une hyperbole. Malheureusement, nous n'avons aucune station dans la région des ondes poussantes. L'onde tirante observée à Kôbe est le simple résultat d'une distribution hyperbolique ; nous voyons le même exemple à la station de Tôkyô à l'occasion du séisme du 3 août 1926.

Pour traiter les données observées à chaque station, nous sommes obligés de considérer leur poids. Il faut compter avec la nature du sismographe aussi bien qu'avec la nature du terrain. Si le terrain d'une station n'est pas constitué par des roches, le sismographe écrit habithellement les perturbations à la surface qui nous empêchent de constater surtout les mouvements initiaux des secousses sismiques. Suivant ces circonstances, il faut exécuter une sélection parmi les données de Kisyôyôran et on verra plusieurs exemples dans les figures déjà données.

En tout cas, les courbes nodales de la distribution des mouvements initiaux sont représentées par les courbes de la section conique. Nous allons, donc, étudier la propagation sphérique des ondes dans l'écorce représentant de telles sortes de courbes nodales quand elles arriveront à la surface terrestre.

5. Hypothèse de l'existence d'une source quadruple au foyer.

Nous avons constaté que les courbes séparant la région des ondes poussantes et la région des ondes tirantes sont représentées par la section d'un cône dont l'angle au sommet est toujours à peu près 45°. Il est, donc, certain qu'il y a dans l'écorce un mécanisme envoyant les ondes sphériques contenant un cône constitué par les ondes poussantes.

Nous voulons ainsi étudier la propagation sphérique des ondes ayant une source dans un milieu infini.[27] Considérons seulement les ondes longitudinales : car nous regardrons seulement les mouvements initiaux des secousses sismiques. La propagation sphérique des ondes est représentée par l'équation fondamentale :

$$(\nabla^2 + k^2)\,\phi = 0$$

où ϕ le potentiel des vitesses et $k^2 = \dfrac{\rho p^2}{\lambda + 2\mu}$. Désignons par ϕ_0, ϕ_1 et ϕ_2 les solutions de cette équation correspondant respectivement aux trois sortes de sources : unique, double et quadruple. Ils sont représentés par

$$\phi_0 = P_0(\cos\theta)\frac{e^{ik(vt-r)}}{r},$$

$$\phi_1 = P_1(\cos\theta)\frac{e^{ik(vt-r)}}{r} f_1(ikr),$$

$$\phi_2 = P_2(\cos\theta)\frac{e^{ik(vt-r)}}{r} f_2(ikr),$$

où f_1 et f_2 sont les fonctions devenant l'unité pour les grandes valeurs de r. Nous donnons, alors, à ces fonctions la valeur un dans le domaine en question.

Faisons attention surtout à la source quadruple $P_2(\cos\theta)$; elle rayonne les ondes poussantes dans un cône ayant l'angle de 55°. (Fig. 12)

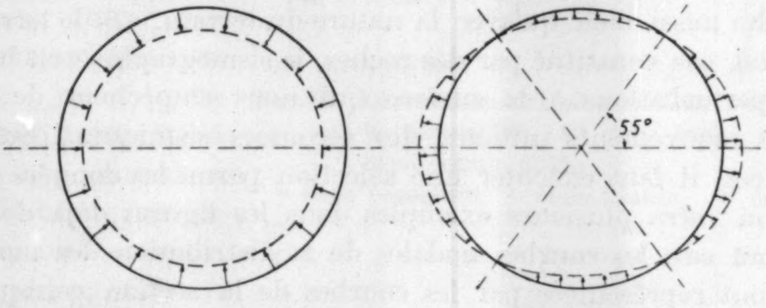

Fig. 12. Aspects généraux de $-P_0(\cos\theta)$ et de $P_2(\cos\theta)$.

27) Le Prof. K. Sezawa a déjà donné les solutions générales dans *Bull. Earthq. Res. Inst.*, 2 (1927), 13.

Quand les ondes envoyées d'une source quadruple arrivent à la surface terrestre, les courbes nodales seront représentées par une section conique. Mais le fait que l'on constate en général que le cône a 45° d'angle au lieu de 55° pour les séismes à foyer peu profond, nous assure qu'il y a une superposition des ondes tirantes de $P_0(\cos\theta)$. Nous constatons ainsi dans le problème à deux dimensions que l'amplitude des ondes initiales aura même valeur de maxima aux quatre directions. (Fig. 13) M. K.

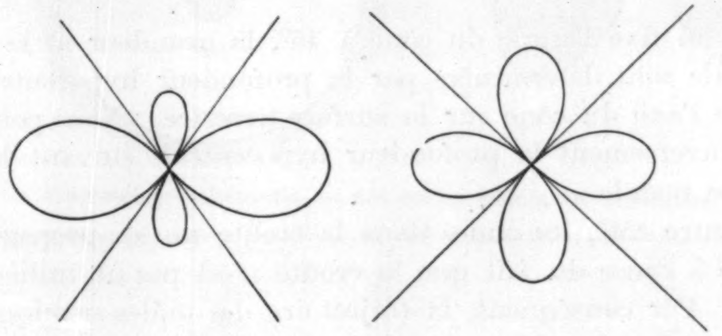

Fig. 13. Amplitudes des mouvements initiaux données par *a*) $P_2(\cos\theta)$ et *b*) $P_2(\cos\theta) - \frac{1}{4}P_0(\cos\theta)$

Honda[28] a constaté cela avec les secousses observées à l'occasion du grand tremblement de terre d'Idu.

Il est certain qu'on peut réaliser une source quadruple avec la séparation brusque de deux point dans le milieu et cette manière de mouvement sera produite à l'hypocentre. Il nous semble que la réalisation d'un cône des ondes poussantes sera impossible avec l'hypothèse de la production d'une faille au foyer. Pour mettre la distribution régionale des mouvements initiaux des secousses sismiques en évidence, nous pensons que le foyer sismique est une source quadruple. Naturellement ce type de source explique seulement le premier rayonnement des ondes du foyer et le mécanisme de la production des autres ondes reste inconnu.

Pour considérer la source quadruple, nous n'avons plus besoin de considérer deux points qui s'éloignent à la fois. Il est suffisant d'avoir le mouvement d'un point-masse avec la théorie de conservation du moment. Certes, comme le moment de ce système était zéro avant la production des ondes sismiques, le mouvement d'un seul point-masse doit produire une source quadruple en action et les harmoniques zonales d'ordre d'impair ne seront pas permises. Quant au mouvement d'une

28) K. Honda, *loc. cit.*

masse nous voulons remarquer le mouvement du magma dans la croûte.

En tout cas, ce que la distribution des mouvements initiaux des secousses sismiques est la simple conséquence de l'existence d'une source quadruple au foyer, nous conduit à établir quelque idée sur l'origine du séisme. L'étude précise de la détermination de la courbe nodale nous afirmera ainsi un modèle plus exact de la production des ondes sismiques.

Quand on fixe l'angle du cône à 45°, la grandeur et la forme de la courbe nodale sont déterminées par la profondeur hypocentrale et l'inclinaison de l'axe du cône sur la surface terrestre. Nous pouvons, donc, considérer inversement la profondeur hypocentrale suivant la grandeur de la courbe nodale.

D'un autre côté, les ondes dans la croûte ne se propagent pas en ligne droite à cause du fait que la croûte n'est pas un milieu homogène et isotrope. Par conséquent, la trajectoire des ondes sismiques tourne sa convexité vers le bas. Nous savons que les études sur la trajectoire des ondes sismiques ont été développées par les sismologues d'Europe surtout pour les séismes lointains ; nous avons, cependant, plusieurs études surtout pour les séismes voisins. MM. T. Matuzawa,[29] K. Wadati,[30] H. Kawasumi,[31] K. Honda,[32] et K. Sagisaka[33] ont publié des mémoires montrant beaucoup de faits remarquables. Certes, il faut introduire ces propriétés de la trajectoire dans les études sur la distribution des mouvements initiaux des secousses sismiques.

Vraiment, les ondes rayonnées obliquement vers le bas paraîtront à la surface plus vite que les autres suivant la distance épicentrale. Nous voulons remarquer spécialement les deux cas suivant ; a) l'axe du cône est vertical, b) l'axe du cône est horizontal. La figure 14 représente schématiquement les distributions considérées.

Nous pouvons relever deux séismes correspondant aux deux exemples[34] : le séisme du 26 nov. 1930 et celui du 1er mai 1930. (Fig. 15) Quant aux discussions sur la forme de la courbe ou sur la manière

---

29) T. MATUZAWA, *Bull. Earthq. Res. Inst.*, **5** (1928), 1.

30) K. WADATI, *Geophys. Mag.*, **1** (1927), 162.

31) H. KAWASUMI, *Jap. Journ. Astro-Geophys.*, **9** (1931), 14 ; *Bull Earthq. Res. Inst.*, **10** (1932), 94.

32) K. HONDA, *Geophys. Mag.*, **4** (1931), 29.

33) K. SAGISAKA, *ibid.*, **4** (1931), 148.

34) Les données sont tirées de Kisyô-yôran aussi que d'études spéciales.

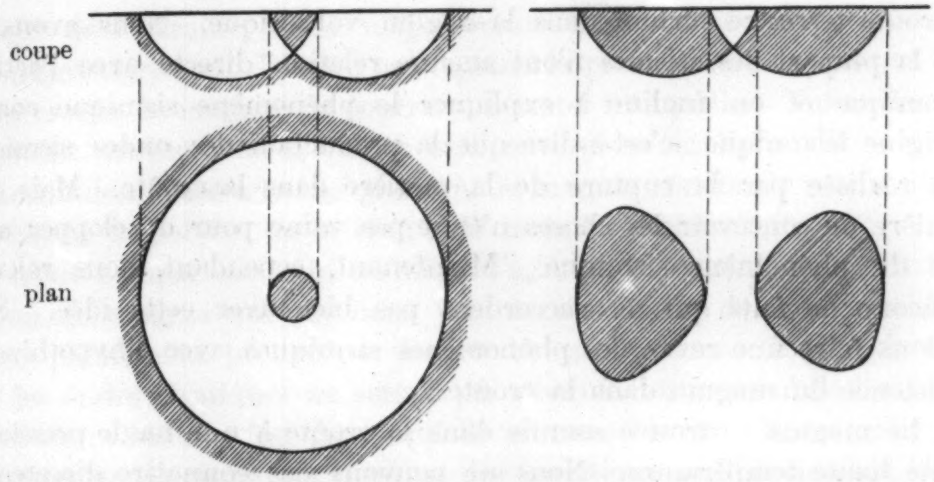

Fig. 14. Trajectoires schématiques des ondes sismiques rayonnées du foyer.

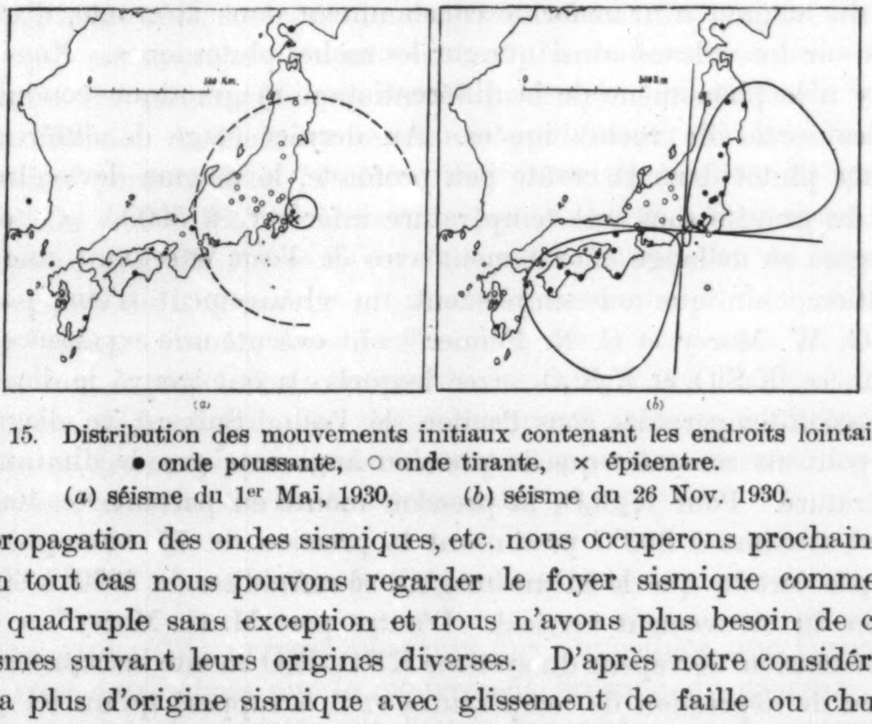

Fig. 15. Distribution des mouvements initiaux contenant les endroits lointains.
• onde poussante, ○ onde tirante, × épicentre.
(*a*) séisme du 1er Mai, 1930, (*b*) séisme du 26 Nov. 1930.

de se propagation des ondes sismiques, etc. nous occuperons prochaine fois.

En tout cas nous pouvons regarder le foyer sismique comme une source quadruple sans exception et nous n'avons plus besoin de classer les séismes suivant leurs origines diverses. D'après notre considération, il n'y a plus d'origine sismique avec glissement de faille ou chute de terrain. Nous voulons ainsi adopter le nom *"séisme plutonique"* pour tous les séismes d'après von Humboldt. Nous allons, en suite considérer le mécanisme du foyer avec le mouvement du magma.

6. Le mouvement du magma et la production des ondes sismiques.

Pour rendre compte d'une source quadruple existant au foyer sismique, nous introduirons le mouvement du magma demeurant au sein de

la croûte terrestre surtout dans la région volcanique. Nous avons dit que la plupart des séismes n'ont aucune relation directe avec l'activité volcanique et on incline à expliquer le phénomène sismique comme d'origine tectonique : c'est-à-dire que la production des ondes sismiques sera réalisée par la rupture de la matière dans la croûte. Mais cette manière de concevoir les choses n'était pas vaine pour développer notre idée du phénomène sismique. Maintenant, cependant, nous relevons beaucoup de faits qui ne s'accordent pas bien avec cette idée. Nous voulons faire une revue des phénomènes sismiques avec l'hypothèse de l'existence du magma dans la croûte.

Le magma se trouve soumis dans la croûte à une haute pression et à une haute température. Nous ne pouvons pas connaître directement son état actuel dans la croûte. Néanmoins, nous pouvons imaginer que l'état du magma se transforme constamment dans la croûte, d'après les études sur les volcans ainsi que sur les roches plutoniques. Nous savons qu'il y a le phénomène de la différentiation magmatique conduisant à diverses sortes de roches ignées. Au dernier étage de différentiation exécutée plutôt dans la croûte peu profonde, le magma deviendra l'eau-mère du granite sous une température inférieure à 500°C. Cette fois-ci le magma se mélange énormèment avec de l'eau effectuant une transformation chimique ou simplement un changement d'état physique. MM. G. W. Morey et C. N. Fenner[35] ont exécuté une expérience sur les substances, K_2SiO_3 et $K_2Si_2O_5$, avec lesquels ils ont trouvé le diagramme de pression-température sous l'action de l'eau. Suivant ce diagramme, nous pouvons constater que la pression augmente avec la diminution de température. Pour $K_2Si_2O_5$ la pression monte en partant de 1000°C et elle est maxima à 600°C produisant la pression de 75 atmosphères. Il n'est pas certain que le même magma se refroidisse de 1000° à 600° sous l'action du mouvement vertical. D'autre part M. G. Morey[36] a montré que la tension de vapeur du système KNO_3-H_2O monte brusquement avec un peu de dépression de température et il a supposé qu'un tel procédé sera exécuté dans le magma qui cause des actions volcaniques. En tout cas, il n'est pas difficile d'imaginer qu'une telle action physique se produise au sein de la croûte.

Dans la croûte, à grande ou à faible profondeur, nous pouvons imaginer des variations d'état du magma surtout dans la région volcanique. Quand l'augmentation de la pression magmatique reste inférieure

35) G. W. MOREY et C. N. FENNER, *Journ. Amer, Chem. Soc.*, **39** (1917), 1173.
36) G. W. MOREY, *Journ. Wash. Acad. Sci.*, **12** (1922), 219.

à celle de la croûte, nous n'apercevrons aucun phénomène constaté à la surface terrestre. D'autre part, quand la pression monte plus que celle de la croûte, le magma ne pourra plus rester tranquille. Naturellement, la croûte résistera ainsi contre une cette pression, mais s'il y a une augmentation incessante de pression, le magma sortira de son réservoir en brisant la portion de la croûte de moindre résistance.

Nous comparons cette manière d'agitation magmatique à une injection du magma surtout dans une certain étage de son refroidissement; phénomène prouvé par les études géologiques. Il est plausible que les ondes sismiques ne seront pas produite au moment de l'augmentation de pression; c'est parce qu'elle est sensiblement lente pour produire des ondes sismiques quoique des variations de l'inclinaison de la surface terrestre soient produites.

D'un autre côté, la sortie du magma donnera un premier choc à la croûte qui se propagera comme le font des ondes sismiques. Certes, cette action du magma fait une source quadruple. La sortie du magma dans la direction de moindre résistance peut causer de la diminution de pression partout dans le réservoir. Cette diminution de pression produira les ondes tirante représentées par $P_0(\cos\theta)$. Nous avons, alors, une superposition de $P_0(\cos\theta)$ sur $P_2(\cos\theta)$. Le rapport de superposition dépendra de la grandeur du réservoir aussi que de la quantité de magma injecté. Comme nous l'avons déjà dit le cône aura un angle de 45° avec une superposition convenable des deux sortes d'ondes. C'est là l'explication de la distribution des mouvements initiaux représentée par deux lignes droites perpendiculaires surtout pour les séismes à foyer peu profond et l'axe du cône reste horizontal.

7. Sur l'origine du séisme.

Nous avons déjà proposé plusieurs fois l'hypothèse que l'origine du séisme n'est autre chose que le mouvement brusque du magma. Cette considération a été constatée par l'étude des phénomènes accompagnés par des secousses sismiques. Nous avons fixé notre idée par les faits obtenus par l'observation des variations de l'inclinaison de la surface terrestre exécutée juste après le grand tremblement de terre de Tango[37] en 1927. En installant deux clinographes auprès de la ville de Miyadu et à Kawana, nous avons observé que des grandes répliques apparaissent à la suite d'une variation de l'inclinaison. (Fig. 16.) Nous avons, donc,

37) M. Ishimoto, *Bull. Earthq. Res. Inst.*, 4 (1927), 203.

conclu cette fois-là que l'augmentation progressive de pression du magma pourra produire l'inclinaison à la surface et l'injection brusque du magma s'ensuit. Naturellement l'injection magmatique produit des ondes sismiques.

Des observations analogues[38] ont été exécuté à Itô et Kawana en profitant de l'apparition d'une foule de séismes près de la ville d'Itô en 1930. Nous avons réussi à obtenir de la même façon des variations de l'inclinaison précédant les séismes principaux.

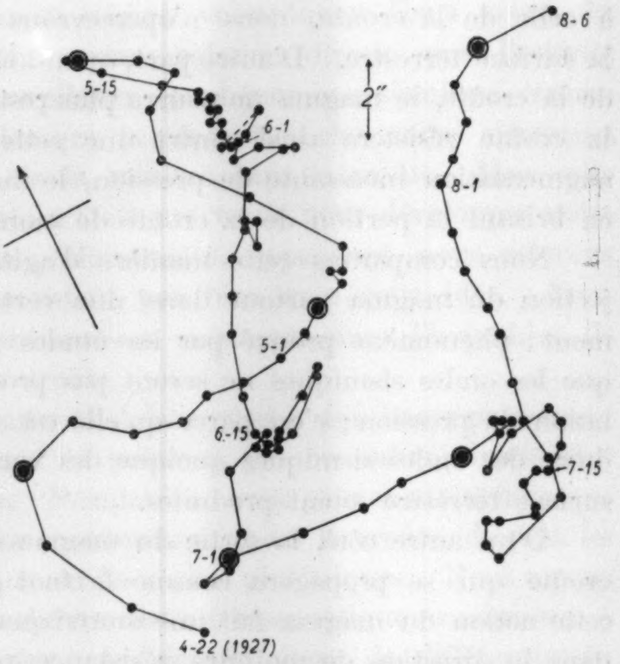

Fig. 16. Variations de l'inclinaison de la surface terrestre observées à Miyadu juste après le grand tremblement de terre de Tango.
⊙ indique le jour où nous avons la réplique dont l'intensité a été assez grande.

Nous faisions des observations analogues[39] dans le tunnel de Tanna depuis le grand tremblement de terre d'Idu en 1930. C'est parce que nous voulons éviter surtout les perturbations thermiques. Ces observations nous montrent aussi l'existence des variations de l'inclinaison précédant de quelques jours l'apparition des séimes locaux. D'un autre côté, nous pouvons citer les observations exécutées par M. W. Inoué[40] à la station de Tukuba. Il a publié un mémoire constatant que les séismes n'apparaissent pas beaucoup dans le cas des grandes variations de l'inclinaison, tandis qu'un grand nombre de séismes apparaissent dans le cas des petites variations de l'inclinaison. En considérant les perturbations thermiques, nous pouvons tirer le phénomène analogue dans les observations exécutées à cet endroit. Certes, les résultats obtenus par les observations de la variation de l'inclinaison nous suggèrent l'hypothèse du mouvement magmatique.

D'un autre côté, les changements topographiques accompagnés par

38) M. ISHIMOTO et R. TAKAHASI, *Bull. Earthq. Res. Inst.*, 8 (1930), 427.
39) pas encore publié.
40) W. INOUYE, *Bull. Earthq. Res. Inst.*, 8 (1930), 346.

les secousses sismiques, nous donnent aussi une certaine confirmation de l'origine du tremblement de terre. Autrefois, on a regardé plutôt les phénomènes de bordure dans les changements topographiques. Certes, on a fait attention aux endroits où le gradient de mouvement reste maximum ou plutôt le mouvement discontinu. Bien qu'il ait le mouvement d'une grande masse d'écorce, nous apercevrons seulement quelques mouvements relatifs aux bordures. La faille que nous remarquons dans la région épicentrale est le simple résultat du mouvement d'une grande masse d'écorce. Les vrais mouvements d'écorce, donc, ont échappé autrefois aux yeux de chercheurs.

Suivant les résultats obtenus surtout par les nivellements de précision, nous constatons toujours l'exhaussement de terrain dans la région épicentrale. Au tremblement de terre d'Oomati[41] en 1917, il y a eu 25 cm d'exhaussement dans la région épicentrale: au tremblement de terre de Sekihara[42] en 1927, il y a eu 2·1 cm d'exhaussement. Pour le grand tremblement de terre de Nôbi[43] en 1891, cependant, la faille observée a été une bordure de la région épicentrale exhaussée. Pour le grand tremblement de terre de Kantô en 1923, l'exhaussement de terrain était visible au bord de la mer en comparant l'encienne plage marquée par les coquilles blanches des huitres. Il est très connu au Chili qu'un exhaussement de terrain apparaît à chaque grand tremblement de terre.

Ces observations nous donnent une certaine idée de la cause du séisme. Nous considérons que l'exhaussement du terrain est réalisé par l'injection magmatique qui produit en même temps les ondes sismiques. En tout cas, nous pensons que l'augmentation de la pression magmatique laisse le magma sortir de son réservoir par une partie peu résistante. Naturellement il y aura un cours principal du magma qui produira l'exhaussement du terrain dans la région épicentrale surtout pour les grands tremblements de terre. Nous constatons, d'un autre côté, que la croûte superficielle est constituée par un groupe de blocs exécutant des mouvements individuels. S'il y a quelque glissement entre les deux blocs, on aperçoit une faille. Nous pouvons dire, en effet, que l'exhaussement de terrain est le phénomène accompagné par la production des failles. L'origine sismique reste toujours dans la croûte, à une assez grande profondeur, tandis que nous voyons quelque-fois le glissement de blocs comme le résultat de l'exhaussement du terrain.

---

41) A. Imamura, *Publ. Earthq. Inv. Comm.*, **25** (1930), 82.
42) A. Imamura, *ibid.*, **25** (1930), 121.
43) A. Imamura, *ibid.*, **25** (1930), 49.

Pour terminer nous remercions le Professeur K. Sezawa qui nous à exécuté une discussion de valeur du mécanisme de la production des ondes sismiques rayonnées par la source quadruple.

Résumé.

D'après les études de la distribution des mouvements initiaux des secousses sismiques, nous avons constaté que les lignes nodales distinguant deux sortes d'ondes, ondes tirantes et ondes poussantes, font toujours des courbes de sections coniques. Nous considérons ainsi qu'il y a une source quadruple au foyer : suivant laquelle l'onde poussante se propage dans l'espace d'un cône. Nous introduisons, donc, le mouvement du magma pour expliquer la source, au lieu du phénomène de la production de faille. Les mouvements du magma ont été déjà considérés pour expliquer les phénomène des variations de l'inclinaison de la surface terrestre, aussi que les changements topographiques accompagnés par les ondes sismiques.

---

30. 地震初動方向分布より震源に四重源の推定

地震研究所 石本巳四雄

1. 1917年志田博士は初動方向、即ち壓し波、引き波の分布が二つの直角に交る節線を境として行はれる事を確め、此の事實を説明する爲めに震源において平行面が急激に遠ざかる運動を推定した。然るに中村(左)博士は島原地震に際して初動方向分布から發震機巧を説明するに當つて、直角に交はる節線に沿つて地殼の横辷りが實現したと爲した。此の結果、此所に二つの發震模型が考へられる事となつたが、震源の淺い地震、即ち初動方向分布を平面問題として取扱ふ限りは何れも同一結果を與へ區別の出來ない性質のものとなる。

2. 確に其れ以後の初動分布研究においては多くは震源において斷層が成生されると考へて議論が進められて居たのである。

3. 初動方向分布を平面問題として取扱ふ事を避ける希望から特に下記三つの深層地震を注意する事とした。

發震時	震央	震源の深さ
昭和六年 (1931) 六月二日	高山附近	240 km
昭和四年 (1929) 六月三日	志摩半島附近	300 km
昭和二年 (1927) 一月十五日	經ケ岬沖合	450 km

而して此等地震初動の節線は何れも圓錐曲線で表はし得る事が判明した。

4. 初動方向の節線が圓錐曲線で表はし得ると云ふ考へから、從來の研究を再び見直して見ると何れも左樣で差支へない事、且つ曲線の中側が常に壓し波に屬する事が判つた。從つて地殼内にお

いては震源に頂點を有する圓錐形中に壓し波の傳播が行はれる事が認定される。

5. 無限に擴る等方等質媒體中における縦波の源は理論上研究されて居るが、此の場合に適合するものは $P_2(\cos\theta)$ で表はされる四重源であり、なほ一般に $P_0(\cos\theta)$ も重複して居るらしく思はれる。此れは $P_0(\cos\theta)$ のみでは圓錐角が 55° であるのに、實際に存在するものは 45° 附近のものが多いからである。なほ地殼内においては深さの増加に從つて地震波の速度も増加する關係上、遠方迄も初動方向分布を考へる時には當然此の事實を顧慮する必要があり、其の影響と思はれる分布狀況も見出し得る。

6. 震源の四重源である事は岩漿の運動を考へる事が最も自然である。岩漿は適當の條件においては温度冷却に伴つて其の蒸氣壓の增加するものであり、然も此の壓力が地殼壓力を凌駕する場合においては、最も弱い方向の壁が破られて岩漿流動が行はれる。斯樣の事實は地質學上岩脈、岩床の成立される機巧として考へられて居るものである。以上の如き機巧を考へるならば放射される彈性波は岩漿流動に伴ふ $P_2(\cos\theta)$ と岩漿溜中における壓力減少による $-P_0(\cos\theta)$ の重複したものとなる事は當然の事であり、否々が地表において觀測する如き節線を生ずるのであらう。

7. 地震の原因が岩漿運動である事は丹後地震後の地表傾斜觀測結果によつて推定したものであるが、其れ以後の觀測も同様の結果を與へて居る。又地震に伴ふ地形變動も水準測量の結果によれば震央附近において常に隆起地帶の見出される結果として岩漿運動を以て說明する事が最も適當であると信ずる。實際吾々が地表において目擊する地變は地下深所における原因に附隨する運動と考へられるからである。

31. *On Two Borings near Atami-mati, Idu Peninsula.*

By Yanosuke ÔTUKA and Hisashi KUNO,
Earthquake Research Institute.

(Read Jan. 19, 1932.—Received March 20, 1932.)

The authors present the following geologic interpretation of two columnar sections obtained by borings made near the Atami hot springs, Idu Peninsula, Central Japan. Of the two cores obtained, one was forwarded by the Nozawa-Gumi Company, Marunouti, Tôkyô, to the Earthquake Research Institute, Tôkyô Imperial University, while the other was obtained by the writers from the Matuo Boring Company at Atami, to whom our thanks are due.

These borings supplemented by actual surface geologic investigations made by H. Kuno, one of the writers, form the data of our study on the presumed underground geologic structure of the region.

The boring machine was of the "Matuo" type, with fishtail bit, so that instead of large complete bore cores we could get only fine powders of the rocks. A large part of the sample was so decomposed by the "hot spring solution" that no satisfactory determination of mineral properties could be made. Fig. 1 is the index map and rough geologic sketch map as surveyed by H. Kuno. A and B of Fig. 2 are the columnar sections.

Boring No. 1. (Fig. 1 and 2, A).

Position of the bore: Northern suburb of Atami-mati (Nisiyama,[1] Nozawa-gumi Bunzyôti).

Height of ground surface above mean sea-level: 150 m.

At depth of 42 m. below the ground surface: Decomposed rocks character.

At depth of 42-45 m. below the ground surface: Pale green tuff containning medium sized fragments (about 2-3 mm. diam.) of dacite. This dacite has the same characters as that of the NONAKA[2] beds, which name has been proposed by H. Kuno.

At depths of 45 m.-300 m. or more below the ground surface: Decomposed rocks belonging to the rheumatica of the Sogayama[3] beds so far as

1) 西山. 2) 野中. 3) 曾我山.

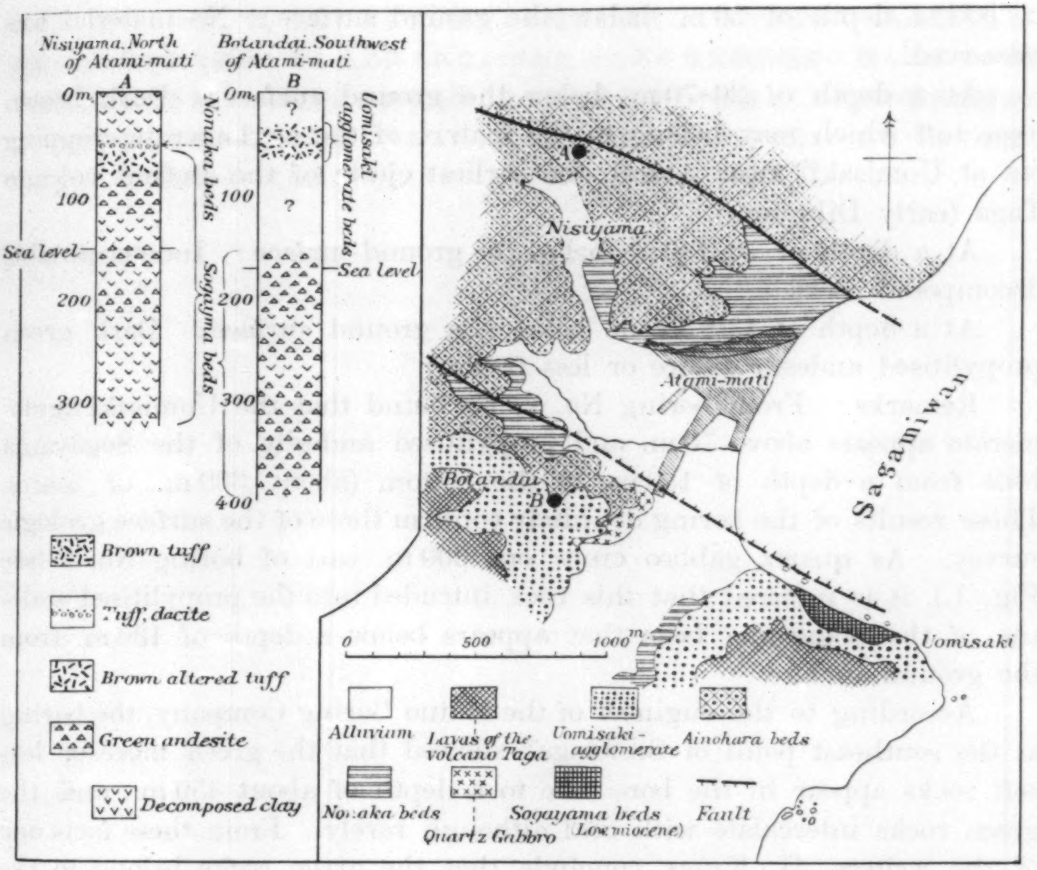

Fig 2. Columnar sections.

Fig. 1. Index map and rough geologic sketch map.

concerns the richness of zeolite veins and other geologic relations.

Remarks:—From the above boring, the dacite of the Nonaka beds appears at a depth of 42–45 m. below the surface. From 45 m. to the bottom, were found decomposed andestic rocks and tuff, which may belong to the Sogayama beds. About 45 m. below the ground surface is probably a geologic boundary plane between the Sogayama beds and the Nonaka beds. The foregoing geologic relations were deduced from the borings.

Boring No. 2. (Fig. 1 and 2, B).

Position of the bore: At Botandai,[4] the southwestern suburb of Atami-mati.

Height of ground surface from the mean sea-level: 170 m.

4) 牡丹臺.

At a depth of 30 m. below the ground surface: No material was preserved.

At a depth of 30–70 m. below the ground surface: Dark brown loose tuff which may belong to the matrix of the agglomerate cropping out at Uomisaki[5] near Atami, the earliest ejecta of the ancient volcano Taga (early Diluvium).

At a depth of 70–130 m. below the ground surface: Indeterminable decomposed rocks.

At a depth of 130–300 m. below the ground surface: Dark green propylitised andesite (more or less fresh).

Remarks: From boring No. 2, we found that the Uomisaki agglomerate appears above 70 m. and propylitised andesite of the Sogayama beds from a depth of 130 m. to the bottom (about 300 m. or more). These results of the boring definitely confirm those of the surface geologic survey. As quartz gabbro crops out 300 m. east of boring No. 2 (see Fig. 1.), it is inferred that this rock intruded into the propylitised andesite of the Sogayama beds that appears below a depth of 130 m. from the ground surface.

According to the engineer of the Matuo Boring Company, the boring at the southeast point of Simotaga[6] showed that the green more or less soft rocks appear in the bore core to a depth of about 450 m., and the green rocks intercalate with coal although rarely. From these facts one of the writers, H. Kuno, conclude that the green rocks belong to the green altered andesite of the Sogayama beds. The writers therefore believe that the Sogayama beds make up the base of the Idu peninsula, at least that region near Atami-mati and Taga village, and also that the younger volcanic materials do not cover this basal rock to any very great depth.

---

31. 伊豆半島、熱海町附近の二つの試錐

地震研究所　大塚彌之助
久野久

末廣所長の御幹旋により、東京丸の内野澤組から送附された熱海町附近の試錐 (Fig. 1, 2, A.) の材料と筆者等が實地踏査の際に寄贈を受けた松尾ボーリング商會に保存されてあつた試錐 (Fig. 1

5) 魚見崎.　6) 下多賀.

2, B.) の材料との報告で、之等によりて、偶々この地域を調査してゐた筆者等の一人久野が地上の關係からは決定的な關係を突き止め得られないでゐたところの地質學的關係に關して多くの事實を知ることができた。この結果は伊豆半島少くとも熱海多賀附近の基盤として久野の曾我山層がかなり廣く分布してゐることを暗示してゐるし、又た若い地質時代の火山岩層がそんなに厚く堆積してゐないことをも暗示してゐる。

32. *Some Experiments on Crack Formation in a Glass Plate.*

By Genrokuro NISHIMURA and Takeo TAKAYAMA,

Earthquake Research Institute.

(Read Nov. 17, 1931, Feb. 16 and March 19, 1932.—Received March 20, 1932.)

1. Using the theoretical results obtained by C. E. Inglis[1] in 1913, A. A. Griffith[2] pointed out the fact that the accumulation of tension stress at sharp corners of crack is the main cause of the growth of that crack in a brittle material, and he also elucidated the rupture phenomenon by the use of energy theory.

Recently Professor T. Terada[3] studied the problem of the crack phenomenon and concluded that this phenomenon was the irregular and irreproducible one and the problem should be studied statistically. From a certain basis concerning their velocities, he classified the cracks in the following two classes :— dynamical crack and statical crack. The latter is such a one that is developed with a velocity which is comparatively small in comparison with the sound velocity of that material ; the former is such a one that is propagated with a velocity comparable with the sound velocity of the material. The one is essentially wave phenomenon and the other is governed by the boundary conditions. He also studied the physical nature of the end point of a propagated straight crack with the analogy of electron. In order to set up his theory, he applied the experimental results obtained independently by R. Taguti,[4] S, Suzuki[5] and M. Hirata.[6] Besides the investigations of the above three authors, the result obtained due to Professor S. Fujiwhara[7] may be noted as another experimental study on crack phenomenon in this country.

We are intending to study the problems in the following three steps. The first is on the mechanism of the generation of crack and the

1) C. E. Inglis, *Trans. Inst. Naval Architects*, **55** (1913).

2) A. A. Griffith, *Phil. Trans. Roy. Soc.*, *A* **221** (1921) & *Proc. 1st. I.N.C. for Applied Mech.*, (1924).

3) T. Terada, *Bull. I.P.C.R.*, **16** (1931), 159~171.

4) R. Taguti, *ibid.*, **10** (1931), 110 (in Japanese).

5) S. Suzuki, *Proc. Phys. Math. Soc.*, Japan, **3** (1921).

6) M. Hirata, *Bull. I.P.C.R.*, **8** (1929), 52 (in Japanese). *ibid.*, **16** (1931), 172.

7) S. Fujiwhara, *Bull. Earthq. Res. Inst.*, **9** (1931), 50, (in Japanese).

growth of the generated crack. The second is on the form of crack, and the third on the velocity of growth of that crack. The first is very complicated, so that we are now contented with the theoretical researches carried out by A. A. Griffith.[8] Secondly the study on the forms of cracks seems to be most interesting to us and there are many problems concerning the forms of cracks. Due to the processes, by which the crack is formed, namely mechanical,[9] heating,[10] electrical[11] etc., applied on a material which may be under initial stress or not, the generated crack has different appearance in each case. The properties and the geometrical form of the material itself and the boundary surfaces are, of course, effective on the formation of crack. Lastly, concerning the velocity of crack Professor K. Sezawa had had, in a former time, the following opinion about the velocity of crack. Referring to the experimental results obtained by late Dr. M. Hagiwara,[12] he stated that the velocity of crack was perhaps limited within the velocity of the elastic wave of the material. From our experiment which is of relatively slow loading-speed, the crack of a material has different velocities according as the magnitudes of the applied loads. In Dr. Hagiwara's experiment the loading speed is nearly instantaneous, so that the elastic deformation is propagated with constant velocity and therefore the crack in pursuit is also transmitted with apparently definite velocity. Needless to say, in the shock phenomenon the shock (elastic) wave is main cause to generate and to grow the crack in the material. If, however, we consider more closely, the crack is not propagated with a definite velocity like elastic waves of the material, but rather the growth of crack is a discontinuous phenomenon with respect to time in the strict sense of the word.

I. General Principle of Experiment.

2. The principal parts of experimental arrangement consist of a Mohr's universal testing machine, a specially designed dynamometer,

---

8) A. A. Griffith, *loc. cit.*

9) R. Taguti, *loc. cit.*

10) M. Hirata, *loc. cit.*

11) T. Terada, M. Hirata and R. Yamamoto, *Proc. Imp. Acad.*, Tokyo, **8** (1932).

12) The elaborate results of Dr. M. Hagiwara's experiments were not published in his lifetime. His experiment is as follows: the principal parts of his experimental arrangement consist of a rifle, a testing glass plate, spark gaps and the photographic apparatus. At the instant when a bullet penetrates the glass plate, instantaneous photographs are taken.

a flat steel plate, and test pieces. In order to discriminate the corners of cracks, we used glass plates, of which the thicknesses were 1∼2 millimetres, as test pieces. The arrangement is shown in Fig. 1.

By the action of Mohr's testing machine the strain energy is accumulated in the glass plate. The glass plate has flat surfaces, the lower surface being contacted with the flat steel base and the upper surface is in a point-contact with a steel ball, of which the diameter is of 1/16″. The mirror, the scale and the telescope system is also employed for the estimation of the load applied to the glass plate from the loading apparatus. Marten's extensometer is attached to the dynamometer as shown in Fig. 1. The load-deformation characteristic of dynamometer is shown in Fig. 2.

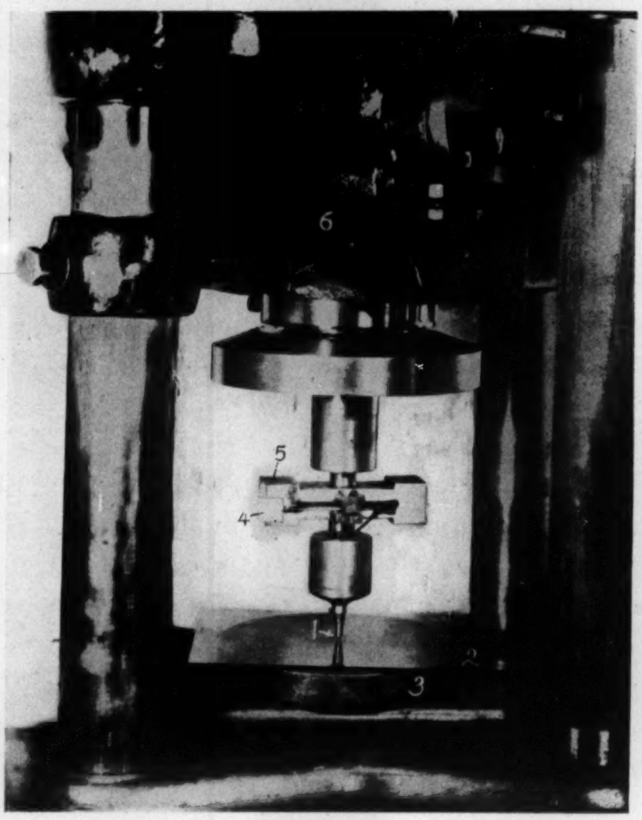

Fig. 1. Experimental arrangement.

[1 : steel ball, 2 : glass plate, 3 : steel plate, 4 : Marten's mirror, 5 : dynamometer.]

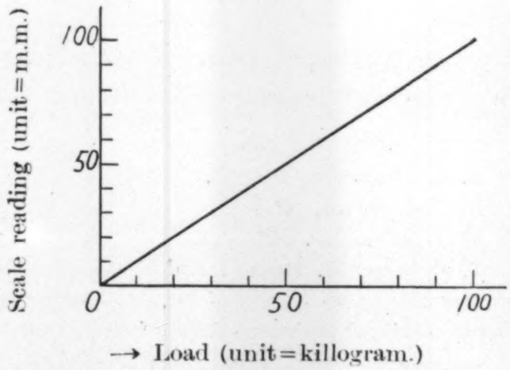

Fig. 2. Load-deformation characteristic ofdynamometer.

As the depression of the surface of glass plate due to the ball was too small to measure its magnitude, the rough magnitude of the depression was measured by counting the number of revolution of the handle of the Mohr's apparatus, neglecting the slip of the transmission

mechanism. The loading speed was maintained nearly constant as possible during each experiment.

We have divided the crack phenomena in three parts occurring in different stages of its growth as well in different regions of the glass plate:— The part occurring in the vicinity of the origin, the part forming radial crack and the part taking place at the edge of the plate. In the second part the velocity of the growth of radial crack became apparently constant. In that stage the relation between the growth of crack and the applied load was obtained. In the part occurring in the vicinity of the origin, where the steel ball was in a point-contact with the glass plate, the state of the plate, from which the radial cracks were originated, was observed. In the third part the cracks occurring near the edge of the glass plate were studied.

II. The Part Occurring in the Vicinity of the Origin.

3. As the cracks in the upper surface of the glass plate were very feeble, we used a microscope for this study.

When we applied the load gradually, the surface which was in a point-contact with the steel ball was gradually deformed elastically. If the load exceeded a certain limit which perphaps corresponded with the elastic limit of glass plate, the permanent indent due to the steel ball was observed microscopically when the load was released. Yet we could not see any type of crack in this state. When the load was more increased, perfectly circular crack, of which the diameter was nearly 0·2 millimetres, was found in the upper surface of glass plate. (See Fig. 3.) At some increase of the load the circular crack of larger diameter was visible and this circular crack was concentric with the former circle and took its position again in the upper surface of the plate. (See Fig. 4.) In this state the former crack disappeared in almost all occasions.

With the more increase of load we could observe a number of spiral cracks around the bounding circle and this number increased with the increase of load. (See Fig. 5, 6, 7, 8[13] & 9.) The crack of this type was named "*spiral crack*" for the convenience, and the former circular "*Circular crack*".

13) C. V. Raman took the same photograph as that of Fig. 8. His experimental method was a dynamical one.
C. V. Raman, "Percussion Figures in Isotropic Solid," *Nature* (1919).

When the *spiral cracks* grew fully, the Newton rings which had been born in advance could be seen distinctly around these cracks. (See Fig. 6, 7, 8.) The number of the Newton rings increased with the increase of load. These rings were the effect due to another type of crack whose form might also be conical. We called this type of crack "*conical crack*". Nearly in this stage we could see another traces of cracks which seemed to run on the surface of *conical crack* like feathers. We called these "*feather cracks*". (See Fig. 5, 6, 7, 8.)

After the growth of these four types of cracks, another type of series of cracks was suddenly branched off nearly from the centre of the *circular crack* and in the interior of the glass plate with feeble sound. These cracks had the nature to grow radially from the loaded position nearly in straight line forms. We called them "*radial cracks*" for convenience. The *radial cracks* ran along the bottom surface of the plate which was in contact with the steel plate. (See Fig. 9.)

The *radial cracks* in their initial stage produced in the plate accompanied with feeble sound had large velocities of transmission, so that their natures could not be well studied: merely their forms and depths could be studied. The *radial cracks* made their forms appear in the bottom surface of the plate, but they did not appear in the upper surface of glass plate. This fact can be seen from the photographs of the *radial cracks* in the vicinity of the origin. The plan views of *radial cracks* are illustrated in Fig. 10b, 11b, 12. Fig. 10b, 11b are the views from the bottom sides and Fig. 10a and 11a that from upper sides. [Upper side corresponds with the surface of the glass plate which is in point-contact with steel ball.] It is also the noteworthy fact[14] that the *radial cracks* had no direct connections with the cracks of other types that were found in the upper surface of glass plate.

The most interesting type of cracks among all various cracks formed in the upper surface of the plate in the vicinity of the origin is the *conical crack*. This type of crack developed in the interior of the plate deeper than other three types. On examining by means of microscope, it was indeed found that the cracks such as *circular*, *spiral* and *feather cracks* resided in the above portions of the surface of the *conical crack*. The *feather cracks*, however, seemed to be on the very surface of the *conical crack* as we have described in the first part of this section. We understand by the patterns of the Newton rings that the breadth of

14) This fact could be ascertained by flowing a drop of ink on the upper surface of the glass plate.

conical crack becomes thiner and thiner towards the outer part of that crack, and it is, of course, of the order of the wave length of light.

When we estimated by microscope the distances between the upper surface of glass plate and the suitable points of the *conical crack*[15] as well as that of the *feather cracks,* we confirmed, together with the patterns of Newton rings, that the *conical crack* superposed with *feather cracks* grew almost in the form of a cone. Now we examine these facts in the following two examples. The observed points a, c, d, e, f, g, h, i, j in Fig. 13b correspond with those in Fig. 13a which schematically shews the photograph Fig. 9. Again the points a, b, c, d, e, f, g, h, i in Fig. 14b correspond with those in Fig. 14a which shews schematically Fig. 15c. The distances at the points e, d, j, h, i in Fig. 15a, and e in Fig. 14, which are not situated on the *feather cracks,* are determined

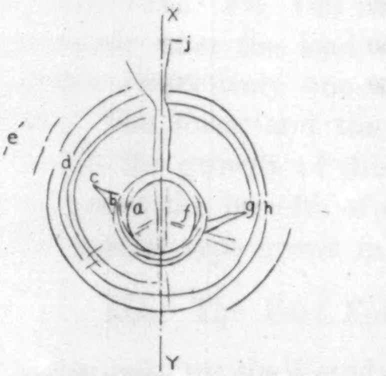

Fig. 13a. (Schematical figure of the photograph Fig. 9.)

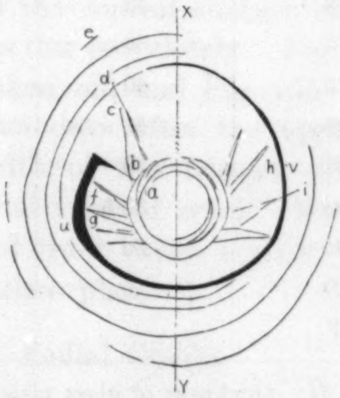

Fig. 14a. (Schematical figure of the photograph Fig. 15c.)

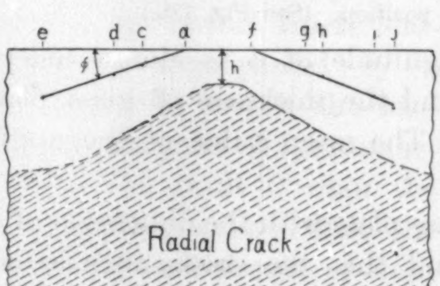

Fig. 13b. Profile of *conical* and *radial crack.*

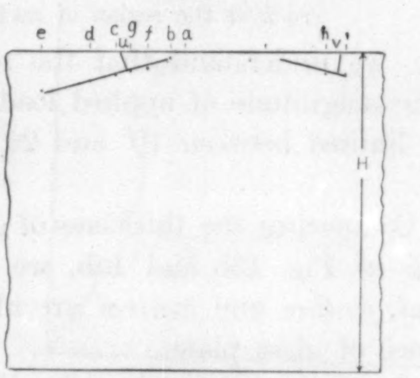

Fig. 14b. Profile of *conical crack.*

15) We confirmed the position of the *conical crack* by flowing a drop of ink on the upper surface of the glass plate.

by flowing a drop of ink in the *conical crack*. The results thus obtained in Fig. 13b and 14b shew us that the observed distances appear to give a nearly straight profile of a cone.

By the method above mentioned, the angle ϕ[16] between the upper surface of glass plate and the surface of *conical crack* was estimated, and the results are shown in the following table. (Table I.) From this

Table I.

No.	Load	H	ϕ	h
54	15 kg	1·40 mm	21°	
52	20	1·41	17	
58	25	1·57	14	
78	33	1·40	19	0·176 mm
75	36	1·80	14	
6	40	1·50	12	
86	41	1·60	18	
47	30			0·167
44	30·5			0·201
45	32			0·173
D				0·164
F				0·167

H: thickness of glass plate.
ϕ: angle between the upper surface of the glass plate and the surface of *conical crack*.
h: shortest distance between the upper surface of plate and the *radial crack* at the region of loaded position. (See Fig. 12b.)

table, we understand that the magnitude of ϕ is almost independent of the magnitude of applied load and the thickness of glass plate, and it is limited between 10° and 20°. The mean value of the angle ϕ is 15°.

Comparing the thickness of glass plate with the dimension of *conical crack* in Fig. 13b and 14b, we find that the cracks such as *circular*, *spiral*, *feather* and *conical* are almost taking their places in the upper surface of glass plate.

Radial crack is schematically shown in Fig. 13b by the hatch.

As we have described, the four types of these cracks in the vicinity

16) To measure this quantity, the refractive index of glass plate was taken into account.

of the upper surface of glass plate have the connections with each other, but they have no direct connections with *radial cracks.*

Again, the interesting fact is that the cracks named *circular, spiral, feather* and *conical* are distributed almost symmetrically about a line passing through the center of the *circular crack* and parallel to the plane of the plate. See Fig. 5, 6, 7, 8, 9, and 15. Two systems of *feather cracks,* each with its proper sense of extension, meet at this line of symmetry. This phenomenon is not due to the effect of the arrangements of the experimental instruments.

Another point to be remarked is that we discovered a new type of crack[17] lasting long after the applied load was taken off. (See Fig. 15a, 15b, 15c, 16.) This new type of crack developed vertically from the surface of *conical crack* in the forms of spiral or near circle between the upper surface of the glass plate and the conical surface of *conical crack*. (See Fig. 14b.) Fig. 14b indicates this fact clearly. Fig. 15a was taken immediately after the load was taken off, and Fig. 15b and Fig. 15c were taken respectively one and two days after the applied load was released. The form and the breadth of the fringes of Newton rings vary with the growth of this special type of crack. We can see from this fact that the breadth of *conical crack* varies according as the crack of this special type grows in the glass plate.

III. The Part Forming Radial Cracks.

4. In this part we shall study the nature of the *radial crack* at distances which are not so near the origin.

When the load reaches point C in Fig. 17, the *radial cracks* suddenly appear accompanied by a feeble sound. No sooner the load decreases to the point D instantaneously from the point C than the *radial cracks* appear, and then the feeding of the load should be stopped. From the stage D, the load decreases exponentially during a short time and attains to a constant value (HI) finally. At this

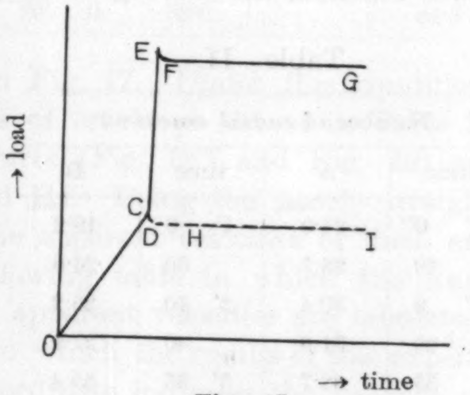

Fig. 17.

17) Prof. T. Terada has also found in his experiment.
T. Terada, M. Hirata and R. Yamamoto, *loc. cit.*

stage the velocity of the growth of crack becomes apparently constant, *i. e.*, the *radial crack* which is started from the point in the plate near the position where the steel ball is in a point-contact has a large velocity for a moment, but after one or two seconds the apparent velocity tends to attain a constant value, which is smaller than that of the initial velocity. The growth of the *radical crack* in this state depends only on the magnitude of the strain energy given in the glass plate. As the order of the velocity of *radial crack* is a few millimeters per minute, the end point of the growing *radial crack* is readily observed. We vanished beforehand the glass plate with lack film uniformly and in experiment we marked with a sharp pencil on the very ends of the growing *radial cracks* successively. The growth of the *radial crack* is not strictly continuous with time, and therefore the apparent velocity in each state of the growth can only be determined by the above method. Using this method, we obtained the apparent extensions of cracks and the apparent velocities of them. And the results shew us that the velocities, the numbers of cracks and the load are in a certain relation which may be reasonable from common sense. But the velocities thus obtained were very small, and we could not obtain the fine result of experiment.

Now to study the natures of these quantities more distinctly, we made the following experiment. After the load reached a certain limit, which corresponded with the stage of the formation of the first *radial cracks* in the plate with a feeble sound, we instantaneously increased the load to the limit in which a second feeble sound was heard. In Fig. 17, *E* is the point corresponding to this second stage. After the point *E* was reached, the feeding of load was stopped, and the load attained

Table II.

Number of *radial cracks*=2

time	A	time	B
1′ 0″	24·0 mm	1′ 0	19·2 mm
40	28·7	50	24·0
2′ 0	30·4	2′ 10	25·2
20	31·0	40	27·1
55	32·7	3′ 35	29·4
3′ 25	33·7	5′ 10	32 0

(*to be continued.*)

Table III.

Number of *radial cracks*=3

time	A	B	C
35″	21·0 mm		
1′ 25	24·9	29·7 mm	
2′ 0	26·4	31·6	
30	28·0	3·33	
3′ 0	29·5	34·0	
4′ 0	31·2	36·0	32·0 mm
5′ 0			34·5
5	34·6	38·1	

(*to be continued.*)

Table II. (*continued.*)

Number of *radial cracks* = 2

time		A	time		B
		mm			mm
4′	0	34·6	6′	43	33·7
5′	0	36·1	7′	32	36·6
6′	0	37·7		55	38·2
7′	12	39·5	8′	32	40·0
8′	0	41·2	9′	0	41·9
	42	44·0		45	43·4
9′	25	45·6	10′	0	44·3
10′	0	46·9		30	45·4
	30	47·9	11′	0	47·0
11′	0	49·2	12′	0	50·0
	30	50·8		30	51·2
12′	0	52·0	13′	0	53·0
	30	53·1		30	54·4
13′	0	54·8	14′	0	55·8
	30	56·7		30	57·2
14′	0	57·8	15′	0	58·8
	30	59·3		30	60·9
15′	0	61·3	16′	0	63·0
	30	63·9		15	65·0
16′	0	66·4		30	66·6
	15	68·0			
	30	70·0			

Table III. (*continued.*)

Number of *radial cracks* = 3

time		A	B	C
		mm	mm	mm
6′	0	36·0	40·0	36·1
7′	0	38·0	41·5	38·0
8′	0	40·5	43·0	40·0
	30	41·9		
9′	0	43·1	44·6	
	12			43·2
	30	43·9		
10′	0	45·1	45·5	
	24			45·9
11′	0	47·8	46·2	48·0
12′	0	50·2		50·0
13′	0	53·4	48·0	
	25			54·9
14′	0	56·3		
	30			58·6
15′	0	59·7		
	30		50·3	62·0
16′	0	63·1		64·0
	30	65·1		66·4
17′	0	66·8		68·5
	30	69·2		70·5
18′	0	71·9	53·8	72·9
	30	74·0		75·2
19′	0	76·6		
	19		56·4	78·2
	30	79·0		81·0
	50		58·8	
20′	0	82·0		84·5

to a constant value (FG) as shown in Fig. 17. Under this condition, we obtained the apparent extensions of cracks as shown in Table II and III. And the following two figures (Fig. 18[18]) and Fig. 19) are obtained by the usage of Table II and III. Using the nearly straight parts of the curves in these figures, the apparent velocities of them are easily found. Thus we obtain the following table in which the load, the numbers of *radial cracks* and the apparent velocities are tabulated. (Table IV.) Table IV gives Fig. 20 in which the results of this experiment are plotted. In this figure the ordinate indicates the velocity of *radial crack*, while the abscissa the load, and the parameter of the curves is the number of the generated *radial cracks*. Of course, the *radial cracks*

18) The results in this figure correspond with the glass plate shown in Fig. 25.

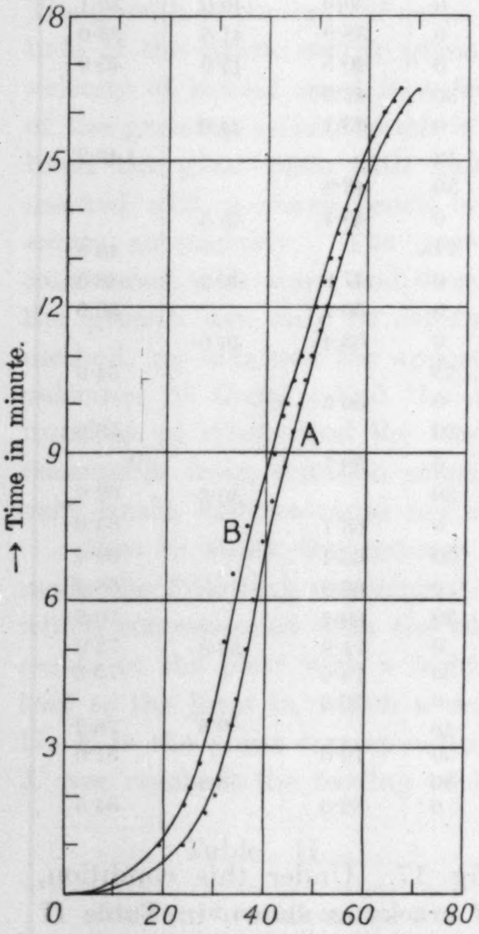

→ Elongation of *radial crack* in m.m.

Fig. 18.

(Two *radial cracks* A, B.)

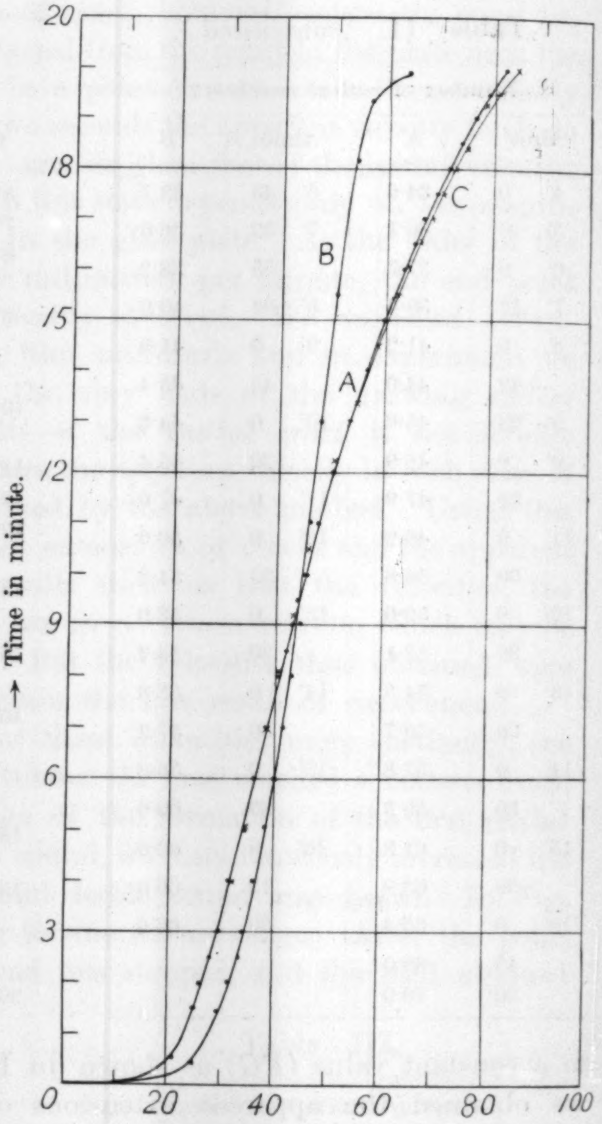

→ Elongation of *radial crack* in m.m.

Fig. 19.

(Three *radial craks* A, B, C.)

which did not extend to the region of the general *radial cracks* were not taken into account. From Fig. 20, we can understand that, when the strain energy given in the glass plate is increased, the velocity of *radial crack* is increased, and nearly proportional to the square of the applied load. When the numbers of *radial cracks* increase, the apparent velocities of them decrease.

Fig. 18, 19, as we have described, shew the relation between the

Table IV. Apparent velocity of *radial crack.*

Load	No.	*Radial Cracks*					
		Total Number	A	B	C	D	E
kg. 40	7	4	0·02	0·02	0·02	0·02	—
48	33	2	1·65	1·7	—	—	—
50	10	2	2·0	2·5	—	—	—
52	29	2	—	0·7	1·3	—	—
60	32	2	5·0	2·4	—	—	—
60	25	2	—	1·1	1·1	—	—
60	21	3	2·6	2·3	2·6	—	—
65	49	2	3·6	3·6	—	—	—
70	26	2	2·3	3·5	—	—	—
70	41	3	2·6	2·5	2·6	—	—
70	47	3	3·4	0·6	3·4	—	—
72	48	4	8·7	8·7	3·2	3·2	—
75	40	4	0·8	4·2	5·0	—	0·5
75	34	2	6·2	6·6	—	—	—
90	39	3	5·2	5·2	5·2	—	—
100	44	2	—	5·3	6·0	—	—
100	45	3	5·0	5·0	5·0	—	—
100	51	3	3·0	3·0	3·0	—	—

{ Load in kg.
Unit of the apparent velocity of *radial crack* in m.m./min.

elongation of *radial crack* and time, and the curves in these figures are apparently straight and apparently continuous. As we have discussed in the preceding section, we know that these are merely the apparent values. In the strict sense of the word, the elongation of the *radial crack* is not continuous with time.

In the surface of a *radial crack* of a broken glass plate, we saw the traces of a number of sharp semi-circular figures as shown in Fig. 21. At the places of these traces the *radial crack* seemed to stop its growth for a moment. By marking with a pencil at the stopping points in the growing state of *radial crack* and comparing these marked points with the traces of semi-circular figures in a broken plate, we confirmed this fact well.

The general forms of the *radial cracks* were very simple and nearly

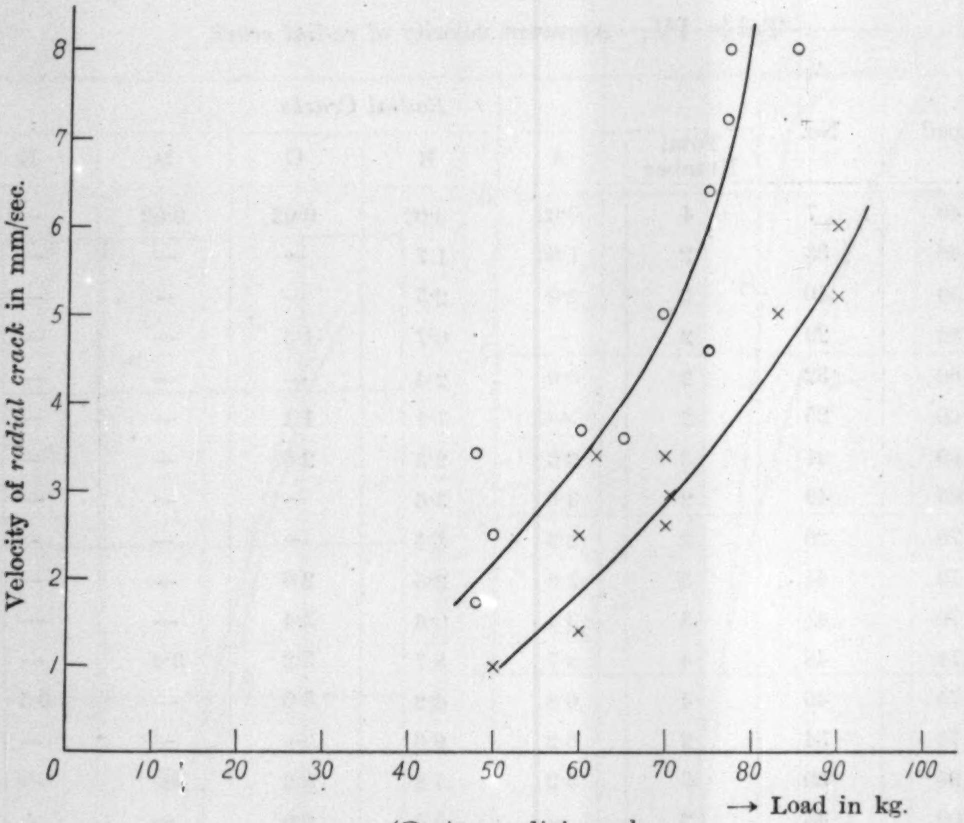

Fig. 20. (○ two *radial cracks*. × three *radial cracks*.)

straight as shown in Fig. 22, 23, 24, 25.

The numbers of *radial cracks* produced in the plate are of important meaning in studying the properties of cracks, and they were, in our case, two, three, four and five. The case of four cracks was very rare. In the case of five cracks, they were generated only in the vicinity of the origin, and they could not extend to farther distances. And the cases of two and three *radial cracks* were very frequently observed.

IV. Radial Cracks at the Edge of Plate.

5. When the *radial cracks* reach near the edge of the plate, their velocities are increased suddenly, and as soon as they reach the edge, a perfect crack extending between the edge and the origin is formed. As we have discussed in the preceding section, the *radial crack* did not appear in the upper surface of the glass plate in its growing state. When the *radial crack* reached the edge, its reflected passage was along

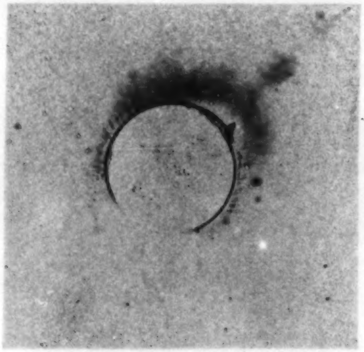

Fig. 3. Circular Crack. ×69
(Load 13 kg.)

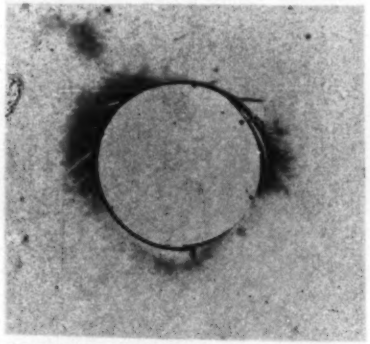

Fig. 4. Circular Crack. ×69
(Load 13 kg.)

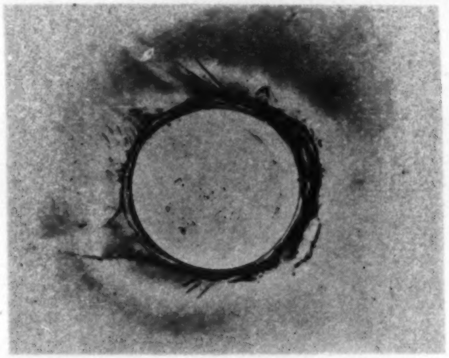

Fig. 5. Spiral Crack, Feather Crack. (Load 13 kg.) ×69

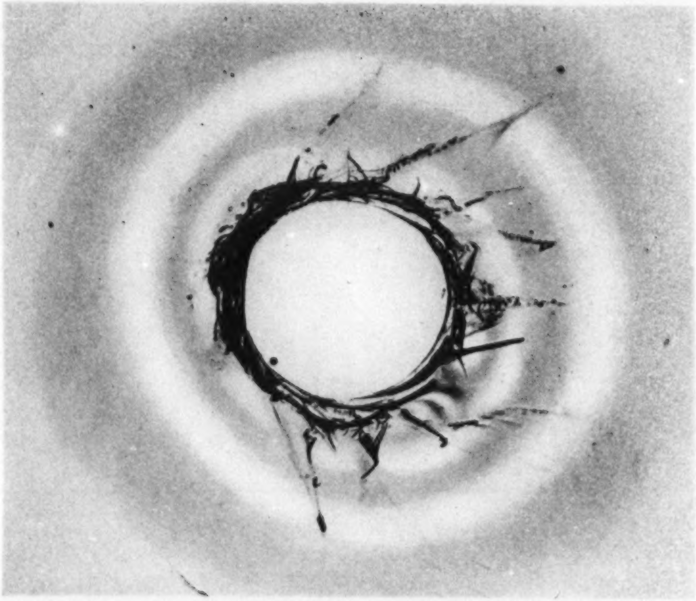

Fig. 6. Spiral, Feather and Conical Cracks. ×69
(Load 30 kg.)

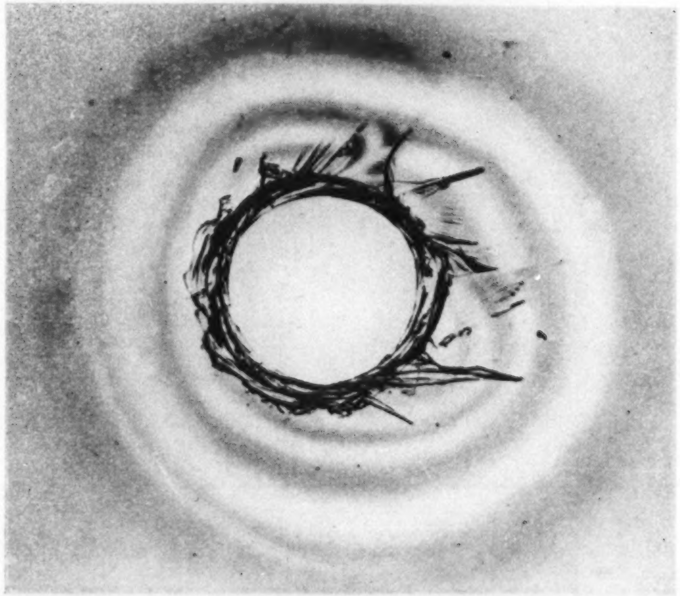

Fig. 7. Spiral, Feather and Conical Cracks. ×69
(Load 25 kg.)

(震研彙報、第十號、圖版、西村、高山)

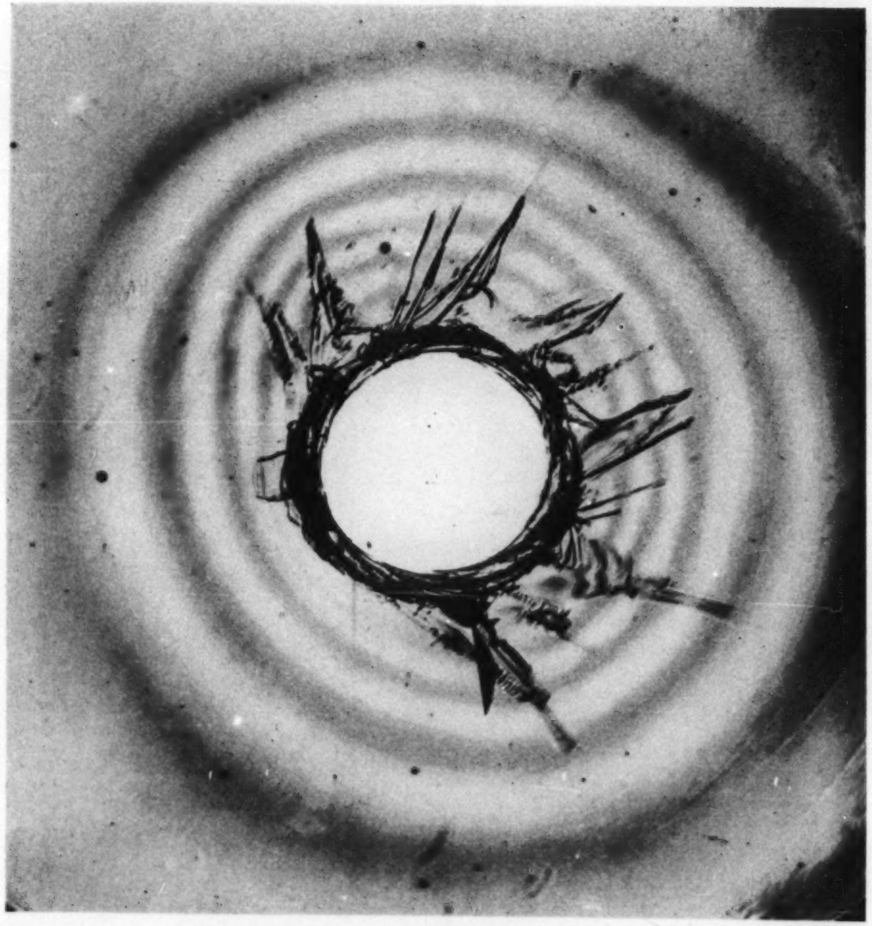

×69
Fig. 8. Spiral, Feather and Conical Cracks. (Load 40 kg.)

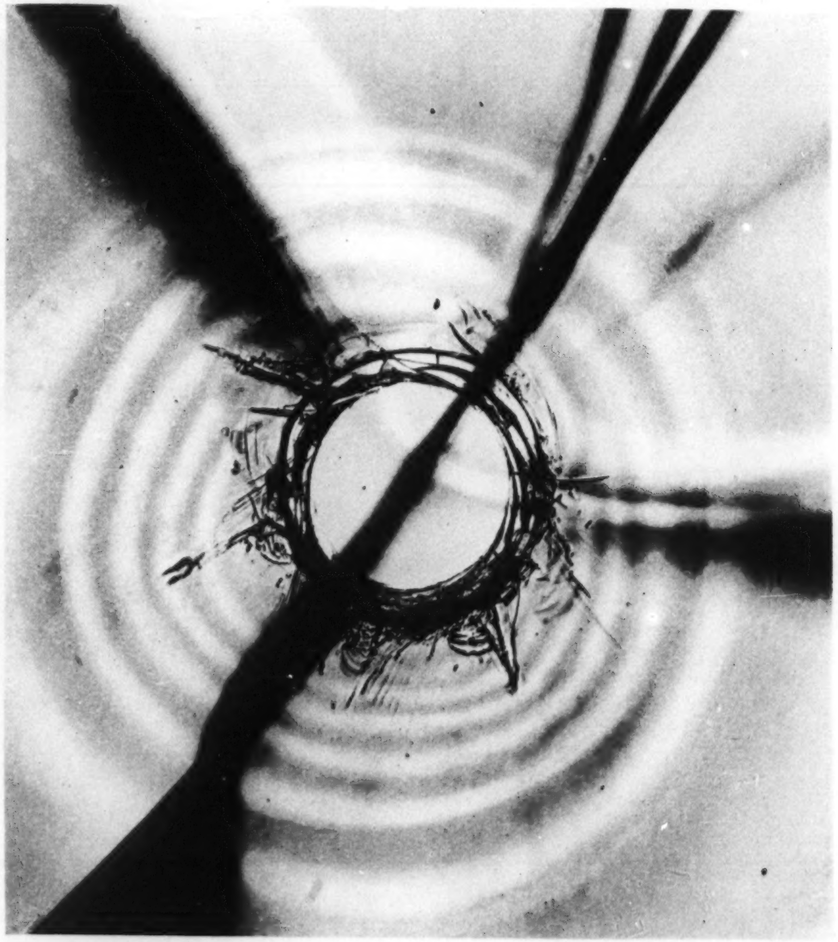

×69
Fig. 9. Spiral, Feather, Conical and Radial Cracks. (Load 33 kg.)

(震研彙報、第十號、圖版、西村、高山)

[Bull. Earthq. Res. Inst., Vol. X, Pl. XLVII.]

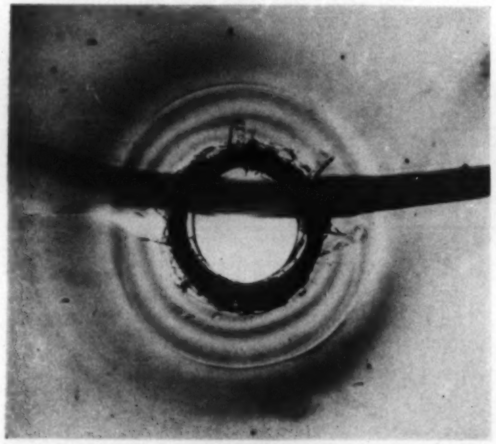

Fig. 10 a. ×35

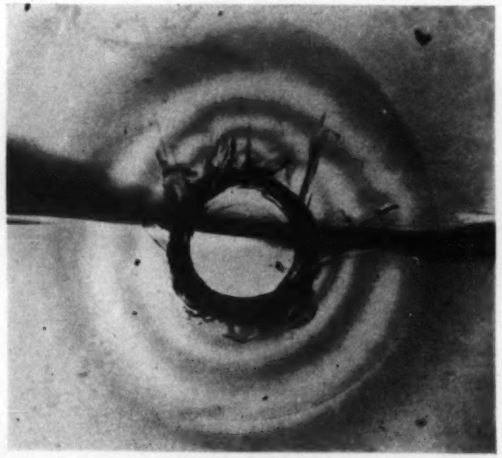

Fig. 11 a. ×35

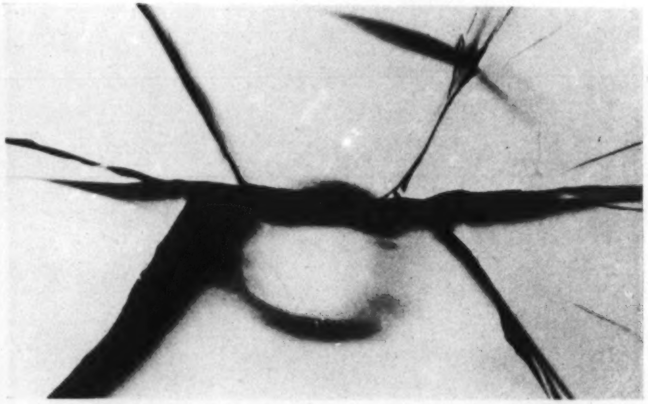

Fig. 12 ×35

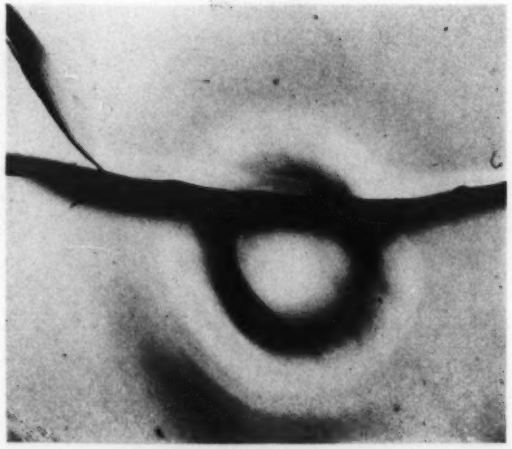

Fig. 10. b ×35

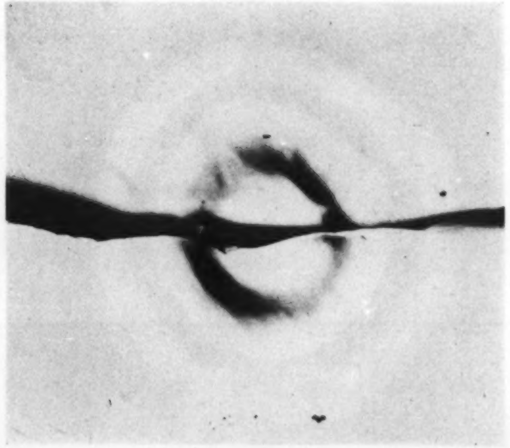

Fig. 11 b. ×35

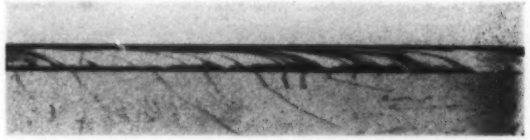

×1·3

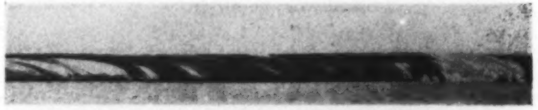

×1·3

Fig. 21. (The surface of Radial Crack of a broken glass plate.)

(震研、彙報、第十號、圖版、西村、高山)

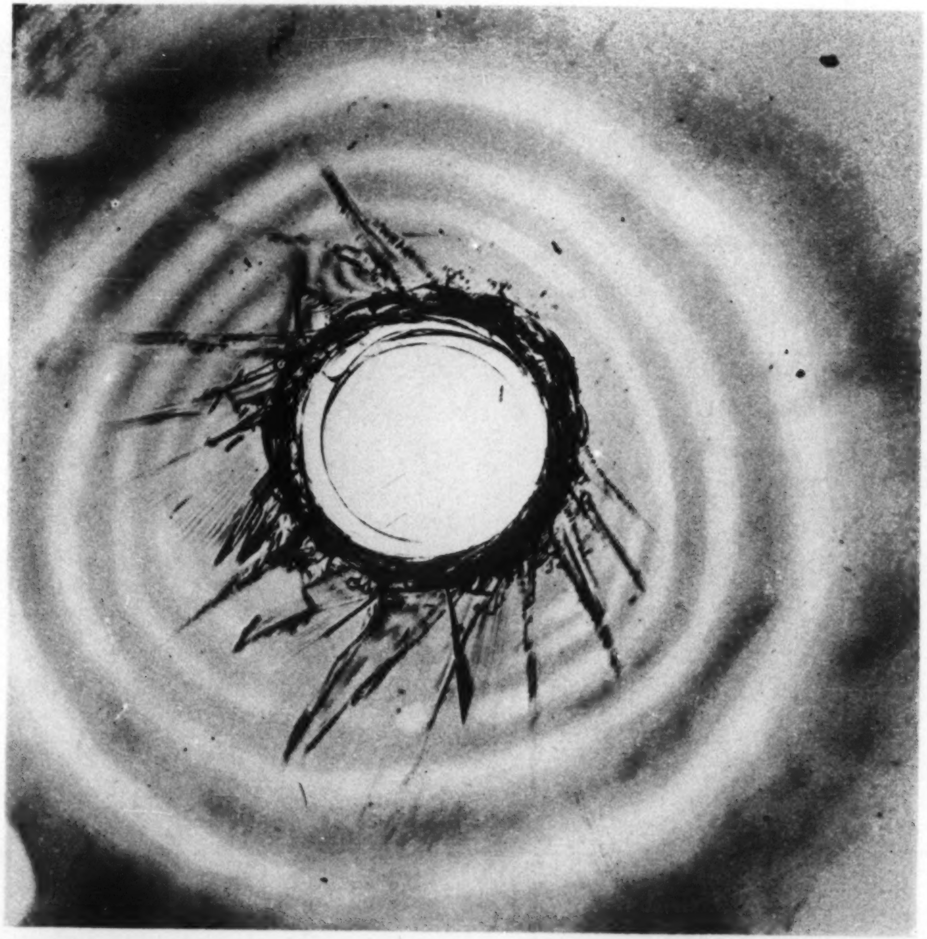

×69

Fig. 15 a. (Immediately after the load was taken off. Load 41 kg.)

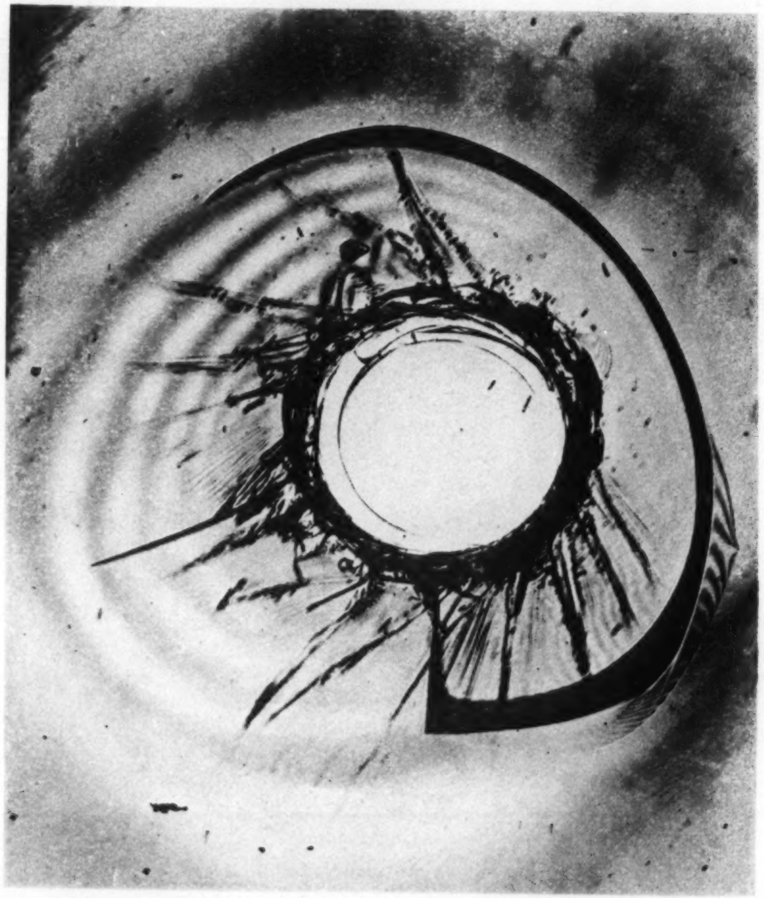

×69

Fig. 15 b. (Same as Fig. 16 a, after one day.)

(震研彙報、第十號、圖版、西村、高山)

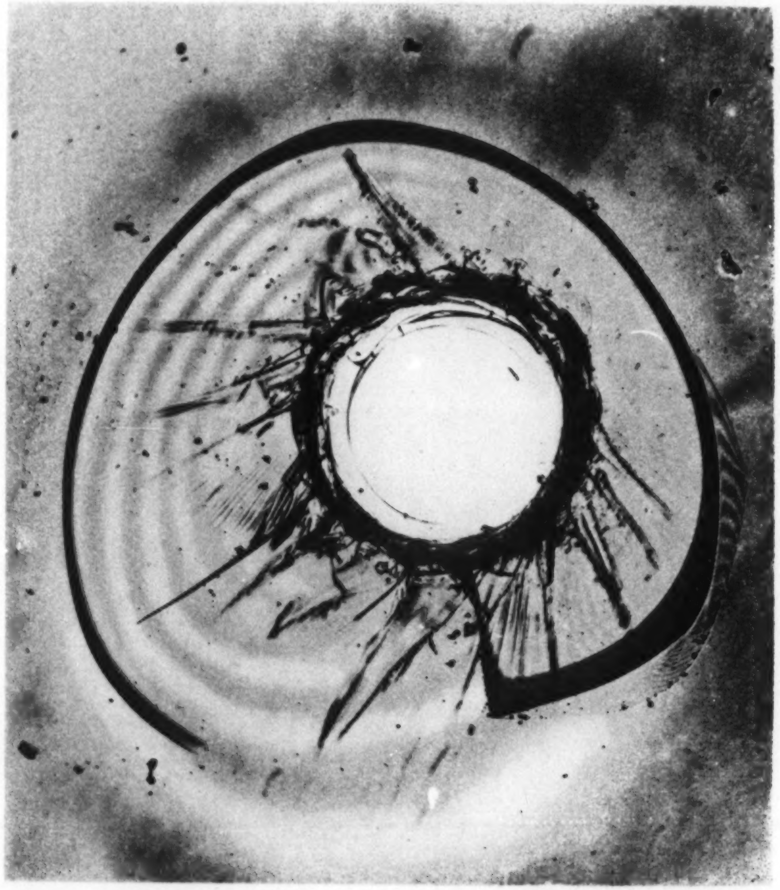

×69

Fig. 15 c. (Same as Fig 15 a, after two days.)

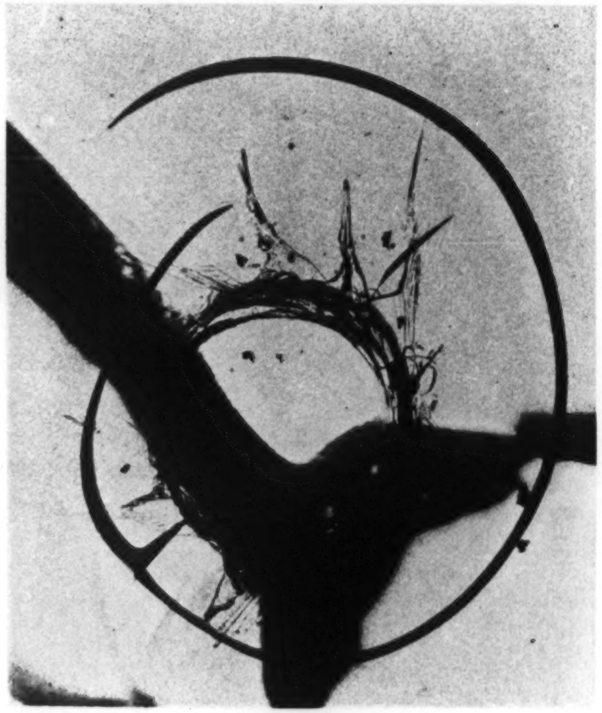

×69

Fig. 16

(震研彙報、第十號、圖版、西村、高山)

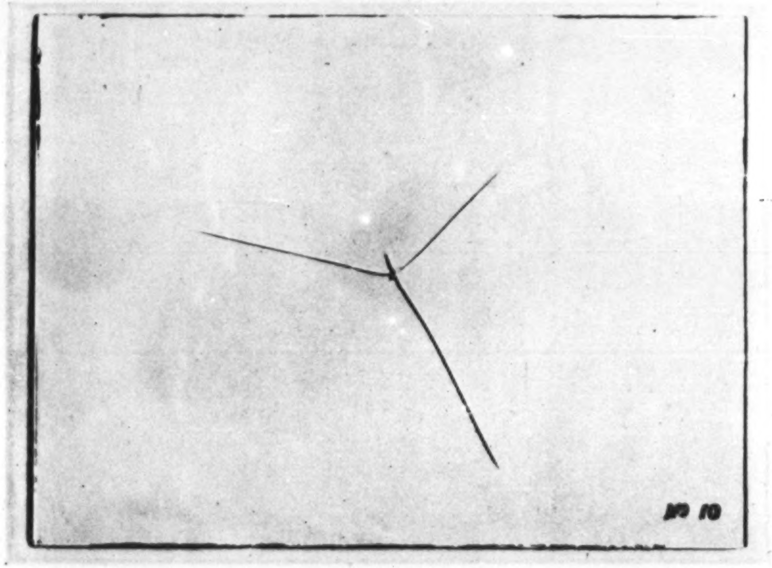

Fig. 22. (Load 50 kg.) $\times \frac{1}{2 \cdot 5}$

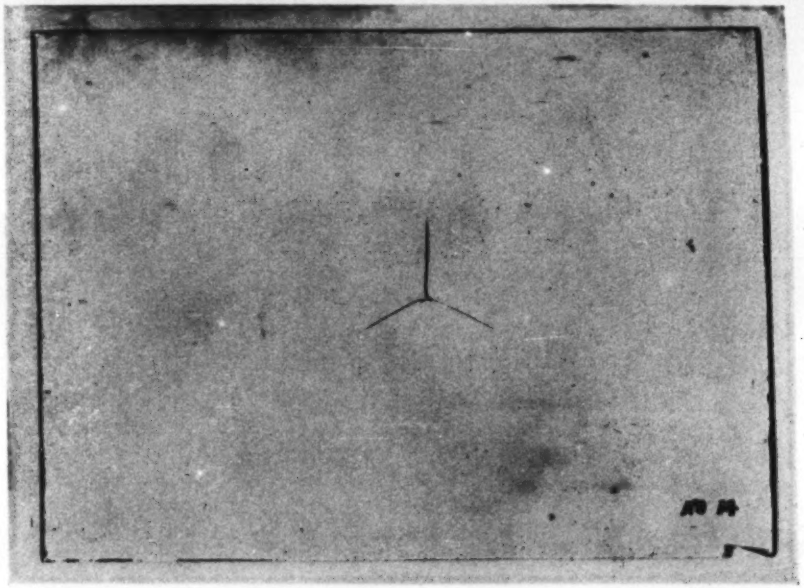

Fig. 23. $\times \frac{1}{2 \cdot 5}$

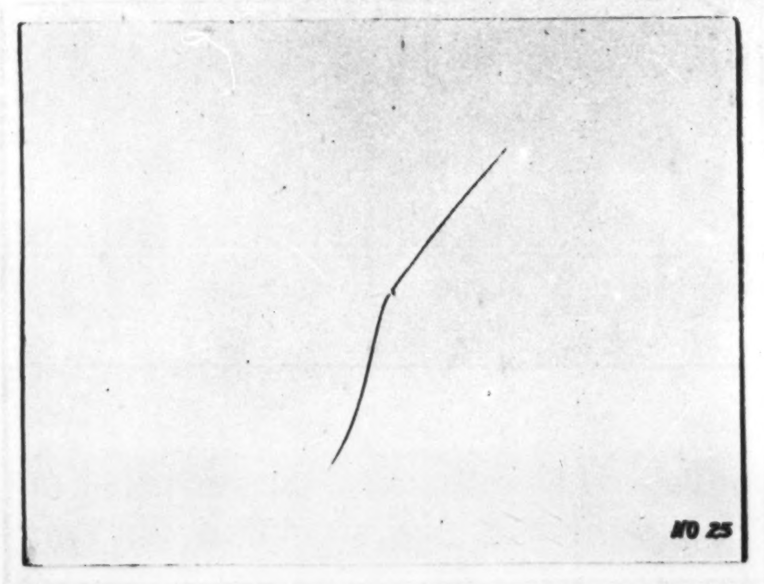

Fig. 24. (Load 60 kg.) $\times \frac{1}{2 \cdot 5}$

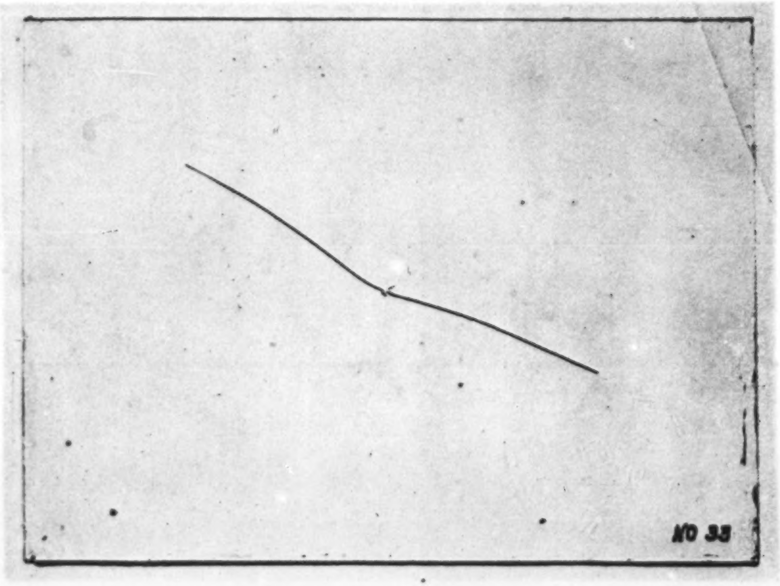

Fig. 25. (Load 48 kg.) $\times \frac{1}{2 \cdot 5}$

（震研彙報、第十號、圖版、西村、高山）

the upper surface, and it instantaneously reached near the position where the steel ball was in a point-contact.

Fig. 26 and 27 shew these mechanisms schematically. When the *radial cracks* started from 0 and were propagated in the directions of OA, OE and OF along the bottom surface of the plate, and one of the *radial cracks* such as OA reached the edge AG of the plate, it was reflected in the directions of AO' instantaneously along the upper surface of the plate. The path (AO') of the reflected *radial crack* is not necessarily coincident with that of the original *radial crack* (OA). Therefore the section of the crack at XY in Fig. 26 has the shape as represented by Fig. 27. In Fig. 27, I, H correspond with I, H in Fig. 26.

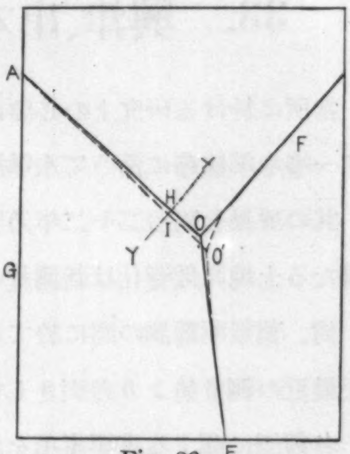

Fig. 26.

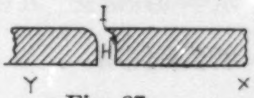

Fig. 27.

Concluding this paper, the authors' cordial thanks are due to Professor T. Terada and Professor K. Sezawa for their kind advices and encouragements during the course of this experiment.

32. 硝子板のワレメに就て

地震研究所 {西村源六郎
高山威雄

ワレメに關しては、ワレメの出來方、ワレメの成長の機構の研究、ワレメの形の研究等があげられるのであるが、著者達は硝子板（厚さ 1 mm.～2 mm.）を鐵板の上におき、直徑 1/16″ の ball で靜荷重をじよじよにかける時、生ずるワレメの形や成長の仕方等に就て、研究してみた。深い理論をたてる迄には今の所行かないが、將來の研究を進める第一步として、此の種の研究に多少でも參考になる所があれば幸甚である。

33. 興津、串本間一等水準線檢測成果報告

當所に於ける研究上の必要により最近陸地測量部に依賴し興津一串本間に別圖に示す一等水準線路に沿うて水準測量を行へり。

其の成果を明治二十二年乃至同三十三年の間に行はれし舊測量結果と比較して求め得たる土地高低變化は新測量の期日と共に別圖に掲げて參考に供す。

尙、舊新兩觀測の間に於て水準線路中の一部分に就き別の觀測結果あり。この結果を最近の測量値より差引きし値を圖中に併せて示せり。

各觀測に關する重要事項を示せば下記の如し。

1. 水準線路延長　五百三十二キロ米

2. 新舊觀測期

舊……興　津――岡　崎……明治三十三年 六 月――十　月

岡　崎――名古屋……明治二十八年 一 月――五　月

名古屋――一身田……明治二十八年 二 月――五　月

一身田――佐　奈……明治二十二年 四 月――八　月

佐　奈――尾　鷲……明治二十八年十一月――廿九年三月

尾　鷲――串　本……明治三十二年 五 月――十一月

新…………………昭 和 六 年 八 月――十一月

舊、新兩觀測の間に於ける別の觀測部分及び其期日

名古屋――一身田――松坂……昭和四年八月――十一月

3. 新觀測値は興津に於ける一等水準點交 70·1 號の眞高四米〇八四五（關東及伊豆兩震災に依る低下〇米一二〇六を加算）を基準とせり。

（昭和七年三月十日　　地震研究所）

串 本 間 —

ts along a Ro

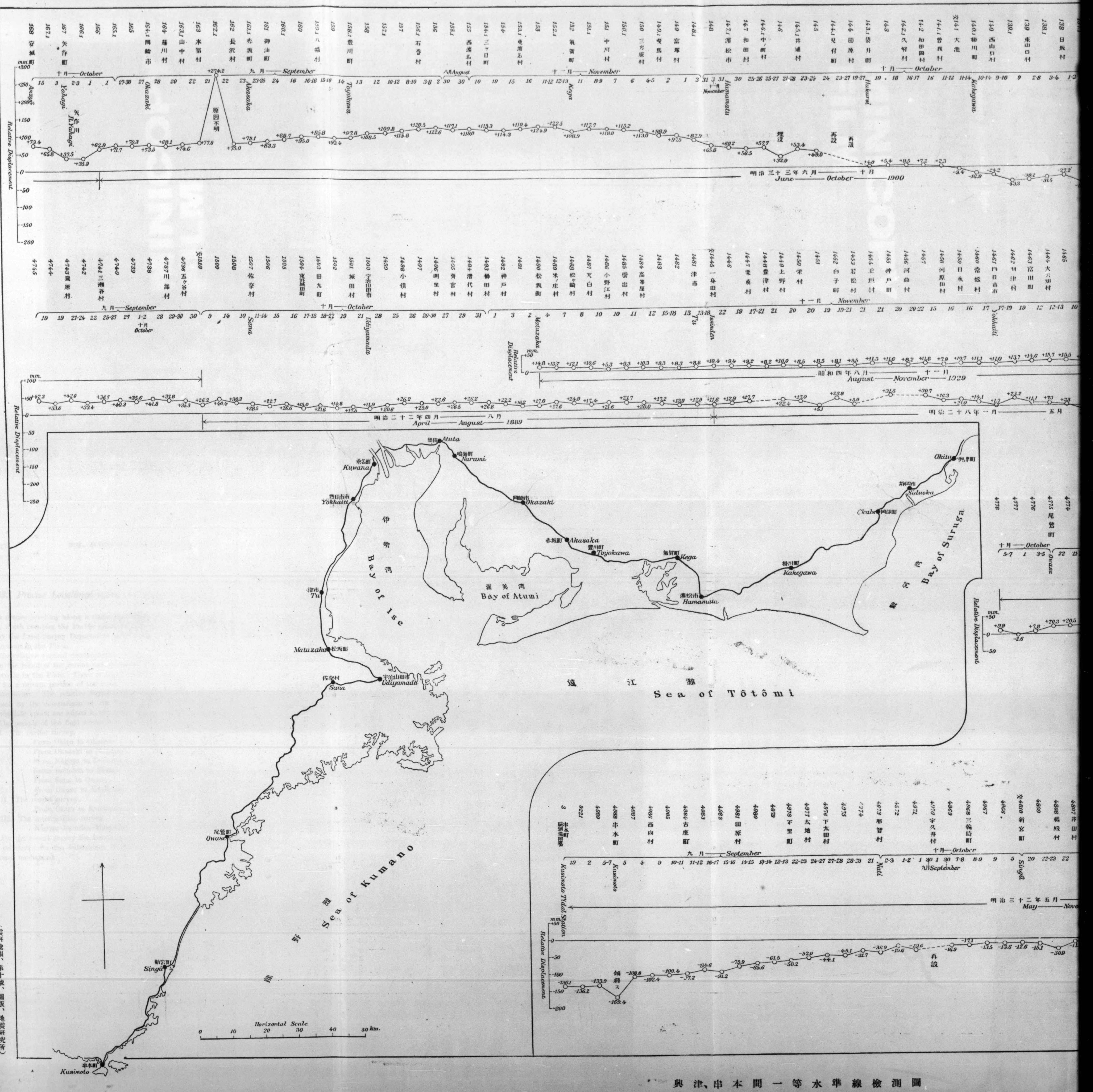

(震研彙報, 第十號, 圖版, 地震研究所)

興津、串本間一等水準線檢測圖

Relative Vertical Displacements of Bench Marks along a Route from Okitu to Kusimoto. (Assuming No. 70.1 to be stationar

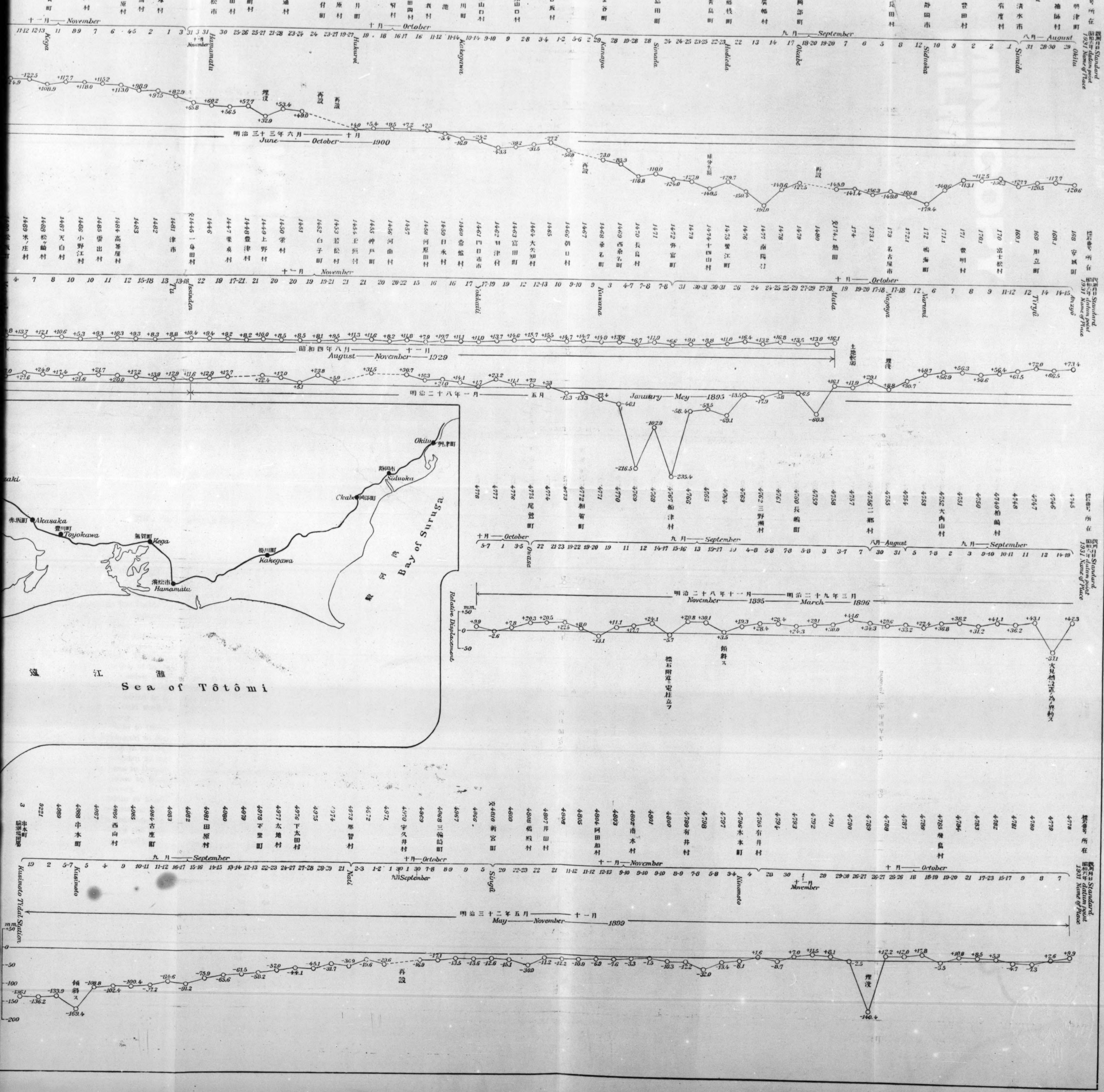

興津、串本間一等水準線檢測圖

Vertical Displacements of Bench Marks along a Route from Okitu to Kusimoto. (Assuming No. 70.1 to be stationary.)

33. *Precise Levellings along a Route from Okitu to Kusimoto.*

A precise levelling along a route extending to 532 kilometers from Okitu to Kusimoto, which occupies the Pacific coast of the middle part of Honsyû, was lately carried out by the Land Survey Department at our request, the route in question being shown in the map in the Plate.

The relative vertical displacements of bench marks obtained by the comparison between the result of the recent measurements and that of the earlier ones are shown in the profile in the Plate. There is another result acquired by a levelling survey that was done for a certain portion of the route in an epoch between the recent and the earlier measurements. The relative vertical displacements of bench marks for this portion obtained by the comparison of the result of the recent measurement and that of the intermediate epoch are added in the same Plate.

The periods of the field works were as follows:

I. The earlier survey.

From Okitu to Okazaki:	June—October, 1900.
From Okazaki to Nagoya:	January—May, 1895.
From Nagoya to Issinden:	February—May, 1895.
From Issinden to Sana:	April—August, 1889.
From Sana to Owase:	November, 1895—March, 1896.
From Owase to Kusimoto:	May—November, 1899.

II. The recent survey.

From Okitu to Kusimoto:	August—November, 1931.

III. The intermediate survey.

Nagoya-Issinden-Matuzaka:	August—November, 1929.

For the recent survey the bench mark No. 70·1 at Okitu, whose true height involving the correction for the subsidence 0·1206 meter was 4·0845 meters above sea level, is assumed unchanged.

(March 10, 1932. Earthquake Research Institute.)

34. Seismometrical Report.

地震觀測報告

(Earthquake Research Institute, Tôkyô, Japan.)

(October 1—December 31, 1931.)

(1) Sensible earthquakes in Tôkyô for the period October 1—December 31, 1931.

List I.

Time = Central standard time of Japan (Civil mean time of the meridian 135°E).

Notation:

Prel. tr. = Preliminary tremors.
N. S. = North-South component.
E. W. = West-East component.
2A = Range of motion.
T = Period of earthquake motion.
λ = Longitude.
φ = Latitude.
D = Depth of focus.

Intensity: 0 (no feeling), I (slight), II (rather weak), III (weak), IV (rather strong), V (strong), VI (violent).

No.	Station	Date	Time of occurrence	Duration: Prel. tr.	Duration: Total	Maximum motion N. S. 2A	N. S. T	E. W. 2A	E. W. T	Direction of initial motion	Epicentre λ (E)	Epicentre φ (N)	D	Intensity
			h m s	s	m	μ	s	μ	s				km	
71	Tôkyô	Oct. 3	2 36 55·2	8·6	15	300	1·3	550	1·4	S34°E, u.	139°20	35°91	24	II
	Kamakura			11·0	8	680	0·8	340	0·8	S6°E				II
	Misaki			13·8	8	467	3·0	400	2·0	S27°E				II
	Kiyosumi			16·2	13	260	4.2	180	2·4					II
	Titibu			4·6	8	1400	1·2	1200	1·2					III
	Tôgane			15·0	14	860	1·0	950	1·0					II
	Tukuba		2 36 58·3	8·6	11					S80°W				II
	Mitaka			7·5	6	600	0·59	590	0·59	S35°E				II

(*to be continued.*)

List I. (*continued.*)

No.	Station	Date	Time of occurrence	Duration: Prel. tr.	Duration: Total	Maximum motion N. S. 2A	Maximum motion N. S. T	Maximum motion E. W. 2A	Maximum motion E. W. T	Direction of initial motion	Epicentre λ (E)	Epicentre φ (N)	D	Intensity
			h m s	s	m	μ	s	μ	s				km	
72	Tôkyô	Oct. 13	21 14 06·0	5·2	3	400	0·39	250	0·39		139°78	35°44	24	II
	Kamakura		21 13 55·6	4·3	2	190	0·65	130	0·65					I
	Misaki			5·1	3	131	1·00	67	1·1					
	Kiyosumi			7·0	1	20	0·3	16	0·3					
	Titibu			10·6	2	20	0·5	22	0·4					
	Tôgane			9·8	2									
	Tukuba													
	Mitaka													
73	Tôkyô	18	4 42 42·0	5·3	2	67	0·48	53	0·48		140·00	35·65	35	I
	Kamakura													
	Misaki			10·0	1	6	0·25	5	0·50					
	Kiyosumi													
	Titibu													
	Tôgane			6·5	1	8	0·3	4	0·35					
	Tukuba		4 42 47·5	8·8	1·3									
	Mitaka													
74	Tôkyô	23	12 16 27·7	8·5	6	76	0·28	64	0·28	S58°E	139·23	36·00	24	I
	Kamakura		12 16 33·5	11·6	3	40	0·67	44	0·67					
	Misaki			14·0	2	18	1·1	9	0·6					
	Kiyosumi			18·6	3	8		6	0·4					
	Titibu			3·4	2	100	0·4	112	0·6					
	Tôgane			14·5	4	58	0·53	56	0·9					
	Tukuba		12 16 35·9	9·1	2·3									
	Mitaka													I
75	Tôkyô	30	3 53 34·7	1·67	12	320	1·00	166	1·00	N41°E, d	141·20	36·10		I
	Kamakura													
	Misaki													
	Kiyosumi			26·0	9	90	2·2	78	1·00					
	Titibu			20·0	6	36	0·80	42	0·80					
	Tôgane			16·0	15	180	0·85	250						
	Tukuba		3 53 24·1	10·0	12									II
	Mitaka													II
76	Tôkyô	31	23 17 01·5	17·3	7	63	1·00	91	0·47		140·00	34·30	20	I
	Kamakura		23 16 58·2	10·4	4	16	0·26	64	0·52					
	Misaki			10·8	5	79	1·6	29						
	Kiyosumi			10·4	8	44	1·3	36	0·95					
	Titibu			16·3	3	8	0·8	8	0·75					
	Tôgane			15·2	10	30	0·5	30	0·8					
	Tukuba		23 17 02·7		4									
	Mitaka													
77	Tôkyô	Nov. 3	4 56 01·5	24·4	10	98	0·77	104	0·78		140·36	34·21	50	I
	Misaki		4 55 58·3	19·0	6	124	0·43	96	0·43					
	Kamakura			16·1	10	345	1·90	517	1·42					
	Kiyosumi			16·2	7	70	1·50	50	1·50					
	Titibu			28·8	6	40	1·13	40	1·13					II
	Tôgane			21·4	7	60	1·04	66	1·04					
	Tukuba			25·7	9									
	Mitaka													

(*to be continued.*)

List I. (*continued.*)

No.	Station	Date	Time of occurrence	Duration: Prel. tr.	Duration: Total	Maximum motion N. S. 2A	N. S. T	E. W. 2A	E. W. T	Direction of initial motion	Epicentre λ (E)	Epicentre φ (N)	D	Intensity
			h m s	s	m	μ	s	μ	s		°	°	km	
78	Tôkyô	Nov. 9	21 33 37·1	9·4	2	76	0·32	56	0·32	S78°E	139·97	35·23	45	I
	Kamakura			7·8	1·3	16		20						
	Misaki													
	Kiyosumi		21 33 37·2	7·1	2	16	0·21	12	0·21					II
	Titibu			13·4	1·5			12	0·68					
	Tôgane			9·3	2	16	0·29	8	0·34					
	Tukuba		21 33 42·3	11·6	1·4									
	Mitaka													
79	Tôkyô	12	15 9 01·5	13·7	16	266	2·36	350	1·65	S58°E	140·57	35·22	50	I
	Kamakura		15 9 00·7	13·0	8	1700	0·60	1440	0·60	N75°E				II
	Misaki			12·5	7	920	1·10	830	1·10					III
	Kiyosumi		15 8 53·6	8·4	14	800	0·58	700	0·58					III
	Titibu			21·8	8	70	1·23	90	1.40					
	Tögane			9·1	14	1460	0·79	710	0·79					II
	Tukuba		15 9 02·1	13·0	12									I
	Mitaka													
80	Tôkyô	12	22 11 22·8	18·0	9	140	0·47	95	0·60		139·59	34·77	50	I
	Kamakura		22 11 16·0	14·6	4	120	0·68	64	0·68					I
	Misaki			14·0	4	139	1·08	200	1·08					
	Kiyosumi			16·0	6	36	1·10	20	1·10					
	Titibu			19·8	4	80	0·87	96	0·87					
	Tôgane			20·7	11	60	0·52	24	0·52					
	Tukuba		22 11 25·5	21·3	6									
	Mitaka													
81	Tôkyô	29	3 36 30·4	8·6	2	52	0·45	40	0·45		140·00	35·51	60	I
	Kamakura													
	Misaki			10·3	3	42	0·50	29	0·50					
	Kiyosumi			9·7	1·5	70	0·37	16	0·43					
	Titibu			15·0	2	8	0·83	6	0·83					
	Tôgane			9·1	2	12	0·39	16	0·39					
	Tukuba													
	Mitaka													
82	Tôkyô	Dec. 2	2 15 43·0	14·1	3	50	0·47	32	0·57		140·58	35·79	80	I
	Kamakura													
	Misaki			18·1	3	8	0·62	8	0·62					
	Kiyosumi			14·8	2	4	0·55	4	0·55					
	Titibu			18·1	1·5			10	0·40					
	Tôgane			11·3	2	8	0·2′	10	0·20					
	Tukuba													
	Mitaka													
83	Tôkyô	2	13 00 25·1	9·4	3	56	0·28	34	0·28		138·79	35·38	10	I
	Kamakura			7·0	3	24	0·47	74	0·47					
	Misaki			9·8	3	29	0·46	65	0·62					
	Kiyosumi		13 00 23·6	9·4	3	2	0·50	4	0·50					
	Titibu			9·8	1·5	20	0·31	25	0·31					
	Tôgane			18·4	3	6	0·90	6	0·90					
	Tububa													
	Mitaka													

(*to be continued.*)

List I. (*continued.*)

No.	Station	Date	Time of occurrence	Duration Prel. tr.	Duration Total	Maximum motion N. S. 2A	N. S. T	E. W. 2A	E. W. T	Direction of initial motion	Epicentre λ (E)	Epicentre φ (N)	D	Intensity
			h m s	s	m	μ	s	μ	s		°	°	km	
84	Tôkyô	Dec. 11	0 57 18·2	10·3	4	44	0·29	46	0·29		140·25	35·22	30	I
	Kamakura		0 57 19·4	9·6	2·5	90	0·56	180	0·56					II
	Misaki													
	Kiyosumi		0 57 14·3	6·1	3	80	0·24	54	0·24					II
	Titibu			17·0	2·5			10	0·33					
	Tôgane			7·4	3	252	0·19	340	0·19	S slight W				II
	Tukuba													
	Mitaka													
85	Tôkyô	15	21 55 16·9	7·4	3	16	0·51	16	0·51		140·05	35·72	50	I
	Kamakura													
	Misaki			10·5	3	10	0·66	19	0·66					
	Kiyosumi			12·2	2	10	0·73	10	0·73					
	Titibu			15·5	2			6	1·1					
	Tôgane			8·3	3	16	0·54	9	0·54					
	Tukuba													
	Mitaka													
86	Tôkyô	16	2 14 57·0	10·8	6	86	0·20	98	0·30		139·95	36·30	55	I
	Kamakura		2 15 01·2	16·1	3	352	0·65	246	0·65					
	Misaki			16·5	4	54	0·74	54	0·92					
	Kiyosumi			16·5	5	20	0·72	20	0·72					
	Titibu			10·8	2·5			104	0·21					
	Tôgane			12·5										
	Tukuba													
	Mitaka													
87	Tôkyô	19	2 14 02·5	8·5	8	200	0·54	194	0·54	N77°E, d	140·26	35·77	45	I
	Kamakura		2 14 04·7	12·8	5	130	0·53	84	0·53					II
	Misaki			12·9	6	186	0·52	111	0·52					I
	Kiyosumi			10·4	6	60	0·78	30	0·78					
	Titibu			15·7	6	82	1·80	30	1·80					
	Tôgane			6·6	5	410	1·16	580	0·98					
	Tukuba													
	Mitaka													
88	Tôkyô	24	23 18 03·5	10·1	2	27	0·51	35	0·54		139·99	35·50	18	I
	Kamakura		23 17 58·3	7·3	1·5	14	0·31	30	0·42					I
	Misaki													
	Kiyosumi													
	Titibu			7·3	1·5	8	0·19	8	0·19					
	Tôgane													
	Tukuba													
	Mitaka													
89	Tôkyô	26	14 15 54·9	8·2	4	72	0·23	50	0·23	S23°W	139·92	36·26	30	I
	Kamakura													
	Misaki													
	Kiyosumi			15·7	4	11	0·48	14	0·48					
	Titibu			9·9	2	54	0·17	46	0·17					
	Tôgane			11·5	3	20	0·56	12	0·56					
	Tukuba													
	Mitaka													

(2) *Important distant earthquake as observed in Tôkyô (Hongô).*

List II.

Date	Phase	Time of Occurrence (G. M. T.)	Amplitude 2A		Period	Probable Epicentre
1931		h m s				
Oct. 3	P	19 22 16·2				15°E, 16°S
	S	19 29 25·2		mm	sec	
	L	19 34 37·0	(EW)	4·6	52	
			(NS)	3·3	63	
	M	19 38 27·0	(EW)	4·4	19	
			(NS)	4·6	21	
	F	22				
Oct. 10	P	0 28 44·0				160°E, 16°S
	S	0 35 56·9				
	L	0 40 54·1	(EW)	4	60	
			(NS)	2·8	50	
	M	0 48 41·2	(EW)	3·2	20	
			(NS)	3·7	15	
			(V)	1·5	18	
	F	2				

Daily frequency of the earthquake felt in Tôkyô during 1931.

List III.

Date	Jan.	Feb.	Mar.	April	May	June	July	Aug.	Sept.	Oct.	Nov.	Dec.
1							1					
2						1	1					2
3										1	1	
4		2	1	1	1							
5	1											
6												
7			2						1			
8							1					
9		1	1			1			1		1	
10			1				2	1				
11						1						1
12			1		1						2	

(to be continued.)

List III. (*continued.*)

Date	Jan.	Feb.	Mar.	April	May	June	July	Aug.	Sept.	Oct.	Nov.	Dec.
13										1		
14						1						
15				1								1
16									1			1
17						3						
18								1	1	1		
19							1	1				1
20		2					1					
21									3			
22												
23	1	1	2			1			1	1		
24				1					3			1
25			1		2	1						
26			1		1		1		1			1
27			1					1				
28							2		2			
29			1								1	
30	1					2	1			1		
31							1			1		
Sum	3	6	12	3	5	11	12	4	14	6	5	8

Total sum=89.

(N. Nasu and Ch. Yasuda.)

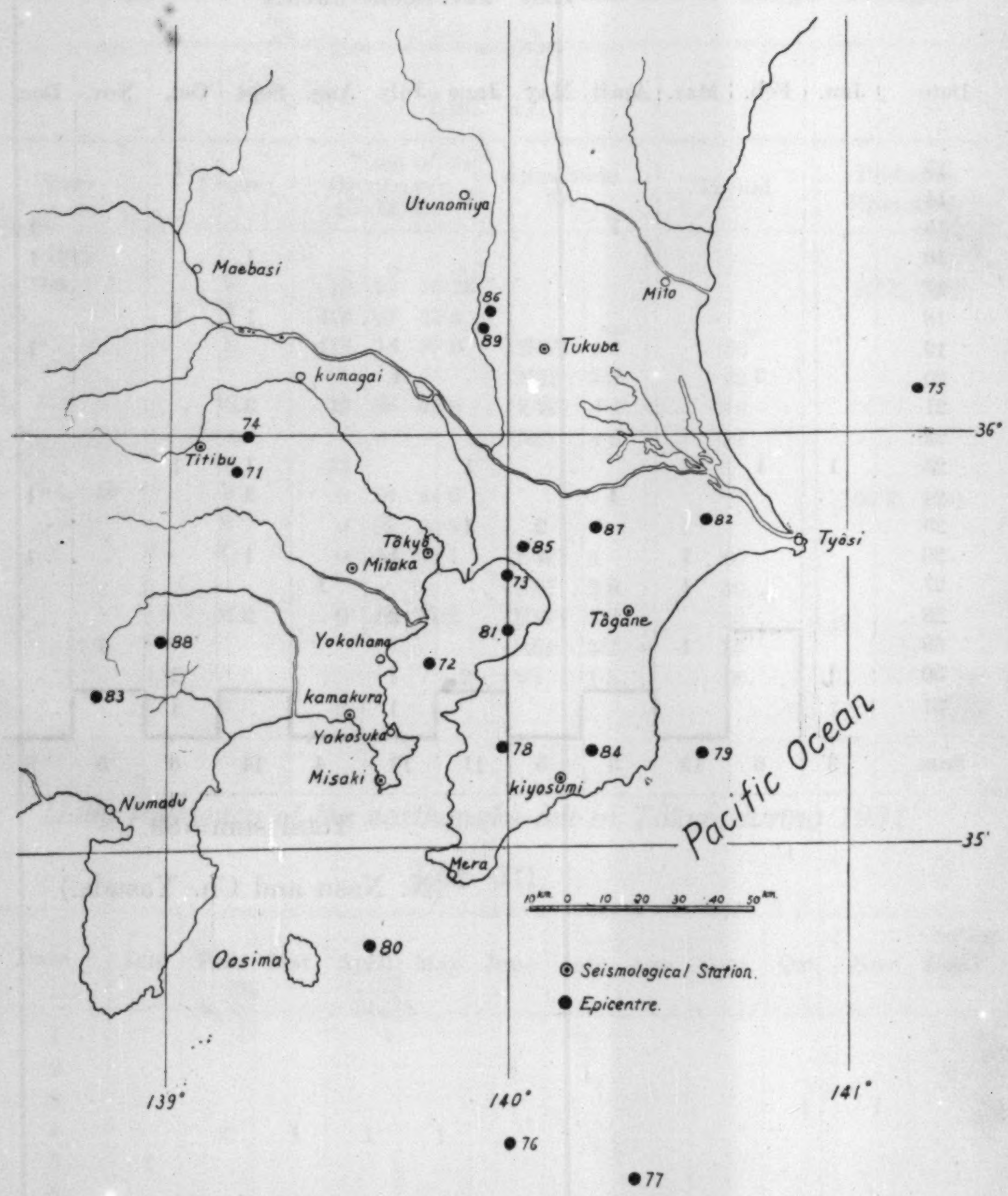

Fig. 1. Distribution of the earthquakes that originated within a distance of 160 kms. from Tôkyô and felt there, for the period October 1–December 31, 1931.
(Figures attached to each epicentre indicate the earthquake number in List I.)

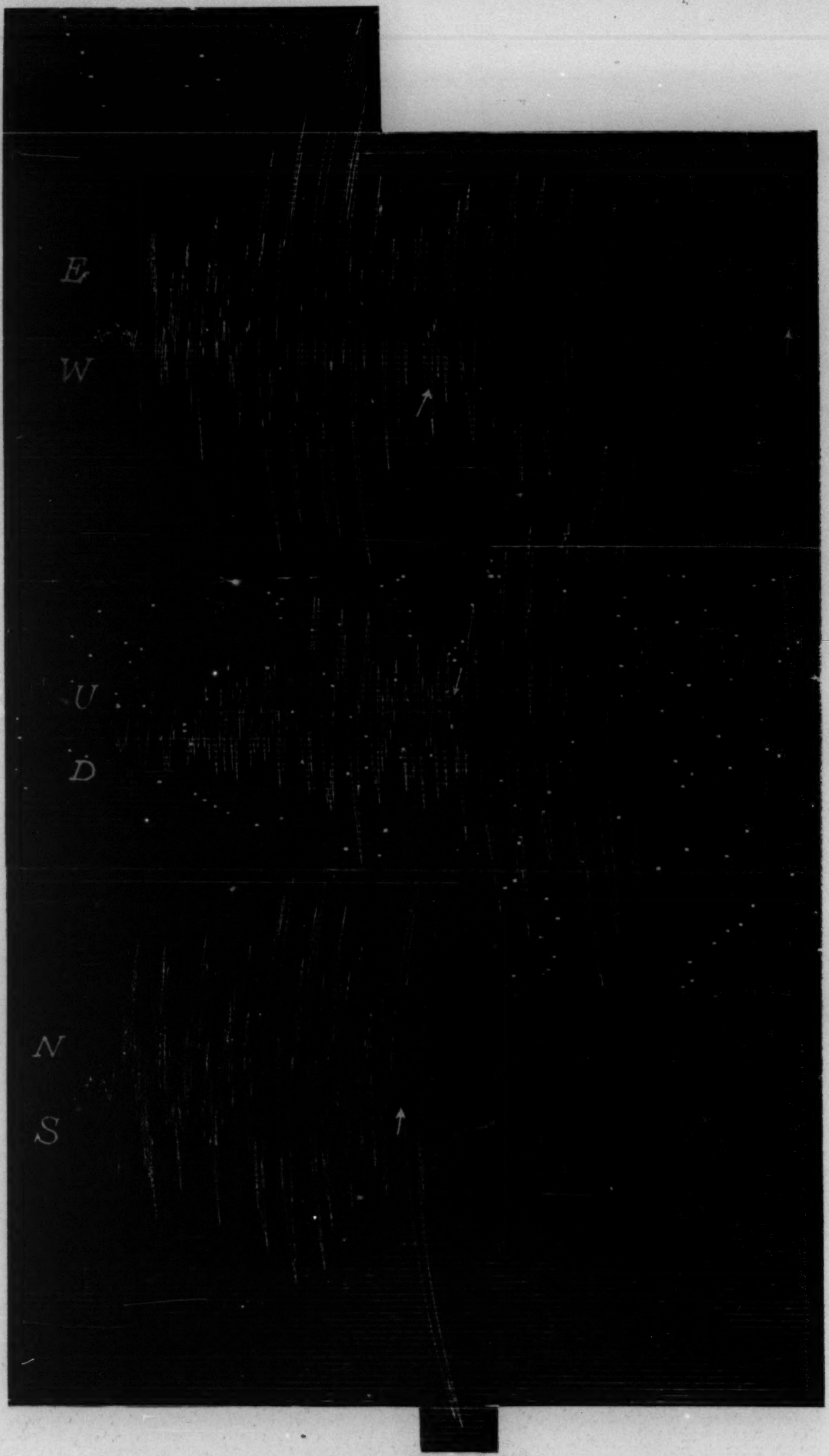

Fig. 2. Tôkyô observation of the earthquake of Oct. 3, 1931.
Instrument = No. 5.

Comp.	Period	Magnification	Damping ratio
N. S.	7 s	50	1·5
E. W.	7	50	1·5
Vert	7	28	1·5

Fig. 3. Titibu observation of the earthquake of Oct. 3, 1931.

Instrumental constants: Natural period = 7 s.
Magnification = 50.
Damping ratio = 1.

(震研彙報、第十號、圖版、震報)

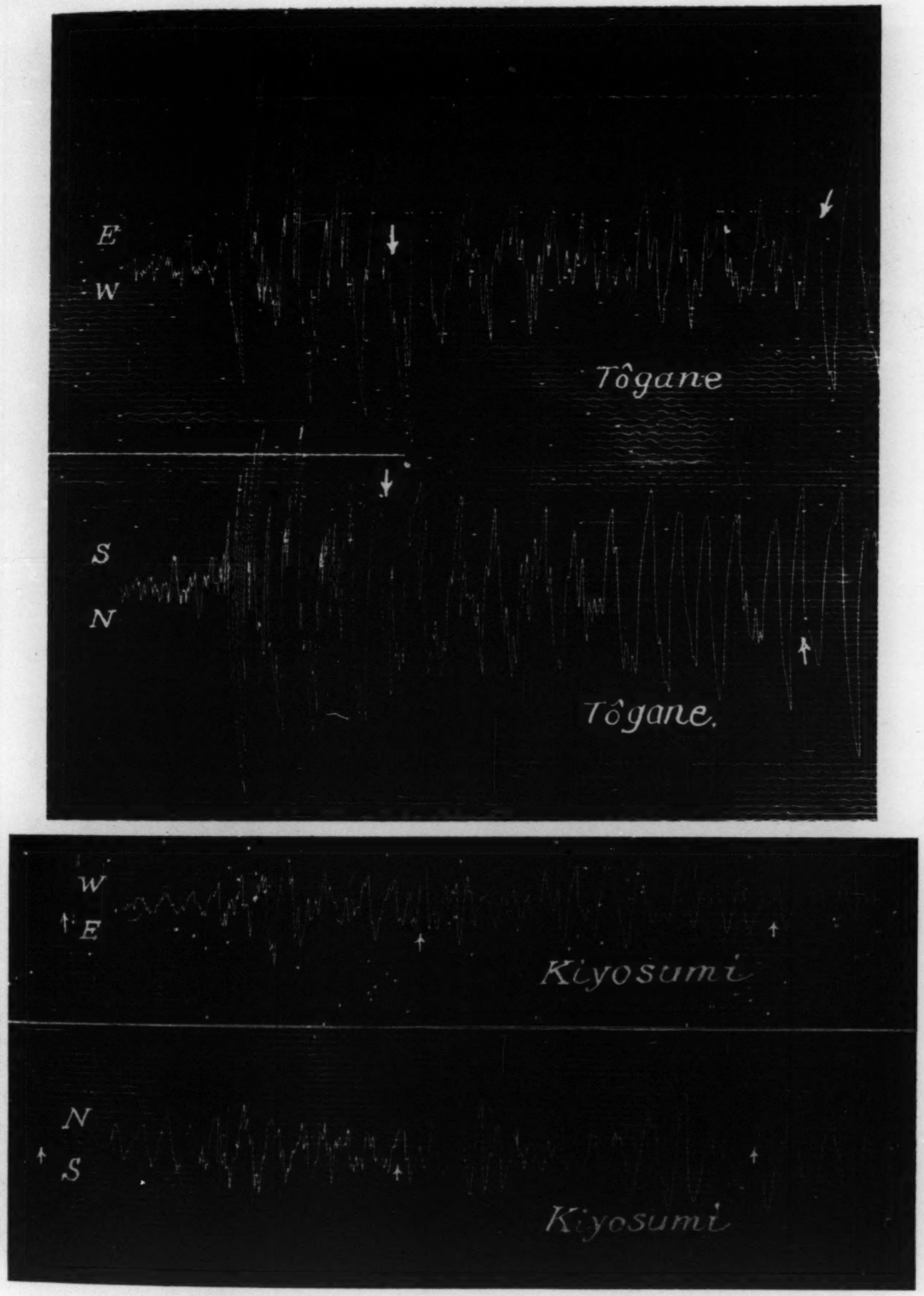

(震研彙報、第十號、圖版、震報)

Fig. 4. Tôgane and Kiyosumi observations of the earthquake of Oct. 3, 1931.
(Small arrow indicates minute-break.)

Instrumental constants:	Tôgane	Kiyosumi
	Natural period = 7 s	Natural period = 7 s
	Magnification = 50	Magnification = 50
	Damping ratio = 1·5	Damping ratio = 1·5

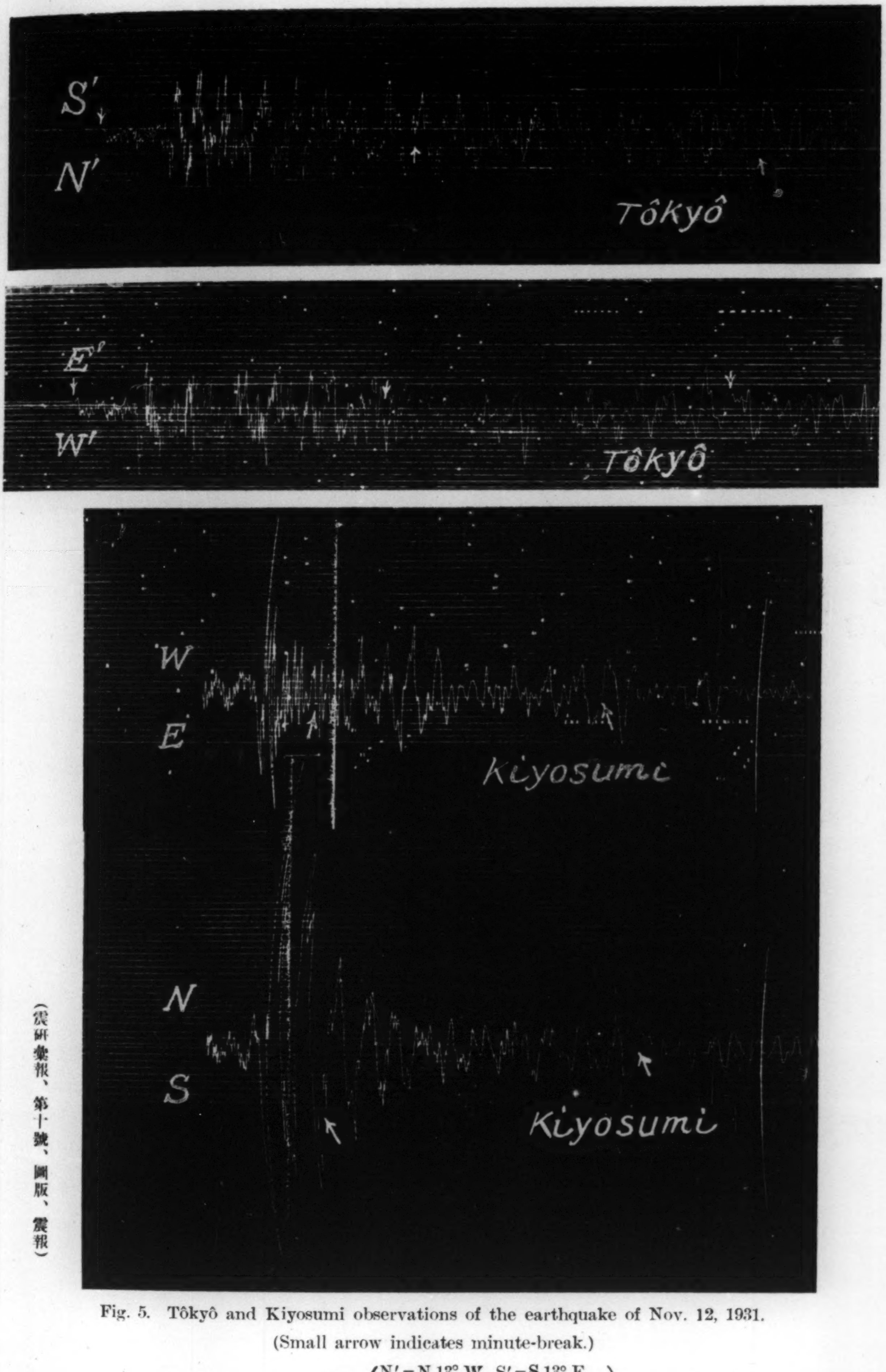

Fig. 5. Tôkyô and Kiyosumi observations of the earthquake of Nov. 12, 1931.
(Small arrow indicates minute-break.)

Instrumental constants: Tôkyô (N' = N 13° W, S' = S 13° E, E' = N 77° E, W' = S 77° W.) Instrument = No. 4.

Kiyosumi. (See Fig. 4.)

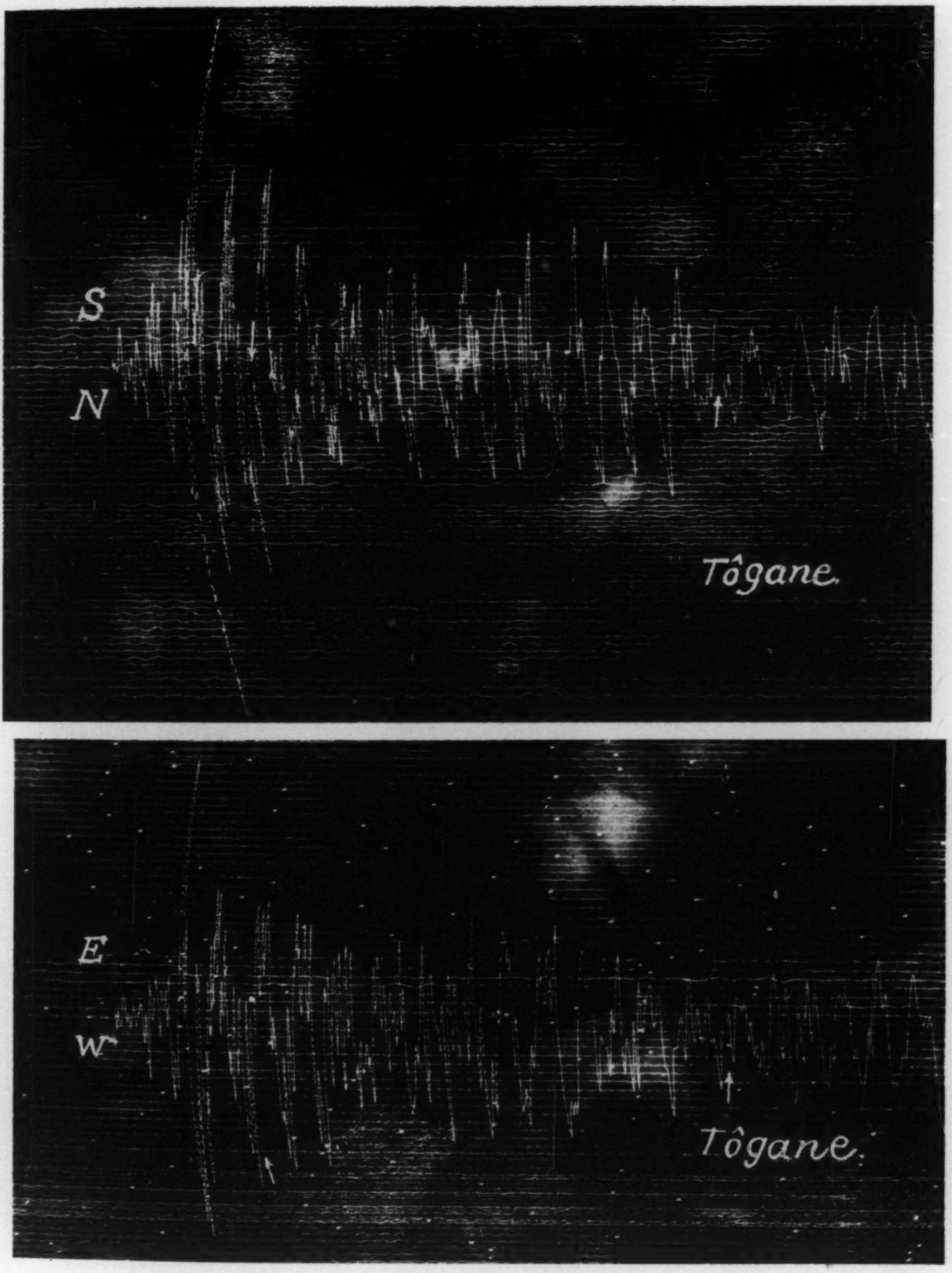

(震研彙報、第十號、圖版、震報)

Fig. 6. Tôgane observation of the earthquake of Nov. 12, 1931.
(Small arrow indicates minute-break.)
Instrumental constants: (See Fig. 4.)

(A)

(B)

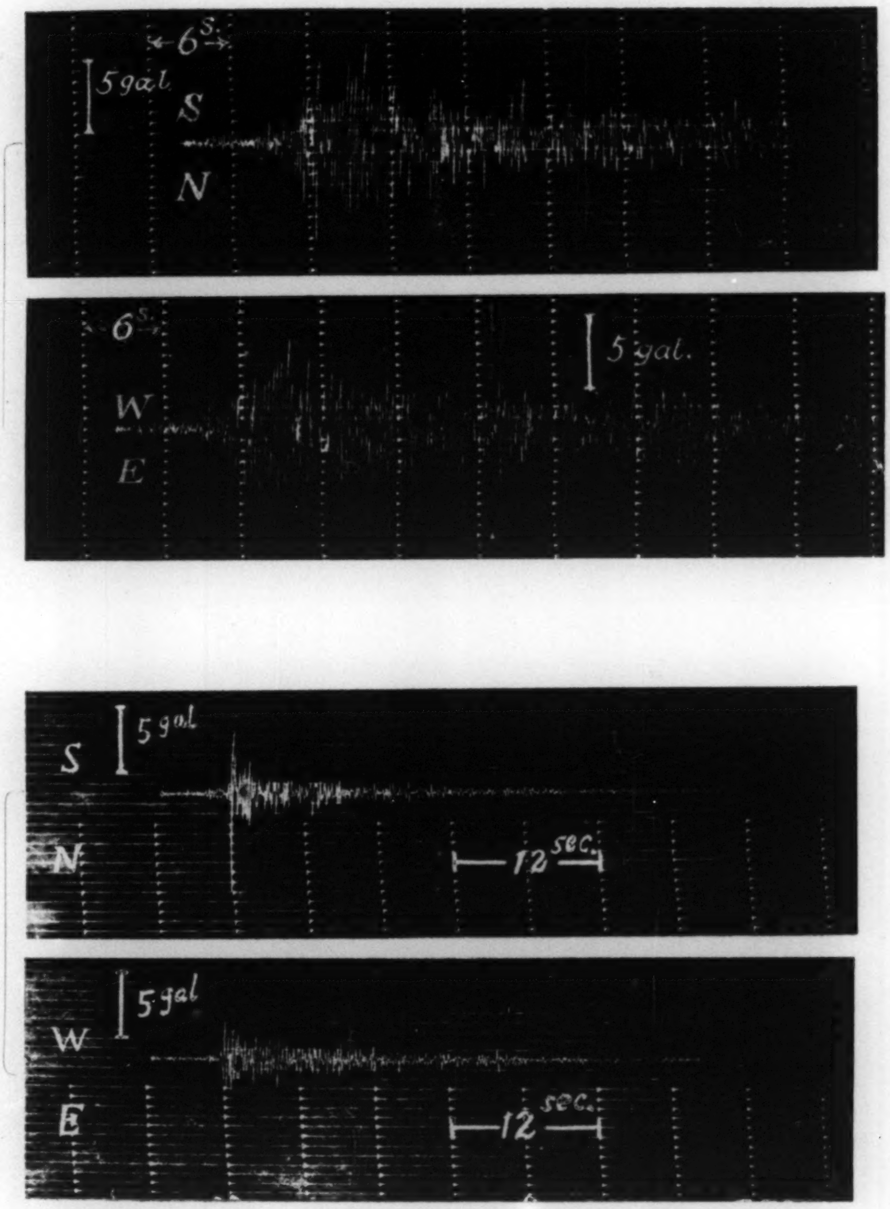

(震研彙報、第十號、圖版、震報)

Fig. 7. Tôkyô observations of the earthquakes of Oct. 3 (A) and Oct. 13. 1931 (B). Ishimoto acceleration seismograph diagrams.

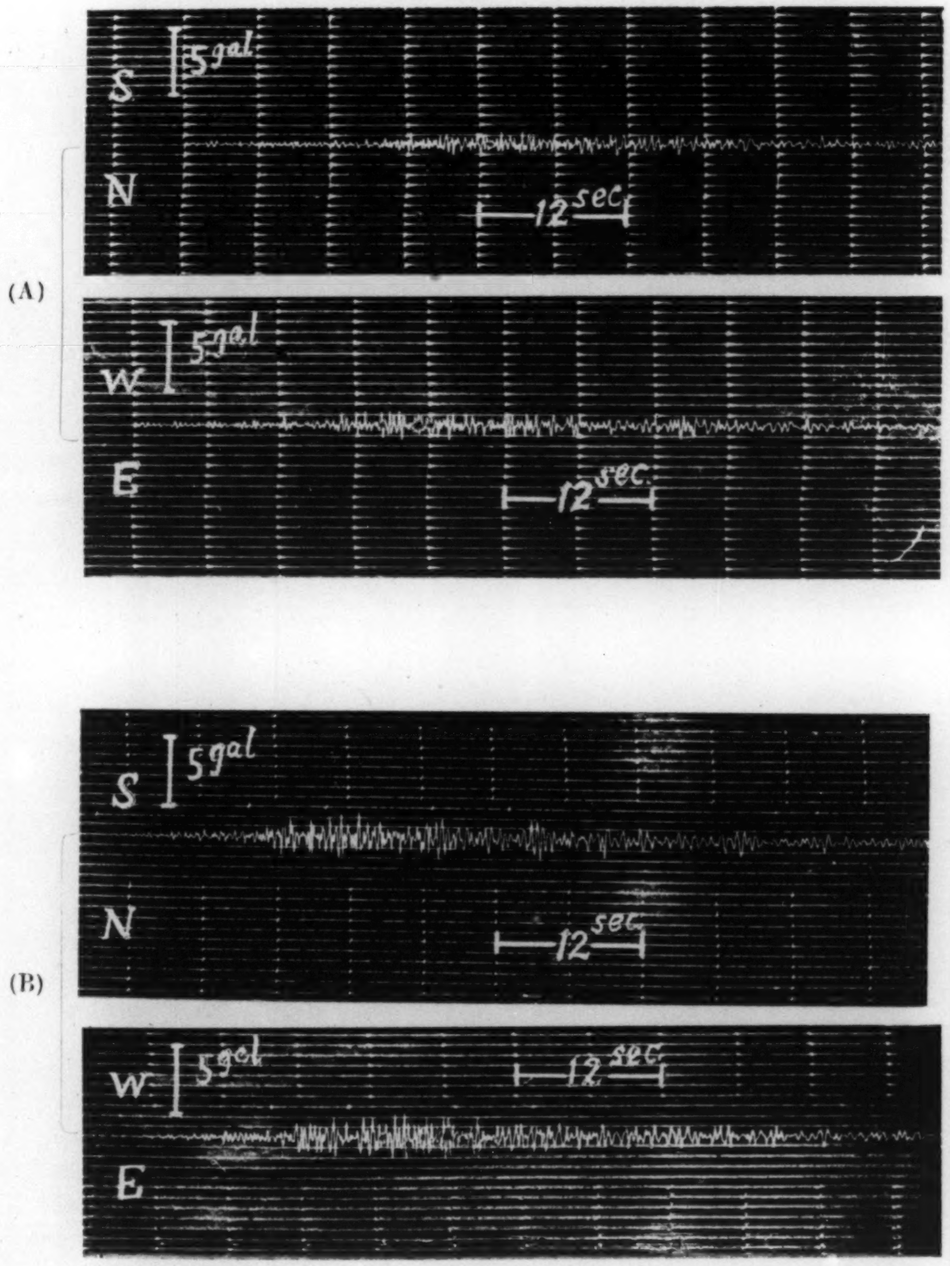

Fig. 8. Tôkyô Observations of the earthquakes of Oct. 30 (A) and Nov. 12 1931 (B). Ishimoto acceleration seismograph diagrams.

(震研彙報、第十號、圖版、震報)

LIBRARY OCT 4 1932 TOKYO

35. *Zwei merkwurdige Wellengruppen bei einigen Erdbeben in Kwantô und die dritte Mitteilung über den vorlaufenden Teil der Erdbebenbewegungen.*

von Takeo MATUZAWA und Takaharu FUKUTOMI.

(Vorgelegt am 17. Mai, 1932.—Eingegangen am 20. Juni, 1932.)

1. Zwei merkwürdige Wellengruppen beim Idu Bebenschwarm in 1930.

Bei fast allen in Tôkyô beobachteten Beben vom Idu Bebenschwarm, über den schon eine Menge Berichte[1] erschienen ist, hatten sich zwei verhältnismäßig langperiodische Wellengruppen gezeigt; z. B. Pl. LIX Fig. 2a. Im vorliegenden ist das Beginn der ersten Gruppe mit U_1 und das der zweiten mit U_2 bezeichnet.

Erstens muß es festgestellt werden, ob diese Bewegungen sich fortpflanzen oder stationär sind. Dazu kann man ohne weiteres Laufzeitverhältnisse benutzen. Die Verteilung der hier benutzten Stationen und die hier behandelten Bebenherde sind in Fig. 1 gezeigt.

---

1) Ausser von R. TAKAHASI zitierten Arbeiten (*Bull. Earthq. Res. Inst.*, 10 (1932) 143) noch;

Berichte über Nord-Idu Beben, *Kensindihô* (Berichte über Erdbeben), 5 (1931).

K. TANAHASI, *Kaiyô-Kisyôdai-Ihô*, 39 (1931), 1–34.

A. IMAMURA, *Bull. Earthq. Res. Inst.*, 9 (1931), 36–43; *Jap. Journ. Astr. Geophys.*, 8 (1930–31), 51–65.

K. SAGISAKA, *Geophysical Magazine*, 4 (1931), 147–155.

H. HONDA, *Geophys. Mag.*, 4 (1931), 185–213; 5 (1932), 69–88.

S. FUJIWHARA u. T. TAKAYAMA, *Gerl. Beitr. z. Geophys.*, 29 (1931), 131–137.

T. TERADA, *Bull. Earthq. Res. Inst.*, 10 (1932), 29–35.

EARTHQ. RES. INST., *Bull. Earthq. Res. Inst.*, 10 (1932), 261–263.

K. IHARA u. K. ISHII, *Journ. of Geography*, 44 (1932).

Geological Map of the North-Idu Earthquake District, *Journ. of Geography*, 44, Nr. 516 (1932).

R. TAYAMA, *Saitô Hôonkwai Hôkoku*, 11 (1931).

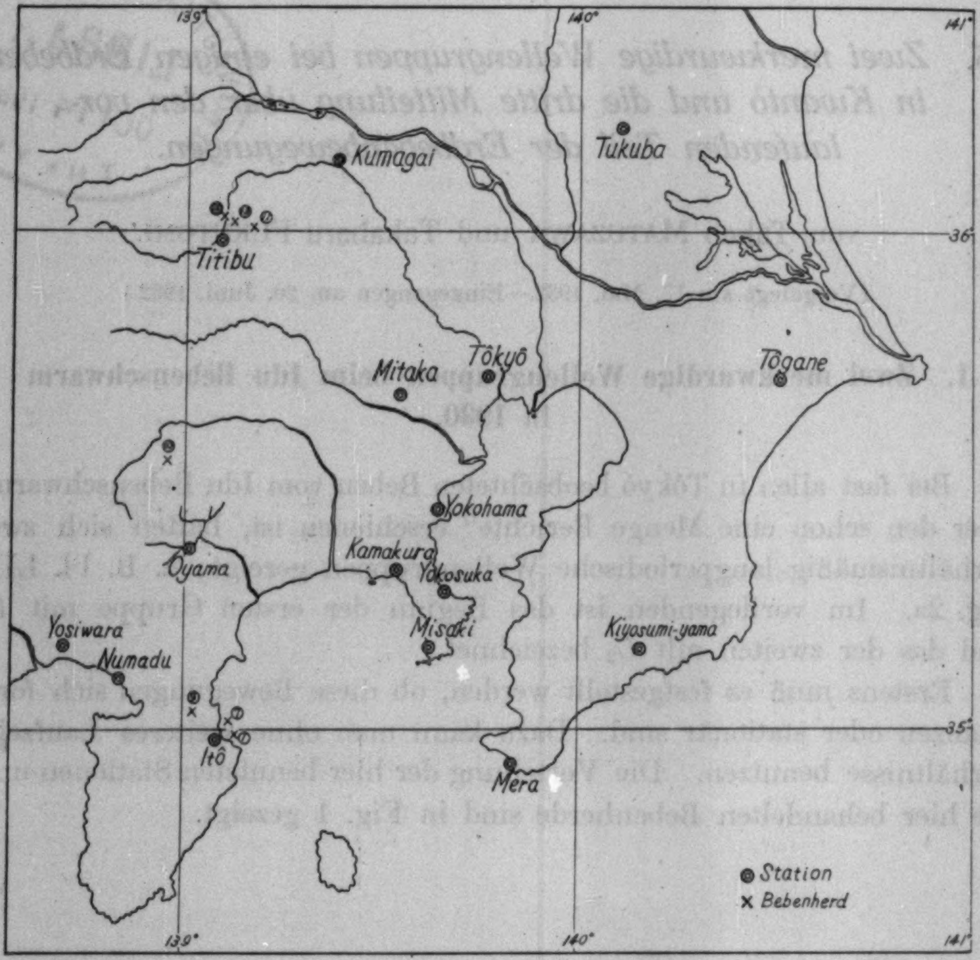

Fig. 1. Ziffer im Kreis bezieht sich auf die Bebennummer im Abschnitt 1 im Text. Alle Beben bis Nr. 6. stimmen beinah mit Nr. 1. überein.

(1) Beben von 1930 III 8. 19^h 54^m $48{\cdot}7^s$ (Hongô Beob.) (Pl. LX, LXI. Fig. 3a, b, c, d)

Tabelle I.

Station	**Kamakura**	**Mitakamura**	**Kiyosumi**	**Hongô (Tôkyô)**	**Tôgane**
Δ km	**51**	**89**	**94**	**97·5**	**146**
$P-U_1$	**15·9**	**25·1**	**26·4**	**33·0**	**41·3**
$P-U_2$	**36·6**	**56·9**	**Beginn unklar.**	**67·2**	**86·0**

P-U bedeutet die Zeitintervalle in Sekunde zwischen dem Beginn des Bebens und dem Anfang der genannten Wellengruppe. Die gegebene

Anfangszeit ist bis auf weiteres die in Hongô, Tôkyô.

(2) Beben von 1930 III 13. 4^h 29^m $44^s \cdot 7$ (Pl. LXII, LXIII, LXIV. Fig. 4a, b, c, d, e, f.)

Tabelle II.

Station	Kamakura	Mitaka	Kiyosumi	Hongô (Tôkyô)	Titibu	Tôgane
Δ	51	84	93	97·5	110	146
$P-U_1$	16·5	24·6	29·0(4·9)	27·6	39·1	48·3(4·0)
$P-U_2$	36·5(6·4)	56·0	58·5(4·9)	73·0		80·0(4·6)

Ziffern in klammern geben die herrschenden Perioden in der Gruppe. In diesem Falle beobachteten wir in Tôkyô noch eine große Bewegungsgruppe U_1' (Pl. LXII. Fig. 4a), $P-U_1'=42\cdot2$ s.

(3) Beben von 1930 III 15. 18^h 34^m 37^s (Pl. LXV, LXVI, LXVII. Fig. 5a, b, c, d, e, f)

Tabelle III.

Station	Misaki	Kamakura	Mitaka	Kiyosumi	Hongô (Tôkyô)	Titibu
Δ	47	51	84	93	97·5	110
$P-U_1$	15·0	Beginn unklar	25·6	25·0	$P-(U_1)$ 44·5(5·3)	37·3(1·9)
$P-U_2$	Beginn unklar	36·5		unklar		

Seismogramme dieses Bebens zeigten besonderes Aussehen als andere Itô-beben. Typisch ist der deutliche Eintritt und die Entwickelung der *S* phase. Die Vermutung liegt nahe, daß der Entstehungsmechanismus dieses Bebens anders als der der anderen wäre.

(4) Beben von 1930 III 21. 23^h 4^m $23^s \cdot 6$.

Tabelle IV.

Station	Kamakura	Mitaka	Hongô (Tôkyô)
Δ	51	84	97
$P-U_1$	16·7	27·0	Beginn unklar
$P-U_2$	Beginn unklar	56·5	72·0

(5) Beben von 1930 III 22. 17^h 50^m $51^s 7$ (Pl. LXVIII. Fig. 6)

Dieses Beben war das allerstärkste vom Itô Bebenschwarm und von S. Sagisaka[2] ausführlich studiert worden. Wegen der Heftigkeit der Erschütterung wurden alle empfindliche Seismographen aus der Ordnung gebracht, und nur Apparate von niedriger Vergrößerung war benutzbar. Wir konnten darum nur Tôkyô Beobachtung ablesen.

Tabelle V. (Tôkyô)

Δ	$P-U_1$	$(P-U_1')$	$P-U_2$
97 km	$28{\cdot}6^s$ $(7{\cdot}75^s)$	$33{\cdot}3^s$ $(7{\cdot}75^s)$	71^s $(6{\cdot}8^s)$

(6) Beben von 1930 III 30. 0^h 6^m $36{\cdot}7^s$.

Tabelle VI.

Station	Kamakura	Mitaka	Kiyosumi	Hongô (Tôkyô)
Δ	51	84	93	97
$P-U_1$	18·3	25·2	28·2(4·78^s)	30·0(3·62)
$P-U_2$	37·0	unklar	53·3(3·8)	72·0(7·75)

(7) Beben von 1930 IV 1. 23^h. (Pl. LXIX, LXX. Fig. 7a, b)

Tabelle VII.

	Misaki	Hongô (Tôkyô)
Δ	47 km	96·0 km
$P-U_1$	$15{\cdot}3^s$	$29{\cdot}6^s$
$P-U_2$	$32{\cdot}2^s$	69·0
		$P-U_3$ 119

U_1 von Misaki ist durch große Schwingungen bedeckt und nicht feststellbar. U_3 in Tôkyô Aufnahme (besonders in der vertikalen Komponente) ist merkwürdig.

2) S. SAGISAKA, *Geophysical Magazine*, 4 (1931), 147-155.

(8) Beben von 1930 V 12. 21^h.

Nur Kamakura Beobachtung war benutzbar.

Tabelle VIII.

Δ	$P-U_1$	$P-U_2$
51 km	$16{\cdot}6^s$	Anfang nicht feststellbar

(9) Beben[3] von 1930 XI 25. $16^h\ 6^m\ 9{\cdot}9^s$ (Herd, nahe bei Ukihasi) (Pl. LIX. Fig. 2a, b.)

Der Herd dieses Bebens ist ziemlich entfernt von denen der oben erwähnten und doch die Entwickelung der genannten Wellengruppen ist musterartig, wie man leicht aus Fig. 2a, b, ersehen kann.

Tabelle IX.

Station	Kamakura	Hongô (Tôkyô)
Δ	56·5	101·5
$P-U_1$	13·7 (6·6)	33·5 (9·3)
$P-U_2$	31·0 (4·1)	66·5 (5·7)

2. Ähnliche Wellengruppen bei einigen anderen Beben.

Es kommt nun in Frage, ob sich diese Wellengruppen bei Beben in anderen Gegenden auch entwickeln können. Daran können wir mehrere gute Beispiele geben wie folgt.

(10) Beben[4] von 1931 VI 11. $15^h\ 16^m\ 19{\cdot}9^s$ (Pl. LXXI, LXXII, Fig. 8a, b, c.)

Dieses Beben war von bedeutender Stärke, darum bei Stationen, die sich nur mit empfindlichen Seismographen versehen haben, konnten wir wegen zu großer Eigenbewegungen der Apparate nicht solche Wellengruppen genau abmessen, obgleich große Wellenschwebungen in ent-

3) A. Imamura, *Bull. Earthq. Res. Inst.*, 9 (1931), 36–43; *Jap. Journ. Astr. Geophys.*, 8 (1930-31), 51-65.

4) N. Nasu u. Ch. Yasuda, *Bull. Earthq. Res. Inst.*, 9 (1931), 511.

sprechenden Lagen in den Seismogrammen wahrgenommen wurden. Wir finden seinen Herd beinah in derselben Lage wie N. Nasu[5] und Ch. Yasuda. (Fig. 1.) Trotzdem könne man in Fig. 8 Existenz der genannten Wellengruppen leicht bemerken.

Tabelle X.

Station	Titibu	Hongô	Tôgane
Δ km	15	76	142
$P-U_1$	Anfang unklar	25	47·5
$P-U_2$	33·2	49·3	Bewegung zu groß zur genauen Messung

(11) Beben von 1931 IX 23. 21^h 46^m 19^s (Pl. LXXIII, LXXIV. Fig. 9a, b, c, d, e, f.)

Tabelle XI.

Station	Mitaka	Hongô	Oyama	Kamakura	Yosiwara	Tôgane
Δ km	50	63	73	83	104	125
$P-U_1$	16 (5·0)	22	21·4	Anfang unklar	33·7	38·6
$P-U_2$	33	38·9	51·5	55·0	unklar	88·5
		U_3 60·0 (5·0)				

(12) Beben von 1931 IX 24. 1^h 22^m $41{\cdot}1^s$ (Pl. LXXV, LXXVI. Fig. 10a, b, c, d, e).

Tabelle XII.

Station	Mitaka	Hongô (Tôkyô)	Misaki	Yosiwara	Oyama	Tôgane	Kiyosumi
Δ km	57	70	107	104	74	133	136
$P-U_1$	15·9	25·2	unklar	unklar	unklar	42·8	unklar
$P-U_2$	39·0	45·7				89·5	
		U_3 55·0					

(13) Beben von 1931 IX 24. 21^h 11^m $26^{\cdot s}$ (Pl. LXXVII, LXXVIII. Fig. 11a, b, c, d, e, f).

5) N. NASU u. Ch. YASUDA, *loc. cit.*

Tabelle XIII.

Station	Mitaka	Hongô (Tôkyô)	Oyama	Kamakura	Misaki	Tôgane
Δ km	54	68	73	86	105	130
$P-U_1$	17·5	22·0	23·0	unklar	33·8	unklar
$P-U_2$	37·4	41·0	50·0		unklar	89·0
		$U_3$66·0 $U_4$80·6 (Vertikal)				

Diese drei Beben[6] sind Beispiele der Nachbeben, die dem starken Beben[7] vom 21. Sept. 1931 folgten, welches den westlichen Teil von Kwantô heimsuchte und durch welches Hunderter von Menschen umgekommen war. Bei diesen Fällen ist Bestimmung der Herde ungenauer als beim Idu Bebenschwarm, weil die Verteilung der Stationen ungünstiger war als beim vorigen Falle. (Fig. 1)

Wie in Figuren (9, 10, 11) ganz anschaulich gezeigt sind, können wir wieder merkwürdige Wellengruppen finden, die man den U_1 and U_2 Gruppen im vorigen Falle entsprechen lassen kann. Wir wollen also vorläufig diese Wellengruppen als dieselbe wie im vorigen Falle ansehen und deren Laufzeitkurven konstruieren.

3. Laufzeitkurven.

In Fig. 12 sind $P-U_1$ (Kreis) und $P-U_2$ (Dreieck) als Ordinate und Herdentfernung als Abszissa eingetragen. Man sehe, daß diese Bewegungen sich fortzupflanzen scheinen. Also wenn man Laufzeitkurve für P-Wellen weiß, dann kann man respektive Kurven für U_1 und U_2 finden.

Laufzeit von P-Wellen beim Nord-Idu Beben von 1930 XI 26. 4^h 02^m ist schon von H. Honda[8] und K. Sagisaka[9] studiert worden. Die Laufzeit beim Itô Beben von 1930 III 22. 17^h 50^m ist außer denselben Autoren auch von K. Hayata[10] studiert worden. Insofern es die beobachteten Materialien anbetrifft, abgesehen von ihren Methoden der Analyse, dürfen wir ruhig innerhalb der Messgenauigkeit ihre Resultate benutzen.

6) N. Nasu und Ch. Yasuda, *Bull Earthq. Res. Inst.*, 10 (1932), 268-269; H. Honda, *Geophys. Mag.*, 5 (1932), 69-88.
7) N. Nasu, *Disin* (Erdbeben), 3 (1931), 27-36.
8) H. Honda, *Kensindihô*, 5 (1931), 93-109.
9) K. Sagisaka, *Kensindihô*, 5 (1931), 55-92; *Geophys. Mag.*, 4 (1931), 185-213.
10) K. Hayata, *Kensindihô*, 5 (1931), 155-170.

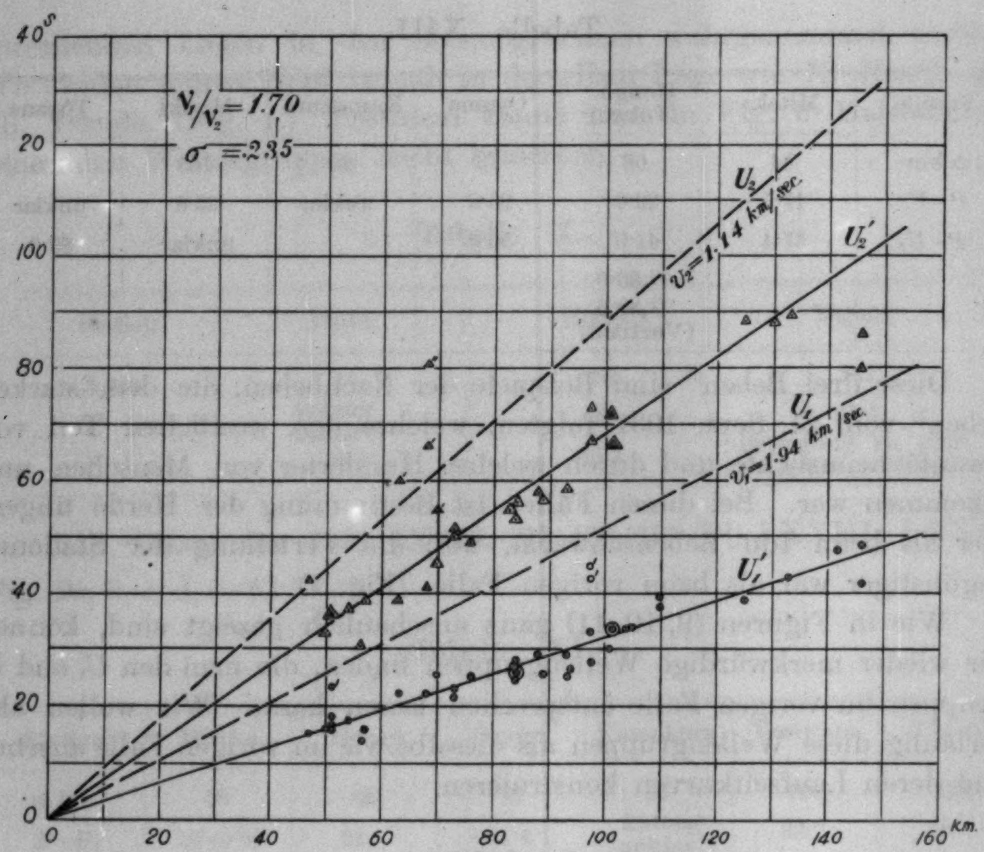

Fig. 12.

Nach H. Honda ist die Laufzeit des Nord-Idu Bebens vom 1930 Nov. 26 wie folgt.

Tabelle XIV.

Δ km	0	10	20	30	40	50	60	70	80	90	100
T sec	0·0	2·8	5·2	7·4	9·5	11·5	13·4	15·1	16·8	18·4	19·9

Damit haben wir Laufzeitkurven für U_1 und U_2 konstruieren können (Fig. 12). Die scheinbare Fortpflanzungsgeschwindigkeiten jeder Gruppe kommen respektiv als $U_1 = 1{\cdot}94$ km/sek. und $U_2 = 1{\cdot}14$ km/sek. heraus, weil sich es dabei ungefähr um geradlinige Kurven handelt.

4. Deutung der U_1 und U_2 Wellengruppen.

Legt man sich die Frage vor, in welcher Weise diese Bewegungen zutage treten, so ist zweierlei denkbar; erstens ließen sie sich respektiv

als Dilatations- und Scherungswellen in einer oberen Schicht deuten, die von ähnlicher Natur sein möge, wie wir[11] einmal vorausgesetzt hatten, zweitens könnten sie Oberflächenwellen vom Love-typ und Rayleigh Typ in geschichteter Erdoberfläche sein.

Existenz solcher oberflächlichen Schicht in Kwantô scheint uns ganz wahrscheinlich, abgesehen von Zahlenwerten, die wir damals angenommen hatten. E. Wanner[12] bestätigte die Verwandtschaft zwischen seismologisch beobachteten Tatsachen ähnlich wie bei uns und der geologisch bekannten Molassenschicht in der Nähe von Zürich.

Nun im Falle, daß sich die Störungsquelle in solcher Schicht befindet, ist die erste Möglichkeit ohne weiteres klar. In der Tat schienen alle die oben erwähnten Beben von geringer Herdtiefe zu sein. (Manchmal geringer als 1 km geschätzt.)

Der zweite Fall ist theoretisch ziemlich kompliziert zu behandeln. Ohne Schichtung ist die Entstehung der Love-Wellen im homogenen Medium überhaupt unmöglich. Dispersion der Rayleigh-Wellen ist auch nicht der Fall, abgesehen von H. Nakano[13] behandelten besonderen Fall. Also wenn man mehrere Wellenzüge mit verschiedener Fortpflanzungsgeschwindigkeit behandeln soll, ist die Voraussetzung der Schichtung unbedingt notwendig. Im geschichteten Medium unterliegen beide Love- und Rayleigh Wellen[14] der Dispersion.

Insofern es den Formalismus anbetrifft, weil die Dispersionsformen der beiden Wellen ähnlich sind (Fig. 13a, b.), können wir uns der Resultate von K. Sezawa[15] und G. Nisimura bedienen, die sie von einer Sorte Welle berechneten, unter der Annahme, daß das Amplitudenverhältnis der vertikalen Komponente zur horizontalen unabhängig von der Wellenlänge sei.

Nach ihnen beschränken sich die Wellenzüge nur im Wellenbereich zwischen der mit Geschwindigkeit in der unteren Schicht sich fortpflanzenden Welle und der Welle mit Geschwindigkeit in der oberen Schicht. Dort ist auch gezeigt, daß eine besondere Welle mit bestimmten Wellenlänge herrscht, die durch die Dispersionsverhältnisse der Medien bestimmt wird.

Einer[16] von uns studierte einmal die Fortpflanzung der Erdbeben-

11) T. Matuzawa, K. Hasegawa u. S. Haeno, *Bull. Earthq. Res. Inst.*, 4 (1928), 85–106.
12) E. Wanner, *Gerl. Beitr. z. Geophys.*, 32 (Köppen Bd. 1) (1931), 231–241.
13) H. Nakano, *Geophys. Mag.*, 1 (1928), 255–303.
14) K. Sezawa, *Bull. Earthq. Res. Inst.*, 3 (1927), 1–18.
15) K. Sezawa u. G. Nishimura, *Bull. Earthq. Res. Inst.*, 8 (1930), 330–335.
16) T. Matuzawa, *Bull. Earthq. Res. Inst.*, 5 (1928), 1–27.

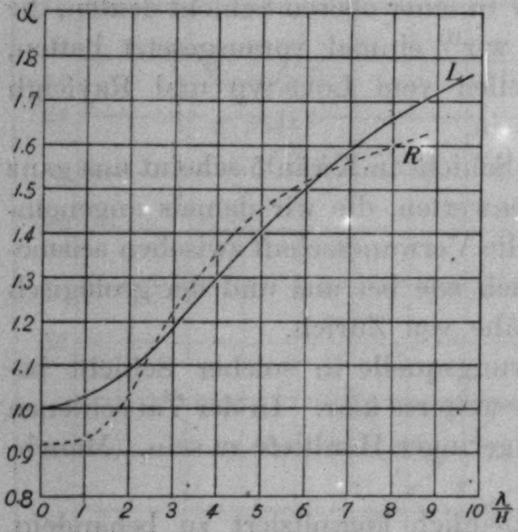

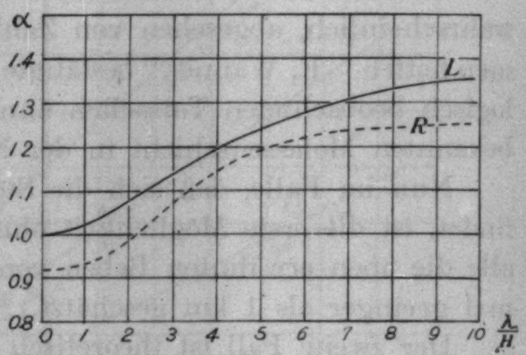

Fig. 13 a. $\left(\frac{\mu_1}{\mu_2}=\frac{1}{5}\ \rho_1=\rho_2,\ \lambda_1=\mu_1,\ \lambda_2=\mu_2\right)$ Fig. 13 b. $\left(\frac{\mu_1}{\mu_2}=\frac{1}{2},\ \rho_1=\rho_2,\ \lambda_1=\mu_1,\ \lambda_2=\mu_2\right)$

Dispersion der Rayleigh (R)- und Love (L) Wellen. α : Geschwindigkeit (Einheit; Geschw. der Scherungswelle in der oberen Schicht.) λ : Wellenlänge. H: Schichtdicke.

wellen in Japan und die Fortpflanzungsgeschwindigkeit der $\overline{P}$ Welle ergab sich zu 5·0 km/sek, die der $\overline{S}$ zu 3·15 km/sek. Also ohne Voraussetzung noch einer dünnen Schicht mit kleiner Wellengeschwindigkeiten kann man überhaupt nicht die U_1 und U_2 Wellen erklären, wenn man sie auf die Oberflächenwellen beziehen will.

Im Falle wie in der vorher erwähnten ersten Möglichkeit wollen wir natürlich nicht die Ko-existenz der Oberflächenwellen ausschließen. Allerdings ist das ganze durch Seismographen registrierte Ensemble nichts anders als ein Potpourri der Körperwellen, Oberflächenwellen, der durch Körperwellen induzierten Oberflächenschwingungen (sich nicht selbständig fortpflanzende Welle) von H. Nakano,[17] der durch mosaikartige Struktur der Erdkruste erzeugten Wiederhallen[18] u. s. w.

Was die U_1 und U_2 Wellen anbelangt, halten wir die erste Möglichkeit für wahrscheinlicher als die zweite, weil das Verhältnis der Fortpflanzungsgeschwindigkeit der U_1 Welle zu der der U_2, 1·70, schwierig zu erklären ist mit der Annahme der Oberflächenwellen. Von der Bewegungsrichtungen der Bodenteilchens wollen wir hier nichts sagen, da die Korrektur der hier gebrauchten Seismogramme etwas schwierig und

17) H. NAKANO, *Jap. Journ. Astr. Geophys.*, **2** (1925), 233–326.
18) K. SEZAWA u. G. NISHIMURA, *Bull. Earthq. Res. Inst.*, **8** (1930), 323–330.

unsicher ist, besonders wenn sich die Bewegungen in der Mitte des gestörten Teils des Seismogrammes befinden.

5. Ergänzung zur $P-P_1$ Beobachtung und Umrechnung der auf die obere Schicht in Kwantô bezogenen Zahlenwerte.

Als wir[19] vor einigen Jahren dieses Problem behandelt hatten, hatten wir keine Idee von makroskopischen Werten, d. h. effektiven Werten der Fortpflanzungsgeschwindigkeit jeder Wellen in der genannten Schicht, darum hatten wir damals vorläufig die durch Laboratoriumsexperiment bestimmten Zahlenwerte als solche angenommen. Jetzt wollen wir die Werte für U_1 und U_2 nämlich 1·94 km/sek. und 1·14 km/sek. respektiv als Geschwindigkeit der Dilatations und der Scherungswelle in der Schicht annehmen. Dann müssen wir den damaligen Wert der Schichtdicke ändern. Die Methode der Rechnung kann dasselbe sein.

Zuerst möchten wir hier das Beobachtungsmaterial ergänzen. Damals hatten wir die P_1 Phase nur in Tôkyô und Kamakura beobachtet. In Kwantô stehen heutzutage neun Stationen zu unser Verfügung. Darum sind wir jetzt imstande, etwas allgemeineres von der Phase zu sprechen. In der nachstehenden Tabelle (Tabelle XV) sehen wir die $P-P_1$ Dauer auf verschiedener Station.

Tabelle XV.

$P-P_1$ Dauer in Sekunde.

Die gestrichene Nummer bezieht sich auf die im ersten Abschnitt erwähnten Beben.

Beben		Tôkyô	Kamakura	Mitaka	Misaki	Titibu	Tôgane	Kiyosumi	Yosiwara (vorläufig)
1	1930 II 21 8h			1·68					
2	III 4 3h			1·35					
3	III 4 5h			1·36					
4, 1′	III 9 4h		1·25	1·29					
5, 2′	III 13 4h			1·47	1·3				
6	III 14 14h	1·45	1·20	1·45	1·15				
7, 3′	III 15 18h	1·55			1·05				
8	III 19 10h	1·6		1·47	1·63				
9, 4′	III 21 23h	1·71	1·15	1·8	1·32				

(*Fortsetzung folgt.*)

19) T. Matuzawa, K. Hasegawa u. S. Haeno, *Bull. Earthq. Res. Inst.*, 4 (1928), 85–106.

Tabelle XV. (*Fortsetzung.*)

Beben		Tôkyô	Kamakura	Mitaka	Misaki	Titibu	Tôgane	Kiyosumi	Yosiwara (vorläufig)
10, 5′	III 22 17h	1·35							
11	III 26 14h		1·46						
12	III 27 1h		1·41						
13, 6′	III 30 0h		1·37	1·38	1·47				
14, 7	IV 1 23h	1·54		1·50	1·68				
15	V 10 2h				1·7				
16, 8′	V 12 21h		1·2			1·54			
17	V 17 5h					1·30		1·65	
18, 9′	XI 25 16h	1·45	1·27						
19, 10′	1931 VI 11 15h						1·5		
20, 11′	IX 23 21h			1·5			1·63		
21, 12′	IX 24 1h			1·32				1·2	1·56
22, 13′	IX 24 21h			1·8			1·75		
Mittel		1·52	1·29	1·49	1·41	1·42	1·62	1·42	1·56

Der Mittelwert für alle Stationen ergiebt sich zu 1·47 sek.

Wir sehen also, daß diese Erscheinung in fast allen Teilen von Kwantô beobachtet wird, abgesehen von Tukuba, wo wir noch nicht sie feststellen kann und zwar die Station auf einem Granitmassive steht. Merkwürdig ist der kleine Wert, 1·29 sek. für Kamakura. Es ist auch ganz bemerkenswert, daß die genannte Phase sich in solcher Stationen wie Tôkyô, Mitaka, Tôgane, ganz deutlich entwickelt, wo sie auf lockeren Boden stehen.

Da unsere Fälle sich um kleine Herdtiefe handeln, können wir die Schichtdicke unter der Voraussetzung des kritischen Einfalswinkels an der unteren Grenze der Schicht berechnen. Die $P-P_1$ Dauer ${}_P\tau_{P_1}$ wird gegeben durch

$$ {}_P\tau_{P_1}=d\left\{\frac{1}{U_2\cos i_{PS}}-\frac{1}{U_1\cos i_{PP}}+\frac{1}{v_1}(\tan i_{PP}-\tan i_{PS})\right\}, $$

worin d, Schichtdicke; U_1, Geschwindigkeit der P Welle in der oberen Schicht; U_2, Geschwindigkeit der S Welle in der oberen Schicht; v_1, Geschwindigkeit der P Welle in der unteren Schicht; $\sin i_{PP}=\frac{U_1}{U_2}$; $\sin i_{PS}=\frac{U_2}{v_1}$; $\sin i_{SS}=\frac{U_2}{v_2}$;

v_2, Geschwindigkeit der S Welle in der unteren Schicht.

Nun haben wir

$v_1 = 5{\cdot}0$ km/sek., $v_2 = 3.15$ km/sek., $U_1 = 1{\cdot}94$ km/sek, $U_2 = 1{\cdot}14$ km/sek.

Daraus kommen heraus

$\sin i_{PP} = 0{\cdot}388$,	$\sin i_{PS} = 0{\cdot}228$,	$\sin i_{SS} = 0{\cdot}362$
$i_{PP} = 22°50'$,	$i_{SP} = 13°10'$,	$i_{SS} = 21°13'$
$\cos i_{PP} = 0{\cdot}922$,	$\cos i_{PS} = 0{\cdot}974$,	$\cos i_{SS} = 0{\cdot}922$
$\tan i_{PP} = 0{\cdot}421$,	$\tan i_{PS} = 0{\cdot}216$,	$\tan i_{SS} = 0{\cdot}388$.

Also $d = 3{\cdot}83$ km.

Dieser Wert ist erheblich kleiner als der damalige Wert 7·0 km. Nun tritt eine wichtige Frage auf, wie wir die damals beobachtete dritte phase[20], die durch „3" gekennzeichnet und als (SP) Welle gedeutet wurde, andeuten sollen.

Wäre die „3" Phase (SP) Welle, müsste laut dieser Zahlenwerte die „3"—S Dauer für Herdentfernung auch ungefähr konstant sein. Wir hätten besser diese Phase als solche[21] ähnlich irgend einer der $PP^*\overline{S}$, $P^*\overline{S}$, $P^*PP^*\overline{S}$, $\overline{P}P^*\overline{S}$, oder $\overline{P}P^*PP^*\overline{S}$ deuten sollen. Um Mißverständnis zu vermeiden, möchten wir hier hinzufügen, daß wir damit nicht dieselbe Phase sondern nur ähnlichen Mechanismus meinen.

In Horizontalkomponenten muß bei den Wechselwellen die Welle, die an die Oberfläche als S Welle eintritt, viel deutlicher sein als die, die als P eintritt und umgekehrt in Vertikalkomponenten, weil der Emergenzwinkel sehr groß (beinah vertikal) werden soll, besonders wenn sich die Station auf lockeren Boden befindet, wie wir schon einmal bemerkt hatten.[22]

Tatsächlich konnte S. Haeno[23] zwei ganz kleine Fortpflanzungsgeschwindigkeitsgruppen in der Nähe von der Universitätsstation in Hongô, Tôkyô, finden. Ganz neu hat T. Suzuki[24] auch eine ähnliche Tatsache durch Messung des wirklichen Emergenzwinkels der Erdbebenwellen an der Oberfläche festgestellt. M. Hasegawa's Kritik[25] an diesen Punkt ist natürlich nicht der Fall, weil er nicht die Brechung der S

---

20) T. Matuzawa, K. Hasegawa u. S. Haeno, *Bull. Earthq. Res. Inst.*, 4 (1928), 85–106.

21) T. Matuzawa, K. Yamada u. T. Suzuki, *Bull. Earthq. Res. Inst.*, 7 (1929), 241–260.

22) T. Matuzawa, K. Hasegawa u. S. Haeno, *Bull. Earthq. Res. Inst.*, 4 (1928), 102.

23) S. Haeno, *Jap. Journ. Astr. Geohys.*, 8 (1931), 39–50.

24) T. Suzuki, *Bull. Earthq. Res. Inst.*, 10 (1932), 517–530.

25) M. Hasegawa, *Zeits. f. Geophys.*, 6 (1930), 94.

Welle behandelte. In anderen Worten hätte er weitere Brechungen der (*PP*) und (*PS*) Wellen vergleichen sollen. Tatsächlich tritt die P_1 phase ganz deutlich auf bei Stationen auf lockerem Boden wie Tôkyô, Mitaka oder Tôgane. Damit ist es auch verständlich, daß nach E. Wanner[26] in Zürich $i_2 = SP$ nur selten identifiziert werden kann trotz der außerordentlichen Deutlichkeit der (*PS*) Phase.

6. Andere Bestätigung mit (*P*−*S*) Dauer beim Itô-Bebenschwarm.

Beim Itô Bebenschwarm in 1930 konnten wir den Bebenherd genau (ungefähr ±2 km) finden, darum lieferte er eine günstige Gelegenheit die (*P*−*S*) Dauer als Funktion der Herdentfernung genau zu studieren. Die auf mehrere Stationen beobachtete (*P*−*S*) Dauer wird in der folgenden Tabelle gezeigt. (Tabelle XVI).

Tabelle XVI.

(*P*−*S*) Dauer beim Itô Bebenschwarm von 1930. Die erste Ziffer, (*P*−*S*) Dauer in sek.; die zweite, Herdentfernung in km.

Erdbeben				Misaki	Kamakura	Mitaka	Kiyosumi	Tôkyô	Titibu
1930	II	21	8h			12·6; 84			
	III	4	3h			11·4; 〃			
	III	4	5h			11·1; 〃			
	III	9	4h		8·31; 51	12·0; 〃			
	III	9	19h		8·55; 〃	10·9; 〃	11·7; 94	13·3;97·5	
	III	13	4h	7·3 ; 49	8·47; 〃		13·1; 93	12·3; 〃	
	III	14	14h	7·5 ; 〃	8·25; 〃	11·5; 〃			12·6;110
	III	15	18h	8·1 ; 〃	8·05; 〃	11·7; 〃	13·0;93·5	14·4; 〃	13·7; 〃
	III	19	10h	7·46; 〃	7·92; 〃	12·3; 〃		11·8; 〃	13·5; 〃
	III	21	23h	7·25; 〃	8·26; 〃	12·8; 〃		14·5; 〃	13·2; 〃
	III	22	17h					13·5; 〃	
	III	26	14h		8·77: 〃			14·1; 〃	
	III	27	1h		8·48; 〃				
	III	30	0h	7·35; 49	8·4 ; 〃	11·7; 84	12·5; 93	13·75;97·5	
	IV	1	23h	7·95; 47		11·8; 81	11·6; 95	13·05;96·0	13·3;105
	V	10	2h	6·6 ; 49	8·5 ; 51				
	V	12	21h	7·3 ; 〃					13·3;110
	V	17	5h				11·0; 93		14·05; 〃

26) E. WANNER, *Gerl. Beitr. z. Geophys.*, **32** (Köppen Bd. 1) (1931), 231.

Nun wollen wir eine lineare Gleichung zwischen Herdentfernung und $(P-S)$ Dauer, $\Delta=a\tau+b$, bestimmen, und zwar innerhalb 90 km Herdentfernung; denn wir müssen Verwechselung der Phasen mit P^*, S^*, u. s. w. vermeiden. Mit der Methode der kleinsten Quadrat sind a und b als $a=8{\cdot}02$ und $b=12{\cdot}74$ km bestimmt. (Fig. 14).

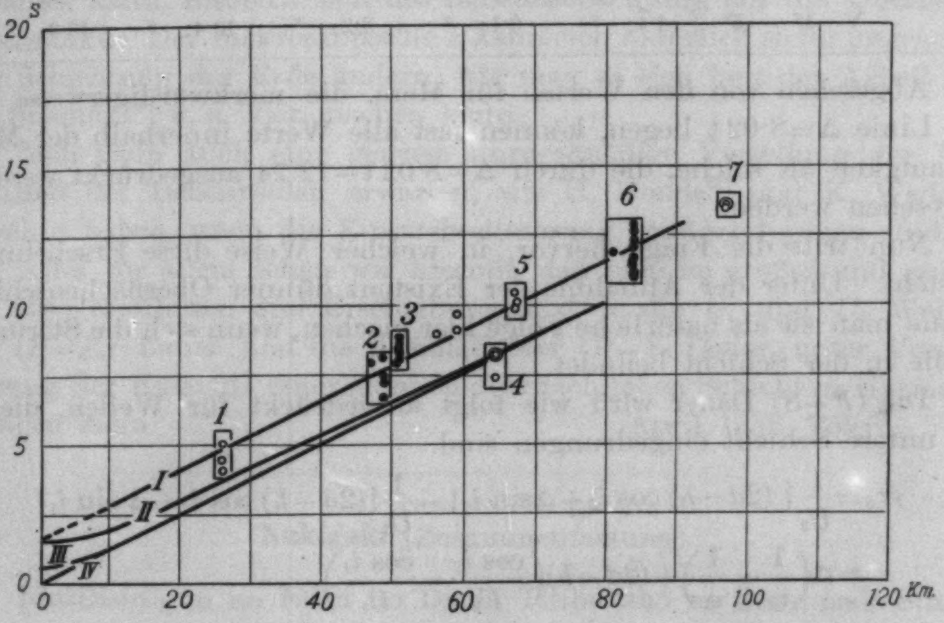

Fig. 14.

Kurve	I;	$\Delta=8{\cdot}02\,t-12{\cdot}74$,	Gruppe 1;	Numadu,	Gruppe 5;	Yokohama,
„	II;	$\sqrt{\Delta^2+12^2}=8{\cdot}02\,t$,	„ 2;	Misaki,	„ 9;	Mitaka,
„	III;	$\sqrt{\Delta^2+4^2}=8{\cdot}02\,t$,	„ 3;	Kamakura,	„ 7;	Tôkyô.
„	IV;	$\Delta=8{\cdot}02\,t$,	„ 4;	Mera,		

Es ist ganz merkwürdig, daß für $\Delta=0$, $\tau=1{\cdot}59$ sek, oder man kann genauer so sagen, daß diese Linie parallel zur Linie $\Delta=8{\cdot}02$ t (Kurve IV in Fig. 14) und zwar um 1·59 Sekunden später läuft. Diese Erscheinung kann nicht durch den Einfluß der Herdtiefe zu tage treten, wie Kurven III (Herdtiefe 4 km), II (Herdtiefe 12 km) deutlich zeigen. Hier muß die Rede sein, daß Misaki Werte kleiner und Kamakura Werte größer als Mittelwert sind.

Um dogmatischen Schluß zu vermeiden, wollen wir auch auf die vom Zentral Meteorologischen Institute veröffentlichten Wert[27] achtgeben. In Fig. 14 sind sie mit Kreis eingetragen worden. In Ziffern ergeben sie sich in der folgenden Tabelle. (Tabelle XVII)

27) *Kisyôyôran* (1930).

Tabelle XVII.

Erdbeben				Numadu	Yokosuka	Mera	Yokohama	Tôkyô
1930	III	9	19h	4·1; 26·1		8·2; 64·6	10·0; 67·4	13·5; 96·9
	III	22	17h	5·0; 〃	9·7; 59·1	7·3; 〃	9·8; 〃	13·4; 〃
	V	17	5h	4·4; 〃	9·1; 〃	8·2; 〃	10·4; 〃	13·6; 〃

Abgesehen von den Werten für Mera, die merkwürdigerweise auf der Linie $\Delta=8{\cdot}02\,t$ liegen, können fast alle Werte innerhalb der Meßgenauigkeit als solche, die durch $\Delta=8{\cdot}02\,t-12{\cdot}74$ ausgedrückt werden, angesehen werden.

Nun tritt die Frage hervor, in welcher Weise diese Erscheinung entsteht. Unter der Annahme der Existenz dünner Oberflächenschicht könne man sie als natürliche Folge klar machen, wenn sich die Störungsquelle in der Schicht befindet.

Die $(P-S)$ Dauer wird wie folgt ausgedrückt für Wellen, die in die untere Schicht eingedrungen sind.

$$ {}_P\tau_S=\frac{1}{U_2}\{(2d-h)\cos i_2+\Delta\sin i_2\}-\frac{1}{U_1}\{(2d-h)\cos i_1+\Delta\sin i_1\} $$

$$ =\Delta\left(\frac{1}{v_2}-\frac{1}{v_1}\right)+(2d-h)\left(\frac{\cos i_2}{U_2}-\frac{\cos i_1}{U_1}\right), $$

worin, d, Schichtdicke; h, Herdtiefe; $\sin i_1=\dfrac{U_1}{v_1}$; $\sin i_2=\dfrac{U_2}{v_2}$.

Nun kann man unseren vorher gesprochenen Wert (1·59 sek.) als $(2d-h)\left(\dfrac{\cos i_2}{U_2}-\dfrac{\cos i_1}{U_1}\right)$ andeuten. Was die Störungsquelle anbetrifft, können wir vielleicht sie nicht punktweise bestimmen, sondern nur makroskopisch innerhalb der Genauigkeit der Größenordnung von Wellenlänge der zur Quellenbestimmung benutzten Welle, was dasselbe in der modernen Atomphysik ist, wie einer[28] von uns einmal bemerkt hatte. Darum wollen wir vorläufig für effektiven Mittelwert von h die Schichtdicke annehmen. Dann ergiebt sich die Schichtdicke zu

$$ d=4{\cdot}09\text{ km (für } h=d) $$

laut des Ausdruckes $d=2{\cdot}05+\dfrac{h}{2}$.

Dieser Wert ist beinah gleich dem vorigen 3·83 km. (für $h=3{\cdot}6$ ist er fast dasselbe.)

28) T. MATUZAWA, *Bull Earthq. Res. Inst.*, 5 (1928), 24–25.

Also mahnt die Methode der Herdbestimmung durch Benutzung der $(P-S)$ Dauer zu einiger Vorsicht. Ähnliche Bemerkung könnte man zur Bestimmung der Proportionalitätskonstante k unter Voraussetzung der Linearität zwischen Epizentralentfernung und $(P-S)$ Dauer $\Delta = k\tau$ hinzufügen, weil man nur makroskopischen Wert[29)] von k bestimmen kann, insofern sich die Bebenbeobachtung auf die Oberfläche beschränkt. Das makroskopische k kann sich natürlich stetig ungeachtet der Schichtung der Erde ändern, wie man es sich laut der Arbeit von A. Imamura[30)] u. a. klar machen kann.

Man kann auch eine gewisse unregelmäßige Verteilung der Eintrittszeit der Bebenwellen erwarten, wie H. Honda[31)] und K. Wadati[32)] erwähnt haben, wenn die Einsatzbestimmung genügend genau sind.

Alles vor allem sehen wir hiermit, daß man im großen und ganzen die oben erwähnten drei Erscheinungen, d. h. die U_1 und U_2 Wellen, die $(P-P_1)$ Dauer und die Anomalie der $(P-S)$ Dauer, unter Voraussetzung der Existenz einer dünnen oberflächlichen Schicht in Harmonie bringen kann. April 1932, Tôkyô.

Nukigaki (Zusammenfassung)

Idu-Disin-gun no Naka no Disin, Titibu-tihô no Disin nado Singen no asai to sinzerareru Disin ni arawareta tokubetuna Nami no Mure U_1, U_2 wo sirabeta. Hyômen tikai aru Atusa no Sô wo kangaeru koto ni yotte korera wo setumei sureba Tyosyara ga mae ni nobeta koto no aru $(P-P_1)$ ya, korera no Disin ni oite mirareta $(P-S)$ no *Anomalie* nado tono Kwankei ga taihen umaku tukerareru.

Summary.

Some earthquakes in western Kwantô, which were believed very shallow seated, revealed two particular wave-groups U_1 and U_2 (Fig. 2). Assuming a thin surface layer and these waves as P and S waves in the layer, we can find close connections between this and other two pheno-

---

29) Werde $k = \frac{v_1 v_2}{v_1 - v_2}$ als mikroskopisch gedeutet, könne man $k = \frac{\delta\Delta}{\delta\tau}$ als makroskopisch ansehen.

30) A. Imamura, F. Kishinouye u. T. Kodaira, *Bull. Earthq. Res. Inst.*, 7 (1930), 471–487.

31) H. Honda, *Kensindihô*, 5, Nr. 1, (1931).

32) K. Wadati, *Geophys. Mag.*, 4 (1931), 259–283.

mena, the $(P-P_1)$ durations, which we discussed before, and the anomaly of $(P-S)$ duration observed in the case of the Itô swarm earthquakes in 1930.

Resumé.

Quelques tremblements de terre dans l'Ouest Kwantô, dont les hypocentres ont été supposés de petite profondeur, ont manifesté deux groupes d'ondes très remarquables, U_1 et U_2 (Fig. 2). En admettant qu'il y aie une couche superficielle dans la terre et considerant cette groupes d'ondes come P et S dans la couches, nous pouvons trouver une connection très intime entre ce phénomène et autres deux, c. d. la durée d'ondes $(P-P_1)$, que nous avons discutée autrefois, et une anomalie de la durée $(P-S)$ observée lors des seisms à Itô 1930.

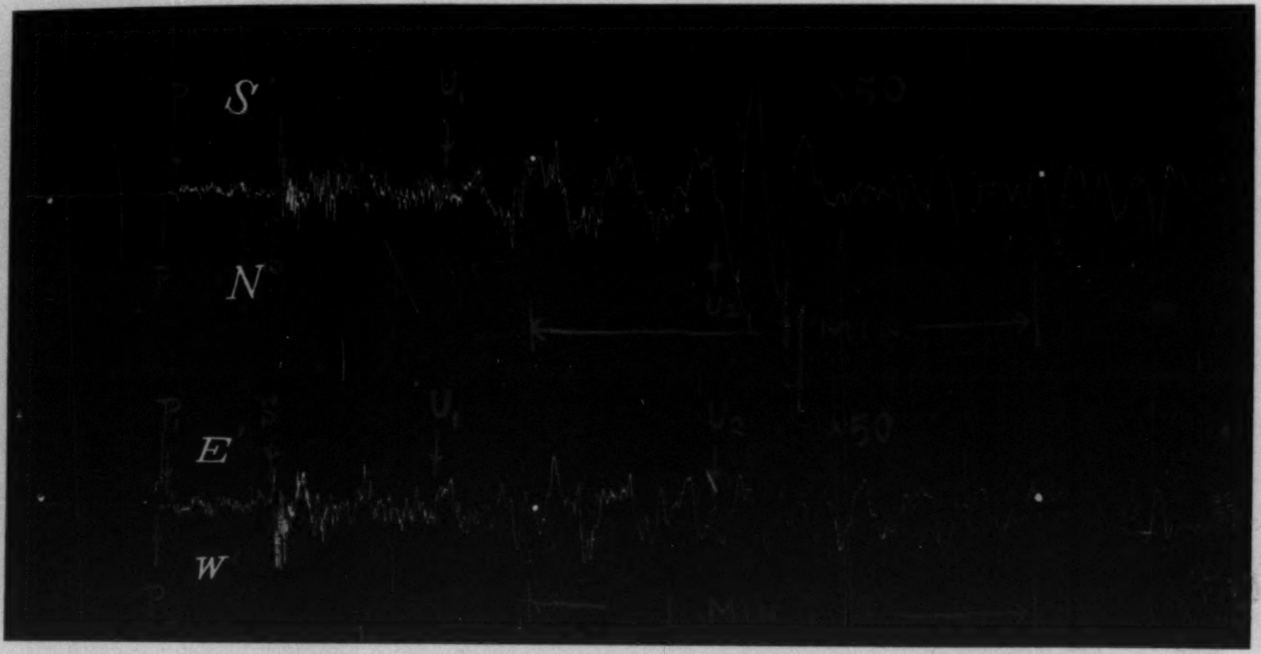

P: 1930 XI 25 16^h 6^m $9^s{\cdot}9$ (Hongô, Tôkyô)

$E'W'$	$V=50$	$T=6^s{\cdot}0$	$v=1{\cdot}4$	$r=1{\cdot}76$
$N'S'$	50	6·1	1·45	1·58

Fig. 2 a.

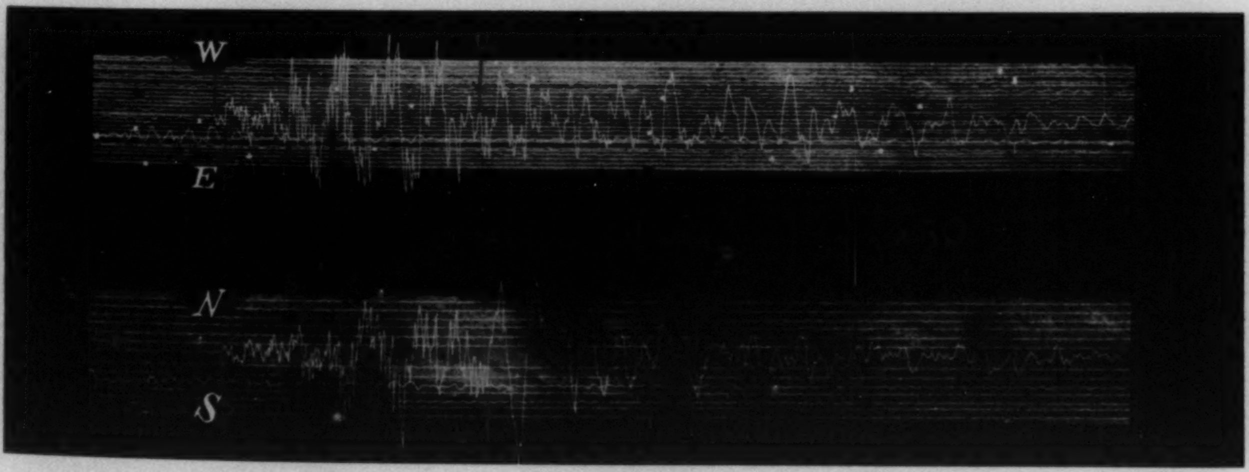

Kamakura, 1930 XI 25 16^h 6^m.

EW	$V=50$	$T=6{\cdot}4$	$v=1{\cdot}5$
NS	$=50$	4·2	1·5

Fig. 2 b.

(震研彙報、第十號、圖版、松澤、福富)

(震研彙報、第十號、圖版、松澤、福富)

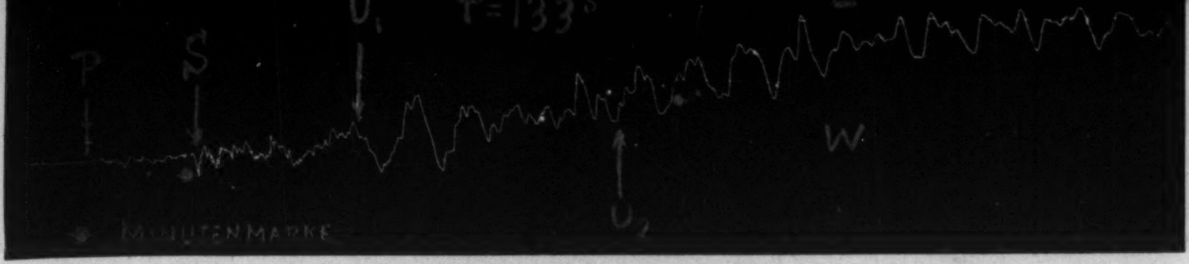

Hongô, 1930 III 9 19^h 54^m $48^s{\cdot}7$.

$V=10$ $T=133^s$ $v=2{\cdot}5$

Fig. 3 a.

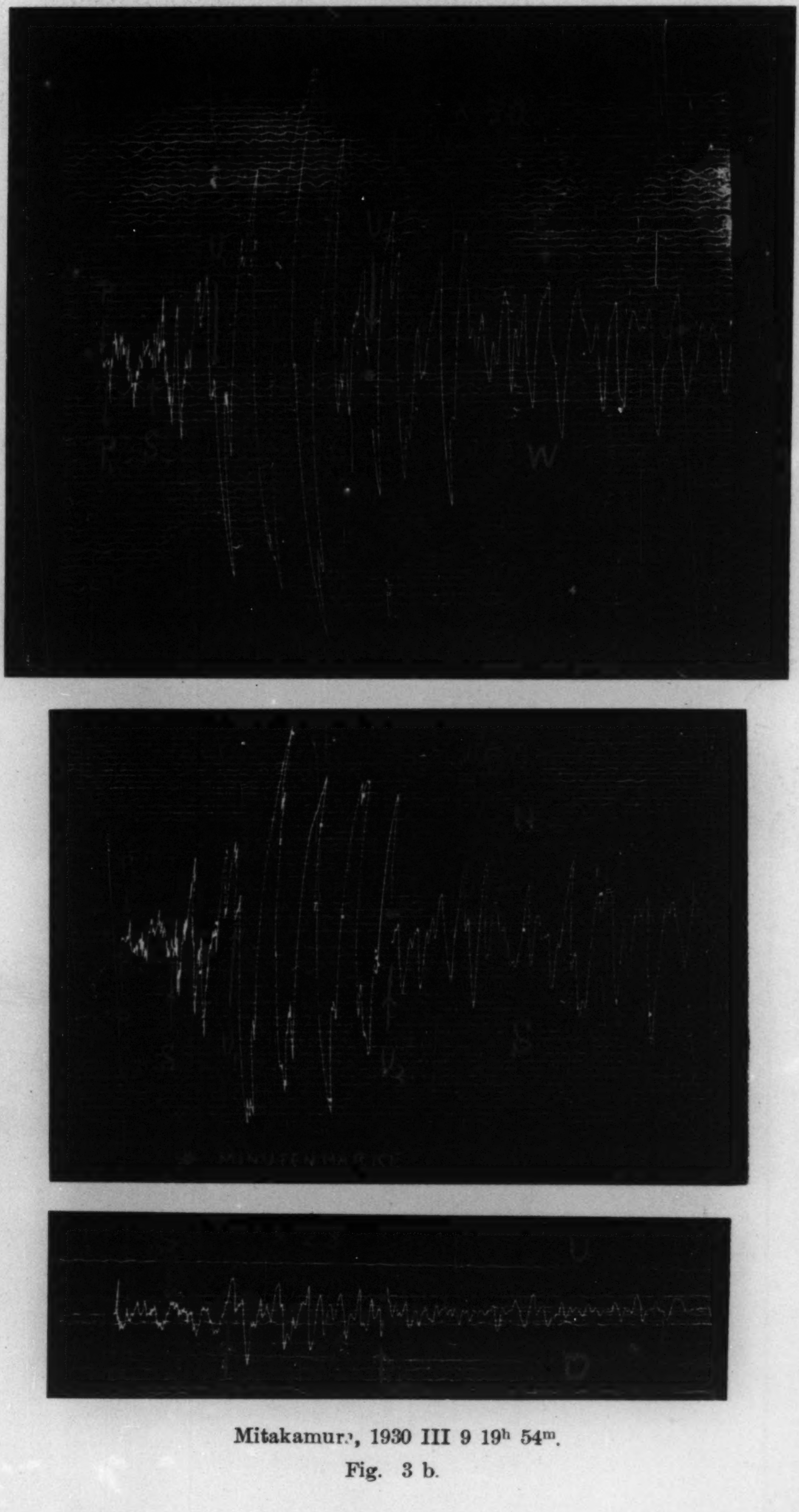

Mitakamura, 1930 III 9 19^h 54^m.

Fig. 3 b.

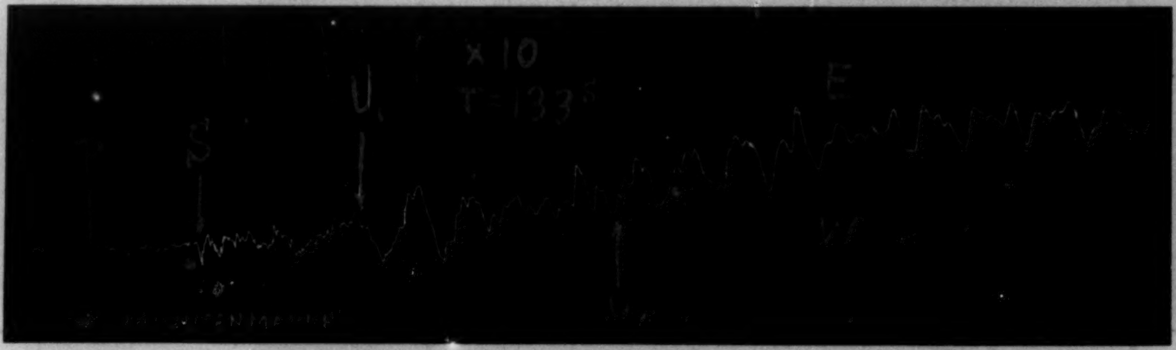

Hongô, 1930 III 9 19^h 54^m $48^s \cdot 7$.

$V=10$ $T=133^s$ $v=2 \cdot 5$

Fig. 3 a.

(震研彙報、第十號、圖版、松澤、福富)

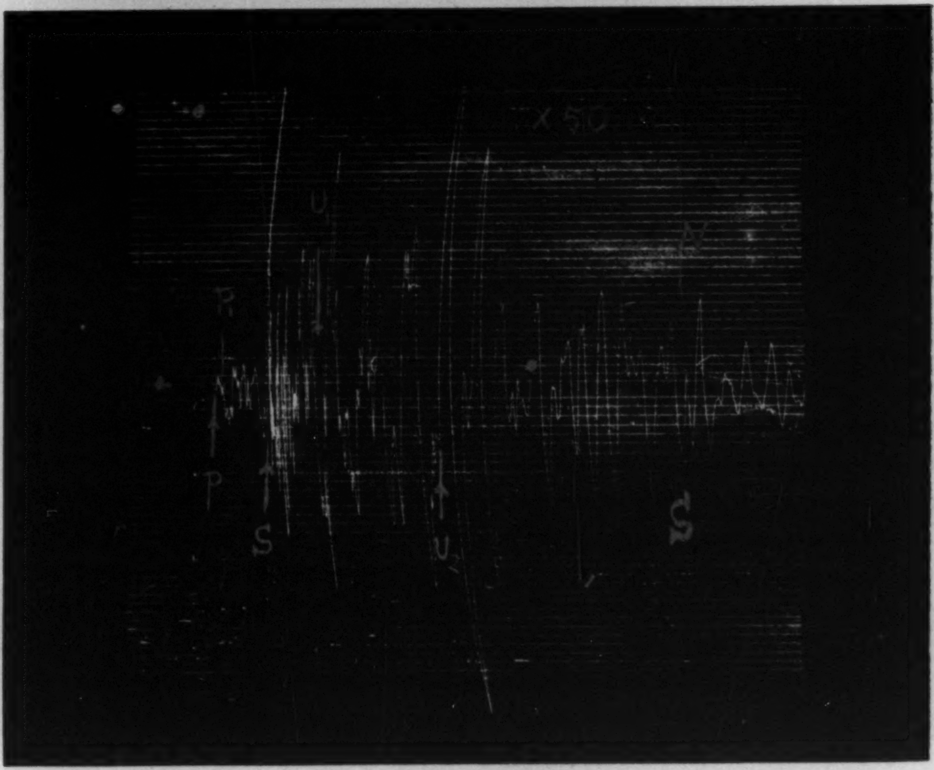

Kamakura, 1930 III 9 19^h 54^m.

$V=50$

Fig. 3 c.

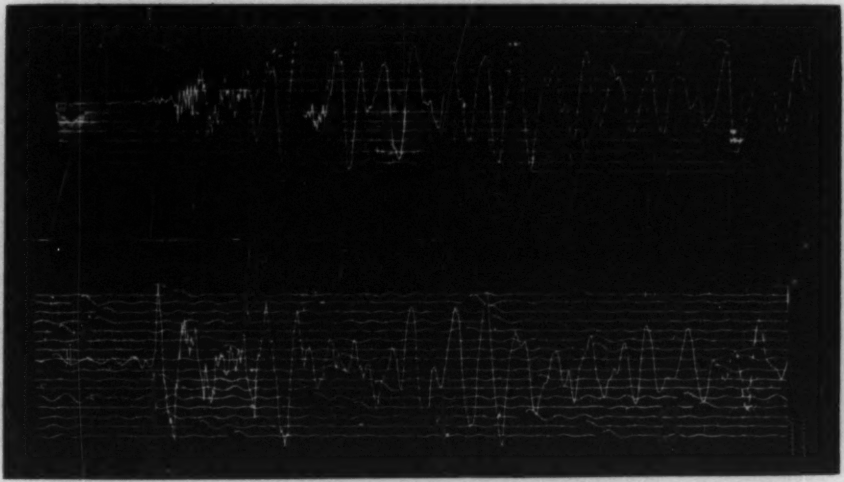

Kiyosumi-yama, 1930 III 9 19^h 54^m.

$V=50$

Fig. 3 d.

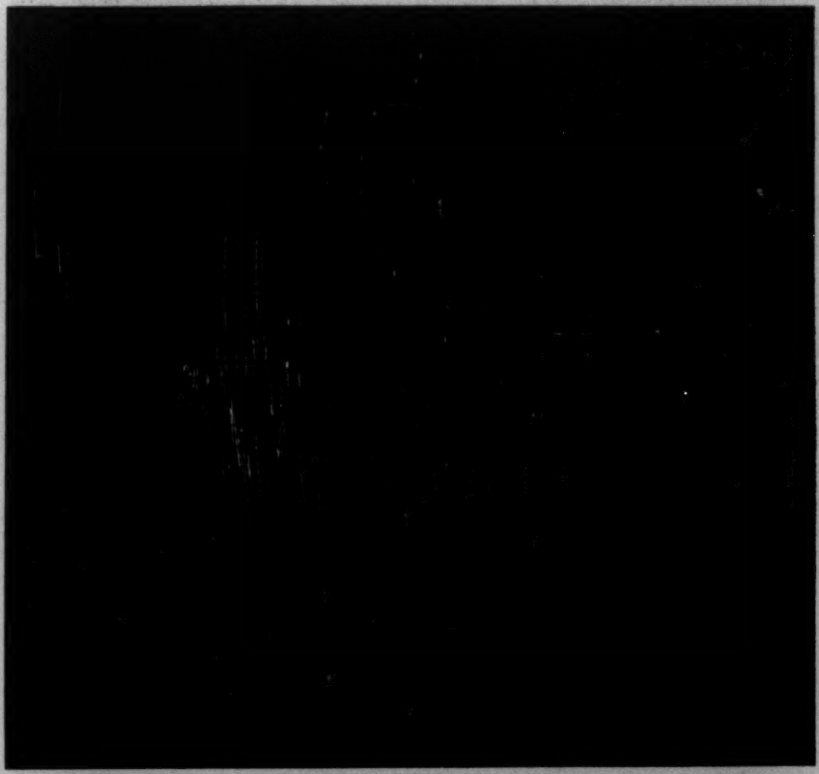

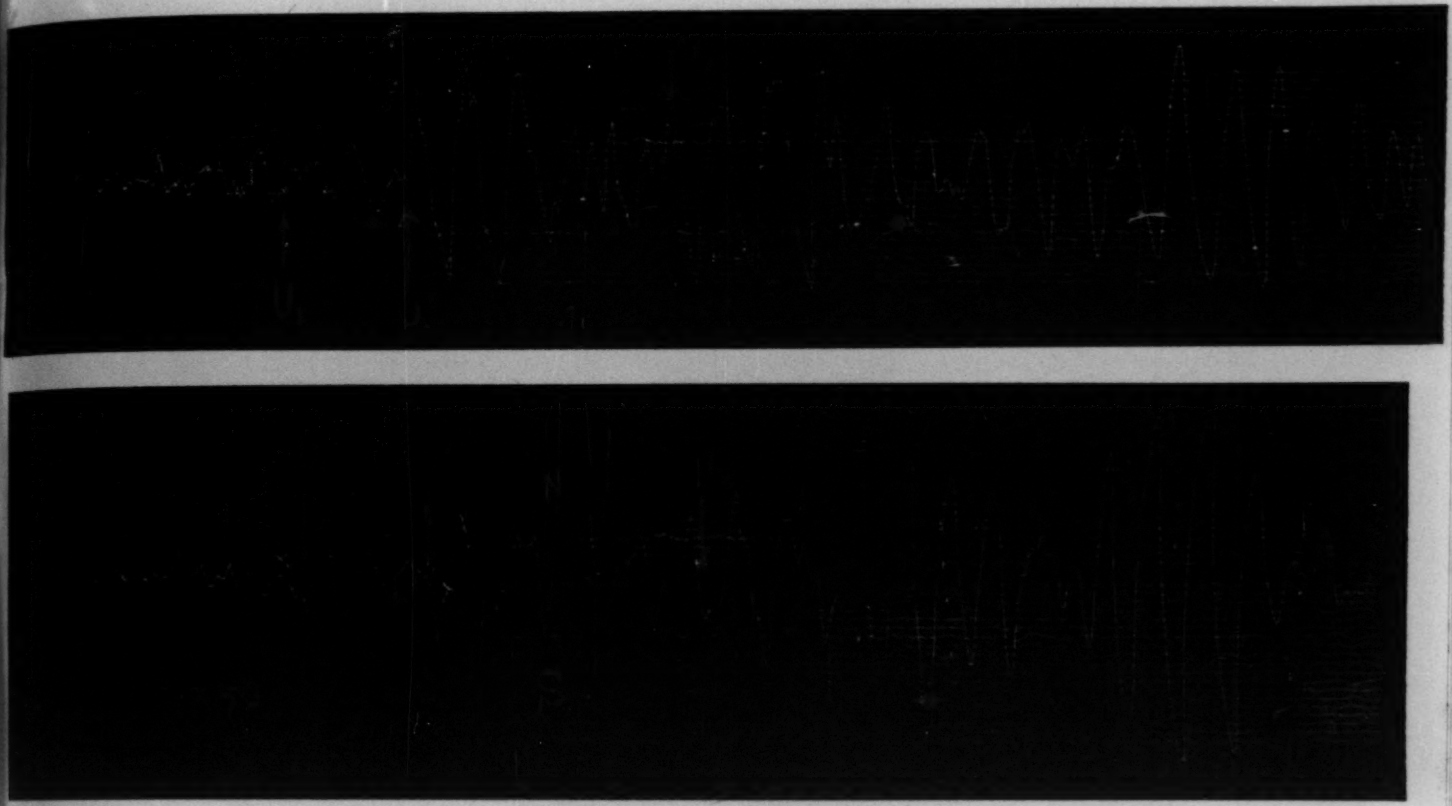

Hongô, 1930 III 13 4^h 29^m $44^s{\cdot}7$.

Fig. 4 a.

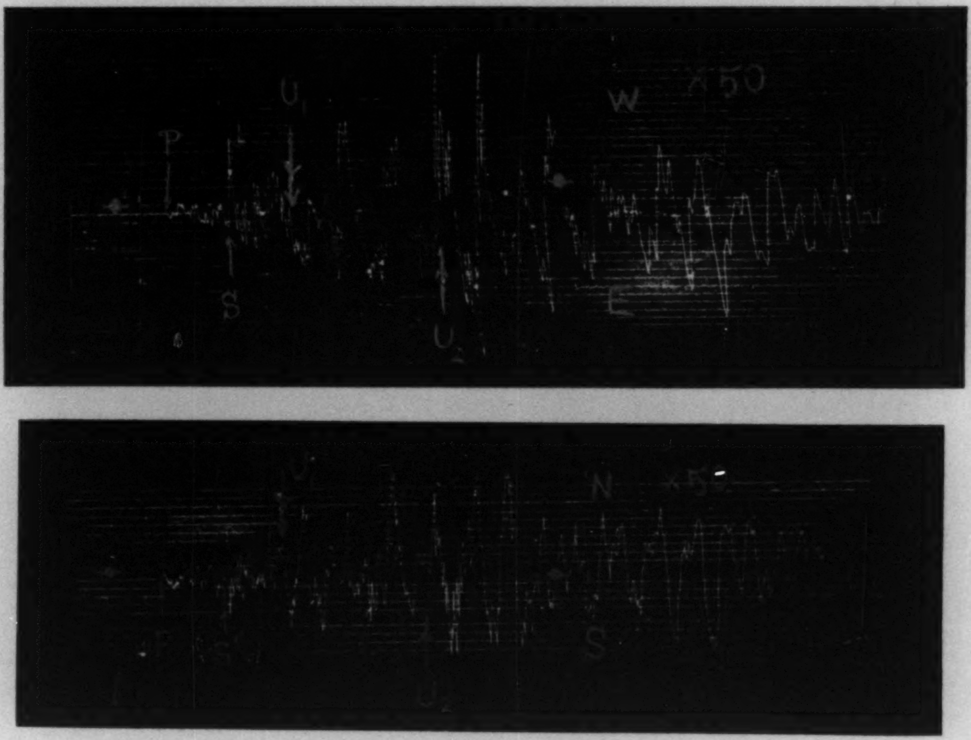

Kamakura, 1930 III 13 4^h 29^m.

Fig. 4 b.

(震研彙報、第十號、圖版、松澤、福富)

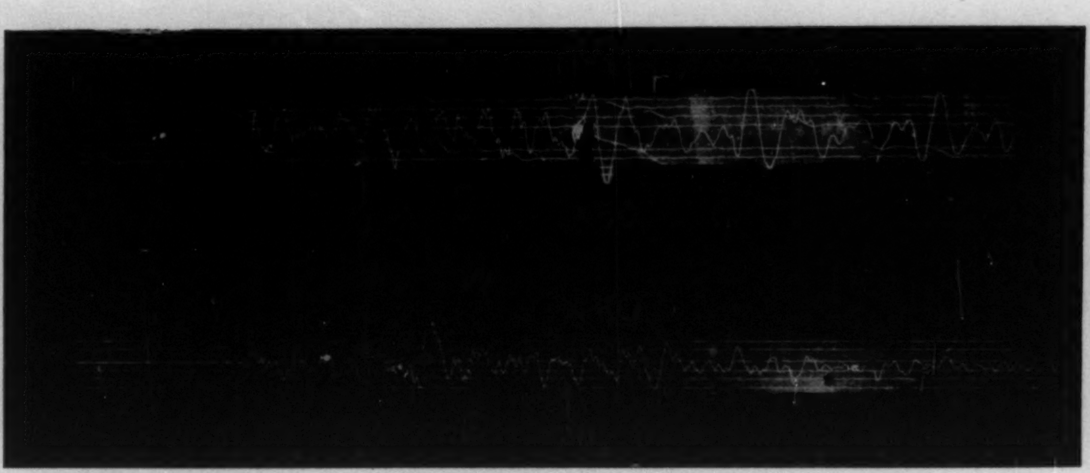

Kiyosumi-yama, 1930 III 13 4^h 29^m.

Fig. 4 c.

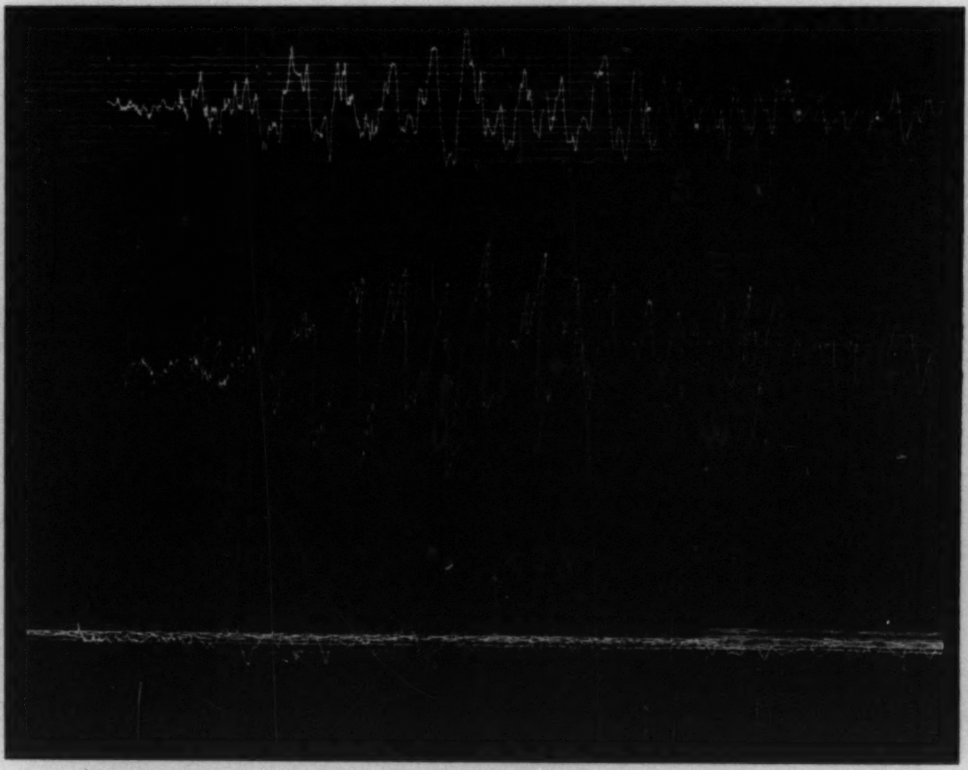

Mitakamura, 1930 III 13^d 4^h 29^m.

Fig. 4 d.

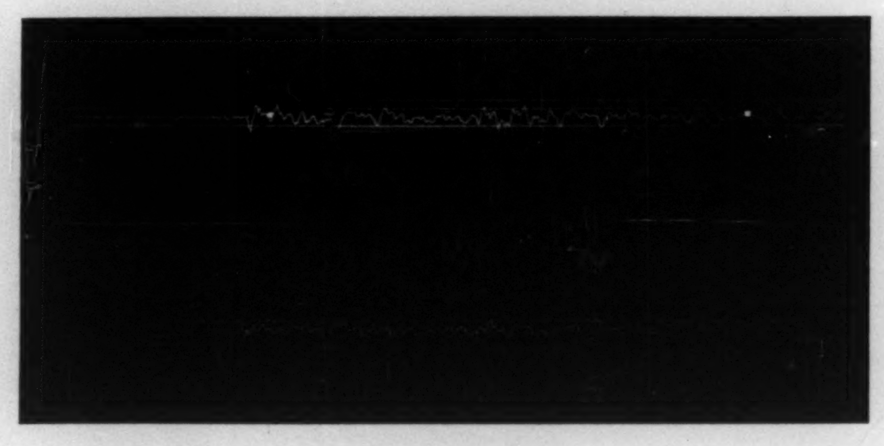

Titibu, 1930 III 13ᵈ 4ʰ 29ᵐ.

Fig 4 e.

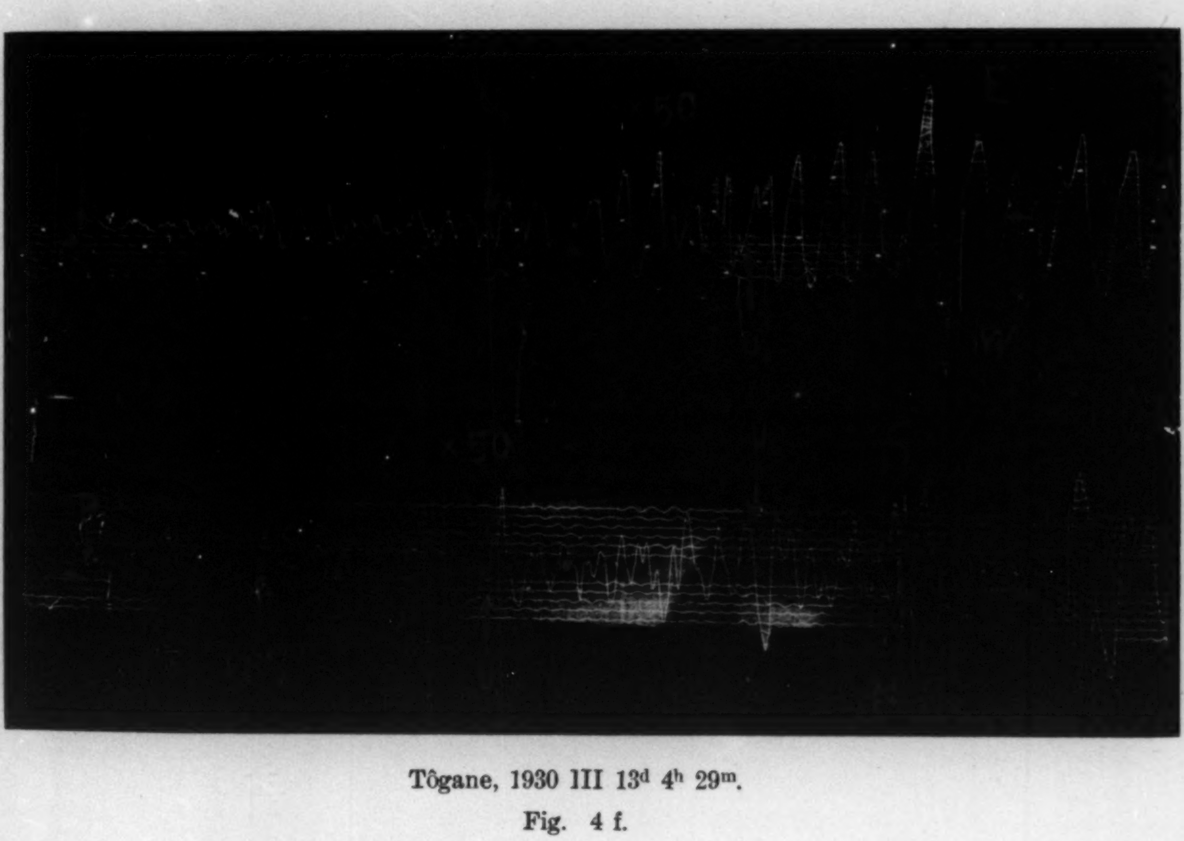

Tôgane, 1930 III 13ᵈ 4ʰ 29ᵐ.

Fig. 4 f.

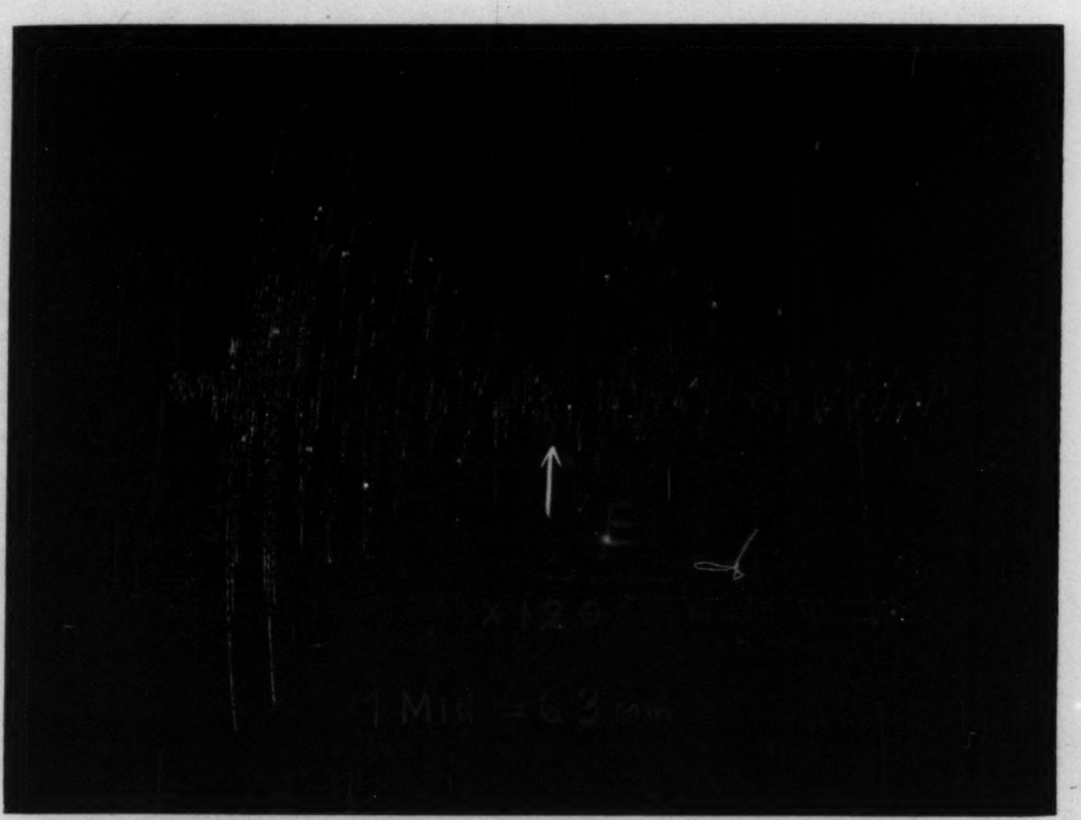

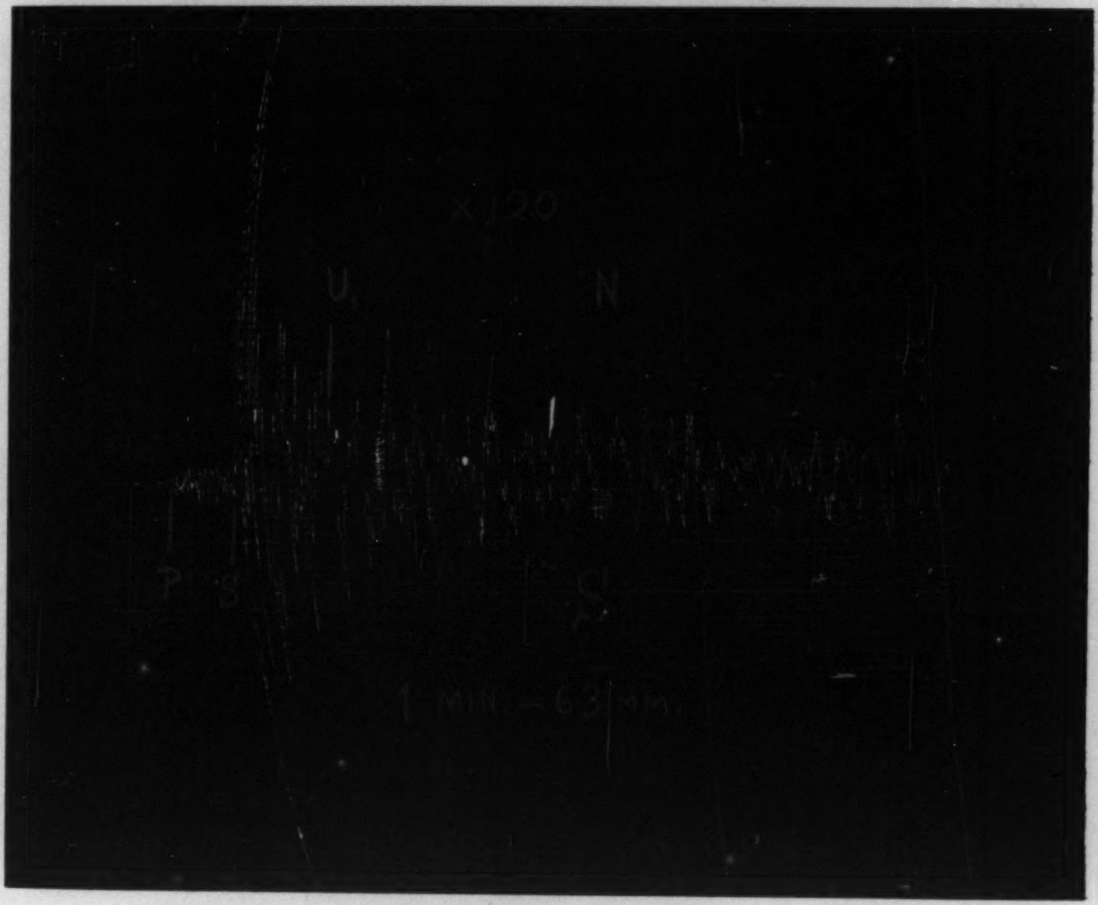

Misaki, 1930 III 15d 18h 34m.

Fig. 5 a.

(震研彙報、第十號、圖版、松澤、福富)

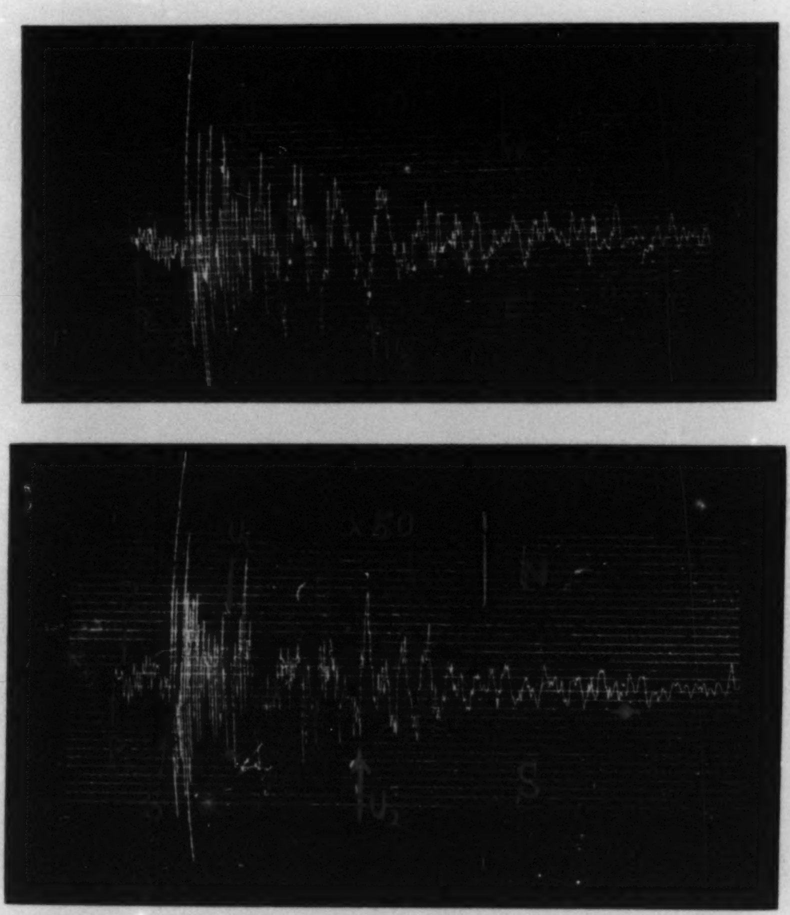

Kamakura, 1930 III 15^d 18^h 34^m.

Fig. 5 b.

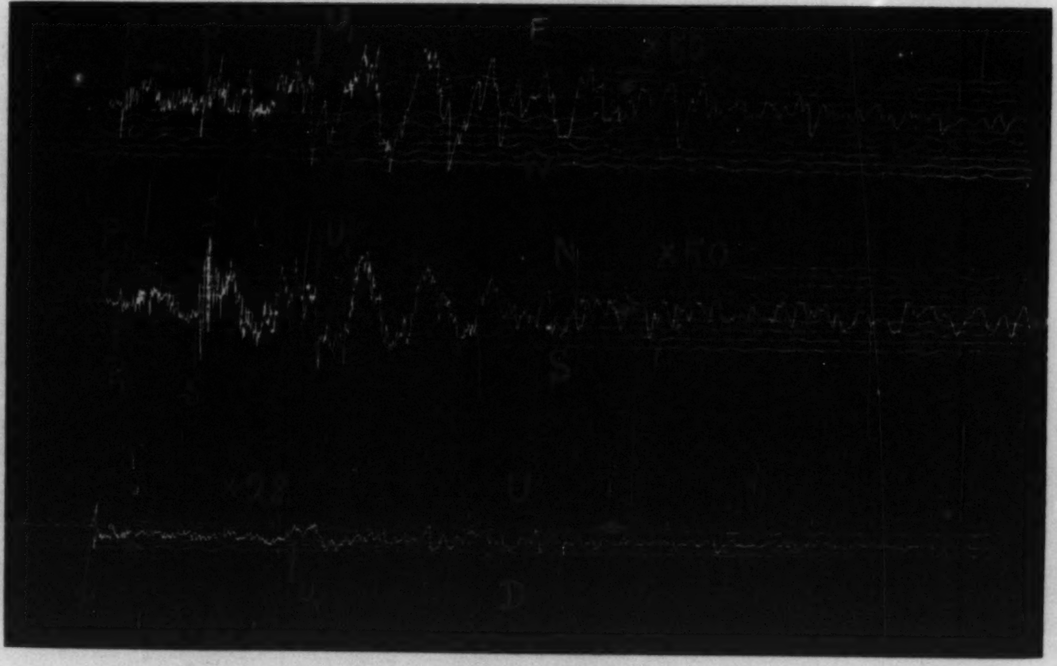

Mitakamura, 1930 III 15^d 18^h 34^m.

Fig. 5 c.

(震研彙報、第十號、圖版、松澤、福富)

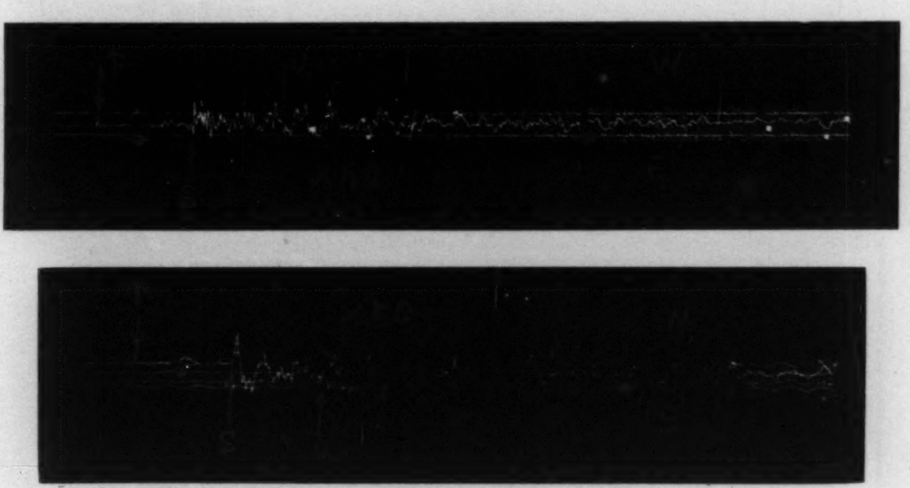

Kiyosumi-yama, 1930 III 15^d 18^h 34^m.

Fig. 5 d.

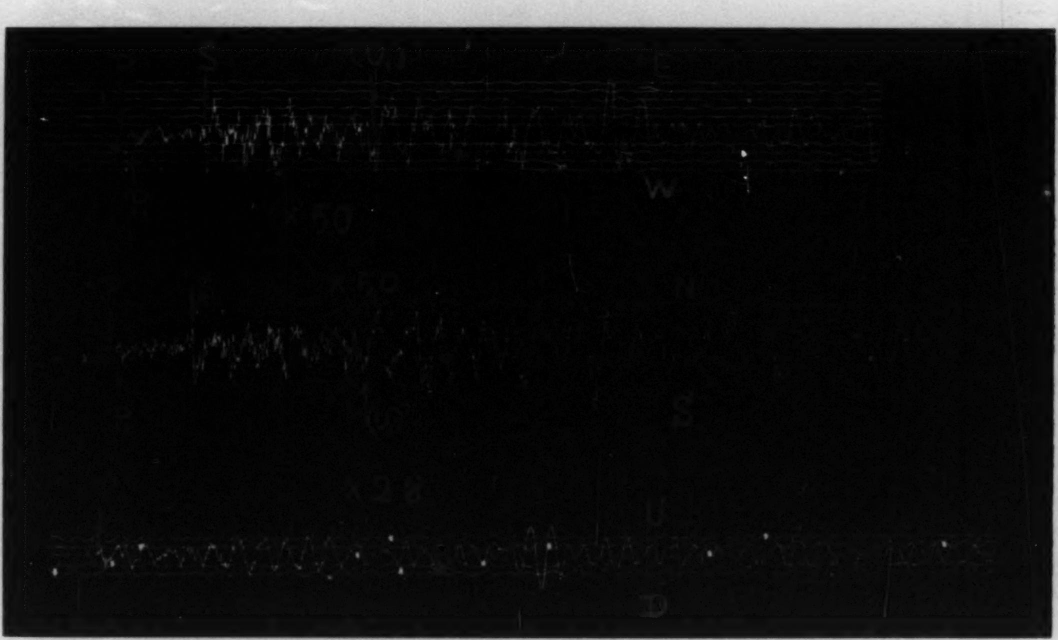

Hongô, 1930 III 15^d 18^h 34^m 37^s.

Fig. 5 e.

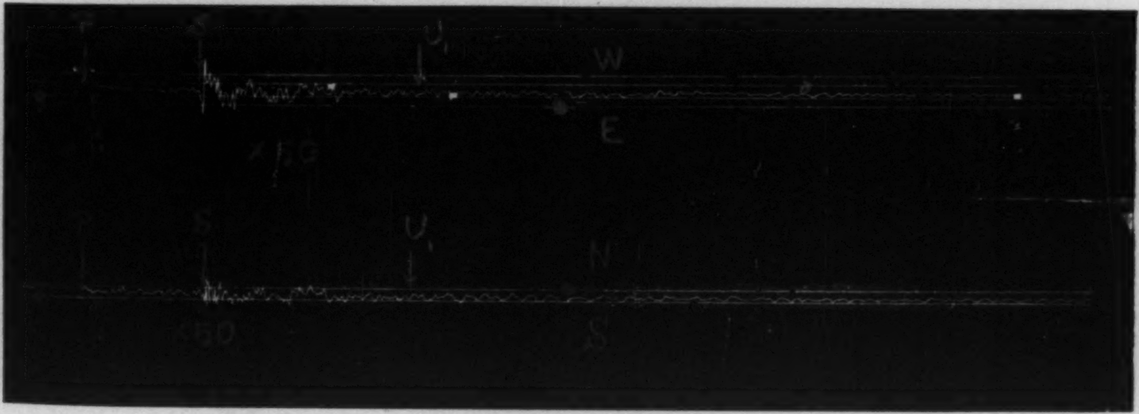

Titibu, 1930 III 15^d 18^h 34^m.

Fig 5 f.

(震研彙報、第十號、圖版、松澤、福富)

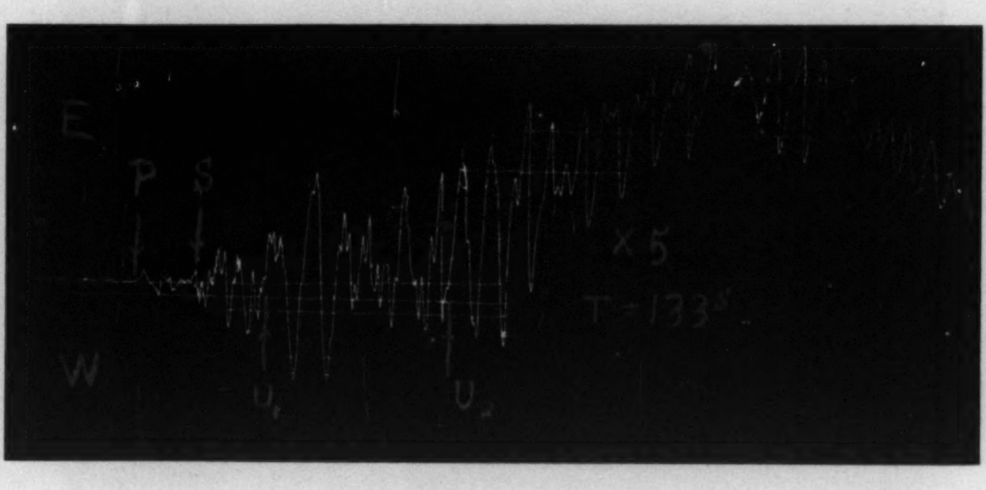

Hongô, 1930 III 22 17h 50m 51·7s.

Fig. 6.

（震研彙報、第十號、圖版、松澤、福富）

Misaki, 1930 IV 1d 23h.

Fig. 7 a.

(震研彙報、第十號、圖版、松澤、福富)

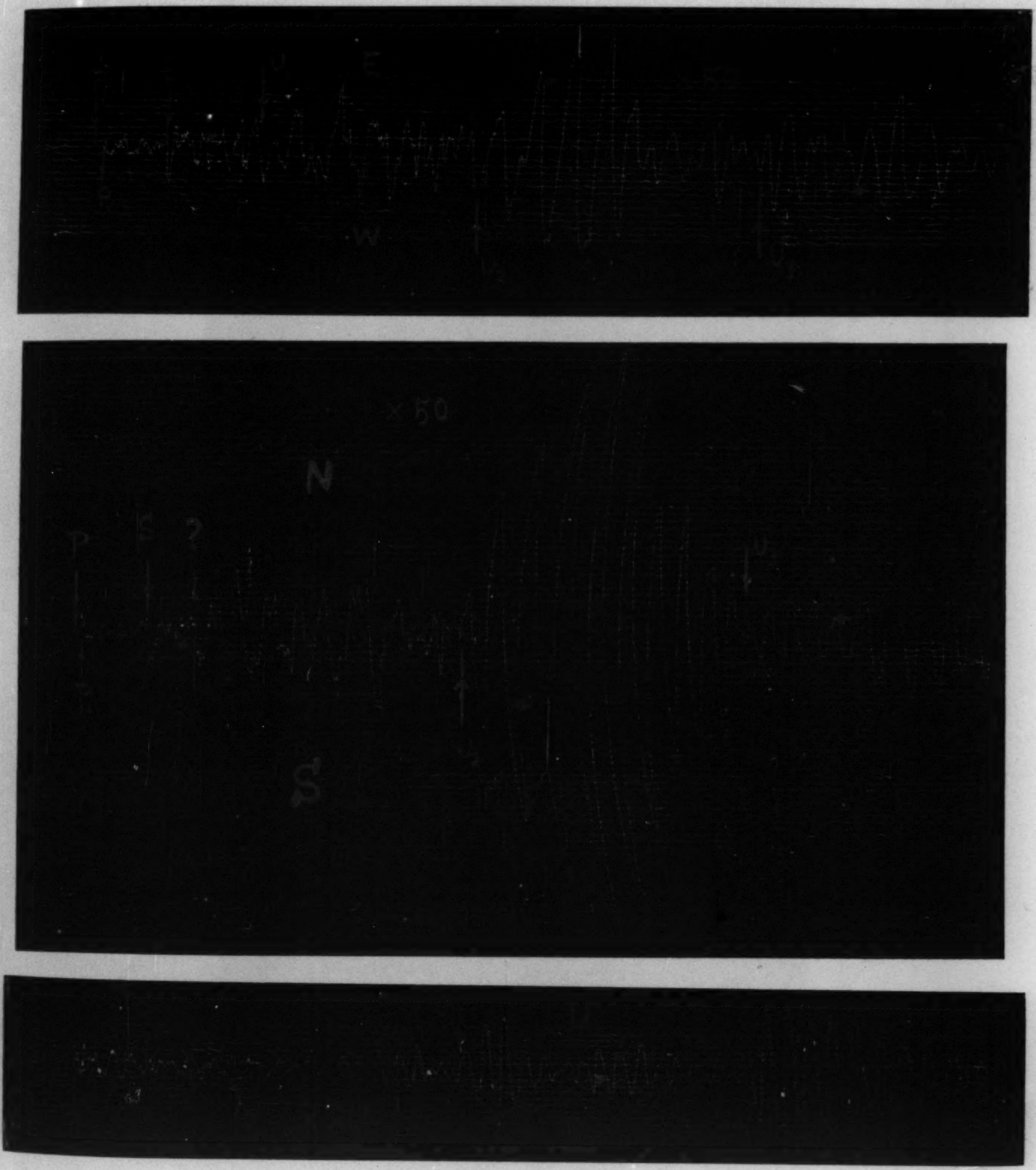

Hongô, 1930 IV 1d 23h.

Fig. 7 b.

(震研彙報、第十號、圖版、松澤、福富)

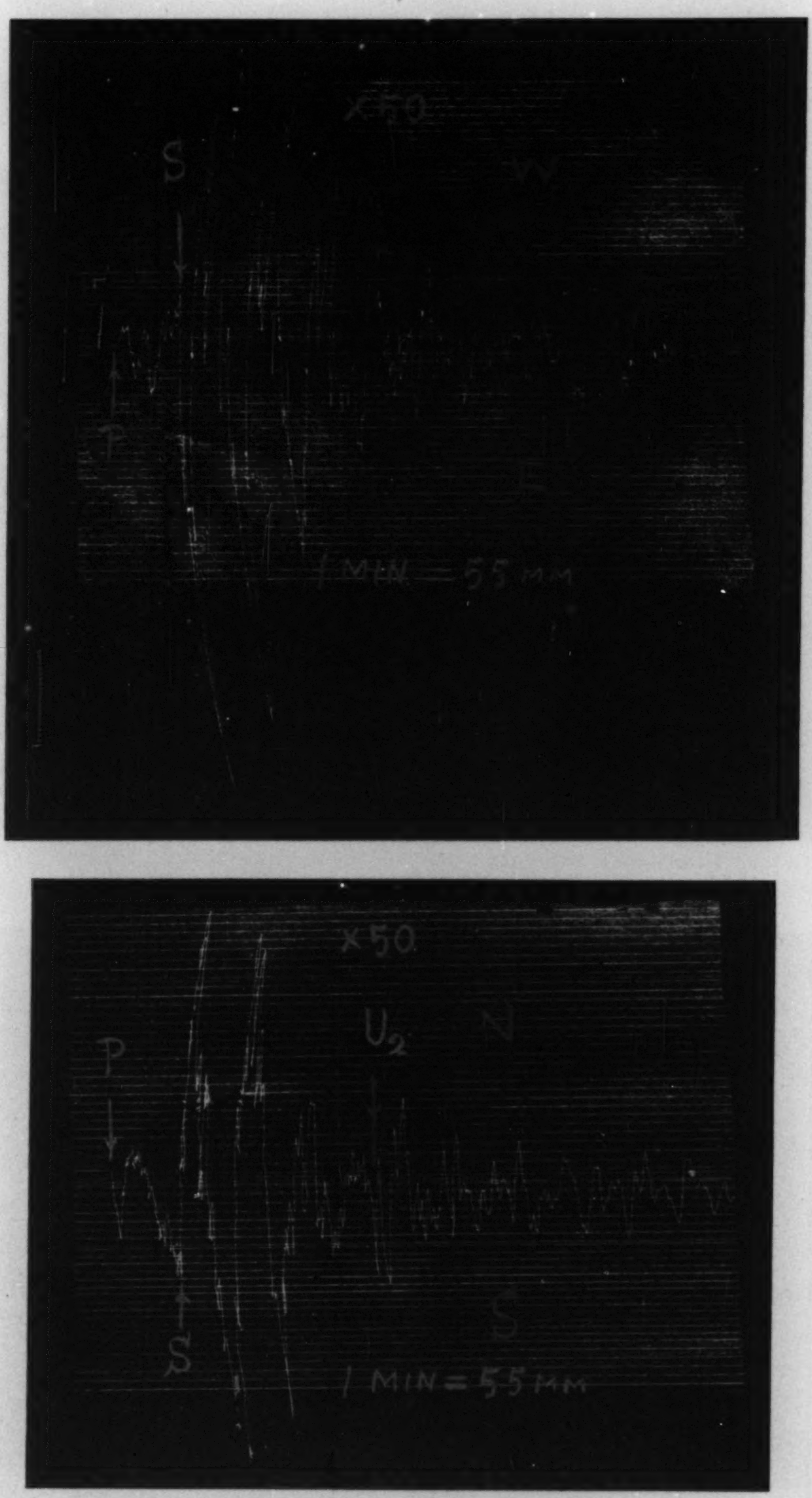

Titibu, 1931 VI 11^{d} 15^{h} 10^{m}.

Fig. 8 a.

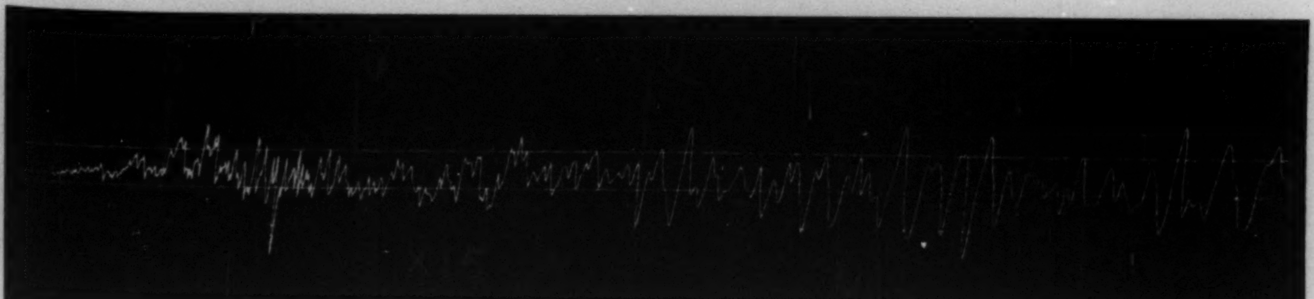

Hongô, 1931 VI 11^{d} 15^{h} 10^{m} $19^{s}\cdot 9$.

Fig. 8 b.

(震研彙報、第十號、圖版、松澤、福富)

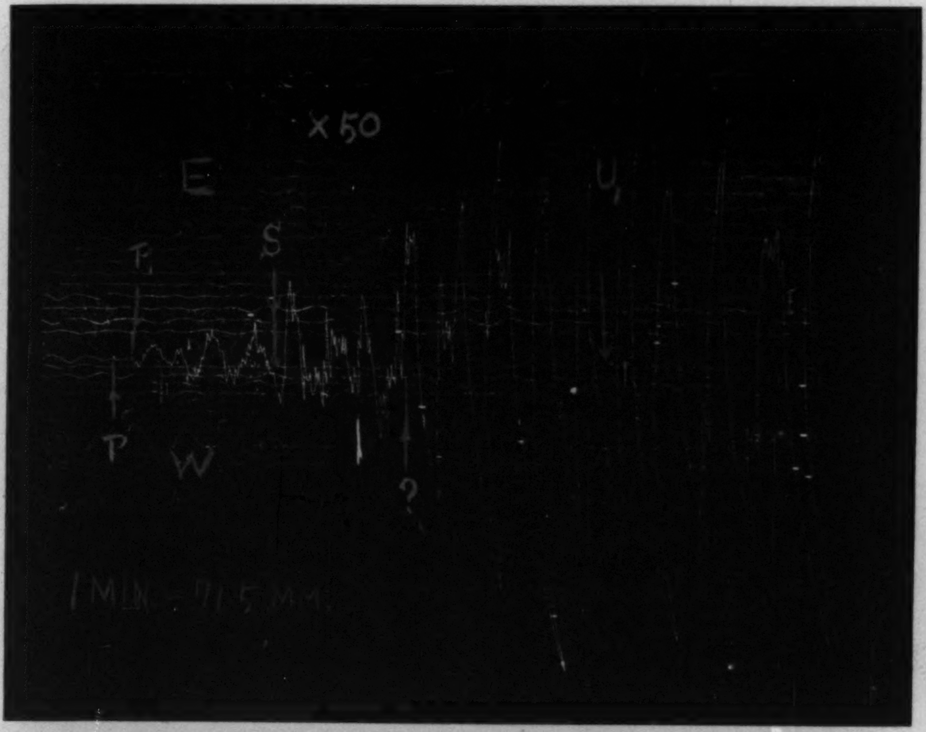

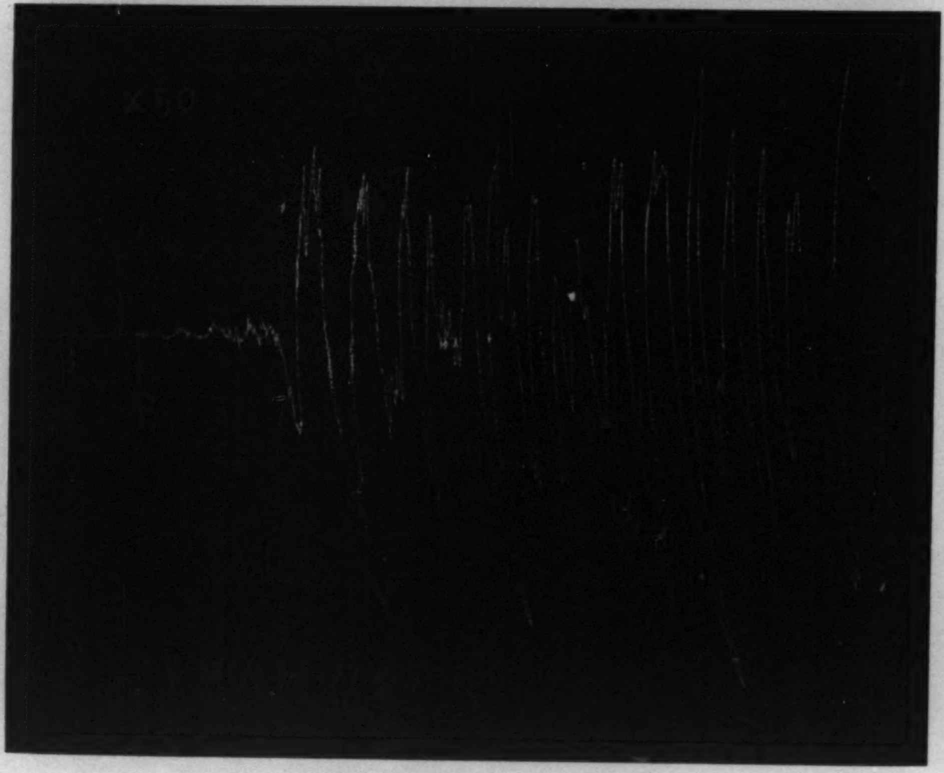

Tôgane, 1931 VI 11^d 15^h 10^m

Fig. 8 c.

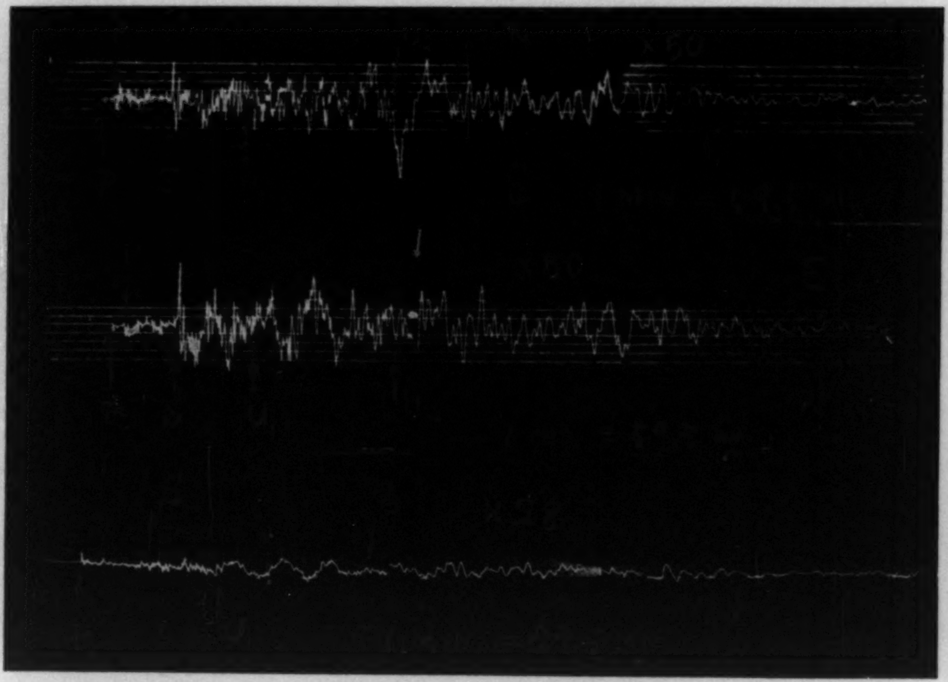

Mitaka, 1931 IX 23ᵈ 21ʰ 46ᵐ.
Fig. 9 a.

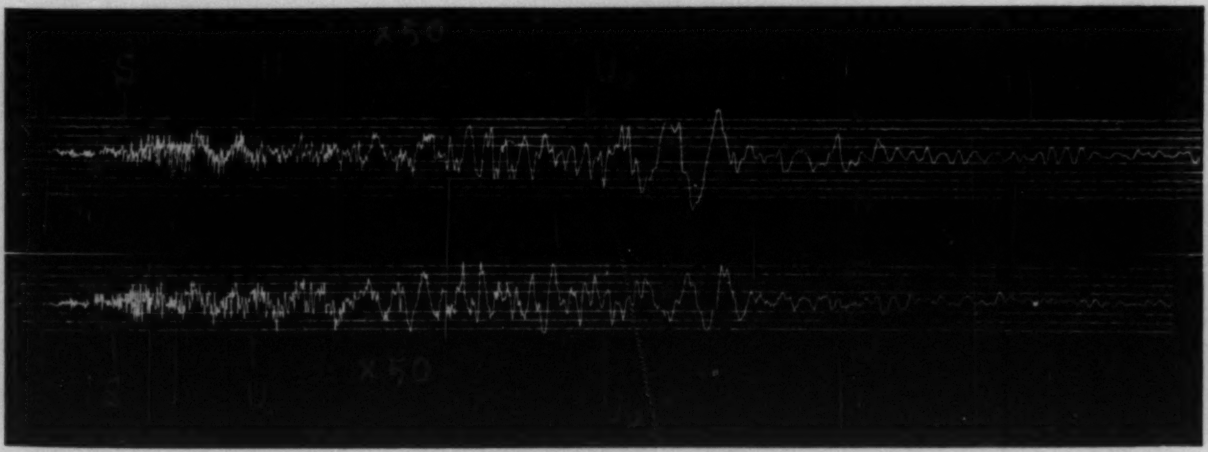

Hongô, 1931 IX 23ᵈ 21ʰ 46ᵐ 19ˢ.
Fig. 9 b.

(震研彙報、第十號、圖版、松澤、福富)

[illegible]

[illegible]

[illegible]

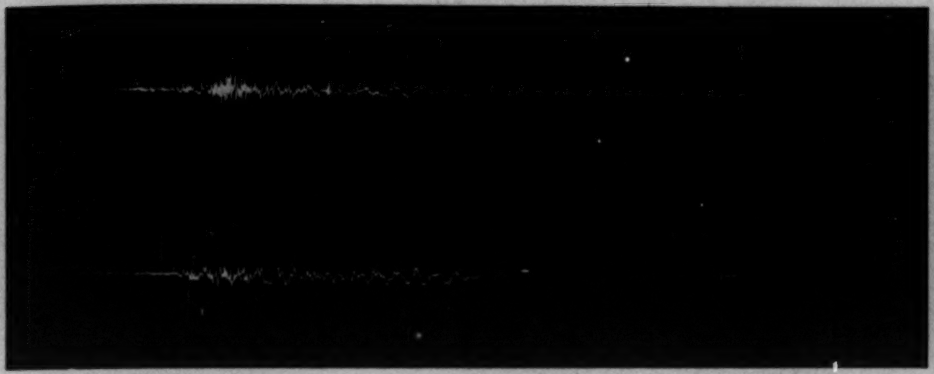

Yosiwara, 1931 IX 23^{d} 21^{h} 46^{m}

Fig. 9 c.

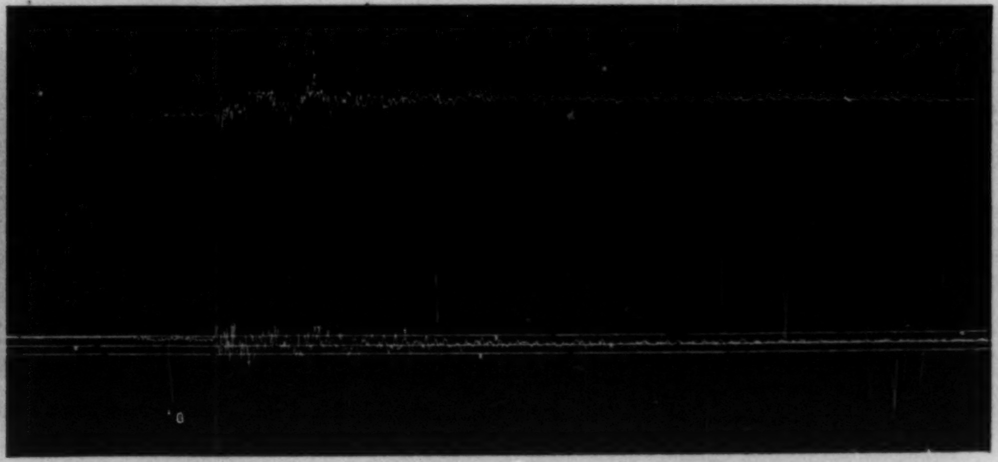

Oyama, 1931 IX 23 21^{h}.

Fig. 9 d.

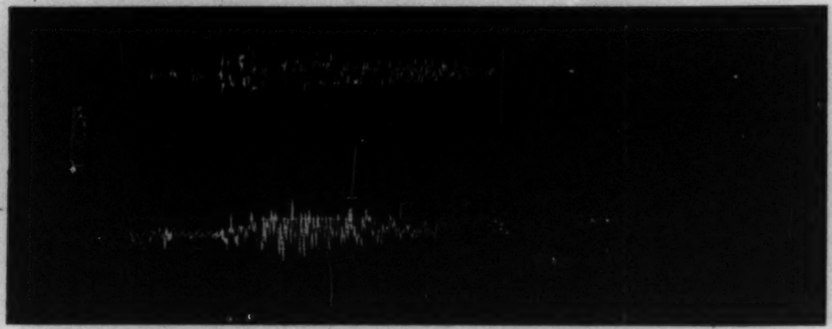

Misaki, 1931 IX 23 21^{h} 46^{m}.

Fig. 9 e.

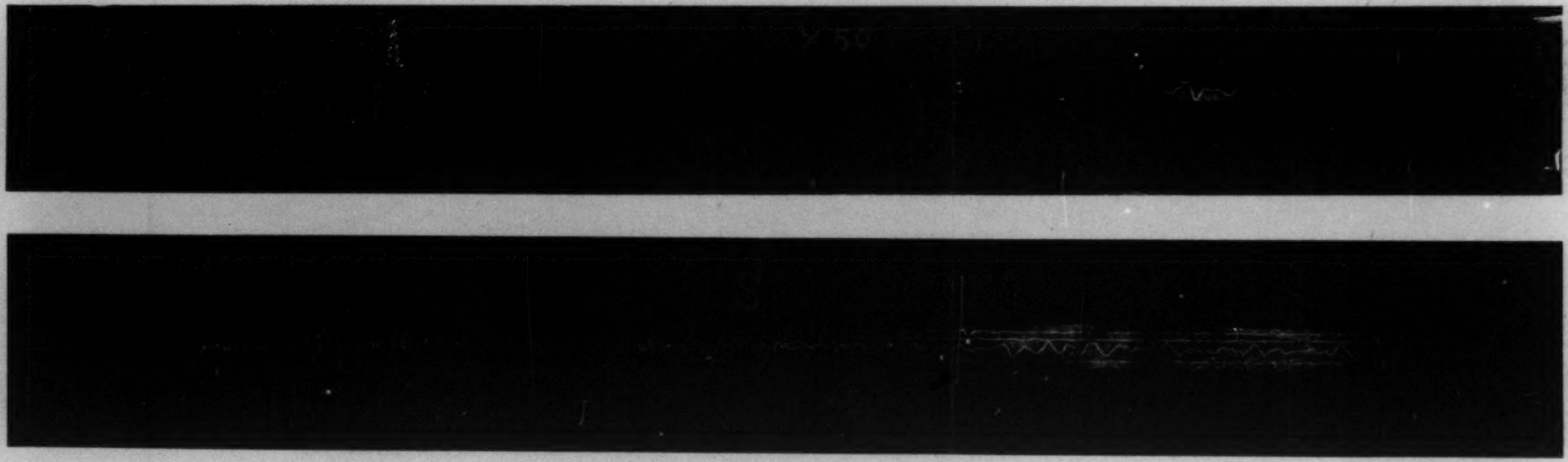

Tôgane, 1931 IX 23^{d} 21^{h} 46^{m}

Fig. 9 f.

(震研彙報、第十號、圖版、松澤、福富)

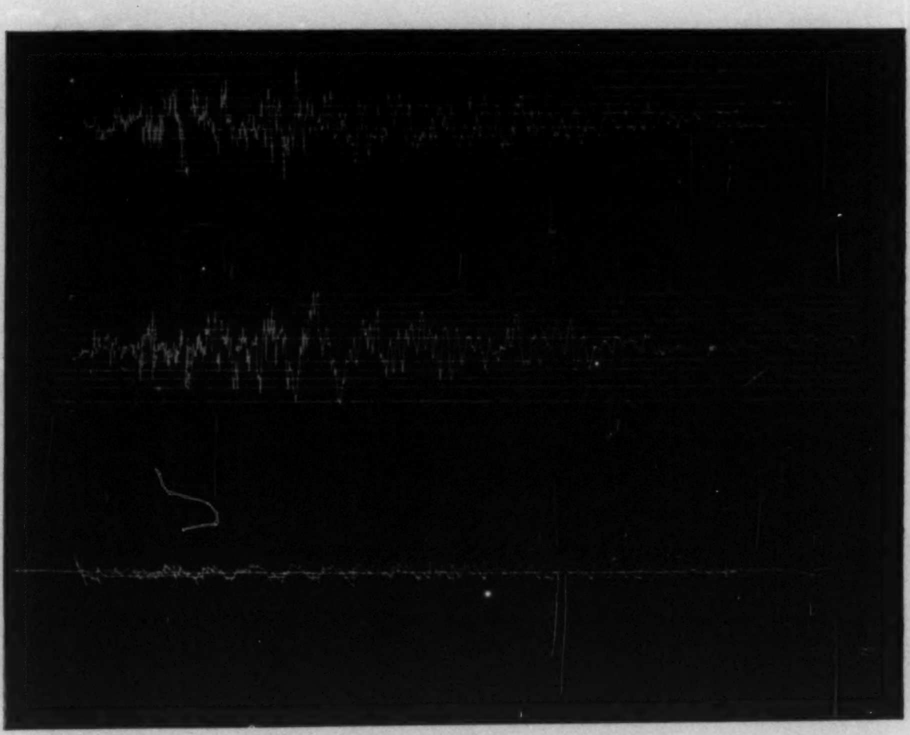

Mitakamura, 1931 IX 24 1^h 22^m.

Fig. 10 a.

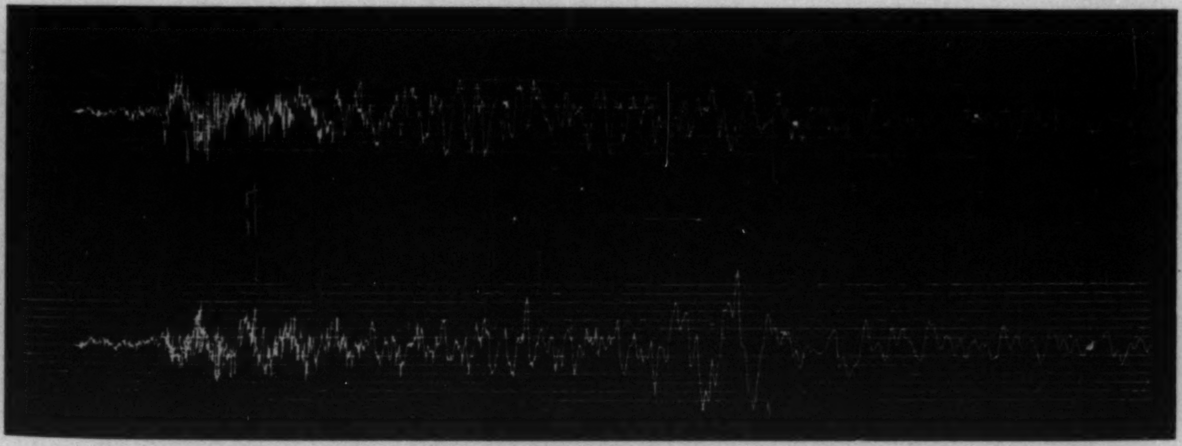

Hongô, 1931 IX 24 1^h 22^m $41^s{\cdot}1$.

Fig. 10 b.

(震研彙報、第十號、圖版、松澤、福富)

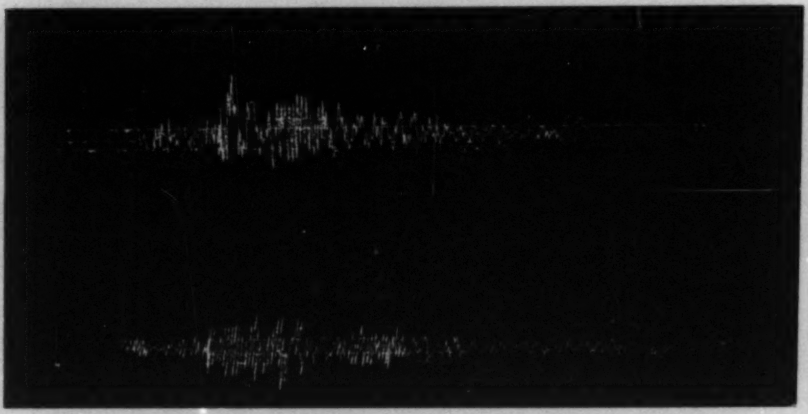

Misaki, 1931 IX 24 1h 22m.

Fig. 10 c.

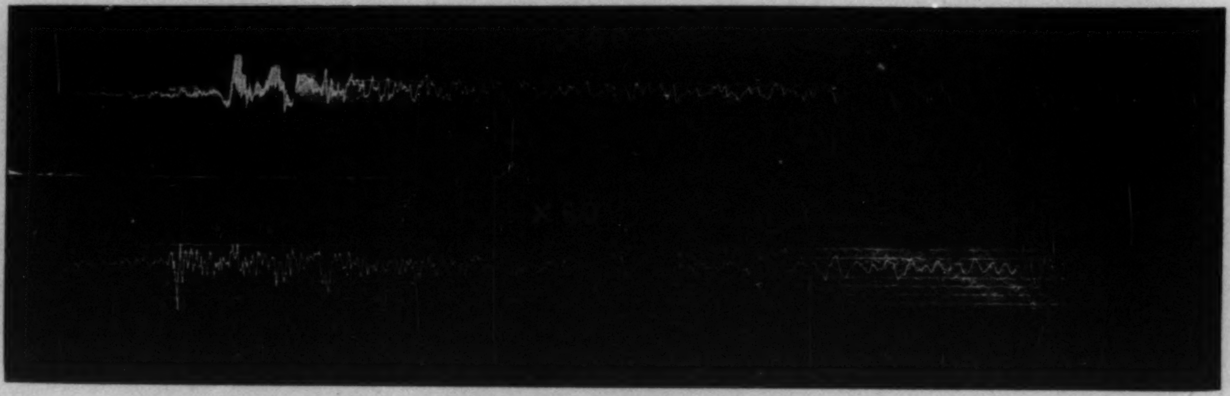

Tôgane, 1931 IX 24 1h 22m.

Fig 10 d.

Kiyosumi-yama, 1931 IX 24d 1h 22m.

Fig. 10 e.

(震研彙報、第十號、圖版、松澤、福富)

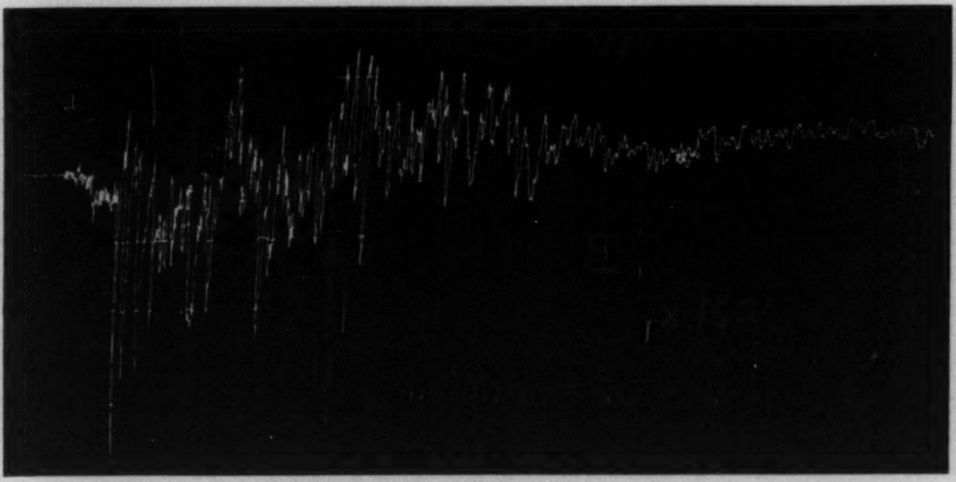

Mitakamura, 1931 IX 24 21h 11m

Fig. 11 a.

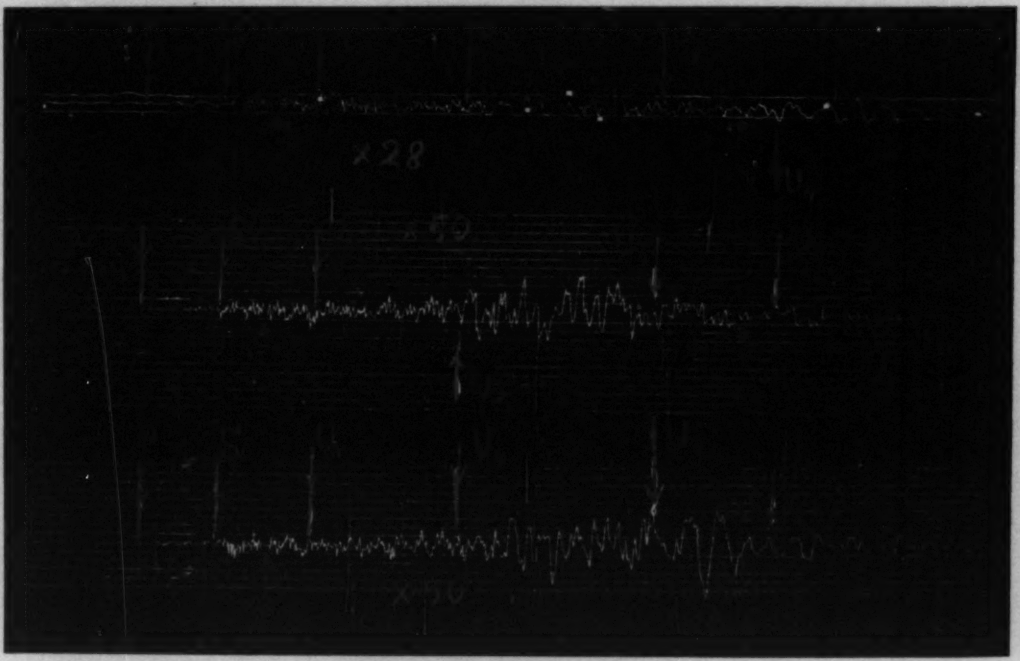

Hongô, 1931 IX 24 21h 11m 26s.

Fig. 11 b.

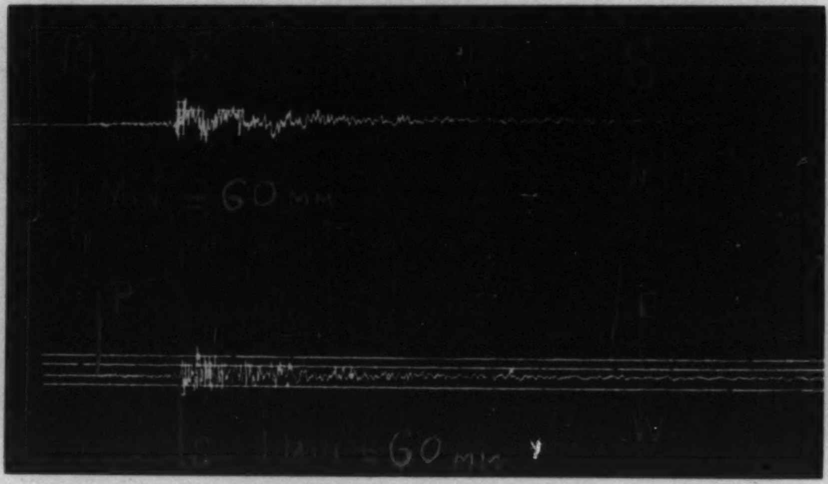

Oyama, 1931 IX 24d 21h 11m.

Fig. 11 c.

（震研彙報、第十號、圖版、松澤、福富）

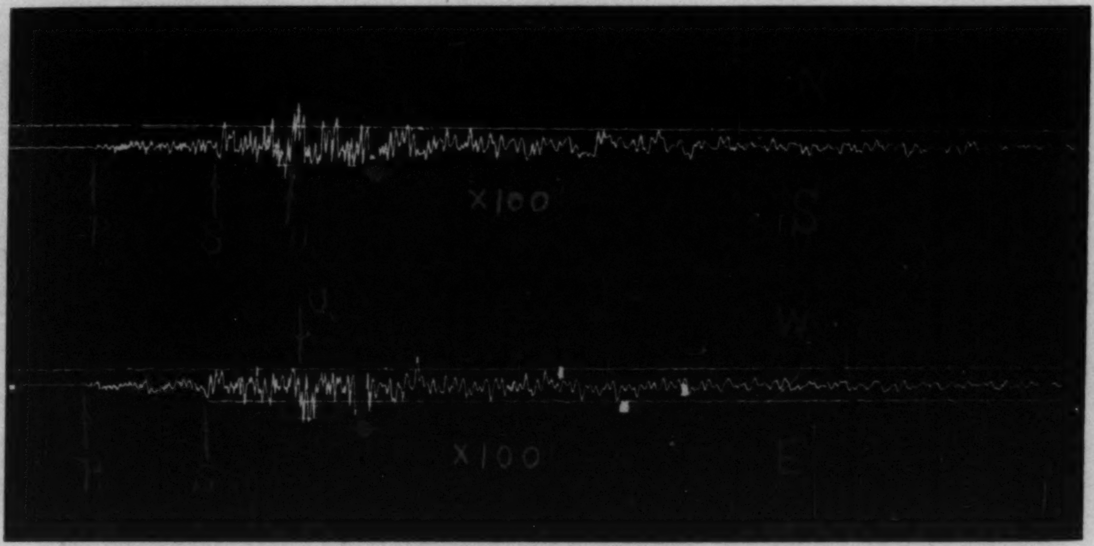

Kamakura, 1931 IX 24ᵈ 21ʰ 11ᵐ.
Fig. 11 d.

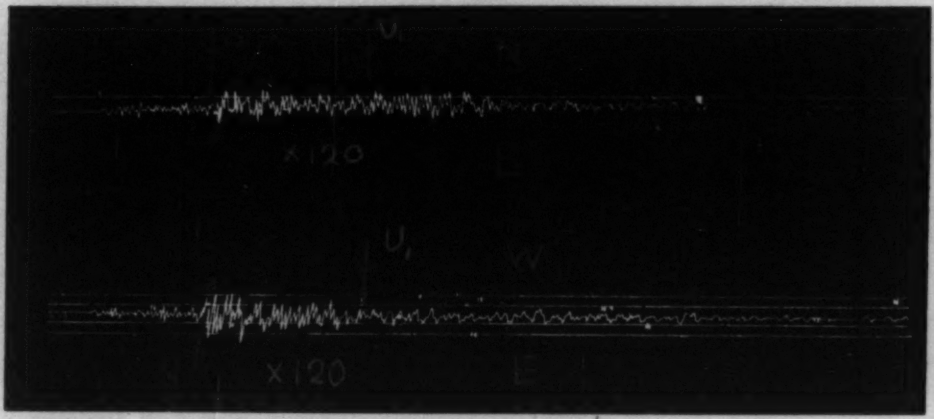

Misaki, 1931 IX 24ᵈ 21ʰ 11ᵐ.
Fig. 11 e.

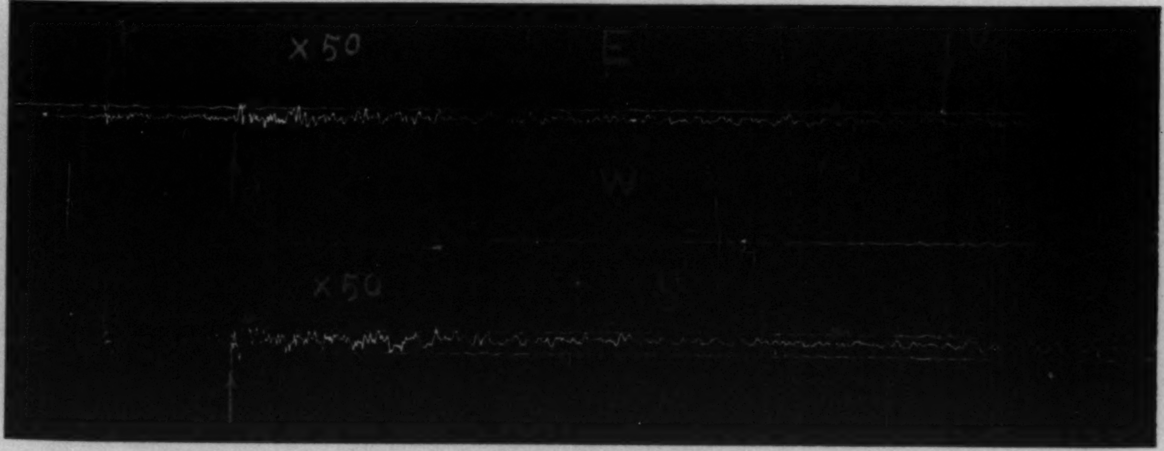

Tôgane, 1931 IX 24ᵈ 21ʰ 11ᵐ.
Fig. 11 f.

(震研彙報、第十號、圖版、松澤、福富)

36. *On the Angle of Incidence of the Initial Motion observed at Hongô and Mitaka.*

By Takeo SUZUKI,

Seismological Institute.

(Read June 21, 1932.—Received June 20, 1932.)

I. Introduction.

It has been already found by Prof. T. Matuzawa[1)] and others that the seismograms of certain earthquakes in the Kwantô district observed at Hongô (Tôkyô) show a typical forerunning part of the commencement of motions. In the horizontal component, during about 1·5 seconds in the beginning the motion is quite small and then followed suddenly by somewhat distinct motions. On the other hand, in the vertical component the beginning phase is quite large compared with the second. Moreover, the time difference 1·5 sec. between the first and the second phase is almost independent of the epicentral distance.

To elucidate this observed fact Prof. Matuzawa introduced a surface layer characteristic to the Kwantô district. When the dilatational wave started from the seismic focus, which is situated deeper than this layer, is incident to the boundary where reflexion and refraction occur, the dilatational and the distortional wave are generated in the upper layer. Prof. Matuzawa considered that the first phase which is mainly vertically polarized, corresponds to the refracted dilatational wave and the second phase which is mainly horizontally polarized, corresponds to the refracted distortional wave. By considering such a mechanism of generation of waves the observed facts i.e. the time relation and the polarization of waves are plausibly explained, assuming the most favourable value of the thickness of the upper layer and velocities of the P and the S wave in it. According to the recent investigation of Prof. Matuzawa[2)] and T. Fukutomi the velocity of the P and that of the S wave in the upper layer are 1·94 km/sec and 1·14 km/sec respectively

---

1) T. MATUZAWA, K. HASEGAWA and S. HAENO, *Bull. Earthq. Res. Inst.*, 4 (1928), 85–106.

T. MATUZAWA, K. YAMADA and T. SUZUKI, *Bull. Earthq. Res. Inst.*, 7 (1929), 241–260.

2) T. MATUZAWA and T. FUKUTOMI, *Bull. Earthq. Res. Inst.*, 10 (1932), 499–516.

and the thickness of this layer comes out 4 km from the duration between the first and the second phase.

Such a remarkable polarization of the first phase shows that the angle of incidence of the first motion is considerably small, that is, the trajectory of the wave is almost vertical near the surface. This may be probably due to sudden decrease of velocity near the surface.

T. Isikawa[3] has investigated the relation between the angle of emergence and the epicentral distance in case of some earthquakes. Dr. H. Kawasumi[4] has determined the angle of emergence by using the reported data adopted from "Kisyô Yôran" published by the Central Meteorological Observatory and found statistically that it is comparatively larger than that expected from the superficial structure of the earth crust introduced by Prof. Matuzawa. The present writer has studied the angle of incidence from the seismograms obtained at two seismological stations Hongô (Seismological Institute) and Mitaka (Astronomical Observatory) with special reference to the velocity of seismic wave near the surface.

II. Observation of the angle of incidence.

The angle of incidence is easily determined by taking the resultant of the first motions in the three components of seismogram. In this method it is most important to compare the corresponding phase in each component. For this purpose a tromometer designed by Prof. A. Imamura is quite suitable. With this instrument the three components are recorded on one and the same recording drum and the minute marks are given on the seismogram as breaks of the line in each component. Therefore, the identification of the corresponding motion in each component is quite easy. The instrumental constants of this seismograph are shown in Table I.

Table I.

component	weight of bob	magnification V	period T	
(EW)	7 kg	50	7 sec	At Mitaka the magnification of the vertical component is 18.
(NS)	7	50	7	
(Vert.)	7	28	7	

3) T. ISIKAWA, *Journ. Meteor. Soc.*, Japan, [ii] 6 (1928), No. 3.

4) H. KAWASUMI, Read before the meeting of Earthquake Research Institute on July 7, 1931.

The angle of incidence thus obtained is not a true one but an apparent one owing to the effect of reflexion of incident wave at the surface. Let $\bar{i}$ be the apparent angle of incidence, then the true one i will be given by the formula

$$\sin^2 i = \left(\frac{V_1}{V_2}\right)^2 \cdot \frac{1-\cos\bar{i}}{2},$$

where V_1 and V_2 are the velocity of the dilatational and the distortional wave respectively. Assuming $V_1/V_2 = 1{\cdot}789$—i.e. Poisson's ratio $\sigma = 0{\cdot}273$, all the observed values of $\bar{i}$ are reduced to i by this formula. The amount

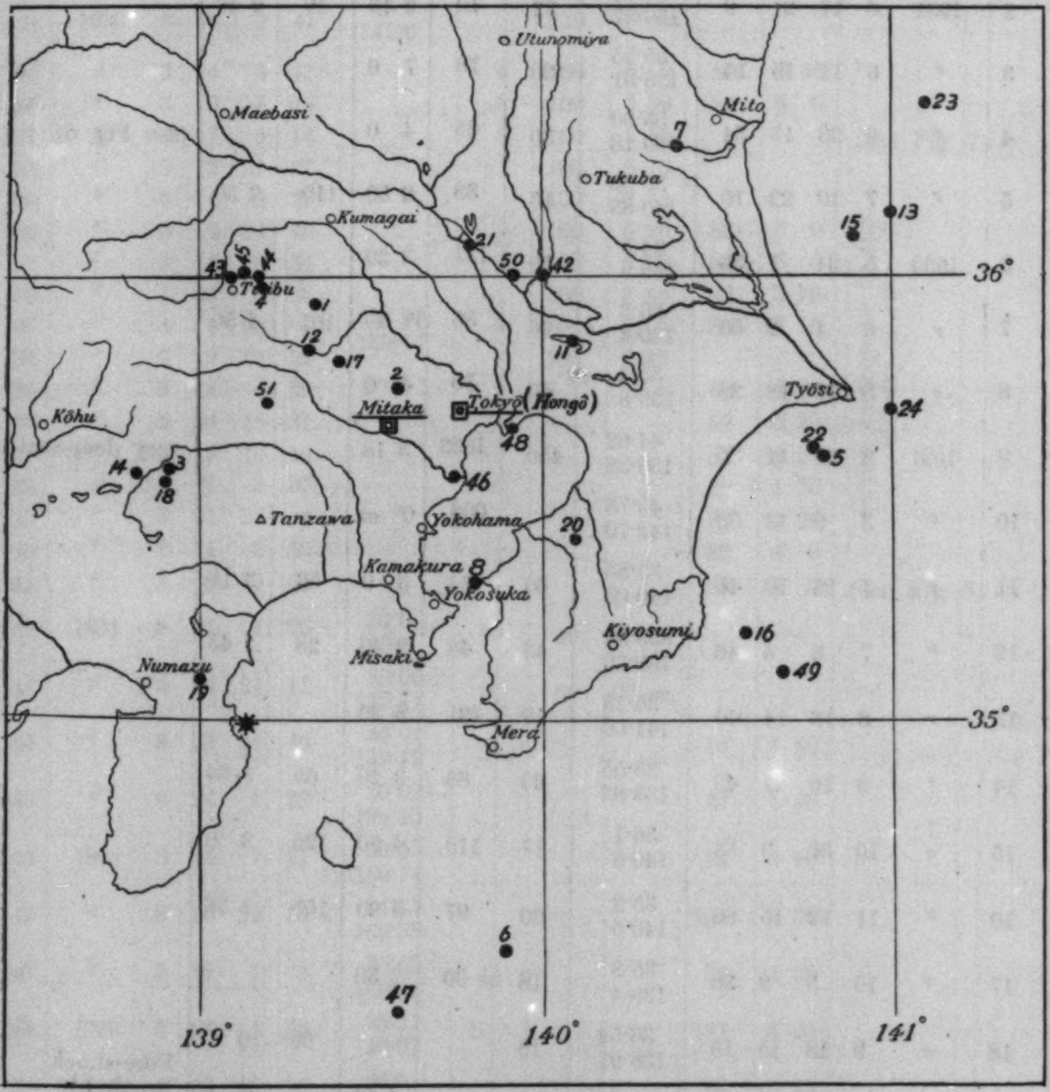

✱ Swarm earthquakes in the vicinity of Itô.

Fig. 1.

of this correction is for example such that if $\bar{i}$ is 5°, i becomes 4° 10′.

The distribution of earthquakes studied by the writer is shown in Fig. 1. The results of observation are tabulated in Table II and shown in Fig. 2 and 3.

Table II.

No.	Commencement at Hongô					Epicentre Latitude Longitude	Focal depth	Hongô		Mitaka		Remarks
	Y	M	D	H	M			Δ	i obs.	Δ	i obs.	
							km	km	° ′	km	° ′	
1	1928	10	5	15	58	35·93 N 139·34 E	43	45	4 0	36	2 45	(see Fig. 4)
2	1931	6	17	21	9	35·74 139·57	32	19	0 15	10	2 40	
3	〃	6	11	15	16	35·55 138·91	20	78	7 0			
4	〃	9	28	13	54	35·96 139·18	30	65	4 0			(see Fig. 6)
5	〃	7	10	22	10	35·59 140·83	15	88	2 50	110	3 30	
6	1930	5	24	1	38	34·5 139·9	50	137	3 20			
7	〃	6	1	2	58	36·3 140·4	46	86	11 40	101	4 50	
8	〃	8	17	18	28	35·3 139·8	45	38	4 0			
9	1931	2	20	14	35	44·62 136·38	450	1032	3 18			very deep-seated
10	〃	3	9	12	50	40·75 142·70		608	0° ca.			
11	〃	7	26	10	41	35·85 140·09	60	34	3 0	52	2 15	
12	〃	7	8	5	46	35·84 139·32	43	46	2 40	28	2 45	
13	〃	8	18	14	40	36·15 141·00	19	121	8 20			
14	〃	9	16	21	43	35·55 138·82	20	86	3 20	65	3 30	
15	〃	10	30	3	53	36·1 140·9	17	110	4 50	126	3 0	
16	〃	11	12	15	09	35·2 140·6	20	97	5 20	105	1 36	
17	〃	10	3	2	36	35·8 139·4	18	50	2 30			
18	〃	9	18	15	13	35·54 138·91	18			59	10 0	
19	1930	11	25	16	6	35·1			4 10		5 0	Fore-shock
20	〃	11	26	4	3	139·0	shallow	100	4 40	79		North Idu earthquake (see Fig. 5)

(*to be continued.*)

Table II. (*continued.*)

No.	Commencement at Hongô					Epicentre Latitude Longitude	Focal depth	Hongô		Mitaka		Remarks
	Y	M	D	H	M			Δ	*i* obs.	Δ	*i* obs.	
							km	km	° ′	km	° ′	
21	1929	7	17	19	49	36·06 139·80	35	40	4 40	49	3 30	
22	1930	5	1	9	58	35·6 140·8	40	92	6 10			
23	1928	8	27			36·40 141·10	20	140	6 10			
24	1930	8	20	2	41	35·7 141·0		110	0° ca.			
25	〃	3	4	5	11		4	100	5 0	82	3 50	
26	〃	3	9	4	39		3	100	5 30	82	4 0	
27	〃	5	17	5	14		3	100	3 50			(see Fig. 7)
28	〃	5	12	21	27			100	6 10			
29	〃	5	14	8	57			100	7 45			
30	〃	3	14	14	18			100	5 20	82	5 0	
31	〃	3	15	18	34			100	6 50	82	5 5	
32	〃	3	30	0	6			100	3 20	82	5 10	
33	〃	4	1	23	4	34·97 139·14	4	100	4 0	82	4 15	swarm earthquake in the vicinity of Itô
34	〃	5	9	12	52			100	6 10			
35	〃	3	13	4	29					82	4 30	
36	〃	2	23	18	31					82	5 30	
37	〃	3	19	10	16					82	4 30	
38	〃	2	21	8	37					82	1 35	
39	〃	3	21	23	4					82	4 26	
40	〃	3	4	3	50					82	4 0	
41	〃	3	9	19	54					82	4 0	(see Fig. 8)
42	1931	9	24	13	26	36·0 140·0	45	40	0° ca.			
43	〃	9	24	21	11	36·00 139·11		65	0° ca.			
44	〃	9	23	21	46	36·01 139·17				51	4 20	
45	〃	9	24	1	22	36·02 139·13				57	5 40	
46	1928	8	14	7	31	35·53 139·74				24	4 50	
47	〃	8	26	22	30	34·35 139·58				144	6 30	
48	〃	9	18	1	1	35·65 139·91	45			32	11 30	
49	1929	3	28	1	32	35·11 140·67				117	3 30	
50	1929	4	23	23	16	36·0 139·91				48	3 35	
51	1931	3	10	3	41	35·7 139·2				31	1 5	

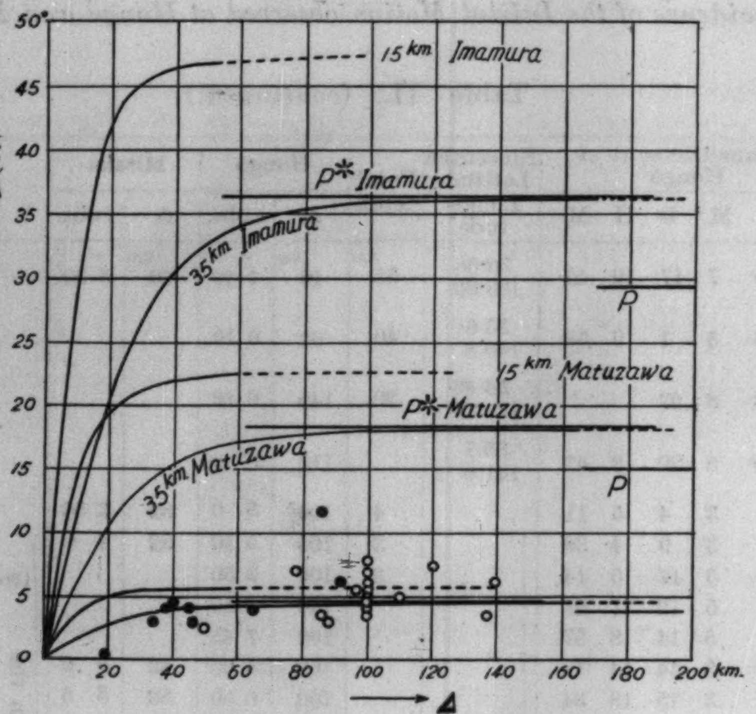

Fig. 2. $\Delta - i$ curve (Hongô).
○ earthquake with its focal depth 0–20 km.
● „ „ „ „ „ 20–50 km.

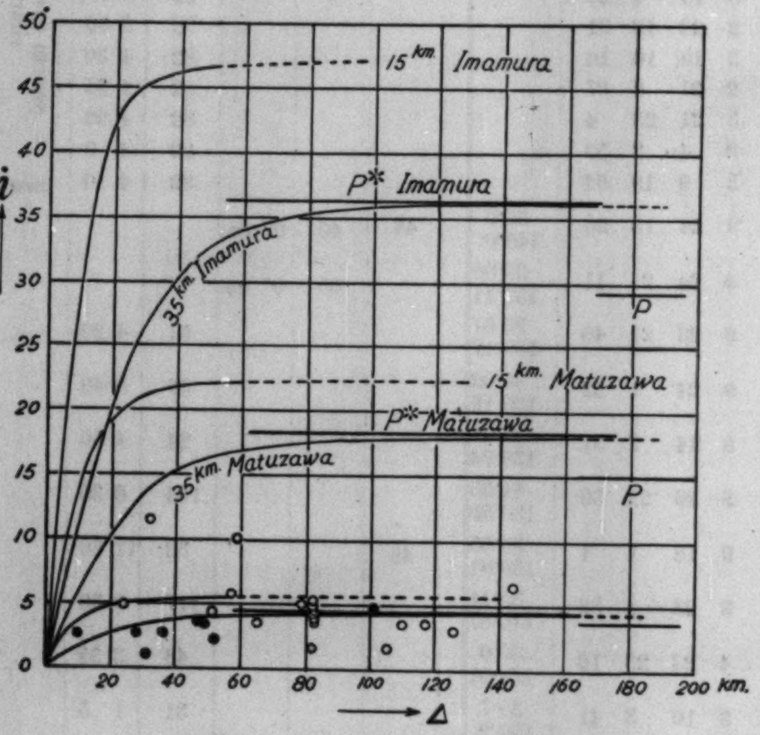

Fig. 3. $\Delta - i$ curve (Mitaka).
○ earthquake with its focal depth 0–20 km.
● „ „ „ „ „ 20–50 km.

In these figures the angle of incidence is plotted against the epicentral distance. Points denoted by ○ and those denoted by ● correspond respectively to the case of focal depth 0–20 km and 20–50 km. As apparent from the figures, the plotted value is nearly independent of the epicentral distance as well as the focal depth, and does not exceed four or five degrees. In illustration, some examples of typical seismogram obtained at Hongô and Mitaka will be shown. (Pl. LXXIX, Fig. 4, Pl. LXXX, Fig. 5, Pl. LXXXI, Fig. 6, Pl. LXXXII, Fig. 7, Pl. LXXXIII, Fig. 8.)

As to be seen from the figures the broad aspect of matter is quite clear. For example, in case of the North Idu earthquake of Nov. 26, 1930 (see Fig. 4), the initial horizontal motion is quite small compared with the vertical one. The time of commencement and the period of the initial motion are quite consistent in both the horizontal and the vertical component as seen from the figure. In horizontal motion a very distinct phase is recognized after 1·5 seconds from the commencement, which is the second phase found by Prof. Matuzawa.

In some ordinary earthquakes which are not so large, the period of the horizontal motion in the beginning phase is often observed different from that of the corresponding vertical one, i.e. the former is shorter than the latter. Even in such a case the horizontal motion with the same period as the vertical can be detected if closely examined. In vertical motion it may be difficult to detect a wave of shorter period on account of its superposition upon waves of longer period. The angle of incidence in such a case is of course determined by taking the resultant of three components with the same period.

The period of the initial motion of earthquakes here studied is nearly the same and ranges between 0·3 sec. and 1·0 sec. If a wave with a period more than 1·5 sec. is incident, then the initial phase is superposed by the transformed wave which is introduced by Prof. Matuzawa, and so that the determination of the angle of incidence may become difficult.

According to T. Isikawa's[5] recent investigation on the North Japan Sea earthquake of Feb. 20, 1931 which is very deep-seated, the angle of emergence of initial motion observed at the stations in Kwantô district is remarkably large compared with that observed at other places. Generally speaking this is quite consistent with the result obtained by the present writer. From T. Isikawa's result the true angle of incidence

5) T. Isikawa, *Journ. Meteor. Soc.*, Japan, [ii] 10 (1932), No. 4.

is calculated with respect to the values at stations in Kwantô district alone and shown in Table III.

Table III.

station	$\bar{e}$	$\bar{i}$	i
Tukubayama	80°0	10°0	8°8
Kakioka	80·0	10·0	8·8
Kumagaya	69·0	21·0	19·0
Tôkyô	73·6	16·4	14·0

The value of i obtained by the writer at Hongô is 3° 18′, as shown in Table II.

III. Discussion.

To explain the observed fact as above stated, the relation between i and Δ must be at first examined in both cases of the mode of superficial stratification of the earth crust introduced by Prof. Matuzawa[6] and by Prof. Imamura[7]. Prof. Imamura has taken into consideration the existence of a superficial sedimentary layer in the upper part of Matuzawa's first layer ($\bar{P}$). Thus, the thickness of the sedimentary layer and its velocity of dilatational wave are determined 10 km and 3·68 km/sec. respectively. The mode of stratification of the earth crust is shown in the following Table (Table IV), referring to the recent investigation of Prof. Matuzawa[8].

Table IV.

	Matuzawa		Imamura	
	depth from the surface	vel. of dil. waves	depth from the surface	vel. of dil. waves
$\bar{P}$	0 km— 4 km 4 —20	1·94 km/sec. 5·0	0 km—10 km (sed. layer)	3·68 km/sec.
P^*	20 —50	6·2		
P	>50	7·5		

6) T. MATUZAWA, *Bull. Earthq. Res. Inst.*, 5 (1928), 1-29; 6 (1929), 177-204.

7) A. IMAMURA, F. KISHINOUYE and T. KODAIRA, *Bull. Earthq. Res. Inst.*, 7 (1929), 471-487.

8) T. MATUZAWA and T. FUKUTOMI, *loc. cit.*, 517.

The relation between the angle of incidence at the earth surface and the epicentral distance can be easily determined, if the focal depth is given, as the problem is quite the same as that of geometrical optics. Numerical calculations were carried out for two cases and shown in Fig. 2 and 3. At first the depth of focus is taken 15 km, i.e. the source of seismic disturbance is in the first layer ($\bar{P}$). In Fig. 2 and 3 the relation is shown by the curves denoted by "15 km Imamura" and "15 km Matuzawa". The former curve shows the $\Delta - i$ relation for Prof. Imamura's assumption and the latter one for Prof. Matuzawa's assumption.

On account of stratification of the earth crust, beyond a certain epicentral distance the first incidence is the wave which is transmitted through the second layer parallel to the surface. For instance, in case of Matuzawa's assumption at a place 62 km from the epicentre the wave denoted by $\bar{P}\,P^*\,\bar{P}$ will first appear, which starts from the first layer and is refracted into the second layer and again into the first layer. Up to this epicentral distance the angle of incidence varies continuously with the distance, but beyond this distance it remains constant and 18° 30′ in the above mentioned case.

In the next place, the depth of focus is taken 35 km i.e. the origin of seismic disturbance is in the second layer (P^*). At small distance the angle of incidence approaches asymtotically to that of $\bar{P}\,P^*\,\bar{P}$ in the preceding case. According to Matuzawa's assumption, beyond the epicentral distance 165 km the first incidence is a wave denoted by $P^*\,P\,P^*\,\bar{P}$ (a wave which starts in the second layer and is refracted into the lower medium and again into the upper layers). In other words, to obtain these curves the travel time of different waves is taken into consideration. The same notice as above holds with respect to other set of curves.

As to be seen from Fig. 2 and 3 the curves thus obtained are not consistent with the observed values which are far smaller than that calculated as above. This may be rather natural. In order to obtain a curve which is well consistent with the observed values, it may be plausible to assume that there exists a quite superficial surface layer in which the velocity of transmission of waves is very small. Although such a factor may have already been taken into account by others, the present writer has examined it only numerically. The velocity of dilatational wave in this layer is easily determined from the observed value of i of the wave $\bar{P}\,P^*\,\bar{P}$. At the epicentral distance 80 km or

so, the mean observed value of i is approximately 4° 30′. Let v be the velocity to be determined, then the following relation is obtained, unless there is any oblique boundary separating two media,

$$\sin i = \frac{v}{6{\cdot}2},$$

where 6·2 km/sec. is the velocity of dilatational wave in the second layer (P^*).

As the observed values of i are nearly the same both at Hongô and Mitaka, the value of v becomes also the same at both places. From above formula v comes out approximately 0·5 km/sec.

Now the velocity is determined 0·5 km/sec. as above, but the thickness of such a layer can not be obtained at all. At any rate there is no doubt that such a layer is only confined to the very surface.

To obtain the $i-\Delta$ relation, the thickness of the layer with velocity 0·5 km/sec. is tentatively assumed 0·5 km, because the thickness of this layer does not much affect the $i-\Delta$ curves. The $i-\Delta$ relation is calculated for two cases of focal depth as before under the mode of stratification of earth crust tabulated as follows. (Table V)

Table V.

Thickness of layers	0·5 km.	4	16	30	>50.5
Vel. of dil. waves	0·5 km/sec.	1·94	5·0	6·2	7·5

The results of calculations are shown in Fig. 2 and 3. In this case also, the curves have been drawn, the travel time of different waves being taken into consideration. From the figures, the observed values seem to be generally well explained in this manner.

Recently it has been suggested by some seismologists[9] that the earth crust has no stratified structure and the velocity of propagation of waves increases with depth continuously. As far as the angle of incidence at the surface alone is concerned, there is no remarkable difference whether the earth crust is stratified or not.

In the earthquakes shown in Table II, the period of the initial motion is nearly from 0·3 sec. to 1·0 sec. When the period is so large as a few tens of seconds, the matter becomes somewhat different. In case of the great Tango earthquake of March 7, 1927 the seismograms

9) K. SAGISAKA, *Geophys. Mag.*, 4 (1931), 147-155.
H. HONDA, *Geophys. Mag.*, 4 (1931), 201.

obtained at Hongô ($\Delta=427$ km) revealed motions with very long period from the beginning. Therefore, the record of the seismograph must undergo certain reductions.

Using the customary notations, the equation of motion of a seismograph is given by

$$\frac{d^2a}{dt^2}+2\varepsilon\frac{da}{dt}+n^2a=-V\frac{d^2x}{dt^2}.$$

If this equation is integrated twice from $t=0$ to $t=t$, then

$$a+2\varepsilon\int_0^t a\,dt+n^2\int_0^t dt\int_0^t a\,dt=-Vx.$$

The displacement of the earth-movement at any time t is obtained by the reduction shown in the left-side of this equation. In case of great Tango earthquake the period of initial motion is approximately 35 sec. and the angle of incidence comes out 58°.

Another example is the strong earthquake of Nov. 2, 1931 which took place in Miyazaki Prefecture in Kyûsyû. The seismogram of the vertical seismograph obtained at Hongô has been already reduced by Dr. H. Kawasumi[10]. From Dr. Kawasumi's result and the record of Imamura's long period horizontal pendulum seismograph, the angle of incidence is determined approximately 50°, the period of the motion being 25 sec. Although these are only two cases, it will be seen that the angle of incidence varies with the period of motion. This fact may suggest that the most superficial structure, varying from place to place, is not effective to the refraction of seismic waves with long period.

It follows from the theory of elasticity, that the law of refraction of elastic waves at the boundary separating two media is independent of the wave length of incident wave. It holds indeed, if the boundary is large enough compared with the wave length or infinitely extended.

On the other hand, suppose that the upper medium is separated by vertical boundaries into blocks, loosely connected with each other, dimensions of which are of the order of magnitude of wave length. In such a case if the elastic wave whose wave length is much larger than the dimension of each block, is incident from the lower medium to the upper one, then the strain distribution in the upper medium may be nearly uniform. Therefore such a surface block behaves as if this is only a part of the lower medium, and does not contribute to the refraction of elastic wave.

10) H. KAWASUMI, *Disin* or *Journ. Seism. Soc.*, Japan, 4 (1932), No. 2, (in Japanese).

In case of earthquakes shown in Table II, their period of initial motion being from 0·3 sec. to 1·0 sec., the most superficial surface whose velocity is 0·5 km/sec. may play an important part. On the other hand it may not be brought into question for the wave of long period as that of great Tango earthquake or of the strong earthquake in Miyazaki Prefecture.

Dr. S. Haeno[11] has obtained 0·25 km/sec. as the velocity of dilatational wave of the ground by the Radio-Seismograph which he has constructed, in his experimental study made in the compound of our university. This value is one half of that obtained by the writer, but the superficial ground may not afford to contribute to the refraction of ordinary seismic waves by the reason as above mentioned.

Dr. N. Nasu[12] has investigated the propagation of artificial disturbance produced by falling a stone on the ground and obtained 0·78 km/sec. as the velocity of the dilatational wave in the experiment made at neighbourhood of our university. This is somewhat greater than that obtained by the writer, but nearly the same in the first approximation.

Now the writer will remark on some observational facts with regards to the seismogram.

At first it is often observed that at the commencement the vertical movement apparently occurs one or two seconds earlier than the horizontal one. This point was found by Visser and Berlage[13] from their observation of distant earthquakes in Batavia. The way of explanation of this phenomenon is similar to that proposed by Prof. Matuzawa.

The apparent earlier commencement of the vertical motion is also often observed in the earthquakes shown in Table II. For instance, in case of the earthquake of March 9, 1931 608 km distant from Tôkyô, the amplitude of the vertical initial motion is 0·1 mm (magnification: 28) and the horizontal one (magnification: 50) is observed with difficulty two seconds after the commencement of the vertical one. The amplitude of the first phase may diminish so much partly due to several refractions and reflexions[14] at boundaries of discontinuity, partly due to the mechanism of occurrence at origin. At any rate, the horizontal motion becomes so small compared with the vertical one, because the

11) S. HAENO, *Journ. Astr. Geophys.*, Japan, 8 (1931), 39–50.

12) N. NASU, *Disin* or *Journ. Seism. Soc.*, Japan, 1 (1929), No. 5, (in Japanese).

13) S. W. VISSER und H. P. BERLAGE, *Gerl. Beitr. z. Geophys.*, 19 (1928), 147–152.

14) H. KAWASUMI and T. SUZUKI, *Disin* or *Journ. Seism. Soc.*, Japan, 4 (1932), No. 5, (in Japanese).

tangent of the angle of incidence is one-tenth or so at Hongô and Mitaka. Therefore, the apparent earlier commencement of the vertical motion than the horizontal one is naturally understood in case of small earthquakes as well as somewhat distant earthquakes.

In the next place, the seismogram of the vertical component does not often reveal any distinction between the preliminary tremor and the principal portion, especially in case of near earthquakes. Fig. 5 [Pl. LXXX] shows the most typical example. On the other hand, the horizontal motion is literally small in the preliminary tremor and becomes suddenly large when the distortional wave is incident. This fact may also be due to nearly vertical trajectory of the wave near the surface. Although it will depend upon the mechanism of occurrence at the origin, whether the *SH*-wave (distortional wave with its plane of vibration parallel to the surface) or the *SV*-wave (the same with its plane of vibration in the incident plane) will be mainly produced, the vibration of the particle will become gradually parallel to the surface from deep place toward the earth-surface even in case of predominance of *SV*-wave. If such a consideration is taken for granted, the observed fact may be plausibly understood.

One more remark will be added to this phenomenon. In case of great Tango earthquake, the three components of the seismogram obtained at Hongô revealed clearly the distinction between the preliminary and the principal portion. It must be remembered that the angle of incidence in this case is 58°.

Summary.

(1) A remarkable forerunner of earthquake motion obtained at Hongô and Mitaka has been fully discussed and plausibly elucidated by Prof. Matuzawa and others. The present writer has studied the angle of incidence of the first motion and it becomes approximately 4° as the mean value at both stations, its fluctuation being small.

(2) From this value of angle of incidence, 0·5 km/sec. is determined as the velocity of dilatational wave in the most superficial layer.

(3) The angle of incidence of the first motion seems to vary with its period such that 4° when the period is 0·4 sec. or so and 50° when the period is about 30 sec.

(4) A few remarks are added to explain some characteristic features of seismogram.

In conclusion the writer wishes to express his heartfelt thanks to

Prof. Matuzawa for his kindness in revising of the original manuscript and valuable advices. Further the writer wishes to record his indebtedness to Dr. H. Kawasumi.

---

36. 本鄉、三鷹に於ける初動入射角に就て

地震學教室　鈴　木　武　夫

(1) 本鄉、三鷹に於ける近地地震の記象に於て初動が著しく鉛直方向に近く偏つて居ることは旣に松澤先生の指摘說明せられた所であるが、筆者は地震記象より初動部分の三成分を合成して初動入射角を求めたるに本鄉、三鷹に於てそれは震央距離や震原の深さにはあまり依らず約四度乃至五度である。

(2) 入射角が小即ち震波線が鉛直に近づくことは地表近くの地震波の速度が深處に較べて小なることに因ると考へられ上述の入射角の値より地表近くの疎密波の速度として 0·5 km/sec. を得た。

(3) 入射角は初動部分の週期が 0·3–1·0 秒位では 4–5 度であるが、週期が 25–30 秒になると 50 度位となる。これは地震波の波長が大となるとその波長より小なる廣がりを持つ地表近くの局部的地層は波の屈折には問題とならない爲であらう。

(4) 初動に於て上下動は水平動より少し早く初まると云ふ觀測事實と、上下動に於ては一般に初期微動と主要動との區別が明瞭でないと云ふ事柄に就て少しく考へて見た。

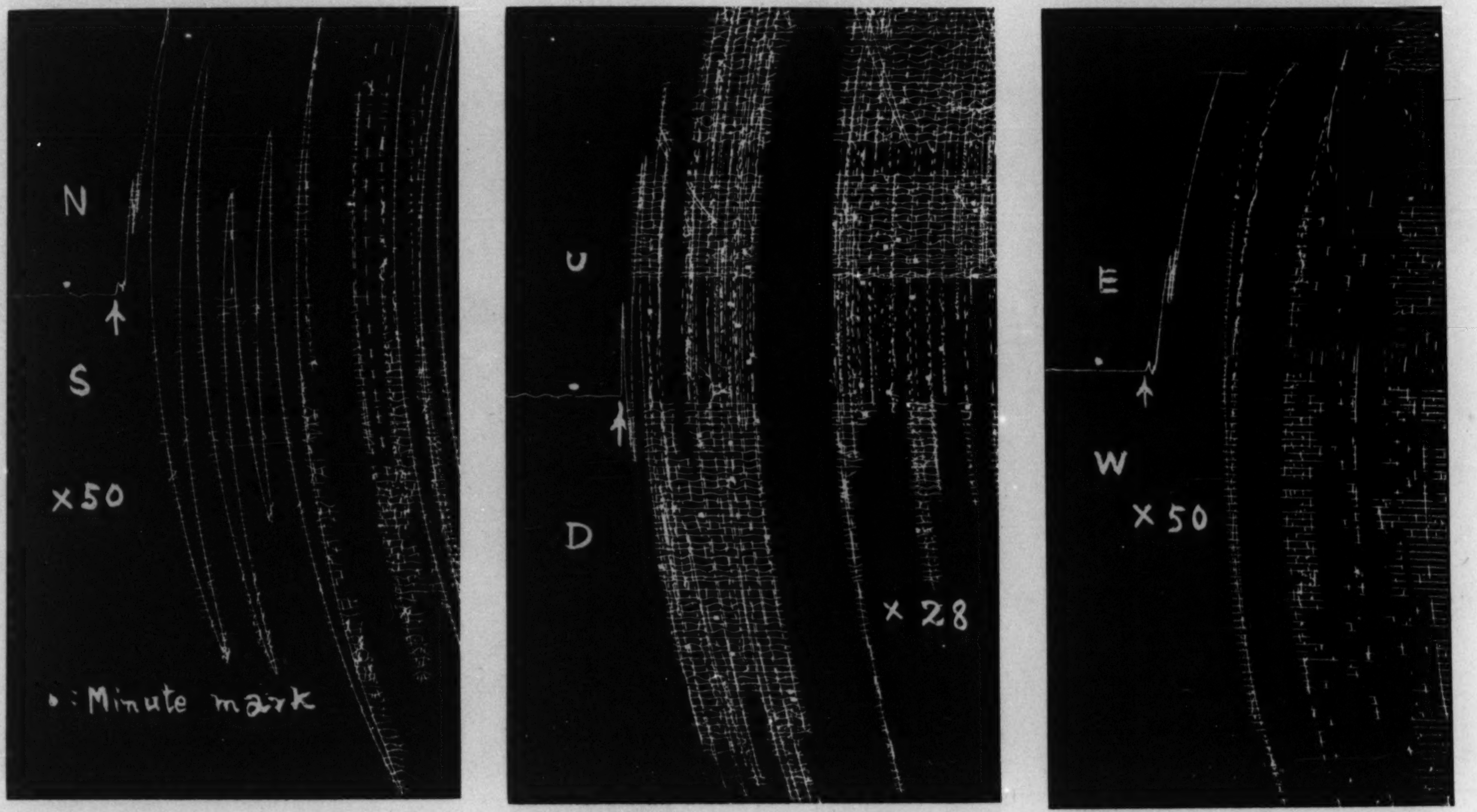

Fig. 4. Earthquake of November 26, 1930. (No. 20)
Recorded at Hongô.

(震研彙報、第十號、圖版、鈴木)

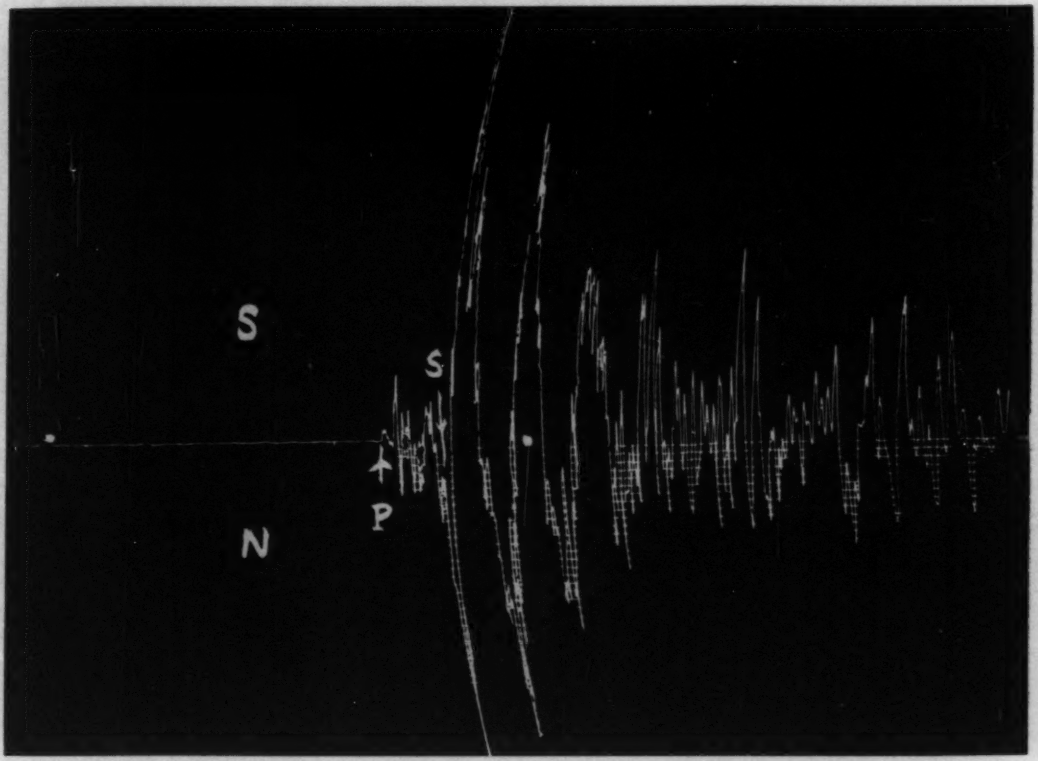

Magnification 50

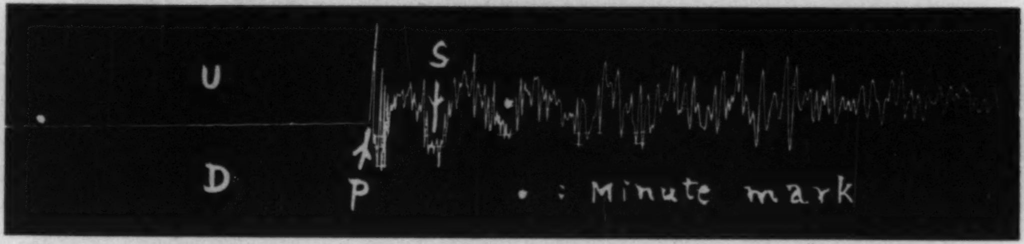

Magnification 18

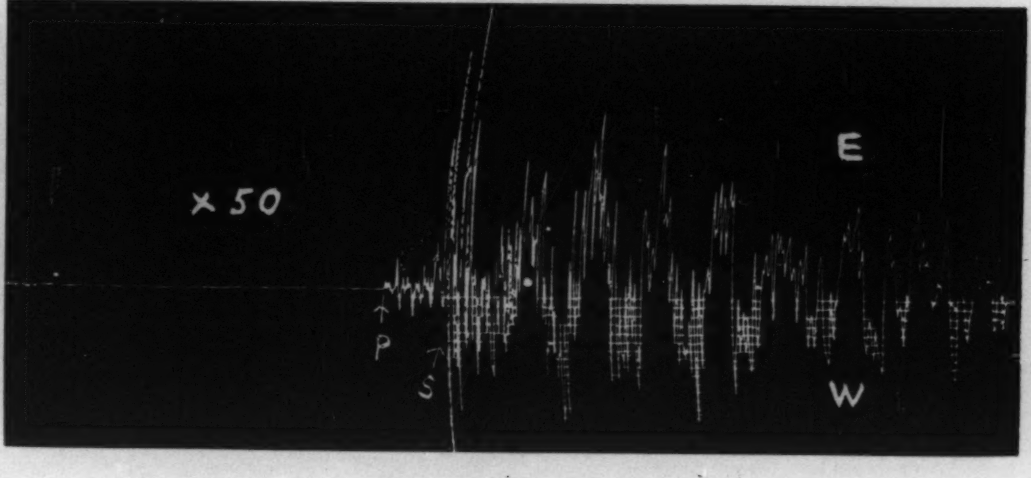

Fig. 5. Earthquake of October 5, 1928. (No. 1)
Recorded at Mitaka.

(震研彙報、第十號、圖版、鈴木)

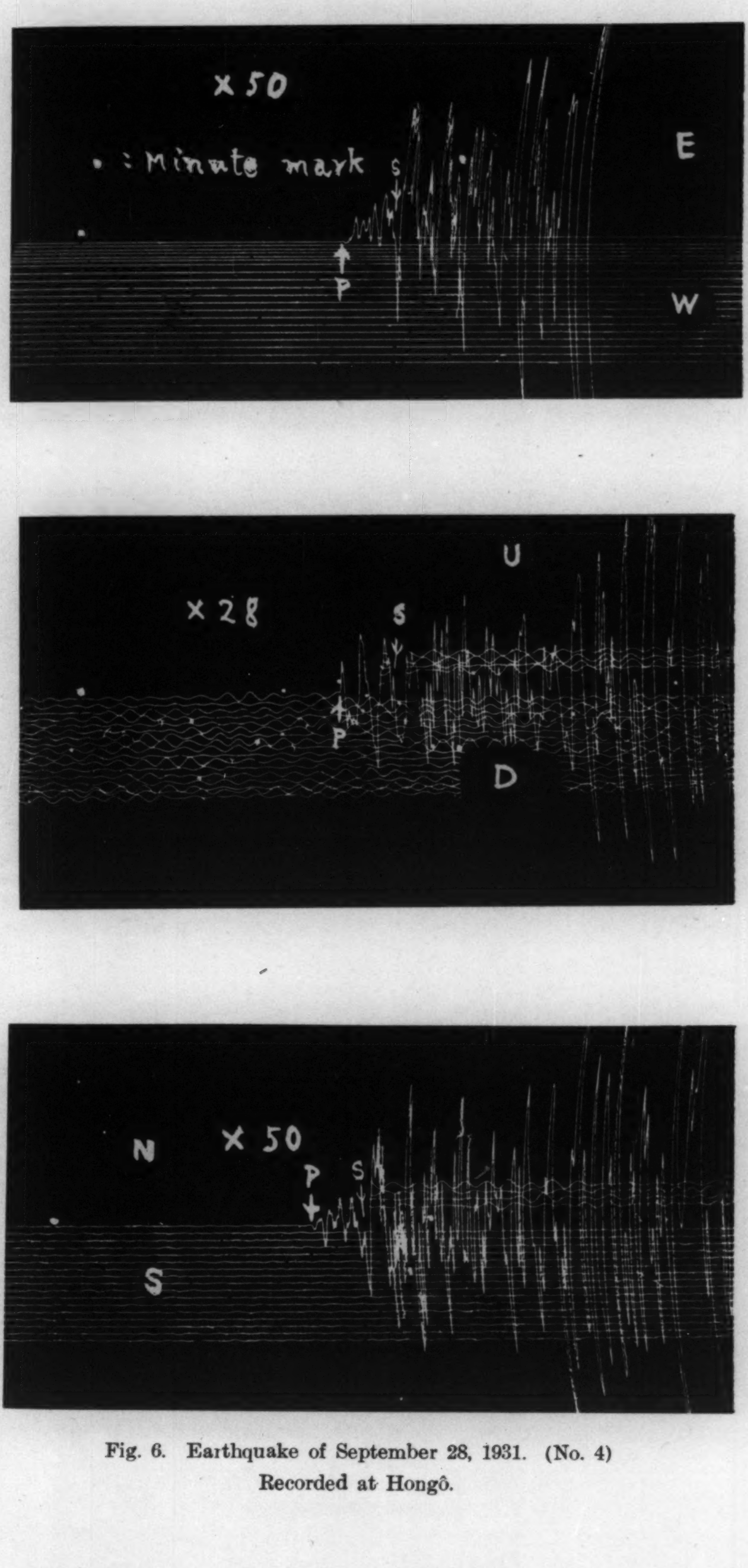

Fig. 6. Earthquake of September 28, 1931. (No. 4)
Recorded at Hongô.

(震研彙報、第十號、圖版、鈴木)

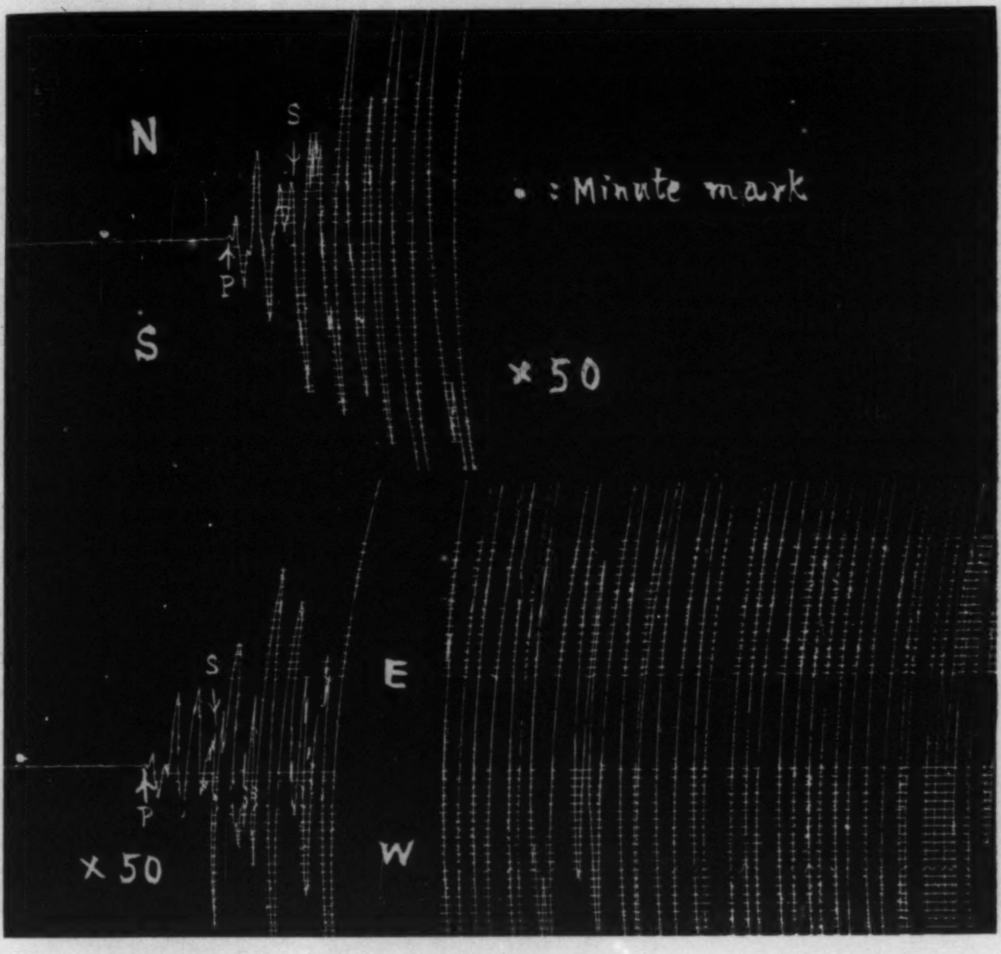

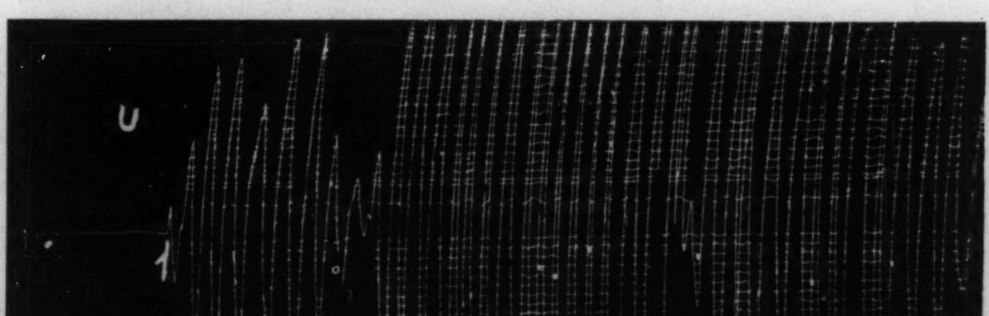

Fig. 7. Earthquake of May 17, 1930. (No. 27)
Recorded at Hongô.

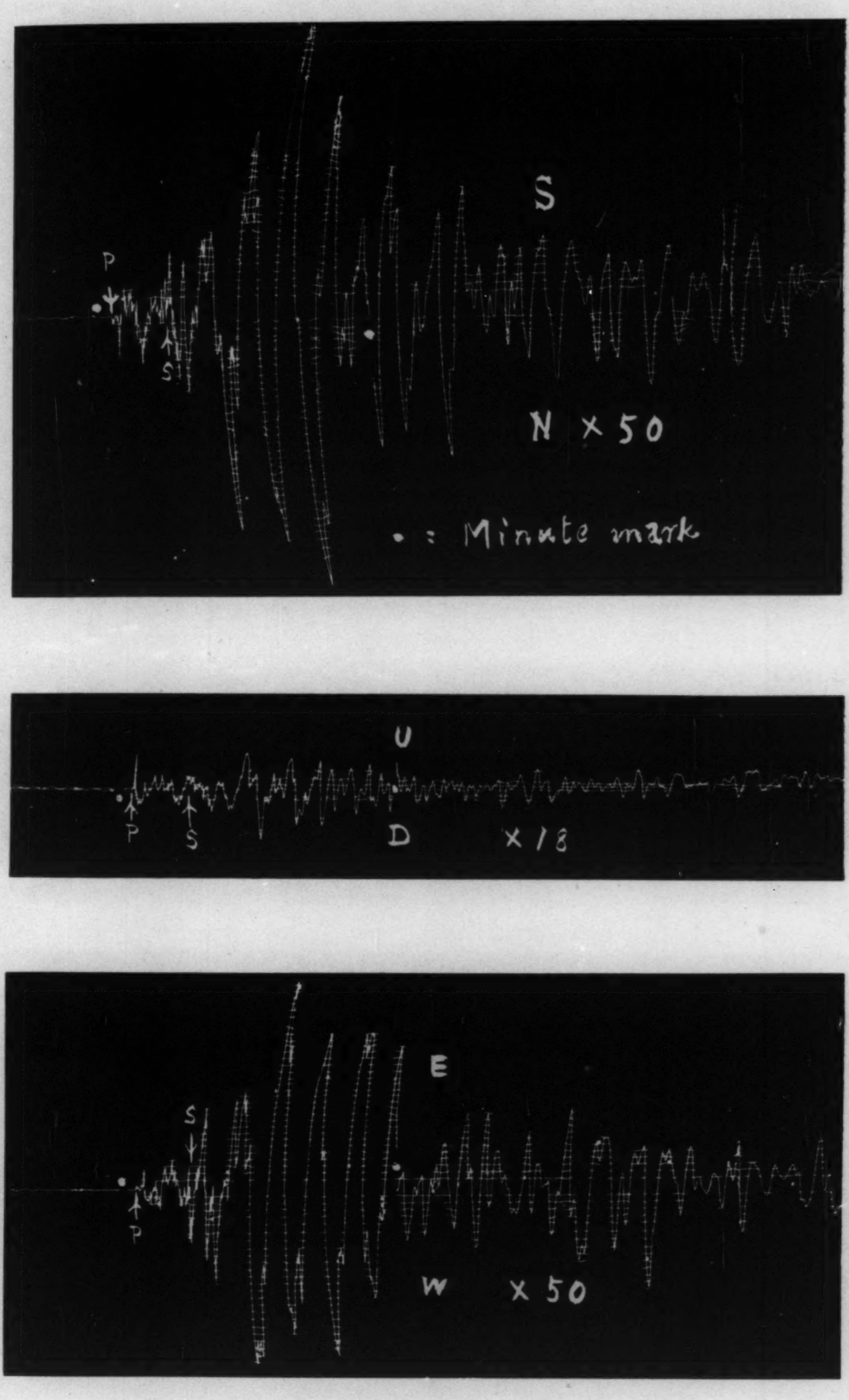

Fig. 8. Earthquake of March 9, 1930. (No. 41)
Recorded at Mitaka.

(震研彙報、第十號、圖版、鈴木)

37. *Tilting Motion of the Earth's Crust observed at Ryozyun (Port Arthur).*

By Ryûtarô TAKAHASI,

Earthquake Research Institute.

(Read Mar. 15, 1932.—Received June 20, 1932.)

1. Introduction. One of the most interesting facts which the recent geophysical investigations in this country revealed, may be that the earth's crust has, at least in some part of it, mozaic structures and that it *does* move incesantly, either related or not related with the occurrences of earthquakes. These developments of our knowledge we owe solely to the introduction of geodetic means to the study of earthquakes and other geophysical phenomena. The existence of secular deformations of the earth's crust and the predominance of mozaic structure in certain regions, have already become the facts of common knowledge in our country. Studies on the size and motion of these land blocks, relations among their size, the frequency of earthquakes and the geological structure, and the general behaviours of their movements after remarkable earthquakes, have been made in so through a manner that there now remain only such problems about land blocks as those regarding their characteristics or the statistics of their movements, except for the study on the fundamental phenomena of their behaviours.

The geodetic surveys which have given invaluable data for these studies were mostly executed, however, in regions more or less disturbed by earthquakes, only few of them having been made in regions entirely free from disturbances of earthquakes. It is, therefore, of great importance to ascertain whether or not the secular deformation of the earth's crust is equally existing in regions entirely free from the earthquake disturbances. In these views, we have started to make observations on the secular movement of the earth's crust at Ryozyun (Port Arthur), where no earthquake has been experienced since the middle of the last century. The secular movement of the earth's crust was known by observing the tilt of the ground by horizontal pendulums. According to the results of the observation so far obtained, we may conclude that there is no sensible secular tilt of the earth's crust at Ryozyun. This conslu-

sion, however, does not worth much confidence because the present observation is too short and was interrupted for about two months under an unavoidable circumstance.

We were fortunate enough, however, in having observed as a by-product the tilting motion of the earth's crust due to tidal loads in the neighbouring seas of the observation station. The present writer has already studied in this Bulletin the similar phenomena observed at other places.[1] Investigations of the tilt of the earth's crust due to tidal loads are very important for the analysis of the earth-tides and, at the same time, for the studies of the structure and rigidity of the earth's crust as well as that of the whole earth. Studies in these lines will give, therefore, much clue to the elucidation of the mechanism and nature of the block movements mentioned above.

2. General description of the observation and the results obtained. The present observation was made in the cellar of the wireless telegraph office, belonging to the Ryozyun Engineering College. The office is situated on a hill in the west suburb of the city of Ryozyun, and is ca. 62 m. high above the mean sea level and is 1·2 km. distant from the nearest coast line. The location of the office is to be seen in Fig. 1.

Fig. 1. Map of Ryozyun. Dotted area indicates sand-banks that appear at low water.

The instrument used in the present observation is a pair of the Ishimoto tiltmeters. The tiltmeter is essentially a horizontal pendulum of the Zöllner suspension, the movable horizontal rod, the suspension fibres and the frame work being all made of fused quartz. Suspension fibres are fused to the frame work and to the movable rod. The instrument is therefore scarcely affected by the variation of temperature of the surrounding air and is also entirely free from elastic after-effect. The angular position of the horizontal rod is recorded continuously by projecting a light beam from a light source and receiving the reflected beam from a mirror attached to the rod on a sheet of photographic paper wound on a revolving drum, the drum being placed

1) *Bull. Earthq. Res. Inst.*, 6 (1929), 85; 7 (1929), 95; 10 (1932), 145.

at the distance of 1 m. from the pendulum. The drum makes one revolution per week by a clock-work contained in its inside, the linear speed being 4·2 cm. per day. Time-marks are recorded twice a day on the record, at 6^h and 18^h, by interrupting the electric current which feeds the light source. The sensibility of the tiltimeter was calibrated before its installation so that we can calculate the sensibility of the instrument at any desired time, or adjust it to any predetermined value, by measuring or regulating suitably the period of free oscillation of the pendulum. Details about the instrument will not be described here as they are fully given in Ishimoto's paper.[2]

The cellar of the wireless telegraph office in which the pendulums were installed has been left as it was digged down to the ground, and is not lined by any material. A concrete box, which is 2 m. × 2 m. × 3 m. in inside dimension, was half embedded into the floor of the cellar, and the tiltmeters were placed directly on the bottom of this concrete box. The concrete box is provided with a wooden entrance door and with a roof covered with a thick layer of sand. The pendulums were installed in the azimuths of 75° and 165°, measured in the clock-wise sense from north to east. The general view of the concrete box and of the installation of the tiltmeters will be obtained by Fig. 2. The sensibility of

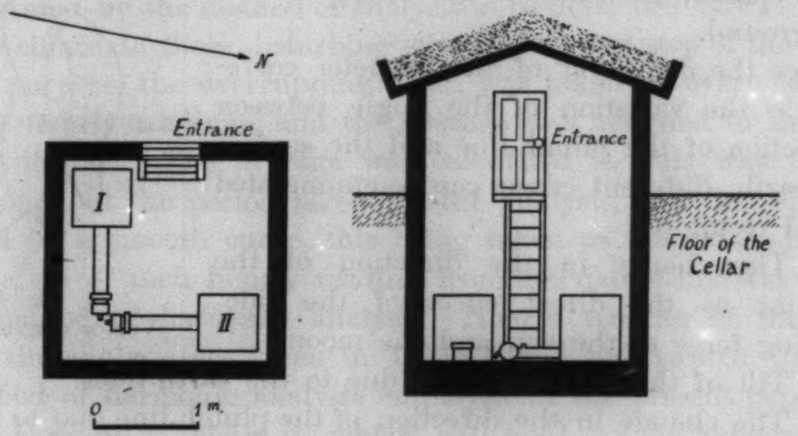

Fig. 2. Observing chamber.

the instrument was adjusted at the beginning of the observation so as it gives the deflection of 2 cm. on the record corresponding to the tilt of 1 second of arc. The sensibility has been calibrated since then many times by measuring the period of free oscillation of the pendulum.

2) M. Ishimoto, *Jap. Journ. Astro. Geophys.*, 6 (1928), 83.

The observation was commenced on Feb. 1, 1931, and has still been continued. In the present paper, however, a part of the observation, extending from April 1, 1931 to Feb. 3, 1932, will only be dealt with. The actual observation, the installation of, and the attendance to the instrument were kindly made by Mr. H. Watanabe, under the guidance of Professor T. Hori, to whom the writer wishes here to express his hearty thanks.

In Fig. 3 (Plate LXXXIV) is given a reproduction of the record obtained by the tiltmeter for the period from Mar. 30 to April 6, 1931. The straight line in the record is the datum-line produced by a fixed mirror placed near the pendulum mirror, and the wavy curve is the record of the tilt of the earth's crust. In this figure as well as in the following, the letters **E**, **W**, **N** and **S** are the directions towards which the ground tilts down. The deflection of the tilt-curve to the side of the letter **E** means, thus, that the crust tilts down to the east side. As can be seen in the figure, the tilt of the earth's crust at Ryozyun is composed of variations respectively with a very long, diurnal and semi-diurnal periods. These features of tilt will be made clearer by making a vector-diagram such as given in Fig. 4. This shows a curve that a rod, planted perpendicularly to the ground, will describe on the celectial sphere, according to the tilting motion of the ground.

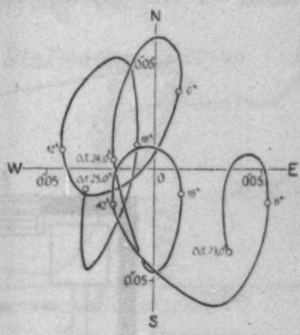

Fig. 4.
Vector diagram of tilt.

Since the deflection of the tiltmeter corresponds to the variation of the angle between the direction of the plumb-line and the surface of the earth, different causes can be enumerated that will result it:

1. The change in the direction of the plumb-line as the direct effect of the tide-generating force of the sun and the moon.
2. Tilt of the earth's surface due to the earth-tides.
3. The change in the direction of the plumb-line due to the deformation of the earth caused by the earth-tides.
4. The change in the direction of the plumb-line due to the attraction of oceanic tides.
5. Tilt due to the load of sea water in oceans.
6. The change in the direction of the plumb-line due to the deformation of the earth produced by tidal loads.
7. The tilt and the change in the direction of the plumb-line due

to the periodic variation of the level of underground water.

8. The atmospheric tides both as load and as attraction.

9. The tilt of the ground due to the thermal stress produced by the variation of the atmospheric temperature and by the sun-shine.

10. Secular or cummulative tilt of land blocks or of the earth's crust.

11. Secular variation of the direction of the plumb-line.

The tiltmeter deflections are thus composed of many defletions which is produced by various causes. It is therefore necessary for the detailed study of the phenomena to analyse the observed deflection into these component deflections. The first three of these items are inseparable in the observation. Some of these causes are very small in amount and need not be taken into consideration. In the following paragraph we will analyse into different components the tilt observed during the period from Oct. 20 to Nov. 17, 1931, in which the tilt due to the annual variation is smallest.

3. Analysis of the observed tilt. We find by further inspection of the record that there is tilt of the period of a few days, besides the tilts already cited. Being due directly or indirectly to meteorological variations, neither these tilts of medium period, nor the long perioded ones can be treated by the method of analysis to be described later. We must therefore eliminate these disturbing tilts in the first step of the analysis. For this purpose, the overrupping mean was taken of every set of 25 successive hourly readings, and the average was assigned to the middle epoch of the set. The average was calculated in this way for every hour throughout the period taken for the analysis, and the values were connected by a smooth curve, this being taken as the datum-line.

Deviation of each hourly reading from this datum-line was analysed by the method of harmonic analysis. Hourly reading of the records used for the analysis are given in Table I and are plotted in Fig. 5. The method of harmonic analysis employed in the present paper is due to A. T. Doodson,[3] details of which will need not be explained here. The results were of course obtained after making all corrections such as those due to the factor of reduction, acceleration in epoch, disturbances among different components, reduction to local time, etc.

Results of the analysis are as follows:

3) A. T. Doodson, *Phil. Transact.*, **227 A** (1927), 223.

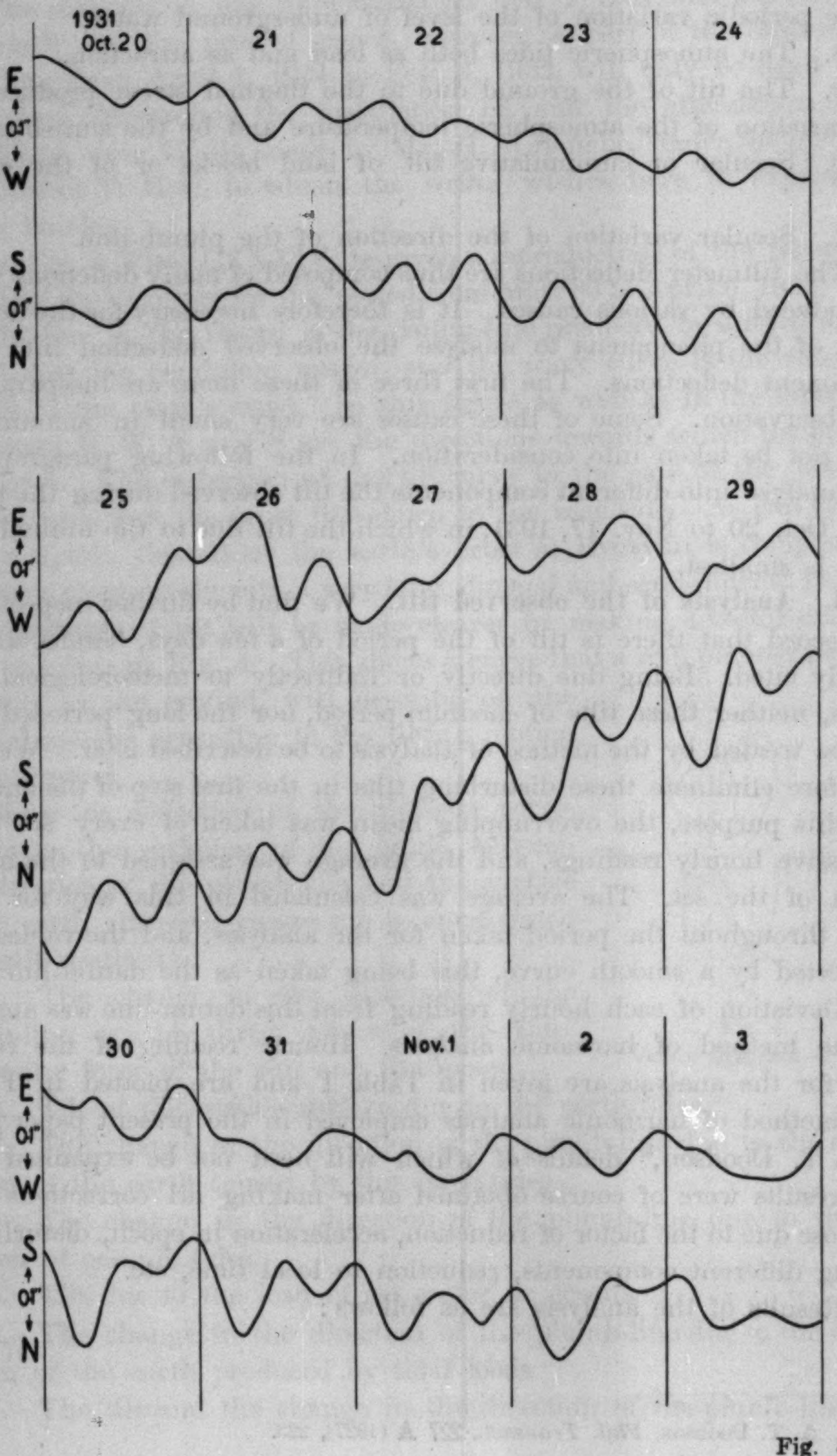
1931
Oct.20
21
22
23
24
E
or
W
S
or
N
25
26
27
28
29
E
or
W
S
or
N
30
31
Nov.1
2
3
E
or
W
S
or
N

Fig. 5.

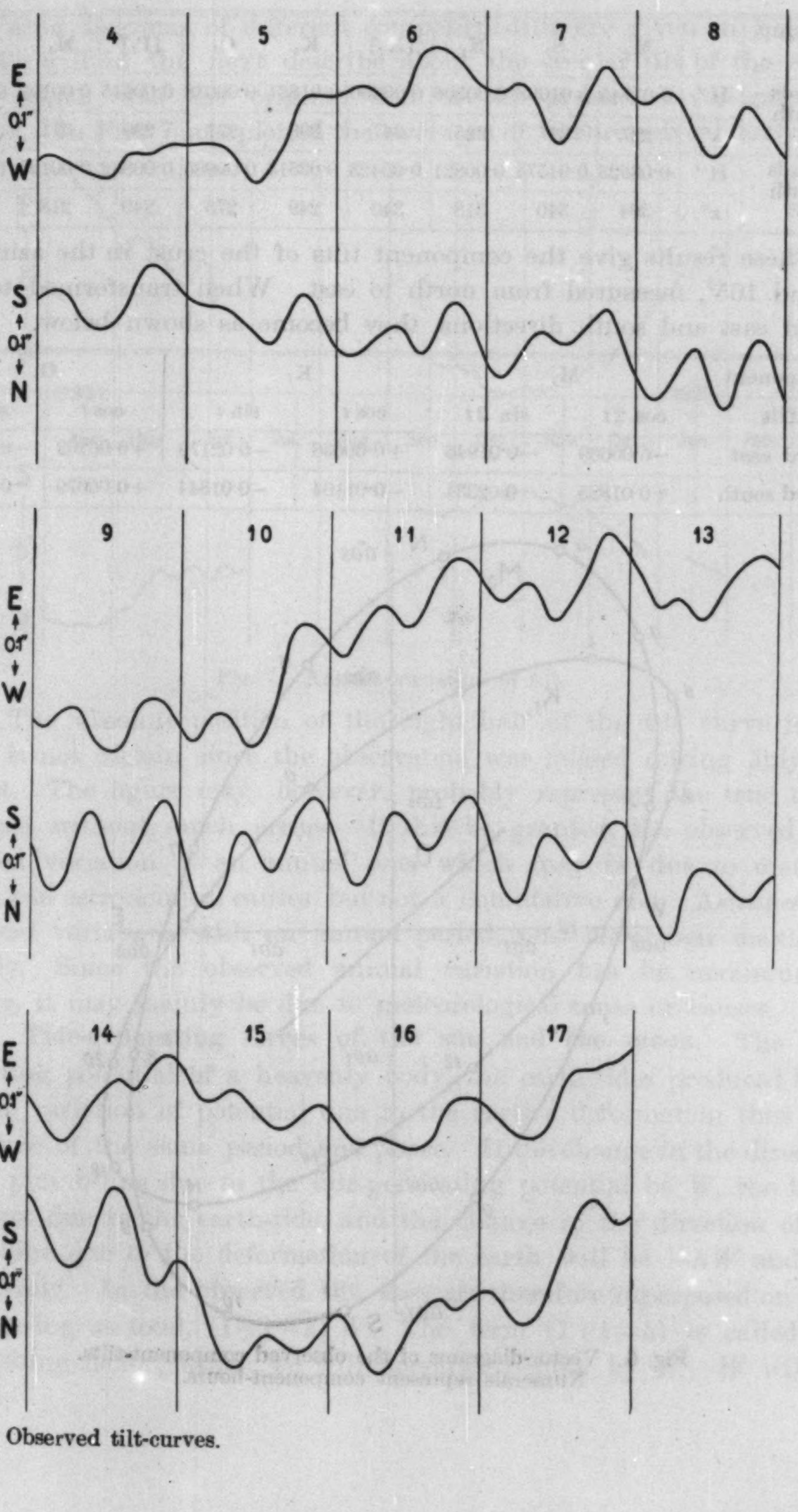

Observed tilt-curves.

Comp. / Tilt		M_2	S_2	N_2	$[K_2]$	K_1	O_1	$[P_1]$	M_4	MS_4
Towards azimuth 75°	H″	0·01745	0·01098	0·00506	0·00296	0·01861	0·00638	0·00615	0·00101	0·00052
	$\kappa°$	227	247	225	247	299	277	299	311	36
Towards azimuth 165°	H″	0·03323	0·01575	0·00821	0·00423	0·02513	0·00985	0·00832	0·00127	0·00097
	$\kappa°$	304	340	318	340	249	276	249	218	317

These results give the component tilts of the crust in the azimuths 75° and 165°, measured from north to east. When transformed to the tilts in east and south directions, they become as shown below.

Component	M_2		K_1		O_1	
Tilt	cos $2t$	sin $2t$	cos t	sin t	cos t	sin t
toward east	−0·00669	−0·01946	+0·00638	−0·02179	+0·00102	−0·00865
toward south	+0·01825	0·02331	−0·01104	−0·01844	+0·00079	−0·00782

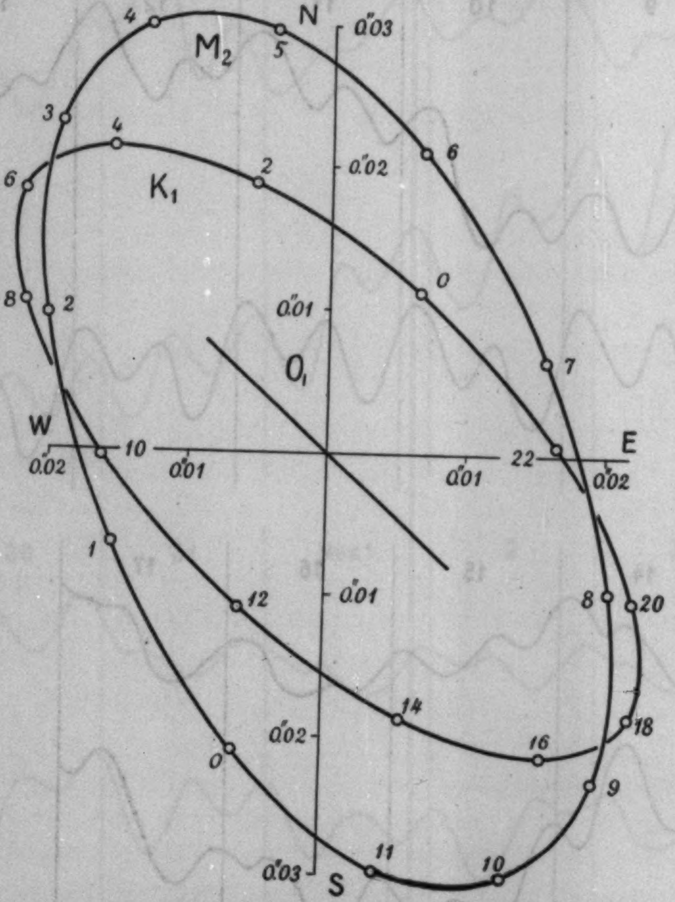

Fig. 6. Vector-diagrams of the observed component-tilts. Numerals represent component-hours.

Vector-diagrams of different component-tilts are given in Fig. 6.

We will in the next describe about the secular tilt of the earth's crust, which was the original aim of the present investigation to observe. In Fig. 7 are plotted the averages of 12 successive hourly read-

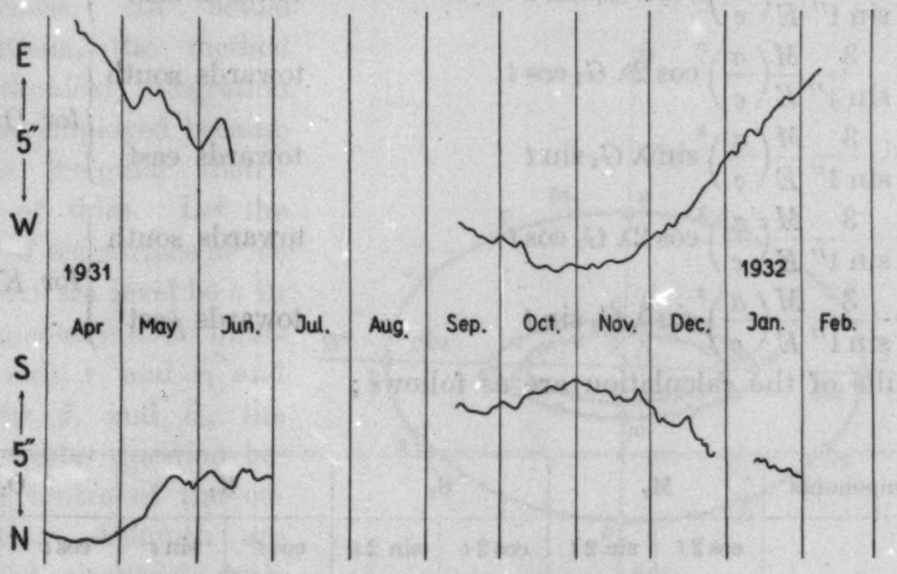

Fig. 7. Annual variation of tilt.

ings. The absolute position of the right half of the tilt curve in the figure is not certain since the observation was missed during July and August. The figure may, however, probably represent the true tilt of the crust without much errors. If this be granted, the observed long perioded variation is an annual one, which may be due to meteorological and astronomical causes, but not a cumulative one. Astronomical and tidal variations with an annual period must have their maximum in July. Since the observed annual variation has its maximum in October, it may mainly be due to meteorological cause or causes.

4. Tide-generating forces of the sun and the moon. The tide-generating potential of a heavenly body, the earth-tides produced by it, and the variation of potential due to the earth's deformation thus produced are of the same period and phase. If the change in the direction of the plumb-line due to the tide-generating potential be W, the tilt of the crust due to the earth-tide, and the change in the direction of the plumb-line due to the deformation of the earth will be $-hW$ and kW respectively. In the observed tilt, they are therefore superposed on each other giving as total, $(1+k-h)\,W$. The term $(1+k-h)$ is called the diminishing factor, which we will hereafter denote by R. W will be

easily calculated by the following expressions.[4]

$$\left.\begin{array}{ll} \dfrac{3}{\sin 1''}\dfrac{M}{E}\left(\dfrac{a}{c}\right)^3\cos\lambda\sin\lambda\, G_1\cos 2t & \text{towards south} \\ -\dfrac{3}{\sin 1''}\dfrac{M}{E}\left(\dfrac{a}{c}\right)^3\cos\lambda\, G_1\sin 2t & \text{towards east} \end{array}\right\}\text{for } M_2;$$

$$\left.\begin{array}{ll} -\dfrac{3}{\sin 1''}\dfrac{M}{E}\left(\dfrac{a}{c}\right)^3\cos 2\lambda\, G_2\cos t & \text{towards south} \\ -\dfrac{3}{\sin 1''}\dfrac{M}{E}\left(\dfrac{a}{c}\right)^3\sin\lambda\, G_2\sin t & \text{towards east} \end{array}\right\}\text{for } O_1;$$

$$\left.\begin{array}{ll} -\dfrac{3}{\sin 1''}\dfrac{M}{E}\left(\dfrac{a}{c}\right)^3\cos 2\lambda\, G_3\cos t & \text{towards south} \\ -\dfrac{3}{\sin 1''}\dfrac{M}{E}\left(\dfrac{a}{c}\right)^3\sin\lambda\, G_3\sin t & \text{towards east} \end{array}\right\}\text{for } K_1.$$

Results of the calculation are as follows:

Components	M_2		S_2		K_1		O_1	
	$\cos 2t$	$\sin 2t$	$\cos 2t$	$\sin 2t$	$\cos t$	$\sin t$	$\cos t$	sin
Towards east	0	$-0''.01178$	0	$-0''.00571$	0	$-0'.00642$	0	$-0''.00482$
Towards south	$0''.00739$	0	$0''.00358$	0	$-0''.00220$	0	$-0''.00165$	0

4) Notations: $G_1=\left(\frac{1}{2}-\frac{5}{4}e^2\right)\cos^4\frac{I}{2}$,

$G_2=\left(\frac{1}{2}-\frac{5}{4}e^2\right)\sin I\cos^2\frac{I}{2}$,

$$G_3=\Big[\left(\frac{1}{4}+\frac{3}{8}e^2\right)^2\sin^4 I+\left(\frac{1}{4}+\frac{3}{8}e_1^2\right)^2 G^2\sin^4\omega+2\left(\frac{1}{4}+\frac{3}{8}e^2\right)\left(\frac{1}{4}+\frac{3}{8}e_1^2\right)$$
$$\times G\sin^2 I\sin^2\omega\cos 2\nu\Big]^{\frac{1}{2}},$$

$G=\dfrac{\text{mass of }\odot}{\text{mass of }☾}\times\left(\dfrac{\text{mean distance of }☾}{\text{mean distance of }\odot}\right)^3=0.46164$,

M mass of moon,
E mass of earth,
a radius of earth,
c mean distance of moon,
λ latitude of the place.
t hour angle of component fictious star or component hour,
e eccentricity of moon's orbit,
I inclination of moon's orbit to equator,
ω inclination of earth's equator to ecliptic,
e_1 eccentricity of earth's orbit,
ν R. A. of intersection of moon's orbit with equator.

5. Attraction of the oceanic tides. The distribution configuration of oceanic water varies with tides. Accordingly, its attraction working at a station varies as well. We must therefore calculate for the present analysis the amount of the deflection of a horizontal pendulum due to this cause. In actual calculations, the method of mechanical integration must be employed because of the irregular distribution of tides. Let the height of sea surface above the mean sea level be h in an elementary area limited by radii r_1 and r_2 and azimuths θ_1 and θ_2, the station under question being the centre of the coordinates. Azimuth are measured clockwise from north to east, as usual. Then the amount of change in the direction of the plumb-line due to the attraction of sea water in this area is given by

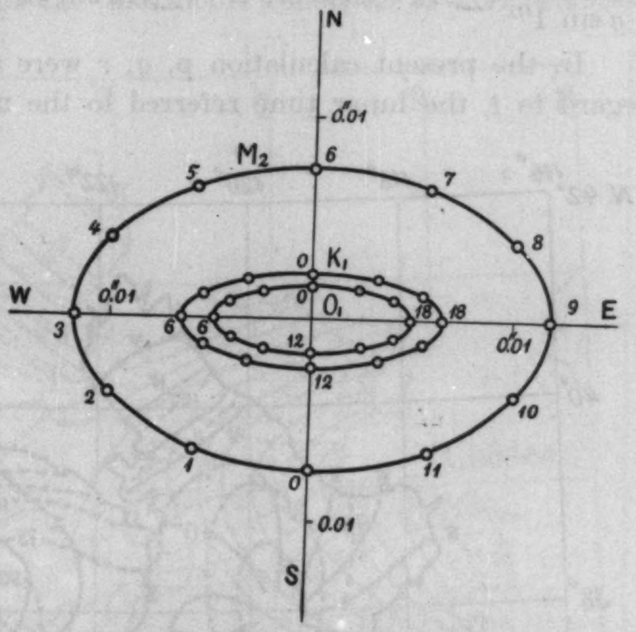

Fig. 8. Component plumb-line deviations due to the attraction of the moon and the sun. Numerals represent component hours.

$$\frac{\gamma\rho h}{g \sin 1''}(\log r_2 - \log r_1)(\cos\theta_2 - \cos\theta_1) \qquad \text{towards east,}$$

$$\frac{\gamma\rho h}{g \sin 1''}(\log r_2 - \log r_1)(\sin\theta_2 - \sin\theta_1) \qquad \text{towards south,}$$

in which γ, ρ and g are the universal gravitation constant, density of sea water and the acceleration of gravity respectively. In the above expressions, h is a function both of time t and the place. If we take, for the sake of brevity, only M_2-tide into consideration,

$$h = H_m \cos(2t - \zeta_m) = H_m \cos\zeta_m \cos 2t + H_m \sin\zeta_m \sin 2t,$$

in which H_m and ζ_m are functions of r and θ.

Now, if we take, in the mechanical integration, the successive steps of r and θ in such manners that

$$\log r_{n+1} - \log r_n = p, \quad \cos\theta_{n+1} - \cos\theta_n = q \quad \text{and} \quad \sin\theta_{n+1} - \sin\theta_n = r,$$

for all values of n, where p, q and r being constants, the above expressions for the plumb-line deflection will be given by

$$\frac{\gamma\rho pq}{g \sin 1''}[(\sum H_m \cos \zeta_m) \cos 2t + (\sum H_m \sin \zeta_m) \sin 2t] \quad \text{towards east,}$$

$$\frac{\gamma\rho pr}{g \sin 1''}[(\sum H_m \cos \zeta_m) \cos 2t + (\sum H_m \sin \zeta_m) \sin 2t] \quad \text{towards south.}$$

In the present calculation p, q, r were all taken to be 0·1, and with regard to t, the lunar time referred to the meridian 135° E was used.

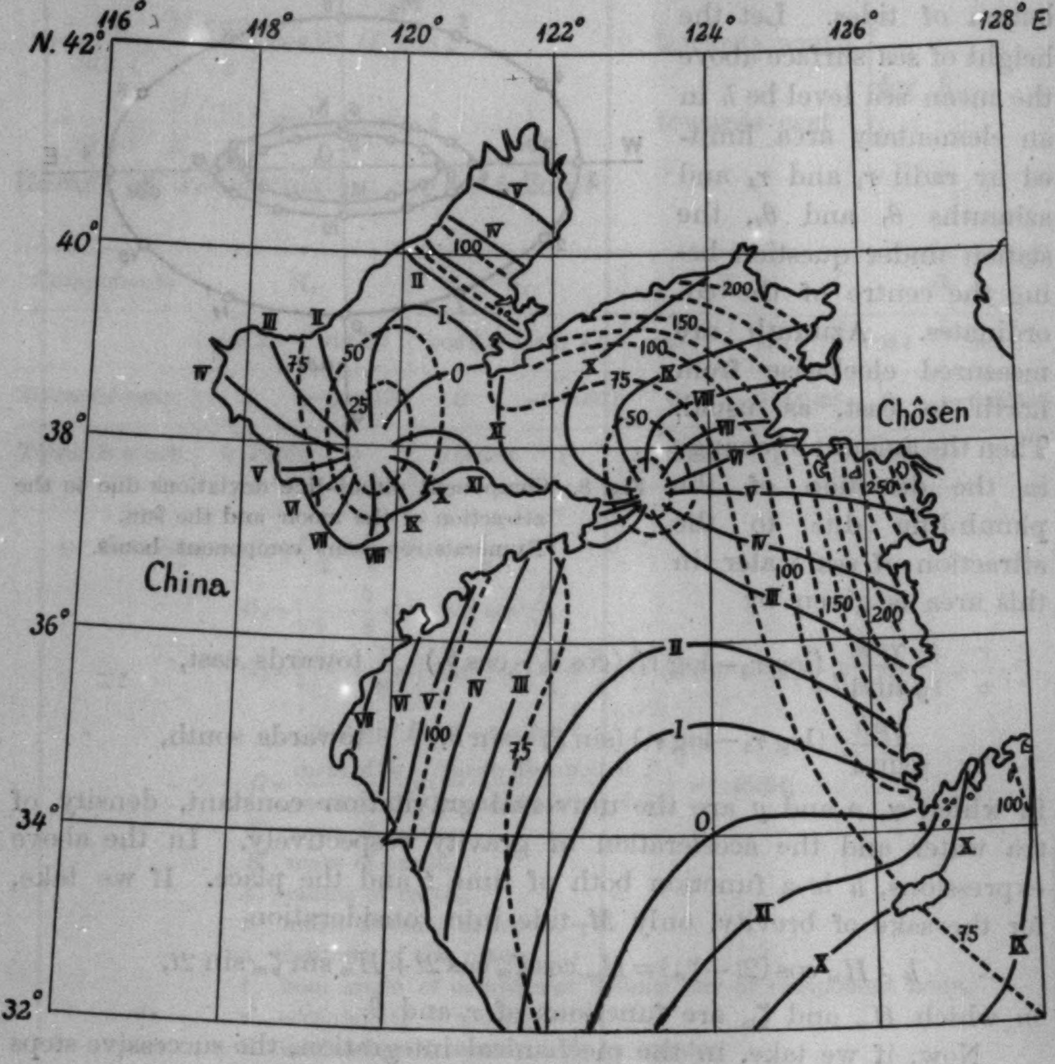

Fig. 9. M_2 **Co-tidal and Co-range Chart.**
Full lines—Co-tidals referred to 135°E meridian
Dotted lines—Co-ranges in cm.

H_m and ζ_m[5] were determined for all parts of the Yellow Sea and its adjacent bays by the tidal constants of the ports situated on the coast of the sea under question, with due regards on the depths and other hydrodynamical conditions of the ocean. In Fig. 9 are shown the co-tidal and co-range lines thus obtained and in Fig. 10 the chart which gives $H_m \cos \zeta_m$ and $H_m \sin \zeta_m$. Harmonic constants of the ports used

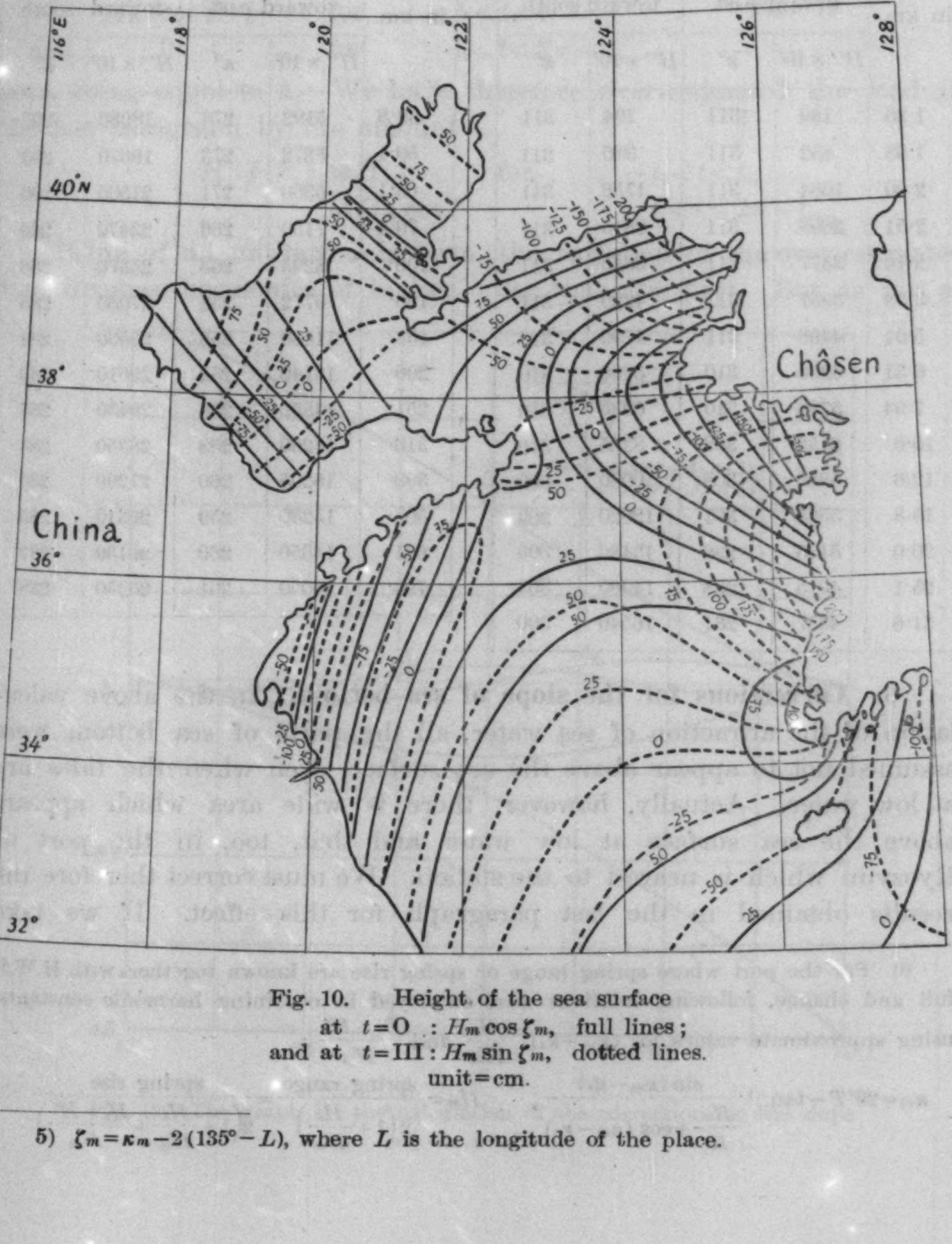

Fig. 10. Height of the sea surface
at $t=0$: $H_m \cos \zeta_m$, full lines;
and at $t=\text{III}$: $H_m \sin \zeta_m$, dotted lines.
unit=cm.

5) $\zeta_m = \kappa_m - 2(135° - L)$, where L is the longitude of the place.

in drawing these charts are given in Table II.[6]

The calculated amount of change in the direction of the plumb-line due to the attraction of tides are given in the following table for successive steps of r. They are already reduced to the local lunar time of Ryozyun.

r in km.	Attraction of M_2-tide			
	toward east		toward south	
	$H' \times 10^7$	κ°	$H' \times 10^7$	κ°
1·26	189	311	194	311
1·58	852	311	980	311
2·00	1684	311	1752	311
2·51	2698	311	2815	311
3·16	3577	311	3845	311
3·98	3957	311	4220	311
5·01	4498	311	4790	310
6·31	5250	310	5800	310
7·94	5780	310	6985	310
10·0	6153	308	8285	310
12.6	5850	305	10080	309
15·8	5525	301	12020	309
20·0	5135	296	13480	306
25·1	4915	288	14900	303
31·6	4857	281	16540	300

r in km.	Attraction of M_2-tide			
	toward east		toward south	
	$H'' \times 10^7$	κ°	$H' \times 10^7$	κ°
39·8	5192	276	18080	297
50·1	5872	273	19670	293
63·1	6300	271	21500	290
79·4	7130	266	23470	288
100·	8295	263	25370	286
126·	9772	258	27080	285
158·	11480	256	28560	284
200·	13140	254	29610	283
251·	14852	256	29430	283
316·	16260	258	28350	283
398·	16295	260	27200	284
501·	15230	259	26310	285
631·	14850	260	26130	287
794·	15090	261	26250	288

6. Corrections for the slope of sea bottom. In the above calculation of the attraction of sea water, all the parts of sea bottom were assumed not to appear above the sea surface, even when the tides are at low water. Actually, however, there is wide area which appears above the sea surface at low water and that, too, in the port of Ryozyun which is nearest to the station. We must correct therefore the results obtained in the last paragraph for this effect. If we take

6) For the port where spring range or spring rise are known together with H.W.I. full and change, following relations were employed in obtaining harmonic constants, using approximate values for $(\kappa_m - \kappa_s)$, $\frac{H_s}{H_m}$ and $\frac{H_0 + H'}{H_m}$:

$$\kappa_m = 29^\circ T - \tan^{-1} \frac{\sin(\kappa_m - \kappa_s)}{\frac{H_m}{H_s} + \cos(\kappa_m - \kappa_s)}, \qquad H_m = \frac{\text{spring range}}{2\left(1 + \frac{H_s}{H_m}\right)} = \frac{\text{spring rise}}{2\left(1 + \frac{H_s}{H_m} + \frac{H_0 + H'}{H_m}\right)}.$$

M_2-tide only into consideration for the sake of simplicity, and assume that the diurnal inequality is negligible, and that the height of sea bottom is kH_m above the mean sea level, where $1 \geqq k \geqq -1$, the load acting upon this area can be represented by the shaded portion of Fig. 11, that is,

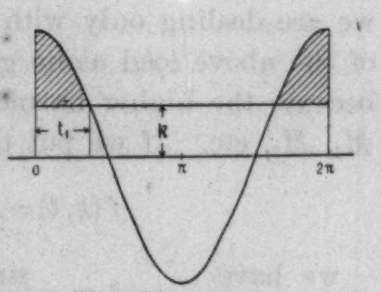

Fig. 11.

$$H_m(\cos t - k) \quad \text{for} \quad -t_1 < t < t_1$$
$$\text{and} \quad 0 \quad \text{for} \quad t_1 < t < 2\pi - t_1,$$

$\cot t_1$ being equal to k. We have therefore over-estimated the load in the last paragraph by the amount

$$H_m f(k, t) \equiv H_m k \qquad \text{for} \qquad -t_1 < t < t_1,$$
$$\equiv H_m \cos t \qquad\qquad t_1 < t < 2\pi - t_1.$$

Being of an un-harmonic form, the variation of the over-estimated load involves harmonics of higher order than the first. But as far as

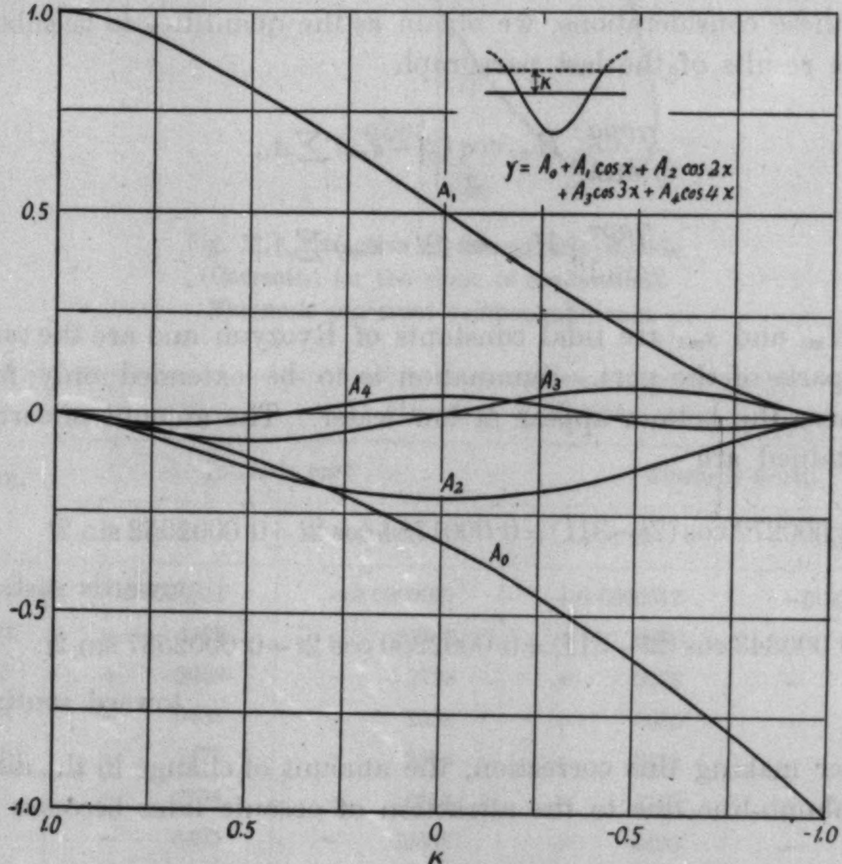

Fig. 12. The graph fo: the calculation of the correction for the slope of the sea-bed.

we are dealing only with M_2-tide, the first harmonics of the variation of the above load alone gives contribution to the results of caluculation, because the higher harmonics are of different periods and contribute to M_4, M_6, etc. If we put then

$$f(k,t)=A_0+A_1\cos t+A_2\cos 2t+\ldots.$$

we have

$$A_0=-\frac{\sin t_1}{\pi}+\frac{t_1\cos t_1}{\pi},$$

$$A_1=\frac{\cos t_1\sin t_1}{\pi}+\left(1-\frac{t_1}{\pi}\right),$$

$$A_n=\frac{2}{\pi(n-1)n(n+1)}(n\cos nt_1\sin t_1-\cos t_1\sin nt_1).$$

In Fig. 12, we have given the values of A_0, A_1, etc. against the values of k taken in abscissa.

By these considerations, we obtain as the quantities to be subtracted from the results of the last paragraph

$$\frac{\gamma\rho pq}{g\sin 1''}H_{m0}\cos(2t-\kappa_{m0})\sum A_1,$$

$$\frac{\gamma\rho pr}{g\sin 1''}H_{m0}\cos(2t-\kappa_{m0})\sum A_1,$$

where H_{m0} and κ_{m0} are tidal constants of Ryozyun and are the same for all the parts of the port. Summation is to be extended only for the area where the bottom appear at low water. The amount of correction thus obtained are

$$0''\!\cdot\!000272\cos(2t-311)=0''\!\cdot\!0001784\cos 2t-0''\!\cdot\!0002052\sin 2t$$

towards east,

$$0''\!\cdot\!000343\cos(2t-311)=0''\!\cdot\!0002250\cos 2t-0''\!\cdot\!0002587\sin 2t$$

toward south.

After making this correction, the amount of change in the direction of the plumb-line due to the attraction of oceanic tides becomes

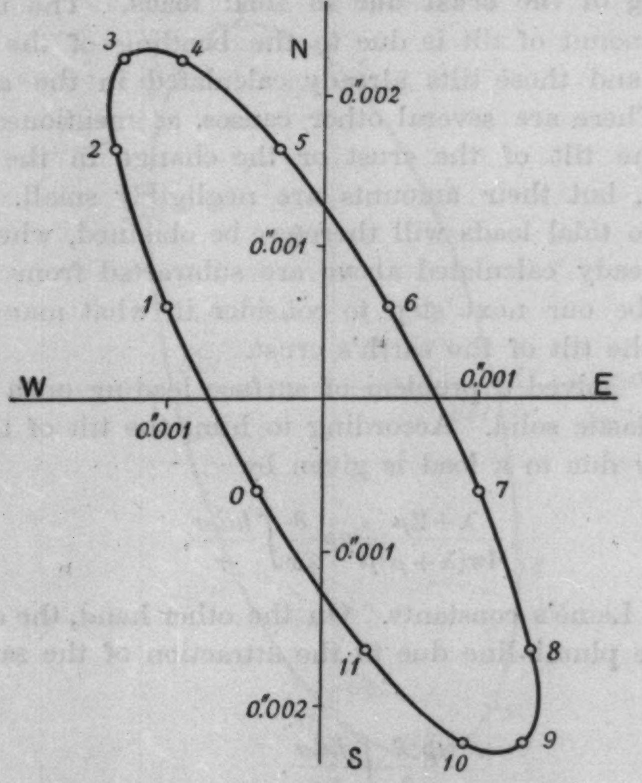

Fig. 13. Attraction of the oceanic M_2-tide.
(Corrected for the slope of sea-bottom)
Numerals represent component hours.

r in km.	Attraction of M_2-tide			
	Towards east		Towards south	
	cos 2*t*	sin 2*t*	cos 2*t*	sin 2*t*
3·98	+0"·0000811	−0"·0000931	+0"·0000517	−0"·0000596
5·01	+ 1162	− 1342	+ 0830	− 1083
10·0	+ 2008	− 2798	+ 3073	− 3763
20·0	+ 0468	− 2558	+ 5680	− 8323
50·1	− 1477	− 3808	+ 5430	− 15513
100·	− 2794	− 6178	+ 4749	− 21813
200·	− 5405	− 10558	+ 4420	− 26223
501·	− 4690	− 12888	+ 4565	− 22813
794·	− 4144	− 12852	+ 5861	− 22379

7. Bending of the crust due to tidal loads. The main part of the observed amount of tilt is due to the bending of the earth's crust by tidal loads and those tilts already calculated in the above several paragraphs. There are several other causes, as mentioned above, that can produce the tilt of the crust or the change in the direction of the plumb-line, but their amounts are negligibly small. The tilt of the crust due to tidal loads will therefore be obtained, when the values which were already calculated above are subtracted from the observed. Thus, it will be our next step to consider in what manner the tidal loads produce the tilt of the earth's crust.

Boussinesq[7] solved a problem of surface loading on a semi-infinite homogeneous elastic solid. According to him, the tilt of the surface of the elastic body due to a load is given by

$$\frac{\lambda+2\mu}{4\pi(\lambda+\mu)\mu}g\rho\frac{\partial}{\partial x}\int\frac{h\,d\sigma}{r},$$

λ and μ being Lamé's constants. On the other hand, the change in the direction of the plumb-line due to the attraction of the same load will be written as

$$\frac{\gamma\rho}{g}\frac{\partial}{\partial x}\int\frac{h\,d\sigma}{r}.$$

Therefore the tilt of the earth's crust due to the tidal load is equal in amount to the deflection of the plumb-line due to the attraction of the load multiplied by

$$\Theta=\frac{\lambda+2\mu}{4\pi(\lambda+\mu)\mu}\frac{g^2}{\gamma}.$$

If we take $\lambda=\mu$, and express μ in units of 10^{10} c. g. s., we have

$$\Theta=\frac{172}{\mu}.$$

Boussinesq's solution holds good, however, only for a homogeneous non-gravitating elastic body, and it is of much questions whether or not it can be applied equally to the actual earth in its unmodified form. In and on the actual earth's crust, there exist many topographical irregularities as well as geological heterogenieties. The earth's crust is very far, from all points of views, from homogeniety. Even if we imagine that these irregularities or heterogenieties exist only within the upper-

7) LOVE, "*Math. Theory Elasticity*," Cambridge Univ. Press (1927), 193.

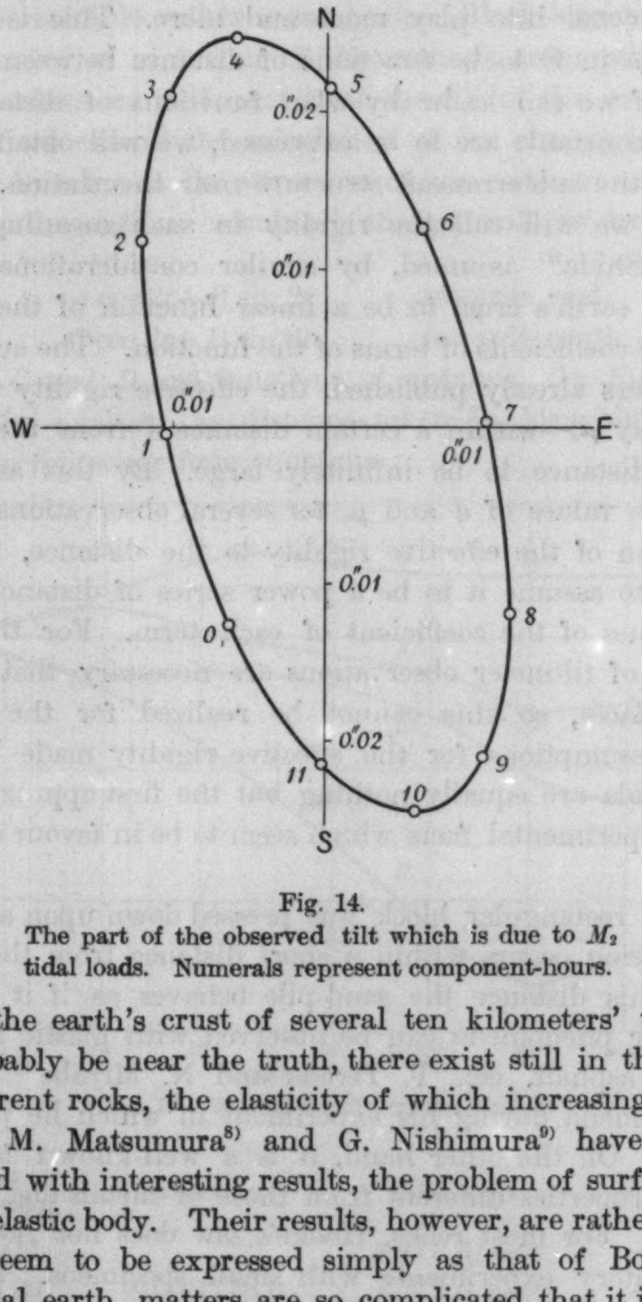

Fig. 14.
The part of the observed tilt which is due to M_2 tidal loads. Numerals represent component-hours.

most part of the earth's crust of several ten kilometers' thickness, and this may probably be near the truth, there exist still in the crust many layers of different rocks, the elasticity of which increasing with depth.

Recently M. Matsumura[8)] and G. Nishimura[9)] have solved independently, and with interesting results, the problem of surface loading on a one-layered elastic body. Their results, however, are rather complicated, and do not seem to be expressed simply as that of Boussinesq was. With the actual earth, matters are so complicated that it is not far from impossibility to treat it mathematically.

It is, however, probable that in producing tilts at a point by a load, only surface layers of the crust partake in the play when the distance between the load and the point is short, and as this distance increases,

8) M. Matsumura, *Journ. Civil Engin. Soc.*, 17 (1931), 813, 1121, (in Japanese).
9) G. Nishimura, *Bull. Earthq. Res. Inst.*, 10 (1932), 23.

deeper layers come into play more and more. This is equivalent to regard λ and μ in Θ to be functions of distance between the load and the station. If we can know by what functions of distance these effective elastic constants are to be expressed, we will obtain a clue to the elucidation of the subterranean structure near the station. In the following pages, we will call the rigidity in such meanings as *effective rigidity*. T. Shida[10] assumed, by similar considerations, the effective rigidity of the earth's crust to be a linear function of the distance and determined the coefficients of terms of the function. The author assumed, in several papers already published, the effective rigidity to have a uniform value—say μ_0—within a certain distance d from the station, and beyond this distance to be infinitely large. By this assumption, he determined the values of d and μ_0 for several observations. For obtaining the relation of the effective rigidity to the distance, it is a customary process to assume it to be a power series of distance and find the numerical values of the coefficient of each term. For this method, a large number of tiltmeter observations are necessary that are executed at different places, so this cannot be realized for the present case. Though the assumptions for the effective rigidity made by the author and by T. Shida are equally nothing but the first approximation, there exist many experimental facts which seem to be in favour of the author's assumption.

If a solid rectangular block was pressed down upon a layer of sand, surface depression occurs within a short distance from the pressed area, but beyond this distance the sand-pile behaves as if it were perfectly rigid. Similar phenomena can be observed with plastic materials such as rice-jelly, asphalt, etc. T. Terada and N. Miyabe[11] have observed similar phenomena during his experiment in which he pressed a sand-pile laterally. On the other hand, it is a well-known fact that rocks have elastic properties different from those of metals and other common elastic bodies. For most rocks, Hooke's law does not hold good, even in the laboratory experiments with small specimens. It will not be absurd to imagine, then, that the crust which is composed of these rocks has peculier elastic characteristics, especially against such long-perioded forces like those treated in this paper, since it is of large scale and in the strong field of gravity. The earth's crust may, in this respect, be

10) T. Shida, *Mem. Coll. Sci., Kyôto Imp. Univ.*, 4 (1910), 1.

11) T. Terada and N. Miyabe, *Bull. Earthq. Res. Inst.*, 4 (1928), 33; 6 (1929), 109; 7 (1929), 65.

considered to resemble rather a sand-pile. Block structure of the crust may also be cited as in favour of the author's assumption.

In these views we will next treat the tilt of the crust observed at Ryozyun. If we extend the calculation of the change in the direction of the plumb-line due to the attraction of sea water to successive steps of distance from the station, calculated change will be expressed by the forms

$$A\cos 2t + B\sin 2t \qquad \text{towards east,}$$
$$C\cos 2t + D\sin 2t \qquad \text{towards south,}$$

where A, B, C and D are functions of distance. In Fig. 15 are given these quantities against the distance taken in logarithmic scale. We have then the following four equations:

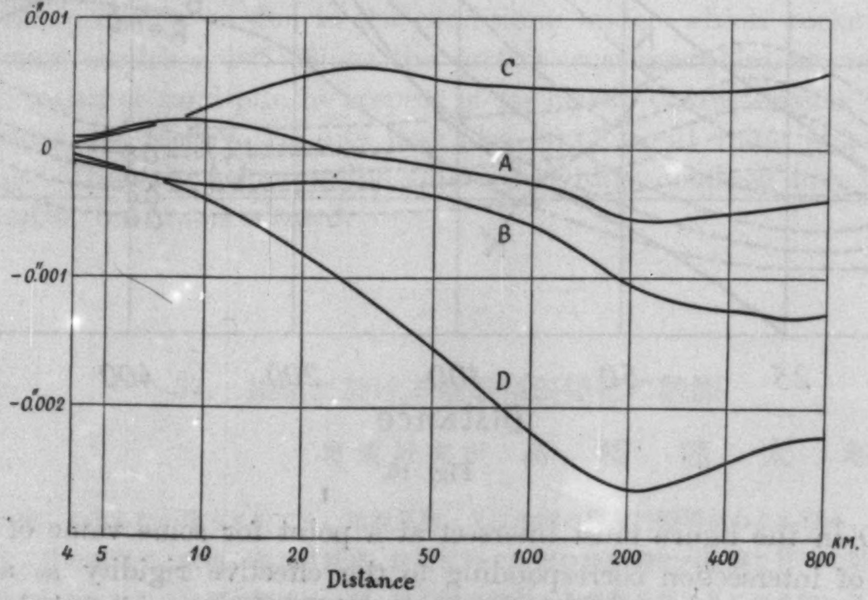

Fig. 15. Attraction of oceanic M_2-tide.

Attraction of oceanic tides	Earth-tides	Tidal loads	Observed values
$-0\overset{''}{\cdot}00041$		$+172\,A/\mu_0 =$	$-0\overset{''}{\cdot}00669$
$-0\cdot00129$	$-0\overset{''}{\cdot}01178\,R$	$+172\,B/\mu_0 =$	$-0\cdot01946$
$+0\cdot00059$	$+0\cdot00739\,R$	$+172\,C/\mu_0 =$	$+0\cdot01825$
$-0\cdot00224$		$+172\,D/\mu_0 =$	$-0\cdot02331,$

or

$$172\,A/\mu_0 \qquad\qquad = -0\overset{''}{\cdot}00628,$$
$$172\,B/\mu_0 \quad -0\overset{''}{\cdot}01178\,R \quad = -0\cdot01817$$
$$172\,C/\mu_0 \quad +0\cdot00739\,R \quad = +0\cdot01766$$
$$172\,D/\mu_0 \qquad\qquad = -0\cdot02107,$$

For the purpose of determining the values of μ_0 and R from these equations we have constructed Fig. 16, taking μ_0 and distance as co-ordinates and R as a parameter. Theoretically the four curves A, B, C

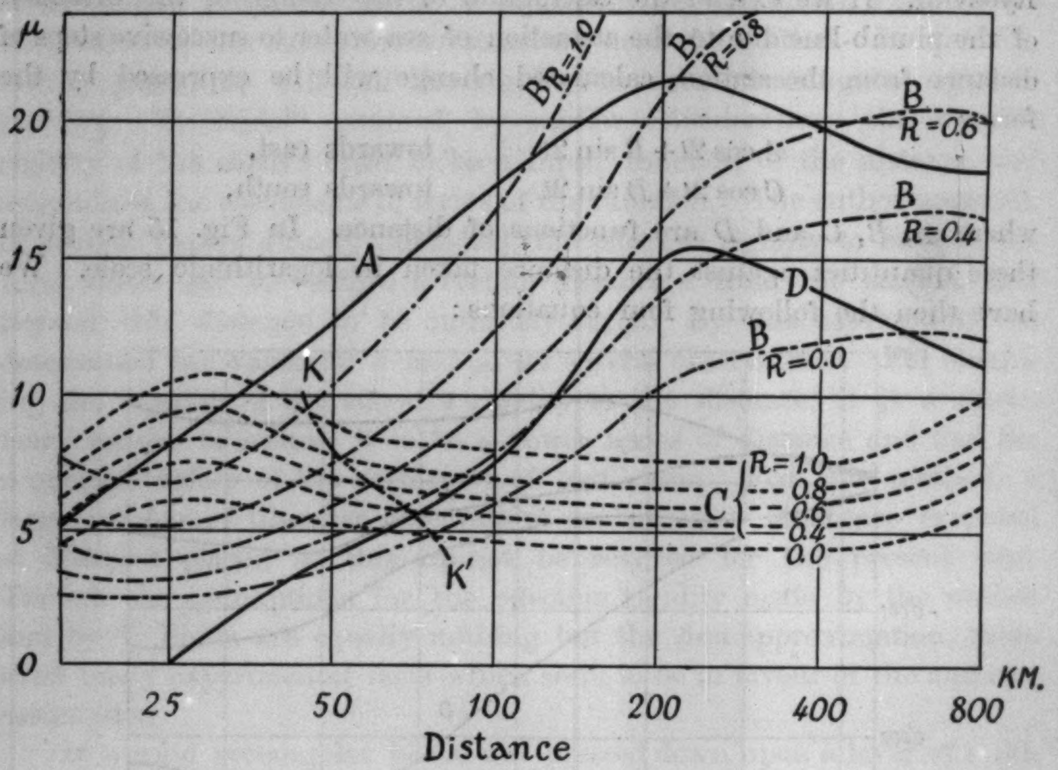

Fig. 16.

and D in the figure must intersect at a point for some value of R, the point of intersection corresponding to the effective rigidity μ_0 and the distance d beyond which the effective rigidity becomes infinitely large. In Fig. 16, we cannot however find such a point; we will therefore determine a point which satisfies the above condition with minimum errors. In the figure, KK' curve is the locus of intersection of B and C curves. We have therefore adopted as the point of minimum errors the point which lies on the curve KK', and is equi-distant from A and D curves, because A and D are nearly parallel. From the co-ordinates of this point, values of μ_0, d and R were obtained as

$$\mu_0 = 6{\cdot}9 \times 10^{10} \quad \text{c. g. s.}$$
$$d = 50 \quad \text{km.}$$
$$R = 0{\cdot}8$$

The value of R, thus obtained, is very near to those which were

hitherto determined by many authors. The present value of R gives 16×10^{11} c. g. s. as the rigidity of the earth. The value of μ_0, obtained here, is very small, being nearly equal to the rigidity of andesite. The effective rigidity at a station is a sort of average value of the rigidities of rocks which lie near or under the station, so it must have a value which is near to those of rocks prevailing at the station. Rocks that are predominant at Ryozyun and its neighbourhood, belonging to paleozoic or archean era, have, however, rigidities which are larger than the value of the effective rigidity here obtained.

This discordance of the values of rigidities is partly due to the deficiencies which may exist in the observation and in the treatment of the results of the observation. The main part of this discordance will, however, probably be due to the conditions under which rocks are in the actual earth's crust. Since the earth's crust resembles, as mentioned above, rather a sand-pile in respect of its elastic characteristics in such conditions, its effective rigidity may also be of small value just like the sand is. Then the value of the effective rigidity obtained here is very reasonable, but never absurd.

---

37. 旅順に於ける地殼傾斜變化の觀測

地震研究所 高 橋 龍 太 郎

地震の殆んど起らない地方に於ても、地塊運動、又は地殼の積年的變形があるか否か、と言ふ事を明にする目的を以て、昭和六年二月以來、旅順に於て地殼の傾斜變化の觀測を行つて居る。此の論文に於て發表したものは其の觀測の一部、即ち觀測當初より昭和七年二月に到る約一年間の期間に對するものである。

觀測の結果に依れば、旅順に於ては今の所積年的の傾斜運動は認められないと言へる樣である。又此の觀測に於て同時に潮汐の負荷に因つて起る地殼の變形が認められた。本論文の主なる部分は此の變形の研究である。

觀測の結果を調和解析によつて分解して、種々の攪亂性分を除去し、其を理論上より得る値と比較して、地殼潮汐の減小率として、0·8 なる値を得た。此の値から計算すると地球の剛性は大凡 16×10^{11} c. g. s. となる。又同時に地殼のみの剛性が $6{\cdot}9\times10^{10}$ c. g. s. と求められた。然し乍ら此の値は旅順附近の岩石の其れと比較する時は著しく小さいのである。論文の最後に於て此の不一致の依つて來るべき原因を論じ、併せて地殼の彈性に論及してある。

Table I. Hourly readings of tiltmeter records.

1931 Pendulum I (Azimuth 75°)

	Oct.									
	20	21	22	23	24	25	26	27	28	29
h	″	″	″	″	″	″	″	″	″	″
0	7·1418	7·0725	7·0344	6·9954	6·9409	6·9276	7·0593	6·9798	7·0655	7·0500
1	434	780	344	923	424	308	585	643	523	305
2	372	842	375	939	479	362	655	588	414	118
3	341	905	437	978	557	448	772	643	351	6·9978
4	279	928	538	7·0102	643	565	889	752	398	954
5	208	811	593	118	713	728	7·1006	876	484	7·0032
6	161	655	601	133	705	939	123	985	577	203
7	107	500	577	118	643	946	232	7·0110	655	344
8	029	336	461	032	565	954	333	188	671	414
9	7·0928	165	305	6·9931	463	876	356	258	671	414
10	842	048	172	759	347	721	201	266	640	352
11	757	024	110	526	238	534	7·0889	219	585	352
12	663	063	032	409	175	410	476	196	585	383
13	577	141	040	471	199	339	6·9985	258	671	468
14	577	203	118	526	315	409	798	344	788	546
15	694	328	196	580	409	557	876	429	936	640
16	811	445	258	658	479	783	7·0063	554	7·1076	718
17	811	562	266	713	510	7·0032	539	694	162	811
18	811	577	258	721	518	235	546	889	201	905
19	772	538	211	713	479	437	577	7·1053	201	990
20	725	429	188	658	409	624	577	146	123	7·1021
21	663	359	126	588	331	772	492	123	021	7·0967
22	655	344	094	526	292	803	266	045	7·0873	819
23	655	344	017	456	276	686	6·9985	7·0811	671	671

			Nov.							
	30	31	1	2	3	4	5	6	7	8
h	″	″	″	″	″	′	″	″	″	″
0	7·0507	7·0188	6·9705	6·9682	6·9697	6·9565	6·9798	7·0585	7·0686	7·0500
1	359	6·9946	635	635	611	635	798	640	648	422
2	274	783	573	565	534	627	806	687	632	422
3	211	666	510	502	479	596	814	733	655	500
4	180	643	432	471	471	557	798	733	710	570
5	180	643	362	417	449	487	775	702	749	585
6	219	635	339	409	378	463	721	648	733	562
7	328	627	409	487	308	409	643	562	609	445
8	344	588	456	557	206	347	534	492	422	274
9	235	534	409	565	128	308	362	429	250	040
10	079	463	292	534	082	261	199	492	6·9985	6·9814
11	6·9915	401	175	440	027	253	175	655	798	635
12	791	331	097	308	019	308	253	928	798	573
13	721	284	035	222	012	471	393	7·1162	939	580
14	674	292	019	129	012	627	549	286	7·0141	713
15	697	362	027	097	004	643	721	349	344	876
16	767	432	051	113	004	635	931	356	531	7·0126
17	900	557	097	175	004	635	7·0196	356	733	328
18	7·0110	643	175	284	004	643	492	310	936	336
19	320	721	292	409	019	689	577	201	7·1037	266
20	453	775	440	510	090	752	577	123	7·0967	110
21	507	791	580	611	175	798	577	7·0990	811	6·9962
22	500	783	650	689	331	798	577	850	679	822
23	398	736	705	721	448	798	577	741	557	674

(to be continued.)

Table I. (*continued.*)

	9	10	11	12	13	14	15	16	17
h	″	″	″	″	″	″	″	″	″
0	6·9518	6·9386	7.0801	7·1894	7·2291	7.2089	7·2688	7·1886	7·1995
1	417	238	671	754	135	7·1980	541	730	941
2	409	175	585	629	7·1933	808	338	590	863
3	487	284	632	551	746	637	159	497	746
4	580	417	780	543	543	473	058	403	629
5	658	565	7·1006	645	434	427	026	349	536
6	721	635	201	754	512	434	042	356	497
7	721	643	349	824	590	528	112	434	442
8	611	565	434	824	590	676	198	442	442
9	347	370	434	738	504	824	198	419	473
10	167	214	341	520	356	948	120	356	543
11	097	105	162	310	271	7.2073	003	325	676
12	027	097	107	224	271	190	7.1886	279	948
13	019	206	123	279	349	283	769	279	7·2213
14	023	432	232	356	512	361	715	279	408
15	175	736	388	512	691	361	668	294	517
16	487	7·0063	575	746	832	276	621	380	525
17	705	492	816	980	972	213	629	551	525
18	822	928	995	7·2229	7·2073	291	668	777	564
19	876	7·1123	7·2151	470	159	463	730	964	603
20	884	138	213	650	229	603	808	7·2019	634
21	830	107	213	626	283	681	894	058	650
22	705	006	159	525	283	751	964	058	681
23	565	7.0905	058	400	213	759	956	050	774

1931 Pendulum II (Azimuth 165°)

	Oct.									
	20	21	22	23	24	25	26	27	28	29
h	″	″	″	″	″	″	″	″	″	″
0	5·4397	5·4264	5·4789	5·4468	5·4060	5·4193	5·5131	5·5758	5·6916	5·8242
1	366	182	652	264	5·3846	5·3984	5·4876	514	661	5·7946
2	366	162	570	121	652	836	692	274	406	554
3	381	295	519	060	519	800	524	080	182	243
4	407	447	560	065	504	907	463	5·4927	008	5·6987
5	407	555	621	137	591	5·4086	478	835	003	819
6	346	575	723	254	754	284	647	922	054	809
7	279	570	835	397	907	545	912	5·5187	202	916
8	223	636	973	585	5·4080	805	5·5243	590	457	5·7273
9	167	713	5·5019	723	172	5·5009	539	973	814	783
10	131	713	5·4978	672	213	090	641	5·6401	5·7191	5·8155
11	106	672	825	494	193	090	636	641	503	466
12	111	600	596	264	014	029	514	656	630	604
13	167	565	437	111	5·3831	5·4866	376	559	559	497
14	295	585	453	009	652	667	218	365	355	268
15	407	672	529	5·3999	601	519	131	263	263	038
16	514	876	621	5·4029	652	468	095	258	222	5·7936
17	641	5·5055	774	111	831	499	136	406	258	936
18	723	182	932	213	5·4009	621	274	610	375	5·8002
19	723	228	5·5080	366	193	830	437	834	554	109
20	682	187	131	519	341	5·5049	590	5·7018	783	232
21	606	131	080	550	494	228	753	120	5·8058	364
22	509	039	5·4876	427	570	335	876	171	222	476
23	381	5·4927	677	213	417	335	891	120	293	543

(*to be continued.*)

Table I. (*continued.*)

			Nov.							
	30	31	1	2	3	4	5	6	7	8
h	″	″	″	″	″	″	″	″	″	″
0	5·8497	5·8650	5·8273	5·7824	5·7936	5·7288	5·7278	5·6406	5·6151	5·5947
1	268	446	166	834	992	350	207	309	5·5998	718
2	5·7951	201	5·7987	752	997	375	161	304	937	559
3	630	5·7911	737	533	936	385	120	314	973	539
4	324	630	503	299	783	375	120	386	5.6126	590
5	084	334	273	038	579	283	115	457	253	743
6	018	181	120	5·6855	344	100	079	528	406	911
7	105	207	095	763	242	5·6931	018	610	508	5·6075
8	350	334	171	804	217	834	5·6947	681	610	202
9	732	528	370	901	222	778	840	743	661	330
10	987	737	503	5·7044	227	768	748	758	610	319
11	5·8186	936	610	222	273	789	630	661	508	049
12	278	5·8166	686	477	329	845	528	457	457	5·5743
13	308	293	732	681	380	931	498	330	483	488
14	293	222	747	834	421	5·7115	590	375	528	335
15	242	120	732	936	426	355	783	513	600	463
16	166	5·7962	656	982	416	579	967	712	681	769
17	125	834	528	911	375	732	5·7140	931	778	5·6029
18	140	763	395	814	324	783	258	5·7079	916	228
19	222	778	314	778	273	788	268	166	5·7018	406
20	344	849	350	758	222	732	151	069	5·6936	477
21	472	987	477	758	212	599	5·6931	5·6865	666	416
22	594	5·8094	574	783	222	477	732	636	432	166
23	665	222	701	860	248	375	523	381	151	5·5855

	9	10	11	12	13	14	15	16	17
h	″	″	″	″	″	″	″	″	″
0	5·5478	5·5641	5·5947	5·6100	5·5845	5·5029	5·3973	5·3009	5·3448
1	151	248	641	5·5845	498	5·4907	927	091	463
2	5·4851	5·4902	335	539	151	636	805	091	443
3	723	570	044	233	5·4810	402	576	5·2938	346
4	754	458	5·4907	5·4922	519	188	244	734	193
5	876	483	866	662	279	5·3973	5·2913	530	040
6	5·5080	590	937	565	091	902	637	367	5·2979
7	437	794	5·5131	621	014	897	448	224	964
8	794	5·5141	442	861	203	958	295	173	004
9	973	539	758	5·5182	596	5·4101	275	234	5·3127
10	993	682	978	549	927	315	352	377	295
11	774	641	5·6049	682	5·5100	570	505	556	550
12	452	457	5·5947	682	141	922	632	775	805
13	243	264	794	559	131	5·5090	724	938	5·4086
14	100	106	641	432	080	126	765	5·3071	366
15	141	049	488	310	5·4983	080	734	168	590
16	284	182	437	218	922	5·4856	663	259	779
17	508	417	503	182	825	570	581	341	896
18	702	677	614	243	723	172	530	341	937
19	896	896	830	417	657	5·3754	515	234	876
20	5·6090	5·6100	5·6008	614	647	596	550	213	749
21	182	228	182	820	738	611	632	275	621
22	136	268	299	896	891	744	754	336	570
23	5·5922	161	304	901	5·5004	907	887	397	652

Table II. Tidal constants of the ports.[12]

Places	Lat.		Long.		H_m	κ_m
Shanghai	31°	21′	121°	30′	95 cm	30°
Wei-hai-wei	37	29	122	13	61	297
Takou	38	59	117	42	94	95
Tang Luan Tsu	37	59	120	42	56	292
Nan Fan Chen Tao	38	21	120	54	60	309
Schichon Tao	39	25	121	15	43	41
Daikokuseki	38	58	121	18	56	359
Yang Tan Wa	38	47	121	08	61	331
Port Arthur	38	48	121	14	83	311
Hsiaoping Tao	38	49	121	31	89	304
Dairen Wan	38	56	121	39	100	297
Tseng Chia Tun	39	08	122	06	115	287
Tsao Tao	39	29	123	05	158	268
Taku Sham road	39	46	123	33	193	272
Autung	40	08	124	24	74	337
Neu-am Po	39	56	124	21	161	297
Tetasa To	39	48	124	25	215	263
Banzo Retto	39	41	124	27	205	253
Napu Somu	39	16	124	43	192	247
Unmu To	39	25	125	07	222	255
Dauchin I.	38	37	125	00	154	226
Pio Sem.	38	40	125	06	167	244
Ping Yang Inlet	38	39	125	35	204	262
Gets naï To	38	03	124	49	106	161
Taityoku To	37	50	124	43	99	157
Kotu Semi	37	44	125	33	198	139
Tyumun To	37	39	126	14	270	139
Chemulpho	37	30	126	34	293	134
Tokutyoku To	37	15	126	09	248	122
Tyonsu Wan	36	23	126	26	226	98

(to be continued.)

12) Taken from "*Tables of Harmonic Constants*," Intern. Hydrogr. Bur. Monaco (1926), and "*Nippon Kinkai no Tyôseki* (*Tides in the Adjacent Seas of Japan.*)" Hydrogr. Bur. Japan (1905).

Table II. (*continued.*)

Place	Lat.		Long.		H_m	κ_m
Weyon To	36°	13′	126°	02′	175 cm	85°
Pikken To	36	07	125	59	179	81
Otyon To	36	02	126	32	213	79
Kokunsan Ganto	35	49	126	25	226	85
Manma To	35	21	126	01	169	60
Koroku To	35	03	126	05	142	43
Hamupyon Wan	35	09	126	21	189	57
Mokuho (Yong Sau)	34	45	126	22	116	51
Pukkan Suido	34	52	126	06	142	34
Paruku Po	34	36	126	01	117	11
Hatai To	34	32	126	03	109	5
Sanse Somu	34	20	126	04	93	346
Tin To (Chin Do)	34	30	126	12	113	31
Tin To (Kapu To)	34	24	126	19	92	342
Gobaro To	34	27	126	25	98	308
Huwapukuni	33	31	126	35	66	301
Soki Po	33	14	126	33	77	271
Ietun Somu	34	10	127	18	92	266
Soan Ko	34	08	126	38	85	295
Tyotyokura	34	22	126	47	107	263
Mato Suido	34	25	126	51	113	285
Sontyuku Po	34	17	127	22	94	276
Kokkumu-Suido	34	30	127	09	110	275
Nano Retto	34	28	127	29	105	268
Kamakkupataan	34	44	127	45	102	252
Suni To	37	45	125	20	154	145

Place	Lat.		Long.		Spring rise	H. W. I. Full and Change	
Ki-kou	38°	35′	117°	32′	320 cm	4 h	30 m
Pei-tang Ho Kou	39	07	117	44	275	3	0
Tchi Ho	39	06	118	50	198	1	20
Luan Ho	39	16	119	70	152	1	30
Tai-shuchi-Ho	39	49	119	30	183	0	15

(*to be continued.*)

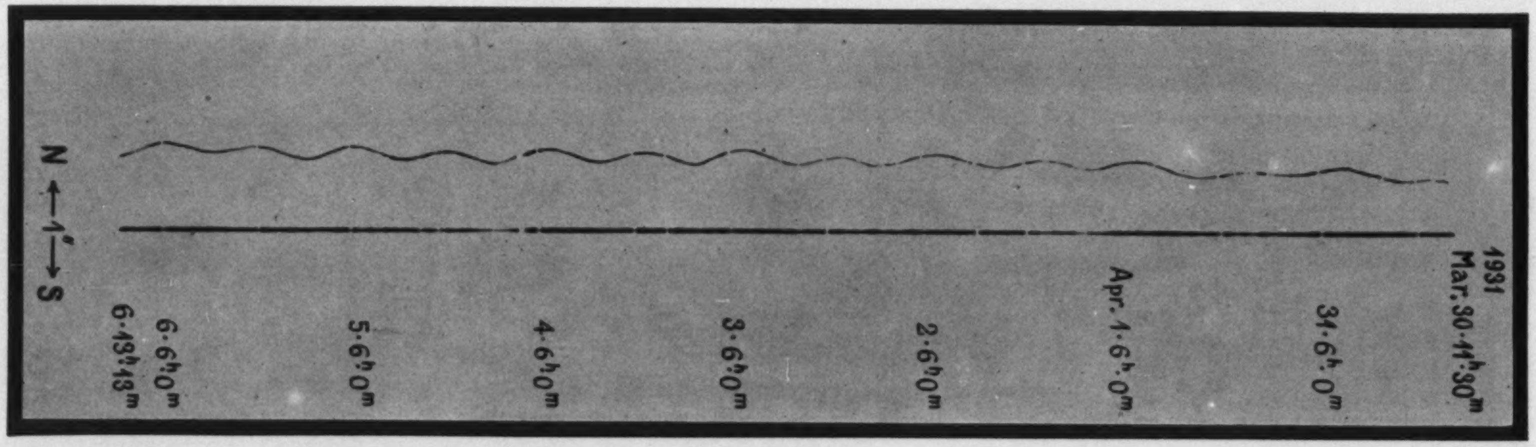

Fig. 3.

Record as obtained by the tiltmeter.

Table II. (*continued.*)

Place	Lat.		Long.		Spring rise	H. W. I. Full and Change	
	°	′	°	′	cm	h	m
Chan-Hai-kouan	39	59	119	49	183	0	00
St. Ubes Pt.	40	18	120	32	230	4	50
Kiu-tcheou	40	48	121	0	328	5	30
In-kou	40	43	122	14	394	5	0
Vansitarts Saddle	40	12	122	0	328	4	20
Collio-San. B.	39	30	121	17	262	2	30
Port-Adams	39	26	121	44	328	2	00
Kin-tcheou B.	39	06	121	42	262	0	15

Place	Lat.		Long.		Spring range	H. W. I. Full and Change	
	°	′	°	′	cm	h	m
Chan-toung Prom.	37	24	122	42	223	4	00
Sang Koon B.	37	08	122	27	226	0	45
Nanking	32	10	118	55	131	10	50
Hang-Tcheou B.	30	14	120	14	450	11	35
Chi-Pou	29	57	121	47	289	1	00
Tai-tcheou I.	28	24	121	52	463	8	50
Min-Kiang Kou	26	02	119	40	624	9	45
Min Kiang	26	03	119	24	633	0	30
Kiao-tcheou	36	00	120	20	374	4	50
Nioutchuang	40	35	122	00	357	4	30
Tieu-tsin	39	09	117	11	136	6	50
Hoang-Ho Kou	37	54	118	34	320	4	00

38. *Change of Depth in the Bay of Tosa.*

By Torahiko TERADA,

Earthquake Research Institute.

(Read May 17, 1932.—Received June 20, 1932.)

In 1928, Hydrographical Department of the Imperial Japanese Navy undertook a thorough revision of the bathymetric chart of the Bay of Tosa. The chart hitherto in use was based on the results of earlier soundings made during 1884–1891. As the result of the revision of sounding survey in the Bay of Sagami carried out just after the Great Kwantô Earthquake has revealed a very remarkable change in the profile of the sea-bed, it is a matter of great interest to carry out a similar revision of sounding in the Bay of Tosa, firstly because no destructive earthquake has been experienced in the latter region since the previous soundings and secondly because we cannot deny the probability of a future occurrence of severe earthquakes in this very region which was already repeatedly frequented by notorious catastrophs such as those of Keityô (1605), Hôei (1707) and Ansei (1854).

The new sounding was carried out during April–August of 1928 and the complete data of the results obtained were kindly placed at the disposal of the research staff of our Institute by the courtesy of Rear-Admiral Yonemura, Director of the Department at that time, to whom the present author is greatly indebted for his interest shown and assistance given during the course of our research work.

The present author has already published some brief notes[1] regarding the changes in depth of sea-bed which were found after the destructive earthquakes of Kwantô (1923), Tazima (1925) and Tango (1927) and attempted some discussions on the probable significance of change in depth thus found. The abnormally large amount of change found in the case of Sagami Bay seems to have been an object of sceptical criticism in some quarter, though the present author believes to have sufficiently proved on the basis of his statistical investigations that the change found must be real in the main. As no destructive earthquake was experienced in the vicinity of the Bay of Tosa in the

1) T. TERADA and N. MIYABE, *Proc. Imp. Acad.*, 4 (1928), 45; T. TERADA and S. HIGASI, *ibid.*, 296 and 394.

interval of time between the old and new sounding, the change in depth, if any, cannot be attributed to any sudden deformation of the sea-bed associated with earthquake, and consequently it must be considered to have been produced gradually and more or less monotonously during the said interval of time. If, therefore, a sensible change in the sea-bed be established as real in the present case of the Bay of Tosa, we may at least assume with a stronger conviction than ever that the greater part of the change in Sagami Bay might also have been produced gradually or chronically. Unfortunately, the depth of the part of the Bay of Tosa recently resurveyed is generally less than 120 m., whereas in the case of the Sagami Bay the greater part is of depth greater than 1000 m. so that any reliable discussion cannot be made on the relative magnitudes of deformation in the two cases.

The method here used of finding the apparent change in depth is as follows:

Contour lines were drawn corresponding to 10, 20,.... 120 m. depths on the old and new charts respectively. Reducing the scale of the new chart (1/75,000) into that of the old one (1/175,000), a rectangular net of 1 cm. mesh was drawn on each of these two charts. The old and new depths at each of the net-points were read off by interpolation and the difference, (new depth) minus (old depth) = Δ, was calculated. Then this difference Δ, i.e. the depression, was plotted on another chart and the lines of equal Δ's were drawn, as shown in Fig. 1. It will be seen at first glance that the middle part of the Bay is generally depressed while the parts near the west and east ends are upheaved. Moreover, it seems that a zone of maximum depression may be discerned running parallel to the entire coast line. Such a zonal character was also observed in the cases of the deformation of sea-bed found after the earthquakes of Kwantô, Tazima and Tango respectively, as was pointed out in the papers cited. On the other hand, such a mode of systematic distribution of Δ can by no means be explained by the accidental errors of sounding.

The bay was divided into four parts (1), (2), (3) and (4) by the three straight lines (shown in Fig. 1) drawn nearly normal to the general trend of coast line at the places near Kaminokae, Urado and Ioki respectively. For each of these parts, the area was again divided into twelve zones bounded by successive contour lines proceeding with 10 m. step, and the mean value of Δ was calculated for each of these zones. This mean Δ for each zone was then plotted along the axis of

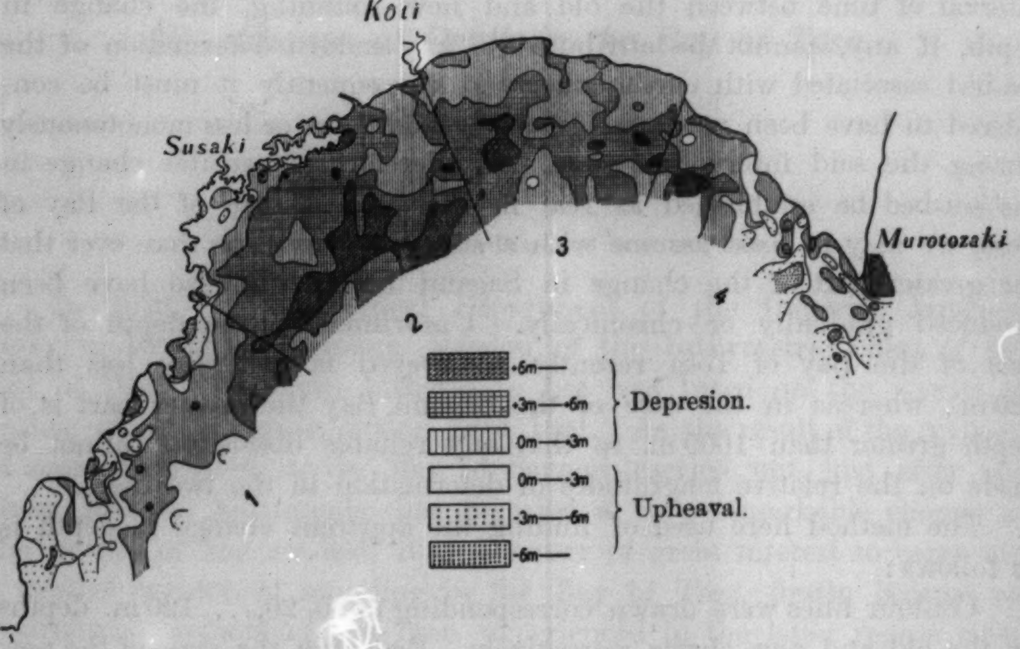

Fig. 1.

ordinates against the corresponding mean depth as abscissa as shown in Fig. 2. It will be seen that for the parts (1), (2) and (3) the slopes of the curves are such that the depression Δ increases off the coast, whereas for the part (4) the opposite is the case. For the depth greater than 40 m. (2) is nearly parallel to (1) and the difference of Δ of the two curves is generally 4 or 5 m. Again, for the depth 20–80 m., (3) resembles (2) in its general trend, while for the depth greater than 80 m., the curve (3) shows a general tendency to run in the same sense as (4). Thus, the apparent

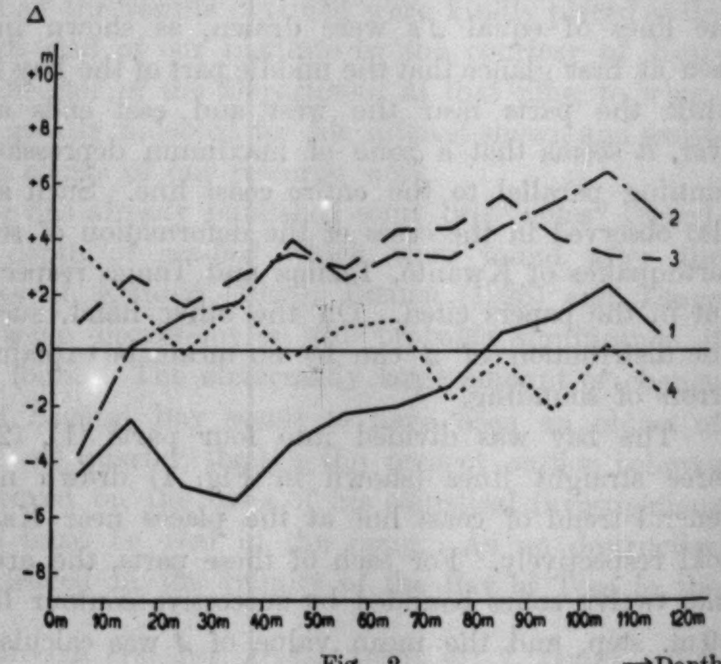

Fig. 2. →Depth

tilting of the sea-bed in (4), i.e. the eastern end of the bay, has taken place in the sense opposite to that of (1) and (2), i.e. the western half of the bay.

Next, the bay was divided into three narrow belts nearly parallel to the coast line and bounded by the three pairs of contour lines, i.e., 0 m.–50 m., 50 m.–80 m. and 80 m.–120 m. Each of these zones was again divided into ten segments of nearly equal length along the length of the zone. The mean depths of these segments belonging to a belt were plotted against the ordinal number of the segments counted from W to E, as shown in Fig. 3. The general mode of warping of the sea bed is made quite clear by the three curves there drawn. The three curves are all of inverted U-shape showing that the bed of the bay is generally bent such that the middle part is depressed while W and E ends are relatively upheaved. By tilting the curve (3), which corresponds to the shallow belt 0–50 m. depth, in such a manner that the eastern end is depressed and the western end is raised, it may be brought to coincide roughly with the curve (2) or (1).

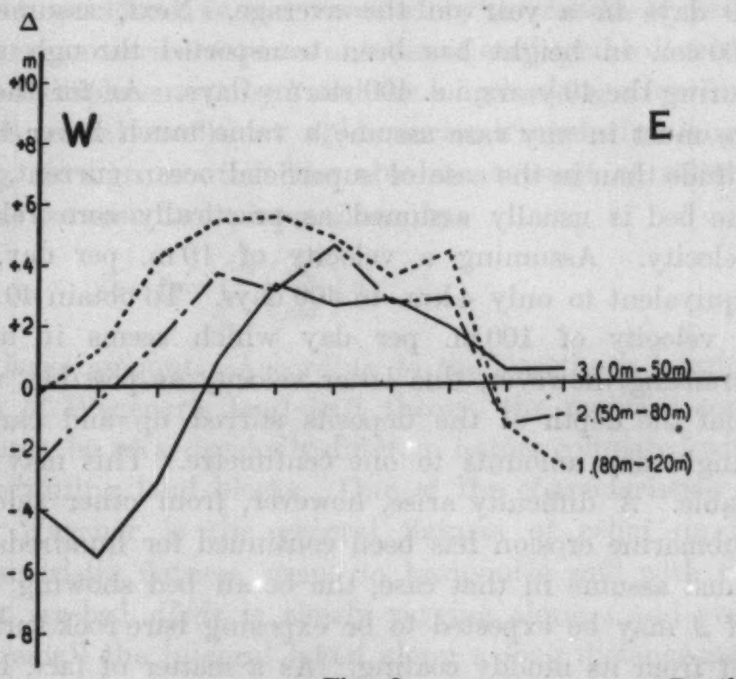

Fig. 3.

As already remarked, such a systematic mode of the change in depth cannot be explained as merely due to the accidental error of sounding. Nor, it is difficult to be attributed to the error due to the inclination of sounding wire. Again, the general slope of the sea bed is small (6/1000 say) so that the effect due to the error in the position of observation may be put out of account. It may, however, be questioned whether the observed change is not due to the horizontal transport of muddy deposits caused by the joint action of waves and current.

The tidal or ocean current must in any case decrease in its velocity

towards the sea-bed and it is highly improbable that the current by itself may cause the transport of any submarine deposit in several ten metres depth. On the other hand, the effect of waves, though periodic, may stir up the lighter deposits to a sensible height and, on this account, the time-integral of the effect of current may turn out sensible under a favourable circumstance, even if the velocity of current may be very small. It is said that on some occasions of very rough sea the muddy deposits are stirred up from a depth of 40 fathoms. Such thing granted as possible, the favourable condition may obtain only rarely throughout the course of a year. Assume that such a condition prevails during 10 days in a year on the average. Next, assume that a deposit of 400 cm. in height has been transported through a distance of 40 km. during the 40 years, i.e. 400 stormy days. As for the velocity of current we must in any case assume a value much lower in the order of magnitude than in the case of superficial ocean current, as the velocity near the bed is usually assumed as practically zero relative to the surface velocity. Assuming a velocity of 10 m. per day, for example, it is equivalent to only 4 km. in 400 days. To obtain 40 km. we must assume a velocity of 100 m. per day which seems in any case improbable. Granting, however, this latter velocity as possible, we must next assume that the depth of the deposits stirred up and carried forth during a single day amounts to one centimetre. This may or may not be probable. A difficulty arise, however, from other side. If such a rate of submarine erosion has been continued for hundreds of centuries, as we must assume in that case, the ocean bed showing large positive values of $\varDelta$ may be expected to be exposing bare rock surface entirely stripped off from its muddy coating. As a matter of fact, however, the part of the bay with positive $\varDelta$ is generally covered either with mud or fine sand as far as may be judged from the hydrographical chart at hand.

In the case of Tazima and Tango earthquakes, the amounts of the vertical deformation of the sea bed were of the same order of magnitude as in the present case of the Bay of Tosa. In the sea off Tango a discontinuity of depth was found along a line forming the prolongation of the Gômura fault. The sense of the relative vertical displacements on the two sides of the line was the same as along the land fault, though the amount of displacement was decidedly larger in sea than on land. Such a discontinuity is also difficult to explain on the basis of mud-transport theory.

The chief origin of scepticism towards the reality of the vertical

deformation obtained by sounding seems to lie in the large absolute magnitude of displacement. It is, however, not the absolute amount of deformation which determines the strain and stress of the earth's crust, but its space-derivative. A depression of 6 m. along a distance of 20 km. in 40 years is equivalent to an annual tilting of about $0{\cdot}8\times10^{-5}$ radian. A tilting of such an amount is by no means rare even on the land area. For an example, Mr. Miyabe[2] has recently found a tilting of just this order, or even a little more, along a local levelling route in Hukagawa, Tokyo. In the case of land, however, the direction of tilting changes rapidly along the horizontal distance, perhaps due to the complicated block structure, as was revealed by the results of recent repeated levelling surveys carried out in a number of earthquake districts. Denoting the vertical displacement by ζ and the length along a levelling route by s, the differential coefficient $d\zeta/ds$ varies irregularly along s frequently changing its sign, so that the absolute amount of relative vertical displacement between two places given by

$$\zeta_2-\zeta_1=\int_{s_1}^{s_2}\left(\frac{d\zeta}{ds}\right)ds$$

can never attain a large amount. According to the hypothesis forming the very foundation of Wegener's land-drift theory, the material composing ocean bed must be of a decidedly different nature compared with the rocky crust constituting land blocks. One of the characteristics of sea-bed quoted by Wegener is the general flatness of relief on its surface. This characteristic flatness seems to harmonize well with the assumption that for sea-bed $d\zeta/ds$ is slowly varying along s and even if its magnitude be small the integral taken along a long distance may attain a sensible amount much greater than the amount ever attainable on land area. Hence, it is not necessary to assume any marked difference in the elastic property of the materials composing land and ocean bed, at least for explaining the observed difference in the order of magnitude of vertical displacement, if we only assume a difference in some structural characters of the earth's crust on land and sea respectively.

In 1904, an ephemeral volcanic island[3] appeared near Minami-

2) The paper is not yet published, but will appear in a near future.

3) T. Wakimizu, *Report of the Imperial Earthquake Investigation Committee*, No. 56 (1903); *Publication of I.E.I.C.*, No. 22C (1908). D. Sato, *Tigakuzassi*, No. 201 and 202 (1905).

Yuwôzima. It rapidly disappeared and a sounding carried out by I.J.N. in 1911 gave a depth of 200 fathoms at the very site of the vanished volcano. In 1914, another volcano[4] emerged nearly at the same spot as before, which disappeared again in the course of a few years. The explanation of this phenomenon seemed difficult at that time. The present author alluded to the effect of wave erosion combined with current as one of the possible cause, as the island was built up of very loose masses of ash and pumice, though it seemed rather doubtful whether the said speedy erosion could reach a depth as large as 200 fathoms. If, however, we could once admit that the earth's crust forming the ocean-bed is capable of vertical displacements far greater in the order of magnitude than ever experienced on land area, another possibility of actual depression must be taken as well into consideration. It will be interesting to repeat occasionally the detailed sounding survey in the vicinity of the former ephemeral volcanic island. On the other hand, it is reported not infrequently in the history of hydrographical survey that a dangerous shoal marked on a chart cannot be traced by a subsequent survey, or that an abnormal depth observed by a previous sounding cannot be detected by a careful revision carried out after many years. In such an occasion, the result of the previous survey was indiscriminately cancelled as erroneous. It seems, however, to be well worth repeating careful revision of sounding with a regular interval of a few years, in the vicinity of the spots where some remarkable discrepancy have been found between two successive soundings.

The difference in magnitude of vertical displacements for land and sea-bed, granted as real, may partly be due to the effect of the bouyancy of water, if we assume that the possible limit of the vertical displacement is laid by the claim of isostasy or of the elastic limit of the earth's crust. Thus, an upheaval of h m. in the case of sea-bed is tantamount to that of $(\rho_1-\rho_3)/\rho_2$ on land where the densities ρ_1, ρ_2 and ρ_3 are respectively for sima, sial and sea water. Taking roughly $\rho_1=3{\cdot}0$, $\rho_2=2{\cdot}7$ and $\rho_3=1$, this amounts to 0·74. Thus, the difference due to this cause may be put out of amount with regard to the present problem, where only the order of magnitude is in question.

Admitting the reality of the vertical displacement of the surface of the earth's crust in the case of the Bay of Tosa, we must also admit

4) I. OGURA, *Report of I.E.I.C.*, No. 79 (1915). T. TERADA, *Tôyôgakugeizassi*, **31** (1914), 149; *Tisitugakuzassi*, **21** (1914), No. 246. T. WAKIMIZU, *Tôyôgakugeizassi*, **37** (1920), 257.

the probability of similar displacements of secular nature in the cases of the beds of the Bay of Sagami, the sea off Tazima and Tango, which are taking place slowly but continuously. This is of no wonder, if we consider that we have already a large number of infallible evidences of such a phenomenon on the land area. It is very interesting to remark that the order of magnitude of the rate of deformation turns out somewhat different for land and sea, if we take the space derivative of the displacement, i.e. the strain, into account, instead of the absolute amount. A further discussion of this point will be given in a next paper.

Returning to the present result of investigation, we may spend a few words with regard to the geotectonic history of the Bay of Tosa. According to the recent investigation of Mr. Watanabe[5] we may draw a curved line of demarcation along the eastern part of the coast of this Bay marking the boundary line separating the region of upheaval from that of depression from each other. These vertical movements are considered to have been completed in a recent geological age. The variation of the vertical displacement along the present coast line, there shown, is in remarkable harmony with the general tendency of the present motion of sea-bed shown by the curves of Fig. 3, i.e., a general upheaval towards Murotozaki and a depression near the middle part of the Bay, though as for the detailed feature, some depression is found in Fig. 1 in the immediate neighbourhood of the shore line near Murotozaki.

H. Kishinouye and T. Kodaira[6] suggested from the result of their investigation regarding the distribution of the slope-angle of sea-bed along the entire coast of Tosa, that the sea-bed in the eastern part of the Bay seems to have been elevated in an unknown past by an amount of twenty to thirty metres relative to the other parts. This is also in harmony, at least partly, with the present result.

In connection with the above investigation of Kishinouye and Kodaira, the present author[7] made some studies on the topographical features of Sikoku, especially of the southern coastal regions of Tosa, and suggested that in a recent geological age the central part of Southern Sikoku seems to have been depressed by a considerable amount, connected with an upheaval of the eastern part.

These results taken together are also in harmony with the result of

---

5) A. Watanabe, *Bull. E.R.I.*, 10 (1932), 209.

6) H. Kishinouye and T. Kodaira, *Bull. E.R.I.*, 4 (1928), 57.

7) T. Terada, *ibid.*, 67.

the present investigation and show that the vertical movement here revealed by sounding appears as a probable continuation or distant echo of what has been taking place since a remote past.

On the occasion of the notorious earthquake of Hôei[8], 1707, the eastern coast of the Tosa Bay was elevated by several syaku (shaku) while some parts of the middle and western coast are said to have been depressed. Again, in the occasion of Ansei Earthquake[9] of 1854 the eastern coast seems to have been subjected to a similar upheaval.

On the other hand, the recent result of precise levelling carried out along the coast of SE Sikoku[10] has revealed the remarkable fact that a region of triangular form, with Murotozaki at its vertex and lengths of thirty to forty km. for its sides, is subjected to a sensible tilting toward S. This is remarkable as this sense of movement of Murotozaki seems to be opposite to that of the different kinds of movement which may be supposed to have occurred in the geological past, while it is the same as is here observed in the sea-bed in the immediate neighbourhood of the coast near Murotozaki.

These different kinds of data regarding the vertical movement of the earth's crust in the southern part of Sikoku seem to throw considerable light on the mechanism of crust deformation upon which the occurrence of earthquakes depends. A further discussion may, however, be reserved for a future, as an extension of relevelling is going on at the present moment towards the western part of the coast of the Tosa Bay and we may expect a substantial addition of data from its results.

---

38. 土佐灣の海底變化

地震研究所 寺 田 寅 彦

昭和三年に行はれた土佐灣水深測量の結果を舊海圖と比較して得た水深變化の量を圖上に記入し其等差線を引いて見ると或系統的な變形の模樣が窺はれる。此の見掛け上の水深變化が果して實際の地殼の垂直變化を示すかどうかといふ疑問に對する若干の考察の徑路を述べ、此れが實測の誤差としても説明し難く、又海底のエロージョンによるとしても説明し難いと考へる理由を述べた。

海底變化の量が陸上で知られた變化に比して異常に大きく思はれ、從つて信じ難く思はれるが、

---

8) M. TERAISI, "*Tosa kokonno Disin* 土佐古今の地震" (1923), issued by Tosa-Sidankwai 土佐史談會; A. IMAMURA, *Disin*, 2 (1930), 81; *Proc. Imp. Acad.*, 6 (1930), 101.

9) M. TERAISI, *loc. cit.*; A. IMAMURA, *Disin* 2 (1930), 357.

10) A. IMAMURA, *loc. cit.*

併し海底の變化の絶對値を考へる代りに、其の水平距離に對する微分係數、即ちストレーンとしての傾斜の量を計量して見ると、陸地で不斷に見られると全く同程度である。唯陸上では傾斜の方向が短距離內で交互に變化するから、此れを水準路に沿ふて積分したものゝ絶對値はいつも小さい。此れに反して海底では此傾斜方向の變化が緩徐であるとすれば、此の積分値が大きくなるのは當然である。海底の起伏が一體に陸上よりも緩徐であることは周知の事實であり、又陸上で認められるやうなブロック構造が海底では認められぬことから考へても、此想像は妥當であり、又一方ウエーゲナーの學說の基礎となつて居る陸塊と海底岩床との特質の差違に關する色々な目標とも合致するのである。

此處で得られた海底の垂直變化の分布が、渡邊光氏の研究された土佐東南部に於ける地質時代の地殼變動、岸上小平兩氏の研究された土佐灣海底の過去の變動、著者の調べた四國南部の過去の變形、又今村氏の調査された寶永安政地震當時の土佐海岸の地變及最近陸地測量部の水準測量の結果等に對して如何なる關係にあるかを解說しておいた。此等の種々の方面の證據から推測される地殼變動の樣式と此處で得た海底變化の樣式とが可也迄相照應することだけから考へても、此水底變化が單なる見掛け上のものでないであらうといふことが諒解される。

此のやうな海底の垂直變化の樣式の可能性を許容するとなれば、そこから色々な推論の可能性が生まれて來る。例へば一九〇四年と一九一四年との兩度に南硫黃島附近に噴出して間もなく消失した新島の出現消失過程の說明にも從來考へたとは稍ちがつた說明が考へ得らるゝので、此れに就て一言し、此の如き疑問の地點に於ける水深測量をなるべく頻繁に繰返して行ひ度いといふ希望を述べてある。

---

39. *Comparison of the Modes of the Vertical Deformations of the Earth's Crust in the Same District during Different Time Intervals.*

By Chûji TSUBOI,

Earthquake Research Institute,

(Received June 20, 1932.)

If a levelling route in a certain district is covered by precise levelling more than thrice in a certain interval of time, we can, by the results of these surveys, compare the modes of the vertical deformations of the earth's crust in the district for at least two different time intervals and in this way we can get informations regarding whether the deformation of the earth's crust in the district is ever going on in one same direction, or goes forward or backward alternately, or gradually changes in its mode, etc. In the present paper, the writer is going to give a few examples of such comparisons, basing solely on the results of measurements obtained recently in our country.

The Case of Positive Correlation.

The case to be mentioned first is that in which the crust deformations in defferent intervals are in a positive correlation. The deformation of the earth's crust found in the Tango district is a typical example of this. Connected with the Tango destructive earthquake of 1927, precise levelling has been repeated five times after the earthquake over the Tango district by

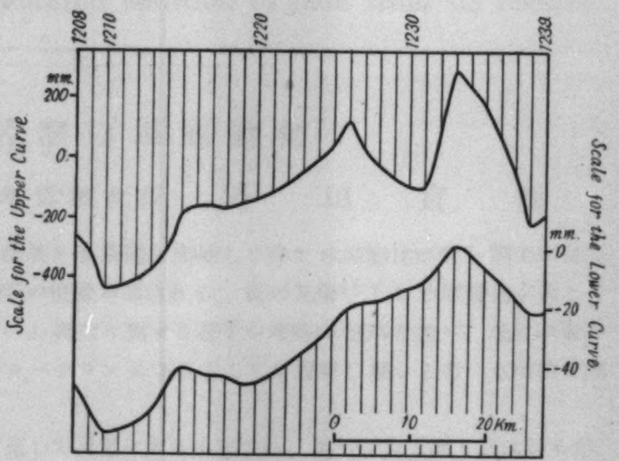

Fig. 1. Overrupping Means of the Change of Height of the Bench Marks in the Tango District at the Time of (Upper Curve) and After (Lower Curve) the Tango Earthquake of 1927.

the experts of the Military Land Survey at the request of the director of our Institute. The results of these surveys were given and discussed in detail in the writer's previous papers[1]. The vertical displacements of the beuch marks in the district that were produced at the time of and after the earthquake are given in Table I, together with their overrupping means. They are in a very close positive correlation as the curves in Fig. 1 show. This is made still clearer by the correlation diagram for the observed values which is given in Fig. 2. The correlation becomes still closer if the overrupping mean values are taken as in Fig. 3. This positive correlation would seem to indicate that the crust deformation at the time of the earthquake did not just match the agency by which it was caused and was somewhat insufficient in its amount.

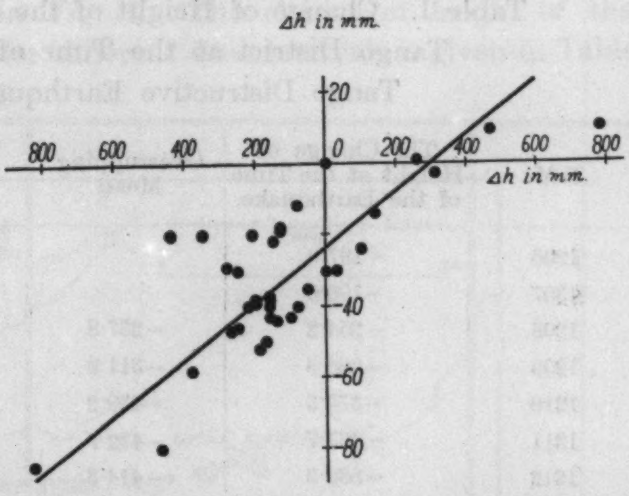

Fig. 2. Correlation Diagram for the Measured Change of Height of the Bench Marks in the Tango District at the Time of (Abscissa) and After (Ordinate) the Tango Earthqake of 1927.

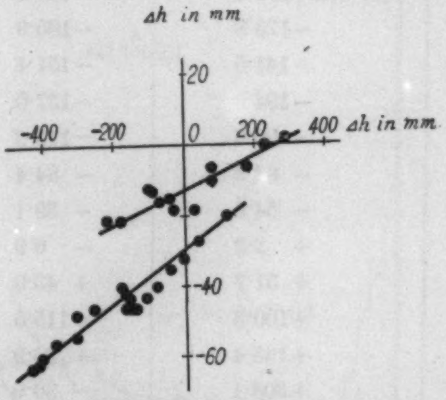

Fig. 3. Correlation Diagram for the Overrupping Means of the Change of Height of the Bench Marks in the Tango District at the Time of (Abscissa) and After (Ordinate) the Tango Earthquake of 1927.

Another example of positive correlation is given by the vertical deformation of the earth's crust along the levelling route from Okitu

1) C. Tsuboi, *Bull. Earthq. Res. Inst.*, **6** (1929), 71 ; **8** (1930), 153 ; **9** (1931), 423.

Table I. Change of Height of the Bench Marks in the Tango District at the Time of and After the Tango Distructive Earthquake of 1927.

B.M.	The Change of Height at the Time of the Earthquake.	Overrupping Mean	Total Change of Height after the Earthquake	Overrupping Mean.
1206	−197·0 mm		−37·7	
1307	−196·0		−39·1	
1208	−254·2	−257·8	−46·1	−45·7
1209	−266·3	−311·9	−47·2	−54·1
1210	−375·3	−439·2	−58·3	−63·2
1211	−467·7	−432·7	−79·6	−61·9
1212	−832·3	−414·3	−84·9	−60·1
1213	−221·9	−371·7	−39·7	−55·8
1214	−174·3	−310·7	−37·9	−47·9
1215	−162·2	−175·5	−37·0	−39·5
1216	−162·9	−165·9	−40·1	−41·5
1217	−156·3	−159·3	−42·7	−42·8
1218	−173·8	−165·9	−49·7	−42·7
1219	−141·5	−151·4	−44·3	−46·2
1220	−194·9	−137·0	−51·7	−45·6
1221	− 90·6	−113·2	−42·6	−42·6
1222	− 84·3	− 84·4	−39·5	−39·7
1223	− 54·6	− 39·1	−34·8	−35·3
1224	+ 2·2	− 0·9	−29·9	−31·6
1225	+ 31·7	+ 43·0	−29·6	−26·5
1226	+100·3	+115·5	−24·2	−20·2
1227	+135·4	+ 26·9	−14·1	−18·2
1228	+308·1	− 30·0	− 3·1	−18·3
1229	−441·0	− 65·3	−20·2	−15·9
1230	−252·8	− 92·4	−29·9	−13·1
1231	− 76·4	−101·4	−12·2	−12·2
1232	0	+ 80·5	0	− 6·4
1233	+263·4	+288·0	+ 1·4	+ 1·5
1234	+468·2	+232·6	+ 8·5	− 0·2
1235	+784·8	+177·1	+ 9·6	− 5 9
1236	−353·0	+ 82·3	−20·3	−10·1
1237	−277·7	− 37·0	−28·6	−15·4
1238	−210 7	−219·5	−19·9	−21·0
1239	−128·6	−179·2	−17·8	−21.4
1240	−127·3		−18·9	
1241	−151·8		−21.7	

to Kôhu which is shown in Fig. 4. The change of height of the bench marks[2] on the route for different time intervals is given in Table II and graphically in Fig. 5.

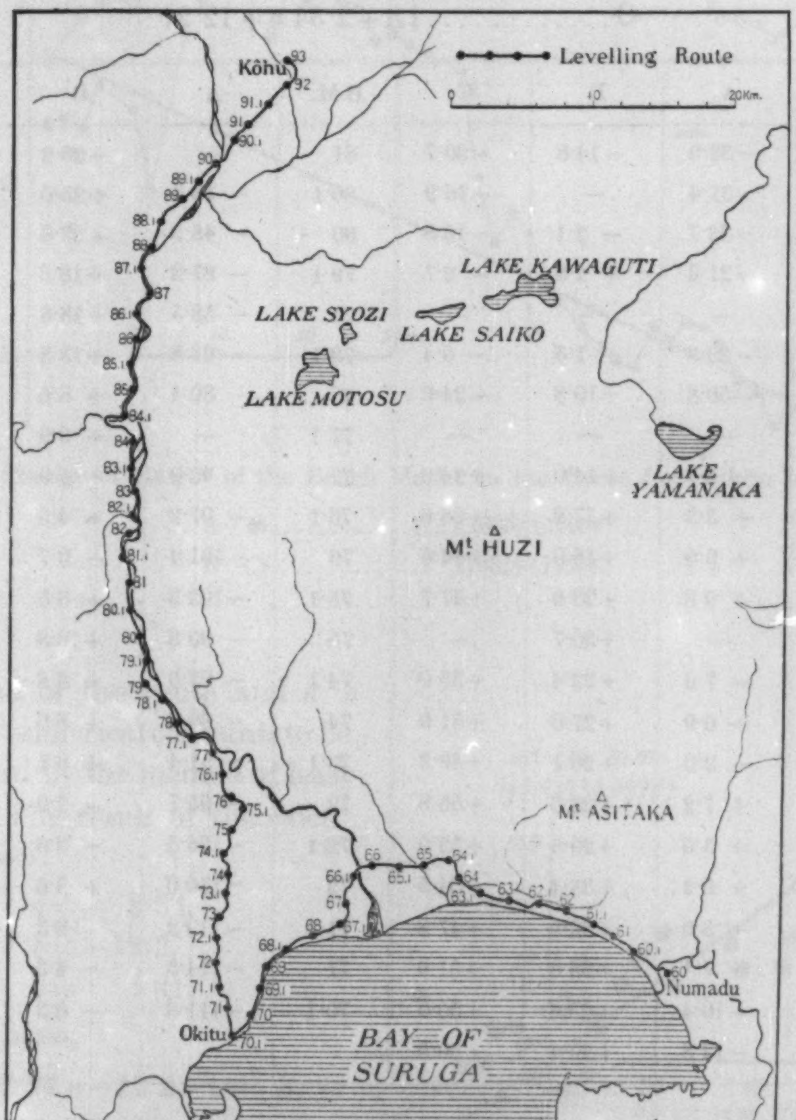

Fig. 4. Levelling Route from Okitu to Kôhu.

2) THE IMPERIAL JAPANESE MILITARY LAND SURVEY, *Bull. Imp. Earthq. Inv. Comm.*, 11 (1930); "*Change of Heights of the Bench Marks in the Meizoseismal Area of the Kwanto Great Earthquake of 1923,*" (1930).

Table II. Change of Height of the Bench Marks on the Levelling Route from Okitu to Kôhu, during Different Time Intervals.

A............(1925–1895)
B............(1931–1925)
C............$\{A+2{\cdot}34\,n+12{\cdot}2\}$

B.M.	A	B	C	B.M.	A	B	C
93	mm −32·9	−14·8	−20·7	81	—	+26·2	—
92	−31·4	—	−16·9	80·1	− 18·3	+25·0	+50·1
91·1	−33·7	− 2·1	−16·8	80	− 48·3	+23·6	+22·4
91	−21·9	+ 2·8	− 2·7	79·1	− 67·3	+18·3	+ 5·7
90·1	—	—	—	79	− 58·5	+18·8	+16·9
90	−29·3	+ 1·5	− 5·4	78·1	− 63·8	+13·8	+13·9
89·1	−50·8	+10·8	−24·6	78	− 80·4	+ 8·6	− 0·3
89	—	—	—	77·1	—	+ 9·9	—
88·1	− 6·7	+14·0	+24·2	77	− 90·9	+ 5·9	− 6·2
88	+ 3·3	+17·2	+36·6	76·1	− 97·2	+ 4·9	−10·1
87·1	+ 9·0	+18·0	+44·6	76	−101·4	− 0·7	−12·0
87	+ 9·8	+23·6	+47·7	75·1	−102·3	+ 5·5	−10·5
86·1	—	+30·7	—	75	− 90·8	+10·8	+ 3·3
86	− 7·6	+22·4	+35·0	74·1	− 93·9	+ 8·8	+ 2·5
85·1	+ 6·9	+27·0	+51·9	74	− 89·8	+ 8·0	+ 9·0
85	+ 2·0	+28·1	+49·3	73·1	− 91·4	+ 6·1	+ 9·7
84·1	+ 7·2	+28·6	+56·8	73	− 95·1	− 2·9	+ 8·4
84	+ 3·0	+29·5	+55·0	72·1	−106·5	− 3·3	− 0·7
83·1	+ 0·2	+33·4	+54·5	72	−110·0	+ 3·6	− 1·9
83	− 8·9	+32·9	+47·8	71·1	−119·2	− 8·3	− 8·7
82·1	− 7·1	+26·6	+51·9	71	−114·5	− 4·3	− 1·7
82	−10·4	+25·6	+50·9	70·1	−111·8	− 6·3	+ 3·4
81·1	−12·8	+29·4	+50·9				

The two curves in Fig. 5 are very much similar in their forms with each other; more precisely, the curve A may be regarded as one which is obtained by the superposition of a linear southward tilting of the earth's crust and the variation that is similar to the curve B. Thus the curve A can be expressed by the equation,

$$A=an+b+kB,$$

where n is the ordinal number of the bench mark counted from the

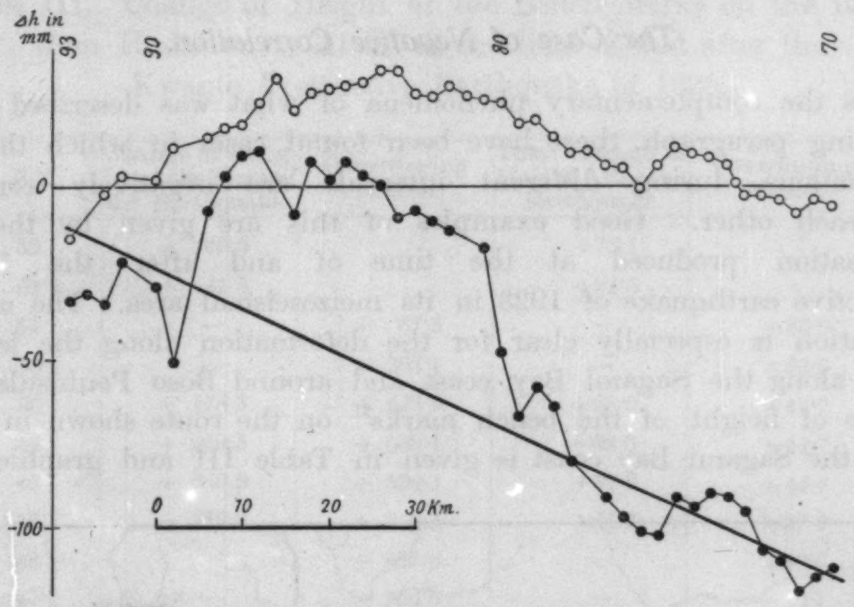

Fig. 5. Change of Height of the Bench Marks on the Route from Okitu to Kôhu.

A ●................(1925)-(1895)

B ○................(1931)-(1925)

north end of the route and a, b and k are numerical constants to be determined by the method of least square. The result of the calculation gave

$$a = -\ 2{\cdot}34,$$
$$b = -12{\cdot}2,$$
$$k = \ \ 1{\cdot}41,$$

thus we have,

$$A = -2{\cdot}34\,n - 12{\cdot}2 + 1{\cdot}41\,B.$$

We can thus expect a close positive correlation between $\{A + 2{\cdot}34\,n + 12{\cdot}2\}$ and B, the values of which being already given in Table II. This is actually the case as the correlation diagram in Fig. 6 indicates.

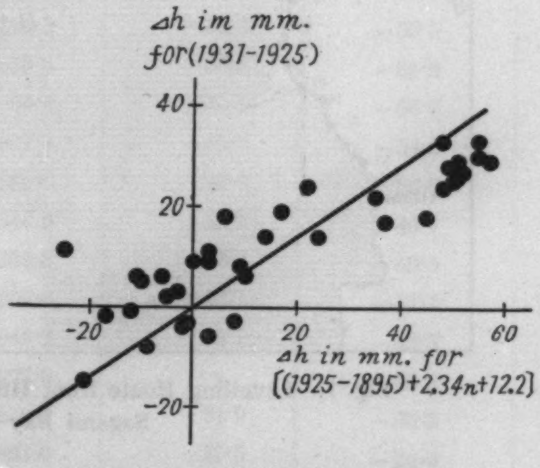

Fig. 6. Correlation Diagram for C [(1925–1895)+2·34 n+12·2] and B (1931–1925).

The Case of Negative Correlation.

As the complementary phenomena of what was described in the preceding paragraph, there have been found cases in which the crust deformations during different intervals are negatively correlated with each other. Good examples of this are given by the crust deformation produced at the time of and after the Kwanto destructive earthquake of 1923 in its meizoseismal area. The negative correlation is especially clear for the deformation along the levelling routes along the Sagami Bay coast and around Boso Peninsula. The change of height of the bench marks[3] on the route shown in Fig. 7 along the Sagami Bay coast is given in Table III and graphically in

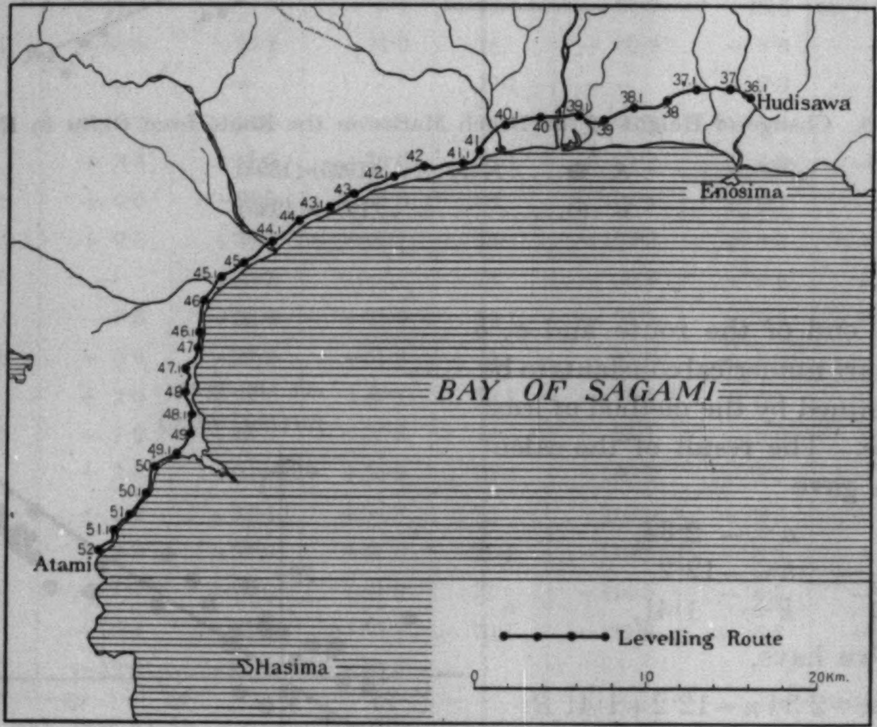

Fig. 7. Levelling Route from Hudisawa to Atami along the Sagami Bay Coast.

3) THE IMPERIAL JAPANESE MILITARY LAND SURVEY, *Bull. Imp. Earthq. Inv. Comm.*, 11 (1930); "*The Results of Precise Levellings executed in the Interval from Feb. 1930 to March 1931*," (1931).

Table III. Change of Height of the Bench Marks on the Route from Hudisawa to Atami at the time of and after the Kwanto Destructive Earthquake of 1928.

B.M.	Change of Height at the Time of the Earthquake.	Overrupping Means.	Total Change of Height After the Earthquake.	Overrupping Means.
52	+ 43·5		+72·1	
51·1	+ 41·5		+94·5	
51	—	+ 87·8	—	+83·9
50·1	—	+ 263·1	—	+63·9
50	+ 178·3	+ 472·5	+65·0	+45·7
49·1	+ 569·5	+ 539·1	+62·3	+44·7
49	+ 669·8	+ 539·1	+39·9	+44·7
48·1	+ 738·9	+ 659·4	+41·4	+37·9
48	—	+ 867·6	—	+40·3
47·1	—	+ 966·5	—	+40·7
47	+1194·1	+1098·3	+40·1	+26·9
46·1	—	+1113·3	—	+26·9
46	+1002·6	+1207·8	+13·8	+ 1·0
45·1	+1143·2	+1344·1	—	−28·2
45	+1491·5	+1438·5	−51·0	−37·5
44·1	+1739·2	+1620·3	−47·5	−54·0
44	+1815·9	+1780·7	−65·4	−54·6
43·1	+1911·5	+1862·3	−52·3	−59·5
43	+1945·3	+1878·4	−56·8	−61·2
42·1	+1899·6	+1865·4	−75·5	−56·7
42	+1819·5	+1807·5	−55·8	−54·6
41·1	+1751·2	+1688·6	−42·9	−53·0
41	+1622·1	+1546·6	−42·2	−46·1
40·1	+1350·6	+1355·8	−48·4	−49·5
40	+1189·7	+1202·6	−41·1	−51·1
39·1	+ 865·5	+1046·2	−72·7	−48·5
39	+ 985·0	+ 927·0	—	−42·8
38·1	+ 840·2	+ 832·3	−31·9	−36·6
38	+ 754·6	+ 824·0	−25·5	−24·6
37·1	+ 716·3	+ 734·3	−16·5	−23·4
37	—		—	
36·1	+ 626·1		−19·7	

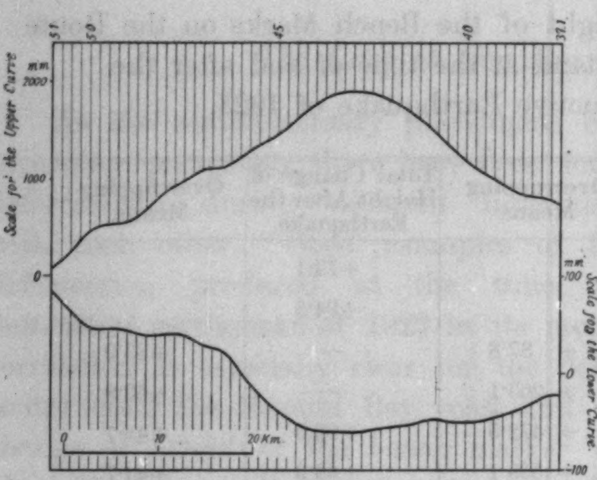

Fig. 8. Overrupping Means of the Change of Height of the Bench Marks on the Route from Hudisawa to Atami at the Time of (Upper Curve) and After (Lower Curve) the Kwantô Earthquake of 1923.

Fig. 8. In Fig. 9 is shown the correlation diagram for the overrupping mean values. As these figures clearly indicate, the correlation between the crust deformations in this district during different time intervals is closely negative. This indicates that the crust deformation after the earthquake of 1923 has been such that to recover what was produced at the time of the earthquake, this being in a remarkable contrast with the case of the Tango earthquake.

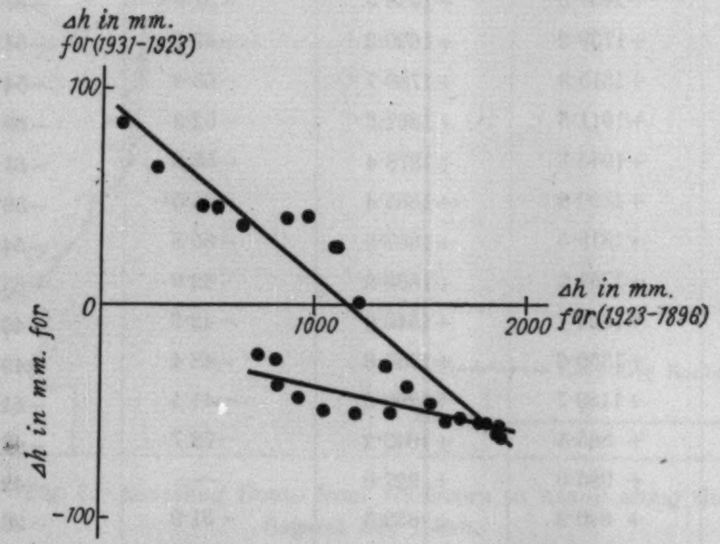

Fig. 9. Correlation Diagram for the Overrupping Means of the Change of Height of the Bench Marks on the Route from Hudisawa to Atami at the Time of (Abscissa) and After (Ordinate) the Kwantô Earthquake of 1923.

The crust deformations in Boso Peninsula at the time of and after the earthquake of 1923 are also in a close negative correlation, as the curves in Fig. 10 show. This has already been pointed out by N. Miyabe.[4] The correlation diagram in Fig. 11 for the overrupping means of the

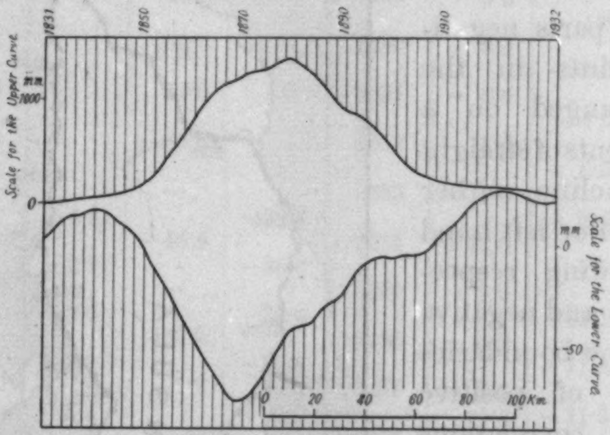

Fig. 10. Overrupping Means of the Change of Height of the Bench Marks on the Route around Boso Peninsula at the Time of (Upper Curve) and After (Lower Curve) the Kwantô Earthquake of 1923.

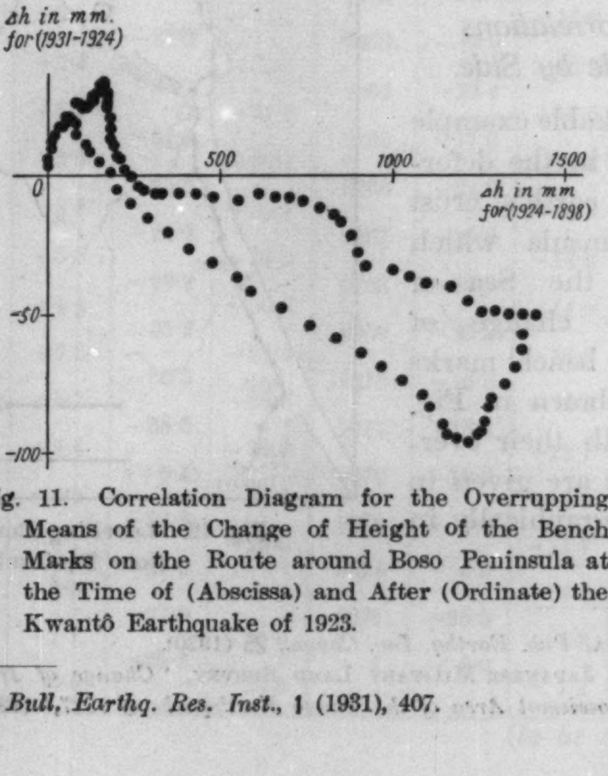

Fig. 11. Correlation Diagram for the Overrupping Means of the Change of Height of the Bench Marks on the Route around Boso Peninsula at the Time of (Abscissa) and After (Ordinate) the Kwantô Earthquake of 1923.

4) N. MIYABE, *Bull. Earthq. Res. Inst.*, 1 (1931), 407.

change of height of the bench marks in the peninsula, however, suggests that in some parts of the peninsula they are positively correlated while in other parts negatively. The points in the figure are arranged on a number of segments of straight line which incline either right hand high or left hand high corresponding respectively to positive and negative correlations. The boundaries of the regions of positive and negative correlations seem to be closely connected with the geological structure of the peninsula.

The Region of Positive and Negative Correlations Situated Side by Side.

The remarkable example of this is seen in the deformation of the earth's crust in Noto Peninsula which projects into the Sea of Japan.[5] The change of height of the bench marks on the route shown in Fig. 12 together with their overrupping means are given in Table IV and graphically in Fig. 13.

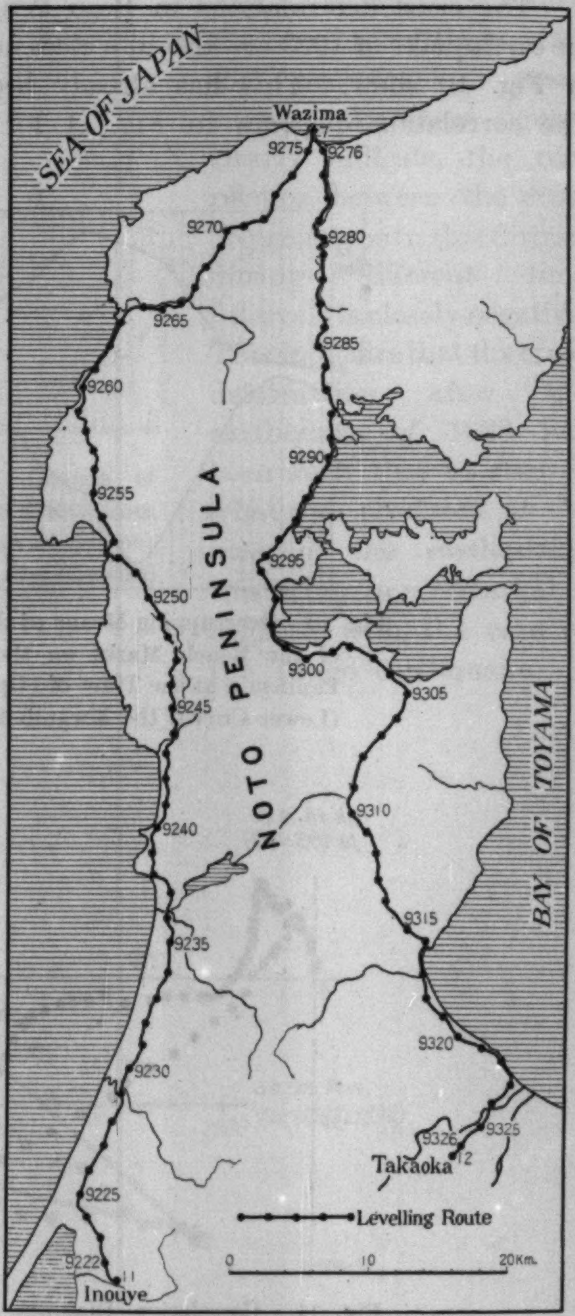

Fig. 12. Levelling Route around Noto Peninsula.

5) A. IMAMURA, *Pub. Earthq. Inv. Comm.*, 25 (1930).
THE IMPERIAL JAPANESE MILITARY LAND SURVEY, "*Change of Height of the Bench Marks in the Meizoseismal Area of the Tango Earthquake of 1927,*" (1929).

Table IV. Change of Height of the Bench Marks in Noto Peninsula.

B.M.	1919 −1917	O.M.	1928 −1917	O.M.	B.M.	1917 −1900	O.M.	1928 −1917	O.M.
11	mm + 8·4		−40·0		9249	+ 3·3		−27·4	
							− 1·8		−24·0
9222	+ 4·8		−39·4		9250	+ 8·4		−22·8	
							− 3·0		−21·9
9223	+ 3·4		−39·0		9251	− 6·4		−24·5	
							− 4·8		−20·5
9224	+ 0·9		−46·0		9252	−13·6		−14·9	
							− 6·0		−18·9
9225	—		—		9253	−11·5		−14·4	
		+4·6		−39·4			− 6·4		−17·0
9226	+11·1		−46·4		9254	−11·0		−16·8	
		+2·2		−38·8			− 7·5		−15·8
9227	(−56·0)		—		9255	− 9·2		−13·1	
		+2·6		−38·4			−11·1		−15·2
9228	+ 8·3		−33·9		9256	− 6·9		−14·3	
		+3·0		−37·5			−11·8		−14·1
9229	+10·9		−31·2		9257	− 7·1		−11·6	
		+3·4		−36·0			−11·6		−14·2
9230	− 1·0		—		9258	− 9·8		− 9·9	
		+2·6		−35·6			−12·4		−14·3
9231	−10·4		−36·0		9259	− 7·6		−15·6	
		+2·7		−33·7			−13·0		−14·5
9232	+ 7·4		−36·3		9260	−27·8		−16·5	
		+2·5		−33·4			−13·8		−14·7
9233	+ 7·5		−32·8		9261	−13·8		—	
		+2·4		−32·5			−15·6		−15·6
9234	+ 3·1		−35·4		9262	−11·3		−16·0	
		+2·0		−31·8			−15·9		−16·0
9235	− 3·9		−33·2		9263	−19·9		−15·2	
		+2·8		−31·5			−16·2		−16·4
9236	+ 2·7		−31·1		9264	−16·4		−18·4	
		+3·6		−31·2			−17·5		−15·9
9237	+ 0·8		−31·0		9265	−17·0		−15·1	
		+3·5		−30·7			−16·4		−17·2
9238	+ 6·5		−25·3		9266	−24·9		−21·8	
		+3·8		−30·7			−16·3		−16·9
9239	+ 7·7		−24·9		9267	−10·9		−15·7	
		+3·8		−30·2			−16·2		−16·6
9240	+ 6·9		−29·2		9268	−12·8		−13·4	
		+4·4		−30·3			−14·8		−16·5
9241	− 2·8		−33·2		9269	−20·3		−11·5	
		+5·3		−29·9			−14·0		−16·8
9242	+ 6·8		−30·5		9270	−16·8		−27·4	
		+5·7		−29·6			−14·7		−15·0
9243	+10·6		−33·6		9271	−13·1		−14·0	
		+4·4		−30·0			−12·7		−14·2
9244	+ 2·5		(+0·4)		9272	−10·2		−13·1	
		+4·0		−30·3			−12·0		−13·9
9245	+ 2·3		−33·8		9273	− 6·0		−14·1	
		+4·1		−29·6			−11·7		−14·1
9246	+11·5		−27·9		9274	− 6·9		−21·5	
		+3·8		−28·6			− 9·2		−14·8
9247	+ 4·6		−27·9		9275	−25·5		+ 2·2	
		+1·7		−26·9			− 7·8		−12·5
9248	− 5·8		−29·3		7	− 4·0		−13·0	
		−0·5		−24·8			− 7·1		−12·3

(*to be continued.*)

Table IV. *(continued.)*

	1921 −1900	O.M.	1928 −1921	O.M.		1921 −1900	O.M.	1928 −1921	O.M.
9276	− 4·1		—		9302	+13·7		−27·7	
		−5·8		−11·5			+ 8·2		−22·7
9277	− 9·8		−14·2		9303	+11·1		−20·8	
		−5·9		−10·5			+ 7·9		−21·8
9278	+ 4·8		−18·5		9304	+ 8·7		−23·5	
		−5·5		− 9·4			+ 7·5		−21·4
9279	− 2·7		− 6·6		9305	+ 2·7		−22·3	
		−2·3		−10·9			+ 7·8		−21·3
9280	− 6·7		−10·9		9306	+ 8·1		−20·2	
		−1·2		−10·7			+ 4·9		−21·4
9281	+ 2·8		− 6·9		9307	+ 5·1		−20·2	
		+0·1		−10·4			+ 4·3		−20·6
9282	− 7·1		− 5·4		9308	+ 7·0		−16·1	
		+1·2		−10·0			+ 4·1		−20·6
9283	− 2·9		−11·5		9309	− 0·2		−19·8	
		+1·8		− 9·0			+ 3·8		−18·1
9284	+ 7·1		−10·9		9310	—		—	
		+0·4		−10·1			+ 3·9		−15·8
9285	+ 6·3		−11·2		9311	−12·3		−22·5	
		+1·6		−10·3			+ 3·4		−14·4
9286	+ 8·6		− 7·8		9312	+ 8·9		—	
		+2·1		−10·8			+ 2·5		−13·7
9287	+ 2·2		—		9313	+ 8·7		—	
		+3·3		−11·4			+ 2·4		−12·9
9288	+10·5		− 9·9		9314	+ 6·2		− 5·6	
		+3·6		−11·6			+ 0·2		−11·8
9289	−17·3		−16·1		9315	+ 3·3		− 6·7	
		+3·6		−12·4			0		−12·5
9290	+ 5·6		−13·4		9316	+ 4·0		−10·1	
		+4·3		−13·5			− 0·9		−11·2
9291	+ 7·8		−10·9		9317	− 3·1		−15·2	
		+3·0		−15·6			− 1·9		− 11·8
9292	+ 5·1		−10·5		9318	+ 6·2		−10·9	
		+3·9		−16·2			− 4·5		−12·5
9293	+ 0·3		−14·0		9319	−20·3		—	
		+3·8		−17·7			− 9·3		−13·3
9294	+ 6·8		−17·5		9320	− 2·0		−16·6	
		+5·9		−18·5			−12·2		−14·2
9295	+13·0		−21·0		9321	− 2·8		−13·2	
		+5·8		−19·4			−14·6		−14·7
6296	− 4·3		−27·1		9322	−19·2		−16·3	
		+6·6		−20·4			−16·5		−14·5
9297	+11·0		−21·2		9323	−19·2		−17·5	
		+7·3		−22·1					
9298	+ 9·6		−25·4		9324	−39·9		−13·6	
		+8·4		−22·8					
9299	+ 4·0		−24·0		9325	−25·5		–	
		+8·6		−23·4					
9300	+ 4·6		−22·5		9326	−19·8		—	
		+7·6		−23·6					
9301	+14·4		−21·0		12	− 22·2		−13·2	
		+8·8		−22·9					

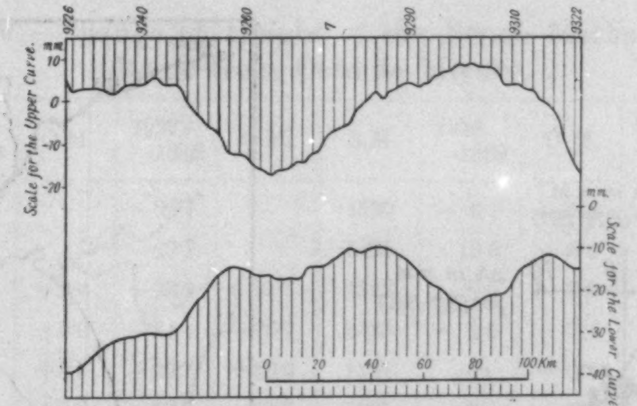

Fig. 13. Overrupping Means of the Change of Height of the Bench Marks on the Route around Noto Peninsula during 1917–1900 (Upper Curve) and 1928–1917 (Lower Curve).

The correlation diagrams of the measured values and their overrupping means are shown in Figs. 14 and 15 respectively. It is an interesting fact that the correlation diagram for the former does not show any clear sign of positive or negative correlation while that for the latter clearly indicates that there are four separate regions in each of which the correlation is negative and positive alternately. The transision from the region of positive correlation to that of negative one is quite distinct.

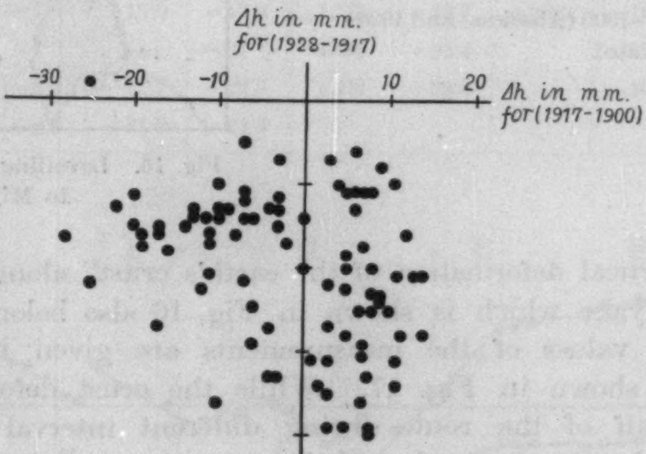

Fig. 14. Correlation Diagram for the Measured Change of Height of the Bench Marks on the Route around Noto Peninsula during 1917–1920 (Abscissa) and 1928–1917 (Ordinate).

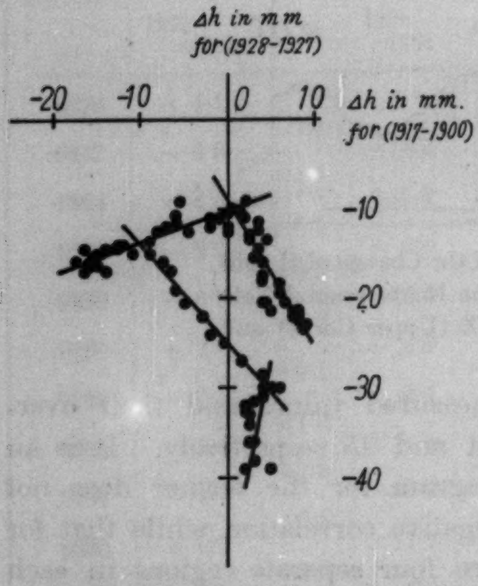

Fig. 15. Correlation Diagram for the Overrupping Means of the Change of Height of the Bench Marks on the Route around Noto Peninsula during 1917-1900 (Abscissa) and 1928-1917 (Ordinate).

Fig. 16. Levelling Route from Ootu to Miyake.

The vertical deformation of the earth's crust[6] along the route from Ootu to Miyake which is shown in Fig. 16 also belongs to this category. The values of the measurements are given in Table V and graphically shown in Fig. 17. While the crust deformation in the southern half of the route during different interval are negatively correlated, that in the northern half positively. As the curves in Fig. 17 shows, the tilting of land blocks in this district are in opposite

---

6) A. IMAMURA, *loc. cit.*

THE IMPERIAL JAPANESE MILITARY LAND SURVEY, "*Change of Height of the Bench Marks in the Meizoseismal Area of the Tango Earthquake of 1927,*" (1929).

Table V. Change of Height of the Bench Marks on the Route from Ootu to Miyake.

B.M.	1918 -1888	O.M.	1927 -1818	O.M.	B.M.	1918 -1888	O.M.	1927 -1918	O.M.
	mm								
213	+13·6		−28·7		1320	− 6·7	− 3·4	− 22·6	−23·5
1300	+ 9·3		−29·7		1321	−10.6	− 6·0	−24·1	−23·2
1301	+ 6·7	+9·4	−23·9	−27·7	1322	− 9·0	− 7·2	−20·4	−21·1
1302	+ 5·7	+9·0	−26·4	−26·7	1323	− 2·6	− 7·4	−17·2	−21·1
1303	+11·7	+8·7	−29·7	−25·6	1324	—	− 6·4	—	−20·4
1304	+11·7	+7·9	−23·9	−23·7	1325	− 7·4	− 3·4	− 22·6	−19·7
1305	+ 7·5	+6·9	−24·3	−23·7	1326	− 6·4	− 2·0	−21·2	−19·7
1306	+ 2·9	+6·6	− 14·0	−22·4	1327	+ 3·0	− 2·0	−17·6	−19·7
1307	+ 0·5	+5·0	− 26·5	−22·1	1328	+ 2·9	+ 3·3	−17·4	−19·6
1308	+10·0	+4·4	− 23·4	− 21·5	1329	—	+10·5	—	−15·1
1309	+ 3·8	+4·5	− 22·2	− 24·0	1330	+13·6	+15·8	−14·0	−13·4
1310	—	+4·6	—	−22·1	1331	+22·6	+21·3	−11·5	−11·9
1311	+ 3·3	+0·8	− 23·8	−20·4	1332	+23·9	+21·3	−10·5	−11·9
1312	+ 0·9	−1·1	−18·9	− 19·6	1333	+25·2	+23·9	− 11·4	−11·1
1313	− 4·9	−1·4	−16·7	−19·0	1334	—	+25·5	—	−11·1
1314	− 3·7	−2·6	−18·8	−17·7	1335	—	+27·5	—	−11·2
1315	− 2·4	−3·5	−16·9	−17·4	1336	+27·5	+27·9	−11·5	−11·2
1316	− 3·1	−1·9	−17·0	−17·9	1337	+29·7	+28·9	−10·8	−11·0
1317	—	−1·2	—	−21·1	1338	+26·4		−11·4	
1318	+ 1·8	−2·3	−18·7	−22·5	1339	+32·0		−10·3	
1319	− 1·2	−4·2	−31·8	−24·3					

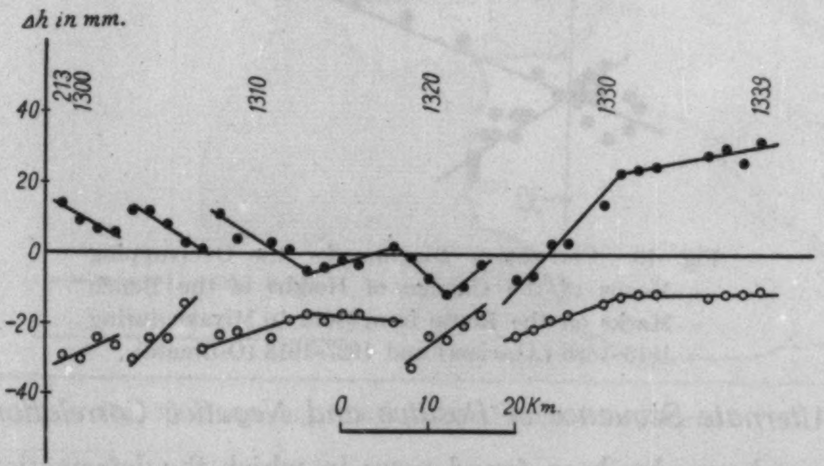

Fig. 17. Change of Height of the Bench Marks on the Route from Ootu to Miyake.
●........(1918–1888) ○........(1927–1918)

sense in the southern half of the route while they are in the same sense in the northern half. This is more clearly indicated by the curves for the overrupping means in Fig. 19. When the correlation diagram for the overrupping means is constructed, we have the diagram shown in Fig. 19. The points in the figure are evidently arranged on two segments of straight line with opposite inclination. The boundary of the two regions of positive and negative correlations lies in the neighbourhood of B. M. 1313.

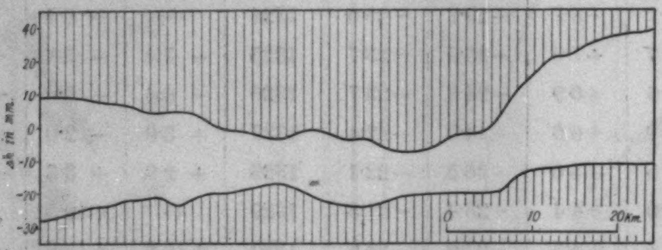

Fig. 18. Overrupping Means of the Change of Height of the Bench Marks on the Route from Ootu to Miyake during 1918–1888 (Upper Curve) and 1927–1918 (Lower Curve).

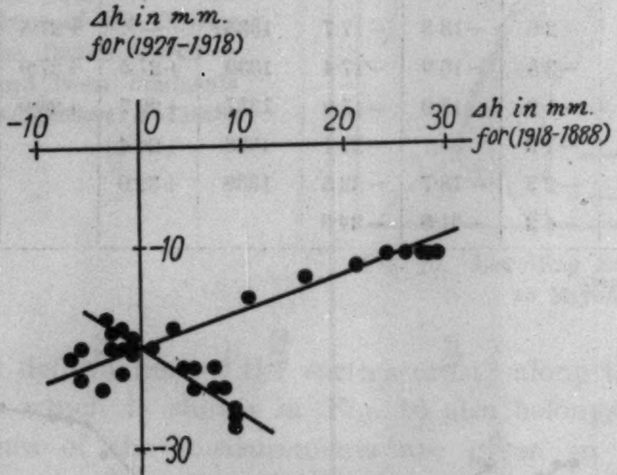

Fig. 19. Correlation Diagram for the Overrupping Means of the Change of Height of the Bench Marks on the Route from Ootu to Miyake during 1918–1888 (Abscissa) and 1927–1918 (Ordinate).

Alternate Sequence of Positive and Negative Correlations.

There have also been found cases in which the deformations of the earth's crust in the same region during different intervals are alter-

nately positively and negatively correlated. This is the case for the deformation of the earth's crust in the Sakurazima volcanic district caused by the eruption of the Sakurazima volcano in 1914. After the eruption, the precise levellings were made in 1914, 1915 and 1918, along the route shown in Fig. 20 in the neighbourhood of the volcano, each survey being referred to as I, II and III hereafter. The results of these measurements are given in the papers of F. Omori and. A. Imamura.[7] We will refer the results of the levelling made in 1892 before the eruption as P. Then (I–P) and (II–I) are positively correlated while (III–II) are negatively correlated to both of them as the curves in Fig. 21 show. This means that soon after the eruption, the deformation of the earth's crust in the district went in the same direction with what was produced at the time of the eruption while some years afterwards the crust deformation was such that to restore the deformation produced before. This is clearly indicated by the correlation diagrams in Figs. 22, 23 and 24.

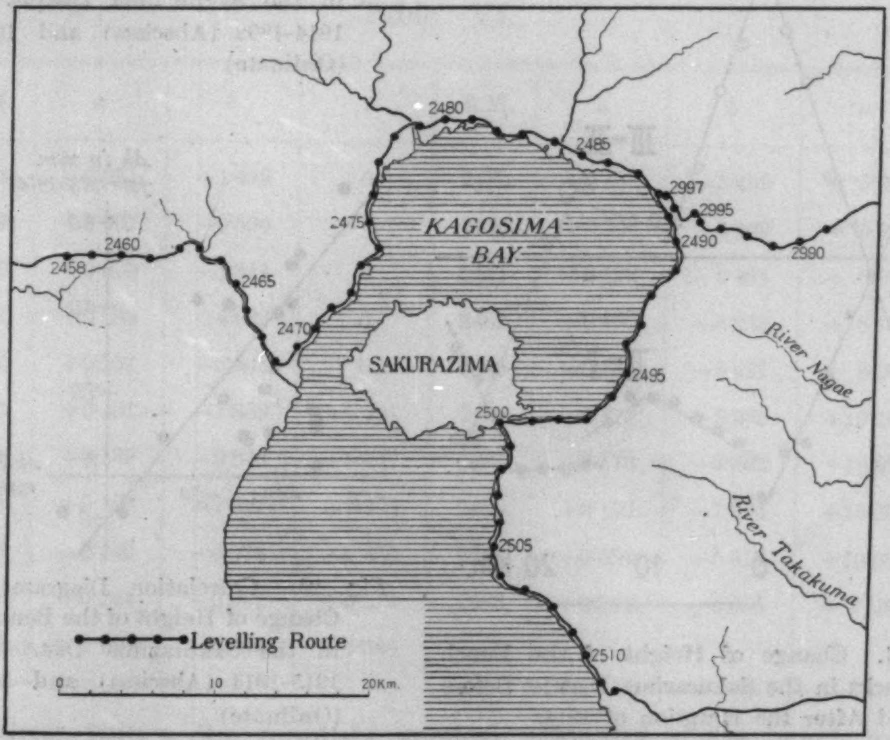

Fig. 20. Levelling Route in the Sakurazima District.

7) F. Omori, *Bull. Imp. Earthq. Inv. Comm.*, **8** (1914–1922).
A. Imamura, *loc. cit.*

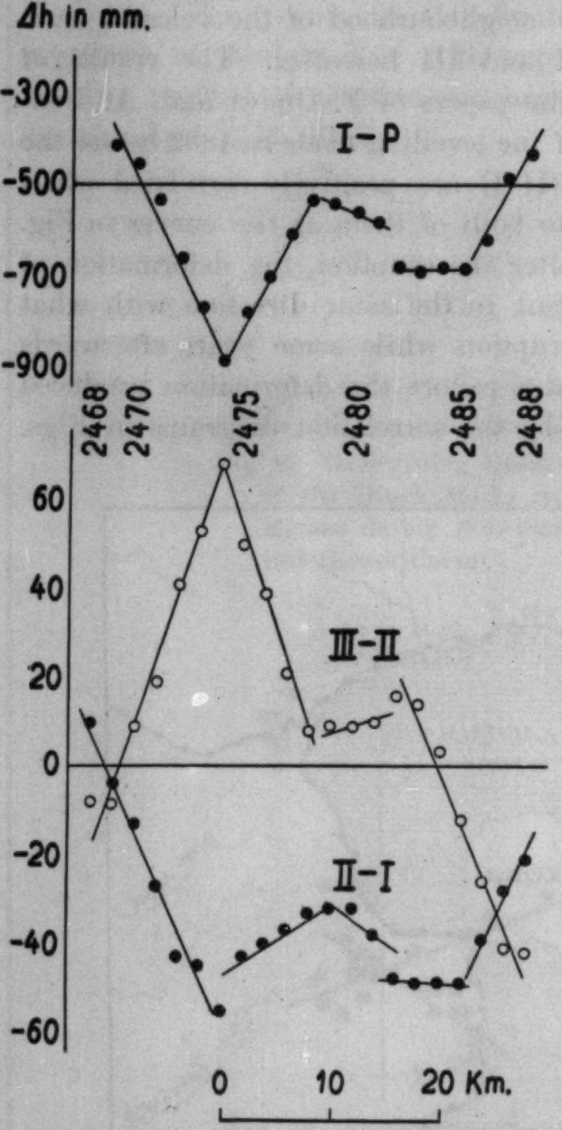

Fig. 21. Change of Height of the Bench Marks in the Sakurazima District Before and After the Eruption of 1914.

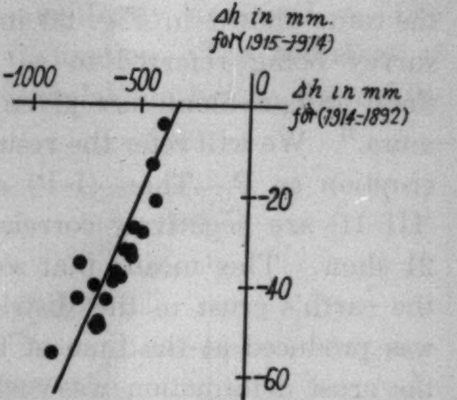

Fig. 22. Correlation Diagram for the Change of Height of the Bench Marks in the Sakurazima District during 1914-1892 (Abscissa) and 1915-1914 (Ordinate).

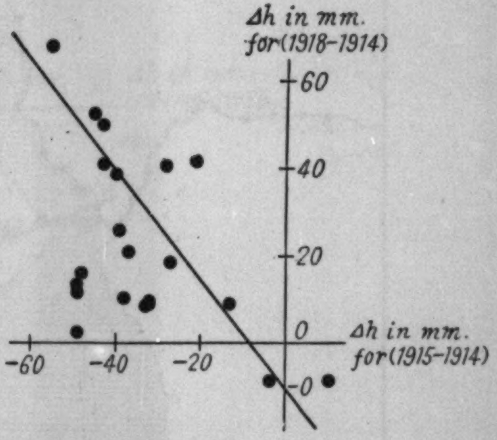

Fig. 23. Correlation Diagram for the Change of Height of the Bench Marks in the Sakurazima District during 1915-1914 (Abscissa) and 1918-1914 (Ordinate).

For the purpose of making clearer the variation with time in the mode of the vertical deformation of the earth's crust in this district, the three measured heights of the bench marks after the eruption were connected by means of curves of second order. This was made by determining three numerical constants in the equation,

$$h = at^2 + bt + c,$$

where h is the height of a bench mark at time t and a, b and c are numerical constants. t is measured from June 1914, one by one for each month. The results of the calculation are given in Table VI.

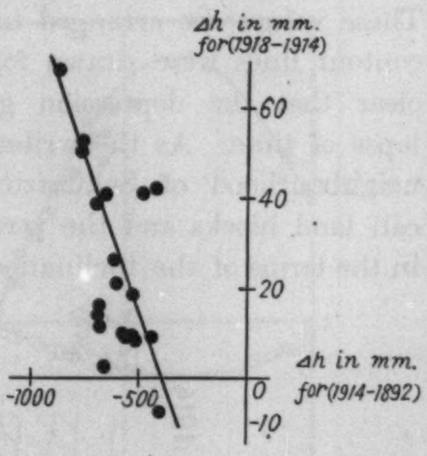

Fig. 24. Correlation Diagram for the Change of Height of the Bench Marks in the Sakurazima District during 1914-1892 (Abscissa) and 1918-1914 (Ordinate).

Table VI.

B.M.	a	b	c	B.M.	a	b	c
2468	−0·031	+1·499	0	2479	+0·103	−5·499	+ 5·396
2469	+0·007	−0·506	0	2480	+0·103	−5·499	+ 5·396
2470	+0·039	−1·944	0	2481	+0·122	−6·491	+ 6·369
2471	+0·083	−4·039	0	2482	+0·156	−8·258	+ 8·102
2472	+0·137	−5·468	0	2483	+0·158	−8·421	+ 8·263
2473	+0·161	−7·882	+7·721	2484	+0·179	−9·955	+19·194
2474	+0·199	−9·646	+9·447	2485	+0·173	−9·892	+19·092
2475	+0·154	−7·527	+7·373	2486	+0·130	−7·804	+15·088
2476	+0·140	−6·976	+6·836	2487	+0·084	−5·510	+10·684
2477	+0·124	−6·397	+6·273	2488	+0·059	−4·085	+ 7·934
2478	+0·106	−5·666	+5·560				

From these values, the monthly vertical velocities of the bench marks in different epochs were calculated according to the relation,

$$\frac{dh}{dt} = 2at + b.$$

These values are arranged in the scheme as shown in Fig. 25 in which contour lines were drawn for equal velocities. In this way it is made clear that the depression gradually changed into upheaval with the lapse of time. As the writer pointed out elsewhere,[8] the district in the neighbourhood of Sakurazima is made up of a number of what we call land blocks and the vertical crust deformation should be expressed in the terms of the inclination of such land blocks. The tiltings of the

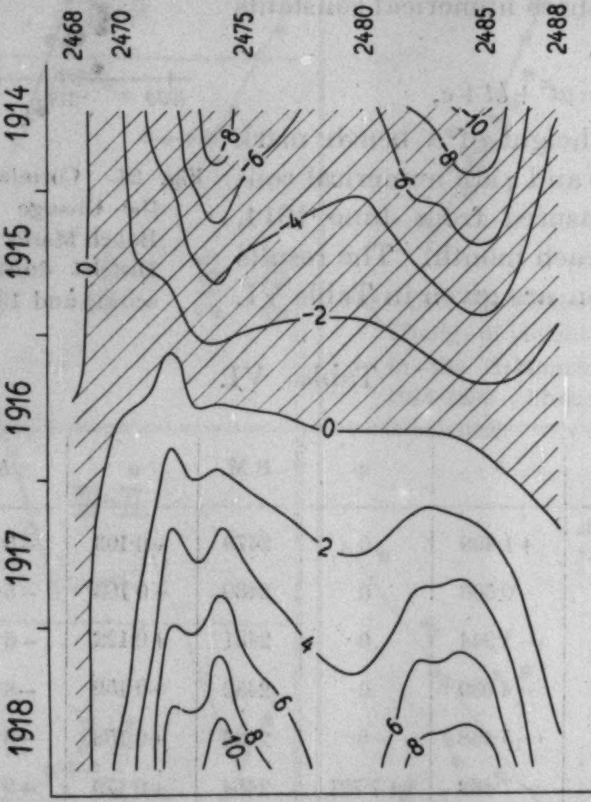

Fig. 25. Monthly Vertical Velocities of Different Bench Marks in the Sakurazima District in mm/month.

land block on which lie the bench marks 2474–2482 during different intervals, for example, were obtained by the Miyabe's method.[9] The tiltings of the land block during (I–P) and (II–I) are naturally of the same sense while that during (III–II) of the opposite sense to both. This is clearly indicated by three sine curves in Fig. 26 and 27 which are constructed by the values in Table VII. The zero gradient of tilting occurs at the azimuth of N 65°E for all three of them but the phase of the curve (I–P) is just opposite to that of (III–II).

8) C. Tsuboi, *Bull. Earthq. Res. Inst.*, **7** (1929), 103.
9) N. Miyabe, *Bull. Earthq. Res. Inst.*, **9** (1931), 256.

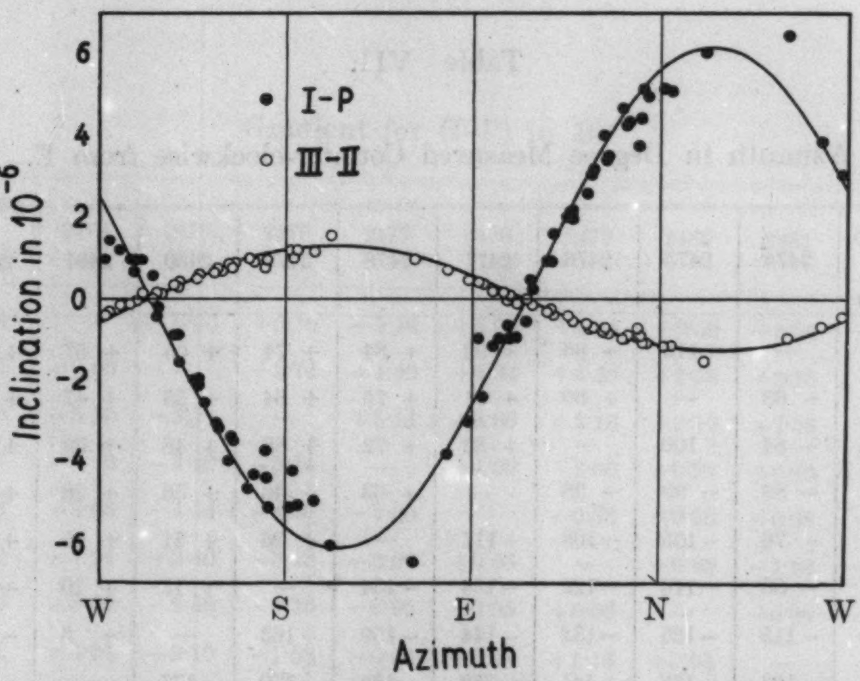

Fig. 26. Sine-Curves Indicating the Tilting of a Land Block in the Sakurazima District.

●........(1914–1892) ○........(1918–1915)

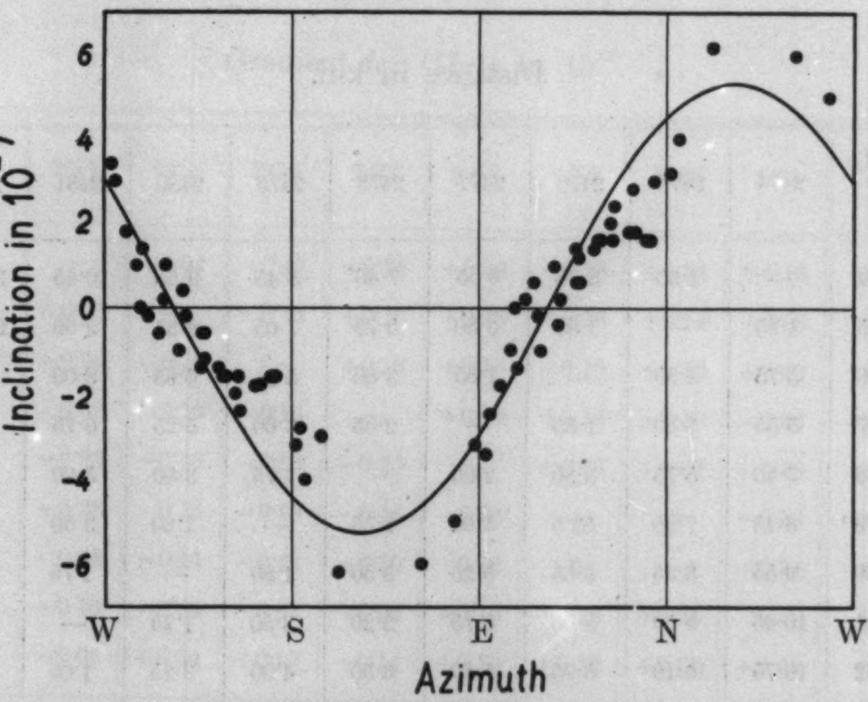

Fig. 27. Sine-Curve indicating the Tilting of a Land Block in the Sakurazima District during (1915–1914).

Table VII.

Azimuth in Degree Measured Counter-clockwise from E.

From \ To	2474	2475	2476	2477	2478	2479	2480	2481	2482
2474	—	+112	+ 96	+ 92	+ 84	+ 74	+ 65	+ 57	+ 48
2475	− 68	—	+ 80	+ 81	+ 75	+ 64	+ 55	+ 47	+ 38
2476	− 84	− 100	—	+ 82	+ 72	+ 58	+ 48	+ 39	+ 29
2477	− 88	− 99	− 98	—	+ 63	+ 46	+ 36	+ 28	+ 18
2478	− 76	− 105	−108	− 117	—	+ 26	+ 21	+ 15	+ 5
2479	− 86	− 116	− 122	− 134	− 154	—	+ 17	+ 10	− 2
2480	−115	−125	−132	−144	− 159	−163	—	+ 3	− 12
2481	−123	− 133	− 141	−152	− 165	−170	−177	—	− 28
2482	−132	− 142	− 151	− 162	− 175	+178	+168	+152	—

Distance in km.

From \ To	2474	2475	2476	2477	2478	2479	2480	2481	2482
2474	—	1·95	3·75	5·55	7·40	8·45	9·55	10·45	10·75
2475	1·95	—	1·95	3·80	5·75	7·05	8·35	9·50	10·10
2476	3·75	1·95	—	1·85	3·80	5·25	6·65	8·00	8·75
2477	5·55	3·80	1·85	—	2·05	3·60	5·25	6·75	7·80
2478	7·40	5·75	3·80	2·05	—	1·75	3·50	5·20	6·50
2479	8·45	7·05	52·5	3·60	1·75	—	1·80	3·50	4·90
2480	9·55	8·35	6·65	5·25	3·50	1·80	—	1·75	3·25
2481	10·45	9·50	8·00	6·75	5·20	3·50	1·75	—	1·65
2482	10·75	10·10	8·75	7·80	6·50	4·90	3·25	1·65	—

Gradient for (I–P) in 10^{-6}.

To / From	2474	2475	2476	2477	2478	2479	2480	2481	2482
2474	—	+6·06	+5·10	+5·16	+5·98	+4·24	+3·50	+3·04	+1·96
2475	−6.06	—	+3·74	+4·42	+4·34	+3·40	+2·58	+2·10	+0·92
2476	−5·10	−3·74	—	+5·14	+4·66	+3·18	+2·16	+1·58	+0·22
2477	−5·16	−4·42	−5·14	—	+4·00	+2·00	+0·92	+0·46	−0·98
2478	−5·98	−4·34	−4·66	−4·00	—	−0·58	−0·98	−0·98	−2·44
2479	−4·24	−3·40	−3·18	−2·00	+0·58	—	−0·68	−1·18	−3·02
2480	−3·50	−2·58	−2·16	−0·92	+0·98	+0·68	—	−0·98	−3·82
2481	−3·04	−2·10	−1·58	−0·46	+0·98	+1·18	+0·98	—	−6·48
2482	−1·96	−0·92	−0·22	−0·98	+2·44	+3·02	+3·82	−6·48	—

Gradient for (II–I) in 10^{-6}.

To / From	2474	2475	2476	2477	2478	2479	2480	2481	2482
2474	—	+0·62	−0·40	+0·32	+0·30	+0·28	+0·24	+0·16	+0·06
2475	−0·62	—	−0·16	+0·16	+0·18	+0·16	+0·14	+0·06	−0·04
2476	−0·40	−0·16	—	+0·16	+0·18	+0·16	+0·12	+0·02	−0·10
2477	−0·32	−0·16	−0·16	—	+0·20	+0·14	+0·10	−0·02	−0·14
2478	−0·30	−0·18	−0·18	−0·20	—	+0·06	+0·02	−0·10	−0·30
2479	−0·28	−0·16	−0·16	−0·14	−0·06	—	0	−0·18	−0·32
2480	−0·24	−0·14	−0·12	−0·10	−0·02	0	—	−0·34	−0·50
2481	−0·16	−0·06	−0·02	+0·02	+0·10	+0·18	+0·34	—	−0·60
2482	−0·06	+0·04	+0·10	+0·14	+0·30	+0·32	+0·50	+0·60	—

Gradient for (III–II) in 10^{-6}.

To / From	2474	2475	2476	2477	2478	2479	2480	2481	2482
2474	—	−1·54	−1·18	−1·18	−1·12	−0·98	−0.86	−0·72	−0·56
2475	+1·54	—	−0·74	−0·92	−0·90	−0·74	−0·62	−0·50	−0·28
2476	+1·18	+0·74	—	−1·12	−0·98	−0·72	−0·56	−0·38	−0·16
2477	+1·18	+0·92	+1·12	—	−0·82	−0·46	−0·32	−0·16	+0·08
2478	+1·12	+0·90	+0·98	+0·82	—	0	−0·14	+0·06	+0·34
2479	+0·98	+0·74	+0·72	+0·46	0	—	−0·02	+0·18	+0·46
2480	+0·86	+0·62	+0·56	+0·32	+0·14	+0·02	—	+0·40	+0·70
2481	+0·72	+0·50	+0·38	+0·16	−0·06	−0·18	−0·40	—	+0·98
2482	+0·56	+0·28	+0·16	−0·08	−0·34	−0·46	−0·70	−0·98	—

Gradual Variation in the Mode of the Crust Deformation.

In all of the above examples, each district seems to have its inherent mode of deformation. In the case of the crust deformation in Ito district along the route shown in Fig. 28 on the eastern coast of Idu Peninsula which is connected with the unusual seismic activity in 1930 in it, the deformation of the crust gradually changed in its mode. This fact was already pointed out in the writer's previous papers[10] in which the results of the surveys were given also. For the purpose of making this circumstance clearer, the successive mean daily velocities of each bench mark was calculated just in the same manner as in the case of Sakurazima. The results of the calculation are graphically shown in Fig. 29. As this diagram clearly indicates, the point at which the vertical velocity is maximum has been migrating northward slowly. It was found on the other hand seismometrically[11] that the epicentre of the earthquakes also migrated northward gradually with time. Thus it seems that the maximum upheaval is, at least for this district, intimately connected with the distribution of the origin of the earthquakes. The maximum vertical velocity itself was also variable,

10) C. TSUBOI, *Proc. Imp. Acad.*, 7 (1931), 153; *Bull. Earthq. Res. Inst.*, 9 (1931), 151.
11) N. NASU, F. KISHINOUYE and T. KODAIRA, *Bull. Earthq. Res. Inst.*, 9 (1931), 22.

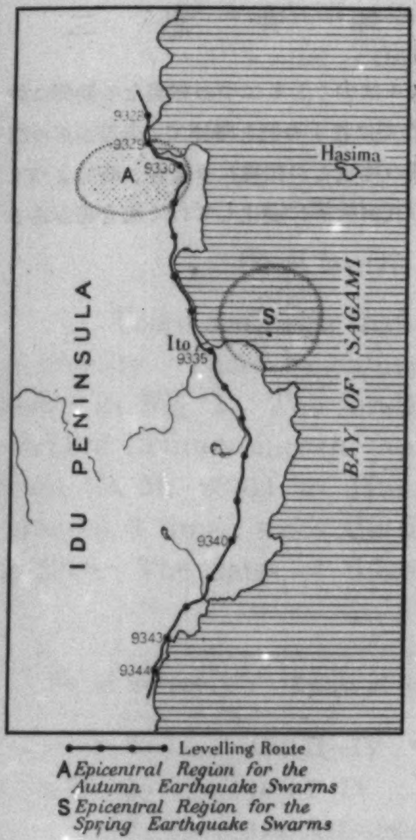

Fig. 28. Levelling Route in the Ito District.

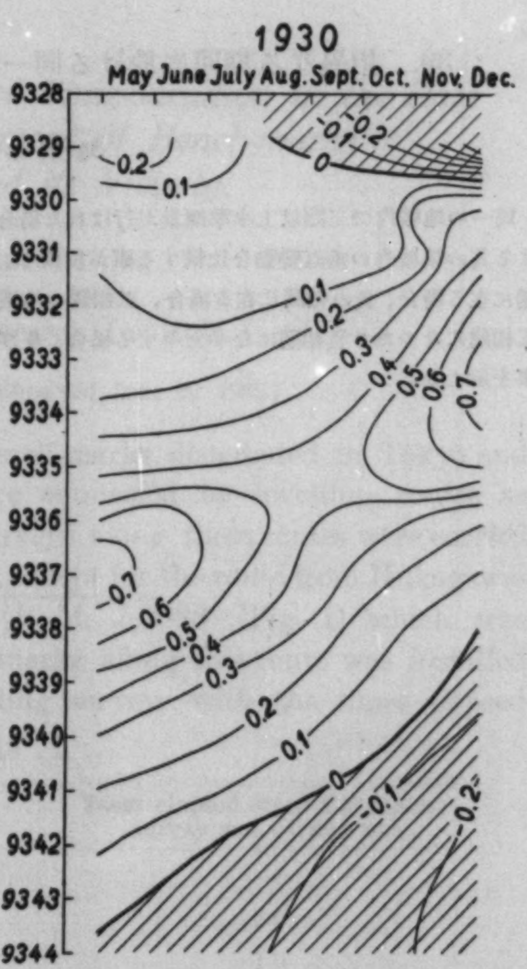

Fig. 29. Daily Vertical Velocities of Different Bench Marks in the Ito District in mm.

being small in summer season of 1930. This is again in good accord with the smallness of the earthquake numbers in the same season.

In conclusion, the writer expresses his sincere thanks to Professor Torahiko TERADA for his interest in this study.

39. 相異なる期間に於ける同一地域の地殼の垂直變動の比較

地震研究所　坪　井　忠　二

同一の地域内で三回以上水準測量が行はれた場合には、我々は少くとも二つの相異なる期間に於ける其の地域内の垂直變動を比較する事が出來る。此の報告では若干の例を擧げて、夫等が正の相關に在る場合、負の相關に在る場合、正相關の地域と負相關の地域とが相隣れる場合、時によつて正相關になつたり負相關になつたりする場合、及び變動の形式が次第に變化して行く場合等がある事を示した。

40. *On Different Types of Time-variation in the Rate of Vertical Displacement of Bench-marks in Tôkyô and its Vicinity.*

By Naomi MIYABE,

Earthquake Research Institute.

(Read May 17, 1932.—Received June 20, 1932.)

1. There are more than 60 bench-marks distributed in Tôkyô and its vicinity. These bench-marks are connected by levelling routes as shown in Fig. 1. The levelling surveys along these routes were carried out 11 or 12 times since the year 1892, except for the route from Hukagawa-Kôen (B. M. 9831) to Hunabasi (B. M. J-3828) (Fig. 1) which was surveyed 5 times, since the bench-marks along this route was installed in 1918. The dates of these levelling surveys with the times elapsed

Table I.

No. of Survey	Dates of Survey	Years elapsed since the former survey was carried out
1	1892·II—IV ***	—
2	1894·I—IV	2·0
3	1895·XII—1896·III	1·9
4	1899·I—IV	3·1
5	1902·III—IV	3·4
6	1909·XII—1910·III	7·9
7	1914·IV—VII	4·2
8	1918·IX—XII	4·3
9	1923·X—1924·II	5·2 *
10	1925·XI—1926·IV	2·0
11	1930·II—III	4·2
12	1931·VII	1·3 **

* The data of the vertical displacements of B. M.'s 9831, 9832, 9833, 9834, 9835, 9836, 9837, 9838, 9839, 9840, 9841, 9842 and 9843 are obtained first in the result of this survey.

** This survey was carried out along the routes.
i) From the Standard Datum Point to Kasukabe (B. M. 2014) via Senzyu;
ii) From Nippori (B. M. 24) to Ômiya (B. M. 482) via Itabasi;
iii) From Bakuro-tyô (B. M. J-5) to Kameido (B. M. 3379);
iv) From Sin-hunamatu-tyô (B. M. J-0) to Suna-mati (B. M. 9834).

*** Numerical figures in roman type denote the month.

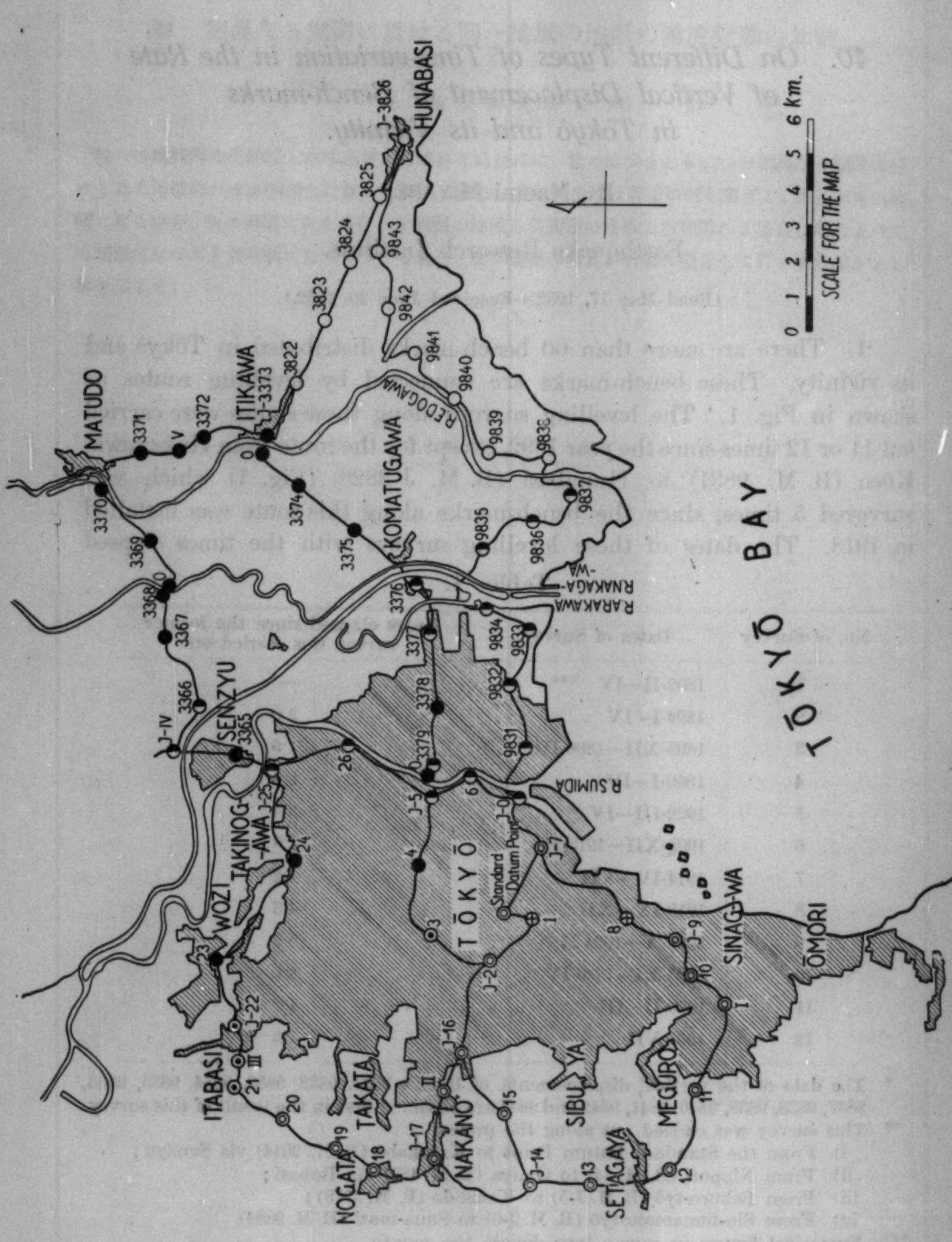

Fig. 1. Distribution of Bench-marks in Tôkyô and its Vicinity.

between successive surveys are shown in Table I.

The present writer intended to investigate the modes of the time variations of the vertical movement of the earth's crust in the vicinity of Tôkyô by utilizing the above data. For this purpose, the time rate of the vertical displacements of each bench-mark for different time intervals were calculated. As the time intervals during which the vertical displacements measured had taken place are not the same for different epochs, the discussions on the time variations of the modes of vertical movements should be based on the time-rates thus obtained.

The data of vertical displacements of the bench-marks employed in the present investigation were taken from Messrs K. Mutô and K. Atumi's paper,[1] the Report on the Results of the Levelling Surveys of 1930[2] and that of 1931.[3]

2. The rate of vertical displacement of each bench-mark is obtained by dividing the vertical displacement ΔH through the corresponding time interval Δt during which the vertical displacement ΔH occurred. Thus, the rates of vertical displacements, $\Delta H/\Delta t$, were calculated and represented numerically in mm./year for each bench-mark with respect to different time intervals and the results are given in Table II. The modes of time variations of vertical displacements of several bench-marks are shown by the curves in Fig. 2.

In Table II or Fig. 2, we notice that there are several different types with regard to the time variations of $\Delta H/\Delta t$. According to the types of curves for $\Delta H/\Delta t$, the bench-marks may conveniently be classified into five different groups. It may also be a remarkable fact that the bench-marks respectively belonging to different groups, above classified, are also distributed in respective groups in different regions. The general characters of modes of time variations of $\Delta H/\Delta t$ for the different groups of bench-marks are pointed out as follows:

i) Type I. As shown in Fig. 2a, the vertical displacements which may be considered as the direct effect of the Kwantô Earthquake of 1923, seem to be generally upward. The rates of the vertical displacements, especially those of depressions, of these bench-marks were discontinuously increased after the Kwantô Earthquake. The bench-marks of which the time variations of $\Delta H/\Delta t$ are of this type are distributed mainly in NE suburb of Tôkyô. Those are B. M. 0 (Yokoami) B. M.

1) K. Mutô and K. Atumi. *Bull. Earthq. Res. Inst.*, 7 (1929), 495.
2) The Report published by the Authorities of the Military Land Survey, (1931).
3) *Bull. Earthq. Res. Inst.*, 9 (1931), 508.

Table II. $\frac{\Delta H}{\Delta t}$ of the Bench-marks in mm./year.

Locality of the Bench-mark	Interval / No. of Bench-mark (B. M.)	1892–1894	1894–1895	1895–1898	1898–1902	1902–1910	1910–1914	1914–1918	1918–1923	1923–1926	1926–1930	1930–1931
Aoi-tyô	1	0·3	-2·0$_5$	0·9	—	1·8	-0·0$_5$	-1·1$_6$	-2·9$_8$	-2·0	-8·8	
Kioi-tyô	J-2	1·6	2·7	-2·0$_6$	-0·6$_7$	—	0·1	0·6$_6$	-2·1$_4$	-0·1$_8$	0·7$_6$	
Huzimi-tyô	3	2·9	0·4$_8$	-4·8$_4$	-0·4	—	-0·9$_8$	0·3	-3·0	-4·0	0·1	
Surugadai	4	1·7	1·1	-3·0	-0·2	—	-0·0$_5$	-0.3$_9$	0·8$_1$	-5·4$_6$	-2·2$_9$	
Bakuro-tyô	J-5	1·1	1·2	-2·4$_7$	-0·3	0·3$_5$	-0·6	—	-2·4$_5$	-7·4$_6$	-5·6$_6$	-2·4
Hama-tyô	6	0·5	-5·3$_8$	-5·2$_8$	-1·0	-2·2	-5·2$_5$	-4·8$_7$	-8·6	-21·3	-20·4	-30·2
Sin-Hunamatu-tyô	J-0	—	-0·3$_9$	-3·4	0·1$_7$	0·1$_8$	-1·3$_5$	-0·5$_5$	-0·6$_9$	-4.2$_6$	-0·9$_8$	-3·0
Tukidi	J-7	0·1	0·0$_6$	-0·8	-1·8$_7$	—	0·7$_9$	-0·3$_4$	-0·1$_8$	-0·8	—	-3·8$_5$
Ta-mati	8	-9·6	11·4	-7·7	-3·0$_7$	-0·4$_7$	-0·9	-0.5$_9$	-0·2$_7$	1·8	-10·1	
Takanawa-kita-mati	J-9	0·3	-2·5	2·6$_9$	-3·2	—	-0·1	0·0$_5$	-1·2$_9$	3·9$_5$	0·4	
Simo-Ôsaki	10	0·8	-0·5$_5$	0·4$_5$	-2·5	-1·4	1·3$_5$	-1·6$_6$	-3·8	3·9	1·9$_4$	
Kirigaya	I	0·5$_5$	0·8$_9$	2·5	-2·1$_7$	-0·4	1·2$_6$	1·0	-3·2	5·2$_8$	2·1$_7$	
Himonya	11	0·8$_5$	1·3	1·4$_7$	-1·7	-0·3$_7$	0·7	0·8$_9$	-5·9$_8$	5·1$_5$	1·8	
Kamiuma	12	0·5$_5$	1·7$_8$	0·4	-2·0$_7$	0·5$_8$	—	1·0	-9·5$_4$	4·8$_4$	2·1	
Daita	13	0.9$_5$	1·1	-1·1	1·5$_7$	0·6	1·7$_9$	0·8$_6$	-10·1$_4$	2·5$_8$	2·3	
Hatagaya	J-14	0·7$_5$	2·4$_4$	-2·0	2·5	—	1·2$_8$	1·0$_7$	-10·0	1·4	1·9	
Hatagaya	15	0·5	2·5$_6$	2·7$_8$	1·3	—	-0·8$_4$	0·1	-8·8$_4$	-0·2$_6$	-1·8	
Asahi-mati	J-16	—	-2·0$_5$	-0·1$_9$	0·1	-0·4	0·4	0·4$_8$	-10·8$_6$	-4·0	-4·2$_5$	
Nakano	J-17	-0·3$_5$	3·6$_6$	-3·1	2·8	-0·9	1·0$_5$	0·8$_4$	-9.2	-3·3$_4$	0·6$_4$	
Kasiwagi	II	0·3	2·9$_4$	-3·0$_9$	1·3	-0·3	0·0$_7$	0·7$_5$	-7·4	-1·6$_9$	1·1$_5$	
Arai	18	-1·5$_5$	5·2$_7$	-3·8	2·9	-1·2$_7$	1·2$_8$	1·0$_7$	-10·6$_9$	-4·0	0·4$_6$	
Otiai	19	-1·7	4·6$_6$	-3·8	0·6	-0·8	0·2	0·8$_4$	-9·2$_4$	-6·0	1·0	
Nagasaki	20	-1·8$_5$	4·0	-3·7	-0·6	-0·5	—	0·5$_9$	-8·3	-7·5$_5$	0·9$_5$	
Simo-Itabasi	21	-0·5$_5$	4·3	-4·6$_5$	-1·8	-1·1$_9$	0·4$_4$	0·1$_4$	-7·7$_6$	-9·4	0·6$_6$	
Simo-Itabasi	III	0·7$_5$	5·0	-5·1$_4$	-1·6	-0·9$_8$	-0·2	0·1$_6$	-6·7$_4$	-9·2$_9$	0·5$_4$	
Simo-Itabasi	J-22	0·0$_5$	3·0	-4·5	-1·5	-1·1$_9$	-0·5$_6$	-0·0$_9$	-5·6$_7$	-9·3	0·0$_5$	-9·5
Wôzi	23	0·7	2·3	-3·9$_7$	-3·0$_7$	-0·5$_8$	—	-0·3$_4$	-1·4	-14·0$_8$	-0·2$_4$	-8·8
Nippori	24	-0·3	3·3	-4·1	-2·9	0·6	—	-0·4	1·5	-13·0$_5$	2·4$_8$	-5·9
Senzyu Minami-gumi	J-25	-0.6	3·8	-7·8	-2·6	-1·2	-4·5	-8·6$_8$	-11·9	-37·1	-23·8	-28·8
Syôden-tyô	26	0·1	1·9	-4.6	-1·6	-0·8	-4·3	-4·4$_5$	-4·4	-25·4$_5$	14·2	-19·6
Senzyu Naka-gumi	3365	-0·4	-4·4	-8·7	-2·4	-0·6	-4·1	-3·8$_8$	-0·8$_4$	-28·3	14·5	-25·4
Senzyu 1-tyôme	J-IV	1·2	3·2	-9·4	-2·3	-0·2	-4·6$_5$	-5·3$_4$	-8·5$_4$	-39·7	-30·0	-37·4

(*to be continued.*)

Table II. (*continued.*)

Locality of the Bench-mark	No. of Bench-mark (B. M.) \ Time Interval	1892–1894	1894–1895	1895–1898	1898–1902	1902–1910	1910–1914	1914–1918	1918–1923	1923–1926	1926–1930	1930–1931
Kosuge	3366	-0·3	5·2	-10·1	-2·8	-0·2	-4.3	—	-10·4$_{5}$	-29·3	-21·2	
Kameari	3367	-0·0$_{5}$	4·9	-9·2	-2·6	0·4	-4·3	—	4·0$_{6}$	-21·5	-19·0	
Kameari	3368	1·1	0·9	—	-3·1	-0·4$_{4}$	-4·9	-3·2$_{7}$	-1·7$_{8}$	-28·1	-22·6	
Sinzyuku	0	0·6	2·4	-8·2	-4·1	-0·2$_{4}$	-6·4	-4·6$_{8}$	-0·1	-25·2	-17·8	
Kanamati	3369	0·4	2·7	-6·0	-3·3	0·6$_{5}$	-4·3	-3·3	5·7$_{5}$	-19·3	-3·3	
Kanamati	3370	0·1	3·9	—	-11·6	-4·1	-7·4	-3·6$_{4}$	9·8$_{5}$	-12·9	-11·0	
Kanamati	0		-1·4									
Matudo	3371	-0·5	-15·8	5·6	-1·2	—	-3·2$_{8}$	-1·0	10·9$_{5}$	-8·4	-2·7	
Matudo	V	-0·5	-16·7	6·9	-1·1	0·5	-2·7$_{4}$	-1·4$_{5}$	11·4	-8·0$_{5}$	-3.4$_{4}$	
Itikawa	3372	-2·2	-15·8	5·8	-1·3	-0·1	-2·8	-1·3$_{4}$	11·2	-7·6	-3·9$_{8}$	
Itikawa	J-3373	-0·4	-16·3	6·6	-3·0	0·7$_{4}$	-2·8$_{8}$	-1·4	11·5$_{6}$	-8·1	-2·4$_{4}$	
Koiwa	0	-4·2	-18·4	-2·7	–	-0·2$_{8}$	-2·7	-1·8	11·3	-11·9$_{5}$	-4·7	
Simo-Koiwa	3374	-1·4	-7·0	3·0	-1·4	-0·6$_{5}$	-2·4	-1·8	7·7	-12·9$_{7}$	-3·3$_{4}$	
Higas - Komatugawa	3375	-2·2	-4·2	-0·5	-1·5	-0·6$_{9}$	-3·1$_{4}$	-2·6$_{8}$	0·4	-42·9	-39·2	
Nisi-Komatugawa	3376	-2·5	-3·6	-3·1	-2·1	-2·3$_{4}$	-9·0$_{5}$	—	-34·9	-57·7	-47·2	
Kameido	3377	0·5	-6·7	-4·8	-3·3	-4·6	-21·2$_{5}$	-26·2	-47·2	-88·8$_{5}$	-58·8	-58·5
Kayaba-tyô	3378	-3·0$_{5}$	-9·1	-9·2	-11·3	-5·8	-18·3	-27·1	-22·0	-52·5	-133·5	-134·0
Koidumi-tyô	3379	0·3	-4·7	-6·9	-6·8	-2·2$_{4}$	-6·6$_{5}$	-17·5	-29·9$_{4}$	-47·0$_{5}$	-37·8	-48·3
Yokoami	0	1·3	1·0	-4·3	-0·1	-0·2	-2·9	-1.5	2·5$_{8}$	-13·1$_{5}$	-11·5$_{6}$	-10·7
Hukagawa-Kôen	9831								-31·8	-37·1$_{5}$	-43·0$_{5}$	-81·5
Higasi-Hirai-tyô	9832								-72·9	-93·8	-91·2	-115·5
Suna-mati	9833								-20·1	-45·6$_{5}$	-38·0	-39·2
Suna-mati	9834								-53·0	-85·0	-55·9	-54·1
Matue-mati	9895								-10·4	-44·5	-29·6	
Kasai	9836								0·1$_{7}$	-23·6	-29·0	
Kasai	9837								0·6	-20·5	-11·8	
Urayasu	9838								0·3$_{5}$	-22·3	-10·5	
MinamiGyôtoku	9839								10·7	-6·8	-2·4	
MinamiGyôtoku	9840								9·3	-11.2	-5·2	
Gyôtoku	9841								10·8	-8·7	-2·9	
Katusika	9842								13·4	-6·8	-1·4	
Katusika	9843								13·8	-6·7	-1·1	
Hunabasi	J-3826								16·6	-5·5	-0·9	

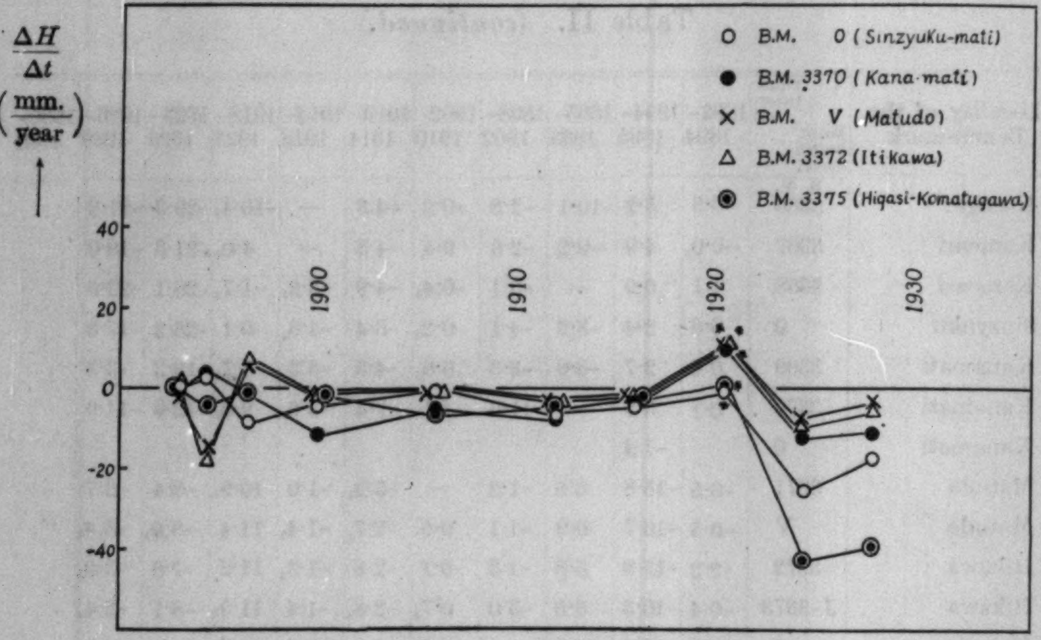

Fig. 2a. The time variation of $\frac{\Delta H}{\Delta t}$: Type I.

Points marked by asterisks represent $\frac{\Delta H}{\Delta t}$, during the corresponding time interval, the Kwantô Earthquake occurred.

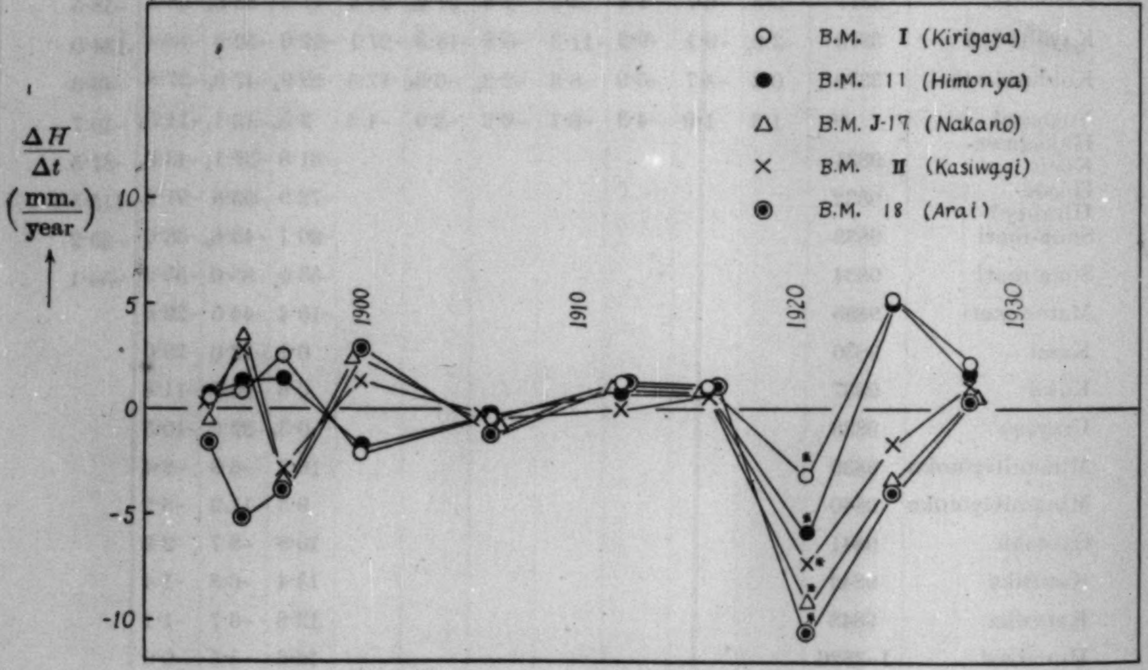

Fig. 2b. The time variation of $\frac{\Delta H}{\Delta t}$: Type II.

The asterisks mean as in the case of Fig. 2a.

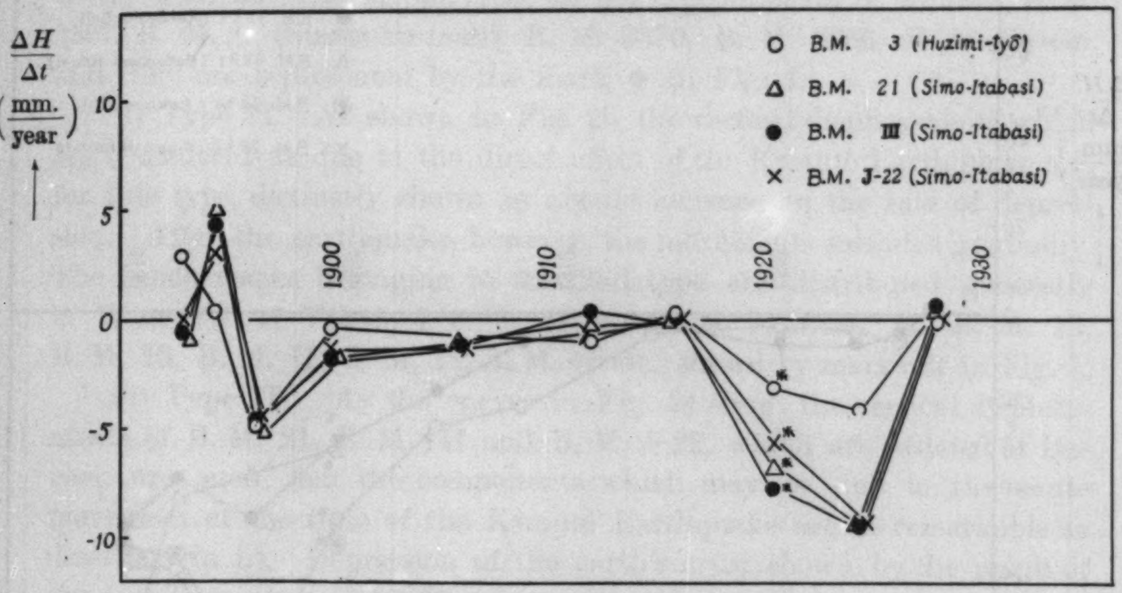

Fig. 2c. The time variation of $\frac{\Delta H}{\Delta t}$: Type III.

The asterisks mean as in the case of Fig. 2a.

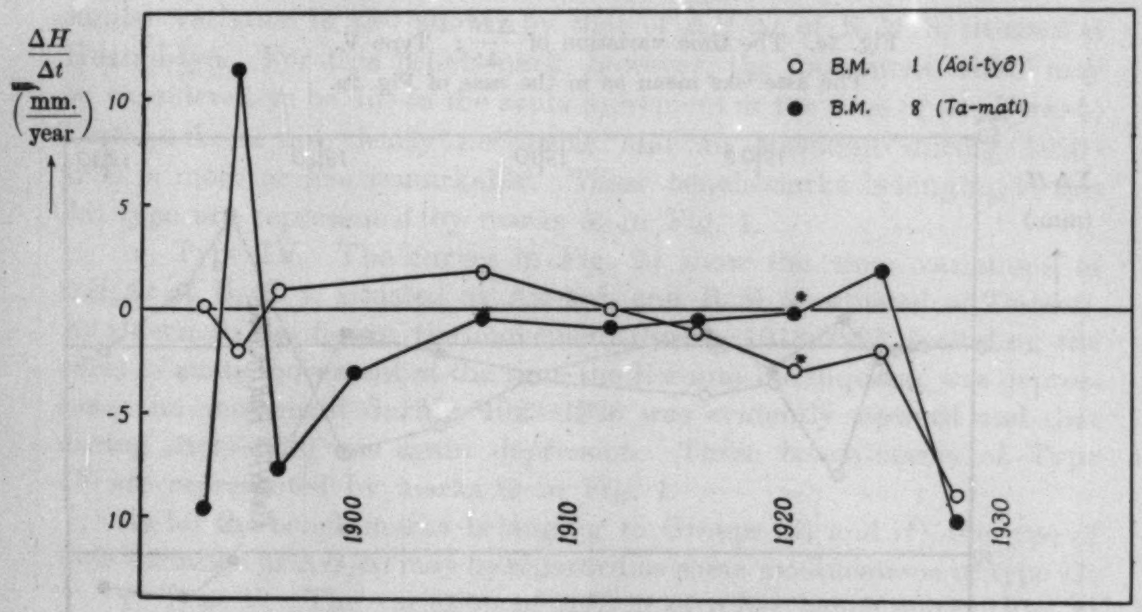

Fig. 2d. The time variation of $\frac{\Delta H}{\Delta t}$: Type IV.

The asterisks mean as in the case of Fig. 2a.

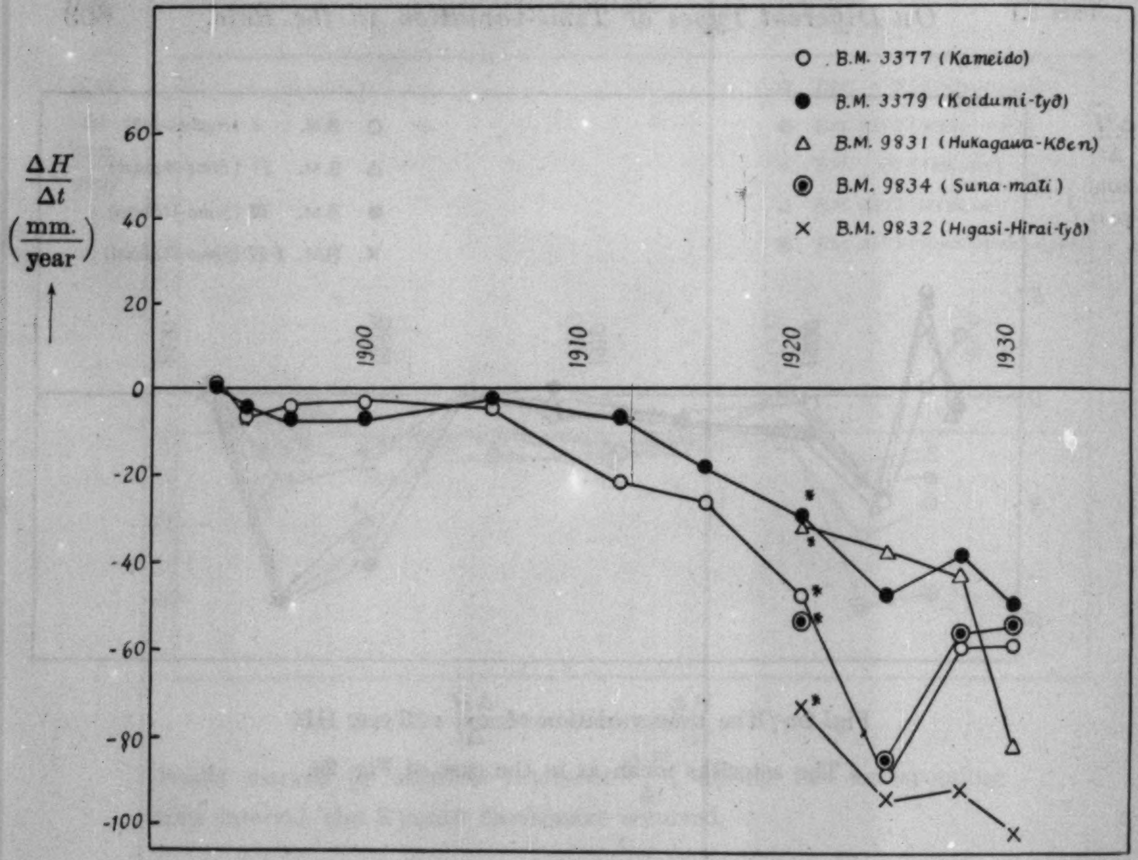

Fig. 2e. The time variation of $\frac{\Delta H}{\Delta t}$: Type V.
The asterisks mean as in the case of Fig. 2a.

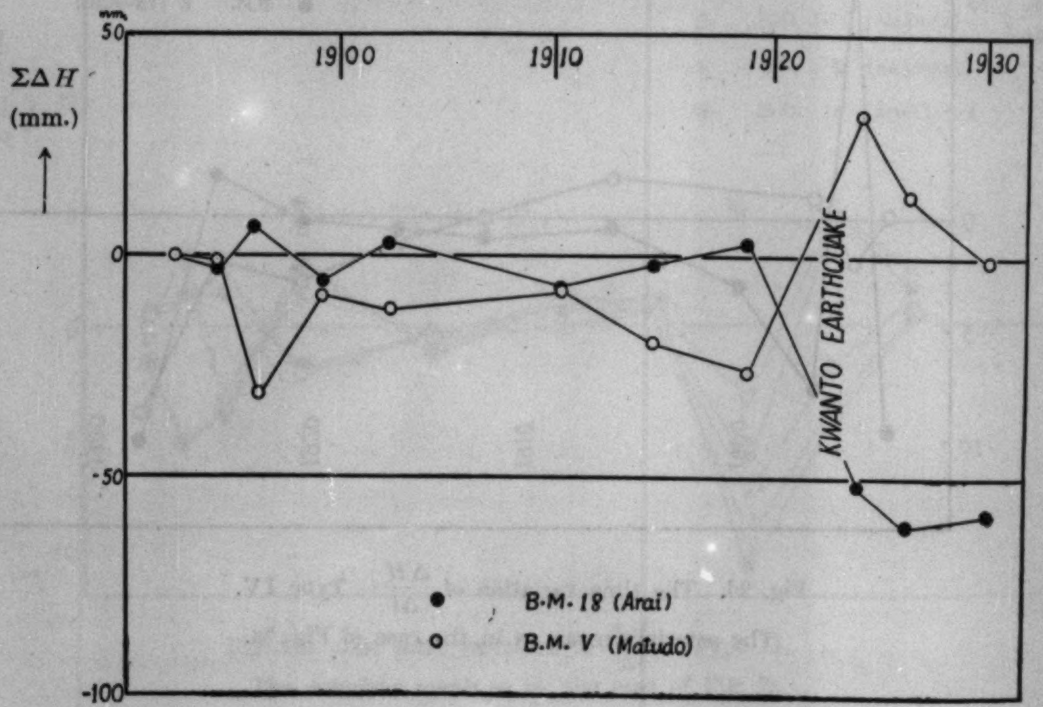

Fig. 2f.
Vertical displacement integrated.

3379, B. M. 3378, B. M. 3377, B. M. 3376, B. M. 3375, B. M. 3368, B. M. 3367 B. M. 0 (Sinzyuku-mati), B. M. 3370, B. M. 3366, B. M. 26 etc. and they are represented by the mark ● in Fig. 1.

ii) Type II. As shown in Fig. 2b, the vertical displacements which are considered as due to the direct effect of the Kwantô Earthquake are, for this type, distinctly shown by abrupt increases in the rate of depression. After the earthquake, however, the movements subsided gradually. The bench-marks belonging to this 2nd type are distributed generally in W or SW of Tôkyô, i. e., B. M. 10, B. M. I, B. M. 11, B. M. 12, B. M. 13, B. M. II, B. M. 18, B. M. 19 etc., shown by marks ◎ in Fig. 1.

iii) Type III. As the curves in Fig. 2c show, the vertical displacements of B. M. 21, B. M. III and B. M. J–22, which are situated at Itabasi, are such that the components which may be due to the acute movement at the time of the Kwantô Earthquake are so remarkable as described in ii). Depression of the earth's crust shown by the result of the levelling survey of 1923 were again shown in the results of the survey of 1926, corresponding to the vertical displacements during 1923–1926. In the result of the survey of 1930, the vertical displacements of these bench-marks are much smaller, i. e., the vertical movement represented by displacements of these bench-marks seems to have ceased. A similar variation is also shown by that of $\Delta H/\Delta t$ of B. M. 3, situated at Huzimi-tyô. For this bench-mark, however, the movement which may be considered to be due to the acute mevement at the time of the Kwantô Earthquake is not clearly noticeable and an elevation during 1926–1930 is more or less remarkable. These bench-marks belonging to this 3rd type are represented by marks ⊙ in Fig. 1.

iv) Type IV. The curves in Fig. 2d show the time variations of $\Delta H/\Delta t$ of B. M. 1, situated at Aio-tyô, and B. M. 8, situated at Ta-mati. As shown in the figure, the movement during 1918–1923, including the effect of acute movement at the time the Kwantô Earthquake, was depression, the movement during 1923–1926 was evidently upward and that during 1926–1930 was again depression. These bench-marks of Type IV are represented by marks ⊕ in Fig. 1.

As for the bench-marks belonging to Groups iii) and iv), the type of time variation of $\Delta H/\Delta t$ may be regarded as some modifications of type II.

v) Type V. The variation of $\Delta H/\Delta t$ of other bench-marks (Fig. 2) are such that the effect of the Kwantô Earthquake, even if it existed, is not evident. The post-seismic rates of depression of these bench-marks, however, are so remarkable in Honzyô, Hukagawa and its vicinity

that even the least value of them amounts to 40 mm. per year in round number.

The bench-marks of which the variations of $\Delta H/\Delta t$ are in such a manner as mentioned above are B. M. J-5, B. M. 6, B. M. J-0, B. M. J-7, B. M. 26, B. M. 3365 etc., represented by marks ◑ in Fig. 1. As for B. M.'s 9831, 9832, 9833 and 9834, the pre-seismic data of the vertical displacements are not sufficient in number for the comparison with the post-seismic series of data, as in the case of the other bench-marks. Hence, these bench-marks are included in Group v, for convenience's sake, as the post-seismic variations of their $\Delta H/\Delta t$ are similar to those of other bench-marks belonging to this group.

The difference in modes of vertical movements of the bench-marks belonging to the different groups are also shown by the curves representing the integrated values of vertical displacements from the time of the first survey. Fig. 2f shows the curves of $Y=\sum\Delta H$ plotted as ordinates taking the time as abscissa, where ΔH means the vertical displacements of the bench-marks during each time interval of the successive surveys. The curves in Fig. 2f show variation of Y of B.M. V, situated at Kana-mati, and B. M. 18, situated at Arai, of which the modes of variations of $\Delta H/\Delta t$ are typical of those of the bench-marks belonging to Group I) and Group II) respectively.

It may be remarked that the types III), IV) and V) of the variations of $\Delta H/\Delta t$ may be regarded as intermediate between the two extreme types I) and II), of which the variations of $\Delta H/\Delta t$ are approximately in negative correlation with each other. For the types III), IV) and V), amounts of $\Delta H/\Delta t$ are generally smaller than those of $\Delta H/\Delta t$ of Types I) and II), and the bench-marks belonging to Groups iii), iv) and v) are distributed in the region situated between the two regions where the bench-marks belonging to Groups i) and ii) are respectively distributed.

3. The distribution of the bench-marks and their types of the time variations of $\Delta H/\Delta t$ suggest us the following mode of deformation of the earth's crust which prevailed in Tôkyô and the environs in the recent years: The crust was first tilted toward SW during 1918–1923, including the effect of the Kwantô Earthquake, if any, and then was tilted in the approximately reversed sense during 1923–1926. According to the results of the surveys carried out after the survey of 1926, i. e., the surveys of 1930 and 1931, the tilting of the earth's crust in this region is generally not remarkable, and yet the conspicuous local depres-

sion in Honzyô and Hukagawa[4] has maitained its activity.

4. A similar mode of deformation of the earth's crust is also obseved in the secular variation of the area of rhombus enclosed by a special set of geodetic base-line which is installed in the compound of the Tôkyô Astronomical Observatory at Mitaka.

All of the lateral sides and one of the diagonals of the rhombus are arranged in the manner as shown in Fig. 3. Since the year 1916 up to 1931, the measurements of the lengths of lateral sides and the diagonal NS with the accuracy up to 0.01 mm have been repeated 18 times. From the results of the measurement, the areal change per unit area of each of the equilateral triangles NES and NWS was calculated for the time intervals corresponding to those of two successive levelling surveys carried out along the routes which contain the bench-marks mentioned in the preceding paragraphs.

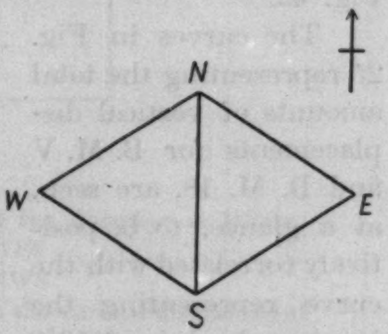

Fig. 3.
The Rhombs of a Special Set of Base-line at Mitaka. $\overline{NE}$, $\overline{ES}$, $\overline{SW}$, $\overline{WN}$ and $\overline{NS}$ being very nearly 100 m.

The calculation of dS/S, the areal change per unit area, is made as Mr. C. Tsuboi[5] shows, by using the relation

$$\frac{dS}{S}=\frac{ds}{75000},$$

Table III. $\frac{dS}{S}$ of Each Triangle of the Rombus at Mitaka.

Time interval	Triangle NES	Triangle NWS	Average
1916·IV–1918·II	$-0{\cdot}083\times10^{-5}$	$0{\cdot}173\times10^{-5}$	$2{\cdot}8\times10^{-7}$ per year
1918·II–1924·I	5·387	4·867	8·7
1924·I–1925·XII	0·053	0·107	4·2
1925·XII–1930·II	0·413	0·640	1·2
1930·II–1931·X	− 0·227	1·640	4·2

4) As for the local depression in Honzyô and Hukagawa Prof. A Imamura discussed, in his investigation, the tilting of Kôtô Block in association with the recent seismic activity in this region. A. Imamura, *Jap. Journ. Astro. Geophys.*, **8** (1931), 177.

The present author has dealt with the same problem and the result will be informed later in this Bulletin.

5) C. Tsuboi, *Proc. Imp. Acad.*, **6** (1930), 367 ; *ibid.*, **7** (1931), 155.

where ds is half the change in periphery of the triangle measured in mm. The calculated values of dS/S for each of the two triangles and their mean values for different time intervals are shown in Table III, and the variation of averaged values of dS/S with respect to time is shown by the curve in Fig. 4a.

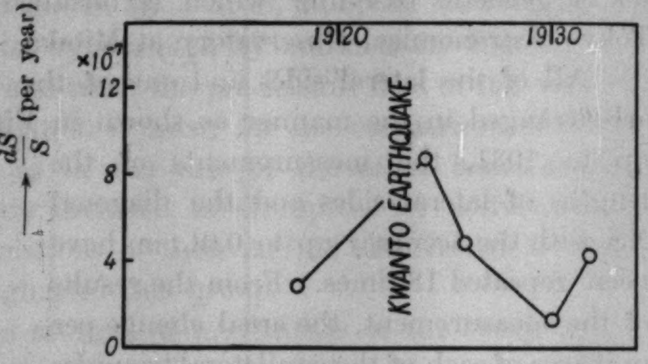

Fig. 4a.

$\frac{dS}{S}$ per year of the Area of the Rhombus at Mitaka.

The curves in Fig. 2f representing the total amounts of vertical displacements for B. M. V and B. M. 18, are seen, at a glance, to be positively correlated with the curve representing the integrated values of dS/S of the area of the rhombus at Mitaka, shown in Fig. 4b.

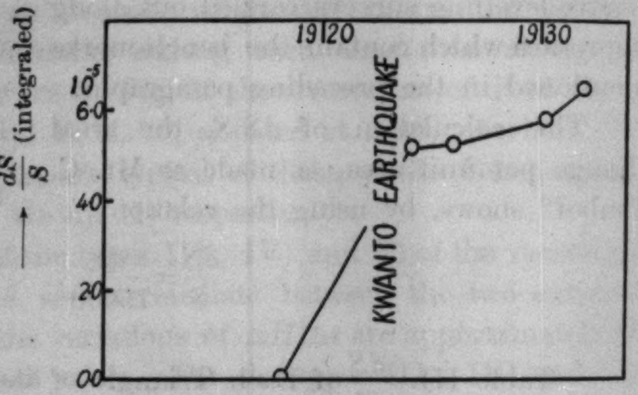

Fig. 4b.

$\frac{dS}{S}$ of the Area of the Rhombus at Mitaka.

As for the rhombus at Mitaka, the vertical displacements of Points E, S and W relative to Point N are also measured 8 times since the year 1916. From these data, the directions and magnitudes of tilting of each triangle are calculated for the different time intervals corresponding to those between two successive surveys along the levelling routes in Tôkyô and the environs.

The vector diagram of the tilting of each triangle is shown in Fig. 5, and numerical values of the magnitudes and azimuths of them are given in Table IV. In this figure, we notice that the tilts of the earth's crust in this region was directed towards SW during 1921 XI–1923 X. If we take the time interval from 1918 X to 1923 X, the tilt of the crust was directed approximately towards W. This tilt of the crust was nearly recovered by the tilt in the reversed sense of the same azimuth during 1923 X–1925 XII. Since then the crust was again tilted to NW.

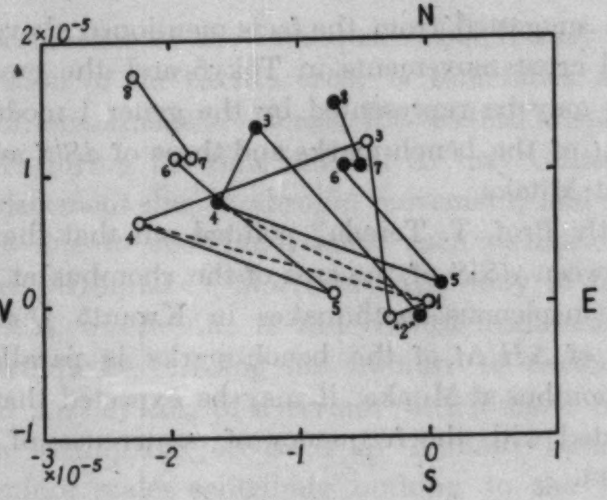

Fig. 5.

Vector Diagram indicating the Tilting of the Area of the Rhombus at Mitaka.

○ Tilting of the Triangle NES

● „ „ „ NWS.

The numerical figures are representing the dates when the vertical displacement of the points E, S, and W are measured.

1 : 1981·X	5 : 1927·XII
2 : 1920·XI	6 : 1929·III
3 : 1921·XI	7 : 1930·II
4 : 1923·X	8 : 1931·X

Table IV. Tilting of the Rombus at Mitaka.

Time Interval	Tilting of NES		Tilting of NWS	
	Magnitude	Azimuth refer-red to N	Magnitude	Azimuth refer-red to N.
1918·X–1920·XI	$0{\cdot}32\times10^{-5}$	250°	$0{\cdot}12\times10^{-5}$	210°
1920·XI–1921·XI	1·33	353	1·92	319
1921·XI–1923·X	1·83	252	0·60	210
1923·X1927·XII	1·62	110	1·86	110
1927·XII–1929·III	1·62	310	1·17	320
1929·III–1930·II	0·12	90	0·12	90
1930·II–1931·X	0·75	314	0·52	340

The fact that the sense of the direction of the tilt of the earth's crust during 1923–1927 was reversed in comparison with the tilt during 1921–1923 or that during 1918–1923, is coincident in sense with the general mode of the time variation of $\Delta H/\Delta t$ of the bench-marks in Tôkyô and the environs.

It may be suggested from the facts mentioned above that there may exist a general crust movements in Tôkyô and the environs including Mitaka, which may be represented by the general mode of time variations of $\Delta H/\Delta t$ of the bench-marks and those of dS/S and tiltings of the earth's crust at Mitaka.

5. Recently Prof. T. Terada[6] pointed out that there is a probable correlation between dS/S of the area of the rhombus at Mitaka and the frequency of conspicuous earthquakes in Kwantô District. Since the time variation of $\Delta H/\Delta t$ of the bench-marks is parallel with that of dS/S of the rhombus at Mitaka, it may be expected that the former will also be correlated with the frequency of occurrence of earthquakes in Kwantô District.

The number of conspicuous earthquakes which occurred in Kwantô District was counted since the year 1911, and the mean values of the numbers of these earthquakes per year were obtained for the time intervals corresponding to those between the successive levelling surveys during which the vertical displacements of the bench-marks were measured had taken place. The result is shown in Fig. 6. It may be remarked that relatively frequent occurrence of conspicuous earthquakes in 1911–1915 compared with the later epoch may partly be due to the difference of the scale of intensity adopted for classifying the earthquakes. Hence, several per cents of the number of earthquakes in 1911–1915 might be discounted. Whatever the matter, the time variation of the frequency of occurrence of earthquakes is noticed to be similar in its general feature with that of $\Delta H/\Delta t$ of the bench-marks.

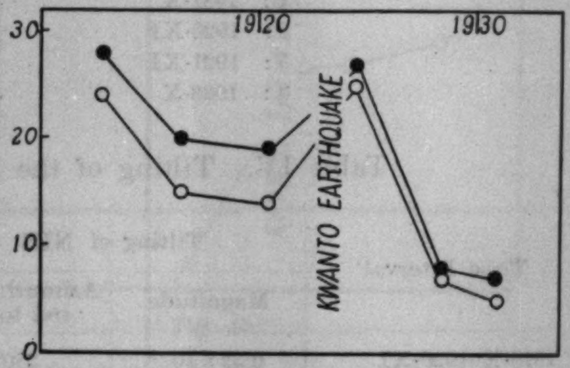

Fig. 6.

Frequency of Conspicuous earthquakes in Kwantô District.

● Including the conspicuous earthquakes of which the epicentres are located in Kasima-nada.

○ Kasima-nada Earthquakes are excluded.

This statistical relation between $\Delta H/\Delta t$ of the bench-marks and the number of occurrence of conspicuous earthquakes, of course, does not lead to a conclusion that the deformation of the earth's crust precedes

6) T. TERADA, *Proc. Imp. Acad.*, 7 (1932), 8.

or follows the occurrence of the earthquake, but it may at least show that the deformation of the earth's crust is sometimes associated with the occurrence of earthquake.[7] Hence, the vertical displacement of the bench-mark, ΔH, during the time interval Δt may consist of $\Delta_c H$, the the vertical displacement due to chronic movement, and $\Delta_a H$, the vertical displacement due to acute movement such as associated with the occurrence of the earthquake. Moreover, $\Delta_a H$ may in its turn consist of Δh_1, $\Delta h_2, \ldots \Delta h_n$, where Δh_n is the vertical displacement associated with a single earthquake, n being the number of earthquakes during the time interval Δt. If Δh_n of a certain bench-mark is constant for any conspicuous earthquake occurred in Kwantô District while the earthquakes of minor scales contribute nothing to the values of Δh_n, $\Delta_a H$ will be linearly proportional to the number of conspicuous earthquakes occurred during the same time interval. Consequently a linear relation between $\Delta H/\Delta t$ of the bench-marks and the frequency of occurrence of the earthquakes may be expected, when $\Delta_c H$ is small. Such a consideration, however, wants verification by evidences from many other sides, which are at present lacking, but for the statistical relation pointed out above.

6. The results of the present investigation are summarized as follows:

a) Five different types in the time variations of $\Delta H/\Delta t$ of the bench-marks in Tôkyô and the environs are pointed out. The majority of the bench-marks show the time variations of types I) and III), of which the modes of the time variations are in approximately opposite senses.

b) From the distribution of the bench-marks having different types of the time variations of $\Delta H/\Delta t$, the general mode of movement or tilting of the earth's crust in this district is suggested, i. e., it might have taken place in such a manner that the crust was tilted to W or SW during 1918–1923, including the effect of acute movement at the time of the Kwantô Earthquake. Then, it was tilted back during 1923–1926, and since that time the general movement is not noticeable, while the local depression in Honzyô and Hukagawa became remarkable.

c) The general mode of the time variations of $\Delta H/\Delta t$ of the bench-marks in this region is similar to those of the time variation of dS/S and also of tiltings of the area of the rhombus at Mitaka. It is

---

7) In his investigation, Prof. A. IMAMURA discussed the tilting of Kôtô Block in association with the occurrence of the earthquake. A. IMAMURA, *Jap. Journ. Astr. Geophys., loc. cit.*, (4).

also similar to the time variation of fluctuations in frequency of occurrence of conspicuous earthquakes in Kwantô District.

In conclusion, the present writer wishes to express his sincere thanks to Professor Torahiko Terada for his kind advices and guidance. Cordeal thanks are also due to Professor Sakuhei Fujiwhara for his kindness in placing the valuable data at the writer's disposal.

---

40. 東京附近に於ける水準點の垂直變動に就て

地震研究所　宮　部　直　巳

東京附近には水準點が六十箇所以上も設置せられてあつて、其等の水準點の高さが、1892 以來十一回乃至十二回観測され、從つて、その各観測年次間に起つた垂直變動量が測定されてゐる。是等の素材によつて東京附近に於ける地殼の垂直變動の模樣を調べてみやうといふ試みが本文の內容である。

この目的の爲めに、先づ測定された垂直變動量 (ΔH) を當該期間に相當する年數 (Δt) で除し、平均の年變動量 $\Delta H/\Delta t$ を各水準點に就いて求め、其の時に對する變化の模樣を調べてみた。その結果は次の如く要約される。

i) $\Delta H/\Delta t$ の時に對する變化の模樣は大體五種の型式に分類することが出來る。即ち：

(a) 關東地震前後の測量より得た結果が、それ以前のものに比して上昇の傾向にあるが、關東地震後の變動は、何れも可なりの沈降を示しつゝあるものが比較的多く、そして、其の樣な變化を示す水準點は主として東京の東部又は東北部に分布してゐる。

(b) 次に、關東地震前後の測量では、かなり著しい沈降を示し、以後その沈降の割合が次第に減少し、若しくは上昇となつて、沈降を恢復しつゝある樣に見えるものがある。斯の如き $\Delta H/\Delta t$ の變化を示す水準點は、主として、東京市の西部又は西南部に分布してゐる。(a) の $\Delta H/\Delta t$ の變化を下町型とすれば、(b) のそれは山手型とも稱すべきものであつて、(a) の變化の略逆向きである。

(c) 下板橋に於ける三個の水準點並に富士見町に於ける B. M. 3 は、關東地震前後の測定で、沈降を示したが、地震後の第一回第二回の測量より得たものも矢張り、沈降の傾向を增長してゐる樣に見え、その後の測量で、垂直變動が零に近づいてゐる。

(d) 又、葵町 (B. M. 1) 及び田町 (B. M. 8)に於ける水準點では、關東地震前後の測量より得たる垂直變動量は左程著しからず、その後に上昇となり更に沈降と變じてゐる。かく、(c) 及 (d) 型は (a) 型と (b) 型との中間、若しくは、寧ろ (b) 型に幾きものであると思惟され、それ等の水準點の位置も、(a) 型の水準點の分布區域と (b) のそれとの略中間に位してゐる。

(e) 以上の諸型式の外に、(a) 型の水準點の分布區域又はその附近に、關東地震前後の測量による垂直變動は、著しからず却つて、震後の沈降の著しくあらはれるものがある。之を第五種の e 型とした。これは寧ろ (a) 型に幾きものと思はれる。

ii) 以上の事實から次の如き東京附近の地殼變動の模樣が想像される。即ち、關東地震を夾む期

間内には、地殻は西又は南西に傾き、地震後は漸次之を恢復して靜穏になつてきた。但、局部的には垂直變動は却つて増大した個所もある。例へば本所深川に於ける著しき沈降はその一である。

iii) 上述の $\Delta H/\Delta t$ の變化の模様は、三鷹村における菱形の面積の伸縮 (dS/S の變化)、その地表面の傾斜、及び關東地方に於ける稍顯著以上の地震の發生の頻度等と統計的には關聯するらしく見える。

以上のことから、東京附近の水準點の垂直變動から期待される地殻變動は、もう少し廣い地域にても存在してゐたやうに考へられる。

41. *Echelle d'intensité sismique et accélération maxima*

par Mishio ISHIMOTO,

Institut de Recherches sur les Tremblements de terre.

(Lu le 21 juin 1932, reçu le 20 juin 1932)

1. Introduction.

Quand nous voulons exprimer l'intensité de secousses sismiques, nous adoptons une échelle d'intensité. Nous classons l'intensité sismique en degrés suivant la sensation humaine ainsi que d'après la destruction des cheminées, des maisons etc. sous l'action des secousses. Certainement il y a une relation serrée entre l'accélération maxima des secousses et la sensation humaine ou la destruction d'un objet. Nous trouvons ainsi une certaine échelle[1], définie suivant l'accélération maxima des secousses. Mais, il est bien regrettable qu'on n'ai pas encore exécuté une comparaison avec la valeur accélérométrique obtenues par l'observation pour toutes les sortes de séismes. Certes, nous déterminons habituellement l'acélération sismique par un calcul sur l'amplitudes et la période dans les inscriptions faites par le sismographe du type ordinaire. Nous remarquons toujours une sorte d'ondes dont l'amplitude devient assez grande pour nous empêcher d'avoir une vraie accélération des secousses. D'un autre côté, le regretté Prof. Omori[2] a exécuté une expérience sur une table oscillante observant le moment où un bloc en bois va glisser ou tomber. Il a déterminé, donc, la valeur de l'accélération maxima produite au moment d'un grand tremblement de terre. Mais, personne après lui n'a utilisé ses résultats. C'est probablement parce qu'il y très peu de cas où les secousses sismiques seront représentées par son échelle. Cette fois-ci les secousses produirent des sinistres.

Parmi les échelles d'intensité sismique, celle de Rossi-Forrel et celle de Mercari sont souvent employées: néanmoins nous citerons ici seulement l'échelle internationale. D'un autre côté, il y a une autre échelle au Japon, adoptée par l'Observatoire Central de Météorologie depuis plusieurs dizaines d'années et utilisée ici. Nous voulons, donc, avancer nos discussions en employant les degrés représentés par cette échelle. Voici un tableou explimant les correspondances entre deux échelles.

---

1) L'échelle de Cancani.

2) F. OMORI, *Publ. Eq. Inv. Com.*, 4 (1910), 69.

Tableau I.

Echelle internationale	Echelle de l'Observatoire Central de Météorologie du Japon.
I Mouvement microséismique noté par les séismographes seulement.	0 Non ressentie par l'homme.
II Secousse enregistrée par les séismographes et constatée seulement par un petit nombre d'observateurs au repos.	I **légère** Secousse constatée par les personnes au repos ou attentives.
III Ebranlement constaté par plusieurs personnes au repos ; assez fort pour que la durée ou la direction puissent être appréciées.	
IV Ebranlement constaté par des personnes en activité, faiblement en plein air, mieux dans les maisons ; ébranlement des objets mobiles, des portes des fenêtres, craquement des planchers.	II **sensible médiocre** Sentie par tout le monde ; ébranlement des fenêtres et des portes.
V Ebranlement constaté en général par toute la population ; ébranlement d'objets plus lourds ; de meubles et de lits ; tintement de quelques sonnettes.	
VI Réveil général des dormeurs; tintement général des sonnettes, oscillations des lustres, arrêt des pendules; ébranlement apparent des arbres. Des personnes effrayées sortent des habitations.	III **assez forte** Ebranlement des maisons, bruit des fenêtres ; arrêt des pendules ; ébranlement des objets suspendus ; ébranlement de l'eau dans les cuvettes.
VII Renversement d'objets mobiles ; chute des plâtras du plafond et des murs ; tintement des cloches dans les églises ; épouvante générale sans dommage aux édifices bien construits.	IV **forte** Ebranlement très fort de maisons ; renversement d'objets mobiles ; l'eau des cuvettes est projetée.
VIII Chute des cheminées ; lézardes dans les murs.	V **très forte** Lézardes dans les murs ; Renversement des tombes, des lanternes de pierre ; chute des cheminées.
IX Destruction partielle ou totale de quelques édifices.	
X Des bâtiments très solides sont détruits. Il se produit des fentes dans le sol. L'eau des rivières, lacs, etc. est projetée.	
XI Catastrophe · Destruction des bâtiments, ponts, digues. Rails tordus, débordement des eaux,	VI **désastreuse** Destruction des bâtiments, montagnes effondrées ; grands changements topographiques apparaissent.
XII Grande catastrophe — Aucune œuvre ne subsiste, montagnes effondrées. ébranlée—Des chutes d'eau se forment, etc.	

Certes, quoique nous faisons les divisions précises dans l'échelle, il n'apporte pas beaucoup de résultats : car il y a des conditions diverses dans les objets soumis aux secuousses: par exemple toutes les maisons ne sont pas construites avec les mêmes matériaux ni avec la même solidité : la stabilité à la chute n'est pas égale pour tous. Nous constatons d'ailleurs que la nature des secousses sismiques varie enormement avec la nature superficielle du terrain. Telles circonstance nous empêchent aussi de faire l'estimation statistique de l'intensité sismique correspondant à chaque endroit. Ainsi nous n'avons que sept degrés dans l'échelle au lieu de douze.

D'un autre côté, il y a l'échelle de Cancani représentée par l'accélération maxima des secousses. Probablement, il a adopté les valeurs d'accélération calculées d'après l'inscription sismographique du type ordinaire. Ses estimations ne s'accordent pas bien, naturellement, avec les résultats obtenus par l'observation directe de l'accélération. Nous allons en parler plus tard.

Or, nous avons construit l'année dernière un sismographe accélérométrique et l'observation se fait continuellement dans notre Institut. Pendant une année, nous avons réussi à enregistrer de nombreux séismes ayant des intensités diverses. Classant ces séismes dans les degrés de l'échelle, nous avons essayé de déterminer l'accélération maxima des secousses correspondant à chaque degré.

Nous avons déjà parlé dans le mémoire précédant[3] de l'accélération sismique observée en deux stations qui se trouvent dans la ville même de Tôkyô et constaté que la période prédominante dans les secousses donne des valeurs différentes correspondant aux deux stations. Nous avons, donc, donné en conclusion que les secousses sismiques de grande accélération ne sont que des ondes du type stationaire produites secondairement à la surface terrestre par l'arrivée des ondes primaires. Ainsi, même dans le domaine de la discussion de l'intensité sismique, nous sommes obligés de tenir compte de ce fait ; autrement ce n'est plus le même phénomène que nous observons. D'une part, si nous fixons le degré de l'intensité sismique d'après la sensation humaine à la partie basse de Tôkyô et d'autre part si nous examinons les inscriptions sismographiques de la station qui se trouve dans la partie haute de la ville, cette manière de comparaison ne pourra nous donner des résultats rigoureux. Heureusement, comme tous les chercheurs de notre Institut habitent dans la partie haute de la ville, il n'apparaîtra pas

3) M. ISHIMOTO, *Bull. Earthq. Res. Inst.*, 10 (1932), 171.

beaucoup de différence entre l'inscription sismique et la sensation humaine.

2. Observation accélérométrique des séismes.

Nous avons déterminé l'accélération maxima pour chaque séisme enregistré par le sismographe accélérométrique installé dans la cave de notre Institut. Nous étudions seulement les deux composantes horizontales. Cette manière d'étude ne sera pas juste sous les conditions réelles. Mais nous constatons que l'accélération de la composantes horizontale devient ordinairement plusieurs fois plus grande que celle de la composante verticale surtout dans la portion principale des secousses. Il nous semble, en effet, que la considération de la composante verticale reste inutile dans le but que nous poursuivons.

Nous avons compté tous les séismes ressentis représentés dans le Bulletin de notre Institut. Le nombre de séismes correspondant à chaque degré est représenté dans le Tableau II.

Tableau II.[4]

degré	nombre de séismes
0	12
I	50
II	17
III	5
IV	2

Comme il n'y a pas eu de séisme des deux degrés V et VI, nous ne pouvons pas dire leur grandeur en valeur de l'accélération. En étudiant dans les inscriptions accélérométriques des séismes non-ressentis, nous avons déterminé leurs accélérations maximas.

On enregistre les accélérations horizontales des séismes par deux composantes et on a, donc, besoin de les composer pour avoir l'accélération maxima des secousses. Cette manipulation est, cependant, assez difficile ; car pour faire cela on doit tenir compte de la phase de secousses qui nous demande 0,01 s. d'exactitude, laquelle n'est par réalisable dans nos inscriptions. Ainsi nous avons mesuré séparément l'accéléra-

4) D'abord on avait mis les deux plus grands séismes dans le degré V; mais après on les a remis dans IV.

tion maxima pour chaque composante. Cette manière de mesure est permise ; car, dans les conditions les plus mauvaises, nous obtenons la mesure 1 au lieu de 1,4 ($=\sqrt{2}$) : mais nous considérons, en tout cas, le logarithme de la valeur d'accélération et cette différence reste, donc, de 15 pourcent, qui est d'une précision suffisante pour notre but. La plus mauvaise condition ne sera pas possible quand les secousses sismiques ébranlent d'une façon assez irrégulière.

Comme nous l'avons déjà constaté, les secousses sismiques se composent toujours à Hongô d'ondes ayant 0,3 s. de période. Nous ressentions les secousses constituées par des ondes de cette période. Si la période prédominante des secousses n'est pas constante pour chaque séisme, la distinction des secousses deviendra plus compliquée.

Comme la période propre d'oscillation du sismographe accélérométrique est de 0,15 s., la sensibilité de l'appareil varie même dans la région de 0,3 s. suivant le degré d'amotissement. Nous exécutons de temps en temps l'étalonnage en employant une fil de caotchouc qui peut exercer une force d'amplitude constante ayant différentes périodes. Nous faisons, ainsi, la correction sur les valeurs de l'accélération maxima suivant les résultatts d'étalonnage.

La détermination du degré de l'intensité à été exécutée par M. T. Yasuda qui a une expérience d'une trentaine d'années. Ses décisions sont représentées aussi dans le Bulletin. M. T. Yasuda habite à la partie haute de la ville et il n'y aura pas de différence entre son expérience et l'inscription sismométrique. Dans le Kisyô-yôran, cependant, on ne note pas le degré surtout pour les petits séismes. Quoiqu'on décide les degrés de secousses dans les autres régions, ils ne sont pas utilisables pour notre but : strictement dit, l'évaluation de l'intensité doit faite au même point où retrouve le sismographe accélérométrique.

En tout cas, comme la fixation de l'intensité dépend entièrement de la sensation humaine, on ne peut pas donner une fixation exacte quand l'intensité tombe juste au milieu de deux degrés consécutifs. Certainement, quant à la distinction du séisme au seuil de sensation il y a tant de conditions sur la perception et la limite devient vague. Nous allons en parler dans le chapitre suivant.

3. Accélération maxima et échelle de l'intensité.

Nous avons arrangé les accélérations maximas de secousses corresopndant aux degrés de l'échelle. Comme la figure 1 représente, les

accélérations maximas se partagent très bien dans les quatre degrés de l'échelle.

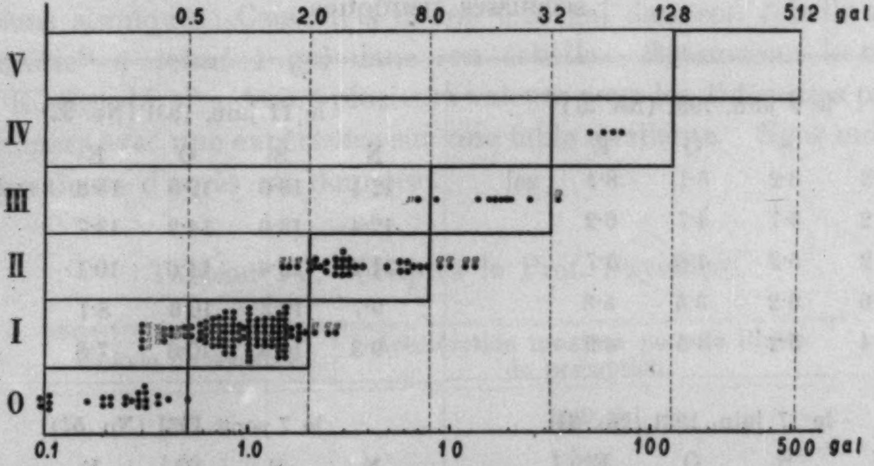

Fig. 1. L'échelle de l'Observatoire Central de Météorologie représentée par l'accélération maxima de secousse.

Ce que nous trouvons une certaine déviation sera expliqué par le fait suivant: 1° il y a une onde solitaire distinguée des autres, 2° la sensation humaine n'est pas toujours la même dans toute la journée, 3° le lieu de perception n'est pas égal, dans ou dehors de la maison, 4° on estime le séisme comparativement petit quand il fréquente et *vice versa*; on verra un bel exemple sur les séismes du 9 Juin (No. 31) et du 18 Sept. (No. 60). Quoique l'acceleration maxima du premier soit plus petite que celle du second, on les a classé inversement dans deux dégrés III et II. Ces conditions nous empêchent d'avoir une conclusion exacte. Ainsi, il est impossible de décider le degré de la secousse suivant une simple accélération maxima surtout quand il y a une onde solitaire dans les secousses. Dans ce cas-là, il est mieux de compter plusieurs nombres d'ondes qui donnent les grandes accélérations. Dans les secousses sismiques du type ordinaire il y a toujours plusieurs d'ondes ayant la grande accélération et une simple accélération maxima d'une onde devient un paramètre pour décider du degré de l'intensité suivant la sensation humaine. Nous montrons, ainsi, deux types de séismes dans le tableau III.

Nous allons, en effet, prendre une valeur moyenne des ondes de plus grande accélération comme paramètre dans les secousses sismiques. Cette définition de l'accélération maxima satisfera notre intention pour déterminer le degré de l'intensité pour tous les séismes. On verra un

Tableau III.

Ondes ayant les plus grandes accélérations dans les secousses sismiques.

le 9 juin, 1931 (No. 31)					le 11 juin, 1931 (No. 32)				
N	S	O	E		N	S	O	E	
5·3	6·2	5·1	8·1	gal	12·4	18·6	19·9	15·2	gal
5·2	5·7	4·7	6·2		12·4	13·6	14·2	13·7	
5·2	5·3	4·6	5·7		11·4	12·4	11·6	10·1	
4·6	5·2	3·5	5·3		9·7	10·3	10·6	8·1	
4·4	5·2	3·5	4·9		9·3	10·3	10·6	7·8	
le 17 juin, 1931 (No. 34)					**le 7 sept. 1931 (No. 57)**				
N	S	O	E		N	S	O	E	
39·1	64·4	60·0	67.7	gal	17·7	26·0	13·7	16·7	gal
37·1	45·6	45·0	58·0		16·0	12·0	12·9	14·2	
35·6	44·0	42·0	58·0		14·0	8·6	10·9	12·0	
33·3	32·4	29·0	56·0		9·5	8·2	10·5	10·9	
25·4	24·4	29·0	50·0		8·6	7·2	9·7	9·3	
le 16 sept. 1931 (No. 59)					**le 18 sept. 1931 (No. 60)**				
N	S	O	E		N	S	O	E	
15·2	21·6	33·6	30·9	gal	9·9	16·9	12·5	7·4	gal
13·2	20·0	19·5	19·5		8·2	6·1	7·2	7·2	
12·8	12·9	17·7	15·0		7·8	6·1	5·1	6·8	
10·3	12·0	16·1	14·2		7·0	5·8	4·8	6·5	
9·5	12·0	12·5	13·7		5·8	5·8	4·8	6·5	
le 21 sept. 1931 (No. 61)					**le 28 sept. 1931 (No. 69)**				
N	S	O	E		N	S	O	E	
41·8	47·4	62·0	50·0	gal	9·9	9·1	6·6	8·9	gal
41·8	40·3	46·3	50·0		7·0	8·1	5·7	5·6	
41·1	39·5	41·4	41·5		6·8	6·6	5·6	5·2	
39·5	39·0	36·4	32·4		6·6	6·2	5·6	4·8	
36·3	37·4	35·1	31·6		5·0	6·2	5·6	4·8	

bel exemple pour le séisme du 16 Sept. 1931 (No. 59); quioque ce séisme aie en une onde solitaire ayant 33,6 gal de l'accélération maxima, son degré a été décidé à III.

Quant à la détermination de la valeur de seuil de la sensation humaine, nous pouvons citer plusieurs études exécutées par les sismologues. Le Prof. Omori[5] a donné 1,7 gal d'accélération d'après les inscriptions sismiques ; Cancani a donné 0,25 gal dans son échelle absolue et McAdie[6] a donné 1 gal dans son échelle. Récemment le regretté Prof. K. Suyehiro[7] a donné plusieurs valeurs pour les différentes périodes de secousses avec une expérience sur une table oscillante. Nous montrons ici les valeurs d'après ses données :

Tableau IV. (d'après le Prof. Suyehiro)

Période de secousse	Accélération maxima pour la limite de perception.
1·49 s.	0·89 gal
1·72	1·34
1·94	1 57
2·18	1·66
2·38	1·73

Suivant ses résultats, la valeur de seuil s'accorde bien avec celle obtenue par le Prof. Omori dans le domaine des grandes périodes tandis qu'elle devient plus petite quand la période approche de zéro.

Comme nous voyons dans la fig. 1, la valeur de seuil est trouvé 0,5 gal. Cette fois-là on estime que les secousses ont 0,3 seconde de période. D'un autre côté, nous entendons seuvent le bruit des fenêtres secouées par un séisme, sans aucune sensation de secousses. Parsuite il est possible qu'il y ait le cas où la nature de la sensation ne soit pas le même et les secousses artificielles ne s'accorderont pas bien avec l'observation directe du phénomène naturel.

Or, nous savons l'existence d'une loi qui peut relier la sensation à la stimulation extérieure. C'est la loi de Fechner. Nous pouvons appliquer cette loi aussi à notre cas. Comme on le voit, dans la Fig. 1, le rapport entre le degré de l'intensité des secousses et l'accélération maxima obéit aussi à cette loi. Quand l'accélération augmente quatre fois, le degré avance d'un. Si nous supposons que la loi de Fechner s'applique même pour les grandes secousses, nous aurons une échelle représentée

5) F. Omori, *Publ. Eq. Inv. Com.*, 11 (1902), 60; 22 A (1908), 37.
6) A. McAdie, *Bull. Seis. Soc. Amer.*, 5 (1915), 123.
7) K. Suyehiro, *Proc. Imp. Acad.*, 5 (1929), 411.

entièrement par la valeur de l'accélération. Voici, le tableau représentant l'échelle de l'Observatoire Central de météorologie avec les accélérations maximas.

Tableau V.

Echelle de l'Observatoire Central de Météorologie représentée par l'accélération maxima.

I	0·5 — 2 gal	d'après les observations à Hongô où la période prédominante dans les secousses est 0,3 seconde.
II	2 — 8	
III	8 — 32	
IV	32 — 128	
V	128 — 512	
VI	512 — ∞	

On comprendera tout de suite que cette échelle ne s'accorde pas bien avec celle de Cancani. Néanmoins, notre échelle se base sur le fait observé directement avec le sismographe accélérométrique.

D'un autre côté, cette échelle coïncide très bien avec les résultats donnés par le Prof. Omori[8] : il a exécuté une expérience sur la table oscillante pour déterminer l'accélération maxima causant le glissement ou la chute d'un bloc de pierre. Ainsi, il a comparé ses résultats aux faits produits par les secousses sismiques et il a déterminé son échelle surtout dans le domaine des intensités catastrophiques des séismes. Nous allons citer ses conclusions :

Tableau VI.

Echelle du Prof. Omori.

I l'Accélération maxima arrive à 30 gal

Beaucoup de personnes s'enfuient en dehors ; fissures aux murs en briques de mauvaise construction ; détachement de plâtras du mur de quelques vieux *dozôs* (magasin japonais) ; renversement d'objets mobiles ; ébranlements des maisons accompagnant des bruits de craquements ; ébranlement apparent des arbres et arbustes; l'eau des piscines est troublée par la boue; **arrêt des pendules**; chute des cheminées de très mauvaise construction.

8) F. OMORI, *loc. cit.*

Tableau VI. (*suite*)

II l'Accélération maxima arrive à 90 gal
Lézardes dans les murs des maisons japonaises ; un peu d'inclinaison aux vielles maisons en bois; chute de pierres tombales et de lanternes en pierre de mauvaise construction ; quelques changements aux sources thermiques etc ; **cheminées d'usine sont intactes en général.**

III l'Accélération maxima arrive à 120 gal
Chute d'un quart des cheminées d'usine; destruction partielle ou totale des bâtiment en briques de mauvaise construction ; destruction totale de quelques vielles maisons en bois et greniers ; **chute de quelques pierres tombales et de lanternes de pierre**; déchirement de *Syôzi* (partie intérieure des maisons japonaises); glissement des tuiles du toit des maisons en bois ; chute de quelques fragments de roche dans la montagne.

IV l'Accélération maxima arrive 200 gal
Chute de toutes les cheminées d'usines; destruction partielle ou totale de la plupart des maisons en briques ; destruction totale de quelques maisons en bois ; les portes et *syôzis* des maisons japonaises sortent de leurs glissières; il se produit plusieurs centimètres de crevasses dans le terrain mou ; destruction légère de quelques digues ; destruction partielle des ponts en bois ; **chute des lanternes de pierre dû type ordinaire.**

V l'Accélération maxima arrive à 250 gal.
Destruction totale de tous les bâtiments en briques de type ordinaire ; **destruction totale de 3% de maison en bois**; chute de quelques *teras* (temples boudhistes) ; destruction sévère des digues; rails tordus légèrement; **chute de pierres tombales du type ordinaire**; détachement *d'isigaki* (mur en pierres) ; crevasses de quelque 50 cm apparaissant au long des digues ; débordement des eaux des lacs, rivières, etc.; quelque perturbation à l'eau des puits ; chutes de terrain dans la montagne.

VI l'Accélération maxima arrive à 400 gal
Chute des *teras* ; **destruction totale de 50% à 80% de maison en bois**; détachement partiel des digues ; dépression des routes en terrain mou arrêtant la circulation; rails tordus ; destruction des grands ponts en fer ; destruction partielle ou totale des ponts en bois ; chute de pierres tombales même de construction stable ; éjections d'eau ou de sable des crevasses ; destruction des magasins creusés en sous-sol ; nombreuses chutes de terrain dans la montagne.

VII l'Accélération maxima dépasse de beaucoup 400 gal
Destruction totale de touts les édifices, sauf quelques maisons en bois; quelques maisons, portes etc. sont projetées ; chutes de terrain de grande importance accompagnant les failles, glissements de terrain etc.

Certainement, le Prof. Omori fait correspondre le degré I de son échelle au degré V de l'échelle de l'Observatoire : pourtant quand nous les lisons attentivement, nous trouvons une autre correspondance qui s'accorde mieux avec les faits produits. (Tableau VII)

Certes, il y a une certaine différence au passage de V et VI dans les deux dernières échelles. Vraiment, d'une part nous avons obtenu

Tableau VII.[9]

Comparaison de trois sortes d'échelles.

Echelle d. l'Obs. Météo.	Echelle d'Omori	Echelle de l'auteur
I		0·5 - 2 gal
II		2 - 8
III	I (-30 gal)	8 - 32
IV	II (30-120)	32 - 128
V	III, IV (120-250)	128 - 512
VI	V, VI, VII (250-∞)	512 - ∞

512 gal pour la limite de V en étendant la loi de Fechner, d'autre part le Prof. Omori regardait la destruction des maisons : son point de vue ne reste plus dans le domaine de la sensation humaine. Il est possible, donc, qu'il y ait une telle différence.

D'un autre côté, on est obligé de considérer la période prédominante des secousses quand on fait attention à la destruction de maisons en bois. Certes, à la partie haute de la ville, les maisons en bois sont comparativement resistantes pour les grandes accélérations car la période prédominante des secousses est de 0,3 seconde. A la partie basse de la ville, cependant, les maisons sont détruites avec une accélération comparativement petite à cause du fait que sa période est assez grande. Suivant ce fait, il y apparaîtra, naturellement, une différence entre les degrés V et VI dans les deux partie de la ville. Il est nécessaire, donc, que l'on soit obligé de considérer la période prédominante des secousses, quand on fait l'estimation de l'accélération maxima pouvant détruire des maisons.

4. Accélération maxima du grand séisme.

Jusqu'aujourd'hui nous déterminons l'accélération maxima d'un séisme suivant l'inscription obtenue par le sismographe du type ordinaire. En effect, nous remarquons toujours des ondes dont l'amplitude et la période sont également grandes dans les secousses. Nous obtenons, ainsi, une valeur de l'accélération maxima comparativement petite pour les

9) Quoique le Prof. Omori aie exécuté son expérience sous les périodes assez grandes, ses résultats s'accordent très bien à ceux obtenus sous les conditions natuelles, c'est-à-dire la période dans les seconsses demeure 0,3 seconde.

grands séismes. Le tableau VIII montre les accélérations maximas obtenues pour les grands séismes apparus récement au voiginage de Tôkyô :

Tableau VIII.

Accélérations maximas des grands séismes. (à Hongô)

Dates.	périodes	accélérations maximas.	auteurs
20 juin (1894)	1·8 s.	88·8 gal	Omori
8 dec. (1921)	1·7	24·6	„
26 avril (1922)	2·0	33·0	„
14 jan. (1923)	1·3	25·0	„
1 sept. (1923)	1·35	97·0	Imamura
15 jan. (1924)	1·8	36·0	„

Bien que tout les séismes soient de degré V et VI, leur accélération maxima reste assez petite. Mais quand nous faisons attention à la période de l'accélération, nous comprenons tout de suite que l'object d' observation ne reste plus le même. Probablement, la période prédominante des secousses de grande accélération était toujours 0,3 seconde à Hongô. Nous savons que toutes les lanternes de pierre ont été renversées par les secousses produites dans la ville au moment du grand séisme de 1923, tandis que l'accélération maxima estimée par l'inscription sismographique était seulement de 97 gal. D'après l'expérience sur la table oscillante, les blocs de pierre ne se renversent jamais sous l'action de secousses dont l'accélération reste à moins de 100 gal.

La comparaison de l'accélération maxima obtenue par deux sortes d'inscriptions, nous montre une grande différence entre eux. En tout cas nous constatons que les accélérations déterminées par le sismographe du type ordinaire ne représente pas le fait réel soutout pour discuter l'action catastrophique de secousses.

5. Remarques.

Pour explimer l'échelle de l'intensité sismique, nous sommes obligés d'employer le sismographe accélérométrique. La période prédominante de secousses ne demeure pas la même partout, mais elle est toujours à peu près constante dans la même région pour tous les séismes. Au

moment d'un grand séisme nous remarquons toujours une destruction groupée de maisons en bois le long d'un fleuve ou d'une vallée. L'accélération produite en ces endroits ne sera pas aussi grande que nous l'imaginons. D'un autre côté, quoique nous ne voyons aucune maison détruite sur la colline, l'accélération maxima sera assez grande. La figure 1 a été déterminé suivant les résultats obtenus à Hongô, et nous ne pouvons pas l'appliquer directement aux autres stations. Pour établir une échelle pour l'intensité sismique, nous devons tenir compte de la période prédominante dans les secousses sismiques dans la région en question.

---

41. 震度階と地震最大加速度

地震研究所 石本巳四雄

1. 地震の强さは人體感覺及び物體の轉倒、破壞等を標準として制定された震度階に據つて表はす事になつて居る。然るに一方震度と最大加速度との間に密接の關係が行はれる事から、二三の絕對震度階の制定も試みられて居る。然し何れも實際の震動加速度を直接觀測したものではない。

2. 著者は昨年來、本鄉臺において直接地震の加速度觀測を行つて居るが、此等を中央氣象臺制定の震度階により決定されたものと比較して見たのである。地震の最大加速度としては水平二成分の値を別々に採用したが、大した不都合は生じない。

3. 第一圖は以上の結果を圖に示したものである。即ち震度と最大加速度との間には Fechner の法則が行はれて居り、其の法則を延長する事によつて次の如く震度階を最大加速度の値で表す事が出來る。

0	無感覺	0—0·5 gal
I	微震	0·5— 2
II	弱震(弱き方)	2— 8
III	弱震	8— 32
IV	强震(弱き方)	32—128
V	强震	128—512
VI	烈震	512—∞

なほ此の範圍に當嵌らぬものは震度決定或ひは最大加速度の採用において多少不備の點のある結果である事が判つた。なほ以上は何れも本鄉觀測であつて、卓越周期が 0·3 秒である事を注意して置く必要がある。

4. 從來の大地震の最大加速度は變位地震計の記象に據つて居た關係上、比較的小なる値を與へて居るが、物體の轉倒、破壞等の觀測に從へば恐らく加速度は數倍大なるものであつたと想像される。但し此の場合の周期も 同じく 0·3 秒程度のものと信ぜられる。

5. 從來の絕對震度は單に最大加速度のみを以て表して居るが、實は各地における大なる加速度を與へる震動は其地方特有の周期であるから、震度を加速度として表す場合、其の周期をも顧慮しなければ完全なものとはならない。

---

42. *On Statistical Distributions of Earthquakes in Kwansai District.*[1]

By Suketosi YAZIMA.

(Read April 26, 1932.—Received June 17, 1932.)

I. Introduction.

In the recent few years, Wakayama and its neighbourhood, it seems, have been frequented by considerable numbers of earthquakes. On the other hand, a destructive one took place in the Province of Tango on 7th. Mar. 1927, which was followed by many after-shocks. Is there any relationship between these two phenomena? or not? This question has been studied by means of statistical analysis of the actual data in the interval of the three years 1927–1929. The present investigation is mainly concerned with the space and time distributions of these earthquakes, correlations among them, and allied statistical phenomena.

II. Data and Classification.

The data of daily occurrence of earthquakes, used here, were obtained from the *Kisyô-Yôran* (Monthly Publication of the Central Meteorological Observatory). In most cases, "felt" (or sensible) earthquakes and "non-felt" (or insensible) ones were treated separately, but sometimes together. In the first place, the space distribution was treated, selecting those of which the origins were located in the following three regions.

(a) Kisyû (Neighbourhood of Wakayama),
(b) Tango Peninsula and its vicinity,
(c) Kwansai in general, excluding (a) and (b).

Fig. 1 shows the extents of these regions. Kwansai, as here defined, may be somewhat broader in extent than the region usually so called. For the sake of convenience, however, such a wide region that extends from Hirosima to Hamamatu and from Sionomisaki to Kanazawa was here considered altogether. This mode of division was made in view of the present purpose of ascertaining first the correlation of Tango and Kisyû earthquakes, and then whether Kisyû earthquakes are of the same type as those in Kwansai in general or not.

---

1) Communicated by T. TERADA.

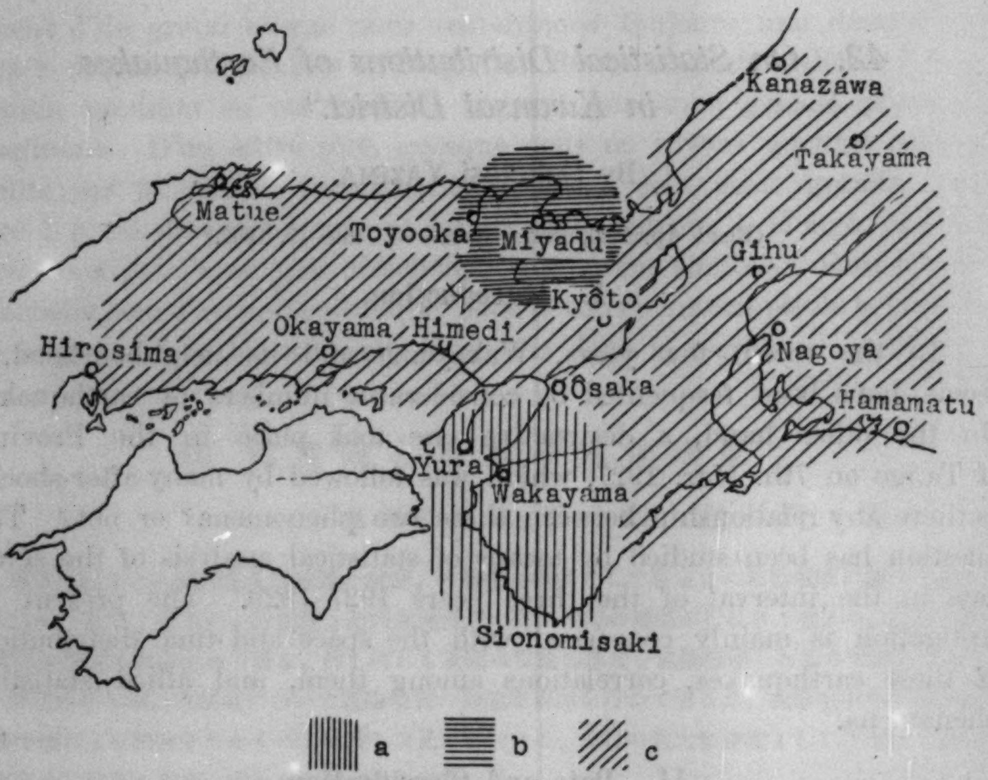

Fig. 1.

In the second place, as for the time distribution, the daily number of occurrence of earthquakes which belong to each region was counted. These data were also plotted in frequency curves (not shown in this paper).

III. Method of Period Investigation.

By the examination of the above mentioned frequency curves, it may be noticed that the activity of earthquake seems to have some periodicity. For a closer examination of this point, the following method of analysis was applied. In case of the hypothetical period $T=n$ days, daily numbers of earthquakes a_1, a_2, a_3.... are arranged in n columns as in ordinary periodogram method (Table I).

Then the means of each column $A_1, A_2, A_3, \ldots A_n$ are calculated and plotted in a diagram against the column number. Fig. 2 shows an example of the diagram. If such a curve shows a single maximum and a single minimum, it may be concluded that the periodicity of $T=n$ days is very remarkable, and the fluctuation is simple harmonic type. If very flat, such periodicity is not sensible at all. At any

Table I.

No.	1	2	3 .... n
	a_1	a_2	a_3 .... a_n
	a_{n+1}	a_{n+2}	a_{n+3} .... a_{2n}
	....	....	....
	....	....	....
	a_{mn+1}	a_{mn+2}	a_{mn+3}............... $a_{(m+1)n}$
Mean	A_1	A_2	A_3 .... A_n

rate, the amplitude of this curve will indicate in some measure the degree of probability for the existence of the period in question. Let

y_m : Mean of A's,

$$y_m=\frac{1}{n}(A_1+A_2+\ldots+A_n),$$

a : Difference of the largest and the least of A's.

Then, the ratio ρ

$$\rho=\frac{a}{y_m}$$

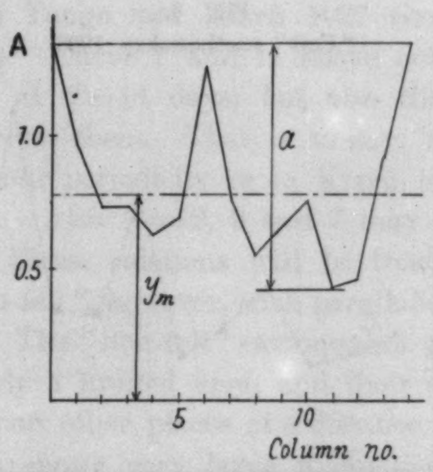

Fig. 2. "Felt" earthquakes in Kisyû, 1927.

may be taken as the measure of periodicity. Various periods which might be supposed to exist, were treated in the same manner, and $\rho-T$ diagrams were drawn for each classified group of earthquakes (Fig. 3a–5c).

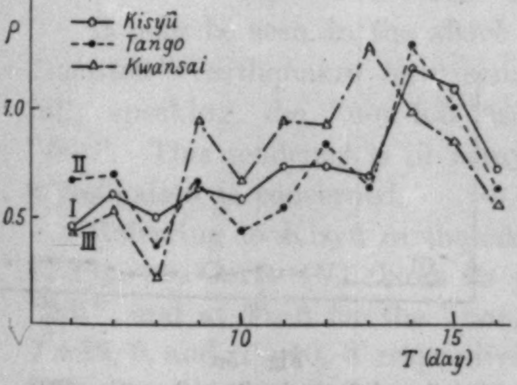

Fig 3a. "Felt" earthquakes, 1927.

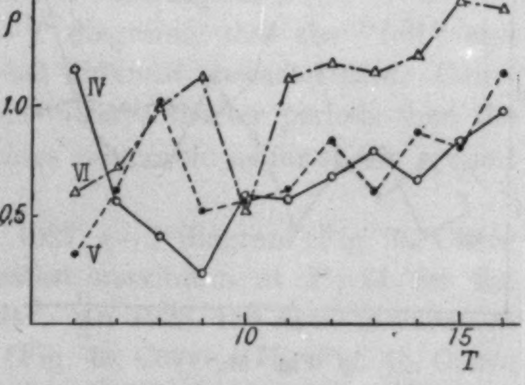

Fig. 3b. "Non-felt" earthquakes, 1927.

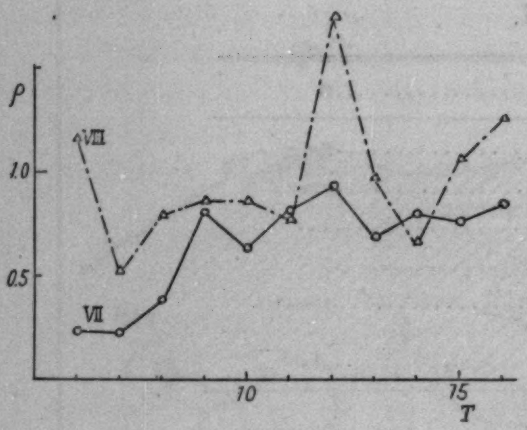

Fig. 4a.
"Felt" earthquakes, 1928

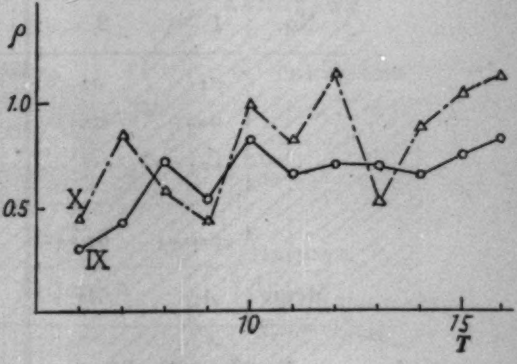

Fig. 4b.
"Non-felt" earthquakes, 1928.

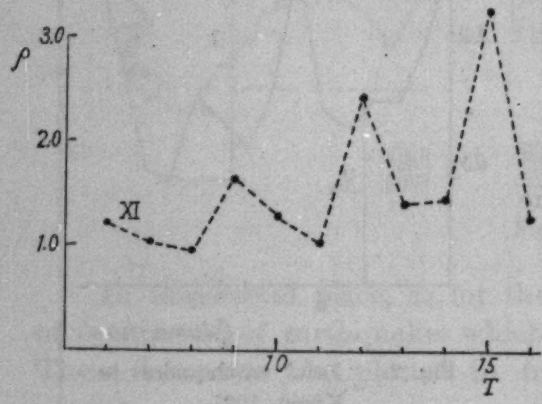

Fig. 4c.
"Felt" and "non-felt" earthquakes, 1928.

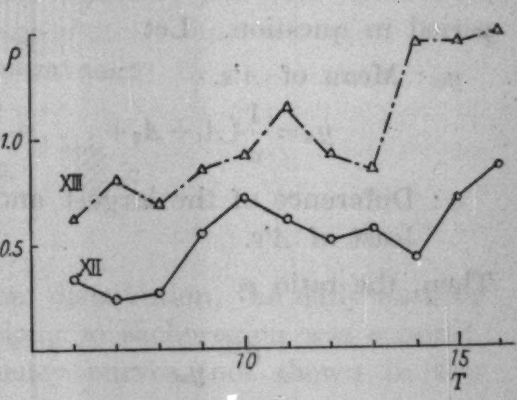

Fig. 5a.
"Felt" earthquakes, 1929.

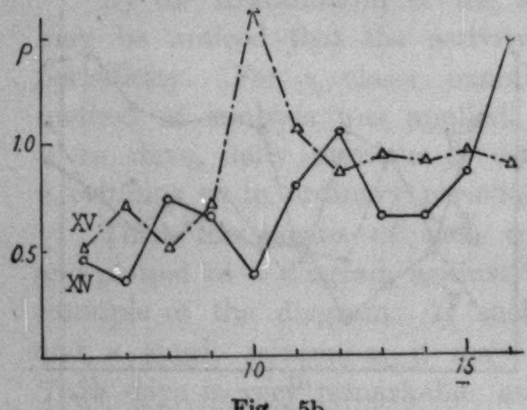

Fig. 5b.
"Non-felt" earthquakes, 1929.

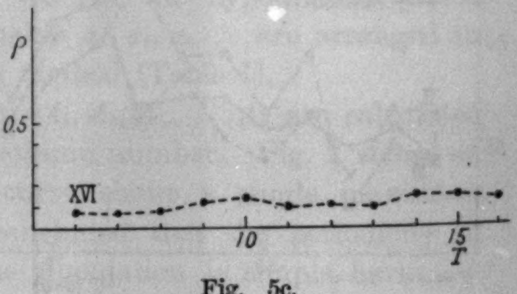

Fig. 5c.
"Felt" and "non-felt" earthquakes, 1929

For Tango earthquakes 1927, the periodogram was commenced with 17th. Apr., for immediately after the destructive shock of 7th. Mar. the decay of after-shocks was very rapid and the period investigation could not be conveniently applied. In 1928 and 1929, the occurrence of either "felt" or "non-felt" earthquakes in Tango was very seldom, so that the periodogram method was applied only to the sum of "felt" and "non-felt" earthquakes in these two years.

IV. General Results of Period Investigations.

(a) Tango and Kisyû Earthquakes.

In the above described $\rho-T$ diagrams, it may be remarked that the periodicity of "felt" earthquakes in Tango and Kisyû 1927 shows much similarity (Fig. 3a, Curve I, II). Curve I and II above noted have not merely the common maxima at $T=14$ days, but also there exists nearly perfect parallelism between them. That is to say, the "felt" earthquakes in Tango have the same periodicity as in Kisyû, and the most remarkable period is 14 days. Also $T=12$, 9 and 7 may be considered as less remarkable periods. Phase relations will be treated in another place. Concerning the "non-felt", however, such parallelism cannot be found (Fig. 3b, Curve IV, V). The "non-felt" earthquakes are of course of local character affecting only a limited area, and their occurrence may have no sensible effects upon other places at a distance.

In 1928, $\rho-T$ diagram for Tango shows very large fluctuations, but it is due to the rarity of occurrence, and does not indicate that a certain period is very remarkable. In 1929, $\rho-T$ diagram is very flat, and differs from that of 1927 or 1928. In this year, after-shocks of the 1927 earthquake did not occur any more, and those which took place do not show any conspicuous periodicity.

(b) "Felt" and "Non-felt" Earthquakes.

It may be seen in the above $\rho-T$ diagrams, that the "felt" and "non-felt" earthquakes have somewhat different characteristics. Generally speaking, the "non-felt" seems to have shorter periods than the "felt". This tendency is in many cases noticeable as far as the present investigation is concerned.

Referring to Kisyû earthquakes 1927, $\rho-T$ diagram (Fig. 3a, Curve I; Fig. 3b, Curve IV) shows its greatest maximum at $T=14$ for the "felt", and at $T=6$ for the "non-felt". In 1928, the same is shown at $T=12$, 9, and $T=10$, 8 respectively (Fig. 4a, Curve VII; Fig. 4b, Curve IX). But in 1929 the things are not so simple as these (Fig. 5a, Curve

XII; Fig. 5b, Curve XIV).

For Tango earthquakes 1927, the "felt" seems to have $T=14$, and the "non-felt" $T=8$ (Fig. 3a, Curve II; Fig. 3b, Curve V). While, $\rho-T$ relations for Kwansai are so complicated that the characteristics of the "felt" and the "non-felt" cannot be expressed in a few words.

(c) Kisyû Earthquakes.

The "felt" earthquakes in Kisyû 1927 have an apparent period of $T=14$ days, while in 1928 $T=12$, and in 1929 $T=10$ (Fig. 3a, 4a, 5a). For the "non-felt" in the same region, $\rho-T$ diagrams have maxima at $T=6$, 8, 10, 12, 16, different in different years, among which some may be the harmonics of others (Fig. 3b, 4b, 5b). In short, it may be concluded that the occurrence of the "felt" earthquakes in Kisyû has rise and fall with the interval of 10 or 14 days, and the "non-felt" with the interval of 6 or 8 days.

Though the present considerations are restricted only to the periodicity of occurrence, yet it may not be very far from truth to say that the Kisyû earthquakes are not of the same mode as Kwansai in general. Each of $\rho-T$ relations indicates sometimes quite different characters. An extreme case is shown in Fig. 5b, where each maximum of one curve nearly corresponds to a minimum of the other. Above considerations are also supported by the following fact. Immediately after the destructive earthquake in Tango (7th. Mar. 1927), the occurrence in Kwansai was evidently affected, but it was not the case in Kisyû.

Annual variation of the Kisyû earthquakes was also investigated, and shown in Fig. 6. But any conclusive result may not be expected from the investigations in such a small interval as three years.

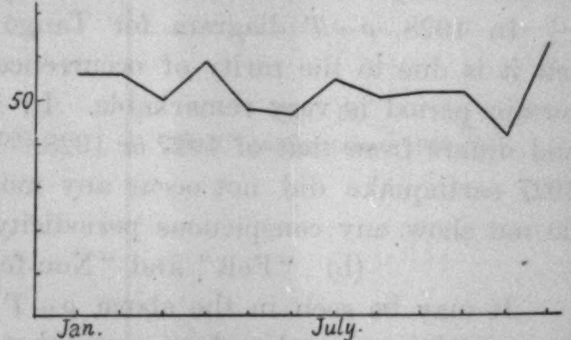

Fig. 6. Annual variation of Kisyû earthquakes.

V. Methods and Results of Phase Investigation.

In the above investigations, it has been known that the Kisyû and Tango earthquakes in 1927 have nearly the same period of occurrence. Hence, a further investigation was made regarding the phase relations between them in the following way.

Let x and y be the daily numbers of earthquakes in Kisyû and Tango respectively. Taking x and y as the rectangular coordinates in a diagram, we obtain a group of points, say $P_1(x_1, y_1)$, $P_2(x_2, y_2)$, etc. If x increases and decreases directly proportional to y, directions of P_1P_2, P_2P_3 etc. will make acute angles with $+x$-axis. If x decreases when y increases and *vice versa*, they will make obtuse angles with the same axis. This relation was first studied. Further, the following method will be also applicable. If x increases and decreases a little preceding y in phase, the points P_1, P_2, P_3 etc. will be so arranged as to make a cycle with clock-wise sense; if y precedes x, then the anti-clock-wise sense will ensue. If sometimes x precedes y and sometimes y precedes x, the cycle will change its sense accordingly. Fig. 7 shows an example of such researches.

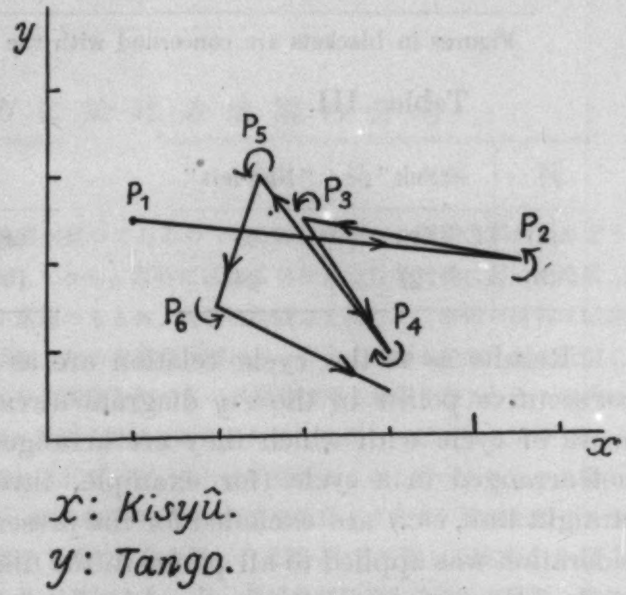

Fig. 7. Phase relation diagram.

Commencing with 1st. Apr. 1927, pairs of daily numbers of Kisyû and Tango earthquakes were plotted in a x-y diagram. Kisyû was always taken as abscissa. Then, connecting two successive points with a straight line, a cluster of lines will be the consequence. The directions of these lines are classified in two cases: i.e. (a) lines make acute angles with $+x$-axis, (b) lines make obtuse angles with the same axis. The former corresponds to the case, in which increase and decrease of Kisyû and Tango earthquakes coincide with each other in sense. The latter is the case, in which an increase of Kisyû earthquakes corresponds to a decrease of Tango earthquakes and *vice versa*. From the diagram above described, frequencies of the two cases were respectively counted (Table II). The same method was applied also to the pairs of earthquakes for every five days, from Mar. to Dec. 1927 (Table III). In 1928. monthly sum of earthquakes was treated in the same manner, owing to the rarity of occurrence (Table IV). For the "felt" earthquakes, the case (b) is always predominant; roughly speaking, frequency of (b) is twice as large as (a).

For the "non-felt", cases (a) and (b) are almost equally distributed. As already shown in our period investigations, the "non-felt" earthquakes in Kisyû and Tango have no apparent correlation, so that the above result concerning the phase relation may be also quite natural.

Table II.

	Apr.	May	Jun.	Jul.	Total
(a)	5 (8)	4 (9)	5 (5)	3 (7)	17 (29)
(b)	10 (8)	7 (10)	6 (9)	6 (4)	29 (31)

Figures in blackets are concerned with the "non-felt" earthquakes.

Table III.

	"Felt"	"Non-felt"
(a)	15	25
(b)	27	24

Table IV.

	"Felt"	"Non-felt"
(a)	2	12
(b)	9	16

Results as to the cycle relation are as follows. Referring to three consecutive points in the x-y diagram already stated, let us consider the sense of cycle with which they are arranged. Such cases that they are not arranged in a cycle (for example, three points are situated on a straight line, etc.) are excluded for the present purpose. The above consideration was applied to all points in the diagram, and frequencies of two cases, (i) clock-wise arrangement and (ii) anti-clock-wise arrangement, were counted. Kisyû was again taken as abscissa. Hence, the former corresponds to the case in which Kisyû earthquakes are advanced in phase. Frequencies of the two cases for the "felt" earthquakes 1927 were arranged in Table V, which indicates predominance of the latter case in general. Though the material used here for deducing the above results is not sufficiently abundant, still the existence of some kind of phase difference between Kisyû and Tango earthquakes may be concluded in statistical sense.

Table V.

	Apr.	May	Jun.	Jul.	Total
(i)	4	9	8	6	27
(ii)	15	8	16	12	51

From the above, it may be seen that the "felt" earthquakes in Kisyû and Tango are nearly in the opposite phase. Namely, the activities of the two regions alternate one after another. Also the same method was applied to Kisyû and Kwansai earthquakes, but the results are not conclusive.

This investigation has been carried out under the kind guidance of Prof. T. Terada, for which the author expresses his best thanks. He is also much indebted to Miss F. Yasuda for her assistance.

---

42. 關西地方に於ける地震の分布

矢 島 祐 利

和歌山附近には引續いて相當の數の地震が起つてゐるので、これに何等かの週期性があるかどうかをペリオドグラムの方法に依つて解析してみた。同時に昭和二年三月七日北丹後に起つた地震と紀州地方のそれとの何等かの關聯といふ豫想のもとに、此等の相關をも扱つた。解析の材料は昭和二年から四年までの三箇年にわたる。昭和二年の有感覺地震については、丹後も紀州も頗る近似した週期性を持つこと、すなはち共に 14 日の週期を持つものが顯著である結果を得た。そこで次に位相の關係を檢べてみると、丹後と紀州の地震の增減は時間的に互に相反して起ることが分つた。無感覺地震については此の樣な關係は認められないが、それは小規模のものと考へられるから斯くあつて然るべきものと見られる。次に、一般に有感覺地震は無感覺地震より大きい週期を持つやうである。例へば昭和二年紀州のものに就いて前者の最も著しい週期 14 日に對して後者は 6 日、昭和三年には 12 日に對して 10 日及び 8 日等である。又、丹後及び紀州を除外した關西一般の地震の週期を計算し、特にこれを紀州地方のものと比較してみると、週期の關係はかなり喰違つてゐる。すなはち紀州地方に起る地震は關西の地震一般とは稍異つた性質を有するが如くである。

---

43. *The Earthquake Swarms of Nagusa and Vicinity.*

By Akitune IMAMURA, Takao KODAIRA and Hisasi IMAMURA.

(Read May 17, 1932.—Received June 20, 1932.)

1. Introduction.

As these earthquakes have been already described by one of the authors in a previous paper,[1] the following *résumé* which is intended to enable an understanding of conditions since the beginning of activities, is necessarily very brief.

From Table I, below, it will be seen that in Wakayama city and neighbourhood there were during the period between 1911 and 1919 an average of not more than 14 sensible shocks a year. Twenty-five shocks were recorded in 1911 and three in 1918. The frequency increased progressively after 1920, in which year as many as 299 shocks were recorded.

Table I. Annual frequency of earthquakes in Wakayama and vicinity.

Year	1906	1907	1908	1909	1910	1911	1912	1913	1914	1915	1916
Frequency	17	15	21	14	7	25	20	7	13	12	12
Year	1917	1918	1919	1920	1921	1922	1923	1924	1925	1926	1927
Frequency	15	3	14	104	154	100	299	195	210	148	142

According to the Wakayama Meteorological Station, where these records were taken, the earthquakes were local in character, while the range of sensibility was circumscribed by an area of less than 20 kms. radius, with the sea-floor of Kii-Awadi Straits as centre.

Although not relevant to our subject, it is interesting to note here that although the inhabitants of the disturbed regions used at first to be alarmed by these frequent tremors, they have become so accustomed to them that it is now the diminution in their frequency that causes anxiety.

As to the origins of these disturbances, they were supposed at first to lie in the sea-floor of the Kii-Awadi Straits, so that two more stations

1) A. IMAMURA, *Jap. Jour. Astro. & Geop.*, 7 (1929), 31.

were added to our seismic net, one at Tomioka, Tokusima Prefecture, and the other at Hukura, Awadi Island; but with the cumulation of observations it became more and more apparent that the majority of the earthquakes emanated from Nagusa and neighbourhood (Kii Peninsula), and not from the Kii-Awadi Straits as originally supposed. To be exact, the focal area is about 10 kms. radius, with either Kimiidera or Hikata as centre. In the circumstances we closed the Hukura station.

This phenomenon of swarms of small earthquakes is not devoid of interest even when viewed merely as manifestations of one form of seismic activity; but when considered in connection with the mechanism of earthquakes and with relation to their distribution in space, it acquires additional interest. They remind us of the dwarfed plants which the Japanese gardener so skilfully produces, so that we are strongly tempted to call them "miniature earthquakes".

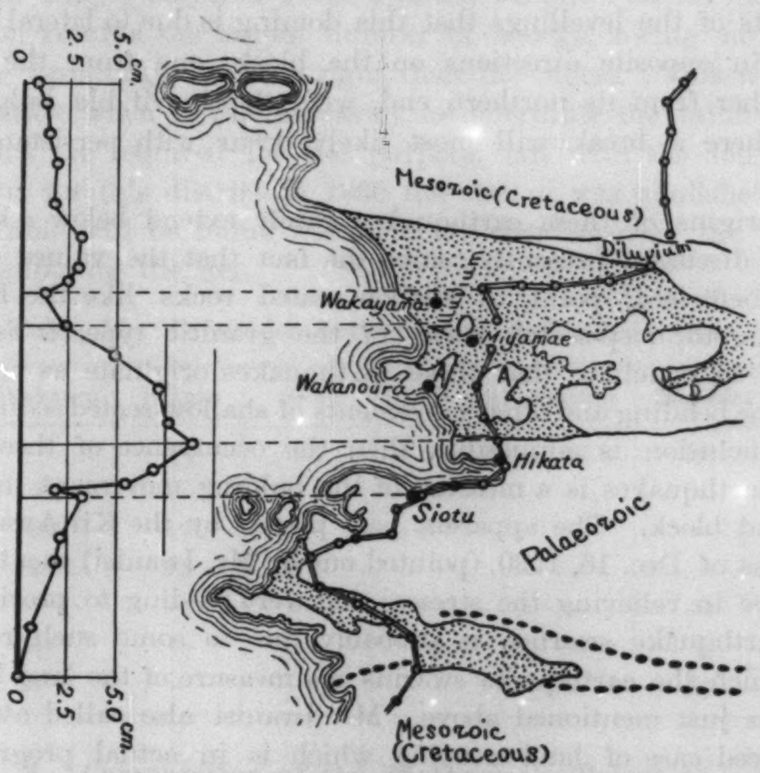

Fig. 1.

2. Changes in land-level at Nagusa and neighbourhood, and the mechanism of the earthquakes.

The two lines of levels that were run along the western coast of

the Kii Peninsula revealed incidentally a marked local change of land-level at Nagusa and neighbourhood—a change that is actually in progress at the present day (Fig. 1). A land block of a diameter of about 10 kms., with Siotu at its southern end and Wakayama city at its northern, is rising with a definite tilt. Although the maximum uplift of 9 cms., it is true, occurred in the 30 years interval that separates the first and second surveys, we have good reasons for concluding that the greater part of the rise took place after 1920. It is a truism that the geological structure of a locality is usually of significance in the interpretation of such phenomena as level-changes that are proceeding, or have proceeded, in that region. In this case in which the land has domed or bulged outward, the summit of the dome is indeed a fault at the junction of a crystalline schist and a Palaeozoic (Titibu) rock; and it is just along this fault line that most of the shocks occur. It appears from results of the levellings that this doming is due to lateral pressures operating in opposite directions on the block, one from the southern and the other from its northern end, with the inevitable bulge at the middle, where a break will most likely occur with persistance of the pressure.

The origins of these earthquakes rarely extend below 4 kms., and as will be discussed presently, since the fact that the values of k, the distance coefficient, point to shallow-seated rocks like the Palaeozoic rather than to deep-seated rocks of the granitic type, it is perhaps reasonable to conclude that these earthquakes originate as accompaniments to the bending and other movements of shallow-seated sedimentaries. If this conclusion is admissible, then the occurrence of these swarms of feeble earthquakes is a measure of the bulging movement in progress on the land block. The apparent part played by the Kii-Awadi Straits earthquakes of Dec. 16, 1930, (pointed out by Mr. Iwanisi) as a temporary safety valve in relieving the stresses that were tending to precipitate the Nagusa earthquake swarms, is probably due to some such relation as that in which the earthquake swarms is a measure of the land bulge that goes on, as just mentioned above. Mr. Iwanisi also called attention to a pronounced case of land-creeping which is in actual progress today at Syôhata, a small village about 9 kms. east of Hikata. As this movement is in all probability connected with the block movement already referred to, Mr. Kishinouye of the Seismological Institute is at present investigating the phenomenon.

3. The Seismic Net.

Because of our error as already mentioned in concluding that the origins of these earthquake swarms embraced a considerable area, our net of observing stations numbered, besides the one at Wakaura, one each at Tanabe, Tomioka, and Hukura. The last-named station is equipped for regular seismological work, while the rest are provided in addition with tiltometers. But with the discovery of the smallness of the focal area soon after beginning concerted observations, a smaller net was established within the originally arranged larger net, resulting in the addition of more stations; one each at Wakaura (base station), Hikata, Kimiidera, and Siotu, making seven stations in all. In addition to these are the auxilliary stations— Miyamae and the Kaisô Middle School and the Wakayama First Female Middle School. The Kimiidera station records the largest number of shocks, owing no doubt to its greater proximity to the origin than the others. This was an important station when it was necessary to determine the value of k, since four stations are required for the purpose, but with the determination of the value for this district in 1930 the station was abolished. In the annexed Table will be found the distances that separate the respective stations composing the net.

Table II. Distances between the stations, in kms.

	Wakaura	Hikata	Siotu	Kimiidera	Tanabe	Tomioka	Hukura
Wakaura	—	5·4	6·5	2·3	55	56	43
Hikata	5·4	—	4·7	3·3	—	—	—
Siotu	6·5	4·7	—	5·7	—	—	—
Kimiidera	2·3	3·3	5·7	—	—	—	—
Tanabe	55	—	—	—	—	70	85
Tomioka	56	—	—	—	70	—	39
Hukura	43	—	—	—	85	85	—

4. Computation of the Distance Coefficient k.

We succeeded in computing the distance coefficient k for eleven of the earthquakes, and these are shown in the next table.

These eleven earthquakes are only those that were accurately recorded by our stations. By taking the feeble motions of the first one

Table III. Computed k values of all Earthquakes observed in 1928.

No,	Time of Occurrence				Duration of Preliminary Tremors				k	Focal Depth
					Wakaura	Kimiide-a	Hikata	Siotu		
	m.	d.	h.	m.	s.	s.	s.	s.		km.
1	VI	3	14	40	1·09	0·87	1·14	1·18	3·20	1·4
2	VI	4	7	20	2·05	1·86	1·71	1·60	3·80	5·8
3	VIII	7	20	10	1·80	1·30	1·40	1·00	2·43	0·6
4	VIII	9	17	8	0·97	1·02	1·48	1·25	3·10	1·1
5	VIII	9	21	14	1·13	0·90	1·04	1·00	3·42	1·5
6	VIII	11	16	33	1·38	0·93	0·82	1·55	3·82	2·8
7	VIII	11	16	57	1·34	0·96	0·86	1·36	3·77	2·9
8	VIII	11	17	4	1·14	0·96	1·06	0·93	3·64	1·9
9	VIII	12	13	25	2·10	1·96	1·80	1·34	3·80	5·1
10	VIII	18	8	40	1·05	0·82	0·98	1·20	3·80	2·6
11	IX	24	11	50	1·74	1·52	1·28	0·96	3·82	3·4

or two seconds as longitudinal waves and those that arrive next and constitute the main portions of the whole motion as transverse waves; and by also assuming that each of these waves were propagated from the origin at speeds uniform throughout their journeys, it is possible to determine the position of the origin of every one of the earthquakes and compute their k values. These origins are shown in Fig. 2, and the k values in Table III.

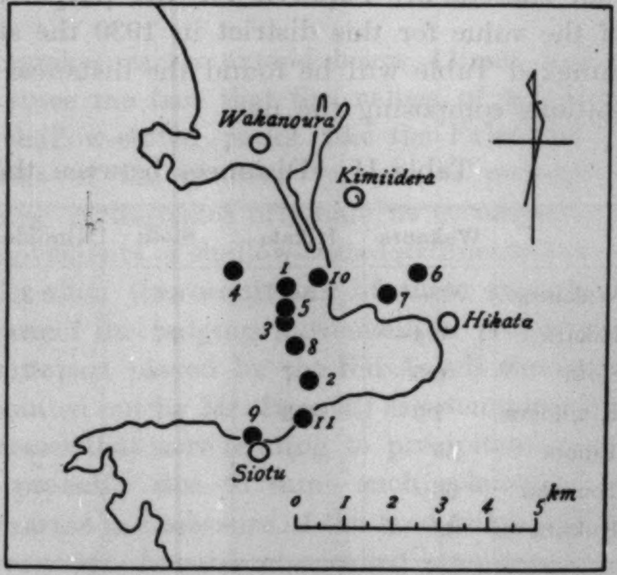

Fig. 2. Origins of the eleven earthquakes.

Coming back to the assumptions of the preceding paragraph, the first question that the reader is likely to ask is whether, in these near earthquakes, the earth movements were treated as consisting of exactly the same types of waves that characterize the larger and more distant

earthquakes. The answer to this question is in the affirmative. The reason is that every one of these earthquakes is exceptionally local in character and feeble in intensity, hence the body that transmits the initial motion,—the prime cause, must also be a small body, whence it follows that the propagated waves are also feeble and merely simple to-and-fro motions. It is therefore logical to assume that the first phase of the longitudinal and transverse waves that arrived at the station were propagated as elastic waves; and observations made at the fairly distant 5th (Wakayama) station confirm the assumption. In other words, the value of k obtained by the observation net and the position of the origin are in accord with the results obtained by the 5th station.

Another point likely to be queried is whether the k values of all the individual earthquakes of the swarm were assumed to be alike. This also is answered in the affirmative. One of the facts on which this assumption rests is the accord in the results of the observations made by the 5th stations, as in the preceding case. Another reason is that the majority of the computations practically agree in giving 3·8 for the value of k, which of course does not mean that all the eleven earthquakes of the table gave identical results. Seven out of the eleven did so, while the values for the remaining four were somewhat smaller, which merely makes their origins shallower—a difference that may indeed point to the presence of a layer of soil overlying the surface rock. See Fig. 3.

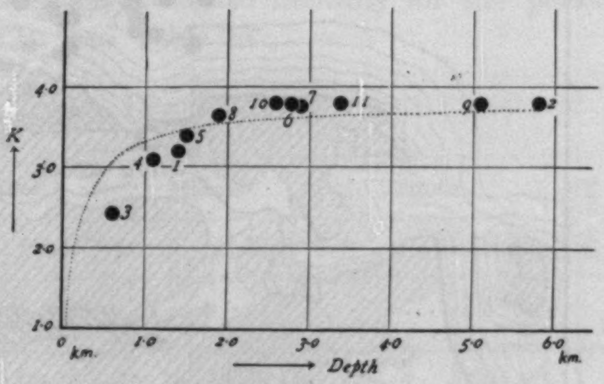

Fig. 3.

By taking for example the thickness of the surface crust to be 50 m. and the value of k to be 1 and the k of the base rock to be 3·8, the curve showing the relation of the focal depth to the apparent value of k takes the form of the dotted line in Fig. 3, a result closely approximating that derived from actual observations.

The small value, 3·8, of k, compared with 8·5, the usual value for granitic rocks, is an important fact to be borne in mind in deducing the seismic focus in this region. Had we employed Omori's formula, taking 7·4 for k, the coefficient of the distance, the result would have

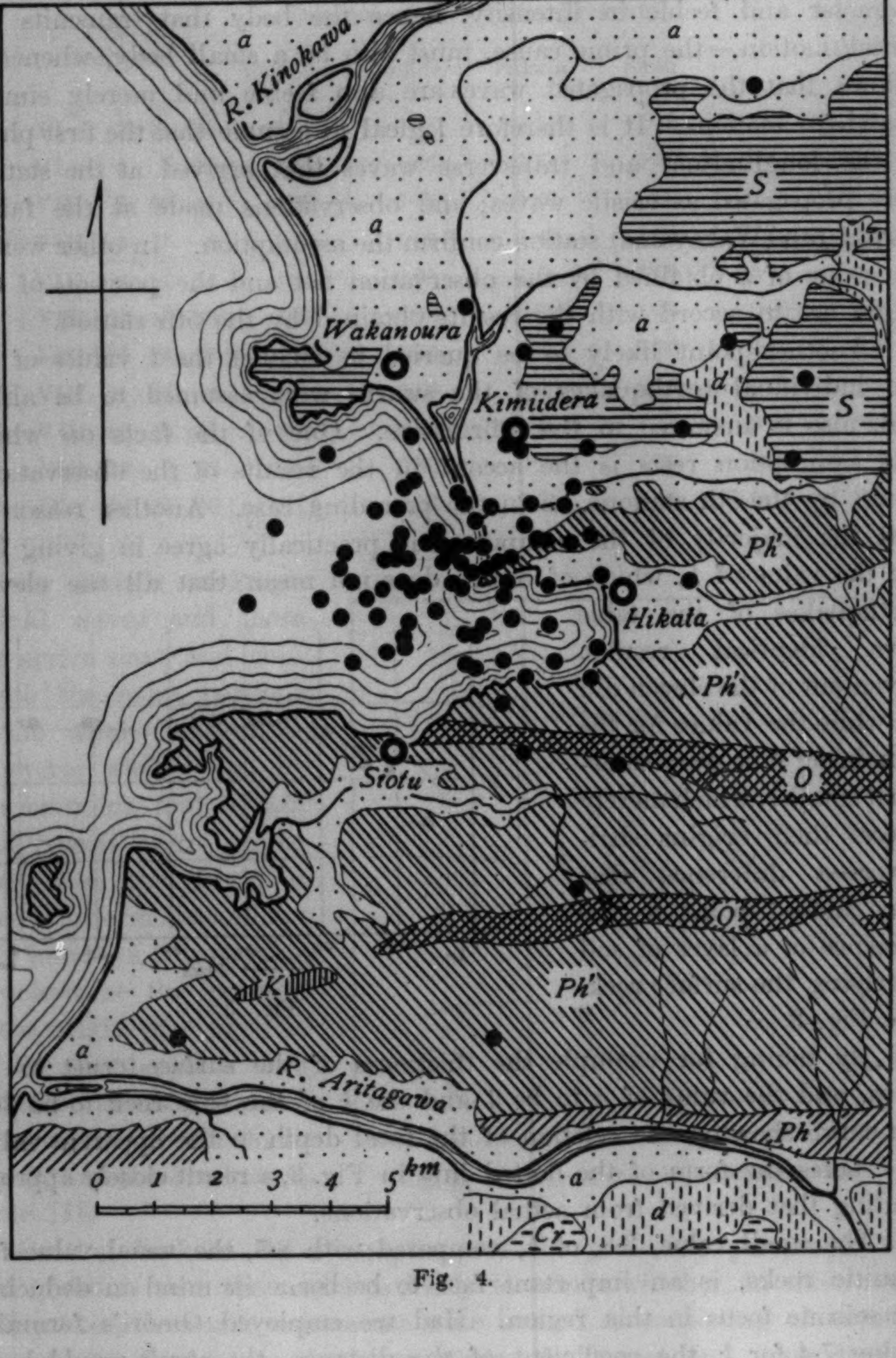
R. Kinokawa
a
a
a
S
Wakanoura
a
Kimiidera
d
S
Ph'
Hikata
Ph'
Siotu
O
O
Ph'
K
a
R. Aritagawa
Ph
0 1 2 3 4 5 km
a
d
Cr

Fig. 4.

given twice the actual distance.

While the derivation of such a small value for k is consonant also with the physical properties of the rock, a Palaeozoic schalstein of Tosa, shows just such a value. Professor Nagaoka in his investigations into the elasticity constants of this rock obtained $v_1=4{\cdot}63$ and $v_2=1{\cdot}80$ (units sec. and km.) whence $k=2{\cdot}95$. The physical constants of rocks from Tosa are not of course expected to be identical in every respect with those of rocks from the Kii Peninsula, but from the similarity of the geological histories of the two regions, the two rocks are not likely to differ to any considerable extent.

As discussed in the foregoing, for our observation net there is no objection to taking 3·8 as the value of k for earthquakes the duration of whose preliminary tremors ranged from 1 to 2 sec. We shall next consider the distribution of the origins as deduced from this value as basis of computation.

5. Distribution of Seismic Origins.

As our observation net began functioning in May 1929, we are able to give the number of sensible shocks recorded monthly for the period of 27 months ending July 1931. See Table IV.

Table IV.

Month	Wakaura					Kimiidera					Hikata					Siotu					Outside the net
	0	I	II	III	IV	0	I	II	III	IV	0	I	II	III	IV	0	I	II	III	IV	
1929																					
V	36	15	0	1	0	42	3	1	0	0	46	13	1	0	0	41	4	0	0	0	1
VI	17	8	1	0	0	45	7	1	0	0	31	8	2	0	0	36	5	1	0	0	1
VII	34	9	3	1	0	83	14	3	0	0	25	12	3	1	0	35	5	1	0	0	1
VIII	18	9	0	0	0	31	15	0	0	0	18	8	2	0	0	24	4	1	0	0	0
IX	29	11	2	0	0	49	19	1	0	0	24	15	0	0	0	25	11	0	0	0	1
X	23	6	0	1	0	51	12	0	1	0	22	14	0	0	0	32	4	1	0	0	0
XI	19	10	0	0	0	18	7	0	0	0	10	6	0	0	0	13	5	0	0	0	0
XII	20	7	1	0	0	41	16	2	0	0	17	12	0	0	0	19	5	0	0	0	0
Total	196	75	7	3	0	360	93	8	1	0	193	88	8	1	0	225	43	4	0	0	4

(*to be continued.*)

Table IV. (*continued.*)

1930																					
I	13	3	1	0	0	9	13	0	0	0	11	5	0	0	0	6	5	0	0	0	0
II	33	16	11	1	1	27	22	14	3	1	29	8	9	1	1	20	9	7	0	1	0
III	24	8	3	1	0	—	—	—	—	—	—	—	—	—	—	20	10	0	0	0	1
IV	9	5	2	0	0	—	—	—	—	—	17	8	3	1	0	20	5	1	0	0	0
V	10	7	1	0	0	—	—	—	—	—	8	14	2	0	0	20	4	1	0	0	1
VI	8	9	0	0	0	—	—	—	—	—	12	6	1	0	0	9	5	1	0	0	0
VII	7	6	2	0	0	—	—	—	—	—	15	7	2	0	0	14	4	1	0	0	0
VIII	12	4	0	0	0	—	—	—	—	—	8	8	0	0	0	6	0	0	0	0	0
IX	6	5	0	0	0	—	—	—	—	—	14	15	0	0	0	4	4	0	0	0	0
X	15	5	2	1	0	—	—	—	—	—	15	9	3	0	0	20	3	2	0	0	0
XI	11	10	3	0	0	—	—	—	—	—	17	16	2	1	0	14	4	0	0	0	0
XII	6	6	0	0	0	—	—	—	—	—	27	14	1	0	0	6	3	1	0	0	1
Total	154	84	25	3	1	—	—	—	—	—	173	111	23	1	0	159	56	14	0	1	3
1931																					
I	22	19	0	0	0	—	—	—	—	—	37	27	0	0	0	8	6	0	0	0	0
II	14	6	0	0	0	—	—	—	—	—	23	15	1	0	0	2	2	0	0	0	2
III	11	7	0	0	0	—	—	—	—	—	22	11	1	0	0	9	2	0	0	0	1
IV	24	15	1	1	0	—	—	—	—	—	36	21	4	0	0	14	4	1	0	0	1
V	16	5	1	0	0	—	—	—	—	—	29	23	3	0	0	21	2	1	0	0	0
VI	15	6	0	0	0	—	—	—	—	—	22	17	1	0	0	13	7	0	0	0	0
VII	11	5	2	1	0	—	—	—	—	—	25	10	3	2	0	4	5	2	0	0	1
Total	112	63	4	2	0	—	—	—	—	—	194	124	13	2	0	71	28	4	0	0	5

The Roman numerals in the second line of the table are the earthquake intensities at stations near the origin. As the period of the main portion of the earthquakes that occurred within the boundary of our net was almost constant, ranging as a general rule from 0·2 sec. to 0·3 sec., the intensity may be regarded as proportional to the amplitude. The maximum amplitude, accordingly, for 0, I, II, III, and IV are 0·01, 0·05, 0·1, 0·5, and 1·5, respectively, so that IV would be classed as "rather strong" and V as "strong". The shocks tabulated under the column headed "Outside the net" occurred within a distance of 50 kms. from the boundary of the net. Of these, that of May, 1929, shook the upper course of the Kino-kawa River, that of December 1930 the coast

of Awadi Island, that of March 1931 the southern coast of Awa (Sikoku) Province, and the others the south of the Arita River. Most of the shocks that occurred before 1919 could safely be supposed to belong to the group in which the origins are rather widely distributed.

The total number of earthquakes registered come to a large figure. The total for Hikata station is 934. Had Kimiidera station been still maintained, the number registered there would have undoubtedly reached 1500 shocks. If from these earthquakes we were to select the 91 shocks that were accurately recorded at more than three stations and examine their origins, the result would be as shown in Fig. 4. The majority of them are seen to belong to what may be called the Nagusa seismic zone, which coincides on one hand with the fault-line (Kamekawa fault) at the junction of the crystalline schists overlying Nagusa and neighbourhood with the lower Titibu Palaeozoic overlying the environs of Hikata, while on the other hand it is as already stated the region which has domed, or bulged outward, as revealed by the results of two levellings.

From these facts it is possible to form some idea of the mechanism of these earthquake-swarms. Upon examining the distribution of the directions of the initial motions of these earthquakes, they appear as though they are the effects of a westerly shear movement of the northern part of the fault line relatively to the south side of the line.

The number of earthquakes whose origins have been thus determined form only 10 per cent of the total number observed, but the results of our studies lead to the inference that the remainder may be safely classed in the same category as the 91 earthquakes of which we have some knowledge. Therefore the origin of these earthquake-swarms must be in Wakaura Bay, near Nagusa and Hikata Bay, and not in the Kii-Awadi Straits as first believed.

6. Progress of the Earthquake Activities.

These earthquake swarms being of a very local nature, the areas of their sensibility scarcely exceed a radius of 20 kms. At the epicentre even the feeblest shocks accompany earth-sounds, the initial tremor lasting about 1 sec., and the whole motion lasting from 1 sec. to not more than 10 sec. The worst do no more than cause cracks in plaster walls, overturn unstable objects, and only rarely throw down stone fencings, so that they could hardly arouse the interest of investigators in Japan, much less of those abroad.

In our opinion these swarms of feeble shocks are the result of stresses that we have reason to believe are now gathering on the floor of the Pacific Ocean off the Kii Peninsula (Nankaido), the seat of devastating convulsions in the past, and which, if we are to keep a watchful vigil of the possible recurrence of another outbreak from this region in the not distant future, is a phenomenon that cannot well be disregarded.

An examination of the records of the Wakayama Meteorological Station (see Table I) shows that, in the first three years following the beginning of observations in 1920, there were no variations in the earthquake frequencies from year to year. But it rose in 1923 when it reached maximum, whence it gradually declined. Our observations extend over a period of 27 months, having begun in May 1929—admittedly too short a period in which to observe the progress of activities—but on carefully studying our results the activity seems to be proceeding in much the same manner as already described in the preceding pages.

Table V. Monthly Frequency of Earthquakes in Wakaura.

Year	1929								1930					
Month	V.	VI	VII	VIII	XI	X	XI	XII	I	II	III	IV	V	VI
Frequency	52	26	47	27	42	30	29	28	17	62	36	16	18	17
	—	—	39	34	35	31	29	33	34	32	30	30	20	16

Year	1930						1931						
Month	VII	VIII	IX	X	XI	XII	I	II	III	IV	V	VI	VII
Frequency	15	16	11	23	24	12	40	20	18	41	22	21	19
	15	16	18	17	22	24	23	26	28	24	24	—	—

Table V shows the monthly earthquake frequency as registered at Wakaura, the first line being the actual number of shocks and the second line the average of 5 months (the month indicated, the 2 months preceding and the 2 months following it). The progress of the frequency can of course be seen directly from the first line. The average figures merely serve to give a general idea of the changes. By taking the average figures it will be seen that in 1930, during the 10 months preceding April activities practically took a uniform course but

suddenly declined during the 6 months that followed. In short these activities reached their peak in 1923, after which they appear to decline.

We believe that the changes in earthquake activities above discussed have also some relation to the tilt which the land block is undergoing. Actually more than one of the strong shocks pointed clearly to this possibility a fact that may indeed have an important bearing on our problem, and which we hope to be able to discuss in a later paper.

---

43. 名草地方の地震群

今 村 明 恒
小 平 孝 雄
今 村 久

1906 年以來 1919 年に至るまでの和歌山地方に於ける有感地震の回數は 1918 年の 3 回を最低とし、1911 年の 25 回を最高として年平均 14 回の程度に過ぎなかつたが、1920 年より急激に其の回數を增加し、年々 100 回を遙かに越えるに到つた。和歌山測候所の觀測に依れば、地震の性質は極めて局部的であつて、有感區域も概して 20 粁の半徑の圓内に極限せられ、震原は主として紀淡海峽にありと云ふことであつた。

吾々の南海道大地震の研究は和歌山附近に發生する此等の小地震群の活動にも連繫すべきもののあることを感じ、1929 年より和歌浦、日方、鹽津、紀三井寺に地震觀測所を設けて、此の地震群の震原分布、發生機構及び活動の經過狀態等の調査を行つてゐる。

1928 年に此の地方に行はれた水準測量の結果は、前回の測量以來 30 年間に鹽津より和歌山に到るまでの約 10 粁の間の地塊が著しい隆起、傾斜を行つて居たことを示し、其の隆起最大價約 9 糎に達してゐた。この地盤の膨みの頂點は北側の結晶片岩の層と南側の秩父古生層との接觸する東西に走る斷層附近に當り、前記各地震觀測所の觀測の結果によりて吾々の得たる小地震群發生區域も紀淡海峽にはあらずして此の地點と全く一致してゐる。なほ地震初動方向の分布狀態より見ると、この地震群に屬する地震は斷層線の北部の地塊が南部に對して關係的に西方への剪斷運動に因つて起されるものゝ樣に思はれる。4 點觀測に依つて確に震原の位置を決定することを得た 11 個の地震より、此の地方の地震波傳播速度に關聯した距離係數の價を求めると殆ど一定の 3·8 と云ふ數を得た。而してこの中震原の比較的淺い 4 個の地震はこれよりも少しく小なる價を與へて居るが、これは地表を被覆する傳播速度の非常に遲い土層の存在に基因するものと見做して差支へないであらう。地質學的に此の地方と同一系統に屬する土佐の古生層輝綠凝灰岩の彈性係數に關する長岡博士の研究より k の價を計算して見ると 2·95 と云ふ數を得る。この地震群に屬する地震は大部分地表より 5 粁以内の淺所に發生するもので、この地方の k の價は地殼上層を構成してゐると云はれる花崗岩層の k の價 8·5 に比べて遙かに小さく、反つてこの 2·95 の價に近いことを示すのは、此等の地震群發生地點が花崗岩層よりも一層淺所に存在することを物語るものであらう。

此の地震群の地震は今日までに知られてゐる限りでは、何れも小規模なもの計りで、其の最も强

いものでも災害としては僅に壁に龜裂を生じ、或は石垣を崩す程度に過ぎない、和歌山測候所の觀測によると有感地震數は 1923 年の 299 回を最高として次第に減少を示してゐるが、吾々の 1929 年 5 月以來 27 ケ月間の觀測の結果より見るも、此の間日方に於て觀測した地震回數 974 回の多きに達してゐるが、矢張り全體として次第に減少の傾向を示してゐる。

過去の南海道沖合に發生した大地震に伴つた紀伊半島の急性的地形變動や、最近の水準測量に依つて明かにされた慢性的地形變動の有樣等を照合して見るに、此の地震群發生の根本原因は現時南海道方面に蓄積されつゝあると想像される歪の局部的發散にあると考へられる點があるので、此の地震群の研究は南海道大地震の將來に對しても輕視することの出來ぬものであらう。

44. 地震に伴ふ發光現象の調査

地震研究所　武　者　金　吉

（昭和七年一月十七日發表——昭和七年六月十五日受理）

I. 廣島縣北部地震の發光現象

1930 年 12 月 20 日廣島縣雙三郡布野を震央とする强震に際し、或る未知の人から發光現象を觀察したと云ふ報告に接したので、直ちに震央を中心とし直徑約 40 キロの圓の內に含まれる中等學校、小學校、及び町村役場に照會して報告を求めた。集つた報告は極めて僅少に過ぎなかつたが、槪略次ぎの如き事實を知る事が出來た。

震央の東微南約 21 キロに位する庄原町では、北方に火事の如き赤き光を認め、之を見た人々の中には、三瓶山の噴火ではないかと云つた人もあつた。この光は瞬間的のものではなかつたらしい。色が赤くて火事に似て居た點、及び瞬間的でなかつた點が、伊豆地震の時に、伊東で地震研究所の那須理學士等によつて觀察された發光現象に酷似する。また庄原町から北微西に當つて火球が昇り上空で消失し、其の後で四邊が明るくなつたのを觀察した人もあつた。火球が消失してから空が明るくなつた例は伊豆地震にもあつた。[1] 其の理由は不明だが、兎に角注意すべき事實である。また同じく庄原町から西北西の方向に、紫電色閃光的放散狀の光を認めた人もある。

震央の北東約 5 キロに位する君田村の或る報告者は、始め南東、ついで北西、東の順に光を認め、其の色は白であつた。また同地の他の報告者は、20 日の强震と 21 日の餘震と兩回に發光を觀察した。前者は北東で、遠方の火事を見る如く、後者は北及び南で、矢張同樣の光であつた。

震央の北東約 11 キロの口北村では、地震を感ずると同時に、山の端から箒を倒さに立てたやうな光が天に冲し、雲に映じ、色は火事の如く、上に至るに從つて淡くなつて居た。なほ其の外に、最初は北西に、次ぎに南東に、次いで北方の山の端から空に向つて一面に明るい光が見られた。

以上の報告を總括すると次ぎの如くなる。

---

1) 武者金吉「昭和五年十一月廿六日伊豆地震に伴ひたる光の現象に就て」地震研究所彙報第九號第二册 (1931), 184。

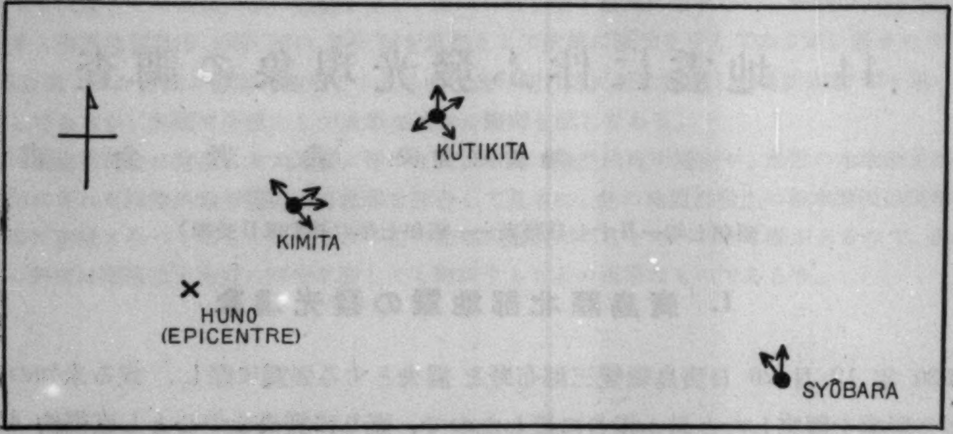

Fig. 1. Directions in which luminous phenomena were observed. (Hirosima Prefecture Eqk.)

(1) 光は唯だ一ケ所だけでなく、何ケ所にも現はれた。

(2) 光の種類は (a) 漠然たる瞬間的の光、(b) 漠然たる非瞬間的の光、(c) 火球狀の光、(d) サーチライト狀の光の四種であつた。

(3) 光の色は區々として一致を見ないが、赤色の卓越する事は注意に値する。

而して地震の當時廣島電氣會社の送電が停止されたと云ふから、斷線した所があつたのかも知れない。從つて送電線の切斷或は接觸による發光もあつた事であらう。併し、伊豆地震の場合と同じく、送電線のスパークのみでこの現象の全部を說明し去る事は、自分には困難と思はれる。

II. 多摩丘陵北西部地震の發光現象

1931 年 6 月 17 日 21 時 9 分 50 秒に發したる、八王子の南 3 キロの地點を震央とする强震には、東京及び近郊に於て發光現象を觀察した者が多かつたので、調査を試みた。資料は東京市の中等學校一と厚木町の中等學校二より得たものが大部分を占める。それに既知未知の人々から惠與された數例、及び寺田敎授御蒐集の分を頂いて、全部で 140 例を得た。先づ各地で光を觀察した方向を地圖に記入して見るに[2]、極めて亂雜で、其の方向が一ケ所或は數ケ所に輻合する所ではなく、卓越せる方向さへも見出し難いと云つて差支ない。發光地點を確める事なぞは全く絕望である。思ふに發光した地點が非常に多かつたのであらう。

2) 厚木高女からの資料 38 には觀察した場所が記載してなかつたので、地圖に記入する事が出來なかつたのは遺憾である。

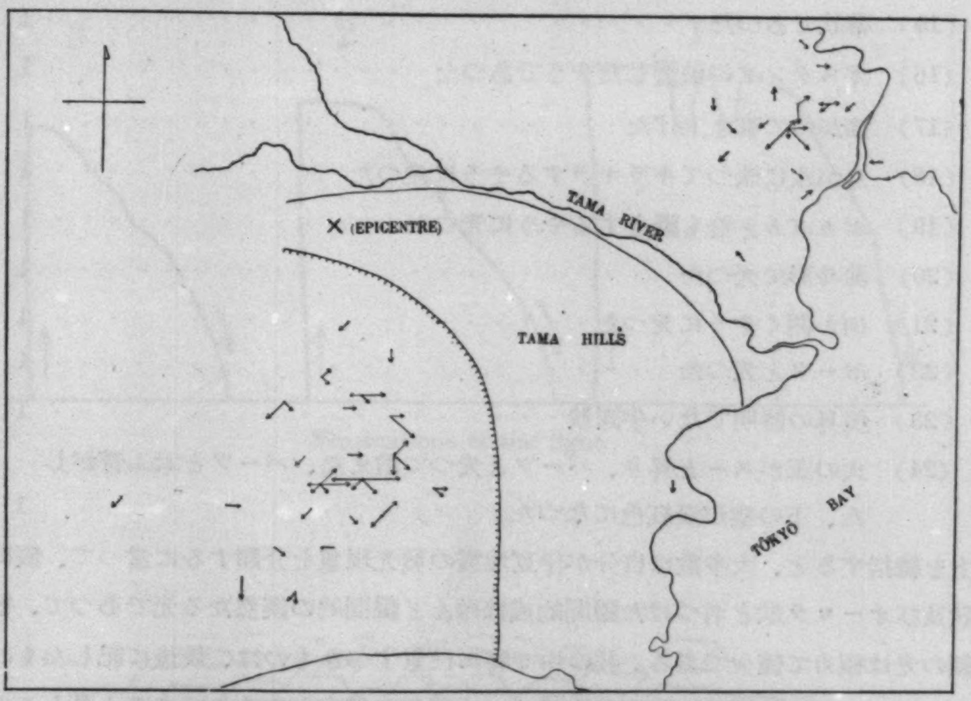

Fig. 2. Directions in which luminous phenomena were observed. (Tama Hills Eqk.)

光り方の種類を分類すると次ぎの如くなる。

(1)	電光のやうに光つた	28
(2)	パツと光つた	26
(3)	一面に光つた	8
(4)	光が横に棚引いた	8
(5)	細長く光つた	6
(6)	波狀に光つた	4
(7)	扇形に擴がつた	3
(8)	一面にボーツと光つた	2
(9)	電光形の如く光つた	1
(10)	横に何か燃えるやうに光つた	1
(11)	稻妻を大きく廣くしたやうに光つた	1
(12)	火の塊を空から落したやうに光つた	1
(13)	圓形に光つた	1
(14)	丸くだんだん大きくなつた	1

(15) 帶狀であつた・・・・・・・・・・・・・・・・・・・・・・・・・・1

(16) ガスタンクの破裂したやうであつた・・・・・・・・・・・・・・・1

(17) 擴がつて噴き上げた・・・・・・・・・・・・・・・・・・・・・・・1

(18) 月が水に映つてキラキラするやうに光つた・・・・・・・・・・・・1

(19) ポカポカと恰も瞬きするやうに光つた・・・・・・・・・・・・・・1

(20) 漏斗形に光つた・・・・・・・・・・・・・・・・・・・・・・・・・1

(21) 何か開くやうに光つた・・・・・・・・・・・・・・・・・・・・・・1

(22) ボーツと光つた・・・・・・・・・・・・・・・・・・・・・・・・・1

(23) 境界の鮮明でない半圓狀・・・・・・・・・・・・・・・・・・・・・1

(24) 火の玉がスーと昇り、パーツと光つて消えた、バーツと云ふ音がした、下の空が淡紅色になつた・・・・1

以上を總括すると、大多數は自分が伊豆地震の發光現象を分類するに當つて、假に電光狀及びオーロラ狀と名づけた瞬間的或は殆んど瞬間的の漠然たる光であつて、他の種類の光は極めて僅少である。其の中で特に注意すべきものは、最後に記したものであつて、これは牛込區肴町停留所附近で一中學生の觀察したものである。若しこの報告が文字通りに信じ得るものとすれば、伊豆地震に靜岡縣庵原郡松野村で天野八代氏の見たものと殆んど同じである。火の玉が消失して後、空が淡紅色を呈したと云ふ點までよく一致する。また廣島縣北部地震に、庄原町で觀察されたものにもよく似て居る。この報告者は自分の直接知つて居る學生で、彼の云ふ所は多分虛僞や誇張ではないであらう。少くも上記の如く彼の眼には見えたのであらう。而して自分は彼に對して天野氏の觀察を話した覺えはない。勿論自分の伊豆地震の報文を讀んだ事はない筈である。但し彼はかなり强度の近視眼である。

次ぎに注意すべきは橫濱市中區相生町より南方に見えた光で、形は第三圖に示す如く、色は中心が靑白に近く、周圍は螢光色に似て、X線の色よりも少し靑味濃く、尙ほ少しく白味を加へた如くであつたと云ふ。發光の回數は三回で、一回の光の繼續時間は 3-4 秒、光と光との間隔は 5-6 秒位、光つて居る間に fluctuation を示した事も、また圖の如くである。音響は伴はなかつた。

光の色を分類し、統計をとると次ぎの如くなる。

(1) 靑色或は靑みがゝつた色・・・・・・・・・・・・・・・・・・・・21

(2) 赤と黃との混合色・・・・・・・・・・・・・・・・・・・・・・・16

(3) 電光の如き色・・・・・・・・・・・・・・・・・・・・・・・・・11

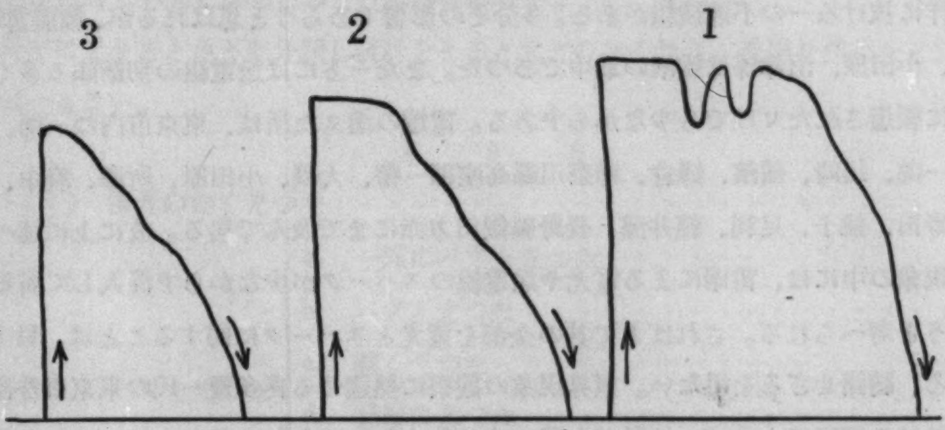

Fluctuations of the light.

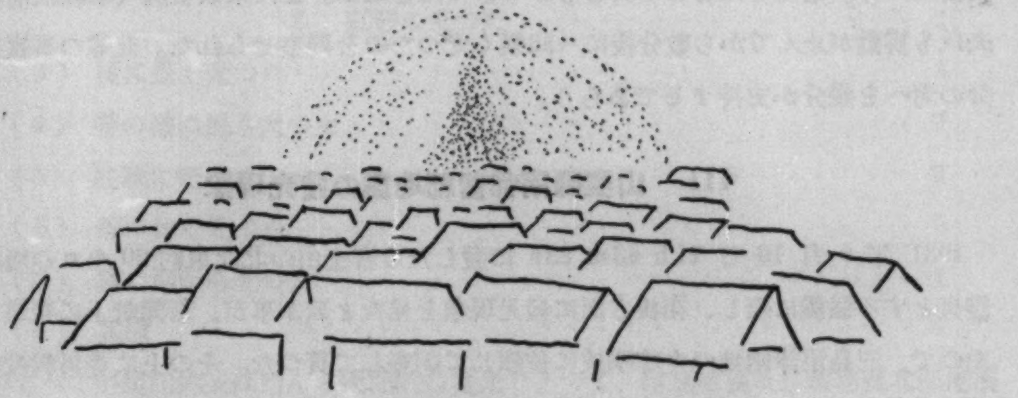

Fig. 3. Luminous phenomena observed in Yokohama.

(4) 黄色或は黄がかつた色 ・・・・・・・・・・・・・・・10
(5) 赤色或は赤みがかつた色 ・・・・・・・・・・・・・・10
(6) 赤と青との混合色 ・・・・・・・・・・・・・・・・・9
(7) 青と黄との混合色 ・・・・・・・・・・・・・・・・・9
(8) 電燈の如き色 ・・・・・・・・・・・・・・・・・・・6
(9) 白色 ・・・・・・・・・・・・・・・・・・・・・・・2
(10) 其他 ・・・・・・・・・・・・・・・・・・・・・・・4

上記の如く青色或は青みがかつた色が最も多く、とりわけ青白色が多く、21 例中の 11 例を占めて居る。

地震の當日 18 時の天氣圖を見るに、日本海上に 760 mm の高氣壓あり、東海道の南方洋上に 758 mm の低氣壓あり、其の中間に、九州をほゞ東西に貫き、瀬戸内海に沿ひ、近畿より本州中部を經て、伊豆半島を斜めに過り、房總半島の南端をかすめて

太平洋に抜ける一の不連續線がある。多分その影響であらうと思はれるが、發震當時、大磯、小田原、沼津等は雷雨の最中であつた。また一方には送電線の切斷頗る多く、新聞に報道されただけでも少なからずある。電燈の消えた所は、東京市内の一部、近郊の一部、川崎、横濱、鎌倉、神奈川縣高座郡一帶、大磯、小田原、所澤、府中、浦和、野田、銚子、足利、輕井澤、長野縣飯田方面にまで及んで居る。故に上に述べた發光現象の中には、雷雨による電光や送電線のスパークが少なからず混入して居るであらうと考へられる。さればとて其の全部を電光とスパークに歸することは、目下のところ、躊躇せざるを得ない。氣界現象の觀察に熟達せる喜多豊一氏の東京市外瀧ノ川に於ける觀察によれば、地動が人體に感じなくなつてもなほ發光を見、しかも其れは雷雨に伴ふ電光とは著しく異るものであつたと云ふ。また東京帝國大學教授清水武夫氏も震動が止んでから數分後に一回强く光つたのを觀察せられた。此等の事實は自分の考へを幾分か支持するであらう。

III. 山梨縣南都留郡地震の發光現象

1931 年 9 月 16 日 21h 43m 23s に發したる富士山の北北東約 20 キロの地點を震央とする强震に際し、箱根方面に發光現象を見たと云ふ事が、新聞紙上に報道されたので、三島沼津兩地の中等學校に依頼して調査して貰つた。その上に寺田教授御蒐集の分其他を加へて 37 の資料が集つた。

光を見た方向を地圖に記入すると、第四圖の如くなり、可なり亂雜ではあるが、箱

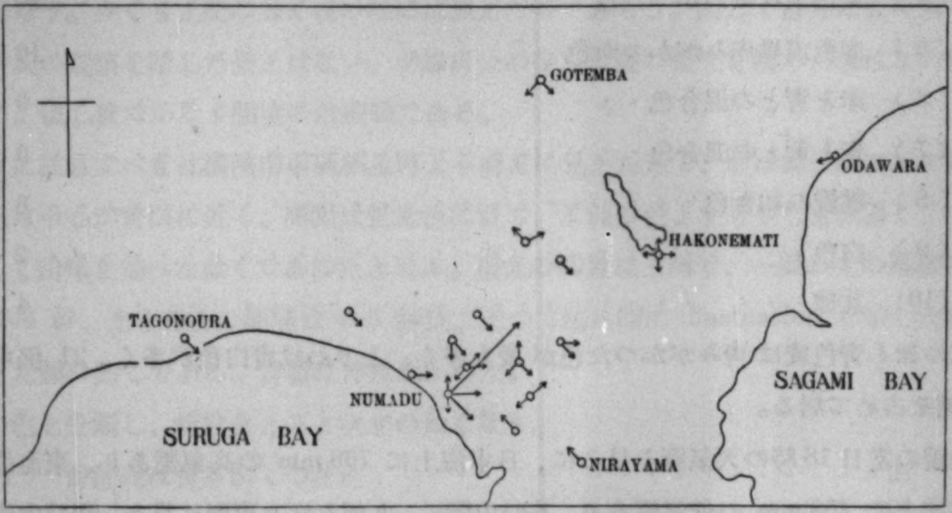

Fig. 4. Directions in which luminous phenomena were observed.
(Yamanasi Prefecture Eqk.)

根方面に著しい光を認めた事だけは爭はれない。

次ぎに光り方と色とを分類し統計をとると次ぎの如くなる。音響を伴つたと云ふ報告は一もない。

光り方

(1)	電光の如く光つた		9
(2)	パツと光つた	a. 一面にパツと光つた	4
		b. パツと光つた	3
		c. 圓く光つた	3
		d. 扇形に光つた	1
		e. 半圓形に光つた	1
		f. 虹形に光つた	1
(3)	横に長く光つた		4
(4)	帶の樣に長く光つた		2
(5)	柱狀に光つた		2
(6)	線の如く光つた		2
(7)	雲の間から光つた		1
(8)	其他		4

其のすべてが瞬間的或は殆んど瞬間的の發光であつて、伊豆地震及び廣島縣北部地震に於て觀察せられた如き非瞬間的のものは、一も報告されなかつた。

光の色

(1)	赤と靑との混合色	6
(2)	黄色或は黄がゝつた色	6
(3)	赤と黄との混合色	6
(4)	靑色或は靑みがゝつた色	5
(5)	靑と黄との混合色	3
(6)	赤色或は赤みがゝつた色	2
(7)	電光の如き色	1
(8)	白色	1
(9)	電燈の如き色	1
(10)	其他	5

光を見た時間は大多數が震動の未だ止まない中である。例外として 8h-9h に見た

と云ふのが１例、發震の數十分後に見たと云ふのが１例ある。また特に重要な報告は箱根町の石内氏から惠與されたもので、同地では地震の數日前から地震後に至るまで、夜間稻妻の如き光が毎晩光つて居た。その光は稻妻の如き光色であつたが、稻妻の如くジクザクの形をなさず、探照燈のやうに、山から山へ頭上を半圓形に光つたと云ふ事である。この報告に誤りがないとすれば、甚だ有趣であり且つ貴重なる資料と云はざるを得ない。

IV. 南日向地震の發光現象

1. 緒　言

1931年11月2日19時3分5秒に、宮崎市を距る東北東90キロの日向灘海底に發した地震は1930年11月26日の伊豆地震に匹敵する程度の地震であつたが[3]、海底地震なりしため、幸ひにして被害の著しいものはなかつた。併しこの地震は、發光現象に關しては、伊豆地震について興味ある資料を我等に提供して呉れた。今、寺田教授、那須理學士、及び自分の蒐集した355例の資料に基いて

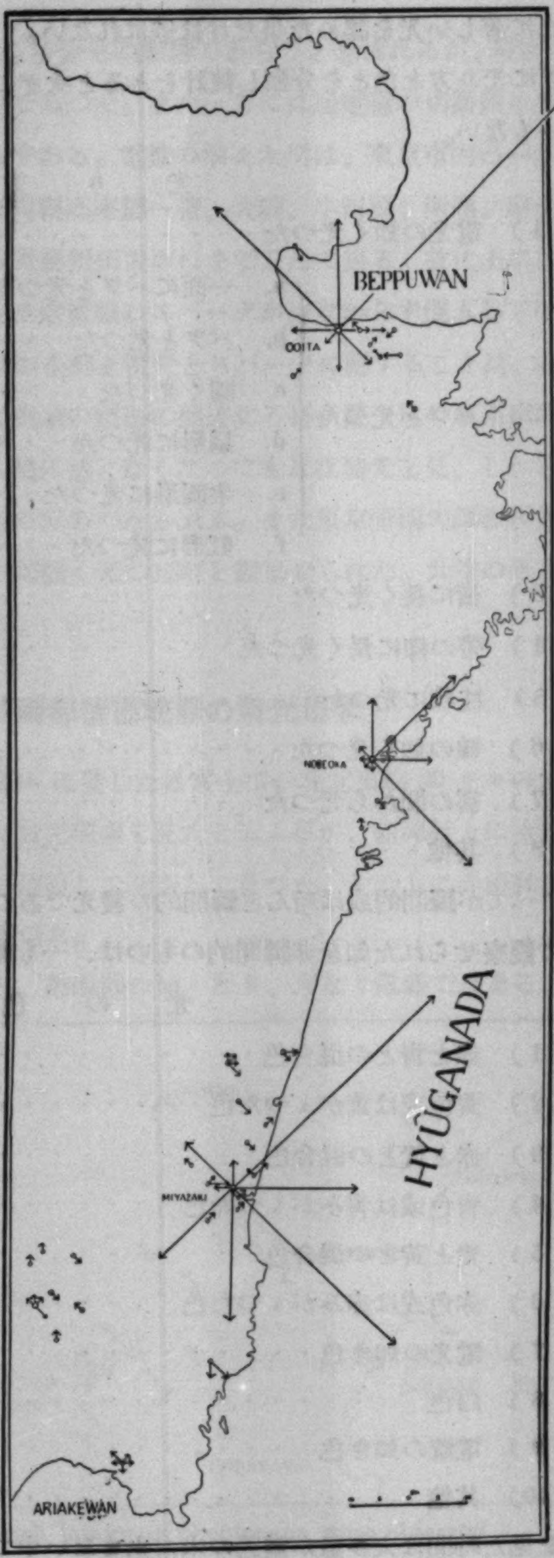

Fig. 5. Directions in which luminous phenomena were observed. (South Hyūga Eqk.)

3) 中央氣象臺國富技師の談話による。

調査した結果を略說すれば、次ぎの如くである。

2. 光の觀察された範圍

光の觀察された範圍は、北は別府灣の北岸から南は有明灣の北岸に至るまで、約200キロに亘つて居る。その間に全く報告のない處が少なからず介在して居るが、報告がないからとて、其等の土地で光が觀察されなかつたと斷定する譯にはゆかない。また光を觀察した者がないと云ふ報告をした二三の町村役場もあるが、充分調査した上の報告かどうかは疑はしい。また西の極限卽ち海岸から最も離れて居る處は、都城附近で、海岸から約40キロであるが、これも始めから成るべく海岸に近い處を選んで照會したのであるから、これを以て眞の西の極限とする事は出來ない。

Fig. 6.

3. 光の見えた方向

各地で光の見えた方向は第五圖に示す通りであつて、大分、延岡、宮崎及び其等の都市の附近に於ては、別府灣或は日向灘の方向に多數の人々が光を見たことが知られる。なほ寺田敎授の御敎示に從ひ、大分、延岡、宮崎及び其等の附近の矢を各〻一括して、三つの group とし、vector diagram を作つて見ると、其の結果は第六圖の如くなつて、其等の各地では、孰れも矢が海の方に向ふことになる。

4. 光り方の種類

光り方の種類を分類すると次ぎの如くなる。

（1）	下より上に放射狀に擴がる光	106
（2）	電光の如き光	47
（3）	地上より空に探照燈を照射したる如き光	23
（4）	横になびくやうな光	7

(5)	棒狀或は箒狀の光	7
(6)	幕狀の光	7
(7)	直線或は曲線形の光	6
(8)	線電の如き形で下より上に動く光	5
(9)	一面に空が赤く見えた	1
(10)	其他分類し難きもの	21

以上の中で (2) は最も曖昧なもので、多分その中には (1) や (4) や (6) が混入して居るであらうことを認めるが、其等を識別する事は困難である。また光り方と光の見えた方向との間に關係があるか無いかを調べて見たが、充分な關係を見出すことは出來なかつた[4]。

5. 光 の 色

光の色の統計をとつて見ると次ぎの如くなる。

(1)	青色或は青みがゝつた色	84
(2)	電光の如き色	31
(3)	黄色或は黄がゝつた色	30
(4)	青と赤との混合色	23
(5)	白色	20
(6)	黄と赤との混合色	20
(7)	赤色或は赤みがゝつた色	14
(8)	黄と青との混合色	11
(9)	電燈の如き色	4
(10)	サーチライトの如き色	1
(11)	石炭瓦斯の燃燒する時の色	1
(12)	其他	28

光り方や光の見えた方向と色との關係もまた調べて見たが、これまた其等の間に判然たる關係の存在すると云ふことは見出されなかつた。

6. 發光を生ぜしめる可能性ある原因

以上述べたる發光現象が惹起される可能性ある原因には、(1) 火事、(2) 雷雨、(3) 山崩れ、(4) 送電線のスパーク、(5) 流星等を擧げる事が出來る。以下その各々について

4) 例外として大分がある。其れについては後に記す。

簡單な検討を試みて見る。

(1) 火事　この地震には前に記した如く、被害の著しいものがなかつた。自分の知る限りに於ては地震のために生じた火事も全くなかつた。また光り方も火事の光とは全然違ふ。故に少くもこの地震については、火事は全く考へる必要がない。山中の炭焼竈ぐらゐは崩壞して發火したかも知れぬが、これ等は殆んど問題にならないであらう。

(2) 雷雨　中央氣象臺發行の天氣圖によると、發震當時には 774 mm の高氣壓が日本海中部にあつて全國その支配の下にあり、雷雨の起り相な形勢は全く見えない。氣象要覽によるも、發震當時に於て九州の東部に雷雨は絕無であつた。從つてこの地震の場合には普通の電光も問題にならない[5]

(3) 山崩れ　山崩れに基く發光現象の存在する事は伊豆地震の發光現象の調査報文にも記載し[6]、また寺田教授の御研究の結果も發表されて居るが[7]、この地震によつて著しい山崩れが生じたかどうかは明でない。地震研究所の那須理學士は多少の山崩れを観察された相であるが、同地方で發行さるゝ新聞が全く問題にして居ない所から見ると、恐らく顯著な山崩れはなかつたのであらう。故に山崩による發光の有無は、目下のところ肯定も否定も出來ないが、其の可能性が乏しいやうに考へられる。

(4) 送電線のスパーク　大分、宮崎、都城では地震と同時に電燈が消えた[8]。同地方で發行される新聞によれば、大分市及び其の附近で高壓線の切斷したものが、七本あつた。延岡町海岸にある日本ベンベルグ絹絲株式會社延岡工場の高壓線からスパークを發した[9]。福島町の變電所からも發光したと傳へられて居る。從つて今回観察された發光の中には、送電線の接觸或は切斷による光が少なからず混じて居るであらう。

---

5) 但し發震の數日前から空中の電氣狀態に異常があつたのではあるまいかと考へられる理由がある。即ち都城市で地震の數日前からラジオに多少の障碍があり、發震當時は感度が非常に微弱になつたと云ふ事である。これは甚だ有趣なる報告であるが、たゞ一例のみで速斷は出來ない。或は其の家のラジオセツトに故障があつたのかも知れない。

また地震前後の雲の變化を調べるために大分測候所に問合せたるところ、所長山川軍治氏より次ぎの如き回答があつた。午後六時雲量 10 KC. CK. 午後十時雲量 10 SC.

6) 武者金吉、「昭和五年十一月廿六日伊豆地震に伴ひたる光の現象に就て」地震研究所彙報第九號第二册 (1931).

7) T. Terada, "On Luminous Phenomena accompanying Earthquakes" 地震研究所彙報第九號第三册 (1931).

8) 今村博士によれば、福岡では電燈が消えなかつたが、佐賀では消えた。中央氣象臺國富技師によれば、下關及び高知でも電燈が消えた。

9) 1000 V の電線三條 (其の間隔 0·45 m 及び 0·90 m) が電柱と電柱との中間にて擦れ合ひ、三線ともスパークした。發光は唯だ一回にて斷線はしなかつたと云ふ。(同工場の報告による)

併し其れだけでこの現象の全部を説明するのは困難である。

(5) 流星　今回の地震の發光の報告の中には、地震のあつた夜に流星が多く見られたと云ふ報告が少くない[10]。理科年表によると、丁度この地震の發した頃は、牡牛座λ流星群の出現する時期に相當する。また報告された光の中にも比較的大なる流星らしきものがないでもない[11]。故に今回の地震に觀察された光の一部は流星であつたかも知れない。併し流星でこの現象の全部を説明する事の出來ないのは勿論である。

强震或は烈震の後では、恐怖した人々が餘震の襲來を怖れて戸外に居ることが多いから、從つて流星を觀察する機會の多いことは云ふまでもない。併し古來の地震記錄には、地震の夜に多くの流星の觀察された例が必ずしも稀でない[12]。例へば 1703 年（元祿 16）關東地震には發震の前から流星が多く見られた[13]。1805 年伊太利 Campagna 及び Molice の地震には、他の發光現象と共に流星が觀察された[14]。1889 年（明治 22）熊本地震には、地震の夜に多くの星が流れた[15]。1908 年 Reggio 及び Messina の地震に、Prof. Di Stefano 夫妻は流星のやうな多くの光の點を目擊した[16]。1911 年 11 月 16 日中歐の地震には、獅子座流星群が著しく現はれた[17]。自分は流星と地震との間に關係があるとは主張しないが、地震の發光現象の中には、或は流星と紛らはしきものも實際に存するかも知れぬ、從つて脚註 (11) に記載した發光現象の如きも、輕々しく流星と斷定を下すことは出來ない。この點に關しては尙ほ將來注意して確めたい。

7. 海上に現はれた發光現象

以上述べた如く、今回の地震の發光現象には、送電線のスパークもあつたであらう。

---

10) 「非常に星が飛んだ」「その夜はわけて流星が他日より多かつたと思ふ」「星が非常に多くいくらでも飛んだ」「流星が多く五つ見た」「星がしきりに隕ちた」「流れ星が落ちました」「流星あり」「澤山の星が飛ぶ」等の報告がある。

11) 延岡町で北方に見えた光の如きは斜めに棒狀をなし、目擊者も「初めは流星かと思はれしも翌朝の新聞にて怪光なりと知る」と附記して居る。

12) この事實は寺田敎授の御注意による。

13) 「廿二日の夜、月の色かわり、ひかり物相見へ、星ながれ候事繁く」（基熙公記）「元祿十六年十一月二十一日、晴天、丑半刻〔即ち地震後〕ヨリ星落飛デ曉ニ至ル」（甘露叢）。

14) I. GALLI, Raccolta e classificazione di fenomeni luminosi osservati nei terremoti.

15) 「南方の恒星絕へず位置を變し（俗に夜這星といふ）晃々として左右斜めに飛行するや數ふるに遑あらず」（翁巷迂叟、熊本明治震災日記）。

16) I. GALLI.

17) AUGUST SIEBERG, Erdbebenkunde 及び MONTESSUS DE BALLORE, Sur les phénomènes lumineux ayant accompagné le tremblement de terre de la Raube Alb. le 16 novembre 1911. (*Comptes Rendus Hebdomadaires des Séance de l'Académie des Sciences*, 1914.)

また其の一部は流星であつたかも知れない。併しそれでは如何にしても説明し得ないのは、海上に現はれた發光である。これは別府灣内に現はれたものと、日向灘の海上に現はれたものとの二つに分けられる。

[A] 別府灣内の發光 (1) 大分新聞によれば、大分市辨天島の海上に數本の電光の柱が立ち、其れが大きい光の幕を張つたやうに見え、其の間僅か十分間だつたが、名狀すべからざる光景を呈したと云ふ。

(2) 大分商業學校教諭今村義市氏によれば、同氏は地震襲來後直ちに、大分市鹽九升町から北東の海上と思はれる邊に、薄赤色の恰も霧のたちこめた空中に垂直に探照燈を照射したやうな光を約一分間觀察した。

(3) 今村教諭以外に、大分市及び其の附近で、別府灣の方向に柱狀、圓筒狀、煙突狀等と形容せられる光を見たと云ふ報告が 24 ある。(其他の方向に見た光は「風呂敷をひろげたやう」「火煙狀」等と形容され、柱狀といふのは一つもない。)

(4) 別府灣北岸の日出町(大分より別府灣を距てゝ北西約 16 キロ)からも、大分市の方向に柱狀の光を見たと報告されて居る。

以上の報告によると、多少記す所に一致しない點もあるが、(1) 大分市辨天島附近の海上に光が現はれ、(2) 其の光はサーチライトを天に向けて照射したやうな形で、(3) しかも其の光は瞬間的のものではなかつたと云ふ事は信じて差支なさ相である。この發光現象を伊豆地震に際して、震央の附近に現はれた光と比較するに、全く符節を合する如くである[18]。

[B] 日向灘海上の發光 (1) 地震研究所の那須理學士が震災地出張の際聽取された所によると、土々呂村の池田丸と云ふ漁船は、丁度地震の時内海(宮崎市の南々東約 17 キロ)の沖合 12 里或は 13 里の所に居つた。ところが午後7時頃、船員一同は自分達の船が急に搖れ出し、舟は立ち、今にも轉覆せんかと思つた。其の時搖れると同時に海面より船員達の眼前に忽ち火柱が立つたので、船員達は皆大恐惶を來し、口々に御題目を唱へるやら、全く生きた心地がなかつたと云ふ。

(2) 土々呂、延岡、宮崎、南那珂郡東鄉村等で光を見た方向は大多數が海の方向である。

この二つの事實から、日向灘海上の發光は多分事實であらうと思はれる。陸上で海

18) 靜岡縣多賀小學校の報告によれば、同地から西北西に當り、探照燈より白光を帶びた柱狀の光が天に冲するのを見た。靜岡縣田方郡中鄉村の清水吉彦氏は、丹那盆地の南方と思はれる地點に斜めに照射するサーチライトの如き光を見たと報告せられて居る。

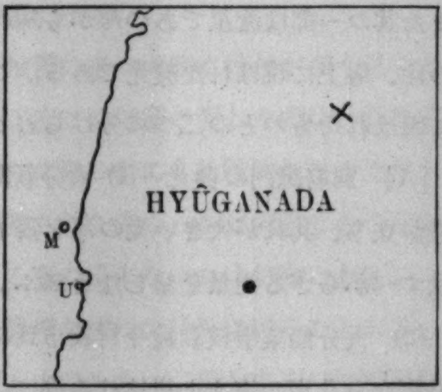

Fig. 7.

× Epicentre.
● Position where a pillar of fire appeared.
M Miyazaki. U Utiumi.

の方に光を見た人々の全部が、海岸から見たのでない事は勿論である。故に目撃者の位置と海岸との間に、送電線の切斷或は接觸による發光でもあつたのではないかと云ふ疑ひはないでもない。實際に其の樣な場合もあつたかも知れないが、最も海岸に近い地點で光を見た一人だと考へられる、延岡の日本窒素會社の小使も「海の方」に光を認めたと云つて居る。延岡驛長の報告にも、「東方海上に當つて普通の稻妻と異る發光が電光形に發しましたが、其の光は稻妻の如く强く眼を射る樣なものでなく、藤色がゝつたもので、其の範圍も相當に廣く、單なる送電線の切斷によるスパークの如き比ではなかつた相です」とある。

(C) 海上發光の例 地震に際して海上に發光の出現した事は獨りこの地震に限つた事ではない。Galli によれば、1783 年 2 月 6 日 Messina 及び Reggio の地震には、海から光が出た。1836 年 4 月 24–25 日の Calabria 地震には、beam 狀の光が波上に現はれ、Talentino 灣の水中に沒した[19]。1923 年關東地震には、東京灣口の邊に火柱が立つたと云はれて居る[20]。また 1930 年の伊東地震群の中の最大の地震の時、伊東附近の海中から火の玉が飛び出した事が、漁夫によつて觀察されて居る[21]。

(D) 海底の火山活動 日向灘に於て火柱を目擊した船員等は、この地震は海底火山の爆發のために相違ないと云つた相である。これは無智な漁民の言として一概に斥ける譯にはゆかない。Sieberg も海面に於ける發光及び火焔現象は海底火山活動と直接に關係して居ると云ひ、[22] Jaggar も前に揭げた東京灣口の火柱を海底噴火のためとした。[23] 併し少くもこの地震の場合には、海底の火山活動で之を證明する事は困難である。發光現象以外に海底火山の活動を肯定すべき資料が全くない。

8. 音 響

音響について記載のある報告は僅か七例に過ぎない。其の中で音響は聞えなかつた

19) I. Galli, Raccolta e classificazione di fenomeni luminosi osservati nei terremoti
20) 1923 年 10 月 17 日報知新聞及び中村(左)博士奥丹後地震報告。
21) 地震研究所那須理學士及び中央氣象臺國富理學士の談話による。
22) Sieberg, Erdbebenkunde.
23) 1923 年 10 月 17 日 報知新聞。

と云ふのが三例、鈍い音がしたと云ふのが二例、砂利溜にトラックを乗り上げた様な音がしたと云ふのが二例ある。思ふに上記の四つの例は、多分地震に伴ふ普通の地鳴であつて、光そのものには音響を伴ふことがなかつたのであらう。

9. 光の現はれた時間

光を觀察した時間を記載してある報告は 147 例ある。併し其の記す所極めて曖昧で、眞相を知るに苦しむが、大體次ぎの如くである。

(a) 發震前に見たもの 26

(b) 發震と同時或は地震の最中に見たもの 99

(c) 地震後に見たもの 22

發震前に光を見たと云ふ中に、「二三分前」「十秒前」「五秒前」「一秒前」等と時間を明記してあるのもあるが、此等は時間の計測に熟練して居ない者の報告であるから、充分に信用は出來ない。また「地震の直前」と云ふのは、嚴密な意味に於ては、發震前とは云ひ難いであらう。斯くの如き怪しげなる報告を除外すると、明らかに發震前に光を見たものは次ぎの四例に過ぎない。

(1) 地震の前夜にも時々ピカピカ光つたやうに思はれた。(宮崎市)

(2) 11 月 2 日 13 時 30 分頃、宮崎縣東諸縣郡倉岡で、紫色の美しい光を放つ雲を見た。

(3) 地震の約 4 時間前に、宮崎市高千穗通から南西の方向に、白色半圓形に近き弧狀の光を見た。

(4) 地震の約 20 分前に、宮崎市外檍村で、東北東の方に前者と同様の光を見た。(3 と 4 は同じ人の觀察)

この中の (1) は報告者自身の記憶が不確實なのだから問題にならない。

(2) は宮崎商業學校の二年生が、自宅の二階で勉强して居ると、窓に紫色の光がさした。怪しんで窓を開いて見ると、紫色の細長い極めて美しい雲が空に浮んで居た。其の雲が北西から東の方へ移動し、約 8 分ばかりの後もとの場所と少し違ふ所に止り、10 秒ほどの後消失した。家族の人々も何事か起る前兆ではないかと云つて心配して居ると、其の晩に地震があつたと云ふのである。

この報告は、雲の動き方の記載が不明瞭ではあるが、極めて著しい紫光を放つ雲が出現した事は事實であらう。多分この現象は彩雲であらう。これが地震の前驅的現象

なりしや否やは、勿論斷言し難いが、地震の前に空や太陽の色が紫色になつたり、火山の噴火の時に、紫色の雲が出たと云ふ記錄があるから、將來の參考に記して置く[24]。

(3) に揭げた地震の 4 時間前と云ふ報告は、其の時間は充分正確でないまでも、大體に於て誤りないものと思はれる。其の時間は凡そ 15 時位に當る。卽ち白晝である。白晝に見えたとすれば、其の光は極めて强烈なものであつたに違ひないが、記載が簡單で詳細を知り得ないのは遺憾である[25]。

(4) に揭げた地震の約 20 分前に光を見たと云ふ檍村は海岸の聚落であり、且つ光の見えた方向が震央の方向である點に於て、この報告は極めて貴重である。地震の前に光の方が先きに現はれたと云ふ事は、古來其の例に乏しくないが、爰にまた其の一例を加へる事が出來た。但し目擊者が唯だ一人であつた事は、やゝ物足りない感がする。

地震と同時或は地震の最中に光を見た者の最も多い事は、今まで自分の調査した他の地震についても同樣であつた。

報告者の用ひて居る「地震の後」と云ふ言葉は、色々な意味に解される。「發震の後、震動の未だ終らぬ中」と云ふ意味にも解される。この場合には地震の最中と同意義になる。「震動を人體に感じなくなるや否や」と云ふ意味にもとれるし、また「震動が感じられなくなつてから相當の時間を經て」卽ち「震動とは全く無關係に光つた」と云ふ意味にもなる。實際に其等の總ての場合が、この言葉の中に含まれて居るのであらう。少くも 11 月 2 日 19 時 3 分 5 秒に發した最初の shock とは無關係に光つたらしい報告には、「八時前後」「九時すぎに一回」「十時頃に一二度光る、其後五分ほどして割合に烈しい地震あり」「十時すぎに一回」「强震後十二時まで五六回見た」等が

---

24) Galli によれば、1832 年 3 月 13 日 Emilia の地震の前に霧が立ちこめて居た、其の後霧が霽れ、空が紫色になり、やがて最も强い shock が來た。また 1905 年 9 月 8 日 Calabria 地震の時には紫色の太陽を見た者があつた。1640 年（寬永 17）6 月 13 日の北海道駒ケ岳噴火の時、松前で見た所によると、「丑寅より紫雲色々出、其雲四方へ散、頓て少々づゝ灰降」とある。1847 年（弘化 3）3 月 24 日の善光寺地震には、11 日前の 3 月 13 日に「日輪の下に飪の如く五色に一の字を引」いたやうな光象（?）が現はれた。1855 年（安政 5）江戸地震には、其の日の早朝下總成田で太陽が濃紫色に見えて、恰も臙脂にて彩つた樣に見えた。また 1856 年（安政 3）北海道駒ケ岳噴火の時には、「俄に震動雷電して、何となく氣分惡くなりけるゆえ、障子を明て表を見るに、向の山に五色の雲起り、人の形のやうなる物其邊を飛行するやうに見えければ、大に驚き、早々障子をしめんとする時、家内震搖して戶障子忽倒けり」とある。

25) 白晝に發光現象の見られた事は前例がないではない。1783 年 2 月 5 日 Messina の地震に、光が白晝見えたと云ふ事が Galli の蒐集の中にある。1923 年（大正 12）9 月 1 日關東地震の起つた日の朝、深川から東京灣の方にピカピカ光るのを認めた人があり、また埼玉縣川口町で、屋根の上で見張りをして居た人が、東京灣方面に見える光（?）の强弱で、餘震の襲來する二三分前に、其の餘震の强さを豫言したと云ふ。

ある。この事は餘震を考慮する事なしには論ずる事が出來ない。確かに餘震に伴つて光が現はれたと考へて不合理でない若干の報告がある[26]。

氣象要覽によると、2 日 24 時までの間に合計 11 回の餘震があつた。

$19^h\ 20^m$	$19^h\ 31^m$	$20^h\ 00^m$	$20^h\ 10^m$,
$20^h\ 23^m$	$20^h\ 24^m$	$20^h\ 33^m$	$20^h\ 41^m$
$20^h\ 46^m$	$21^h\ 11^m$	$22^h\ 45^m$	

故に「八時前後」の光は 20 h 00 m の最大餘震に伴つたものかも知れず、「九時すぎ」の光は 21 h 11 m、「十時頃」及び「十時すぎ」の光は 22 h 45 m の餘震に伴つたものかも知れない。全く震動を感じない時（人體にも地震計にも）にも發光するや否やは、是非確めたい問題の一であるが、報告者の記載して居る時間の不正確なるため、未だ斷定を下し難い。併し震動と無關係に光の出現する事もあるらしいと考へられるやうな資料はこの地震についても二三ある[27]。

10. 結　語

要するにこの地震に伴つた發光現象の中には、送電線のスパークもあるべく、また其の中の少數は比較的大なる流星であつたかも知れないが、少くも日向灘と別府灣に現はれた光は、其等の原因に歸する事は困難である。此等を我々の云ふ地震に伴ふ發光現象と考へる事は決して不合理ではないであらう。其等の光が海中から或は海上に發したと云ふ點が特に我等の興味をそゝるのである。

V. 總　括

自分は曩に伊豆地震の發光現象を調査して、地震に伴ふ發光現象の存在する事を、或る程度まで證明することが出來た。其後四回の地震について同じ現象の調査を試みた結果によると、自分の主張は毫も動搖しないのみならず、反つて益々自分の確信は强められるに至つた。其れと同時に、地震に伴ふ發光現象として報告せられたものゝ中には種々なる不純物の混在する事を認めざるを得ない。從つて其等の寄せ集めの中

26) 「最初二、三、四回を算する餘震の時は、この發光現象の起るに引續いて、其の都度餘震が來ましたので、『あツまた光つた、ソレ地震』と云ふ風に、家をとび出した者もありました」「光つた後で地震がした、再び光る其のあとで搖れた」。

27) 「始めは光る每に搖れましたが、後からは光るだけでした」「後たびたび光つたが地震は起らなかつた」「一回の地震が終つて、二回目の地震が始まる前、一回と二回の間に光が多く光つた」但し本震が 19 h 3 m 5 s に發し、第一回の餘震が 19 h 20 m に發したから、最後の例はこの場合論據とするに不適當かも知れぬ。

から genuine のものを選び出す事が自分の將來の仕事でなければならぬ。この目的のためには、機會ある毎に正確な資料を蒐集し、共れについて檢討を試みることが必要である。この現象の characteristics が充分明らかにされた後に於てこそ、發光の機巧も始めて眞に闡明されるやうになるのではあるまいか。

---

44. *Investigations into the Luminous Phenomena accompanying Earthquakes.*

By Kinkiti MUSYA,

Earthquake Research Institute.

Last year the present author published the result of his investigations into the luminous phenomenon accompanying the Idu Earthquake, Nov. 26, 1930. He also investigated the similar phenomena observed in other four earthquakes that have since occurred in Japan. The following are the results of these later investigations.

I. The Luminous Phenomena observed in the Hirosima Prefecture Earthquake, Dec. 20, 1930.

A few days after the Hirosima Prefecture Earthquake the author received a report from a stranger in the district that luminous phenomena were observed in Syôbara-mati at the time of the earthquake. So the author at once made inquiries of the middle and primary schools, as well as town and village offices which are within a radius of about 20 km from Huno, the epicentre. The data thus collected were very few, but the author could learn the following facts.

In Syôbara-mati, about 21 km E by S of the epicentre, a reddish luminosity just like a fire seen from afar was observed towards N (Fig. 1, p. 650). Some who saw the phenomenon suspected of the eruption of the Sambe volcano. This luminosity was not instantaneous. In respect of the reddish colour and non-instantaneousness, it closely resembles that observed by Mr. Nasu of our institute in Ito in the Idu Earthquake, Nov. 26, 1930. In Syôbara-mati, towards N by W, a fire-ball was reported to have ascended high in the sky and then disappeared. Afterwards the sky grew light in general. A dimly lighted sky after the disappearance of a fire-ball was also observed at Matuno-mura, Ibara-gun, Siduoka prefecture, in the Idu Earthquake. Though the cause cannot be explained by the author, it seems to be noticeable. And in the same town, towards WNW, a purplish radiating flash was also seen. A villager of Kimita, about 5 km NE of the epicentre, observed the phenomena, in SE at first, then NW, and then E. Their colour is reported to have been whitish. Another man in the same village observed luminosities, on both the 20th and 21st. The former was seen in NE, and was just like a fire seen from a distant place. The latter's directions were W and S, and they were like the former. In Kutikita-mura, about 11 km NE of the epicentre, as soon as the shock was felt, a reddish light like a besom standing upside-down was seen

behind the mountains. Besides the above a broad expanse of light was observed behind the mountains.

The above report may be summed up as follows.

(1) The luminous phenomena were seen in several directions.

(2) The luminosities were (a) indefinite, instantaneous luminosity, (b) indefinite, non-instantaneous luminosity, (c) fire-ball, and (d) searchlight-shaped.

(3) The colours of the luminosities was various, but a reddish colour predominated.

Since the power-transmission of the Hirosima Electric Co. was cut off at the time of the earthquake, there might have been the snapping of high-voltage wires. So there might have been flashes caused by the snapping or touching of wires. But to the present author it seems rather difficult to attribute all of those phenomena to this cause.

2. The Luminous Phenomena observed in the Tama Hills Earthquake, June 17, 1931.

At 21h 9m 50s, on June 17, 1931, a remarkable earthquake occurred, the epicentre of which was reported to have situated in the north-western part of the Tama Hills. At that time the luminous phenomena were observed in Tôkyô and its vicinity. The data regarding them were obtained from a middle school in Tôkyô and a middle school and a girls' school in Atugi-mati, Kanagawa prefecture. Their number amounts to 140, including those collected by Prof. Terada and a few other data.

As is shown on the appended map (Fig. 2, p. 651), the arrows which show the directions of the lights are far from converging at one point or several points. Even the predominating directions cannot be found. It probably means that the sources of those lights were very many.

The varieties of the luminosities observed are as follows. (The words used by observers or reporters are very ambiguous, so different expressions may mean the similar phenomenon).

(1)	Lightning-like flash	28
(2)	Indefinite instantaneous light	26
(3)	A part of the sky was illuminated	8
(4)	Streamed horizontally	6
(5)	Oblong light	6
(6)	Wave-like flash	4
(7)	Radiating light	3
(8)	A dim light spread on the sky	2
(9)	Zig-zag-shaped flash	1
(10)	Flame-like light which streamed horizontally	1
(11)	Light larger than ordinary lightning	1
(12)	Flash as if a lump of fire fell from the heavens	1
(13)	Vague round-shaped light	1
(14)	Gradually enlarging round-shaped light	1
(15)	Band-like light	1
(16)	Flash just like an explosion of a gas tank	1
(17)	Gradually enlarging radiating light	1
(18)	Just like the water glistening in the moonlight	1
(19)	Just like twinkling	1
(20)	Funnel-shaped light	1
(21)	Just like something is unfolded	1

(22) A dim light 1
(23) Indefinite semi-circular light 1
(24) A fire-ball rose in the sky and disappeared. A sound like "Bah...." was heard. The lower sky was coloured pink-red for some time after the disappearance of the light 1

To sum up, most of the luminosities observed in this earthquake are indefinite instantaneous or almost instantaneous luminosities, and other kinds of luminosities are very small in number. The last-mentioned one is especially noticeable. It is observed by a middle school student on the street at Sakana-mati, Usigome, Tôkyô. If the report can be believed to the letter, it closely resembles that observed by a girl named Y. Amano in the Idu Earthquake, 1930. There is a coincidence in the fact that the sky turned pink after the disappearance of a fire-ball. It also resembles that observed in Syôbara-mati in the Hirosima Prefecture Earthquake. The author knows the boy who supplied the datum, and believes that he is not a liar or a tall talker. He probably tells the actual impression which the phenomenon made upon him. And if the author remembers rightly, the boy had never been told about the observation by Amano. Of course he had not read the paper written by the author. But as the boy is pretty strongly near-sighted, his observation cannot be given enough credence.

The luminosity observed in Yokohama, too, is noteworthy. It was seen in S. The form of the luminosity is shown in Fig. 3 (p. 653), its colour being rather pale in the centre, and more bluish than X-rays on the margin. It appeared three times at intervals of about 5–6 s, and the duration was 3–4 s each time. They showed fluctuations while the luminescence continued. No sound was heard.

The colours of the light observed are as follows.

(1) Blue or bluish 21
(2) Various blended colours of red and yellow 16
(3) A colour just like that of lightning 11
(4) Yellow or yellowish 10
(5) Red or reddish 10
(6) Various blended colours of red and blue 9
(7) Various blended colours of blue and yellow 9
(8) A colour just like electric light 6
(9) White or whitish 2
(10) Others 4

Consulting the weather chart for that time it is found that a discontinuity line lies in the neighbourhood of the epicentral region. Probably influenced by it, in Ôiso Odawara, Numadu, etc. thunderstorms were reported at the time of the earthquake. Therefore part of the luminosities observed may have been ordinary lightning. On the other hand, many snappings of power transmission lines were reported. In part of Tôkyô and its vicinity, Kawasaki, Yokohama, Kamakura, most part of Kôza-gun (Kanagawa prefecture), Ôiso, Odawara, Tokorozawa, Hutyû, Urawa, Noda, and even so far as Asikaga, Karuizawa, and Iida (Nagano prefecture), the electric current was interrupted. Therefore part of the above-mentioned luminosities may have been sparks from the snapping or touching of wires. But at the present time the author is inclined not to attribute all of the phenomena to ordinary lightning or sparks of power-transmission wires. According to the observation in Takinogawa near Tôkyô by Mr. Kita, a student of physics and careful observer of atmospheric phenomena, the luminosities appeared even when the shock became unfelt to the human body. Those lights did not at all

resemble ordinary lightning accompanying thunderstorms. And Prof. Simidu of the Imperial University of Tôkyô observed a light a few minutes after the vibration ceased. These facts may support the author's opinion to some extent.

III. The Luminous Phenomena observed in the Earthquake in Minamituru-gun, Yamanasi Prefecture, Sept. 16, 1931.

When a remarkable earthquake occurred at 21h 43m 23s, on Sept. 16, 1931, (the epicentre of which was situated at the point about 20 km NNE of Mt. Huji,) it was reported from Misima, Siduoka prefecture, that intense luminosity was observed in the direction of the Hakone volcano. So the author made inquiries of four middle and girls' schools in Numadu and Misima. The data which were sent to the author in response amounted to 37, including those collected by Prof. Terada.

The arrows in the appended map (Fig. 4, p. 654) show the direction in which the luminous phenomena were seen. The directions of the arrows are very irregular. But the fact that remarkable luminescence was seen towards the Hakone volcano is beyond doubt.

The varieties of the luminosities observed as follows.

(1)	Lightning-like flash	9
(2)	Indefinite instantaneous or almost instantaneous luminosity	
	a. A part of the sky was lighted up	4
	b Indefinite flash	3
	c. Dim round-shaped luminosity	3
	d Radiating light	1
	e. Semi-circular light	1
	f. Rain-bow-shaped light	1
(3)	Long horizontal luminosity	4
(4)	Band-like luminosity	2
(5)	Pillar-like luminosity	2
(6)	Linear luminosity	2
(7)	Flash in the clouds	1
(8)	Others	4

All were instantaneous or almost instantaneous and non-instantaneous ones like those observed in the Idu Earthquake and the Hirosima Prefecture Earthquake were not reported at all.

The colours of the luminosities observed are as follows.

(1)	Various blended colours of red and blue	6
(2)	Yellow or yellowish	6
(3)	Various blended colours of red and yellow	6
(4)	Blue or bluish	5
(5)	Various blended colours of blue and yellow	3
(6)	Red or reddish	2
(7)	A colour just like lightning	1
(8)	White or whitish	1
(9)	A colour just like electric light	1
(10)	Others	5

The time when the luminosities were observed was mostly during the shock. There is one case in which the phenomenon was observed between 8-9 p.m. (that is before the earthquake), and another report states that the phenomenon was witnessed in less

than one hour after the shock. Especially important is the report which came from Hakone-mati, a small town in the caldera of the Hakone extinct volcano. According to Mr. Isiuti in the town, a luminosity appeared a few days previous to the earthquake, and lasted till after the earthquake. Every evening lightning-like flashes were seen. They were not zig-zag-shaped, but were like a searchlight sweeping overhead from mountain to mountain in a semi-circle. If this report is true, it is very important and interesting.

IV. The Luminous Phenomena observed in the South Hyûga Earthquake, Nov. 2, 1931.

Introduction.

The severe earthquake which occurred at 19h 3m 5s, on Nov. 2, 1931, supplied the author the most interesting data on the luminous phenomena, next only to the Idu Earthquake, 1930. The results of the investigations based upon 355 data including those collected by Prof. Terada and Mr. Nasu of our institute, are given below.

The extent of the area where the phenomena were observed.

The localities where the phenomena were observed range from the northern coast of Beppu-wan (the Bay of Beppu) in the north to the northern coast of Ariake-wan (the Bay of Ariake). The length between the two extremities is about 200 km. There are not a few places from which no report could be obtained. But if the schools or public offices in those places had been kind enough, the gaps might have been filled up. The western limit, on the other hand, from where the phenomena were reported is Miyakonojô, about 40 km of the shore of Hyûganada. But the author sent inquiries to towns and villages comparatively near the sea, so it is doubtful whether the abovementioned city is really the western limit.

The directions in which the phenomena were observed.

The directions in which the phenomena were observed in various places are shown in the appended map (Fig. 5, p. 656). They are varied, but it is noticeable that in Ooita, Nobeoka, Miyazaki and their vicinity, most observers saw the phenomena towards Hyûganada in which the epicentre of the earthquake situated or towards Beppu-wan.

Varieties of the luminescence.

The luminescence observed can be classified as follows.

(1)	Radiating from the horizon	106
(2)	Lightning-like	47
(3)	Like a searchlight turned to the sky	23
(4)	Streaming across the sky	7
(5)	Beam-like or besom-like	7
(6)	Curtain-like	7
(7)	Straight or curved line	6
(8)	Like streak-lightning rising to the sky	5
(9)	Lighting the sky red	1
(10)	Others	21

Of these, (2) is most ambiguous, perhaps (1), (4), and (6) are mixed with it, but the author cannot distinguish between them.

The colours of the lights.

The colours of the lights observed are as follows.

(1)	Blue or bluish	84
(2)	A colour just like lightning	31
(3)	Yellow or yellowish	30
(4)	Various blended colours of blue and red	23
(5)	White or whitish	20
(6)	Various blended colours of yellow and red	20
(7)	Red or reddish	14
(8)	Various blended colours of yellow and blue	11
(9)	A colour just like electric light	4
(10)	A colour just like searchlight	1
(11)	A colour just like flames of coal-gas	1
(12)	Others	28

The possible causes of the phenomena.

As the possible causes of the above-mentioned phenomena, the author may cite (1) fire, (2) thunderstorm, (3) land-slide, (4) electric sparking, (5) meteor. Concerning each of them, a brief examination will be tried.

(1) Fire. So far as the author is informed, no fire was reported at the time of this earthquake. Besides, the phenomena observed are quite different from fire. So they cannot be accounted for by fire.

(2) Thunderstorm. According to the weather chart for 18h of that day and the *Kisyô-yôran*, there was no thunderstorm all over the affected area. Therefore it is out of question that the phenomena were not ordinary lightning. (For a few days previous to the earthquake a radio-set was out of order, a report says, and at the time of the shock its sensitivity became very weak. This report is very interesting, but only one report is insufficient to prove the abnormal condition of electricity in the atmosphere at that time.)

(3) Landslide. No news of landslides could be found in the newspapers issued in that district, so it may be concluded that at least no remarkable landslide occurred. Therefore, though luminescence owing to landslides can be neither affirmed nor denied in this case, yet the author's opinion is inclined to a negative conclusion as regards their being the possible cause of the luminescence.

(4) Electric sparking. As soon as the shock was felt, electric light went out in Ooita, Miyazaki, and Miyakonojô. According to a paper, in Ooita and its vicinity, seven power-transmission lines were snapped. In a factory in Nobeoka, a brilliant spark was emitted from power-transmission lines, though the lines were not snapped. In Hukusima-mati a spark was observed in a transformer sub-station. Therefore part of luminosities may be attributed to electric sparking. But all the luminous phenomena, it seems to the present author, cannot be explained by electric sparking.

(5) Meteor. Many meteors were observed by not a few persons on the evening of the earthquake. Of the luminosities observed, too, there are some which seem to be meteors. So part of the luminosities might have been meteors. But it is beyond doubt that the author cannot explain all the phenomena by meteors. There are not a few cases in which many shooting stars were seen at the time of shock in Japan and other countries. This fact is noticeable.

Luminosities observed on the sea.

The luminosities that appeared on the sea cannot be explained by the causes mentioned above. They were witnessed both in Beppuwan and Hyûganada.

[A] Luminous phenomena seen over Beppuwan.

(1) The *Ooita Shimbun* reported that a few pillar-like lights appeared off Benten-Jima, Ooita, and they were just like a hanging curtain, the scene being sublime beyond description.

(2) According to Mr. Imamura, a teacher of the Ooita Commercial School, he observed to NE a light red luminosity as if a searchlight were turned upward in the foggy sky, immediately after the shock was felt. The light lasted about one minute.

(3) Besides Mr. Imamura, in Ooita and its vicinity, 24 persons reported that pillar-like, a cylindrical, or chimney-like luminosities were observed by them in the direction of the bay.

(4) In Hidi-mati, a pillar-like luminosity was seen towards Ooita.

Judging from the above-mentioned reports, though the accounts do not exactly agree with one another, it seems to be not too much to say that a searchlight-shaped luminosity appeared off Ooita in the Beppuwan at the time of the earthquake, and the light was non-instantaneous. This phenomenon closely resembles that observed in the epicentral region in the Idu Earthquake, 1930.

[B] Luminous phenomena observed in Hyûganada.

(1) According to Mr. Nasu of our institute, a very interesting phenomenon was witnessed in Hyûganada.. A fishing boat called the *Ikedamaru* was engaged in fishing on the sea about 50 km off Utiumi, a town on the coast of Hyûganada. At about 7 p.m. the boat began to pitch so heavily all of a sudden that they thought she was near being capsized. At the same time, to the crew's consternation, a large pillar of fire shot up from the surface of the sea near the boat. (Fig. 7, p. 662)

(2) In Nobeoka, Totori, Miyazaki and their vicinity, luminous phenomena were observed by many people towards Hyûganada.

From the above-mentioned facts, the author concludes that the luminosity perhaps really appeared on Hyûganada. The appearance of light from the surface of sea is not without examples. In the Kwantô Earthquake in 1923, a pillar (or pillars) of flames was reported from the mouth of Tôkyô Bay. In the Itô swarm-earthquakes in 1930, a fisherman observed a fire-ball burst out of the sea off Itô-mati.

These luminosities which appeared on the sea cannot be attributed to the activity of submarine volcanoes. There is no ground at all to affirm it except for the luminous phenomena, and Hyûganada is not a volcanic region, though near Beppu-wan there are a number of volcanoes and a famous spa called Beppu.

Sound.

Only seven reports mention sound phenomena. Three of them are negative and the others affirmative. But the author thinks the sound reported was ordinary sound phenomena accompanying earthquakes, and had nothing to do with the luminescence.

The time of observation.

Though 147 reports mention the time of observation, the words used by the observers are extremely ambiguous, so the author cannot see the matter in a true light. At any rate, the reports may be summarized as follows.

(a) Before the shock 26
(b) Simultaneously with or during the time the shock was on...... 99
(c) After the shock 22

But, in a strict sense, the cases in which luminous phenomena were observed before the earthquake are only four.

(1) In the previous evening there seemed to have been flashes of light from time to time.

(2) At about 1h 30m p.m. on Nov. 2, an intensely brilliant purplish bank of cloud was observed near Miyazaki.

(3) About 4 hours previous to the disturbance (that is about 3h p.m.) whitish semi-circular light was seen in Miyazaki towards SW.

(4) About 20 minutes before the earthquake, a similar light was observed near Miyazaki towards ENE.

Of the above, (4) is most important, because the direction points evidently to the epicentre. Moreover, the place of observation is near the seashore.

The cases in which the phenomena were observed simultaneously with or during the time the shock was on were greatest in number. The same can be said of the other earthquakes investigated by the present author.

The term "after the shock" is very ambiguous. It may mean "after the earthquake began and during the time the shock was on," or "directly the vibration ceased," or "when the shock became quite unfelt." Practically all the cases mentioned above may be included in the term "after the shock." There are some reports which seem to tell that the phenomena and aftershocks occurred at the same time, on the other hand, there are some reverse reports, too. Though special importance has been attached to this respect by the author, he cannot yet bring it to light, owing to the ambiguous terminology used by observers.

Conclusion

In short, the luminous phenomena accompanying the earthquake in question are not free from various sorts of mixture, but there are some which it seems impossible for the present author to explain by electric sparking or meteors, etc. At least the author should like to believe that the luminosities which appeared on the sea are directly related to the earthquake by some unknown mechanism.

V. Conclusive Remarks.

In the foregoing pages the author has stated his latest investigations into, and his views on the luminous phenomena accompanying earthquakes. In fine, he is convinced of the existence of the phenomena, and he thinks he has been able to prove it to some extent. At the same time, he admits that there are various mixtures are contained in the data of the phenomena collected by the author and others. It should therefore be his future task to select genuine elements out of the medley. For this purpose, it is needful for the author to collect exact data and examine them, every time he finds an opportunity in the future. It may be at the time when the characteristics of the phenomena are grasped that the mechanism of the luminescence will be brought to light in the true sense of the term.

45. *A Study of the Osaka Landslide.*

By Nobuji NASU,

Earthquake Research Institute.

(Read Feb. 16, 1932.—Received June 20, 1932.)

Introduction. On November 27 last year, several rows of earth cracks, a few centimetres long and about a half centimetre wide, were noticed by the people of Katakami, a village 20 km. southeast of the city of Osaka. These cracks, which were on an orchard of recently cultivated slanting ground dipping towards the River Yamatogawa, gradually increased in both length and width with time. Later, other cracks were found in the neighbourhood. It was then recognized that the land block on which the village was situated, about 330,000 m^2. in area, was slowly sliding downwards in a southerly direction. Thenceforth, the sliding speed increased daily until Feb. 20, when it reached maximum, after which it showed a gradual decrease. The sliding land mass is an irregularly shaped area, bounded on all sides except on the southeast by a zone of cracks. In the beginning of June, as the result of the present sliding movement, the cracks at the front of the sliding area grew as large as 20 m. in width. In the course of time, since the cracks were first noticed, a huge trench-like hollow, 500 m. long and 80 m. wide, had formed at the western margin of the slipping area. About the end of January, local upheavals of the river-bed and of road surfaces along the river banks became noticeable. The gradual upheaval of the river bed, together with avalanches of large quantities of rock and earth into the nothern side of the river, thus narrowing it and at the same time raising the level of the upper stream, created fears of flood among the inhabitants. The houses in the sliding area having listed heavily to one side, owing to the earth-tilts that accompanied the landslide. Many of them were rendered uninhabitable.

Outline of the topography and geology of the slipping region. The district that is slipping is situated on the northern side of the River Yamatogawa, which cuts across a mountain range running in a north-south direction. This mountain has the form of a saddle, in the hollow of which is situated the hamlet of Tôge. The slope of the sliding region is about 15°.

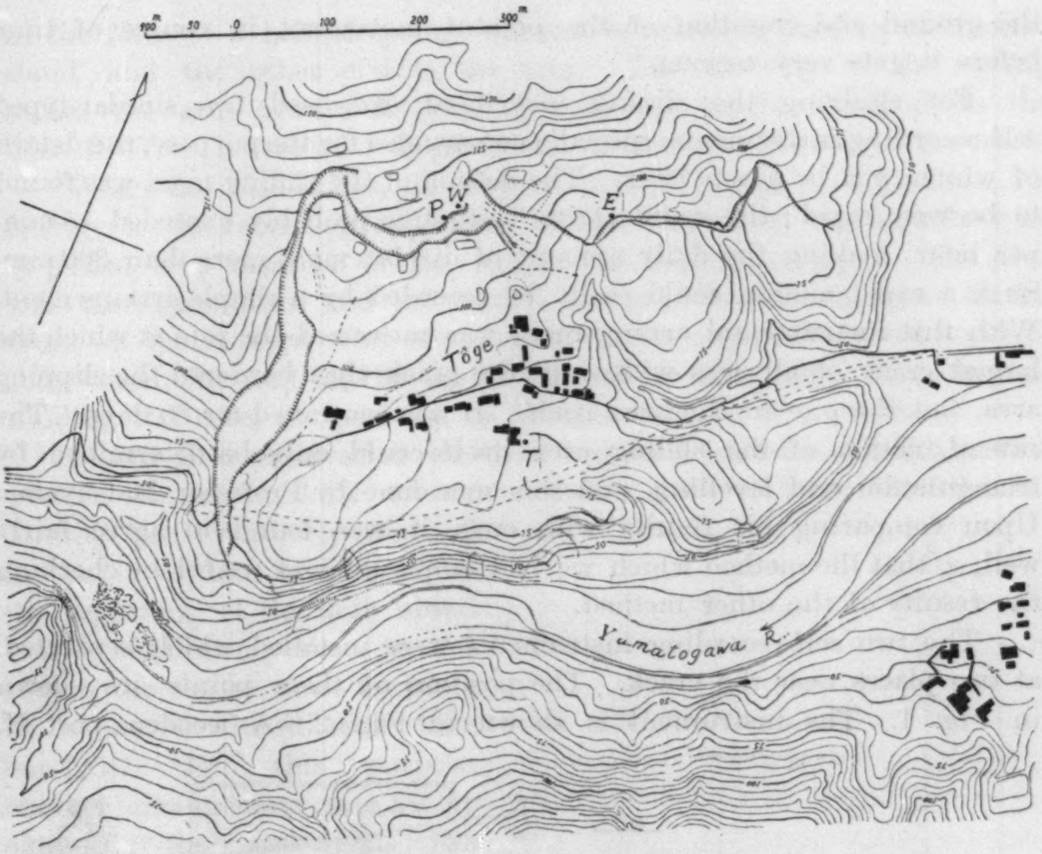

Fig. 1. Map showing the slipping district. (From a Government Railway map.) Points E and W indicate the positions of self-recording instrument; P the photographic recording instrument; T the tiltmeter station.

According to Professor Makiyama, the uppermost surface of the sliding area is covered by younger andesite. Below it is a layer of agglomerate and gravel with the older andesite underneath it. This older andesite is well developed in a wide region lying to the south of this district.

Observation of the landslide. To measure the extent of slide with reference to time, different methods have been used by different observers. Professor Matsuyama, of the Kyôto Imperial University, carried out triangulations and ran precise levels over the whole of the affected area, and determined the directions in which the bench marks were moving and the time in which they did so. It might incidentally be mentioned that, on the basis of these observations, he has predicted settlement of

1) M. Matsuyama, "Observation of the Katakami Landslide," *Tikyû*, 17, No. 5 (1932), (in Japanese).

the ground and cessation of the present movement in course of time before it gets very serious.

For studying the sliding movement, we used two similar-typed self-recording instruments, specially constructed for the purpose, the details of which will be given later. The motion of the sliding mass was found to be very rapid; the speed at its maximum probably exceeded 15 mm. per hour, making the daily amount of displacement more than 300 mm. Such a rapid motion could easily be recorded by a simple arrangement. With this instrumental arrangement was measured the rate at which the largest crack of all was widening–the crack that bordered the slipping area, not the one in the area itself. It was continued for 80 days. The rate of motion of the sliding area itself could only be determined by triangulation and levelling, and this was done by Professor Matsuyama. Upon comparing his results with ours, it was found to agree fairly well, so that the method which we had employed was useful in checking the results of the other method.

The two self-recording instruments were installed, widely separated, at two places near the crack. The position of these points are shown in Fig. 1. The instrument is shown in Fig. 2. A wooden post *H*,

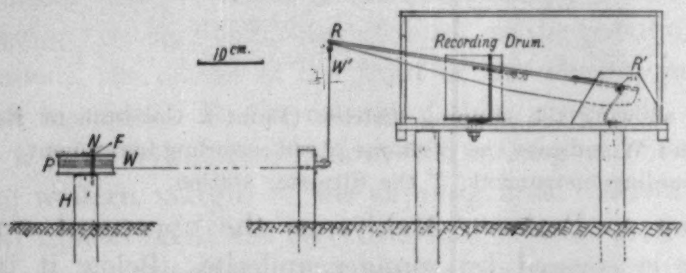

Fig. 2. Side-view of the self-recording instrument.

about 1 m. long, is driven into the sliding ground some distance from the margin of the crack. On the top of this post is attached a pulley *P* with its rotating axis vertical. A nail *N* driven through hole *F* in the pulley into the top of the post prevents rotation of the pulley except when required, when it is withdrawn. A steel wire, 0·4 mm. diameter and a few metres long, is wound around this pulley. The end of this wire is fixed to the end of the lever arm RR'. An inked pen is fixed to the middle point of RR'. The recording drum encloses an ordinary Richard's clock which makes one revolution a day. The arm RR' rotates in a vertical plane about the horizontal axis, passing through R'. Around the axle of the lever arm is wound a steel wire

in the form of a helical spring, one end of which is fixed to the wooden stand and the other end to the arm. The elasticity of the spring causes the arm always to leap upward and produce tension on the wire WW'. The recorder is placed on the undisturbed side of the crack.

When the land slides, the wooden post H changes its position relatively to the recording apparatus, so that the extent to which the wire is pulled is a measure of the length the land has slipped. The arm RR' then goes down and the motion of the ground is registered on the drum on the reduced scale of one-half. After expiration of 24 hours of observation, the nail on the top of the post is withdrawn, when by unwinding the wire, the pen can be brought back to zero position.

In our first observation we used two such instruments, but at the western station the daily amount of sliding grew so large that the recording pen eventually went off the paper within 24 hours from the beginning of the daily observation, indicating that at this station the record must be taken on a more reduced scale than one-half. For this purpose, another arrangement was set up alongside the instrument just mentioned. As shown in Fig. 3, in this arrangement the wire from post H was fastened to end L of the new lever arm, LL'. The lever rotates in a horizontal plane about the vertical axis passing through O, the arm ratio LO to $L'O$ being 2·5 : 1·0. The wire from the recording arm RR' is fixed to L'. This enabled the motion to be registered on the scale of one-fifth.

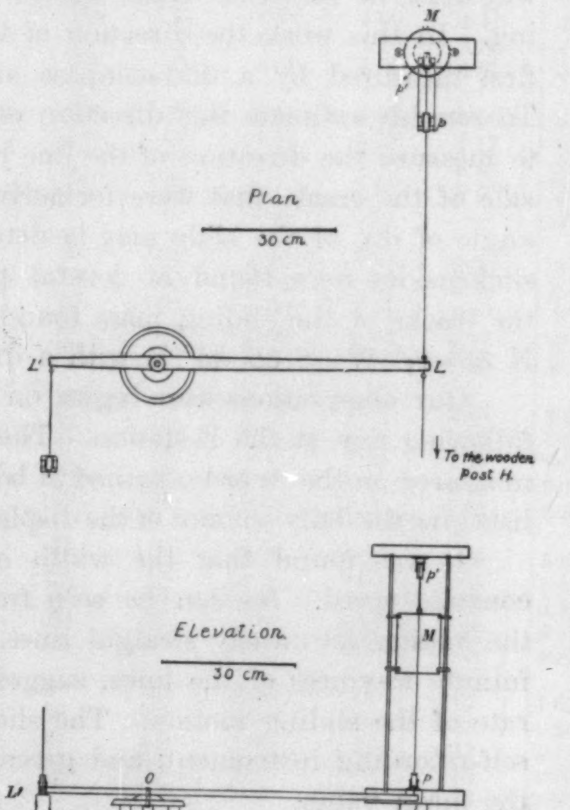

Fig. 3. Arrangement added to the instrument at E-Station.

Another advantage from this arrangement is that the wire between post H and arm RR' in the old arrangement, as shown in Fig.

2, was often shaken by strong winds, with the result that the curves were zig-zag, thus making it impossible to determine the motion of the ground. The difficulty was increased with the lengthening of the wire between H and RR'. To avoid it, a stronger tension was applied to the wire. To effect this, another wire is fastened to L and stretched to the opposite side of the wooden post H, passing over two pulleys p and p'. At the end of this wire is suspended a heavy mass M, weighing 4 kg. The weight moves upward along the two guides when the post moves away from the recorder. The tension of the wire may be varied by changing the weight. In this way, we managed to keep the wire always taut and free from wind effects.

In setting up the instrument, the direction of the sliding motion of the ground was carefully ascertained and the wire stretched in such a way that its direction shall always coincide with the direction of sliding. In this work the direction of the motion of the wooden post was first measured by a dial-compass and wire stretched in that direction. To roughly estimate this direction of the sliding motion, it is sufficient to measure the direction of the line joining any two points, one on each side of the crack, that were formerly closer together. In doing so, the angle of dip of the slide may be determined. In the present movement, slickensides were found at several places. For example, at station-E, the tracks of the sliding mass found on the slickenside had a strike of N 35°-45° W—S 35°-45° E with a dip of 30°-35° S.

Our observations were begun on Feb. 1 at the W-station and on the following day at the E-station. The daily amount of displacement was measured on the record obtained at both stations E and W. The following lists give the daily amount of the displacement and the hourly rate of sliding.

It was found that the width of the cracks increased with fairly constant speed. As can be seen from Fig. 4, a, b, c, d, the records of the motion are nearly straight lines, although close examination reveals minute waviness of the lines, suggesting more or less fluctuation in the rate of the sliding motion. The sliding speed as determined with the self-recording instrument, and given in Lists 1 and 2 may be said to be the mean value.

From the beginning of the observations, the mean speed increased gradually until Feb. 20, when the sliding motion reached maximum, after which the motion declined rather slowly, a feature that was also pointed out by Professor Matsuyama.[2] Professor Matsuyama calculated

2) M. MATSUYAMA, *loc. cit.*

List 1.

The Daily amount and the hourly rate of sliding at the E-station.

Date	Daily amount sliding	sliding 6 hours				Hourly rate of sliding			
		0^h-6^h	6^h-12^h	12^h-18^h	18^h-24^h	0^h-6^h	6^h-12^h	12^h-18^h	18^h-24^h
	mm	mm	mm	mm	mm	mm	mm	mm	mm
Feb. 1	—	—	—	—	—	—	—	—	—
2	60	14	14	16	16	2·33	2·33	2·67	2·67
3	65	15	17	17	16	2·50	2·83	2·83	2·67
4	72	18	18	18	18	3·00	3·00	3·00	3·00
5	78	19	19	20	20	3·17	3·17	3·33	3·33
6	85	20	21	22	22	3·33	3·50	3·67	3·67
7	91	22	22	23	24	3·67	3·67	3·83	4·00
8	97	24	24	25	24	4·00	4·00	4·17	4·00
9	104	25	25	27	27	4·17	4·17	4·50	4·50
10	110	27	27	28	28	4·50	4·50	4·67	4·67
11	117	28	29	30	30	4·67	4·83	5·00	5·00
12	124	31	31	31	31	5·17	5·17	5·17	5·17
13	126	32	32	32	30	5·33	5·33	5·33	5·00
14	—	—	34	34	34	—	5·67	5·67	5·67
15	—	34	34	—	35	5·67	5·67	—	5·83
16	142	35	35	36	36	5·83	5·83	6·00	6·00
17	144	36	36	36	36	6·00	6·00	6·00	6·00
18	143	36	35	37	35	6·00	5·83	6·17	5·83
19	146	36	36	37	37	6·00	6·00	6·17	6·17
20	151	38	38	38	37	6·33	6·33	6·33	6·17
21	150	37	37	38	38	6·17	6·17	6·33	6·33
22	148	37	37	37	37	6·17	6·17	6·17	6·17
23	145	37	36	36	36	6·17	6·00	6·00	6·00
24	146	37	36	36	37	6·17	6·00	6·00	6·17
25	140	35	35	35	35	5·83	5·83	5·83	5·83
26	139	35	35	35	34	5·83	5·83	5·83	5·67
27	138	34	35	34	35	5·67	5·83	5·67	5·83
28	133	34	34	33	32	5·67	5·67	5·50	5·33
29	125	32	32	30	31	5·33	5·33	5·00	5·17
March 1	118	30	30	29	29	5·00	5·00	4·83	4·83
2	113	29	28	28	28	4·83	4·67	4·67	4·67
3	108	28	27	26	27	4·67	4·50	4·33	4·50
4	102	26	26	25	25	4·33	4·33	4·17	4·17
5	96	25	24	23	24	4·17	4·00	3·84	4·00
6	90	25	24	20	21	4·17	4·00	3·33	3·50
7	87	22	23	22	20	3·67	3·83	3·67	33·3
8	85	22	22	21	20	3·67	3·73	3·50	33·3
9	78	20	21	19	18	3·33	3·50	3·17	30·0
10	71	18	18	17	18	3·00	3·00	2·83	30·0
11	72	18	18	18	18	3·00	3·00	3·00	30·0

(to be continued.)

List 1. (*continued.*)

Date		Daily amount sliding	Distance slid in 6 hours				Hourly rate of sliding			
			0^h-6^h	6^h-12^h	12^h-18^h	18^h-24^h	0^h-6^h	6^h-12^h	12^h-18^h	18^h-24^h
		mm	mm	mm	mm	mm	mm	mm	mm	mm
	12	70	17	17	18	18	2·83	2·83	3·00	3·00
	13	69	16	18	18	17	2·67	3·00	3·00	2·83
	14	66	17	17	17	15	2·83	2·83	2·83	2·50
	15	64	16	16	16	16	2·67	2·67	2·67	2·67
	16	58	14	15	14	15	2·33	2·50	2·33	2·50
	17	56	14	14	14	14	2·33	2·33	2·33	2·33
	18	55	14	13	14	14	2·33	2·17	2·33	2·33
	19	50	13	13	12	12	2·17	2·17	2·00	2·00
	20	50	12	14	12	12	2·00	2·33	2·00	2·00
	21	48	12	12	12	12	2·00	2·00	2·00	2·00
	22	42	12	11	9	10	2·00	1·83	1·50	1·67
	23	41	11	10	9	11	1·83	1·67	1·50	1·83
	24	42	10	11	11	10	1·67	1·83	1·83	1·67
	25	43	11	11	11	10	1·83	1·83	1·83	1·67
	26	42	10	10	11	11	1·67	1·67	1·83	1·83
	27	37	11	8	10	8	1·83	1·33	1·67	1·33
	28	30	7	6	8	9	1·17	1·00	1·33	1·50
	29	35	9	10	9	7	1·50	1·67	1·50	1·17
	30	37	9	11	8	9	1·50	1·83	1·33	1·50
	31	35	10	10	8	7	1·67	1·67	1·33	1·17
April	1	32	8	8	8	8	1·33	1·33	1·33	1·33
	2	35	9	9	9	8	1·50	1·50	1·50	1·33
	3	31	8	7	8	8	1·33	1·17	1·33	1·33
	4	32	8	8	8	8	1·33	1·33	1·33	1·33
	5	29	7	7	8	7	1·17	1·17	1·33	1·17
	6	26	7	6	6	7	1·17	1·00	1·00	1·17
	7	24	6	6	6	6	1·00	1·00	1·00	1·00
	8	25	7	6	6	6	1·17	1·00	1·00	1·00
	9	24	6	7	6	5	1·00	1·00	1·00	0·83
	10	20	5	5	5	5	0·83	0·83	0·83	0·83
	11	18	5	4	5	4	0·83	0·67	0·83	0·67
	12	20	5	5	5	5	0·83	0·83	0·83	0·83
	13	21	6	5	5	5	1·00	0·83	0·83	0·83
	14	20	5	5	5	5	0·83	0·83	0·83	0·83
	15	22	5	6	5	6	0·83	1·00	0·83	1·00
	16	19	5	5	5	4	0·83	0·83	0·83	0·67
	17	18	5	4	4	5	0·83	0·67	0·67	0·83
	18	22	5	5	6	6	0·83	0·83	1·00	1·00
	19	22	6	6	5	5	1·00	1·00	0·83	0·83
	20	18	5	5	4	4	0·83	0·83	0·67	0·67

List 2.

The daily amount and the hourly rate of sliding at the W-station.

Date		Daily amount of sliding	Distance slid in 6 hours				Hourly rate of sliding			
			0^h-6^h	6^h-12^h	12^h-18^h	18^h-24^h	0^h-6^h	6^h-12^h	12^h-18^h	18^h-24^h
		mm	mm	mm	mm	mm	mm	mm	mm	mm
Feb.	1	101	22	24	28	27	3·67	4·00	4·67	4·50
	2	130	28	30	36	36	4·67	5·00	6·00	6.00
	3	149	35	39	39	36	5·83	6·50	6·50	6·00
	4	166	40	40	46	40	6·67	6·67	7·67	6·67
	5	166	40	38	43	45	6·67	6·33	7·17	7·50
	6	185	46	45	47	47	7·67	7·50	7·83	7·83
	7	197	49	47	51	50	8·17	7·83	8·50	8·33
	8	207	50	52	54	51	8·33	8·67	9·00	8·50
	9	229	52	52	62	63	8·67	8·67	10·33	10·50
	10	245	60	60	65	60	10·00	10·00	10·83	10·00
	11	255	63	62	62	68	10·50	10·33	10·33	11·33
	12	281	68	68	73	72	11·33	11·33	12·17	12·00
	13	290	72	72	73	73	12·00	12·00	12·17	12·17
	14	298	71	73	76	78	11·83	12·17	12·67	13·00
	15	312	76	76	77	83	12·67	12·67	12·83	13·83
	16	337	78	82	87	90	13·00	13·67	14·50	15·00
	17	332	83	84	82	83	13·83	14·00	13·67	13·83
	18	322	80	80	82	80	13·33	13·33	13·67	13·33
	19	319	79	78	78	84	13·17	13·00	13·00	14·00
	20	333	84	84	82	83	14·00	14·00	13·67	13·83
	21	—	83	—	—	84	13·83	—	—	14·00
	22	320	85	89	74	72	14·17	14·83	12·33	12·00
	23	286	75	74	67	70	12·50	12·33	11·17	11·67
	24	—	75	82	—	67	12·50	13·67	—	11·17
	25	292	63	77	77	75	10·50	12·83	12·83	12·50
	26	297	77	75	75	70	12·83	12·50	12·50	11·67
	27	279	73	71	68	67	12·17	11·83	11·33	11·17
	28	280	76	70	68	66	12·67	11·67	11·33	11·00
	29	256	65	65	63	63	10·83	10·83	10·50	10·50
March	1	246	62	62	62	60	10·33	10·33	10·33	10·00
	2	228	59	55	57	57	9·83	9·17	9·50	9·50
	3	222	57	57	55	53	9·50	9·50	9·17	8·83
	4	210	53	53	53	51	8·83	8·83	8·83	8·50
	5	188	50	48	45	45	8·33	8·00	7·50	7·50
	6	177	45	47	45	40	7·50	7·83	7·50	6·68
	7	—	45	—	—	—	7·50	—	—	—
	8	—	—	—	40	38	—	—	6·67	6·33
	9	146	33	38	40	35	5·50	6·33	6·67	5.83
	10	146	33	38	40	35	5·50	6·33	6·67	5·83
	11	125	33	32	30	30	5·50	5·33	5·00	5·00

(to be continued.)

List 2. (*continued.*)

Date	Daily amount of sliding	Distance slid in 6 hours				Hourly rate of distance slid			
		0^h-6^h	6^h-12^h	12^h-18^h	18^h-24^h	0^h-6^h	6^h-12^h	12^h-18^h	18^h-24^h
	mm	mm	mm	mm	mm	mm	mm	mm	mm
March 12	—	—	—	—	26	—	—	—	4·33
13	115	30	30	25	30	5·00	5·00	4·17	5·00
14	112	27	35	25	25	4·50	5·83	4·17	4·17
15	109	32	27	25	25	5·33	4·50	4·17	4·17
16	107	30	30	25	22	5·00	5·00	4·17	3·67
17	—	24	22	—	20	4·00	3·67	—	3·33
18	88	22	23	20	23	3·67	3·83	3·33	3·83
19	88	22	26	22	18	3·67	4·33	3·67	3·00
20	85	20	22	21	22	3·33	3·67	3·50	3·67
21	88	20	23	20	25	3·33	3·83	3·33	4·17
22	68	18	20	15	15	3·00	3·33	2·50	2·50
23	75	20	20	17	18	3·33	3·33	2·83	3·00
24	70	20	15	18	17	3·33	2·50	3·00	2·83
25	79	20	25	17	17	3·33	4·18	2·83	2·83
26	61	16	17	15	13	2·67	2·83	2·50	2·17
27	—	15	17	—	10	2·50	2·83	—	1·67
28	67	15	17	18	17	2·50	2·83	3·00	2·83
29	77	22	18	17	20	3·67	3·00	2·83	3·33
30	63	22	15	13	13	3·67	2·50	2·17	2·17
31	60	17	15	13	15	2·83	2·50	2·17	2·50
April 1	54	15	15	12	12	2·50	2·50	2·00	2·00
2	—	10	15	—	—	1·67	2·50	—	—
3	—	—	—	—	—	—	—	—	—
4	—	—	—	—	12	—	—	—	2·00
5	47	12	13	12	10	2·00	2·17	2·00	1·67
6	45	12	13	10	10	2·00	2·17	1·67	1·67
7	—	8	10	—	—	1·33	1·67	—	—
8	—	—	—	—	—	—	—	—	—
9	—	—	—	—	10	—	—	—	1·67
10	42	10	12	12	8	1·67	2·00	2·00	1·33
11	41	11	10	12	8	1·83	1·67	2·00	1·33
12	34	8	8	8	10	1·33	1·33	1·33	1·67
13	32	12	6	6	8	2·00	1·00	1·00	1·33
14	41	12	9	10	10	2·00	1·50	1·67	1·67
15	39	9	9	11	10	1·50	1·50	1·83	1·67
16	37	12	10	6	9	2·00	1·67	1·00	1·50
17	34	12	8	7	7	2·00	1·33	1·17	1·17
18	36	10	7	10	9	1·67	1·17	1·67	1·50
19	43	9	15	8	11	1·50	2·50	1·33	1·83
20	43	10	15	8	10	1·67	2·50	1·33	1·67

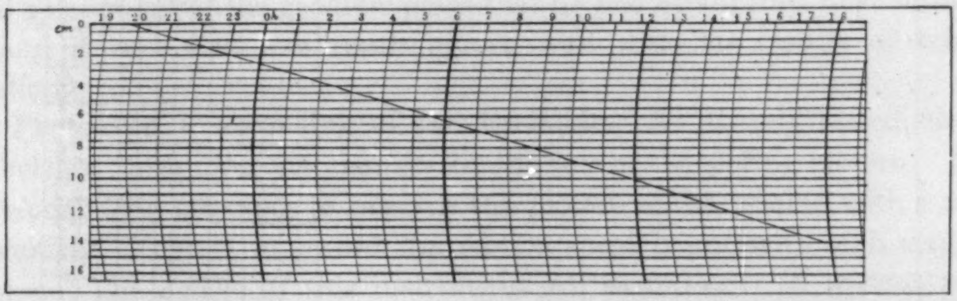

a

From Feb. 4. 19h45m to Feb. 5. 17h40m.

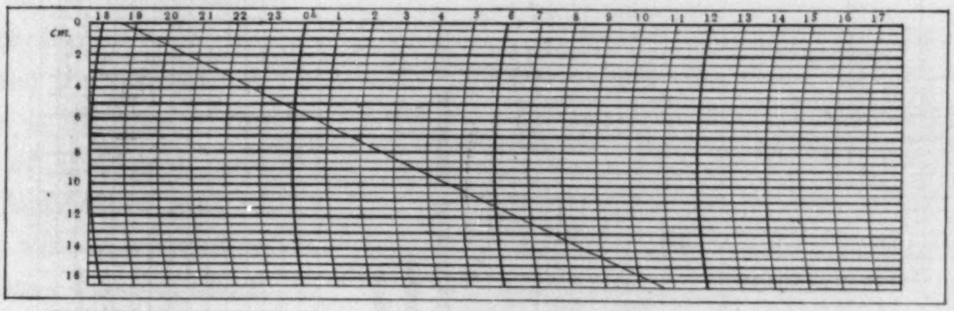

b

From Feb. 9. 18h30m to Feb. 10. 10h50m.

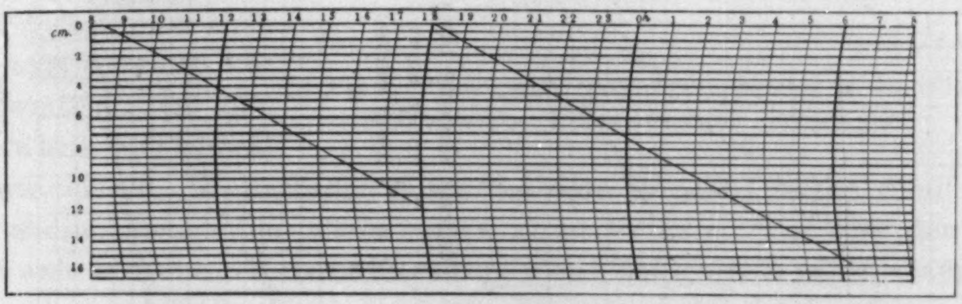

c

From Feb. 14. 8h30m to Feb. 15. 6h15m.

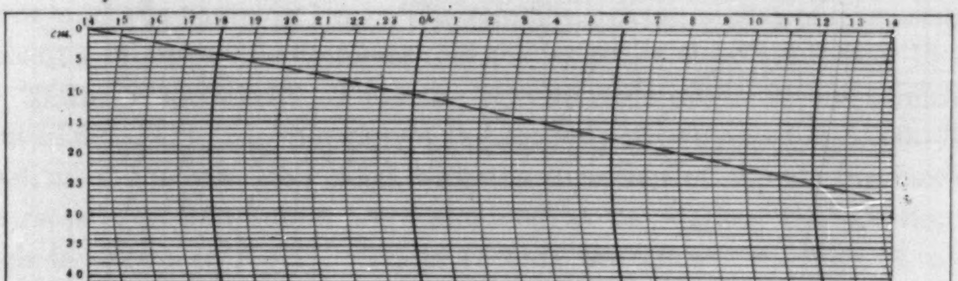

d

From Feb. 27. 14h00m to Feb. 28. 13h40m.

Fig. 4. Records of the widening motion of the crack taken at W-station. Figures about 1/3 actual size.

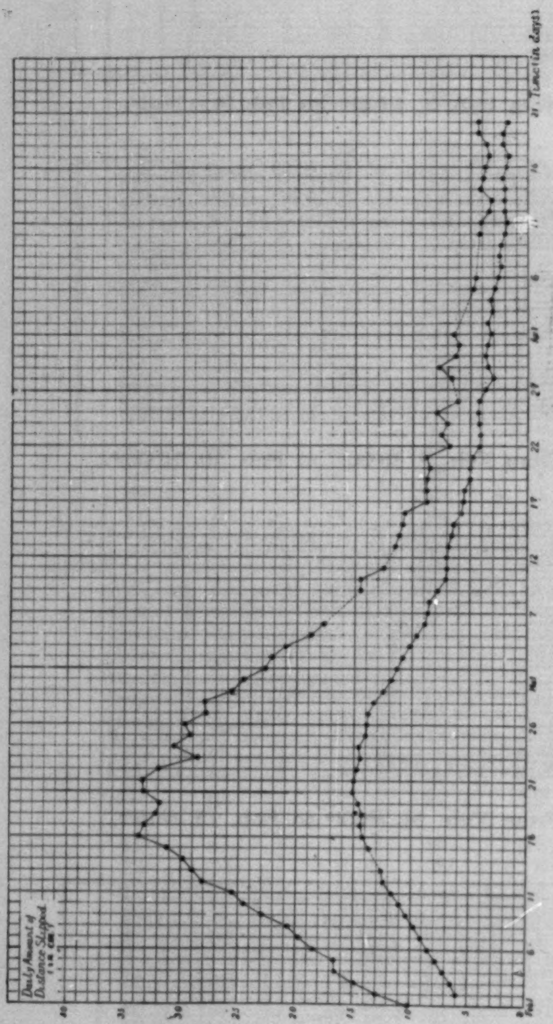

Fig. 5. Diagram showing the daily amount of distance slid.
upper curve: W-station.
lower curve: E-station.

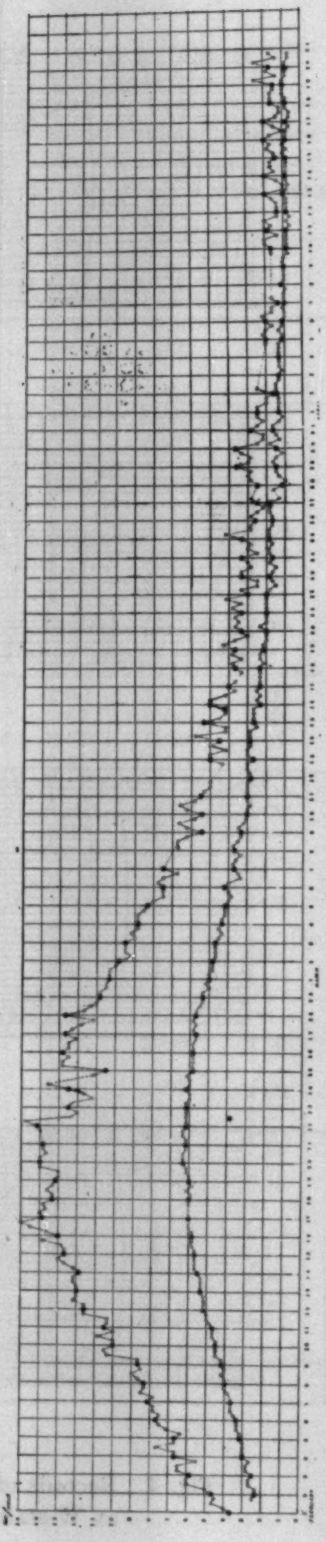

Fig. 6. Hourly rate of sliding.
upper curve: W-station.
lower curve: E-station.

the displacement of the geodetic point that he had established near station-W and showed that our result agrees well with his results of triangulation.

Photographic recording of the landslide. As already stated, there are certain instantaneous changes in the rate of the sliding motion. We therefore made attempts to observe the motion of the ground with a new instrument designed to record the motion speedily and with high magnification. The details of this instrument are as follows. A wooden post is driven into the sliding side of the ground, as in the case of the former instrument. A wire is clamped to the top of this post, and to the other end of this wire is suspended a heavy mass of about 5 kg., as shown in Fig. 7. The wire passes over a steel roller RR', the axis of which lies horizontally. On this axis a lens-mirror (focal length=50 cm.) is attached. When the wire is pulled as the result of the sliding motion the mirror rotates about its axis. The diameter of this axle is 2 mm. A recording drum with photographic paper wrapped around it is set at a distance of 1 m. from the surface of the mirror. A point-source lamp illuminates this mirror. The distance between the mirror and the lamp is 1 m. The recording drum makes one revolution in about 4 minutes, the diameter and the length of the drum being 18 cm. and 25 cm., respectively. Thus the rate of registration in one minute is about 14 cm. The magnification of the motion thus obtained is 2,000. The direction of the wire coincided with the direction of the sliding motion. The records of the motion were obtained at the station, the position of which is shown in Fig. 1. These records are shown in Figs. 8, a, b, c, d.

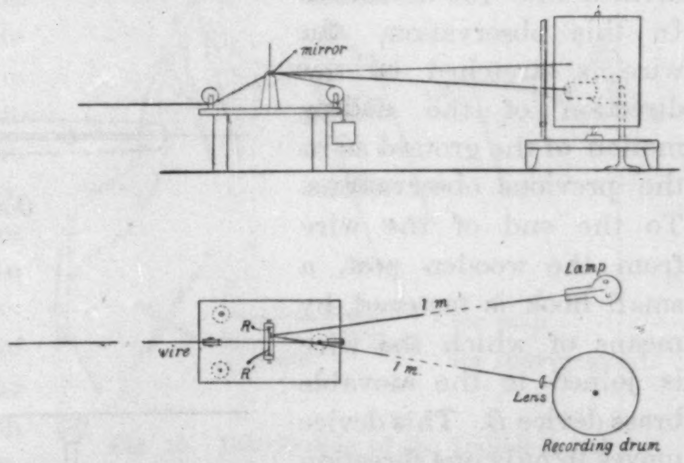

Fig. 7. Photographic recording apparatus for landslide observation. Upper=elevation, lower=plan.

From these records it is apparent that the motion did not have a constant speed, but varied considerably from time to time. In the figures are seen several sudden changes in the inclination of the curve. The

fluctuations in the sliding speed were also confirmed in the following manner.

Observation of the sliding motion by means of the dial-gauge. As is well known, the displacement of the contact point of the dial-gauge is measured by reading the displaced amount of the indicator on the graduated circle. In our case a displacement of 1 mm. of the contact point is equivalent to one revolution of the indicator. The circumference of the circle is divided into 100 divisions. In this observation, the wire is stretched in the direction of the sliding motion of the ground as in the previous observations. To the end of the wire from the wooden post, a small hook is fastened, by means of which the wire is joined to the movable brass device B. This device moves in only one direction through rectangular opening $EFCD$, while to its opposite end a helical spring is attached. This spring gives the desired tension to the wire upon adjusting its length by means of the screw S. The brass stand is fixed to the ground by embedding the tripod firmly in it. When the land makes a sliding motion, it pulls the wire and moves the brass device. The contact point of the gauge touching this device rotates the indicator. The exact time required for a definite amount of sliding distance was measured by a stop-watch. The instrument being portable, the sliding speed could be determined wherever desired.

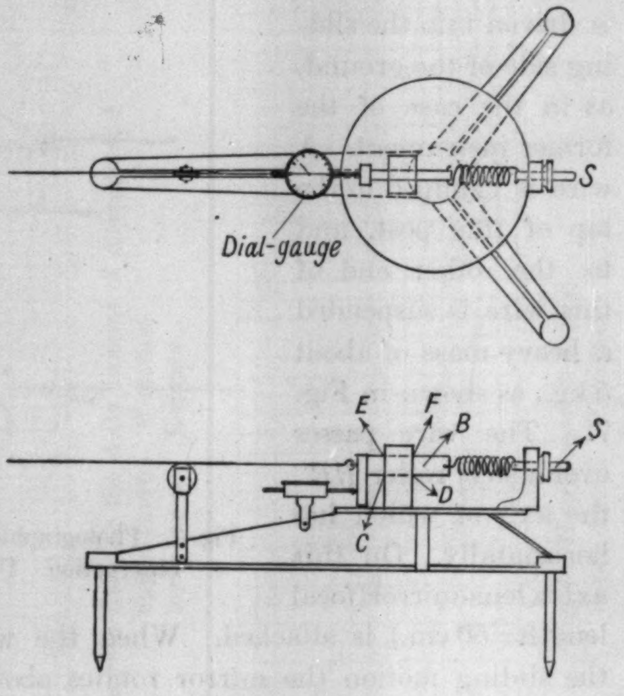

Fig. 9.

In the case of the present landslide, the sliding speed was considerable. The time required to slide 1 mm. as measured at places where sliding was most active being less than ten minutes. Measurements were also made at places where the speed was not so great, in which case the time required to slide less than 1 mm. was measured.

It must here be added that in using this instrument, where the sliding speed is small, difficulties arise, for at such places, owing to the long time required for the observation, influences of temperature variation disturb the results. Our experience has shown, however, that when this instrument is set on firm (stationary) ground, the indicator of the gauge showed no deflection greater than one division during a half-hour or an hour, and that on the whole there is little effect of sunshine or wind.

Observations with this instrument were made twice during February; the first observation on the 18th and the second on the 28th. The sliding times and the sliding distances measured are shown in Lists 3 and 4. The direction and the magnitude of the hourly rate of the sliding distance at each point are shown in Figs. 10 and 11.

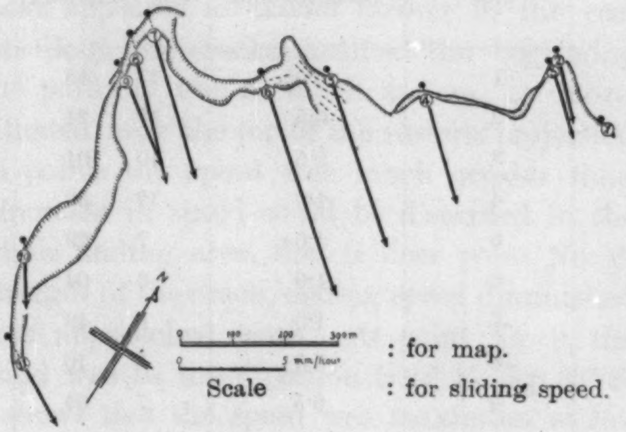

Fig. 10. Distribution of the sliding speed on Feb. 18.

The direction of the sliding motion at each station was determined by means of the dial-compass, which shows fair agreement with Professor Matsuyama's result. For example, Matsuyama's value of the sliding direction of bench-mark M_2[3] takes a value between S 50° E and S 54° E, while in our observation it was S 50° E at point No. 6 in Fig. 11; and at M_8,[3] one of Matsuyama's bench marks, the direction was between S 59° E and S 54° E, against which value we obtained S

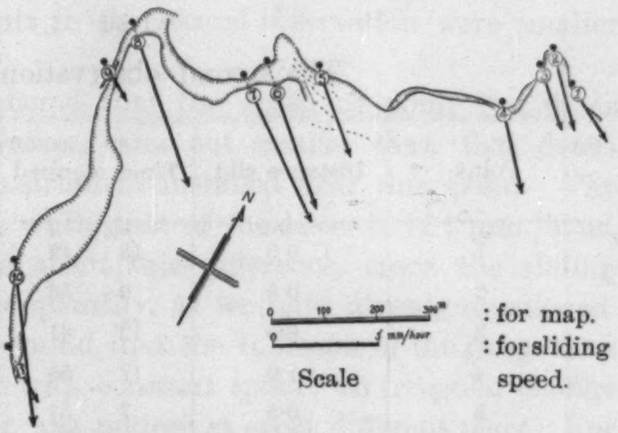

Fig. 11. Distribution of the sliding speed on Feb. 28.

3) MATSUYAMA's bench-mark M_2 was 80 m. away from point No. 6 (Fig. 11) eastward. Bench-mark M_8 was 50 m. away from point No. 11 (Fig. 11) north-eastward.

60° E. In the last two figures, the positions of the post are indicated with circles, together with their serial number, while the positions of the gauge are shown by dots. The arrows are drawn in the directions

List 3.

The first observation, Feb. 18.

Point	Distance slid	Time required		Hourly rate of slide	Direction
	mm	m	s	mm	
1	0·05	17	15	0·2	S 60° E
2	0·5	10	24	2·9	S 45° E
3	0·5	10	04	3·0	S 48° E
4	1·0	12	35	4·8	S 48° E
5	1·0	7	29	7·9	S 50° E
6	1·0	6	04	9·9	S 50° E
7	1·0	8	48	6·8	S 48° E
8	0·5	5	10	5·8	S 45° E
9	0·5	7	04	4·3	S 54° E
10	0·5	12	59	2·3	S 33° E
11	0·5	18	57	3·2	S 60° E

List 4.

The second observation, Feb. 28.

Point	Distance slid	Time required		Hourly rate of slide	Direction
	mm	m	s	mm	
1	0·5	13	12	2·3	S 60° E
2	0·5	9	56	3·0	S 45° E
3	0·5	12	41	2·4	S 50° E
4	1·0	17	50	3·4	S 55° E
5	0·5	7	51	3·8	S 50° E
6	0·5	5	25	5·6	S 50° E
7	0·5	4	42	6·4	S 55° E
8	1·0	8	34	7·0	S 45° E
9	0·5	22	57	1·3	S 58° E
10	1·0	8	46	6·8	S 60° E
11	0·25	11	45	1·3	S 37° E

of the sliding motion, their lengths being proportional to the sliding speed.

In Fig. 11, we see that at point No. 1, the eastern extremity of the zone of cracks, the motion was much slower than at any other place. In fact, the total amount of dislocation of the narrow pathway that passed through this point No. 1 was found to be about 50 cm. at the time it was observed on Feb. 18, beyond which the trace of the cracks could hardly be traced. It should be added that since this observation (Feb. 18) was made, the cracks appeared to extend farther to the east with increased sliding motion along the cracks, until at the beginning of June the dislocation of the pathway was as much as 3 m. or more. Stations Nos. 2 and 3 are situated near the top of the eastern projection of the sliding area, at which points the speed was much greater than at point No. 1, but further increase in speed could be discerned in the region at the top of the whole sliding area, that is near point No. 6. At points along the western margin of the crack, sliding speed diminished as the positions of the points approached south. At point No. 9, the motion of the depressed ground was in the direction S 23° E, dip 33° S.

The second observation shows that the speed was maximum at No. 8, instead of at No. 6 as in the first observation. There is more or less difference in the distribution of the sliding speed in these two observations, but the speed was greater at the top of the whole sliding area. The sliding speeds of all points in the second observation were smaller than those in the first.

It must here be remembered that the speed of point No. 6, as determined in the first observation, came out smaller than that determined by the self-recording instrument installed near this point. The former value is 9·9 mm./hour, while that of the latter is 11·2 mm./hour. There is nothing remarkable about this difference, since the sliding speed is not always a constant quantity, as we have already mentioned. As a matter of fact, we have found that the indicator of the gauge does not invariably move smoothly with constant speed; an irregular change in the motion of the indicator was noticed at every different place. For example, at point No. 6, the indicator sometimes travelled over five or ten divisions of the graduated circle in only two or three seconds, and afterwards moved leisurely at a rate of ten or twenty seconds to pass one division. At points where the motion was slower than at point No. 6, the number of divisions traversed within a given time diminished in proportion to the speed of the landslide. All these anomalies, of course,

have nothing to do with instrumental peculiarities.

Variations similar to the foregoing, but in the sliding motion of the ground, takes place in comparatively long time-intervals, such as two or three hours. It was often found in the records obtained by the instrument first described, that the inclination of short segments of the curves showed different values for each segment of the curve. It is therefore to be understood that Figs. 11 and 12 show the distribution of the sliding speed for only a few hours. It might be added here that a series of our observation takes about 3 hours.

Observation of the sliding mass for earth-tilts. The fact that houses in the disturbed area, since the beginning of the sliding, had leaned so much out of the vertical as to render it difficult in the course of a month to close the doors, naturally suggested earth-tilt. For the purpose of measuring the tilts, we installed two horizontal component seismographs at T, see Fig. 1, and registered the two horizontal components of the tilting motion. These component pendulums were of the mechanical registration type, with natural oscillation periods between 2·0 and 6·0 seconds, their mechanical magnification being 20 times.

At the beginning of observations, that is Feb. 3, tilting went on at the rate of 1·49′ a day in the NS component and 0·74′ in the EW component. But since then the amount of the tilting incresed daily as the sliding speed increased. The pendulums, whose periods were first adjusted to 4·5 seconds, became too sensible to register such a large amount of tilting and often went off the smoked paper during a day's observation. The periods were reduced therefore to 3·5 seconds on Feb. 16. The daily amounts of tilt are given in List 5, with the changes

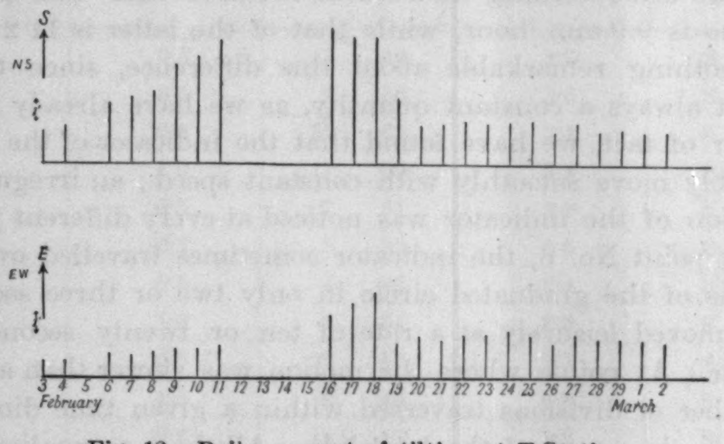

Fig. 12. Daily amount of tilting at T-Station.

List 5.

The daily and hourly amounts of tilt.

(Angle in minutes)

Date		NS comp. (dip S)		EW comp. (dip E)	
		ϕ/day	ϕ/hour	φ/day	φ/hour
Feb.	3	1·49′	0·06′	0·74′	0·03′
	4	1·76	0·07	0·72	0·03
	5				
	6	2·88	0·12	1·02	0·04
	7	3·17	0·13	0·89	0·04
	8	3·41	0·14	1·12	0·05
	9	4·59	0·19	1·23	0·05
	10	5·05	0·21	1·29	0·05
	11	5·89	0·25	1·44	0·06
	12				
	13				
	14				
	15				
	16	6·36	0·27	2·83	0·12
	17	5·92	0·25	3·48	0·15
	18	6·00	0·25	3·98	0·17
	19	3·05	0·13	1·58	0·07
	20	1·87	0·08	1·91	0·08
	21	1·88	0·08	1·69	0·07
	22	2·06	0·09	1·94	0·08
	23	1·91	0·08	1·99	0·08
	24	1·99	0·08	2·15	0·09
	25	2·04	0·09	1·94	0·08
	26	1·56	0·07	1·53	0·06
	27	1·95	0·08	1·95	0·08
	28	1·56	0·07	1·73	0·07
	29	1·67	0·07	1·76	0·07
March	1	1·51	0·06	1·69	0·07
	2	1·56	0·06	1·59	0·07

shown in Fig. 12. The total amount of tilt is unknown as no observation were made on Feb. 5 and during the 4 days following Feb. 12. inclusive. The direction of the tilting motion during the first half of Feburary was downwards towards the SSE, but in the latter half it veered to the SE.

Conclusion. This landslide, which is still going on, is believed to be the largest that has been experienced in Japan. From the view point of geology and geography, it has nothing new to teach us. The only serious aspect of it is the potential danger to civil engineering works. No landslide has yet been studied quantitatively with instruments of precision. It gave Professor Matsuyama an opportunity of establishing a method of studying the phenomenon of landslides in a scientific manner. Our method, however, which demands much less labour and smaller outfit, will be found convenient and suitable when nothing more than the general course of the sliding movement of the land mass is sought.

---

45. 大阪地辷の研究

地震研究所 那須信治

大阪府下峠區地辷の發現當初よりの經過の概要を述べ、地辷に對する簡單なる器械觀測方法を記して置いた。その大要は次の通りである。

地辷地帶の周緣部の主裂罅の運動を特殊の自記裝置により二箇所に於て二月一日より四月二十日に至る八十日間觀測した。その結果二月二十日頃地辷運動は最高潮に達し、日々移動量は三三・四糎に達した。それより順次減退を示してゐることがわかつた。

自記記錄によれば地辷り運動は比較的正しく直線に記錄されてゐる。即ち一日中の速度は略等速度のように見える。然しこれを瞬間的によく見るとやゝ不規則な速度變化がある。この現象を研究するために地辷運動を二千倍に擴大しこれを早廻しの寫眞記錄裝置により記錄した。その結果速度は前述の如く瞬間的には可成り大なる變化があることを認めた。

次にダイヤル、ゲージを裝置した携帶用の移動測定器を考案し、周緣部に沿つて十一箇所に於ける運動速度の大小を研究した。この測定では地辷速度の大なるところでは一粍を辷るに要する時間を、又速度が大ならざるところでは〇・五粍或はそれ以下を辷るに要する時間を測定した。この觀測は二月中二回施行した。これらの時間より各點に於ける一時間の地辷移動量を求めた。二回の觀測の結果、地辷地帶の上部(頂點にあたるところ)附近に於て移動量は最大であつた。

次に地表傾斜觀測を地辷地帶の中央部に於て二月三日より三月二日迄繼續して行つた。日々の傾斜量は地辷速度の增減と略同一步調を以て增減を示した。

此研究の主眼は地辷運動を記錄し、或はダイヤル、ゲージ等によりて測定し、比較的短時間中に於ける運動の消長を知るにある。日々移動量の測定等には三角測量及水準測量等を以てするを最良の方法とするも瞬時の運動の研究には本文に携げたような方法を取るより仕方がない。しかしながら主裂罅より遠い地辷地帶內部の點の瞬間的の運動はこゝに述べてある方法を以てしては知ること

a

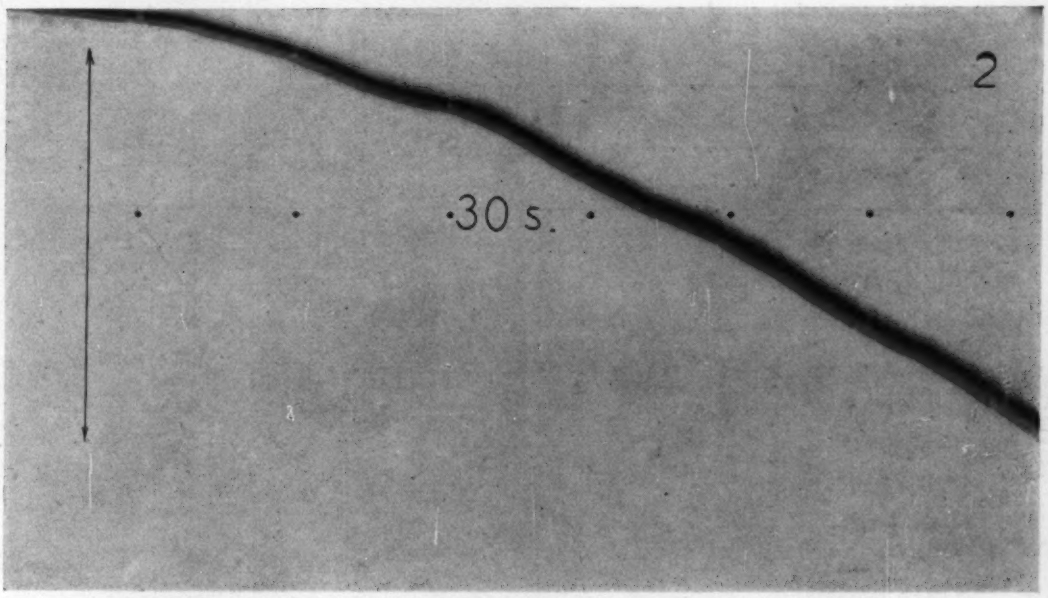

(3/14 of actual)

b

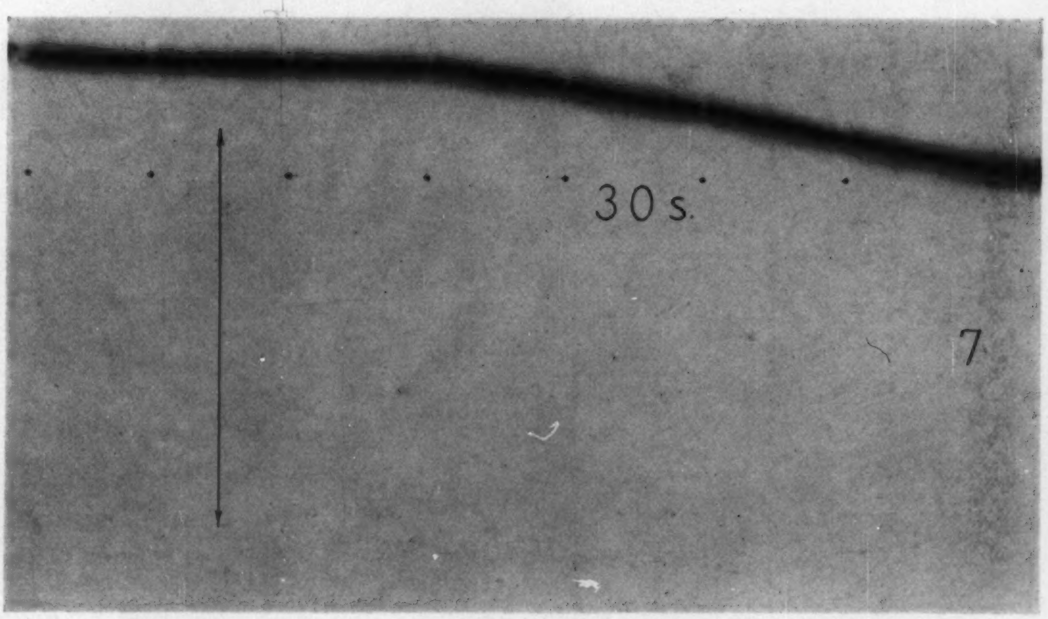

(3/14 of actual)

Fig. 8. a. b. Photographic records of the sliding motion. Lengths of arrows corresponds to the actual distance slid of 1/10 mm. Time between two dots = 30 sec.

(震研彙報、第十號、圖版、那須)

c

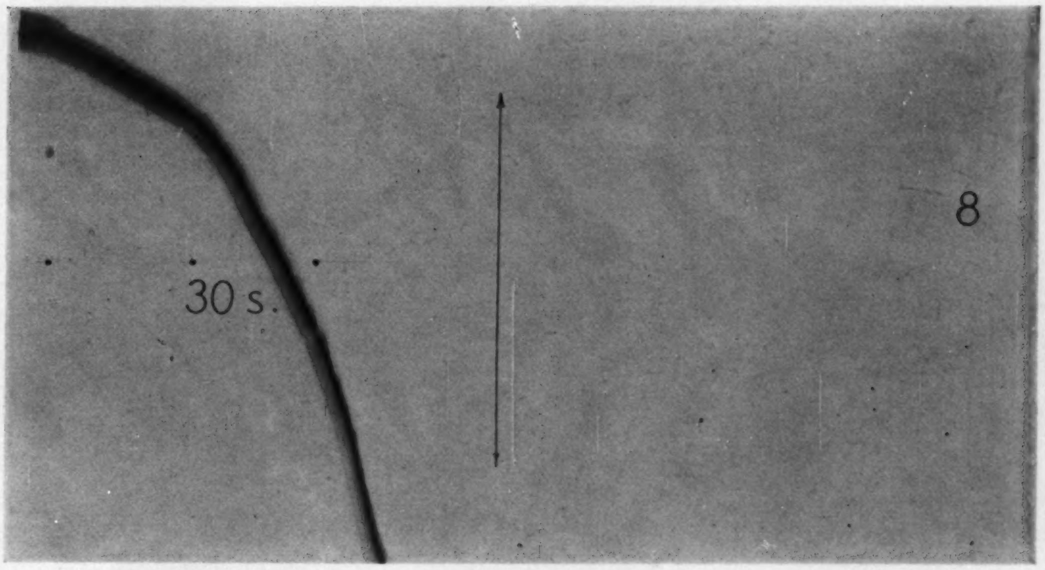

(3/14 of actual)

d

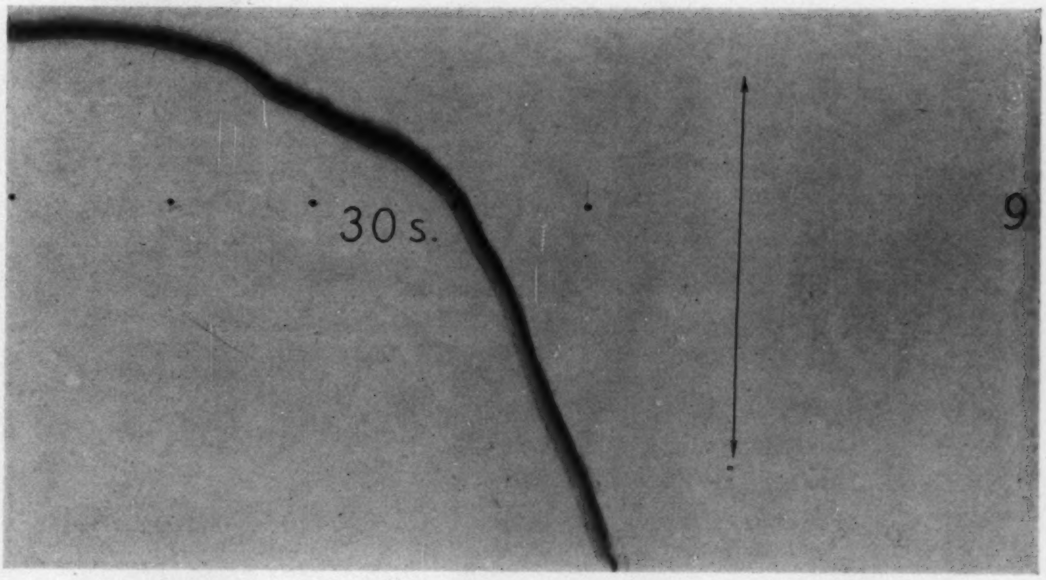

(3/14 of actual)

Fig. 8. c. d. Photographic records of the landslide. Length of the arrows corresponds to the actual distance slid of 1/10 mm. Time between two dots = 30 sec.

(震研彙報、第十號、圖版、那須)

不可能である故に此研究は周緣部の運動に就いてのみ行つた。地亡運動全般の經過を知るには此の方法でも相當の結果を擧げ得ると思ふ。

46. *Landslide at Tôge, Katagami-mura, Osaka-Hu.*[1]

By Naomi MIYABE,

Earthquake Research Institute.

(Read Feb. 16, 1932.—Received June 20, 1932.)

1. Towards the end of November 1931, a phenomenon of a most alarming nature was discovered at Tôge, a village in Osaka prefecture. An area of nearly 74 acres, containing the village of Tôge, was found to be sliding slowly downwards in a southerly direction towards the Yamatogawa[2] (river). Many cracks had formed on the boundary zones of the moving and stationary regions as well as in the middle of the sliding ground itself, and these seemed to grow in size and number every day. Not long after the discovery, the inside wall of the Kamenose[3] railway tunnel that passes underneath the sliding region, caved in and temporarily interrupted traffic. This paper is a report of studies of the landslide made by the writer on the spot.

2. The map, Fig. 1, shows the location of the village of Tôge and the topographical features of its environs. It will be seen from the figure that the slope on which the village is situated is gentler than the opposite slope across the Yamatogawa (river). The topographical feature of this gentle slope, together with the curious trend of the river-course, suggests frequent landslides here in recent geological time.

The area not slipping is bounded by a zone of major cracks, while in the area itself minor cracks have developed here and there. The distribution of these cracks are shown in Fig. 2, and parts of them also in Figs. 5, 6, and 7 (Pl. LXXXVII & LXXXVIII).

On tracing the trend of the zone of major cracks, its continuity is interrupted by a sudden change in direction at the point marked E in the Fig. 2. In observing these cracks, Mr. Nasu[4] noticed that the cracks at a place westward of point E differed in rate of growth from those at a place eastward of it. For case of reference, therefore, the cracks have been divided into two groups, the Eastern and Western, in accordance with their location and mode of growth.

---

1) 大阪府堅上村峠.
2) 大和川.
3) 龜ノ瀬.
4) N. NASU, *Bull. Earthq. Res. Inst.*, this vol.

Fig. 1. Topographical Feature in the Vicinity of the Village of Tôge.

In the Western group, the cracks at A (Fig. 2) consist of several parallel fissures *en échelon,* which might have been produced by a shear movement. These cracks are traceable southward down to R, where the uplifted bed (probably a result of the landslide) of the Yamatogawa river is exposed. At the place marked M, popularly called "Owankake" and "Ubagakake", considerable quantities of sand and gravel drop from time to time into the river below.

The cracks B and C which were the first to be discovered, have grown since then and become the largest of them all. The movement of the area that is sliding is recognized at these places by the opening of cracks and formation of steps, and has been found to be in the direction approximately perpendicular to the trend of the cracks at these places. It is here also that the horizontal and vertical movements of the sliding earth mass have been most marked. Shear type cracks are observed in the region lying between C and D.

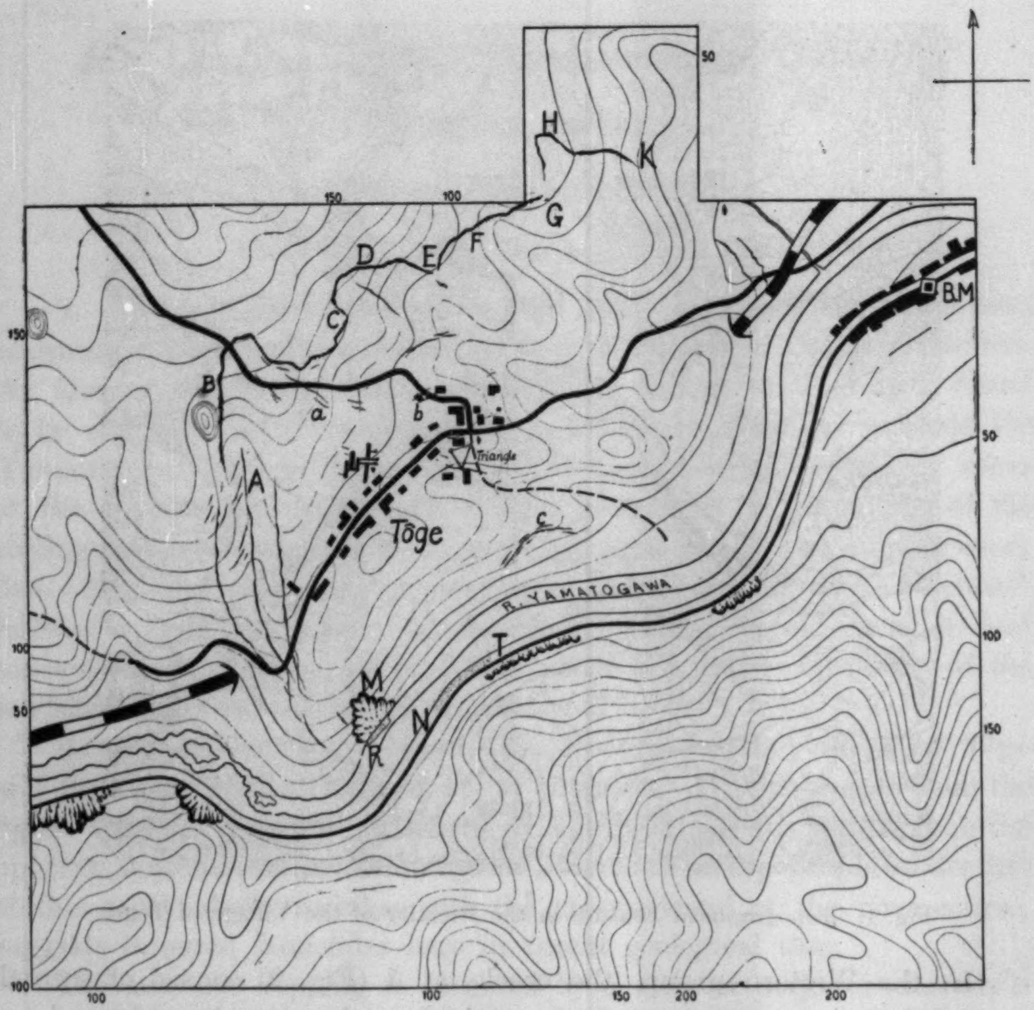

Fig. 2. Distribution of Cracks in the Vicinity of the Village of Tôge, Osaka-Hu.

The existence of these shear cracks between C and D and the cracks *en échelon* between A and B, is consistent with the presence of tension cracks between B and C, and consequently with the implication that the movement of the sliding earth mass is being directed perpendicular to the trend of the cracks at B and C, that is, from N to S.

As already mentioned, the trend of the cracks of the Eastern group, i.e., the cracks EFGHK (Fig. 2), are traceable over the rice fields and the railway track from K to the eastern portal of the Kamenose railway tunnel.

On the southern side of the Yamatogawa (river) a continuation of a sliding earth is observed at an upheaval of several metres of a part of a highway, the prefectural road joining Osaka and Nara, and denoted

by NT in Fig. 2 (cf. photo Fig. 8, Pl. LXXXVIII). This fact seems to strengthen the conclusion that the movement of the earth mass is in such a manner that it as a whole slides over some curved surface down to the south as shown schematically in Fig. 3.

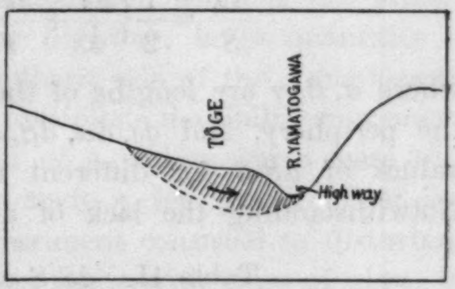

Fig. 3.

As has been already mentioned, in addition to the cracks in the boundary zones, many cracks or groups of cracks are observed in the sliding area itself, the outstanding ones being those marked *a* and *b* and some others near *c*.

3. Since the landslide is slowly proceeding, houses in the village of Tôge, in the sliding area, have been more or less damaged, probably because of deformation of the sliding earth mass.

The writer has measured the lengths and angles of a triangle framed in Tôge (Fig. 4) for the purpose of investigating the variations in the deformation of the earth's surface with respect to time. These measurements were carried out three times since the 1st of February this year, with results as shown in Table I.

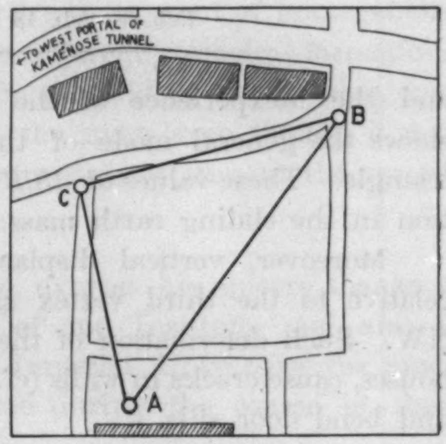

Fig. 4.

Table I. The Result of the Triangulation.

Date of Measurement	Lengths and Changes in Length of Lateral Sides						Heights referred to *A*	
	$\overline{AB}$	$\delta(\overline{AB})$	$\overline{BC}$	$\delta(\overline{BC})$	$\overline{CA}$	$\delta(\overline{CA})$	*B*	*C*
Feb. 1. p.m.	m 38·718		m 31·107		m 18·947		m 1·331	m 1·220
		cm +4·6		cm −2·9		cm +2·5		
Feb. 3. p.m.	38·764		31·078		18·972		1·325	1·182
		+9·8		+1·7		+10·3		
Feb. 13. p.m.	38·862		31·095		19·075		1·429	0·938

From these results, elongations and contractions of the lateral sides of the triangle for different time intervals were obtained by means of a simple calculation, whence the horizontal deformation of the triangular area its computed by the formula

$$\frac{dS}{S}=\frac{1}{2}\left\{\frac{ds}{s}+\frac{ds-d\alpha}{s-\alpha}+\frac{ds-d\beta}{s-\beta}+\frac{ds-d\gamma}{s-\gamma}\right\},$$

where α, β, γ are lengths of the lateral sides of the triangle, s is half the periphery, and ds, $d\alpha$, $d\beta$, $d\gamma$, are their changes. The calculated values of dS/S for different time intervals are shown in Table II. Notwithstanding the lack of accuracy incident to instrumental errors

Table II. dS/S calculated from the data in Table I.

Time interval	dS/S
Feb. 1—Feb. 3	$-1{\cdot}8\times10^{-4}$
Feb. 3—Feb. 13	$5{\cdot}7\times10^{-3}$

and the inexperience of the observer, the result obtained as above shows the general mode of time-variation of the deformation of the triangle. These values of dS/S point to considerable horizontal deformation in the sliding earth mass.

Moreover, vertical displacements of two vertices of the triangle relative to the third vertex show that the triangle tilted to the N or NW. Such deformation of the sliding earth mass may probably damage houses, cause cracks in walls (cf. photo Fig. 9, Pl. LXXXIX), tilt pillars, and bend door sills.

4. As to the real cause of the present landslide, we have no direct evidence of any kind. But so far as our observations go, the phenomenon seems to be due in large measure to mechanical action of the materials constituting the present sliding earth mass and its neighbourhood.

According to Prof. Makiyama, the geological structure of this region consists, as Prof. Matuyama[5] has also described, of three layers, namely, a lower andesite which had come from some mature volcano in the south, an intermediate agglomerate or conglomerate, and an upper layer of recent andesite. In the upper layer, slaty jointing is the dominant feature (cf. photo Fig. 10, Pl. LXXXIX), its uppermost parts being so badly weathered that almost all of it has transformed into clay. In such a condition of things, a minute change in the field of gravity, or in that of the other mechanical forces at work in maintaining the present state

5) M. MATUYAMA, *Tikyû*, 17 (1932), 323, (in Japanese).

of the earth's surface, may produce phenomenon such as the present landslide. In the construction of a new highway, large quantities of earth have been removed from the southern side of the Yamatogawa, and it is possible that this has helped to precipitate the sliding movement.

We could compare the deformation of a sliding earth mass with the results of an experiment[6] that was made a few years ago at our Institute with layers of sand. The experiment consisted in disturbing horizontal layers of sand packed in a box made with sides of glass, by gradually pulling away with uniform speed one of the end sides of the rectangular box, when the sand mass slips down forming irregular step faults[7] (cf. photo Fig. 11, Pl. LXXXIX). These irregular formation of step faults may have been due partly to slight lack of homogeneity in the sand mass. In the actual case of the earth's crust, want of homogeneity, such as the varying surface configurations, different geological formations, and the presence of cocluded waters in the sliding earth mass, may complicate the mode of deformation of the mass even though it may be sliding as a whole with uniform mean speed, as seen in the records that were obtained by Mr. Nasu.[8]

In conclusion, the writer desires to express his sincere thanks to Professors T. Terada and M. Ishimoto of our Institute, and also to Professor M. Matuyama of the Kyôto Imperial University, for much valuable advices and suggestions received during the course of these studies.

---

46. 大阪府堅上村峠に於ける地辷に關する調査報告

地震研究所 宮 部 直 巳

昨年 (1931 年) 十一月の末頃から大阪府下堅上村峠附近の傾斜地に地割を生じ、それが次第に生長してゆく樣に見えた。其後、この地域を通過する關西本線龜ノ瀬隧道にも龜裂を生じ、局部的には崩壞するに至つたので、關西本線の運行が停止されこの部分だけ徒歩によつて聯絡することゝなつた。

---

6) T. Terada and N. Miyabe, *Bull. Earthq. Res. Inst.*, **4** (1928), 33; **6** (1929), 109; **7** (1929), 65.

7) These experiments thus far are not comprehensive enough to justify discussions of them as being in any way analogous to the phenomenon of the present landslide. Further experiments are contemplated.

8) N. Nasu, *Bull. Earthq. Res. Inst.*, this vol., *loc. cit.*, (4).

筆者は二月初旬から中旬にかけて調査を命ぜられた。本文はその結果の簡單な報告である。

第二圖は滑落地域における龜裂の分布を示したものであるが、龜裂の大いさ、數等は其後次第に增加しつゝあるので現在の龜裂の分布とは多少異るかもしれない。

二月中旬には、地域内の家屋が損傷を被るやうになり、壁の龜裂（寫眞第九圖）、柱の傾斜、敷居の撓曲等が見られた。これは、恐らく滑落地域内の土地の變形によるものであらうと思はれる。地域内に設けた假の三角形により、その邊長の時變化からその附近の土地の變形を算出したものは第一、二表に示されてゐる。これによつても、可成の程度の變形があつたことを推察することが出來る。

この地辷の眞因は[illegible]ところ不明であるが、今まで見た所では、土地を構成する地層の性質が關係の深いことは推察出來る。この附近の土地の[illegible]なる安山岩層中には第一〇圖寫眞に示す樣なスレート樣節理が[illegible]達して居て、崩れやすく、最上層は殆ど風化して粘土化してゐる。

かく地層の[illegible]崩れやすく壞れやすいところへ、この地形を保つてゐる外力に些少の變化でも起つたならば、[illegible]樣な地辷りが起り得るのではなからうか。例へば、大和川南岸の縣道工事に際して切取ら[illegible] mass の有無といふやうな事でも、このやうな現象を起す爲めの所謂 triggar action と[illegible]可能性があるかもしれない。

この地[illegible]類似な現象の一つとして、吾々が嘗つて行つた砂層の崩壞に關する實驗の結果を想起する[illegible]出來る。

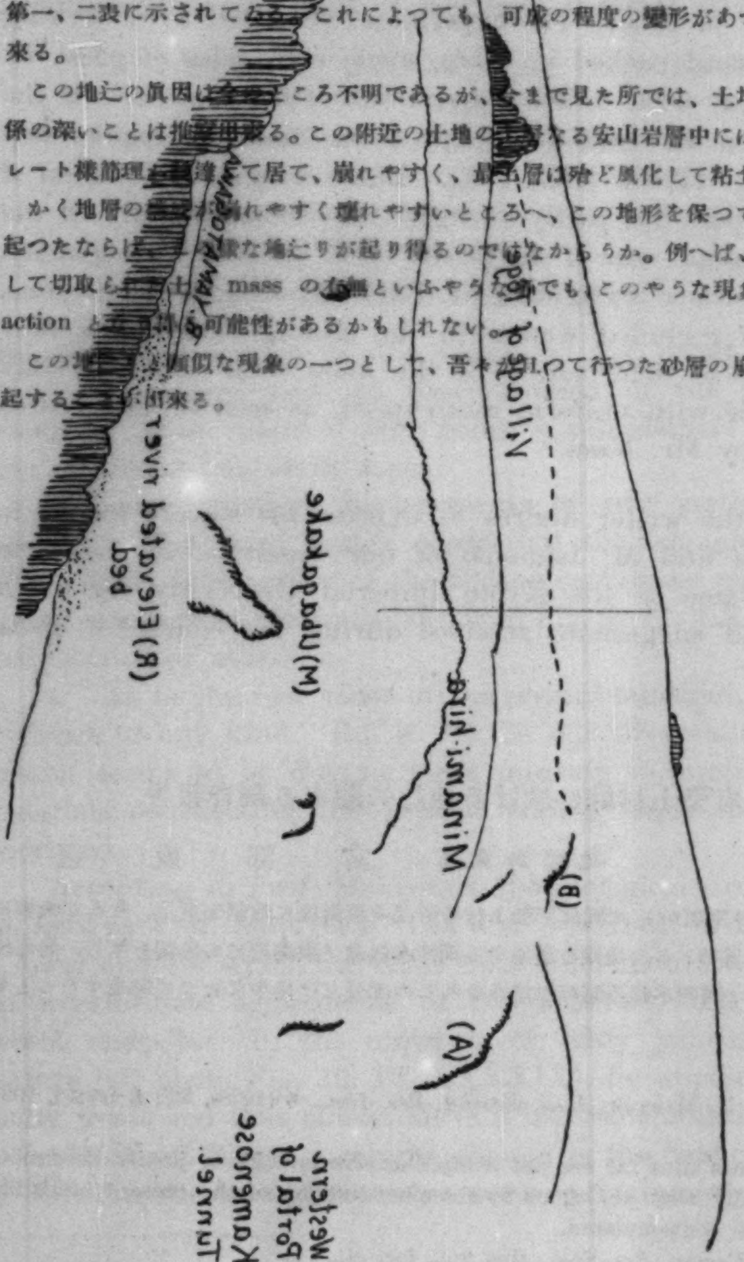

(震研彙報、第十號、圖版、宮部)

Fig. 5. General view of the sliding area.
(Photo. on the 13th of February, from SW across the Yamatogawa.

筆者は二月初旬から中旬にかけて調査を命ぜられた。本文はその結果の簡單な報告である。

第二圖は滑落地域における龜裂の分布を示したものであるが、龜裂の大いさ、數等は其後次第に増加しつゝあるので現在の龜裂の分布とは多少異るかもしれない。

二月中旬には、地域内の家屋が損傷を被るやうになり、壁の龜裂（寫眞第九圖）、柱の傾斜、敷居の撓曲等が見られた。これは、恐らく滑落地域内の土地の變形によるものであらうと思はれる。地域内に設けた假の三角形につき、その邊長の時變化からその附近の土地の變形を算出したものは第一、二表に示されてゐる。これによつても、可成の程度の變形があつたことを推察することが出來る。

この地辷の眞因は今のところ不明であるが、今まで見た所では、土地を構成する地層の性質が關係の深いことは推察出來る。この附近の土地の上層なる安山岩層中には第一〇圖寫眞に示す樣なスレート樣節理が發達して居て、崩れやすく、最上層は殆ど風化して粘土化してゐる。

かく地層の構成が崩れやすく壞れやすいところへ、この地形を保つてゐる外力に些少の變化でも起つたならば、この樣な地辷りが起り得るのではなからうか。例へば、大和川南岸の縣道工事に際して切取られた土の mass の有無といふやうな事でも、このやうな現象を起す爲めの所謂 triggar action となり得る可能性があるかもしれない。

この地辷りと類似な現象の一つとして、吾々が且つて行つた砂層の崩壞に關する實驗の結果を想起することが出來る。

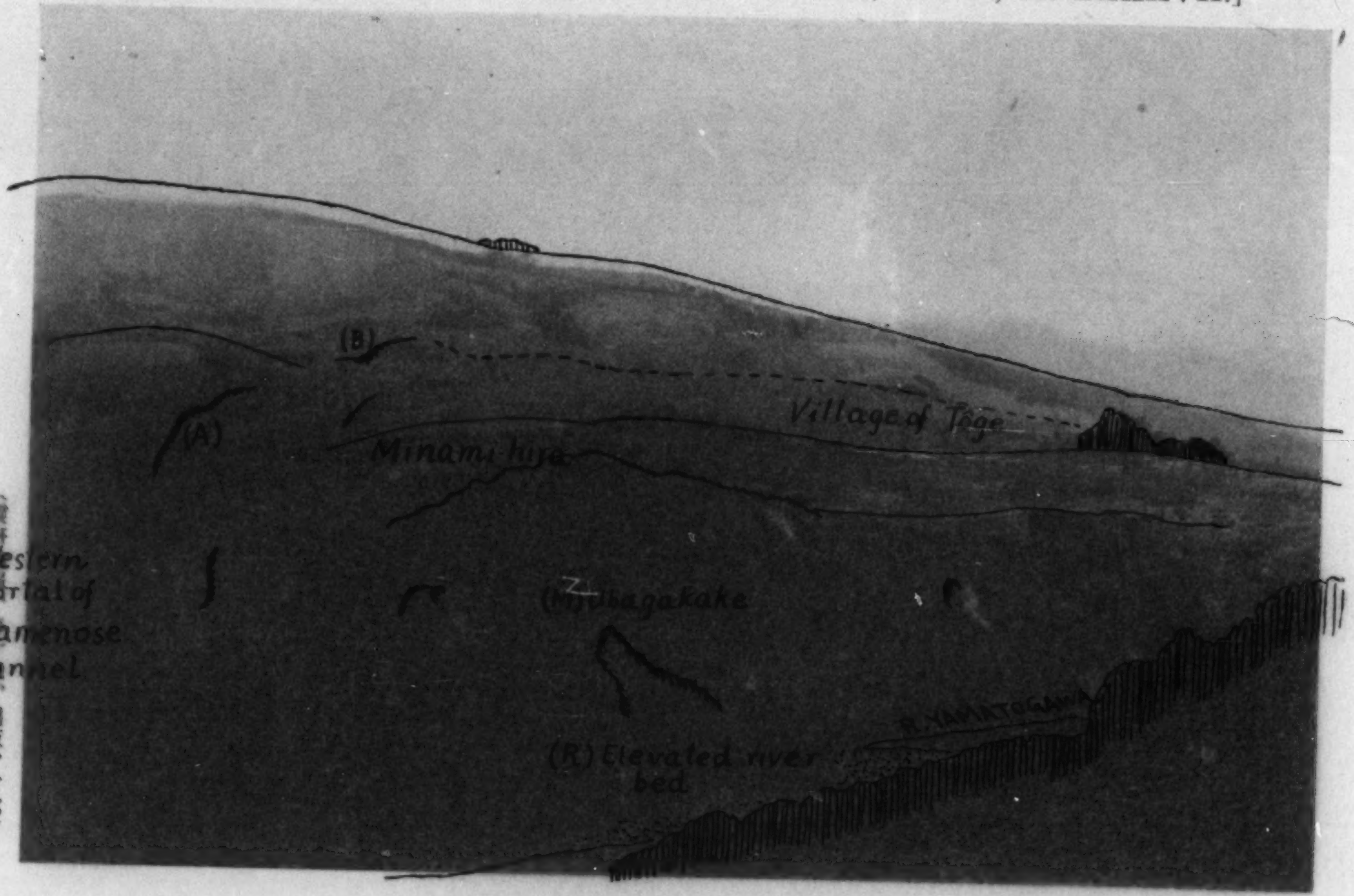

Fig. 5. General view of the sliding area.
(Photo. on the 13th of February, from SW across the Yamatogawa.

(震研、圓阪、宮部)

Fig. 6. Crack near C, where Mr. Nasu's self-recording instrument was installed.
(Photo. on the 3rd of February).

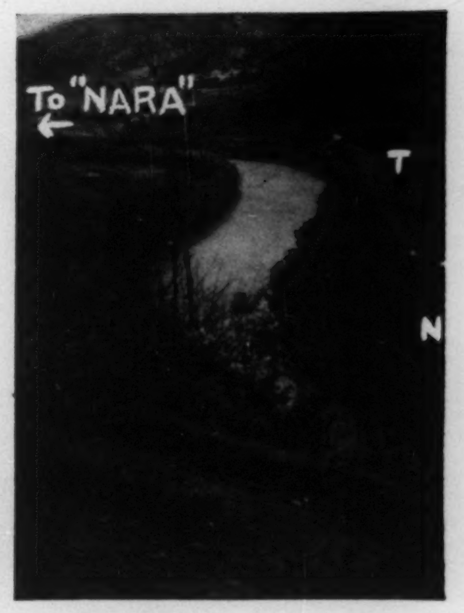

Fig. 8. The Yamatogawa viewed from Minamihara.
(Photo. on the 3rd of February).

Fig. 7. Crack in the sliding area.
(Photo. on the 3rd of February).

Fig. 9. A house attacked by the deformation of the earth's mass. (Photo. on the 13th of February).

Fig. 10. Slaty Joints.

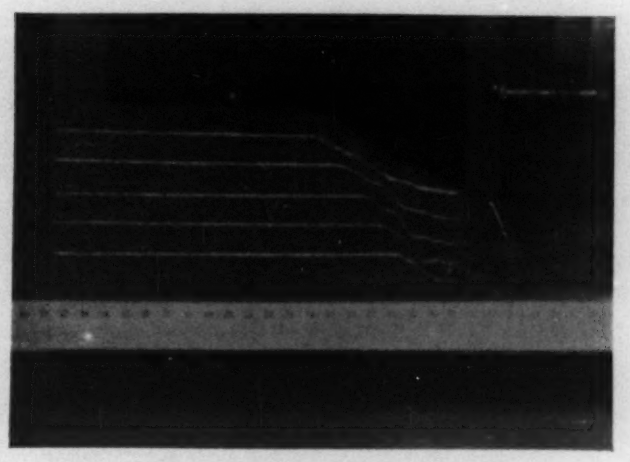

Fig. 11. Deformation of the Sand mass produced by receding the wall.

(震研彙報、第十號、圖版、宮部)

47. *Post Pliocene Crustal Movements in the Outer Zone of Southwest Japan and in the "Fossa Magna."*

(1)

By Yanosuke ÔTUKA,

Earthquake Research Institute.

(Read Nov. 17, 1931.—Received June 20, 1932.)

Introduction.

In a previous paper[1] the writer compared the geologic structure of the lower Pliocene strata in the Outer zone of Southwest Japan with that in the Fossa Magna, and arrived at the following conclusions:

The lower Pliocene or Pliocene strata are usually monoclinal at low angles either to the southwest or to the southeast, with the exception of a few small displacements in other directions, while the contemporaneous deposits in the Fossa Magna form a complex anticlinorium, each pericline having a trend parallel to that of the Fossa Magna. There are many thrust- and normal-faults associated with these folds. Volcanism was frequently active. The structural lines of the lower Pliocene deposits conform neither to the general trend of the Honsyû arc nor to the main structural lines of the Outer zone of Southwest Japan, but with the trend of contour lines of a summit-level in the Outer zone of Southwest Japan. Moreover, the inclination of the bedding plane of the Pliocene strata is steeper than that of the surface of the summit-level, which dips in the same direction. The writer inferred from these facts that an extensive crustal movement in the form of broad swells took place in the Outer zone of Southwest Japan along a line parallel to the Ryûkyû arc rather than to the Honsyû arc.

The land surface that is represented in outline by the summit-level was denuded during post lower Pliocene, seeing that the lower Pliocene strata are cut by the surface of the summit-level. After that came crustal deformation in the form of broad swells by which the denuded surface was upwarped to the same height as the surface of the summit-level, and this may have continued into the post-Pliocene.

It is a question whether the structural movements in this geologic

1) Y. ÔTUKA, "Early Pliocene Crustal Movement in the Outer Zone of Southwest Japan and in Naumann's Fossa Magna," *Bull. Earthq. Res. Inst.*, 9 (1931), 340-352.

region in the form of broad swells as stated above have continued since the Pliocene to recent times. In this first half of the paper (the second to follow at a later date) will be discussed the geologic structures and the geomorphologic characters that point to crustal deformation during post-Pliocene. Since the Pliocene, the Outer zone of Southwest Japan has been deformed by a marked type of crustal deformations, and the old upwarped land surfaces have worn away through atmospheric denudation, while the old downwarped sea bottoms are covered by fresh deposits. In profile, the old imaginary surfaces that existed as dry land as well as under the sea are seen to have increased their amplitudes, just like stationary waves (Fig. 1).

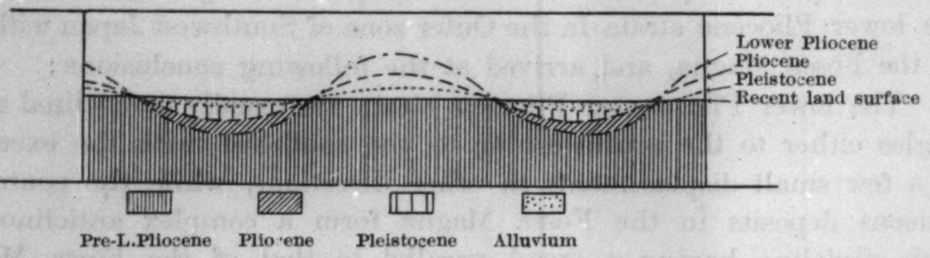

Fig. 1. Ideal section of the areas being deformed in the form of broad swells.

In view of the fact that crustal deformations, such as described in the previous paper, have been found in lower Pliocene strata in the Outer zone of Southwest Japan, the writer considers it reasonable to expect to find similar deformations in the geological structure of post-Pliocene deposits, in the very same part of Japan as well as in the Fossa Magna. These deformations in the crust of the two regions just mentioned will be treated in the latter half of this paper (to follows at a later date), when the crustal disturbances will be considered with reference to the result of precise levels that were run in the two regions.

The Stratigraphic Correlation of the Post Pliocene Strata in the Outer Zone of Southwest Japan with that in the Fossa Magna.

Before discussing the crustal deformations of these region, their general stratigraphy will be outlined. The stratigraphic correlation of the Neogene formations in these regions, which were listed in the writer's previous paper (Table I), needs some corrections in the light of new facts that have come to our knowledge since last year. In Table II are ten stratigraphic columns for these region, which were compiled

from different sources, and is the new scheme of stratigraphic correlation of the Neogene strata in these regions. The post-Pliocene stratigraphy being fully discussed in the "Dai Si Ki" (The Quaternary) of Iwanami Kôza,[2] it will not be repeated here, although certain features of it will be explained in later sections.

For convenience, the Outer zone of Southwest Japan, i.e., the Southern part of the median dislocation line of Southwest Japan, will be divided into five regions as follows:—(a) Tôtômi,[3] (b) Kii,[4] (c) southeastern Sikoku,[5] (d) southwestern Sikoku, (e) Hyûga[6] coastal plain; and the Fossa Magna into three, (f) Suruga,[7] (g) Idu[8] and Sagami[9] and (h) Sinano.[10] In six of these regions,—a, c, e, f, g, h, the Pliocene strata are exposed as already mentioned, while with the exception of southwestern Sikoku, the post-Pliocene strata are exposed in all of them. (Fig. 2.)

Table I. (1931, 9. Y. Ôtuka.)

Locality / Geologic Age	(1) Miyazaki	(2) Kôti	(3) Kakegawa	(4) Asigara	(5) Nagano
Upper Diluvium	Gravel beds	Gravel beds	Gravel beds	Volcanic lava and ash	
Lower Diluvium	Freshwater deposits		Ogasa conglomerate	Gravel beds	
Upper Pliocene			Soga beds	(Ninomiya beds) Nisikoiso beds	
Lower Pliocene	Takanabe group { Heki beds, Kôonzi beds, Sadowara beds }	Suzuki's Pliocene	Kakegawa series	Asigara beds	Sigarami beds
		Umbonium mysticum Zone	Horinouti series		Ogawa beds
Miocene	Tuma group		Sagara beds	Misaka beds	

Post Pliocene Crustal Deformation in the Outer Zone of Southwest Japan.

In order clearly to understand the post-Pliocene crustal deformation in the Outer zone of Southwest Japan, the geologic and geomorphologic features of the respective regions will first be discussed, after which the

2) Y. Ôtuka, "Daisiki" (The Quaternary), *Iwanami Kôza*, (1931), (in Japanese).
3) 遠江. 4) 紀伊. 5) 四國. 6) 日向. 7) 駿河. 8) 伊豆. 9) 相模. 10) 信濃.

Table II. New scheme of stratigraphic correlation of the Neogene strata in the Outer zone of Southwest Japan and in the Fossa Magna. (1932, 6. Y. Ôtuka.)

Province / geologic age	a Tôtômi I. Makinoga-hara.	a II Mikataga-hara.	a III Ogasa hill	a IV. Atumi peninsula	b Kii	c SE Sikoku	e Hyûga	f Suruga	g Idu Sagami	h Sinano
Du.	Makinoga-hara upheaved fluviatile plain	Mikataga-hara upheaved dalta plain		Atumi penin. raised coastal plain	Coastal terraces	Coastal terraces	Coastal terraces	Base of Hudi volc.		
du_I.	Makinoga-hara gravel beds	Mikataga-hara gravel beds		Upper division of Atumi beds					Hakone volcanic ashes	Gravels of River terraces
dl_{II}.	Huruya shell beds	Sahamma shell beds		Lower division of Atumi beds	Sakisima beds		Tôriyama-hama beds		Hirai pumiceous beds	Siokawa beds
dl_I.	Ogasa conglomerate	Ogasa conglomerate	Ogasa conglomerate					Kunôsan & Kanbara conglomerate	Suruga & Kuroiwa conglomerate	
pd.		Soga beds	Soga beds						Zyô beds	Kabutoiwa plant beds
pu.								Kunôsan beds	Kasiwa-tôge beds	
p.	Horinouti series	Kakegawa Series				Tôno-hama group	Takanabe group	Asigara beds		Sigarami & Ogawa beds
m.	Tamari beds						Tuma group			

Du=topographic surfaces of upper Pleistocene; duI=lower half of upper Pleistocene; dlII=upper half of lower Pleistocene; dlI=lower half of lower Pleistocene; pd=transitional formations between lower Pleistocene and upper Pliocene; pu=upper Pliocene (Lower Carabrian); p=Pliocene (middle and lower); m=Miocene (upper).

marked features of the crustal deformation of the post-Pliocene in these regions will be readily grasped.

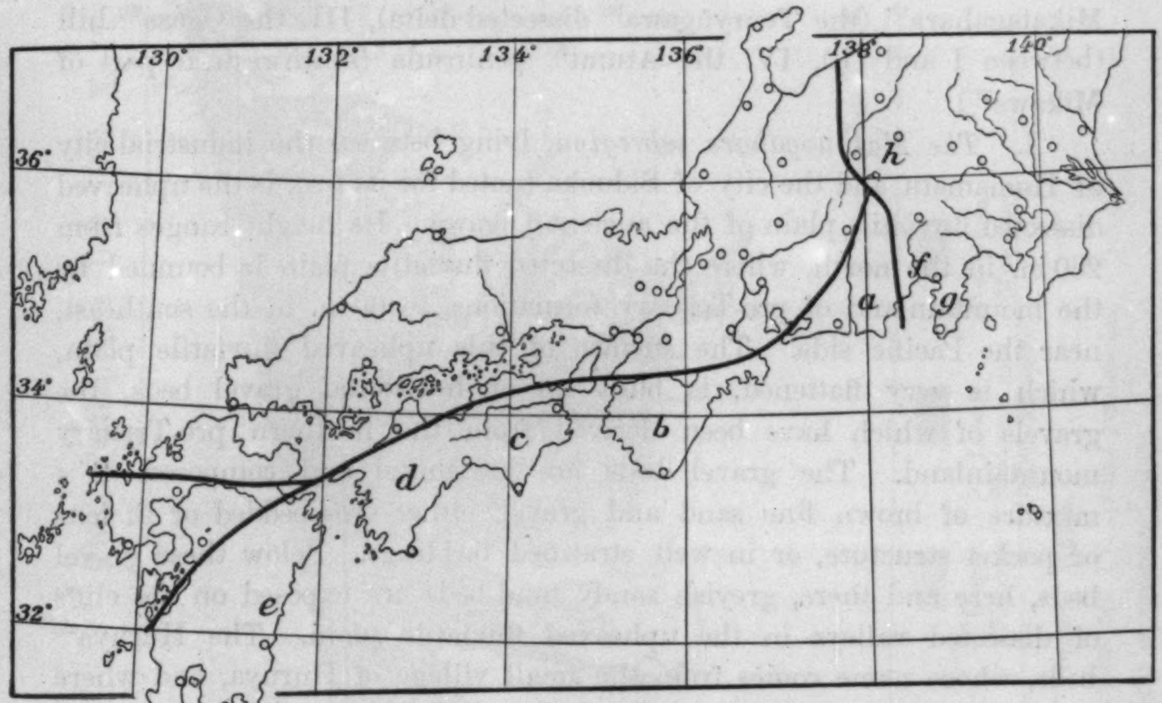

Fig. 2. Index map showing the regions discussed in this paper.

a = Tôtômi, b = Kii, c = Southeastern Sikoku, d = Southwestern Sikoku, e = Hyûga
Outer Zone of Southwest Japan.

f = Suruga, g = Idu, h = Sinano
Fossa Magna.

(a). "Tôtômi" region. The stratigraphy of the Tôtômi districts, as shown in the list (Table II), was surveyed by the late S. Miura,[11] the late K. Nakajima,[12] and later studied by Ishii,[13] Chitani[14] and Makiyama.[15] It is from the writing of the three last-named that the writer has arranged the succession of strata for this region in Table II, column a I, II, III, IV. (Fig. 3).

11) S. Miura, Expl. Text Geol. Map Japan. "Toyohashi" sheet, 1:200.000, (1889), (in Japanese).

12) K. Nakajima, Expl. Text Geol. Map Japan, "Shidzuoka" sheet, 1:200.000, (1886), (in Japanese).

13) K. Ishii, Expl. Text Geol. Map Japan, "Irakozaki" sheet, 1:75.000, (1927).

14) Y. Chitani, Expl. Text Geol. Map Japan, "Sagara" sheet, 1:75.000, (1927); Expl. Text Geol. Map Japan, "Shidzuoka" sheet, 1:75.000, (1932).

15) J. Makiyama, "Stratigraphy of the Kakegawa Pliocene in Tôtômi," *Mem. Col. Sci., Kyôtô Imp. Univ.*, Ser. B, 7, 1 (1931).

This region is divided for convenience into four sub-regions:— I. Makinogahara[16] (eastern portion of the Ôigawa[17] dissected delta), II. Mikatagahara[18] (the Tenryûgawa[19] dissected delta), III. the Ogasa[20] hill (between I and II.), IV. the Atumi[21] peninsula (southwestern part of Mikawa[22]).

I. *The Makinogahara subregion,* lying between the industrial city of Hamamatu and the city of Siduoka (noted for its tea), is the upheaved dissected fluviatile plain of the ancient Ôigawa. Its height ranges from 280 m. in the north, where the dissected fluviatile plain is bounded by the mountainland of pre-Tertiary formations, to 60 m. in the southeast, near the Pacific side. The surface of this upheaved fluviatile plain, which is very flattened, is built up of horizontal gravel beds, the gravels of which have been derived from the northern pre-Tertiary mountainland. The gravel beds are horizontal and composed of a mixture of brown fine sand and gravel, either crossbedded or in lens or pocket structure, or in well stratified beddings. Below these gravel beds, here and there, greyish sandy mud-beds are exposed on the cliffs of dissected valleys in the upheaved fluviatile plain. The Huruya[23] beds, whose name comes from the small village of Huruya, and where the muddy beds are exposed in a typical manner, contain some fossil shells, such as *Ostrea gigas* Thunberg and *Anadara granosa* Linné. These are common species in the Sahamma beds, to which reference will be made later. These beds are underlain unconformably by either the highly dipping Kakegawa[24] series, the Horinouti[25] series, or the Ôigawa series. Near Takaoyama,[26] the older conglomerate beds project like an isolated hill from underneath the surface of the Makinogahara dissected fluviatile plain. This dissected plain, which is bounded on the west by the Ogasa hill, is therefore not considered a typical dissected delta spreading from north to south without any barriers. On the east side of the Ôigawa, the Makinogahara dissected plain disappears. From the distribution of the dissected plains, Watanabe[27] has explained this disappearance by a flexuose deformation of an ancient delta plain, as a result of which the east side of the Ôigawa is flexured downward. But this explanation is based on the assumption that the Makinogahara

---

16) 牧野原. 17) 大井川, gawa=river. 18) 三方ケ原. 19) 天龍川. 20) 小笠. 21) 渥美. 22) 三河. 23) 古谷.
24) 掛川. 25) 堀之内. 26) 高尾山.
27) A. WATANABE, "Some considerations concerning the Japanese raised deltas," *Geogr. Rev.*, Japan, 5, 1 (1929), (in Japanese).

(震研彙報、第十號、圖版、大塚)

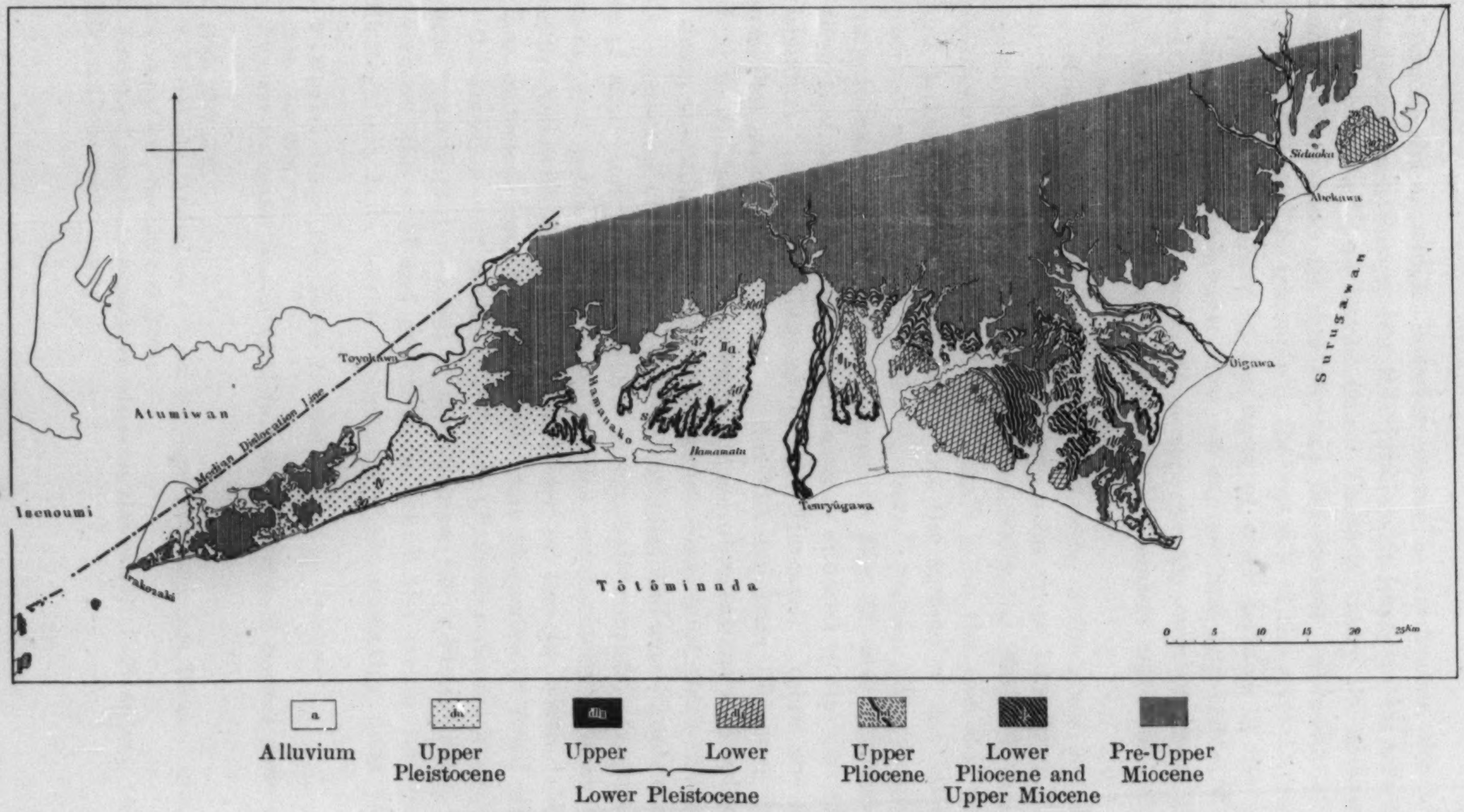

Fig. 3. Geologic map of "Tôtômi" region.

1. Makinogahara, II. Mikatagahara, III. Ogasa hill IV. Atumi peninsula.

Numbers in roman type indicate the height of upheaved plain.

(After Chitani, Makiyama and Ishii.)

was a typical delta, which however seems to contradict the above flexuous deformation theory, but this problem is likely to be solved by Murata's later studies[28] on fluvial fans. There is really no dislocation or flexuose deformation in this region; the eastern extension of the fluviatile plain should be traceable in the east side of the river Ôi(gawa), at least, in the valleys there in the form of river terraces of the same level as that of Makinogahara. But we cannot find any traces of this upheaved plain or of terraces in a topographic map of these areas (scale 1/25.000). So the writer accepts Watanabe's opinions in the absence of anything better.

II. *Mikatagahara subregion.* On each side of the river mouth of the Tenryû, which, like the Ôigawa, originates from lake Suwa,[29] the broad upheaved dissected delta plain is about 100 m. or 200 m. in height. Of these dissected terraces, the Iwatagahara[30] is on the east side of the river and Mikatagahara on the west. As the surface of the latter is well preserved, we call this the "Mikatagahara" region. The height of the terrace increases northwards, as shown in Fig. 3*, and is somewhat lower than that of the Iwatagahara, which is situated to the east of it. Near Sahamma,[31] a small village along lake Hamana,[32] there are some exposures that show the structure of the Mikatagahara dissected delta. According to J. Makiyama,[33] who has made observations and collected fossils there, the upper half of the exposure consists of thick fluviatile deposits, consisting of boulders, gravels, pebbles, and small intercalating pockets of sand and clay, while the lower half consists of estuarine clay, sand, and pebbles. The two divisions are distinctly separated by crossbedded yellowish sand of about a meter or less in width. Makiyama has collected from the lower division 45 species of fossil shells, besides the remains of a mammal, *Elephas* (*Palaeoloxodonta*) *naumanni* Makiyama,[34] an important fossil of the Japanese lower Pleistocene. The upper division, the sand and gravel beds, which the writer has called the Mikatagahara beds, forms the surface of the dissecting delta plain.

28) T. Murata, *Geogr. Rev.*, Japan, 7, 7 and 8 (1931), (in Japanese).
29) 諏訪. 30) 磐田ヶ原.
* Numbers in roman type in fig. 3 indicate the height of terraces above mean sea-level.
31) 佐濱. 32) 濱名.
33) J. Makiyama, "Notes on a Fossil Elephant from Sahamma, Tôtômi," *Mem. Col. Sci., Kyôto Imp. Univ.*, Ser. B, 1, 2 (1924).
34) Formerly "*Loxodonta namadicus naumanni* Makiyama," J. Makiyama, *Chikyû*, 12, 5 (1929), (in Japanese.)

The shell bearing lower division, which for convenience is called the Sahamma beds, are observed in the southwestern part of the Mikatagahara, but not in the eastern part of the Iwatagahara district. As common species of the lower division, are collected *Ostrea gigas* Thunberg, *Anadara granosa* Linné from the Huruya beds also. Therefore the Sahamma shell beds of the lower Pleistocene may be contemporaneous with the Huruya beds, whence the upper division, the Mikatagahara beds may, together with the Makinogahara gravel beds, be Pleistocene in age. Consequently the surface of the Mikatagahara dissected delta and the surface of the Makinogahara dissected fluviatile plain may both be of the same age. Hence these two regions have a similar geologic history. But considering the distribution of the heights of the upheaved surfaces and the distribution of the shell beds, their crustal deformations

Fig. 4. Summit-level of Ogasa Hill. (Contour line is referred to the highest points in the 1250 m. nets.)

must have taken place in different directions, namely the Makinogahara flexing toward the southeast and the Mikatagahara and the Iwatagahara southwest.

III. *The Ogasa hill.* The Ogasa hill being higher than the two dissected plains just mentioned, occupies a mid-position as regards height between the Mikatagahara and the Makinogahara. The hill surface inclines slightly toward the southwest and the highest ridges of the northeastern limit of the hill borders is bounded by steep escarpments. Fig. 4 is the summit-level of the hill surface contour line showing a broad tilted deltaic surface and steep escarpments. The hill is mainly built up of conglomerate beds, called by our geologists the Ogasa conglomerate beds. These beds generally dip less than 10° southwest, while in places the amount of dip is steeper than the inclination of the hill surface. The gravels that form the conglomerates are rocks of the Mikura series, porphyrite, granite, and Palaeozoic rocks derived from the northern mountainland. Under the conglomerates are the Soga[35] beds, shallow sea deposits with alternations of sand and mud, with basal conglomerates at its western base. The Ogasa conglomerates overlap the Soga beds in the southeast areas and conceal it from the ground surface, but in the southwest area the latter is extensively exposed below the Ogasa conglomerate beds and above the next older Kakegawa series. The writer takes this occasion to rectify an error in his previous paper on the stratigraphic relationship between the Kakegawa and the Horinouti series. It has been corrected in correlation Table II. Instead of the Kakegawa series being underlain by the Horinouti series, the upper part of the latter is contemporaneous with the former.[36] The distribution of the Kakegawa series and the younger formation in these regions is shown in Fig. 3, drawn after the geologic maps of Chitani,[37] Ishii[38] and Makiyama.[36] According to this map, the dips of these strata incline in the same direction, and are steepest in the oldest formation, the Horinouti series, but become less so as the younger formations are reached. But their strikes are almost parallel to all the formations now under discussion. From these considerations it would seem that since the lower Horinouti period, the earthcrust has been gradually flexed in the same direction, i.e., southward and

35) 曽我.
36) J. Makiyama, *op. cit.*, (1931).
37) Y. Chitani, *op. cit.*, (1927), and (1932).
38) K. Ishii, *op. cit.*, (1927).

westward.

From the present position of the reliefs, by which the Ogasa hill is higher than the Makinogahara and the Mikatagahara, some believe that an upwarping of the earth's crust took place with its axis situated on Ogasa hill. But in the writer's opinion, Makinogahara is the fluviatile plain that was formed in the "vale[39] of the cuesta" like topography of Ogasa hill, and believes there is an earth-flexure near the mouth of the Ôigawa, because the asymmetrical structure of the post-lower Pliocene strata does not reconcile with the views above mentioned.

IV. *The Atumi Peninsula.* The Mikatagahara dissected plain extends southwestward and forms a raised coastal plain of the Atumi peninsula, a long and narrow land with a straight contraposed shoreline along the Pacific side of Japan.

The Peninsula is bounded on its north side by the median dislocation line. The height of the raised coastal plain at the headland, Irakozaki,[40] is only 6 m., but as one goes eastward, its height gradually increases to about 60 m. or more. Fig. 3 shows the distribution of their heights. The structure of the raised coastal plain may be observed on sea cliffs along the Pacific coast. The brown sand and fine gravel beds may be seen in the upper half of the exposures, with alternations of fossil bearing fine sand and mud exposed in the lower half, both of which rest unconformably on Palaeozoic rocks. Prof. Yokoyama[41] has described 48 species of fossil shells from the lower division, which is continuous with the Sahamma shell beds. Though Prof. Yokoyama concluded by the Lyellian method, that the age of the lower division is upper Pliocene, it is continuous with the Sahama beds which yielded *Elephas* (*Paleoloxodonta*) *naumanni* Makiyama, a lower Pleistocene fossil. Owing to the ancient surface inequalities in the Palaeozoic rock, the Pleistocene gravel beds could not have completely covered the surface of the lower member. The Palaeozoic land projected above the surface of the Pleistocene gravel beds like tops of islands. But these Palaeozoic lands are gradually drowned in the sea at the mouth of the Ise-no-umi.

From the geologic structure and the distribution of heights of relief in the above four districts, the writer believes that gradual crustal deformation in the form of broad swells was actively in progress since

39) C. A. Cotton, "Geomorphology of New Zealand," (1926).
40) 伊良湖岬.
41) M. Yokoyama, *Jour. Fac. Sci., Imp. Univ.*, Tokyo, Sec. II, 1, 9 (1926), 369-375.

[Bull. Earthq. Res. Inst., Vol. X, Pl. XCI.]

(震研彙報、第十號、圖版、大塚)

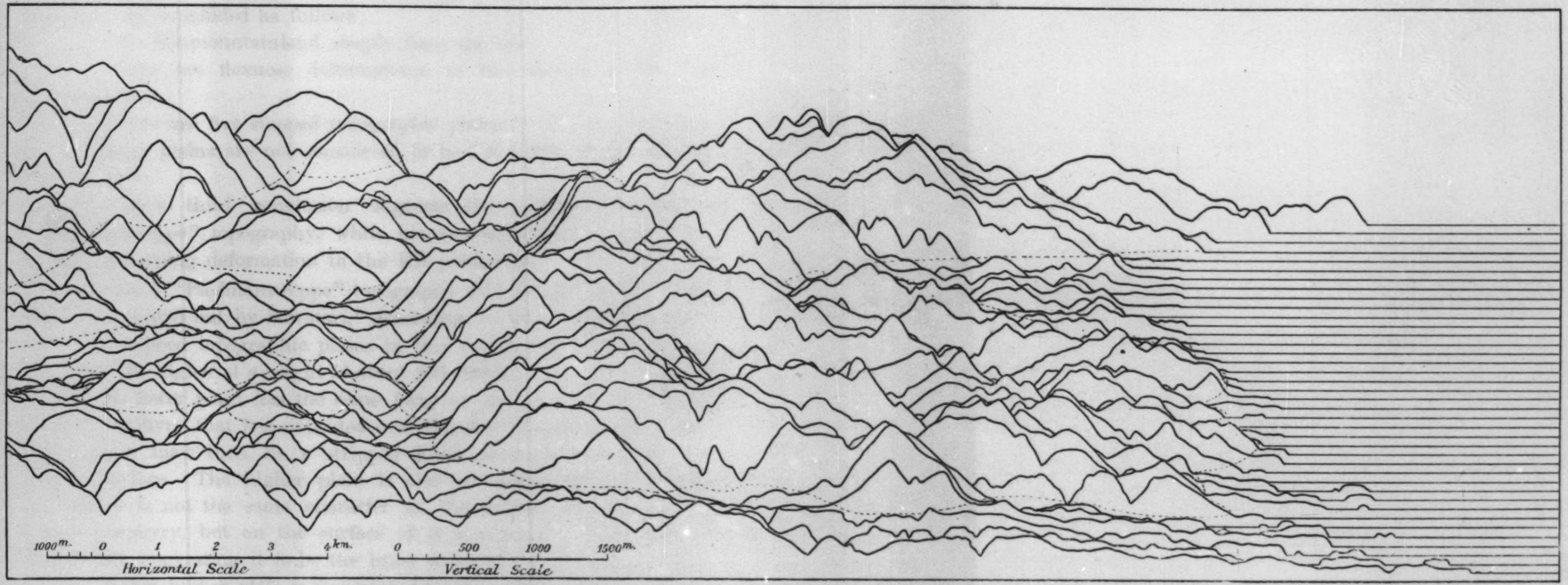

Fig. 5. Projected profiles of the southeastern Kii (near Singû) arranged in equal intervals. Ridge tops are projected upon 39 parallel vertical planes which are put at about right angles to the general trend of the shoreline at intervals of 1000 m. "............" lines are the approximate boundary lines of the erosion surfaces which are suggested by the arranged projected profiles.

early Pliocene. In other words, the northeast part of these regions gradually upwarped while the southwest part gradually downwarped.

(*b*) ***Kii Peninsula.*** In the Kii Peninsula, which is a part of Richthofen's "Kuma Kii mountainland," there are no Pliocene deposits, so we have only the topographic features to aid us in deducing the upwarping movement of the Kii Peninsula. According to W. Penck,[42] broad upwarping of the earthcrust and intermittent changes of erosion base are favourable for the formation of his "Piedmonttreppe." Recently Miyasaki[43] has studied the distribution of mountain heights in these districts and concluded as follows:

1. The Kii-mountainland steeply faces the sea.
2. There are flexuose deformations on the margin of the Kii mountainland.
3. There are five stepped topographic plains in the Kii mountainland. These plains are not considered to be the result of the solitary erosion cycle.

Miyasaki's third conclusion suggests the existence of Penck's "Piedmonttreppe" topography, while his second conclusion practically admits upwarping deformation in the Kii peninsula.

Fig. 5 is a "Piedmonttreppe" topography near Singû[44] in Kii, which was first pointed out by Sawatari,* according to whom there are more than two stepped topographic plains in this region, the lower one surrounding the higher at a height of about 400–200 m, while the boundary line of the lower plain has the same form as the base of the flow of granite porphyry that has extruded over the older erosion surface. The lower plain may then be a stripped fossil plain—a re-exposed old erosion surface. The higher plain is also an erosion surface because the surface is not the same character as the surface of the flow of granite-porphyry, but on the surface of it is exposed a facies of high crystalinity, suggesting it to be the inner facies of the flow mass. The surface of this higher plain is represented by the surface of the summit-level, as shown in the writer's previous paper. The inclination of the old erosion surface is steeper than that of the surface of the summit-level. In other words, the old erosion surface has been flexed

42) W. Penck, "Die morphologische Analyse," (1924).

43) K. Miyasaki, *Geogr. Rev.*, Japan, **6**, 9 (1930).

44) 新宮.

* He studied the geology of the granite porphyry cropping out near Kinomoto (木本). This granite porphyry is coloured as liparite in other geologic maps.

seaward. To determine the crustal deformation from the terrace distribution along the margin of the Kii mountainland is not easy; for if the configuration of the shoreline has been affected by crustal movements, it might be the combined result of two types of possible earth flexures, the one in a N-S direction and the other E-W. That is, the shoreline may be a nodal line of two orthotomic flexuose crustal movements.

(*c*) ***Southeastern Sikoku.*** The relations between the Pliocene formations and the summit-level in these regions were discussed in the previous paper. A. Watanabe,[45] who recently discussed this region in detail in this bulletin from the geomorphologic point of view, also believes that an upwarp occurred here.

(*d*) ***Southwestern Sikoku.*** Southwestern Sikoku also is a region where the same type of crustal deformation as just described is expected to have occurred, but here, as in the Kii-mountainland, no younger formations are exposed, so that crustal deformations if any, can only be deduced from geomorphologic evidence.

The writer[46] in 1925 noticed the peculiar digitate way in which the tributaries of the Simanto[47] river were distributed, and tried to explain the peculiarity by regarding it as an upwarped surface dissected in old age. As his report is in Japanese, a few extracts will here be made from it.

> The inclosed meander and the various forms of valleys have been studied in detail by Winslow, Gilbert, Davis, Rich, Tarr, and Vacher. Recently, Moore,[48] after summarising the views of other writers, classified the inclosed meander into incised or ingrown meander, ingrown-intrenched meander, and intrenched meander, and referred to the Colorado river for the peculiar distribution of various types of inclosed meanders.
>
> From the writings of the above-mentioned authors, the writer has extracted the following relationships holding between the form of valley, the volume of water, the gradient of river-floor, the load, the hardness of the rocks, etc., as in Table III. According to these relations, when the dissected area, as shown in section in Fig. 6,

45) A. Watanabe, *Bull. Earthq. Res. Inst.*, **10**, 1 (1932).

46) Y. Ôtuka, *Geogr. Rev.*, Japan, **3**, 5 (1927), (in Japanese).

47) 四萬十川.

48) R, C. Moore, *Jour. Geol.*, **34**, 1 and 2 (1926).

Table III.

	Volume of water		Gradient		Load		Hardness of rock	
	large	small	increase	decrease	excess	defect	soft	hard
Velocity of erosion	quick	slow	quick	slow	quick	slow	quick	slow
Lateral erosion	increase	decrease	downward increase	increase	increase	decrease	increase	decrease
Vertical erosion	increase	decrease	increase	decrease	increase	increase	increase	increase
Types of inclosed meanders	ingrown or ingrown-intrenched meander	shrink	decrease the swings	ingrown or ingrown-intrenched meander	ingrown or ingrown-intrenched meander	intrenched meander	ingrown or ingrown-intrenched meander	intrenched meander

is upwarped gradually as in Fig. 7, it follows that the erosion bases of the valleys (b in Fig. 6 and 7) near the axis of the upwarp is lowered more rapidly than that of the other two valleys (a and c in Fig. 6 and 7) distant from the axis; for the base levels of the

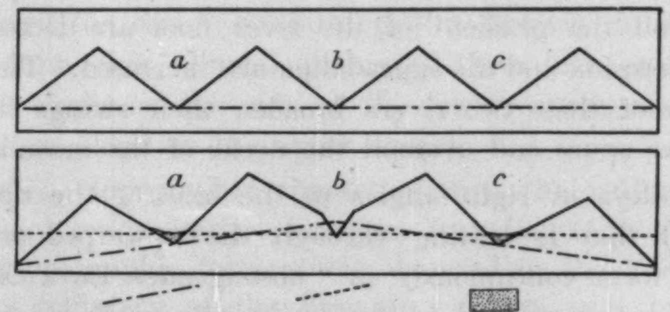

Fig. 6.

Fig. 7.

Early horizontal plane. Late erosion base. Sedimentary deposits.

former valley is upheaved relatively to that of the latter two, so that in the former valley, W. Penck's "aufsteigende Entwicklungsform" may be seen and in the latter the "absteigende Entwicklungsform." If these three valleys belong to one river system, the contrast in the valley forms as mentioned above is heightened because the local erosion bases of a river system do not remain in the same condition for long.

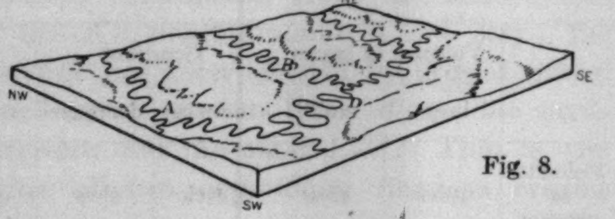

Fig. 8.

Fig. 8 shows a relief dissected in old stage, on which a meandering river flows with three courses parallel and one course perpendicular to the three. If an upwarping erosion deformation occurs on the relief in such a manner that the axis of the upwarping is parallel to the trend of the three parallel valleys, and such that the axis lies in the middle of them, the middle river course (B in Fig. 8) is rejuvenated and is represented by the "aufsteigende Entwicklungsform", while in the other two valleys on each side of the middle one (A and C in Fig. 8), the erosion bases of which are lowered relatively to that of the middle one, still retain the old stage topography, and is represented by "absteigende Entwicklungsform." In the former valley, therefore, the current velocity, the downward lateral erosion and the vertical erosion, the load, the transportation of the load, and the gradient of the river-floor are increased, and smooth meandering valleys in the middle course changed into those of sharp zigzag form; whereas in the latter valley, the current velocity, the vertical erosion, the load, the transportation of the load, and the gradient of the river floor are decreased, while the lateral erosion and the aggradation are increased. Then the meander courses of these two rivers broaden their swings and cut off the meander spurs and overspil the necks of the meander spurs.

Valleys at right angles to the axis of the upwarping (D in Fig. 8) that is cutting through the upwarped area, change the valley form continuously in "absteigendes Entwicklungsform" in the upper course and in the "aufsteigendes Entwicklungsform" in the middle, and in "absteigendes" in the lower courses. But the middle region of the "aufsteigendes Entwicklungsform" does not increase in gradient of valley floor and does not transport the waste,

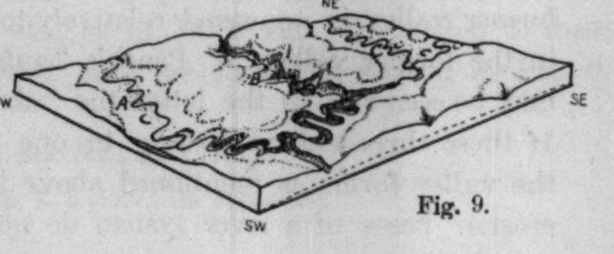

Fig. 9.

most of which is unloaded in the upper course, the "absteigendes Entwicklungsform" region, so that the the lateral erosion is small. For these conditions the formation of the intrenched meander is most suitable. Fig. 9 shows the results of topographic developments of the upwarped relief shown in Fig. 8.

The topographic features of the drainage of Simanto-river, is exactly like that shown in Fig. 9. The Yusuhara-gawa,[49] where it confluxes with the Simanto at Tanono,[50] shows a very sharp zigzag course, and cut-off spurs are observed at heights of about 200 m. above the recent valley floor. The tendency of the increasing amplitude of the meander swing is not observable in this valley. Near Nisituno-mura[51] an ingrown intrenched meander is seen to be scarped. The valley was deepened by vertical and downward lateral erosion. These characteristics are represented in valley B shown in Fig. 9.

The Matubaragawa,[52] which is the upper course of the Simanto river that originates from Mt. Kakusyonomori,[53] and which runs through the Kubokawa[54] basin, is where the broad alluvial plain spreads out. The rivers flow freely on the broad alluvial plain, being restricted only by the low valley wall. Near the town of Kubokawa, the secondary inclosed meanders are developeing into a "valley in valley" topography, a topography that becomes quite distinct toward the east. Examining the isolated hills or spurs projecting from this alluvial plain, all these hills or spurs have their slip-off slopes on the side of the lower course, and the steep attacked-surface slope on the upper course.

From these topographic characters then the valleys must be considered as having similar characters to valley C in Fig. 9.

Similar topographic features are observed in the Yosinogawa,[55] the western tributary of the Simanto. There is a broad basin along the Yosino as in the case of the Kubokawa basin, and cut off spurs and over-spil spurs have developed in the basin floor.

Near Hirose,[56] where the Simanto flows in an East-West course as in valley D in Fig. 9, the river runs through an ingrown meander. The flood-plains on both sides of the river floor gradually decrease from Kubokawa to Hirose, and in the lower course or near Hirose, it is seen only on the inner side of the loop where the

---

49) 檮原川. 50) 田野々. 51) 西都野村. 52) 松原川.
53) 鶴松森. 54) 窪川. 55) 吉野川. 56) 弘瀬.

current flows slowly. All the spurs have distinct slip-off slopes on the side of the lower course. In the lower course of Ôno,[57] the Simanto runs in a typical intrenched meander valley. Each side of the vally wall whose heights reach 320 m, 435 m, and 320 m respectively are steep and symmetrical. The course of the Simanto between Hirose and Naro[58] then corresponds to valley C in Fig. 9. If these analogies of the four valleys of the Simanto to the valleys in Fig. 9 are true, southwestern Sikoku must be deformed by an upwarping in shown in Fig. 10.

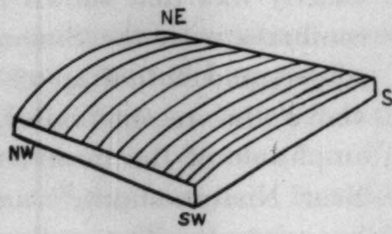

Fig. 10.

Judging from the above extracts from the writer's previous paper, and from the submerged topography of the coast around Southwestern Sikoku, the existence of signs of upwarping movements in this region may be regarded as established.

(*e*) *The Hyûga coastal plain.* From the foregoing results the upwarping crustal deformations taking place in the above four districts have been established. The writer now desires to know whether or not similar types of crustal deformations exist in the most western region of Southwest Japan, and also in the Ryûkyû[59] arc. Explanations of the stratigraphy and the structure of the Hyûga coastal plain were given briefly in the writer's previous paper.[60] The rock facies of these groups are as follows (Table II):—

Lower Pleistocene	The Tôriyamahama[61] beds.	Muddy sand and mud beds with basal conglomeratic gravel beds at its base, and in places containing estuary shells.
	unconformity	
Neogene	The Takanabe[62] group.	The Heki[63] beds; sandy mud beds with marine fossils. The Koonzi[64] beds; thin alternations of mud and sand. The Sadowara[65] beds; alternations of sand and mud, and fine conglomeratic sand at its base (Flysch type).
	uncomformity	
	The Tuma[66] group.	Black muddy beds with pelagic fauna.

57) 大野. 58) 奈路 59) 琉球.
60) Y. ÔTUKA, *op. cit.*, (1931).
61) 通山濱. 62) 高鍋. 63) 日置. 64) 光音寺. 65) 佐土原. 66) 妻.

Late Miocene and middle and lower Pliocene strata are arranged in such order that the younger formations lie in the east and the older in the west, generally parallel to the boundary line between the Osuzu[67] mountainland and the Hyûga coastal plain, the boundary line almost coinciding with the line of unconformity running NNE-SSW. The Takanabe group may be contemporaneous with the Kakegawa series and the Horinouti series of Makiyama; the Heki beds of the group may be more or less younger than the Dainiti[68] horizon of the lower Kakegawa series.

The general strikes of the Takanabe and Tuma groups are arranged in directions varying from NNE to SSE and dipping E. But the dips are steep in the base and low in the upper horizon. In other words, the older the strata the steeper is the inclination toward the east. Between the Tuma group and the Takanabe group, two cycles of sedimentation are seen to have occurred during the middle Neogene, judging from the great change of rock facies between the base of the Takanabe group and the upper limit of the Tuma group. This boundary may have been caused by the same level change or by the epeirogenic earth movements that led to the abrupt change of facies between the base of the Kakegawa series of the Horinouti series and the upper limits of the Sagara beds or the Tamari beds, in the Tôtômi districts.

The eastern slope of mount Zyômegi is the same plain continued from the basal plain of the Tama group.

As the inclination of the eastern slope of mount Zyômegi,[69] which amounts to 10° in its eastern part accords with the dips of the basal plain of the Tuma group, the eastern slope may be Cotton's "stripped fossil plain," or the surface that is re-exposed from the basal surface on the Tuma group by differential erosion due to the solid Mesozoic rocks and the loose young Tertiary strata. From the foregoing considerations, the crustal deformation of the Hyûga coastal plain took place in the form of gradual tilting of the crust toward the east, during which two cycles of sedimentation were repeated.

On these two Neogene formations, the horizontal Tôriyamahama beds are scattered in patches. Hitherto the writer was of the opinion that these beds were fresh water deposits, judging from its rock facies, but according to Takeyama, who recently visited these regions, estuary fossils have been collected from the same beds near Tonogôri[70]. The

---

67) 尾鈴. 68) 大日. 69) 上面木. 70) 都於郡.

age of the crustal movement, when the Tertiary beds tilted 10° is uncertain, but it is probably the same age as that of the pre-Tôriyamahama beds.

o our geologists and geomorphologists, the practical uniformity in the heights of the summits recalls remnants of a subdued form of peneplain which was uplifted and dissected at full maturity. Then the question arises, when was the low relief surface formed? The Tôriyamahama strata, as mentioned in the previous paper, are sediments in the valleys which are dissected in the denuded surface of the Tertiary beds. The age of Tôriyamahama beds is younger than that of the denuded surface of the Tertiary which may be contemporaneous with or later than the age of the so-called peneplain surface. The age of the so-called peneplain is consequently older than that of the Tôriyamahama beds, that is, it may be late Pliocene or early Pleistocene, and the deformation of the Tertiary deposits antedates the so-called peneplain. And if the so-called peneplain did suffer such crustal deformations, Penck's "piedmonttreppe" should form in these regions.

Of the "Piedmonttreppe" in these regions, the writer awaits with no small interest the result from Miyasaki's study of the geomorphology of these regions.

We shall now study the coastal terraces bordering the Hyûga coast line, in order to find the same type of crust deformation as above discussed, that took place during the post-Tertiary. If there is tilting and uplifting of the crust, as shown in Fig. 11, the first terrace BB′ would be tilted and upheaved with formation of the lower surface of the second terrace CC′, but in the next interval, the first and second terrace BB′ and CC′ are tilted and upheaved by the same crustal movement, and the third new terrace surface DD′ relatively to the new erosion base level formed, when the first, second, and third terraces are deformed with formation of the fourth EE′ and so on. The inclination of the oldest terrace therefore assumed the largest angle, while of the youngest terraces, the recent fluviatile plain may assume the lowest.

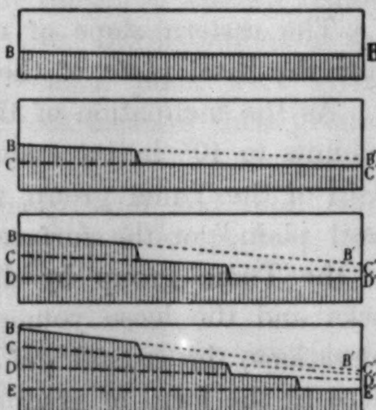

Fig. 11. Developement of terrace surfaces.

With these facts in mind, the writer measured the grades of these

coastal terraces spreading over the regions concerned. He[71] had already classified these coastal terraces into the following: Pre-Tyausubaru,[72] Tyausubaru, Sanzaibaru,[73] Nyutabaru,[74] and the recent Fluviatile plain of the Omaru[75] and the Hitotuse.[76] (Fig. 12.)

The grades of these terraces were compared in the following manner:

1. Interfluviatile areas between the Omaru and the Hitotuse are selected and jotted down on paper and an XY vertical plane is drawn almost parallel to these two river courses, namely at right angles to the shoreline.

2. Then the vertical planes 1, 2, 3, ...n are drawn at right angles to the vertical plane XY at intervals of 500 m.

3. The mean height of the respective terrace surfaces intersecting the vertical planes 1, 2, 3, 4,....n, is projected on the vertical plane XY. (Fig. 12).

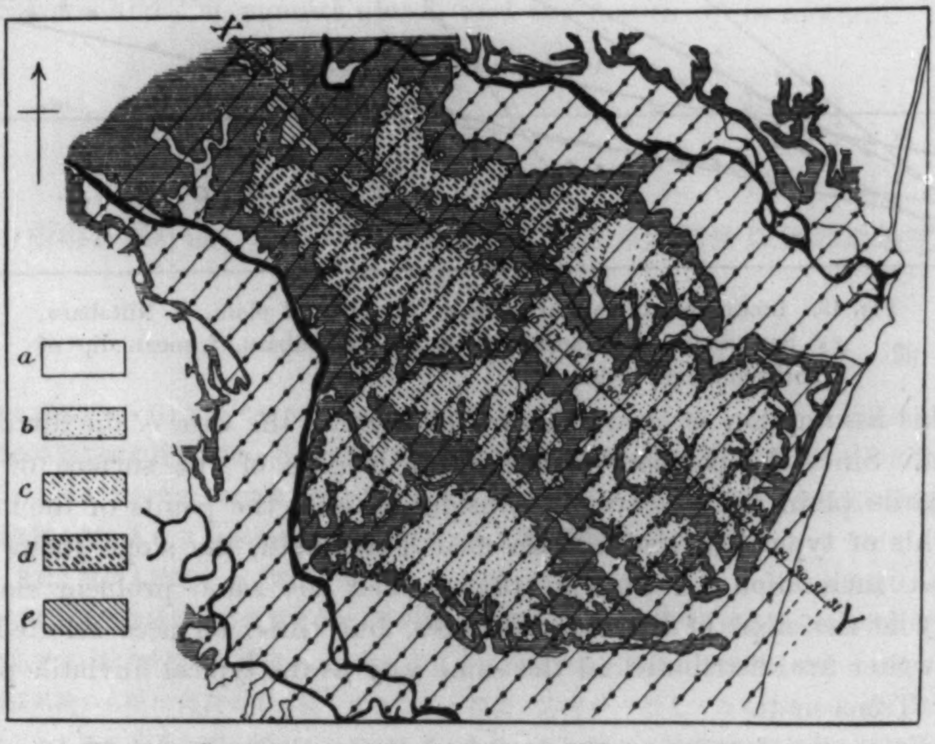

Fig. 12. Coastal terraces bordering the Hyûga coast line.

a. Alluvial plain. d. Tyausubaru.
b. Niitabaru. e Pre-Tyausubaru.
c. Sanzaibaru.

71) Y. Ôtuka, "Some Geologic Problems in the Southwestern Coast of Kyûsyû," *Geog. Rev.*, Japan, 6, 7 (193), (0in Japanese).

72) 茶臼原. 73) 三財原. 74) 新田原. 75) 小丸. 76) 一ツ瀬.

If the surfaces of the respective terraces were ideal planes, the projected points of the mean height of the respective terraces at the XY plane may be arranged in a straight line. Now the slope of the respective terraces can be compared with the inclination of these straight lines on the XY plane. Fig. 13, shows these line. From Fig. 13, it is seen that the oldest terrace, the pre-Tyausubaru, is the most steeply inclined, while the younger ones become less so in order of age.

The recent fluviatile plain of the Hitotusegawa is a solitary exception, but this is due in the writer's opinion to the fact that the surfaces of the terraces are ideal planes, without any flexuose deformation. But in reality this assumption of the flatness of the terraced surfaces or of the fluviatile plain is open to criticism. The untenability

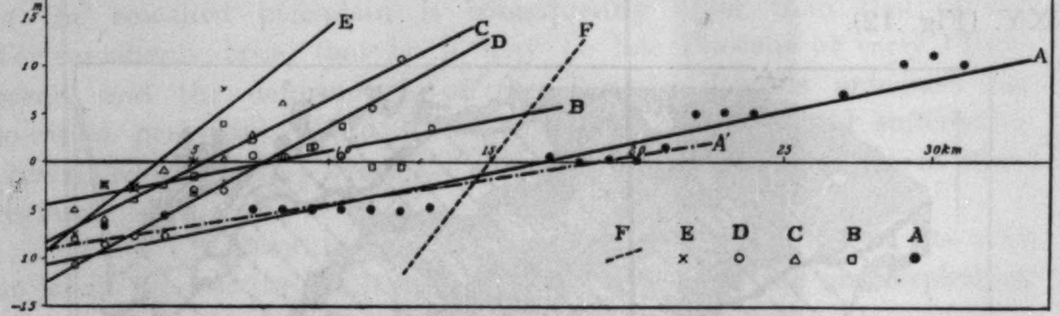

Fig. 13. Inclination of coastal terraces. a. Alluvial plain, b. Niitabaru, c. Sanzaibaru, d. Tyausubaru, e, Pre-Tyausubaru, f. mean dip of Tôriyamahama beds.

of this assumption is clearly shown at least in the case of the fluviatile plain. Since the positions of the mean heights of the surface of the fluviatile plain are concave, in considering only the points of the mean heights of typical fluviatile plain near Tuma-mati, the slope shows the lowest inclination (A in Fig. 13), so that the same problem should apply to the slope of the older terraces, but these terraces selected by the writer are distributed in the same way as the typical fluviatile plain near Tuma-mati.

From the foregoing, the writer believes that since early Pliocene, gradual deformation took place, the change being confined to that part between the two nodes as shown in Fig. 1, as a dominant type of crustal deformation in the Outer zone of Southwest Japan. And recent land areas, such as the Tôtômi region, the Kii mountainland, southeastern and southwestern Sikoku, and the Hyûga coastal region are upwarped and recent embayments, while the mouth of the Ise-no-umi, the embay

ment between Kii and Sikoku, Tosa bay, and Hyûganada, and Pacific coast have downwarped since the Pliocene. This type of crustal deformation is not observed in the eastern part of the river Ôi near where the western limits of the Fossa Magna or where the Itoigawa Siduoka geotectonic line is situated.

Quite recently, Prof. T. Terada[77] has reported a change in the bottom of Tosa bay during the last about 40 years, as deduced from soundings made by the Naval Hydrographic Department. According to him, the sea bottom of Tosa bay has deepened about 6 m. about its deepest part, while on the other hand the sea shore has shallowed.

Results of repeated precise levellings also show the upwarped characters of the land in the Outer zone of Southwest Japan. It is also worthy of notice that the epicentres of earthquakes are packed together in some of the downwarped areas, e.g., the Hyûganada, the embayment between the Sikoku and Kii mountainland, and the mouth of Ise-no-umi.

(*To be Continued.*)

---

47. 西南日本外帶とフオッサ・マグナとに於ける鮮新世以後の地殼運動 (其一)

地震研究所　大塚彌之助

筆者の前論文(1931)に於て知り得た材料から西南日本外帶と フオツサ マグナ とに於ける鮮新世以後の地殼運動の性質に就いて述べてある。この論文はその西南日本外帶に關するものに就いて述べてあるものであつて、前論文で知り得た西南日本外帶のウネリの樣な波狀の地殼運動は鮮新世の地殼運動と解するよりも鮮新世以後も繼續してゐる地殼運動と解する方がよいやうなこととなつた。便宜上取扱ふ地域を a. 遠江、b. 紀伊、c. 東南四國、d. 西南四國、e. 日向海岸段丘の五區域に分けた。遠江地域に於ては堀之內統・掛川統・曾我層・小笠山礫岩層・佐濱貝層或は古谷貝層或は渥美半島下部・及び牧野ヶ原礫層或は三方原礫層或は渥美半島上部層の地質構造に就いて述べ、最古の地質系統から順に傾斜の度の緩くなることと傾斜の方向が一致してゐることから古い地層の堆積時代から順に南及び西へ傾き下つてゐることを知つた。更にこの地方に發達する海岸段丘に就いて、その高度分布を調べて、同樣なことを知り得た。そして略ぼ大井川を境として東部が東南へ撓曲してゐると言ふことは渡邊氏の意見に贊成する。

紀伊では若い地層の發達がないので、宮崎氏の論文と最近佐渡氏によりて注意された新宮附近の山麓階に就いての地形學的研究を試みて、大體宮崎氏の意見に贊成することができた。

---

77) T. Terada, "Change of Depth in the Bay of Tosa." *Proc. Imp. Acad.*, 8, 5 (1932).

四國東南部は渡邊氏の論文によることとした。

四國西南部は筆者の四萬十川の流路に關する古い論文によりて大體を知ることができた。

日向の海岸平野に就いては段丘及び地質構造に依つたが之等は地理學評論第八卷第二號に述べたことを再錄した迄の事である。

最後に最近寺田博士によりて紹介された土佐灣海底變化及び水準測量の結果が簡單に紹介されてある。

そして之等の事から現在西南日本外帶では鮮新世初期から陸地になつてゐる部分は次第に曲隆し、海になつてゐる部分は次第に曲窪してゐて、同時に太平洋の方へ即ち南方へ撓曲し下つて行く樣な地殼運動が見られることがわかつた。曲隆された古い地表面は次第に浸蝕し去られて、air saddle の樣に空中に曲隆した表面として想像されるだけである。

48. *On the Stress Distribution in the Vicinity of a Horizontal Circular Hole in a Gravitating Wedge-Shaped Elastic Solid.*

By Genrokuro NISHIMURA and Takeo TAKAYAMA,

Earthquake Research Institute.

(Read May 17, 1932.—Received June 20, 1932.)

1. The problem of the stress distribution in the neighbourhood of a circular hole in a gravitating semi-infinite solid has recently been studied by N. Yamaguti[1] and T. Sugihara[2] independently. N. Yamaguti studied the case of a horizontal circular hole for the purpose of investigating the stability of a horizontal tunnel, and T. Sugihara discussed an inclined circular hole in relation to the mining engineering.

It may be of some importance to study the effect of topography on the stability of a tunnel, and the present paper shall make some contribution to this problem. The paper consists of two parts: in the first part we studied the equilibrium of a gravitating wedge-shaped solid having no hole in its interior, and the second part treated of the stress distribution in the vicinity of a horizontal circular tunnel in a gravitating wedge-shaped solid having the vertex of right-angle.

Part I. The Equilibrium of a Gravitating Wedge-Shaped Elastic Solid.

2. The stress distribution in a gravitating wedge-shaped solid without a hole was studied by M. Lévy[3] and N. Mononobe,[4] and others. Taking the earthquake intensity into account, Professor N. Mononobe discussed a technically important problem in relation to the construction of a gravity dam. Independent of above authors, we have obtained the stress distribution in a gravitating wedge-shaped solid as a preliminary calculation for the investigation of the effect of a hole on that solid.

1) N. YAMAGUTI, *Jour. Civil Eng.*, Tokyo, **15** (1929), 291.
2) T. SUGIHARA, *Jour. Mining Inst., Japan*, **47** (1931), 560, (in Japanese).
3) M. LÉVY, *C. R.*, Paris, **127** (1898), 10.
4) N. MONONOBE, 水理と土木, **2** (1929) & **3** (1930).

We use the rectangular coordinates (x, y, z), taking the positive sense of x-axis upward and y-axis horizontal. Let the origin o be at the vertex of a gravitating wedge-shaped solid of which the surfaces are defined by the following two equations:

$$\left.\begin{aligned} y &= -x\cot\varphi, \\ y &= x\cot\theta. \end{aligned}\right\} \quad \ldots\ldots(1)$$

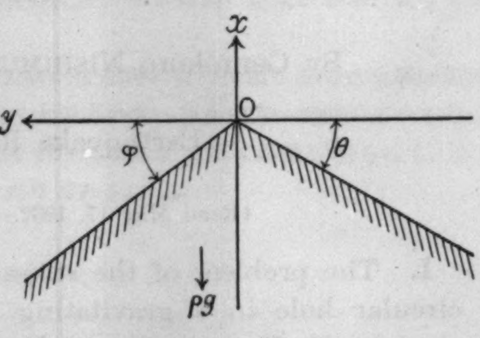

Fig. 1.

Now the equations of equilibrium of the gravitating solid are expressed by the following forms:

$$\left.\begin{aligned} \frac{\partial \widehat{xx}}{\partial x}+\frac{\partial \widehat{xy}}{\partial y} &= \rho g, \\ \frac{\partial \widehat{xy}}{\partial x}+\frac{\partial \widehat{yy}}{\partial y} &= 0, \end{aligned}\right\} \quad \ldots\ldots(2)$$

where ρ and g are the density and the gravity constant of the solid, and $\widehat{xx}$, $\widehat{yy}$, the normal components of stress, and $\widehat{xy}$ is the shearing component of stress.

The components of stress $\widehat{xx}$, $\widehat{yy}$, $\widehat{xy}$ are expressed by the following relations:

$$\left.\begin{aligned} \widehat{xx} &= \lambda\left(\frac{\partial u}{\partial x}+\frac{\partial v}{\partial y}\right)+2\mu\frac{\partial u}{\partial x}, \\ \widehat{yy} &= \lambda\left(\frac{\partial u}{\partial x}+\frac{\partial v}{\partial y}\right)+2\mu\frac{\partial v}{\partial y}, \\ \widehat{xy} &= \mu\left(\frac{\partial v}{\partial x}+\frac{\partial u}{\partial y}\right), \end{aligned}\right\} \quad \ldots\ldots\ldots\ldots\ldots\ldots(3)$$

where u, v are the x- and y-components of displacement of the solid, and λ, μ are the Lame's elastic constants of that solid.

In equation (2), we substitute for the components of stress the expression (3); and we thus obtain the following equations:

$$\left.\begin{aligned} (\lambda+2\mu)\frac{\partial \Delta}{\partial x}-2\mu\frac{\partial \varpi}{\partial y} &= \rho g, \\ (\lambda+2\mu)\frac{\partial \Delta}{\partial y}+2\mu\frac{\partial \varpi}{\partial x} &= 0, \end{aligned}\right\} \quad \ldots\ldots\ldots\ldots\ldots(4)$$

where

$$\left.\begin{aligned} \Delta &= \frac{\partial u}{\partial x}+\frac{\partial v}{\partial y}, \\ 2\varpi &= \frac{\partial v}{\partial x}-\frac{\partial u}{\partial y}, \end{aligned}\right\} \quad \ldots\ldots\ldots\ldots\ldots\ldots(5)$$

Now there are may particular solutions of (4), and we take the following forms of $\varDelta$ and 2ϖ satisfying (4) for the present study:

$$\left.\begin{aligned} \varDelta &= A_0 + A_1 x + A_2 y, \\ 2\varpi &= B_0 - \frac{(\lambda+2\mu)}{\mu} A_2 x + \frac{\{(\lambda+2\mu)A_1 - \rho g\}}{\mu} y, \end{aligned}\right\} \quad \ldots\ldots (6)$$

where A_0, B_0, A_1 and A_2 are the arbitrary constants to be determined by the boundary conditions of elastity of the solid.

We can find the following two differential equations in relation to u, v, $\varDelta$ and 2ϖ from the relations (5):

$$\left.\begin{aligned} \frac{\partial^2 u}{\partial x^2} + \frac{\partial^2 u}{\partial y^2} &= \frac{\partial \varDelta}{\partial x} - 2\frac{\partial \varpi}{\partial y}, \\ \frac{\partial^2 v}{\partial y^2} + \frac{\partial^2 v}{\partial y^2} &= \frac{\partial \varDelta}{\partial y} + 2\frac{\partial \varpi}{\partial x}. \end{aligned}\right\} \quad \ldots\ldots\ldots\ldots\ldots (7)$$

Substituting the relations (6) for the expressions of $\varDelta$ and 2ϖ in the right-hand terms of the equations (7), we obtain the particular solutions of u and v as follows:

$$\left.\begin{aligned} u &= \frac{A_1}{2} x^2 - B_0 y - \frac{\{(\lambda+2\mu)A_1 - \rho g\}}{2\mu} y^2, \\ v &= A_0 y + \frac{A_2}{2} y^2 - \frac{(\lambda+2\mu)}{2\mu} A_2 x^2. \end{aligned}\right\} \quad \ldots\ldots\ldots\ldots (8)$$

As the complementary solutions u, v of (7), we take the following expressions which are favourable for the present study:

$$\left.\begin{aligned} u &= C_0 + C_1 x + C_2 y + C_3 xy - \frac{C_4}{2} x^2 + \frac{C_4}{2} y^2, \\ v &= C_0' - C_1 y + C_2 x + C_4 xy + \frac{C_3}{2} x^2 - \frac{C_3}{2} y^2, \end{aligned}\right\} \quad \ldots\ldots\ldots\ldots (9)$$

where C_0, C_0', C_1, C_2, C_3 and C_4 are also the arbitrary constants to be determined by the elasticity conditions. The expressions (8) and (9) satisfy, of course, the equations of equilibrium of the solid expressed by (4).

Using (6), (8) and (9), we obtain the following forms of the components of stress $\widehat{xx}$, $\widehat{yy}$, $\widehat{xy}$ by the relations of (3);

$$\left.\begin{aligned} \widehat{xx} &= \lambda A_0 + 2\mu C_1 + (\lambda+2\mu)A_1 x + \lambda A_2 y + 2\mu C_3 y - 2\mu C_4 x, \\ \widehat{yy} &= (\lambda+2\mu)A_0 - 2\mu C_1 + \lambda A_1 x + (\lambda+2\mu)A_2 y + 2\mu C_4 x - 2\mu C_3 y, \\ \widehat{xy} &= \mu(2C_2 - B_0) - (\lambda+2\mu)A_2 x - \{(\lambda+2\mu)A_1 - \rho g\} y + 2\mu C_4 y + 2\mu C_3 x. \end{aligned}\right\} \quad (10)$$

Now the two surfaces of the solid expressed by (1) are completely free from traction, and therefore the normal and shearing stresses in these two surfaces must be zero. Then, by these boundary conditions, we have the following equations in regard to the arbitrary constants:

$$A_0=C_1=C_2=B_0=0, \qquad \text{(11)}$$

$$\{\lambda\tan\varphi\sin^2\varphi+3(\lambda+2\mu)\sin\varphi\cos\varphi\}A_1+\{\lambda\cos^2\varphi +3(\lambda+2\mu)\sin^2\varphi\}A_2+2\mu\{\cos^2\varphi-\sin^2\varphi\}C_3+2\mu\tan\varphi \times\{\sin^2\varphi-3\cos^2\varphi\}C_4=\rho g\sin 2\varphi, \qquad \text{(12)}$$

$$\{(\lambda+4\mu)\sin^2\varphi-(\lambda+2\mu)\cos^2\varphi\}A_1+\{(\lambda+2\mu)\sin^2\varphi\tan\varphi -(\lambda+4\mu)\cos^2\varphi\tan\varphi\}A_2+2\mu\tan\varphi\{3\cos^2\varphi-\sin^2\varphi\}C_3 +2\mu\{\cos^2\varphi-3\sin^2\varphi\}C_4=-\rho g\cos 2\varphi, \qquad \text{(13)}$$

$$\{\lambda\sin^2\theta+3(\lambda+2\mu)\cos^2\theta\}\tan\theta\, A_1-\{3(\lambda+2\mu)\sin^2\theta +\lambda\cos^2\theta\}A_2+2\mu\{3\sin^2\theta-\cos^2\theta\}C_3 +2\mu\{\sin^2\theta-3\cos^2\theta\}\tan\theta\, C_4=\rho g\sin 2\theta, \qquad \text{(14)}$$

$$\{(\lambda+4\mu)\sin^2\theta-(\lambda+2\mu)\cos^2\theta\}A_1+\{(\lambda+4\mu)\cos^2\theta- -(\lambda+2\mu)\sin^2\theta\}\tan\theta\, A_2-2\mu\tan\theta\{3\cos^2\theta-\sin^2\theta\}C_3 -2\mu\{3\sin^2\theta-\cos^2\theta\}C_4=-\rho g\cos 2\theta. \qquad \text{(15)}$$

From these equations we can easily obtain A_1, A_2, C_3 and C_4, and find the final results $\widehat{xx}$, $\widehat{yy}$, $\widehat{xy}$ satisfying all elasticity conditions from the equations (10). These results are the most general ones for the gravitating wedge-shaped solid having any vertex angle.

For the special case where the vertex has right-angle as shewn in Fig. 2 in which the relation between the new axes OX, OY of the rectangular coordinates (X, Y) and the ox, oy is shewn, we can easily obtain the expressions as follows:

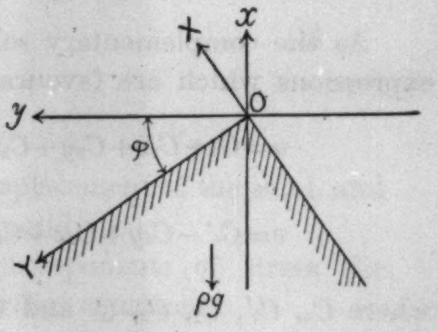

Fig. 2.

$$\left.\begin{aligned}\widehat{xx}&=(\lambda+2\mu)\rho g\frac{\vartheta_{A1}}{\vartheta}x+\lambda\rho g\frac{\vartheta_{A2}}{\vartheta}y+2\mu\rho g\frac{\vartheta_{C3}}{\vartheta}y-2\rho g\frac{\vartheta_{C4}}{\vartheta}x,\\ \widehat{yy}&=\lambda\rho g\frac{\vartheta_{A1}}{\vartheta}x+(\lambda+2\mu)\rho g\frac{\vartheta_{A2}}{\vartheta}y+2\mu\rho g\frac{\vartheta_{C4}}{\vartheta}x-2\mu\rho g\frac{\vartheta_{C3}}{\vartheta}y,\\ \widehat{xy}&=-(\lambda+2\mu)\rho g\frac{\vartheta_{A2}}{\vartheta}x-\left\{(\lambda+2\mu)\frac{\vartheta_{A1}}{\vartheta}-1\right\}\rho g y+2\mu\rho g\frac{\vartheta_{C4}}{\vartheta}y+2\mu\rho g\frac{\vartheta_{C3}}{\vartheta}x,\end{aligned}\right\} \qquad \text{(16)}$$

$$\frac{\vartheta}{4\mu^2}=\left|\begin{array}{l}
\{3(\lambda+2\mu)\cos\varphi\sin^2\varphi+\lambda\cos^3\varphi\},\ \{3(\lambda+2\mu)\cos^2\varphi\sin\varphi+\lambda\sin^3\varphi\},\\
\quad\{\sin^3\varphi-3\sin\varphi\cos^2\varphi\},\ \{\cos^3\varphi-3\sin^2\varphi\cos\varphi\}\\
\{-(\lambda+4\mu)\sin\varphi\cos^2\varphi+(\lambda+2\mu)\sin^3\varphi\},\ \{(\lambda+4\mu)\cos\varphi\sin^2\varphi\\
\quad-(\lambda+2\mu)\cos^3\varphi\},\ \{\cos^3\varphi-3\cos\varphi\sin^2\varphi\},\ \{3\sin\varphi\cos^2\varphi-\sin^3\varphi\}\\
\{-3(\lambda+2\mu)\cos^2\varphi\sin\varphi-\lambda\sin^3\varphi\},\ \{3(\lambda+2\mu)\cos\varphi\sin^2\varphi+\lambda\cos^3\varphi\},\\
\quad\{\cos^3\varphi-3\sin^2\varphi\cos\varphi\},\ \{-\sin^3\varphi+3\sin\varphi\cos^2\varphi\}\\
\{(\lambda+4\mu)\sin^2\varphi\cos\varphi-(\lambda+2\mu)\cos^3\varphi\},\ \{(\lambda+4\mu)\sin\varphi\cos^2\varphi\\
\quad-(\lambda+2\mu)\sin^3\varphi\},\ \{-3\sin\varphi\cos^2\varphi+\sin^3\varphi\},\ \{-3\cos\varphi\sin^2\varphi+\cos^3\varphi\}
\end{array}\right|, \tag{17}$$

$$\frac{\vartheta_{A1}}{4\mu^2}=\left|\begin{array}{l}
2\sin^2\varphi\cos\varphi,\ \{3(\lambda+2\mu)\cos^2\varphi\sin\varphi+\lambda\sin^3\varphi\},\\
\quad\{\sin^3\varphi-3\sin\varphi\cos^2\varphi\},\ \{\cos^3\varphi-3\sin^2\varphi\cos\varphi\}\\
-\sin\varphi(\cos^2\varphi-\sin^2\varphi),\ \{(\lambda+4\mu)\cos\varphi\sin^2\varphi-(\lambda+2\mu)\cos^3\varphi\},\\
\quad\{\cos^3\varphi-3\cos\varphi\sin^2\varphi\},\ \{3\sin\varphi\cos^2\varphi-\sin^3\varphi\}\\
-2\sin\varphi\cos^2\varphi,\ \{3(\lambda+2\mu)\cos\varphi\sin^2\varphi+\lambda\cos^3\varphi\},\\
\quad\{\cos^3\varphi-3\sin^2\varphi\cos\varphi\},\ \{-\sin^3\varphi+3\sin\varphi\cos^2\varphi\}\\
-\cos\varphi(\cos^2\varphi-\sin^2\varphi),\ \{(\lambda+4\mu)\sin\varphi\cos^2\varphi-(\lambda+2\mu)\sin^3\varphi\}\\
\quad\{-3\sin\varphi\cos^2\varphi+\sin^3\varphi\},\ \{-3\cos\varphi\sin^2\varphi+\cos^3\varphi\},
\end{array}\right|, \tag{18}$$

$$\frac{\vartheta_{A2}}{4\mu^2}=\left|\begin{array}{l}
\{3(\lambda+2\mu)\cos\varphi\sin^2\varphi+\lambda\cos^3\varphi\},\ 2\sin^2\varphi\cos\varphi,\\
\quad\{\sin^3\varphi-3\sin\varphi\cos^2\varphi\},\ \{\cos^3\varphi-3\sin^2\varphi\cos\varphi\}\\
\{-(\lambda+4\mu)\sin\varphi\cos^2\varphi+(\lambda+2\mu)\sin^3\varphi\},\ -\sin\varphi(\cos^2\varphi-\sin^2\varphi),\\
\quad\{\cos^3\varphi-3\cos\varphi\sin^2\varphi\},\ \{3\sin\varphi\cos^2\varphi-\sin^3\varphi\}\\
\{-3(\lambda+2\mu)\cos^2\varphi\sin\varphi-\lambda\sin^3\varphi\},\ -2\sin\varphi\cos^2\varphi,\\
\quad\{\cos^3\varphi-3\sin^2\varphi\cos\varphi\},\ \{-\sin^3\varphi+3\sin\varphi\cos^2\varphi\}\\
\{(\lambda+4\mu)\sin^2\varphi\cos\varphi-(\lambda+2\mu)\cos^3\varphi\},\ -\cos\varphi(\cos^2\varphi-\sin^2\varphi),\\
\quad\{-3\sin\varphi\cos^2\varphi+\sin^3\varphi\},\ \{-3\cos\varphi\sin^2\varphi+\cos^3\varphi\},
\end{array}\right|, \tag{19}$$

$$\frac{\vartheta_{C3}}{2\mu}=\left|\begin{array}{l}
\{3(\lambda+2\mu)\cos\varphi\sin^2\varphi+\lambda\cos^3\varphi\},\ \{3(\lambda+2\mu)\cos^2\varphi\sin\varphi+\lambda\sin^3\varphi\},\\
\quad 2\sin^2\varphi\cos\varphi,\ \{\cos^3\varphi-3\sin^2\varphi\cos\varphi\}\\
\{-(\lambda+4\mu)\sin\varphi\cos^2\varphi+(\lambda+2\mu)\sin^3\varphi\},\ \{(\lambda+4\mu)\cos\varphi\sin^2\varphi\\
\quad-(\lambda+2\mu)\cos^3\varphi\},\ -\sin\varphi(\cos^2\varphi-\sin^2\varphi),\ \{3\sin\varphi\cos^2\varphi-\sin^3\varphi\}\\
\{-3(\lambda+2\mu)\cos^2\varphi\sin\varphi-\lambda\sin^3\varphi\},\ \{3(\lambda+2\mu)\cos\varphi\sin^2\varphi+\lambda\cos^3\varphi\},\\
\quad-2\sin\varphi\cos^2\varphi,\ \{-\sin^3\varphi+3\sin\varphi\cos^2\varphi\}\\
\{(\lambda+4\mu)\sin^2\varphi\cos\varphi-(\lambda+2\mu)\cos^3\varphi\},\ \{(\lambda+4\mu)\sin\varphi\cos^2\varphi\\
\quad-(\lambda+2\mu)\sin^3\varphi\},\ -\cos\varphi(\cos^2\varphi-\sin^2\varphi),\ \{-3\cos\varphi\sin^2\varphi+\cos^3\varphi\}
\end{array}\right|, \tag{20}$$

$$\frac{\vartheta_{C4}}{2\mu}=\begin{vmatrix} \{3(\lambda+2\mu)\cos\varphi\sin^2\varphi+\lambda\cos^3\varphi\}, & \{3(\lambda+2\mu)\cos^2\varphi\sin\varphi+\lambda\sin^3\varphi\}, & \{\sin^3\varphi-3\sin\varphi\cos^2\varphi\}, & 2\sin^2\varphi\cos\varphi \\ \{-(\lambda+4\mu)\sin\varphi\cos^2\varphi+(\lambda+2\mu)\sin^3\varphi\}, & \{(\lambda+4\mu)\cos\varphi\sin^2\varphi-(\lambda+2\mu)\cos^3\varphi\}, & \{\cos^3\varphi-3\cos\varphi\sin^2\varphi\}, & -\sin\varphi\{\cos^2\varphi-\sin^2\varphi\} \\ \{-3(\lambda+2\mu)\cos^2\varphi\sin\varphi-\lambda\sin^3\varphi\}, & \{3(\lambda+2\mu)\cos\varphi\sin^2\varphi+\lambda\cos^3\varphi\}, & \{\cos^3\varphi-3\sin^2\varphi\cos\varphi\}, & -2\sin\varphi\cos^2\varphi \\ \{(\lambda+4\mu)\sin^2\varphi\cos\varphi-(\lambda+2\mu)\cos^3\varphi\}, & \{(\lambda+4\mu)\sin\varphi\cos^2-(\lambda+2\mu)\sin^3\varphi\}, & \{-3\sin\varphi\cos^2\varphi+\sin^3\varphi\}, & -\cos\varphi\{\cos^2\varphi-\sin^2\varphi\} \end{vmatrix}. \quad (21)$$

For ascertaining the stress distribution in the solid we take a numerical example. Assuming $\lambda=\mu$ (Poisson's ratio$=1/4$), we calculate ϑ, ϑ_{A1}, ϑ_{A2}, ϑ_{C3} and ϑ_{C4} in accordance with the various magnitudes of angle φ; and the results are tabulated in the following table. (Table I.)

Table I.

φ	0°	20°	30°	45°	60°	70°	90°
$\frac{\vartheta_{A1}}{\vartheta}$	$\frac{1}{4}\frac{\rho g}{\mu}$	$\frac{1}{4}\frac{\rho g}{\mu}$	$\frac{1}{4}\frac{\rho g}{\mu}$	$\frac{1}{4}\frac{\rho g}{\mu}$	$\frac{1}{4}\frac{\rho g}{\mu}$	$\frac{1}{4}\frac{\rho g}{\mu}$	$\frac{1}{4}\frac{\rho g}{\mu}$
$\frac{\vartheta_{A2}}{\vartheta}$	0	0	0	0	0	0	0
$\frac{\vartheta_{C3}}{\vartheta}$	0	$0{\cdot}123\frac{\rho g}{\mu}$	$0{\cdot}108\frac{\rho g}{\mu}$	0	$-0{\cdot}108\frac{\rho g}{\mu}$	$-0{\cdot}123\frac{\rho g}{\mu}$	0
$\frac{\vartheta_{C4}}{\vartheta}$	$-\frac{1}{8}\frac{\rho g}{\mu}$	$-0{\cdot}0219\frac{\rho g}{\mu}$	$0{\cdot}062\frac{\rho g}{\mu}$	$\frac{1}{8}\frac{\rho g}{\mu}$	$0{\cdot}062\frac{\rho g}{\mu}$	$-0{\cdot}0210\frac{\rho g}{\mu}$	$-\frac{1}{8}\frac{\rho g}{\mu}$

Using the expressions (16) and Table I, we obtain the stress components $\widehat{xx}$, $\widehat{yy}$ $\widehat{xy}$ as shewn in Table II and Fig. 3a, 3b, 3c.

Table II.

(unit$==\rho g$)

φ	0°	20°	30°	45°	60°	70°	90°
$\widehat{xx}$	x	$0{\cdot}794x+0{\cdot}246y$	$0{\cdot}626x+0{\cdot}216y$	$0{\cdot}5x$	$0{\cdot}626x-0{\cdot}216y$	$0{\cdot}794x-0{\cdot}246y$	x
$\widehat{yy}$	0	$0{\cdot}206x-0{\cdot}246y$	$0{\cdot}374x-0{\cdot}216y$	$0{\cdot}5x$	$0{\cdot}374x+0{\cdot}216y$	$0{\cdot}206x+0{\cdot}246y$	0
$\widehat{xy}$	0	$0{\cdot}246x+0{\cdot}206y$	$0{\cdot}216x+0{\cdot}374y$	$0{\cdot}5y$	$-0{\cdot}216x+0{\cdot}374y$	$-0{\cdot}246x+0{\cdot}206y$	0

In Fig. 3a, 3b, and 3c, the abscissae shew the angle φ and the ordinates the magnitudes of the x- and y-components of the components of stress $\widehat{xx}$, $\widehat{yy}$, $\widehat{xy}$ respectively. In Fig. 3a, $\widehat{xx}$ (x) and $\widehat{xx}$ (y) represent the x- and y-components of stress $\widehat{xx}$ respectively, and therefore the magnitude of $\widehat{xx}$ at any point in the solid is gixen by the algebraic sum of $\widehat{xx}$ (x) and $\widehat{xx}$ (y).

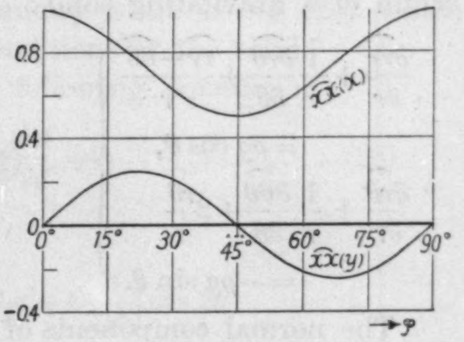

Fig. 3a.

From Table II, we can easily calculate the tangential components of stress $\widehat{YY}$ on the surface OY of the solid:

$$\widehat{YY}_{on\ OY} = -\rho g\, Y \sin\varphi. \quad \ldots.(22)$$

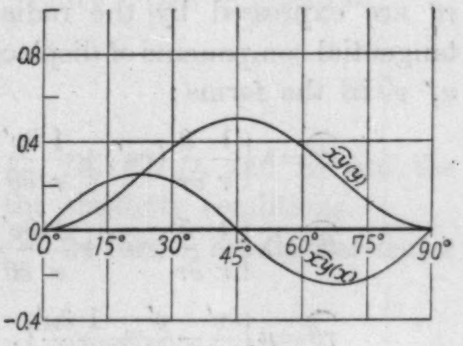

Fig. 3b.

This form is simple to know effect of φ on the properties of tangential stress $\widehat{YY}$. The compression stress only exists on the surface OY.

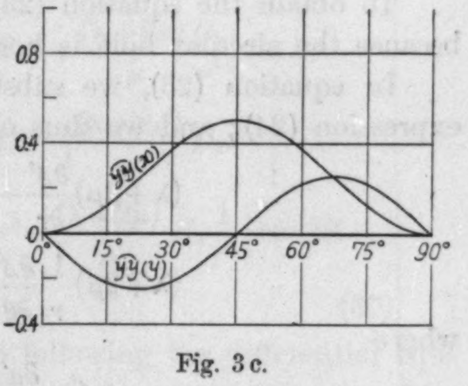

Fig. 3c.

Part II. The Stress Distribution in the Vicinity of a Horizontal Circular Hole in a Gravitating Wedge-Shaped Solid.

3. In this part we studied the stress distribution in the vicinity of a horizontal hole of which the radius is a, and the centre O' is at the point $(x=-\xi,\ y=\eta)$ as shewn in Fig. 4.

The vertex angle of the solid is assumed to be right-angle for the sake of simplicity as in the preceding section.

Now we must first obtain the general expressions of stresses which satisfy the equations of equilibrium of the solid. Using the cylindrical coordinates $(r,\ \theta,\ z)$, of which the axis z is coincident with the axis of the circular hole and the azimuthal angle θ is taken counterclockwise from the axis $o'x'$ as shewn in Fig. 4, we have the equations of equili-

brium of a gravitating solid:

$$\left.\begin{aligned}&\frac{\partial \widehat{rr}}{\partial r}+\frac{1}{r}\frac{\partial \widehat{r\theta}}{\partial \theta}+\frac{\widehat{rr}-\widehat{\theta\theta}}{r}\\&\qquad=\rho g\cos\theta,\\&\frac{\partial \widehat{r\theta}}{\partial r}+\frac{1}{r}\frac{\partial \widehat{\theta\theta}}{\partial \theta}+2\frac{\widehat{r\theta}}{r}\\&\qquad=-\rho g\sin\theta.\end{aligned}\right\}\quad\ldots\ldots(23)$$

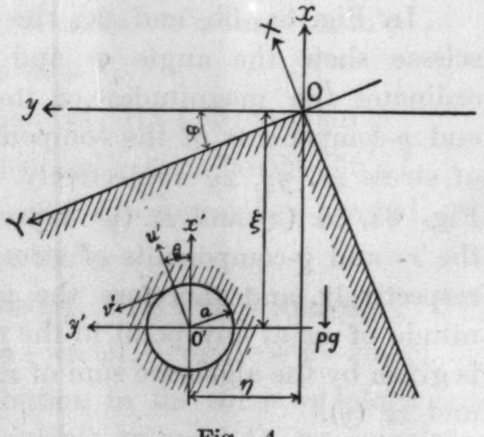

Fig. 4.

The normal components of stress $\widehat{rr}$, $\widehat{\theta\theta}$ and the shearing component $\widehat{r\theta}$ are expressed by the radial and tangential components of displacement u', v' in the forms:

$$\left.\begin{aligned}\widehat{rr}&=\lambda\left\{\frac{1}{r}\frac{\partial}{\partial r}(ru')+\frac{1}{r}\frac{\partial v'}{\partial \theta}\right\}+2\mu\frac{\partial u'}{\partial r},\\\widehat{\theta\theta}&=\lambda\left\{\frac{1}{r}\frac{\partial}{\partial r}(ru')+\frac{1}{r}\frac{\partial v'}{\partial \theta}\right\}+2\mu\left\{\frac{1}{r}\frac{\partial v'}{\partial \theta}+\frac{u'}{r}\right\},\\\widehat{r\theta}&=\mu\left\{\frac{\partial v'}{\partial r}-\frac{v'}{r}+\frac{1}{r}\frac{\partial u'}{\partial \theta}\right\}.\end{aligned}\right\}\quad\ldots\ldots\ldots(24)$$

To obtain the equation (23) we neglect the axial variation of stress, because the circular hole is horizontal.

In equation (23), we substitute for the components of stress the expression (24); and we thus obtain the following equations:

$$\left.\begin{aligned}&(\lambda+2\mu)\frac{\partial \Delta'}{\partial r}-\frac{2\mu}{r}\frac{\partial \varpi'}{\partial \theta}=\rho g\cos\theta,\\&(\lambda+2\mu)\frac{1}{r}\frac{\partial \Delta'}{\partial \theta}+2\mu\frac{\partial \varpi'}{\partial r}=-\rho g\sin\theta,\end{aligned}\right\}\quad\ldots\ldots(25)$$

where

$$\left.\begin{aligned}\Delta'&=\frac{\partial u'}{\partial r}+\frac{u'}{r}+\frac{1}{r}\frac{\partial v'}{\partial \theta},\\2\varpi'&=\frac{\partial v'}{\partial r}+\frac{v'}{r}-\frac{1}{r}\frac{\partial u'}{\partial \theta}.\end{aligned}\right\}\quad\ldots\ldots\ldots\ldots(26)$$

Among the particular solutions satisfying (25), we take the particular solution which is useful for the present study as follows:

$$\left.\begin{aligned}\Delta'&=0,\\2\varpi'&=-\frac{\rho g}{\mu}r\sin\theta.\end{aligned}\right\}\quad\ldots\ldots\ldots\ldots(27)$$

Next we must obtain the complementary solutions of (25) which are necessary to satisfy the boundary conditions of the soild.

Now the equations (25) give us the following equation:

$$\frac{\partial^2 \Delta'}{\partial r^2}+\frac{1}{r}\frac{\partial \Delta'}{\partial r}+\frac{\partial^2 \Delta'}{r^2\partial\theta^2}=0, \qquad \text{(28)}$$

the solutions of which are expressed by

$$\Delta'=B_0+\left\{\frac{F_1}{r}+B_1r+\frac{C_1}{r}\right\}\cos\theta+\left\{B_2r^2+C_2\frac{1}{r^2}\right\}\cos 2\theta$$
$$+\left\{B_3r^3+\frac{C_3}{r^3}\right\}\cos 3\theta+\left\{D_1r+\frac{E_1}{r}\right\}\sin\theta+\left\{D_2r^2+\frac{E_2}{r^2}\right\}\sin 2\theta$$
$$+\left\{D_3r^3+\frac{E_3}{r^3}\right\}\sin 3\theta, \qquad \text{(29)}$$

where B_0, B_1, C_1, B_2, C_2, B_3, C_3, F_1, D_1, E_1, D_2, E_2, D_3 and E_3 are the arbitrary constants to be determined by the elasticity conditions.

Using (29) we obtain the expressions of $2\varpi'$ which are the particular solutions of (25) as follows:

$$2\varpi'=\left\{\frac{(\lambda+2\mu)}{\mu}B_1r+\frac{(\lambda+2\mu)}{\mu}C_1\frac{1}{r}\right\}\sin\theta+\left\{\frac{(\lambda+2\mu)}{\mu}B_2r^2\right.$$
$$\left.+\frac{(\lambda+2\mu)}{\mu}C_2\frac{1}{r^2}\right\}\sin 2\theta+\left\{\frac{(\lambda+2\mu)}{\mu}B_3r^3+\frac{(\lambda+2\mu)}{\mu}\frac{C_3}{r^3}\right\}\sin 3\theta$$
$$-\left\{\frac{(\lambda+2\mu)}{\mu}D_1r+\frac{(\lambda+2\mu)}{\mu}E_1\frac{1}{r}\right\}\cos\theta-\left\{\frac{(\lambda+2\mu)}{\mu}D_2r^2\right.$$
$$\left.+\frac{(\lambda+2\mu)}{\mu}\frac{E_2}{r^2}\right\}\cos 2\theta-\left\{\frac{(\lambda+2\mu)}{\mu}D_3r^3+\frac{(\lambda+2\mu)}{\mu}E_3\frac{1}{r^3}\right\}\cos 3\theta. \qquad \text{(30)}$$

After some reductions we obtain the following the differential equations in relation to u', v' and Δ', $2\varpi'$ from the relations expressed by (26):

$$\frac{\partial^2(ru')}{\partial r^2}+\frac{1}{r}\frac{\partial(ru')}{\partial r}+\frac{1}{r^2}\frac{\partial^2 ru')}{\partial\theta^2}=\frac{1}{r}\frac{\partial(r^2\Delta')}{\partial r}-2\frac{\partial\varpi'}{\partial\theta}, \qquad \text{(31)}$$

$$\frac{\partial^2(rv')}{\partial r^2}+\frac{1}{r}\frac{\partial(rv')}{\partial r}+\frac{1}{r^2}\frac{\partial^2(rv')}{\partial\theta^2}=\frac{\partial\Delta'}{\partial\theta}+\frac{2}{r}\frac{\partial(r\varpi')}{\partial r}. \qquad \text{(32)}$$

Substituting (27) for the expressions of Δ' and $2\varpi'$ in the equations (31), (32), we obtain the particular solutions of (31) and (32) as follows:

$$\left.\begin{aligned} u' &= \frac{\rho g}{8\mu} r^2 \cos\theta, \\ v' &= -\frac{3\rho g}{8\mu} r^2 \sin\theta. \end{aligned}\right\} \qquad (33)$$

These expressions satisfy, of course, the equilibrium equations (25).

Substituting (29) and (30) for the expressions of Δ' and $2\varpi'$ in the right-hand terms of the equations (31) and (32), we obtain the particular solutions which are, of course, the particular solutions of (25) in the following forms:

$$\left.\begin{aligned} u' &= \frac{1}{2}B_0 r + \left[\frac{(-\lambda+\mu)}{8\mu}B_1 r^2 + \left\{\frac{(\lambda+3\mu)}{2\mu}\, ln\,\frac{r}{a} + \frac{1}{2}\right\}F_1\right]\cos\theta \\ &\quad - \left\{\frac{\lambda}{6\mu}B_2 r^3 + \frac{(\lambda+2\mu)}{2\mu}\frac{C_2}{r}\right\}\cos 2\theta - \left\{\frac{(3\lambda+\mu)}{16\mu}B_3 r^4 \right. \\ &\quad \left. + \frac{(3\lambda+5\mu)}{8\mu}\frac{C_3}{r^2}\right\}\cos 3\theta + \frac{(-\lambda+\mu)}{8\mu}D_1 r^2 \sin\theta - \left\{\frac{\lambda}{6\mu}D_2 r^3 \right. \\ &\quad \left. + \frac{(\lambda+2\mu)}{2\mu}\frac{E_2}{r}\right\}\sin 2\theta - \left\{\frac{(3\lambda+\mu)}{16\mu}D_3 r^4 + \frac{(3\lambda+5\mu)}{8\mu}\frac{E_3}{r^2}\right\}\sin 3\theta, \\ v' &= \left[\frac{(3\lambda+5\mu)}{8\mu}B_1 r^2 - \left\{\frac{(\lambda+3\mu)}{2\mu}\, ln\,\frac{r}{a} + \frac{(\lambda+2\mu)}{2\mu}\right\}F_1\right]\sin\theta \\ &\quad + \left\{\frac{(2\lambda+3\mu)}{6\mu}B_2 r^3 + \frac{1}{2}\frac{C_2}{r}\right\}\sin 2\theta + \left\{\frac{(5\lambda+7\mu)}{16\mu}B_3 r^4 \right. \\ &\quad \left. - \frac{(\lambda-\mu)}{8\mu}\frac{C_3}{r^2}\right\}\sin 3\theta - \frac{(3\lambda+5\mu)}{8\mu}D_1 r^2 \cos\theta - \left\{\frac{(2\lambda+3\mu)}{6\mu}D_2 r^3 \right. \\ &\quad \left. + \frac{1}{2}\frac{E_2}{r}\right\}\cos 2\theta - \left\{\frac{(5\lambda+7\mu)}{16\mu}D_3 r^4 - \frac{(\lambda-\mu)}{8\mu}\frac{E_3}{r^2}\right\}\cos 3\theta. \end{aligned}\right\} \qquad (34)$$

As the complementary solutions of (31) and (32) which are favourable to the present study, we obtain the following u' and v';

$$\left.\begin{aligned} u' &= \frac{B_0''}{r} + \frac{C_1''}{r^2}\cos\theta + \left\{B_2'' r + \frac{C_2''}{r^3}\right\}\cos 2\theta + \left\{B_3'' r^2 + \frac{C_3''}{r^4}\right\}\cos 3\theta \\ &\quad + \frac{D_1''}{r^2}\sin\theta + \left\{D_2'' r + \frac{E_2''}{r^3}\right\}\sin 2\theta + \left\{D_3'' r^2 + \frac{E_3''}{r^4}\right\}\sin 3\theta, \\ v' &= \frac{C_1''}{r^2}\sin\theta - \left\{B_2'' r - \frac{C_2''}{r^3}\right\}\sin 2\theta - \left\{B_3'' r^2 - \frac{C_3''}{r^4}\right\}\sin 3\theta \\ &\quad - \frac{D_1''}{r^2}\cos\theta + \left\{D_2'' r - \frac{E_2''}{r^3}\right\}\cos 2\theta + \left\{D_3'' r^2 - \frac{E_3''}{r^4}\right\}\cos 3\theta. \end{aligned}\right\} \qquad (35)$$

The general expressions of the components of the displacement thus obtained, (33), (34) and (35), satisfy, of course, the equations of equilibrium of the elastic solid (25). Using these general expressions we get the general expressions of stress $\widehat{rr}$, $\widehat{\theta\theta}$, and $\widehat{r\theta}$ as in the following forms:

$$\widehat{rr}=(\lambda+\mu)B_0-2\mu\frac{B_0''}{r^2}+\left[\frac{1}{2}\rho gr+\frac{(\lambda+\mu)}{2}B_1r-\frac{4\mu}{r^3}C_1''+\frac{(2\lambda+3\mu)}{r}F_1\right]\cos\theta$$
$$+\left[2\mu B_2''+\frac{2(\lambda+\mu)}{r^2}C_2-\frac{6\mu}{r^4}C_2''\right]\cos 2\theta+\left[-\frac{(\lambda+\mu)}{2}B_3r^3+4\mu B_3''r\right.$$
$$\left.+\frac{5(\lambda+\mu)}{2}\frac{C_3}{r^3}-\frac{8\mu}{r^5}C_3''\right]\cos 3\theta+\left[\frac{(\lambda+\mu)}{2}D_1r+\frac{(2\lambda+3\mu)}{r}E_1-\frac{4\mu}{r^3}E_1''\right]\sin\theta$$
$$+\left[2\mu D_2''+\frac{2(\lambda+\mu)}{r^2}E_2-\frac{6\mu}{r^4}E_2''\right]\sin 2\theta+\left[-\frac{(\lambda+\mu)}{2}r^3D_3+4\mu D_3''r\right.$$
$$\left.+\frac{5(\lambda+\mu)}{2r^3}E_3-\frac{8\mu}{r^5}E_3''\right]\sin 3\theta, \qquad\qquad (36)$$

$$\widehat{\theta\theta}=(\lambda+\mu)B_0+2\mu\frac{B_0''}{r^2}+\left[\frac{3}{2}(\lambda+\mu)B_1r-\frac{\rho g}{2}r+\frac{4\mu}{r^3}C_1''-\frac{\mu}{r}F_1\right]\cos\theta$$
$$+\left[2(\lambda+\mu)B_2r^2-2\mu B_2''+\frac{6\mu}{r^4}C_2''\right]\cos 2\theta+\left[\frac{5}{2}(\lambda+\mu)B_3r^3-4\mu B_3''r\right.$$
$$\left.-\frac{(\lambda+\mu)}{2}\frac{C_3}{r^3}+\frac{8\mu}{r^5}C_3''\right]\cos 3\theta+\left[\frac{3}{2}(\lambda+\mu)D_1r-\frac{\mu}{r}E_1+\frac{4\mu}{r^3}E_1''\right]\sin\theta$$
$$+\left[2(\lambda+\mu)D_2r^2-2\mu D_2''+\frac{6\mu}{r^4}E_2''\right]\sin 2\theta+\left[\frac{5}{2}(\lambda+\mu)D_3r^3-4\mu D_3''r\right.$$
$$\left.-\frac{(\lambda+\mu)}{2}\frac{E_3}{r^3}+\frac{8\mu}{r^5}E_3''\right]\sin 3\theta, \qquad\qquad (37)$$

$$\widehat{r\theta}=\left[-\frac{\rho gr}{2}+\frac{(\lambda+\mu)}{2}B_1r-\frac{4\mu}{r^3}C_1''-\frac{\mu}{r}F_1\right]\sin\theta+\left[(\lambda+\mu)B_2r^2-2\mu B_2''\right.$$
$$\left.+(\lambda+\mu)\frac{C_2}{r^2}-\frac{6\mu}{r^4}C_2''\right]\sin 2\theta+\left[\frac{3(\lambda+\mu)}{2}B_3r^3-4\mu B_3''r\right.$$
$$\left.+\frac{3}{2}\frac{(\lambda+\mu)}{r^3}C_3-\frac{8\mu}{r^5}C_3''\right]\sin 3\theta+\left[-\frac{(\lambda+\mu)}{2}D_1r+\frac{\mu}{r}E_1+\frac{4\mu}{r^3}E_1''\right]\cos\theta$$
$$+\left[-(\lambda+\mu)r^2D_2+2\mu D_2''-(\lambda+\mu)\frac{E_2}{r^2}+\frac{6\mu}{r^4}E_2''\right]\cos 2\theta$$
$$+\left[-\frac{3(\lambda+\mu)}{2}D_3r^3+4\mu D_3''r-\frac{3}{2}\frac{(\lambda+\mu)}{r^3}E_3+\frac{8\mu}{r^5}E_3''\right]\cos 3\theta \ldots (38)$$

These expressions of the components of stress satisfy, of course, the equations of equilibrium of the solid under the gravitating field expressed

by (23). Using these expressions of traction we shall study the stresses in the vicinity of a horizontal hole in the wedge-shaped solid of which the vertex has right-angle. We have obtained the expressions (16) of the stress distribution in the wedge-shaped solid having the vertex of right-angle in the preceding section. When we transform these components of stress $\widehat{xx}$, $\widehat{yy}$, $\widehat{xy}$ into the components of stress $\widehat{rr}$, $\widehat{\theta\theta}$, $\widehat{r\theta}$ in the cylindrical coordinates (r, θ) of which the relation with the rectangular coordinates (x', y') has already been explained, we have the following forms:

$$\begin{aligned}\widehat{rr}=&\left[-(\lambda+\mu)\rho g\xi\frac{\vartheta_{A1}}{\vartheta}+(\lambda+\mu)\rho g\eta\frac{\vartheta_{A2}}{\vartheta}\right]+\left[\frac{(\lambda+\mu)}{2}\rho g\frac{\vartheta_{A1}}{\vartheta}+\frac{\rho g}{2}\right]r\cos\theta\\&+\left[\left\{-\mu\frac{\vartheta_{A1}}{\vartheta}+2\mu\frac{\vartheta_{C4}}{\vartheta}\right\}\xi+\left\{-\mu\frac{\vartheta_{A2}}{\vartheta}+2\mu\frac{\vartheta_{C3}}{\vartheta}\right\}\eta\right]\rho g\cos 2\theta\\&+\left[\frac{(\lambda+3\mu)}{2}\frac{\vartheta_{A1}}{\vartheta}-2\mu\frac{\vartheta_{C4}}{\vartheta}-\frac{\rho g}{2}\right]\rho gr\cos 3\theta+\frac{(3\lambda+4\mu)}{4}\frac{\vartheta_{A2}}{\vartheta}\rho gr\sin\theta\\&+\left[\left\{(\lambda+2\mu)\frac{\vartheta_{A2}}{\vartheta}-2\mu\frac{\vartheta_{C3}}{\vartheta}\right\}\xi+\left\{-(\lambda+2\mu)\frac{\vartheta_{A1}}{\vartheta}+2\mu\frac{\vartheta_{C4}}{\vartheta}+1\right\}\eta\right]\rho g\sin 2\theta\\&+\left[-\frac{(\lambda+3\mu)}{2}\frac{\vartheta_{A2}}{\vartheta}+2\mu\frac{\vartheta_{C3}}{\vartheta}\right]\rho gr\sin 3\theta,\quad\ldots\ldots\ldots(39)\end{aligned}$$

$$\begin{aligned}\widehat{\theta\theta}=&\left[-(\lambda+\mu)\frac{\vartheta_{A1}}{\vartheta}\xi+(\lambda+\mu)\frac{\vartheta_{A2}}{\vartheta}\eta\right]\rho g+\left[\frac{3}{2}(\lambda+\mu)\frac{\vartheta_{A1}}{\vartheta}-\frac{1}{2}\right]\rho gr\cos\theta\\&+\left[\left\{\mu\frac{\vartheta_{A1}}{\vartheta}-2\mu\frac{\vartheta_{C4}}{\vartheta}\right\}\xi+\left\{\mu\frac{\vartheta_{A2}}{\vartheta}-2\mu\frac{\vartheta_{C3}}{\vartheta}\right\}\eta\right]\rho g\cos 2\theta\\&+\left[-\frac{(\lambda+3\mu)}{2}\frac{\vartheta_{A1}}{\vartheta}+2\mu\frac{\vartheta_{C4}}{\vartheta}+\frac{1}{2}\right]\rho gr\cos 3\theta+\frac{3(\lambda+\mu)}{2}\frac{\vartheta_{A2}}{\vartheta}\rho gr\sin\theta\\&-\left[\left\{(\lambda+2\mu)\frac{\vartheta_{A2}}{\vartheta}-2\mu\frac{\vartheta_{C3}}{\vartheta}\right\}\xi+\left\{-(\lambda+2\mu)\frac{\vartheta_{A1}}{\vartheta}+2\mu\frac{\vartheta_{C4}}{\vartheta}+1\right\}\eta\right]\rho g\sin 2\theta\\&+\left[\frac{(\lambda+3\mu)}{2}\frac{\vartheta_{A2}}{\vartheta}-2\mu\frac{\vartheta_{C3}}{\vartheta}\right]\rho gr\sin 3\theta,\quad\ldots\ldots\ldots(40)\end{aligned}$$

$$\begin{aligned}\widehat{r\theta}=&\left[\frac{(\lambda+\mu)}{2}\frac{\vartheta_{A1}}{\vartheta}-\frac{1}{2}\right]\rho gr\sin\theta\\&+\left[\left\{\mu\frac{\vartheta_{A1}}{\vartheta}-2\mu\frac{\vartheta_{C4}}{\vartheta}\right\}\xi+\left\{\mu\frac{\vartheta_{A2}}{\vartheta}-2\mu\frac{\vartheta_{C3}}{\vartheta}\right\}\eta\right]\rho g\sin 2\theta\\&+\left[-\frac{(\lambda+3\mu)}{2}\frac{\vartheta_{A1}}{\vartheta}+2\mu\frac{\vartheta_{C4}}{\vartheta}+\frac{1}{2}\right]\rho gr\sin 3\theta-\frac{(\lambda+\mu)}{2}\frac{\vartheta_{A2}}{\vartheta}\rho gr\cos\theta\\&+\left[\left\{(\lambda+2\mu)\frac{\vartheta_{A2}}{\vartheta}-2\mu\frac{\vartheta_{C3}}{\vartheta}\right\}\xi+\left\{-(\lambda+2\mu)\frac{\vartheta_{A1}}{\vartheta}+2\mu\frac{\vartheta_{C4}}{\vartheta}+1\right\}\eta\right]\rho g\cos 2\theta\end{aligned}$$

$$+\left[-\frac{(\lambda+3\mu)}{2}\frac{\vartheta_{A2}}{\vartheta}+2\mu\frac{\vartheta_{C3}}{\vartheta}\right]\rho g r\cos 3\theta. \qquad \ldots\ldots\ldots\ldots(41)$$

In the present study the boundary conditions of elasticity are as follows: (Referring to Fig. 3.)

1. On the two surfaces OY and OX the normal and shearing components of stress are zero.
2. On the surface of the horizontal circular hole, the normal and shearing components of stress are zero.

It is difficult to satisfy these conditions completely, and it is, however, our object to investigate the stress distribution in the vicinity of the hole, and therefore we may take the following conditions instead of of the above two conditions:

1. The stress at the whole space far from the horizontal hole in the wedge-shaped solid is equal to that expressed by (39), (40) and (41).
2. The surface of this hole is completely free from traction.

These are denoted by

$$r=\infty;\quad \left.\begin{array}{ll}\widehat{rr}=\widehat{rr} & \text{expressed by (39),}\\ \widehat{\theta\theta}=\widehat{\theta\theta} & \text{expressed by (40),}\\ \widehat{r\theta}=\widehat{r\theta} & \text{expressed by (41),}\end{array}\right\} \qquad \ldots\ldots\ldots\ldots(42)$$

$$r=a;\quad \left.\begin{array}{l}\widehat{rr}=0,\\ \widehat{r\theta}=0.\end{array}\right\} \qquad \ldots\ldots\ldots\ldots\ldots\ldots\ldots\ldots\ldots\ldots(43)$$

Using the expressions of stress, (36), (37) and (38), which are the general solutions of the equilibrium of the solid, and the conditions (42) and (43), we find the values of the arbitrary constants as follows:

From (42);

$$\left.\begin{array}{l}
B_0=\rho g\left\{-\frac{\vartheta_{A1}}{\vartheta}\xi+\frac{\vartheta_{A2}}{\vartheta}\eta\right\},\ B_1=\rho g\frac{\vartheta_{A1}}{\vartheta},\ B_3=0,\ D_2=0,\ D_3=0.\\
B_2''=\frac{\rho g}{2\mu}\left[\left\{-\mu\frac{\vartheta_{A1}}{\vartheta}+2\mu\frac{\vartheta_{C4}}{\vartheta}\right\}\xi+\left\{-\mu\frac{\vartheta_{A2}}{\vartheta}+2\mu\frac{\vartheta_{C3}}{\vartheta}\right\}\eta\right],\\
B_3''=\frac{\rho g}{4\mu}\left[\frac{(\lambda+3\mu)}{2}\frac{\vartheta_{A1}}{\vartheta}-2\mu\frac{\vartheta_{C4}}{\vartheta}-\frac{1}{2}\right],\ D_3''=\frac{\rho g}{4\mu}\left\{-\frac{(\lambda+3\mu)}{2}\frac{\vartheta_{A2}}{\vartheta}+2\mu\frac{\vartheta_{C3}}{\vartheta}\right\},\\
D_2''=\dfrac{\left[\left\{(\lambda+2\mu)\frac{\vartheta_{A2}}{\vartheta}-2\mu\frac{\vartheta_{C3}}{\vartheta}\right\}\xi+\left\{-(\lambda+2\mu)\frac{\vartheta_{A1}}{\vartheta}+2\mu\frac{\vartheta_{C4}}{\vartheta}+1\right\}\eta\right]\rho g}{2\mu}.
\end{array}\right\}(44)$$

From (43) :—

$$
\left.
\begin{aligned}
&B_0''=-\frac{(\lambda+\mu)}{2\mu}\left\{\frac{\vartheta_{A1}}{\vartheta}\xi-\frac{\vartheta_{A2}}{\vartheta}\eta\right\}\rho g a^2,\ F_1=-\frac{\rho g a^2}{2(\lambda+2\mu)},\\
&C_1''=\frac{(\lambda+\mu)}{8\mu}\rho g\frac{\vartheta_{A1}}{\vartheta}a^4-\frac{(\lambda+\mu)}{8\mu(\lambda+2\mu)}\rho g a^4,\ E_1=0,\\
&E_1''=\frac{\rho g(\lambda+\mu)}{8\mu}\frac{\vartheta_{A2}}{\vartheta}a^4,\ E_2=-\frac{2\rho g a^2}{(\lambda+\mu)}\\
&\qquad\times\left[\left\{(\lambda+2\mu)\frac{\vartheta_{A2}}{\vartheta}-2\mu\frac{\vartheta_{C3}}{\vartheta}\right\}\xi+\left\{-(\lambda+2\mu)\frac{\vartheta_{A1}}{\vartheta}+2\mu\frac{\vartheta_{C4}}{\vartheta}+1\right\}\eta\right],\\
&E_2''=-\frac{\rho g a^4}{2\mu}\left[\left\{(\lambda+2\mu)\frac{\vartheta_{A2}}{\vartheta}-2\mu\frac{\vartheta_{C3}}{\vartheta}\right\}\xi+\left\{-(\lambda+2\mu)\frac{\vartheta_{A1}}{\vartheta}\right.\right.\\
&\qquad\left.\left.+2\mu\frac{\vartheta_{C4}}{\vartheta}+1\right\}\eta\right],\\
&C_3=-\frac{2\rho g a^4}{(\lambda+\mu)}\left[\frac{(\lambda+3\mu)}{2}\frac{\vartheta_{A1}}{\vartheta}-2\mu\frac{\vartheta_{C4}}{\vartheta}-\frac{1}{2}\right],\\
&C_3''=-\frac{\rho g a^6}{2\mu}\left[\frac{(\lambda+3\mu)}{2}\frac{\vartheta_{A1}}{\vartheta}-2\mu\frac{\vartheta_{C4}}{\vartheta}-\frac{1}{2}\right],\\
&E_3=-\frac{2\rho g a^4}{(\lambda+\mu)}\left\{-\frac{(\lambda+3\mu)}{2}\frac{\vartheta_{A2}}{\vartheta}+2\mu\frac{\vartheta_{C3}}{\vartheta}\right\},\\
&E_3''=-\frac{\rho g a^6}{2\mu}\left\{-\frac{(\lambda+3\mu)}{2}\frac{\vartheta_{A2}}{\vartheta}+2\mu\frac{\vartheta_{C3}}{\vartheta}\right\}.\\
&C_2=-\frac{2\rho g a^2}{(\lambda+\mu)}\left[\left\{-\mu\frac{\vartheta_{A1}}{\vartheta}+2\mu\frac{\vartheta_{C4}}{\vartheta}\right\}\xi+\left\{-\mu\frac{\vartheta_{A2}}{\vartheta}+2\mu\frac{\vartheta_{C3}}{\vartheta}\right\}\eta\right],\\
&C_2''=-\frac{\rho g a^4}{2\mu}\left[\left\{-\mu\frac{\vartheta_{A1}}{\vartheta}+2\mu\frac{\vartheta_{C4}}{\vartheta}\right\}\xi+\left\{-\mu\frac{\vartheta_{A2}}{\vartheta}+2\mu\frac{\vartheta_{C3}}{\vartheta}\right\}\eta\right].
\end{aligned}
\right\}\quad(45)
$$

Substituting these values (44) and (45) for B_0, B_1, B_3, D_2, D_3, B_2'', B_3'', D_2'', D_3'', B_0'', F_1, C_1'', C_2, C_2'', E_1, E_1'', E_2, E_2'', C_3, C_3'', E_3 and E_3'' in the expressions (36), (37) and (38), we obtain the final results of the stress which are favourable to the present study as follows:

$$
\begin{aligned}
\widehat{rr}&=(\lambda+\mu)\rho g\left\{\xi\frac{\vartheta_{A1}}{\vartheta}-\eta\frac{\vartheta_{A2}}{\vartheta}\right\}\left\{-1+\frac{a^2}{r^2}\right\}\\
&+\rho g\left[\frac{(\lambda+\mu)}{2}\frac{\vartheta_{A1}}{\vartheta}\left(r-\frac{a^4}{r^3}\right)+\frac{1}{2}\left\{r-\frac{(2\lambda+3\mu)}{(\lambda+2\mu)}\frac{a^2}{r}+\frac{(\lambda+\mu)}{(\lambda+2\mu)}\frac{a^4}{r^3}\right\}\right]\cos\theta\\
&+\rho g\left[\left\{-\mu\frac{\vartheta_{A1}}{\vartheta}+2\mu\frac{\vartheta_{C4}}{\vartheta}\right\}\xi+\left\{-\mu\frac{\vartheta_{A2}}{\vartheta}+2\mu\frac{\vartheta_{C3}}{\vartheta}\right\}\eta\right]\left\{1-\frac{4a^2}{r^2}+\frac{3a^4}{r^4}\right\}\cos 2\theta
\end{aligned}
$$

$$+\rho g\left[\frac{(\lambda+3\mu)}{2}\frac{\vartheta_{A2}}{\vartheta}-2\mu\frac{\vartheta_{C4}}{\vartheta}-\frac{1}{2}\right]\left\{r-\frac{5a^4}{r^3}+\frac{4a^6}{r^5}\right\}\cos 3\theta$$

$$+\rho g\frac{(\lambda+\mu)}{2}\frac{\vartheta_{A2}}{\vartheta}\left(r-\frac{a^4}{r^3}\right)\sin\theta$$

$$+\rho g\left[\left\{(\lambda+2\mu)\frac{\vartheta_{A2}}{\vartheta}-2\mu\frac{\vartheta_{C3}}{\vartheta}\right\}\xi+\left\{-(\lambda+2\mu)\frac{\vartheta_{A1}}{\vartheta}+2\mu\frac{\vartheta_{C4}}{\vartheta}+1\right\}\eta\right]$$

$$\times\left\{1-\frac{4a^2}{r^2}+\frac{3a^4}{r^4}\right\}\sin 2\theta$$

$$+\rho g\left[-\frac{(\lambda+3\mu)}{2}\frac{\vartheta_{A2}}{\vartheta}+2\mu\frac{\vartheta_{C3}}{\vartheta}\right]\left\{r-5\frac{a^4}{r^3}+4\frac{a^6}{r^5}\right\}\sin 3\theta, \quad \ldots\ldots\ldots(46)$$

$$\widehat{\theta\theta}=-(\lambda+\mu)\rho g\left\{\xi\frac{\vartheta_{A1}}{\vartheta}-\eta\frac{\vartheta_{A2}}{\vartheta}\right\}\left\{1+\frac{a^2}{r^2}\right\}$$

$$+\rho g\left[\frac{(\lambda+\mu)}{2}\frac{\vartheta_{A1}}{\vartheta}\left(3r+\frac{a^4}{r^3}\right)+\frac{1}{2}\left\{-r+\frac{\mu a^2}{(\lambda+2\mu)r}-\frac{(\lambda+\mu)}{(\lambda+2\mu)}\frac{a^4}{r^3}\right\}\right]\cos\theta$$

$$+\rho g\left[\left\{\mu\frac{\vartheta_{A1}}{\vartheta}-2\mu\frac{\vartheta_{C4}}{\vartheta}\right\}\xi+\left\{\mu\frac{\vartheta_{A2}}{\vartheta}-2\mu\frac{\vartheta_{C3}}{\vartheta}\right\}\eta\right]\left\{1+\frac{3a^4}{r^4}\right\}\cos 2\theta$$

$$+\rho g\left[\frac{(\lambda+3\mu)}{2}\frac{\vartheta_{A1}}{\vartheta}-2\mu\frac{\vartheta_{C4}}{\vartheta}-\frac{1}{2}\right]\left\{-r+\frac{a^4}{r^3}-\frac{4a^6}{r^5}\right\}\cos 3\theta$$

$$+\frac{(\lambda+\mu)}{2}\rho g\frac{\vartheta_{A2}}{\vartheta}\left\{3r-\frac{a^4}{r^3}\right\}\sin\theta$$

$$+\rho g\left[\left\{-(\lambda+2\mu)\frac{\vartheta_{A2}}{\vartheta}+2\mu\frac{\vartheta_{C3}}{\vartheta}\right\}\xi+\left\{(\lambda+2\mu)\frac{\vartheta_{A1}}{\vartheta}-2\mu\frac{\vartheta_{C4}}{\vartheta}-1\right\}\eta\right]$$

$$\times\left\{1+\frac{3a^4}{r^4}\right\}\sin 2\theta$$

$$+\rho g\left[-\frac{(\lambda+3\mu)}{2}\frac{\vartheta_{A2}}{\vartheta}+2\mu\frac{\vartheta_{C3}}{\vartheta}\right]\left\{-r+\frac{a^4}{r^3}-4\frac{a^6}{r^5}\right\}\sin 3\theta, \quad \ldots\ldots\ldots(47)$$

$$\widehat{r\theta}=\rho g\left[\frac{(\lambda+\mu)}{2}\frac{\vartheta_{A1}}{\vartheta}\left\{r-\frac{a^4}{r^3}\right\}+\frac{1}{2}\left\{-r+\frac{\mu}{(\lambda+2\mu)}\frac{a^2}{r}+\frac{(\lambda+\mu)}{(\lambda+2\mu)}\frac{a^4}{r^3}\right\}\right]\sin\theta$$

$$+\rho g\left[\left\{-\mu\frac{\vartheta_{A1}}{\vartheta}+2\mu\frac{\vartheta_{C4}}{\vartheta}\right\}\xi+\left\{-\mu\frac{\vartheta_{A2}}{\vartheta}+2\mu\frac{\vartheta_{C3}}{\vartheta}\right\}\eta\right]$$

$$\times\left\{-1-\frac{2a^2}{r^2}+\frac{3a^4}{r^4}\right\}\sin 2\theta$$

$$+\rho g\left[\frac{(\lambda+3\mu)}{2}\frac{\vartheta_{A1}}{\vartheta}-2\mu\frac{\vartheta_{C4}}{\vartheta}-\frac{1}{2}\right]\left\{-r-\frac{3a^4}{r^3}+\frac{4a^6}{r^5}\right\}\sin 3\theta$$

$$-\rho g\frac{(\lambda+\mu)}{2}\frac{\vartheta_{A2}}{\vartheta}\left\{r-\frac{a^4}{r^3}\right\}\cos\theta$$

$$+\rho g\left[\left\{(\lambda+2\mu)\frac{\vartheta_{A2}}{\vartheta}-2\mu\frac{\vartheta_{C3}}{\vartheta}\right\}\xi+\left\{-(\lambda+2\mu)\frac{\vartheta_{A1}}{\vartheta}+2\mu\frac{\vartheta_{C4}}{\vartheta}+1\right\}\eta\right]$$

$$\times\left\{1+\frac{2a^2}{r^2}-\frac{3a^4}{r^4}\right\}\cos 2\theta$$

$$+\rho g\left[-\frac{(\lambda+3\mu)}{2}\frac{\vartheta_{A2}}{\vartheta}+2\mu\frac{\vartheta_{C3}}{\vartheta}\right]\left\{r+3\frac{a^4}{r^3}-4\frac{a^6}{r^5}\right\}\cos 3\theta. \quad \text{........(48)}$$

As $\widehat{\theta\theta}_{r=a}$ on the surface of the hole play an important *rôle* on the failure of the tunnel, it may be of some importance to investigate the properties of the stress distribution around tne surface of the horizontal hole. For this purpose we assume $\lambda=\mu$ (Poisson's ratio$=1/4$). Then the tangential stress $\widehat{\theta\theta}_{r=a}$ on the surface of the hole is expressed by the following simplified form:

$$\widehat{\theta\theta}_{r=a}=\Theta+\Phi+\Psi, \quad \text{.....................(49)}$$

where

$$\frac{\Theta}{\rho g a}=\left(4\frac{\vartheta_{A1}}{\vartheta}-\frac{2}{3}\right)\cos\theta-4\left\{4\frac{\vartheta_{A1}}{\vartheta}-4\frac{\vartheta_{C4}}{\vartheta}-1\right\}\cos 3\theta-8\frac{\vartheta_{C3}}{\vartheta}\sin 3\theta, \quad (50)$$

$$\frac{\Phi}{\rho g a}=-4\frac{\vartheta_{A1}}{\vartheta}+4\left\{\frac{\vartheta_{A1}}{\vartheta}-2\frac{\vartheta_{C4}}{\vartheta}\right\}\cos 2\theta+8\frac{\vartheta_{C3}}{\vartheta}\sin 2\theta, \quad \text{............(51)}$$

$$\frac{\Psi}{\rho g a}=-8\frac{\vartheta_{C3}}{\vartheta}\cos 2\theta+4\left\{3\frac{\vartheta_{A1}}{\vartheta}-2\frac{\vartheta_{C4}}{\vartheta}-1\right\}\sin 2\theta. \quad \text{..............(52)}$$

Substituting the relations in Table I for the expressions of $\frac{\vartheta_{A1}}{\vartheta}$, $\frac{\vartheta_{A2}}{\vartheta}$, $\frac{\vartheta_{C3}}{\vartheta}$ and $\frac{\vartheta_{C4}}{\vartheta}$ in the right-hand terms of Θ, Φ, Ψ, we obtain Table III in which Θ, Φ, and Ψ expressed by terms θ only are tabulated in the cases of $\varphi=0°$, $20°$, $30°$, $45°$, $60°$ and $70°$.

Table III.

φ	0°	20°	30°	45°	60°	70°
Θ	$\frac{1}{3}\cos\theta$ $-\cos 3\theta$	$\frac{1}{3}\cos\theta$ $-0{\cdot}175\cos 3\theta$ $-0{\cdot}984\sin 3\theta$	$\frac{1}{3}\cos\theta$ $+0{\cdot}496\cos 3\theta$ $-0{\cdot}864\sin 3\theta$	$\frac{1}{3}\cos\theta$ $+\cos 3\theta$	$\frac{1}{3}\cos\theta$ $+0{\cdot}496\cos 3\theta$ $+0{\cdot}864\sin 3\theta$	$\frac{1}{3}\cos\theta$ $-0{\cdot}175\cos 3\theta$ $+0{\cdot}984\sin 3\theta$
Φ	-1 $+2\cos 2\theta$	-1 $+1{\cdot}175\cos 2\theta$ $+0{\cdot}984\sin 2\theta$	-1 $+0{\cdot}504\cos 2\theta$ $+0{\cdot}864\sin 2\theta$	-1	-1 $+0{\cdot}504\cos 2\theta$ $-0{\cdot}864\sin 2\theta$	-1 $+1{\cdot}175\cos 2\theta$ $-0{\cdot}984\sin 2\theta$
Ψ	0	$-0{\cdot}984\cos 2\theta$ $-0{\cdot}825\sin 2\theta$	$-0{\cdot}864\cos 2\theta$ $-1{\cdot}496\sin 2\theta$	-2 $\times\sin 2\theta$	$0{\cdot}864\cos 2\theta$ $-1{\cdot}496\sin 2\theta$	$0{\cdot}984\cos 2\theta$ $-0{\cdot}825\sin 2\theta$

The magnitudes Θ, Φ and Ψ in Table III are easily calculated, and the results are tabulated in Table IV, V, and VI, and illustrated in Fig. 5, 6, 7, 8, 9, 10, 11, 12, 13, 14, 15, 16, 17, 18, 19, 20, 21.

The following properties may be seen from these tables and figures:

1. When $\varphi=0°$ and 45°, the distribution of Θ and Φ are symmetrical about the axis $o'x'$ (vertical axis). Φ has especially a constant value $(-\rho g\xi)$ uniformly distrbuted on the surface of the hole in the case of $\varphi=45°$.

2. The curves denoting Φ and Ψ have regular forms of certain constant amplitudes of fluctuation for differnt θ, and their mean lines are the lines of $\Phi=-\rho g\xi$ and $\Psi=0$ respectively in all cases of φ. The curve denoting Θ, however, has irregular amplitudes.

3. The amplitudes of the curves of Φ and Ψ are variable according to the magnitude of φ. The curve denoting Φ has the largest amplitude when $\varphi=0°$ or 90°; and the amplitude of Ψ takes the largest value when $\varphi=45°$.

4. The positions of maxima and minima of the amplitudes of Θ, Φ, Ψ shift regularly and systematically along θ-axis between $\theta=0°$ and $\theta=360°$ according to the variation of φ between 0 and 90°.

5. Ψ has no effect upon the stress distribution when $\varphi=0$. When $\varphi=45°$, Ψ takes the largest values 200 $\rho g\eta$ (with positive sign) at $\theta=135°$ and $\theta=315°$, and also similar values (with negative sign) at $\theta=45°$ and 225°.

Next we shall study the numerical variation of $\widehat{\theta\theta}_{r=a}$ according to different values of ξ, η and φ. Before entering this investigation, the

Table IV. $\left(\text{Magnitude of } \frac{\theta}{\rho g a}.\right)$

θ \ φ	0°	20°	30°	45°	60°	70°
0°	−0·67	0·16	0·83	1·33	0·83	0·16
10	−0·54	−0·32	0·24	1·19	1·19	0·67
20	−0·19	−0·63	−0·24	0·81	1·31	1·08
30	0·29	−0·70	−0·58	0·29	1·15	1·27
45	0·94	−0·34	−0·65	−0·47	0·50	1·06
60	1·17	0·34	−0·33	−0·83	−0·33	0·34
70	0·98	0·76	0·20	−0·75	−0·75	−0·23
80	0·56	1·00	0·61	−0·44	−0·94	−0·71
90	0	0·98	0·86	0	−0·86	−0·98
100	−0·56	0·71	0·89	0·44	−0·56	−1·00
110	−0·98	0·22	0·66	0·75	−0·12	−0·76
120	−1·17	−0·34	0·33	0·83	0·33	−0·34
135	−0·94	−1·05	−0·57	0·47	0·72	0·34
150	−0·29	−1·27	−1·15	−0·29	0·58	0·70
160	0·19	−1·08	−1·26	−0·81	0·19	0·63
170	0·54	−0·66	−1·10	−1·19	−0·33	0·32
180	0·67	−0·16	−0·83	−1·33	−0·83	−0·16
190	0·54	0·32	−0·24	−1·19	−1·19	−0·67
200	0·19	0·63	0·24	−0·81	−1·31	−1·08
210	−0·29	0·70	0·58	−0·29	−1·15	−1·27
225	−0·94	0·34	0·65	0·47	−0·50	−1·06
240	−1·17	−0·34	0·33	0·83	0·33	−0·34
250	−0·98	−0·76	−0·20	0·75	0·75	0·23
260	−0·56	−1·00	−0·61	0·44	0·94	0·71
270	0	−0·98	−0·86	0	0·86	0·98
280	0·56	−0·71	−0·89	−0·44	0·56	1·00
290	0·98	−0·22	−0·66	−0·75	0·12	0·76
300	1·17	0·34	−0·33	−0·83	−0·33	0·34
315	0·94	1·05	0·57	−0·47	−0·72	−0·34
330	0·29	1·27	1·15	0·29	−0·58	−0·70
340	−0·19	1·08	1·26	0·81	−0·19	−0·63
350	−0·54	0·66	1·10	1·19	0·33	−0·32
360	−0·67	0·16	0·83	1·33	0·83	0·16

Table V. (Magnitude of $\frac{\Phi}{\rho g \xi}$.)

θ \ φ	0°	20°	30°	45°	60°	70°
0°	1·00	0·18	−0·50	−1	−0·50	0·18
10	0·88	0·44	−0·23	−1	−0·82	−0·24
20	0·53	0·53	−0·06	−1	−1·17	−0·73
30	0	0·44	0	−1	−1·50	−1·27
45	−1·00	−0·02	−0·14	−1	−1·86	−1·98
60	−2·00	−0·74	−0·50	−1	−2·00	−2·44
70	−2·53	−1·27	−0·83	−1	−1·94	−2·53
80	−2·88	−1·77	−1·18	−1	−1·77	−2·44
90	−3·00	−2·18	−1·50	−1	−1·50	−2·18
100	−2·88	−2·44	−1·77	−1	−1·18	−1·76
110	−2·53	−2·53	−1·94	−1	−0·83	−1·27
120	−2·00	−2·44	−2·00	−1	−0·50	−0·73
135	−1·00	−1·98	−1·86	−1	−0·14	−0·02
150	0	−1·27	−1·50	−1	0	0·44
160	0·53	−0·73	−1·17	−1	−0·06	0·53
170	0·87	−0·23	−0·82	−1	−0·23	0·44
180	1·00	0·18	−0·50	−1	−0·50	0·18
190	0·87	0·44	−0·23	−1	−0·82	−0·24
200	0·53	0·53	−0·06	−1	−1·17	−0·73
210	0	0·44	0	−1	−1·50	−1·27
225	−1·00	−0·02	−0·14	−1	−1·86	−1·98
240	−2·00	−0·74	−0·50	−1	−2·00	−2·44
250	−2·53	−1·27	−0·83	−1	−1·94	−2·53
260	−2·88	−1·77	−1·18	−1	−1·77	−2·44
270	−3·00	−2·18	−1·50	−1	−1·50	−2·18
280	−2·88	−2·44	−1·77	−1	−1·18	−1·76
290	−2·53	−2·53	−1·94	−1	−0·83	−1·27
300	−2·00	−2·44	−2·00	−1	−0·50	−0·73
315	−1·00	−1·98	−1·86	−1	−0·14	−0·02
330	0	−1·27	−1·50	−1	0	0·44
340	0·53	−0·73	−1·17	−1	−0·06	0·53
350	0·88	−0·23	−0·82	−1	−0·23	0·44
360	1·00	0·18	−0·50	−1	−0·50	0·18

Table VI. $\left(\text{Magnitude of } \frac{\Psi}{\rho g \eta}.\right)$

θ \ φ	0°	20°	30°	45°	60°	70°
0°	0	−0·98	−0·86	0	0·86	0·98
10	〃	−1·21	−1·32	−0·68	0·30	0·64
20	〃	−1·29	−1·62	−1·29	−0·30	0·22
30	〃	−1·21	−1·72	−1·73	−0·86	−0·22
45	〃	−0·83	−1·50	−2·00	−1·50	−0·83
60	〃	0·23	−0·86	−1·73	−1·73	−1·21
70	〃	0·23	−0·30	−1·29	−1·62	−1·28
80	〃	0·64	0·30	−0·68	−1·32	−1·21
90	〃	0·98	0·86	0	−0·86	−0·98
100	〃	1·21	1·32	0·68	−0·30	−0·64
110	〃	1·29	1·62	1·29	0·30	−0·22
120	〃	1·21	1·72	1·73	0·86	0·22
135	〃	0·83	1·50	2·00	1·50	0·83
150	〃	0·22	0·86	1·73	1·73	1·21
160	〃	−0·23	0·30	1·29	1·62	1·28
170	〃	−0·64	−0·30	0·68	1·32	1·21
180	〃	−0·98	−0·86	0	0·86	0·98
190	〃	−1·21	−1·32	−0·68	0·30	0·64
200	〃	−1·29	−1·62	−1·29	−0·30	0·22
210	〃	−1·21	−1·72	−1·73	−0·86	−0·22
225	〃	−0·83	−1·50	−2·00	−1·50	−0·83
240	〃	−0·22	−0·86	−1·73	−1·73	−1·21
250	〃	0·23	−0·30	−1·29	−1·62	−1·28
260	〃	0·64	0·30	−0·68	−1·32	−1·27
270	〃	0·98	0·86	0	−0·86	−0·98
280	〃	1·21	1·32	0·68	−0·30	−0·64
290	〃	1·29	1·62	1·29	0·30	−0·22
300	〃	1·21	1·72	1·73	0·86	0·22
315	〃	0·83	1·50	2·00	1·50	0·83
330	〃	0·23	0·86	1·73	1·73	1·21
340	〃	−0·23	0·30	1·29	1·62	1·28
350	〃	−0·64	−0·30	0·68	1·32	1·21
360	〃	−0·98	−0·86	0	0·86	0·98

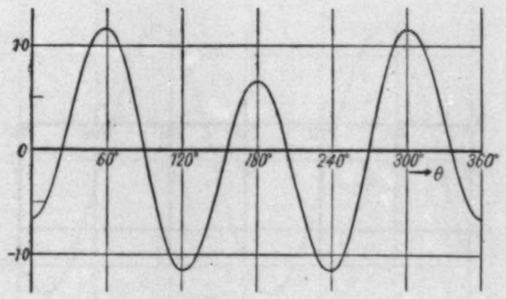

Fig. 5. Magnitude of $\frac{\Theta}{\rho g a}$ when $\varphi=0$.

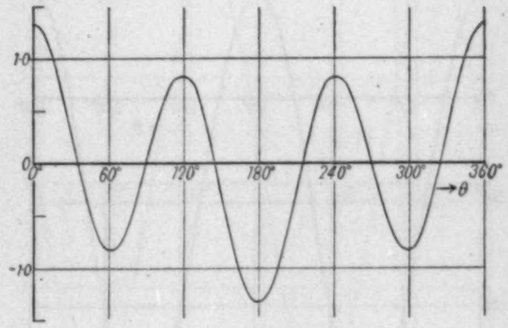

Fig. 8. Magnitude of $\frac{\Theta}{\rho g a}$ when $\varphi=45°$.

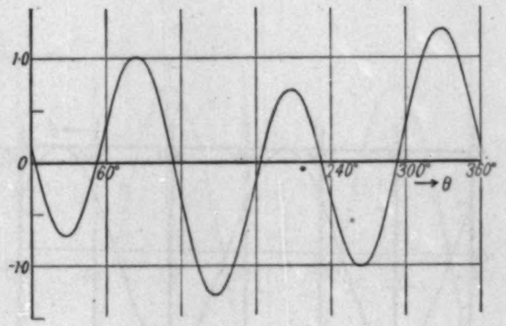

Fig. 6. Magnitude of $\frac{\Theta}{\rho g a}$ when $\varphi=20°$.

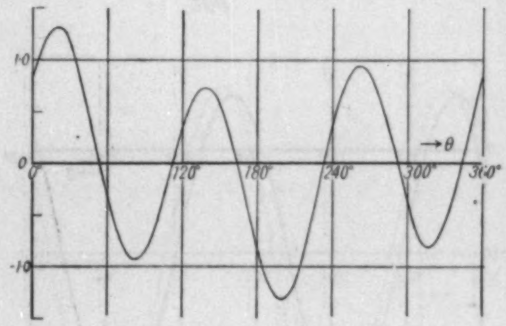

Fig. 9. Magnitude of $\frac{\Theta}{\rho g a}$ when $\varphi=60°$.

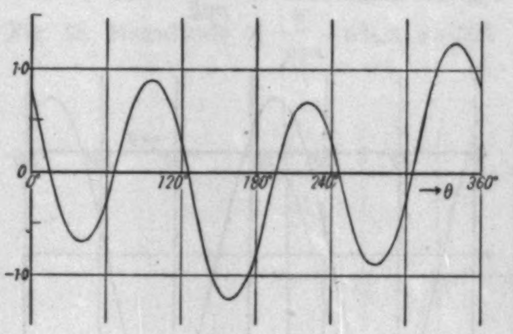

Fig. 7. Magnitude of $\frac{\Theta}{\rho g a}$ when $\varphi=30°$.

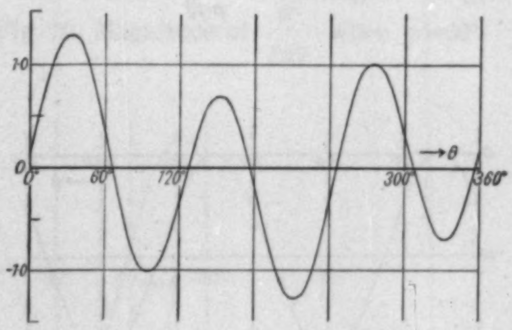

Fig. 10. Magnitude of $\frac{\Theta}{\rho g a}$ when $\varphi=70°$.

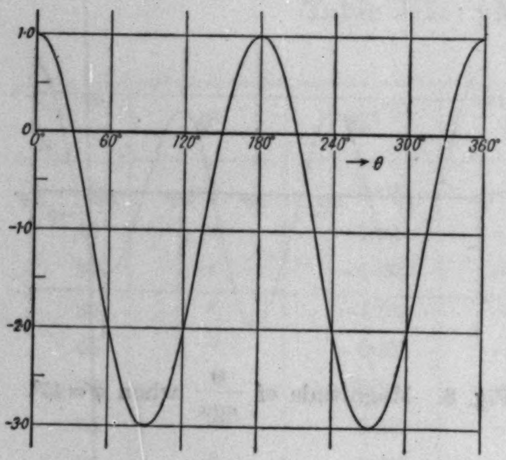

Fig. 11. Magnitude of $\frac{\Phi}{\rho g \xi}$ when $\varphi=0°$.

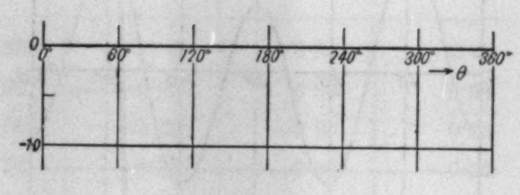

Fig. 14. Magnitude of $\frac{\Phi}{\rho g \xi}$ when $\varphi=45°$.

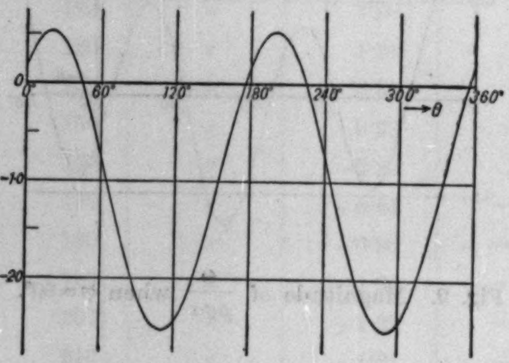

Fig. 12. Magnitude of $\frac{\Phi}{\rho g \xi}$ when $\varphi=20°$.

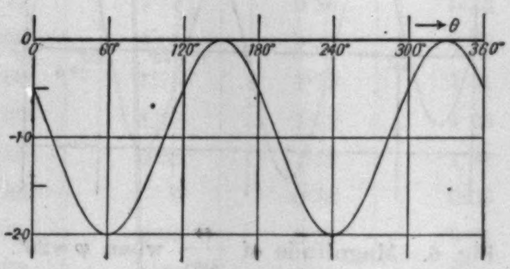

Fig. 15. Magnitude of $\frac{\Phi}{\rho g \xi}$ when $\varphi=60°$.

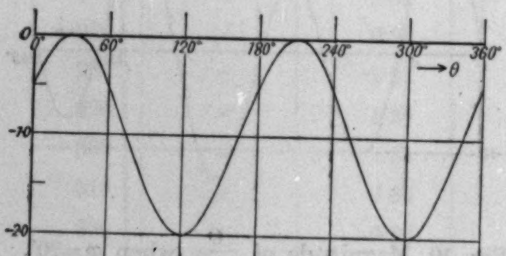

Fig. 13. Magnitude of $\frac{\Phi}{\rho g \xi}$ when $\varphi=30°$.

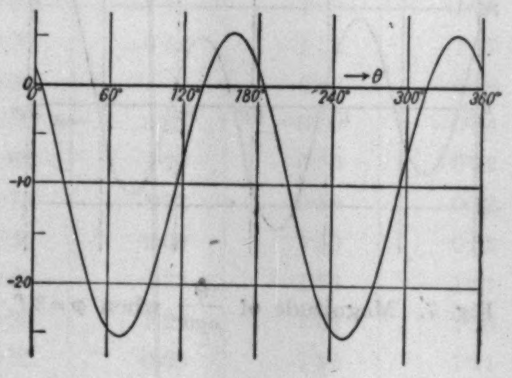

Fig. 16. Magnitude of $\frac{\Phi}{\rho g \xi}$ when $\varphi=70°$.

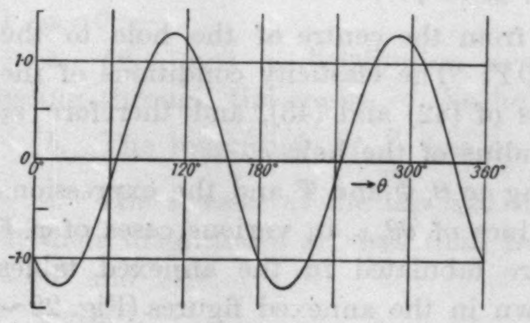

Fig. 17. Magnitude of $\dfrac{\Psi}{\rho g \eta}$ when $\varphi=20°$.

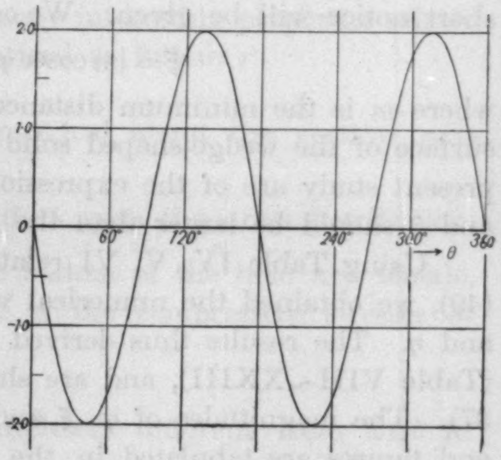

Fig. 19. Magnitude of $\dfrac{\Psi}{\rho g \eta}$ when $\varphi=45°$.

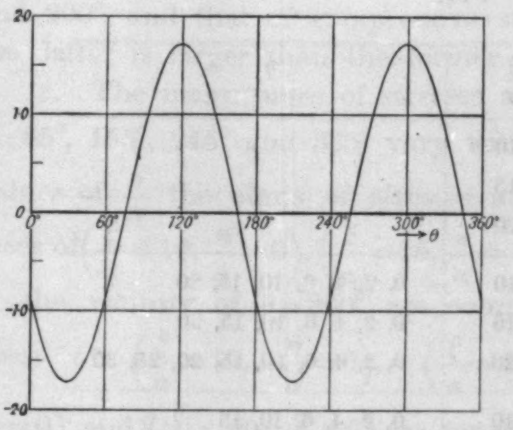

Fig. 18. Magnitude of $\dfrac{\Psi}{\rho g \eta}$ when $\varphi=30°$.

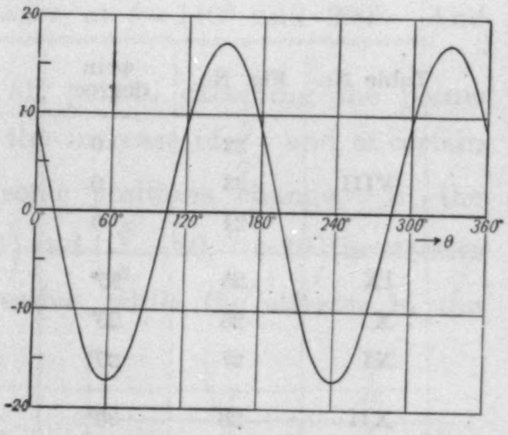

Fig. 20. Magnitude of $\dfrac{\Psi}{\rho g \eta}$ when $\varphi=60°$.

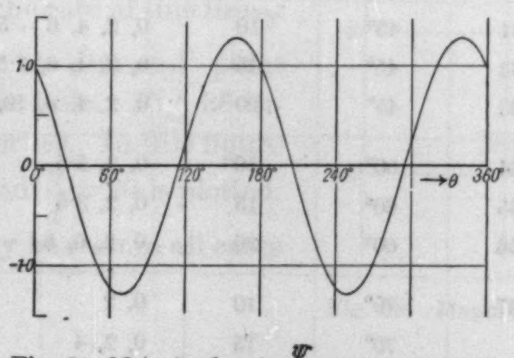

Fig. 21. Magnitude of $\dfrac{\Psi}{\rho g \eta}$ when $\varphi=70°$

short notice will be given. We can easily obtain the following relation:

$$\xi = \{m \operatorname{cosec} \varphi + \eta\} \tan \varphi, \qquad (53)$$

where m is the minimum distance from the centre of the hole to the surface of the wedge-shaped solid OY. The elasticity conditions of the present study are of the expressions of (42) and (43), and therefore m and ξ should be larger than the radius of the hole a.

Using Table IV, V, VI relating to θ, Φ and Ψ and the expressions (49), we obtained the numerical values of $\widehat{\theta\theta}_{r=a}$ in various cases of φ, ξ and η. The results thus derived are tabulated in the annexed tables (Table VIII~XXIII), and are shewn in the annexed figures (Fig. 22~37). The magnitudes of φ, ξ and η of which we treated in these tables and figures are tabulated in the following table, for the convenience sake. (Table VII.)

Table VII.

Table No.	Fig. No.	φ in degree	$\frac{\xi}{a}$	$\frac{\eta}{a}$
	22	0	10	
VIII	23	0	15	
	24	0	20	
IX	25	20°	10	0, 2, 4, 6, 10, 15, 20
X	26	20°	15	0, 2, 4, 6, 10, 15, 20
XI	27	20°	20	0, 2, 4, 6, 10, 15, 20, 25, 30
XII	28	30°	10	0, 2, 4, 6, 10, 13
XIII	29	30°	15	0, 2, 4, 6, 10, 13, 20
XIV	30	30°	20	0, 2, 4, 6, 10, 13, 15, 20, 25
XV	31	45°	10	0, 2, 4, 6, 7·5
XVI	32	45°	15	0, 2, 4, 6, 7·5
XVII	33	45°	20	0, 2, 4, 6, 10, 15
XVIII	34	60°	10	0, 2, 3·5
XIX	35	60°	15	0, 2, 3·5
XX	36	60°	20	0, 2, 6, 8
XXI	37	70°	10	0, 2
XXII		70°	15	0, 2, 4
XXIII		70°	20	0, 2, 4, 6

These tables and figures shew us many interesting properties related to $\widehat{\theta\theta}_{r=a}$, and some of them are summarized as follows:

1) $\varphi=0$:—

a. $\widehat{\theta\theta}_{r=a}$ has a distribution symmetrical about the vertical axis passing through the centre of the hole.

b. The magnitude of $\frac{\eta}{a}$ has no effect upon the stress distribution.

c. The stresses at the top and the bottom of the hole are tensile, but their magnitudes are less than that of the compressive stresses at $\theta=90°$ and $270°$.

2) $\varphi=20°$:—

a. The distribution of $\widehat{\theta\theta}_{r=a}$ is completely different from that in the case of $\varphi=0$ and it is much affected by the variation of $\frac{\eta}{a}$.

b. Wen $\frac{\eta}{a}$ is zero, the maxima of tensile stresses occur at $\theta=20°$ and $200°$, and that of compressive stresses at $\theta=110°$ and $290°$. And the latter is larger than the former.

c. The magnitudes of stresses at all points, excepting the points $\theta=65°$, $155°$, $245°$ and $335°$ vary with the increase of $\frac{\eta}{a}$, and at certain values of $\frac{\eta}{a}$ the signs of stresses at some positions change. In the cases of $\left(\frac{\xi}{a}=10, \frac{\eta}{a}=6\right)$, $\left(\frac{\xi}{a}=15, \frac{\eta}{a}=10\right)$ and $\left(\frac{\xi}{a}=20, \frac{\eta}{a}=10\right)$ the stresses in the vicinity of $\theta=200°$ are compressive, while the stresses in the cases of $\left(\frac{\xi}{a}=10, \frac{\eta}{a}=0\right)$, $\left(\frac{\xi}{a}=15, \frac{\eta}{a}=0\right)$ and $\left(\frac{\xi}{a}=20, \frac{\eta}{a}=0\right)$ are tensile.

d. $\widehat{\theta\theta}_{r=a}$ increases linearly with the increase of $\frac{\xi}{a}$, but the rate of this linear increase is different at different point on the surface of the hole. Fig. 38 indicates us these properties. In this figure the case of $\varphi=20°$ and $\frac{\eta}{a}=20$ is plotted. (These properties may be seen in all cases of φ.)

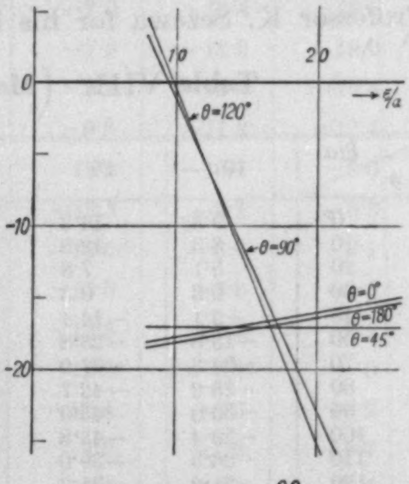

Fig. 38. Magnitude of $\frac{\theta\theta_{r=a}}{\rho g a}$ when $\varphi=20°$ and $\frac{\eta}{a}=20$.

3) $\varphi=45°$:—

a. When $\frac{\eta}{a}=0$, the stresses are of

course distributed symmetrically about the vertical plane passing through the centre of the hole.

b. When $\frac{\eta}{a}=0$, the stresses are compressive, and they have no remarkable variations of the distribution as in the case of $\varphi=0$.

c. Of course, the positions of maximum and minimum magnitudes of stresses are different from that in the cases of $\varphi=20°$ and $30°$.

3. We have now studied the stress distribution in the neighbourhood of a horizontal circular hole in a gravitating wedge-shaped solid, and may resume some results obtained from the calculations:

1. The maximum values of tension and compression are different in each case of φ, and their positions are also different.

2. The variations of $\frac{\xi}{a}$ and $\frac{\eta}{a}$ give no effect upon the variations of the positions of the maxima and minima of the stresses.

3. According to the variation of $\frac{\eta}{a}$ the sign of stress may change.

4. There are some positions on the surface of the hole where the values of stress do not change in spite of the variation of $\frac{\eta}{a}$.

5. The magnitude of stress at a point on the surface of the hole is proportional to the depth of the centre of the hole from the vertex of the solid.

6. The rate of the linear increase of the stress with the depth of the hole is different at different point on the surface of the hole.

In conclusion, the authors must express their sincere thanks to Professor K. Sezawa for his kind guidance.

Table VIII. $\left(\text{Magnitude of } \frac{\widehat{\theta\theta}_{r=a}}{\rho g a} \text{ when } \varphi=0°.\right)$

θ \ ξ/a	10	15	20	θ \ ξ/a	10	15	20
0°	9·3	14·3	19·3	190	9·2	13·8	17·9
10	8·3	12·8	17·1	200	5·5	8·2	10·8
20	5·1	7·8	10·4	210	−0·3	−0·3	−0·3
30	0·3	0·3	0·3	225	−10·9	−15·9	−20·9
45	−9·1	−14·1	−19·1	240	−21·2	−31·2	−41·2
60	−18·8	−28·8	−38·8	250	−26·3	−39·0	−51·6
70	−24·3	−37·0	−49·6	260	−29·4	−43·8	−58·2
80	−28·2	−42·7	−57·0	270	−30·0	−45·0	−60.0
90	−30·0	−45·0	−60·0	280	−28·2	−42·6	−57·0
100	−29·4	−43·8	−58·2	290	−24·3	−37·0	−49·6
110	−26·3	−39·0	−51.6	300	−18·8	−28·8	−38·8
120	−21·2	−31·2	−41·2	315	−9·1	−14·1	−19·1
135	−10·9	−15 9	−20·9	330	0·3	0·3	0·3
150	−0·3	−0·3	−0·3	340	5·1	7·8	10·4
160	5·5	8·2	10·8	350	8·3	12·8	17·1
170	9·2	13·8	17·9	360	9·3	14·3	19·3
180	10·7	15·7	20·7				

Table IX. $\left(\text{Magnitude of } \frac{\widehat{\theta\theta}_{r=a}}{\rho g a} \text{ when } \varphi=20^\circ \text{ and } \frac{\xi}{a}=10.\right)$

θ \ η/a	0	2	4	6	10	15	20
0°	2·0	0	−1·9	−3·9	−7·8	−12·8	−17·7
10	4·1	1·7	−0·7	−3·2	−8·1	−14·0	−20·0
20	4·7	2·2	−0·5	−3·0	−8·2	−14·6	−21·0
30	3·7	1·3	−1·1	−3·6	−8·4	−14·4	−20·4
45	−0·5	−2·2	−3·8	−5·5	−8·8	−12·9	−17·0
60	−7·1	−7·6	−8·0	−8·5	−9·4	−10·6	−11·8
70	−11·9	−11·5	−11·0	−10·5	−9·6	−8·5	−7·4
80	−16·7	−15·4	−14·1	−12·8	−10·3	−7·1	−3·8
90	−20·8	−18·8	−16·9	−14·9	−11·0	−6·0	−1·1
100	−23·7	−21·7	−18·9	−16·4	−11·6	−5·6	0·4
110	−25·1	−22·5	−19·9	−17·4	−12·2	−5·8	0·6
120	−24·7	−22·4	−19·9	−17·4	−12·6	−6·6	−0·6
135	−20·9	−19·2	−17·6	−15·9	−12·6	−8·5	−4·4
150	−14·0	−13·6	−13·1	−12·6	−11·8	−10·5	−9·3
160	−8·4	−8·9	−9·3	−9·8	−10·7	−11·8	−12·9
170	−2·9	−4·3	−5·5	−6·8	−9·3	−12·5	−15·8
180	1·6	0	−2·3	−4·3	−8·2	−13·2	−18·1
190	4·7	2·3	−0·1	−2·6	−7·4	−13·4	−19·4
200	5.9	3·3	0·7	−1·8	−7·0	−13·4	−19·8
210	5·1	2·7	0·3	−2·2	−7·0	−13·0	−19.0
225	0·1	−1·6	−3·2	−4·9	−8·2	−12·3	−16·4
240	−7·7	−8·1	−8·6	−9·1	−9·9	−11·2	−12·4
250	−13·5	−13·0	−12·6	−12·1	−11·2	−10·1	−9·0
260	−18·7	−17·4	−16·1	−14·8	−12·3	−9·1	−5·8
270	−22·8	−20·9	−18·9	−16·9	−13·0	−8·0	−3·1
280	−25·1	−22·7	−20·3	−17·8	−13·0	−7·0	−1·0
290	−25·5	−22·9	−20·3	−17·8	−12·6	−6·2	0·2
300	−24·1	−21·7	−19·3	−16·8	−12·0	−6·0	0
315	−18·7	−17·1	−15·4	−13·7	−10·4	−6·3	−2·2
330	−11·4	−10·9	−10·5	−10·0	−9·2	−7·9	−6·7
340	−7·2	−6·7	−8·1	−8·6	−9·5	−10·6	−11·7
350	−1·7	−2·9	−4·3	−5·6	−8·1	−11·3	−14·6
360	2·0	0	−1·9	−3·9	−7·8	−12·8	−17·7

Table X. $\left(\text{Magnitude of } \frac{\widehat{\theta\theta}_{r=a}}{\rho g a} \text{ when } \varphi=20^\circ \text{ and } \frac{\xi}{a}=15.\right)$

θ \ η/a	0	2	4	6	10	15	20	25
0°	2·8	0·8	−1·1	−3·1	−7·0	−12·0	−16·9	−21·8
10	6·3	3·9	1·5	−1·0	−5·8	−11·8	−17·8	−23·9
20	7·4	4·8	2·2	−0·3	−5·5	−11·9	−18·3	−24·8
30	5·9	3·8	1·2	−1·4	−6·2	−12·3	−18·2	−24·3
45	−0·5	−2·2	−3·8	−5·5	−8·8	−12·9	−17·0	−21·1
60	−10·7	−11·2	−11·6	−12·1	−13·0	−14·2	−15·4	−16·5
70	−18·2	−17·7	−17·3	−16·8	−15·9	−14·8	−13·7	−12·7
80	−25·5	−24·2	−22·9	−21·6	−19·1	−15·9	−12·6	−9·4
90	−31·6	−29·6	−27·7	−25·7	−21·8	−16·8	−11·9	−7·0
100	−35·9	−33·5	−31·1	−28·6	−23·8	−17·8	−11·8	−5·7
110	−37·8	−35·2	−32·6	−30·1	−24·9	−18·5	−12·1	−5·6
120	−36·9	−34·5	−32·1	−29·6	−24·8	−18·8	−12·8	−6·7
135	−30·9	−29·2	−27·6	−25·9	−22·6	−18·5	−14·4	−10·3
150	−20·3	−19·8	−19·4	−18·9	−18·0	−16·8	−15·6	−14·5
160	−12·1	−12·6	−13·0	−13·5	−14·4	−15·5	−16·8	−17·6
170	−4·1	−5·4	−6·7	−8·0	−10·5	−13·7	−17·0	−20·2
180	2·4	0·4	−1·5	−3·5	−7·4	−12·4	−17·3	−22·2
190	6·9	4·5	2·1	−0·4	−5·2	−11·2	−17·2	−23·0
200	8·6	6·0	3·4	0·9	−4·3	−10·7	−17·1	−23·6
210	7·3	4·9	2·5	0	−4·8	−10·8	−16·8	−22·9
225	0·1	−1·2	−3·2	−4·9	−8·2	−12·3	−16·4	−20·5
240	−11·3	−11·8	−12·2	−12·7	−13·5	−14·8	−16·0	−17·1
250	−19·8	−19·3	−18·9	−18·4	−17·5	−16·4	−15·3	−14·3
260	−27·5	−26·2	−24·9	−23·6	−21·1	−17·9	−14·6	−11·4
270	−33.6	−31·6	−29·7	−27·7	−23·8	−18·8	−13·9	−9·0
280	−37·3	−34·9	−32·5	−30·0	−25·2	−19·2	−13·2	−7·1
290	−38·2	−35·6	−33·0	−30·5	−25·3	−18·9	−12·5	−6·0
300	−36·3	−33·9	−31·5	−29·0	−24·2	−18·2	−12·2	−6·1
315	−28·7	−27·1	−25·4	−23·7	−20·4	−16·3	−12·2	−8·1
330	−17.7	−17·2	−16·8	−16·3	−15·5	−14·2	−13·0	−11·9
340	−9·9	−10·4	−10·8	−11·3	−12·2	−13·3	−14·4	−15·4
350	−2·8	−4·1	−5·4	−6·7	−9·2	−12·4	−15·7	−18·9
360	2·8	0·8	−1·1	−3·1	−7·0	−12·0	−16·9	−21·8

Table XI. (Magnitude of $\frac{\widehat{\theta\theta}_{r=a}}{\rho g a}$ when $\varphi=20°$ and $\frac{\xi}{a}=20$.)

θ \ η/a	0	2	4	6	10	15	20	25	30
0°	3·7	1·7	−0·2	−2·2	−6·1	−11·1	−16·0	−20·9	−25·8
10	8·5	6·1	3·7	1·2	−3·6	−9·6	−15·6	−21·7	−27·7
20	10·1	7·5	4·9	2·4	−2·8	−9·2	−15·6	−22·1	−28·5
30	8·1	5·6	3·3	0·8	−4·0	−10·0	−16·0	−22·1	−28·1
45	−0·6	−2·3	−3·9	−5·6	−8·9	−13·0	−17·1	−21·2	−25·4
60	−14·4	−14·9	−15·3	−15·8	−16·7	−17·9	−19·1	−20·2	−21·4
70	−24·5	−24·0	−23·6	−23·1	−22·2	−21·1	−20·0	−19·0	−17·7
80	−34·3	−33·0	−31·7	−30·4	−27·9	−24·7	−21·4	−18·2	−15·0
90	−42·5	−40·5	−38·6	−36·6	−32·7	−27·7	−22·8	−17·9	−13·0
100	−48·1	−45·7	−43·3	−40·8	−36·0	−30·0	−24·0	−17·9	−11·9
110	−50·5	−47·9	−45·3	−42·8	−37·6	−31·2	−24·8	−18·3	−12·3
120	−49·1	−46·7	−44·3	−41·8	−37·0	−31·0	−25·0	−18·9	−12·9
135	−40·8	−39·1	−37·5	−35·8	−32·5	−28·4	−24·3	−20·2	−16·0
150	−26·6	−26·1	−25·7	−25·2	−24·4	−23·1	−21·9	−20·8	−19·6
160	−15·6	−16·1	−16·5	−17·0	−17·9	−19·0	−20·1	−21·1	−22·4
170	−5·3	−6·5	−7·9	−9·2	−11·7	−14·9	−18·2	−21·4	−24·6
180	3·3	1·3	−0·6	−2·6	−6·5	−11·5	−16·4	−21·3	−26·2
190	9·1	6·7	4·3	1·8	−3·0	−9·0	−15·0	−21·1	−27·1
200	11·2	8·6	6·0	3·5	−1·7	−8·1	−14·5	−21·0	−27·0
210	9·5	7·1	4·7	2·2	−2·6	−8·6	−14·6	−20·7	−26·7
225	−0·1	−1·8	−3·4	−5·1	−8·4	−12·5	−16·6	−20·7	−24·9
240	−15·0	−15·5	−15·9	−16·4	−17·2	−18·5	−19·7	−20·8	−22·0
250	−26·0	−25·5	−26·9	−24·6	−23·7	−22·6	−21·5	−20·5	−19·2
260	−36·2	−34·9	−33·6	−32·3	−29·8	−26·6	−23·3	−20·1	−16·9
270	−44·5	−42·5	−40·6	−38·6	−34·7	−29·7	−24·8	−19·9	−15·0
280	−49·6	−47·2	−44·8	−42·3	−37·5	−31·5	−25·5	−19·4	−13·4
290	−50·8	−48·2	−45·6	−43·1	−37·9	−31·5	−25·1	−18·6	−12·6
300	−48·6	−46·1	−43·8	−41·3	−36·5	−30·5	−24·5	−18·4	−12·4
315	−38·6	−36·9	−35·3	−33·6	−30·3	−26·2	−22·1	−18·0	−13·8
330	−24·0	−23·5	−23·1	−22·6	−21·8	−20·5	−19·3	−18·2	−17·0
340	−13·6	−14·1	−14·5	−15·0	−15·8	−17·0	−18·1	−19·1	−20·4
350	−3·9	−5·2	−6·5	−7·8	−10·3	−13·5	−16·8	−20·0	−23·2
360	3·7	1·7	−0·2	−2·2	−6·1	−11·1	−16·0	−20·9	−25·8

Table XII. $\left(\text{Magnitude of } \frac{\widehat{\theta\theta}_{r=\gamma}}{\rho g a} \text{ when } \varphi=30^\circ \text{ and } \frac{\xi}{a}=10.\right)$

θ \ η/a	0	2	4	6	10	13	15
0°	−4·2	−5·9	−7·7	−9·4	−12·8	−15·4	−17·1
10	−2·1	−4·8	−7·4	−10·1	−15·3	−19·3	−22·0
20	−0·8	−4·1	−7·3	−10·6	−17·0	−21·9	−25·2
30	−0·6	−4·1	−7·5	−10·9	−17·8	−23·0	−26·5
45	−2·1	−5·1	−8·1	−11·1	−17·1	−21·5	−24·5
60	−5·3	−7·0	−8·7	−10·5	−13·9	−16·5	−18·2
70	−8·1	−8·7	−9·3	−9·9	−11·1	−12·0	−12·6
80	−11·2	−10·6	−10·0	−9·4	−8·2	−7·3	−6·7
90	−14·1	−12·4	−10·6	−8.9	−5·5	−2·9	−1·2
100	−16·9	−14·2	−11·6	−8·9	−3·7	0·3	3·0
110	−18·7	−15·4	−12·2	−8·9	−2·5	2·4	5·7
120	−19·7	−16·2	−12·8	−9·4	−2·5	2·7	6·2
135	−19·2	−16·2	−13·2	−10·2	−4·2	0·2	3·2
150	−16·2	−14·5	−12·8	−11·0	−7·6	−5·0	−3·3
160	−13·0	−12·4	−11·8	−11·2	−10·0	−9·1	−8·5
170	−9·3	−9·9	−10·5	−11·1	−12·3	−13·2	−13·8
180	−5·8	−7·5	−9·3	−11·0	−14·4	−17·0	−18·7
190	−2·5	−5·2	−7·8	−10·5	−15·7	−19·7	−22·4
200	0·1	−3·2	−6·4	−9·7	−16·1	−21·0	−24·3
210	0·6	−2·9	−6·3	−9·7	−16·6	−21·8	−25·3
225	−0·7	−3·7	−6·7	−9·7	−15·7	−20·1	−23·1
240	−4·7	−6·4	−8·1	−9·9	−13·3	−15·9	−17·6
250	−8·5	−9·1	−9·7	−10·3	−11·5	−12·4	−13·0
260	−12·4	−11·8	−11·2	−10·6	−9·4	−8·5	−7·9
270	−15·9	−14·2	−12·4	−10·7	−7·3	−4·7	−3·0
280	−18·5	−15·8	−13·2	−10·5	−5·3	−1·3	1·4
290	−20·1	−16·8	−13·6	−10·3	−3·9	1·0	4·3
300	−20·3	−16·8	−13·4	−10·0	−3·1	2·1	5·6
315	−18·0	−15·0	−12·0	−9·0	−3·0	1·4	4·4
330	−13·8	−12·1	−10·4	−8·6	−5·2	−2·6	−0·9
340	−10·4	−9·8	−9·2	−8·6	−7·4	−6·5	−5·9
350	−7·1	−7·7	−8·3	−8·9	−10·1	−11·0	−11·6
360	−4·2	−5·9	−7·7	−9·4	−12·8	−15·4	−17·1

Table XIII. $\left(\text{Magnitude of } \frac{\widehat{\theta\theta}_{r=a}}{\rho g a} \text{ when } \varphi = 30^\circ \text{ and } \frac{\xi}{a} = 15.\right)$

θ \ η/a	0	2	4	6	10	13	15	20
0°	−6·6	−8·3	−10·1	−11·8	−15·2	−17·8	−19·5	−23·8
10	−3·3	−6·0	−8·8	−11·3	−16·5	−20·5	−23·2	−29·7
20	−1·1	−4·4	−7·6	−10·9	−17·3	−22·2	−25·5	−33·5
30	−0·6	−4·1	−7·5	−10·9	−17·8	−23·0	−26·5	−35·0
45	−2·7	−5.7	−8·7	−11·7	−17·7	−22·1	−25·1	−32·7
60	−7·9	−9·6	−11·3	−13·1	−16·5	−19·1	−20·8	−25·1
70	−12·3	−12·9	−13·5	−14·1	−15·3	−16·2	−16·8	−18·3
80	−17·0	−16·4	−15·8	−15·2	−14·0	−13·1	−12·5	−11·0
90	−21·7	−20·0	−18·2	−16·5	−13·1	−10·5	−8·8	−4·5
100	−25·6	−22·9	−20·3	−17·6	−12·4	−8·4	−5·7	0·8
110	−28·5	−25·2	−22·0	−18·7	−12·3	−7·4	−4·1	3·9
120	−29·7	−26·2	−22·8	−19·4	−12·5	−7·3	−3·8	4·7
135	−28·6	−25·6	−22·6	−19·6	−13·6	−9·2	−6·2	1·4
150	−23·6	−21·9	−20·2	−18·4	−15·0	−12·4	−10·7	−6·0
160	−18·8	−18·2	−17·6	−17·0	−15·8	−14·9	−14·3	−12·8
170	−13·4	−14·0	−14·6	−15·2	−16·4	−17·3	−17·9	−19·4
180	−8·2	−9·9	−11·7	−13·4	−16·8	−19·4	−21·1	−25·4
190	−3·7	−6·4	−9·0	−11·7	−16·9	−20·9	−23·6	−30·1
200	−0·7	−4·0	−7·2	−10·5	−16·9	−21·8	−25·1	−33·1
210	0·6	−2·9	−6·3	−9·7	−16·6	−21·8	−25·3	−33·8
225	−1·3	−4·3	−7·3	−10·3	−16·3	−20·7	−23·7	−31·3
240	−7·3	−9·0	−10·7	−12·5	−15·9	−18·5	−20·2	−24·5
250	−12·7	−13·3	−13·9	−14·5	−15·7	−16·6	−17·2	−18·7
260	−18·2	−17·6	−17·0	−16·4	−15·2	−14·3	−13·7	−12·2
270	−23·5	−21·8	−20·0	−18·3	−14·9	−12·3	−10·6	−6·3
280	−27·4	−24·7	−22·1	−19·4	−14·2	−10·2	−7·5	−1·0
290	−29·9	−26·6	−23·4	−20·1	−13·7	−8·8	−5·5	2·5
300	−30·3	−26·8	−23.4	−20·0	−13·1	−7·9	−4·4	4·1
315	−27·4	−24·4	−21·4	−18·4	−12·4	−8·0	−5·0	2·6
330	−21·2	−19·5	−17·8	−16·0	−12·6	−10·0	−8·3	−4·0
340	−16·2	−15·6	−15·0	−14·4	−13·2	−12·3	−11·7	−10·2
350	−11·2	−11·8	−12·4	−13·0	−14·2	−15·1	−15·7	−17·2
360	−6·6	−8·3	−10·1	−11·8	−15·2	−17·8	−19·5	−23·8

Table XIV. $\left(\text{Magnitude of } \frac{\widehat{\theta\theta}_{r=a}}{\rho g a} \text{ when } \varphi=30^\circ \text{ and } \frac{\xi}{a}=20.\right)$

θ \ η/a	0	2	4	6	10	13	15	20	25
0°	−9·1	−10·8	−12·6	−14·3	−17·7	−20·3	−22·0	−26·3	−30·7
10	−4·4	−7·1	−9·7	−12·4	−17·6	−21·6	−24·3	−30·8	−37·5
20	−1·4	−4·7	−7·9	−11·2	−17·6	−22·5	−25·8	−33·8	−42·0
30	−0·6	−4·1	−7·5	−10·9	−17·8	−23·0	−26·5	−35·0	−43·7
45	−3·4	−6·4	−9·4	−12·4	−18·0	−22·8	−25·8	−33·4	−40·8
60	−10·4	−12·1	−13·8	−15·6	−19·0	−21·6	−23·3	−27·6	−31·9
70	−16·4	−17·0	−17·6	−18·2	−19·4	−20·3			−23·9
80	−23·0	−22·4	−21·8	−21·2	−20·0	−19·1	−18·5	−17·0	−15·5
90	−29·1	−27·5	−25·7	−24·0	−20·6	−18·0	−16·2	−11·9	−7·5
100	−34·5	−31·8	−29·2	−26·5	−21·3	−17·3	−14·6	−8·1	−1·4
110	−38·1	−34·8	−31·6	−28·3	−21·9	−17·0	−13·7	−5·7	2·5
120	−39·7	−36·2	−32·8	−29·4	−22·5	−17·3	−13·8	−5·3	3·4
135	−38·0	−34·9	−31·9	−28·9	−22·9	−18·5	−15·6	−8.0	−0·6
150	−30·7	−29·0	−27·3	−25·5	−22·1	−19·5		−13·1	−9·2
160	−24·7	−24·1	−23·5	−22·9	−21·7	−20·8	−20·2	−18·7	−17·2
170	−17·5	−18·1	−18·7	−19·3	−20·5	−21·4	−22·0	−23·5	−25·0
180	−10·7	−12·4	−14·2	−15·9	−19·3	−21·9	−23·6	−27·9	−32·3
190	−4·8	−7·5	−10·1	−12·8	−18·0	−22.0	−24·7	−31·2	−37·9
200	−1·0	−4·3	−7·5	−10·8	−17·2	−22·1	−25·4	−33·4	−41·6
210	0·6	−2·9	−6·3	−9·7	−16·6	−21·8	−25·3	−33·8	−42·5
225	−2·0	−5·0	−8·0	−11·0	−17·0	−21·4	−24·4	−32·0	−39·4
240	−9·8	−11·5	−13·2	−15·0	−18·4	−21·0	−22·7	−27·0	−31·3
250	−16·8	−17·4	−18·0	−18·6	−19·8	−20·7	−21·3	−22·8	−24·3
260	−24·2	−23·6	−23·0	−22·4	−21·2	−20·3	−19·7	−18·2	−16·7
270	−30·9	−29·2	−27·4	−25·7	−22·3	−19·7	−18·0	−13·7	−9·3
280	−36·2	−33·6	−31·0	−28·3	−23·1	−19·1	−16·3	−9·8	−3·1
290	−39·5	−36·2	−33·0	−29·7	−23·3	−18·4	−15·1	−7·1	1·1
300	−40·3	−36·8	−33·4	−30·0	−23·1	−17·9	−14·4	−5·9	2·8
315	−36·7	−33·7	−30·7	−27·7	−21·7	−17.3	−14·3	−6·7	0·7
330	−28·3	−26·6	−24·9	−23·1		−17·1	−15·4	−11·1	−6·8
340	−22·1	−21·5	−20.9	−20·3	−19·1	−18·2	−17·6	−16·1	−14·6
350	−15·3	−15·9	−16·5	−17·1	−18·3	−19·2	−19·8	−21·3	−22·8
360	−9·1	−10·8	−12·6	−14·3	−17·7	−20·3	−22·0	−26·3	−30·7

Table XV. (Magnitude of $\frac{\widehat{\theta\theta}_{r=a}}{\rho g a}$ when $\varphi=45°$ and $\frac{\xi}{a}=10.$)

θ \ η/a	0	2	4	6	7·5
0°	−8·7	−8·7	−8·7	−8·7	−8·7
10	−8·8	−10·2	−11·5	−12·9	−13·9
20	−9·2	−11·8	−14·3	−16·9	−18·9
30	−9·7	−13·2	−16·6	−20·1	−22·7
45	−10·5	−14·5	−18·5	−22·5	−25·5
60	−10·8	−14·3	−17·7	−21·2	−23·8
70	−10·8	−13·4	−15·9	−18·5	−20·5
80	−10·4	−11·8	−13.1	−14·5	−15·5
90	−10·0	−10·0	−10·0	−10·0	−10·0
100	−9·6	−8·2	−6·9	−5·5	−4·5
110	−9·2	−6·6	−4·1	−1·5	0·5
120	−9·2	−5·7	−2·3	1·2	3·8
135	−9·5	−5·5	−1·5	2·5	5·5
150	−10·3	−6·8	−3·4	0·1	2·7
160	−10·8	−8·2	−5·7	−3·1	−1·1
170	−11·2	−9·8	−8·5	−7·1	−6·1
180	−11·3	−11·3	−11·3	−11·3	−11·3
190	−11·2	−12·6	−13·9	−15·3	−16·3
200	−10·8	−13·4	−15·9	−18·5	−20·5
210	−10·3	−13·8	−17·2	−20·7	−23·3
225	−9·5	−13·5	−17·5	−21·5	−24·5
240	−9·2	−12·7	−16·1	−19·6	−22·2
250	−9·2	−11·8	−14·3	−16·9	−18·9
260	−9·6	−11·0	−12·3	−13·7	−14·7
270	−10·0	−10·0	−10·0	−10·0	−10·0
280	−10·4	−9·0	−7·7	−6·3	−5·3
290	−10·8	−8·2	−5·7	−3·1	−1·1
300	−10·8	−7·3	−3·9	−0·4	2·2
315	−10·5	−6·5	−2·5	1·5	4·5
330	−9·7	−6·2	−2·8	0·7	3·3
340	−9·2	−6·6	−4·1	−1·5	0·5
350	−8·8	−7·4	−6·1	−4·7	−3·7
360	−8·7	−8·7	−8·7	−8·7	−8·7

Table XVI. (Magnitude of $\frac{\widehat{\theta\theta}_{r=a}}{\rho g a}$ when $\varphi=45°$ and $\frac{\xi}{a}=15$.)

θ \ η/a	0	2	4	6	7·5	10
0°	−13·7	−13·7	−13.7	−13·7	−13·7	−13·7
10	−13·8	−15·2	−16·5	−17·9	−18·9	−20·6
20	−14·2	−16·8	−19·3	−21·9	−23·9	−27·1
30	−14·7	−18·2	−21·6	−25·1	−27·7	−32·0
45	−15·5	−19·5	−23·5	−27·5	−30·5	−35·5
60	−15·8	−19·3	−22·7	−26·2	−28·8	−33·1
70	−15·8	−18·4	−20·9	−23·5	−25·5	−28·7
80	−15·4	−16·8	−18·1	−19·5	−20·5	−22·2
90	−15·0	−15·0	−15·0	−15·0	−15·0	−15·0
100	−14·6	−13·2	−11·9	−10·5	−9·5	−7·8
110	−14·2	−11·6	−9·1	−6·5	−4·5	−1·3
120	−14·2	−10·7	−7·3	−3·8	−1·2	3·1
135	−14·5	−10·5	−6·5	−2·5	0·5	7·5
150	−15·3	−11·8	−8·4	−4·9	−2·3	2·0
160	−15·8	−13·2	−10·7	−8·1	−6·1	−2·9
170	−16·2	−14·8	−13·5	−12·1	−11·1	−9·4
180	−16·3	−16·3	−16·3	−16·3	−16·3	−16·3
190	−16·2	−17·6	−18·9	−20·3	−21·3	−23·0
200	−15·8	−18·4	−20·9	−23·5	−25·5	−28·7
210	−15·3	−18·8	−22·2	−25·7	−28·3	−32·6
225	−14·5	−18·5	−22·5	−26·5	−29·5	−34·5
240	−14·2	−17·7	−21·1	−24·6	−27·2	−31·5
250	−14·2	−16·8	−19·3	−21·9	−23·9	−27·1
260	−14·6	−16·0	−17·3	−18·7	−19·7	−21·4
270	−15·0	−15·0	−15·0	−15·0	−15·0	−15·0
280	−15·4	−14·0	−12·7	−11·3	−10·3	−8·6
290	−15·8	−13·2	−10·7	−8·1	−6·1	−2·9
300	−15·8	−12·3	−8·9	−5·4	−2·8	1·5
315	−15·5	−11·5	−7·5	−3·5	−0·5	4·5
330	−14·7	−11·2	−7·8	−4·3	−1·7	2·6
340	−14·2	−11·6	−9·1	−6·5	−4·5	−1·3
350	−13·8	−12·4	−11·1	−9·7	−8·7	−7·0
360	−13·7	−13·7	−13·7	−13·7	−13·7	−13·7

Table XVII. $\left(\text{Magnitude of } \frac{\widehat{\theta\theta}_{r=a}}{\rho g a} \text{ when } \varphi=45^\circ \text{ and } \frac{\xi}{a}=20.\right)$

θ \ η/a	0	2	4	6	7·5	10	15
0°	−18·7	−18·7	−18·7	−18·7	−18·7	−18·7	−18·7
10	−18·8	−20·2	−21·5	−22·9	−23.9	−25·6	−29·0
20	−19·2	−21·8	−24·3	−26·9	−28·9	−32·1	−38·5
30	−19·7	−23·2	−26·6	−30·1	−32·7	−37·0	−45·7
45	−20·5	−24·5	−28·5	−32·5	−35·5	−40·5	−50·5
60	−20·8	−24·3	−27·7	−31·2	−33·8	−38·1	−46·8
70	−20·8	−23·4	−25·9	−28·5	−30·5	−33·7	−40·1
80	−20·4	−21·8	−23·1	−24·5	−25·5	−27·2	−30·6
90	−20·0	−20·0	−20·0	−20·0	−20·0	−20·0	−20·0
100	−19·6	−18·2	−16·9	−15·5	−14·5	−12·8	−9·4
110	−19·2	−16·6	−14·1	−11·5	−9·5	−6·3	0·1
120	−19·2	−15·7	−12·3	−8·8	−7·2	−1·9	6·8
135	−19·5	−15·5	−11·5	−7·5	−4·5	0·5	10·5
150	−20·3	−16·8	−13·4	−9·9	−7·3	−3·0	7·7
160	−20·8	−18·2	−15·7	−13·1	−11·1	−7·9	−1·5
170	−21·2	−19·8	−18·5	−17·1	−16·1	−14·4	−11·0
180	−21·3	−21·3	−21·3	−21·3	−21·3	−21·3	−21·3
190	−21·2	−22·6	−23·9	−25·3	−26·3	−28·0	−31·4
200	−20·8	−23·4	−25·9	−28·5	−30·5	−33·7	−40·1
210	−20·3	−23·8	−27·2	−30·7	−33·3	−37·6	−46·3
225	−19·5	−23·5	−27·5	−31·5	−34·5	−39·5	−49·5
240	−19·2	−22·7	−26·1	−29·6	−32·2	−36·5	−45·2
250	−19·2	−21·8	−24·3	−26·9	−28·9	−32·1	−38·5
260	−19·6	−21·0	−22·3	−23·7	−24·7	−26·4	−29·8
270	−20·0	−20·0	−20·0	−20·0	−20·0	−20·0	−20·0
280	−20·4	−19·0	−17·7	−16·3	−15·3	−13·6	−10·2
290	−20·8	−18·2	−15·7	−13·1	−11·1	−7·9	−1·5
300	−20·8	−17·3	−13·9	−10·4	−7·8	−3·5	5·2
315	−20·5	−16·5	−12·5	−8·5	−5·5	−0·5	9·5
330	−19·7	−16·2	−12·8	−9·3	−6·7	−2·4	6·3
340	−19·2	−16·6	−14·1	−11·5	−9·5	−6·3	0·1
350	−18·8	−17·4	−16·1	−14·7	−13·7	−12·0	−8·6
360	−18·7	−18·7	−18·7	−18·7	−18·7	−18·7	−18·7

Table XVIII $\left(\text{Magnitude of } \dfrac{\widehat{\theta\theta}_{r=a}}{\rho g a} \text{ when } \varphi=60^\circ \text{ and } \dfrac{\xi}{a}=10.\right)$

θ \ η/a	0	2	3·5	θ \ η/a	0	2	3·5
0°	−4·2	−2·4	−1·0	190	−9·4	−8·8	−8·3
10	−7·0	−6·4	−5·9	200	−13·0	−13·6	−14·1
20	−10·4	−11·0	−11·5	210	−16·2	−18·0	−19·3
30	−13·8	−15·6	−16·9	225	−19·1	−22·1	−24·3
45	−18·1	−21·1	−23·3	240	−19·7	−23·1	−25·7
60	−20·3	−23·5	−26·0	250	−18·7	−21·9	−24·5
70	−20·1	−23·3	−25·9	260	−16·8	−19·4	−21·4
80	−18·6	−21·2	−23·2	270	−14·1	−15·9	−17·3
90	−15·9	−17·7	−19·1	280	−11·2	−11·8	−12·3
100	−12·4	−13·0	−13·5	290	−8·2	−7·6	−7·1
110	−8·4	−7·8	−7·3	300	−5·3	−3·5	−2·2
120	−4·7	−2·9	−1·6	315	−2·1	0·9	3·1
135	−0·7	2·3	4·5	330	−0·6	2·8	5·4
150	0·6	4·0	6·6	340	−0·8	2·5	5·0
160	−0·4	2·8	5·4	350	−2·0	0	2·6
170	−2·6	0	2·0	360	−4·2	−2·4	−1·0
180	−5·8	−4·0	2·6				

Table XIX. $\left(\text{Magnitude of } \dfrac{\widehat{\theta\theta}_{r=a}}{\rho g a} \text{ when } \varphi=60^\circ \text{ and } \dfrac{\xi}{a}=10.\right)$

θ \ η/a	0	2	3·5	6	θ \ η/a	0	2	3·5	6
0°	−6·7	−4·9	−3·5	−1·5	190	−13·5	−12·9	−12·4	−11·7
10	−11·1	−10·5	−10·0	−9·3	200	−18·8	−19·4	−19·9	−20·6
20	−16·2	−16·8	−17·3	−18·0	210	−23·6	−25·4	−26·7	−28·8
30	−21·2	−23·0	−24·3	−26·4	225	−28·5	−31·5	−33·7	−37·2
45	−27·5	−30·5	−32·7	−36·2	240	−29·7	−33·1	−35·7	−40·0
60	−30·3	−33·7	−36·3	−40·6	250	−28·5	−31·7	−34·3	−38·3
70	−29·9	−33·1	−35·7	−39·7	260	−25·6	−28·2	−30·2	−33·5
80	−27·4	−30·0	−32·0	−35·3	270	−21·5	−23·3	−24·7	−26·7
90	−23·5	−25·3	−26·7	−28·7	280	−17·1	−17·7	−18·2	−18·9
100	−18·3	−18·9	−19·4	−20·1	290	−12·4	−11·8	−11·3	−10·6
110	−12·6	−12·0	−11·5	−10·8	300	−7·9	−6·1	−4·8	−2·7
120	−7·3	−5·5	−4·2	−2·1	315	−3·1	−0·1	2·1	5·6
135	−1·7	1·3	3·5	7·0	330	−0·6	2·8	5·4	9·7
150	0·6	4·0	6·6	10·9	340	−1·1	2·1	4·7	8·7
160	−0·7	2·5	5·1	9·1	350	−3·2	−0·6	1·4	4·7
170	−3·8	−1·2	0·8	4·1	360	−6·7	−4·9	−3·5	−1·5
180	−8·3	−6·5	−5·1	−3·1					

Table XX. (Magnitude of $\dfrac{\widehat{\theta\theta}_{r=a}}{\rho g a}$ when $\varphi=60°$ and $\dfrac{\xi}{a}=20.$)

θ \ η/a	0	2	3·5	6	8
0°	−9·1	−7.3	−5·9	−3·9	−2·2
10	−15·2	−14·6	−14·1	−13·4	−12·8
20	−22·1	−22·7	−23·2	−23·9	−24·5
30	−28·7	−30·5	−31·8	−33·9	−35·6
45	−36·8	−39·8	−42·0	−45·5	−48·8
60	−40·3	−43·7	−46·3	−50·6	−54·1
70	−39·5	−42·7	−45·3	−49·3	−52·5
80	−36·2	−38·8	−40·8	−44·1	−46·8
90	−31·0	−32·8	−34·2	−36·2	−37·9
100	−24·2	−24·8	−25·3	−26·0	−26·6
110	−16·7	−16·1	−15·6	−14·9	−14·3
120	−9·8	−8·0	−6·7	−4·6	−2·9
135	−2·1	0·9	3·1	6·6	9·9
150	0·6	4·0	6·6	10·9	14·4
160	−1·0	2·2	4·8	8·8	12·0
170	−4·3	−1·7	0·3	3·6	6·3
180	−9·1	−7·3	−5·9	−3·9	−2·2
190	−17·6	−17·0	−16·5	−15·8	−15·2
200	−24·7	−25·3	−25·8	−26·5	−27·1
210	−31·1	−32·9	−34·2	−36·3	−38·0
225	−37·8	−40·8	−43·0	−46·5	−49·8
240	−39·7	−43·1	−45·7	−50·0	−53·5
250	−38·1	−41·3	−43·9	−47·9	−51·1
260	−34·4	−37·0	−39·0	−42·3	−45·0
270	−29·2	−31·0	−32·4	−34·4	−36·1
280	−23·0	−23·6	−24·1	−24·8	−25·4
290	−16·5	−15·9	−15·4	−14·7	−14·1
300	−10·4	−8·6	−7·3	−5·2	−3.5
315	−3·5	−0·5	1·7	5·2	8·5
330	−0·6	2·8	5·4	9·7	13·2
340	−1·4	1·8	4·4	8·4	11·6
350	−4·3	−1·7	0·3	3·6	6·3
360	−9·1	−7·3	−5·9	−3·9	−2·2

Table XXI. $\left(\text{Magnitude of } \frac{\widehat{\theta\theta}_{r=a}}{\rho g a} \text{ when } \varphi=70^\circ \text{ and } \frac{\xi}{a}=10.\right)$

θ \ η/a	0	2	θ \ η/a	0	2
0°	2·0	4·0	190	−3·1	−1·9
10	−1·7	−0·5	200	−8·4	−8·0
20	−6·2	−5·8	210	−13·9	−14·4
30	−11·4	−11·8	225	−20·9	−22·5
45	−18·7	−20·3	240	−24·7	−27·1
60	−24·1	−26·5	250	−25·1	−27·7
70	−25·5	−28·1	260	−23·7	−26·1
80	−25·1	−27·5	270	−20·8	−22·8
90	−22·8	−24·8	280	−16·6	−17·8
100	−18·6	−19·8	290	−11·9	−12·3
110	−13·5	−13·9	300	−7·0	−6·6
120	−7·6	−7·2	315	−0·5	1·1
135	0·1	1·7	330	3·7	6·1
150	5·1	7·5	340	4·7	7·3
160	5·6	8·5	350	4·1	6·5
170	4·7	7·1	360	2·0	4·0
180	1·6	3·6			

Table XXII. $\left(\text{Magnitude of } \frac{\widehat{\theta\theta}_{r=a}}{\rho g a} \text{ when } \varphi=70^\circ \text{ and } \frac{\xi}{a}=15.\right)$

θ \ η/a	0	2	4	θ \ η/a	0	2	4
0°	2·8	4·8	6·7	190	−4·2	−3·0	−1·6
10	−2·8	−1·6	−0·2	200	−12·1	−11·7	−11·2
20	−9·9	−9·5	−9·0	210	−20·3	−20·7	−21·2
30	−17·7	−18·1	−18·6	225	−30·9	−32·5	−34·2
45	−28·7	−30·3	−32·0	240	−36·9	−39·5	−41·7
60	−36·3	−38·7	−41·1	250	−37·8	−40·4	−42·9
70	−38·2	−40·8	−43·3	260	−35·8	−38·2	−40·6
80	−37·2	−39·6	−42·0	270	−31·6	−33·6	−35·5
90	−33·6	−35·6	−37·5	280	−25·4	−26.6	−28·0
100	−27·4	−28·2	−30·0	290	−18·2	−18·6	−19·1
110	−19·8	−20·2	−20·7	300	−10·7	−10·3	−9·8
120	−11·3	−10·9	−10·4	315	−2·7	−1·1	0·6
135	0·1	1·7	3·4	330	6·0	8·4	10·8
150	7·3	9·7	12·1	340	7·4	10·0	12·5
160	8·6	11·2	13·7	350	6·2	8·6	11·0
170	6·8	9·2	11·6	360	2·8	4·8	6·7
180	2·4	4·4	6·3				

Table XXIII. $\left(\text{Magnitude of } \frac{\widehat{r\theta}_{r=a}}{\rho g a} \text{ when } \varphi=70^\circ \text{ and } \frac{\xi}{a}=20.\right)$

θ \ η/a	0	2	4	6
0°	3·7	5·7	7·6	9·6
10	−4·0	−2·8	−1·4	−0·1
20	−13·6	−12·2	−12·7	−12·3
30	−24·0	−24·4	−24·9	−25·3
45	−38·6	−40·2	−41·9	−43·6
60	−48·5	−50·9	−53·3	−55·7
70	−50·9	−53·5	−56·0	−58·6
80	−49·4	−51·8	−54·2	−56·6
90	−44·5	−46·5	−48·4	−50·4
100	−36·3	−37·5	−38·9	−40·2
110	−26·1	−26·5	−27·0	−27·4
120	−15·0	−14·6	−14·1	−13·7
135	0·0	1·6	3·3	5·0
150	9·5	11·9	14·3	16·7
160	11·3	13·9	16·4	19·0
170	10·0	12·4	14·8	17·2
180	3·3	5·3	7·2	9·2
190	−5·4	−4·2	−2·8	−1·5
200	−15·8	−15·4	−14·9	−14·5
210	−26·6	−27·0	−27·5	−27·9
225	−40·8	−42·4	−44·1	−45·8
240	−49·1	−51·5	−53·9	−56·3
250	−50·5	−53·1	−55·6	−58·2
210	−48·0	−50·4	−52·8	−55·2
270	−42·5	−44·5	−46·4	−43·4
280	−34·3	−35·5	−36·9	−38·2
290	−24·5	−24·9	−25·4	−25·8
300	−14·4	−14·0	−13·5	−13·1
315	−0·6	1·0	2·7	4·6
330	8·1	10·5	12·9	15·3
340	10·1	12·7	15·2	17·8
350	8·4	10·8	13·2	15·6
360	3·7	5·7	7·6	9·6

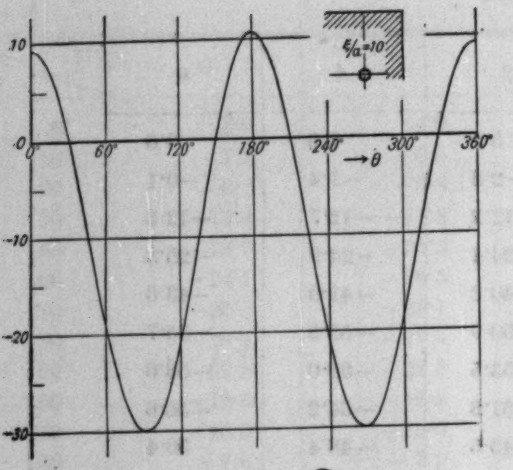

Fig. 22. Magnitude of $\frac{\widehat{\theta\theta}_{r=a}}{\rho g a}$ when $\varphi=0°$ and $\frac{\xi}{a}=10$.

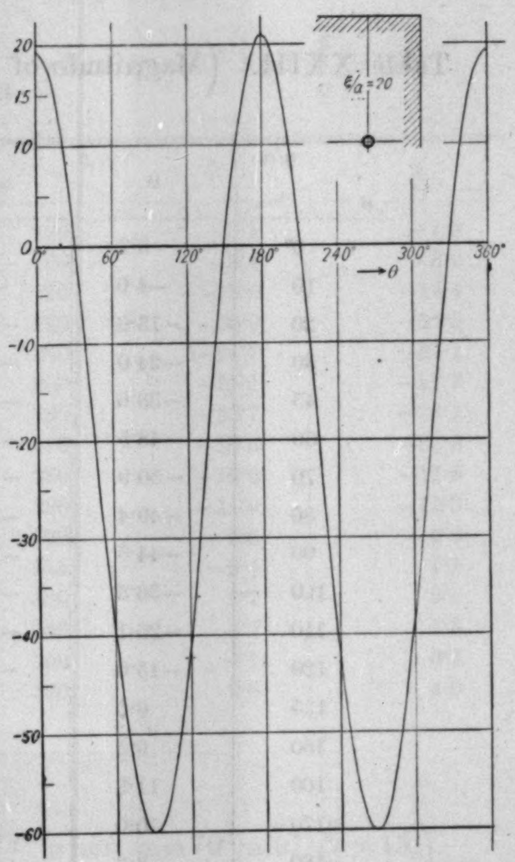

Fig. 24. Magnitude of $\frac{\widehat{\theta\theta}_{r=a}}{\rho g a}$ when $\varphi=0°$ and $\frac{\xi}{a}=20$.

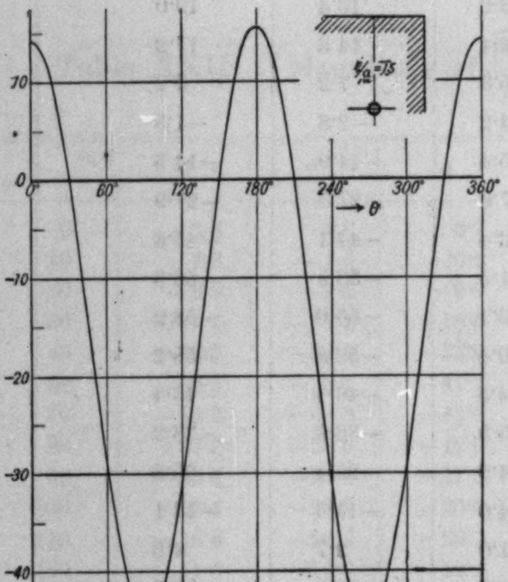

Fig. 23. Magnitude of $\frac{\widehat{\theta\theta}_{r=a}}{\rho g a}$ when $\varphi=0°$ and $\frac{\xi}{a}=15$.

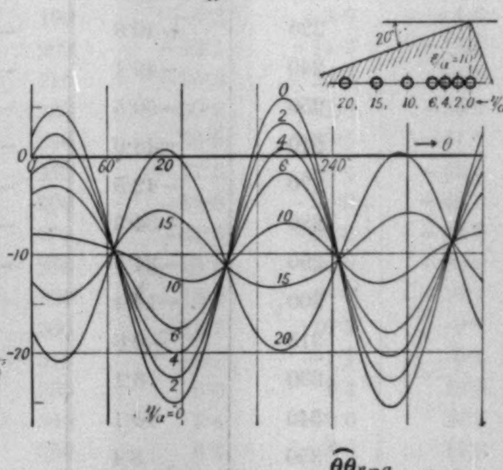

Fig. 25. Magnitude of $\frac{\widehat{\theta\theta}_{r=a}}{\rho g a}$ when $\varphi=20°$, and $\frac{\xi}{a}=10$.

$\left(\frac{\eta}{a}=0,\ 2,\ 4,\ 6,\ 10,\ 15,\ 20.\right)$

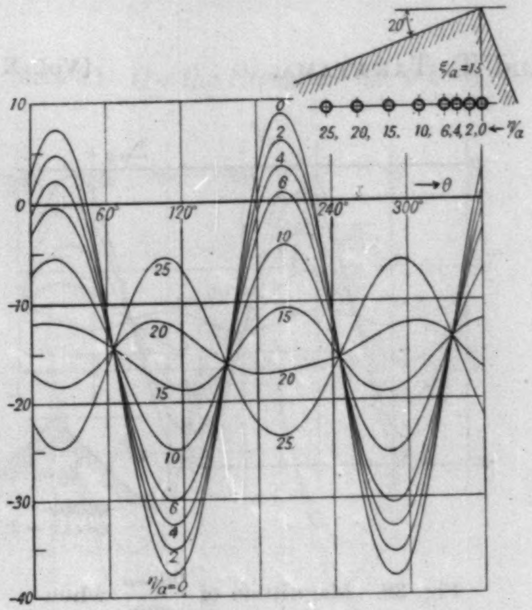

Fig. 26. Magnitude of $\frac{\widehat{\theta\theta}_{r=a}}{\rho g a}$ when

$\varphi=20°$ and $\frac{\xi}{a}=15°$

$\left(\frac{\eta}{a}=0,\ 2,\ 4,\ 6,\ 10,\ 15,\ 20,\ 25.\right)$

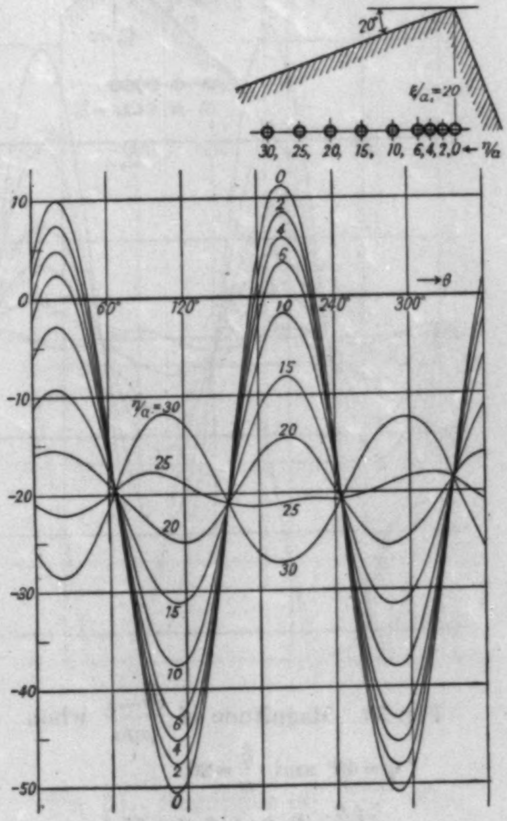

Fig. 27. Magnitude of $\frac{\widehat{\theta\theta}_{r=a}}{\rho g a}$ when

$\varphi=20°$ and $\frac{\xi}{a}=20.$

$\left(\frac{\eta}{a}=0,\ 2,\ 4,\ 6,\ 10,\ 15,\ 20,\ 25,\ 30.\right)$

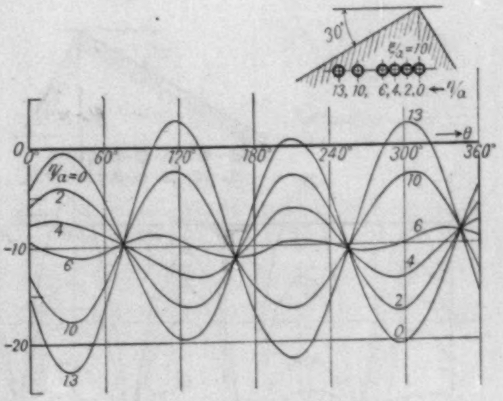

Fig. 28. Magnitude of $\frac{\widehat{\theta\theta}_{r=a}}{\rho g a}$ when

$\varphi=30°$ and $\frac{\xi}{a}=10.$

$\left(\frac{\eta}{a}=0,\ 2,\ 4,\ 6,\ 10,\ 13.\right)$

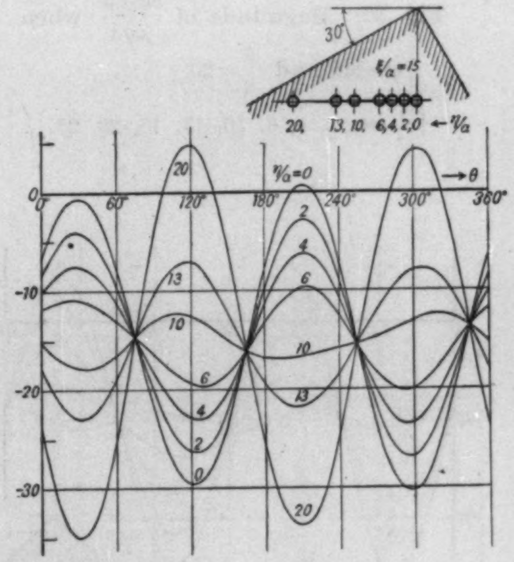

Fig. 29. Magnitude of $\frac{\widehat{\theta\theta}_{r=a}}{\rho g a}$ when

$\varphi=30°$ and $\frac{\xi}{a}=15.$

$\left(\frac{\eta}{a}=0,\ 2,\ 4,\ 6,\ 10,\ 13,\ 20.\right)$

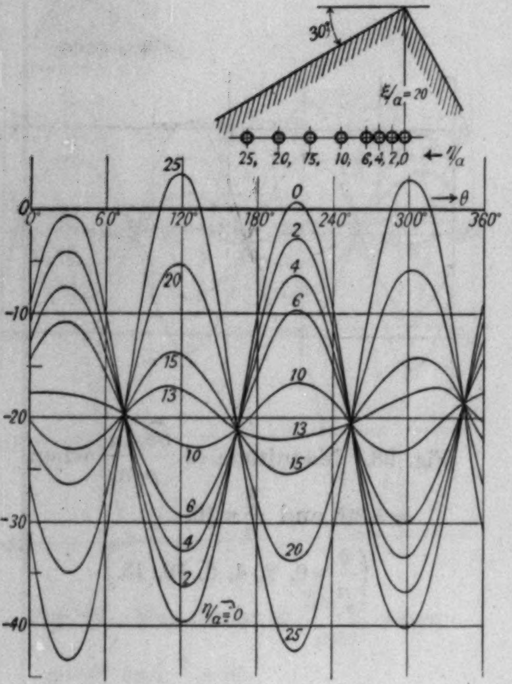

Fig. 30. Magnitude of $\frac{\widehat{\theta\theta}_{r=a}}{\rho g a}$ when

$\varphi=30°$ and $\frac{\xi}{a}=20.$

$\left(\frac{\eta}{a}=0,\ 2,\ 4,\ 6,\ 10,\ 13,\ 15,\ 20,\ 25.\right)$

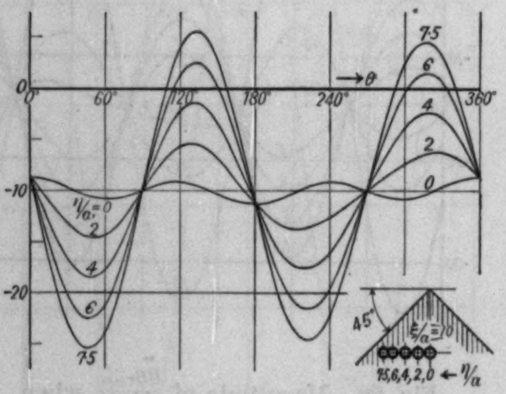

Fig. 31. Magnitude of $\frac{\widehat{\theta\theta}_{r=a}}{\rho g a}$ when

$\varphi=45°$ and $\frac{\xi}{a}=10.$

$\left(\frac{\eta}{a}=0,\ 2,\ 4,\ 6,\ 7{\cdot}5.\right)$

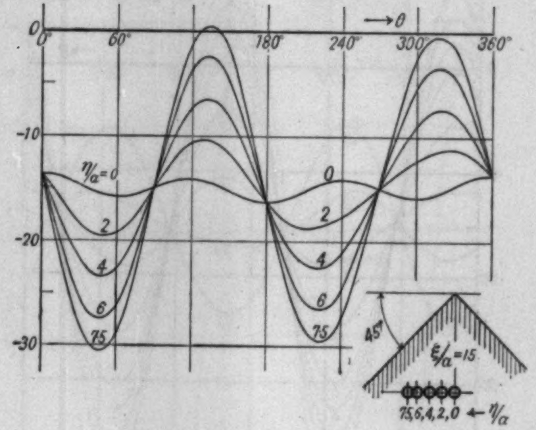

Fig. 32. Magnitude of $\frac{\widehat{\theta\theta}_{r=a}}{\rho g a}$ when

$\varphi=45°$ and $\frac{\xi}{a}=15.$

$\left(\frac{\eta}{a}=0,\ 2,\ 4,\ 6,\ 7{\cdot}5.\right)$

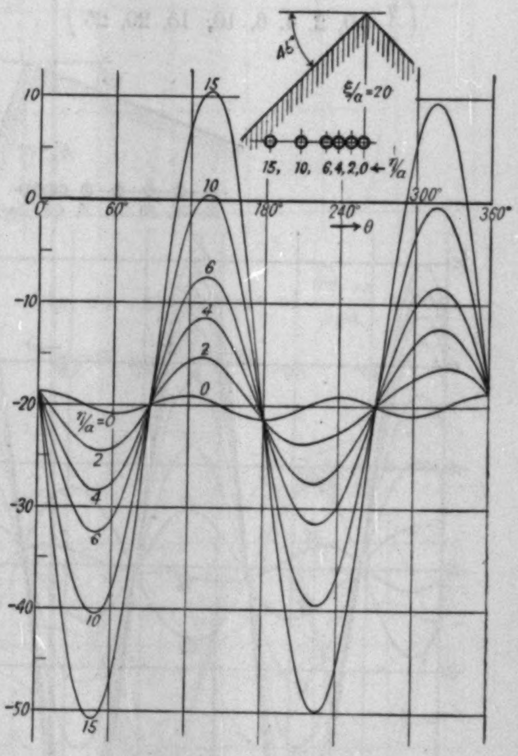

Fig. 33. Magnitude of $\frac{\widehat{\theta\theta}_{r=a}}{\rho g a}$ when

$\varphi=45°$ and $\frac{\xi}{a}=20.$

$\left(\frac{\eta}{a}=0,\ 2,\ 4,\ 6,\ 10,\ 15.\right)$

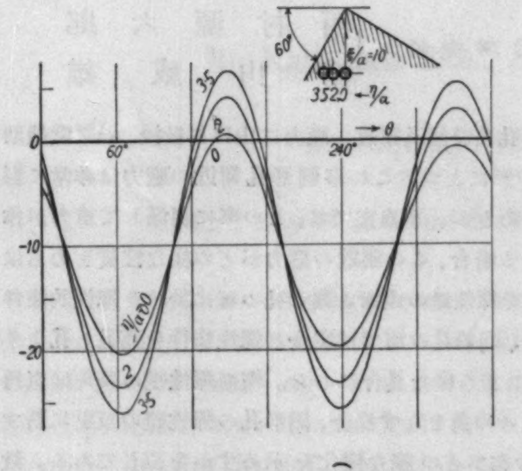

Fig. 34. Magnitude of $\frac{\widehat{\theta\theta}_{r=a}}{\rho g a}$ when $\varphi=60°$ and $\frac{\xi}{a}=10$. $\left(\frac{\eta}{a}=0,\ 2,\ 3{\cdot}5.\right)$

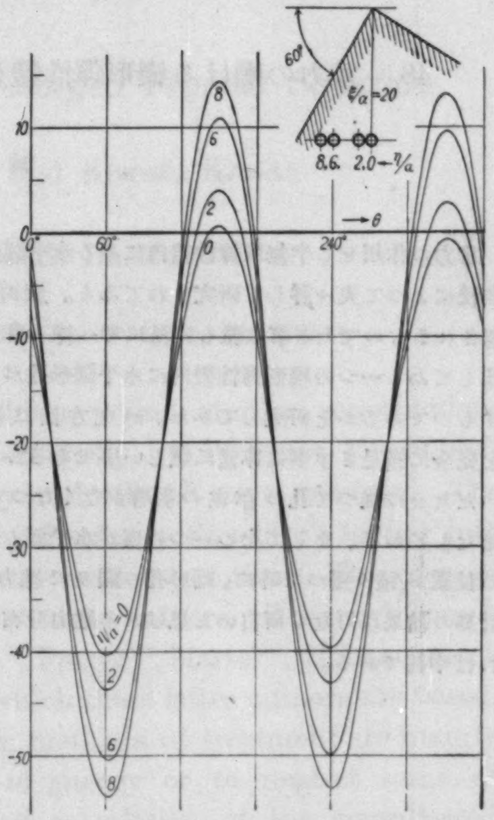

Fig. 36. Magnitude of $\frac{\widehat{\theta\theta}_{r=a}}{\rho g a}$ when $\varphi=60°$ and $\frac{\xi}{a}=20$. $\left(\frac{\eta}{a}=0,\ 2,\ 6,\ 8.\right)$

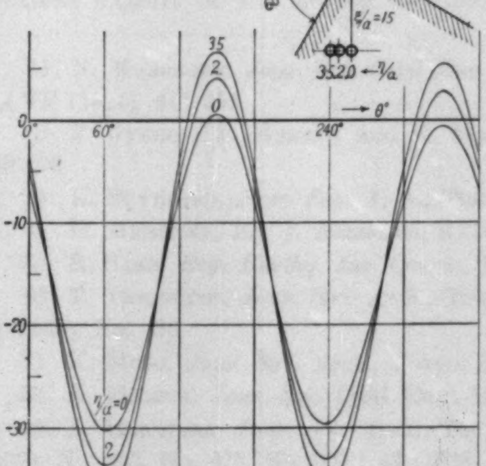

Fig. 35. Magnitude of $\frac{\widehat{\theta\theta}_{r=a}}{\rho g a}$ when $\varphi=60°$ and $\frac{\xi}{a}=15$. $\left(\frac{\eta}{a}=0,\ 2,\ 3{\cdot}5.\right)$

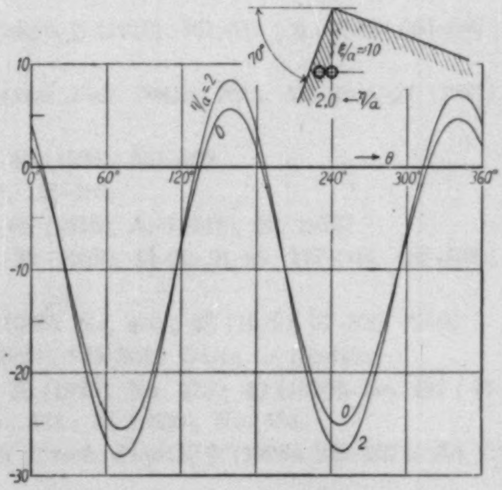

Fig. 37. Magnitude of $\frac{\widehat{\theta\theta}_{r=a}}{\rho g a}$ when $\varphi=70°$ and $\frac{\xi}{a}=10$. $\left(\frac{\eta}{a}=0,\ 2.\right)$

48. 重力の働ける楔形彈性體を貫通する水平圓形孔附近の應力

地震研究所 { 西村源六郎
高山威雄

重力の作用せる半無限彈性體内にある水平圓形孔及び傾孔附近の應力は山口昇教授、杉原武德助教授によつて夫々詳しく研究されてゐる。表面の形によつてこれ等圓形孔附近の應力は非常に影響されるものである事は誰も容易に考へ得る事であるが、本論文では、この事に關係して重力が作用してゐる一つの楔形彈性體内に水平圓形孔がある場合、この附近の應力がどの様な性質をあらはすものであるかを研究してみた。研究方法は楔形彈性體の表面と圓形孔の面に於ける彈性的條件を完全に滿足さす事は非常に煩しい事であるから、圓形孔の面では完全に彈性條件を滿足し孔よりへだたるに從つて孔の存在の影響がなくなつてしまう樣な具合にした。楔形彈性體の頂角は直角をなしており、そしてその一つの面が水平面と色々の角をなす場合、圓形孔の彈性體の頂點に對する位置が種々變つた時に、圓形孔の圍りで應力分布がどの樣な變化を示めすかを論じてある。數計算の結果は可なり面白いと思はれる應力分布の性質を示してゐるが、多少でも參考になる所があれば幸甚である。

49. *Vibrations of a Singled-storyed Framed Structure.*

By Katsutada SEZAWA and Kiyoshi KANAI,

Earthquake Research Institute.

(Read May 17 and June 21, 1932.—Received June 20, 1932.)

The problem of vibrations of a chimney and similar constructions due to seismic waves was studied theoretically by Professor Mononobe[1] about twelve years ago and by Byerly and others[2] very recently. The same problem was again dealt with by Professor Suyehiro[3] taking into account of the initial condition of the vibratory motion. The case of framed structure was also treated of by many authors: Reissner[4] Sano[5], Taniguchi[6], Muto[7], Majima[8], Mizuhara[9], Prager[10], Martel[11], Hohenemser[12] and others. But the standpoints, on which these latter authors are based, are not theoretically rigorous, as their methods of treatment are mainly to apply approximately the principle of energy or to neglect some of boundary conditions. Indeed, the exact calculation of the complicated framed structure is very difficult in general. We have obtained the solution of the vibration problem of a single-storyed framed structure.

We have calculated the natural periods of a framed structure with endless extent of the series of successive spans, the distribution of the

1) N. MONONOBE. *Jour. Soc. Civil Eng.*, Tokyo, 5 (1919), 561–647; 6 (1920), 581–690; *ZAMM* (1921), 445–451.

2) P. BYERLY, J. HESTER and K. MARSHALL. *Bull. Seism. Soc.*, America, 21 (1931), 268–276.

3) K. SUYEHIRO, *Jour. Soc. Arch.*, Tokyo, 40 (1926), 531–559.

4) H. REISSNER, *ZS. f. Bauwesen*, 8 (1903), 135–162.

5) R. SANO, *Rep. Earthq. Inv. Comm.*, No. 83 (1916), A, 1–141; B, 1–137.

6) T. TANIGUCHI, *Jour. Soc. Arch.*, Tokyo, 39 (1925), 43–62, 91–99, 177–206, 487–498; 40 (1926), No. 480.

7) K. MUTO, *Jour. Soc. Arch.*, Tokyo, 39 (1925), No. 476; 43 (1929), 67–106, 49–66.

8) K. MAJIMA, *Jour. Soc. Civil Eng.*, 12 (1926), 229–304: *Disin to Kentiku.*

9) A. MIZUHARA, *Jour. Soc. Arch.*, Tokyo, 39 (1925), No. 475; 40 (1926), No. 487; 41 (1927), No. 493, No. 476, No. 501; 43 (1929), No. 522; 44 (1930), No. 534.

10) W. PRAGER, *Bauing.*, 8 (1927), 129; *ZS. f. tech. Physik*, 9 (1928), 223–227; *ZS. f. tech. Physik*, 10 (1929), 275–280.

11) R. R. MARTEL, *Proc. WEC*, 3 (1929, Tokyo).

12) K. HOHENEMSER, *Ing. Arch.*, 1 (1930), 271–292.

deflections as well as bending moments in the structure due to forcep oscillations, and the natural periods and the forced oscillation of the case of two spans.

I. Natural Periods of Framed Structure of an Infinite Number of Spans.

In this paper the following notations are employed.

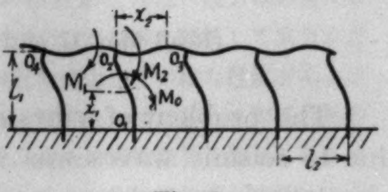

Fig. 1.

$\rho_1,\ \rho_2$ = densities of pillar and beam respectively,

$E_1,\ E_2$ = Young's Moduli of ....,

$a_1,\ a_2$ = effective areas of ....,

$k_1,\ k_2$ = radii of gyration of the sections of.........................,

$l_1,\ l_2$ = effective lengths of pillar and the intercepted portion of the beam respectively,

$y_1,\ y_2$ = transverse deflections of pillar and beam at x_1 and x_2 respectively,

M_0, M_1, M_2 = bending moments of pillar and beam at joint O_2.

The equation of motion of the bar O_1O_2 is expressed by

$$E_1k_1^2\frac{\partial^4 y_1}{\partial x_1^4}+\rho_1\frac{\partial^2 y_1}{\partial t^2}=0. \tag{1}$$

If we write $y_1=u_1 \cos pt$, then

$$\frac{d^4u_1}{dx_1^4}=m_1^4u_1, \tag{2}$$

where

$$m_1^4=\frac{\rho_1 p^2}{E_1k_1^2}. \tag{3}$$

The solution of (2) is

$$u_1=A_1 \cos m_1x_1+B_1 \sin m_1x_1+C_1 \cosh m_1x_1+D_1 \sinh m_1x_1. \tag{4}$$

The boundary conditions at O_1, which is the clamped end of the pillar, are written by

$$x_1=0\ ;\quad u_1=0,\quad \frac{du_1}{dx_1}=0. \tag{5}$$

Substituting from (4) in (5), we get

$$u_1=A_1(\cos m_1x_1-\cosh m_1x_1)+B_1(\sin m_1x_1-\sinh m_1x_1). \tag{6}$$

The boundary conditions at the other ends O_2 are

$$x_1=l_1\,;\quad -E_1a_1k_1^2\frac{d^2u_1}{dx_1^2}=M_0,\quad -E_1a_1k_1^2\frac{d^3u_1}{dx_1^3}=\rho_1a_2l_2p^2u_1. \qquad (7),\,(8)$$

The equation of the motion of the member 0_20_3 (or 0_40_2) is expressed by

$$E_2k_2^2\frac{\partial^4 y_2}{\partial x_2^4}+\rho_2\frac{\partial^2 y_2}{\partial x_2^2}=0. \qquad (9)$$

If we write $y_2=u_2\cos pt$, then

$$\frac{d^4u_2}{dx_2^4}=m_2^4u_2, \qquad (10)$$

where

$$m_2^4=\frac{\rho_2p^2}{E_2k_2^2}. \qquad (11)$$

The solution of (10) is

$$u_2=A_2\cos m_2x_2+B_2\sin m_2x_2+C_2\cosh m_2x_2+D_2\sinh m_2x_2. \qquad (12)$$

The conditions at the clamped joint, $x_2=0,\ x_1=l_1$, are

$$u_2=0,\quad \frac{du_2}{dx_2}=\frac{du_1}{dx_1},\quad -E_2a_2k_2^2\frac{d^2u_2}{dx_2^2}=M_2\,; \qquad (13),\,(14),\,(15)$$

and the condition at the clamped joint $x_2=l_2,\ x_1=l_1$, are

$$u_2=0,\quad \frac{du_2}{dx_2}=\frac{dv_1}{dx_1},\quad -E_2a_2k_2^2\frac{d^2u_2}{dx_2^2}=M_1. \qquad (16),\,(17),\,(18)$$

The condition of the fixing moment at 0_2 (or 0_3) is written by

$$M_0+M_1-M_2=0. \qquad (19)$$

Applying the conditions and the relations in (7) (8), (13), (14), (15), (16), (17), (18), (19) to the equations (6) and (12), it is possible to find the ratios of the constants $A_1, B_1, A_2, B_2, C_2, D_2$ besides M_0, M_1, M_2, and to determine the values of m_1 and m_2 which give us the frequency p.

Write

$$m_1l_1\equiv\alpha,\quad m_2l_2\equiv\beta,\quad \frac{\rho_2a_2l_2p^2}{E_1a_1k_1^2m_1^3}\equiv\gamma,\quad \frac{m_2}{m_1}=\xi,\quad \frac{E_2a_2k_2^2m_2^2}{E_1a_1k_1^2m_1^2}\equiv\eta\,; \qquad (20)$$

then, from the conditions (8) we get

$$A_1[(\sin\alpha-\sinh\alpha)+\gamma(\cos\alpha-\cosh\alpha)]$$
$$=B_1[(\cos\alpha+\cosh\alpha)-\gamma(\sin\alpha-\sinh\alpha)]. \qquad (21)$$

From (13), (14) we find

$$(B_2+D_2)\,\xi=-A_1(\sin\alpha+\sinh\alpha)+B_1(\cos\alpha-\cosh\alpha), \qquad (22)$$

while (16) gives us

$$A_2(\cos\beta-\cosh\beta)+B_2\sin\beta+D_2\sinh\beta=0. \qquad (23)$$

By means of (17) and (22) we obtain

$$A_2(\sin\beta+\sinh\beta)+B_2(1-\cos\beta)+D_2(1-\cosh\beta)=0. \qquad (24)$$

Finally, using the relations (7), (15), (18) and the condition (19), we get

$$A_1(\cos\alpha+\cosh\alpha)+B_1(\sin\alpha+\sinh\alpha)+A_2\eta(-2+\cos\beta+\cosh\beta)$$
$$+B_2\eta\sin\beta-D_2\eta\sinh\beta=0. \qquad (25)$$

Eliminating A_1, B_1, A_2, B_2, D_2 between (21), (22), (23), (24), (25), we arrive at the relation,

$$2\{(\cos\alpha\sinh\alpha+\sin\alpha\cosh\alpha)+\gamma(\cos\alpha\cosh\alpha-1\}$$
$$\times\{\sin\beta(\cosh\beta-1)+\sinh\beta(1-\cos\beta)\}=\frac{\xi}{\eta}\{(\cos\alpha\cosh\alpha+1)$$
$$+\gamma(\cos\alpha\sinh\alpha-\sin\alpha\cosh\alpha)\}(\cos\beta\cosh\beta-1). \qquad (26)$$

From this equation and the relations in (20), we can find the frequency p or the period of vibrations $\frac{2\pi}{p}$.

When the stiffness of the pillar is very high compared with that of the beam, the condition, $\frac{\eta}{\xi}=0$ holds, so that

$$\cos\beta\cosh\beta-1=0. \qquad (27)$$

This is the frequency equation of the beam, whose both ends are clamped in position and inclination. In a special case, where there is no beam, we know that $\frac{\eta}{\xi}=0$ and $\gamma=0$, so that we get

$$\cos\alpha\cosh\alpha+1=0. \qquad (28)$$

This is the frequency equation of a clamped-free bar and gives the equation of a clamped-free bar.

When the stiffness of the beam is very high in comparison with that of the pillar and the mass of the beam is large, we may put $\frac{\xi}{\eta}=0$, $\frac{1}{\gamma}=0$, so that

$$\cos\alpha\cosh\alpha-1=0. \qquad (29)$$

This is the frequency equation of a bar whose both ends are clamped in position and in slope.

As it is very difficult to solve (26) in general, we have employed the method of trial and error to get frequencies of various cases. Again, we have limited the calculation to the determination of the fundamental free vibration of the cases, $\frac{\rho_1}{\rho_2}=\frac{1}{4}, \frac{1}{2}, 1$, besides the conditions that $l_1=l_2$, $E_1=E_2$, and $a_1=a_2$. The result is shown as follows.

$$\frac{\rho_1}{\rho_2}=1, \qquad \frac{1}{2}, \qquad \frac{1}{4}.$$

$$\left(\frac{\rho_1 p^2}{E_1 k_1^2}\right)^{\frac{1}{4}} l_1=1{\cdot}645 \qquad 1{\cdot}429 \qquad 1{\cdot}224$$

II. Forced Vibrations of Framed Structure of an Infinite Number of Spans.

When the bottom of each pillar is oscillating horizontally with amplitude b and with period $\frac{2\pi}{p'}$, the boundary conditions at the end 0_1, which is the clamped end of the pillar, are written by

$$x_1=0\,; \quad u_1=b, \quad \frac{du_1}{dx_1}=0\,; \tag{5'}$$

and other conditions are the same as those in the preceding case.

As the types of the solutions we write $y_1=u_1 \cos p't$, $y_2=u_2 \cos p't$, so that m_1^4, m_2^4 should have the meanings such that

$$m_1^4=\frac{\rho_1 p'^2}{E_1 k_1^2}, \quad m_2^4=\frac{\rho_2 p'^2}{E_2 k_2^2}. \qquad (3'), (11')$$

Substituting from (4) in (5′), we get

$$u_1=A_1 (\cos m_1x_1-\cosh m_1x_1)+B_1 (\sin m_1x_1-\sinh m_1x_1) + b \cosh m_1x_1. \tag{6'}$$

Applying the conditions and relations in (7), (8), (9), (13), (14), (15), (16), (17), (18), (19) to the equations (6′) and (12), it is possible to find the values of the constants A_1, B_1, A_2, B_2, C_2, D_2 besides M_0, M_1, M_2. Write

$$m_1 l_1 \equiv \alpha, \quad m_2 l_2 \equiv \beta, \quad \frac{\rho_2 a_2 l_2 p'^2}{E_1 a_1 k_1^2 m_1^3} \equiv \gamma, \quad \frac{m_2}{m_1} \equiv \xi, \quad \frac{E_2 a_2 k_2^2 m_2^2}{E_1 a_1 k_1^2 m_1^2} \equiv \eta\,; \tag{20'}$$

then, from (6′) and (8) we get

$$A_1 \{(\sin\alpha-\sinh\alpha)+\gamma(\cos\alpha-\cosh\alpha)\}-B_1\{(\cos\alpha+\cosh\alpha) -\gamma(\sin\alpha-\sinh\alpha)\}=-b(\sinh\alpha+\gamma\cosh\alpha). \tag{21'}$$

From (12) and (13) we find

$$C_2+A_2=0. \tag{21''}$$

By means of (12) and (14) we obtain

$$(B_2+D_2)+A_1(\sin\alpha+\sinh\alpha)-B_1(\cos\alpha-\cosh\alpha)=b\sinh\alpha. \tag{22'}$$

From (16) we get

$$A_2(\cos\beta-\cosh\beta)+B_2\sin\beta+D_2\sinh\beta=0. \tag{23'}$$

Again, from (17) and (22)

$$A_2(\sin\beta+\sinh\beta)+B_2(1-\cos\beta)+D_2(1-\cosh\beta)=0. \qquad (24')$$

(7), (15), (18), (19) give us

$$A_1(\cos\alpha+\cosh\alpha)+B_1(\sin\alpha+\sinh\alpha)+A_2\eta(-2+\cos\beta+\cosh\beta)$$
$$+B_2\eta\sin\beta-D_2\eta\sinh\beta=b\cosh\alpha. \qquad (25')$$

Thus we find from (21′), (22′), (23′), (24′), (25′)

$$A_1=\frac{\begin{array}{l} b[\xi(1-\cos\beta\cosh\beta)\{(\cos\alpha\cosh\alpha-\sin\alpha\sinh\alpha+1)-2\gamma\sin\alpha\cosh\alpha\} \\ \quad +2\eta\{\sin\beta(\cosh\beta-1)\sinh\beta(1-\cos\beta)\} \\ \quad \times\{2\cos\alpha\sinh\alpha+\gamma(\cos\alpha\cosh\alpha-\sin\alpha\sinh\alpha-1)\}] \end{array}}{\begin{array}{l} 2[\xi(1-\cos\beta\cosh\beta)\{(1+\cos\alpha\cosh\alpha)+\gamma(\cos\alpha\sinh\alpha-\sin\alpha\cosh\alpha)\} \\ \quad +2\eta\{\sin\beta(\cosh\beta-1)+\sinh\beta(1-\cos\beta)\} \\ \quad \times\{(\sin\alpha\cosh\alpha+\cos\alpha\sinh\alpha)+\gamma(\cos\alpha\cosh\alpha-1)\}] \end{array}}, \qquad (26')$$

$$B_1=\frac{\begin{array}{l} b[\xi(1-\cos\beta\cosh\beta)\{(\sin\alpha\cosh\alpha+\cos\alpha\sinh\alpha)+2\gamma\cos\alpha\cosh\alpha\} \\ \quad +2\eta\{\sin\beta(\cosh\beta-1)+\sinh\beta(1-\cos\beta)\} \\ \quad \times\{2\sin\alpha\sinh\alpha+\gamma(\cos\alpha\sinh\alpha+\sin\alpha\cosh\alpha)\}] \end{array}}{\begin{array}{l} 2[\xi(1-\cos\beta\cosh\beta)\{(1+\cos\alpha\cosh\alpha)+\gamma(\cos\alpha\sinh\alpha-\sin\alpha\cosh\alpha)\} \\ \quad +2\eta\{\sin\beta(\cosh\beta-1)+\sinh\beta(1-\cos\beta)\} \\ \quad \times\{(\sin\alpha\cosh\alpha+\cos\alpha\sinh\alpha)+\gamma(\cos\alpha\cosh\alpha-1)\}] \end{array}}, \qquad (27')$$

$$A_2=\frac{\begin{array}{l} b\{\sin\beta(1-\cosh\beta)-(1-\cos\beta)\sinh\beta\} \\ \quad \times\{(\sin\alpha-\sinh\alpha)+\gamma(\cos\alpha-\cosh\alpha)\} \end{array}}{\begin{array}{l} 2[\xi(1-\cos\beta\cosh\beta)\{(1+\cos\alpha\cosh\alpha)+\gamma(\cos\alpha\sinh\alpha-\sin\alpha\cosh\alpha)\} \\ \quad +2\eta\{\sin\beta(\cosh\beta-1)+\sinh\beta(1-\cos\beta)\} \\ \quad \times\{\sin\alpha\cosh\alpha+\cos\alpha\sinh\alpha)+\gamma(\cos\alpha\cosh\alpha-1)\}] \end{array}}, \qquad (28')$$

$$B_2=\frac{\begin{array}{l} b\{\sinh\beta(\sin\beta+\sinh\beta)-(1-\cosh\beta)(\cos\beta-\cosh\beta)\} \\ \quad \times\{(\sin\alpha-\sinh\alpha)+\gamma(\cos\alpha-\cosh\alpha)\} \end{array}}{\begin{array}{l} 2[\xi(1-\cos\beta\cosh\beta)\{(1+\cos\alpha\cosh\alpha)+\gamma(\cos\alpha\sinh\alpha-\sin\alpha\cosh\alpha)\} \\ \quad +2\eta\{\sin\beta(\cosh\beta-1)+\sinh\beta(1-\cos\beta)\} \\ \quad \times\{\sin\alpha\cosh\alpha+\cos\alpha\sinh\alpha)+\gamma(\cos\alpha\cosh\alpha-1)\}] \end{array}}, \qquad (29')$$

$$D_2=\frac{\begin{array}{l} b\{(1-\cos\beta)(\cos\beta-\cosh\beta)-\sin\beta(\sin\beta+\sinh\beta)\} \\ \quad \times\{(\sin\alpha-\sinh\alpha)+\gamma(\cos\alpha-\cosh\alpha)\} \end{array}}{\begin{array}{l} 2[\xi(1-\cos\beta\cosh\beta)\{(1+\cos\alpha\cosh\alpha)+\gamma(\cos\alpha\sinh\alpha-\sin\alpha\cosh\alpha)\} \\ \quad +2\eta\{\sin\beta(\cosh\beta-1)+\sinh\beta(1-\cos\beta)\} \\ \quad \times\{\sin\alpha\cosh\alpha+\cos\alpha\sinh\alpha)+\gamma(\cos\alpha\cosh\alpha-1)\}] \end{array}}, \qquad (30')$$

The distributions of the deflections of pillar and the beam are shown by the equations.

$$y_1=\frac{\begin{array}{l} b\cos p't[\xi(1-\cos\beta\cosh\beta)\{(\cos\alpha\cosh\alpha-\sin\alpha\sinh\alpha+1)-2\gamma\sin\alpha\cosh\alpha\} \\ \quad +2\eta\{\sin\beta(\cosh\beta-1)+\sinh\beta(1-\cos\beta)\} \\ \quad \times\{2\cos\alpha\sinh\alpha+\gamma(\cos\alpha\cosh\alpha-\sin\alpha\sinh\alpha-1)\}] \\ \quad \times(\cos m_1x_1-\cosh m_1x_1) \end{array}}{\begin{array}{l} 2[\xi(1-\cos\beta\cosh\beta)\{(1+\cos\alpha\cosh\alpha)+\gamma(\cos\alpha\sinh\alpha-\sin\alpha\cosh\alpha)\} \\ \quad +2\eta\{\sin\beta(\cosh\beta-1)+\sinh\beta(1-\cos\beta)\} \\ \quad \times\{(\sin\alpha\cosh\alpha+\cos\alpha\sinh\alpha)+\gamma(\cos\alpha\cosh\alpha-1)\}] \end{array}}$$

$$+\frac{\begin{array}{l} b\cos p't[\xi(1-\cos\beta\cosh\beta)\{(\sin\alpha\cosh\alpha+\cos\alpha\sinh\alpha)+2\gamma\cos\alpha\cosh\alpha\} \\ \quad +2\eta\{\sin\beta(\cosh\beta-1)+\sinh\beta(1-\cos\beta)\} \\ \quad \times\{2\sin\alpha\sinh\alpha+\gamma(\cos\alpha\sinh\alpha+\sin\alpha\cosh\alpha)\}] \\ \quad \times(\sin m_1x_1-\sinh m_1x_1) \end{array}}{\begin{array}{l} 2[\xi(1-\cos\beta\cosh\beta)\{(1+\cos\alpha\cosh\alpha)+\gamma(\cos\alpha\sinh\alpha-\sin\alpha\cosh\alpha)\} \\ \quad \times+2\eta\{\sin\beta(\cosh\beta-1)+\sinh\beta(1-\cos\beta)\} \\ \quad \times\{(\sin\alpha\cosh\alpha+\cos\alpha\sinh\alpha)+\gamma(\cos\alpha\cosh\alpha-1)\}] \end{array}}$$

$$+ b\cos p't \cosh m_1x_1, \tag{31'}$$

$$y_2=\frac{\begin{aligned}&b\cos p't\,\{(\sin\alpha-\sinh\alpha)+\gamma(\cos\alpha-\cosh\alpha)\}\\&\quad\times[\{\sin\beta(1-\cosh\beta)-(1-\cos\beta)\sinh\beta\}(\cos m_2x_2-\cosh m_2x_2)\\&\quad+\{\sinh\beta(\sin\beta+\sinh\beta)-(1-\cosh\beta)(\cos\beta-\cosh\beta)\}\sin m_2x_2\\&\quad+\{(1-\cos\beta)(\cos\beta-\cosh\beta)-\sin\beta(\sin\beta-\sinh\beta)\}\sinh m_2x_2]\end{aligned}}{\begin{aligned}&2[\xi(1-\cos\beta\cosh\beta)\{(1+\cos\alpha\cosh\alpha)+\gamma(\cos\alpha\sinh\alpha-\sin\alpha\cosh\alpha)\}\\&\quad+2\eta\{\sin\beta(\cosh\beta-1)+\sinh\beta(1-\cos\beta)\}\\&\quad\times\{(\sin\alpha\cosh\alpha+\cos\alpha\sin\alpha)+\gamma(\cos\alpha\cosh\alpha-1)\}]\end{aligned}}. \tag{32'}$$

When the condition,

$$\begin{aligned}&2\{(\cos\alpha\sinh\alpha+\sin\alpha\cosh\alpha)+\gamma(\cos\alpha\cosh\alpha)\}\\&\quad\times\{\sin\beta(\cosh\beta-1)+\sinh\beta(1-\cos\beta)\}\\&\quad=\frac{\xi}{\eta}\{(\cos\alpha\cosh\alpha+1)+\gamma(\cos\alpha\sinh\alpha-\sin\alpha\cosh\alpha)\}\\&\qquad\qquad\times(\cos\beta\cosh\beta-1)\end{aligned} \tag{30}$$

is satisfied, each denominator of the expressions of y_1 and y_2 vanishes. As the above expression gives the frequency equation of the natural vibrations of framed structure, this gives the condition of resonance vibration of that structure.

The distributions of the displacements in the cases, where $E_1=E_2$; $l_1=l_2$; $a_1=a_2$; $\frac{\rho_1}{\rho_2}=1, \frac{1}{2}, \frac{1}{4}$; and frequencies of vibrations nearly satisfy

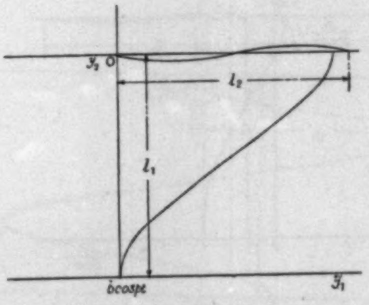

Fig. 2. $\frac{\rho_1}{\rho_2}=1$, $\alpha=1{\cdot}645$

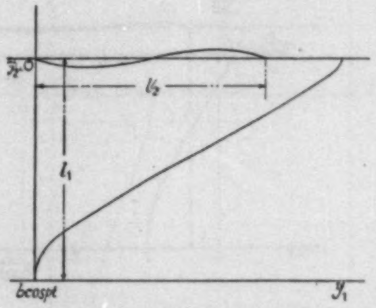

Fig. 3. $\frac{\rho_1}{\rho_2}=\frac{1}{2}$, $\alpha=1{\cdot}429$

$\left(\frac{\rho_1p'^2}{E_1k_1^2}\right)^{\frac{1}{4}}l_1=1{\cdot}645,\ 1{\cdot}429,\ 1{\cdot}224$ for respective values of $\frac{\rho_1}{\rho_2}$ given above, are shown in Figs. 2, 3, 4. These figures indicate merely the proportions of displacements, but not their absolute magnitudes.

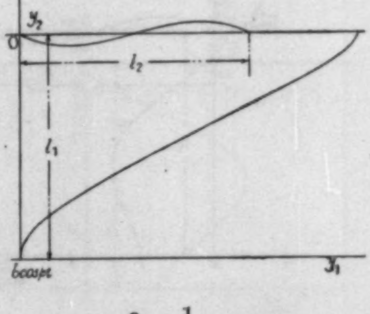

Fig. 4. $\frac{\rho_1}{\rho_2}=\frac{1}{4}$, $\alpha=1{\cdot}224$

The distributions of displacements and bending moments in the cases, $\frac{\rho_1}{\rho_2}=1$, $\alpha=1, 2, 2\cdot5, 3, 4, 10$; $\frac{\rho_1}{\rho_2}=\frac{1}{2}$, $\alpha=1, 1\cdot5, 1\cdot8, 4, 8$; $\frac{\rho_1}{\rho_2}=\frac{1}{4}$, $\alpha=1, 1\cdot5, 4, 8$ are shown in Figs. 5—34 and in Table I—XII. In these y_1, y_2, M_1, M_2 are the deflections and bending moments in pillar and beam respectively, and $\alpha=\left(\frac{\rho_1 p'^2}{E_1 k_1^2}\right)^{\frac{1}{4}} l_1$.

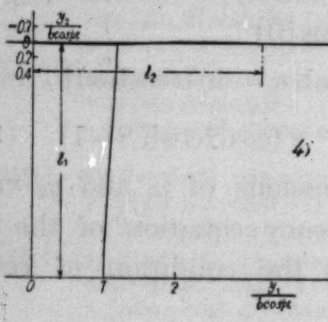

Fig. 5. $\frac{\rho_1}{\rho_2}=1$, $\alpha=1$.

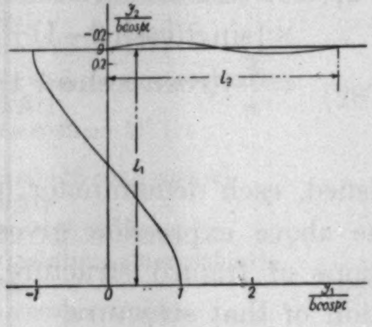

Fig. 6. $\frac{\rho_1}{\rho_2}=1$, $\alpha=2$.

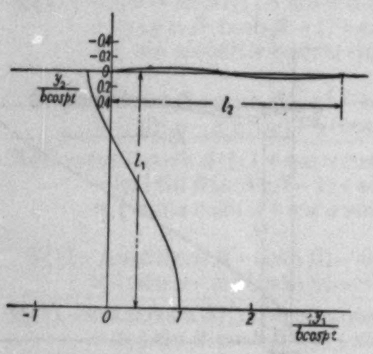

Fig. 7. $\frac{\rho_1}{\rho_2}=1$, $\alpha=2\cdot5$

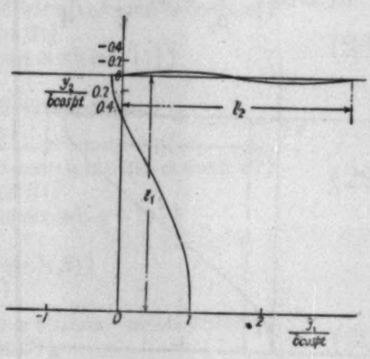

Fig. 8. $\frac{\rho_1}{\rho_2}=1$, $\alpha=3$.

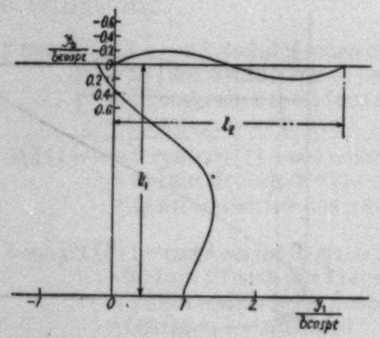

Fig. 9. $\frac{\rho_1}{\rho_2}=1$, $\alpha=4$

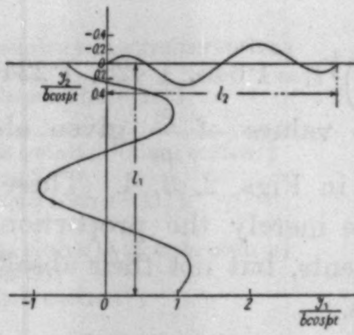

Fig. 10. $\frac{\rho_1}{\rho_2}=1$, $\alpha=10$.

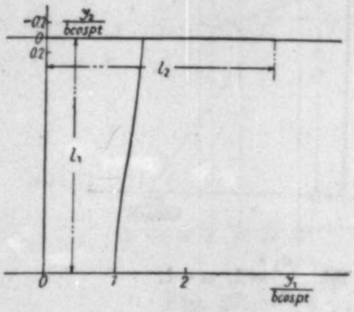

Fig. 11. $\frac{\rho_1}{\rho_2}=\frac{1}{2}$, $\alpha=1$.

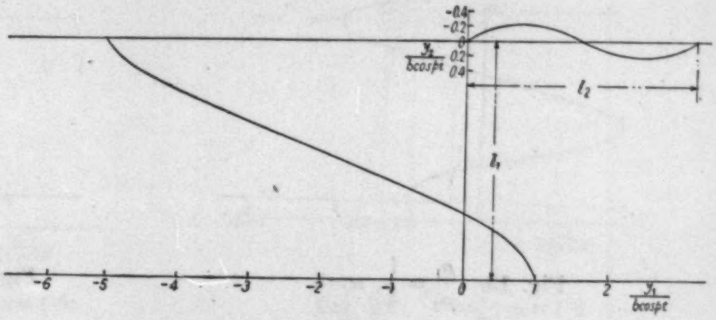

Fig. 12. $\frac{\rho_1}{\rho_2}=\frac{1}{2}$, $\alpha=1{\cdot}5$.

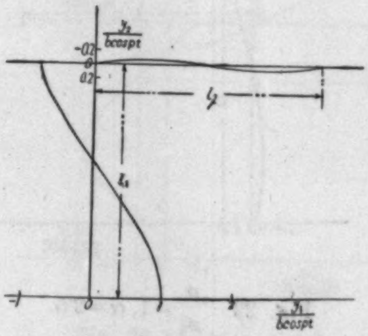

Fig. 13. $\frac{\rho_1}{\rho_2}=\frac{1}{2}$, $\alpha=1{\cdot}8$.

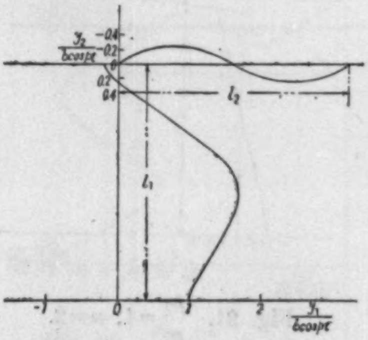

Fig. 14. $\frac{\rho_1}{\rho_2}=\frac{1}{2}$, $\alpha=4$.

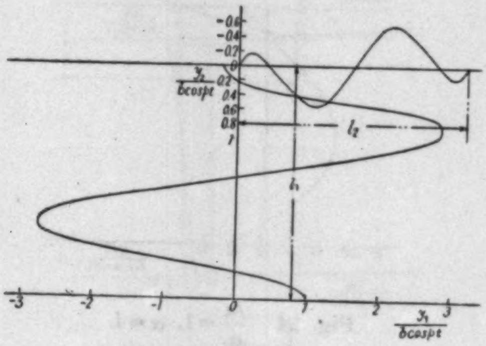

Fig. 15. $\frac{\rho_1}{\rho_2}=\frac{1}{2}$, $\alpha=8$.

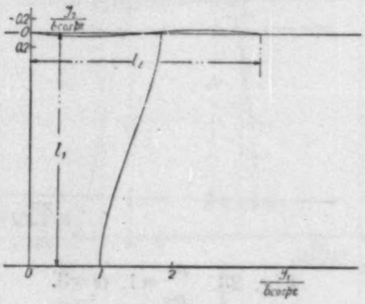

Fig. 16. $\frac{\rho_1}{\rho_2}=\frac{1}{4}$, $\alpha=1$.

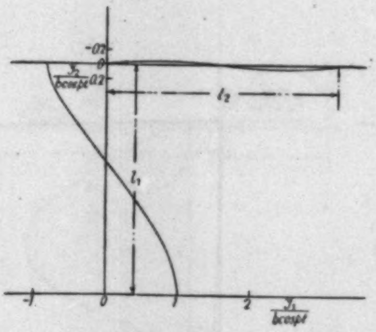

Fig. 17. $\frac{\rho_1}{\rho_2}=\frac{1}{4}$, $\alpha=1{\cdot}5$.

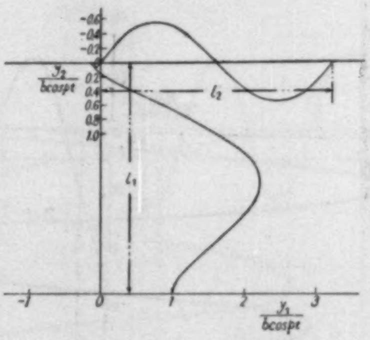

Fig. 18. $\frac{\rho_1}{\rho_2}=\frac{1}{4}$, $\alpha=4$

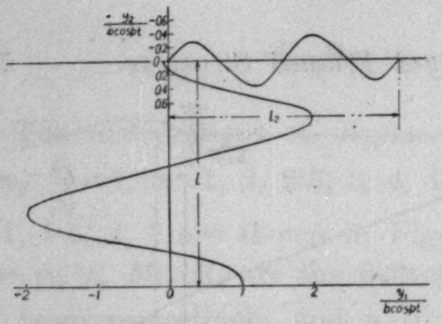

Fig. 19. $\frac{\rho_1}{\rho_2}=\frac{1}{4}$, $\alpha=8$.

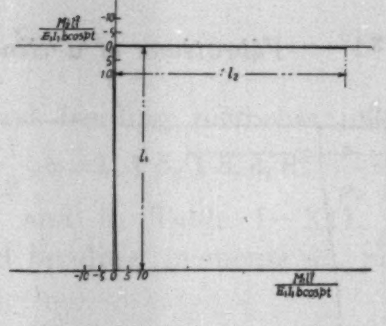

Fig. 20. $\frac{\rho_1}{\rho_2}=1$, $\alpha=1$.

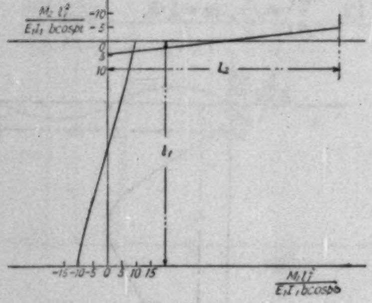

Fig. 21. $\frac{\rho_1}{\rho_2}=1$, $\alpha=2$.

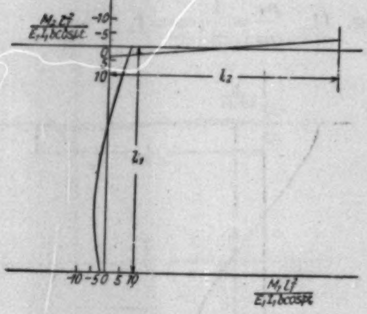

Fig. 22. $\frac{\rho}{\rho_2}=1$, $\alpha=2\cdot5$.

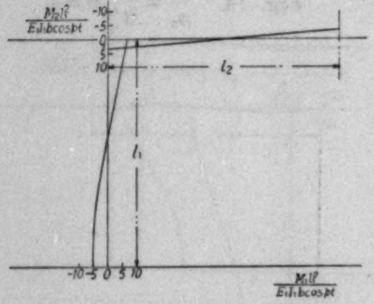

Fig. 23. $\frac{\rho_1}{\rho_2}=1$, $\alpha=3$.

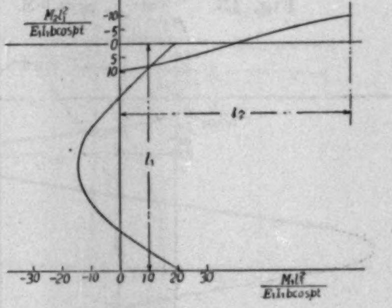

Fig. 24. $\frac{\rho_1}{\rho_2}=1$, $\alpha=4$.

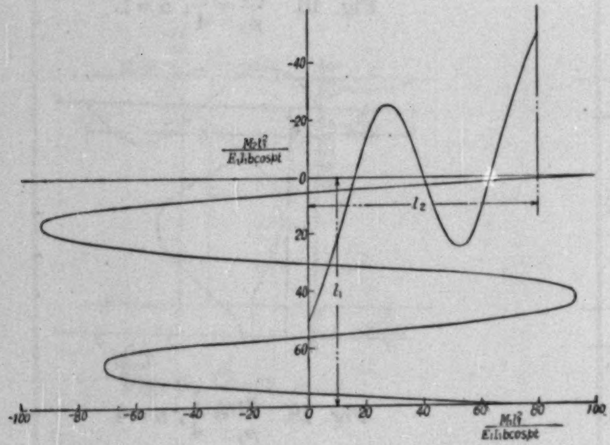

Fig. 25. $\frac{\rho_1}{\rho_2}=1$, $\alpha=10$.

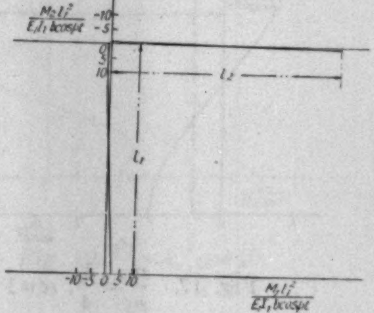

Fig. 26. $\frac{\rho_1}{\rho_2}=\frac{1}{2}$, $\alpha=1$.

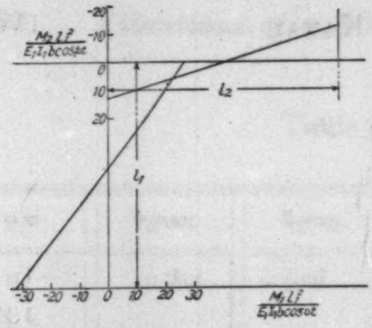

Fig. 27. $\frac{\rho_1}{\rho_2}=\frac{1}{2}$, $\alpha=1{\cdot}5$.

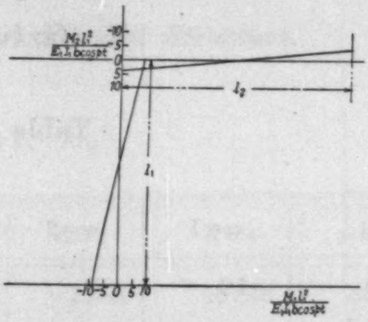

Fig. 28. $\frac{\rho_1}{\rho_2}=\frac{1}{2}$, $\alpha=1{\cdot}8$.

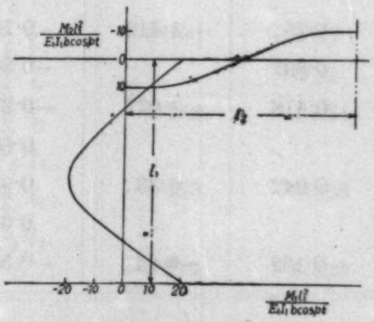

Fig. 29. $\frac{\rho_1}{\rho_2}=\frac{1}{2}$, $\alpha=4$.

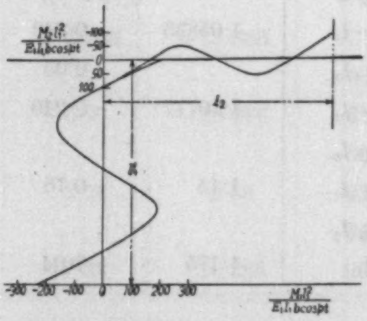

Fig. 30. $\frac{\rho_1}{\rho_2}=\frac{1}{2}$, $\alpha=8$.

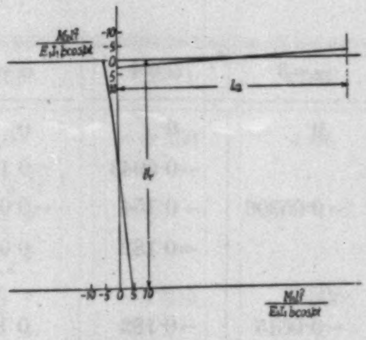

Fig. 31. $\frac{\rho_1}{\rho_2}=\frac{1}{4}$, $\alpha=1$.

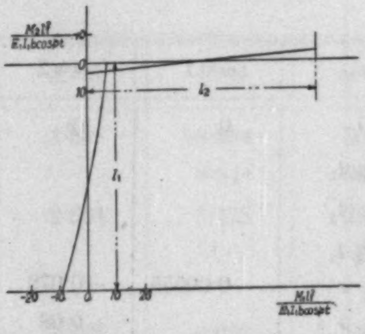

Fig. 32. $\frac{\rho_1}{\rho_2}=\frac{1}{4}$, $\alpha=1{\cdot}5$.

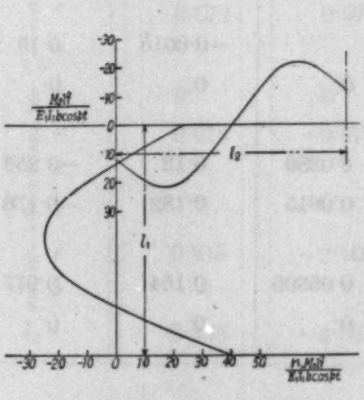

Fig. 33. $\frac{\rho_1}{\rho_2}=\frac{1}{4}$, $\alpha=4$.

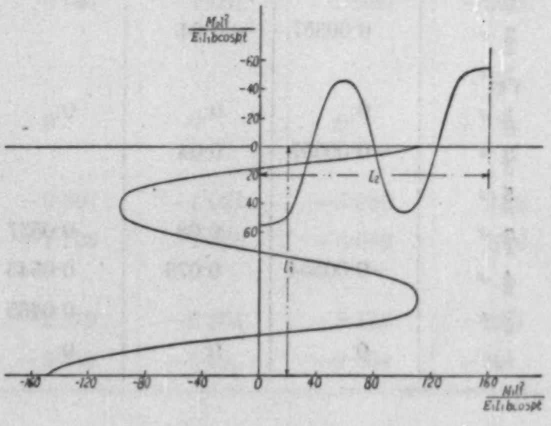

Fig. 34. $\frac{\rho_1}{\rho_2}=\frac{1}{4}$, $\alpha=8$.

Table I. $\frac{\rho_1}{\rho_2}=1$, y_1.

x_1	$\alpha=1$	$\alpha=2$	$\alpha=2{\cdot}5$	$\alpha=3$	$\alpha=4$	$\alpha=10$
0	1·1	1·	1·	1·	1·	1·
$\frac{1}{10}l_1$						1·17
$\frac{1}{5}l_1$	1·0174	0·811	0·91	0·948	1·242	0·9722
$\frac{3}{10}l_1$						0·127
$\frac{2}{5}l_1$	1·05835	0·342	0·623	0·75	1·412	−0·73
$\frac{1}{2}l_1$		0·05		0·597		−0·88
$\frac{3}{5}l_1$	1·10717	−0·249	0·247	0·418	1·077	−0·2
$\frac{7}{10}l_1$						0·667
$\frac{4}{5}l_1$	1·15	−0·75	−0·118	0·042	0·33	0·93
$\frac{9}{10}l_1$						0·34
l_1	1·175	−1·04	−0·34	−0·162	−0·24	−0·56

Table II. $\frac{\rho_1}{\rho_2}=1$, y_2.

x_2	$\alpha=1$	$\alpha=2$	$\alpha=2{\cdot}5$	$\alpha=3$	$\alpha=4$	$\alpha=10$
0	0·	0·	0·	0·	0·	0·
$\frac{1}{16}l_2$					−0·0943	−0·112
$\frac{1}{8}l_2$			−0·0465	−0·05306	−0·154	−0·077
$\frac{3}{16}l_2$					−0·182	0·043
$\frac{1}{5}$ 〃	0·00555	−0·078	−0·0545			
$\frac{1}{4}$ 〃		−0·08	−0·0537	−0·0615	−0·182	0·176
$\frac{5}{16}$ 〃					−0·158	0·26
$\frac{3}{8}$ 〃				−0·0389	−0·12	0·253
$\frac{2}{5}$ 〃	0·00357	−0·04				
$\frac{7}{16}$ 〃					−0·0615	0·15
$\frac{1}{2}$ 〃	0·	0·	0·	0·	0·	0·
$\frac{3}{5}$ 〃	−0·00357	0·04				
$\frac{5}{8}$ 〃				0·0389	0·12	−0·253
$\frac{3}{4}$ 〃		0·08	0·0537	0·0615	0·182	−0·176
$\frac{4}{5}$ 〃	−0·00554	0·078	0·0545			
$\frac{7}{8}$ 〃			0·0465	0·05306	0·154	0·077
l_2	0·	0·	0·	0·	0·	0·

Table III. $\frac{\rho_1}{\rho_2}=1$, M_1.

x_1	$\alpha=1$	$\alpha=2$	$\alpha=2·5$	$\alpha=3$	$\alpha=4$	$\alpha=10$
0	0·984	−10·6	−5·125	−1·395	20·848	89·1
$\frac{1}{10}l_1$						−47·8
$\frac{1}{5}l_1$	0·585	−7·0	−4·54	−4·0	−2·848	−70·9
$\frac{3}{10}l_1$				$(\frac{1}{3}l_1)$ −4·05		−3·2
$\frac{2}{5}l_1$	0·196	−2·88	−2·565	−3·546	−13·888	77·
$\frac{1}{2}l_1$		−0·72				90·
$\frac{3}{5}l_1$	−0·152	1·364	0·3625	−0·9	−10·976	21·4
$\frac{7}{10}l_1$						−66·1
$\frac{4}{5}l_1$	−0·453	5·628	3·67	3·24	2·56	−92·7
$\frac{9}{10}l_1$						−34·
l_1	−0·714	9·308	6·631	7·38	19·328	99·7

Table IV. $\frac{\rho_1}{\rho_2}=1$, M_2.

x_2	$\alpha=1$	$\alpha=2$	$\alpha=2·5$	$\alpha=3$	$\alpha=4$	$\alpha=10$
0	−0·358	4·66	3·315	3·69	9·664	50·
$\frac{1}{16}l_2$					8·944	38·
$\frac{1}{8}$ 〃			2·519	2·864	8·128	22·1
$\frac{3}{16}$ 〃						3·4
$\frac{1}{5}$ 〃	−0·215	2·808				
$\frac{1}{4}$ 〃			1·705	1·978	6·032	−13·6
$\frac{5}{16}$ 〃						−24·
$\frac{3}{8}$ 〃			0·867	1·021	3·280	−24·2
$\frac{2}{5}$ 〃	0·072	0·976				
$\frac{7}{16}$ 〃						−15·
$\frac{1}{2}$ 〃	0·	0·	0·	0·	0·	0·
$\frac{3}{5}$ 〃	0·072	−0·976				
$\frac{5}{8}$ 〃			−0·867	−1·021	−3·280	24·2
$\frac{3}{4}$ 〃			−1·705	−1·978	−6·032	13·6
$\frac{4}{5}$ 〃	0·215	−2·808				
$\frac{7}{8}$ 〃			−2·519	−2·864	−8·128	−22·1
l_2	0·358	−4·66	−3·315	−3·69	−9·664	−50·

Table V. $\frac{\rho_1}{\rho_2}=\frac{1}{2}$, y_1.

x_1	$\alpha=1$	$\alpha=1{\cdot}5$	$\alpha=1{\cdot}8$	$\alpha=4$	$\alpha=8$
0	1·	1·	1·	1·	1·
$\frac{1}{10}l_1$					
$\frac{1}{5}l_1$	1·0332	0·437	0·8415	1·326	−1·668
$\frac{3}{10}l_1$					−2·726
$\frac{2}{5}$ ″	1·1077	−0·9245	0·448	1·637	−2·288
$\frac{1}{2}l_1$					
$\frac{3}{5}$ ″	1·2002	−2·6	−0·043	1·361	1·573
$\frac{7}{10}l_1$					2·77
$\frac{4}{5}$ ″	1·2905	−4·11	−0·501	0·555	2·41
$\frac{9}{10}$ ″					
l_1	1·349	−5·	−0·77	−0·204	−0·224

Table VI. $\frac{\rho_1}{\rho_2}=\frac{1}{2}$, y_2.

x_2	$\alpha=1$	$\alpha=1{\cdot}5$	$\alpha=1{\cdot}8$	$\alpha=4$	$\alpha=8$
0	0·	·0	0·	0·	0·
$\frac{1}{16}l_2$					−0·165
$\frac{1}{8}$ ″		−0·182	−0·0532	0·208	−0·006
$\frac{3}{16}$ ″				0·25	
$\frac{1}{5}$ ″	0·01505				
$\frac{1}{4}$ ″	0·01042	−0·208	−0·0637	−0·253	0·426
$\frac{5}{16}$ ″				−0·2225	0·56
$\frac{3}{8}$ ″				−0·165	0·521
$\frac{2}{5}$ ″	0·00543				
$\frac{7}{16}$ ″					
$\frac{1}{2}$ ″	0·	0·	0·	0·	0·
$\frac{3}{5}$ ″	−0·00543				
$\frac{5}{8}$ ″				0·165	−0·521
$\frac{3}{4}$ ″	−0·01042	0·208	0·0637	0·253	−0·426
$\frac{4}{5}$ ″	−0·01505				
$\frac{7}{8}$ ″		0·182	0·0532	0·208	0·006
l_2	0·	0·	0·	0·	0·

Table VII. $\frac{\rho_1}{\rho_2}=\frac{1}{2}$, M_1.

x_1	$\alpha=1$	$\alpha=1{\cdot}5$	$\alpha=1{\cdot}8$	$\alpha=4$	$\alpha=8$
0	1·84	−32·175	−8·91	21·312	−233·856
$\frac{1}{10}l_1$					
$\frac{1}{5}l_1$	1·1228	−20·036	−5·911	−1·52	72·32
$\frac{3}{10}$ ″					181·376
$\frac{2}{5}$ ″	0·448	−7·796	−2·56	−16·064	141·056
$\frac{1}{2}$ ″					
$\frac{3}{5}$ ″	−0·192	4·277	1·001	−14·4	−94·656
$\frac{7}{10}$ ″					−161·152
$\frac{4}{5}$ ″	−0·773	15·775	4·484	0·72	−121·344
$\frac{9}{10}$ ″					
l_1	−1·382	26·26	7·90	21·568	197·184

Table VIII. $\frac{\rho_1}{\rho_2}=\frac{1}{2}$, M_2.

x_2	$\alpha=1$	$\alpha=1{\cdot}5$	$\alpha=1{\cdot}8$	$\alpha=4$	$\alpha=8$
0	−0·693	13·137	3·957	10·80	98·656
$\frac{1}{16}l_2$					69·421
$\frac{1}{8}$ ″		9·908	2·991	10·544	35·48
$\frac{3}{16}$ ″				9·888	
$\frac{1}{5}$ ″	−0·414				
$\frac{1}{4}$ ″	−0·351	6·616	2·029	8·745	−29·506
$\frac{5}{16}$ ″				7·105	−45·888
$\frac{3}{8}$ ″				5·001	−47·156
$\frac{2}{5}$ ″	−0·109				
$\frac{7}{16}$ ″					
$\frac{1}{2}$ ″	0·	0·	0·	0·	0·
$\frac{3}{5}$ ″	0·109				
$\frac{5}{8}$ ″				−5·001	47·156
$\frac{3}{4}$ ″	0·351	−6·616	−2·029	−8·745	29·506
$\frac{4}{5}$ ″	0·414				
$\frac{7}{8}$ ″		−9·908	−2·991	−10·544	−35·48
l_2	0·693	−13·137	−3·957	−10·80	−98·656

Table IX. $\frac{\rho_1}{\rho_2}=\frac{1}{4}$, y_1.

x_1	$\alpha=1$	$\alpha=1\cdot5$	$\alpha=4$	$\alpha=8$
0	1·	1·	1·	1·
$\frac{1}{10}l_1$				
$\frac{1}{5}l_1$	1·077	0·832	1·52	-0·844
$\frac{3}{10}$ 〃				
$\frac{2}{5}$ 〃	1·263	0·42	2·148	-1·64
$\frac{1}{2}$ 〃		0·165	2·194	
$\frac{3}{5}$ 〃	1·492	−0·09	1·997	0·833
$\frac{7}{10}$ 〃				
$\frac{4}{5}$ 〃	1·699	−0·564	1·	1·725
$\frac{9}{10}$ 〃				
l_1	1·816	0·843	−0·144	−0·076

Table X. $\frac{\rho_1}{\rho_2}=\frac{1}{4}$, y_2.

x_2	$\alpha=1$	$\alpha=1\cdot5$	$\alpha=4$	$\alpha=8$
0	0·	0·	0·	0·
$\frac{1}{16}l_2$				
$\frac{1}{8}$ 〃	0·0345	−0·0477	−0·424	-0·275
$\frac{3}{16}$ 〃				
$\frac{1}{5}$ 〃				
$\frac{1}{4}$ 〃	0·0398	−0·0546	−0·554	0·126
$\frac{5}{16}$ 〃				
$\frac{3}{8}$ 〃			−0·376	0·366
$\frac{2}{5}$ 〃				
$\frac{7}{16}$ 〃				
$\frac{1}{2}$ 〃	0·	0·	0·	0·
$\frac{3}{5}$ 〃				
$\frac{5}{8}$ 〃			0·376	−0·366
$\frac{3}{4}$ 〃	−0·0398	0·0546	0·554	−0·126
$\frac{4}{5}$ 〃				
$\frac{7}{8}$ 〃	−0·0398	0·0477	0·424	0·275
l_2	0·	0·	0·	0·

Table XI. $\frac{\rho_1}{\rho_2}=\frac{1}{4}$, M_1.

x_1	$\alpha=1$	$\alpha=1{\cdot}5$	$\alpha=4$	$\alpha=8$
0	4·425	−9·518	39·793	−148·698
$\frac{1}{10}\,l_1$				
$\frac{1}{5}\,l_1$	2·72	−6·109	1·4144	37·011
$\frac{3}{10}$ ″				
$\frac{2}{5}$ ″	1·0535	−2·52	−21·333	102·406
$\frac{1}{2}$ ″			−24·84	
$\frac{3}{5}$ ″	0·56	1·125	−22·779	−49·709
$\frac{7}{10}$ ″				
$\frac{4}{5}$ ″	2·113	4·77	−4·536	−90·893
$\frac{9}{10}$ ″				
l_1	4.95	7·135	23·806	110·432

Table XII. $\frac{\rho_1}{\rho_2}=\frac{1}{4}$, M_2.

x_2	$\alpha=1$	$\alpha=1{\cdot}5$	$\alpha=4$	$\alpha=8$
0	−2·49	3·51	11·903	55·05
$\frac{1}{16}\,l_2$				
$\frac{1}{8}$ ″	−1·87	2·66	19·392	48·563
$\frac{3}{16}$ ″			20·974	
$\frac{1}{5}$ ″				
$\frac{1}{4}$ ″	−1·27	1·791	20·472	−12·826
$\frac{5}{16}$ ″				
$\frac{3}{8}$ ″			13·109	−45·99
$\frac{2}{5}$ ″				
$\frac{7}{16}$ ″				
$\frac{1}{2}$ ″	0·	0·	0·	0·
$\frac{3}{5}$ ″				
$\frac{5}{8}$ ″			−13·109	45·99
$\frac{3}{4}$ ″	1·27	−1·791	−20·472	12·826
$\frac{4}{5}$ ″				
$\frac{7}{8}$ ″	1·87	−2·66	−19·392	−48·563
l_2	2·49	−3·51	−11·903	−55·05

The important facts, which may be found from these results, are enumerated as follows.

i) The greatest amplitude of horizontal vibrations of the pillar occurs at its top in resonance condition.

ii) When the frequency of vibrations of seismic waves is higher than those of natural vibration of the pillar, the amplitudes of the top of the pillar and hence those of the horizontal movement of the beam is not so great as the horizontal movement of the ground. This nature is more distinctly revealed when ρ_2 is greater than ρ_1.

iii) In the forced vibrations of higher frequency the deflection curves of pillars as well as those of beams become wavy. The amplitudes of the horizontal vibrations of the beams in this case, too, are not large.

iv) The bending moment at low frequency is small and uniformly increasing along its length, so that the moment is very similar to that obtained in the manner of the statical problem. This fact was also cited in Professor Suyehiro's paper[10] concerning the vibration of a chimney.

v) At the frequency which is higher than the natural one the bending moment varies in an oscillatory type along the beam and the pillar. The moments take greater values as ρ_2/ρ_1 increases. The moments increase too as the increase of the frequency of the forced vibrations.

III. Natural Periods of Framed Structure of Two Spans.

Let u_1, u_1', u_1'', u_2, u_2' be the amplitudes of pillars and beams at x_1, x_1', x_1'', x_2, x_2' respectively, M_0, M_0', M_0'', M_2, M_1, M_2', M_1' be the bending moments at O_2, O_4, O_6 respectively, x_1, x_1', x_1'', x_2, x_2' be the coordinates along O_1O_2, O_3O_4, O_5O_6, O_2O_4, O_4O_6 respectively, then the solution of the vibrations of the member, O_1O_2, fulfilling the conditions at the bottom end of this bar is written by

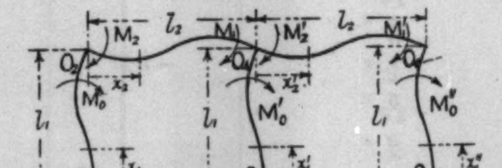

Fig. 35.

$$u_1 = A_1 (\cos m_1 x_1 - \cosh m_1 x_1) + B_1 (\sin m_1 x_1 - \sinh m_1 x_1). \tag{31}$$

The conditions at the other end are

$$x_1 = l_1, \quad -E_1 a_1 k_1^2 \frac{d^2 u_1}{dx_1^2} = M_0, \quad -E_1 a_1 k_1^2 \frac{d^3 u_1}{dx_1^3} = \frac{\rho_2 a_2 l_2 p^2 u_1}{2}. \qquad (32), (33)$$

10) K. SUYEHIRO, *loc. cit.*

The solution of the vibrations of the beam, O_2O_4, is expressed by

$$u_2 = A_2 \cos m_2x_2 + B_2 \sin m_2x_2 + C_2 \cosh m_2x_2 + D_2 \sinh m_2x_2. \qquad (34)$$

The boundary conditions at one end, O_2, are denoted by

$$x_2=0,\ x_1=l_1\ ;\ u_2=0,\ \frac{du_2}{dx_2}=\frac{du_1}{dx_1},\ -E_2a_2k_2^2\frac{d^2u_2}{dx_2^2}=M_2. \qquad (35), (36), (37)$$

The condition of the fixing moment at this joint is

$$M_0 - M_2 = 0. \qquad (38)$$

The boundary conditions at the other end are written by

$$x_2=l_2,\ x_1'=l_1\ ;\ u_2=0,\ \frac{du_2}{dx_2}=\frac{du_1'}{dx_1'},\ -E_2a_2k_2^2\frac{d^2u_2}{dx_2^2}=M_1, \qquad (39), (40), (41)$$

where u_1' is the solution of the member, O_3O_4, and has the same type as that of u_1 such that

$$u_1' = A_1'(\cos m_1x_1' - \cosh m_1x_1') + B_1'(\sin m_1x_1' - \sinh m_1x_1'). \qquad (42)$$

The boundary conditions of the pillar, O_3O_4, at the joint are

$$x_1'=l_1\ ;\ -E_1a_1k_1^2\frac{d^2u_1}{dx_1'^2}=M_0',\quad -E_1a_1k_1^2\frac{d^3u_1'}{dx_1'^3}=\rho_2a_2l_2p^2u_1'. \qquad (43), (44)$$

The form of the solution of the beam, O_4O_6, is written by

$$u_2' = A_2' \cos m_2x_2' + B_2' \sin m_2x_2' + C_2' \cosh m_2x_2' + D_2' \sinh m_2x_2'. \qquad (45)$$

The boundary conditions of this bar at O_4 are denoted by

$$x_2'=0,\ x_1=l_1\ ;\ u_2'=0,\ \frac{du_2'}{dx_2'}=\frac{du_1'}{dx_1'},\ -E_2a_2k_2^2\frac{d^2u_2'}{dx_2'^2}=M_2'. \qquad (46), (47), (48)$$

The condition of the fixing moment at the point, O_4, is

$$M_0' + M_1 - M_2' = 0. \qquad (49)$$

The solution of the vibration of the pillar, O_5O_6, is expressed by

$$u_1'' = A_1''(\cos m_1x_1'' - \cosh m_1x_1'') + B_1''(\sin m_1x_1'' - \sinh m_1x_1''). \qquad (50)$$

The conditions of this pillar at the top end are given by

$$x_1''=l_1\ ;\ -E_1a_1k_1^2\frac{d^2u_1''}{dx_1''^2}=M_0'',\ -E_1a_1k_1^2\frac{d^3u_1''}{dx_1''^3}=\frac{\rho_2a_2l_2p^2u_1''}{2}. \qquad (51), (52)$$

The condition of the beam at the end, O_6, are

$$x_2'=l_2,\ x_1''=l_1\ ;\ u_2'=0,\ \frac{du_2'}{dx_2'}=\frac{du_1''}{dx_1''},\ -E_2a_2k_2^2\frac{p^2u_2'^2}{dx_2^2}=M_1'. \qquad (53),(54),(55)$$

The condition of the fixing moment at the joint, O_6, is

$$M_0'' + M_1' = 0. \qquad (56)$$

Write

$$m_1l_1\equiv\alpha,\ m_2l_2\equiv\beta,\ \frac{\rho_2a_2l_2p^2}{E_1a_1k_1^2m_1^3}\equiv\gamma,\ \frac{m_2}{m_1}\equiv\xi,\ \frac{E_2a_2k_2^2m_2^2}{E_1a_1k_1^2m_1^2}\equiv\eta,$$

then, from (31) and (33) we find

$$A_1\{2(\sin\alpha-\sinh\alpha)+\gamma(\cos\alpha-\cosh\alpha)\}-B_1\{2(\cos\alpha+\cosh\alpha)-\gamma(\sin\alpha-\sinh\alpha)\}=0. \quad (57)$$

Again, from (34) and (35)

$$C_2+A_2=0, \quad (58)$$

while (31), (34), (36) give us

$$\xi(B_2+D_2)+A_1(\sin\alpha+\sinh\alpha)-B_1(\cos\alpha-\cosh\alpha)=0. \quad (59)$$

From (39)

$$A_2(\cos\beta-\cosh\beta)+B_2\sin\beta+D_2\sinh\beta=0. \quad (60)$$

From (42), (34), (40) we find

$$\xi\{-A_2(\sin\beta+\sinh\beta)+B_2\cos\beta+D_2\cosh\beta\}+A_1'(\sin\alpha+\sinh\alpha)-B_1'(\cos\alpha-\cosh a)=0. \quad (61)$$

By means of (32), (37), (38) we get

$$A_1(\cos\alpha+\cosh\alpha)+B_1(\sin\alpha+\sinh\alpha)-2\eta A_2=0. \quad (62)$$

(42), (44) give us

$$A_1'\{(\sin\alpha-\sinh\alpha)+\gamma(\cos\alpha-\cosh\alpha)\}-B_1'\{(\cos\alpha+\cosh\alpha)-\gamma(\sin\alpha-\sinh\alpha)\}=0. \quad (63)$$

(45), (46) give us

$$C_2'+A_2'=0, \quad (64)$$

while (42), (45), (47) give us

$$\xi(B_2'+D_2')+A_1'(\sin\alpha+\sinh\alpha)-B_1'(\cos\alpha-\cosh\alpha)=0. \quad (65)$$

From (53)

$$A_2'(\cos\beta-\cosh\beta)+B_2'\sin\beta+D_2'\sinh\beta=0. \quad (66)$$

By means of (45), (50), (54) we find

$$\xi\{-A_2'(\sin\beta+\sinh\beta)+B_2'\cos\beta+D_2'\cosh\beta\}+A_1''(\sin\alpha+\sinh\alpha)-B_1''(\cos\alpha-\cosh\alpha)=0. \quad (67)$$

From (43), (41), (48), (49)

$$A_1'(\cos\alpha+\cosh\alpha)+B_1'(\sin\alpha+\sinh\alpha)+\eta\{A_2(\cos\beta+\cosh\beta)+B_2\sin\beta-D_2\sinh\beta-2A_2'\}=0. \quad (68)$$

From (50), (52)

$$A_1''\{2(\sin\alpha-\sinh\alpha)+\gamma(\cos\alpha-\cosh\alpha)\}-B_1''\{2(\cos\alpha+\cosh\alpha)-\gamma(\sin\alpha-\sinh\alpha)\}=0. \quad (69)$$

By means of (51), (55), (56) we obtain

$$A_1''(\cos\alpha+\cosh\alpha)+B_1''(\sin\alpha+\sinh\alpha)$$
$$+\eta\{A_2'(\cos\beta+\cosh\beta)+B_2'\sin\beta-D_2'\sinh\beta\}=0. \quad (70)$$

From (61), (65)

$$A_2(\sin\beta+\sinh\beta)-B_2\cos\beta-D_2\cosh\beta+B_2'+D_2'=0. \quad (71)$$

Eliminating A_1 between (57), (59), we find

$$(B_2+D_2)\xi\{2(\sin\alpha-\sinh\alpha)+\gamma(\cos\alpha-\cosh\alpha)\}$$
$$+2B_1\{2(\cos\alpha\sinh\alpha+\sin\alpha\cosh\alpha)-\gamma(1-\cos\alpha\cosh\alpha)\}=0. \quad (72)$$

Eliminaing A_1 between (57) and (62)

$$B_1\{2(1+\cos\alpha\cosh\alpha)+\gamma(\cos\alpha\sinh\alpha-\sin\alpha\cosh\alpha)\}$$
$$-A_2\eta\{2(\sin\alpha-\sinh\alpha)+\gamma(\cos\alpha-\cosh\alpha)\}=0. \quad (73)$$

Eliminating B_1 between (72), (73) we obtain

$$(B_2+D_2)\xi\{2(1+\cos\alpha\cosh\alpha)+\gamma(\cos\alpha\sinh\alpha-\sin\alpha\cosh\alpha)\}$$
$$+2A_2\eta\{2(\cos\alpha\sinh\alpha+\sin\alpha\cosh\alpha)-\gamma(1-\cos\alpha\cosh\alpha)\}=0. \quad (74)$$

Eliminating A_1' between (63), (65) we get

$$(B_2'+D_2')\xi\{(\sin\alpha-\sinh\alpha)+\gamma(\cos\alpha-\cosh\alpha)\}$$
$$+2B_1'\{(\cos\alpha\sinh\alpha+\sin\alpha\cosh\alpha)-\gamma(1-\cos\alpha\cosh\alpha)\}=0. \quad (75)$$

Eliminating A_1' between (63), (68)

$$2B_1'\{1+\cos\alpha\cosh\alpha)+\gamma(\cos\alpha\sinh\alpha-\sin\alpha\cosh\alpha)\}$$
$$+\eta\{A_2(\cos\beta+\cosh\beta)+B_2\sin\beta-D_2\sinh\beta-2A_2'\}$$
$$\times\{(\sin\alpha-\sinh\alpha)+\gamma(\cos\alpha-\cosh\alpha)\}=0. \quad (76)$$

Eliminating A_1'' between (69), (70)

$$2B_1''\{2(1+\cos\alpha\cosh\alpha)+\gamma(\cos\alpha\sinh\alpha-\sin\alpha\cosh\alpha)\}$$
$$+\eta\{A_2'(\cos\beta+\cosh\beta)+B_2'\sin\beta-D_2'\sinh\beta\}$$
$$\times\{2(\sin\alpha-\sinh\alpha)+\gamma(\cos\alpha-\cosh\alpha)\}=0. \quad (77)$$

Eliminating B_2 between (60), (74) we obtain

$$D_2\xi(\sin\beta-\sinh\beta)\{2(1+\cos\alpha\cosh\alpha)+\gamma(\cos\alpha\sinh\alpha-\sin\alpha\cosh\alpha)\}$$
$$+A_2[2\eta\sin\beta\{2(\cos\alpha\sinh\alpha+\sin\alpha\cosh\alpha)-\gamma(1-\cos\alpha\cosh\alpha)\}$$
$$-\xi(\cos\beta-\cosh\beta)\{2(1+\cos\alpha\cosh\alpha)+\gamma(\cos\alpha\sinh\alpha-\sin\alpha\cosh\alpha)\}]=0. \quad (78)$$

Eliminating B_2 between (60), (76)

$$B_1'\{(1+\cos\alpha\cosh\alpha)+\gamma(\cos\alpha\sinh\alpha-\sin\alpha\cosh\alpha)\}$$
$$+\eta(A_2\cosh\beta-D_2\sinh\beta-A_2')\{(\sin\alpha-\sinh\alpha)+\gamma(\cos\alpha-\cosh\alpha)\}=0. \quad (79)$$

Eliminating B_2 between (60), (71)

$$A_2(1-\cos\beta\cosh\beta+\sin\beta\sinh\beta)+D_2(\cos\beta\sinh\beta-\sin\beta\cosh\beta)$$
$$+(B_2'+D_2')\sin\beta=0. \quad (80)$$

Eliminating B_2' between (66), (67)

$$A_2'\xi(1-\cos\beta\cosh\beta+\sin\beta\sinh\beta)+D_2'\xi(\cos\beta\sinh\beta-\sin\beta\cosh\beta)$$
$$-A_1''\sin\beta(\sin\alpha+\sinh\alpha)+B_1''\sin\beta(\cos\alpha-\cosh\alpha)=0. \quad (81)$$

Eliminating B_2' between (66), (75)

$$\xi\{(\sin\alpha-\sinh\alpha)+\gamma(\cos\alpha-\cosh\alpha)\}\{A_2'(\cos\beta-\cosh\beta)-D_2'(\sin\beta-\sinh\beta)\}$$
$$-2B_1'\sin\beta\{(\cos\alpha\sinh\alpha+\sin\alpha\cosh\alpha)-\gamma(1-\cos\alpha\cosh\alpha)\}=0. \quad (82)$$

Eliminating B_2' between (66), (77)

$$B_1''\{2(1+\cos\alpha\cosh\alpha)+\gamma(\cos\alpha\sinh\alpha-\sin\alpha\cosh\alpha)\}$$
$$+\eta(A_2'\cosh\beta-D_2'\sinh\beta)\{2(\sin\alpha-\sinh\alpha)+\gamma(\cos\alpha-\cosh\alpha)\}=0. \quad (83)$$

Eliminating B_2' between (66), (80)

$$A_2(1-\cos\beta\cosh\beta+\sin\beta\sinh\beta)+D_2(\cos\beta\sinh\beta-\sin\beta\cosh\beta)$$
$$-A_2'(\cos\beta-\cosh\beta)+D_2'(\sin\beta-\sinh\beta)=0. \quad (84)$$

Eliminating A_1'' between (69), (81)

$$\xi\{2(\sin\alpha-\sinh\alpha)+\gamma(\cos\alpha-\cosh\alpha)\}$$
$$\times\{A_2'(1-\cos\beta\cosh\beta+\sin\beta\sinh\beta)+D_2'(\cos\beta\sinh\beta-\sin\beta\cosh\beta)\}$$
$$-2B_1''\sin\beta\{2(\cos\alpha\sinh\alpha+\sin\alpha\cosh\alpha)-\gamma(1-\cos\alpha\cosh\alpha)\}=0. \quad (85)$$

Eliminating B_1'' between (83), (85)

$$-D_2'[2\eta\sin\beta\sinh\beta\{2(\cos\alpha\sinh\alpha+\sin\alpha\cosh\alpha)-\gamma(1-\cos\alpha\cosh\alpha)\}$$
$$-\xi(\cos\beta\sinh\beta-\sin\beta\cosh\beta)$$
$$\times\{2(1+\cos\alpha\cosh\alpha)+\gamma(\cos\alpha\sinh\alpha-\sin\alpha\cosh\alpha)\}]=0. \quad (86)$$

Eliminating D_2 between (78), (84)

$$\xi(\sin\beta-\sinh\beta)\{2(1+\cos\alpha\cosh\alpha)+\gamma(\cos\alpha\sinh\alpha-\sin\alpha\cosh\alpha)\}$$
$$\times\{-A_2'(\cos\beta-\cosh\beta)+D_2'(\sin\beta-\sinh\beta)\}+2A_2\sin\beta$$
$$\times[\xi(1-\cos\beta\cosh\beta)\{2(1+\cos\alpha\cosh\alpha)+\gamma(\cos\alpha\sinh\alpha-\sin\alpha\cosh\alpha)\}$$
$$-\eta(\cos\beta\sinh\beta-\sin\beta\cosh\beta)$$
$$\times\{2(\cos\alpha\sinh\alpha+\sin\alpha\cosh\alpha)-\gamma(1-\cos\alpha\cosh\alpha)\}]=0. \quad (87)$$

Eliminating D_2 between (79), (87)

$$\eta\{(\sin\alpha-\sinh\alpha)+\gamma(\cos\alpha-\cosh\alpha)\}\{A_2(\sinh\beta-\sin\beta)$$
$$+A_2'(-2\cos\beta\sinh\beta+\sinh\beta\cosh\beta+\sin\beta\cosh\beta)$$
$$+D_2'\sinh\beta(\sin\beta-\sinh\beta)\}+B_1'(\cos\beta\sinh\beta-\sin\beta\cosh\beta)$$
$$\times\{(1+\cos\alpha\cosh\alpha)+\gamma(\cos\alpha\sinh\alpha-\sin\alpha\cosh\alpha)\}=0. \quad (88)$$

Eliminating A_2 between (87), (88), we find finally

$$\begin{aligned}
&4\eta^3\sin\beta\sinh\beta(\cos\beta\sinh\beta-\sin\beta\cosh\beta)\\
&\quad\times\{2(\cos\alpha\sinh\alpha+\sin\alpha\cosh\alpha)-\gamma(1-\cos\alpha\cosh\alpha)\}^2\\
&\quad\times\{(\cos\alpha\sinh\alpha+\sin\alpha\cosh\alpha)-\gamma(1-\cos\alpha\cosh\alpha)\}\\
&-\xi\eta^2\{2(\cos\alpha\sinh\alpha+\sin\alpha\cosh\alpha)-\gamma(1-\cos\alpha\cosh\alpha)\}\\
&\quad\times[(\cos\beta\sinh\beta-\sin\beta\cosh\beta)^2\\
&\quad\times\{2(\cos\alpha\sinh\alpha+\sin\alpha\cosh\alpha)-\gamma(1-\cos\alpha\cosh\alpha)\\
&\quad\times\{(1+\cos\alpha\cosh\alpha)+\gamma(\cos\alpha\sinh\alpha-\sin\alpha\cosh\alpha)\}]\\
&+2\{2(\cos\beta\sinh\beta-\sin\beta\cosh\beta)^2-(\sin\beta-\sinh\beta)^2\}\\
&\quad\times\{2(1+\cos\alpha\cosh\alpha)+\gamma(\cos\alpha\sinh\alpha-\sin\alpha\cosh\alpha)\}\\
&\quad\times\{(\cos\alpha\sinh\alpha+\sin\alpha\cosh\alpha)-\gamma(1-\cos\alpha\cosh\alpha)\}]\\
&+2\eta\xi^2(1-\cos\beta\cosh\beta)(\cos\beta\sinh\beta-\sin\beta\cosh\beta)\\
&\quad\times\{2(1+\cos\alpha\cosh\alpha)+\gamma(\cos\alpha\sinh\alpha-\sin\alpha\cosh\alpha)\}\\
&\quad\times[\{2(\cos\alpha\sinh\alpha+\sin\alpha\cosh\alpha)-\gamma(1-\cos\alpha\cosh\alpha)\}\\
&\quad\times\{(1+\cos\alpha\cosh\alpha)+\gamma(\cos\alpha\sinh\alpha-\sin\alpha\cosh\alpha)\}\\
&\quad+\{2(1+\cos\alpha\cosh\alpha)+\gamma(\cos\alpha\sinh\alpha-\sin\alpha\cosh\alpha)\}\\
&\quad\times\{(\cos\alpha\sinh\alpha+\sin\alpha\cosh\alpha)-\gamma(1-\cos\alpha\cosh\alpha)\}]\\
&-\xi^3(1-\cos\beta\cosh\beta)^2\{2(1+\cos\alpha\cosh\alpha)+\gamma(\cos\alpha\sinh\alpha-\sin\alpha\cosh\alpha)\}^2\\
&\quad\times\{1+\cos\alpha\cosh\alpha)+\gamma(\cos\alpha\sinh\alpha-\sin\alpha\cosh\alpha)\}=0. \qquad (89)
\end{aligned}$$

The natural period of the vibrations may be determined from this equation. We have calculated the three cases of $\frac{\rho_1}{\rho_2}$ as follows. ($l_1=l_2$, $E_1=E_2$, $a_1=a_2$)

	$\frac{\rho_1}{\rho_2}=$	$\frac{1}{4}$	$\frac{1}{2}$	1
$\alpha=\left(\frac{\rho_1 p^2}{E_1 k_1^2}\right)^{\frac{1}{4}} l_1$	for two spans $=$	1·117	1·365	1·73
	for inf. no. of spans $=$	1·224	1·429	1·645

It may be seen that the periods of vibrations of the structure with two spans are approximately equal to those of the structure with an infinite number of spans. For smaller ratio of $\frac{\rho_1}{\rho_2}$ the value of α for two spans is somewhat less than that of α for an infinite number of spans, while for larger ratio of $\frac{\rho_1}{\rho_2}$ the inverse is the case.

IV. Forced Vibrations of Framed Structure of Two Spans.

We take the case where the bottom of each pillar is oscillating horizontally with amplitude b and with the period $\frac{2\pi}{p'}$. Then the boundary conditions at the bottom ends of the pillars are denoted by

$$\left.\begin{aligned} x_1=0\,; \quad u_1=b, \quad \frac{du_1}{dx_1}=0. \\ x_1'=0\,; \quad u_1'=b, \quad \frac{du_1'}{dx_1'}=0. \\ x_1''=0\,; \quad u_1''=b. \quad \frac{du_1''}{dx_1''}=0. \end{aligned}\right\} \quad (90)$$

and other conditions are the same as in the preceding case.

Write

$$m_1 l_1 \equiv \alpha, \ m_2 l_2 \equiv \beta, \ \frac{\rho_2 a_2 l_2 p'^2}{E_1 a_1 k_1^2 m_1^3} \equiv \gamma, \ \frac{m_2}{m_1} \equiv \xi, \ \frac{E_2 a_2 k_2^2 m_2^2}{E_1 a_1 k_1^2 m_1^2} \equiv \eta,$$

then, from (31), (33)

$$A_1\{2(\sin\alpha-\sinh\alpha)+\gamma(\cos\alpha-\cosh\alpha)\}-B_1\{2(\cos\alpha+\cosh\alpha) \\ -\gamma(\sin\alpha-\sinh\alpha)\}=-b(2\sinh\alpha+\gamma\cosh\alpha) \quad (57')$$

From (34), (35)

$$C_2+A_2=0. \quad (58')$$

From (31), (34), (36), we have

$$\xi(B_2+D_2)+A_1(\sin\alpha+\sinh\alpha)-B_1(\cos\alpha-\cosh\alpha)=b\sinh\alpha \quad (59')$$

From (39)

$$A_2(\cos\beta-\cosh\beta)+B_2\sin\beta+D_2\sinh\beta=0. \quad (60')$$

From (42), (34), (40)

$$\xi\{-A_2(\sin\beta+\sinh\beta)+B_2\cos\beta+D_2\cosh\beta\}+A_1'(\sin\alpha+\sinh\alpha) \\ -B_1'(\cos\alpha-\cosh\alpha)=b\sinh\alpha \quad (61')$$

From (32), (37), (38)

$$A_1(\cos\alpha+\cosh\alpha)+B_1(\sin\alpha+\sinh\alpha)-2\eta A_2=b\cosh\alpha \quad (62')$$

From (42), (44)

$$A_1'\{(\sin\alpha-\sinh\alpha)+\gamma(\cos\alpha-\cosh\alpha)\}-B_1'\{(\cos\alpha+\cosh\alpha) \\ -\gamma(\sin\alpha-\sinh\alpha)\}=-b(\sinh\alpha+\gamma\cosh\alpha) \quad (63')$$

(45), (46) give us

$$C_2'+A_2'=0. \quad (64')$$

From (42), (45), (47)

$$\xi(B_2'+D_2')+A_1'(\sin\alpha+\sinh\alpha)-B_1'(\cos\alpha-\cosh\alpha)=b\sinh\alpha \quad (65')$$

From (53)

$$A_2'(\cos\beta-\cosh\beta)+B_2'\sin\beta+D_2'\sinh\beta=0. \quad (66')$$

From (45), (50), (54)

$$\xi\{-A_2'(\sin\beta+\sinh\beta)+B_2'\cos\beta+D_2'\cosh\beta\}+A_1''(\sin\alpha+\sinh\alpha)$$
$$-B_1''(\cos\alpha-\cosh\alpha)=b\sinh\alpha \quad (67')$$

By means of (43), (41), (48), (49) we find

$$A_1'(\cos\alpha+\cosh\alpha)+B_1'(\sin\alpha+\sinh\alpha)$$
$$+\eta\{A_2(\cos\beta+\cosh\beta)+B_2\sin\beta-D_2\sinh\beta-2A_2'\}=b\cosh\alpha \quad (68')$$

From (50), (52)

$$A_1''\{2(\sin\alpha-\sinh\alpha)+\gamma(\cos\alpha-\cosh\alpha)\}$$
$$-B_1''\{2(\cos\alpha+\cosh\alpha)-\gamma(\sin\alpha-\sinh\alpha)\}=-b(2\sinh\alpha+\gamma\cosh\alpha) \quad (69')$$

From (51), (55), (56)

$$A_1''(\cos\alpha+\cosh\alpha)+B_1''(\sin\alpha+\sinh\alpha)$$
$$+\eta\{A_2'(\cos\beta+\cosh\beta)+B_2'\sin\beta-D_2'\sinh\beta\}=b\cosh\alpha \quad (70')$$

From (61′), (65′)

$$A_2(\sin\beta+\sinh\beta)-B_2\cos\beta-D_2\cosh\beta+B_2'+D_2'=0. \quad (71')$$

Eliminating A_1 between (57′), (59′),

$$(B_2+D_2)\xi\{2(\sin\alpha-\sinh\alpha)+\gamma(\cos\alpha-\cosh\alpha)\}$$
$$+2B_1\{2(\cos\alpha\sinh\alpha+\sin\alpha\cosh\alpha)-\gamma(1-\cos\alpha\cosh\alpha)\}$$
$$=b\{4\sin\alpha\sinh\alpha+\gamma(\cos\alpha\sinh\alpha+\sin\alpha\cosh\alpha)\} \quad (72')$$

Eliminating A_1 between (57′), (62′),

$$B_1\{2(1+\cos\alpha\cosh\alpha)+\gamma(\cos\alpha\sinh\alpha-\sin\alpha\cosh\alpha)\}$$
$$-A_2\eta\{2(\sin\alpha-\sinh\alpha)+\gamma(\cos\alpha-\cosh\alpha)\}$$
$$=b\{(\cos\alpha\sinh\alpha+\sin\alpha\cosh\alpha)+\gamma\cos\alpha\cosh\alpha\} \quad (73')$$

Eliminating B_1 between (72′), (73′),

$$(B_2'+D_2')\xi\{2(1+\cos\alpha\cosh\alpha)+\gamma(\cos\alpha\sinh\alpha-\sin\alpha\cosh\alpha)\}$$
$$+2A_2\eta\{2(\cos\alpha\sinh\alpha+\sin\alpha\cosh\alpha)-\gamma(1-\cos\alpha\cosh\alpha)\}$$
$$=-b\{2(\sin\alpha-\sinh\alpha)+\gamma(\cos\alpha-\cosh\alpha)\} \quad (74')$$

Eliminating A_1' between (63′), (65′), we get

$$(B_2'+D_2')\xi\{(\sin\alpha-\sinh\alpha)+\gamma(\cos\alpha-\cosh\alpha)\}$$
$$+2B_1'\{(\cos\alpha\sinh\alpha+\sin\alpha\cosh\alpha)-\gamma(1-\cos\alpha\cosh\alpha)\}$$
$$=b\{2\sin\alpha\sinh\alpha+\gamma(\cos\alpha\sinh\alpha+\sin\alpha\cosh\alpha)\} \quad (75')$$

Eliminating A_1' between (63′), (68′),

$$2B_1'\{(1+\cos\alpha\cosh\alpha)+\gamma(\cos\alpha\sinh\alpha-\sin\alpha\cosh\alpha)\}$$
$$+\eta\{A_2(\cos\beta+\cosh\beta)+B_2\sin\beta-D_2\sinh\beta-2A_2'\}$$
$$\times\{(\sin\alpha-\sinh\alpha)+\gamma(\cos\alpha-\cosh\alpha)\}$$
$$=b\{(\cos\alpha\sinh\alpha+\sin\alpha\cosh\alpha)+2\gamma\cos\alpha\cosh\alpha\} \quad (76')$$

Eliminating A_1'' between (69′), (70′),

$$2B_1''\{2(1+\cos\alpha\cosh\alpha)+\gamma(\cos\alpha\sinh\alpha-\sin\alpha\cosh\alpha)\}$$
$$+\eta\{A_2'(\cos\beta+\cosh\beta)+B_2'\sin\beta-D_2'\sinh\beta\}$$
$$\times\{2(\sin\alpha-\sinh\alpha)+\gamma(\cos\alpha-\cosh\alpha)\}$$
$$=2b\{(\cos\alpha\sinh\alpha+\sin\alpha\cosh\alpha)+\gamma\cos\alpha\cosh\alpha\} \quad (77')$$

Eliminating B_2 between (60'), (74'),

$$D_2\xi(\sin\beta-\sinh\beta)\{2(1+\cos\alpha\cosh\alpha)+\gamma(\cos\alpha\sinh\alpha-\sin\alpha\cosh\alpha)\}$$
$$+A_2[2\eta\sin\beta\{2(\cos\alpha\sinh\alpha+\sin\alpha\cosh\alpha)-\gamma(1-\cos\alpha\cosh\alpha)\}$$
$$-\xi(\cos\beta-\cosh\beta)\{2(1+\cos\alpha\cosh\alpha)+\gamma(\cos\alpha\sinh\alpha-\sin\alpha\cosh\alpha)\}$$
$$=-b\sin\beta\{2(\sin\alpha-\sinh\alpha)+\gamma(\cos\alpha-\cosh\alpha)\} \quad (78')$$

Eliminating B_2 between (60'), (76'),

$$B_1'\{1+\cos\alpha\cosh\alpha)+\gamma(\cos\alpha\sinh\alpha-\sin\alpha\cosh\alpha)\}$$
$$+\eta(A_2\cosh\beta-D_2\sinh\beta-A_2')\{(\sin\alpha-\sinh\alpha)+\gamma(\cos\alpha-\cosh\alpha)\}$$
$$=\frac{1}{2}b\{(\cos\alpha\sinh\alpha+\sin\alpha\cosh\alpha)+2\gamma\cos\alpha\cosh\alpha\} \quad (79')$$

Eliminating B_2 between (60'), (71'),

$$A_2(1-\cos\beta\cosh\beta+\sin\beta\sinh\beta)+D_2(\cos\beta\sinh\beta-\sin\beta\cosh\beta)$$
$$+(B_2'+D_2')\sin\beta=0. \quad (80')$$

Eliminating B_2' between (66'), (67'),

$$A_2'\xi(1-\cos\beta\cosh\beta+\sin\beta\sinh\beta)+D_2'\xi(\cos\beta\sinh\beta-\sin\beta\cosh\beta)$$
$$-A_1''\sin\beta(\sin\alpha+\sinh\alpha)+B_1''\sin\beta(\cos\alpha-\cosh\alpha)$$
$$=-b\sin\beta\sinh\alpha \quad (81')$$

Eliminating B_2' between (66'), (75'),

$$\xi\{(\sin\alpha-\sinh\alpha)+\gamma(\cos\alpha-\cosh\alpha)\}$$
$$\times\{A_2'(\cos\beta-\cosh\beta)-D_2'(\sin\beta-\sinh\beta)\}$$
$$-2B_1'\sin\beta\{(\cos\alpha\sinh\alpha+\sin\alpha\cosh\alpha)-\gamma(1-\cos\alpha\cosh\alpha)\}$$
$$=-b\sin\beta\{2\sin\alpha\sinh\alpha+\gamma(\cos\alpha\sinh\alpha+\sin\alpha\cosh\alpha)\} \quad (82')$$

Eliminating B_2' between (66'), (77'),

$$B_1''\{2(1+\cos\alpha\cosh\alpha)+\gamma(\cos\alpha\sinh\alpha-\sin\alpha\cosh\alpha)\}$$
$$+\eta(A_2'\cosh\beta-D_2'\sinh\beta)\{2(\sin\alpha-\sinh\alpha)+\gamma(\cos\alpha-\cosh\alpha)\}$$
$$=b\{(\cos\alpha\sinh\alpha+\sin\alpha\cosh\alpha)+\gamma\cos\alpha\cosh\alpha\} \quad (83')$$

Eliminating B_2' between (66'), (80'),

$$A_2(1-\cos\beta\cosh\beta+\sin\beta\sinh\beta)+D_2(\cos\beta\sinh\beta-\sin\beta\cosh\beta)$$
$$-A_2'(\cos\beta-\cosh\beta)+D_2'(\sin\beta-\sinh\beta)=0. \quad (84')$$

Eliminating A_1'' between (69'), (81'),

$$\xi\{2(\sin\alpha-\sinh\alpha)+\gamma(\cos\alpha-\cosh\alpha)\}$$
$$\times\{A_2'(1-\cos\beta\cosh\beta+\sin\beta\sinh\beta)+D_2'(\cos\beta\sinh\beta-\sin\beta\cosh\beta)\}$$

$$-2B_1''\sin\beta\{2(\cos\alpha\sinh\alpha+\sin\alpha\cosh\alpha)-\gamma(1-\cos\alpha\cosh\alpha)\}$$
$$=-b\sin\beta\{4\sin\alpha\sinh\alpha+\gamma(\cos\alpha\sinh\alpha+\sin\alpha\cosh\alpha)\} \quad (85')$$

Eliminating B_1'' between (83'), (85'),

$$A_2'[2\eta\sin\beta\cosh\beta\{2(\cos\alpha\sinh\alpha+\sin\alpha\cosh\alpha)-\gamma(1-\cos\alpha\cosh\alpha)\}$$
$$+\xi(1-\cos\beta\cosh\beta+\sin\beta\sinh\beta)$$
$$\times\{2(1+\cos\alpha\cosh\alpha)+\gamma(\cos\alpha\sinh\alpha-\sin\alpha\cosh\alpha)\}]$$
$$-D_2'[2\eta\sin\beta\sinh\beta\{2(\cos\alpha\sinh\alpha+\sin\alpha\cosh\alpha)-\gamma(1-\cos\alpha\cosh\alpha)\}$$
$$-\xi(\cos\beta\sinh\beta-\sin\beta\cosh\beta)$$
$$\times\{2(1+\cos\alpha\cosh\alpha)+\gamma(\cos\alpha\sinh\alpha-\sin\alpha\cosh\alpha)\}]$$
$$=b\sin\beta\{2(\sin\alpha-\sinh\alpha)+\gamma(\cos\alpha-\cosh\alpha)\} \quad (86')$$

Eliminating D_2 between (78'), (84'),

$$\xi(\sin\beta-\sinh\beta)\{2(1+\cos\alpha\cosh\alpha)+\gamma(\cos\alpha\sinh\alpha-\sin\alpha\cosh\alpha)\}$$
$$\times\{-A_2'(\cos\beta-\cosh\beta)+D_2'(\sin\beta-\sinh\beta)\}$$
$$+2A_2\sin\beta[\xi(1-\cos\beta\cosh\beta)\{2(1+\cos\alpha\cosh\alpha)$$
$$+\gamma(\cos\alpha\sinh\alpha-\sin\alpha\cosh\alpha)\}-\eta(\cos\beta\sinh\beta-\sin\beta\cosh\beta)$$
$$\times\{2(\cos\alpha\sinh\alpha+\sin\alpha\cosh\alpha)-\gamma(1-\cos\alpha\cosh\alpha)\}]$$
$$=b\sin\beta(\cos\beta\sinh\beta-\sin\beta\cosh\beta)\{2(\sin\alpha-\sinh\alpha)$$
$$+\gamma(\cos\alpha-\cosh\alpha)\} \quad (87')$$

Eliminating D_2 between (79'), (84'),

$$\eta\{(\sin\alpha-\sinh\alpha)+\gamma(\cos\alpha-\cosh\alpha)\}\{-A_2(\sin\beta-\sinh\beta)$$
$$+A_2'(-2\cos\beta\sinh\beta+\sinh\beta\cosh\beta+\sin\beta\cosh\beta)$$
$$+D_2'\sinh\beta(\sin\beta-\sinh\beta)\}$$
$$+B_1'(\cos\beta\sinh\beta-\sin\beta\cosh\beta)$$
$$\times\{(1+\cos\alpha\cosh\alpha)+\gamma(\cos\alpha\sinh\alpha-\sin\alpha\cosh\alpha)\}$$
$$=\frac{1}{2}b(\cos\beta\sinh\beta-\sin\beta\cosh\beta)$$
$$\times\{(\cos\alpha\sinh\alpha+\sin\alpha\cosh\alpha)+2\gamma\cos\alpha\cosh\alpha\} \quad (88')$$

From (82'), (86'), (87'), (88') we find the coefficients, B_1', A_2, A_2', D_2'. The other coefficients are derived from these constants thus determined. The result are shown below.

i) The denominator of each constant is given by twice the expression of (88)

ii) The numerator of $\frac{A_1}{b}$ is

$$4\eta^3\sin\beta\sinh\beta(\cos\beta\sinh\beta-\sin\beta\cosh\beta)$$
$$\times\{2(\cos\alpha\sinh\alpha+\sin\alpha\cosh\alpha)-\gamma(1-\cos\alpha\cosh\alpha)\}$$
$$\times\{(\cos\alpha\sinh\alpha+\sin\alpha\cosh\alpha)-\gamma(1-\cos\alpha\cosh\alpha)\}$$
$$\times\{4\cos\alpha\sinh\alpha-\gamma(1-\cos\alpha\cosh\alpha+\sin\alpha\sinh\alpha)\}$$

$$+\eta^2\xi\Big\{(\sin\beta-\sinh\beta)(\cos\beta\sinh\beta-\sin\beta\cosh\beta)$$
$$\times\{2(\cos\alpha\sinh\alpha+\sin\alpha\cosh\alpha)-\gamma(1-\cos\alpha\cosh\alpha)\}$$
$$\times\{(\sin\alpha-\sinh\alpha)+\gamma(\cos\alpha-\cosh\alpha)\}$$
$$\times\{2(\cos\alpha+\cosh\alpha)-\gamma(\sin\alpha-\sinh\alpha)\}$$
$$+2(\sin\beta-\sinh\beta)^2\{2(1+\cos\alpha\cosh\alpha)+\gamma(\cos\alpha\sinh\alpha-\sin\alpha\cosh\alpha)\}$$
$$\times\{(\cos\alpha\sinh\alpha+\sin\alpha\cosh\alpha)-\gamma(1-\cos\alpha\cosh\alpha)\}$$
$$\times\{4\cos\alpha\sinh\alpha-\gamma(1-\cos\alpha\cosh\alpha+\sin\alpha\sinh\alpha)\}$$
$$-(\cos\beta\sinh\beta-\sin\beta\cosh\beta)^2$$
$$\times[4\{2(\cos\alpha\sinh\alpha+\sin\alpha\cosh\alpha)-\gamma(1-\cos\alpha\cosh\alpha)\}$$
$$\times\{(\cos\alpha\sinh\alpha+\sin\alpha\cosh\alpha)-\gamma(1-\cos\alpha\cosh\alpha)\}$$
$$\times\{(1+\cos\alpha\cosh\alpha-\sin\alpha\sinh\alpha)-\gamma\sin\alpha\cosh\alpha\}$$
$$+2\{2(1+\cos\alpha\cosh\alpha)+\gamma(\cos\alpha\sinh\alpha-\sin\alpha\cosh\alpha)\}$$
$$\times\{(\cos\alpha\sinh\alpha+\sin\alpha\cosh\alpha)-\gamma(1-\cos\alpha\cosh\alpha)\}$$
$$\times\{4\cos\alpha\sinh\alpha-\gamma(1-\cos\alpha\cosh\alpha+\sin\alpha\sinh\alpha)\}$$
$$+\{2(\cos\alpha\sinh\alpha+\sin\alpha\cosh\alpha)-\gamma(1-\cos\alpha\cosh\alpha)\}$$
$$\times\{(1+\cos\alpha\cosh\alpha)+\gamma(\cos\alpha\sinh\alpha-\sin\alpha\cosh\alpha)\}$$
$$\times\{4\cos\alpha\sinh\alpha-\gamma(1-\cos\alpha\cosh\alpha+\sin\alpha\sinh\alpha)\}]\Big\}$$
$$+\eta\xi^2(1-\cos\beta\cosh\beta)\Big\{(\cos\beta\sinh\beta-\sin\beta\cosh\beta)$$
$$\times[4\{2(1+\cos\alpha\cosh\alpha)+\gamma(\cos\alpha\sinh\alpha-\sin\alpha\cosh\alpha)\}$$
$$\times\{(\cos\alpha\sinh\alpha+\sin\alpha\cosh\alpha)-\gamma(1-\cos\alpha\cosh\alpha)\}$$
$$\times\{(1+\cos\alpha\cosh\alpha-\sin\alpha\sinh\alpha)-\gamma\sin\alpha\cosh\alpha\}$$
$$+2\{2(\cos\alpha\sinh\alpha+\sin\alpha\cosh\alpha)-\gamma(1-\cos\alpha\cosh\alpha)\}$$
$$\times\{(1+\cos\alpha\cosh\alpha)+\gamma(\cos\alpha\sinh\alpha-\sin\alpha\cosh\alpha)\}$$
$$\times\{(1+\cos\alpha\cosh\alpha-\sin\alpha\sinh\alpha)-\gamma\sin\alpha\cosh\alpha\}$$
$$+\{2(1+\cos\alpha\cosh\alpha)+\gamma(\cos\alpha\sinh\alpha-\sin\alpha\cosh\alpha)\}$$
$$\times\{(1+\cos\alpha\cosh\alpha)+\gamma(\cos\alpha\sinh\alpha-\sin\alpha\cosh\alpha)\}$$
$$\times\{4\cos\alpha\sinh\alpha-\gamma(1-\cos\alpha\cosh\alpha+\sin\alpha\sinh\alpha)\}]$$
$$-(\sin\beta-\sinh\beta)\{2(1+\cos\alpha\cosh\alpha)+\gamma(\cos\alpha\sinh\alpha-\sin\alpha\cosh\alpha)\}$$
$$\times\{(\sin\alpha-\sinh\alpha)+\gamma(\cos\alpha-\cosh\alpha\}$$
$$\times\{2(\cos\alpha+\cosh\alpha)-\gamma(\sin\alpha-\sinh\alpha)\}\Big\}$$
$$-2\xi^3(1-\cos\beta\cosh\beta)^2\{2(1+\cos\alpha\cosh\alpha)+\gamma(\cos\alpha\sinh\alpha-\sin\alpha\cosh\alpha)\}$$
$$\times\{(1+\cos\alpha\cosh\alpha)+\gamma(\cos\alpha\sinh\alpha-\sin\alpha\cosh\alpha)\}$$
$$\times\{(1+\cos\alpha\cosh\alpha-\sin\alpha\sinh\alpha)-\gamma\sin\alpha\cosh\alpha\}$$

iii) The numerator of $\dfrac{B_1}{b}$ is

$$4\eta^3\sin\beta\sinh\beta(\cos\beta\sinh\beta-\sin\beta\cosh\beta)$$
$$\times\{2(\cos\alpha\sinh\alpha+\sin\alpha\cosh\alpha)-\gamma(1-\cos\alpha\cosh\alpha)\}$$

$$\times\{(\cos\alpha\sinh\alpha+\sin\alpha\cosh\alpha)-\gamma(1-\cos\alpha\cosh\alpha)\}$$
$$\times\{4\sin\alpha\sinh\alpha+\gamma(\cos\alpha\sinh\alpha+\sin\alpha\cosh\alpha)\}$$
$$+\eta\xi^2\Big\{2(\sin\beta-\sinh\beta)^2\{2(1+\cos\alpha\cosh\alpha)+\gamma(\cos\alpha\sinh\alpha-\sin\alpha\cosh\alpha)\}$$
$$\times\{(\cos\alpha\sinh\alpha+\sin\alpha\cosh\alpha)-\gamma(1-\cos\alpha\cosh\alpha)\}$$
$$\times\{4\sin\alpha\sinh\alpha+\gamma(\cos\alpha\sinh\alpha+\sin\alpha\cosh\alpha)\}$$
$$+(\sin\beta-\sinh\beta)(\cos\beta\sinh\beta-\sin\beta\cosh\beta)$$
$$\times\{2(\cos\alpha\sinh\alpha+\sin\alpha\cosh\alpha)-\gamma(1-\cos\alpha\cosh\alpha)\}$$
$$\times\{(\sin\alpha-\sinh\alpha)+\gamma(\cos\alpha-\cosh\alpha)\}$$
$$\times\{2(\sin\alpha-\sinh\alpha)+\gamma(\cos\alpha-\cosh\alpha)\}$$
$$-(\cos\beta\sinh\beta-\sin\beta\cosh\beta)^2$$
$$\times[4\{2(\cos\alpha\sinh\alpha+\sin\alpha\cosh\alpha)-\gamma(1-\cos\alpha\cosh\alpha)\}$$
$$\times\{(\cos\alpha\sinh\alpha+\sin\alpha\cosh\alpha)-\gamma(1-\cos\alpha\cosh\alpha)\}$$
$$\times\{(\cos\alpha\sinh\alpha+\sin\alpha\cosh\alpha)+\gamma\cos\alpha\cosh\alpha\}$$
$$+2\{2(1+\cos\alpha\cosh\alpha)+\gamma(\cos\alpha\sinh\alpha-\sin\alpha\cosh\alpha)\}$$
$$\times\{(\cos\alpha\sinh\alpha+\sin\alpha\cosh\alpha)-\gamma(1-\cos\alpha\cosh\alpha)\}$$
$$\times\{4\sin\alpha\sinh\alpha+\gamma(\cos\alpha\sinh\alpha+\sin\alpha\cosh\alpha)\}$$
$$+\{2(\cos\alpha\sinh\alpha+\sin\alpha\cosh\alpha)-\gamma(1-\cos\alpha\cosh\alpha)\}$$
$$\times\{(1+\cos\alpha\cosh\alpha)+\gamma(\cos\alpha\sinh\alpha-\sin\alpha\cosh\alpha)\}$$
$$\times\{4\sin\alpha\sinh\alpha+\gamma(\cos\alpha\sinh\alpha+\sin\alpha\cosh\alpha)\}]\Big]$$
$$+\eta\xi^2(1-\cos\beta\cosh\beta)\Big\{(\cos\beta\sinh\beta-\sin\beta\cosh\beta)$$
$$\times[4\{2(1+\cos\alpha\cosh\alpha)+\gamma(\cos\alpha\sinh\alpha-\sin\alpha\cosh\alpha)\}$$
$$\times\{(\cos\alpha\sinh\alpha+\sin\alpha\cosh\alpha)-\gamma(1-\cos\alpha\cosh\alpha)\}$$
$$\times\{(\cos\alpha\sinh\alpha+\sin\alpha\cosh\alpha)+\gamma\cos\alpha\cosh\alpha\}$$
$$+2\{2(\cos\alpha\sinh\alpha+\sin\alpha\cosh\alpha)-\gamma(1-\cos\alpha\cosh\alpha)\}$$
$$\times\{(1+\cos\alpha\cosh\alpha)+\gamma(\cos\alpha\sinh\alpha-\sin\alpha\cosh\alpha)\}$$
$$\times\{(\cos\alpha\sinh\alpha+\sin\alpha\cosh\alpha)+\gamma\cos\alpha\cosh\alpha\}$$
$$+\{2(1+\cos\alpha\cosh\alpha)+\gamma(\cos\alpha\sinh\alpha-\sin\alpha\cosh\alpha)\}$$
$$\times\{(1+\cos\alpha\cosh\alpha)+\gamma(\cos\alpha\sinh\alpha-\sin\alpha\cosh\alpha)\}$$
$$\times\{4\sin\alpha\sinh\alpha+\gamma(\cos\alpha\sinh\alpha+\sin\alpha\cosh\alpha)\}]$$
$$-(\sin\beta-\sinh\beta)\{2(1+\cos\alpha\cosh\alpha)+\gamma(\cos\alpha\sinh\alpha-\sin\alpha\cosh\alpha)\}$$
$$\times\{(\sin\alpha-\sinh\alpha)+\gamma(\cos\alpha-\cosh\alpha)\}$$
$$\times\{2(\sin\alpha-\sinh\alpha)+\gamma(\cos\alpha-\cosh\alpha)\}\Big\}$$
$$-2\xi^3(1-\cos\beta\cosh\beta)^2\{2(1+\cos\alpha\cosh\alpha)+\gamma(\cos\alpha\sinh\alpha-\sin\alpha\cosh\alpha)\}$$
$$\times\{(1+\cos\alpha\cosh\alpha)+\gamma(\cos\alpha\sinh\alpha-\sin\alpha\cosh\alpha)\}$$
$$\times\{(\cos\alpha\sinh\alpha+\sin\alpha\cosh\alpha)+\gamma\cos\alpha\cosh\alpha\}$$

iv) The numerator of $\dfrac{A_1'}{b}$ is

$$
\begin{aligned}
&4\eta^3 \sin\beta \sinh\beta (\cos\beta \sinh\beta - \sin\beta \cosh\beta) \\
&\quad \times \{2(\cos\alpha \sinh\alpha + \sin\alpha \cosh\alpha) - \gamma(1 - \cos\alpha \cosh\alpha)\}^2 \\
&\quad \times \{2\cos\alpha \sinh\alpha - \gamma(1 - \cos\alpha \cosh\alpha + \sin\alpha \sinh\alpha)\} \\
&+\eta^2\xi\{2(\cos\alpha \sinh\alpha + \sin\alpha \cosh\alpha) - \gamma(1 - \cos\alpha \cosh\alpha)\} \\
&\quad \times [2(\cos\beta \sinh\beta - \sin\beta \cosh\beta)(\sin\beta - \sinh\beta) \\
&\quad \times \{(\cos\alpha + \cosh\alpha) - \gamma(\sin\alpha - \sinh\alpha)\} \\
&\quad \times \{2(\sin\alpha - \sinh\alpha) + \gamma(\cos\alpha - \cosh\alpha)\} \\
&\quad -(\cos\beta \sinh\beta - \sin\beta \cosh\beta)^2 \\
&\quad \times \{2(\cos\alpha \sinh\alpha + \sin\alpha \cosh\alpha) - \gamma(1 - \cos\alpha \cosh\alpha)\} \\
&\quad \times \{(1 + \cos\alpha \cosh\alpha - \sin\alpha \sinh\alpha) - 2\gamma \sin\alpha \cosh\alpha\} \\
&\quad -2\{2(\cos\beta \sinh\beta - \sin\beta \cosh\beta)^2 - (\sin\beta - \sinh\beta)^2\} \\
&\quad \times \{2(1 + \cos\alpha \cosh\alpha) + \gamma(\cos\alpha \sinh\alpha - \sin\alpha \cosh\alpha)\} \\
&\quad \{2\cos\alpha \sinh\alpha - \gamma(1 - \cos\alpha \cosh\alpha + \sin\alpha \sinh\alpha)\}] \\
&+2\eta\xi^2(1 - \cos\beta \cosh\beta)\{2(1 + \cos\alpha \cosh\alpha) + \gamma(\cos\alpha \sinh\alpha - \sin\alpha \cosh\alpha)\} \\
&\quad \times \Big\{(\cos\beta \sinh\beta - \sin\beta \cosh\beta) \\
&\quad \times [\{2(1 + \cos\alpha \cosh\alpha) + \gamma(\cos\alpha \sinh\alpha - \sin\alpha \cosh\alpha)\} \\
&\quad \times \{2\cos\alpha \sinh\alpha - \gamma(1 - \cos\alpha \cosh\alpha + \sin\alpha \sinh\alpha)\} \\
&\quad + \{2(\cos\alpha \sinh\alpha + \sin\alpha \cosh\alpha) - \gamma(1 - \cos\alpha \cosh\alpha)\} \\
&\quad \times \{(1 + \cos\alpha \cosh\alpha - \sin\alpha \sinh\alpha) - 2\gamma \sin\alpha \cosh\alpha\}] \\
&\quad -(\sin\beta - \sinh\beta)\{(\cos\alpha + \cosh\alpha) - \gamma(\sin\alpha - \sinh\alpha)\} \\
&\quad \times \{2(\sin\alpha - \sinh\alpha) + \gamma(\cos\alpha - \cosh\alpha)\}\Big\} \\
&-\xi^3(1 - \cos\beta \cosh\beta)\{2(1 + \cos\alpha \cosh\alpha) + \gamma(\cos\alpha \sinh\alpha - \sin\alpha \cosh\alpha)\}^2 \\
&\quad \times \{(1 + \cos\alpha \cosh\alpha - \sin\alpha \sinh\alpha) - \gamma \sin\alpha \cosh\alpha\}
\end{aligned}
$$

v) The numerator of $\dfrac{B_1'}{b}$ is

$$
\begin{aligned}
&4\eta^3 \sin\beta \sinh\beta (\cos\beta \sinh\beta - \sin\beta \cosh\beta) \\
&\quad \times \{2(\cos\alpha \sinh\alpha + \sin\alpha \cosh\alpha) - \gamma(1 - \cos\alpha \cosh\alpha)\}^2 \\
&\quad \times \{2\sin\alpha \sinh\alpha + \gamma(\cos\alpha \sinh\alpha + \sin\alpha \cosh\alpha)\} \\
&+\eta^2\xi\{2(\cos\alpha \sinh\alpha + \sin\alpha \cosh\alpha) - \gamma(1 - \cos\alpha \cosh\alpha)\} \\
&\quad \times [2(\sin\beta - \sinh\beta)(\cos\beta \sinh\beta - \sin\beta \cosh\beta) \\
&\quad \times \{2(\sin\alpha - \sinh\alpha) + \gamma(\cos\alpha - \cosh\alpha)\} \\
&\quad \times \{(\sin\alpha - \sinh\alpha) + \gamma(\cos\alpha - \cosh\alpha)\} \\
&\quad -(\cos\beta \sinh\beta - \sin\beta \cosh\beta)^2 \\
&\quad \times \{2(\cos\alpha \sinh\alpha + \sin\alpha \cosh\alpha) - \gamma(1 - \cos\alpha \cosh\alpha)\} \\
&\quad \times \{(\cos\alpha \sinh\alpha + \sin\alpha \cosh\alpha) + 2\gamma \cos\alpha \cosh\alpha\} \\
&\quad -2\{2(\cos\beta \sinh\beta - \sin\beta \cosh\beta)^2 - (\sin\beta - \sinh\beta)^2\} \\
&\quad \times \{2(1 + \cos\alpha \cosh\alpha) + \gamma(\cos\alpha \sinh\alpha - \sin\alpha \cosh\alpha)\}
\end{aligned}
$$

$$\times\{2\sin\alpha\sinh\alpha+\gamma(\cos\alpha\sinh\alpha+\sin\alpha\cosh\alpha)\}]$$
$$-2\eta\xi^2(1-\cos\beta\cosh\beta)\{2(1+\cos\alpha\cosh\alpha)+\gamma(\cos\alpha\sinh\alpha-\sin\alpha\cosh\alpha)\}$$
$$\times\Big\{(\sin\beta-\sinh\beta)\{2(\sin\alpha-\sinh\alpha)+\gamma(\cos\alpha-\cosh\alpha)\}$$
$$\times\{(\sin\alpha-\sinh\alpha)+\gamma(\cos\alpha-\cosh\alpha)\}$$
$$-(\cos\beta\sinh\beta-\sin\beta\cosh\beta)$$
$$\times[\{2(\cos\alpha\sinh\alpha+\sin\alpha\cosh\alpha)-\gamma(1-\cos\alpha\cosh\alpha)\}$$
$$\times\{(\cos\alpha\sinh\alpha+\sin\alpha\cosh\alpha)+2\gamma\cos\alpha\cosh\alpha\}$$
$$+\{2(1+\cos\alpha\cosh\alpha)+\gamma(\cos\alpha\sinh\alpha-\sin\alpha\cosh\alpha)\}$$
$$\times\{2\sin\alpha\sinh\alpha+\gamma(\cos\alpha\sinh\alpha+\sin\alpha\cosh\alpha\}]\Big\}$$
$$-\xi^3(1-\cos\beta\cosh\beta)^2\{2(1+\cos\alpha\cosh\alpha)+\gamma(\cos\alpha\sinh\alpha-\sin\alpha\cosh\alpha)\}^2$$
$$\times\{(\cos\alpha\sinh\alpha+\sin\alpha\cosh\alpha)+2\gamma\cos\alpha\cosh\alpha\}]$$

vi) $A_1''=A_1$

vii) $B_1''=B_1$

viii) The numerator of $\dfrac{A_2}{b}$ is

$$-4\eta^2\sin\beta\sinh\beta(\cos\beta\sinh\beta-\sin\beta\cosh\beta)$$
$$\times\{2(\cos\alpha\sinh\alpha+\sin\alpha\cosh\alpha)-\gamma(1-\cos\alpha\cosh\alpha)\}$$
$$\times\{(\cos\alpha\sinh\alpha+\sin\alpha\cosh\alpha)-\gamma(1-\cos\alpha\cosh\alpha)\}$$
$$\times\{2(\sin\alpha-\sinh\alpha)+\gamma(\cos\alpha-\cosh\alpha)\}$$
$$+\eta\xi[(\cos\beta\sinh\beta-\sin\beta\cosh\beta)^2$$
$$\times\{2(\cos\alpha\sinh\alpha+\sin\alpha\cosh\alpha)-\gamma(1-\cos\alpha\cosh\alpha)\}$$
$$\times\{(1+\cos\alpha\cosh\alpha)+\gamma(\cos\alpha\sinh\alpha-\sin\alpha\cosh\alpha)\}$$
$$\times\{2(\sin\alpha-\sinh\alpha)+\gamma(\cos\alpha-\cosh\alpha)\}$$
$$+4\sin\beta\sinh\beta(1-\cos\beta\cosh\beta)$$
$$\times2(1+\cos\alpha\cosh\alpha)+\gamma(\cos\alpha\sinh\alpha-\sin\alpha\cosh\alpha)\}$$
$$\times\{(\cos\alpha\sinh\alpha+\sin\alpha\cosh\alpha)-\gamma(1-\cos\alpha\cosh\alpha)\}$$
$$\times\{2(\sin\alpha-\sinh\alpha)+\gamma(\cos\alpha-\cosh\alpha)\}$$
$$+(\sin\beta-\sinh\beta)(\cos\beta\sinh\beta-\sin\beta\cosh\beta)$$
$$\times\{2(1+\cos\alpha\cosh\alpha)+\gamma(\cos\alpha\sinh\alpha-\sin\alpha\cosh\alpha)\}$$
$$\times\{2(\cos\alpha\sinh\alpha+\sin\alpha\cosh\alpha)-\gamma(1-\cos\alpha\cosh\alpha)\}$$
$$\times\{(\sin\alpha-\sinh\alpha)+\gamma(\cos\alpha-\cosh\alpha)\}]$$
$$-\xi^2(1-\cos\beta\cosh\beta)\{2(1+\cos\alpha\cosh\alpha)+\gamma(\cos\alpha\sinh\alpha-\sin\alpha\cosh\alpha)\}$$
$$\times[(\cos\beta\sinh\beta-\sin\beta\cosh\beta)$$
$$\times\{(1+\cos\alpha\cosh\alpha)+\gamma(\cos\alpha\sinh\alpha-\sin\alpha\cosh\alpha)\}$$
$$\times\{2(\sin\alpha-\sinh\alpha)+\gamma(\cos\alpha-\cosh\alpha)\}$$
$$+(\sin\beta-\sinh\beta)\{2(1+\cos\alpha\cosh\alpha)+\gamma(\cos\alpha\sinh\alpha-\sin\alpha\cosh\alpha)\}$$
$$\times\{(\sin\alpha-\sinh\alpha)+\gamma(\cos\alpha-\cosh\alpha)]$$

ix) The numerator of $\dfrac{B_2}{b}$ is

$$2\eta^2\sinh\beta(\cos\beta\sinh\beta-\sin\beta\cosh\beta)$$
$$\times\{2(\cos\alpha\sinh\alpha+\sin\alpha\cosh\alpha)-\gamma(1-\cos\alpha\cosh\alpha)\}$$
$$\times[\{2(\cos\alpha\sinh\alpha+\sin\alpha\cosh\alpha)-\gamma(1-\cos\alpha\cosh\alpha)\}$$
$$\times\{(\sin\alpha-\sinh\alpha)+\gamma(\cos\alpha-\cosh\alpha)\}$$
$$+2\cos\beta\{(\cos\alpha\sinh\alpha+\sin\alpha\cosh\alpha)-\gamma(1-\cos\alpha\cosh\alpha)\}$$
$$\times\{2(\sin\alpha-\sinh\alpha)+\gamma(\cos\alpha-\cosh\alpha)\}]$$
$$-\eta\xi[4\cos\beta\sinh\beta(1-\cos\beta\cosh\beta)$$
$$\times\{2(1+\cos\alpha\cosh\alpha)+\gamma(\cos\alpha\sinh\alpha-\sin\alpha\cosh\alpha)\}$$
$$\times\{(\cos\alpha\sinh\alpha+\sin\alpha\cosh\alpha)-\gamma(1-\cos\alpha\cosh\alpha)\}$$
$$\times\{2(\sin\alpha-\sinh\alpha)+\gamma(\cos\alpha-\cosh\alpha)\}$$
$$+\{2\sinh\beta(1-\cos\beta\cosh\beta)+(\cos\beta\sinh\beta-\sin\beta\cosh\beta)(\cos\beta-\cosh\beta)\}$$
$$\times\{2(1+\cos\alpha\cosh\alpha)+\gamma(\cos\alpha\sinh\alpha-\sin\alpha\cosh\alpha)\}$$
$$\times\{2(\cos\alpha\sinh\alpha+\sin\alpha\cosh\alpha)-\gamma(1-\cos\alpha\cosh\alpha)\}$$
$$\times\{(\sin\alpha-\sinh\alpha)+\gamma(\cos\alpha-\cosh\alpha)\}$$
$$+(1-\cos\beta\cosh\beta-\sin\beta\sinh\beta)(\cos\beta\sinh\beta-\sin\beta\cosh\beta)$$
$$\times\{2(\cos\alpha\sinh\alpha+\sin\alpha\cosh\alpha)-\gamma(1-\cos\alpha\cosh\alpha)\}$$
$$\times\{(1+\cos\alpha\cosh\alpha)+\gamma(\cos\alpha\sinh\alpha-\sin\alpha\cosh\alpha)\}$$
$$\times\{2(\sin\alpha-\sinh\alpha)+\gamma(\cos\alpha-\cosh\alpha)\}]$$
$$+\xi^2(1-\cos\beta\cosh\beta)\{2(1+\cos\alpha\cosh\alpha)+\gamma(\cos\alpha\sinh\alpha-\sin\alpha\cosh\alpha)\}$$
$$\times[(\cos\beta-\cosh\beta)\{2(1+\cos\alpha\cosh\alpha)+\gamma(\cos\alpha\sinh\alpha-\sin\alpha\cosh\alpha)\}$$
$$\times\{(\sin\alpha-\sinh\alpha)+\gamma(\cos\alpha-\cosh\alpha)\}$$
$$+(1-\cos\beta\cosh\beta-\sin\beta\sinh\beta)$$
$$\times\{(1+\cos\alpha\cosh\alpha)+\gamma(\cos\alpha\sinh\alpha-\sin\alpha\cosh\alpha)\}$$
$$\times\{2(\sin\alpha-\sinh\alpha)+\gamma(\cos\alpha-\cosh\alpha)\}]$$

x) The numerator of $\dfrac{D_2}{b}$ is

$$-2\eta^2\sin\beta(\cos\beta\sinh\beta-\sin\beta\cosh\beta)$$
$$\times\{2(\cos\alpha\sinh\alpha+\sin\alpha\cosh\alpha)-\gamma(1-\cos\alpha\cosh\alpha)\}$$
$$\times[\{2(\cos\alpha\sinh\alpha+\sin\alpha\cosh\alpha)-\gamma(1-\cos\alpha\cosh\alpha)\}$$
$$\times\{(\sin\alpha-\sinh\alpha)+\gamma(\cos\alpha-\cosh\alpha)\}$$
$$+2\cosh\beta\{(\cos\alpha\sinh\alpha+\sin\alpha\cosh\alpha)-\gamma(1-\cos\alpha\cosh\alpha)\}$$
$$\times\{2(\sin\alpha-\sinh\alpha)+\gamma(\cos\alpha-\cosh\alpha)\}]$$
$$+\eta\xi[4\sin\beta\cosh\beta(1-\cos\beta\cosh\beta)$$
$$\times\{2(1+\cos\alpha\cosh\alpha)+\gamma(\cos\alpha\sinh\alpha-\sin\alpha\cosh\alpha)\}$$
$$\times\{(\cos\alpha\sinh\alpha+\sin\alpha\cosh\alpha)-\gamma(1-\cos\alpha\cosh\alpha)\}$$
$$\times\{2(\sin\alpha-\sinh\alpha)+\gamma(\cos\alpha-\cosh\alpha)\}$$
$$+\{(\cos\beta-\cosh\beta)(\cos\beta\sinh\beta-\sin\beta\cosh\beta)+2\sin\beta(1-\cos\beta\cosh\beta)\}$$

$$\times\{2(1+\cos\alpha\cosh\alpha)+\beta(\cos\alpha\sinh\alpha-\sin\alpha\cosh\alpha)\}$$
$$\times\{2(\cos\alpha\sinh\alpha+\sin\alpha\cosh\alpha)-\gamma(1-\cos\alpha\cosh\alpha)\}$$
$$\times\{(\sin\alpha-\sinh\alpha)+\gamma(\cos\alpha-\cosh\alpha)\}$$
$$-(1-\cos\beta\cosh\beta+\sin\beta\sinh\beta)(\cos\beta\sinh\beta-\sin\beta\cosh\beta)$$
$$\times\{2(\cos\alpha\sinh\alpha+\sin\alpha\cosh\alpha)-\gamma(1-\cos\alpha\cosh\alpha)\}$$
$$\times\{(1+\cos\alpha\cosh\alpha)+\gamma(\cos\alpha\sinh\alpha-\sin\alpha\cosh\alpha)\}$$
$$\times\{2(\sin\alpha-\sinh\alpha)+\gamma(\cos\alpha-\cosh\alpha)\}]$$
$$+\xi^2(1-\cos\beta\cosh\beta)\{2(1+\cos\alpha\cosh\alpha)+\gamma(\cos\alpha\sinh\alpha-\sin\alpha\cosh\alpha)\}$$
$$\times[(1-\cos\beta\cosh\beta+\sin\beta\sinh\beta)$$
$$\times\{(1+\cos\alpha\cosh\alpha)+\gamma(\cos\alpha\sinh\alpha-\sin\alpha\cosh\alpha)\}$$
$$\times\{2(\sin\alpha-\sinh\alpha)+\gamma(\cos\alpha-\cosh\alpha)\}$$
$$-(\cos\beta-\cosh\beta)\{2(1+\cos\alpha\cosh\alpha)+\gamma(\cos\alpha\sinh\alpha-\sin\alpha\cosh\alpha)\}$$
$$\times\{(\sin\alpha-\sinh\alpha)+\gamma(\cos\alpha-\cosh\alpha)\}]$$

xi) The numerator of $\dfrac{A_2'}{b}$ is

$$-2\eta^2\sin\beta\sinh\beta(\cos\beta\sinh\beta-\sin\beta\cosh\beta)$$
$$\times\{2(\cos\alpha\sinh\alpha+\sin\alpha\cosh\alpha)-\gamma(1-\cos\alpha\cosh\alpha)\}^2$$
$$\times\{(\sin\alpha-\sinh\alpha)+\gamma(\cos\alpha-\cosh\alpha)\}$$
$$+\eta\xi\{2(\cos\alpha\sinh\alpha+\sin\alpha\cosh\alpha)-\gamma(1-\cos\alpha\cosh\alpha)\}$$
$$\times[(\sin\beta-\sinh\beta)(\cos\beta\sinh\beta-\sin\beta\cosh\beta)$$
$$\times\{(1+\cos\alpha\cosh\alpha)+\gamma(\cos\alpha\sinh\alpha-\sin\alpha\cosh\alpha)\}$$
$$\times\{2(\sin\alpha-\sinh\alpha)+\gamma(\cos\alpha-\cosh\alpha)\}$$
$$+\{2\sin\beta\sinh\beta(1-\cos\beta\cosh\beta)+(\cos\beta\sinh\beta-\sin\beta\cosh\beta)^2\}$$
$$\times\{2(1+\cos\alpha\cosh\alpha)+\gamma(\cos\alpha\sinh\alpha-\sin\alpha\cosh\alpha)\}$$
$$\times\{(\sin\alpha-\sinh\alpha)+\gamma(\cos\alpha-\cosh\alpha)\}]$$
$$-\xi^2(1-\cos\beta\cosh\beta)\{2(1+\cos\alpha\cosh\alpha)+\gamma(\cos\alpha\sinh\alpha-\sin\alpha\cosh\alpha)\}$$
$$\times[(\sin\beta-\sinh\beta)\{(1+\cos\alpha\cosh\alpha)+\gamma(\cos\alpha\sinh\alpha-\sin\alpha\cosh\alpha)\}$$
$$\times\{2(\sin\alpha-\sinh\alpha)+\gamma(\cos\alpha-\cosh\alpha)\}$$
$$+(\cos\beta\sinh\beta-\sin\beta\cosh\beta)$$
$$\times\{2(1+\cos\alpha\cosh\alpha)+\gamma(\cos\alpha\sinh\alpha-\sin\alpha\cosh\alpha)\}$$
$$\times\{(\sin\alpha-\sinh\alpha)+\gamma(\cos\alpha-\cosh\alpha)\}]$$

xii) The numerator of $\dfrac{B_2'}{b}$ is

$$2\eta^2\sinh\beta(\cos\beta\sinh\beta-\sin\beta\cosh\beta)$$
$$\times\{2(\cos\alpha\sinh\alpha+\sin\alpha\cosh\alpha)-\gamma(1-\cos\alpha\cosh\alpha)\}$$
$$\times[\cos\beta\{2(\cos\alpha\sinh\alpha+\sin\alpha\cosh\alpha)-\gamma(1-\cos\alpha\cosh\alpha)\}$$
$$\times\{(\sin\alpha-\sinh\alpha)+\gamma(\cos\alpha-\cosh\alpha)\}$$
$$+2\{(\cos\alpha\sinh\alpha+\sin\alpha\cosh\alpha)-\gamma(1-\cos\alpha\cosh\alpha)\}$$

$$\times\{2(\sin\alpha-\sinh\alpha)+\gamma(\cos\alpha-\cosh\alpha)\}]$$

$$-\eta\xi[4\sinh\beta(1-\cos\beta\cosh\beta)$$
$$\times\{2(1+\cos\alpha\cosh\alpha)+\gamma(\cos\alpha\sinh\alpha-\sin\alpha\cosh\alpha)\}$$
$$\times\{(\cos\alpha\sinh\alpha+\sin\alpha\cosh\alpha)-\gamma(1-\cos\alpha\cosh\alpha)\}$$
$$\times\{2(\sin\alpha-\sinh\alpha)+\gamma(\cos\alpha-\cosh\alpha)\}$$

$$+\{4\cos\beta\sinh\beta(1-\cos\beta\cosh\beta)+(\sin\beta-\sinh\beta)(\cos\beta-\cosh\beta)\}$$
$$\times\{2(1+\cos\alpha\cosh\alpha)+\gamma(\cos\alpha\sinh\alpha-\sin\alpha\cosh\alpha)\}$$
$$\times\{2(\cos\alpha\sinh\alpha+\sin\alpha\cosh\alpha)-\gamma(1-\cos\alpha\cosh\alpha)\}$$
$$\times\{(\sin\alpha-\sinh\alpha)+\gamma(\cos\alpha-\cosh\alpha)\}$$

$$+(\cos\beta-\cosh\beta)(\cos\beta\sinh\beta-\sin\beta\cosh\beta)$$
$$\times\{2(\cos\alpha\sinh\alpha+\sin\alpha\cosh\alpha)-\gamma(1-\cos\alpha\cosh\alpha)\}$$
$$\times\{(1+\cos\alpha\cosh\alpha)+\gamma(\cos\alpha\sinh\alpha-\sin\alpha\cosh\alpha)\}$$
$$\times\{2(\sin\alpha-\sinh\alpha)+\gamma(\cos\alpha-\cosh\alpha)\}]$$

$$+\xi^2(1-\cos\beta\cosh\beta)\{2(1+\cos\alpha\cosh\alpha)+\gamma(\cos\alpha\sinh\alpha-\sin\alpha\cosh\alpha)\}$$
$$\times[(1-\cos\beta\cosh\beta-\sin\beta\sinh\beta)$$
$$\times\{2(1+\cos\alpha\cosh\alpha)+\gamma(\cos\alpha\sinh\alpha-\sin\alpha\cosh\alpha)\}$$
$$\times\{(\sin\alpha-\sinh\alpha)+\gamma(\cos\alpha-\cosh\alpha)\}$$
$$+(\cos\beta-\cosh\beta)\{(1+\cos\alpha\cosh\alpha)+\gamma(\cos\alpha\sinh\alpha-\sin\alpha\cosh\alpha)\}$$
$$\times\{2(\sin\alpha-\sinh\alpha)+\gamma(\cos\alpha-\cosh\alpha)\}]$$

xiii) The numerator of $\dfrac{D_2'}{b}$ is

$$-2\eta^2\sin\beta(\cos\beta\sinh\beta-\sin\beta\cosh\beta)$$
$$\times\{2(\cos\alpha\sinh\alpha+\sin\alpha\cosh\alpha)-\gamma(1-\cos\alpha\cosh\alpha)\}$$
$$\times[\cosh\beta\{2(\cos\alpha\sinh\alpha+\sin\alpha\cosh\alpha)-\gamma(1-\cos\alpha\cosh\alpha)\}$$
$$\times\{(\sin\alpha-\sinh\alpha)+\gamma(\cos\alpha-\cosh\alpha)\}$$
$$+2\{(\cos\alpha\sinh\alpha+\sin\alpha\cosh\alpha)-\gamma(1-\cos\alpha\cosh\alpha)\}$$
$$\times\{2(\sin\alpha-\sinh\alpha)+\gamma(\cos\alpha-\cosh\alpha)\}]$$

$$+\eta\xi[4\sin\beta(1-\cos\beta\cosh\beta)$$
$$\times\{2(1+\cos\alpha\cosh\alpha)+\gamma(\cos\alpha\sinh\alpha-\sin\alpha\cosh\alpha)\}$$
$$\times\{(\cos\alpha\sinh\alpha+\sin\alpha\cosh\alpha)-\gamma(1-\cos\alpha\cosh\alpha)\}$$
$$\times\{2(\sin\alpha-\sinh\alpha)+\gamma(\cos\alpha-\cosh\alpha)\}$$

$$+\{4\sin\beta\cosh\beta(1-\cos\beta\cosh\beta)+(\sin\beta-\sinh\beta)(\cos\beta-\cosh\beta)\}$$
$$\times\{2(1+\cos\alpha\cosh\alpha)+\gamma(\cos\alpha\sinh\alpha-\sin\alpha\cosh\alpha)\}$$
$$\times\{2(\cos\alpha\sinh\alpha+\sin\alpha\cosh\alpha)-\gamma(1-\cos\alpha\cosh\alpha)\}$$
$$\times\{(\sin\alpha-\sinh\alpha)+\gamma(\cos\alpha-\cosh\alpha)\}$$

$$+(\cos\beta-\cosh\beta)(\cos\beta\sinh\beta-\sin\beta\cosh\beta)$$
$$\times\{2(\cos\alpha\sinh\alpha+\sin\alpha\cosh\alpha)-\gamma(1-\cos\alpha\cosh\alpha)\}$$

$$\times\{(1+\cos\alpha\cosh\alpha)+\gamma(\cos\alpha\sinh\alpha-\sin\alpha\cosh\alpha)\}$$
$$\times\{2(\sin\alpha-\sinh\alpha)+\gamma(\cos\alpha-\cosh\alpha)\}]$$
$$+\xi^2(1-\cos\beta\cosh\beta)\{2(1+\cos\alpha\cosh\alpha)+\gamma(\cos\alpha\sinh\alpha-\sin\alpha\cosh\alpha)\}.$$
$$\times[(1-\cos\beta\cosh\beta+\sin\beta\sinh\beta)$$
$$\times\{2(1+\cos\alpha\cosh\alpha)+\gamma(\cos\alpha\sinh\alpha-\sin\alpha\cosh\alpha)\}$$
$$\times\{(\sin\alpha-\sinh\alpha)+\gamma(\cos\alpha-\cosh\alpha)\}$$
$$-(\cos\beta-\cosh\beta)\{(1+\cos\alpha\cosh\alpha)+\gamma(\cos\alpha\sinh\alpha-\sin\alpha\cosh\alpha)\}$$
$$\times\{2(\sin\alpha-\sinh\alpha)+\gamma(\cos\alpha-\cosh\alpha)\}]$$

The general expressions of the displacements of all members are

$$y_1=\{A_1(\cos m_1x_1-\cosh m_1x_1)+B_1(\sin m_1x_1-\sinh m_1x_1)\}\cos p't,$$
$$y_1'=\{A_1'(\cos m_1x_1'-\cosh m_1x_1')+B_1'(\sin m_1x_1'-\sinh m_1x_1')\}\cos p't,$$
$$y_1''=\{A_1''(\cos m_1x_1''-\cosh m_1x_1'')+B_1''(\sin m_1x_1''-\sinh m_1x_1'')\}\cos p't,$$
$$y_2=\{A_2(\cos m_2x_2-\cosh m_2x_2)+B_2\sin m_2x_2+D_2\sinh m_2x_2\}\cos p't,$$
$$y_2'=\{A_2'(\cos m_2x_2'-\cosh m_2x_2')+B_2'\sin m_2x_2'+D_2'\sinh m_2x_2'\}\cos p't.$$

As an example of calculation we have taken up the case $\rho_1/\rho_2=1$, $\alpha=1$ and plotted the result in the following figure. From this result, it may be seen that the distribution of the displacement is the same as that in the case of the framed structure with an infinite number of spans. The transverse deflection of the beam is very small in comparison with that

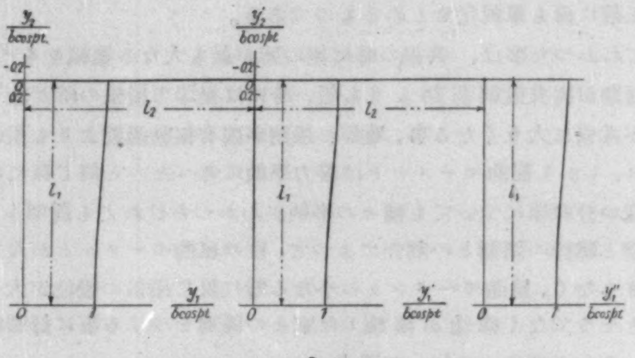

Fig. 36. $\frac{\rho_1}{\rho_2}=1,\quad \alpha=1.$

of the pillar. This fact has been found also in the case of the structure of infinite number of spans. At any rate, it is not without importance that the natural periods as well as the deformation due to forced vibration of a framed structure with two spans are the same as those of the structure with an infinite number of spans. It is clear that the case of three or more spans far approximates to that of the infinite number of

spans, so that it seems that the treatment of the case of an infinite number of spans covers practically all the problems of horizontal vibrations of framed structures with any number (larger than two) of spans in general.

---

49. 單層架構構造の震動

地震研究所 { 妹澤克惟
金井清

架構構造の振動問題は内外の多くの學者によつて手をつけられて居るが、力學上や境界條件の立場から見て完全なものが殆ど見つからない。著者の一人が帶板を有するタービン翼の振動問題に試みた方法は建築構造が水平地震動を受ける場合の振動にも應用出來る事がわかつた。それで著者等は建築其他の構造物にあてはまる樣な種々の場合を計算して見た所が其手續きは非常に面倒ではあつたけれども、しかし重要なる二三の結論に到達した。

計算を行つた場合といふのは張間が無限にある時の固有振動と其强制振動、張間が二つある時の同じく固有振動と强制振動とでわるが、張間が二つある時のすべての問題は其が無限にある時のそれに近いといふ事がわかつた事は、張間が二つ以上幾個ある時でも無限にある時と同じに見て計算をしてよいといふ事を示すものであつて、現在の計算が何等の假定のなき根據を有するものだけに今後の斯る計算を正確に而も單純化せしめるものである。

又振動問題としてわかつた事は、共振の時に梁の所が最も大なる振幅をもつ事はいふ迄もなく、地震の週期的振動週期が固有振動週期よりも短い時には梁即ち屋根の所が餘り搖れなくて寧ろ柱の屈曲モーメントが非常に大きくなる事、地震の週期が固有振動週期よりも長い時には屋根が地動と同じく大きく搖れ、しかし屈曲モーメントは靜力學的に考へたのと同じ樣になる事などもわかつた。其他質量や剛度の分布等についても種々の事柄がわかつたけれども説明を省略して置いた。終りに、地震動の週期と建物の週期との割合によつて、柱の屈曲モーメントが大になつた時には屋根の變位がそれ程大きくなく、屈曲モーメントの小なる時に反て屋根の變位が大きくなる事は地震の時に瓦の落ちた家とそうでなく構造が破壞した家との區別をつける事に好都合であらうといふ事を寺田先生から敎へられた事をつけ加へて置く。

Corrigenda to the Bull. Earthq. Res. Inst.

Volume	Part	Page	Line	for	read	Discoverer
IX	4	400	3			
〃	〃	405	14	$e^{\left(\frac{1}{4}+\frac{p}{2k}\right)}$	$e^{-\left(\frac{1}{2}+\frac{p}{2k}\right)}$	
〃	〃	406	23			C. Tsuboi
〃	〃	403	7			
〃	〃	405	16	$e^{\left(\frac{1}{6}+\frac{p}{2k}\right)}$	$e^{-\left(\frac{2}{3}+\frac{p}{2k}\right)}$	
〃	〃	406	24			
X	2	305	4, 7, 9, 11, 13, 15	$(-1)^m \frac{d^m P_n(\cos\theta)}{d\theta^m}$	$P_n^m(\cos\theta)$	H. Kawasumi
〃	2	306	1, 3, 5			

These errors are not effective on remaining parts of the respective papers.

50. *Reflection and Refraction of Seismic Waves in a Stratified Body.*

AERONAUTICAL RESEARCH INSTITUTE
LIBRARY
JAN 7
TOKYO

By Katsutada SEZAWA and Kiyoshi KANAI,

Earthquake Research Institute.

(Read Sept. 20, 1932.—Received Sept. 20, 1932.)

Recently Dr. T. Suzuki[1] found from records of seismic observation the fact that the apparent angle of incidence of longitudinal waves of short vibration periods is relatively small while that angle corresponding to large periods is not small. He concluded that this fact may be due to the refractive character of surface layer of the earth. His result suggested us to solve the problem of reflection and refraction of obliquely incident seismic waves at the boundary surfaces of a stratified semi-infinitely body.

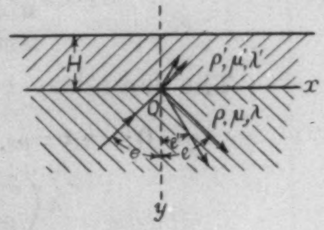

Fig. 1.

Let ϕ, ψ, ϕ', ψ' be wave functions of longitudinal and transverse waves in the bottom medium and the stratified layer. If the primary incident waves are longitudinal and expressed by

$$\phi = Ae^{if(x-\alpha y-nt)} \quad \cdots\cdots\cdots\cdots\cdots\cdots \quad (1)$$

where α is cotangent of the angle of incidence and fn is circular frequency of the vibratory motion of waves, the general expressions of ϕ, ψ, ϕ', ψ' are denoted by

$$\left.\begin{aligned} \phi &= Ae^{if(x-\alpha y-nt)} + A_1 e^{if(x+\alpha y-nt)}, \\ \psi &= B_1 e^{if(x+\beta y-nt)}, \\ \phi' &= (Ce^{\gamma y} + De^{-\gamma y})\, e^{if(x-nt)}, \\ \psi' &= (Ee^{\delta y} + Fe^{-\delta y})\, e^{if(x-nt)}. \end{aligned}\right\} \quad \cdots\cdots\cdots (2)$$

in which β is cotangent of the reflective angle of the reflected transverse waves; and A_1, B_1, C, D, E, F are arbitrary constants to be determined.

From the equations of the vibratory motion of elastic bodies:

---

1) T. SUZUKI, *Bull. Earthq. Res. Inst.*, 10 (1932), 517–530.

$$\left.\begin{aligned} \rho\frac{\partial^2\phi}{\partial t^2}&=(\lambda+2\mu)\left(\frac{\partial^2\phi}{\partial x^2}+\frac{\partial^2\phi}{\partial y^2}\right),\quad \rho\frac{\partial^2\psi}{\partial t^2}=\mu\left(\frac{\partial^2\psi}{\partial x^2}+\frac{\partial^2\psi}{\partial y^2}\right),\\ \rho'\frac{\partial^2\phi'}{\partial t^2}&=(\lambda'2\mu')\left(\frac{\partial^2\phi'}{\partial x^2}+\frac{\partial^2\phi'}{\partial y^2}\right),\quad \rho'\frac{\partial^2\psi'}{\partial t^2}=\mu'\left(\frac{\partial^2\psi'}{\partial x^2}+\frac{\partial^2\psi'}{\partial y^2}\right),\end{aligned}\right\}\quad\cdots(3)$$

we find

$$\left.\begin{aligned} n^2&=\frac{\lambda+2\mu}{\rho}(1+\alpha^2)=\frac{\mu}{\rho}(1+\beta^2),\\ r^2&=f^2\left(1-\frac{\rho' n^2}{\lambda'+2\mu'}\right),\quad s^2=f^2\left(1-\frac{\rho' n^2}{\mu'}\right).\end{aligned}\right\}\quad\cdots\cdots\cdots(4)$$

The horizontal and vertical components of the displacements in the bottom medium and in the layer are determined from

$$\left.\begin{aligned} u_1&=\frac{\partial\phi}{\partial x}+\frac{\partial\psi}{\partial y},\quad v_1=\frac{\partial\phi}{\partial y}-\frac{\partial\psi}{\partial x},\\ u_2&=\frac{\partial\phi'}{\partial x}+\frac{\partial\psi'}{\partial y},\quad v_2=\frac{\partial\phi'}{\partial y}-\frac{\partial\psi'}{\partial x}.\end{aligned}\right\}\quad\cdots\cdots\cdots\cdots(5)$$

The boundary conditions are such that

$$\left.\begin{aligned} y=0;\quad & u_1=u_2,\quad v_1=v_2,\\ & \lambda\left(\frac{\partial u_1}{\partial x}+\frac{\partial v_1}{\partial y}\right)+2\mu\frac{\partial v_1}{\partial y}=\lambda'\left(\frac{\partial u_2}{\partial x}+\frac{\partial v_2}{\partial y}\right)+2\mu'\frac{\partial v_2}{\partial y},\\ & \mu\left(\frac{\partial v_1}{\partial x}+\frac{\partial u_1}{\partial y}\right)=\mu'\left(\frac{\partial v_2}{\partial x}+\frac{\partial u_2}{\partial y}\right),\end{aligned}\right\}\quad(6)$$

$$\left.\begin{aligned} y=-H;\quad & \lambda'\left(\frac{\partial u_2}{\partial x}+\frac{\partial v_2}{\partial y}\right)+2\mu'\frac{\partial v_2}{\partial y}=0,\\ & \frac{\partial v_2}{\partial x}+\frac{\partial u_2}{\partial y}=0.\end{aligned}\right\}\quad\cdots\cdots\cdots\cdots\cdots\cdots(7)$$

Substituting from (2), (5) in (6), (7), we get

$$A_1+\beta B_1-C-D+i\frac{s}{f}E-i\frac{s}{f}F=-A,$$

$$\alpha A_1-B_1+i\frac{r}{f}C-i\frac{r}{f}D+E+F=\alpha A,$$

$$-\left\{\frac{\lambda}{\mu}(1+\alpha^2)+2\alpha^2\right\}A_1+2\beta B_1-\left\{\frac{\lambda'}{\mu}\left(\frac{r^2}{f^2}-1\right)+\frac{2\mu'}{\mu}\cdot\frac{r^2}{f^2}\right\}C-\left\{\frac{\lambda'}{\mu}\left(\frac{r^2}{f^2}-1\right)\right.$$

$$\left.+\frac{2\mu'}{\mu}\cdot\frac{r^2}{f^2}\right\}D+2i\frac{\mu'}{\mu}\cdot\frac{s}{f}E-2i\frac{\mu'}{\mu}\cdot\frac{s}{f}F=\left\{\frac{\lambda}{\mu}(1+\alpha^2)+2\alpha^2\right\}A,$$

$$2\alpha A_1+(\beta^2-1)B_1+2i\frac{\mu'}{\mu}.\frac{r}{f}C-2i\frac{\mu'}{\mu}.\frac{r}{f}D+\frac{\mu'}{\mu}\left(\frac{s^2}{f^2}+1\right)E$$
$$+\frac{\mu'}{\mu}\left(\frac{s^2}{f^2}+1\right)F=2\alpha A,$$

$$\left\{\frac{\lambda'}{\mu'}\left(\frac{r^2}{f^2}-1\right)+2\frac{r^2}{f^2}\right\}e^{-rH}C+\left\{\frac{\lambda'}{\mu'}\left(\frac{r^2}{f^2}-1\right)+2\frac{r^2}{f^2}\right\}e^{rH}D-2i\frac{s}{f}e^{-sH}E$$
$$+2i\frac{s}{f}e^{sH}F=0,$$

$$2i\frac{r}{f}e^{-rH}C-2i\frac{r}{f}e^{rH}D+\left(\frac{s^2}{f^2}+1\right)e^{-sH}E+\left(\frac{s^2}{f^2}+1\right)e^{sH}F=0. \quad (8)$$

From these equations the values of A_1, B_1, C, D, E, F are determined as functions of A, fH, α. For the sake of simplicity we put $\rho=\rho'$, $\lambda=\mu$, $\lambda'=\mu'$, $\mu=2\mu'$, $\alpha=\cot\frac{\pi}{4}$. Then we get

$$A_1=[\{1186{\cdot}354-341{\cdot}320\cos(a+b)-2304{\cdot}171\cos(a-b)\}$$
$$+i\{307{\cdot}890\sin(a+b)-2491{\cdot}920\sin(a-b)\}]\frac{A}{G},$$

$$B_1=2\{976{\cdot}565+333{\cdot}954\cos(a+b)+343{\cdot}954\cos(a-b)\}\frac{A}{G},$$

$$C=3[\{161{\cdot}618-28{\cdot}625\cos(a+b)-620{\cdot}688\cos(a-b)\}$$
$$+i\{28{\cdot}625\sin(a+b)-620{\cdot}688\sin(a-b)\}]\frac{A}{G},$$

$$D=3[\{95{\cdot}286+991{\cdot}055\cos(a+b)+17{\cdot}932\cos(a-b)\}$$
$$+i\{-991{\cdot}055\sin(a+b)-17{\cdot}932\sin(a-b)\}]\frac{A}{G},$$

$$E=3[\{558{\cdot}342+88{\cdot}330\cos(a+b)+93{\cdot}829\cos(a-b)\}$$
$$+i\{88{\cdot}330\sin(a+b)-93{\cdot}829\sin(a-b)\}]\frac{A}{G},$$

$$F=3[\{16{\cdot}126-149{\cdot}820\cos(a+b)-55{\cdot}320\cos(a-b)\}$$
$$+i\{149{\cdot}820\sin(a+b)-55{\cdot}320\sin(a-b)\}]\frac{A}{G},$$

$$\ldots\ldots\ldots(9)$$

where

$$G=\{611{\cdot}904+4104{\cdot}738\cos(a+b)+441{\cdot}887\cos(a-b)\}$$
$$+i\{-3978{\cdot}738\sin(a+b)+192{\cdot}852\sin(a-b)\},\ldots.(10)$$

and $a=rH$, $b=sH$.

The displacement of a point ($x=0$) on the surface $y=H$ is obtained by using (2) and (5). We are to take real parts of complex forms of

expressions of u_2 and v_2. These real parts correspond with the primary waves:

$$\left.\begin{aligned} u_{10} &= -Af\sin f(x-\alpha y-nt), \\ v_{10} &= Af\alpha\sin f(x-\alpha y-nt). \end{aligned}\right\} \qquad \cdots\cdots\cdots\cdots(11)$$

As the length (L) of the primary waves is $2\pi f/\sqrt{1+\alpha^2}$, we find $fH=\dfrac{2\pi}{\sqrt{1+\alpha^2}}\dfrac{H}{L}$. We have calculated three cases of fH, namely $fH=1$, $fH=100$, $fH=\dfrac{1}{100}$, the result being shown in Figs. 2, 3, 4. In these figures, the respective upper curves indicate the variation of u- and v-components with respect to time, while the lower ones give the orbits of a certain point on the surface of the body, U_0 being the amplitude of the primary waves.

It will be seen that when the primary waves are long compared with the thickness of the layer, the motion of a point on the surface is approximately similar to that of these primary waves. The apparent incidence angle on the surface is somewhat different from the incidence angle of the primary waves. When the length of primary waves is

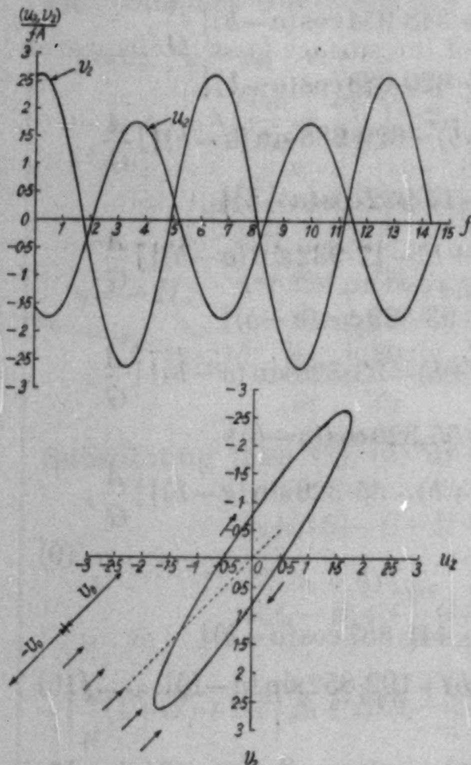

Fig. 2.

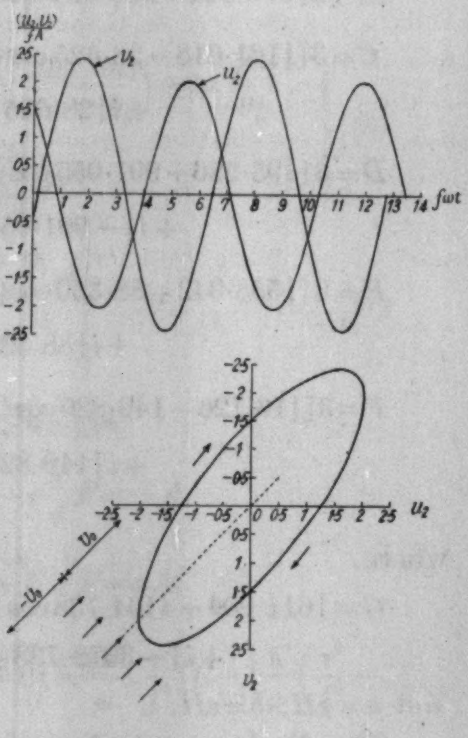

Fig. 3.

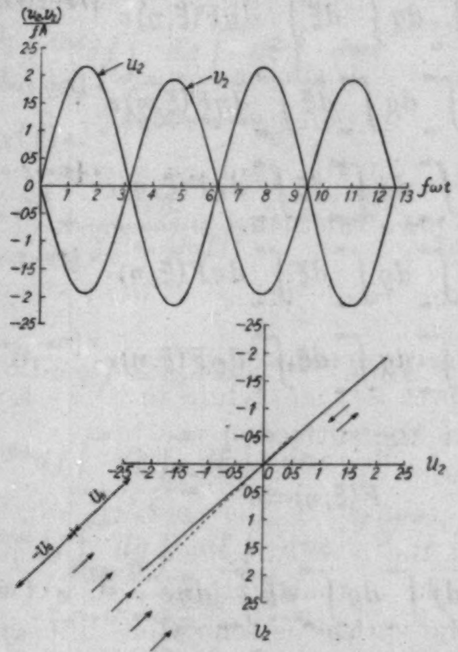

Fig. 4.

small in comparison with the thickness of the surface layer, the apparent angle of incidence becomes small as Dr. Suzuki pointed out. It is remarkable fact that the ratio of length of the minor axis to that of the major axis is relartively great for small wave length. For very large wave length the length of the minor axis is approximately zero.

The movement of ground due to an arbitrary disturbance may be found by applying Fourier's integral expression, namely

$$F(x,y)=\frac{1}{\pi^2}\int_0^\infty dp\int_0^\infty dq\int_{-\infty}^\infty d\xi\int_{-\infty}^\infty d\eta F(\xi,\eta)\cos p(x-\xi)\cos q(y-\eta)$$

$$=\frac{1}{4\pi^2}\int_{-\infty}^\infty dp\int_{-\infty}^\infty dq\int_{-\infty}^\infty d\xi\int_{-\infty}^\infty d\eta F(\xi,\eta)\,e^{ip(x-\xi)}\,e^{-iq(y-\eta)}. \quad \ldots.(12)$$

We find thus

$$\phi_1=F(x,y,t)=\frac{1}{4\pi^2}\int_{-\infty}^\infty df\int_{-\infty}^\infty d(f\alpha)\int_{-\infty}^\infty d\xi\int_{-\infty}^\infty d\eta F(\xi,\eta)\,e^{if(x-\xi)}\,e^{-i(f\alpha)(y-\eta)}\,e^{-if\kappa t}$$

$$(f\alpha=g)$$

$$=\frac{1}{4\pi^2}\int_{-\infty}^\infty e^{-if\kappa t}df\int_{-\infty}^\infty dg\int_{-\infty}^\infty d\xi\int_{-\infty}^\infty d\eta F(\xi,\eta)\,e^{i\{f(x-\xi)-g(y-\eta)\}},$$

$$\phi=\phi_1+\frac{1}{4\pi^2}\int_{-\infty}^\infty \frac{A_1}{A}e^{-if\kappa t}df\int_{-\infty}^\infty dg\int_{-\infty}^\infty d\xi\int_{-\infty}^\infty d\eta F(\xi,\eta)\,e^{i\{f(x-\xi)+g(y+\eta)\}},$$

$$\psi=\frac{1}{4\pi^2}\int_{-\infty}^{\infty}\frac{B_1}{A}e^{-ifnt}df\int_{-\infty}^{\infty}dg\int_{-\infty}^{\infty}d\xi\int_{-\infty}^{\infty}d\eta F(\xi,\eta)\,e^{i\left\{f(x-\xi)+g\left(\frac{\beta}{\alpha}y+\eta\right)\right\}},$$

$$\phi'=\frac{1}{4\pi^2}\int_{-\infty}^{\infty}\frac{C}{A}e^{-ifnt}df\int_{\infty}^{\infty}dg\int_{-\infty}^{\infty}d\xi\int_{-\infty}^{\infty}d\eta F(\xi,\eta)\,e^{i\{f(x-\xi)+g\eta\}+\frac{g}{\alpha}\sqrt{1-\frac{\rho' n^2}{\lambda'+2\mu'}}\,y}$$

$$+\frac{1}{4\pi^2}\int_{-\infty}^{\infty}\frac{D}{A}e^{-ifnt}df\int_{-\infty}^{\infty}dg\int_{-\infty}^{\infty}d\xi\int_{-\infty}^{\infty}d\eta F(\xi,\eta)\,e^{i\{f(x-\xi)+g\eta\}-\frac{g}{\alpha}\sqrt{1-\frac{\rho' n^2}{\lambda'+2\mu'}}\,y},$$

$$\psi'=\frac{1}{4\pi^2}\int_{-\infty}^{\infty}\frac{E}{A}e^{-ifnt}df\int_{-\infty}^{\infty}dg\int_{-\infty}^{\infty}d\xi\int_{-\infty}^{\infty}d\eta F(\xi,\eta)\,e^{i\{f(x-\xi)+g\eta\}+\frac{g}{\alpha}\sqrt{1-\frac{\rho' n^2}{\mu'}}\,y}$$

$$+\frac{1}{4\pi^2}\int_{-\infty}^{\infty}\frac{E}{A}e^{-ifnt}df\int_{-\infty}^{\infty}dg\int_{-\infty}^{\infty}d\xi\int_{-\infty}^{\infty}d\eta F(\xi,\eta)\,e^{i\{f(x-\xi)+g\eta\}-\frac{g}{\alpha}\sqrt{1-\frac{\rho' n^2}{\mu'}}\,y}$$

$$\qquad\qquad\qquad\qquad\qquad\qquad\qquad\qquad\qquad\qquad\dots\dots\dots\dots(13)$$

Put

$$F(\xi,\eta)=e^{-\frac{(\xi-a\eta)^2}{c^2}},\quad\dots\dots\dots\dots(14)$$

then we get

$$\phi_1=\frac{1}{4\pi^2}\int_{-\infty}^{\infty}e^{-ifnt}df\int_{-\infty}^{\infty}dg\int_{-\infty}^{\infty}d\xi\int_{-\infty}^{\infty}d\eta\, e^{-\frac{(\xi-a\eta)^2}{c^2}}e^{i\{f(x-\xi)-g(y-\eta)\}}$$

$$=\frac{c}{4\pi^{3/2}\alpha}\int_{-\infty}^{\infty}e^{-if(x-nt)}df\int_{-\infty}^{\infty}e^{-\frac{c^2}{4a^2}g^2+ig\left(\frac{\xi}{a}-y\right)}dg\int_{-\infty}^{\infty}e^{-if\xi}d\xi$$

$$=\frac{1}{2\pi}\int_{-\infty}^{\infty}e^{-if(x-nt)}df\int_{-\infty}^{\infty}e^{-\frac{(\xi-a\eta)^2}{c^2}-if\xi}d\xi$$

$$=\frac{c}{2\sqrt{\pi}}\int_{-\infty}^{\infty}e^{-\frac{c^2}{4}f^2-if(x-ay-nt)}df$$

$$=e^{-\frac{(x-ay-nt)^2}{c^2}}.$$

Similarly we obtain

$$\phi=\phi_1+\frac{1}{4\pi^2}\int_{-\infty}^{\infty}\frac{A_1}{A}e^{-ifnt}df\int_{-\infty}^{\infty}dg\int_{-\infty}^{\infty}d\xi\int_{-\infty}^{\infty}e^{-\frac{(\xi-a\eta)^2}{c^2}}e^{i\{f(x-\xi)+g(y+\eta)\}}d\eta$$

$$=\phi_1+\frac{c}{2\sqrt{\pi}}\int_{-\infty}^{\infty}F(f)\,e^{-\frac{c^2}{4}f^2+if(x+ay-nt)}df$$

$$=e^{-\frac{(x-ay-nt)^4}{c^2}}$$

$$+a_1e^{-\frac{(x+ay-nt)^2}{c^2}}+\frac{cb_1}{\sqrt{c^2+4h_1H^2}}e^{-\frac{(x+ay-nt)^2}{c^2+4h_1H^2}}+\frac{cd_1}{\sqrt{c^2+4k_1H^2}}e^{-\frac{(x+ay-nt)^2}{c^2+4k_1H^2}},$$

$$\qquad\qquad\qquad\qquad\qquad\qquad\qquad\qquad\qquad\qquad\dots\dots\dots\dots(16)$$

where use is made of the approximate formula

$$\frac{A_1}{A}=F(f)=a_1+b_1e^{-h_1(fH)^2}+d_1e^{-k_1(fH)^2}.\quad\dots\dots\dots(17)$$

In the same manner of treatment we get

$$\psi=\frac{1}{4\pi^2}\int_{-\infty}^{\infty}\frac{B_1}{A}e^{-ifnt}df\int_{-\infty}^{\infty}dg\int_{-\infty}^{\infty}d\xi\int_{-\infty}^{\infty}d\eta\, c^{-\frac{(\xi-\alpha\eta)^2}{c^2}}e^{i\left\{f(x-\xi)+g\left(\frac{\beta}{\alpha}y+\eta\right)\right\}}$$

$$=\frac{c}{2\sqrt{\pi}}\int_{-\infty}^{\infty}\chi(f)\,e^{-\frac{c^2}{4}f^2+if(x+\beta y-nt)}df$$

$$=a_2e^{-\frac{(x+\beta y-nt)^2}{c^2}}+\frac{cb_2}{\sqrt{c^2+4h_2H^2}}e^{-\frac{(x+\beta y-nt)^2}{c^2+4h_2H^2}}+\frac{cd_2}{\sqrt{c^2+4k_2H^2}}e^{-\frac{(x+\beta y-nt)^2}{c^2+4k_2H^2}},$$

$$\qquad\ldots\ldots\ldots\ldots(18)$$

where

$$\frac{B_1}{A}=\chi(f)=a_2+b_2e^{-h_2(fH)^2}+d_2e^{-k_2(fH)^2},$$

$$\phi'=\frac{1}{4\pi^2}\int_{-\infty}^{\infty}\frac{C}{A}e^{-ifnt}df\int_{-\infty}^{\infty}dg\int_{-\infty}^{\infty}d\xi\int_{-\infty}^{\infty}d\eta\, e^{-\frac{(\xi-\alpha\eta)^2}{c^2}}e^{i\{f(x-\xi)+g\eta\}+\frac{g}{\alpha}\sqrt{1-\frac{\rho' n^2}{\lambda'+2\mu'}}\,y}$$

$$+\frac{1}{4\pi^2}\int_{-\infty}^{\infty}\frac{D}{A}e^{-ifnt}df\int_{-\infty}^{\infty}dg\int_{-\infty}^{\infty}d\xi\int_{-\infty}^{\infty}d\eta\, e^{-\frac{(\xi-\alpha\eta)^2}{c^2}}e^{i\{f(x-\xi)+g\eta\}-\frac{g}{\alpha}\sqrt{1-\frac{\rho' n^2}{\lambda'+2\mu'}}\,y}$$

$$=\frac{c}{2\sqrt{\pi}}\int_{-\infty}^{\infty}\Phi(f)\,e^{-\frac{c^2}{4}f^2+if\left(x+\sqrt{\frac{\rho' n^2}{\lambda'+2\mu'}-1}\,y-nt\right)}df$$

$$+\frac{c}{2\sqrt{\pi}}\int_{-\infty}^{\infty}\Phi'(f)\,e^{-\frac{c^2}{4}f^2+if\left(x-\sqrt{\frac{\rho' n^2}{\lambda'+2\mu'}-1}\,y-nt\right)}df$$

$$=a_3e^{-\frac{\left(x+\sqrt{\frac{\rho' n^2}{\lambda'+2\mu'}-1}\,y-nt\right)^2}{c^2}}+\frac{cb_3}{\sqrt{c^2+4h_3H^2}}e^{-\frac{\left(x+\sqrt{\frac{\rho' n^2}{\lambda'+2\mu'}-1}\,y-nt\right)^2}{c^2+4h_3H^2}}$$

$$+\frac{cd_3}{\sqrt{c^2+4k_3H^2}}e^{-\frac{\left(x+\sqrt{\frac{\rho' n^2}{\lambda'+2\mu'}-1}\,y-nt\right)^2}{c^2+4k_3H^2}}$$

$$+a_4e^{-\frac{\left(x-\sqrt{\frac{\rho' n^2}{\lambda'+2\mu'}-1}\,y-nt\right)^2}{c^2}}+\frac{cb_4}{\sqrt{c^2+4h_4H^2}}e^{-\frac{\left(x-\sqrt{\frac{\rho' n^2}{\lambda'+2\mu'}-1}\,y-nt\right)^2}{c^2+4h_4H^2}}$$

$$+\frac{cd_4}{\sqrt{c^2+4k_4H^2}}e^{-\frac{\left(x-\sqrt{\frac{\rho' n^2}{\lambda'+2\mu'}-1}\,y-nt\right)^2}{c^2+4k_4H^2}},\quad\ldots\ldots(19)$$

where

$$\left.\begin{aligned}\frac{C}{A}&=\Phi(f)=a_3+b_3e^{-h_3(fH)^2}+d_3e^{-k_3(fH)^2},\\ \frac{D}{A}&=\Phi'(f)=a_4+b_4e^{-h_4(fH)^2}+d_4e^{-k_4(fH)^2},\end{aligned}\right\}\ldots\ldots\ldots\ldots(20)$$

$$\psi'=\frac{1}{4\pi^2}\int_{-\infty}^{\infty}\frac{E}{A}e^{-ifnt}df\int_{-\infty}^{\infty}dg\int_{-\infty}^{\infty}d\xi\int_{-\infty}^{\infty}d\eta\, e^{-\frac{(\xi-\alpha\eta)^2}{c^2}}e^{i\{f(x-\xi)+g\eta\}+\frac{g}{\alpha}\sqrt{1-\frac{\rho' n^2}{\mu'}}\,y}$$

$$+\frac{1}{4\pi^2}\int_{-\infty}^{\infty}\frac{F}{A}e^{-ifnt}df\int_{-\infty}^{\infty}dg\int_{-\infty}^{\infty}d\xi\int_{-\infty}^{\infty}d\eta\, e^{-\frac{(\xi-\alpha\eta)^2}{c^2}}e^{i\{f(x-\xi)+gy\}-\frac{g}{a}\sqrt{1-\frac{\rho' n^2}{\mu'}}\,y}$$

$$=\frac{c}{2\sqrt{\pi}}\int_{-\infty}^{\infty}\Psi(f)\,e^{-\frac{c^2}{4}f^2+if\left(x+\sqrt{\frac{\rho' n^2}{\mu'}-1}\,y-nt\right)}df$$

$$+\frac{c}{2\sqrt{\pi}}\int_{-\infty}^{\infty}\Psi'(f)\,e^{-\frac{c^2}{4}f^2+if\left(x-\sqrt{\frac{\rho' n^2}{\mu'}-1}\,y-nt\right)}df$$

$$=a_5 e^{-\frac{\left(x+\sqrt{\frac{\rho' n^2}{\mu'}-1}\,y-nt\right)^2}{c^2}}+\frac{cb_5}{\sqrt{c^2+4h_5H^2}}e^{-\frac{\left(x+\sqrt{\frac{\rho' n^2}{\mu'}-1}\,y-nt\right)^2}{c^2+4h_5H^2}}$$

$$+\frac{cd_5}{\sqrt{c^2+4k_5H^2}}c^{-\frac{\left(x+\sqrt{\frac{\rho' n^2}{\mu'}-1}\,y-nt\right)^2}{c^2+4k_5H^2}}$$

$$=a_6 e^{-\frac{\left(x-\sqrt{\frac{\rho' n^2}{\mu'}-1}\,y-nt\right)^2}{c^2}}+\frac{cb_6}{\sqrt{c^2+4h_6H^2}}e^{-\frac{\left(x-\sqrt{\frac{\rho' n^2}{\mu'}-1}\,y-nt\right)^2}{c^2+4h_6H^2}}$$

$$+\frac{cd_6}{\sqrt{c^2+4k_6H^2}}e^{-\frac{\left(x-\sqrt{\frac{\rho' n^2}{\mu'}-1}\,y-nt\right)^2}{c^2+4k_6H^2}}, \quad \dots\dots\dots(21)$$

where

$$\left.\begin{aligned}\frac{E}{A}&=\Psi(f)=a_5+b_5e^{-h_5(fH)^2}+d_5e^{-k_5(fH)^2},\\ \frac{F}{A}&=\Psi'(f)=a_6+b_6e^{-h_5(fH)^2}+d_6e^{-k_5(fH)^2}.\end{aligned}\right\}\quad\dots\dots\dots\ (22)$$

By means of the formula:

$$\left.\begin{aligned}u_1&=\frac{\partial\phi}{\partial x}+\frac{\partial\psi}{\partial y},\quad v_1=\frac{\partial\phi}{\partial y}-\frac{\partial\psi}{\partial x},\\ u_2&=\frac{\partial\phi'}{\partial x}+\frac{\partial\psi'}{\partial y},\quad v_2=\frac{\partial\phi'}{\partial y}-\frac{\partial\psi'}{\partial x},\end{aligned}\right\}\quad\dots\dots\dots\dots(5')$$

the expressions of displacements become

$$u_1=-\frac{2(x-\alpha y-nt)}{c^2}e^{-\frac{(x-\alpha y-nt)^2}{c^2}}$$

$$-2(x+\alpha y-nt)\left\{\frac{a_1}{c^2}e^{-\frac{(x+\alpha y-nt)^2}{c^2}}+\frac{cb_1}{(c^2+4h_1H^2)^{3/2}}e^{-\frac{(x+\alpha y-nt)^2}{c^2+4h_1H^2}}\right.$$

$$\left.+\frac{cd_1}{(c^2+4k_1H^2)^{3/2}}e^{-\frac{(x+\alpha y-nt)^2}{c^2+4k_1H^2}}\right\}$$

$$
-2\beta(x+\beta y-nt)\left\{\frac{a^2}{c^2}e^{-\frac{(x+\beta y-nt)^2}{c^2}}+\frac{cb_2}{(c^2+4h_2H^2)^{3/2}}e^{-\frac{(x+\beta y-nt)^2}{c^2+4h_2H^2}}+\frac{cd_2}{(c^2+4k_2H^2)^{3/2}}e^{-\frac{(x+\beta y-nt)^2}{c^2+4k_2H^2}}\right\},
\qquad \ldots\ldots\ldots\ldots(23)
$$

$$
v_1=\frac{2\alpha(x-\alpha y-nt)}{c^2}e^{-\frac{(x-\alpha y-nt)^2}{c^2}}
-2\alpha(x+\alpha y-nt)\left\{\frac{a_1}{c^2}e^{-\frac{(x+\alpha y-nt)^2}{c^2}}+\frac{cb_1}{(c^2+4h_1H^2)^{3/2}}e^{-\frac{(x+\alpha y-nt)^2}{c^2+4h_2H^2}}+\frac{cd_1}{(c^2+4k_1H^2)^{3/2}}e^{-\frac{(x+\alpha y-nt)^2}{c^2+4k_2H^2}}\right\}
$$

$$
+2(x+\beta y-nt)\left\{\frac{a_2}{c^2}e^{-\frac{(x+\beta y-nt)^2}{c^2}}+\frac{cb_2}{(c^2+4h_2H^2)^{3/2}}e^{-\frac{(x+\beta y-nt)^2}{c^2+4h_2H^2}}+\frac{cd_2}{(c^2+4k_2H^2)^{3/2}}e^{-\frac{(x+\beta y-nt)^2}{c^2+4k_2H^2}}\right\},
\qquad \ldots\ldots\ldots\ldots(24)
$$

$$
u_2=-2\Bigl(x+\sqrt{\frac{\rho' n^2}{\lambda'+2\mu'}-1}\,y-nt\Bigl\{\frac{a_3}{c^2}e^{-\frac{\left(x+\sqrt{\frac{\rho' n^2}{\lambda'+2\mu'}-1}\,y-nt\right)^2}{c^2}}
+\frac{cb_3}{(c^2+4h_3H^2)^{3/2}}e^{-\frac{\left(x+\sqrt{\frac{\rho' n^2}{\lambda'+2\mu'}-1}\,y-nt\right)^2}{c^2+4h_3H^2}}+\frac{cd_3}{(c^2+4k_3H^2)^{3/2}}e^{-\frac{\left(x+\sqrt{\frac{\rho' n^2}{\lambda'+2\mu'}-1}\,y-nt\right)^2}{c^2+4k_3H^2}}\Bigr\}
$$

$$
-2\left(x-\sqrt{\frac{\rho' n^2}{\lambda'+2\mu'}-1}\,y-nt\right)\left\{\frac{a_4}{c^2}e^{-\frac{\left(x-\sqrt{\frac{\rho' n^2}{\lambda'+2\mu'}-1}\,y-nt\right)^2}{c^2}}
+\frac{cb_4}{(c^2+4h_4H^2)^{3/2}}e^{-\frac{\left(x-\sqrt{\frac{\rho' n^2}{\lambda'+2\mu'}-1}\,y-nt\right)^2}{c^2+4h_4H^2}}+\frac{cd_4}{(c^2+4k_4H^2)^{3/2}}e^{-\frac{\left(x-\sqrt{\frac{\rho' n^2}{\lambda^2+2\mu'}-1}\,y-nt\right)^2}{c^2+4k_4H^2}}\right\}
$$

$$
-2\sqrt{\frac{\rho' n^2}{\mu'}-1}\left(x+\sqrt{\frac{\rho' n^2}{\mu'}-1}\,y-nt\right)\left\{\frac{a_5}{c^2}e^{-\frac{\left(x+\sqrt{\frac{\rho' n^2}{\mu'}-1}\,y-nt\right)^2}{c^2}}
+\frac{cb_5}{(c^2+4h_5H^2)^{3/2}}e^{-\frac{\left(x+\sqrt{\frac{\rho' n^2}{\mu'}-1}\,y-nt\right)^2}{c^2+4h_5H^2}}+\frac{cd_5}{(c^2+4k_5H^2)^{3/2}}e^{-\frac{\left(x+\sqrt{\frac{\rho' n^2}{\mu'}-1}\,y-nt\right)^2}{c^2+4k_5H^2}}\right\}
$$

$$
+2\sqrt{\frac{\rho' n^2}{\mu'}-1}\left(x-\sqrt{\frac{\rho' n^2}{\mu'}-1}\,y-nt\right)\left\{\frac{a_6}{c^2}e^{-\frac{\left(x-\sqrt{\frac{\rho' n^2}{\mu'}-1}\,y-nt\right)^2}{c^2}}\right.
$$

$$+\frac{cb_6}{(c^2+4h_6H^2)^{3/2}}e^{-\frac{\left(x-\sqrt{\frac{\rho' n^2}{\mu'}-1}\,y-nt\right)^2}{c^2+4h_6H^2}}+\frac{cd_6}{(c^2+4k_6H^2)^{3/2}}e^{-\frac{\left(x-\sqrt{\frac{\rho' n^2}{\mu'}-1}\,y-nt\right)^2}{c^2+4k_6H^2}}\Bigg\},$$

$$\ldots\ldots\ldots\ldots(25)$$

$$v_2=-2\sqrt{\frac{\rho' n^2}{\lambda'+2\mu'}-1}\left(x+\sqrt{\frac{\rho' n^2}{\lambda'+2\mu'}-1}\,y-nt\right)\Bigg\{\frac{a_3}{c^2}e^{-\frac{\left(x+\sqrt{\frac{\rho' n^2}{\lambda'+2\mu'}-1}\,y-nt\right)^2}{c^2}}$$

$$+\frac{cb_3}{(c^2+4h_3H^2)^{3/2}}e^{-\frac{\left(x+\sqrt{\frac{\rho' n^2}{\lambda'+2\mu'}-1}\,y-nt\right)^2}{c^2+4h_3H^2}}+\frac{cd_3}{(c^2+4k_3H^2)^{3/2}}e^{-\frac{\left(x+\sqrt{\frac{\rho' n^2}{\lambda 2+2\mu'}-1}\,y-nt\right)^2}{c^2+4k_3H^2}}\Bigg\}$$

$$+2\sqrt{\frac{\rho' n^2}{\lambda'+2\mu'}-1}\left(x-\sqrt{\frac{\rho' n^2}{\lambda'+2\mu'}-1}\,y-nt\right)\Bigg\{\frac{a_4}{c^2}e^{-\frac{\left(x-\sqrt{\frac{\rho' n^2}{\lambda'+2\mu'}-1}\,y-nt\right)^2}{c^2}}$$

$$+\frac{cb_4}{(c^2+4h_4H^2)^{3/2}}e^{-\frac{\left(x-\sqrt{\frac{\rho' n^2}{\lambda'+2\mu'}-1}\,y-nt\right)^2}{c^2+4h_4H^2}}\ \frac{cd_4}{(c^2+4k_4H^2)^{3/2}}e^{-\frac{\left(x-\sqrt{\frac{\rho' n^2}{\lambda'+2\mu'}-1}\,y-nt\right)^2}{c^2+4k_4H^2}}\Bigg\}$$

$$+2\left(x+\sqrt{\frac{\rho' n^2}{\mu'}-1}\,y-nt\right)\Bigg\{\frac{a_5}{c^2}e^{-\frac{\left(x+\sqrt{\frac{\rho' n^2}{\mu'}-1}\,y-nt\right)^2}{c^2}}$$

$$+\frac{cb_5}{(c^2+4h_5H^2)^{3/2}}e^{-\frac{\left(x+\sqrt{\frac{\rho' n^2}{\mu'}-1}\,y-nt\right)^2}{c^2+4h_5H^2}}+\frac{cd_5}{(c^2+4k_5H^2)^{3/2}}e^{-\frac{\left(x+\sqrt{\frac{\rho' n^2}{\mu'}-1}\,y-nt\right)^2}{c^2+4k_5H^2}}\Bigg\}$$

$$+2\left(x-\sqrt{\frac{\rho' n^2}{\mu'}-1}\,y-nt\right)\Bigg\{\frac{a_6}{c^2}e^{-\frac{\left(x-\sqrt{\frac{\rho' n^2}{\mu'}-1}\,y-nt\right)^2}{c^2}}$$

$$+\frac{cb_6}{(c^2+4h_6H^2)^{3/2}}e^{-\frac{\left(x-\sqrt{\frac{\rho' n^2}{\mu'}-1}\,y-nt\right)^2}{c^2+4h_6H^2}}+\frac{cd_6}{(c^2+4k_6H^2)^{3/2}}e^{-\frac{\left(x-\sqrt{\frac{\rho' n^2}{\mu'}-1}\,y-nt\right)^2}{c^2+4k_6H^2}}\Bigg\}.$$

$$\ldots\ldots\ldots\ldots(26)$$

The movement of the ground surface may be obtained by putting $x=0$, $y=-H$ in the expressions of u_2, v_2. The result is shown as follows:

$$u_2=2\left(\sqrt{\frac{\rho' n^2}{\lambda'+2\mu'}-1}\,H+nt\ \Bigg\{\frac{a_3}{c^2}e^{-\frac{\left(\sqrt{\frac{\rho' n^2}{\lambda'+2\mu'}-1}\,H+nt\right)^2}{c^2}}\right.$$

$$+\frac{cb_3}{(e^2+4h_3H^2)^{3/2}}e^{-\frac{\left(\sqrt{\frac{\rho' n^2}{\lambda'+2\mu'}-1}\,H+nt\right)^2}{c^2+4h_3H^2}}+\frac{cd_3}{(c^2+4k_3H^2)^{3/2}}e^{-\frac{\left(\sqrt{\frac{\rho' n^2}{\lambda'+2\mu'}-1}\,H+nt\right)^2}{c^2+4k_3H\,3}}\Bigg\}$$

$$-2\left(\sqrt{\frac{\rho' n^2}{\lambda'+2\mu'}-1}\,H-nt\ \Bigg\{\frac{a_4}{c^2}e^{-\frac{\left(\sqrt{\frac{\rho' n^2}{\lambda'+2u'}-1}\,H-nt\right)^2}{c^2}}\right.$$

$$+\frac{cb_4}{(c^2+4h_4H^2)^{3/2}}e^{-\frac{\left(\sqrt{\frac{\rho n'^4}{\lambda'+2\mu'}-1}\,H-nt\right)^2}{c^2+4h_4H^2}}+\frac{cd_4}{(c^2+4k_4H^2)^{3/2}}e^{-\frac{\left(\sqrt{\frac{\rho' n^2}{\lambda'+2\mu'}-1}\,H-nt\right)^2}{c^2+4k_4H^2}}\Bigg\}$$

$$+2\sqrt{\frac{\rho' n^2}{\mu'}-1}\left(\sqrt{\frac{\rho' n^2}{\mu'}-1}\,H+nt\right)\Bigg\{\frac{a_5}{c^2}e^{-\frac{\left(\sqrt{\frac{\rho' n^2}{\mu'}-1}\,H+nt\right)^2}{c^2}}$$

$$+\frac{cb_5}{(c^2+4h_5H^2)^{3/2}}e^{-\frac{\left(\sqrt{\frac{\rho' n^2}{\mu'}-1}\,H+nt\right)^2}{c^2+4h_5H^2}}+\frac{cd_5}{(c^2+4k_5H^2)^{3/2}}e^{-\frac{\left(\sqrt{\frac{\rho' n^2}{\mu'}-1}\,H+nt\right)^2}{c^2+4k_5H^2}}\Bigg\}$$

$$+2\sqrt{\frac{\rho' n^2}{\mu'}-1}\left(\sqrt{\frac{\rho' n^2}{\mu'}-1}\,H-nt\right)\Bigg\{\frac{a_6}{c^2}e^{-\frac{\left(\sqrt{\frac{\rho' n^2}{\mu'}-1}\,H-nt\right)^2}{c^2}}$$

$$+\frac{cb_6}{(c^2+4h_6H^2)^{3/2}}e^{-\frac{\left(\sqrt{\frac{\rho' n^2}{\mu'}-1}\,H-nt\right)^2}{c^2+4h_6H^2}}+\frac{cd_6}{(c^2+4k_6H^2)^{3/2}}e^{-\frac{\left(\sqrt{\frac{\rho' n^2}{\mu'}-1}\,H-nt\right)^2}{c^2+4k_6H^2}}\Bigg\},\qquad\ldots\ldots\ldots\ldots(27)$$

$$v_2=2\sqrt{\frac{\rho' n^2}{\lambda'+2\mu'}-1}\left(\sqrt{\frac{\rho' n^2}{\lambda'+2\mu'}-1}\,H+nt\right)\Bigg\{\frac{a_3}{c^2}e^{-\frac{\left(\sqrt{\frac{\rho' n^2}{\lambda'+2\mu'}-1}\,H+nt\right)^2}{c^2}}$$

$$+\frac{cb_3}{(c^2+4h_3H^2)^{3/2}}e^{-\frac{\left(\sqrt{\frac{\rho' n^2}{\lambda'+2\mu'}-1}\,H+nt\right)^2}{c^2+4h_3H^2}}+\frac{cd_3}{(c^2+4k_3H^2)^{3/2}}e^{-\frac{\left(\sqrt{\frac{\rho' n^2}{\lambda'+2\mu'}-1}\,H+nt\right)^2}{c^2+4k_3H^2}}\Bigg\}$$

$$+2\sqrt{\frac{\rho' n^2}{\lambda'+2\mu'}-1}\left(\sqrt{\frac{\rho' n^2}{\lambda'+2\mu'}-1}\,H-nt\right)\Bigg\{\frac{a_4}{c^2}e^{-\frac{\left(\sqrt{\frac{\rho' n^2}{\lambda'+2\mu'}-1}\,H-nt\right)^2}{c^2}}$$

$$+\frac{cb_4}{(c^2+4h_4H^2)^{3/2}}e^{-\frac{\left(\sqrt{\frac{\rho' n^2}{\lambda'+2\mu'}-1}\,H-nt\right)^2}{c^2+4h_4H^4}}+\frac{cd_4}{(c^2+4k_4H^2)^{3/2}}e^{-\frac{\left(\sqrt{\frac{\rho' n^2}{\lambda'+2\mu'}-1}\,H-nt\right)^2}{c^2+4k_4H^2}}\Bigg\}$$

$$-2\left(\sqrt{\frac{\rho' n^2}{\mu'}-1}\,H+nt\right)\Bigg\{\frac{a_5}{c^2}e^{-\frac{\left(\sqrt{\frac{\rho' n^2}{\mu'}-1}\,H+nt\right)^2}{c^2}}$$

$$+\frac{cb_5}{(c^2+4h_5H^2)^{3/2}}e^{-\frac{\left(\sqrt{\frac{\rho' n^2}{\mu'}-1}\,H+nt\right)^2}{c^2+4h_5H^2}}+\frac{cd_5}{(c^2+4k_5H^2)^{3/2}}e^{-\frac{\left(\sqrt{\frac{\rho' n^2}{\mu'}-1}\,H+nt\right)^2}{c^2+4k_5H^2}}\Bigg\}$$

$$+2\left(\sqrt{\frac{\rho' n^2}{\mu'}-1}\,H-nt\right)\Bigg\{\frac{a_6}{c^2}e^{-\frac{\left(\sqrt{\frac{\rho' n^2}{\mu'}-1}\,H-nt\right)^2}{c^2}}$$

$$+\frac{cb_6}{(c^2+4h_6H^2)^{3/2}}e^{-\frac{\left(\sqrt{\frac{\rho' n^2}{\mu'}-1}\,H-nt\right)^2}{c^2+4h_6H^2}}+\frac{cd_6}{(c^2+4k_6H^2)^{3/4}}e^{-\frac{\left(\sqrt{\frac{\rho' n^2}{\mu'}-1}\,H-nt\right)^2}{c^2+4k_6H^2}}\Bigg\}.\qquad\ldots\ldots\ldots\ldots(28)$$

It seems that the movement of the ground due to arbitrary waves is quite similar to that due to the waves of harmonic type of infinite extent.

---

50. 地表に一つの層があるときの地震波の反射及屈折

地震研究所 妹澤克惟
金井清

地表に一つの層があるときに水平面に對して斜の方向から來た地震波が層の境界面で反射屈折する模樣を彈性力學的に正確なる方法でしらべた。その結果

1. 地表の層の厚さに比して地震波の波長が極めて長いときには地表上の點の運動は Knott などがやつたやうに振動方向が大體に於て入射波の方向に向く事がわかつた。
2. 地震の層の厚さに比して地震波の波長が短く、且つ入射波が無限につゞく正弦波のときには、地表の運動は、若し上層の彈性が低いときには振動方向が垂直の方へ向いてくるものであつて、この結果は鈴木理學士の實驗結果と大體に於て一致してゐる。
3. 地震波が層の厚さに比して短いとき程、表面上の點の振動軌跡の楕圓形に於て短軸の方が零よりも少しづつ大なる値となることがわかつた。

---

51. On Variations in the Length of the Mitaka Comparison Base Line.

By Katsuhiko MUTO and Kunihiko SINO,

Imperial Japanese Military Land Survey.

(Read April 26, 1932.—Received Sept. 16, 1932.)

It was recently noticed that the length of the Mitaka 25 meter comparison base line varied as the air temperature varied. These constant changes being a serious matter, investigations were made with a view to ascertain whether they were due to constructional defects in connection with the original measurement of the base line or to actual movements of the earth's crust.

1. This base line was laid down in 1915. As the specifications covering the constructional work at the time of the original measurement was lost in the fire that followed the great 1923 earthquake, there is uncertainty about the exact underground construction of the terminal of the base line, but from such parts of the exterior as are visible, it seems that it was constructed in the same way as that of the Sagamino base line. See Fig. 1.

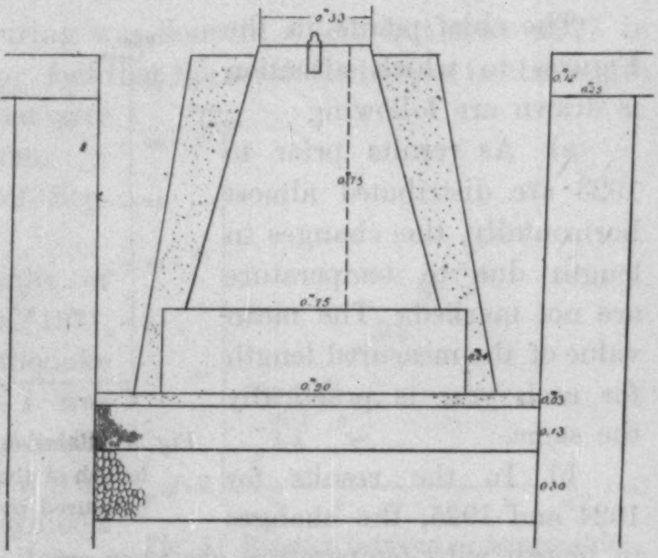

Fig. 1. Sketch of a terminal of the Base.

In 1931 the greater part of the inner concrete floor was cut away from the foundation in order to prevent the former from being unduly influenced by the latter.

2. Results of measurements.

The Mitaka comparison base has been often measured in testing

the Jäderin wires. Figs. 2–5 represent the relation between the length of the base and the temperature as observed in free air. The base

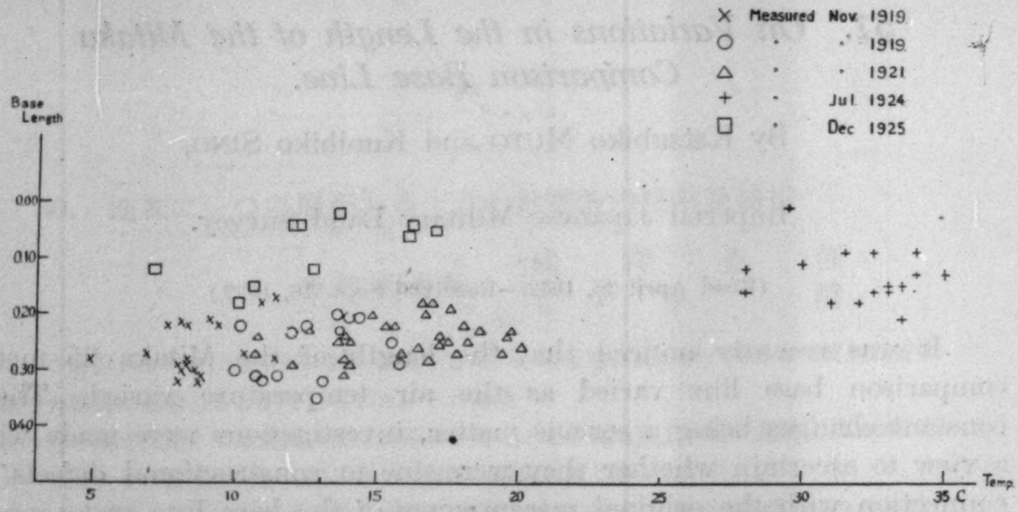

Fig. 2. Relation between air temperature and the length of the 25 m. Comparison Base Line as measured by a Guillaume 5 m. apparatus.

apparatus used was the Guillaume 5 m. Standard Scale, and the method of measurement invariably the same.

The chief points in the Figures to which attention is drawn are following:

a) As results prior to 1923 are distributed almost horizontally, the changes in length due to temperature are not marked. The mean value of the measured length for each year is practically the same.

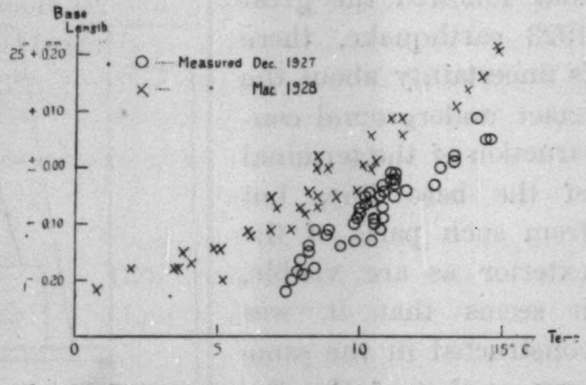

Fig. 3. Relation between air temperature and the length of the 25 m. Comparison Base Line as measured by a Guillaume 5 m. apparatus.

b) In the results for 1924 and 1925, the changes in length with temperature are very small but the mean length during 1924 is elongated as compared with values prior to 1923, while the mean length for 1925 is considerably larger than that for 1924.

c) Since 1927 the length has changed in a remarkable manner with variations of temperature. The length of the base has increased gradually every year. Fig. 8 shows the yearly change in the length of

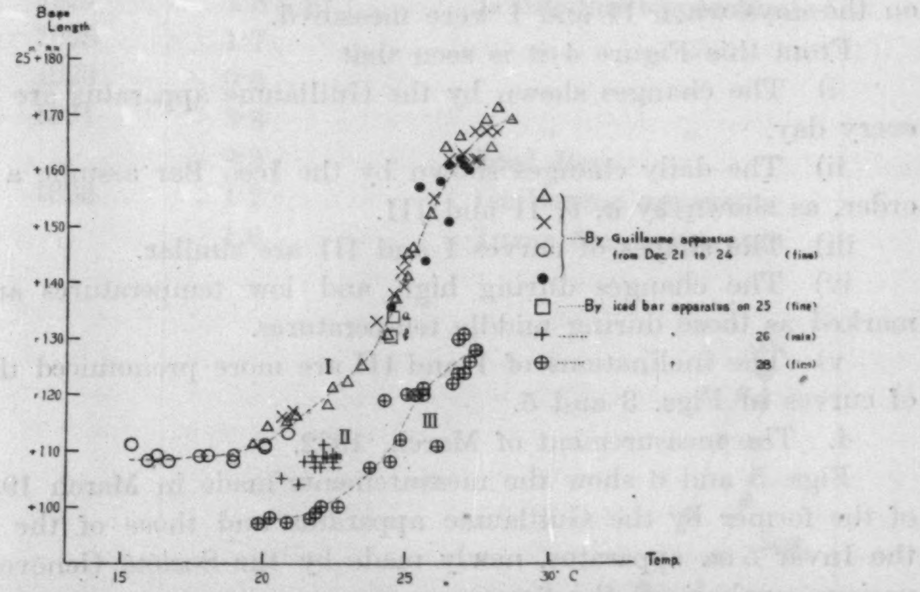

Fig. 4. Relation between air temperature and the length of the 25 m. Base Line as measured by a 5 m. Guillaume apparatus and a 5 m. Invar apparatus.

the base line at 10°C.

Previous to 1925, measuring was done in a tent but since 1927 in a house. It is an interesting fact that the marked changes in the length appeared in measurements that were made in the comparison room.

3. The measurement of September, 1931.

Fig. 4 shows the results of measurements taken in Sept. 1931, at the request of the Earthquake Research Institute. Curve I was obtained by the Guillaume apparatus and curves II and III by a 5 m. Iced Bar. The different symbols on curve I show the different days on which the measurements were taken. The weather during the measurement of I was fair, of II rainy, and of III clear.

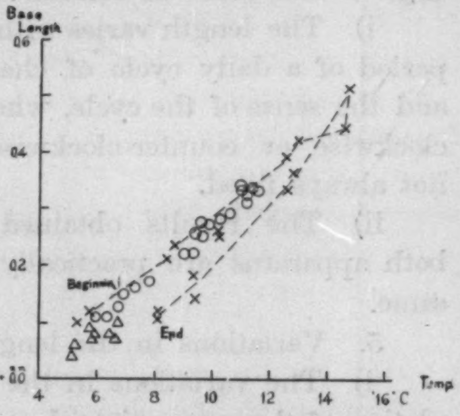

Fig. 5. Relation between air temperature and the Base Line as measured by a 5 m. Guillaume apparatus in March 1932.

The two points marked *a* and *b* in I near 24°5 were obtained by the Iced Bar the day before measurement of II. The weather was fine

on the days when II and I were measured.

From this Figure 4 it is seen that

i) The changes shown by the Guillaume apparatus are the same every day.

ii) The daily changes shown by the Iced Bar assume a step like order, as shown by *a*, *b*, II and III.

iii) The shapes of curves I and III are similar.

iv) The changes during high and low temperatures are not so marked as those during middle temperatures.

v) The inclinations of I and III are more pronounced than those of curves in Figs. 3 and 5.

4. The measurement of March, 1932.

Figs. 5 and 6 show the measurements made in March 1932; those of the former by the Guillaume apparatus and those of the latter by the Invar 5 m. apparatus, newly made by the Société Genêvoise. The various symbols in the figures represent the different days on which the measurements were taken. The same method of measurement was used with both apparatus.

The chief points of interest in Figs. 5 and 6 are as follows:

i) The length varies with the period of a daily cycle of changes and the sense of the cycle, whether clockwise or counter-clockwise, is not always fixed.

ii) The results obtained by both apparatus are practically the same.

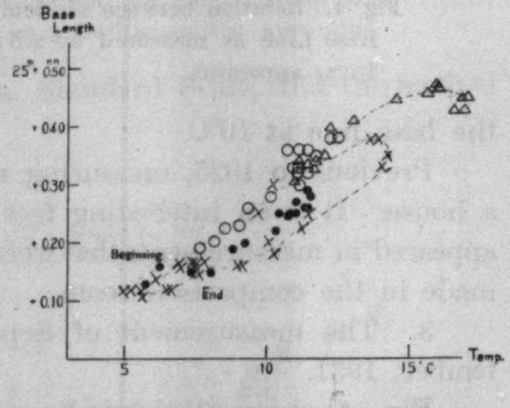

Fig. 6. Relation between air temperature and the length of the 25 m. Base Line as measured by an Invar apparatus in March 1932.

5. Variations in the length of the comparison base.

i) The variations in the length of the base began with the completion of the comparison house. This daily variation in sympathy with the air temperature resembles the variation in the temperature of the ground surface relatively to the air temperature. Fig. 7 shows the temperature variations of the ground surface with reference to the air temperature.

The maximum elongations of the base through temperature since 1927 are as follows:

1927	$1{\cdot}8\times10^{-6}$	Guillaume apparatus
1928	1·7	„ „
1929	0·8	„ „
1931	3·8	„ „
„	2·8	Iced Bar
1932	1·7	Guillaume apparatus
„	1.8	Invar 5 m. apparatus

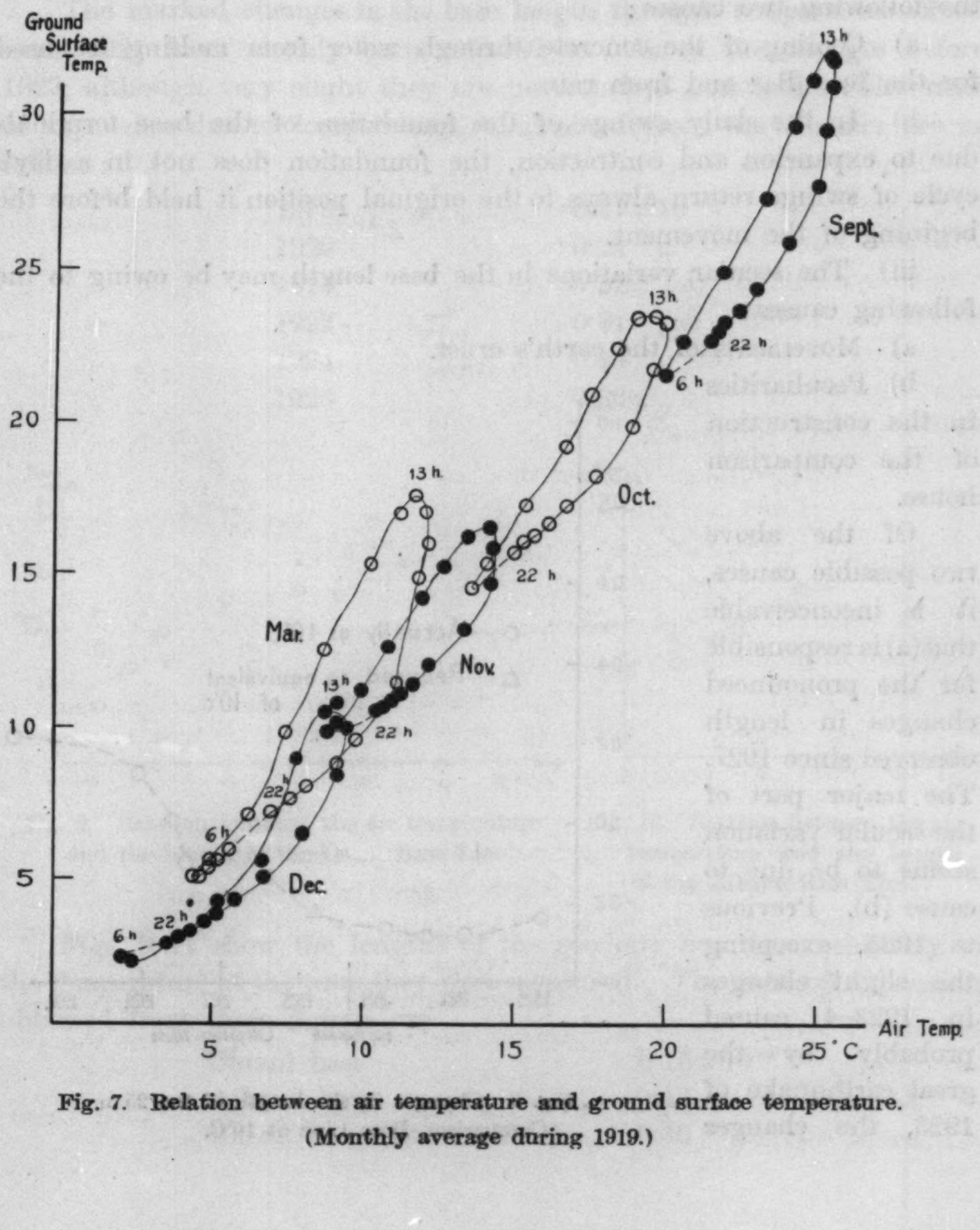

Fig. 7. Relation between air temperature and ground surface temperature. (Monthly average during 1919.)

These rates of elongation closely resemble the coefficient of expansion of concrete, which is $2{\cdot}5-4{\cdot}0\times10^{-6}$. The absence of any particular difference in the results from the Guillaume apparatus, the Iced Bar, and the Invar apparatus are significant. From these considerations the chief cause of variation in the measured length seems to lie not in the measuring apparatus, but in the expansion and contraction of the concrete floor of the comparison house.

ii) The step-like changes in the measured length may be due to the following two causes:

a) Cooling of the concrete through water from melting ice used for the Iced Bar and from rain.

b) In the daily swings of the foundation of the base terminals due to expansion and contraction, the foundation does not in a day's cycle of swings return always to the original position it held before the begining of the movement.

iii) The secular variations in the base length may be owing to the following causes:

a) Movements of the earth's crust.

b) Peculiarities in the construction of the comparison house.

Of the above two possible causes, it is inconceivable that (a) is responsible for the pronounced changes in length observed since 1927. The major part of the secular variation seems to be due to cause (b). Previous to 1925, excepting the slight changes in 1923-4 caused probably by the great earthquake of 1923, the changes

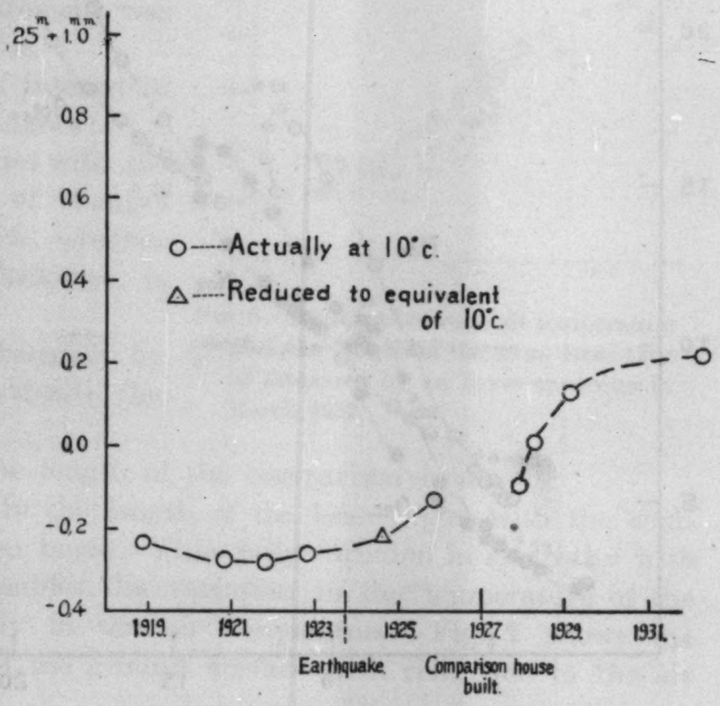

Fig. 8. Changes in the length of the 25 m. Comparison Base Line at 10°C.

were insignificant. The chief cause of (b) is probably changes in the positions of the terminals due to expansion and contraction of the concrete floor.

As shown in Fig. 8, the results of 1931 are very different from those of other years. They show the seasonal variations of the base. The cause of these variations may also be the cause of changes in the position of the terminals as already mentioned.

6. Expansion and contraction of the ground.

The marked changes in the base length through temperature effects since 1927 have already been referred to. As to the changes before 1927, although very slight they are nevertheless noticeable. The rates of expansion due to temperature as obtained from the Figures are as follows:

1919	$0{\cdot}31 \times 10^{-6}$
1920	0·24 „
1921	0·27 „
1922	0·31 „
1924	0·46 „
1925	0·32 „

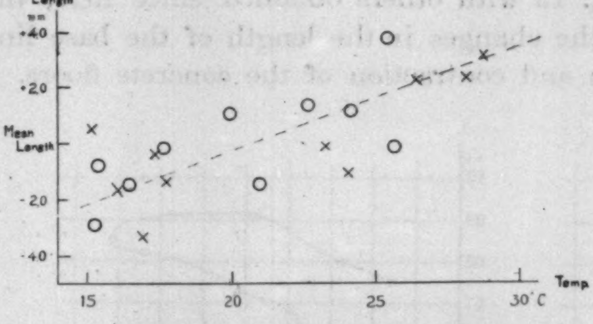

Fig. 9. Relation between the air temperature and the length of the Otani Base Line.

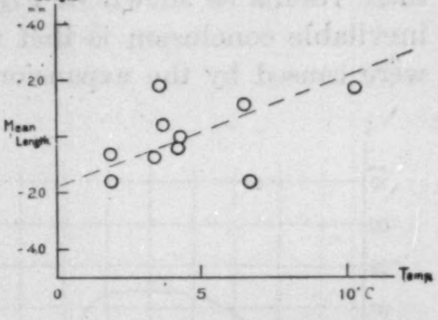

Fig. 10. Relation between the air temperature and the length of the Aibano Base Line.

Figs. 9–11 show the lengths of the geodetic base line relatively to the temperature at the time they were measured. The rates of expansion obtained from these figures are

Ootani base	$0{\cdot}15 \times 10^{-6}$
Aibano base	0·13 „
100 m. base (ES) at Mitaka	0·46 „

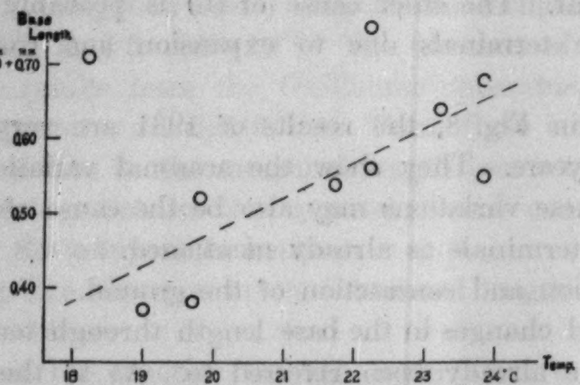

Fig. 11. Relation between the air temperature and the length of the Mitaka 100 m. Rhombic Base Line.

As these values coincide tolerably well with the values of the comparison base, they may be taken as the expansion coefficients of the ground.

The expansion and contraction of the concrete floors being considered the chief cause of the changes in length of the comparison base as already mentioned, two 25 m. base lines were set up on July 18/9, one in front and the other back of the comparison house on the concrete floors outside of the house, and measured on July 29/30. Comparing these results as shown in Fig. 12 with others obtained since 1927, the inevitable conclusion is that the changes in the length of the base line were caused by the expansion and contraction of the concrete floors.

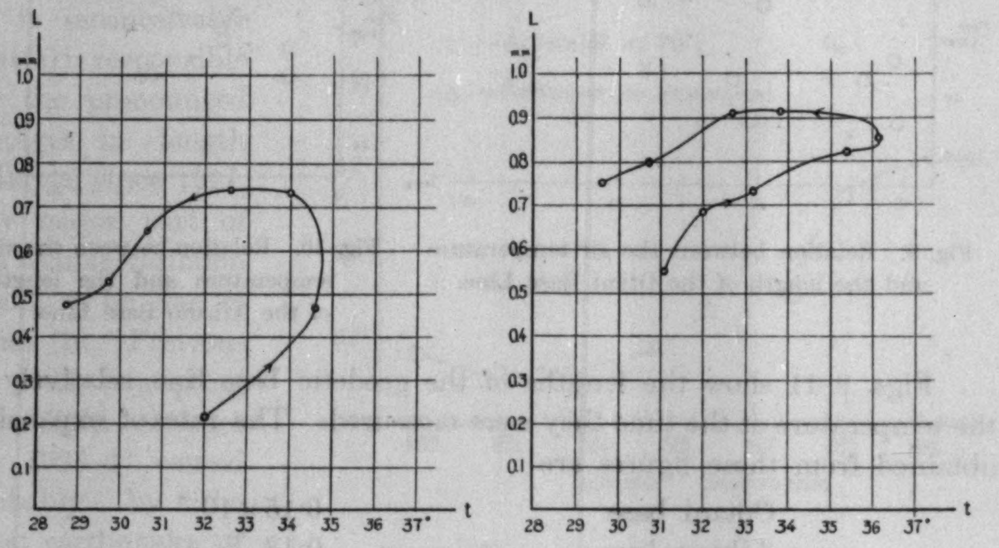

Front. Back.

Fig. 12. Changes in the length of the 25 m. concrete floor.

51. 三鷹村二十五米比較基線長の變化について

陸地測量部 { 武藤勝彦
篠邦彦

三鷹村 25 米比較基線長が温度によつてかなり著しい變化をすることは大分前から知られて居た。この變化が何に基因するかをしらべた結果その大部分の原因は比較室のコンクリート床の温度による伸縮にあることを知つた。又温度による比較室建設前の微弱な變化其他の野外基線長の變化から土地の温度に對する伸長率を求めた。尚最後にコンクリート床の温度による伸縮をたしかめるため新たにコンクリート床自身の上に直接25米の基線をとつて測定した結果をつけ加へてある。

52. *A Note on the Tilting Motion of the Earth's Crust observed at Zinsen (Chemulpo).*

By Ryûtarô TAKAHASI,

Earthquake Research Institute.

(Read May 17, 1932.—Received Sept. 20, 1932)

1. Introduction.

What is written in this paper is the revision of Sekiguchi's pioneer observation[1], but not the observation made by the present author himself. In 1916, Sekiguchi, while he was in the Meteorological Observatory of Zinsen, noticed the existence of the tilting motion of the earth's crust from the periodic variation of line-intervals of the records obtained by the Omori horizontal pendulum seismograph, installed in the observatory. This periodic tilting motion of the earth's crust was naturally attributed to the load of tides in the port of Zinsen and its neighbouring seas, where the tidal range is as large as 10 metres.

Sekiguchi calculated then the rigidity of the earth's crust, by comparing the observed amount of tilt with that theoretically deduced. In his treatment, however, there are assumptions, especially in tidal materials, which seem to the present author to be rather rough.

The present author felt much anxious about that the results obtained under such assumptions will deviate much from the truth. In these anxieties, the author made a revision of Sekiguchi's observation, making use of the co-tidal and co-range charts of the Yellow Sea and its adjacent bays, which he has compiled in his previous research,[2] and also of a method of analysis different from that used by Sekiguchi. The author has thus obtained something new, which will be described in the following paragraphs.

2. Sekiguchi's observation and the instrument used.

The instrument used in Sekiguchi's observation is the Omori horizontal pendulum, installed in the cellar of the Zinsen Meteorological

1) R. SEKIGUCHI, *Mem. Imp. Marine Obs.*, 1 (1922), 1.
2) *Earthq. Res. Inst.*, 10 (1932), 531.

Observatory (Lat. 37° 28′ 30″ N ; Long. 126° 37′ 36″ E) in the azimuth as to record EW component of earthquake vibrations. The magnification coefficient of the seismograph was 150, the period of the free oscillation of the pendulum being 28 sec. The sensibility of the seismograph for the tilt of the ground in EW direction is given therefore by

$$V=\frac{150\,gT_0^2\sin 1''}{4\pi^2}\ \text{cm./sec. of arc},$$

where g and T_0 are the acceleration of gravity and the period of the free oscillation of the pendulum respectively. Giving numerical values to g, T_0 and π in the above expression, we have

$$V=14{\cdot}1.$$

The recording drum of the seismograph revolved once in 30 minuits and it slided towards east with the revolution. The recording pen of the seismograph described therefore a series of straight lines, the interval of these lines varying with the velocity of tilting of the ground.

The air temperature in the cellar of the observatory was very steady during the period of the observation, diurnal variations being scarcely recognized. The humidity of the air was constantly at the point of saturation.

The location of the observatory is to be seen in Fig. 5, below.

The period of the observation extended from Jan. 1 to Mar. 27, 1916, that is, over three complete lunations. It was observed that there occurre dusually two maximum and two minimum line-intervals of the seismogram in a day, synchronously to the ebb and flood of tides in the port of Zinsen.

3. Reduction of the observed data.

Supposing for a while that the diurnal inequality of tilt is negligible, let the tilt towards *west* of the ground be expressed by

$$\psi=\psi_m\cos(2T+2h-2s-\varepsilon_m)+\psi_s\cos(2T-\varepsilon_s),$$

where ψ_m is the amplitude of M_2 component-tilt, ψ_s that of S_2 component-tilt, T the hour angle of the mean sun, h the mean longitude of the sun, s the mean longitude of the moon and ε_m and ε_s the phase lags. If we put again

$$2T+2h-2s=\sigma_m t,$$

where σ_m is the angular velocity of M_2 component, then t is approximately equal to the mean solar time reckoned from the upper culmina-

tion of the moon, and we have

$$\psi=\psi_m\cos(\sigma_m t-\varepsilon_m)+\psi_s\cos\{(\sigma_m t-\varepsilon_m)+(\zeta-a)\},$$

in which $\zeta=2(s-h)$ and $a=\varepsilon_s-\varepsilon_m$.
This expression can be written

$$\psi=R\cos(\sigma_m t-\varepsilon_m+\theta),$$

if

$$R^2=\psi_m^2+\psi_s^2+2\psi_m\psi_s\cos(\zeta-a),$$

and

$$\theta=\tan^{-1}\frac{\psi_s\sin(\zeta-a)}{\psi_m+\psi_s\cos(\zeta-a)}.$$

On the other hand the line-interval of the seismogram is given by

$$W=I-V\frac{d\psi}{dt}\Delta t,$$

where I is the pitch of the screw attached to the recording drum of the seismograph, Δt the time of one complete revolution of the recording drum.
We have therefore

$$W_{\text{max.}}-W_{\text{min.}}=\frac{2\pi}{180}\sigma_m V\Delta t\cdot R.$$

The times of occurrence of the maximum and minimum widenings of the line-interval that follow the upper culmination of the moon are given respectively by

$$t_{\text{max.}}=\frac{\varepsilon_m-\theta+90^\circ}{\sigma_m},$$

$$t_{\text{min.}}=\frac{\varepsilon_m-\theta+270^\circ}{\sigma_m}.$$

The time of occurrence of the maximum *eastward* tilt t_1 is $\frac{\varepsilon_m-\theta+180^\circ}{\sigma_m}$; hence we have

$$t_1=\frac{t_{\text{max.}}+t_{\text{min.}}}{2}.$$

In Sekiguchi's paper, values of $W_{\text{max.}}-W_{\text{min.}}$ and t_1 are given for each day. We will cite them in the next, together with the time, referred to the meridan 135° E, of the moon's culmination over the meridian of Zinsen.

Table I.

Table for $W_{max.} - W_{min.}$, t_1 and the time of moon's transit over the meridian of Zinsen, the time used being referred to the meridian 135° E.

Date	☾'s Transit	t_1	$W_{max.}-W_{min.}$	Date	☾'s Transit	t_1	$W_{max.}-W_{min.}$
	h m	h m	mm		h m	h m	mm
Dec. 31	19 54	12 06	3·5	Jan. 15	20 51	12 08	1·5
Jan. 1	8 20	12 09	2·7	16	9 16	12 59	2·0
1	20 39	11 41	3·2	16	21 41	13 19	2·5
2	9 19	12 41	3·2	17	10 06	13 13	1·5
2	21 50	12 39	4·4	17	22 32	12 28	4·1
3	10 22	11 52	3·5	18	10 57	12 48	4·3
3	22 55	11 34	5·0	18	23 22	11 53	5·8
4	11 29	12 00	4·4	19	11 47	12 43	5·2
4	—	—	—	19	—	—	—
5	0 02	11 26	4·6	20	0 12	11 48	7·0
5	12 36	12 10	6·1	20	12 35	13 39	5·0
6	1 07	11 37	6·8	21	0 59	12 01	5·0
6	13 39	11 06	5·6	21	13 22	11 53	3·2
7	2 07	10 56	4·0	22	1 45	11 45	1·2
7	14 36	10 38	4·0	22	14 08	11 53	2·0
8	3 02	10 42	4·2	23	2 28	12 32	0·7
8	15 29	10 46	2·5	23	14 49	12 25	1·0
9	3 53	10 51	4.0	24	3 11	13 04	1·2
9	16 17	11 58	3·2	24	15 32	11 58	1·0
10	4 40	10 50	3·6	25	3 54	13 06	0·3
10	17 03	11 27	4·5	25	16 15	12 00	0·5
11	5 25	10 20	2·8	26	4 37	13 08	0·1
11	17 47	11 43	3·0	26	17 00	11 45	0·4
12	6 09	11 21	1·7	27	5 23	13 06	0·3
12	18 31	10 29	2·0	27	17 48	11 42	0·0
13	6 53	9 21	2·8	28	6 13	12 32	1·5
13	19 16	10 14	3·0	28	18 40	11 51	0·1
14	7 39	11 36	1·3	29	7 07	12 38	1·0
14	20 03	12 27	2·0	29	19 36	11 54	0·0
15	8 27	13 19	1·5	30	8 06	11 24	0·6

(to be continued.)

Table I (*continued.*)

Date	☾'s Transit	t_1	$W_{max}-W_{min}$.	Date	☾'s Transit	t_1	$W_{max}-W_{min}$.
	h m	h m	mm		h m	h m	mm
Jan. 30	20 35	12 37	1·8	Feb. 16	22 54	12 51	0·4
31	9 09	12 20	1·5	17	11 17	12 27	0·2
31	21 41	12 33	3·7	17	23 40	12 49	0·2
Feb. 1	10 14	12 31	2·8	18	—	—	—
1	22 45	12 13	5·0	18	12 02	12 27	0·5
2	11 17	12 42	4·1	19	0 25	13 05	2·8
2	23 47	12 11	6·5	19	12 47	11 43	3·5
3	—	—	—	20	1 19	11 51	4·6
3	12 17	12 27	4·5	20	13 30	11 44	3·0
4	0 45	12 14	6·0	21	1 52	11 38	4·0
4	13 13	(11 28)	(8·2)	21	14 14	13 16	4·5
5	1 38	11 56	5·0	22	2 36	11 54	5 3
5	14 04	11 26	6·0	22	14 59	11 31	7·0
6	2 28	11 31	7·1	23	3 22	12 08	4·0
6	14 52	11 38	6·2	23	15 46	11 14	5·0
7	3 15	11 29	3·3	24	4 10	11 35	5·4
7	15 38	12 21	0·5	24	16 36	11 54	5·0
8	4 01	11 29	3·5	25	5 02	11 57	1·6
8	16 24	12 06	5·2	25	17 30	11 29	3·2
9	4 47	10 58	5·0	26	5 59	11 01	2·8
9	17 10	11 35	2·8	26	18 29	11 01	1·8
10	5 33	11 57	2·8	27	6 59	10 46	1·8
10	17 57	13 03	1·0	27	19 30	10 14	2·6
11	6 21	11 09	0·5	28	8 10	11 13	1·7
11	18 45	12 45	0·4	28	20 33	11 42	1·8
12	7 10	10 50	1·0	29	9 03	(12 31)	(2·4)
12	19 35	12 40	0·0	29	21 33	(12 22)	(3·8)
13	8 00	11 45	0·8	Mar. 1	10 03	12 12	2·8
13	20 25	12 04	0·0	1	22 31	11 43	2·2
14	8 50	11 39	1·0	2	10 59	11 46	3·8
14	21 16	12 44	0·3	2	23 25	11 50	4·9
15	9 41	12 18	0·3	3	11 51	11 39	3·8
15	22 06	12 54	0·1	3	—	—	—
16	10 30	12 15	0·3	4	0 15	11 44	4·0

(*to be continued.*)

Table I. (*continued.*)

Date		☾'s Transit		t_1		$W_{max.}-W_{min.}$	Date		☾'s Transit		t_1		$W_{max.}-W_{min.}$
		h	m	h	m	mm			h	m	h	m	mm
Mar.	4	12	40	11	35	4·7	Mar.	16	22	19	(12	53)	(1·8)
	5	1	03	11	26	4·0		17	10	41	12	43	3·8
	5	13	27	11	17	4·6		17	23	03	11	27	4·9
	6	1	48	11	09	3·0		18	11	25	12	45	3·5
	6	14	14	11	31	3·5		18	23	47	11	43	5·0
	7	2	37	11	38	2·8		19	12	09	11	51	4·5
	7	15	00	12	15	2·0		19	—		—		—
	8	3	23	10	51	2·8		20	0	31	11	28	4·7
	8	15	47	12	27	2·0		20	12	54	11	51	4·6
	9	4	11	11	03	2·0		21	1	17	11	28	5·0
	9	16	36	11	24	2·0		21	13	41	11	18	5·2
	10	5	01	(11	02)	(3·6)		22	2	06	11	09	5·2
	10	17	26	11	34	1·0		22	14	32	11	28	4·1
	11	5	51	10	23	1·0		23	2	58	11	02	4·6
	11	18	17	11	43	0·0		23	15	26	10	49	5·2
	12	6	42	10	17	2·0		24	3	54	10	36	3·0
	12	19	08	10	52	1·3		24	16	23	10	36	2·5
	13	7	33	9	57	0·8		25	4	53	11	36	2·9
	13	19	58	11	32	1·1		25	17	24	10	35	1·3
	14	8	23	9	37	0·8		26	5	55	(11	55)	(1·5)
	14	20	47	12	13	2·3		26	18	26	(11	26)	(1·0)
	15	9	10	12	50	2·0		27	6	57	11	03	1·0
	15	21	34	12	26	2·0		27	19	26	10	33	0·0
	16	9	56	12	32	2·1							

The quantities to be computed are ψ_m and ε_m. We will calculate them in the next by making use of the above data and mathematical relations.

We cannot, however, treat at once those data given in Table I. Being as read off from seismograms, they involve, besides variations to be found, many undesired disturbances such as diurnal inequality, phase inequality and meteorological ones. Consequently, we must, at the first step of the computation, eliminate all inequalities other than the phase inequality, by grouping the observed data according to the time of moon's transit. As the period of the observation is short, being only

three months, complete elimination cannot be expected, but the greater part of the inequalities may be got rid of, if $W_{max.}-W_{min.}$ and t_1 are arranged according to such a schedule as is given by the Hydrographic Department of the British Admiralty for the computation of non-harmonic tidal constants.

Grouping and averaging of the data written in Table I give the following results.

☾'s Transit	$W_{max.}-W_{min.}$	t_1		Note
h	mm	h	m	
0	4·3	12	04	The time of ☾'s transit is referred to 135° E. meridian.
1	5·2	11	50	
2	4·2	11	36	
3	3·7	11	37	
4	2·9	11	37	
5	2·6	11	29	
6	1·4	11	37	
7	1·4	10	58	
8	1·4	11	40	
9	1·9	12	20	
10	2·5	12	35	
11	3·7	12	12	

The values of $W_{max.}-W_{min.}$ and t_1, obtained here, must now be free from all inequalities other than the phase inequality. $W_{max.}-W_{min.}$ and t_1 are not of course independent but are related to each other. As can be seen from the expressions of R and θ, points that represent the values of $W_{max.}-W_{min.}$ and the corresponding values of $\sigma_m t_1$, in polar co-ordinates, must all fall on a circle, having its centre at $\left(\frac{2\pi}{180}\sigma_m\psi_m V\Delta t,\ \varepsilon_m+180^\circ\right)$ and having for its radius $\frac{2\pi}{180}\sigma_m\psi_s V\Delta t$. These relations can be easily understood by the aid of Fig. 1.

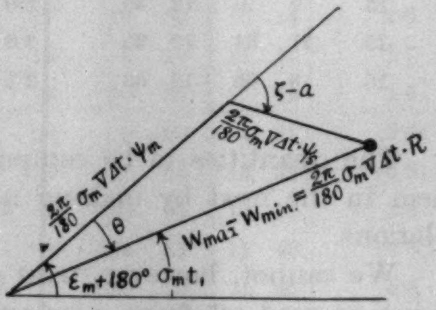

Fig. 1.

We can find, therefore, ψ_m and ε_m from the co-ordinates of the centre of the circle, ψ_s from the magnitude of the radius of the circle, and ε_s from the positions of the points on the circle.

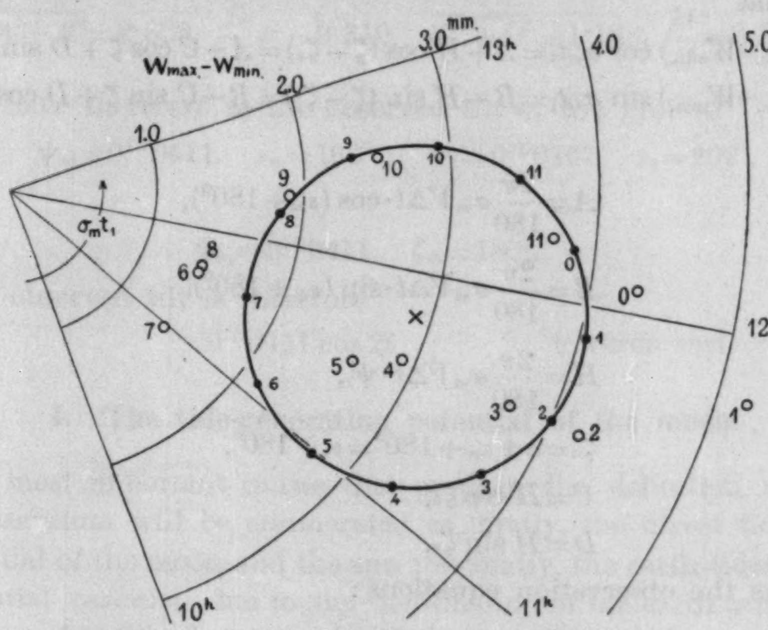

Fig. 2. ○....not adjusted ●....adjusted
Numerals represent the time of moon's transit.

Actually, however, the points do not fall always on a circle, but are distributed irregularly, as are shown in Fig. 2 and 3, because of the

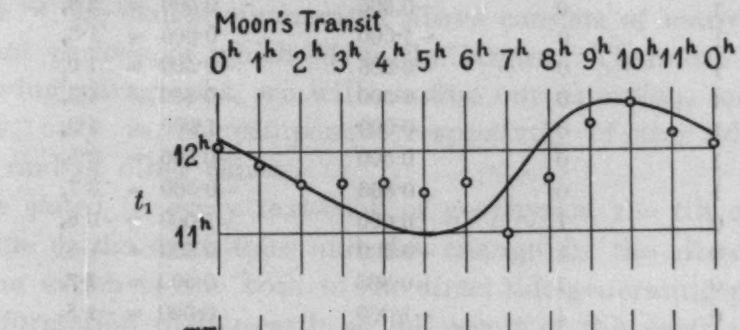

Fig. 3.

disturbances and inequalities not yet completely eliminated. We must therefore determine the circle of minimum errors by the method of least squares and obtain therefrom the values of ψ_m and ε_m.

Putting that

$$(W_{max.}-W_{min.})\cos\sigma_m t_1 = A+H\cos(\zeta-\zeta_0)=A+C\cos\zeta+D\sin\zeta,$$

$$(W_{max.}-W_{min.})\sin\sigma_m t_1 = B-H\sin(\zeta-\zeta_0)=B-C\sin\zeta+D\cos\zeta,$$

where

$$A=\frac{2\pi}{180}\sigma_m V\Delta t\cdot\cos(\varepsilon_m+180°),$$

$$B=\frac{2\pi}{180}\sigma_m V\Delta t\cdot\sin(\varepsilon_m+180°),$$

$$H=\frac{2\pi}{180}\sigma_m V\Delta t\cdot\psi_s,$$

$$\zeta_0=a+\varepsilon_m+180°=\varepsilon_s+180°,$$

$$C=H\cos\zeta_0,$$

$$D=H\sin\zeta_0,$$

we have as the observation equations:

A	B	C	D	
1	0	1·000	0·000	= 4·2,
1	0	0·866	0·500	= 4·9,
1	0	0·500	0·866	= 3·8,
1	0	0·000	1·000	= 3·4,
1	0	−0·500	0·866	= 2·6,
1	0	−0.866	0·500	= 2·3,
1	0	−1·000	0·000	= 1·3,
1	0	−0·866	−0·500	= 1·0,
1	0	−0·500	−0·866	= 1·3,
1	0	0·000	−1·000	= 1·9,
1	0	0·500	−0·866	= 2·5,
1	0	0·866	−0·500	= 3·7,
0	1	0·000	1·000	= −0·8,
0	1	−0·500	0·866	= −1·5,
0	1	−0·866	0·500	= −1·7,
0	1	−1·000	0·000	= −1·5,
0	1	−0·866	−0·500	= −1·2,
0	1	−0·500	−0·866	= −1·2,
0	1	0·000	−1·000	= −0·6,
0	1	0·500	−0·866	= −0·9,
0	1	0·866	−0·500	= −0·5,
0	1	1·000	0·000	= −0·1,
0	1	0·866	0·500	= 0·2,
0	1	0·500	0·866	= −0·4,

from which we obtain

$$A=2{\cdot}740,\quad B=-0{\cdot}850,\quad C=1{\cdot}086 \quad\text{and}\quad D=0{\cdot}430,$$

that is

$$\sqrt{A^2+B^2}=2{\cdot}869,\quad \frac{B}{A}=-0{\cdot}310,\quad \sqrt{C^2+D^2}=1{\cdot}168,\quad \frac{D}{C}=0{\cdot}396.$$

We have therefore as the observed tilt of the ground

$$\psi_m=0{\cdot}''0411,\quad \varepsilon_m=163^\circ\,;\quad \psi_s=0{\cdot}''0167,\quad \varepsilon_s=202^\circ,$$

or

$$\psi_m=0{\cdot}''0411,\quad \zeta_m=180^\circ.$$

The observed tilt is therefore

$$0{\cdot}''0411\cos 2t \qquad \text{towards east.}$$

4. The tide-generating potential of the moon.

The most important causes that produce the deflection of a horizontal pendulum will be enumerated as, firstly, the direct tide-generating potential of the moon and the sun ; secondly, the earth-tides ; thirdly, the potential variation due to the deformation of the earth caused by the earth-tides ; fourthly ; the gravitational attraction of the oceanic tides ; fifthly and finally, the deformation of the earth's crust due to tidal loading. There are of course many other causes which can also produce the deflection of a horizontal pendulum, but their contributions to the deflection are very small, compared with the causes just referred to.

Each of the causes enumerated above consists of many components of different periods, of which M_2 is the largest. Therefore in this and the following paragraphs, we will confine our attention, for the sake of simplicity, only to M_2 component respectively of the tide-generating potential and of other causes.

As is stated in every text-book of geophysics, the tilt of the earth's surface due to the earth-tides and the change in the direction of the plumb-line which is due both to the direct tide-generating potential and to the deformation of the earth as the result of the earth-tides, are of the same period and phase. They come, therefore, into the observed amount of apparent tilt as total, namely, as $(1-h+k)W$, if we denote the change in the direction of the plumb-line due to the direct tide-generating potential of the moon by W. The quantity $(1-h+k)$ is what is generally called the diminishing factor, and is denoted by D.

W will be calculated easily by the formula

$$-\frac{3}{\sin 1''}\frac{M}{E}\left(\frac{a}{c}\right)^3\left(\frac{1}{2}-\frac{5}{4}e^2\right)\cos^4\frac{I}{2}\cos\lambda\sin 2t \quad \text{towards east,}$$

where M=mass of moon,
E=mass of earth,
a=radius of earth,
c=mean distance of moon,
λ=latitude of the place,
e=eccentricity of moon's orbit,
and I=inclination of moon's orbit to equator.

For the central day of the period of the observation we have

$$I=26\cdot^\circ 89$$

so the calculated value of W is

$$-0\cdot''01221 \sin 2t \quad \text{towards east,}$$

in which t is the local lunar time. For the sake of convenience of the comparison which will be made later, we will here convert t to the lunar time referred to the meridian 135°E. Then the above expression becomes

$$-0\cdot''01221 \sin(2t-17)=-0\cdot''01169 \sin 2t+0\cdot''00353 \cos 2t.$$

5. Attraction of the oceanic tides.

In the calculation of the deflection of a horizontal pendulum due to the attraction of the oceanic tides in the Yellow sea and its adjacent bays, Sekiguchi divided these seas into three parts, according to their tides. In A section, which is the area east-side of the meridian of 120° E and north-side of the parallel of latitude 37°20′ N, tidal constants were assumed to be the same everywhere, namely, $H_m=9\cdot 6$ ft., $\zeta_m=149°$. In B section, which is the area including the portion lying on the east side of the straight line connecting Amminto ($\varphi=36°35'$N, $\lambda=126°13'$ E) and Coppeki point ($\varphi=38°07'$ N, $\lambda=124°39'$ E) and excluding the section A, tidal constants were assumed to be $H_m=8\cdot 2$ ft., $\zeta_m=149°$ everywhere. As for the section C, which includes the remaining part of the Yellow Sea and the Gulf of Pechili, he assumed that $H_m=3\cdot 5$ ft. everywhere and that ζ_m increases uniformly with the latitude and is independent with the longitude.

Actually, however, the distribution of tides in the Yellow Sea is such that is shown in Fig. 4. This is the co-tidal and co-range chart of the Yellow Sea, as determined from the tidal constants of the ports situated on the coast of the sea under question, with due regards to the

depth and other hydrodynamical conditions of the sea. The present author calculated, by the method of mechanical integration, and using this tidal chart, the change in the direction of the plumb-line due to the attraction of the tides in the Yellow Sea by the aid of the following formulae:

$$-\frac{\gamma\rho h}{g\sin 1''}(\log r_2-\log r_1)(\cos\theta_2-\cos\theta_1) \text{ towards east,}$$

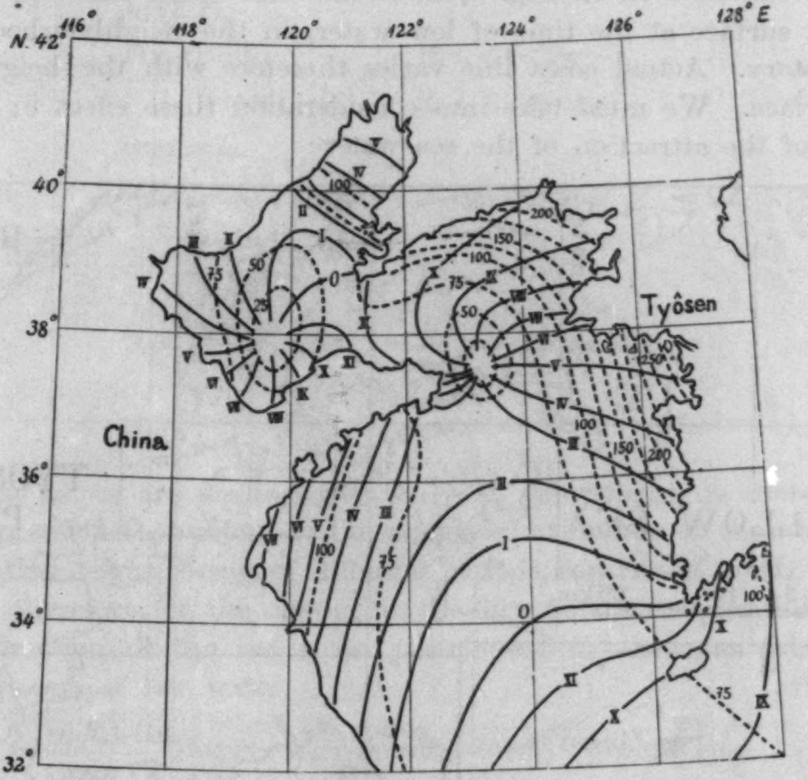

Fig. 4.

M$_2$ co-tidal and co-range chart.
Full lines—Co-tidals referred to 135° E. meridian.
Dotted lines—Co-ranges in cm.

where r = the distance from the observatory,

θ = the azimuth measured from the north in the clock-wise sense,

γ = the gravitational constant,

ρ = the density of the sea water,

and h = the height of tides above the mean sea level.

In the above expression, h is the function of the place, that is, both

of r and θ and can be calculated easily by the data given in Fig. 4 as follows:

$$h = H_m \cos\zeta_m \cos 2t - H_m \sin\zeta_m \sin 2t.$$

Results of the calculation are given in the next paragraph.

6. The correction for the slope of the sea bottom.

As can be seen in Fig. 5, there are vast areas that appear above the sea surface at the time of low water, in the neighbourhood of the observatory. Actual coast line varies therefore with the height of the sea surface. We must take into consideration these effect in the calculation of the attraction of the sea water.

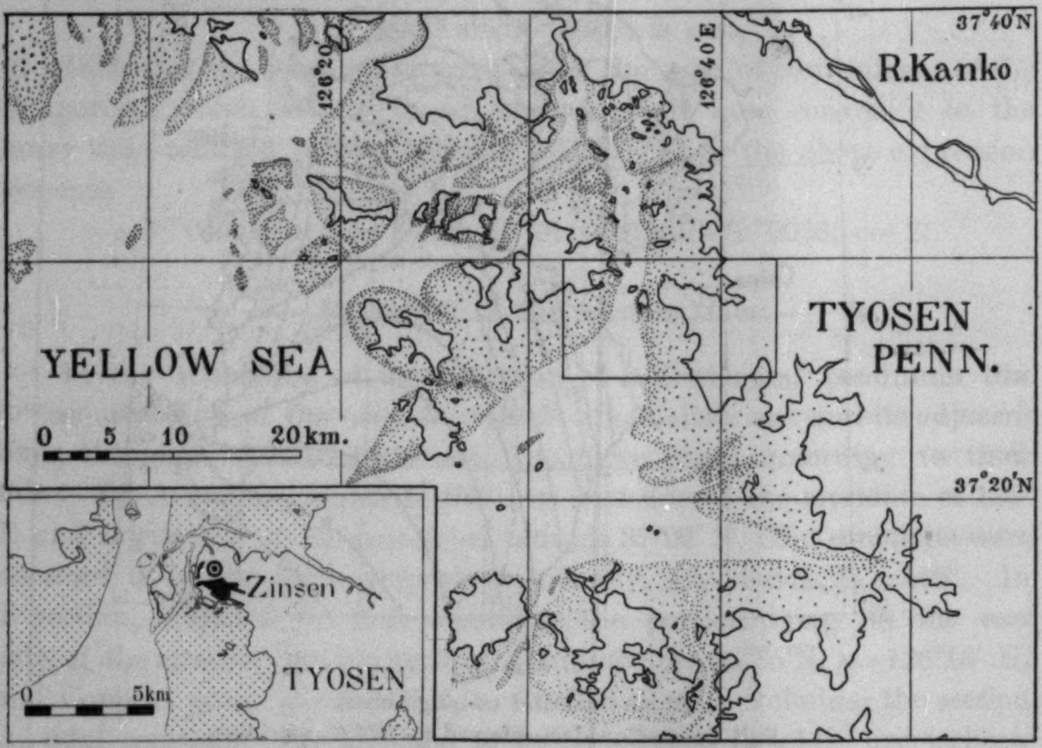

Fig. 5. The location of the observatory is indicated by ⊙. Dotted areas indicate sand-banks that appear at low water.

Sekiguchi assumed the form of the sea near the observatory to be a rectangle, with the depth uniformly increasing towards west, and the observatory being situated on the extension of the meadian line of the sea. The distance of the observatory from the nearest coast line was assumed to be 5 km. On these assumptions, he calculated mathematically the effect of the slope of the sea bottom.

In the present paper, the effect of the slope of the sea bottom was treated in a different manner, which seems to be more true to the actual condition of the sea.

Let us consider, for the sake of simplicity, only M_2 tide, and assume that the height of the sea bottom above the mean sea level be kh at a place, where h is the range of tides at the place under question and $1>k>-1$, then the variation of the water height at the place is given by

$$hf(k, t),$$

where $\quad f(k, t)=0, \qquad \text{if } t_1<t<2\pi-t_1,$

$$=\cos t-k, \qquad \text{if } -t_1<t<t_1,$$

and $\quad \cos t_1=k.$

If we put $\quad f(k, t)=A_0+A_1\cos t+A_2\cos 2+\ldots$

then we have

$$A_0=-\frac{\sin t_1}{\pi}+\frac{t_1\cos t}{\pi},$$

$$A_1=\frac{\cos t_1\sin t_1}{\pi}+\left(1-\frac{t_1}{\pi}\right),$$

$$A_n=\frac{2}{\pi(n-1)\,n(n+1)}(n\cos nt_1\sin t_1-\cos t_1\sin nt_1).$$

As far as we are dealing with only M_2 component, A_1 alone of the above expressions contribute to the calculated attraction of the sea water, because other terms, being of different periods, contribute to M_4, M_6, etc. We have therefore for the change in the direction of the plumb-line due to the attraction of the sea water distributed in the area where the bottom appears at low water,

$$-\frac{\gamma\rho hA_1(k)}{g\sin 1''}(\log r_2-\log r_1)(\cos\theta_2-\cos\theta_1) \quad \text{toward east.}$$

In the actual calculation, successive steps of r and θ were taken in such a way as

$$(\log r_{n+1}-\log r_n)=0{\cdot}1, \quad (\cos\theta_{n+1}-\cos\theta_n)=0{\cdot}1,$$

for all values of n, so we have

$$\frac{0{\cdot}01\gamma\rho}{g\sin 1''}\sum A_1(k)\cdot h$$

$$=\frac{0{\cdot}01\gamma\rho}{g\sin 1''}[\sum A_1(k)H_m\cos\zeta_m\cos 2t+\sum A_1(k)H_m\sin\zeta_m\sin 2t],$$

which will hold good not only for the areas under question but also to the remaining part of the ocean, if we consider

$$A_1(k)=1, \quad \text{if} \quad k<-1.$$

The results of the calculation are given in Table II for the successive steps of r, and is poltted in Fig. 6.

Table II.

Attraction of oceanic tides (Slope correction inclusive).

r No.	Distance km.	cos $2t$ $\times 10^{-7}$	sin $2t$ $\times 10^{-7}$
1	0·64	850″	− 472″
2	0·80	3907	− 2168
3	1.00	8517	− 4725
4	1·3	13236	− 7343
5	1·5	17148	− 9514
6	2·0	21498	−11930
7	2·5	27266	−15131
8	3	33520	−18602
9	4	39673	−22044
10	5	44764	−24895
11	6	48932	−27221
12	8	52587	−29249
13	10	56203	−31219
14	13	60938	−33628
15	16	64791	−35770
16	20	68319	−37597
17	25	73002″	−39993″
18	32	78840	−42953
19	40	84591	−45706
20	50	88825	−48171
21	64	92628	−50515
22	80	95861	−52670
23	100	98319	−54854
24	128	100034	−56814
25	160	101353	−58147
26	200	102246	−58464
27	256	102126	−58171
28	320	101193	−58127
29	400	100549	−58663
30	512	100367	−59378
31	640	100281	−59709
32	800	100148	−59616

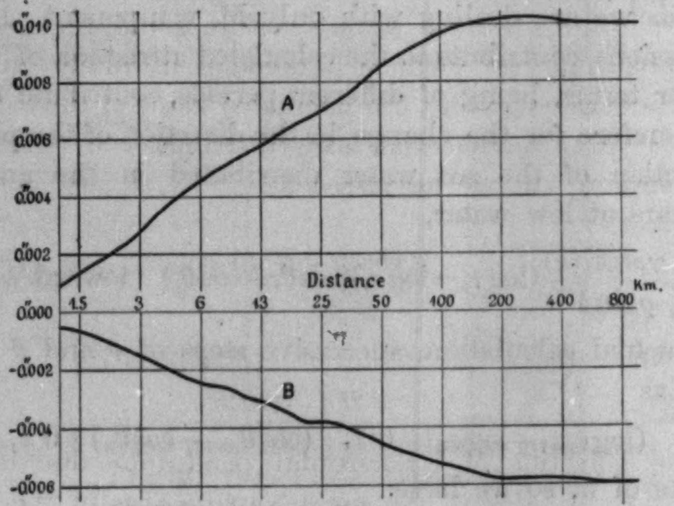

Fig. 6.

7. Tilt of the earth's surface due to tidal loads.

We have already calculated above the amount of contributions of the first four causes to the deflection of a pendulum, out of the five important causes enumerated in **3**. The last cause now to be considered

is the tilt of the earth's surface due to tidal loads distributed in the neighbouring seas of the observatory; we will calculate this contribution in this paragraph.

According to Boussinesq's solution of the problem of surface loading, tilt of the surface of an semi-infinite elastic body due to a surface load are equivalent to the direction change of the vertical due to the attraction of the load, multiplied by

$$\Theta = \frac{(\lambda+2\mu)}{4\pi(\lambda+\mu)\mu}\frac{g^2}{\gamma} = \frac{172}{\mu},$$

if we take $\lambda=\mu$ and express μ in unit of 10^{10} c. g. s.

In the case of the actual earth's crust, however, Boussinesq's solution does not hold good because of the irregularities and heterogenieties of the structure existing in the crust. It is nearly impossible to treat mathematically the problem of the tilt of the earth's surface at a station due to a surface loading. The present author introduced in his previous paper, the idea of the *effective rigidity* as a method of approximate solution of the problem. He calls μ in Θ as the effective rigidity of the earth's crust when it is considered to be the function of the distance between the load and the station, and assumes that the effective rigidity has a certain uniform value—say μ_0—within some distance d from the station, and beyond that distance it becomes infinitely large.

Under these assumptions, the calculated value of the tilt of the earth's crust at Zinsen due to the tidal loads distributed in the neighbouring seas of the station, can be expressed as

$$\frac{172}{\mu_0}(A\cos 2t + B\sin 2t),$$

where

$$A\cos 2t + B\sin 2t$$

expresses the deflection of a horizontal pendulum due to the gravitational attraction of tides in the neighbouring seas of the station, when the calculation is extended to the successive steps of distance. A and B in the above expression are therefore functions of the distance from the station, and are plotted in Fig. 6.

Comparing the coefficients of the cosine terms and sine terms of the observed tilt with those of the calculated one, we obtain the following two equations:

Observed values		Attraction of the moon and the earth-tides	Attraction of the sea water	Tilt due to tidal load
$0''\!\cdot\!0411$	=	$0''\!\cdot\!0035\,D$	$+0''\!\cdot\!0100$	$+172\,A/\mu_0$,
0	=	$-0''\!\cdot\!0117\,D$	$-0''\!\cdot\!0060$	$+172\,B/\mu_0$,

or, to be the same thing,

$$+0''\!\cdot\!0311=+0''\!\cdot\!0035\,D+172\,A/\mu_0,$$
$$+0''\!\cdot\!0060=-0''\!\cdot\!0117\,D+172\,B/\mu_0.$$

As can be seen in Fig. 6, the functions A and B are approximately proportional to each other, the ratio of the value of A to that of B being the same for all values of distance. We can therefore eliminate from the above two equations the terms which include the effective rigidity, the most vague quantity in the equation, making use of this relation existing between A and B.
Then we have

$$D=-2\cdot6.$$

The generally accepted value of D is 0·8, which gives for the rigidity of the earth 13×10^{11} c. g. s. or so. Negative values of D or the values of it greater than the unity are theoretically meaningless. This absurdity in the value of D is probably due to the fact that there is phase-lag between the actual and the calculated values of the tilt of the earth's crust due to tidal loading. These features will be clearly seen in Fig. 7, a vector diagram like that used in the theory of the of the alternating electric current.

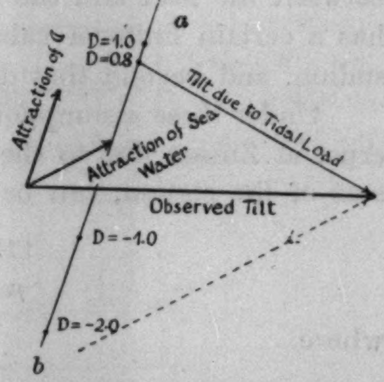

Fig. 7. Vector diagram of the observed and calculated tilts.

In the figure, the resultant vector of the attraction of the moon and the earth-tide is taken on the line $a\ b$, which is parallel to the attraction of the moon. Then, if we assume that the tilt due to tidal loading is in phase (dotted line in the figure) with the attraction of the sea water, the value of D must be $-2\cdot6$ in order to give the observed tilt. On the contrary, if we assume that $D=0\cdot8$, then the tilt due to tidal loading becomes out of phase with the attraction of sea water, the phase-lag being about 2 hours.

When we disregard this phase-lag, and assume that the value of D is 0·8, and also that the effective rigidity of the crust is the same for all

distances from the station, we obtain as the rigidity of the crust $6{\cdot}2 \times 10^{11}$ c. g. s., which value does not vary much even if we assume different values for D. This value of the rigidity of the earth's crust is very near to the value of the crust assumed by Sekiguchi.

In conclusion, the writer wishes to express his most cordial thanks to Dr. R. Sekiguchi for his generosity of permitting the writer to make this revision, using the results of his observation.

---

52. 仁川に於て觀測された地殼の傾斜運動に就いて

地震研究所 高橋龍太郎

此の論文に記載せるものは、著者自身に依つて爲された觀測ではなく、1916 年に關口鯉吉氏に依つて爲された觀測を計算し直したものである。關口氏の計算に於ては潮汐及び仁川附近の海岸に非常に多く分布する干出の取扱に就いて稍〻粗末ではないかと思はれる假定が二三存在する。著者は此の點に關して多少の變更を試み、且つ關口氏と異つた計算方法を用ひて計算をやり直して見たのである。其の結果は次の如く、大體に於て關口氏の得られたものと同一であるが、多少の異なる點も無いでもない様である。

計算の結果に依れば、仁川の地殼は、潮差二米突余の太陰半日潮と、其の起潮力に對して振幅 0·″041 の傾斜運動を爲してゐるが、潮汐と其れの荷重に因つて生ずる地殼の撓曲との間には約二時間の位相差が存在するのである。地殼潮汐の減少率を 0·8 とし、且つ此の位相差を考へぬ事にすれば、地殼の剛性として $6{\cdot}2 \times 10^{11}$ c. g. s. なる値を得る事になる。

---

53. *On Depression of the Earth's Crust in Honzyô and Hukagawa, Tokyo.*

By Naomi MIYABE,

Earthquake Research Institute.

(Read July 21, 1932.—Received Sept. 20, 1932.)

1. The result of the recent precise levelling along the routes passing through Honzyô and Hukagawa, Tokyo, shows remarkable depressions of the bench-marks distributed in this region. Among them, B. M. 9832, situated at Higasi-Hirai-tyô, and B. M. 3378, situated at Kayaba-tyô, were depressed more than 15 cm. during 1930–1931. A zone including these two bench-marks are regarded as the zone of maximum depression. In the preceding paper,[1] it was pointed out that the zone of maximum depression was coincident with the zone in which several wells yielding methane gas were located. The zone of maximum depression was shown also as coincident with a valley in the Tertiary surface features, reproduced from the data obtained by the authorities of the Reconstruction Bureau. In his recent investigation, Prof. A. Imamura has regarded this zone of maximum depression as the west boundary of Kôtô Block.[2]

2. As the matter of fact, the bench-marks in Honzyô and Hukagawa have been depressed considerably since the Kwantô Earthquake of 1923.

On the other hand, there is not a portion in Honzyô and Hukagawa where the level of the ground surface is much higher than 3 m. above the mean sea level. If, therefore, the general feature of the ground surface is represented by the present heights of the bench-marks in this region and the depression of the earth's crust continues with the rate with which it is now being depressed, it is a matter of worry to predict that the ground of this region may surely go down into the water in scores of years hereafter. Total amounts of depressions during 1925–1931 and the heights in 1925 and in 1931 of the bench-marks in this region are given in Table I.

As shown in the table, the heights of the bench-marks have been

1) N. MIYABE, *Proc. Imp. Acad.*, 7 (1931), 344.
2) A. IMAMURA, *Jap. Journ. Astro. Geophys.*, 8 (1931), 177.

Table I.

B. M.	Locality	Heitght 1926	Displacement (1926—1931)	Height (1931—VII.)
		m.	mm.	m.
0	Yokoami	1·8241	− 62·4	1·7617
3379	Koidumi-tyô	1·1776	−221·2	0·9564
3378	Kayaba-tyô	0·9432	−734·5	0·2087
3377	Kameido	1·6711	−319·0	1·3521
9831	Hukagawa Kôen	1·3283	−287·2	1·0411
9832	Higasi Hirai-tyô	0·8350	−532·6	0·3024
9833	Sunamati	0·9303	−210·9	0·7194
9834	„	0·1339	−304·7	−0·1708
			(1926—1930)	(1930—II-III.)
		m.	mm.	m.
3375	Higasi Komatugawa	1·2877	−160·9	1·1268
3376	Nisi „	0·6871	−193·8	0·4933
9835	Matue-mati	2·5138	−124·2	2·3996
9836	Kasai-mura	1·7273	−121·5	1·6058

so much lowered that, in 1931, B. M. 3378 (Kayaba-tyô) stands at 0·2087 m., B. M. 9832 (Higasi-Hirai-tyô) at 0·3024 m. and B. M. 9834 (Suna-mati) at −0·1708 m. above the mean sea level. Hence, if the houses are built on the ground surface at such a height that is represented by the present heights of the bench-marks, it is possible that they should be inundated at high tide, since the maximum range of the semi-diurnal tide in Tokyo Bay a little exceeds 2 m. In autumn of the last year (1931), the newspaper reported for several times that the houses in Hukagawa were inundated at high tide. In Fig. 1, the shaded areas represent the flooded areas at high tide of the last autumn. It is said that the houses are inundated at high tide in the season, from summer to autumn, in these two or three years, and that the height of the flood in the last autumn was so conspicuous that a similar case was never experienced before, but for the cases due to heavy rains.

The land of Honzyô and Hukagawa was reclaimed after the Kwantô Earthquake of 1923, to keep the level of the ground surface at least 8 feet above the A. P. Level.[3] As the maximum range of the semi-diurnal tide in the Tokyo Bay does not much exceed 2 m., the land of Honzyô and Hukagawa should not be inundated at high tide, provided that

3) The A. P. Level is the level by 1·1344 m. lower than the mean sea level of Tokyo Bay which is taken as the standard datum for the heights of all bench-marks.

there had been neither a considerable depression of the land nor an abnormal rise of the water surface.

3. Mareographs are installed at several places in Hukagawa and the levels of the water are continuously recorded since before the Kwantô Earthquake under the supervision of the authorities of the Civil Engineering Bureau of the Municipality of Tokyo. Among these, the mareograph at Heikyû-tyô (marked by × in Fig. 1) is situated nearest to the zone of maximum depression mentioned in the preceding paper. By the courtesy of the municipal authorities of Tokyo, the author was able to review the mareograms taken at Heikyû-tyô.

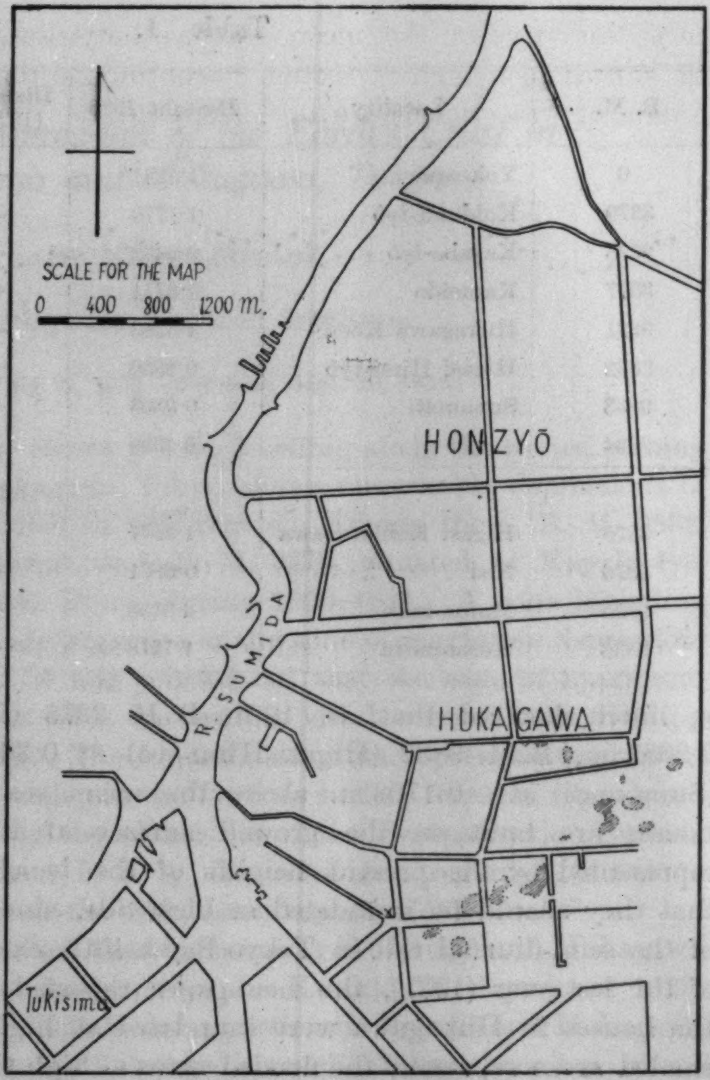

Fig. 1. Distribution of Flooded Areas in Hukagawa, Last Autumn (Nov. 1931).

In order to obtain the curve of the mean sea level at Heikyû-tyô, the heights of the water level was read on the mareograms at every hour. Heights of the water level thus obtained were averaged for every 29 days to diminish terms of semi-diurnal, diurnal and fortnight periods and the resulting curve is shown in Fig. 2. It must be remarked that the mareograms are not taken during the time interval April—May of 1926, as the mareograph was in disorder. After May 1926, the heights of the water level on the mareogram is referred to a different zero-line.

Hence, the curve of the mean sea level afterwards 1926 should be a little shifted to a higher position to continue to the curve obtained from the data of water levels during 1923–1926.

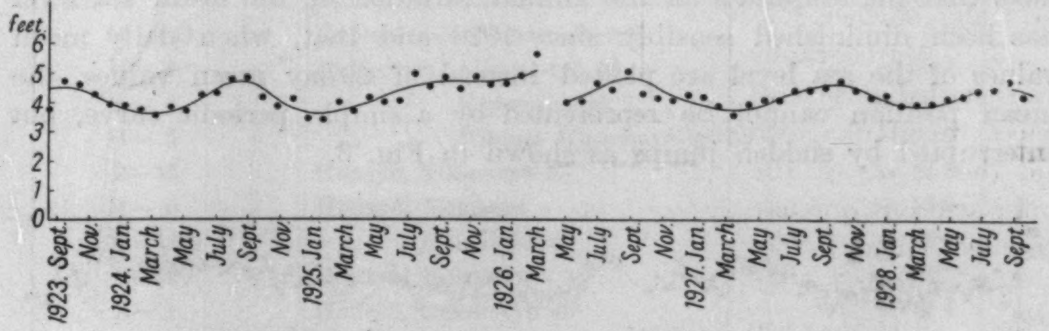

Fig. 2. 29 Day Mean Sea Level at Heikyû-tyô, Hukagawa.

Following facts are noticed in the curve of the mean sea level in Fig. 2.

a) The mean sea level oscillates with an approximate annual period. It is highest towards the end of summer and lowest towards the end of winter, the amplitude being about 30 cm. or less. This fact agrees with the phenomenon that the inundation in Hukagawa at high tide is experienced most frequently in summer and autumn.

b) In addition to the annual period in the change of the mean sea level there exists a secular change, as will be seen in Fig. 2. The mean sea level in 1926 is about 20 cm. higher than that in 1923. During the same period of time, the vertical displacements of B. M. 9831 was −74·5 mm. The gradual rise of the mean sea level at Heikyû-tyô is, therefore, 2·7 times the amount of depression of B. M. 9831 during 1923–1926. This value of the ratio is approximately the same with the ratio of the amount of depression of B. M. 9831 to that of B. M. H–15 measured as had occurred during 1929–1932, the latter ratio being 2·4. As the bench-mark H–15 is situated very near the portion where the mareograph under consideration is situated, the secular upheaval of the mean sea level noticed in the mareograms taken at Heikyû-tyô may be regarded as the depression of the earth's crust, if the crust movement had been continued in the same sense since 1923, as that observed during 1929–1932. As for the vertical displacements of the bench-marks during 1929–1932, descriptions and discussions are given afterwards.

As a matter of fact, we cannot notice any sign of secular upheaval of the mean sea level in the curve afterwards 1926, while the earth's

crust was deformed continuously in the same region. Here, it may be conjectured[4] that there had been an intentional adjustment of the referrence lines on the recording paper. The conjecture is based on the facts that the amplitude of the annual variation of the mean sea level has been diminished sensibly since 1926 and that, when daily mean values of the sea level are plotted instead of 29day mean values, the mean position cannot be represented by a simple periodic curve, but interrupted by sudden jumps as shown in Fig. 3.

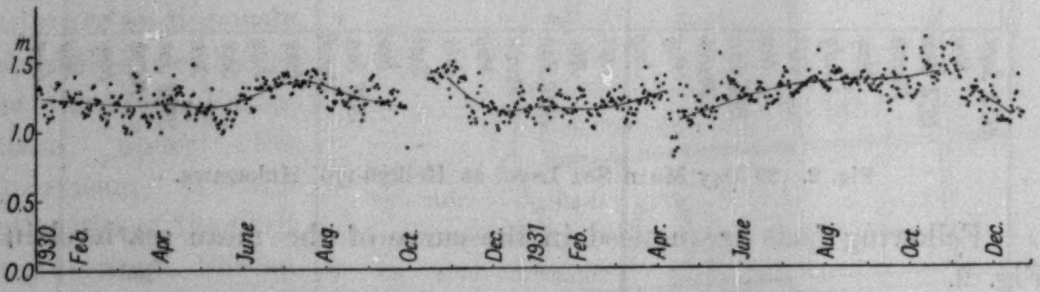

Fig. 3. Daily Mean Sea Level at Haikyû-tyô, Hugagawa.

4. On account of frequent inundations in Hukagawa at high tide and remarkable depressions of the bench-marks shown as the results of recent precise levellings carried out by the authorities of the Military Land Survey, the municipal authorities of Tokyo decided to carry out a revision of precise levelling survey in the region of Honzyô and Hukagawa, where the former survey was carried out by the same authorities in Nov. 1929.

There are 42 bench-marks distributed in Honzyô and Hukagawa including Tukisima, 33 of which are installed by the municipal authorities,[5] 4 of which by the authorities of the Reconstruction Bureau[6] and the remaining 5 bench-marks are installed by the authorities of the Military Land Survey.[7]

The geographical distribution of these bench-marks is shown in Fig. 4.

The revision of the precise levelling was carried out in Jan.-April of this year (1932), and the vertical displacements of these bench-marks measured which had occurred during these 2·3 years. The amounts of vertical displacements of these bench-marks are given in Table II.

4) The conjecture was ascertained afterwards.
5) Shown by marks ● and numerals with prefix H or Z.
6) Shown by marks ○ and numerals with prefix R.
7) Shown by marks ⊙ and numerals with prefix M.

Table II.

B.M.	Locality	Vertical Displacement ΔH. During Nov. 1929—March 1932.
M—J-O	Kyôbasi, Sin Hunamatu-tyô	− 3·9^{mm}
H— 1	Hukagawa, Aikawa-tyô 18	− 69·1
H— 4	„ Kiyozumi-tyô 7	−186·9
H— 5	„ Mihuna Kuramaye-tyô 33	−163·9
Z—15	Honzyô, Titose-tyô 55	− 37·9
M— 0	Honzyô, Yokoami	− 13·9
M—3379	„ Koizumi-tyô	− 92·0
R−32	Honzyô, Yokoami	− 99·7
Z— 1	Honzyô, Omote-tyô 43	− 10·4
Z— 2	„ Nakanogô-Kawara-mati 1	− 17·5
Z— 8	„ Nakanogô-Narihira-tyô	—
Z— 6	„ Yanagisima-Moto-mati 186	−175·0
Z— 7	„ Yanagisima-mati	−206·7
M—3378	Honzyô, Kayaba-tyô	−234·5
H— 8	Hukagawa, Honmura-tyô	−235·6
H— 9	„ Senda-mati	−298·0
M—9832	Hukagawa, Higasi-Hirai-tyô	−208·0
H—12	Hukagawa, Higasi-Hirai-tyô	−152·6
H—13	„ Kiba-mati 13	−371·2
M−9831	Hukagawa, Hukagawa-Kôen	−137·4
R—35	Hukagawa, Monzen-Yamamoto-tyô	−216·9
Z— 3	Honzyô, Sumida-Kôen	− 39·1
Z— 4	„ Susaki-tyô 179	− 97·5
Z— 5	„ Ukedi-mati 75	—
Z—10	„ Isiwara-tyô III-2	−151·6
Z— 9	„ Taihei-tyô I-62	−209·7
Z—14	„ Hayasi-tyô I-2	−119·6
Z−11	„ Midori-tyô II-3	−168·0
Z—12	„ Kikukawa-tyô I-3	−313·5
Z—13	„ Hayasi-tyô II-89	−190·1
H— 7	Hukagawa, Higasi-Ôgibasi 25	−145·7
H— 2	„ Zaimoku-tyô 12	−221·1
H— 3	„ Nisi-Hirano-tyô 6	−177·5
H— 6	„ Higasi-Daiku-mati 62	−226·0
H—10	„ Miyosi-tyô 1	−124·6
H—11	„ Nisi-Hirai-tyô 73	−152·1
H—14	„ Susaki-Benten-tyô I-17	−118·9

(*to be continued.*)

Table II. (*continued.*)

B.M.	Locality	Vertical Displacement ΔH. During Nov. 1929—March 1932
H—15	Hukagawa, Huruisiba	$-322{\cdot}0^{mm}$
H—16	„ Hamazono-tyô	−128·6
H—17	„ Ettyûzima-mati 8	−228·2
H—18	„ Ettyûzima-mati 1	− 54·1
R—15	Kyôbasi, Sin-Tukudazima	9·0
R—13	„ Tukisima	6·0

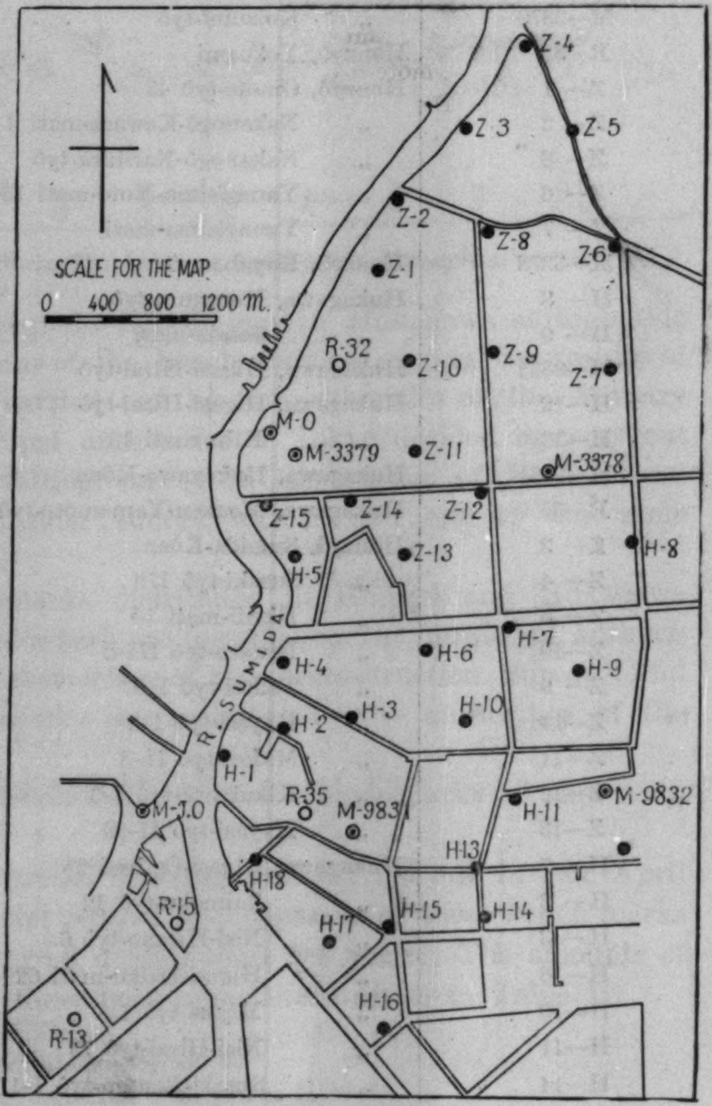

Fig. 4. Distribution of Bench-marks in Honzyô and Hukagawa.

Errors of the measurements are, of course, not so small. But, as the amounts of the vertical displacements are large enough, the general feature of the deformation of the earth's crust may not be much affected by these errors.

In analysing the present data of vertical displacements of the bench-marks distributed in Honzyô and Hukagawa, the whole area is divided into six regions. Corresponding to Regions I, II, III and IV respectively, Blocks with their magnitudes and azimuths of their tiltings are determined by using as the data the vertical displacements of the bench-marks, through the relation

$$\tan \varphi = \tan \varphi_m \cos (\theta - \theta_m),$$ [8]

where φ_m and θ_m are magnitude and azimuth of tilting of Block respectively.

The azimuths and magnitudes of tiltings of these blocks are determined graphically as shown in Figs. 5a, 5b, 5c and 5 d. The numerical values of φ_m and θ_m of tiltings and the mean vertical displacements, $\overline{\Delta H}$, of these blocks are given in Table III.

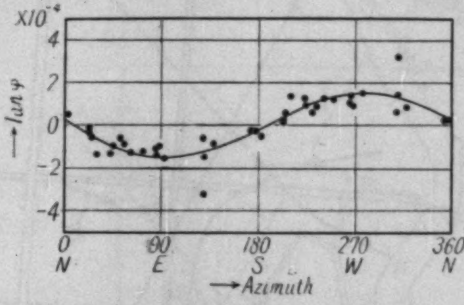

Fig. 5 a. Graph determining φ_m and θ_m of Block I.

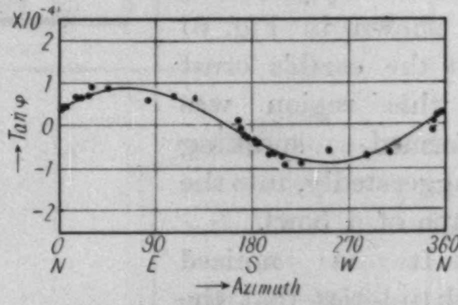

Fig. 5 b. Graph determining φ_m and θ_m of Block II.

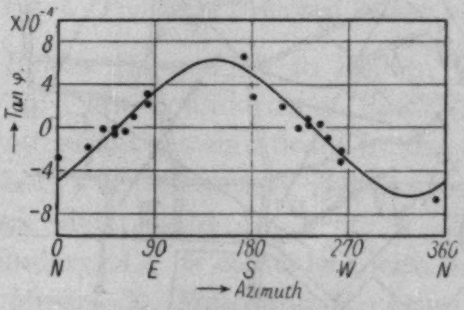

Fig. 5 c. Graph determining φ_m and θ_m of Block III.

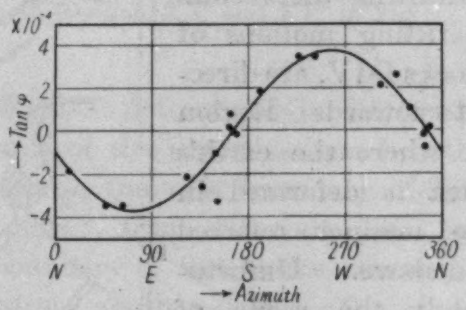

Fig. 5 d. Graph determining φ_m and θ_m of Block IV.

Table III. Magnitudes and Directions of Tiltings and Mean Vertical Movements of Blocks.

Block	Direction of Tilt. Referred to N. θ_m	Magnitude of Tilt. φ_m in 10^{-4}	Mean Vertical Move. $\overline{\Delta H}$ in mm.
I	99° (S 81° E)	1·5	− 97·5
II	247° (S 67° W)	0·86	−252·2
III	326° (N 34° W)	6·3	−241·2
IV	76° (N 76° E)	3·7	−157·9
V	—	—	−167·1

8) N. Miyabe, *Proc. Imp. Acad.*, 7 (1931), 150. *Bull. Earthq. Res. Inst*, 9 (1931), 256.

As for the Region V, a plane or a tilted block cannot be determined as in the case of Regions I–IV. But the contours lines of equal depression are so simply drawn (as shown in Fig. 6) that the earth's crust in this region was deformed, speaking exaggeratedly, into the shape of a bowl.

It is noticed with interest that the arrows in Fig. 6, representing the vectors of tilting motions of Blocks I–IV, are directed towards Region V, where the earth's crust is deformed in the manner referred to above. Unfortunately the mode of deformation of the earth's crust in the sixth region, i. e., the northern most region is not clearly determined for the lack of the data of vertical displacements of the bench-marks Z–5 and Z–8.

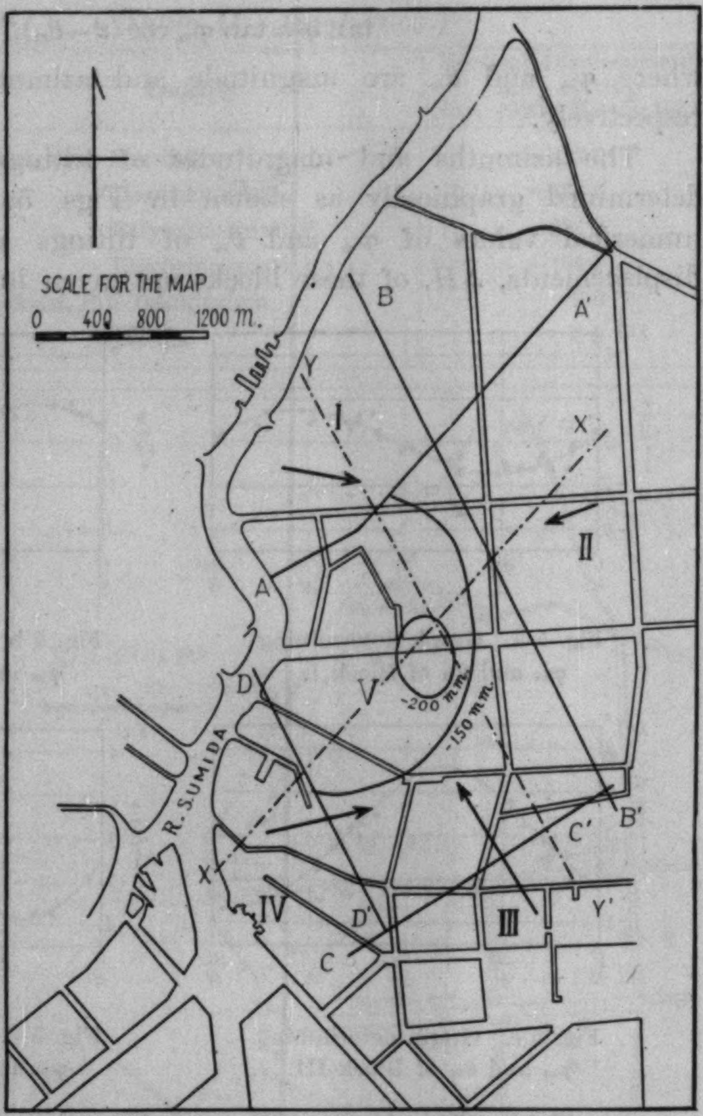

Fig. 6. Block Movements and Deformation of the Earth's Crust in Honzyô and Hukagawa.

In Fig. 7, profiles of sections XX' and YY' in Fig. 6 are shown with much exaggerated vertical scale. Blocks III and IV are strongly tilted towards NW and NE respectively and the zones including the boundaries of these two blocks to Region V are exceedingly depressed. Amount of depression in this zone exceeds 30 cm. in these 2·3 years.

It may be remarked that the regions which inundated at high tide are approximately coincident with the zones including the boundaries

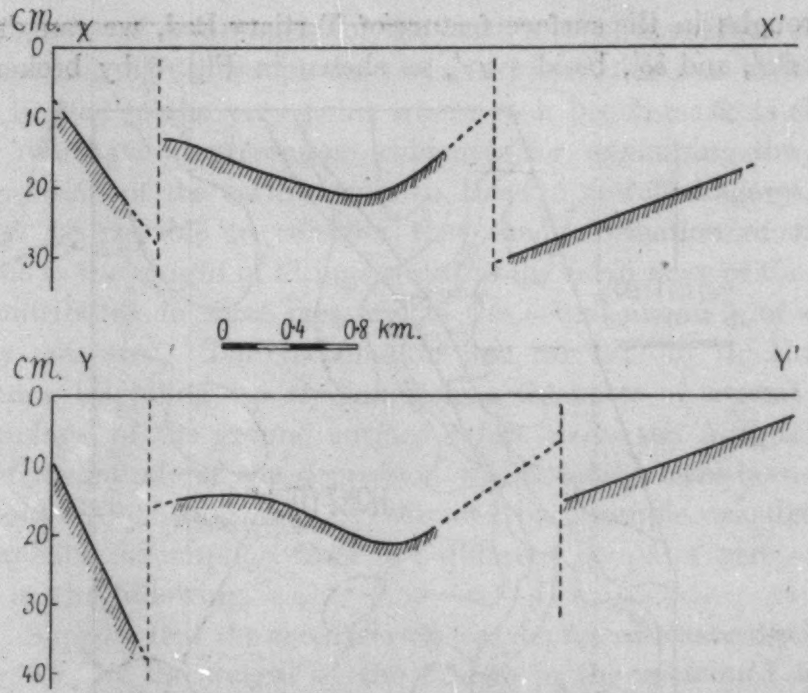

Fig. 7. Profiles of Deformed Surface of Earth (Section XX' and YY' in Fig. 4).

of Blocks III and IV to Region V.

5. The boundaries of Blocks or Regions determined in the present investigation are significant in the results of the investigations by other authors; i.e., Boundary BB' corresponds to the west boundary of Kôtô Block determined by Prof. A. Imamura[9] from different data, and Boundary AA' is coincident with the boundary of the blocks determined by Messrs. K. Muto and K. Atumi[10] from another data.

In the preceding paper,[11] we have pointed out the coincidence of the zone of maximum depression including B.M. 9832 and B.M. 3378 with a valley in the Tertiary surface features. To investigate the matter in more detail, the surface feature of the Tertiary Bed in the region of Honzyô and Hukagawa was thoroughly reproduced from the data obtained by the authorities of the Reconstruction Bureau. The map of Fig. 8 shows the surface features of the Tertiary Bed in Honzyô and Hukagawa thus reproduced. In the figure, $\gamma\gamma'$ denote the valley in the Tertiary surface features previously remarked. This central line denoting the course of the valley is directed from NE to SW. By connecting

9) A. Imamura, *loc. cit.* 2).

10) K. Muto and K. Atumi, *Bull. Earthq. Res. Inst.*, 7 (1929), 495.

11) N. Miyabe, *loc. cit.* 1).

axis of troughs in the surface feature of Tertiary Bed, we can draw the lines $\alpha\alpha'$, $\beta\beta'$, and $\delta\delta'$, besides $\gamma\gamma'$, as shown in Fig. 8 by broken lines.

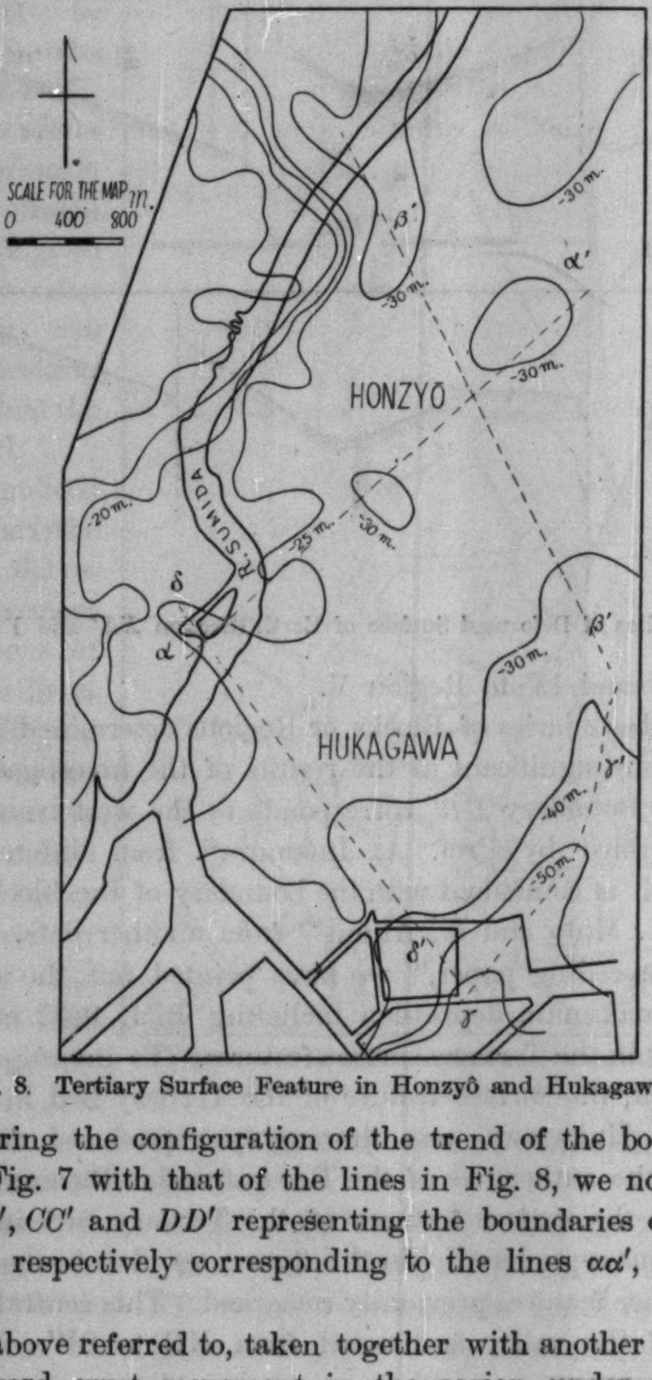

Fig. 8. Tertiary Surface Feature in Honzyô and Hukagawa.

In comparing the configuration of the trend of the boundary lines of blocks in Fig. 7 with that of the lines in Fig. 8, we notice that the lines AA', BB', CC' and DD' representing the boundaries of the blocks in Fig. 7 are respectively corresponding to the lines $\alpha\alpha'$, $\beta\beta'$, $\gamma\gamma'$ and $\delta\delta'$ in Fig. 8.

The fact above referred to, taken together with another fact that the rate of downward crust movement in the region under consideration seems to be accelerated in these several years,[12] suggests us that the

12) N. MIYABE, *Bull. Earthq. Res. Inst.*, 10 (1932), 597.

present mode of deformation of the earth's crust is neither simply due to the settling of fillings in the reclaimed land nor due to local disturbances limited to the very point where each bench-mark is situated.

6. We have at present no evidences for explaining the course of the depression of the earth's crust in Honzyô and Hukagawa. It may, however, be possible to consider that the deformation of the earth's crust due to the weight of fillings added to the earth mass of the reclaimed land contributes, in some measure, to the actual amounts of depression recently measured. The reclamation was carried out in Honzyô and Hukagawa by piling up the muds to a thickness of several metres to keep the level of the ground surface 8 feet above the A. P. Level. The order of magnitude of the depression which might have been caused by the weight of the fillings may be estimated by a simple calculation based on a probable assumption from two different points of view, as will be shown in the following.

a) Suppose that the earth's crust was depressed elastically by surface loading, i.e., by the weight of the fillings in the reclaimed land, then we have the following expression for the vertical displacement, w, after Boussinesq,

$$w = -\frac{1}{4\pi\mu}\frac{\partial^2}{\partial z^2}\int r\,dP + \frac{2\lambda+3\mu}{4\pi\mu(\lambda+\mu)}\int\frac{dP}{r}.$$

Assuming that the surface loading is uniform over the circular area of radius R, the vertical displacement, w, at the periphery of the circular area is given by Prof. H. Nagaoka,[13] in the form

$$w = \frac{\lambda+2\mu}{\pi\mu(\lambda+\mu)}\rho g h R,$$

where $\rho g h$ corresponds to the load on a unit area, ρ is the density and h is the thickness of the fillings. In the present case, the following numerical values may be adopted as probable:

$$\rho = 2{\cdot}0.$$

$$\delta = 1/4 \text{ (Poisson's ratio).}$$

$$g = 9{\cdot}8\times10^2\,\text{cm./sec.}$$

$$h = 5\,\text{m.}$$

$$R = 2\,\text{km.}$$

$$\mu \fallingdotseq 10^{10}\,\text{c.g.s.}^{14)}$$

---

13) *c.f.* H. Nagaoka, *Publ. Imp. Earthq. Inv. Com.*, No. 22 B (1906), 1.

14) Prof. S. Kusakabe has shown that E (Young's modulus) of the wet sandstone is $3{\cdot}2\times10^{10}$ c.g.s.; S. Kusakabe, *ibid.*, No. 22 B (1906), 27.

Then we have

$$w \fallingdotseq 12 \text{ cm.}$$

The estimated depression in this case is a little smaller than the actual depression, but of the same order of magnitude. The amount of depression estimated above, indicates the depression at the periphery of the area of surface loading. Hence, the amount of depression at the centre[15] of the area will be a little greater, i.e., closer to the actual amount of depression.

b) Suppose that the earth's crust consisted of a material like a mass of sand, and the density is uniform. By piling up the fillings to the thickness of h, the region surrounding the reclaimed land was upheaved, i.e., the reclaimed land was depressed, say, by w. Then we have the relation, after the theory developed by Prandtl,

$$\frac{w}{h}=\frac{1-\sin\rho}{1+\sin\rho}e^{-\pi\tan\rho},$$

where ρ is an angle of repose of the sandy crust.

Substituting

$$h=5 \text{ m.},$$

and

$$\rho=30°,$$

in the above relation, we have

$$w \fallingdotseq 28 \text{ cm.}$$

The estimated amount of depression, in this case, is closer to the actual amount of depression.

Thus, the estimated amounts of depression as calculated above are of the same in order of their magnitudes with each other and also with those of actual depression. Hence, it may be thought possible, if not probable, that the actual depression measured by the revision of the levelling survey contains an effect due to elastic or plastic deformation of the earth's crust caused by the surface loading, i.e., the weight of the fillings in the reclaimed land.

In conclusion, the present writer wishes to express his sincere thanks to Professor Torahiko Terada for his kind advices and guidance

---

15) The amount of depression at the centre is given by

$$w=\frac{\lambda+2\mu}{\pi\mu(\lambda+\mu)}\rho g h R.E(0).$$

Substituting the numerical values referred to above, we have

$$w \doteq 18 \text{ cm.}$$

and to Late Professor Kyoji Suyehiro for his kind advices and encouragements. Cordial thanks are also due to Messrs. Y. Otuka, T. Takayama, S. Kawasima and T. Watanabe, for their valuable assistances, and to the Municipal Authorities of Tokyo for their kindness in placing the valuable data at the writer's disposal.

---

53. 本所及び深川に於ける土地の沈降

地震研究所　宮部直巳

本所深川方面に在る陸地測量部の水準點が年々著しく沈降することは既に前報告に於いて注意した所であるが、昨年（昭和六年）秋には、大潮の滿潮時に深川方面一帶が海水の浸入を受けるに至つた。この浸水は、尤も、それ以前にもあつたのであるが、昨年は一層甚だしかつたといふことである。一方に於いて、平久町に設置されてゐる檢潮儀の記錄からは平均海水面が 1923—1926 の間に徐々に上昇してゐたことが知られた。此に於いて、東京市土木局では、本年（昭和七年）一月から四月に亘つて、本所深川方面の水準測量を遂行した。水準點は陸地測量のものの外、復興局及び東京市土木局のものを加へて合計四十二個あり、從つて、その水準測量の結果、深川方面の土地の變形狀況が一層詳細に知られることになつた。本文に於いては主としてその結果を取扱つたものである。

敍上の水準測量によつて知られた各水準點の垂直變動を解析した結果は次の如く要約される。

i) 本所深川一帶を六個の部分に分けることが出來、その中の四個については、各部分内にある水準點の垂直變動量を、その各部分がそれぞれ傾斜せる地塊であるとして說明し得る。是等四個の地塊は第五の部分を圍繞して存し、而も、各地塊の傾斜の方向は何れもこの中心部分を指してゐる。又この中心部分における變形は凹形の椀の如き形を示してゐる。

ii) 各地塊の境界は夫々他の方面よりも意味あるものの如く、その一は、今村博士の定められた江東地塊の西緣と一致し、他の一は、武藤、熱海兩氏が、他のデータから定められたものと一致する。又是等の境界線は、復興局に於いて調査されたデータから決定されたこの方面の第三紀層の表面地形にあらはれてゐる低地を連ねた線とも略〻一致する。

以上の垂直變動が何によつて起されたかは未知の問題に屬するけれども、地表を埋立てた埋土の荷重による、彈性的又は可塑性的變形として期待される變動量は、測量の結果得たものと、オーダーに於いては一致する。從つて斯樣な意味の變形もこの場合全然無視して考慮の外に置くことは出來ないのではないかと思はれる。

---

54. ピボットに働く摩擦力率の測定

地震研究所　石 本 巳 四 雄
萩 原 尊 禮
吉 田 幸 雄

(昭和七年七月五日發表——昭和七年九月二十日受理)

緒言

從來地震計の性能を論ずるに當つて、固體摩擦としては煤紙上を滑る描針に於ける摩擦力のみを問題として居たが、地震動を槓桿を用ひて擴大する時その回轉軸には多くピボットを使用する關係上其處に働く固體摩擦をも考慮することが必要である。然し此のピボットに働く摩擦力率に關しては充分の調査が見當らぬため、今回此の摩擦力率の大きさ、性質を測定するため實驗を試みることとした。

裝置

測定に用ひた裝置は第一圖に示す如く、A、B の兩部分より成り、A は臺に固定せられ、B は刄先 C に依り A の上に支へられて居る。質量 F 及 G の位置を適當に加減し、B 部分の重心を刄先 C に持ち來たす。而して CE' の距離と CD の距離とは等しいから、D に於ける重錘の重量に等しい力がピボットの兩端に働くことになる。又ピボット P には輕いアルミニウムの棒 M を附し一種の振子を形成せしめる。

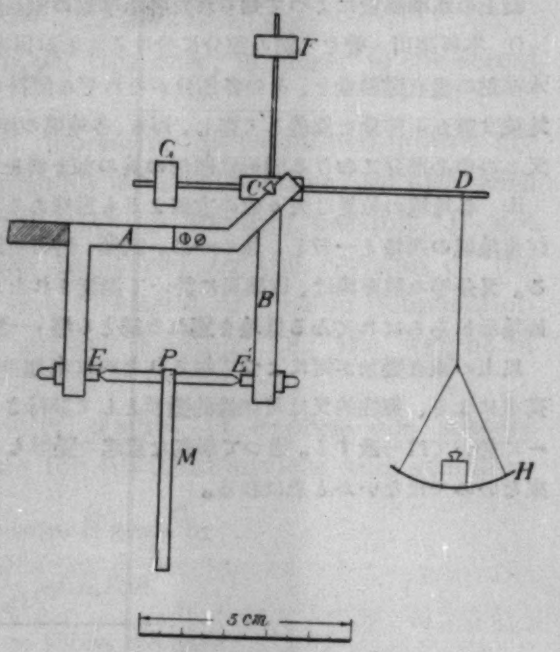

第1圖　實驗の裝置

此の振子の運動を考へるに、振幅が相當小であり又空氣の抵抗を度外視すれば次の式で表される

$$I\frac{d^2\theta}{dt^2}+mgh\theta\pm R=0,$$

但し. $\frac{d\theta}{dt}>0$ のとき $+R$, $\frac{d\theta}{dt}<0$ のとき $-R$

此處に θ は振子の廻轉角、I は振子の慣性能率、m は振子の質量、h は振子の廻轉軸より重心に至る距離、g は重力常數、R はピボットに働く固體摩擦力率、t は時間である。

從つて $t=0$ に於いて $\frac{d\theta}{dt}=0$, $\theta=\theta_0$ とすれば

$$\theta\pm\rho=(\theta_0\pm\rho)\cos\sqrt{\frac{mgh}{I}}\,t,$$

$$\rho=\frac{R}{mgh}.$$

從つて一往復振動に依る振幅の減小は 4ρ となり、θ_0 に比較して ρ が小である時は、或る定つた角 θ_0 から振子を振動せしめて振子が靜止するに至る迄の振動回數を N と置けば次の關係が得られる。

$$4N\rho\fallingdotseq\theta_0,$$

從つて

$$R\fallingdotseq\frac{mgh\theta_0}{4N}.$$

此の式に依り、θ_0 及び N を測定することに依り簡單に摩擦力率 R を決定することが出來る。

實驗に用ひたピボットは燒入鋼鐵製で、先端の鈍、鋭及び其の中間の三種、受けの皿は眞鍮、鋼鐵、瑪瑙の三種を採用し、是等を色々に組合せピボットに加はる壓力を變化せしめて測定を行つた。上述の方法から求めた結果がどの程度まで正確であるかを知るため、ピボットの受皿が鋼鐵の場合に就き、振子の運動を寫眞裝置により廻轉ドラム上のブロマイド紙に記錄せしめ、一般の固體摩擦の値を出す時と同樣の方法に依り摩擦力率の値を定めて見た。二方法に依つて得られた結果を比較すると極めて良く一致し、寧ろ前者の方が簡單であつて多くの數値が得られ其の平均を取ることに依つて滿足すべき値を得ることが出來ることが判つた。尚寫眞記錄の上からは空氣に依る摩擦の影響を省略して良いことも確められた。

實驗の結果

實驗はピボットに加はる壓力の小なる場合より開始し次第に壓力を增加し、或る値に達して後又壓力を次第に減少せしめて始めの壓力に戻した。普通一つの場合に就き五回の測定をなしその平均の値を採用することとした。第二圖はその一例としてピボ

ットの鈍なる場合に就いて得られた結果を示すものである。此の圖より明かなる如

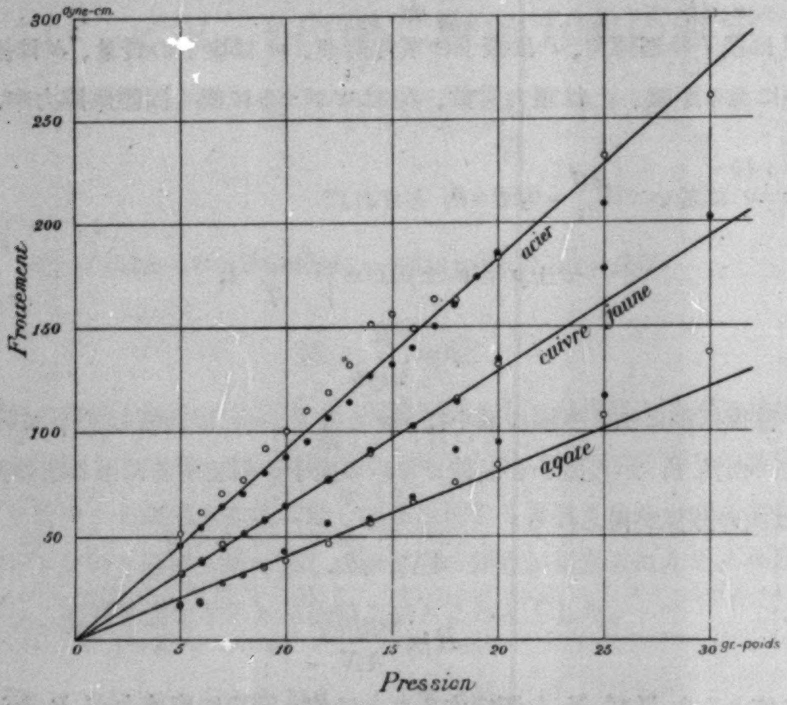

第 2 圖　壓力と摩擦力率との關係（ピボット鈍）
○壓力を增加せしめた場合
●壓力を減少せしめた場合

く、摩擦力率は後に述べる特別な場合を除いてはピボットに加はる壓力に大體比例することが判る。各の場合に就き得られた壓力 10 gr-poids に對する摩擦力率の平均の値は次の表に示す如くである。即ち、瑪瑙の受皿が摩擦力最も少く眞鍮、鋼鐵は遙かに大きい値を示して居る。

壓力 10 gr-poids に對する摩擦力率
Pression exercée à la portée est 10 gr-poids

ピボット (Pivot)	受皿 (portée)			比 (proportion)
	鋼鐵 (acier)	眞鍮 (cuivre jaune)	瑪瑙 (agate)	agate / acier (cuivre jaune)
鈍 (obtu)	93·1 dyne-cm	63·2	39·9	0·43 (0·63)
中 (intermédiare)	51·5	4·61	5·73	0·11 (0·12)
銳 (aigu)	2·02	2·44	0·664	0·33 (0·27)

論　議

ピボットに働く摩擦力率はピボット、受皿の形狀並に其等の物質間の摩擦係數に依

つて異るものと考へられる。今第三圖に示せる如く、ピボットに加はる力をP、ピボットと受皿の接觸面に働く壓力をp、接觸面の面積を s、ピボットの軸と受皿の面との爲す角を θ、接觸部の摩擦係数を μ とし、尚ピボットの先端の形狀を球の一部と考へ其の半徑を r とすれば、

$$P=sp\sin\theta,$$

從つて摩擦として作用する力の能率 M は

$$M=\mu.\,ps.\,r\cos\theta$$
$$=\mu rP\cot\theta.$$

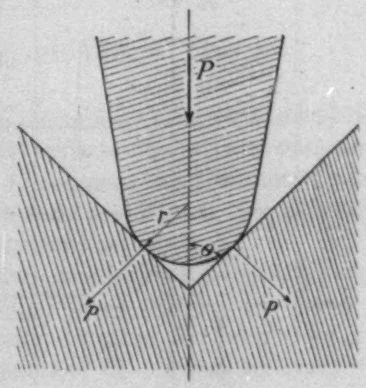

第 3 圖

實驗に使用したピボットの尖端を寫眞に依り擴大して求めた r の値は鈍は 0·22 mm、中は 0·12 mm、鋭は 0 に近く測定出來ない程度である。又 θ を測定する爲、先づ受皿の圓錐形面に當つて反射する光を目標として顯微鏡を備へ、然る後此の面とは圓錐の軸に對して對稱の位置にある圓錐面が反射光を送るに至るまで、受皿を光線を含む平面に直角な軸の廻りに廻轉せしめ、其の廻轉角を測定することに依り兩面間の角 (2θ) を定めた。かくして得た θ の値は鋼鐵 42·°8 眞鍮 49·°5、瑪瑙 52·°5 である。

ピボットが鈍であつて受皿が瑪瑙の場合に就いて $\mu=0{\cdot}1$ として是等の値から $P=10$ gr. poids に對する M の値を計算して見ると 16·5 dyne-cm となる。吾々の實驗に於いてはかかる力がピボットの兩端に働く結果、摩擦力率は $2M$ 卽ち 33·0 dyne-cm となるから、實驗より得たる 39·9 dyne-cm とほぼ一致することが判る。他の場合に就いても同樣であるが、受皿の中央に近づくと θ が上に得た値より大きくなるため、ピボットが鈍でない場合は計算値よりも實際に得た値の方が小である。

先端の鋭なピボットの摩擦力率は或る大さの壓力を加へて後再び壓力を減ずるとも前の値に歸ることなく大なる値を採る。之は或る壓力に達すればピボットの先端は其の壓力に耐へることなく、變形し損傷せられる爲めと考へられる。第四圖は先端の鋭なピボット、受皿瑪瑙の場合に得られた結果を示すものである。之は始め鋼鐵燒入ピボットの先端は良く磨かれ鋭く尖つたものに壓力を 5 gr. poids より始めて次第に增加し 20 gr. poids に至つて後壓力を次第に減小せしめ 5 gr. poids まで歸り、次に又壓力を增加して 25 gr. poids に至り再び壓力を減少せしめ元に歸り、かかる操作を 100 gr. poids の壓力まで行つた場合の摩擦力率變化の狀況を示すものである。或

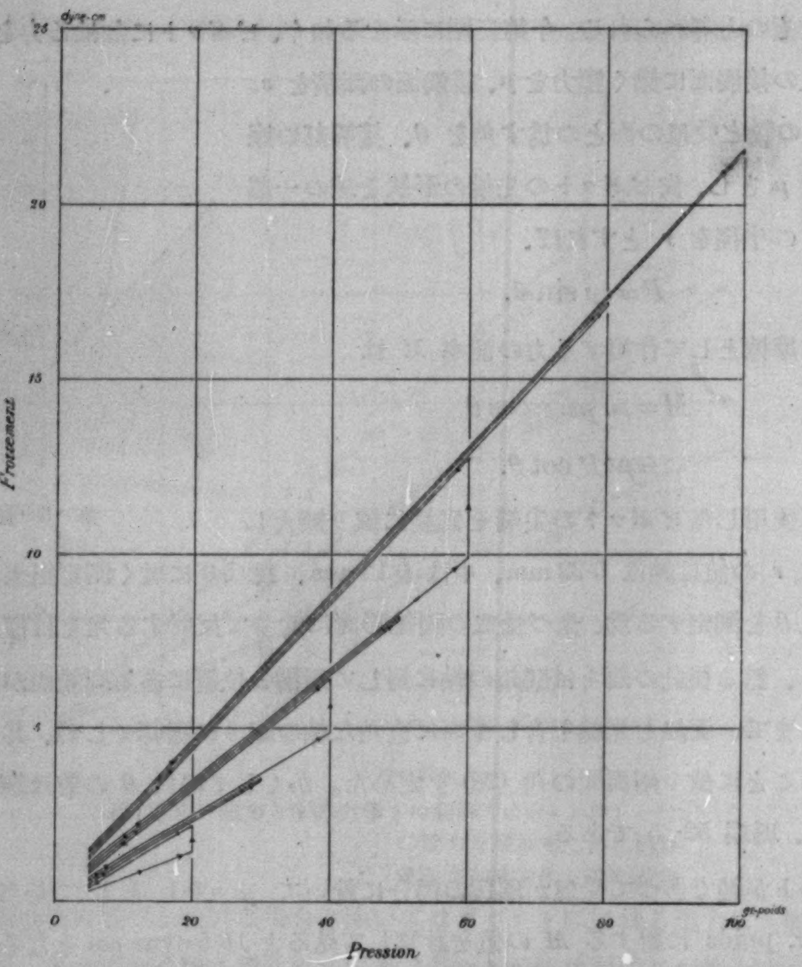

第 4 圖　ピボットの先端を鋭く磨いた場合、壓力を次第に增減せる時の摩擦力率の變化

る壓力に達すると急に摩擦力率は增加するが、共の後次の變化が無い限り、壓力と摩擦力率は比例して增減する。このことから、ピボットの先端を鋭く磨ぐときは摩擦力率は小であるが壓力に對して甚だ不安定で損傷し易い、而して損傷を受けると摩擦力率を增加するが一度損傷を受けたものは次の損傷を起す壓力の範圍內で常に壓力と比例する關係を保つて居ることが知られる。

普通吾々が槓桿の支へに用ふる場合は槓桿の重量を零と考へても壓力は 10 gr.poids 程度のものであるから、鋼鐵燒入ピボット、瑪瑙の皿の場合壓力 10 gr. poids に對して 1·0 dyne-cm と云ふ程度の値ならば 20 gr. poids 以內で安定なものと見ることが出來る。又槓桿に重量がある場合には其の重量がピボットに掛かることとなるから、若し其の重量が相當大なる場合は大なる摩擦力率が豫想せられる。從つて之は地震計設計上成るべく注意して避くべきことである。

54. Mesure du moment de frottement au pivot

par Mishio Ishimoto, Takahiro Hagiwara, et Yukio Yosida.

Quand on veut discuter le frottement du solide dans le mécanisme d'un sismographe, on remarque toujours simplement le frottement à l'extrémité de la plume faisant contacte avec le papier. D'un autre coté, on doit compter encore le moment de frottement au pivot, s'il y en a, qui se fait le centre de rotation des leviers amplifiant. On a donc executé une expérience pour déterminer la valeur de frottement au pivot.

On a pris un petit pendule dont le centre de rotation est constitué par un pivot, auquel la pression longitudinale s'applique par intermédiaire de sa portée. En comptant le nombre d'oscillation libre du pendule dans certain domaine de l'angle, on a constaté la valeur du frottement qui se varie suivant la quantité de pression exercée.

On a employé trois sortes de pivots en acier dont les extrémités ont des aigreurs différents. Les expériences ont été faites avec des portées constituées par en acier, en laiton ou en agate. On constate que le frottement au pivot est toujours proportionel à la pression dans une certain limite. Le tableau représente les valeurs du moment de frottement aux trois pivots rapportés aux portées de matériaux différents. Cette fois-ci la pression est tenu 10 gramme-poids. Le moment de frottement calculé d'après la forme de l'extrémités de pivot et celle de la portée etc. s'accorde très bien avec les résultats obtenus par les expériences. Les extrémités du pivot se casse quand la pression augmente plus qu'a certaine valeur. Quoique le frottement devienne grande dans cet état, il tient une valeur proportionelle à la pression jusqu'au 2me casseur réalisé par une plus grande pression.

55. *On Some Pebbles collected from the Floor of the Japan Sea.*

By Hiromichi TSUYA,

Earthquake Research Institute.

(Read July 5, 1932.—Received Sept. 20, 1932.)

Introduction.

In sounding the Japan Sea, a surveying ship of the Hydrographic Department of the Imperial Japanese Navy collected in August, 1931, at 39°50′ N., 133°50′ E., a granite pebble from the sea-floor at a depth of 453 m. This is in the northern part of a submarine ridge known as the Yamato Bank[1] (see Fig. 1), which, besides including the islands of Oki,[2] extends northwards from the northern coast of southwest Japan. Its depth is 500–700 m. and is in the Japan Sea deep. According to Mr. H. Niino, dredging operations (Kamiya method) carried out by the Imperial Fisheries Experimental Station of Tokyo, on the continental shelf bordering Japan, have revealed the presence of considerable gravels and sands in that part of the Japan Sea where the granite pebble was discovered, and also on the sea-floor off the tip of the Noto Peninsula.[3] These facts show the distribution of pebbles on the bottom of the Japan Sea to be more than local.

The purpose of this paper is to call attention to the present discovery rather than offer a definite explanation of the presence of pebbles on the Japan Sea floor. The find is of interest because at no depth so great as 500 m. had the deposition of such pebbles been expected. A possible explanation is submergence of that part of the Japan Sea, where the pebbles were discovered.

Microscopic studies and petrographic comparisons of these pebbles with allied rocks from neighbouring shores may furnish a clue to the sources whence they have been derived, as well as to their geological age, and consequently to the age of the submergence, if submergence there has been.

This paper deals mainly with the granite pebble. Preliminary exami-

1) 大和堆. 2) 隠岐. 3) 能登半島.

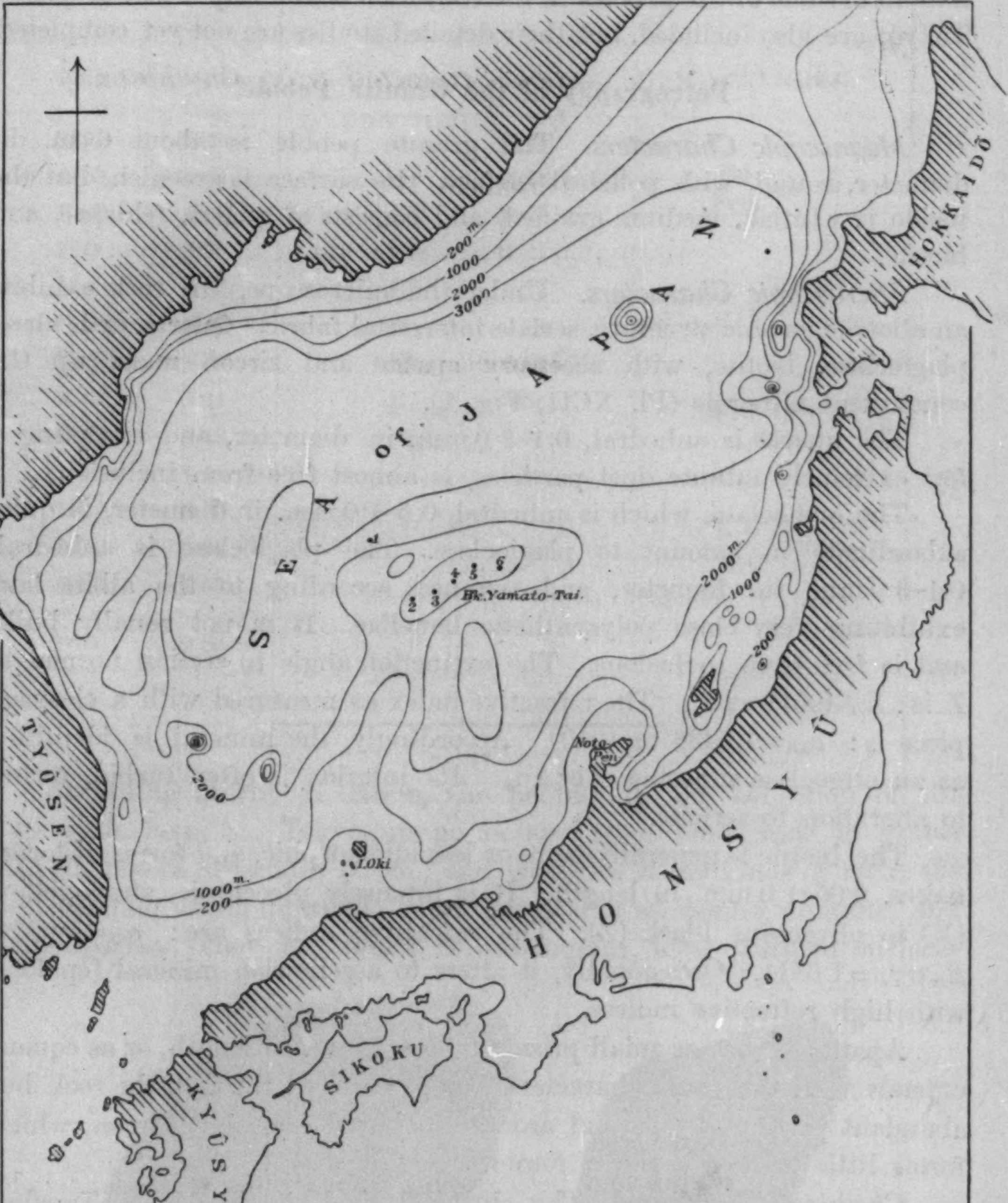

Fig. 1. Index map showing location of the pebbles.
Granite pebble from loc. No. 1; the other pebbles from locs. No. 2 and 5.

nations of some of the pebbles in the collection of the Imp. Fish. Exp. St., Tokyo, are also included, but their detailed studies are not yet completed.

Petrography of the Granite Pebble.

Megascopic Characters. The granite pebble is about 6 cm. in diameter, round, with polished surface. Its surface is greenish, but the inside is whitish, medium-grained, and consists of quartz, feldspar, and biotite.

Microscopic Characters. Under the microscope, the rock exhibits an allotriomorphic structure, seriate intersertal fabric. Quartz, orthoclase, plagioclase, biotite, with accessory apatite and zircon make up the constituent minerals (Pl. XCII, Fig. 1).

The quartz is anhedral, 0·1–3·0 mm. in diameter, and excepting a few extremely minute dust particles, is almost free from inclusions.

The orthoclase, which is anhedral, 0·5–1·0 mm. in diameter, is quite subordinate in amount to plagioclase. The plagioclase is anhedral, 0·1–3·0 mm. in diameter, and twinned according to the albite law, exhibiting very close polysynthetic lamellae. It is not zonally built, and is free from inclusions. The extinction angle in section normal to Z is: $X \wedge (001) = 2{\cdot}5°$. The refractive index as measured with a cleavage piece is: $n_{1D} = 1{\cdot}5438$ on (010). Accordingly, the mineral is identified as an oligoclase-andesine $Ab_{70}An_{30}$. Its interior is often turbid, owing to alteration to sericite.

The biotite is generally more or less idiomorphic, and forms distorted flakes, 0·05–1·0 mm. in length. It is intensely pleochroic, straw-yellow (X) to olivaceous black (Z). The refractive indices are: $\alpha_D = 1{\cdot}6029$, $\beta_D \fallingdotseq \gamma_D = 1{\cdot}6511$. Occasionally, it alters to a yellowish mineral (epidote) with high refractive indices.

Apatite occurs as small prisms, 0·05–0·1 mm. in length, or as equant crystals with the usual characters, being scattered through the rock but abundant particularly in and around the biotite crystals. Zircon, which forms little prisms, is rarely found.

Chemical Characters. The chemical analysis (by Mr. S. Tanaka) of the rock gave the results as shown in Table I.

According to the C. I. P. W. quantitative system, the rock belongs to *yellowstonose* (1. 4.″ 3. 4(5)). It may thus be classified with granodiorite or the quartz-diorite family rather than be called a typical granite. The normative plagioclase has the composition of oligoclase-andesine $Ab_{70}An_{30}$, being identical with the modal one.

Table I.

Bulk Composition	Wt. %	Norm Composition		Ratios
SiO_2	69·20	Q	27·45	
Al_2O_3	16·61	Or	9·68	$\frac{Sal}{Fem}=15{\cdot}32$
Fe_2O_3	0·67	Ab	40·37	
FeO	1·70	An	17·25	
MgO	0·85	C	1·22	$\frac{Q}{F}=0{\cdot}43$
CaO	3·67	Hy	4·22	
Na_2O	4·76	Mt	0·93	
K_2O	1·11	Il	0·61	
H_2O+	0·73	Ap	0·31	$\frac{K_2O'+Na_2O'}{CaO'}=1{\cdot}44$
−	0·16			
TiO_2	0·29			
P_2O_5	0·11			$\frac{K_2O'}{Na_2O'}=0{\cdot}16$
MnO	0·03			
Total	99·89			

According to Mr. H. Niino, the pebbles in the collection of the Imp. Fish. Exp. St., Tokyo, range in size from sand-grade to gravel with diameters exceeding 50 cm., and comprise many kinds of rock, the most common being quartzite, chert, graywacke sandstone, andesite, and plagioliparite. They are round or subangular, with polished surfaces

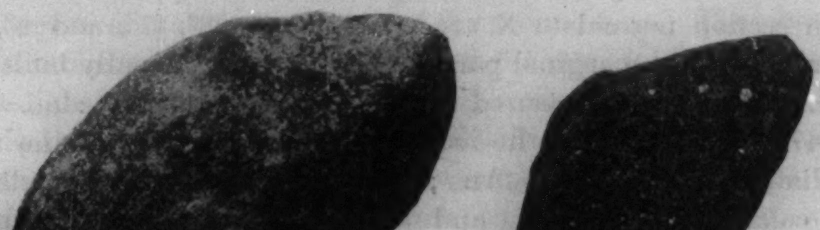

Fig. 2. Pebbles of augite-hypersthene-andesite (left) and olivine-basalt (right). Natural size.

(see Fig. 2). The writer obtained through the kindness of Mr. H. Niino some of these pebbles, of which the following will be briefly described.

1. Micropegmatite. 2. Hornblende-dacite.
3. Augite-hypersthene-andesite. 4. Olivine-augite-basalt.
5. Olivine-basalt.

1. *Micropegmatite.* (Pl. XCII, Fig. 2) Megascopically, this rock is gray, and almost aphanitic, but contains some megascopic feldspar. Microscopically, it is holocrystalline, and consists of phenocrystic plagioclase scattered through an equigranular mass that exhibits both micropegmatitic and microspherulitic—granophyric—texture. The phenocrystic plagioclase is euhedral to subhedral, 0·5–2·0 mm. in diameter, and is twinned according to Carlsbad, albite, and pericline laws. Zonal structure due to chemical difference is entirely absent. The maximum symmetrical extinction angle, which is about 15°, indicates an oligoclase-andesine, $Ab_{70}An_{30}$. The equigranular mass consists of quartz, orthoclase, and plagioclase, often exhibiting micrographic intergrowths of feldspar and quartz, and regular spherulitic aggregates of feldspar fibres. Besides the minerals above mentioned, we see pale greenish anhedral flakes of chlorite, 0·1–0·3 mm. in diameter.

2. *Hornblende-dacite.* (Pl. XCII, Fig. 3) Megascopically, this rock is gray, compact, aud sempatic with phenocrysts of plagioclase, quartz, and hornblende. Microscopically, it consists of phenocrysts of plagioclase, quartz, and hornblende, with accessory apatite and magnetite, scattered through a devitrified groundmass. The plagioclase phenocryst, which is euhedral to subhedral, 0·5–1·0 mm. in diameter, is twinned according to the albite and Carlsbad laws. Zonal structure due to chemical difference is moderately exhibited. Optic character: positive. Extinction angles in section normal to X are: $Y \wedge (010) = 28°$, 17°, and 6°, in the central, middle, and marginal parts respectively of a zonally built crystal. The refractive indices measured with a cleavage flake are: $n_{1D} = 1{\cdot}5432$, $n_{2D} = 1{\cdot}5470$. Accordingly, the mineral is identified as andesine with an intermediate composition $Ab_{69}An_{31}$; while the zonally built crystals have a more calcic core $Ab_{49}An_{50}$ and a more sodic shell $Ab_{75}An_{25}$. The hornblende, which is euhedral to subhedral, occurs usually in prismatic habit with a length of less than 1 mm., but the mineral is entirely altered to chlorite and epidote, with an aggregate of minute grains of iron-ore. Quartz is subhedral, 0·3–1·5 mm. in diameter but is sometimes much indented with inlets of the groundmass. The cryptocrystalline groundmass is traversed by secondary quartz veinlets.

3. *Augite-hypersthene-andesite.* (Pl. XCII, Fig. 4) The majority of the pebble specimens in the writer's hands consists of this rock. Megascopically, it is dark gray to black, with greenish tints, compact, and porphyritic with phenocrysts of plagioclase and pyroxene. Microscopically, it is docrystalline in crystallinity, and dopatic. The chief constituent minerals are plagioclase, hypersthene, and augite, with accessory magnetite and interstitial glass. Plagioclase occurs as phenocrysts and as a constituent of the groundmass. The phenocrystic one is euhedral to subhedral, less than 1·5 mm. in diameter, and is developed in prismatic and of nearly equant habits, showing simple and polysynthetic twin-lamellae according to the albite, Carlsbad, and pericline laws. Zonal structure due to chemical difference is often very faintly exhibited. Extinction angles in section normal to Z are: $X \wedge (010) = -31°$ in the core and $-20°$ in the shell. Optic character: positive. The refractive indices measured with a cleavage piece are: $n_{1D} = 1{\cdot}5640$ and $n_{1D} = 1{\cdot}5683$ on (010). Accordingly, the mineral is identified as labradorite $Ab_{32}An_{68}$ with a more sodic shell. The plagioclase in the groundmass is dominantly lath-shaped, 0·1 mm. in length, and commonly twinned in two or three lamellae. In symmetrically cut sections the extinction angles do not exceed 24°, indicating an andesine with composition nearly equal to the shell part of the phenocrystic plagioclase.

Hypersthene occurs as euhedral phenocrysts of stout prismatic form, measuring 0·2–0·5 mm. along the longest direction, and is traversed by cracks perpendicular to the c-axis and sometimes by notable prismatic cleavage lines. The optical plane is parallel to the c-axis. Pleochroism is moderately exhibited with the following axial colors: X—brown, Y—yellowish brown, and Z—pale green. Monoclinic pyroxene is found as phenocrysts and as a constituent of the groundmass. The phenocrystic augite is subhedral, equant in habit, 0·2–0·5 mm. in diameter, and pale green to light yellow brown. It exhibits very faint zonal structure due to chemical difference. Parallel growth with rhombic pyroxene is rarely observed. The refractive index as measured with a cleavage flake is: $n_{1D} = 1{\cdot}6922$. The monoclinic pyroxene in the groundmass occurs in slender prismatic habit, 0·05–0·1 mm. in length, and is often twinned in two or three lamellae. Magnetite is scattered through the rock as equant grains, less than 0·1 mm. in diameter. The glass base, which is uniformly brown, is preserved with remarkable freshness. The rock, in bulk composition, contains 58·00 wt. per cent SiO_2.

4. *Olivine-augite-andesite.* (Pl. XCII, Fig. 5) This is a dense, dull

black rock with a few visible crystals of pyroxene. Microscopically, it is docrystalline in crystallinity, and is dopatic, with microphenocrysts of olivine and augite. Phenocrystic plagioclase is absent. The olivine is euhedral to subhedral, 0·05–0·2 mm. in diameter, and is much altered to a pale greenish substance with low double refraction and in parts to a reddish brown substance with higher double refraction. These alteration products of olivine are commonly surrounded by minute grains of iron-ore, preserving the outer form of the original mineral. There are numerous phenocrysts of augite with stout prismatic habit, 0·2–0·5 mm. in length, with a few up to 1·0 mm. The mineral, which is pale brown, often twinned after (100), shows remarkable undulatory extinction. The larger phenocrysts of the mineral exhibit faint zoning due to chemical difference. The refractive index as measured with a cleavage piece is: $n_{1D}=1·6932$. Plagioclase, monoclinic pyroxene, and magnetite, with interstitial glass, make up the groundmass. The plagioclase occurs as simple or once-twinned prismoids, 0·03–0·15 mm. in length, and is in part disposed in fluxional arrangement. The mineral is too fine for accurate determination, but in symmetrically cut sections the extinction angles do not exceed 30°, indicating an acid labradorite ($Ab_{45}An_{55}$). The monoclinic pyroxene in the groundmass is pale brown, occurring as minute grains, less than 0·01 mm. in diameter, and also as prismoids, 0·03–0·1 mm. in length. Minute grains of magnetite are disseminated through the groundmass. The interstitial glass base is colorless. In bulk composition the rock contains 54·80 wt. per cent SiO_2.

5. *Olivine-basalt.* (Pl. XCII, Fig. 6) Megascopically, this rock is dark gray to black, compact, and aphanitic without a trace of phenocrysts. Microscopically, it is non-porphyritic, docrystalline in crystallinity with hyalopilitic texture, and consists of plagioclase, monoclinic pyroxene, and magnetite, with interstitial glass, except a few altered microphenocrysts of olivine. The altered olivine phenocrysts are anhedral, 0·4–0·7 mm. in diameter, and although generally pale green with low double refraction (antigorite?) are in parts yellow to reddish brown, and strongly pleochroic with higher double refraction (iddingsite). They are sometimes surrounded with grains of monoclinic pyroxene. The plagioclase occurs as simple or multiple-twinned prismoids of less than 0·15 mm. in length, but anhedral crystals up to 0·2 mm. in diameter are also present. The larger plagioclase crystals often exhibit zonal growth due to chemical difference. The mineral is too fine for accurate determination, but its extinction angle in an oriented section indicates a labradorite. The

monoclinic pyroxene, which is pale greenish brown, occurs as grains of less than 0·1 mm. in diameter and also as rods of 0·1 mm. length. Undulatory extinction of the mineral is strongly exhibited. Magnetite occurs as grains with diameters less than 0·05 mm. The colorless glass base encloses a fine dusty substance. In bulk composition the rock contains 53·00 wt. per cent SiO_2.

Comparison with Rocks of Neighbouring Shores.

The Japan Sea region comprising the Japan Sea coast-belts of Tyûgoku,[4] Oki Islands, Uturyôtô Island,[5] Saisyûtô Island,[6] Gotô Islands,[7] Tyosen (Korea), etc., forms a petrographic province characterised by the occurrence of various volcanic alkali-rocks effused during late-Tertiary and post-Tertiary. The pebbles as described above, however, do not contain any material characteristic of alkali-rocks, though they were collected from the sea-floor adjacent to or possibly included in the area of the province. All are of calc-alkali type, similar to what is extensively distributed in the Japanese Islands, such as Tyûgoku and elsewhere.

Compared with a specimen of the biotite-granite exposed extensively in the Tyûgoku district, the granite pebble shows finer grains of components, more calcic composition of the plagioclase, and lower refractive indices of the biotite. It is however not neccessary, nor is it to be expected that they shall be characteristic of the original granite, the parent mass of the pebble, for the granite mass might have had various petrographic characters according to the petrogenic process that went on during the cooling of the body; and further, as is seen from the examples in Table II, the components of one part of a granite mass might not have the optic properties that are found in another.

Under these circumstances, our petrographic study has not determined whether the granite pebble is derived from a certain mass now exposed in the Japanese Islands or not. The only thing of which we are positive is that the granite pebble has, as is clear from the foregoing description and from Table II, the general petrographic characters common to many Japanese granites, and which differ in many respects from the granites exposed on the continental side of the Japan Sea. The chemical composition of the pebble indicates that the rock belongs in the granodiorite or the quartz-diorite family rather than typical granite, containing as it does much normative plagioclase similar in

---

4) 中國. 5) 鬱陵島. 6) 濟州島. 7) 五島列島.

Table II.

	Ab% in Plagioclase	Biotite, $\beta_D \doteqdot \gamma_D$
1	70	1·6511
2	83	1·6720
3	66	1·648
4	77	1·651
5	80	1·652–1·653
6	82	1·653–1·654
7	63–75	1·648
8	67–78	1·652
9	60–76	1·655

1. Japan Sea, 39°50′ N., 133° 50′ E. (Biotite-granite pebble from the sea-floor)
2. Morimoto, Prov. Tango.[8)] (Biotite-granite)
3–6. Kasagiyama, Prov. Yamato.[9)] (Biotite-granite)
7–9. Tukubasan, Prov. Hitati.[10)] (Biotite-granite)

composition to the modal one ($Ab_{70}An_{30}$). The last character may be seen also in many Japanese granites.

The micropegmatite pebble is similar in petrographic characters to some of the dike-rocks intimately associated with many Japanese granite masses.

Of the pebbles of volcanic rocks, the augite-hypersthene-andesite bears a striking resemblance to the palaeotypal pyroxene-andesite (or palaeo-andesite) which occurs extensively in Tyûgoku and elsewhere as lava-flows, covered unconformably by lower Neogene (?) Tertiary formations. The pebble does not however show the alterations to which the palaeotypal andesite has occasionally been subjected.

As to the pebbles of dacite and basalt, we may also expect a close comparison with rocks of respective rock-type among the Japanese volcanics; and while petrographic evidences may point to an essentially Neogene Tertiary or Quaternary age, it is still premature to assign any exact dates to these pebbles.

Igneous-rock pebbles being the subject of this paper, accounts of

8) 丹後國森本.
9) 大和國笠置山, *cf.* M. HOTTA, *MS.*, 1927.
10) 常陸國筑波山, *cf.* K. SUGI, *Jour. Geol. Soc.*, Tokyo, 34 (1927), 358.

other pebbles should be left for another occasion, but it may here be remarked that some of the pebbles are probably derived from sedimentary rocks similar to some of the upper palaeozoic formations distributed in Tyûgoku and elsewhere.

Summary and Conclusions.

Many pebbles of igneous rocks, both plutonic and effusive, and of sedimentary rocks were collected from a submarine ridge known as the Yamato Bank in the Japan Sea. They are round or subangular with well polished surface, and vary in size from sand-grade to gravel over 50 cm. in diameter. If these pebbles had been found only in a limitted area lying on the track of steamships, their presence might be attributed to ballast thrown overboard from passing vessels. But the distribution of the pebbles is evidence of its improbability. Neither is it likely that ocean currents transport pebbles of this size so far from the present shores. On the other hand, there can be no wearing down of the surface of hard rocks on the sea-floor with a depth of 500–600 m. The only alternative is that the sea-floor that yielded these pebbles was at one time either a land-surface or a shallow sea near the shore, when they were formed by erosive action of the water flowing over their respective parent rock-masses, the shores submerging later to their present depths.

All the pebbles described in this paper have the general petrographic characters common to their respective rock-types now exposed in the Japanese Islands. Hence it is inferred that the pebbles are derived from land which is now below the sea and which is geologically connected with the Japanese Islands, or that it was transported from some part of the present Japanese Islands before its submergence to where they lie on the sea-floor at present.

The granite pebbles does not show characteristics that could be correlated with any Japanese granite whose geological age has been established; while the andesite and basalt pebbles have characteristics common to the late-Tertiary and Quaternary volcanics in the Japanese Islands. It is therefore highly probable that the sea-floor where these pebbles exist was a land-surface or a very shallow sea near the shore during the post-Neogene. If the latest land-submergence had occurred in a very remote geological past, the pebbles could not have remained for long, geologically speaking, in the condition in which they are found at present without the aid of some auxiliary agent such as earthquake disturbances at the sea-bottom, since a sea-floor with a depth of 500–

600 m. acts as a settling basin for fine sediments and may be covered with deposits of mud and marine organisms soon after submergence. The wide distribution of the pebbles cannot be explained as due to such an auxiliary agent. Thus, the only explanation for the presence of the pebbles is *land-submergence in very recent geological time.*

The writer may here remark that recent land-submergence, to which he has ascribed the existence of pebbles at the bottom of the Japan Sea, was already deduced by Dr. H. Yabe from other evidence. According to him,[11] "the sea-floor now encircling the Japanese Islands to the depth of some 720 m., in the average, was once a land surface, and the land submerged below the sea level in a time geologically not very remote from the present. Prior to this great submergence of land, the Japanese Islands were elevated some 720 m. more than they are at present, and directly connected with the Asiatic continent." (See Fig. 3) He further believes that "the land connection of the Japanese Islands to the Asiatic continent was in full swing during the PN stage and continued to the end of the T stage."[12]

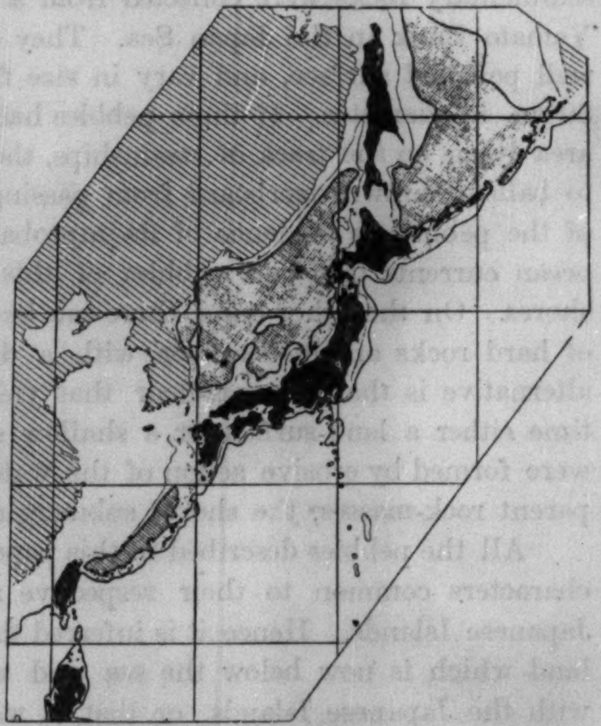

Fig. 3. Map showing distribution of land and sea before the submergence of some 720 m. of the sea-floor encircling the Japanese Islands (After Yabe).

Dr. Yabe's view cited above is essentially based upon the facts that along the coast of the Japanese Islands there are two submarine shelves of different depths, and that each of the submarine shelves carry traces of drowned valleys on its surface.[13] According to him, of the two submarine shelves the higher continental shelf is 150 m. deep on an

11) H. YABE, *Proc. Imp. Acad.*, 5 (1929), 167.
12) H. YABE, *Ibid.*, 430.
13) H. YABE and R. TAYAMA, *Record Oceanogr. Works*, Japan, 2 (1929-30), 1.

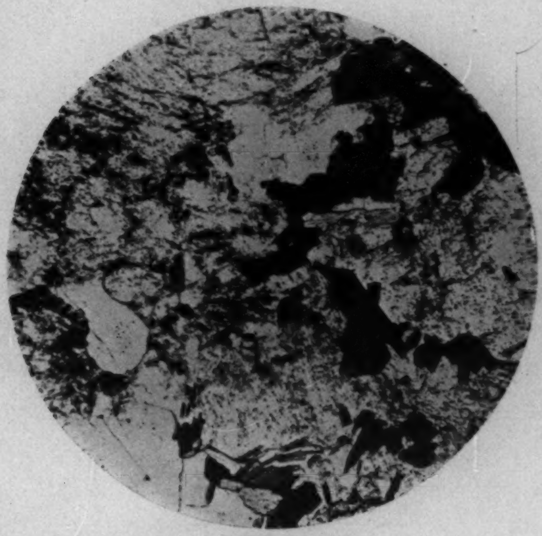

Fig. 1. Biotite-granite. × 41.
See p. 3.

Fig. 2. Micropegmatite. × 41.
See p. 6.

Fig. 3. Hornblende-dacite. × 30.
See p. 6.

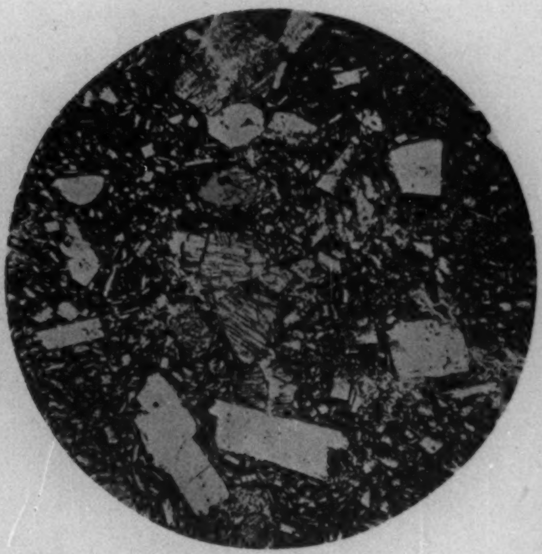

Fig. 4. Augite-hypersthene-andesite. × 41.
See p. 7.

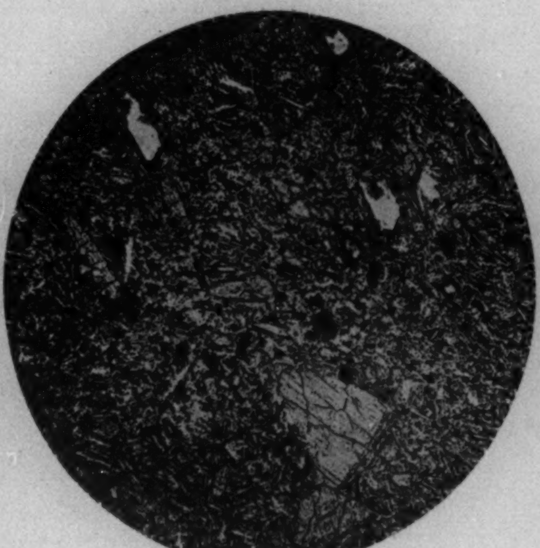

Fig. 5. Olivine-augite-andesite. × 41.
See p. 9.

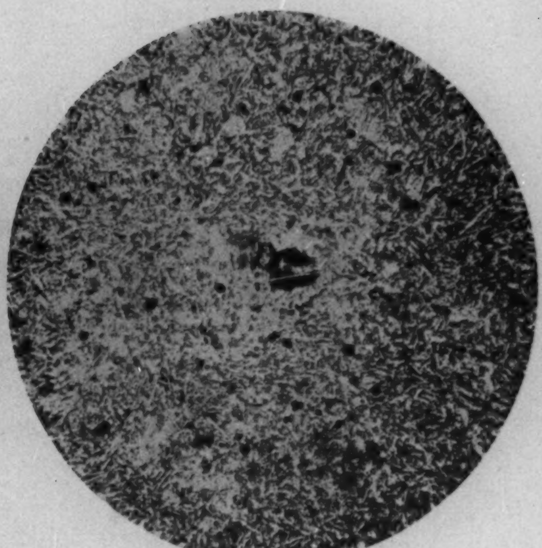

Fig. 6. Olivine-basalt. × 41.
See p. 9.

Microphotographs of the Pebbles collected from the Japan Sea Floor.

（震研彙報、第十號、圖版、津屋）

average along its outer margin, and the lower one, which is far less incomplete in form than the other, extends down to 720 m. These two are regarded by him as the prolongations respectively of the T and PN terraces[14] on the present land-surface of the Japanese Islands.

Thus, the present discovery of the pebbles and the inferences drawn from a petrographic study made of them may be strong evidences in support of Dr. Yabe's views concerning the epeirogenetic or eustatic movement of the Japanese Islands in recent geologic times, regardless of the cause, the magnitude, or the mechanism of the movement. Further studies of these pebbles may supply data that will afford more weighty evidence in favor of some particular age-span for the latest land-stage of the seas now bordering the present Japanese Islands.

In conclusion the writer desires to express his sincere thanks to Lieutenant-Commander Asahina, who supplied him with a piece of the granite pebble, and also to Mr Niino, through whose kindness the writer obtained many pebbles from the collection of the Imperial Fisheries Experimental Station of Tokyo.

---

55. 日本海海底より採集せられたる礫に就いて

地震研究所　津　屋　弘　逵

昭和 6 年 8 月海軍水路部の一測量艦が日本海の測量に從事中、北緯 39°50′、東經 133°50′ 附近の深さ 453 m. の海底（所謂大和堆の北方）より一花崗岩礫を採集した。該礫は直徑約 5 cm. で圓味を帶び、中粒顯晶質で、石英、正長石、斜長石及び黑雲母を主成分として有する。日本內地の花崗岩に類似し、斜長石（オリゴクレース）の多いこと及び化學成分より見ると花崗岩といふよりむしろ花崗閃綠岩といふ方が適當かも知れない。

東京水產試驗場では以前より日本沿海海底の物質を採集してゐて、その採集品の中に多くの砂礫がある。之等は新野弘理學士によつて整理されてゐるが、同學士より得た數種の標本中には砂岩、硅岩等の水成岩の他にマイクロペグマタイト、角閃石・石英安山岩、複輝石・安山岩、橄欖石・輝石安山岩、橄欖石・玄武岩等の礫がある。之等は上述の花崗岩礫の發見せられた所より少し東南方の 500 m. 內外の深さの海底に於て採集せられたもののみであるが、新野學士によれば隱岐島の北方、能登半島の北方、佐渡の北西方等の何れも 500 m. 內外の深さの海底より多量の砂礫が採集せられてゐる。

かゝる礫が 500 m. 內外の海底に容易に採集し得る狀態にて存在することは非常に重大な意味を有することで、恐らく最近の陸地沈降を示すものであらう。礫の種類より見ればこの沈降は新第三紀又はそれ以後といふことが推定される。更に多くの礫を岩石學的に調べて日本內地の岩石と比較すると或はもつと限定された陸地沈降時代を知ることが出來るかも知れない。

---

14) PN and T are abbreviated notations designating respectively Pre-Narita terrace and Tama terrace.

56. *Recent Activity of the Long-Dormant Akita-Komagatake*[1] *Volcano in North-East Japan.*

By Yanosuke ÔTUKA,

Earthquake Research Institute.

(Read Sept. 20, 1932.—Received Sept. 20, 1932.)

Introduction.

The long-dormant volcano, Akita-Komagatake, which suddenly became active towards the end of July last, is part of the long mountain range running in a north-south direction and forming the backbone of North-East Japan. This volcano, with Hatimantai[2] and Ebosidake[3], constitute the three conspicuous peaks that rise from this range; the volcano, which is 1800m. high, being the highest of the three. The position of the volcano is approximately 5 km. southwest of the volcano Iwate[4] (Ganzyu[5] in some maps), which lies north-west of the city of Morioka[6] and about 2·5 km. east-north-east of the celebrated lake Tazawa[7] (see index map, fig. 1).

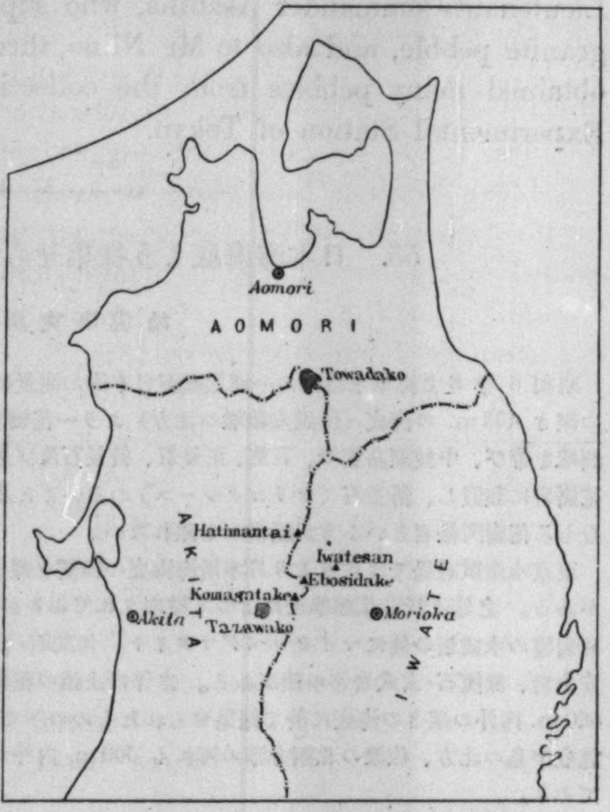

Fig. 1. Index map showing the position of the Komagatake or Akita-Komagatake.

1) 秋田駒ヶ嶽. 2) 八幡平. 3) 烏帽子嶽. 4) 岩手. 5) 巖鷲. 6) 盛岡. 7) 田澤.

Brief Geology and Morphology of the Volcano.

North-East Japan is divided into two zones, the Outer and Inner, by the lowlands of the rivers Mabeti[8], Kitakami[9], and Abukuma[10]. The Neogene strata in the Outer zone which thinly cover the basement complex are slightly deformed, while the same strata in the Inner zone consist of thick pyroclastic materials; their geologic structures being complicated by crustal movements and volcanic activities. During the Quaternary they were extruded and covered by many volcanoes. The volcano and vicinity are in the Inner zone.

The basal rocks of this region consist of pyroclastic rocks and hard mud-stones, resembling the so-called green tuff formation and the siliceous shale, respectively, of the Akita-Yamagata[11] oilfields.

For convenience the writer will call these pyroclastic rocks and hard mud-stone the Sakamoto[12] formation. The Neogene formation, which is the bluish-grey tuffaceous muddy sand out-cropping near Hasiba[13] village, probably rests on the Sakamoto formation. Fossil shells reported by S. Nomura[14] from this formation suggest middle Neogene age.

These Neogene formations strike N. 40°W. and dip 40° or more NW. In the Sakamoto valley the greenish tuffaceous beds are often intercalated in the hornfels as hard mud-stone beds. At the summit of the Kunimi[15] pass (894. 4 m.), this formation assumes a folded structure (Fig. 2). Its strike and dip vary, but the former is generally N. 20°-30°E. Fig. 3 is a schematic geologic map of the Akita-Komagatake after the late Sakurai.[16]

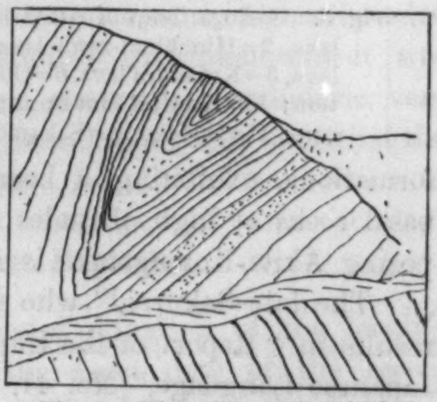

Fig. 2. Fig. shows the folded structure of Neogene strata.

These basal Neogene rocks crop out on the Kunimi pass and at the Kunimi hot springs, where the basal rocks (N. 20° W.: N. 10°) have been metamorphosed by sulphur bearing gases or solutions. Mt. Sasamori consists of these basal

---

8) 馬淵. 9) 北上. 10) 阿武隈. 11) 秋田山形. 12) 坂本. 13) 橋場.

14) S. Nomura, 「化石標本蒐集報告」, *Bull. Saitô-Hôonkai Museum*, 8 (1931). Following species are reported: *Anadara trilineata amicula* (Yokoyama), *Ostrea gravitesta* Yokoyama, *Mytilus crassitesta* Lischke, *Dosinia* cf. *kaneharai* Yokoyama.

15) 國見.

16) H. Sakurai, "Geology of the Iwate volcanic group", *Sinsai Yobô Chôsakai Hôbun* (*Report of the Imperial Earthquake Investigation Comittee in Japanese Language*), 44 (1903).

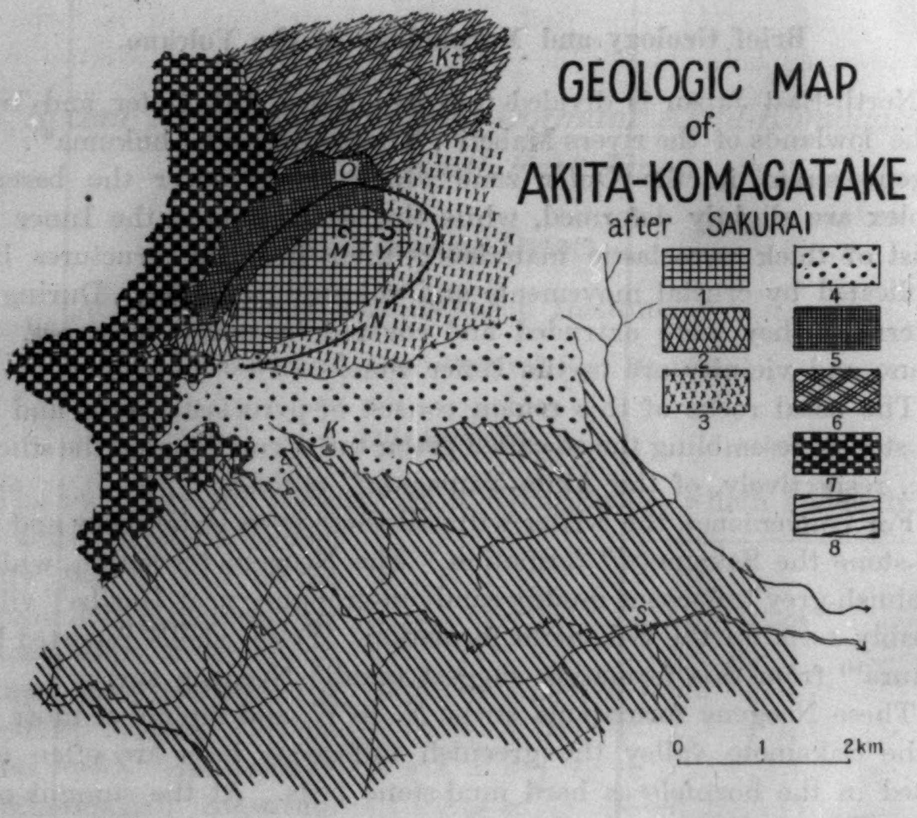

Fig. 3. Geologic map of Akita-Komagatake after H. Sakurai (1903). 1 = Me lake lava, 2 = Hinokinai-zawa lava, 3 = Ooyakesuna lava, 4 = Southern Komagatake lava, 5 = Katakura lava, 6 = Oodake lava, 7 = Midusawa lava, 8 = Sakamoto formation; K = Kunimi Hot Springs, Kt = Katakura-sawa, M = Medake, N = Yokonagane, O = Oodake, S = Sakamoto valley, Y = Yokodake.

formations, exhibiting a beautiful stratification. The development of basal rocks at high altitudes suggests that the volcanic materials composing Akita-Komagatake is not thick.

The late Sakurai,[16] who studied this volcano in 1903, published his results in "Report of the Imperial Earthquake Investigation Comittee in Japanese Language," No. 44, illustrated with excellent geologic maps. He states that the basal Neogene develops also on the north and south side of the mountain.

The Akita-Komagatake is a volcano that rose during the Quaternary on the erosion reliefs of basal rocks. It consists of two central cones, Medake[17] and Yokodake,[18] surrounded by the sommas Yokonagane,[19]

17) 女岳. 18) 横岳 (not of topographic map of Military Land Survey, Sidukuisi (雫石) sheet, 1/50000).

19) 横長根 ("Yokodake" of topographic map (Sidukuisi sheet)).

Ôdake[20] and the 1115·7 m. peak. A broad atrio, which is formed of lava flows, spreads out on the south side of these two central cones. Fig. 6 shows the lava-flows which were exposed on the wall of the recent explosion pits. The late Sakurai classified the lava-flows of the Akita-Komagatake into the following kinds:

Medake lava (Olivine-Hypersthene-Andesite),
Hinokinai-zawa[21] lava (Hypersthene-Augite-Andesite),
Ooyakesuna[22] lava (Olivine-Hypersthene-Andesite),
Southern Komagatake lava (Olivine-Hypersthene-Augite-Andesite),
Katakura[23] lava (Olivine-Hypersthene-Andesite),
Ôdake lava (Hypersthene-Augite-Andesite),
Midusawa lava (Hypersthene-Andesite).

The lava flows forming the surface of the atrio, the hypersthene bearing Olivine Andesites (Sakurai's Medake lava), is the most recent in age.

Past References to the Activity of the Volcano.*

This volcano must have continued its activities for a very long time in the remote past. The rich sulphur beds of the Katakura valley on the northeast side of the mountain are mute witnesses of these bygone activities. Beyond the escape of gases from these sulphur beds observed 50 years ago[25], the volcano has been perfectly quiescent so far as recorded history is concerned. When Sakurai studied this mountain it was absolutely devoid of any sign of activity; not even a solfataric vent could be found on the crater. It would seem from these data that the volcano has been dormant for untold ages.

Exact Date of the Recent Explosion.

On account of the secluded and isolated situation of the locality concerned, there is disagreement about the exact date of the recent explosions. On the morning of July 21, 1932, visitors to the Kunimi-hot springs, only 2·5 km. east of the new explosion pits, felt shocks (or

20) 男岳.
21) 檜木内澤. 22) 大焼砂. 23) 片倉. 24) 水澤.
25) *Chigaku Zassi* (*Journal of Geography*) II, 22 (1890), (in Japanese).
* In 1891, the following report appeared in the "Journal of Geography" in Japan, vol. 3, p. 43:—People living near the Akita-Komagatake volcano spoke about the volcano having rumbled and ejected hot stones from the crater during December, 1890. But no particular sighns of such could be seen.

earthquakes), but that day and the two days which followed were so inclement that no one ascended the volcano. On July 24 some mountaineers crossed the mountain along the somma on their way from Obonai[26] to the Kunimi hot springs. The day was so cloudy that they failed to notice the new activity, but they were puzzled to find their clothes discoloured black by fine dust in going over the Yokonagane. (Fig. 4).

The discovery by the other party of the new explosion pits on the atrio the following day (25), which turned out fine, caused great excitement at the Kunimi hot springs and the village of Obonai.

Several Japanese newspapers erroneously reported the new explosion of the Akita-Komagatake as having occurred on July 25 and 26[27], while others gave the dates as the 27th and 29th[28].

From the informations obtained at Obonai village and elsewhere the writer concludes that the new explosion occurred on July 21.

The New Explosion.

Position. As stated above, the new explosion occurred in the "Atrio" (locally called Isibora or Isipora)[29] surrounded by the "Somma," at the southern foot of Medake, one of the central cones. The southern most explosion pit lies about 700 m. east of the 1115·7 m. triangulation point, or 500 m. south of the top of Medake. These pits lie between about 1000–1150 m. above sea-level. (Fig. 4).

Distribution of the New Explosion Pits.

On the atrio, explosion pits were hitherto unknown. The 11 or more new explosion pits are arranged in a line in direction about N. 45° E. for about 600 m., as shown in Fig. 4; the southernmost one lying at a distance of 700 m. from the triangulation point 1115·7 m. in a N. 84° E. direction. Fig. 4 is a sketch map showing their distribution. Fig. 5, which is a photograph taken from the southern side of the central cone Medake, gives a complete view of the new explosion pits.

For convenience, they are numbered from 1 to 11, counting from south to north (Fig. 4). Their descriptions follow.

Explosion pit No. 1: (Fig. 6 and 8). Explosion pit No. 1, which

26) 生保内.
27) *Iwate Nippô*, Aug. 6, 1832; *Akita Sakigake Shinpô*, July 31, & Aug. 2, 1932.
28) *Hôchi Shimbun*, July 28, 1932; *Nippon*, Aug. 2, 1932.
29) 石ボラ.

is the largest and deepest of all, is nearly subpentagonal. Its long axis is about 18 m. The pit wall is vertical except for small collapses, one each on the northern and the western walls. The three lava flows (Hypersthene bearing Olivine andesite) which form the surface of the atrio are clearly seen on the pit wall. Fig. 6 shows a complete view of the first explosion pit and the lava flows. The floor of the pit is filled partly with water and partly with mud, which on drying has formed beautiful suncrack figures. Fig. 8 shows the floor. Surrounding the pit, large andesite blocks (about 1 m. or more in diameter) and lapilli and ashes are scattered about, the thickness of the last-named in places being about 3 m. Most of these blocks, lapillus, and ashes are fragments of the Hypersthene bearing Olivine andesite seen exposed on the pit wall. The root-like forms seen on the upper part of the pit wall in Fig. 6 are Ditake[30] (a species of bamboo) buried by the ejecta. The pit being now quiet no gases are emitted.

Explosion pit No. 2. Explosion pit No. 2, which ranks second in size, lies north of the first. It appears from fig. 5 that the second pit is a continuation of the first. The long oval horse-shoe form opens toward the south. While the southern wall of the pit is either low or level with the surrounding surface, the northern wall is similar to those of pit No. 1. Mud fills the pit floor and overflows the lower southern wall. Activity having subsided no gases are being emitted.

Explosion pit No. 3. This pit, which is situated northeast of pit No. 2, is also of an oval, horse-shoe form opening southward. The northern wall of the pit is about 3 m. high. Explosion ejecta around the pit have buried tall trees, such as Didake, Sugi[31], and Sirakaba[32] etc., only their tops being visible above the new ground surface. The longer axis of the pit is about 35 m. and the shorter 23 m.

Explosion pit No. 4. Explosion pit No. 4 is situated northeast of No. 3. It forms an irregular quadrilateral, as shown in fig. 4; its south and north ends being closed crevice-like. The floor of the pit here is also filled with mud.

Explosion pit No. 5. Explosion pit No. 5, which lies northwest of No. 4, is relatively small, shallow, and almost round. Its radius is about 12 m. Mud also fills the floor of this pit from which gases issue no longer.

Explosion pit No. 6. Explosion pit No. 6, situated 100 m. east of

30) 地竹. 31) 杉, (a species of cedar). 32) 白樺, (a species of birch).

No. 5, is relatively large and nearly ellipse, with its longer axis about 30 m. long and the shorter about 15 m. The pit wall (about 3 m. high) is a low ridge formed by materials ejected from the pit. The topography is that of a small "Maar" near the Rhine in Germany. The east part of the outer slope of the low ridge is eroded by a gully, forming cliffs. Fig. 9 shows the explosion pit and the inner slope of the low ridge. Its full view is seen in fig. 4. Water and mud fill the floor of the explosion pit.

Explosion pit No. 7. This pit, situated 40 m. east of No. 6, is round, about 15 m. in diameter, with its horse-shoe formed part opening toward the south. The only wall, which is on the northern side, is 5 m. high. Although pit No. 6 is now quiescent, some vapour still issues from a fissure under the northern wall of pit No. 7.

Explosion pit No. 8. Pit No. 8 is very small, round with its horse-shoe formed part opening toward N. E. E. Its diameter is about 4 m. and its depth about 1 m. The floor of the pit is filled with mud and water. It lies 70 m. east of No. 7.

Explosion pits Nos. 9 to 11. These three active pits emit gaseous H_2O, and SO_2. The distribution of the fumaroles are shown in fig. 4. These three pits are connected, forming a long narrow active explosion fissure about 200 m. long; pits Nos. 9 and 10 lying close together. Their depths are about 10 m. or more, and their widths about 23 m. No. 11, the northernmost one, is about 16 m. wide and about 7 m. deep. Nos. 10 and 11 are connected by a narrow fissure, from which also issue SO_2 and H_2O. Fig. 10 shows pit No. 9. and its fumarole.

Distribution of the Ejecta.

The materials ejected are distributed along the atrio and the eastern region of Akita-Komagatake, and are mainly confined to the eastern parts of the explosion pits, near which the large blocks (about 1 m. or more in diameter) are scattered. Fine gray ash, about 5 cm. deep, is deposited on the ridge of Yokonagane. In Iwate prefecture, lying north of the volcano, occurred a slight ashfall. Fig. 4 gives some idea of the effects of the ejecta, destroying the vegetation buried by it, as shown in the light coloured parts of Fig. 5 and 7.

Damage.

Owing to the isolated character of the district, the amount of damage

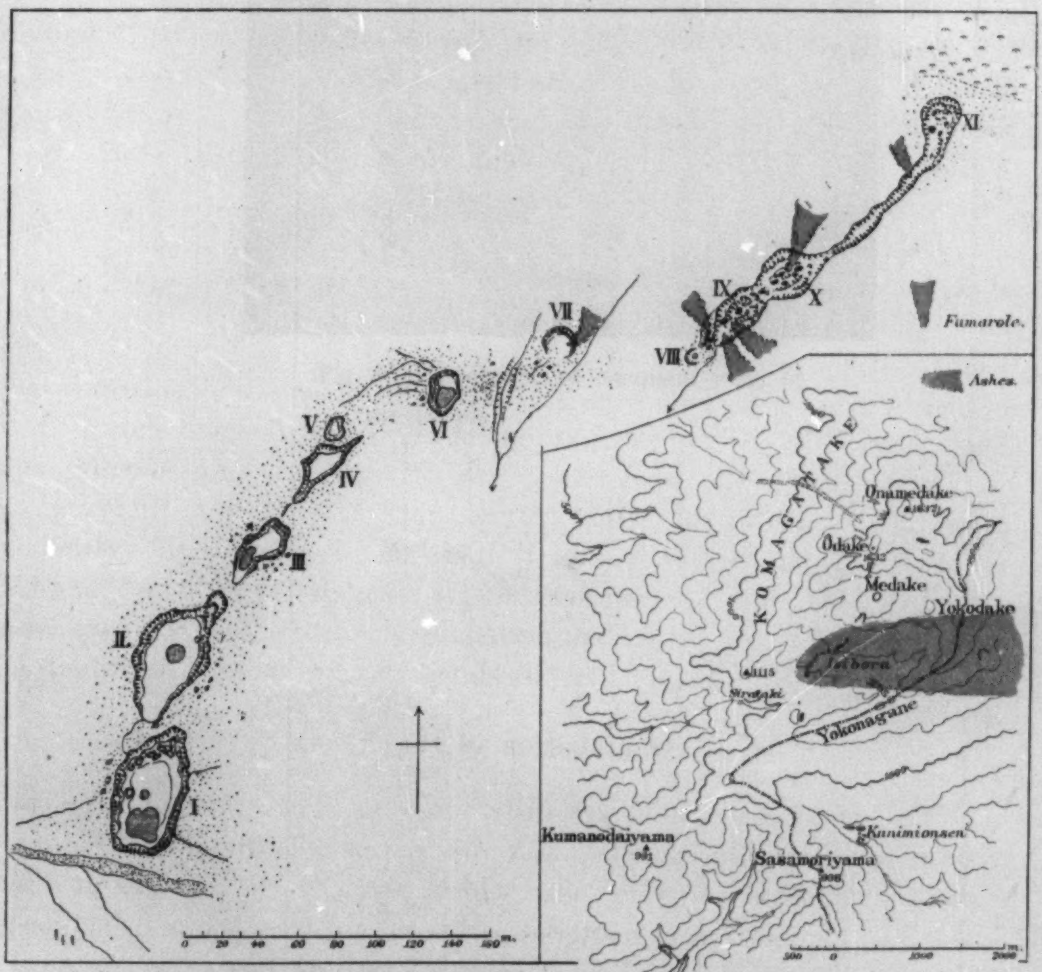

Fig. 4. Sketch map showing the distribution of the explosion pits and ashes.

(震研彙報、第十號、圖版、大塚)

Fig. 6. Photograph of complete view of the 1st pit.

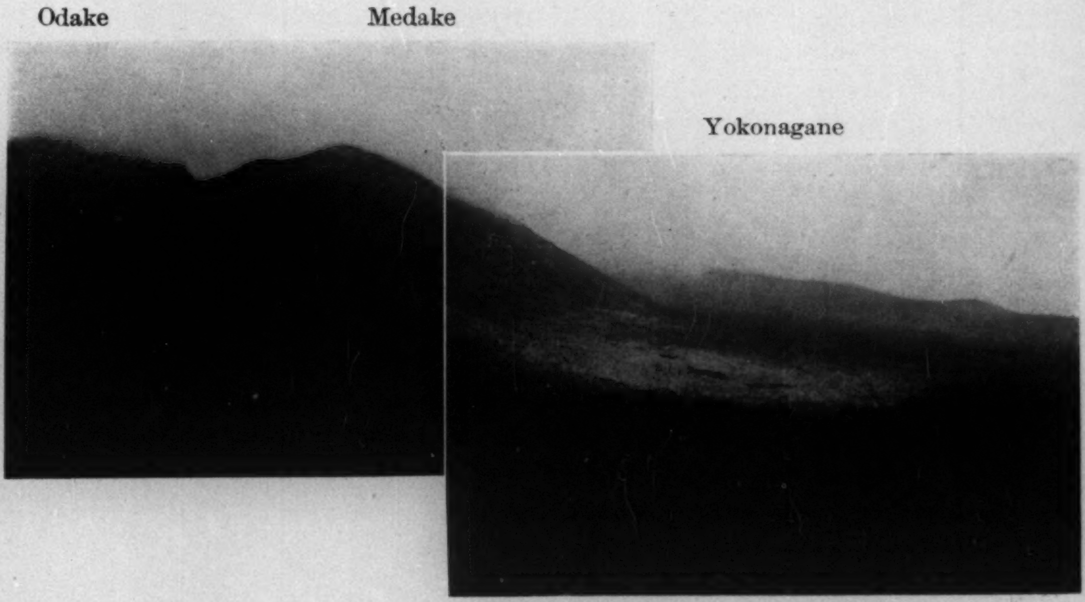

Fig. 7. Photograph of complete view of the explosion area.

（震研彙報、第十號、圖版、大塚）

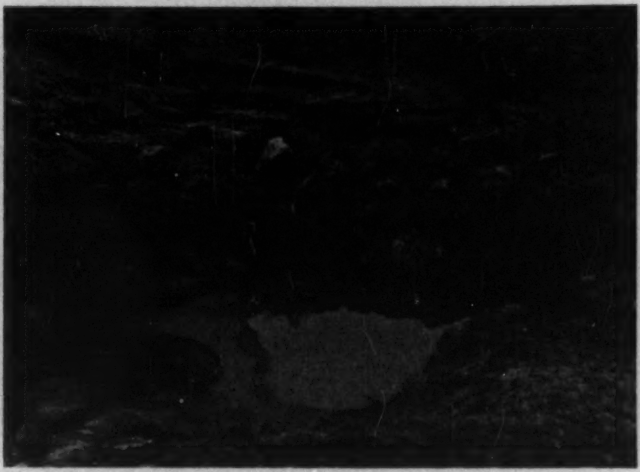

Fig. 9. Photograph of 6th pit.

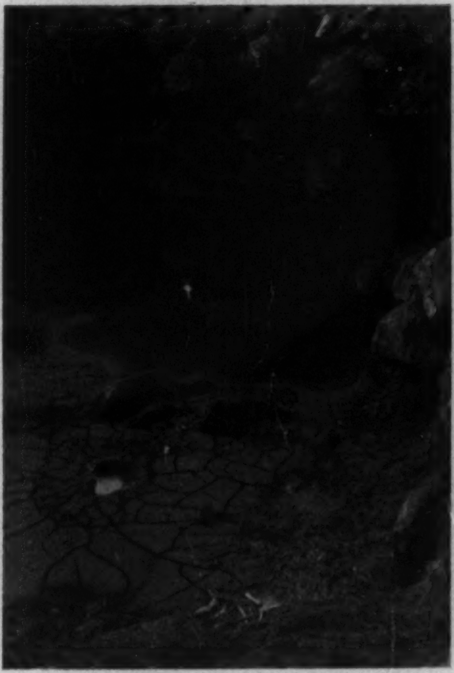

Fig. 8. The floor of the 1st pit.

Fig. 10 The 9th explosion pit and its fumaroles.

Fig. 5. Complete view of the new explosion pits.

(震研彙報、第十號、圖版、大塚)

is small, being limited to destruction of vegetation over an area of 2 km. The cool springs gushing out from the end of the atrio (locally called Ootubo[33]) changed into carbonated springs but without rising in temperature.* The temperature of the Kunimi hot springs rose after the explosion. A few days after the explosion, a guide was temporarily suffocated on the atrio by arsenic ?-impregnated gas.

Local earthquakes were felt at the town of Oomagari[34] which is situated on the Alluvial plain, 12 km. S. W. of the volcano, both before and after the explosion.

Summary.

The recent activity of the long-dormant volcano Akita-Komagatake was of the explosive type. The explosion occurred some time between July 20 and 24. The writer believes that the date is July 21, 1932. Eight or more seperate explosion pits and 3 connected pits were formed. They are all quiet now with the exception of pit No. 7 and the three connected ones (Nos. 9, 10, and 11), which were emitting vapours of H_2O, SO_2, and H_2S ?, when the writer visited them. On account of its isolated situation the damage was small.

The linear arrangement of the explosion pits seems to suggest a tectonic line lying immediately under the land surface.

---

56. 休火山秋田駒ヶ岳の活動

地震研究所　大塚彌之助

休火山秋田駒ヶ岳の最近活動した結果が述べてある。活動は爆裂で、1932 年 7 月 20 日から 25 日の間に行はれた。種々の點から綜合して、21 日に爆裂が行はれたと信ぜられる。爆裂孔は合計 11 個で、その内 8 箇はそれぞれ獨立した爆裂孔で、殘りの 3 つは溝狀の裂罅で續いてゐる。南から數へて 7 番目と 9, 10, 11 番目とは未だ水蒸氣、亞硫酸ガスを噴出してゐるが、他は泥水で充たされて、全く靜止してゐる。最大のものは徑 70 m. に達してゐる。被害は降灰區域の僅な部分の植物にあつたのみ。

尙、この爆裂後國見溫泉の溫度が高まり、大ツボの淸水は炭酸泉に變質した。

今度の爆裂は極めて表面的であること、及び爆裂孔が一列に並んでゐることは面白い。

---

33) 大ツボ.　34) 大曲.

* Some mountaineers noted that the spring dried up during the few days before the explosion.

57. *Experimental Investigation of Lateral Earth Pressure during Earthquakes.*

By Nagaho MONONOBE, and Haruo MATSUO,

Earthquake Research Institute and Research Office of Public Works, Department of Home Affairs.

(Read May 17, 1932.—Received Sept. 5, 1932.)

I. Introduction.

The previous experiment[1] with a shaking box, $1 \cdot 33 \times 1 \cdot 33 \times 2 \cdot 74$ m. in size and 8 tons in weight, proved that the max. lateral earth pressure against a wall during earthquakes may be calculated practically by applying common static earth pressure theories assuming g_e acts upon the back filling for this case instead of g for static case, both in its magnitude and direction. Here g_e represents the resulting acceleration of g, i.e. the acceleration of gravity, and the max. seismic acceleration.

But in the course of that experiment some unknown phenomenon were observed and they are traced here by more precise observations with a smaller swinging box, $0 \cdot 40 \times 0 \cdot 43 \times 1 \cdot 10$ m. in size and 560 kg. in weight, measuring the pressure against walls of $0 \cdot 40 \times 0 \cdot 30$ m. and several different sizes. The earth used was dry sand and the box was subjected to horizontal vibrations only.

II. Arrangements for Experiment.

Swinging Box. The box, filled with sand in the space $40 \times 43 \times 110$ cm., is suspended from a rigid steel frame by 4 strips of steel and the frame is supported with 2 solid concrete piers (Fig. 1 and Pl. XCVII (1)). Thus it is given horizontal vibration parallel to the figure and the pressures against the walls are measured with piezo-electric pressure gauges. The frame of the box is made of steel angles and plates, the 2 longitudinal sides are of glass plates, so as the interior be observed from outside. Free test walls, made of boards, are set vertically on both ends of the box, the widths of which are 40 cm. at one end and 20 cm.

1) *Proc. of the World Engineering Congress*, Tokyo, 1929, Paper No. 388; *Public Works*, Part 1.

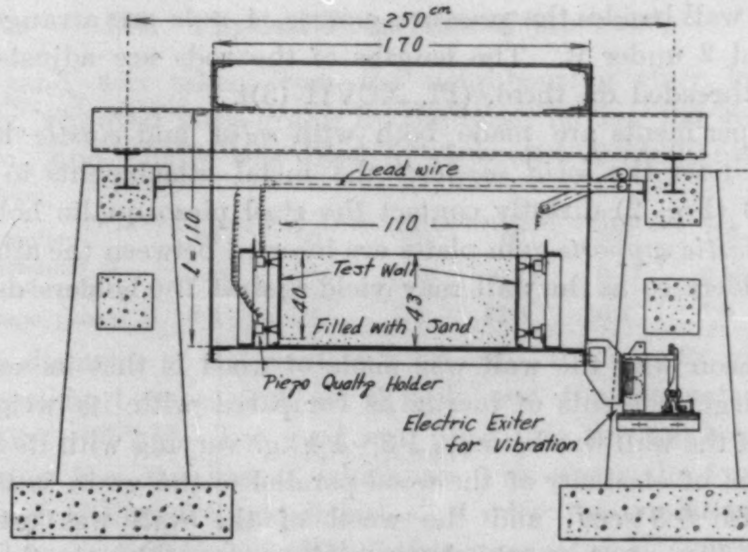

Fig. 1. Test box with the supports.

at the other. The period of vibration of the box is between 0·5∼2·0 sec. and is controlled with the steel strips changing the section between 3×3/16″ and 3 3/4×7/16″. The maximum horizontal acceleration of the horizontal vibration is about 3000 mm/sec/sec. or nearly 0·3 by the earthquake scale. Here the earthquake scale represents the ratio of the max. acceleration of vibration to the acceleration of gravity. The vibration most frequently adopted here is as follows; period $T=0{\cdot}88$ sec., max. amplitude 5·75 cm., the earthquake scale k_h being 0·3. The vibration for the box is given sometimes by hand and sometimes by electromagnetic action.

The weight of the box with sand is 560 kg.

Test Walls. The height of the walls are between 10 cm. and 40 cm. and Fig. 2 shows an example of the wall of which tests are made most frequently. According to the figure the wall is supported horizontally with A and B and vertically C and D. For the measurement of the deflection of the wall, strain dial gauges graduated 0·01 mm. are arranged at points 1∼9 and 10 in Fig. 2. (See also Pl. XCVII (2)). As it was necessary in the course of the experiment, to

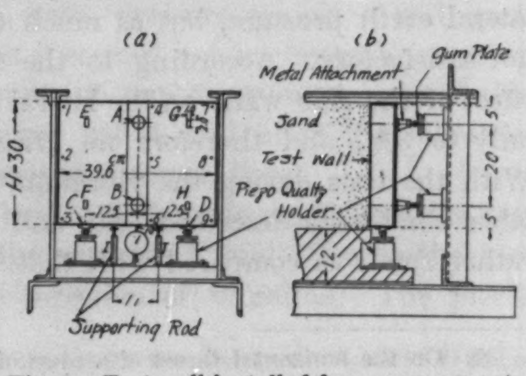

Fig. 2. Test wall installed for measurement.

support the wall besides the pressure gauges, 4 rods are arranged before the wall and 2 under it. The lengths of the rods are adjustable with the screws threaded on them. (Pl. XCVII (3)).

The experiments are made both with *solid* and *elastic* horizontal supports. Under the *solid supports* the metal attachments to the wall at A and B (Fig. 2) directly contact the steel piezo qualtz holders and under the *elastic supports* gum plates are inserted between the attachments and the holders so as the wall may yield against the holders during the vibration.

The reason why the wall was made of wood is that its section has relatively large moments of inertia as compared with its weight. The weight W of the wall was between $1{\cdot}3 \sim 4{\cdot}4$ kg. varying with its thickness. The modulus of elasticity of the wood parallel to the grain is $90{\cdot}3\,t/cm^2$. and crosswise $5{\cdot}8\,t/cm^2$. and the wood of the wall was used grains horizontal. The effect on the horizontal pressure due to the mass of the wall during the vibration is $k_h W$, and the vibration of the earth pressure is determined by subtracting $k_h W$ from the horizontal pressure measured.

Pressure Gauges. The dynamometers with steel springs or oils are not appropriate for the measurement of the pressure which varies with small periods, and here the piezo-electric pressure gauges are adopted. The electric charges exhibited at the sides of the qualtz plates when subjected to pressures are measured by delicate string electrometers. The displacement of the string is magnified by the telescope and its image is taken in a photographic plate. Two electrometers are used and the pressures on the support A and B or C and D are measured simultaneously.

Effect of Side Walls. Various arrangements to eliminate the effect of the side walls were made by previous conductors of the tests on the lateral earth pressure, but as much as the authors are aware they seems not satisfactory. According to the tests made by G. H. Darwin[2] the effect of the side walls on the lateral pressure is rather small amounting only to 3%, and therefore no arrangement for that was made here. With the tests during the vibration, the pressure was much affected by other conditions described later and the effect of the side walls seems rather small as compared with that.

---

2) On the horizontal thrust of a mass of sand, *Min. of Proc. of the Inst. of C. E.*, 71 (1882-3), 350.

III. Physical Properties of the Sand.

The sand was taken from the neighbouring river bed, washed thoroughly, removed large grains by the mesh having the clear distance of 0·5 mm., and finally was dried in an oven. A mechanical analysis is as follows,

Sieve number	20	30	40	50	80	100	200
Clear distances of the mesh (mm.)	0·85	0·50	0·36	0·29	0·17	0·14	0·074
Percentage passed	0·2	0·8	7·2	72·8	10·4	7·9	0·7

The mean diameter of the sand is 0·225 mm., the specific gravity 2·70, the unit weight between 1·25∼1·48 kg/l., and the percentage of voids between 53·7∼45·2%. The sand was filled into the test box by gravity from another box, the base of which was 1 m. above the top of the test box, through a hose 2·2 cm. diameter. Under the condition tested the unit weight was 1·29 kg/l. and the percentage of void 52·3%.

The result of the measurement of the internal co-efficient of friction of the sand was as follows:

$$p = 0{\cdot}56\, w + 0{\cdot}00159,$$

where p horizontal shear on the unit area in kg/cm². and w unit vertical pressure. Under the condition tested the angle of internal friction was $\varphi = 32°40'$. The co-efficient of friction of the sand against the wall was measured in the same way:

$$p = 0{\cdot}557\, w + 0{\cdot}00037,$$

$$\varphi_0 \fallingdotseq 30°.$$

Angle of natural slope was between 31°30′∼34°30′, varying with the packing of the sand, and the condition under which the test was carried out was rather nearer to the former.

IV. Lateral Static Pressure against a Vertical Wall.

Several laboratory tests of the static pressure against a wall gave quite satisfactory results,[3] and at first it seemed not necessary to measure the *static* pressure. But in the course of our experiment, remarkable difference between the static pressures before and after the vibration was observed and it became necessary to measure them.

Method of measurement. The box is first made empty and the test wall is carefully set vertically on the supports C and D so as the face of the wall is perpendicular to the direction of vibration. The pieces

3) Among these we remenber with full respect the test made by Mr. J. Feld, *Proc. of Am. S. C. E*, (1923), 615-660.

of the attachments on the wall to transmit the horizontal pressure to the wall at A and B are so adjusted as they are just in contact with the piezo holders when the wall is vertical. (Fig. 2). Narrow strips of cloth are provided at the ends of the wall to prevent the escape of sand, and the box is filled in horizontal layers as described in the preceding article. The time necessary to finish the filling is about 5 minutes. Then the two electrometers are first connected to the piezo qualtz holders at C and D, and the two vertical supporting rods I and J (Fig. 2) are screwed off alternately, so as they are just in contact with the wall. Observing carefully the strings of the electrometers we can distinguish whether the rods touch the wall or not. Then the adjusting pieces against the holders are screwed in and the pressure against the wall is transmitted to the rods. Thus the pressure is observed by the minus readings of the electrometers. After the measurement of C and D the readings at A and B are taken simultaneously in the same way. The pressure measured immediately after the filling is called *the pressure before the vibration* and that after it *the pressure after the vibration*. The vibration was as follows:

Period $T=0{\cdot}88$ sec.; amplitude (half) $r=5{\cdot}75$ cm., this corresponds $k_h=0{\cdot}3$ by the earthquake scale (§ II); time of the vibration about 2 m.

Tests were made both with *solid* and *elastic* horizontal supports (§ II), the vertical supports at C and D being always *solid*. For elastic supports the diameter of the gum plates were always 20 mm. The walls used and the thicknesses of gum plates were as follows:

Test No.	Test wall		Thickness of the gum plates at the supports.	
	Dimension $b\times h\times d$ (cm.)	Weight (kg.)	A (mm.)	B (mm.)
No. 4	39·6×30×6	3·63	solid	solid
„ 20	„	„	4	0·8
„ 21	„	„	8	1·6
„ 34	„	„	16	3·2
„ 23	39·6×30×1·5	1·36	4	0·8
„ 24	„	„	8	1·6
„ 25	„	„	16	3·2

Lateral Static Pressure. From the readings at C and *D* the weight of the wall was excluded and togather with the readings at A and B the pressure was expressed by the co-efficients of earth pressure. The notations are

C_{oh}=co-efficient of the horizontal component; i.e., the sum of readings at A and B is divided by $\frac{1}{2}wH^2b$, where

w=unit weight of the sand 1·29 kg/l.

H=height of the wall; 30 cm.

b=width of the wall; 40 cm.

C_{ov}=co-efficient of the vertical component; i.e., the weight of the wall is subtracted from the sum of the readings at C and D and this is divided by $\frac{1}{2}wH^2b$.

C_o=co-efficient of the resultant.

$\tan\delta=C_{ov}/C_{oh}$

h_c=height of the point of application measured from the base of the wall.

$$M_{oh}=C_{oh}\times\frac{h_c}{H}$$

Pressures before the vibration measured are as follows:

Test No.	C_{oh}	h_c/H	M_{oh}	C_{ov}	C_o	C_{ov}/C_{oh}	δ
4	0·276	0·397	0·1095	0·142	0·310	0·514	27°10′
20	0·242	0·337	0·0816	0·145	0·282	0·601	31° 0′
21	0·254	0·337	0·0856	0·154	0·296	0·605	31°10′
34	0·246	0·377	0·0927	—	—	—	—
23	0·278	0·374	0·1040	0·127	0·305	0·455	34°30′
24	0·248	0·310	0·0770	0·146	0·289	0·590	30°30′
25	0·243	0·400	0·0971	0·149	0·285	0·613	31°30′
Mean	0·255	0·362	0·0925	0·144	0·295	0·563	29°20′

After the vibration these values are

Test No.	C_{oh}	h_c/H	M_{oh}	C_{ov}	C_o	C_{ov}/C_{oh}	δ
4	0·362	0·294	0·1064	0·128	0·382	0·354	19°30′
20	0·336	0·370	0·1240	0·132	0·361	0·394	21°30′
21	0·354	0·354	0·1252	0·124	0·374	0·350	19°15′
34	0·332	0·370	0·1242	0·149	0·368	0·445	24° 0′
23	0·334	0·370	0.1235	0·090	0·346	0·270	15°10′
24	0·334	0·357	0·1190	0·127	0·357	0·380	20°50′
25	0·382	0·410	0·1565	0·114	0·399	0·298	16°30′
Mean	0·348	0·361	0·1256	0·124	0·370	0·356	19°35′

The results extend pretty wide range and the values of the solid supports can not be distinguished from those of the elastic supports, yet there is remarkable difference between those before and after the vibration.

The ratios of the mean values of the two cases are:

	C_{oh}	C_{ov}	C_o	$\tan\delta$
Ratio = (After)/(Before)	1·36	0·86	1·25	0·63

The most remarkable difference is the increase of the horizontal component and the decrease of the angle δ. (Fig. 3).

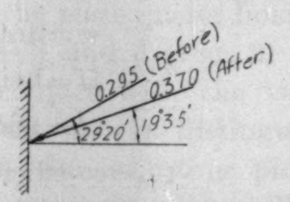

Fig. 3. Static pressures before and after the vibration.

This is considered that during the vibration the sand settles down and some passive pressure occurs against the wall. The values of the active pressure calculated with the wedge theory for this case, $\varphi=32°40'$ $\varphi_0=\delta=30°$, are

$$C_{oh}=0{\cdot}234, \quad C_{ov}=0{\cdot}135, \quad C_o=0{\cdot}270, \quad \delta=30°,$$

these approximating the values before the vibration.

V. Variation of Lateral Pressure at the Beginning of Vibration.

After the test wall is set vertically, supported by A, B, C, and D, and filled with sand as described in § III, the box is given horizontal vibrations and records of the pressure variation are taken on the photographic plates. Two electrometers are used and the records at A and B or C and D are taken simultaneously.

As the pressure variation at the beginning differed much from that after several minutes vibration, the two cases are discussed separately, here the former and in the next paragraph the latter.

The pressure variation also differed with the condition of horizontal supports, i.e. between the solid and the elastic supports, they are also separately dealt with.

Elastic Horizontal Supports. With the elastic supports the thicknesses of the gum plates are so arranged as the wall may yield during the vibration around the back base line as shown in Fig. 4.

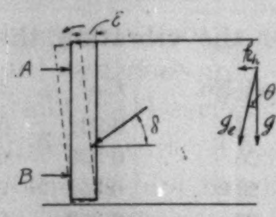

Fig. 4. Yielding of wall under elastic supports.

According to Fig. 5 which shows a typical record of the pressure at the beginning of the vibration, the mean value of the horizontal pressure increases gradually besides the periodical

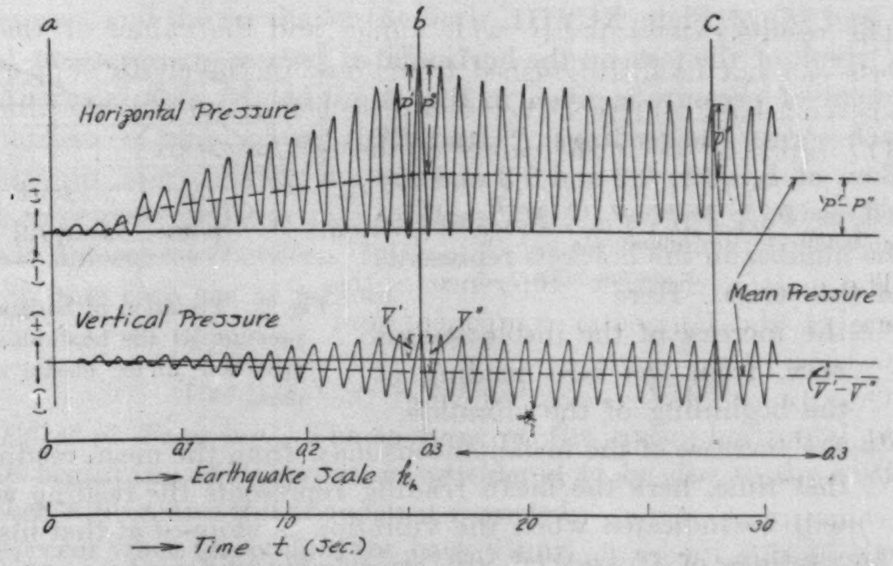

Fig. 5. Typical record of pressure at the beginning of vibration.

variation of the pressure as the amplitude of the vibration increases (between *a* and *b* of the figure). Where the amplitude reaches its max., at *b* in the figure, the increasing tendency of the mean pressure almost stops and when the amplitude of vibration is kept constant after that, the amplitude of the pressure variations tends to decrease (between *b* and *c*).

The mean value of the vertical pressure tends somewhat to decrease (between *a* and *b*) and when the max. amplitude of vibration is reached (at *b*) the decreasing tendency stops and after that the same pressure variation is repeated (after *b*).

The test was made under the following conditions:

Dimensions of the wall; $b=39{\cdot}6$ cm., $h=30$ cm., $d=1{\cdot}5$ cm.

Weight, 1·36 kg.

Thickness of the gum plate at $A=8$ mm., at $B=1{\cdot}6$ mm.

Period of vibration $T=0{\cdot}88$ sec.; max. amplitude (half) $r=5{\cdot}75$ cm., this corresponds $k_h=0{\cdot}3$.

For each test the following series of vibrations were given:

Series (1). The amplitude is made gradually large untill it becomes $k_h=0{\cdot}3$; this vibration is kept about 5 seconds and then gradually retarded and stopped.

Series (2). The same series of vibrations as (1) are repeated after the series (1).

Series (3). If necessary, the same vibrations again repeated after the series (2). Records of horizontal pressure of series (1) and (2) are shown

in (4) and (5) of Plate XCVIII.

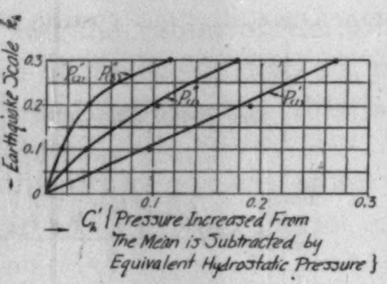

Fig. 6. Variation of horizontal pressure at the beginning of vibration under elastic supports.

A result of the tests on the horizontal component of pressure is given in Fig. 6. For each series, the readings P' and P'' are taken at $k_h = 0{\cdot}1$, $0{\cdot}2$ and $0{\cdot}3$ and are denoted as $P_{(1)}'$, $P_{(1)}''$, $P_{(2)}''$, $P_{(3)}''$ and so on ; the number in the brackets represents that of the series. Here

P' = the increase of the instantaneous max. from the zero reading at the beginning of the vibration,

P'' = the increase of the instantaneous max. from the mean reading at that time, here the mean reading represents the reading which will be indicated when the vibration is stopped at that instant.

The readings of P' and P'' are remarkably different on series (1) but on (2) and (3) they differ but little and for these P'' only is taken. The effect of the wall to the horizontal pressure is $k_h W$, W being the weight of the wall, and this is subtracted from the readings and they are represented by the co-efficient of earth pressure C_h'.

The increase of the mean horizontal pressure during the vibration which is represented by $P_{(1)}' - P_{(1)}''$ in the figure is little influenced by the condition of supports and the mean values of 5 tests both of elastic and solid supports are

$k_h = 0{\cdot}1$	$0{\cdot}2$	$0{\cdot}3$
$C_h = 0{\cdot}038$	$0{\cdot}076$	$0{\cdot}106$

The difference of P'' at a and b (Fig. 5) is here represented (Fig. 6) by $P_{(1)}'' - P_{(2)}''$ or $P_{(1)}'' - P_{(3)}''$ and the max. values are

$k_h = 0{\cdot}1$	$0{\cdot}2$	$0{\cdot}3$
$C_h = 0{\cdot}04$	$0{\cdot}06$	$0{\cdot}08$

From the record of the vertical pressure the decrease of the mean vertical pressure is measured as

$k_h = 0{\cdot}1$	$0{\cdot}2$	$0{\cdot}3$
$C_v = 0{\cdot}007$	$0{\cdot}014$	$0{\cdot}020$

and as for the vertical components there is little difference between $P_{(1)}''$ and $P_{(2)}''$.

Solid Horizontal Supports. Tests were also made by the solid horizontal supports, the other conditions being exactly the same as the

former case, and the results for the horizontal pressures are shown in Fig. 7.

As was already related the amount of increase of the mean horizontal pressure are aproximately the same as the former case, and the max. values of the differences between $P_{(1)}''$ and $P_{(2)}''$ in this case are as follows,

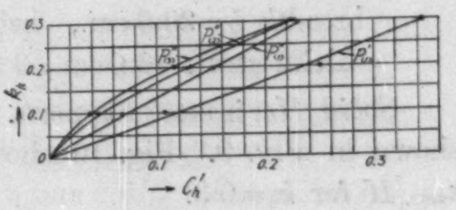

Fig. 7. Variation of horizontal pressure at the beginning of vibration under solid supports.

$k_h=0{\cdot}1$	$0{\cdot}2$	$0{\cdot}3$
$C_h=0{\cdot}035$	$0{\cdot}050$	$0{\cdot}020$

Effect of Tamping. The increase of the mean horizontal pressure at the beginning of vibration is considered to be due to the settling of the back filling, and this increase is expected to disappear when tamping of the back filling is made. Tests were made under the condition and a result is shown in Fig. 8.

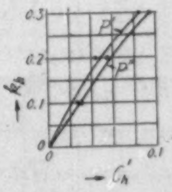

Fig. 8. Variation of horizontal pressure when tamping was made.

The tamping was made by falling an iron weight covering an area 10×10 cm. (weight $2{\cdot}1$ kg.) on the sand surface from the height of 10 cm. at every $2{\cdot}5$ cm. layer and one fall for every 10×10 cm. area of sand surface. According to the figure, the increasing tendency of the mean horizontal pressure disappears and the tamping seems very effective. But the absolute max. pressure against the wall is the sum of P' and the initial static pressure. This test shows that the sum of this case is larger than that when tamping was not made and from this point of view tamping seems not always effective. The most effective *ideal tamping* is that the back filling is tamped to that degree of packing that it is brought when the filling undergoes the earthquake assumed. For structures, even most careful tamping seems to be within this ideal state and it seems not necessary to guard against too much tamping.

VI. Variation of Lateral Pressure under Stable Condition.

After several minutes vibration, the mean pressure becomes constant and the same variation is repeated under the same amplitude of vibration. Under this condition, the relation of the deformation of the wall to the difference between the max. and the mean of the pressure was investigated. Dimensions of test walls are

breadth $b=39{\cdot}6$ cm., heights $h=40$ cm., 30 cm. and 20 cm.,
thicknesses $t=6{\cdot}0$ cm., 3·0 cm. and 1·5 cm.

Solid Horizontal Supports. An example of the results of tests is shown in Fig. 9. Fig. 10 shows the relation of C_h' or M_h' to $\varepsilon_{max.}$ or $\varepsilon_{max.}/H$ for $k_h=0{\cdot}3$.

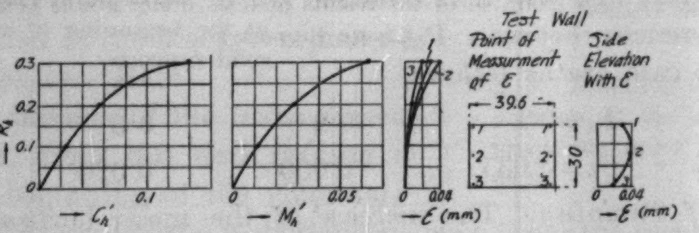

Fig. 9. An example of the results of tests under stable condition.
(Solid supports; $b=39.6$, $h=30$, $t=1.5^{cm}$)

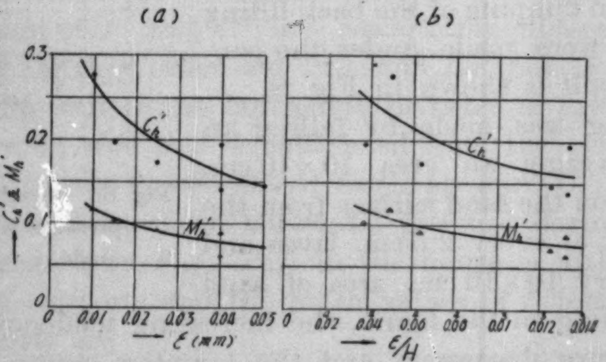

Fig. 10. Relation between ε and C_h' etc. under stable condition.
(Solid supports; $k_h=0.3$)

The larger $\varepsilon_{max.}$ or $\varepsilon_{max.}/H$, the smaller C_h' or M_h' becomes. The means of all measured values are as follows,

k_h	C_h'	C_v'
0·1	0·034	0·012
0·2	0·093	0·023
0·3	0·195	0·037

The relations between these values and the static pressures are to be discussed in § VII.

Elastic Horizontal Supports. Tests were made under the arrangement that the wall may yield as shown in Fig. 4, and the readings were taken as shown in Fig. 11. The relations $\varepsilon_{max.}$ and $\varepsilon_{max.}/H$ to C_h' and M_h' for each tests corresponding $k_h=0{\cdot}3$ are plotted in Fig. 12. As a special case of this, the results of solid supports are also plotted in

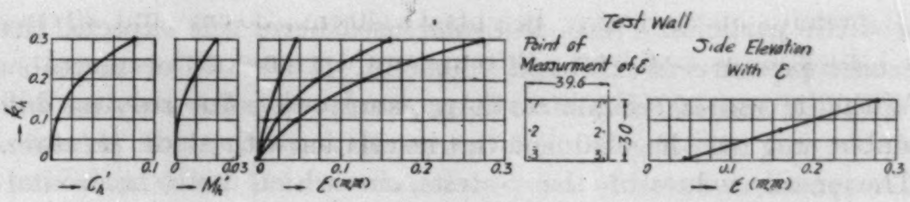

Fig. 11. An example of the results of tests under stable condition. (Elastic supports)

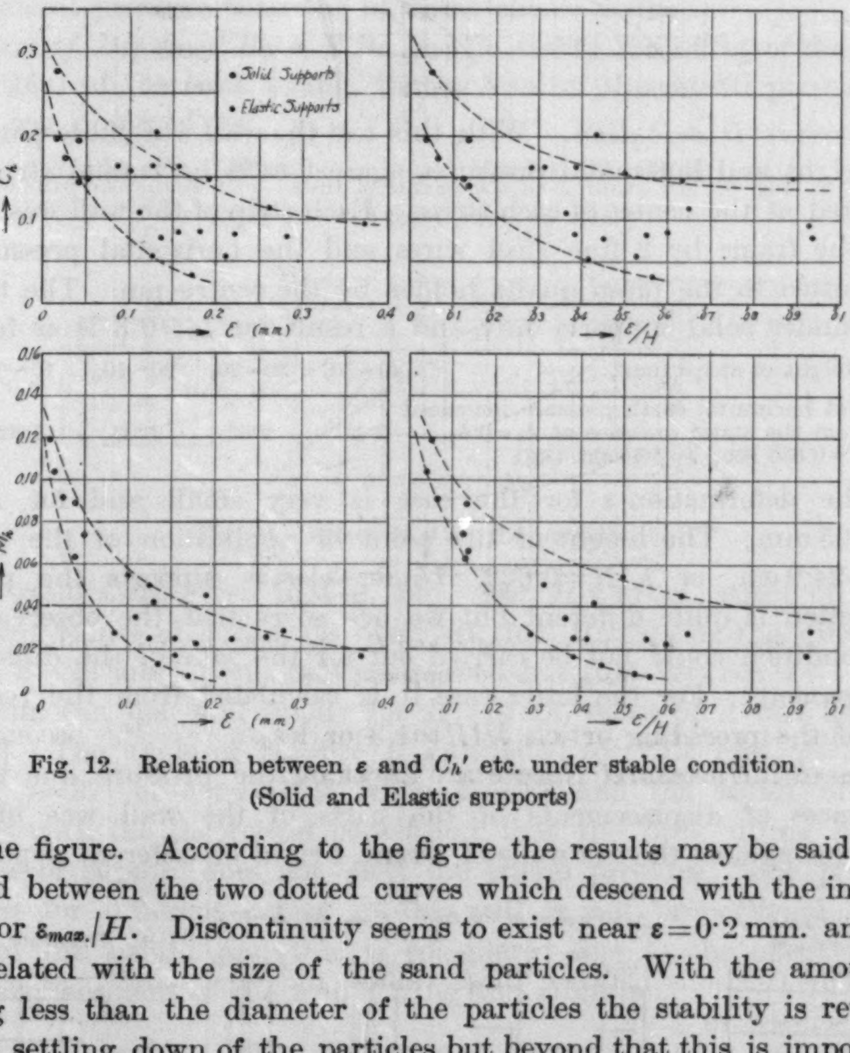

Fig. 12. Relation between ε and C_h' etc. under stable condition. (Solid and Elastic supports)

the same figure. According to the figure the results may be said to be involved between the two dotted curves which descend with the increase of $\varepsilon_{max.}$ or $\varepsilon_{max.}/H$. Discontinuity seems to exist near $\varepsilon=0{\cdot}2$ mm. and this to be related with the size of the sand particles. With the amount of yielding less than the diameter of the particles the stability is retained without settling down of the particles but beyond that this is impossible. Dr. Terzaghi relates[4] concluding his experiment on static earth pressure that the min. co-efficient of earth pressure is obtained when $\varepsilon_{max.}/H=0{\cdot}001$. This, however, seems not to be determined independently with the size

4) *Engineering*, May 30, 1930.

of the earth particles. With the sand used here, it is expected that the min. static pressure is exhibited when $\varepsilon_{max.}/H=0\cdot0006$ or thereabouts.

With the test of seismic earth pressure one point only for one k_h is obtainable and not the chain of the results as with static pressure.

The mean values of the 5 tests, in which both horizontal and vertical components were taken, are

k_h'	C_h'	C_v'
0·1	0·008	0·029
0·2	0·026	0·068
0·3	0·071	0·118

Pressure Distribution. With this test the wall was cut to parts of 10 cm. height and horizontal pressures against each horizontal strips were measured at the centre of each strips. Each strip of the wall was hanged from the frame by 2 fine steel wires and the horizontal pressure was transmitted to the piezo qualtz holder by the centre pin. The test was made under solid supports only and a result for $k_h=0\cdot3$ is as follows:

Height of strips (cm),	40∼30,	30∼20,	20∼10,	10∼0.	
Net horizontal earth pressure increased from the static pressure at $k_h=0\cdot3$; $T=0\cdot855$ sec; $r=5\cdot45$ cm. (kg).	2·42	2·62	2·02	1·82	$\Sigma=8\cdot88$

The deformation ε for the case is very small and for $k_h=0\cdot3$, $\varepsilon \fallingdotseq 0\cdot005$ mm. The height of the point of application of the pressure is $h_c=24\cdot9$ cm. or $h_c/H=0\cdot622$. Under elastic supports the point of application is quite different but we are sorry that the observation of this condition could not be carried out for the sake of the difficulty of arrangements. For the latter case it is calculated from the results of tests of the preceding article $h_c/H=1/3$ or less.

Special Horizontal Supports. Effect on the pressure due to small differences of displacements of the parts of the wall was observed. Pressures against the test walls of 10 cm. height of different depths were

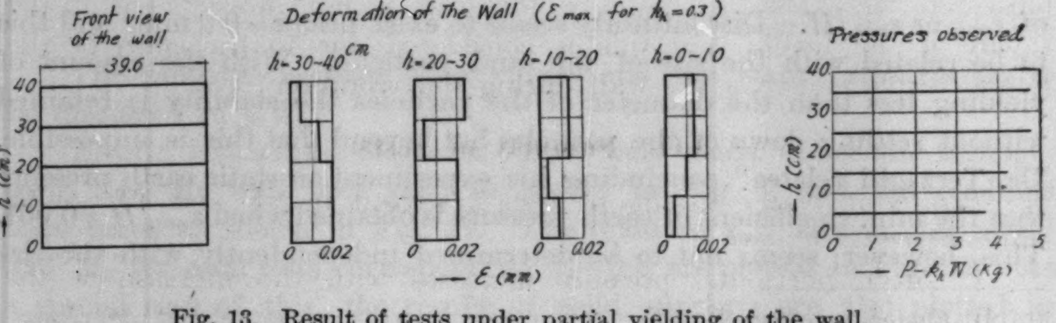

Fig. 13. Result of tests under partial yielding of the wall.

observed by allowing less displacement of the wall than the adjacent parts. Results of 4 tests are given in Fig. 13. For the part measured $\varepsilon \doteqdot 0{\cdot}005$ mm. where for the adjacent part $\varepsilon = 0{\cdot}01 \sim 0{\cdot}02$ mm. when $k_h = 0{\cdot}3$. Total sum of the pressures increased from the means for 4 different parts is 17·3kg. where the corresponding value of the preceding paragraph is 8·8 kg. This shows that the pressure is much influenced by the displacement of the adjacent walls and that the solid wall undergoes larger lateral pressure than the adjacent elastic walls.

Effect of Depth of Back Filling. To testify the effect of the depth d (Fig. 14a) of the back filling, the increase of the lateral pressure for $k_h = 0{\cdot}3$ was observed for

$$d = 12,\ 20,\ 110 \text{ cm.} \qquad H = 10,\ 20,\ 30,\ 40 \text{ cm.}$$

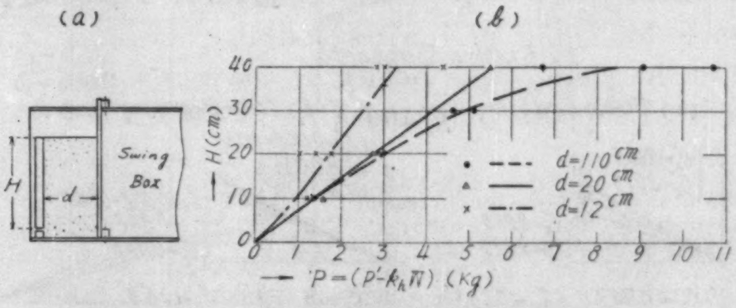

Fig. 14. Effect of d on the pressure.

and the results are given in Fig. 14b. For $H=40$ cm. effect on P of 3 different values of d can be observed, for $H=20$ cm. the difference between $d=20$ and 12 cm. can be observed but that between $d=110$ cm. and 20 cm. can not, and finally for $H=10$ cm. effect of d can little be observed. The angle of rupture is calculated for this case $\varphi = 32°40'$, $\varphi_0 = 30°$, $\gamma = 37°$ or $\cot\gamma = 1{\cdot}33$ when $k_h = 0{\cdot}3$ and the result of tests coincides with the theoretical conclusion that the back filling outside the plane of rupture does not effect the lateral pressure. The pressure measured for different height of the wall is not proportional to the square of the height and this is considered due to the effect of the lateral displacement of the wall during the vibration.

VII. Summay of Tests.

Results of Tests. Results of tests described in § V and VI can be summarized as follows.

1. Mean horizontal pressure increases with the increase of the amplitude of vibration, and mean vertical pressure somewhat decreases.

2. The increase or decrease of the mean pressure during the vibration remains as it is after vibration.

3. Taking the vibration of a certain k_h, the difference between the instantaneous max. and the mean of the horizontal pressure at the beginning is larger than that after several minutes vibration; the difference of the vertical pressures remains always constant for the same k_h.

4. The difference between the mean and the instantaneous min. of the horizontal pressure is almost 75% of the difference between the max. and the mean (see Pl. XCVIII (6)), where for the vertical pressure the two differences are always the same. The instantaneous max. and min. together with the mean pressure, viz. the static pressure, are shown in Fig. 15; in which values under elastic supports (I), solid supports (II),

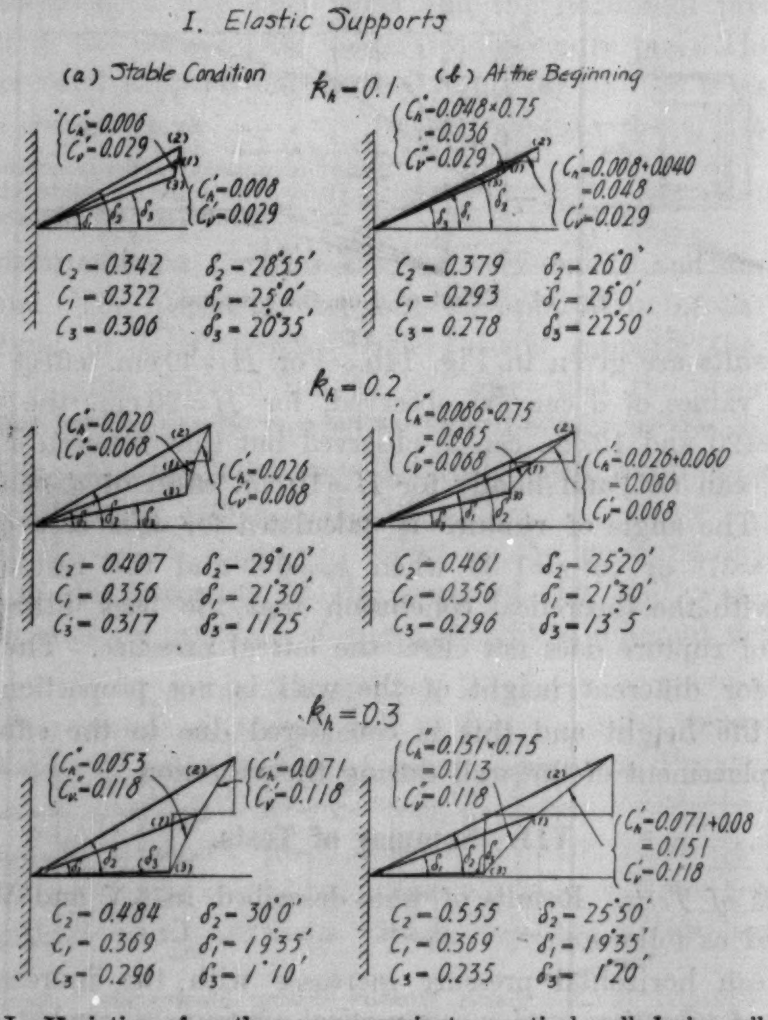

Fig. 15-I. Variation of earth pressure against a vertical wall during vibration.

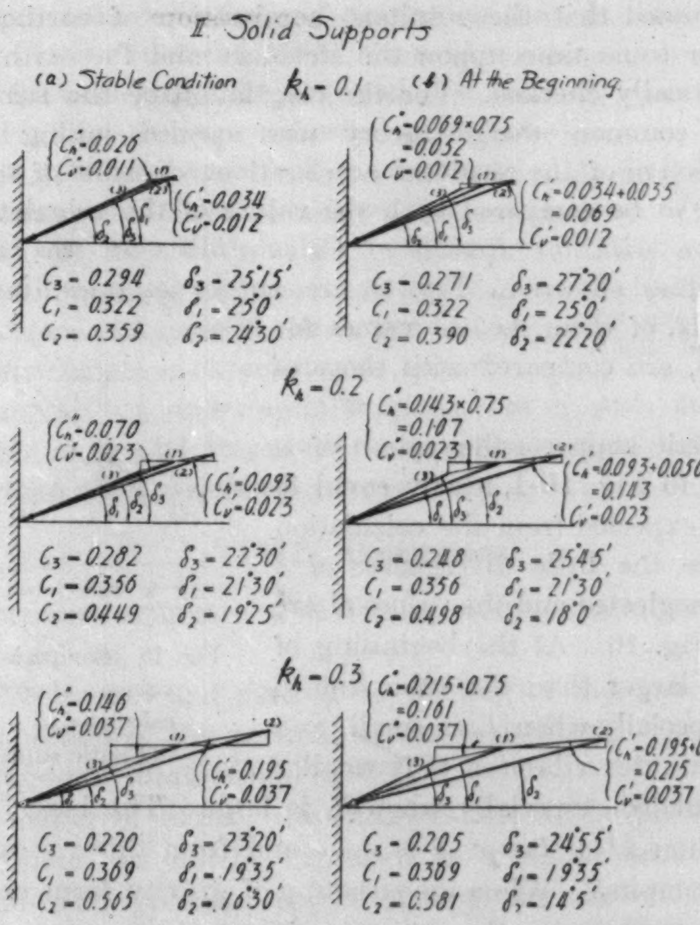

Fig. 15-II Variation of earth pressure against a vertical wall during vibration.

and for each at the beginning (b), and after several minutes vibration (a) are given. These values are the means of several tests and not the exact values.

The pressure against the wall when the max. horizontal acceleration of vibration is directed towards the wall is shown as (2) in each figures and when directed against is (3) and the *mean pressure*, viz. the pressure which is expected when stopped at that instant, is shown as (1).

In general the structure is most dangerous under the condition (2) and for the design of earthquake-proof structures this state is considered.

Method of Calculation of Seismic Earth Pressure. A method of calculation for the design of the earthquake-proof structures was introduced by one of the authors[5] shortly after the Great Earthquake of

5) N. Mononobe, "On the Earth Pressure during Earthquake," *Journal of the Japanese Civil Engineering Society*, 10 (1924), No. 5, (in Japanese).

1923. He assumed that the resultant acceleration of earthquake and gravity acts for some time uppon the structure and the earth, and the stability is statically checked. For the calculation of the seismic earth pressure, the common wedge theory was applied taking the most dangerous direction of the resultant acceleration. Results of tests above mensioned are to be compared with the values of the calculation.

Comparison with the Results of Calculation. As was mentioned already the values shown in Fig. 15 are not exact ones, but for the present the max. of them, i.e. the values for (2) in Fig. 15, are compared with those of calculation.

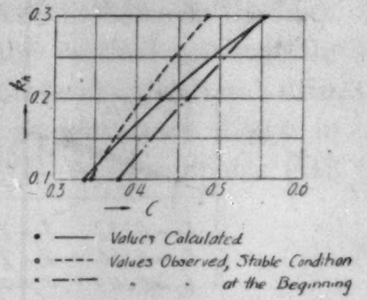

Fig. 16. Comparison of the values observed with calculated. (Elastic supports)

Under elastic supports the values of δ_1 are, according to Fig. 15–I, nearly equal to 30°—which is expected from the calculation —and therefore the little divergences of δ from 30° are neglected and the values C are compared in Fig. 16. At the beginning of vibration C is larger than the value due to calculation, especially when k_h is small, and after several minutes vibration C is smaller than that calculated, especially when k_h is large. The latter case also corresponds when *ideal tamping* is done and from this we can see the advantage of tamping. When the structure of gravity form or L shape is subjected to earthquake, the pressure against it is expected to have the tendency above mensioned rather than that next described.

For solid supports the observed values of δ are quite different and therefore the two components are shown separately in Fig. 17. In this

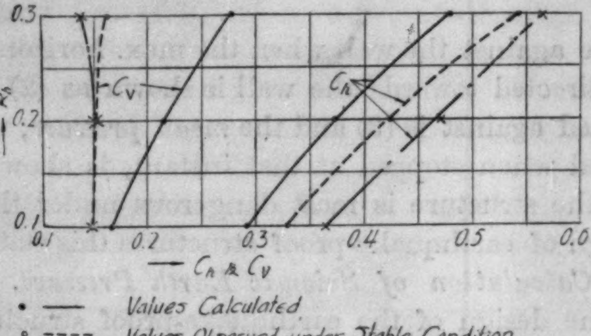

Fig. 17. Comparison of the values observed with calculated. (Solid supports)

case, contrary to the former case δ_2 is smaller than δ_3. This seems due to the different kind of deformation of the wall. Under the elastic supports the wall yields as shown in Fig. 18 (a) when subjected to the acceleration g_e—this causing max. δ—but under solid supports the wall yields as shown in Fig. 18 (b). According to Fig. 17 the horizontal components observed are larger than calculated. In general the amount of ε/H of the structure is expected to be larger than that of the test under solid supports, but if such amount of ε/H should occur in a solid structure, the pressure against it is expected to be larger than that calculated.

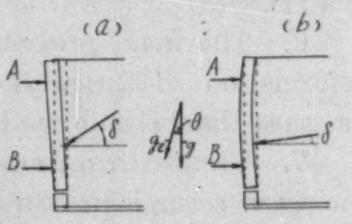

Fig. 18. Yielding of the wall under elastic supports (a) and solid supports (b).

VIII. Conclusions.

The pressure against a wall during vibration is influenced by many conditions such as,

1. The amount and manner of yielding of the wall,
2. Condition of the packing of the back filling,
3. Time of vibration and so on,

and, as a matter of course, the exact values of the pressure including these conditions can not be expressed in a simple formula. But concerning the max. pressure, results of tests deviate but little from the values calculated, except some special cases, and the authors would conclude that the values of the calculation may be taken as approximating the max. pressure against the wall during the vibration, so long as the exact values of the effects of the conditions are not determined by further experiments.

The conclusions drawn from the experiments are

1. Under the vibration of a certain k_h, structures are subjected to max. seismic lateral pressure at the beginning of the vibration. (§ V).

2. The lateral static pressure after vibration is larger than that before vibration and this is considered to be due to the passive pressure caused by *settling* of the filling. (§ IV and V)

3. For smaller k_h, the effect of the settling is large and for which the max. lateral pressure larger than calculated is measured. (§ VII)

4. Carefull tamping has the advantage to reduce the max. pressure at the beginning of vibration. (§ V).

5. The max. pressure against the structure, for which ideal tamping

of the back filling is carried out, is somewhat smaller than that calculated. (§ VII).

6. The max. pressure during the vibration is much effected by the deformation of the wall and solid walls undergo larger seismic earth pressure than elastic walls. (§ VI).

7. The earth outside the plane of rupture calculated does not effect the max. seismic pressure. (§ VI).

---

57. 地震時土壓の實驗的研究

地震研究所 物部長穗
松尾春雄

地震時土砂が構造物壁面に及ぼす壓力變化の狀態を明かならしむる爲、振動函(寸法、內法 40×43×110 cm.) に乾燥せる砂を滿し之に水平振動を與へ、振動の方向に直角に支へたる垂直壁に作用する壓力の變化をピエゾ電氣壓力計にて記錄し、その時間的變化を研究した。試驗の結果を綜合すれば次の如くである。

1. 擁壁が地震を受くる場合、之に働く土壓力は最大震度に達したる初期に於て最大である。

2. 振動後に於ける靜止土壓力は、振動中の土砂の沈定の爲、振動前の靜止土壓力より大なる値を示す。

3. 土砂沈定の影響は震度が小なる時比較的大にして、振動中の最大壓力の測定値は、震度が小なる場合には計算値より一般に大である。

4. 裏込土砂の搗き固めを十分にする事は、振動初期の增加壓力を小にする效果がある。

5. 「理想的の搗き固め」をなした場合に限り、地震時壓力は計算値より小である。

6. 振動中の最大土壓は壁の歪と大なる關係を有し、殆ど變形なき剛性壁には特に大なる地震時土壓が働く。

7. 計算せる地震時崩壞面より外方にある土砂は、最大土壓には影響を及ぼさない。

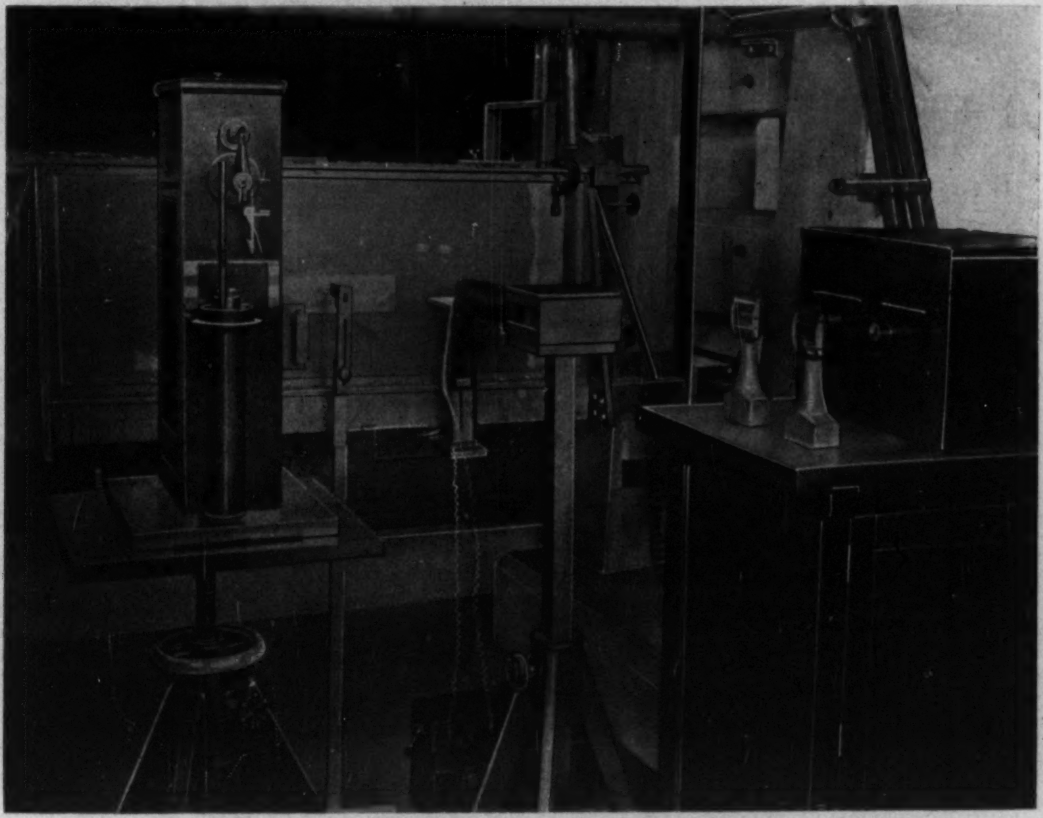

(1) Test box and measuring apparatus.

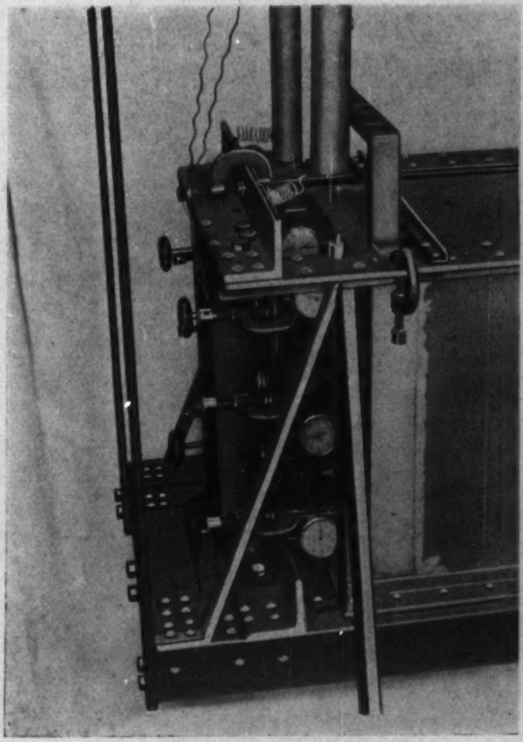

(2) Measuring apparatus of the deflection of the wall.

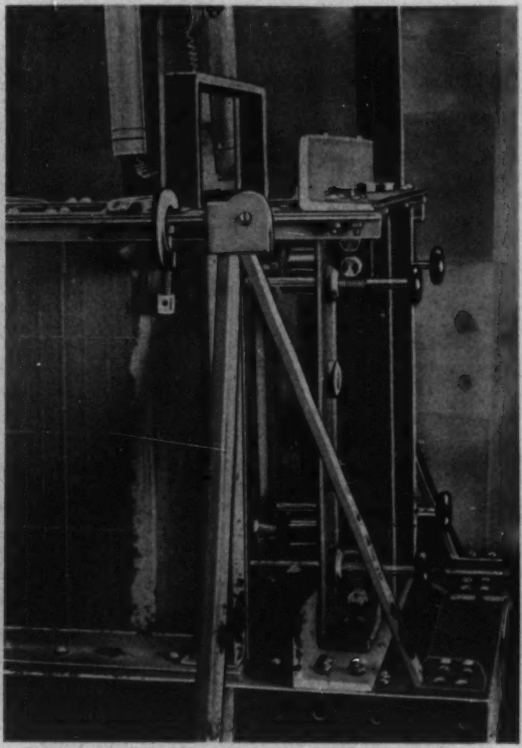

(3) Auxiliary supporting rods of the wall.

(震研彙報、第十號、圖版、物部、松尾)

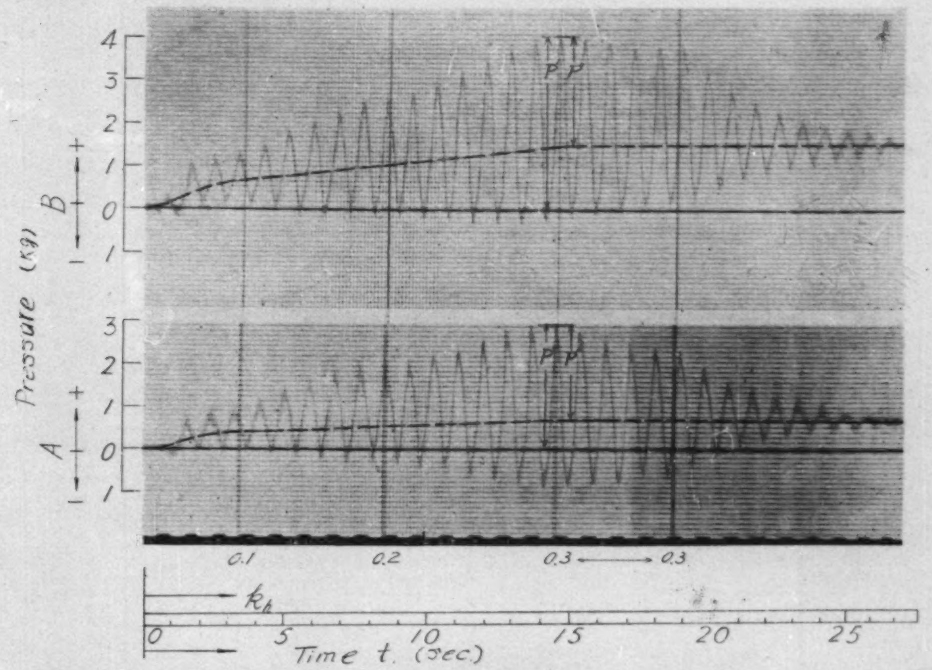

(4) Record of horizontal pressure at the beginning of vibration, Series (1)

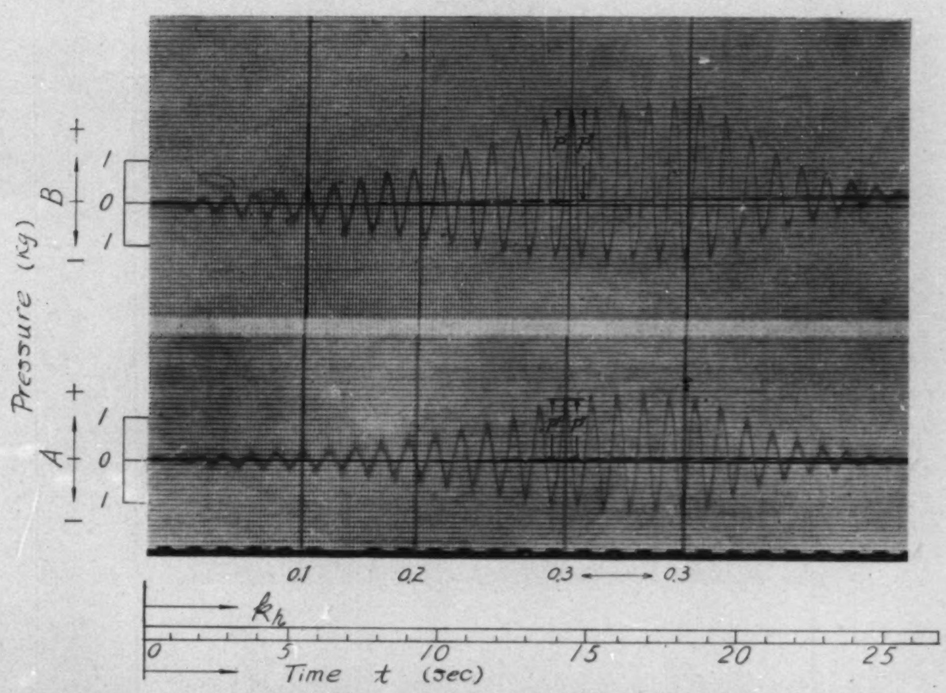

(5) Record of horizontal pressure at the beginning of vibration, Series (2).

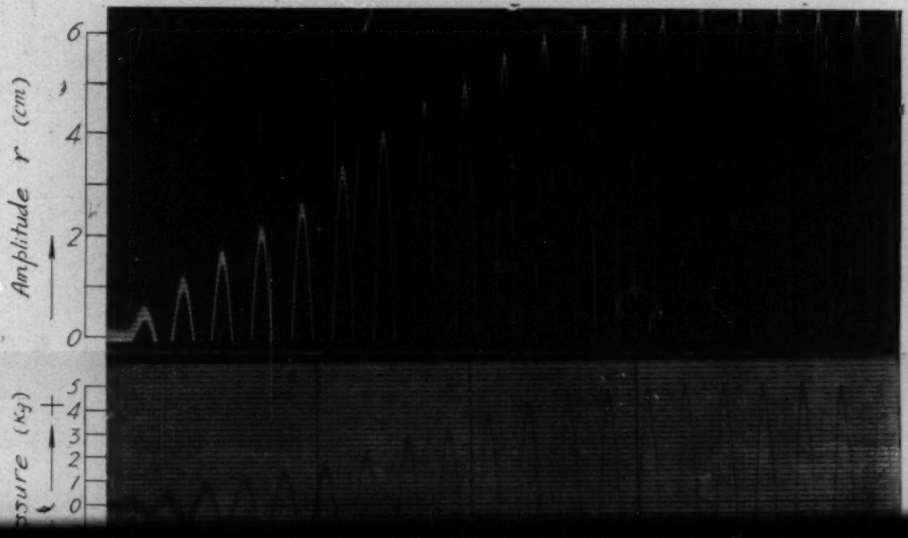

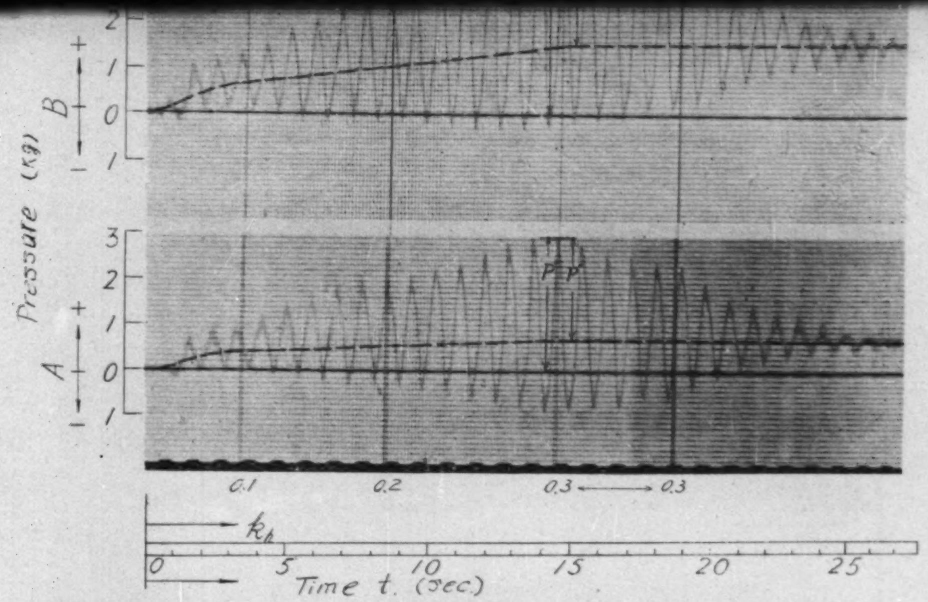

(4) Record of horizontal pressure at the beginning of vibration, Series (1)

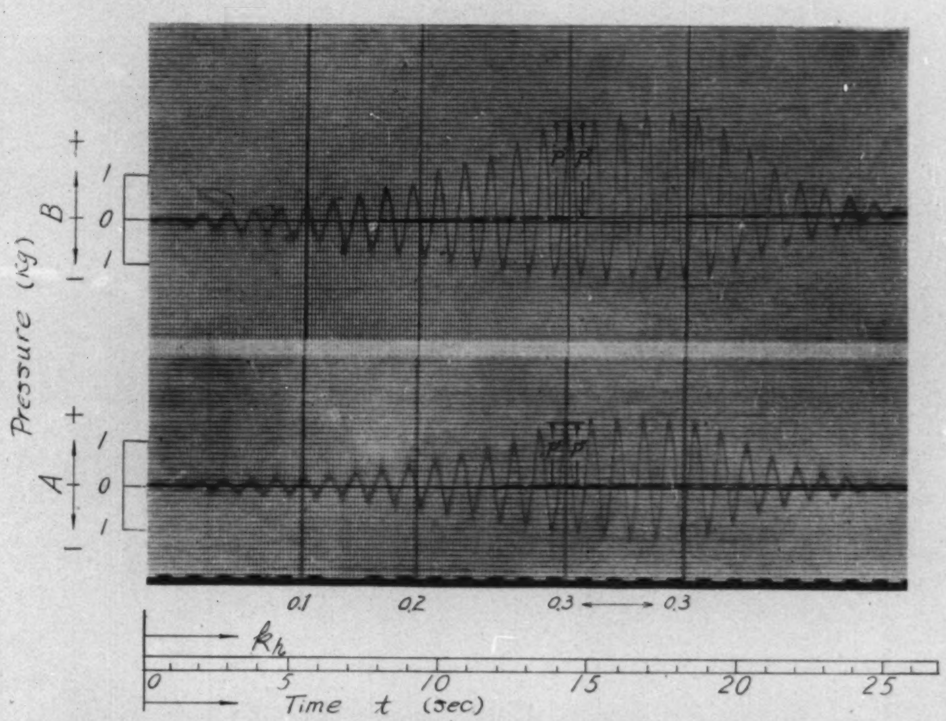

(5) Record of horizontal pressure at the beginning of vibration, Series (2).

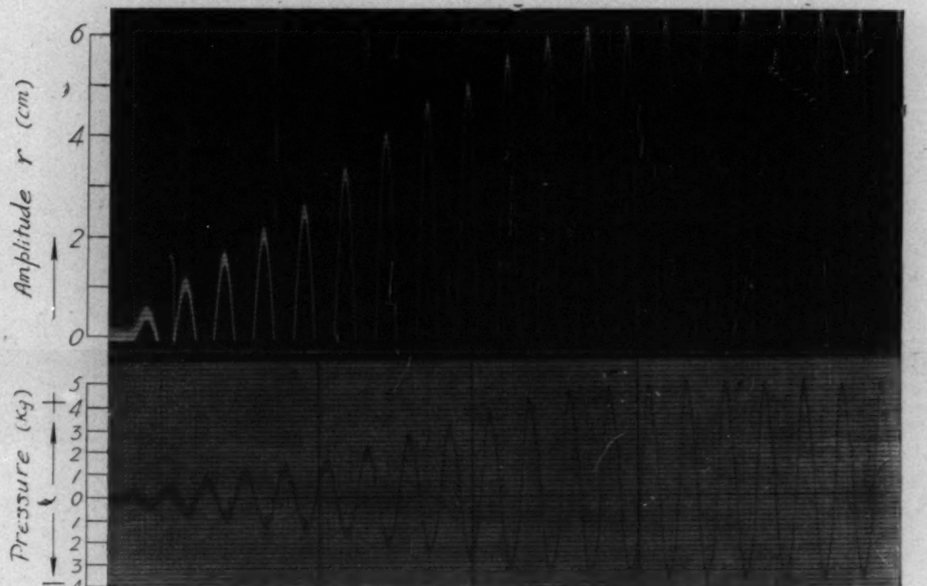

(6) Record of the vibration of the box and the horizontal pressure variation.

(震研彙報、第十號、圖版、物部、松尾)

58. *Vibrations of a Two- or Three-storeyed Structure.*

By Katsutada SEZAWA and Kiyoshi KANAI,

Earthquake Research Institute.

(Read Sept. 20, 1932.—Received Sept. 20, 1932.)

In this paper we are going to find theoretically the period of natural vibrations of a two- or three-storeyed structure. Our method of treatment is somewhat different from those of the authors cited in our former paper.[1] The structure in question is assumed to be a clamped-free bar carrying concentrated masses at positions corresponding to its horizontal members. It is clear from our paper or common sense that the deformation of the horizontal members or of beams due horizontal vibrations is very small and such members may be treated as rigid bodies, so that our case may be applied to the problem of a building or of a bridge. The case of a single concentrated mass was dealt with by Mononobe[2], Prescott[3] and Muto[4]. Although the problem of vibrations of the case of many masses was studied approximately by a few others, its accurate solution has not yet been studied.

1. Free Vibrations of a Bar having Two Concentrated Masses.

Two parts, OA and AB, of the bar are assumed uniform along their respective lengths, O, B, A being clamped and free ends and an intermediate point of the bar respectively. The following notations are used:

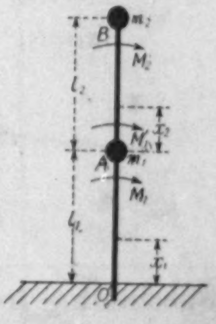

Fig. 1.

m_1, m_2=concentrated masses at A and B,

l_1, l_2= distances between 0 and A, and that between A and B,

$\rho_1, E_1, a_1, I_1, y_1$=density, Young's modulus, area and moment of inertia of cross section, and transverse deflection of the part OA,

1) K. SEZAWA and K. KANAI, "Vibrations of a Single-storied Framed Structure," *Bull. Earthq. Res. Inst.*, 10 (1932), 767–803.

2) N. MONONOBE, *Journ. Soc. Civil Eng.*, Tokyo, 6 (1920), 581–690.

3) J. PRESCOTT, *Applied Elasticity* (London, 1924), 213.

4) K. MUTO, *ZAMM*, 10 (1930), 346.

$\rho_2, E_2, a_2, I_2, Y_2$ = similar respective ones of the part AB,
M_1, M_1', M_2 = bending moments of the parts OA and AB at the points A and B.
F_1, F_1', F_2 = shearing forces of the parts OA and AB at A and B.

The equations of motion of the parts OA and AB are expressed by

$$E_1 I_1 \frac{\partial^4 y_1}{\partial x_1^4} + \rho_1 a_1 \frac{\partial^2 y_1}{\partial t^2} = 0\ ; \quad E_2 I_2 \frac{\partial^4 y_2}{\partial x_2^4} + \rho_2 a_2 \frac{\partial^2 y_2}{\partial t^2} = 0. \quad \ldots\ldots (1)$$

If we write $y_1 = u_1 \cos pt$, $y_2 = u_2 \cos pt$, $n_1^4 = \dfrac{\rho_1 p^2}{E_1 k_1^2}$, $n_2^4 = \dfrac{\rho_2 p^2}{E_2 k_2^2}$ we get

$$\left.\begin{aligned} u_1 &= A_1 \cos n_1 x_1 + B_1 \sin n_1 x_1 + C_1 \cosh n_1 x_1 + D_1 \sinh n_1 x_1, \\ u_2 &= A_2 \cos n_2 x_2 + B_2 \sin n_2 x_2 + C_2 \cosh n_2 x_2 + D_2 \sinh n_2 x_2, \end{aligned}\right\} \ldots (2)$$

We know that

$$\left.\begin{aligned} -\left(E_1 I_1 \frac{\partial^2 y_1}{\partial x_1^2}\right)_{x_1=l_1} &= M_1, \quad -\left(E_1 I_1 \frac{\partial^3 y_1}{\partial x_1^3}\right)_{x_1=l_1} = F_1, \\ -\left(E_2 I_2 \frac{\partial^2 y_2}{\partial x_2^2}\right)_{x_2=0} &= M_1', \quad -\left(E_2 I_2 \frac{\partial^3 y_2}{\partial x_2^3}\right)_{x_2=0} = F_1', \\ -\left(E_2 I_2 \frac{\partial^2 y_2}{\partial x_2^2}\right)_{x_2=l_2} &= M_2, \quad -\left(E_2 I_2 \frac{\partial^3 y_2}{\partial x_2^3}\right)_{x_2=l_2} = F_2. \end{aligned}\right\} \ldots\ldots (3)$$

The boundary conditions are such that

$$x_1 = 0\ ; \quad y_1 = 0, \quad \frac{\partial y_1}{\partial x_1} = 0, \quad \ldots\ldots\ldots\ldots\ldots\ldots\ldots (4)$$

$$\left.\begin{aligned} x_1 = l_1,\ x_2 = 0\ ; \quad & M_1 - M_1' = 0, \quad F_1' = F_1 + m_1 \frac{\partial^2 y_1}{\partial t^2}, \\ & y_1 = y_2, \quad \frac{\partial y_1}{\partial x} = \frac{\partial y_2}{\partial x}, \end{aligned}\right\} \ldots\ldots\ldots (5)$$

$$x_2 = l_2\ ; \quad M_2 = 0, \quad F_2 + m_2 \frac{\partial^2 y_2}{\partial t^2} = 0. \quad \ldots\ldots\ldots\ldots\ldots\ldots (6)$$

Substituting from (2), (3) in (4), (5), (6), we get finally

$$\begin{aligned} &\xi\{(1+\cos\alpha\cosh\alpha) + \gamma_1(\cos\alpha\sinh\alpha - \sin\alpha\cosh\alpha)\}\{(1+\cos\beta\cosh\beta) \\ &\quad + \gamma_2(\cos\beta\sinh\beta - \sin\beta\cosh\beta)\} + \eta\{(\cos\alpha\sinh\alpha + \sin\alpha\cosh\alpha) \\ &\quad - \gamma_1(1-\cos\alpha\cosh\alpha)\}\{(\cos\beta\sinh\beta - \sin\beta\cosh\beta) - 2\gamma_2\sin\beta\sinh\beta\} \\ &\quad - 2\xi\eta\sin\alpha\sinh\alpha\{\sin\beta\sinh\beta + \gamma_2(\cos\beta\sinh\beta + \sin\beta\cosh\beta)\} \\ &\quad + \xi^2\eta(\cos\alpha\sinh\alpha - \sin\alpha\cosh\alpha)\{(\cos\beta\sinh\beta + \sin\beta\cosh\beta) \\ &\quad + 2\gamma_2\cos\beta\cosh\beta\} + \xi\eta^2(1-\cos\alpha\cosh\alpha)\{(1-\cos\beta\cosh\beta) \end{aligned}$$

$$-\gamma_2(\cos\beta\sinh\beta-\sin\beta\cosh\beta)\}=0, \quad \ldots\ldots\ldots\ldots\ldots\ldots\ldots\ldots(7)$$

where

$$\left.\begin{aligned}&\alpha=n_1l_1,\ \beta=n_2l_2,\ \xi=\frac{n_2}{n_1},\ \eta=\frac{E_2I_2n_2^2}{E_1I_1n_1^2},\\&\gamma_1=\frac{m_1p^2}{E_1I_1n_1^3},\ \gamma_2=\frac{m_2p^2}{E_2I_2n_2^3}.\end{aligned}\right\}\ldots\ldots\ldots(8)$$

From the relations (7) and (8) we find the frequency of vibrations p.

When $m_1=0$, $m_2=0$, $\rho_1=\rho_2$, $l_1=l_2$, $k_1=k_2$, $E_1=E_2$, $a_1=a_2$, we have $\xi=1$, $\eta=1$, $\alpha=\beta$, $\gamma_1=0$, $\gamma_2=0$, so that we get

$$1+\cos z\cosh z=0, \quad \ldots\ldots\ldots\ldots\ldots\ldots\ldots\ldots(9)$$

where $z=2l_1n_1$. This is the frequency equation of a clamped-free bar whose length is $2l_1$.

When $m_1=0$, $\rho_1=\rho_2$, $l_1=l_2$, $k_1=k_2$, $E_1=E_2$, $a_1=a_2$, we have $\xi=1$, $\eta=1$, $\alpha=\beta$, $\gamma_1=0$, so that we get

$$(1+\cos z\cosh z)+cz(\cos z\sinh z-\sin z\cosh z)=0, \quad \ldots(10)$$

where $z=2l_1n_1$, $cz=\dfrac{m_2p^2}{E_2I_2n_2^3}\equiv\gamma_2$. This is the frequency equation of a bar clamped at one end and carrying a concentrated mass at its free end.

As it is very difficult to solve (7), we have used the method of trial and error to get frequencies of various cases. This method is quite similar to that of our preceding paper[5]. Again, we have limited the calculation to the determination of the respective frequencies of the fundamental vibrations of the cases, $\dfrac{m_1}{\rho_1a_1l_1}=4,\ 2,\ 1,\ \dfrac{1}{2}$, besides the conditions that $m_1=m_2$, $\rho_1=\rho_2$, $l_1=l_2$, $k_1=k_2$, $E_1=E_2$, $a_1=a_2$. The result is shown as follows:

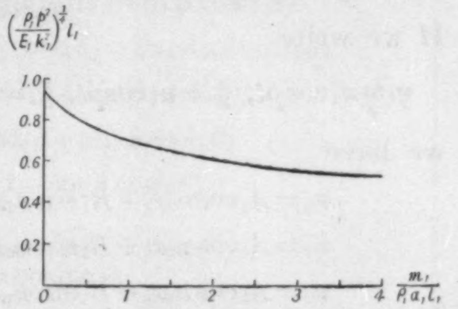

Fig. 2.

$\dfrac{m_1}{\rho_1a_1l_1}$ =	4	2	1	$\frac{1}{2}$	0
$\left(\dfrac{\rho_1p^2}{E_1k_1^2}\right)^{\frac{1}{4}}l_1$ =	0·526	0·612	0·698	0·777	0·938

These values are plotted in Fig. 2.

5) K. Sezawa and K. Kanai, *loc. cit.*

2. Free Vibrations of a Bar having Three Concentrated Masses.

Three parts OA, AB, and BC of the bar are assumed uniform along their respective lengths, O, C, A, B being clamped and free ends and intermediate points of the bar respectively. Notations used are as follows:

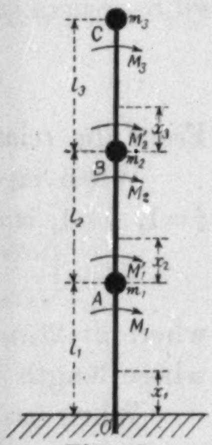

Fig. 3.

m_1, m_2, m_3=concentrated masses at A, B and C,

l_1, l_2, l_3=distances OA, AB and BC,

ρ_1, E_1, a_1, I_1, y_1=density, Young's modulus, area of cross section, moment of inertia of cross section, and the transverse deflection of the part OA,

ρ_2, E_2, a_2, I_2, y_2=similar ones of the part AB,

ρ_3, E_3, a_3, I_3, y_3=similar ones of the part BC,

M_1, M_1', M_2, M_2', M_3=bending moments of the parts OA, AB, BC at the points A, B, C,

F_1, F_1', F_2, F_2' F_3=shearing forces of the parts OA, AB, BC at the point A, B, C.

The equations of motion of the parts OA, AB, BC are expressed by

$$E_1I_1\frac{\partial^4 y_1}{\partial x_1^4}+\rho_1a_1\frac{\partial^2 y_1}{\partial t^2}=0,\quad E_2I_2\frac{\partial^4 y_2}{\partial x_2^4}+\rho_2a_2\frac{\partial^2 y_2}{\partial t^2}=0,$$

$$E_3I_3\frac{\partial^4 y_3}{\partial x_3^4}+\rho_3a_3\frac{\partial^2 y_3}{\partial t^2}=0. \quad\ldots\ldots\ldots\ldots\ldots\ldots(11)$$

If we write

$$y_1=u_1\cos pt,\quad y_2=u_2\cos pt,\quad y_3=u_3\cos pt,\quad n_1^4=\frac{\rho_1p^2}{E_1k_1^2},\quad n_2^4=\frac{\rho_2p^2}{E_2k_2^2},\quad n_3^4=\frac{\rho_3p^2}{E_3k_3^2},$$

we have

$$\left.\begin{aligned}n_1&=A_1\cos n_1x_1+B_1\sin n_1x_1+C_1\cosh n_1x_1+D_1\sinh n_1x_1,\\ n_2&=A_2\cos n_2x_2+B_2\sin n_2x_2+C_2\cosh n_2x_2+D_2\sinh n_2x_2,\\ n_3&=A_3\cos n_3x_3+B_3\sin n_3x_3+C_3\cosh n_3x_3+D_2\sinh n_3x_3.\end{aligned}\right\}\ldots(12)$$

We know that

$$\left.\begin{aligned}&-\left(E_1I_1\frac{\partial^2 y_1}{\partial x_1^2}\right)_{x_1=l_1}=M_1, &&-\left(E_1I_1\frac{\partial^3 y_1}{\partial x_1^3}\right)_{x_1=l_1}=F_1,\\ &-\left(E_2I_2\frac{\partial^2 y_2}{\partial x_2^2}\right)_{x_2=0}=M_1', &&-\left(E_2I_2\frac{\partial^3 y_2}{\partial x_2^3}\right)_{x_2=0}=F_1',\\ &-\left(E_2I_2\frac{\partial^2 y_2}{\partial x_2^2}\right)_{x_2=l_2}=M_2, &&-\left(E_2I_2\frac{\partial^3 y_2}{\partial x_2^3}\right)_{x_2=l_2}=F_2,\end{aligned}\right\}\ldots\ldots(13)$$

$$\left.\begin{aligned}-\left(E_3I_3\frac{\partial^2y_3}{\partial x_3^2}\right)_{x_3=0}&=M_2', & -\left(E_3I_3\frac{\partial^3y_3}{\partial x_3^3}\right)_{x_3=0}&=F_2',\\ -\left(E_3I_3\frac{\partial^2y_3}{\partial x_3^2}\right)_{x_3=l_3}&=M_3, & -\left(E_3I_3\frac{\partial^3y_3}{\partial x_3^3}\right)_{x_3=l_3}&=F_3.\end{aligned}\right\}$$

The boundary conditions are such that

$$x_1=0\ ;\ y_1=0,\ \frac{\partial y_1}{\partial x_1}=0, \qquad \text{(14)}$$

$$\left.\begin{aligned}x_1=l_1,\ x_2=0\ ;\ M_1-M_1'=0,\ F_1'=F_1+m_1\frac{\partial^2y_1}{\partial t^2},\\ y_1=y_2,\qquad \frac{\partial y_1}{\partial x_1}=\frac{\partial y_2}{\partial x_2},\end{aligned}\right\} \qquad \text{(15)}$$

$$\left.\begin{aligned}x_2=l_2,\ x_3=0\ ;\ M_2-M_2'=0,\ F_2'=F_2+m_2\frac{\partial^2y_2}{\partial t^2},\\ y_2=y_3,\qquad \frac{\partial y_2}{\partial x_2}=\frac{\partial y_3}{\partial x_3},\end{aligned}\right\} \qquad \text{(16)}$$

$$x_3=l_3\ ;\ M_3=0,\ F_3+m_3\frac{\partial^2y_3}{\partial t^2}=0. \qquad \text{(17)}$$

Substituting from (12), (13) in (14), (15), (16), (17) and carrying out a complex calculation we get finally

$$\begin{aligned}&\xi\{(1+\cos\alpha\cosh\alpha)+\gamma_1(\cos\alpha\sinh\alpha-\sin\alpha\cosh\alpha)\}\\
&\quad\times[\zeta\{(1+\cos\beta\cosh\beta)+\gamma_2(\cos\beta\sinh\beta-\sin\beta\cosh\beta)\}\{(1+\cos\delta\cosh\delta)\\
&\quad+\gamma_3(\cos\delta\sinh\delta-\sin\delta\cosh\delta)\}+\vartheta\{(\cos\beta\sinh\beta+\sin\beta\cosh\beta)\\
&\quad-\gamma_2(1-\cos\beta\cosh\beta)\}\{(\cos\delta\sinh\delta-\sin\delta\cosh\delta)-2\gamma_3\sin\delta\sinh\delta\}\\
&\quad-2\zeta\vartheta\sin\beta\sinh\beta\{\sin\delta\sinh\delta+\gamma_3(\cos\delta\sinh\delta+\sin\delta\cosh\delta)\}\\
&\quad+\zeta^2\vartheta(\cos\beta\sinh\beta-\sin\beta\cosh\beta)\{(\cos\delta\sinh\delta+\sin\delta\cosh\delta)\\
&\quad+2\gamma_3\cos\delta\cosh\delta\}+\zeta\vartheta^2(1-\cos\beta\cosh\beta)\{(1-\cos\delta\cosh\delta)\\
&\quad-\gamma_3(\cos\delta\sinh\delta-\sin\delta\cosh\delta)\}]\\
&+\eta\{(\cos\alpha\sinh\alpha+\sin\alpha\cosh\alpha)-\gamma_1(1-\cos\alpha\cosh\alpha)\}\\
&\quad\times[\zeta\{(\cos\beta\sinh\beta-\sin\beta\cosh\beta)-2\gamma_2\sin\beta\sinh\beta\}\{(1+\cos\delta\cosh\delta)\\
&\quad+\gamma_3(\cos\delta\sinh\delta-\sin\delta\cosh\delta)\}+\vartheta\{2\cos\beta\cosh\beta\\
&\quad+\gamma_2(\cos\beta\sinh\beta-\sin\beta\cosh\beta)\}\{(\cos\delta\sinh\delta-\sin\delta\cosh\delta)-2\gamma_3\sin\delta\sinh\delta\}\\
&\quad-2\zeta\vartheta(\cos\beta\sinh\beta+\sin\beta\cosh\beta)\{\sin\delta\sinh\delta+\gamma_3(\cos\delta\sinh\delta+\sin\delta\cosh\delta)\}\\
&\quad-2\zeta^2\vartheta\sin\beta\sinh\beta\{(\cos\delta\sinh\delta+\sin\delta\cosh\delta)+2\gamma_3\cos\delta\cosh\delta\}\\
&\quad-\zeta\vartheta^2(\cos\beta\sinh\beta-\sin\beta\cosh\beta)\{(1-\cos\delta\cosh\delta)\\
&\quad-\gamma_3(\cos\delta\sinh\delta-\sin\delta\cosh\delta)\}]\end{aligned}$$

$$
\begin{aligned}
&-2\xi\eta\sin\alpha\sinh\alpha\\
&\quad\times[\zeta\{\sin\beta\sinh\beta+\gamma_2(\cos\beta\sinh\beta+\sin\beta\cosh\beta)\}\{(1+\cos\delta\cosh\delta)\\
&\quad+\gamma_3(\cos\delta\sinh\delta-\sin\delta\cosh\delta)\}-\vartheta\{(\cos\beta\sinh\beta-\sin\beta\cosh\beta)\\
&\quad-\gamma_2\sin\beta\sinh\beta\}\{(\cos\delta\sinh\delta-\sin\delta\cosh\delta)-2\gamma_3\sin\delta\sinh\delta\}\\
&\quad+2\zeta\vartheta\cos\beta\cosh\beta\{\sin\delta\sinh\delta+\gamma_3(\cos\delta\sinh\delta+\sin\delta\cosh\delta)\}\\
&\quad+\zeta^2\vartheta(\cos\beta\sinh\beta+\sin\beta\cosh\beta)\{(\cos\delta\sinh\delta+\sin\delta\cosh\delta)+2\gamma_3\cos\delta\cosh\delta\}\\
&\quad-\zeta\vartheta^2\sin\beta\sinh\beta\{(1-\cos\delta\cosh\delta)-\gamma_3(\cos\delta\sinh\delta-\sin\delta\cosh\delta)\}]\\
&+\xi^2\eta(\cos\alpha\sinh\alpha-\sin\alpha\cosh\alpha)\\
&\quad\times[\zeta\{(\cos\beta\sinh\beta+\sin\beta\cosh\beta)+2\gamma_2\cos\beta\cosh\beta\}\{(1+\cos\delta\cosh\delta)\\
&\quad+\gamma_3(\cos\delta\sinh\delta-\sin\delta\cosh\delta)\}+\vartheta\{2\sin\beta\sinh\beta+\gamma_2(\cos\beta\sinh\beta\\
&\quad+\sin\beta\cosh\beta)\}\{(\cos\delta\sinh\delta-\sin\delta\cosh\delta)-2\gamma_3\sin\delta\sinh\delta\}\\
&\quad+2\zeta\vartheta(\cos\beta\sinh\beta-\sin\beta\cosh\beta)\{\sin\delta\sinh\delta+\gamma_3(\cos\delta\sinh\delta+\sin\delta\cosh\delta)\}\\
&\quad+2\zeta^2\vartheta\cos\beta\cosh\beta\{(\cos\delta\sinh\delta+\sin\delta\cosh\delta)+2\gamma_3\cos\delta\cosh\delta\}\\
&\quad-\zeta\vartheta^2(\cos\beta\sinh\beta+\sin\beta\cosh\beta)\{(1-\cos\delta\cosh\delta)\\
&\quad-\gamma_3(\cos\delta\sinh\delta-\sin\delta\cosh\delta)\}]\\
&+\xi\eta^2(1-\cos\alpha\cosh\alpha)\\
&\quad\times[\zeta\{(1-\cos\beta\cosh\beta)-\gamma_2(\cos\beta\sinh\beta-\sin\beta\cosh\beta)\}\{(1+\cos\delta\cosh\delta)\\
&\quad+\gamma_3(\cos\delta\sinh\delta-\sin\delta\cosh\delta)\}-\vartheta\{(\cos\beta\sinh\beta+\sin\beta\cosh\beta)\\
&\quad+\gamma_2(1+\cos\beta\cosh\beta)\}\{(\cos\delta\sinh\delta-\sin\delta\cosh\delta)-2\gamma_3\sin\delta\sinh\delta\}\\
&\quad+2\zeta\vartheta\sin\beta\sinh\beta\{\sin\delta\sinh\delta+\gamma_3(\cos\delta\sinh\delta+\sin\delta\cosh\delta)\}\\
&\quad-\zeta^2\vartheta(\cos\beta\sinh\beta-\sin\beta\cosh\beta)\{(\cos\delta\sinh\delta+\sin\delta\cosh\delta)\\
&\quad+2\gamma_3\cos\delta\cosh\delta\}+\zeta\vartheta^2(1+\cos\beta\cosh\beta)\{(1-\cos\delta\cosh\delta)\\
&\quad-\gamma_3(\cos\delta\sinh\delta-\sin\delta\cosh\delta)\}]=0, \qquad\qquad (18)
\end{aligned}
$$

where

$$\alpha=n_1l_1,\quad \beta=n_2l_2,\quad \delta=n_3l_3,\quad \xi=\frac{n_2}{n_1},\quad \eta=\frac{E_2I_2n_2^2}{E_1I_1n_1^2},$$

$$\zeta=\frac{n_3}{n_2},\quad \vartheta=\frac{E_3I_3n_3^2}{E_2I_2n_2^2},\quad \gamma_1=\frac{m_1p^2}{E_1I_1n_1^3},\quad \gamma_2=\frac{m_2p^2}{E_2I_2n_2^3},\quad \gamma_3=\frac{m_3p^2}{E_3I_3n_3^3}.$$

The natural period of vibrations is determined from the equation (18). We have calculated four cases of $m_1/\rho_1a_1l_1$ as follows:

$$(\rho_1=\rho_2=\rho_3,\ E_1=E_2=E_3,\ k_1=k_2=k_3,\ a_1=a_2=a_3,\ m_1=m_2=m_3,\ l_1=l_2=l_3)$$

$$\frac{m_1}{\rho_1 a_1 l_1} = 4 \quad 2 \quad 1 \quad \frac{1}{2} \quad 0$$

$$\left(\frac{\rho_1 p^2}{E_1 k_1^2}\right)^{\frac{1}{4}} l_1 = 0{\cdot}371 \quad 0{\cdot}428 \quad 0{\cdot}485 \quad 0{\cdot}535 \quad 0.625$$

These values are plotted in Fig. 4.

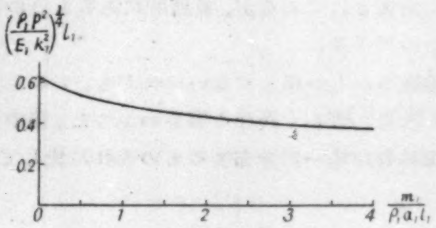

Fig. 4.

3. Resumé.

For the purpose of comparison the present calculated values and some other well known results together are tabulated below:

The values of $\left(\frac{\rho_1 p^2}{E_1 k_1^2}\right)^{\frac{1}{4}} l_1$

$\frac{m_1}{\rho_1 a_1 l_1}$		4	2	1	$\frac{1}{2}$	0
One concentrated mass	I	0·908	1·077	1·23	1·46	1·875
	II	(1·255)	(1·428)	(1·577)	(1·691)	(1·875)
Two concentrated mass	I	0·526	0·612	0·698	0·777	0·938
	II	(0·628)	(0·713)	(0·788)	(0·847)	(0·938)
Three concentrated mass	I	0·371	0·428	0·485	0·535	0·625
	II	(0·418)	(0·475)	(0·525)	(0·565)	(0·625)

I: Exact calculation.
II: Concentrated mass being distributed uniformly along the bar.

58. 二層又は三層架構の屈曲振動

地震研究所 妹澤克惟
金井清

構造物の床部を載荷物と見做した場合の棒の屈曲振動の計算を行つた。棒の一端に載荷物のある場合は物部博士によつて既に研究されてゐるが、數箇所にあるものの正確な計算はまだやつてなかつたので、この研究を試みたのである。

この計算では棒の固有振動數のみしか出してないけれども、しかし其振動數は集中質量を棒の長さに沿うて均一に分布させた場合と著しく異なる事がわかつた。集中質量の全質量が棒の全質量の二倍位のときでも正確なる振動數は均一に分布せるものそれに比して二割位も少ない事がわかつた。